Atlas of Sellar, Suprasellar, and Parasellar Lesions

plus videos

Editor-in-chief
Narayanan Janakiram

Associate Editors
Dharambir S. Sethi
Shilpee Bhatia Sharma

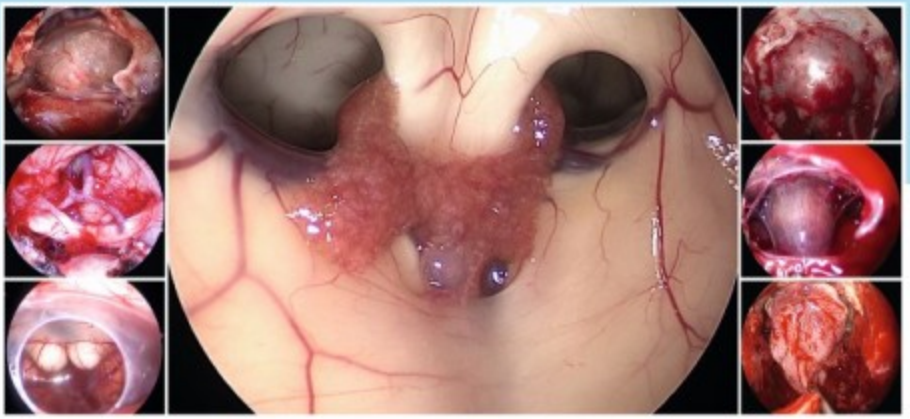

Thieme

Thieme

Atlas of Sellar, Suprasellar, and Parasellar Lesions

Editor-in-Chief

Narayanan Janakiram, DLO, MS
Skull Base Surgeon
Managing Director
Royal Pearl Hospital
Tiruchirapalli
Tamil Nadu, India

Associate Editors

Dharambir S. Sethi, MBBS, FRCSEd
Senior Consultant
Ear, Nose, and Throat Surgeon
Novena ENT–Head and Neck Surgery Specialist Centre
Mount Elizabeth Novena Hospital
Visiting Consultant
Department of Otolaryngology
Singapore General Hospital
Bukit Merah, Singapore

Shilpee Bhatia Sharma, MS
Consultant
Department of Otolaryngology
Royal Pearl Hospital
Tiruchirapalli
Tamil Nadu, India

1097 illustrations

Thieme
Delhi • Stuttgart • New York • Rio de Janeiro

Publishing Director: Ritu Sharma
Development Editor: Dr Gurvinder Kaur
Director-Editorial Services: Rachna Sinha
Project Manager: Marcus Laithangbam, Apoorva Goel
Production Editor: Rohit Bharadwaj
Vice President Sales and Marketing: Arun Kumar Majji
Managing Director & CEO: Ajit Kohli

© 2020. Thieme. All rights reserved.

Thieme Medical and Scientific Publishers Private Limited.
A - 12, Second Floor, Sector - 2, Noida - 201 301,
Uttar Pradesh, India, +911204556600
Email: customerservice@thieme.in
www.thieme.in

Cover design: Thieme Publishing Group
Typesetting by RECTO Graphics, India

Printed in India by Nutech Print Services

5 4 3 2 1

ISBN: 978-93-88257-53-4

Important note: Medicine is an ever-changing science undergoing continual development. Research and clinical experience are continually expanding our knowledge, in particular, our knowledge of proper treatment and drug therapy. Insofar as this book mentions any dosage or application, readers may rest assured that the authors, editors, and publishers have made every effort to ensure that such references are in accordance with **the state of knowledge at the time of production of the book.**

Nevertheless, this does not involve, imply, or express any guarantee or responsibility on the part of the publishers in respect to any dosage instructions and forms of applications stated in the book. **Every user is requested to examine carefully** the manufacturers' leaflets accompanying each drug and to check, if necessary, in consultation with a physician or specialist, whether the dosage schedules mentioned therein or the contraindications stated by the manufacturers differ from the statements made in the present book. Such examination is particularly important with drugs that are either rarely used or have been newly released in the market. Every dosage schedule or every form of application used is entirely at the user's own risk and responsibility. The authors and publishers request every user to report to the publishers any discrepancies or inaccuracies noticed. If errors in this work are found after publication, errata will be posted at www.thieme.com on the product description page.

Some of the product names, patents, and registered designs referred to in this book are in fact registered trademarks or proprietary names even though specific reference to this fact is not always made in the text. Therefore, the appearance of a name without designation as proprietary is not to be construed as a representation by the publisher that it is in the public domain.

This book, including all parts thereof, is legally protected by copyright. Any use, exploitation, or commercialization outside the narrow limits set by copyright legislation without the publisher's consent is illegal and liable to prosecution. This applies in particular to photostat reproduction, copying, mimeographing or duplication of any kind, translating, preparation of microfilms, and electronic data processing and storage.

This book is dedicated to my mentors, Professor Amin B. Kassam, Professor Ricardo Carrau, and Professor Dharamvir S. Sethi, who have been instrumental in imparting their knowledge to me.

To my mother Kalyani and my father Narayanan, who have been exemplary parents and my driving force and constant source of inspiration, integrity, and perseverance.

To my son Sathyanarayanan J. D. for his continuous pursuit and eagerness to explore new frontiers which continues to inspire me.

Contents

Videos viii

Foreword ix

Preface x

About the Author xi

Contributors xii

1. Endoscopic Pituitary Surgery: My 25-Year Journey (1994–2019) 1
Dharambir S. Sethi

2. Anatomical Perspectives of the Sellar, Suprasellar, and Parasellar Regions 11
Shilpee Bhatia Sharma, Abhilasha Karunasagar, Narayanan Janakiram

3. Radiological Protocols in Sellar, Suprasellar, and Parasellar Regions 33
R. Bavaharan Rajalingam, Narayanan Janakiram, Joseph Nadakkavukaran

4. Perioperative Management for Anterior Skull Base Tumors 60
Vignesh G.

5. Anesthetic Considerations in the Surgery for Sellar, Suprasellar, and Parasellar Lesions 63
Balamurugan Chinnasamy

6. Reconstructive Options in the Surgery for Sellar, Suprasellar, and Parasellar Lesions 68
Joseph Nadakkavukaran, Shilpee Bhatia Sharma, Narayanan Janakiram

6A. Temporoparietal Fascial Flap for Skull Base Reconstruction 97
Alberto Schreiber, Puya Dehgani-Mobaraki

7. Endoscopic Approach to Sellar Lesions 99
Nisha Shrivastava, Shilpee Bhatia Sharma, Narayanan Janakiram

8. Endoscopic Approach to Suprasellar Lesions 182
Dipen Thakkar, Shilpee Bhatia Sharma, Narayanan Janakiram

9. Endoscopic Approach to Parasellar Lesions 306
Chaithra B. G., Shilpee Bhatia Sharma, Narayanan Janakiram

10. Intraoperative Magnetic Resonance Imaging in Endonasal Surgery for Pituitary Adenoma 394
Beng-Ti Ang, Dharambir S. Sethi

11. Endoscopic Surgery for Sellar and Parasellar Lesions: A Tailored Approach 398
Michel Roethlisberger, Vicknes Waran, Prepageran Narayanan

12. Skull Base Approaches to the Lesions of Sellar and Parasellar Regions: Anatomy, Techniques, and Insights 417
Iype Cherian, Hira Burhan

13. Surgery on Sellar and Parasellar Lesions 428
Atul Goel

14. Radiation Therapy for Pituitary Tumors 435
Bhargavi Ilangova, Murali Venkatraman, Murugan Logamuthukrishnan, Babu Rajendran

Index 456

Videos

Video 7.1	Pituitary macroadenoma	104
Video 7.2	Pituitary abscess	124
Video 7.3	Fibrous pituitary macroadenoma: Fibrous lesion	140
Video 7.4	Pituitary macroadenoma extending to left sphenoid sinus	147
Video 7.5	Pituitary tuberculosis	155
Video 7.6	Rathke's cleft cyst 1	161
Video 7.7	Rathke's cleft cyst 2	167
Video 7.8	Sellar craniopharyngioma	174
Video 8.1	Pituitary macroadenoma with suprasellar extension	188
Video 8.2	Pituitary adenoma: Fibrous type	193
Video 8.3	Pituitary macroadenoma with suprasellar extension	199
Video 8.4	Revision pituitary macroadenoma with suprasellar extension	207
Video 8.5	Planum/ Tuberculum meningioma – 1	247
Video 8.6	Planum/ Tuberculum meningioma – 2	253
Video 8.7	Craniopharyngioma	266
Video 8.8	Craniopharyngioma	274
Video 8.9	Craniopharyngioma	280
Video 9.1	Pituitary macroadenoma with acromegaly	313
Video 9.2	Pituitary macroadenoma with inferomedial compartment involvement of the cavernous sinus	320
Video 9.3	Pituitary macroadenoma with superomedial compartment involvement of the cavernous sinus	324
Video 9.4	Revision pituitary macroadenoma: Fibrous type with parasellar extension	329
Video 9.5	Revision pituitary macroadenoma with acromegaly	337
Video 9.6	Cavernous hemangioma: Cavernous sinus	374
Video 12.1	Modified Dolenc's Approach, Part 1	417
Video 12.2	Modified Dolenc's Approach, Part 2	418

Foreword

I think that this book about Endoscopic Neurosurgery is a scientific work that everyone who practices endoscopic approaches to the skull base should read. The book in its contents demonstrates the surgical experience of the authors, acquired over the years. It is a very complete book and it guides the reader through the knowledge of the different pathologies, the surgical techniques to endoscopically remove the tumors of the Sellar, Suprasellar, and Parasellar regions, and also gives them the knowledge of the reconstructive techniques of the skull base. The text is very clear and is excellently illustrated with diagrams, drawings, photographs, and videos of the highest quality. This is a book that I recommend reading and having as a reference book, for when we need to perform an endoscopic approach in different typical pathologies of the skull base and especially of the sellar region. I want to personally congratulate the authors of the different chapters and especially their main author Professor Narayanan Janakiram for this excellent book. I am convinced that this publication will be of relevance to and be disseminated among the global neurosurgical and scientific community, receiving recognition from them.

Roberto R. Herrera, MD, PhD
Board of Director
Walter Dandy Neurosurgical Society
Chairman
Neurosurgery Department
Belgrano Adventist Clinic
Buenos Aires
Consultant Neurosurgeon
Private Rosario Hospital
Rosario, Santa Fe
Pergamino Diagnostic Institute Director
Pergamino, Buenos Aires, Argentine Republic

Preface

Skull base surgeons have always been fascinated by endoscopic approaches to various parts of the skull base. Lesions of the sellar, suprasellar, and parasellar regions are technically challenging, and rigorous training is required to perform these surgeries and avoid complications. Mastering this impeccable technique involves a steep learning curve which in turn needs perseverance and dedication.

In an effort to standardize the approaches to these areas, we thought of bringing out a color atlas that would give the reader a clear idea of our philosophy in the management of lesions involving these complex regions.

In response to a perceived need for greater exposure to the endoscopic technique necessary to treat lesions of the sellar, suprasellar, and parasellar regions, we have put together a collection of carefully chosen images which would cover the spectrum of surgeries in these areas. However, working directly in the operating room with an experienced endoscopic team will always remain an irreplaceable part of training in this field.

Skull base surgery is a team effort which involves close coordination between various specialties such as neurosurgery, otolaryngology, endocrinology, radiology, ophthalmology, and anesthesiology. In this book, we have tried to bring all these specialties into a common arena so that the reader gets an overall perspective of the problem dealt with. Yet, no matter how well written, no standard text can fully capture the art and spirit of a surgical procedure. Hence, the addition of surgical videos which will serve as an invaluable tool for expanding the educational process by demonstrating the nuances involved and microsurgical anatomy that cannot be captured by text or still images alone.

In this book, we have dealt with endoscopic management of lesions such as pituitary macroadenomas, craniopharyngiomas, meningiomas, and several other lesions involving the sellar, suprasellar, and parasellar regions. We have tried to standardize the steps by portraying various case examples which will help in improving the reader's surgical technique, thus giving good results without complications. We have compiled author experiences not only from Royal Pearl Hospital but also from several other pioneering centers in this field.

Most of the techniques described in the book are the result of my training with my mentors—Professor Amin Kassam and Professor Ricardo Carrau. They were instrumental in training me and instilling in me the obsession for dexterity, patience, and prudent attention to details in every aspect of the surgery performed. They instilled in me a sophisticated understanding of intracranial anatomy and finesse during surgical manipulation to avoid undue complications which are inherent in surgeries performed in these areas.

I hope this book will help the current generation of skull base surgeons in understanding the nuances of this discipline, thus benefitting the patient suffering from ailments involving these areas.

Narayanan Janakiram

About the Author

Narayanan Janakiram, MS, DLO, is Managing Director of Royal Pearl Hospital, Trichy, Tamil Nadu, India. He is internationally acclaimed for his work in skull base surgery. He is a pioneer in the field of endoscopic management of juvenile nasopharyngeal angiofibroma. Dr. Janakiram has authored several chapters, articles, and books pertaining to skull base surgery, including a book on juvenile nasopharyngeal angiofibroma and a book titled *Step-by-Step Approach to Endoscopic Cadaveric Dissection* by Thieme Publishers.

Contributors

Alberto Schreiber, MD, PhD
Consultant
Unit of Otorhinolaryngology—Head and Neck Surgery
ASST Spedali Civili Brescia
University of Brescia
Brescia, Italy

Atul Goel, MD, MCh
Professor and Head
Department of Neurosurgery
KEM Hospital and Seth GS Medical College
Mumbai, India

Babu Rajendran, MD, DMRT, DNB
Senior Consultant
Department of Radiation Oncology
Apollo Cancer Institutes
Chennai, India

Balamurugan Chinnasamy, DA
Consultant
Department of Anaesthesiology
Royal Pearl Hospital
Tiruchirapalli
Tamil Nadu, India

Beng-Ti Ang, MBBS, FRCSEd (SN)
Senior Consultant and Head
Department of Neurosurgery
Singapore General Hospital
Bukit Merah, Singapore

Bhargavi Ilangovan, DMRT, DNB, FRCR
Junior Consultant
Department of Radiation Oncology
Apollo Cancer Institutes
Chennai, India

Chaithra B. G., MS, DNB
Junior Consultant
Department of Otolaryngology
Royal Pearl Hospital
Tiruchirapalli
Tamil Nadu, India

Dharambir S. Sethi, MBBS, FRCSEd
Senior Consultant
Ear, Nose, and Throat Surgeon
Novena ENT—Head and Neck Surgery Specialist Centre
Mount Elizabeth Novena Hospital
Visiting Consultant
Department of Otolaryngology
Singapore General Hospital
Bukit Merah, Singapore

Dipen Thakkar, MS
Junior Consultant
Department of Otolaryngology
Royal Pearl Hospital
Tiruchirapalli
Tamil Nadu, India

Hira Burhan, MBBS
Resident
Institute of Neurosciences
Nobel Medical College and Teaching Hospital
Biratnagar, Nepal

Iype Cherian, MCh
Director and Chair
Institute of Neurosciences
Nobel Medical College and Teaching Hospital
Biratnagar, Nepal

Joseph Nadakkavukaran, MS
Junior Consultant
Royal Pearl Hospital
Tiruchirapalli
Tamil Nadu, India

Karunasagar Abhilasha, MS
Junior Consultant
Department of Otolaryngology
Royal Pearl Hospital
Tiruchirapalli
Tamil Nadu, India

Michel Roethlisberger, MD, FMH
Senior Consultant
Department of Neurosurgery
Faculty of Medicine
University of Basel
Basel, Switzerland
Consultant Specialist in SkullBase Surgery
Department of Neurosurgery and Otorhinolaryngology
Faculty of Medicine
University of Malaya
Kuala Lumpur, Malaysia

Murali Venkatraman, MSc, PhD
Chief Medical Physicist
Department of Medical Physics
Apollo Cancer Institutes
Chennai, India

Murugan Logamuthukrishnan, MCh
Senior Consultant
Department of Neurosurgery
Apollo Cancer Institutes
Chennai, India

Narayanan Janakiram, DLO, MS
Skull Base Surgeon
Managing Director
Royal Pearl Hospital
Tiruchirapalli
Tamil Nadu, India

Nisha Shrivastava, MS
Junior Consultant
Department of Otolaryngology
Royal Pearl Hospital
Tiruchirapalli
Tamil Nadu, India

Prepageran Narayanan, FRCSEd, FRCS (Glas), MS
Professor
Department of Otorhinolaryngology
Faculty of Medicine
University of Malaya
Kuala Lumpur, Malaysia

Puya Dehgani-Mobaraki, MD
Consultant
Unit of Otorhinolaryngology—Head and Neck Surgery
Gubbio–Gualdo Tadino Hospital
Association "Naso Sano"
Umbria Regional Registry of Volunteer Activities
Corciano, Italy

R. Bavaharan Rajalingam, DNB, FRCR
Consultant Interventional Radiologist
Managing Director
Magnum Imaging and Diagnostics Pvt. Ltd.
Tiruchirapalli
Tamil Nadu, India

Shilpee Bhatia Sharma, MS
Consultant
Department of Otolaryngology
Royal Pearl Hospital
Tiruchirapalli
Tamil Nadu, India

Vicknes Waran
Neurosurgery Division
Faculty of Medicine
University of Malaya
Kuala Lumpur, Malaysia

Vignesh G., MD, DM
Consultant Endocrinologist
Endocrine and Diabetes Centre
Tiruchirappalli
Tamil Nadu, India

1 Endoscopic Pituitary Surgery: My 25-Year Journey (1994–2019)

Dharambir S. Sethi

Introduction

The use of endoscopes for the diagnosis and treatment of sinusitis and a wide range of other sinonasal conditions has been well established since its advent in the 1980s. It is without doubt that endoscopes provide excellent illumination, magnification, and panoramic-angled views. Application of the endoscopes in the nasal cavity and the sinuses led to a better understanding of the sinonasal anatomy and physiology. With the advent of endoscopic sinus surgery, better understanding of the endoscopic sinonasal anatomy, and familiarity with the endoscopic instrumentation, the use of endoscopes to perform surgery on adjacent areas such as the skull base came as a natural progression.

Reports of endoscopic repair of CSF leaks started emerging in the late 1980s. By early 1990s, surgeons started using endoscopes to remove pituitary tumors. This was the beginning of a new frontier. Twenty-five years later, endoscopic pituitary surgery has become well established and a state-of-the-art operation. With advances in technology and instruments in the early part of the last decade combined with our experience in pituitary surgery and closure of CSF leaks, surgeons were able to push the boundaries beyond the sella that led to the evolution of endoscopic skull base surgery. Available today, in most centers involved in the endoscopic skull base surgery are the state-of-the-art equipments like high-definition endoscopic camera systems, transnasal neurodrills, endoscrubs, intraoperative navigation, intraoperative magnetic resonance imaging (iMRI), iCT scanners, transnasal Doppler, and several hemostatic agents. But that was not how we embarked on pituitary surgery 25 years ago. When we started with pituitary surgery the amenities available were very basic. Armed with a single-chip camera system and routine endoscopic sinus surgery instruments and some trans-sphenoidal instruments designed for microscopic trans-sphenoidal pituitary surgery, is how we started. There were no microdebrider, transnasal skull base drills, neuronavigations, or the hemostatic agents that are available today.

This chapter is a brief description of this journey.

The Early Beginnings (1994–2000)

It was in August 1993, when I had just returned from Johns Hopkins University School of Medicine after completing a year of clinical fellowship in Rhinology and Endoscopic Sinus Surgery, that the Head of Neurosurgery at Singapore General Hospital, Dr Prem Pillay, asked me if it was possible to remove pituitary tumors using endoscopes. A review of the literature showed only one published article on endoscopic pituitary surgery by Dr Jankowski.[1] I managed to get into touch with Dr Jankowski and learnt that they had done five cases of endoscopic pituitary tumors and since then had stopped doing this surgery. With paucity of literature on this subject and no previous experience, I decided to do a cadaver study to understand the anatomy of the sphenoid sinus and the feasibility of performing pituitary surgery using the endoscopes. The study was completed late 1993. The results were encouraging and were subsequently published.[2] In December 1993, we performed our first endoscopic pituitary operation (**Fig. 1.1a–d**). The approach used for this case was transethmoid.[3]

Arguing that it was not necessary to perform an ethmoidectomy on normal sinuses to approach the sella, we decided to access the sella via the trans-septal approach which most of us were very familiar with (**Fig. 1.2a–f**). The objective was preservation of the anatomy of the normal sinuses. The trans-septal approach was quick but had limitations. It was difficult for two surgeons to work together through the long narrow tunnel.[4,5] We abandoned the trans-septal approach and developed the bilateral sphenoidotomy approach. This approach was direct and required the identification of the

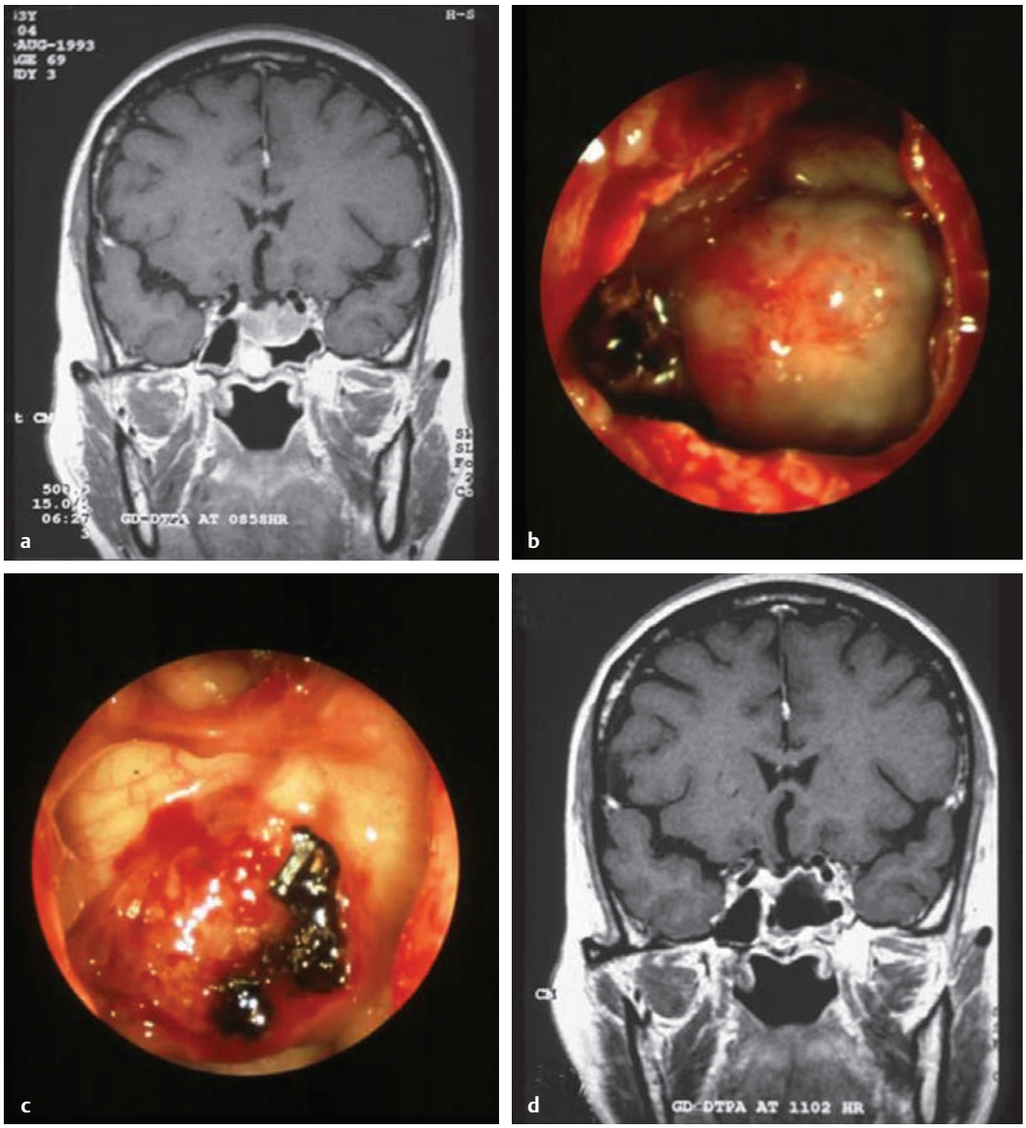

Fig. 1.1 **(a)** Preoperative MRI scan showing the expansion of the Sella. **(b)** Intraoperative view of the sella. **(c)** Three-week postoperative endoscopic view of the sella. **(d)** Postoperative MRI scan showing tumor has been completely removed.

sphenoid ostium in the sphenoethmoid recess bilaterally. The sphenoid ostium was then widened bilaterally to create a wide sphenoidotomy. The sphenoidotomy extended superiorly from the planum to the floor inferiorly. The lateral limits were the superior turbinates of either side. Concerns of olfactory loss following the removal of the superior turbinates were prevalent among the rhinologists of that era. To facilitate instrumentation from the contralateral side, about 1 cm of the posterior nasal septum was removed. This maneuver created a wide corridor, enabled instruments to be passed from the other side and two surgeons to work at the same time. This approach was subsequently reported as our "four-handed approach" (**Fig. 1.3a–f**). Extreme precaution was taken for mucosal preservation in the sphenoid sinus which resulted in excellent mucosal healing.

In the next 18 months we operated on 50 patients with pituitary tumors. These included mainly patients with pituitary macroadenomas, where the objective was mainly to decompress the tumor. The MRI scan of one of the patients done in 1995 is shown in **Fig. 1.4a, b**.

In June 1995, at the International Joint Congress on Minimally Invasive Surgery in Otolaryngology and Neurosurgery held in Pittsburgh, we presented our initial experience of 50 patients who underwent endoscopic pituitary surgery.[6] It is at this meeting that I met Dr Jho, a neurosurgeon and Dr Ricardo Carrau, an otolaryngologist,

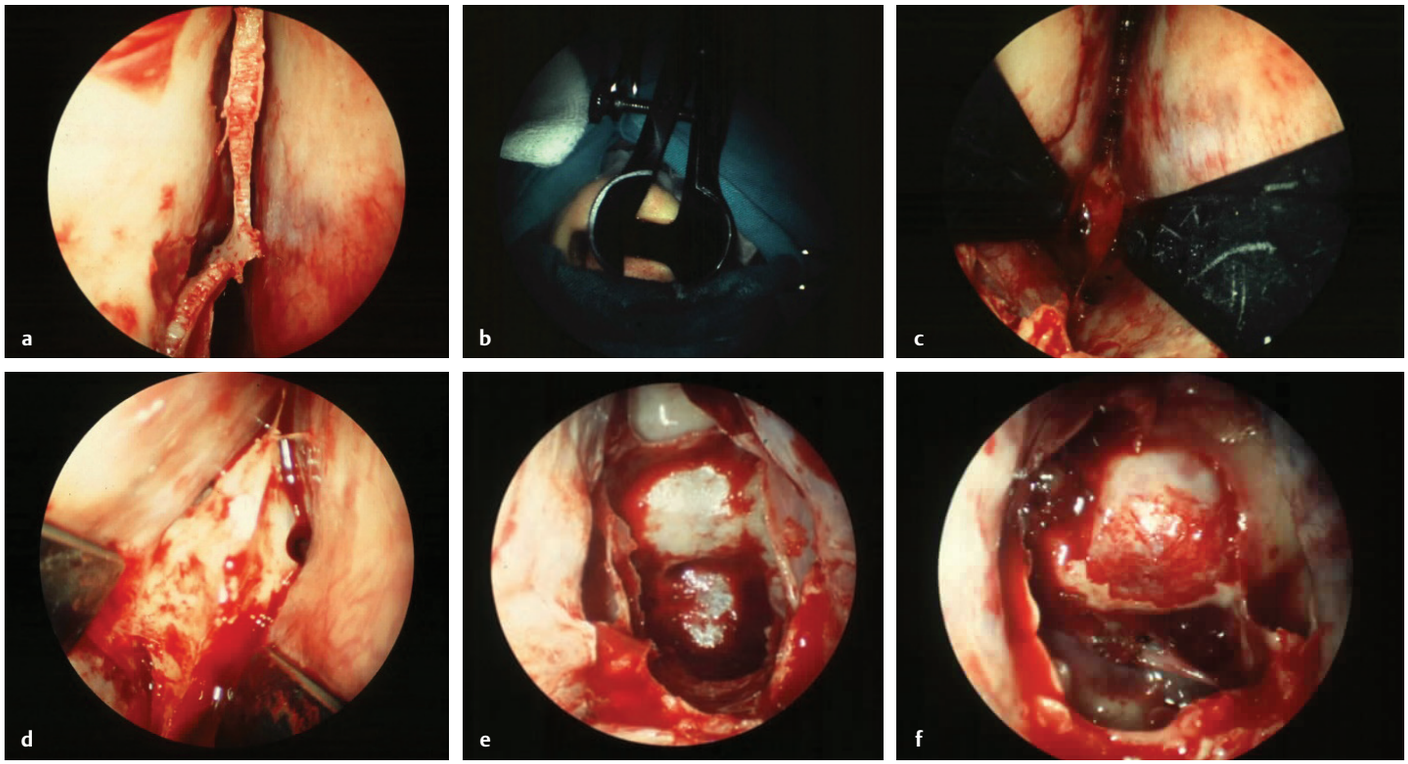

Fig. 1.2 Endoscopic trans-septal approach. **(a)** The cartilaginous septum has been dislocated from the bony nasal septum. **(b)** Mini self-retaining retractor used to retract the mucoperichondrial flaps. **(c)** The bony nasal septum has been removed to expose the sphenoid keel. **(d)** Zoomed-in view of the sphenoid keel and the sphenoid ostium. **(e)** Exposure of the sella. **(f)** Floor of the sella removed. Dura exposed.

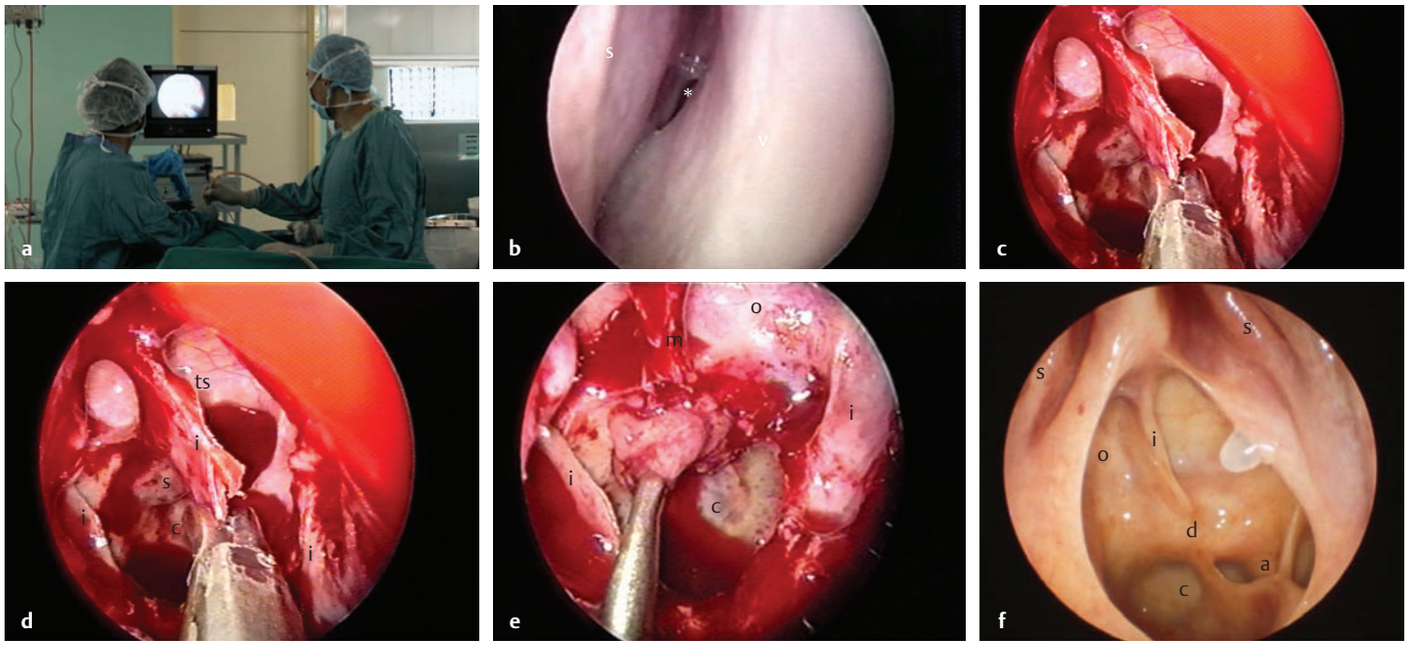

Fig. 1.3 The bilateral sphenoidotomy four-handed approach. **(a)** Basic operative setup in 1995. The ENT surgeon stands on the right-hand side and the neurosurgeon on the left. The video monitor is placed at the head end of the patient. The anesthesiologist is on the caudal end. **(b)** Sphenoid ostium (white asterisk) identified in the sphenoethmoid recess. S, superior turbinate, v, vomer. **(c, d)** Bilateral sphenoidotomy has been done and part of the posterior nasal septum removed. ts, tuberculum sella; i, intersinus septum; s, sella; c, clivus. **(e)** Tumor being removed. **(f)** Postoperative sphenoidotomy. s, superior turbinates; o, optic nerve; a, paraclival carotid artery; i, intersinus septum; c, clivus.

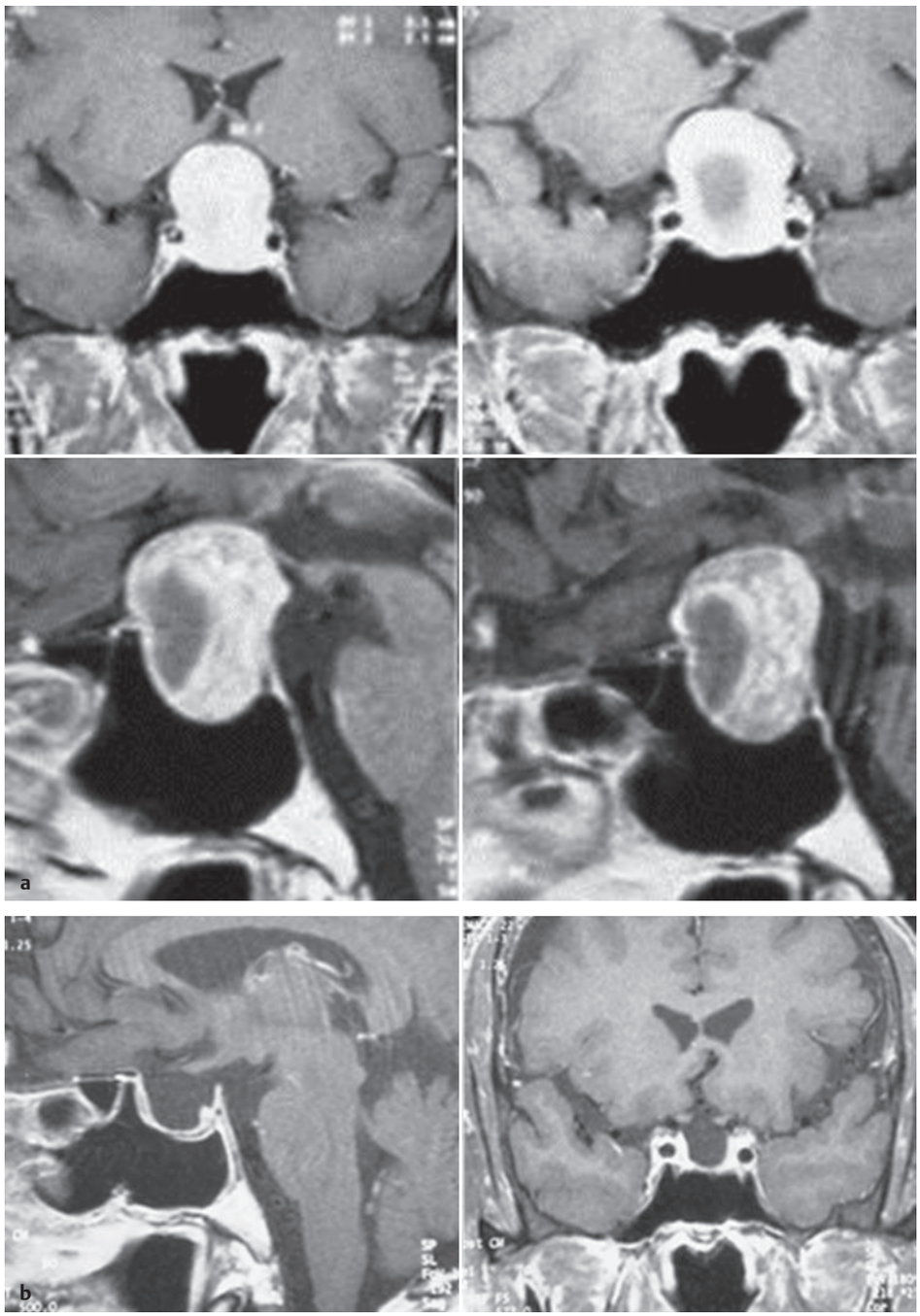

Fig. 1.4 **(a)** Pre- and **(b)** postoperative MRI scan of a patient with pituitary macroadenoma.

who were doing similar work at University of Pittsburgh Medical Center. They started using endoscope as an adjunct to microscopic techniques and then changed to pure endoscopic techniques.[7] In 1997 they reported on 50 patients, 46 of whom were treated via a pure endoscopic approach.

The same year, in 1995, I was given the opportunity to present on endoscopic pituitary surgery as a plenary speaker at the Third International Sinus Symposium in Cairns, Australia and at the Annual American Academy of Otolaryngology – Head & Neck Surgery meeting, in New Orleans and subsequently at the American Rhinologic Society meeting in Orlando. There was tremendous interest and enthusiasm shown in endoscopic pituitary surgery both among the neurosurgeons and otolaryngologists. It became clear the endoscopic pituitary surgery was just the beginning of a new era.

In January 1997, I had the opportunity to meet Professor Aldo Stamm at a workshop on endoscopic sinus surgery in Mumbai, India. Well known for his microscopic techniques for sinus and skull base surgery, he was impressed with what endoscopic techniques had to offer. I was honored to be invited to Sao Paulo, Brazil in November the same year as the key faculty to conduct the first endoscopic sinus surgery course (**Fig. 1.5a, b**). With his amazing surgical skills and past neurosurgical training, Professor Stamm contributed significantly to the field of endoscopic skull base surgery, in the years that followed.

By 1998, several reports on endoscopic pituitary surgery started emerging. Of note is the work done by Paolo Cappabianca and Enrico de Divitiis from Naples who reported their experience with the use of pure endoscopic technique introducing the term "functional endoscopic pituitary surgery" or FEPS.[8]

The Next Decade (2000–2010)

In the years that followed, Professor Paolo Cappabianca and his team made significant contributions to the development of endoscopic pituitary surgery. They developed dedicated endoscopic instruments,[9] reported technical improvements,[10,11] and contributed significantly to the scientific basis[12,13,14] and critical assessment of the techniques.[15,16,17,18] The acceptance of endoscopic pituitary surgery was supported by reports by many others from around the world.

By the year 2000 there had been several technological advances. The three-chip camera system offered improved image quality, intranasal powered instrumentation, that was introduced in the mid-1990s, had improved, and transnasal neurodrills became available. With other technical adjuncts such as neuronavigation and microvascular Doppler ultrasonography surgeons were able to extend endoscopic pituitary surgery to lesions outside of the sella turcica introducing the concept of extended approaches to the skull base.

Our initial experience with endoscopic pituitary surgery showed two limitations. They were residual tumors left behind in patients with large suprasellar extension, particularly those extending to the anterior skull base, and tumors that were extending or encircling the cavernous sinus.

These limitations were overcome by novel techniques described by several surgeons.

Kaptain et al in 2001 reported extended approach for sellar tumors with extension into the anterior cranial fossa and/or suprasellar cistern by extending the exposure to include removal of a portion of planum sphenoidale, tuberculum sella, and division of the superior intercavernous sinus.[19]

Giorgio Frank and Ernesto Pasquini, a neurosurgeon and otolaryngologist from Bologna, developed the ethmoid–pterygoid–sphenoid endoscopic approach for the treatment of pituitary tumors that were extending to cavernous sinus or occurred primarily in the cavernous sinus.[20]

Several reports on the use of pure endonasal endoscopic technique for the treatment of various pathological conditions of the skull base[21,22,23,24] emerged from University of Pittsburgh Medical Center in 2005. The skull base team comprised of Amin Kassam, a neurosurgeon, and Ricardo L. Carrau and Carl Snyderman, otolaryngologists. These extended approaches allowed a wide resection of tumors of the skull base but also resulted in large skull base defects. Inability to deal with the large skull base defects in the skull base resulted in high morbidity and mortality ranging

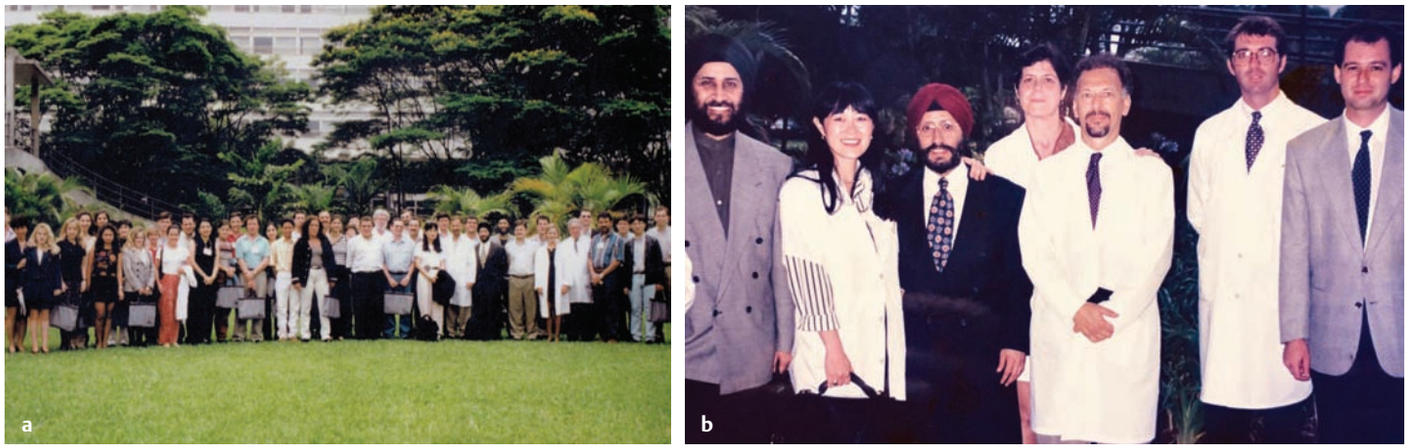

Fig. 1.5 **(a, b)** Microendoscopic Sinus Surgery Course, Sao Paulo, November 5–8, 1997.

from 10 to 40%. The most common complication was postoperative cerebrospinal fluid fistula and its potential infective complications such as meningitis and ventriculitis. Several techniques were described to close these defects. These included the use of free grafts and fascia lata or temporalis in an underlay or overlay fashion with double or triple layers and use of biologic substitutes among others.[25,26,27,28] All these grafts were nonvascularized and results were variable, depending on whether the graft gained sufficient vascular supply from the adjacent tissue.

The University of Pittsburgh, in 2005, started using a vascularized nasoseptal flap pedicled on the sphenopalatine artery. The flap was developed by Drs Gustavo Hadad and Louis Bassagaisteguy from Argentina who had been using it since 1999. The University of Pittsburgh team, in 2006, reported their results of using this flap in 43 patients with a 95% success rate. Of the 43 patients, only two had minor postoperative CSF leak that was successfully treated with the focal fat grafts.[29] This vascularized nasoseptal flap has since become the work horse to repair the large skull base defects following endoscopic skull base surgery.[30,31]

Due credit must also be given to the team from the University of Pittsburgh for introducing a standard training program for endoscopic skull base surgery. The program included the adoption of a modular and incremental training of endonasal surgeons in both otorhinolaryngology and neurosurgery with the objective of developing the surgeon's knowledge and expertise to minimize the risk of complications.[32]

In 2007, we acquired the iMRI facility at our institution at the Singapore General Hospital (**Fig. 1.6a, b** and **Table 1.1**). This package included iMRI suite, iCT scanner suite, four ambulatory navigation systems, and four mounted neuronavigation systems. The iMRI comprised the Siemens MAGNETOM Espree superconductive 1.5-Tesla high-field magnet with a length of 120 cm and an inner bore diameter of 70 cm equipped with a gradient system with a field strength of up to 33 mT/m (effective 57mT/m) and a slew rate of up to 100 T/m/s (173 T/m/s effective).

We started using the iMRI as an adjunct to endoscopic pituitary surgery in 2008. In the first year we used it for 42 patients with suprasellar extension. We were able to improve the gross tumor resection from 78.5 (33 patients) to 93% (39 patients) (**Fig. 1.6c**). Based on our initial experience we felt that iMRI was a useful adjunct but a fully endoscopic technique with careful visualization of the resected cavity followed by directed and systematic examination of the sellar space to identify residual tumor was critical to obtain good results for the management of pituitary

Table 1.1 Unpublished data of our early experience with iMRI

N = 42	Gross total resection
Initial resection	33 (78.5%)
After re-exploration	39 (93%)

Fig. 1.6 **(a)** Endoscopic pituitary surgery in progress in iMRI suite (2008). **(b)** Patient undergoing intraoperative MRI (2008).

macroadenomas. We found the iMRI to be more useful in dealing with very large macroadenomas which as a result of tumor expansion led to the distortion and gross redundancy of the diaphragm sella. We noted that with progressive tumor removal, the descent of the diaphragm in an irregular fashion led to the residual pockets of tumor being obscured. Intimate contact of redundant folds of diaphragm created an endoscopic appearance of complete symmetric descent. iMRi assisted us in identifying these residual tumors, in such situations. Teasing apart the folds often revealed tumor tissue of significant size in some cases. We still continue to use the iMRI for selected pituitary macroadenomas at the Singapore General Hospital.

In 2010 from January 13 to January 17, a group of rhinologists and neurosurgeons met in Stubai Valley, Austria. Chaired by Professor Stammberger and Professor Valerie Lund, this group formed the advisory board for European Position Paper on the endoscopic management of tumors of the nose, paranasal sinuses, and skull base. The paper was subsequently published in June 2010.[33] Among other objectives the intent of the paper was: (1) to provide an evidence-based review of the diagnostic methods; (2) to provide an evidence-based review of endoscopic techniques in the context of other available treatments; (3) to propose algorithms for the management of the disease; (4) to propose guidance for outcome measurements for research and encourage prospective collection of data.

The Current Decade (2011–2019)

There were further technological advances in the operative instrumentation and the development of several novel techniques. There have been refinements and further improvements in imaging, camera definitions, navigation, transnasal neurodrills, and surgical technique (**Fig. 1.7a, b**).[34]

From a single-chip camera in the early 1990s, we now have the latest high-definition (HD) state-of-the-art camera systems and 4K monitors providing amazing picture quality.

The concept of pituitary surgery has changed from just decompression to almost complete gross tumor resection (**Fig. 1.8a**). Involvement of the cavernous sinus with tumor, especially when it is completing encircling the cavernous carotid artery, was once considered inoperable (**Fig. 1.8b, c**). Today many surgeons are able to achieve this feat of removal of the tumor from the cavernous sinus with considerable dexterity.

Three-dimensional endoscopes have become much more user friendly and are a recent addition in the armamentarium of the trans-sphenoidal surgical approach for pituitary, anterior skull base and parasellar lesions. Preliminary studies suggest it is useful alternative to two-dimensional HD endoscope, is more efficient surgically, and has a short learning curve.[35]

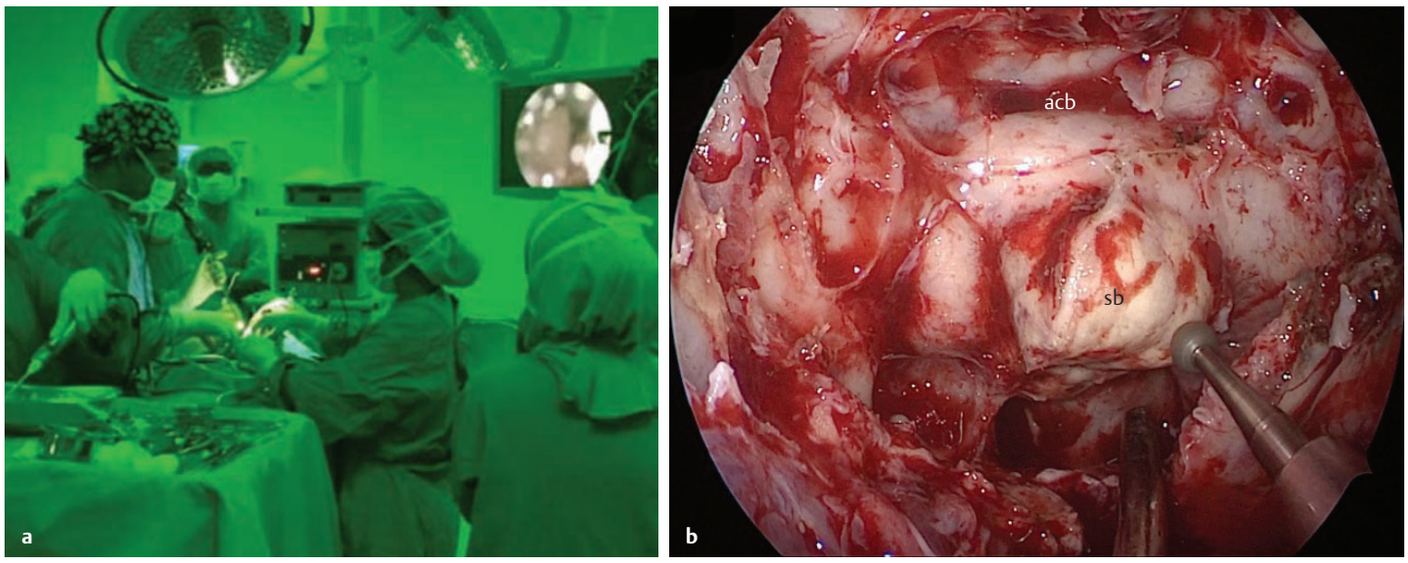

Fig. 1.7 **(a)** Operative setup during endoscopic pituitary surgery. **(b)** S3 neurodrill in use in endoscopic pituitary surgery. sb, sellar bone; acb, anterior cranial base.

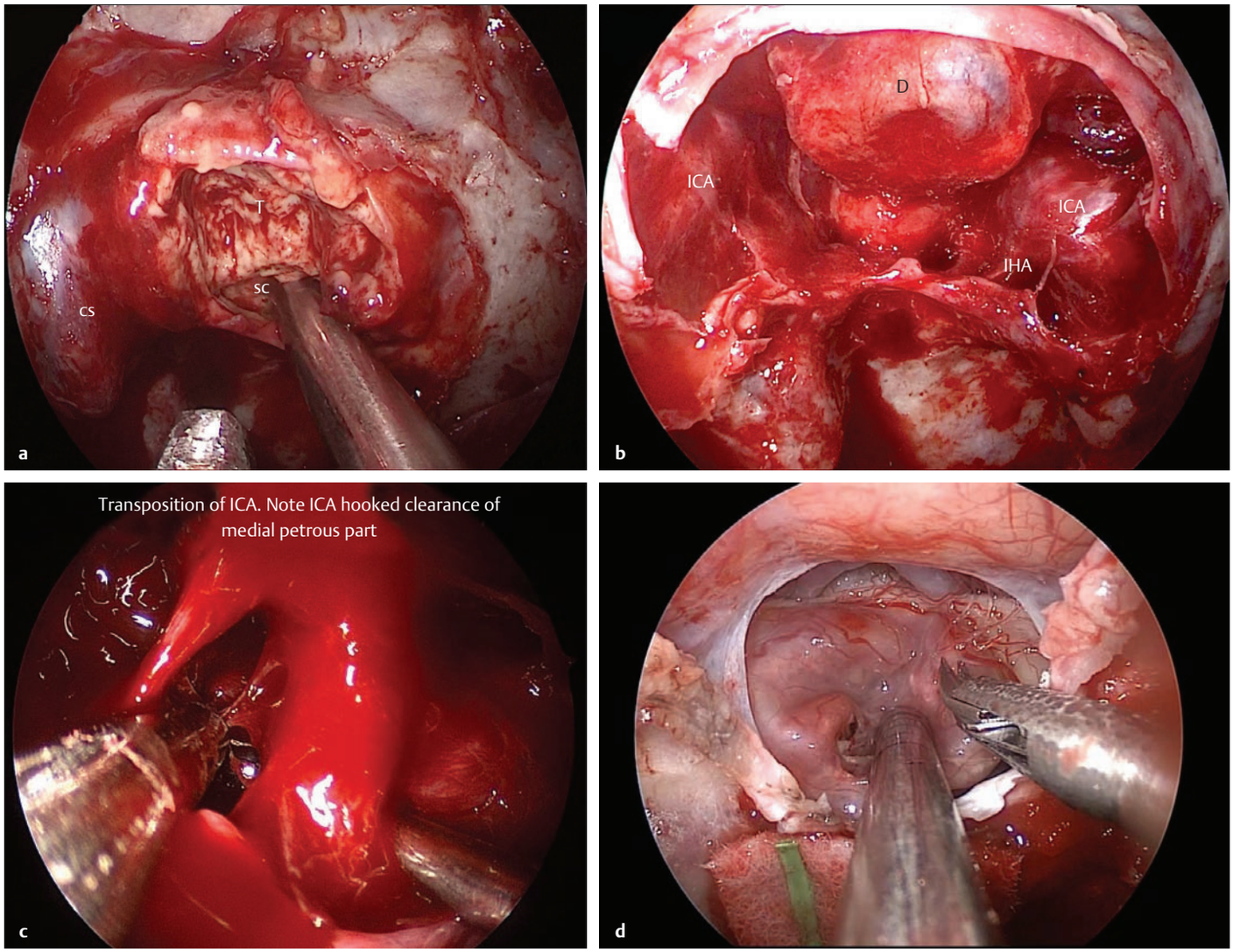

Fig. 1.8 **(a)** Endoscopic pituitary surgery. sc, sellar cavity; T, tumor; cs, cavernous sinus. **(b)** Complete tumor removal from the cavernous sinus. D, diaphragma; ICA, internal carotid artery; IHA, inferior hypophyseal artery. **(c)** 360-degree clearance of the tumor achieved by carotid transposition. **(d)** Intradural dissection of a craniopharyngioma.

To overcome a common problem experienced by many surgeons, the collision of the endoscope with surgical instrumentation resulting in limited surgical freedom, malleable endoscopes have been designed and are being assessed. Malleable endoscopes offer the potential advantage of reducing surgical collision by adjusting the camera head out of the way from entrance of the nasal cavity.[36]

One of the more recent fields of skull base surgery to be developed is transorbital endoscopic surgery[37] (**Fig. 1.9a, b**). Several emerging applications of transorbital endoscopic approaches to the skull base for the treatment of selected extradural and intradural lesions have been described. These approaches are directed to the anterior and middle cranial base. They may represent safe and feasible techniques with great potential for new applications in the nearby future.

Robotic technology has been accepted into surgeon's armamentarium, with its implementation into abdominal, thoracic, and head and neck surgery. However, the application of surgical robotics to the skull base has yet to be achieved. Preclinical research is ongoing and work is in progress.[38]

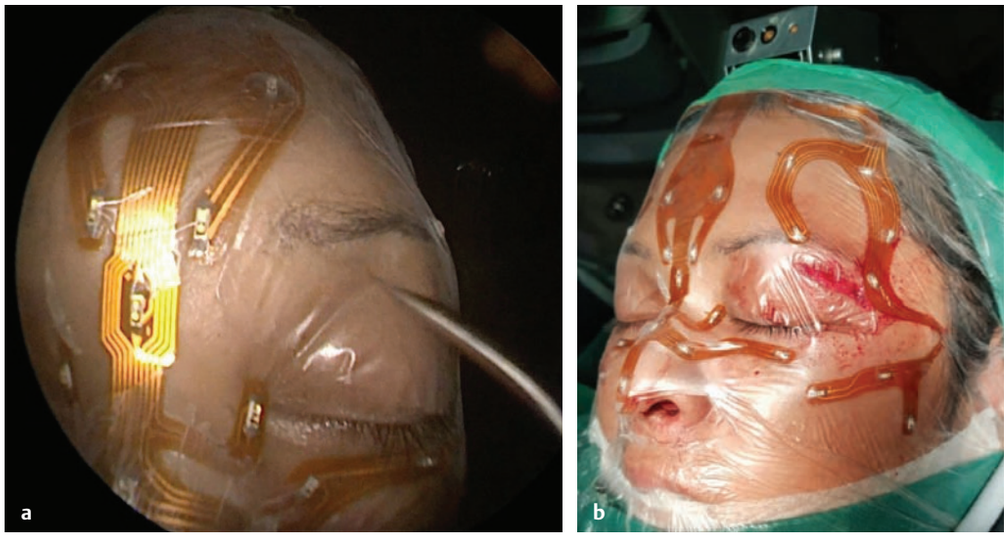

Fig. 1.9 **(a, b)** Transorbital endoscopic approach with neuronavigation.

Conclusion

Endoscopic pituitary surgery had a humble beginning but soon gained acceptance. Significant advances over the next 25 years in imaging technology, surgical instrumentation, knowledge of the skull base anatomy, and reconstructive techniques resulted in extended endoscopic approaches to the skull base and the evolution of endoscopic skull base surgery. Driven by some visionary surgeons who pioneered novel techniques and by technological advances, it has reached to where it stands today. However, the importance of the learning curve in the endoscopic sinus surgery and the use of multidisciplinary approach should not be forgotten. Three-dimensional and robotic endoscopic skull base surgery may be the next frontier.

Acknowledgments

I would like to thank the neurosurgeons that I have worked with in the past 25 years. They are Dr Prem Pillay, Dr Alvin Hong, Dr John Thomas, and Dr Krishan Kumar.

References

1. Jankowski R, Auque J, Simon C, Marchal JC, Hepner H, Wayoff M. Endoscopic pituitary tumor surgery. Laryngoscope 1992; 102(2):198–202
2. Sethi DS, Stanley RE, Pillay PK. Endoscopic anatomy of the sphenoid sinus and sella turcica. J Laryngol Otol 1995;109(10): 951–955
3. Sethi DS, Pillay PK. Endoscopic management of lesions of the sella turcica. J Laryngol Otol 1995;109(10):956–962
4. Sethi DS, Prem K. Pillay; endoscopic pituitary surgery – a minimally invasive technique. Am J Rhinol 1996;10(3):141–147
5. Sethi DS, Prem K. Pillay: endoscopic surgery for pituitary tumours. Oper Tech Otolaryngol – Head Neck Surg 1996;7(3): 264–268
6. Sethi DS. International Joint Congress on Minimally Invasive Surgery in Otolaryngology and Neurosurgery. June 17–20, 1995; Pittsburgh, PA
7. Carrau RL, Jho HD, Ko Y. Transnasal-transsphenoidal endoscopic surgery of the pituitary gland. Laryngoscope 1996;106(7): 914–918
8. Cappabianca P, Alfieri A, de Divitiis E. Endoscopic endonasal transsphenoidal approach to the sella: towards functional endoscopic pituitary surgery (FEPS). Minim Invasive Neurosurg 1998;41(2):66–73
9. Cappabianca P, Alfieri A, Thermes S, Buonamassa S, de Divitiis E. Instruments for endoscopic endonasal transsphenoidal surgery. Neurosurgery 1999;45(2):392–395, discussion 395–396
10. Cappabianca P, Cavallo LM, Valente V, et al. Sellar repair with fibrin sealant and collagen fleece after endoscopic endonasal transsphenoidal surgery. Surg Neurol 2004;62(3):227–233, discussion 233
11. Cappabiance P, Frank G, Pasquini E, et al. Extended endonasal trans-sphenoidal approaches to the suprasellar region, planum sphenoidale and clivus. In: de Divitiis E, Cappabianca P, eds. Endoscopic Endonasal Trans-sphenoidal Surgery. Wien: Springer-Verlag; 2003
12. Cappabianca P, Cavallo LM, de Divitiis E. Endoscopic endonasal transsphenoidal surgery. Neurosurgery 2004;55(4):933–940, discussion 940–941
13. Cavallo LM, Cappabianca P, Galzio R, Iaconetta G, de Divitiis E, Tschabitscher M. Endoscopic transnasal approach to

the cavernous sinus versus transcranial route: anatomic study. Neurosurgery 2005;56(2, Suppl):379–389, discussion 379–389
14. de Divitiis E, Cappabianca P. Microscopic and endoscopic transsphenoidal surgery. Neurosurgery 2002;51(6):1527–1529, author reply 1529–1530
15. Cappabianca P, Cavallo LM, Colao A, et al. Endoscopic endonasal transsphenoidal approach: outcome analysis of 100 consecutive procedures. Minim Invasive Neurosurg 2002;45(4):193–200
16. Cappabianca P, Cavallo LM, Mariniello G, de Divitiis O, Romero AD, de Divitiis E. Easy sellar reconstruction in endoscopic endonasal transsphenoidal surgery with polyester-silicone dural substitute and fibrin glue: technical note. Neurosurgery 2001;49(2):473–475, discussion 475–476
17. Cavallo LM, Briganti F, Cappabianca P, et al. Hemorrhagic vascular complications of endoscopic transsphenoidal surgery. Minim Invasive Neurosurg 2004;47(3):145–150
18. de Divitiis E, Cappabianca P, Cavallo LM. Endoscopic transsphenoidal approach: adaptability of the procedure to different sellar lesions. Neurosurgery 2002;51(3):699–705, discussion 705–707
19. Kaptain GJ, Vincent DA, Sheehan JP, Laws ER Jr. Transsphenoidal approaches for the extracapsular resection of midline suprasellar and anterior cranial base lesions. Neurosurgery 2001;49(1):94–100, discussion 100–101
20. Frank G, Pasquini E. Approach to the cavernous sinus. In: de Devitiis E, Cappabianca P, eds. Endoscopic Endonasal Transsphenoidal Surgery. Wien. Springer-Verlag. 2003:159–175
21. Kassam A, Snyderman CH, Mintz A, Gardner P, Carrau RL. Expanded endonasal approach: the rostrocaudal axis. Part I. Crista galli to the sella turcica. Neurosurg Focus 2005;19(1):E3
22. Kassam A, Snyderman CH, Mintz A, Gardner P, Carrau RL. Expanded endonasal approach: the rostrocaudal axis. Part II. Posterior clinoids to the foramen magnum. Neurosurg Focus 2005;19(1):E4
23. Kassam AB, Gardner P, Snyderman C, Mintz A, Carrau R. Expanded endonasal approach: fully endoscopic, completely transnasal approach to the middle third of the clivus, petrous bone, middle cranial fossa, and infratemporal fossa. Neurosurg Focus 2005;19(1):E6
24. Kassam AB, Snyderman C, Gardner P, Carrau R, Spiro R. The expanded endonasal approach: a fully endoscopic transnasal approach and resection of the odontoid process: technical case report. Neurosurgery 2005;57(1, Suppl):E213, discussion E213
25. McMains KC, Gross CW, Kountakis SE. Endoscopic management of cerebrospinal fluid rhinorrhea. Laryngoscope 2004;114(10):1833–1837
26. Kirtane MV, Gautham K, Upadhyaya SR. Endoscopic CSF rhinorrhea closure: our experience in 267 cases. Otolaryngol Head Neck Surg 2005;132(2):208–212
27. Locatelli D, Rampa F, Acchiardi I, Bignami M, Pistochini A, Castelnuovo P. Endoscopic endonasal approaches to anterior skull base defects in pediatric patients. Childs Nerv Syst 2006;22(11):1411–1418
28. Shah AR, Pearlman AN, O'Grady KM, Bhattacharyya TK, Toriumi DM. Combined use of fibrin tissue adhesive and acellular dermis in dural repair. Am J Rhinol 2007;21(5):619–621
29. Hadad G, Bassagasteguy L, Carrau RL, et al. A novel reconstructive technique after endoscopic expanded endonasal approaches: vascular pedicle nasoseptal flap. Laryngoscope 2006;116(10):1882–1886
30. Harvey RJ, Smith JE, Wise SK, et al. Intracranial complications before and after endoscopic skullbase reconstruction. Am J Rhinol 2007;22:619–621
31. Harvey RJ, Nogueira JF Jr, Schlosser RJ, Patel SJ, Vellutini E, Stamm AC. Closure of large skull base defects after endoscopic transnasal craniotomy. Clinical article. J Neurosurg 2009;111(2):371–379
32. Snyderman C, Kassam A, Carrau R, Mintz A, Gardner P, Prevedello DM. Acquisition of surgical skills for endonasal skull base surgery: a training program. Laryngoscope 2007;117(4):699–705
33. Lund VJ, Stammberger H, Nicolai P, et al; European Rhinologic Society Advisory Board on Endoscopic Techniques in the Management of Nose, Paranasal Sinus and Skull Base Tumours. European position paper on endoscopic management of tumours of the nose, paranasal sinuses and skull base. Rhinol Suppl 2010;22:1–143
34. Lobo B, Heng A, Barkhoudarian G, Griffiths CF, Kelly DF. The expanding role of the endonasal endoscopic approach in pituitary and skull base surgery: a 2014 perspective. Surg Neurol Int 2015;6(6):82
35. Barkhoudarian G, Del Carmen Becerra Romero A, Laws ER. Evaluation of the 3-dimensional endoscope in transsphenoidal surgery. Neurosurgery 2014;73:74–79
36. Elhadi AM, Zaidi HA, Hardesty DA, et al. Malleable endoscope increases surgical freedom compared with a rigid endoscope in endoscopic endonasal approaches to the parasellar region. Neurosurgery 2014;10(Suppl 3):393–399, discussion 399
37. Locatelli D, Pozzi F, Turri-Zanoni M, et al. Transorbital endoscopic approaches to the skull base: current concepts and future perspectives. J Neurosurg Sci 2016;60(4):514–525
38. Kupferman ME, Hanna E. Robotic surgery of the skull base. Otolaryngol Clin North Am 2014;47(3):415–423

2 Anatomical Perspectives of the Sellar, Suprasellar, and Parasellar Regions

Shilpee Bhatia Sharma, Abhilasha Karunasagar, Narayanan Janakiram

Introduction

The versatility of the transsphenoid route forms the foundation of the expanded endonasal approaches to sellar, parasellar, and suprasellar region.[1,2,3] Endoscopic techniques have contributed to decreased morbidity, mortality, and cosmetic deformity, leading to a shift in surgical paradigm.[3,4,5] The advances in technology, however, have not replaced having a comprehensive understanding of anatomy, which has always been the foundation of surgery. Acquisition of surgical skills, endoscopic views, and orientation of landmarks are of paramount importance to avoid complications. In this chapter, the authors briefly describe the anatomy of the sellar, suprasellar, and parasellar regions from an endoscopic perspective.

Development

The cranial base develops in three stages: the membranous, the cartilaginous, and stage of ossification.

In the cartilaginous phase, sphenoid bone develops from orbitosphenoid (lesser wing and anterior clinoid process), alisphenoid (greater wing of sphenoid), anterior presphenoid ossification center (sphenoid body anterior to tuberculum), and posteriorly from postsphenoid ossification center which constitutes two hypophyseal cartilaginous center (sphenoid body posterior to tuberculum, sella turcica, dorsum sella)[6] (**Fig. 2.1**). The orbitosphenoid consists of two crura which form the boundary of the optic canal (the crus anterius) and the crus posteriorus.[7]

The ossification is complex and is derived from 18 or 19 ossification centers (**Tables 2.1 and 2.2**). There are four ossification centers in postsphenoid—one pair of medial centers (sella floor and dorsum sella) and the rest lateral centers (lingula sphenoidalis and carotid sulcus). In 80% of the cases, the development is from joining of two medial centers followed by their joining with lateral centers at the end of fifth month of gestation and with the presphenoid at the end of 6 months.

The fusion with orbitosphenoid and alisphenoid starts at the beginning of 6 and 9 months, respectively and is completed by 10 months of birth. The fusion of presphenoid centers with the opposite side and orbitosphenoid takes place progressively from fourth month to ninth month.[7] The zone of fusion is at the level of tuberculum sella.[8] The fusion plates develop at the point of union and offer resistance

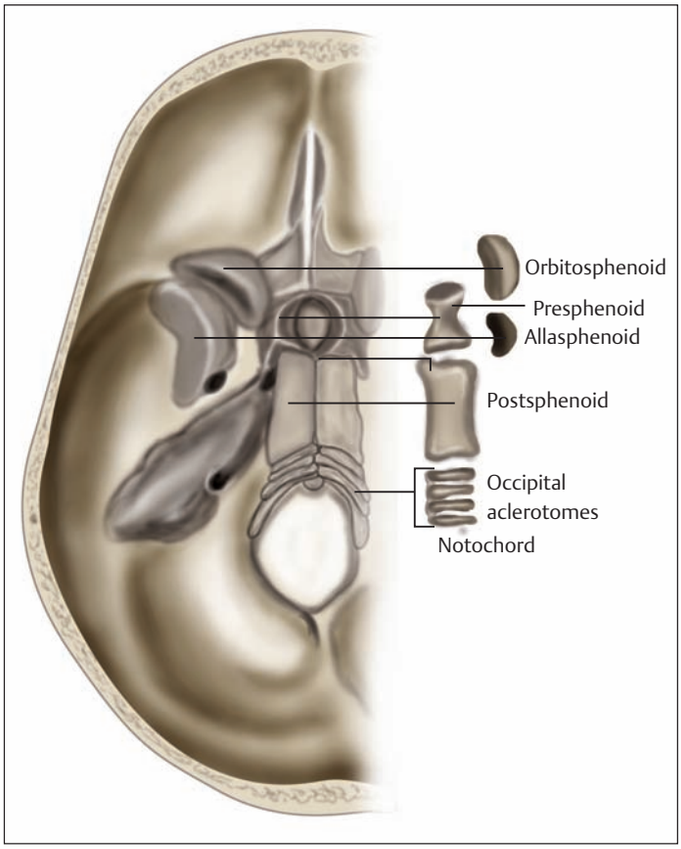

Fig. 2.1 Embryonic cartilage precursors of the sphenoid bone.

Table 2.1 Embryology of sphenoid ossification center

Presphenoid		Postsphenoid	
Ninth week	Small wing ossification center appears	Eighth week	Great wing of sphenoid
Fifth month	Sphenoid conchae appears		Membrane ossification for orbital, lateral pterygoid middle cranial fossa part
3–4 years	Hollowing appears	Ninth week	Sella turcica center appears
Fourth year	Fuse with labyrinths of ethmoid		Medial pterygoid ossification center
9–12 years	Unite with sphenoid	Third month	Hamulus ossification
		Fourth month	Lingula center appears
Eighth month: pre- and postsphenoid join			
First year: great wings and body unite. Jugum sphenoidale formed			
25th year: sphenoid joins with occipital bone			

Table 2.2 Sphenoid foramen and its contents

Foramen	Content
Foramen ovale	Mandibular division of trigeminal nerve Middle meningeal vein Lesser superficial petrosal nerve Accessory middle meningeal artery
Foramen spinosum	Middle meningeal artery Middle meningeal vein Meningeal branch of V3
Foramen rotundum	Maxillary division of V2
Foramen lacerum	Meningeal branch of ascending pharyngeal artery Vidian nerve and vein Emissary vein
Vidian canal	Vidian nerve Artery of vidian canal
Foramen Vesalius	Emissary vein Accessory meningeal artery
Canal of Arnold	Lesser superficial petrosal nerve
Optic canal	Ophthalmic artery Optic nerve
Superior orbital fissure	Cranial nerves III, IV, V (ophthalmic division V1), VI Superior ophthalmic vein Recurrent meningeal branch of lacrimal artery Orbital branch of middle meningeal artery

to pneumatization leading to the formation of crests and septae[8] (**Fig. 2.2**).

At birth, sphenoid sinus is composed of three segments—central segment (body and lesser wings) and two lateral segments (greater wing and pterygoid process). The sphenoid sinus is filled with red erythropoietic marrow at birth.[9] The unossified cartilage is present in the sphenoid body, sphenooccipital and sphenopetrous junction, and foramen lacerum.[6] During the first postnatal year, greater wings fuse with the body around the vidian canal.[6]

The red erythropoietin is converted to yellow in presphenoid plate between 7 months and 2 years and then extends posteriorly toward the basisphenoid plate.[8] The process of pneumatization starts as early as 4 months of age (generally around age 3 years) but does not reach maturity until approximately age 10 to 14 years.[10] The sphenooccipital synchondrosis is not ossified till 16th to 18th year of life. The pneumatization can extend into the occipital bone after 18 years of life[10] (**Fig. 2.3**).

The area of planum sphenoidale center is formed after 1 year of birth by fusion of median orbitosphenoid process.[7] The presphenoid continues to grow in height and eventually fuses with the anterosuperior roots of lesser wings of the sphenoid. This fusion results in the formation of planum sphenoidale and its posterior growth pattern are variable. The posterior edge of planum is called limbus and region of presphenoid not overlapped by planum remains as the chiasmatic sulcus. Usually the plane of the angle that tuberculum-chiasmatic-sulcus and limbus makes with the horizontal plane is 45 degrees. In cases where limbus grows posteriorly, the chiasmatic sulcus is vertical with the long anterior wall of the sphenoid. It is more horizontal in the case of the tuberculum overgrowing upward (**Fig. 2.4**).[11] The fusion between presphenoid and planum sphenoidale is completed at 6 years of life.[7]

The ethmoid sinuses are fully developed by birth, but the labyrinth is partially ossified. The perpendicular plate

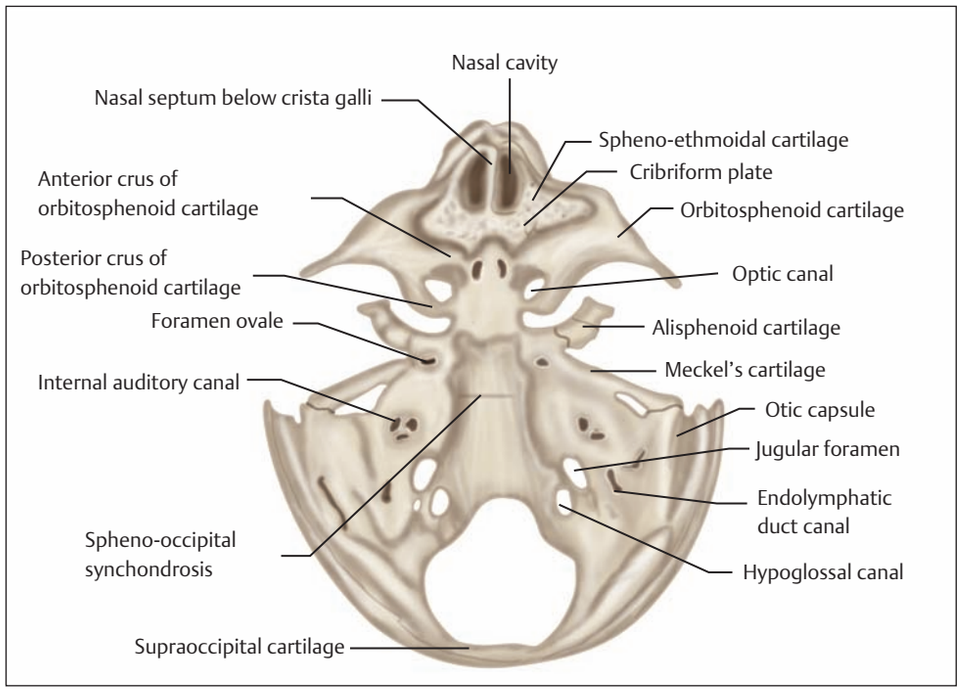

Fig. 2.2 Ossification of the fetal sphenoid bone.

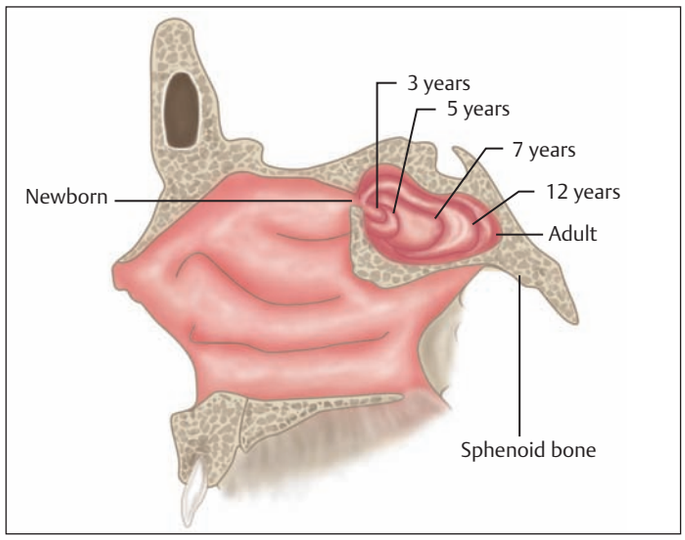

Fig. 2.3 Development of the sphenoid sinus.

ossification starts in the first year of life and fuses with the labyrinth in the second year of life, followed by cribriform plate and crista galli. The single ethmoid bone develops at 3 years of age. The maxillary sinus is fully pneumatized by 2 to 5 years, but sphenoid sinus continues to pneumatize till adolescence.[8] The normal variants of the central skull base have been discussed in **Fig. 2.5 and Table 2.2.**

Sphenoid Bone

The word sphenoid is derived from Greek word sphen, meaning a wedge.[12] The sphenoid bone resembles a bird with outstretched wings, wedge-shaped, and centrally placed in the skull base. It articulates with numerous bones, possesses many foramina, and has important neurovascular relationships. The sphenoid bone is located at the center of the skull base, in front of the temporal and occipital bones and posterior to the frontal and ethmoid bones.

It consists of a central body which is cuboidal in shape, two lesser wings extending from the superolateral surface of the body, two greater wings which spread upward from the lower part of the body, and two pterygoid processes with their median and lateral pterygoid plates directed downward from the body (**Fig. 2.6**).

Body

The body is cubical and contains sphenoid sinus separated by a septum. The superior surface of the body anteriorly the planum sphenoidale articulates in the front articulates with the cribriform plate of the ethmoid forming anterior cranial fossa. Laterally, it forms the optic canal and blends with the anterior clinoid process. The chiasmatic sulcus

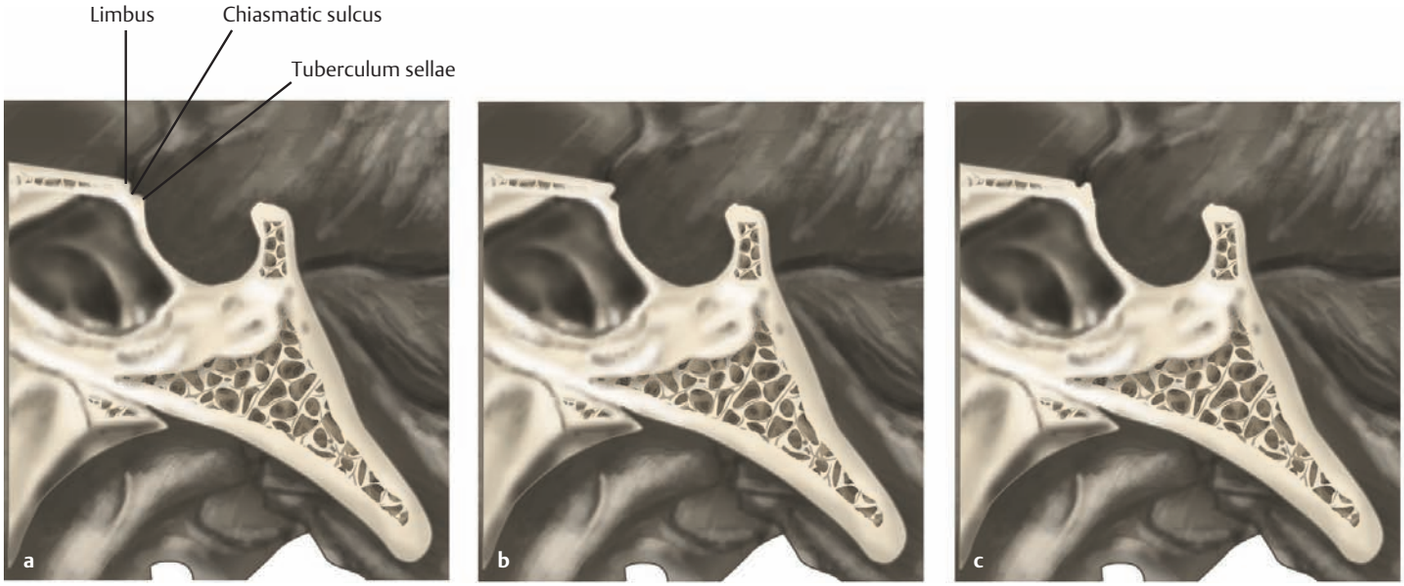

Fig. 2.4 Chiasmatic tuberculum planum angle. **(a)** C-T-P angle is 45 degrees to the horizontal plane. **(b)** Chiasmatic sulcus is vertically aligned. **(c)** Chiasmatic sulcus is horizontally oriented.

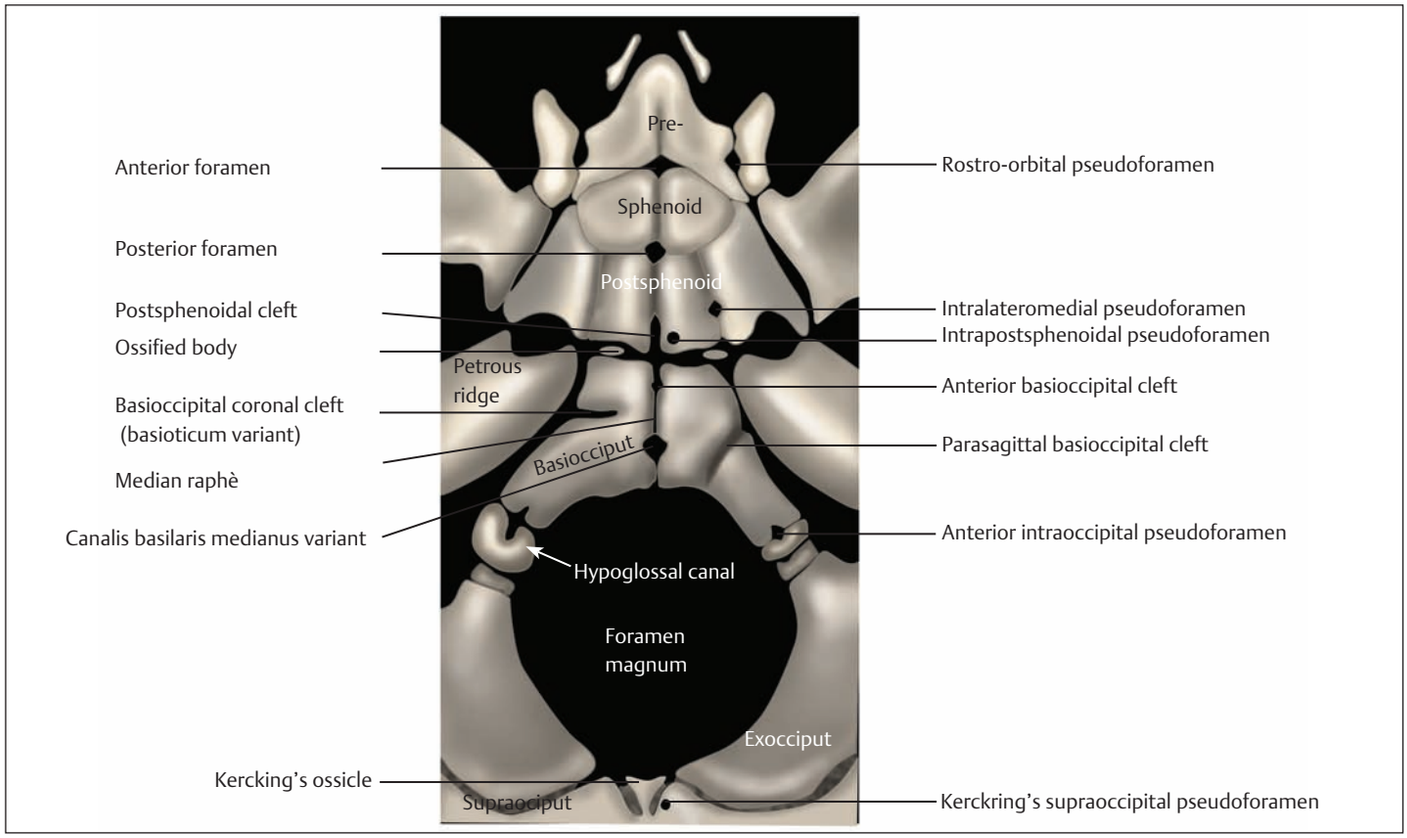

Fig. 2.5 Normal variants of the skull base.

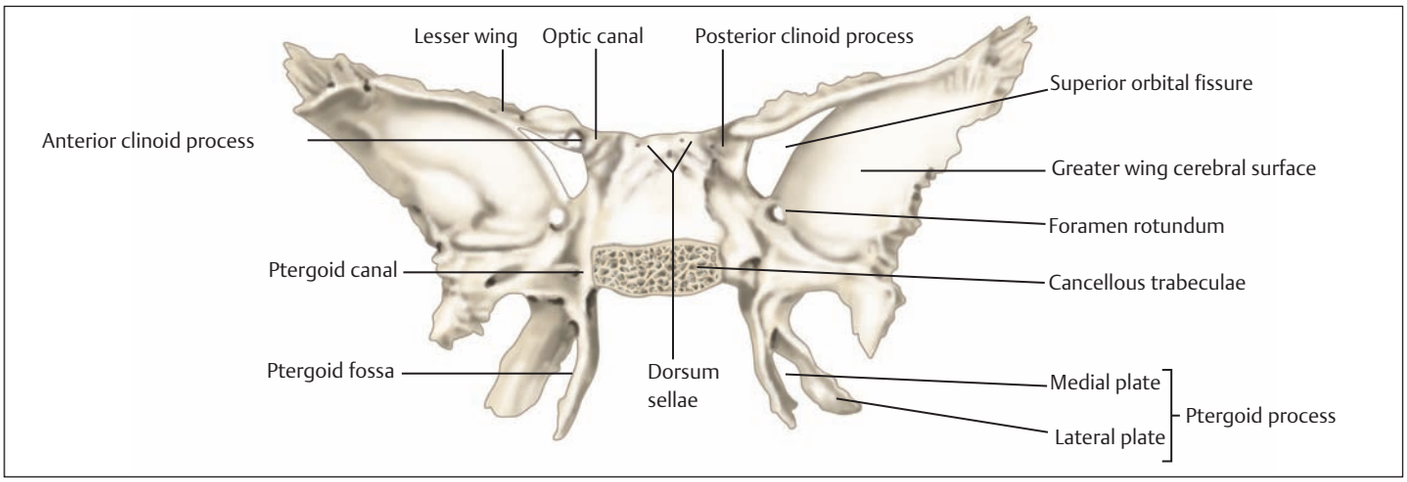

Fig. 2.6 Posterior view of the sphenoid bone.

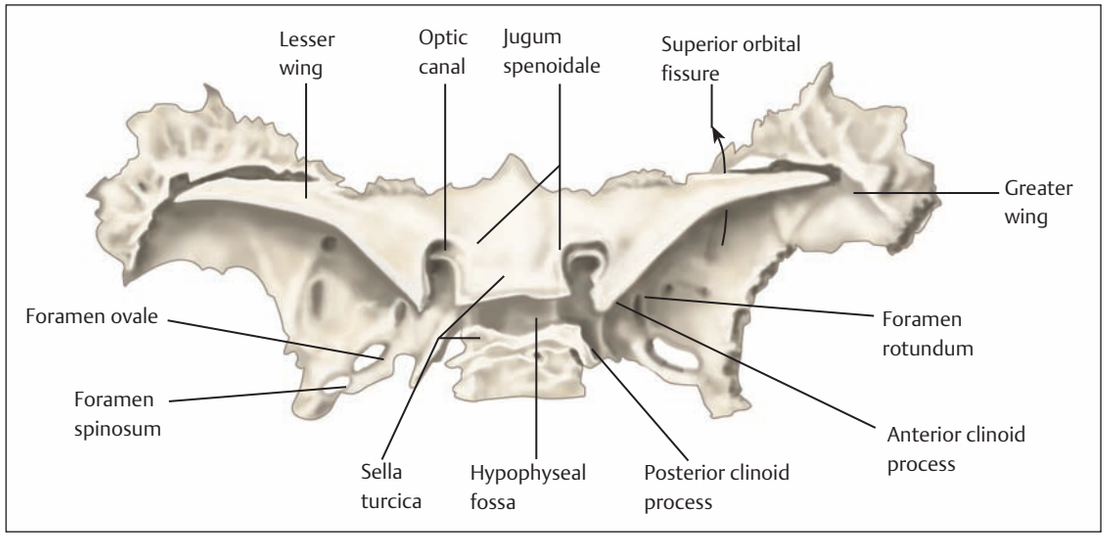

Fig. 2.7 Superior view of the sphenoid bone.

forms the slight depression in the posterior boundary of the planum sphenoidale and extends laterally to the optic canals. The anterior ridge forms the limbus sphenoidale forming the posterior limit of planum sphenoidale and tuberculum sella lies posteriorly (**Fig. 2.7**).

The sella turcica is a depression in the sphenoid bone and contains pituitary gland. A middle clinoid process forms the anterior boundary of sella, two eminences on either side, and posterior by dorsum sella with two tubercules—posterior clinoid process. The posterior clinoids are narrower than anterior, and tentorium is anchored to it. The internal carotid artery (ICA) passes between anterior and middle clinoid process and pierces dura at that level. On each side of the dorsum sellae is a notch for the abducent nerve and below the notch a sharp process, which articulates with the apex of the temporal bone and forms the medial boundary of the foramen lacerum. The clivus below the dorsum sellae is a shallow depression, the clivus, which slopes obliquely backward and continuous with the groove on the basilar portion of the occipital bone (**Fig. 2.8**).

The Lateral Surface

The lateral surface unites with the greater wing of sphenoid and pterygoid plates. Above the attachment of each great wing is a wide groove it lodges ICA and is named carotid groove. The ridge of the bone in the posterior part of the lateral margin of the groove in between the body and great wing is called lingula (**Fig. 2.8**).

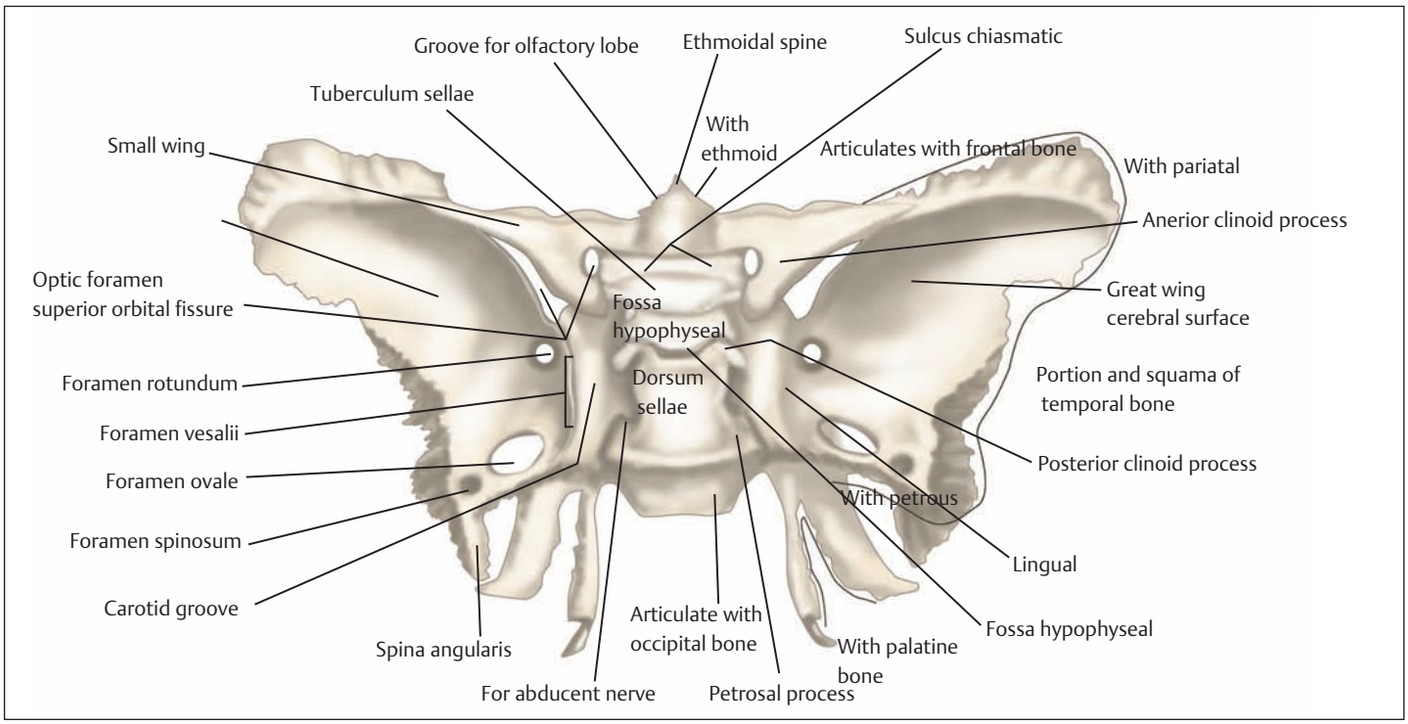

Fig. 2.8 Upper surface of the sphenoid bone.

The Posterior Surface

This is quadrangular in shape and ossifies with the occipital bone between 18 years and 25 years of life.

Inferior Surface

In the inferior surface, in the middle is a triangular spine—sphenoid rostrum, which articulates with the sphenoid crest on the anterior surface. On either side is the vaginal process, directed medialward from the base of the medial pterygoid plate (**Fig. 2.9a, b**).

Anterior Surface

The anterior surface of the body in the midline has a sphenoid crest which articulates with the perpendicular plate of the ethmoid. On either side of the crest, sphenoid ostium leads to sphenoid sinuses. The lateral margin of the anterior surface articulates with the posterior ethmoid cells and the lower margin articulates with the orbital process of the palatine bone and upper with the orbital plate of the frontal bone (**Fig. 2.9a, b**).

The Greater Wing

The greater wings arise from the sides of the body and are curved upward, lateralward, and backward; the posterior part of each projects as a triangular process which fits into the angle between the squama and the petrous portion of the temporal and presents at its apex a downwardly directed process, the spina angularis (sphenoid spine). The greater wing has many surfaces and forms the portion of middle cranial fossa, orbit, temporal, infratemporal, and pterygopalatine fossa (**Fig. 2.8**).

The superior surface forms part of the middle fossa of the skull; it is deeply concave and presents depressions for the convolutions of the temporal lobe of the brain. At its anterior and medial part is a circular aperture, the foramen rotundum, for the transmission of the maxillary nerve. Behind and lateral to this is the foramen ovale, for the transmission of the mandibular nerve, the accessory meningeal artery, and sometimes the lesser superficial petrosal nerve. Medial to the foramen ovale, a small aperture, the foramen Vesalii, may occasionally be seen opposite the root of the pterygoid process; it opens below near the scaphoid fossa and transmits a small vein from the cavernous sinus. Lastly,

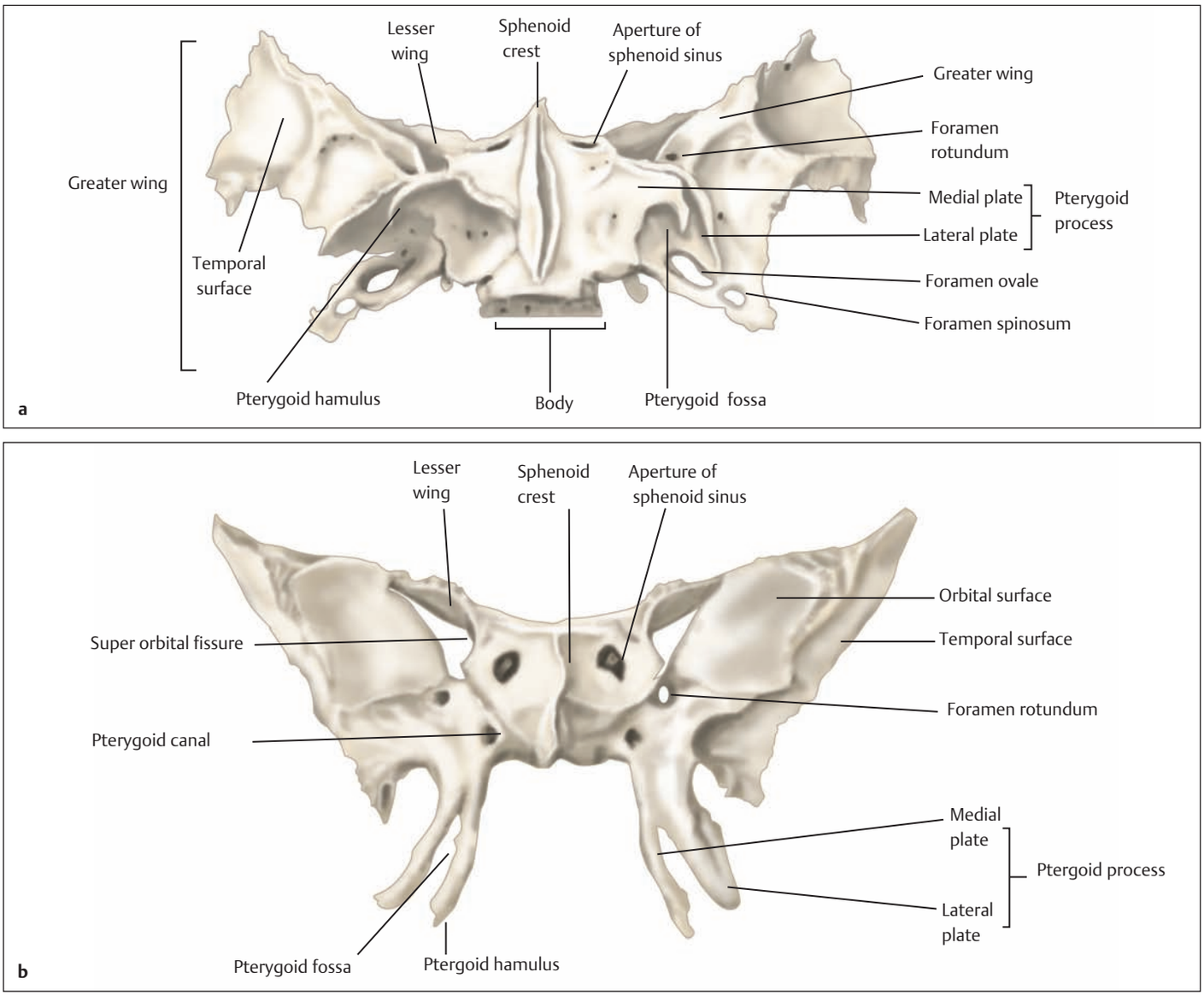

Fig. 2.9 **(a)** Inferior view of the sphenoid bone. **(b)** Anterior view of the sphenoid bone.

in the posterior angle, near to and in front of the spine, is a short canal, sometimes double, the foramen spinosum, which transmits the middle meningeal vessels and a recurrent branch from the mandibular nerve (**Fig. 2.8**).

The lateral surface is divided by a transverse ridge, the infratemporal crest, into two portions. The superior or vertical temporal portion forms a part of the temporal fossa, and gives attachment to the Temporalis; the inferior or horizontal infratemporal, smaller in size and concave, enters into the formation of the infratemporal fossa, and, together with the infratemporal crest, affords attachment to the lateral pterygoid muscle. The foramen ovale and foramen spinosum pierce it, and at its posterior part is the spina angularis, which is frequently grooved on its medial surface for the chorda tympani nerve. To the spina angularis are attached the sphenomandibular ligament and the Tensor veli palatini. Medial to the anterior extremity of the infratemporal crest is a triangular process which serves to increase the attachment of the lateral pterygoid muscle; extending downward and medialward from this process on to the front part of the lateral pterygoid plate is a ridge which forms the anterior limit of the infratemporal surface, and in the articulated skull, the posterior boundary of the pterygomaxillary fissure (**Fig. 2.10**).

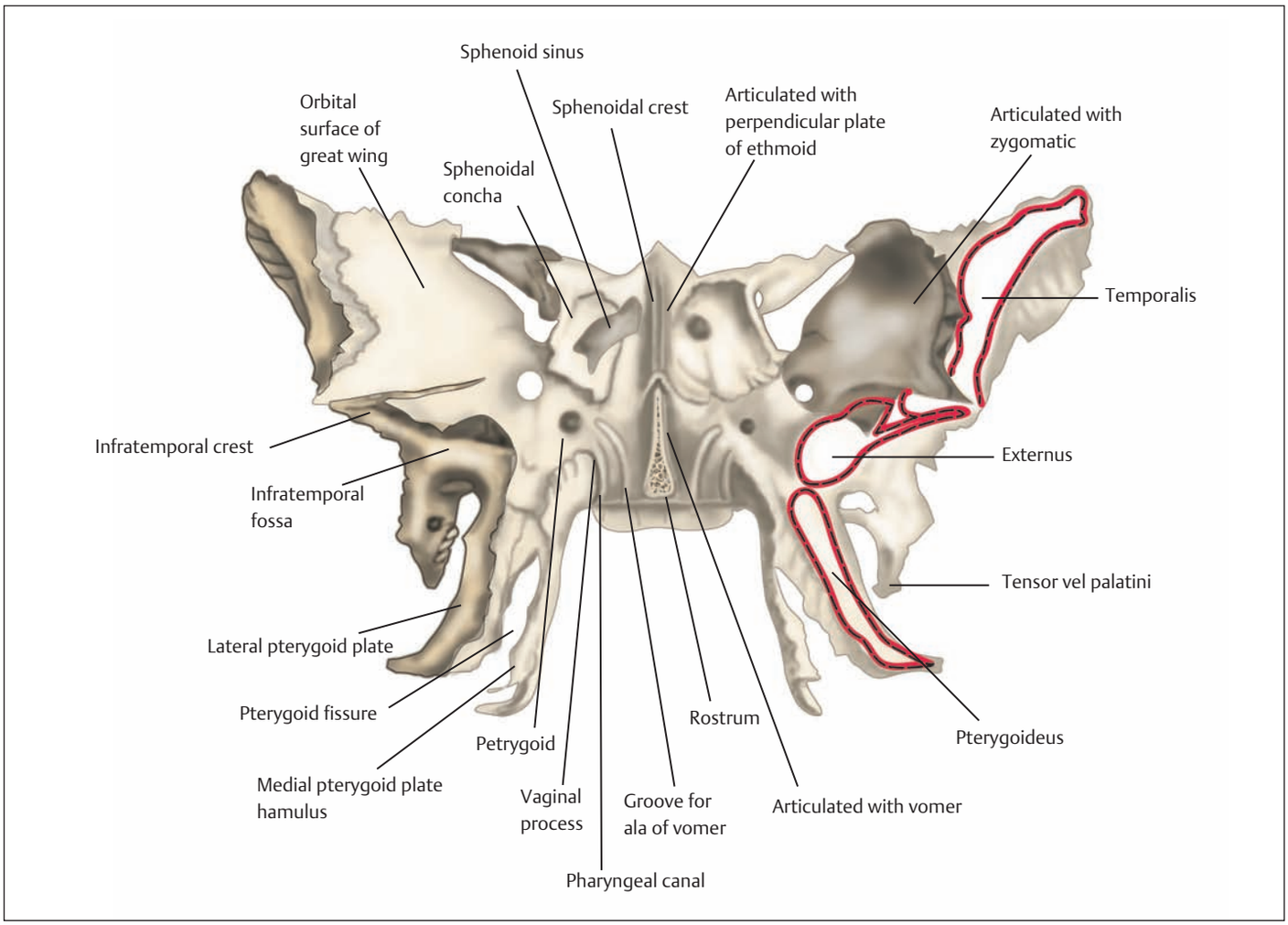

Fig. 2.10 Anterior surface of the sphenoid bone.

The orbital surface of the great wing, smooth and quadrilateral in shape, is directed forward and medialward and forms the posterior part of the lateral wall of the orbit. Its upper serrated edge articulates with the orbital plate of the frontal. Its inferior rounded border forms the posterolateral boundary of the inferior orbital fissure. Its sharp medial margin forms the lower boundary of the superior orbital fissure. Its lateral margin is serrated and articulates with the zygomatic bone. Below the medial end of the superior orbital fissure is a grooved surface, which forms the posterior wall of the pterygopalatine fossa, and is pierced by the foramen rotundum (**Fig. 2.8**).

The Lesser Wing

The lesser wings or orbitosphenoids are two thin triangular plates, which arise from the planum sphenoidale laterally and form the posterior floor of the anterior cranial fossa. The inferior surface forms the back part of the roof of the orbit and the upper boundary of the superior orbital fissure. The anterior border is serrated for articulation with the frontal bone. The posterior border, smooth and rounded, is received into the lateral fissure of the brain; the medial end of this border forms the anterior clinoid process, which gives attachment to the tentorium cerebelli; it is sometimes

joined to the middle clinoid process by a spicule of bone, and when this occurs the termination of the groove for the ICA is converted into a foramen (caroticoclinoid). The lesser wing is connected to the body by two roots, the upper thin and flat, the lower thick and triangular; between the two roots is the optic foramen, for the transmission of the optic nerve and ophthalmic artery (**Fig. 2.8**).

Pterygoid Processes

The pterygoid processes, one on either side, descend perpendicularly from the regions where the body and great wings unite. Each process consists of a medial and a lateral plate, the upper parts of which are fused anteriorly; a vertical sulcus, the pterygopalatine groove, descends on the front of the line of fusion. The plates are separated below by an angular cleft, the pterygoid fissure, the margins of which are rough for articulation with the pyramidal process of the palatine bone. The two plates diverge behind and enclose between them is a **V**-shaped fossa, the pterygoid fossa, which contains the medial pterygoid plate and Tensor veli palatini. Above this fossa is a small, oval, shallow depression, the scaphoid fossa, which gives origin to the Tensor veli palatini. The anterior surface of the pterygoid process is broad and triangular near its root, where it forms the posterior wall of the pterygopalatine fossa and presents the anterior orifice of the pterygoid canal (**Fig. 2.10**).

Medial Pterygoid Plate

The medial pterygoid plate is narrower and longer than the lateral; lower extremity into a hook-like process, the pterygoid hamulus, around which the tendon of the Tensor veli palatini glides. The lateral surface of this plate forms part of the pterygoid fossa; the medial surface constitutes the lateral boundary of the choana or posterior aperture of the corresponding nasal cavity. It is attached superiorly by pharyngobasilar fascia and superior constrictor muscle of the pharynx inferiorly (**Fig. 2.10**).

At the junction of the pterygoid processes and the sphenoid body lies the Vidian (pterygoid) canal, which opens into the pterygoid fossa. The anterior surface of the process forms the posterior boundary of the pterygopalatine fossa, where the pterygopalatine ganglion is located.

Lateral Pterygoid Plate

The lateral pterygoid plate is broad, thin, and everted; its lateral surface forms part of the medial wall of the infratemporal fossa, and gives attachment to the lateral pterygoid muscle; its medial surface forms part of the pterygoid fossa, and gives attachment to the medial pterygoid muscle (**Fig. 2.9**).

Intrinsic Ligaments of the Sphenoid

The more important of these are the pterygospinous, stretching between the spina angularis and the lateral pterygoid plate; the interclinoid, a fibrous process joining the anterior to the posterior clinoid process; and the caroticoclinoid, connecting the anterior to the middle clinoid process. These ligaments occasionally ossify. The multiple foramina in sphenoid bone are described in **Table 2.3**.

Sphenoid Sinus

The sphenoid sinus is a surgical window for expanded endoscopic approaches to sella, suprasellar, and parasellar regions. It is surrounded by the vital anatomical structures such as an ICA, optic nerves, and cranial nerves. The sphenoid sinus varies in size, shape, and septation. The knowledge of the three-dimensional endoscopic anatomy and orientation of landmarks is of paramount importance to avoid morbidity and mortality. The development of endoscopic approach has induced a deeper understanding of the sphenoid sinus central. The transsphenoid approach to sella, suprasellar, and parasellar regions is greatly influenced by the anatomical variations of the sphenoid sinus.

The sphenoid sinus is a pair which lie in the sphenoid bone. It is bounded anteriorly by ethmoid air cells, laterally cavernous sinuses and its contents, inferiorly posterior choana, posteriorly clivus and superiorly pituitary fossa and planum sphenoidale.[13,14,15] The sinus is related to the optic nerve superolaterally, ICA posterolaterally,[15] and maxillary vidian nerve inferiorly (**Fig. 2.11**). Both sinuses are separated by intersphenoid septum which is not necessarily located in the midline with drainage in the sphenoethmoidal recess into the nasopharynx. The intrasphenoid septations inside

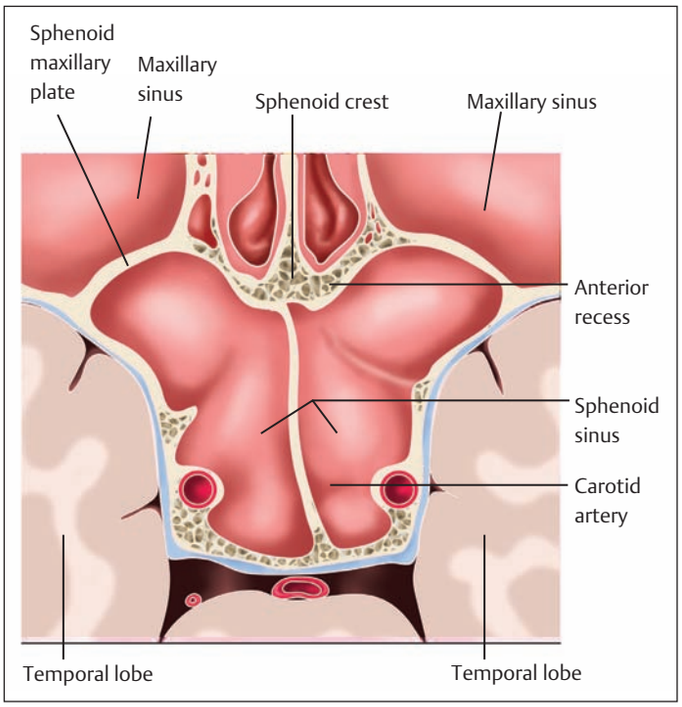

Fig. 2.11 Anatomical relationships of the sphenoid sinus.

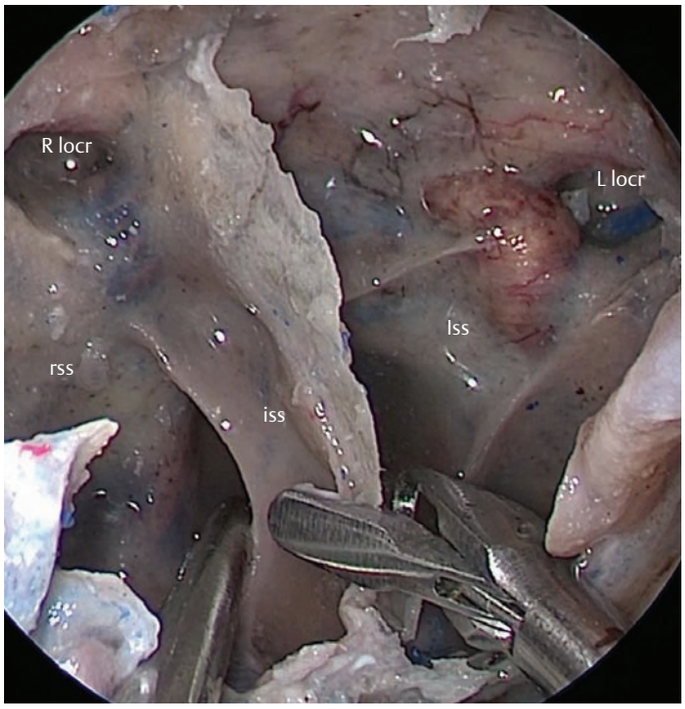

Fig. 2.12 Intersphenoid septum with insertion in the right internal carotid artery in sphenoid sinus.

sphenoid sinus divide it into compartments (**Fig. 2.12**). They are divided into intersphenoid and accessory septations. In general, one or more intersphenoid septations are present with great variation. The insertion of the septation in the neurovascular structure increases the risk of injury (**Fig. 2.12**). Recent studies show that during endoscopic sinus surgery the sphenoid septum is unreliable as a guide to midline and attachment to the optic nerve and/or ICA. The average volume of the sphenoid sinus is between 3 mL and 10 mL.[16]

Ramalho et al noticed that 52% had septations attached to the ICA; this prevalence was higher in the well- pneumatized sphenoid sinus (62.4%).[17] This data is in contrast with Fernandez-Miranda et al which showed a prevalence of 85% among at least one septation in the ICA.[18] Renn and Rhoton found intersphenoid septations next to the ICA channel in 32% of the cadavers.[19] Sethi et al described intersphenoid septations in the ICA in 40% of the 30 cadavers in an endoscopic study in 1995.[20] Unal et al and Abdullah et al reported 30% and 31% of septations of the sphenoid sinus attached to the wall of the ICA, respectively, using CT scans.[21]

Pneumatization Patterns of the Sphenoid Sinus

Many classifications have been devised to understand pneumatization patterns of the sphenoid sinus (**Figs. 2.13 and 2.14**).[22,23] The transsphenoid surgery has expanded approaches to complex regions such as cavernous sinus, suprasellar, and middle cranial fossa, facilitated by sphenoid sinus pneumatization patterns. The sphenoid sinus is highly pneumatized, that distorts anatomy. Thus, knowledge of the pneumatization pattern is essential for anatomical orientation with technical adjuncts applied only as a verification tool. Wang et al[24] reported predominance of sellar pneumatization type followed by postsellar and presellar types and conchal being the least common. Sphenoid sinus agenesis is a rare condition reported as 0.67% by Sonbay et al[25] and 0.26% by Cakur et al.[26] It is occasionally reported isolated[27] and usually is associated with craniofacial syndromes or primary ciliary dyskinesia.[28] There appears to be a difference regarding the ethnicity in the pneumatization patterns.

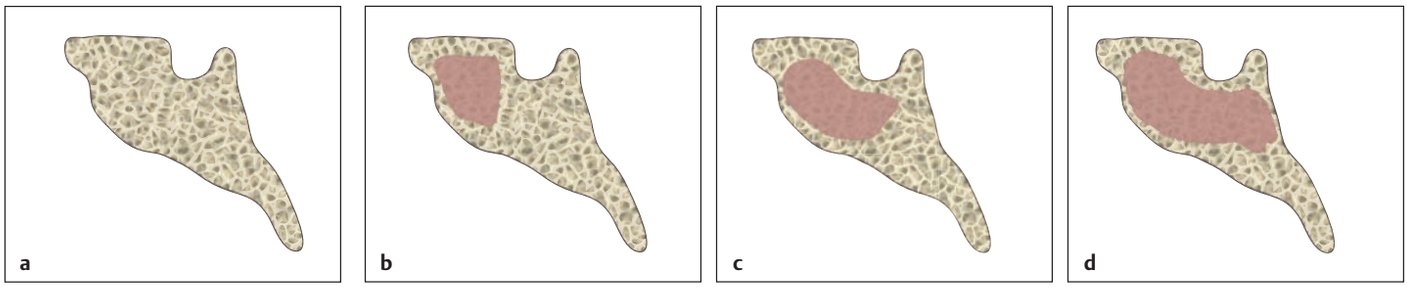

Fig. 2.13 Traditional sphenoid sinus pneumatization classification. **(a)** Conchal-ossified sella with no air cavity. **(b)** Presellar: the air cavity is limited to the vertical line anterior to the anterior wall of the sella. **(c)** Sellar: well-pneumatized till the posterior wall of the sella. **(d)** Postsellar: the pneumatization extends to the posterior wall of the sella.

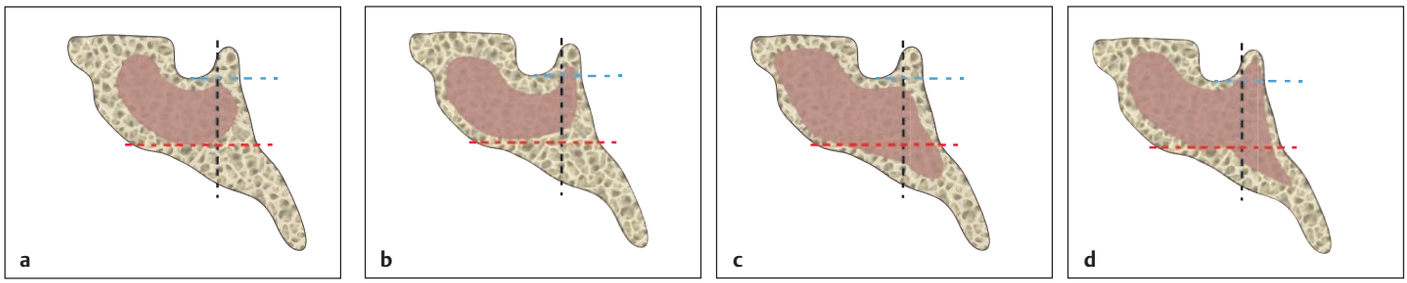

Fig. 2.14 Clival extension of the sphenoid pneumatization. **(a)** Subdorsum: limited till posterior wall of the sella. **(b)** Dorsum type: extends into dorsum sella. **(c)** Occipital type: extends behind posterior wall and below the upper edge of the vidian nerve. **(d)** Combined occipito-dorsum type. Black dashed line parallel to the posterior wall of the sella. Blue dashed line parallel to the sellar floor. Red dashed line parallel to the vidian canal.

Table 2.3 Theories of sphenoid center ossification

Cope et al	Planes of fusion at ossification centers as boundary line	• Presphenoid • Intermediate • Postsphenoid
Elwany et al	Tuberculum sella as vertical line	• Presellar • Postsellar
Hamberger et al	Pneumatization pattern based on relationship with sella turcica	• Conchal • Presellar • Sellar
Hammer et al	Divided seller into Incomplete Complete	• Conchal • Presellar • Sellar • Postsellar
Wang et al		• Sphenoid body • Lateral type • Posterior type • Superior type • Anterior type • Combined

Sphenoid Ostium

The sphenoid ostium located on the anterior wall of the sphenoid sinus communicates with the posterior nasal cavity through sphenoethmoidal recess. Multiple intranasal landmarks have been described for localization of the sphenoid ostium[29,30] (**Table 2.4**). The natural ostium is located approximately at the midpoint of the sphenoid face[30] (**Fig. 2.15**). Millard and Orlandi reported sphenoid osmium to be always medial to the superior turbinate; other studies report 17 to 1.36% of the sphenoid osmium lateral to the superior turbinate.[29] Recent reports showed relationships between pneumatization of the sphenoid sinus and sphenoid sinus ostium. It was noticed that the distance between the planum and ostium is shorter in presellar and sellar pneumatization patterns.[31]

Table 2.4 Landmarks for sphenoid os identification

Posteroinferior end of the superior turbinate	Most reliable landmark
0.8–1 cm from inferior end of superior turbinate	
1.5–3 cm for the choana	
1 cm from midline	
25–34 degrees with distance of 55–62 mm from nasal sill	
Medial to superior turbinate 100% of time	
Medial end of roof of maxillary sinus is always below skull base	
The sphenoid ostium is just above the height of medial maxillary sinus roof	

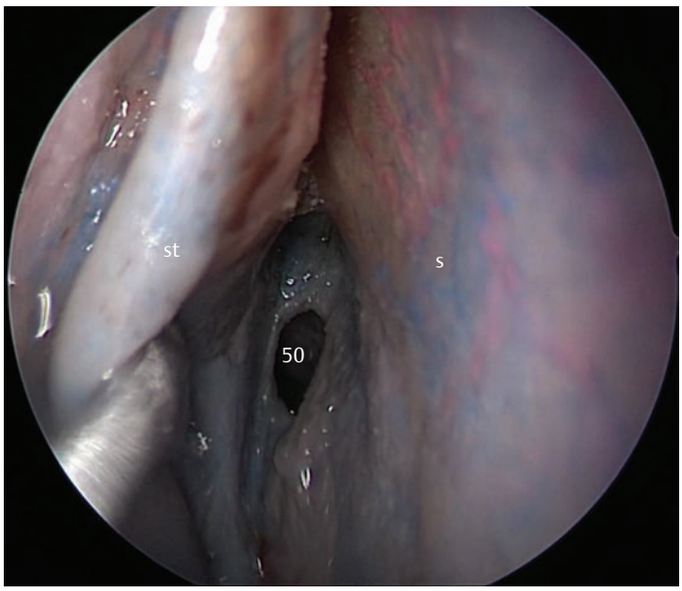

Fig. 2.15 The relationship of the superior turbinate to the sphenoid os.

Onodi Cell

The Onodi cell is an anatomical variant in which the most posterior ethmoid air cell extends posteriorly to lie lateral,and/or superior to the sphenoid sinus.It can reach the optic nerve and/or the internal carotid artery. It is difficult to determine accurately the presence or absence of the Onodi cell, as well as its shape, based on axial or coronal views only. It is important for surgeons to understand the position of the Onodi cell in relation to the optic nerve, ICA, and pituitary gland. However, a large Onodi cell is often confused with the sphenoid sinus, which makes sphenoid sinus surgery difficult. The most posterior wall of

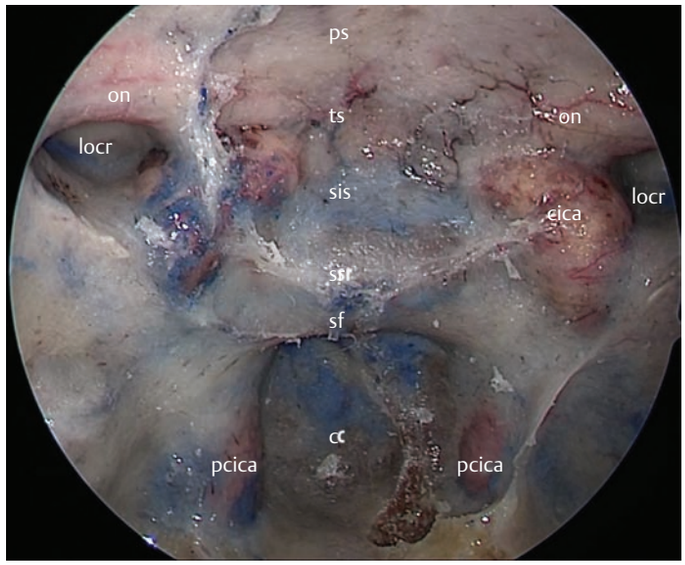

Fig. 2.16 Anatomy of the posterior wall of the sphenoid.

the ethmoid sinus or the Onodi cell is the anterior wall of the sphenoid sinus. In studies based on CT, Onodi cell incidence is mostly low (8–24%).[32] However, in their detailed study based on sagittal CT, Tomovic et al reported that the incidence of the Onodi cell was 65.3%,[33] although they did not provide details about their method of identification. Meanwhile, in studies based on cadavers, Onodi cell incidence is reported to be 42 to 60%.[34,35]

Posterior Wall of the Sphenoid Sinus

The clival indentation is a consistent surgical landmark bounded superiorly by seller floor and laterally by the ICA[36] (**Fig. 2.16**). Alferidi et al[36] divided the anatomy of the posterior wall of the sphenoid sinus into five compartments: midline, bilateral, paramedian, bilateral, and lateral. The structures in the midline above the clival indentation are sellar protuberance, the tuberculum sella, and the planum sphenoidale.

The Planum Sphenoidale

The medial anterior surface of the body of the sphenoid bone is flat and named planum sphenoidale forming the posterior part of the anterior cranial fossa. It connects the two lesser wings of the sphenoid in the midline, bounded anteriorly by the posterior ethmoids and lies above the tuberculum sella (**Fig. 2.17**). The posterior aspect of the planum is called limbus, and just behind it, there is a

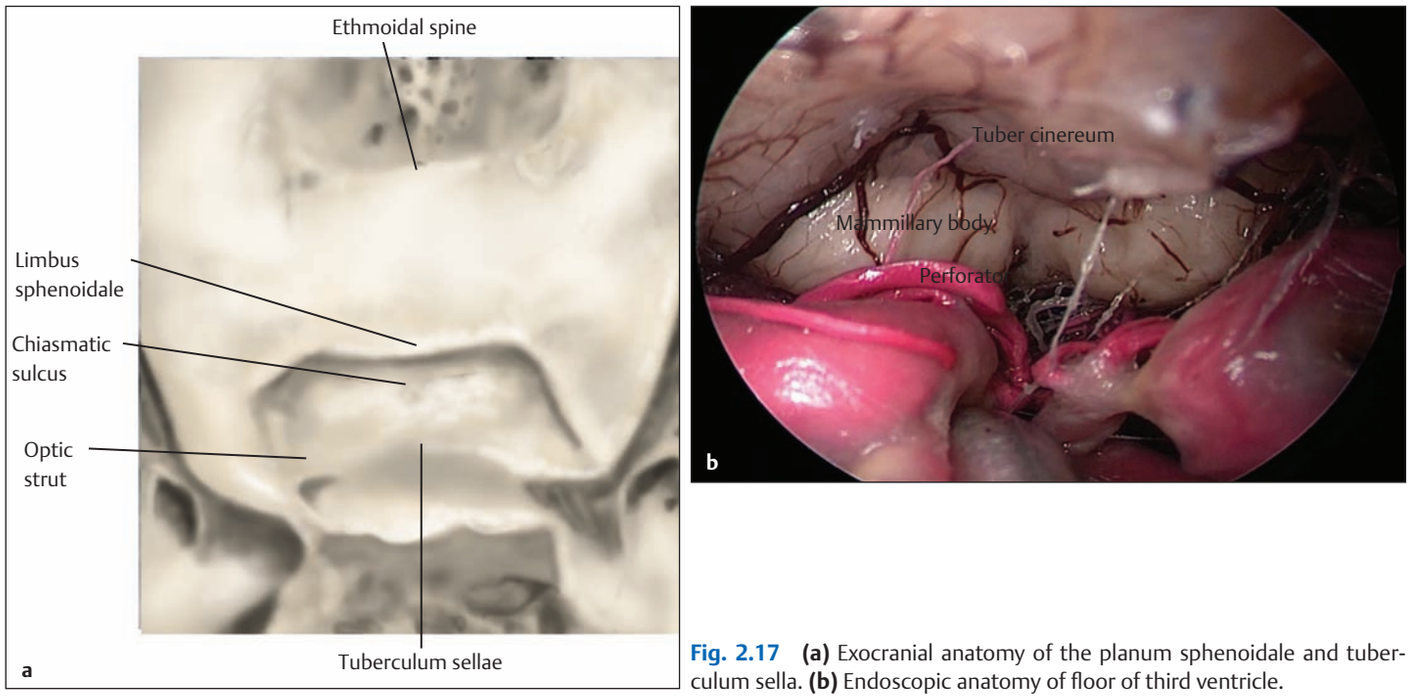

Fig. 2.17 **(a)** Exocranial anatomy of the planum sphenoidale and tuberculum sella. **(b)** Endoscopic anatomy of floor of third ventricle.

chiasmatic groove, then a bony prominence tuberculum sella, and then sella turcica.

The Tuberculum Sella

The region of the tuberculum sella comprises space between anteriorly limited by two anterior clinoids and posteriorly by dorsum sella and anteriorly by planum sphenoidale (**Fig. 2.17**). Endoscopically, it is bound anteriorly by the line joining the two opticocarotid recesses, inferiorly by the line pressing the superior margin of the sella and laterally by the medial aspect of the paraclinoidal carotid arteries (**Fig. 2.16**). The lateral portion of the tuberculum is referred to as medial opticocarotid recess and is reported as a vital landmark in the transsphenoid approach (**Fig. 2.19**).

The surgical boundaries of transtuberculum approach inferiorly line passing in the superior third of sella, laterally by the medial aspect of the parasellar tract of carotid arteries superiorly by the line joining the superior margin of the optic canal which intracranially is seen as limbus sphenoidale (**Figs. 2.17 and 2.18**). This level has a dural fold named falciform ligament and any bone removal anterior to it is addressed as transplanum approach (**Fig. 2.18**). The TS is drilled from medial to lateral toward medial opticocarotid recess (MOCR) to again access to suprasellar/supradiaphragmatic cisterns. According to

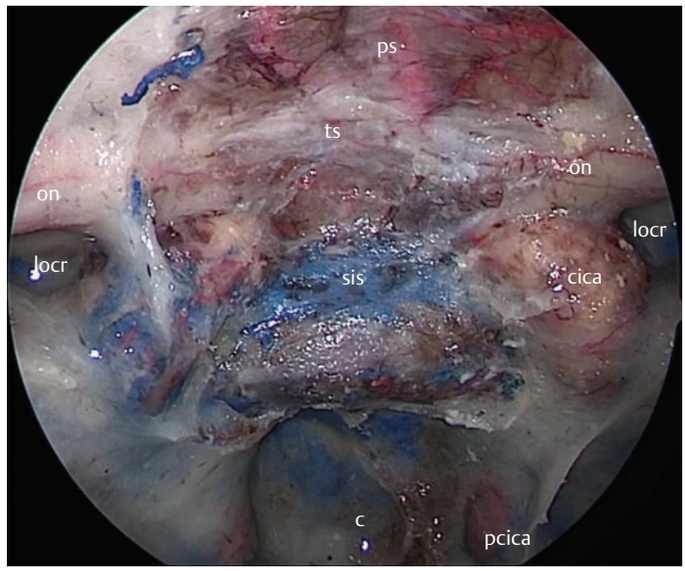

Fig. 2.18 Falciform ligament: fold of the dura seen demarking the tuberculum and planum approaches.

Fujii et al, the mean thickness of tuberculum is 1.0 mm (0.2–4.3 mm) and that of planum is 0.6 mm (0.2–1.4 mm).[37] The shortest distance between the paired arteries is usually located at the level of tuberculum sella.

At the paramedian vertical compartment, carotid protuberance are viewed and are subdivided into paraclival caudally and parasellar rostrally (**Fig. 2.20**).

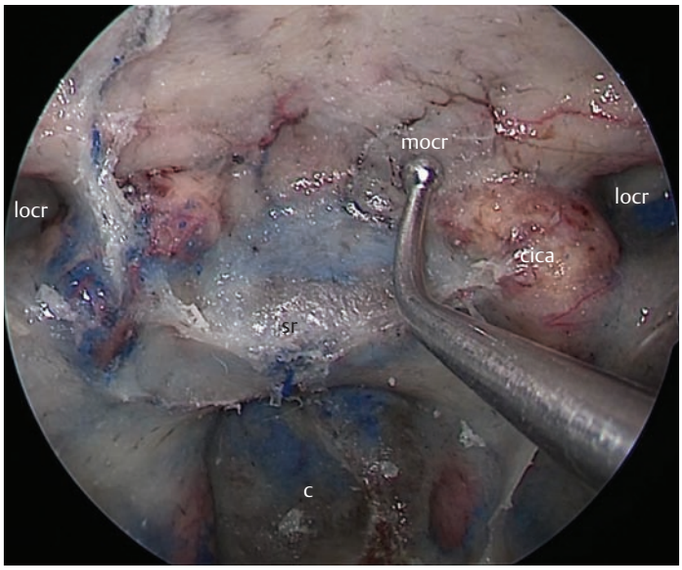

Fig. 2.19 Endoscopic view of the lateral-most boundary of transtuberculum approach: medial opticocarotid recess.

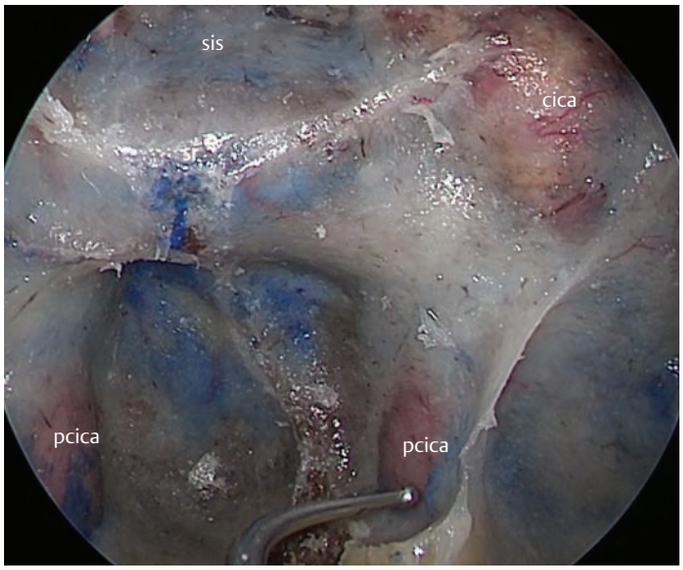

Fig. 2.20 The paramedian compartment showing paraclival carotid and parasellar carotid protuberances.

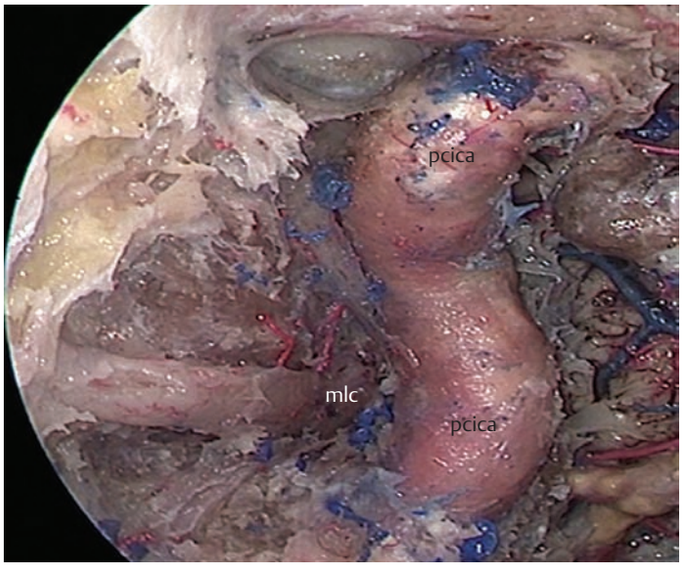

Fig. 2.21 Endoscopic image showing the course of paraclival internal carotid artery (foramen magnum) and parasellar internal carotid artery.

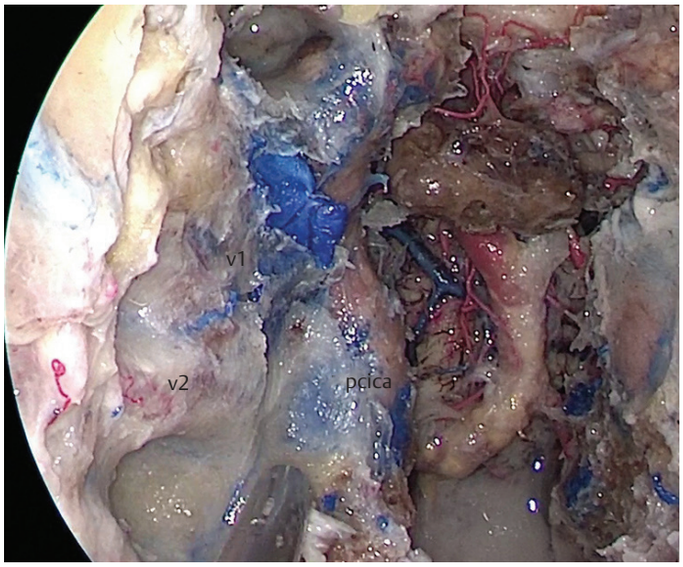

Fig. 2.22 Endoscopic image showing the removal of lingual process of the sphenoid below V2.

The Paraclival Internal Carotid Artery

The paraclival segment extends from the posterolateral part of the foramen lacerum up to the inferior of the sellar floor, which coincides with the superior limit of the medial petrous apex (**Fig. 2.21**). The paraclival carotid artery is divided into two segments: extracavernous and intracavernous by an imaginary line at the superior level of lingular recess (**Fig. 2.22**).

The Parasellar Internal Carotid Artery

The parasellar is the only segment located inside the cavernous sinus and extends from the medial petrous apex to the proximal dural ring. The parasellar part of ICA is widely separated from the carotid sulcus and is without dural constraints like medial petrous apex, clivus, and lingular process for a paraclival and optic strut, anterior clinoid, and distal dural ring in case of the paraclinoidal

segment (**Fig. 2.19**). The space between the parasellar carotid and carotid sulcus is the space extending below and lateral to the sellar floor as well as a posterosuperior compartment of the cavernous sinus. The parasellar carotid artery is in close proximity to the neural component in the cavernous sinus.

Medial Opticocarotid Recess

The MOCR is a landmark in accessing the parasellar and suprasellar regions. It is identified at the confluence of sella, tuberculum, carotid protuberance, optic canal, and planum sphenoidale (**Fig. 2.16**). It is an osseous depression formed between the medial projection of optic nerve superiorly, medial portion of the paraclinoid ICA (as it travels intradurally) inferiorly, and medially superolateral surface of the sella.[38] The middle clinoid process is situated at the inferomedial edge of the carotid sulcus at lateral aspect of the sella. The middle clinoid process is a separate structure from MOCR (**Fig. 2.19**) removal of bone over MOCR allows early identification of the optic nerve and paraclinoid ICA.

Paraclinoidal Carotid

The paraclival segment is small but crucial from the anatomy point of view with multiple landmarks to guide resections intraoperatively. This segment extends from proximal to the distal dural ring of the ICA. The lateral tubercular recess is bony indentation at the lateral most part of the tuberculum sellae and is bounded laterally by the medial surface of the paraclival carotid artery. The osseous arch connecting the LOCR and LTR is called distal osseous arch and overlies the distal dural ring.

The lateral vertical compartment of the posterior wall of the sphenoid sinus is well-defined, with four bony protrusions and three bony depressions. From rostral to caudal, the four bony protuberances are the optic canal, the cavernous sinus apex, the trigeminal maxillary division (V2), and the trigeminal mandibular division (V3). The three bony depressions are the carotico-optic recess, the depression between the cavernous sinus apex and V2, and the depression between V2 and V3 (**Fig. 2.20**).

Optic Canal

The optic canal is bounded medially by the body of the sphenoid, the lower border by optic strut, and the upper border by the anterior root of the sphenoid bone. The anterior root joins medially limbus sphenoidale and laterally anterior clinoid process. It extends anteriorly into the orbital apex.

Lateral Opticocarotid Recess

The LOCR is an osseous depression at the lateral most edge of the tuberculum sellae.[36,38] It represents the pneumatization of the ventral surface of the optic strut. It is bounded superiorly by the floor of optic canal, inferior surface by superior orbital fissure, and the medial surface by the bone overlying the lateral portion of the carotid prominence. The bone overlying the carotid is thinned or dehiscent in most of the cases. The junction of superior and medial surface is seen exocranial and is called infraoptic arch.

Optic Strut

The optic strut constitutes posterior root of lesser wing of the sphenoid bone.[36,38] It extends from the inferomedial aspect of the base of anterior clinoid process to the body of sphenoid. It is bounded inferiorly by the superior orbital fissure, superiorly by the optic nerve and posteriorly by the carotid sulcus.

The superior surface slopes downward and forward from its intracranial edge to form the floor of the optic canal. The inferior surface is part of the roof of the superior orbital fissure. The posterior surface of the optic strut faces downward and widens as it slopes medially to blend with the carotid sulcus of the sphenoid body. The junction between the superior and posterior surfaces of the optic strut forms a slightly concave edge at the superior most level of the floor of the optic canal.

Pituitary Gland

The pituitary gland or hypophysis cerebri, a reddish gray ovoid body, that lies in the pituitary fossa of the sphenoid bone covered superiorly by the diaphragma sellae.[39,40,41] The pituitary gland is surrounded by the critical neurovascular structures, such as superiorly by optic nerve, optic chiasm, and anterior circulation; the cavernous sinus, ICA, cranial nerves laterally; brainstem, and posterior circulation posteriorly (**Fig. 2.23**). The pituitary gland is divided into an anterior (adenohypophysis), a posterior (neurohypophysis), and an intermediate lobe. The adenohypophysis is composed of encompassing the anterior lobe, pars intermedia, and pars tuberalis. The pars tuberalis is a part of anterior gland that forms the collar around the stalk.

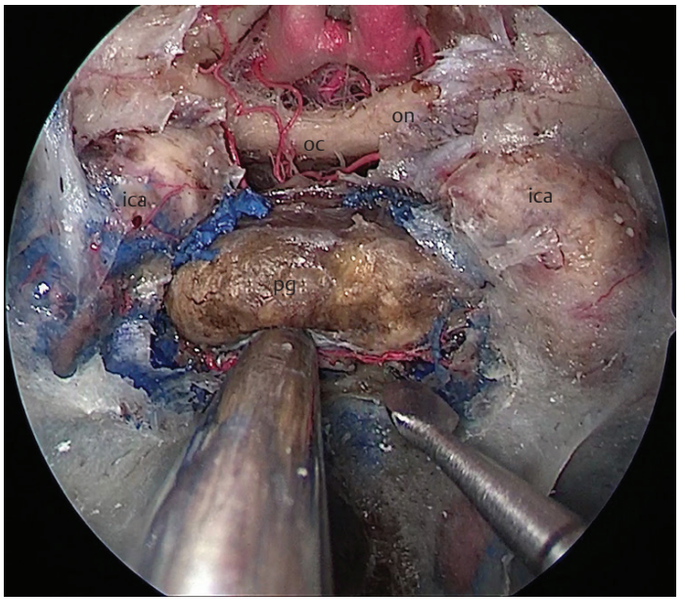

Fig. 2.23 Endoscopic image showing the relationships of pituitary gland.

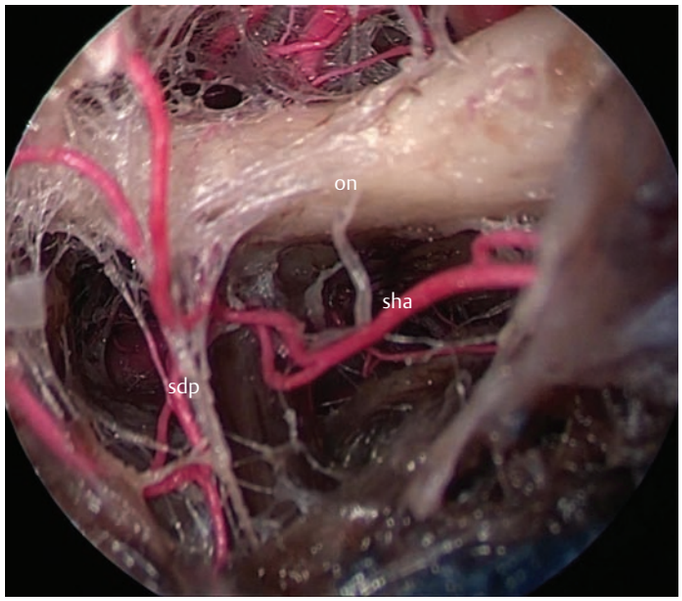

Fig. 2.24 Note the superior hypophyseal artery to the stalk of the pituitary gland. on, optic nerve; sha, superior hypophyseal artery.

The pars intermedia, a narrow zone between the anterior and posterior lobe rudimentary in humans, often contains a microscopic remnant of Rathke's cleft. The posterior lobe, infundibular stalk, and median eminence form neurohypophysis. The hypophysis is connected to the brain via the infundibulum, a tubular structure arising from the tuber cinereum and median eminence of the hypothalamus. The stalk divides as pars tuberalis and posterior pars infundibularis. The anterior lobe is firmer but easily separated from the anterior and lateral sellar walls. The posterior lobe is soft and gelatinous, more firmly adherent to the gland, and difficult to remove. Autonomic nerves supplying the anterior gland and posterior gland are exclusively composed of hypothalamic nerve fibers. The adenohypophysis and hypothalamus share a complex portal blood supply, carrying trophic and inhibitory hormones from hypothalamus, regulating the release of anterior hormones.

The anterior gland receives its blood supply from the superior hypophyseal arteries which arise from the medial aspect of the supraclinoidal segment of the carotid artery approximately 5-mm distal to the ophthalmic artery (**Fig. 2.24**). Each superior hypophyseal artery typically gives off three branches: one to the optic nerve (recurrent branch), one to the undersurface of the optic chiasm and upper infundibulum (anastomotic branch), and one to the lower infundibulum and diaphragm (descending branch). The branch to the upper infundibulum anastomoses with the branch from the contralateral superior hypophyseal artery to form a capillary network. A portal venous system drains the capillary plexus of the superior hypophyseal arteries, which delivers blood to the anterior gland. This allows the delivery of hypothalamic prohormones to the adenohypophysis. The posterior gland has been thought to receive most of its blood supply from the inferior hypophyseal arteries. The inferior hypophyseal artery is a branch of the meningohypophyseal trunk, which is the first branch of the internal carotid within the cavernous sinus (**Fig. 2.25**). Recent evidence, however, has shown that sacrifice of both inferior hypophyseal arteries does not cause posterior pituitary dysfunction (i.e., diabetes insipidus), suggesting alternative vascular supply by the superior hypophyseal arterial system.[8] Venous drainage from the anterior and posterior gland comes together and drains into the cavernous sinus.

Most of the pituitary gland is covered by two layers of dura: an outer periosteal layer and inner meningeal layer. These two layers separate laterally to form parts of the cavernous sinus. Anteriorly, the outer periosteal layer continues laterally to form the anterior sphenoid wall of the cavernous sinus, and the inner meningeal layer stays attached to the gland and turns posteriorly toward the dorsum sella to form the medial wall of the cavernous sinus. This medial wall also serves as the lateral wall of the sella. It is commonly compressed and occasionally even invaded by the pituitary tumors. Also, the presence of two dural layers in

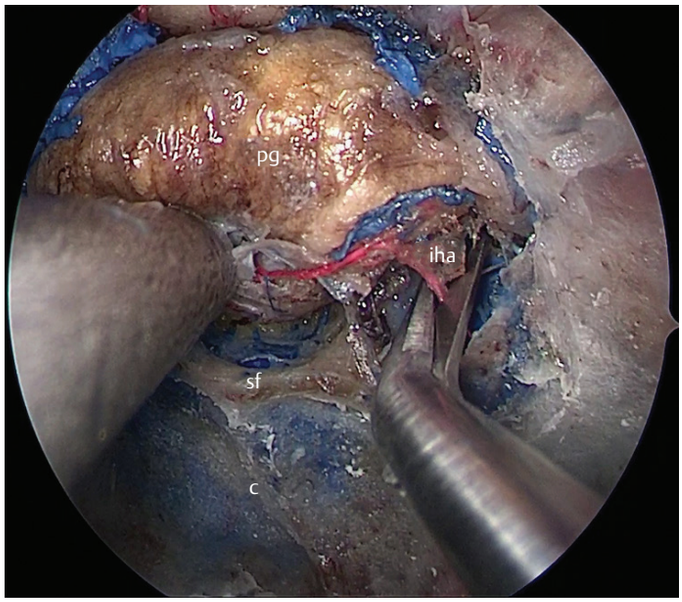

Fig. 2.25 Endoscopic image showing the ligation of inferior hypophyseal artery.

the sellar region is the basis for the presence of intercavernous venous connections, which can exist anywhere along the anterior, posterior, or inferior aspects of the gland.

Diaphragma Sella

The diaphragma sella is a dural sheath composed of two leaves of dura that form the roof of the pituitary gland. It is rectangular in shape, and it is usually convex in 54% of the patients, flat in 42%, and concave in 4%. It is usually complete except centrally where the pituitary stalk descends from the third ventricle. The diaphragma sella is thinner around the infundibulum and thicker around the periphery. The opening in the diaphragm is usually larger than the size of the pituitary stalk, and there is remarkable variability in the size and morphology of the opening. In one study, the diaphragm opening was greater than 5 mm in 56% of the cases, round in 54% of the cases, and elliptical in 46% of the patients. The size and morphology of the diaphragm opening determine the dumbbell growth pattern of a pituitary adenoma. A large central or peripheral deficiency of the diaphragma is also thought to predispose the patient to an empty sella, where the arachnoid crosses into the sella and if opened may result in a cerebrospinal fluid leak after pituitary surgery.

Suprasellar Anatomy

The suprasellar space extends from the diaphragma inferiorly to the floor of the third ventricle superiorly. Access to the suprasellar space is obtained by removing the tuberculum sella, prechiasmatic sulcus, and posterior planum sphenoidale. The suprasellar space is divided into the infrachiasmatic, suprachiasmatic, and retrochiasmatic areas[39,40,41,42,43] (**Figs. 2.17 and 2.26a,b**).

Within the infrachiasmatic space is found the inferior surface of the optic chiasm and the infundibulum in the midline. The infundibulum is covered by the suprasellar cistern arachnoid anteriorly and by the membrane of Liliequist posteriorly. The optic nerves course anterolaterally from the chiasm to enter the optic canal. The ophthalmic artery is the first branch of the supraclinoidal carotid above the distal dural ring. It arises from the ventral surface of the carotid to enter the optic canal where it travels inferior to the optic nerve. The superior hypophyseal artery arises just distal to the ophthalmic artery on the medial aspect of the supraclinoidal carotid. The same arachnoid membrane that covers the infundibulum anteriorly also surrounds the superior hypophyseal artery branches. Tuberculum sellae meningiomas that extend into this area, displace the infundibulum and superior hypophyseal arteries, posteriorly.

After opening of the lamina terminalis the suprachiasmatic route can help visualize the infundibular area of the third ventricle, thalamus and with angled endoscopes interthalamic fissure can be seen.

The suprachiasmatic space extends above the optic chiasm. The posterior aspect of each olfactory tract is found here as they divide to become the olfactory striae just above each optic nerve. The A1 segment of the anterior cerebral artery runs from the carotid bifurcation to the midline just above the optic chiasm. It anastomoses to its counterpart here via the anterior communicating artery. From here, the A2 segments arise and enter the interhemispheric fissure. There are two important arterial branches in the suprachiasmatic space. One is the recurrent artery of Heubner, which travels from the midline to the anterior perforated substance. The other is the fronto-orbital artery, which is the first cortical branch of the A2 segment and is often involved with tumors in this area. Planum meningiomas typically occupy this anatomical region and displace the optic chiasm and associated vascular structures posteriorly and/or inferiorly.

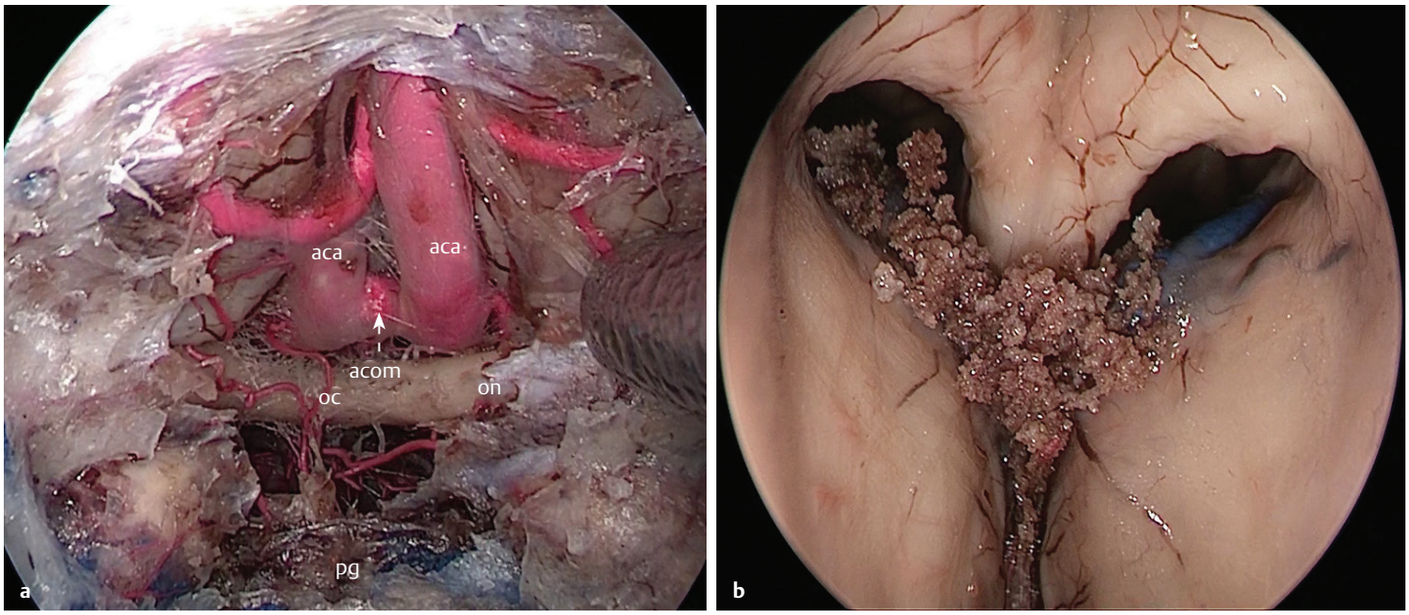

Fig. 2.26 **(a)** Endoscopic anatomy of the suprasellar region. **(b)** Endoscopic image showing endoscopic approach to floor of third ventricle.

The retrochiasmatic or retro-infundibular space extends from the infundibulum anteroinferiorly to the posterior perforated substance and cerebral peduncles posteriorly. It is bounded by the floor of the third ventricle superiorly. The Liliequist membrane provides access to the interpeduncular cistern where the basilar apex is visible posteriorly. The posterior communicating arteries run in the lateral recess of the interpeduncular cistern along with the oculomotor nerves, which is seen traveling between the superior cerebellar artery and posterior cerebral artery. Craniopharyngiomas often occupy this anatomical space.

The infrachiasmatic route is the door to the floor of the third ventricle through tuber cinereum between the pituitary stalk and the mammillary bodies. The transection of the stalk and pituitary transposition aids visualization of outer surface of floor of the third ventricle. The body of the fornix can be visualized midline and continues upwards and laterally. The inferolateral surface of the foramen of Monro is formed by ipsilateral thalamus. The choroid plexus is seen within the foramen of Monro and communicates with lateral ventricle through choroidal fissure and anterior commissure is visualized anteriorly (**Fig 2.26b**). The posterior portion of ventricle can be accessed by passing under the interthalamic commissure in an attempt to visualize pineal gland, suprapineal recess, posterior commissure, habenular commissure, habenular trigona, and cerebral aqueduct.

Optic Chiasm

The normal chiasm overlies the diaphragma sellae and the pituitary gland, the prefixed chiasm overlies the tuberculum, and the postfixed chiasm overlies the dorsum. In approximately 70% of our cases, the chiasm is in the normal position; of the remaining 30%, approximately half are 30%, a half "postfixed".

Parasellar Anatomy

Parasellar region is a part of middle cranial base situated between sella and temporal fossa. It is considered the critical and smallest part of the skull base with highest concentration of the neurovascular structures as it houses the cavernous sinuses. The bony structures contributing to form parasellar area are the petrous apex of the temporal bone and the sphenoid bone. The sphenoid bone, the major bone structure responsible for supporting the cavernous sinuses, presents to the parasellar area the anterior clinoid process and the lateral part of the sphenoid body, along which the greater sphenoid wing attaches.[44,45,46,47,48]

The cavernous sinus is venous confluence encased by dural layers. The cavernous sinuses are bounded by the petrous apex and dorsum sellae posteriorly and by the superior orbital fissure anteriorly. The paired cavernous

sinuses have dural walls enclosing venous spaces through which a segment of ICA and cranial nerves courses.

Each cavernous sinus has four walls. The roof faces the basal cisterns. The posterior wall faces the upper part of the posterior fossa. The medial wall, which separates the cavernous sinus from the contents of sella and sphenoid sinus, is formed by a thin dural layer, and this anatomical fact enables sellar tumors to extend toward the cavernous sinus. The lateral wall faces the medial temporal lobe.[1]

After opening the floor of the sella turcica, the dura mater covering the pituitary gland is identified. At this level, there are two distinct layers of dura. One layer adjacent to the bone, periosteal dura, covering the floor of the sella turcica, extends laterally beyond the sella, lines the carotid sulcus where it forms part of the medial wall of CS and then continues as the floor of CS. The dural layer adjacent to the pituitary gland itself separates the gland from the medial compartment of the CS. Superiorly, this layer reflects to form the two layers of the diaphragma sella. This reflection creates the central opening of the diaphragma sella through which the infundibulum passes. This layer continues laterally as the outer dural layer (dura propria) of the roof and lateral wall of the CS. Thus, the medial wall of the CS is formed by the dural layer of the pituitary gland without bony support. In its lower aspect, the medial wall of the CS is formed by the periosteal dura of the sella turcica and is supported by the bone of the lateral wall of the sphenoid sinus.

It is common that venous channels occupy the space between the two layers of dura in the sella turcica. These venous channels communicate between the two cavernous sinuses. Typically, these venous channels form both an anterior and a posterior intercavernous sinus, which, in combination with the two cavernous sinuses is referred as the circular sinus.

The endoscopic endonasal approach has opened new routes to the ventral skull base, including the CS. The wider view provided by the endoscope enables the surgeon to inspect the medial wall and the inside of the CS directly using a medial-to-lateral trajectory. The author describes the different compartments of the CS in relation to the intracavernous carotid artery based on the classification proposed by Fernandaz et al[48] (**Fig. 2.27**). It is the modification of classification proposed by Harris and Rhoton in 1976.[46]

Superior Compartment of Cavernous Sinus

The superior compartment of the CS lies superior to the horizontal cavernous ICA and posterior to the anterior genu. It is limited by the roof of the CS superiorly and

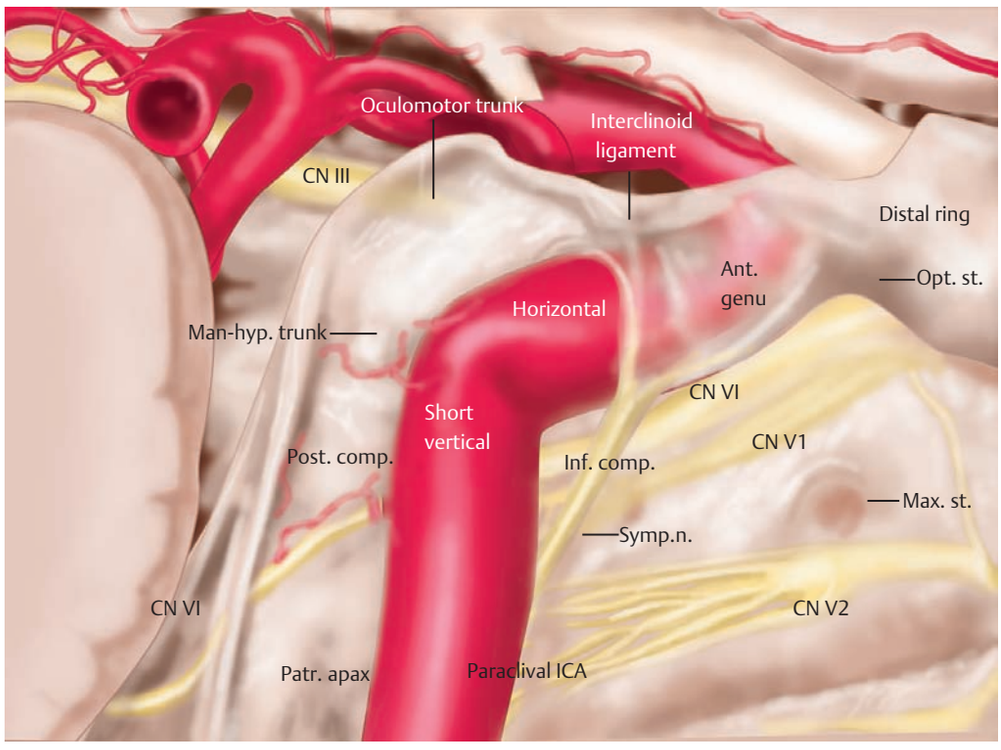

Fig. 2.27 Endoscopic anatomy of the cavernous sinus and its compartments.

laterally: the ventral surface of the paraclinoidal ICA anterolaterally (which corresponds to the clinoidal triangle), and the dura of the oculomotor triangle posterolaterally.

The oculomotor nerve runs in the lateral wall which correlates with the oculomotor triangle. This oculomotor nerve segment travels between two layers of dura in the oculomotor triangle and is thus defined as the interdural segment, but it is also defined as the oculomotor cistern. As the nerve travels anteriorly, it is incorporated into the most superior aspect of the lateral wall of the CS. The entry point of the oculomotor nerve into the lateral wall of the CS is just lateral to the anterior genu of the ICA. The interclinoid ligament is a key landmark to be identified within the roof of the superior compartment of the CS. The paraclinoidal ICA runs medial and anterior to the interclinoid ligament, and the oculomotor nerve runs just lateral and posterior.

Posterior Compartment of Cavernous Sinus

The posterior compartment of the CS is located posterior to the short vertical cavernous ICA and anterior to the lateral petroclival dura, forming the posterior wall of the CS. The transition between the short vertical and horizontal subsegments of the cavernous ICA (posterior cavernous ICA genu) marks the transition between the superior and posterior compartments.

The meningohypophyseal trunk arises from the posterior wall of the posterior genu of the ICA at this transitional level. The inferior hypophyseal artery has a lateromedial trajectory toward the dura of the sellar floor, while the dorsal meningeal artery has a posterior and inferomedial trajectory toward the dura of the dorsum sella. These two arteries, along with the tentorial artery, may arise together from the meningohypophyseal trunk or as independent branches directly from the ICA. The gulfar segment of the abducens nerve is located at the most inferior portion of this compartment as it passes through Dorello's canal to enter the CS, just behind the ICA. This nerve segment is above the most medial aspect of the petrous apex and is bounded posteriorly by the petrosphenoid or Gruber's ligament.[7] It is critical to note that the abducens nerve sits at the confluence (or gulf) of the inferior and superior petrosal sinuses with the basilar plexus as they enter the CS. Once it enters the CS, the nerve does not have any dural layer protecting it.

Lateral Compartment of Cavernous Sinus

The lateral compartment of the CS lies lateral to the anterior genu and horizontal ICA subsegments. The upper limit of this compartment is formed by the proximal dural ring that covers the inferior surface of the optic strut. The maxillary strut separates the superior orbital fissure from the foramen rotundum and marks the inferior limit of the lateral compartment along with the V2 prominence. At the anterior limit of the optic and maxillary struts, the CNs have entered the superior orbital fissure and exited the CS (**Fig. 2.28**).

This compartment contains the third and fourth CNs, and the first division of the trigeminal nerve, which are located at the lateral wall of the CS. As mentioned above, the distal cavernous segment of the abducens nerve is located at the transition between inferior and lateral compartments. The arterial branches of the inferolateral trunk (arising from the inferior surface of the horizontal cavernous ICA) can be identified in this region running from medial to lateral where they distribute along the lateral wall of the CS.

Inferior Compartment of Cavernous Sinus

The inferior compartment of the CS is located inferior to the horizontal and anterior genu subsegments of the ICA

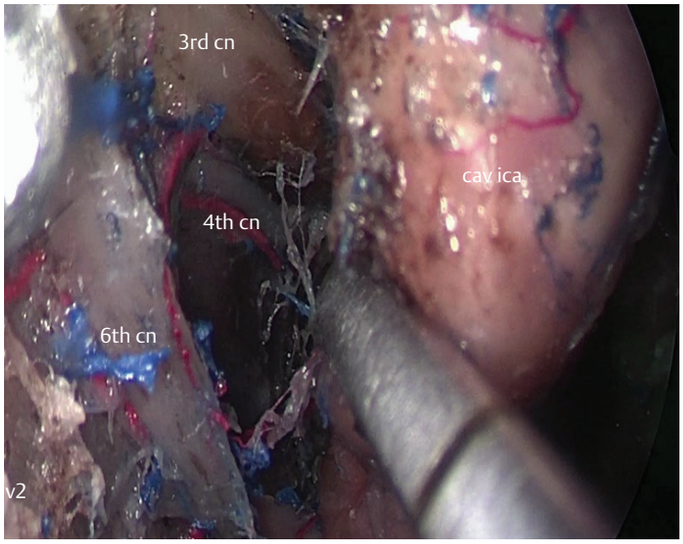

Fig. 2.28 Endoscopic image showing the final exposure for the transpterygoid approach to cavernous sinus.

and anterior to the short vertical subsegment. The anterior wall of this compartment is the anterior wall of the CS. It continues laterally with the lateral compartment.

The sympathetic nerve or plexus is in this compartment around the ICA as it travels from the short vertical ICA to the horizontal ICA. The distal cavernous segment of the abducens nerve is just inferior and lateral to the horizontal ICA subsegment, at the transition between the inferior and lateral compartments. The sympathetic nerve is located medially in relation to the abducens nerve and has an oblique trajectory, running from the surface of the ICA to join the abducens nerve, which has a more horizontal trajectory at this segment.

Conclusion

Endonasal endoscopic approaches provide improved visualization and access to the different areas of ventral skull base along its irregular bony topography, which, in turn, facilitates better tumor clearance. Accurate orientation to endoscopic anatomy, thorough knowledge of anatomical variations, surgical expertise, and appropriate instrumentation are the primal prerequisites for dealing with the skull base pathologies via these approaches. Mastering sophisticated endoscopic skull base techniques translates into superior surgical outcome. This can be best achieved by continued endoscopic cadaveric skull base dissections, at least in the training phase. Anatomical dissections enable the dissector to familiarize with endoscopic anatomical topography, two dimensional views, and acquire appropriate practical skills. These orient the trainees/dissectors to identify important anatomical landmarks and avoid critical neurovascular structures.

References

1. Kassam A, Snyderman CH, Mintz A, Gardner P, Carrau RL. Expanded endonasal approach: the rostrocaudal axis. Part I. Crista galli to the sella turcica. Neurosurg Focus 2005;19(1):E3
2. Kassam A, Snyderman CH, Mintz A, Gardner P, Carrau RL. Expanded endonasal approach: the rostrocaudal axis. Part II. Posterior clinoids to the foramen magnum. Neurosurg Focus 2005;19(1):E4
3. Koutourousiou M, Fernandez-Miranda JC, Stefko ST, Wang EW, Snyderman CH, Gardner PA. Endoscopic endonasal surgery for suprasellar meningiomas: experience with 75 patients. J Neurosurg 2014;120(6):1326–1339
4. Romano A, Zuccarello M, van Loveren HR, Keller JT. Expanding the boundaries of the transsphenoidal approach: a microanatomic study. Clin Anat 2001;14(1):1–9
5. Cappabianca P, Cavallo LM, Esposito F, De Divitiis O, Messina A, De Divitiis E. Extended endoscopic endonasal approach to the midline skull base: the evolving role of transsphenoidal surgery. Adv Tech Stand Neurosurg 2008;33:151–199
6. Kuta AJ, Laine FJ. Imaging the sphenoid bone and basiocciput: anatomic considerations. Semin Ultrasound CT MR 1993;14(3): 146–159
7. Szolar D, Preidler K, Ranner G, et al. The sphenoid sinus during childhood: establishment of normal developmental standards by MRI. Surg Radiol Anat 1994;16(2):193–198
8. Scuderi AJ, Harnsberger HR, Boyer RS. Pneumatization of the paranasal sinuses: normal features of importance to the accurate interpretation of CT scans and MR images. AJR Am J Roentgenol 1993;160(5):1101–1104
9. Aoki S, Dillon WP, Barkovich AJ, Norman D. Marrow conversion before pneumatization of the sphenoid sinus: assessment with MR imaging. Radiology 1989;172(2):373–375
10. Van Alyea OE. Sphenoid sinus. Arch Otolaryngol 1941;34: 225–253
11. Som PM, Naidich TP. Development of the skull base and calvarium: an overview of the progression from mesenchyme to chondrification to ossification. Neurographics 2013;3(4): 169–184
12. Anderson JE. Grant's Atlas of Anatomy. Baltimore, MD: Williams & Wilkins; 1978
13. Kayalioglu G, Govsa F, Erturk M, Pinar Y, Ozer MA, Ozgur T. The cavernous sinus: topographic morphometry of its contents. Surg Radiol Anat 1999;21(4):255–260
14. Lanza DC, Kennedy DW. Endoscopic sinus surgery. In: Bailey BJ, ed. Head and Neck Surgery—Otolaryngology. Philadelphia, PA: J.B. Lippincott; 1993:389–398
15. Sinnatamby C. Last's Anatomy: Regional and Applied. 11th ed. Edinburgh: Churchill Livingstone; 2006
16. Sareen D, Agarwal AK, Kaul JM, et al. Study of sphenoid sinus anatomy in relation to endoscopic surgery. Int J Morphol 2005;23(3):261–266
17. Ramalho CO, Marenco HA, de Assis Vaz Guimarães Filho F, et al. Intrasphenoid septations inserted into the internal carotid arteries: a frequent and risky relationship in transsphenoidal surgeries. Rev Bras Otorrinolaringol (Engl Ed) 2017;83(2): 162–167
18. Fernandez-Miranda JC, Prevedello DM, Madhok R, et al. Sphenoid septations and their relationship with internal carotid arteries: anatomical and radiological study. Laryngoscope 2009;119(10):1893–1896
19. Renn WH, Rhoton AL Jr. Microsurgical anatomy of the sellar region. J Neurosurg 1975;43(3):288–298

20. Sethi DS, Stanley RE, Pillay PK. Endoscopic anatomy of the sphenoid sinus and sella turcica. J Laryngol Otol 1995;109(10): 951–955
21. Hamid O, El Fiky L, Hassan O, Kotb A, El Fiky S. Anatomic variations of the sphenoid sinus and their impact on transsphenoid pituitary surgery. Skull Base 2008;18(1):9–15
22. Hamberger CA, Hammer G, Norlen G, Sjogren B. Transantrosphenoidal hypophysectomy. Arch Otolaryngol 1961;74:2–8
23. Hammer G, Radberg C. The sphenoidal sinus. An anatomical and roentgenologic study with reference to transsphenoid hypophysectomy. Acta Radiol 1961;56:401–422
24. Wang J, Bidari S, Inoue K, Yang H, Rhoton A Jr. Extensions of the sphenoid sinus: a new classification. Neurosurgery 2010;66(4):797–816
25. Sonbay D, Saka C, Akin I, Gunsoy B, Gokler A. Prevalence of sphenoid sinus agenesis in adults: a CT scan study. B-ENT 2010;6(3):167–169
26. Cakur B, Sümbüllü MA, Yılmaz AB. A retrospective analysis of sphenoid sinus hypoplasia and agenesis using dental volumetric CT in Turkish individuals. Diagn Interv Radiol 2011;17(3): 205–208
27. Keskin G, Ustündag E, Ciftçi E. Agenesis of sphenoid sinuses. Surg Radiol Anat 2002;24(5):324–326
28. Pifferi M, Bush A, Caramella D, et al. Agenesis of paranasal sinuses and nasal nitric oxide in primary ciliary dyskinesia. Eur Respir J 2011;37(3):566–571
29. Millar DA, Orlandi RR. The sphenoid sinus natural ostium is consistently medial to the superior turbinate. Am J Rhinol 2006; 20(2):180–181
30. Hidir Y, Battal B, Durmaz A, Karaman B, Tosun F. Optimum height from the roof of the choana for seeking the sphenoid ostium. J Craniofac Surg 2011;22(3):1077–1079
31. Perondi GE, Isolan GR, de Aguiar PH, Stefani MA, Falcetta EF. Endoscopic anatomy of sellar region. Pituitary 2013;16(2): 251–259
32. Yanagisawa E, Weaver EM, Ashikawa R. The Onodi (sphenoethmoid). Ear Nose Throat J 1998;77(8):578–580
33. Tomovic S, Esmaeili A, Chan NJ, et al. High-resolution computed tomography analysis of the prevalence of Onodi cells. Laryngoscope 2012;122(7):1470–1473
34. Kantarci M, Karasen RM, Alper F, Onbas O, Okur A, Karaman A. Remarkable anatomic variations in paranasal sinus region and their clinical importance. Eur J Radiol 2004;50(3):296–302
35. Thanaviratananich S, Chaisiwamongkol K, Kraitrakul S, Tangsawad W. The prevalence of an Onodi cell in adult Thai cadavers. Ear Nose Throat J 2003;82(3):200–204
36. Alferidi A, Jho HD. Endoscopic endonasal cavernous sinus surgery: an anatomic study. Neurosurgery 2001;48(4):827–836, discussion 836–837
37. Fujii K, Chambers SM, Rhoton AL Jr. Neurovascular relationships of the sphenoid sinus. A microsurgical study. J Neurosurg 1979;50(1):31–39
38. Labib MA, Prevedello DM, Fernandez-Miranda JC, et al. The medial opticocarotid recess: an anatomic study of an endoscopic "key landmark" for the ventral cranial base. Neurosurgery 2013; 72(1, Suppl Operative)66–76, discussion 76
39. Fernandez-Miranda JC, Gardner PA, Rastelli mm Jr, et al. Endoscopic endonasal transcavernous posterior clinoidectomy with interdural pituitary transposition. J Neurosurg 2014; 121(1):91–99
40. Fernandez-Miranda JC, Gardner PA, Snyderman CH, et al. Craniopharyngioma: a pathologic, clinical, and surgical review. Head Neck 2012;34(7):1036–1044
41. Rhoton AL Jr. The anterior and middle cranial base. Neurosurgery 2002; 51(4, Suppl):S273–S302
42. Everton KL, Rassner UA, Osborn AG, Harnsberger HR. The oculomotor cistern: anatomy and high-resolution imaging. AJNR Am J Neuroradiol 2008;29(7):1344–1348
43. Rhoton AL Jr. Anatomy of the pituitary gland and sellar region. In: Thapar K, Kovacs K, Scheithauer B, Lloyd RV, eds. Diagnosis and Management of Pituitary Tumors. Totowa, NJ: Humana Press, Inc; 2001:13–40
44. Martins C, Yasuda A, Campero A, Rhoton AL Jr. Microsurgical anatomy of the oculomotor cistern. Neurosurgery 2006; 58:ONS-220–ONS-227
45. Khan AA, Niranjan A, Kano H, Kondziolka D, Flickinger JC, Lunsford LD. Stereotactic radiosurgery for cavernous sinus or orbital hemangiomas. Neurosurgery 2009;65(5):914–918, discussion 918
46. Harris FS, Rhoton AL. Anatomy of the cavernous sinus. A microsurgical study. J Neurosurg 1976;45(2):169–180
47. Micko AS, Wöhrer A, Wolfsberger S, Knosp E. Invasion of the cavernous sinus space in pituitary adenomas: endoscopic verification and its correlation with an MRI-based classification. J Neurosurg 2015;122(4):803–811
48. Fernandez-Miranda JC, Zwagerman NT, Abhinav K, et al. Cavernous sinus compartments from the endoscopic endonasal approach: anatomical considerations and surgical relevance to adenoma surgery. J Neurosurg 2018;129(2):430–441

3 Radiological Protocols in Sellar, Suprasellar, and Parasellar Regions

R. Bavaharan Rajalingam, Narayanan Janakiram, Joseph Nadakkavukaran

Introduction

The skull base is a compact and complex space that has many important neurovascular structures. Varied pathologies develop in skull base. Computed tomography (CT) maintains a role in the evaluation of many entities; it delineates osseous erosion with great detail and characterizes calcified tumor matrices. Magnetic resonance imaging (MRI) is the mainstay in the neuroimaging assessment of most pathologies occurring at the skull base. With multiplanar sequences and higher soft-tissue resolution, MRI has proven superior in imaging the skull base. MRI can provide information on the presence of lipids, paramagnetic and diamagnetic elements, and tumor cellularity. In addition, currently available MRI techniques are able to generate high spatial resolution images that allow visualization of cranial nerves and their involvement by adjacent pathology. The information obtained from such examinations may aid in the distinction of these disease processes and in the accurate delineation of their extent prior to biopsy or treatment planning.[1]

Anatomy

The primary component of the sella turcica is the sphenoid bone with a component from the basiocciput. Anteriorly, it is bounded by a bony ridge, the tuberculum sella, and posteriorly by the dorsum sella and the posterior clinoid processes. The anterior clinoid processes of the lesser wing of the sphenoid are lateral to the tuberculum sella and project posteriorly. The roof of the sella is formed by a dural extension called the diaphragma sella. This lines the sella turcica, envelopes the pituitary gland, and forms the incomplete superior border. Laterally, there are the venous sinusoids of the cavernous sinuses, and middle clinoid processes are variably present.

The sella is a saddle-shaped concavity in the sphenoid body that is devoid of a bony covering laterally and superiorly. The pituitary gland is lodged in the sella, which is composed of the adenophysis and neurohypophysis. The pars distalis, pars intermedia, and pars tuberalis form the adenohypophysis. The neurohypophysis is made up of the pars nervosa, infundibular stalk, and the infundibula proper. The height (craniocaudal dimension) of the pituitary gland varies with age and gender (**Table 3.1**).

Sella turcica is bounded laterally by cavernous sinuses, which are large venous plexuses between inner and outer layers of dura mater. The cavernous sinuses are interconnected through channels crossing the midline along the anterior, inferior, and posterior pituitary surfaces. A reflection of the inner dural layer above the pituitary gland forms the diaphragma sellae, which has a variable-sized opening for the infundibulum.

The hypothalamus and pituitary gland are connected by important neurovascular connections. Axons of supraoptic and paraventricular nuclei of the hypothalamus traverse the infundibular stalk and extend into the neurohypophysis. The secretory granules carrying vasopressin and oxytocin appear as the “bright spot” of the posterior lobe of the pituitary gland on T1-weighted unenhanced MRI. Releasing and inhibiting factors produced in the neurons in the hypothalamus are transported to the adenohypophysis by the

Table 3.1 Normal craniocaudal dimensions in relation to age, gender, and varying physiological conditions

Category	Craniocaudal dimension (in mm)
Children	6
Male	8
Female	
Postmenopausal	8
Premenopausal	10
Lactating	12

tuberhypophyseal neural tract and the hypophyseal portal system. Ectopic posterior pituitary gland may be seen superior to the sella and can be seen at various levels in the pituitary hypothalamic axis (**Figs. 3.1–3.3**)

Bilateral cavernous sinuses extend from the petrous segment of the temporal bone to the orbit. The cavernous segment of the internal carotid arteries and their meningohypophyseal trunks travel through these paired duraperiosteal spaces. Cranial nerves III (oculomotor), IV (trochlear), V1 (ophthalmic division of the trigeminal nerve), and V2 (maxillary division of the trigeminal nerve) course along its lateral aspect and the most medial structures are the internal carotid artery and cranial nerve VI (abducens nerve). The mandibular division of the trigeminal nerve (V3) lies external to the cavernous sinus and exits through foramen ovale vertically oriented beneath Meckel's cave. Bilateral Meckel's caves are inferolateral to each of the cavernous sinuses.

Above the sellar region lies the suprasellar cistern. Several critical structures traverse this area, including the circle of Willis, optic nerves and optic chiasm, hypothalamus, pituitary infundibulum, and the infundibular and suprachiasmatic recesses of the third ventricle.

Imaging

CT is useful in the delineation of the osseous margins of the sella. It is helpful in evaluating the bony changes related to pathologic processes. CT may be the only option in patients who cannot have an MRI examination (e.g., those with pacemakers, incompatible hardware, and severe

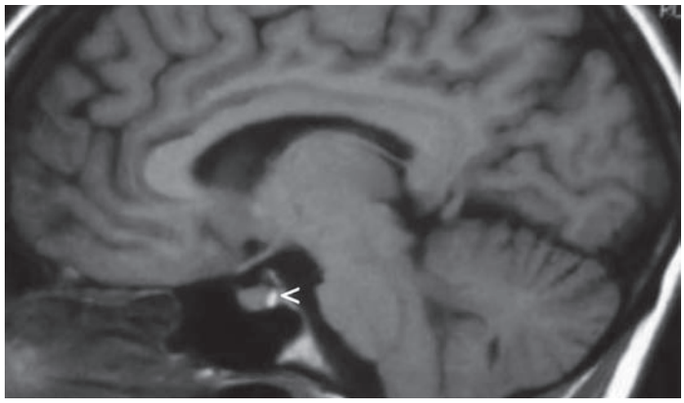

Fig. 3.1 Sagittal T1W MRI shows normal pituitary gland with normal posterior pituitary bright spot (*white arrow*).

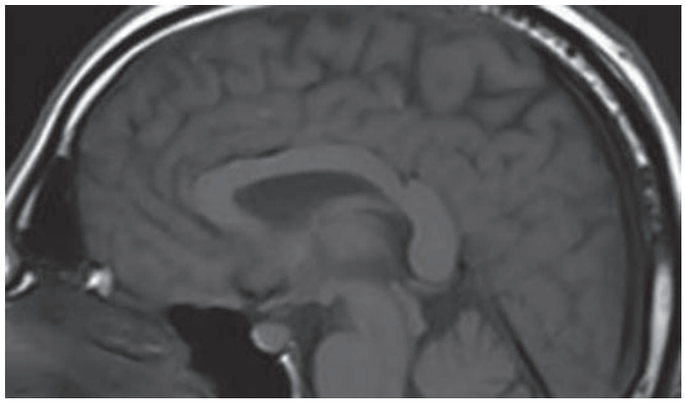

Fig. 3.2 Sagittal T1W MRI shows absent posterior bright spot.

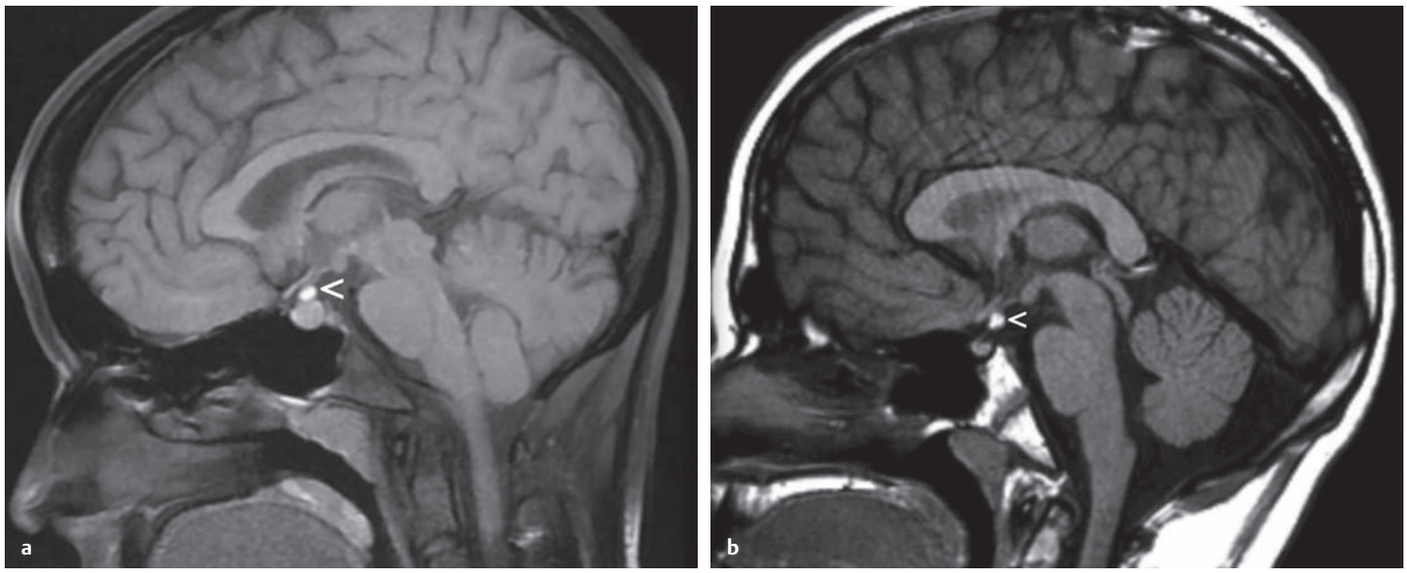

Fig. 3.3 **(a,b)** Sagittal T1W MRI shows ectopic suprasellar posterior pituitary gland (*white arrow*).

claustrophobia). Thin section of 0.625-mm axial spirally acquired images can be reformatted into sagittal and coronal images. The examination may be obtained without contrast for dedicated bony assessment. Contrast CT angiographic and venous phases can be obtained for evaluation of the carotids and cavernous sinus, respectively, in relation to the pathology, which is very useful in surgical management.

The following checklist is to be kept in mind while reading a CT scan (0.6–1 mm slices) (**Figs. 3.4–3.16**):

- Coronal cuts thin sections:
  - Concha bullosa (**Fig. 3.14**).
  - Septal deviation (**Figs. 3.4 and 3.14**).
  - Sinus diseases (**Fig. 3.5**).
  - Onodi cell.
  - Sphenoid sinus pneumatization (conchal, presellar, sellar) (**Figs. 3.6–3.8**).
  - Crista galli (**Fig. 3.13**).
  - Type of ethmoid roof (**Figs. 3.10–3.12**).
- Axial cuts:
  - Erosion of the dorsum sella by the tumor.
  - Extension of the tumor to the retro-genu area and the cavernous sinus (in contrast-enhanced CT).
- Sagittal cuts:
  - Planum tuberculum angle in cases of meningioma.

MRI provides detailed information about the contents of the sellar and parasellar regions. It is the fundamental preoperative and postoperative imaging modality.

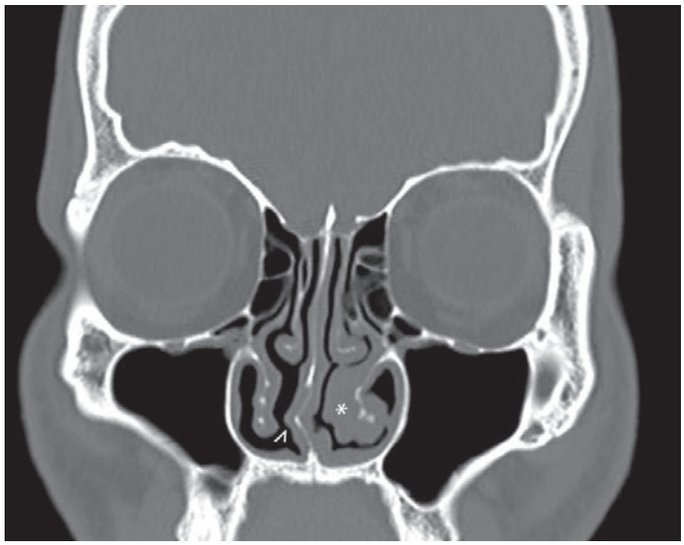

Fig. 3.4 Deviated nasal septum to the left- and right-sided inferior turbinate hypertrophy.

Fig. 3.5 Soft-tissue polypoidal mucosal thickening of the right maxillary sinus extending into the nasal cavity.

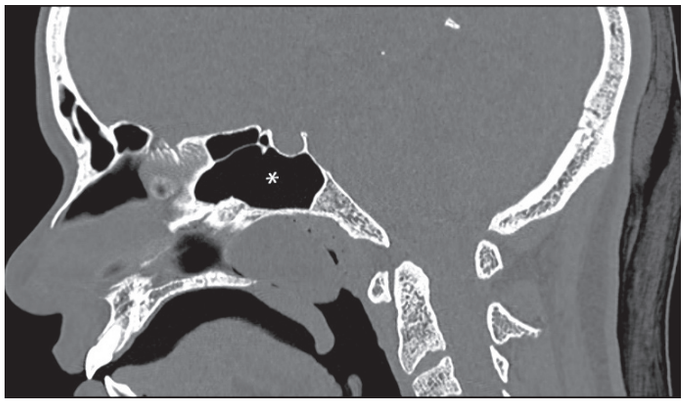

Fig. 3.6 Sellar type of sphenoid pneumatization.

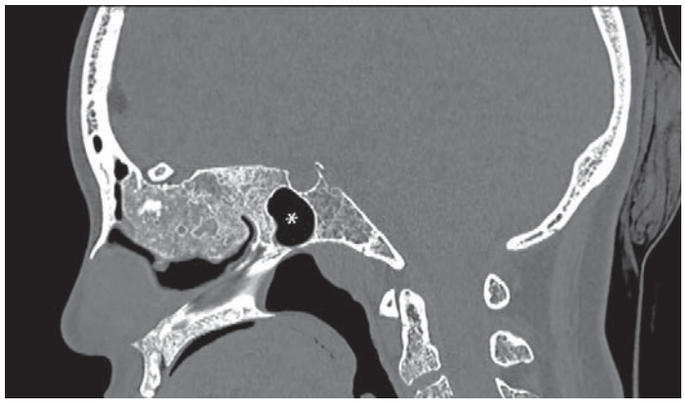

Fig. 3.7 Presellar type of sphenoid pneumatization.

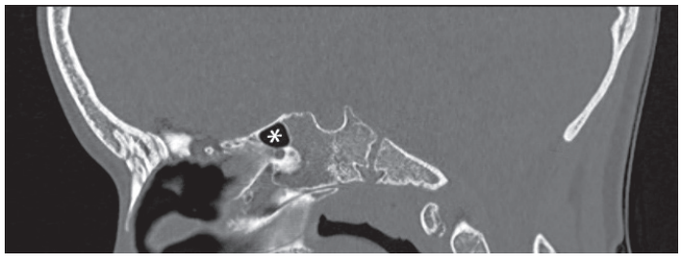

Fig. 3.8 Conchal type of sphenoid pneumatization.

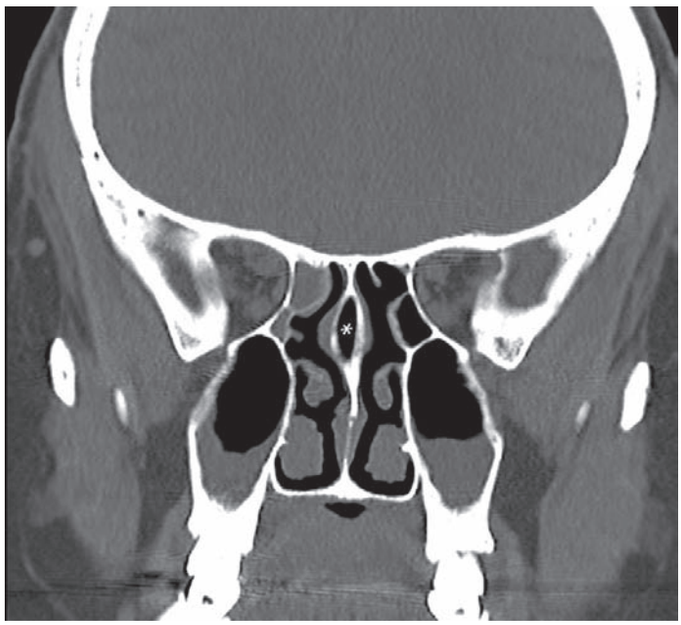

Fig. 3.9 Sphenoid rostral pneumatization.

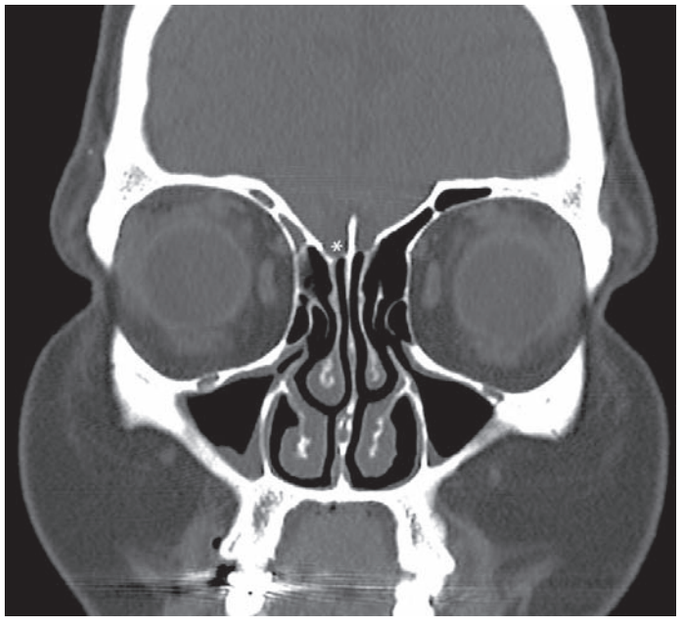

Fig. 3.10 Type 1 ethmoid roof according to Kero's classification.

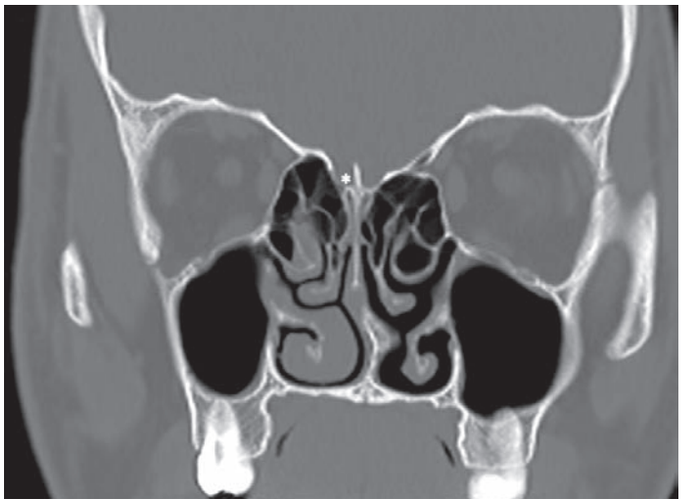

Fig. 3.11 Type 2 ethmoid roof according to Kero's classification.

Fig. 3.12 Type 3 ethmoid roof according to Kero's classification.

Sagittal and coronal images with a small field of view in thin sections (£3 mm) are obtained through the sella turcica to include the parasellar structures, including the suprasellar cistern, cavernous sinuses, Meckel's cave, and hypothalamus. Postgadolinium-enhanced sequences are obtained with fat saturation to improve contrast between pathology and the basicranium.

MRI Protocol

- Precontrast:
  - Sagittal T1 → 3-mm sections.
  - Axial T2 → 3-mm sections.
  - Coronal T1 → 3-mm sections.

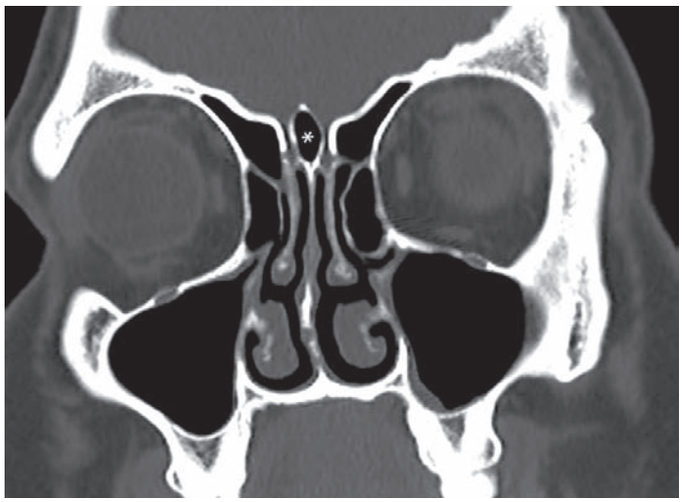

Fig. 3.13 Pneumatic crista galli.

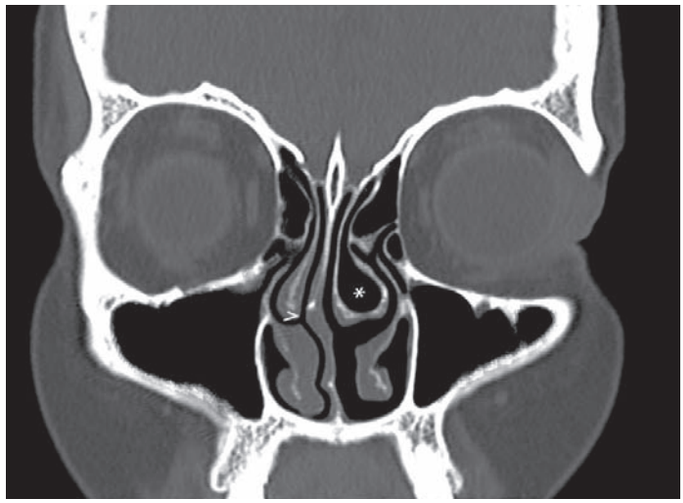

Fig. 3.14 Concha bullosa on right side with deviated nasal septum and inferior turbinate hypertrophy on the left side.

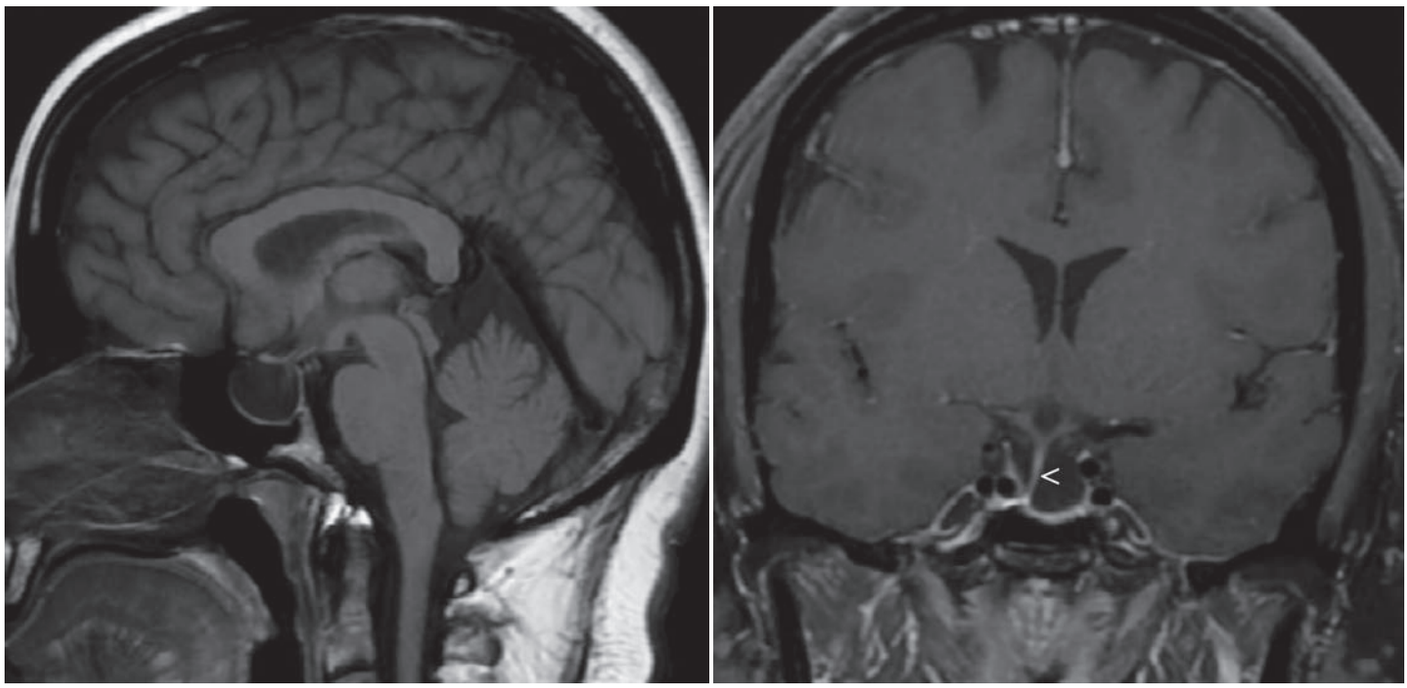

Fig. 3.15 Empty sella T1W sagittal and T1W postcontrast coronal images show CSF intensity in the sella with compressed pituitary gland and normal appearing stalk (*white arrow*).

- Coronal T2 → 3-mm sections.

- Postcontrast:
  - Dynamic coronal T1 → five slices taken every 10 seconds.
  - Coronal T1 → 3-mm sections.
  - Sagittal T1 → 3-mm sections.
  - Axial T13D fat saturation postcontrast → 3D volume data from the sinus level to vertex.

Dynamic Contrast MRI

It has been proven to be the best imaging tool in the evaluation of pituitary adenomas. A three-dimensional Fourier transformation gradient echo or fast turbo spin echo (TSE) sequence may be used for dynamic study. A dose of 0.05 mmol/kg of gadolinium is injected intravenously. After a bolus injection of intravenous gadolinium, six consecutive

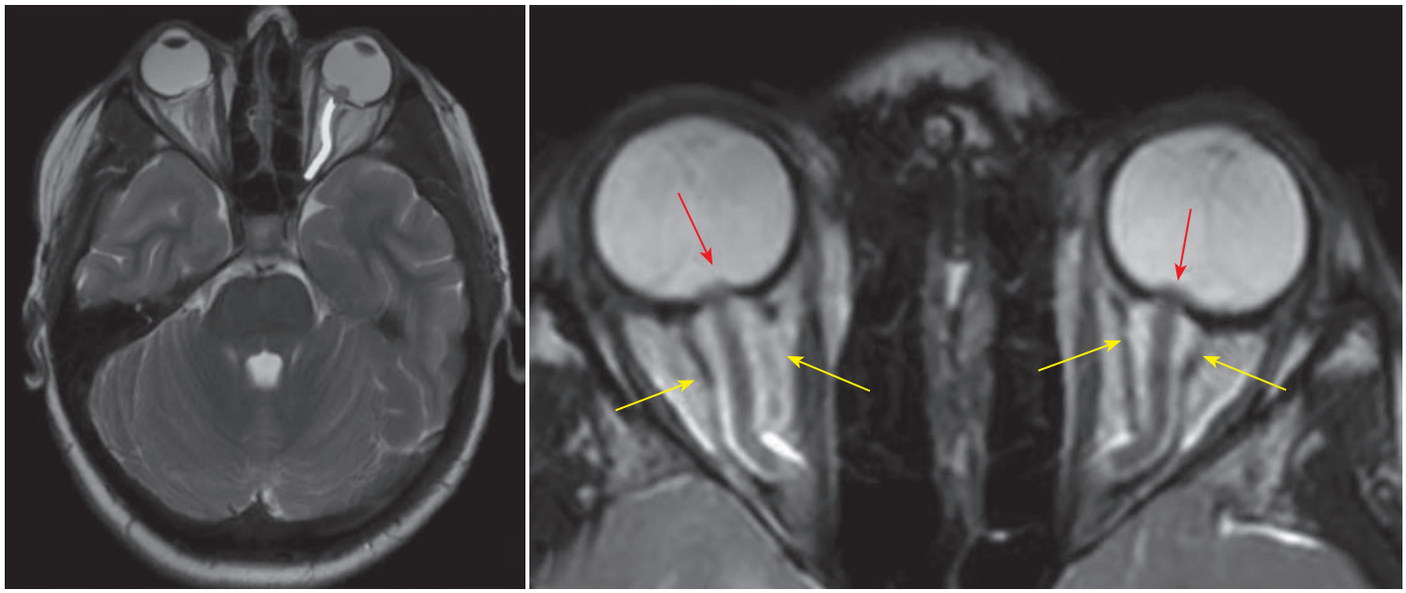

Fig. 3.16 Axial T2 images of brain and orbit show features suggestive of idiopathic intracranial hyperintension.

sets of five images are obtained in coronal plane every 10 seconds. The enhancement occurs first in the pituitary stalk and then in the pituitary tuft (the junction point of the stalk and gland), and finally there is centrifugal opacification of the entire anterior lobe. Within 30 to 60 seconds, the entire gland shows homogeneous enhancement. The maximum image contrast between the normal pituitary tissue and microadenomas is attained about 30 to 60 seconds after the bolus injection of the intravenous contrast. Most microadenomas appear as relatively nonenhancing (dark) lesions within an intensely enhancing pituitary gland.[2]

The peak enhancement of the pituitary adenomas occurs at 60 to 200 seconds, usually after the most marked enhancement of the normal pituitary gland, and persists for a longer duration.[3] Delayed scan (30–60 minutes after contrast injection) may demonstrate a reversal of the image contrast obtained at 30 to 60 seconds on dynamic scanning. This is because the contrast from the normal pituitary gland fades but diffuses into the microadenoma that stands out as a hyperintense focus.[4] Yuh et al[5] have documented early enhancement in the microadenomas, long before the anterior lobe, which is attributed to pituitary adenomas having a direct arterial blood supply similar to that of posterior pituitary lobe.[6] Addition of dynamic sagittal plane images to the routine coronal study increases the overall detection rate of pituitary microadenomas.[7] Dynamic contrast MRI is not only useful in evaluating the pituitary microadenomas but also has an equally important role in assessing the macroadenomas, invasion of cavernous sinus by the macroadenomas, and differentiating residual/recurrent tumor from postoperative tissues.[8–10]

Generating differential diagnoses can be difficult because of the complexity of the structures in the sellar and suprasellar region. Dividing this region into the pituitary fossa, cavernous sinuses, and the suprasellar cisterns can be helpful. However, many disease processes can involve multiple components of the sellar and parasellar region, and it can sometimes be difficult to delineate the origin of large neoplasms and extensive disease processes. Identification of normal structures, such as the pituitary gland, in relation to the pathology can be helpful in determining the etiology.

Systematic Approach to Sellar and Suprasellar Mass Lesions by MRI

- Identify the sella turcica, pituitary gland, and its stalk in T1 sagittal and T2 coronal sequences.
- Epicenter of the lesion (whether it is in the sella or suprasellar, below or lateral to the sella).
- If it is in the sella → Is sella enlarged? (Depth more than 12 mm and anteroposterior dimension more than 15 mm.)
- Once the location of the mass is clear, analyze the signal intensity patterns: is the lesion cystic, solid, fat, or hemorrhage? (**Table 3.2**)

Table 3.2 MRI characteristic appearance of contents of the tumor

Content		MRI characteristics		
		T1	T2	Other
1	Clear cyst (follows CSF signal intensity)	Hypointense	Hyperintense	Hypointense on FLAIR
2	Hemorrhage			
	Hyperacute (<12 h, oxyhemoglobin)	Isointense	Hyperintense	Hyperintense on FLAIR Gradient blooming
	Acute (deoxyhemoglobin) (12 h–2 d)	Isointense	Hypointense	Hypointense on FLAIR Gradient blooming
	Subacute (methemoglobin)			
	Early (2–7 d)	Hyperintense	Hypointense	Hypointense on FLAIR Gradient blooming
	Late (7 d–1 mo)	Hyperintense	Hyperintense	Hyperintense on FLAIR Gradient blooming
	Chronic (hemosiderin, ferritin) (>1 mo)	Hypointense	Hypointense	Hypointense on FLAIR Gradient blooming
3	Proteinaceous content			
	<10%	Hypointense	Hyperintense	Hyperintense on FLAIR
	20–25%	Hyperintense	Hyperintense	Hyperintense on FLAIR
	>25%	Hyperintense	Hypointense	Hypointense on FLAIR
4	Fat	Hyperintense	Hyperintense	Hyperintense on FLAIR and suppressed on fat-saturation images
5	Solid	Hypointense	Hyperintense to isointense (depending on cellularity and histology)	Hyperintense on FLAIR

Abbreviations: CSF, cerebrospinal fluid; FLAIR, Fluid-attenuated inversion recovery; MRI, magnetic resonance imaging.

- Does it contain any abnormal vessels? If need be, do MRI angiogram or CT angiogram.
- Differential diagnosis (**Table 3.3**).

The following lesions show diffusion restriction on MRI:

- Acute infarct/hemorrhage.
- Epidermoid.
- Lymphoma.
- Choroid plexus lesion.
- Medulloblastoma.
- Primitive ectodermal tumors.
- Abscess.
- Acute demyelination disorders.
- High-grade gliomas.
- Carbon monoxide poisoning.

Empty Sella

The "empty sella" appearance is due to the patulous diaphragma sella and the extension of the suprasellar subarachnoid space. The superior margin of the pituitary is flattened or concave, the sella turcica is often enlarged, and occasionally there may be intrasellar herniation of the anteroinferior portion of the third ventricle or optic nerves/chiasm. There is usually no functional impairment of the pituitary gland. However, a partially empty sella appearance can be seen in a premenopausal female with additional signs and symptoms of pseudotumor cerebri.[11] Pituitary microadenomas have also been reported to coexist with an empty sella[12] (**Figs. 3.15 and 3.16**).

Rathke's Cleft Cysts

Rathke's cleft cysts are congenital cystic lesions in the sellar region (25%), suprasellar region (5%), or both (70%), which are lined by cuboidal or columnar cells. The MR signal intensity and CT attenuation of these lesions are variable due to the amount of proteinaceous material within them. Occasionally, they can show peripheral enhancement on contrast study (**Fig. 3.17**).

Pituitary Hyperplasia

Pituitary gland is hyperplastic when its size is more than the normal craniocaudal dimensions (**Table 3.1**) with normal constituency and homogeneous contrast enhancement.

Table 3.3 Various pathologies involving different anatomical sites

Area	Possible pathologies
Pituitary gland	Pituitary adenoma Rathke's cleft cyst Craniopharyngioma
Pituitary stalk	Rathke's cleft cyst Craniopharyngioma Germinoma Eosinophilic granuloma Metastases
Optic chiasm	Glioma Demyelination
Hypothalamus	Glioma Hamartoma Germinoma Eosinophilic granuloma
Carotid artery	Aneurysm Ectasia
Cavernous sinus	Schwannoma Caroticocavernous fistula
Meninges	Meningioma Inflammation
Sphenoid sinus/skull base	Squamous cell carcinoma Chordoma Sarcoma Metastases Inflammation/infection

It can be a physiologic manifestation during pregnancy or lactation due to hypertrophy of prolactin cells. It can also occur in the setting of hypofunction of the thyroid gland, adrenal glands, or gonads as a result of the lack of negative feedback.[13] Nodular or diffuse pituitary hyperplasia can also be seen as a cause of Cushing's disease.

Pituitary Adenomas

Pituitary adenomas account for 10 to 15% of intracranial tumors.[14] Pituitary adenomas can be classified as:

- Microadenomas (<10 mm) and macroadenomas (>10 mm). Microadenomas may be difficult to detect due to their size but nonetheless be highly symptomatic, while macroadenomas have the potential to exert mass effect.
- Adenomas can also be classified according to their cellular origin into lactotrophs, somatotrophs, gonadotrophs, corticotrophs, and thyrotrophs.
- In an epidemiologic study, 74% of macroadenomas and 22% of microadenomas were nonfunctioning.[15] Functioning adenomas secrete prolactin in 25 to 41% and adrenocorticotropic and growth hormones in 5 and 2.8% of cases, respectively.[16]

Identification of small lesions may benefit from dynamic contrast-enhanced MRI or, rarely, CT techniques (usually when MRI cannot be performed) based on the differential rate of enhancement of adenomas compared to pituitary tissue. Normal pituitary parenchyma shows homogeneous enhancement at 60 to 80 seconds following administration of contrast material.[17] Maximum image contrast between adenomas and pituitary tissue occurs at about 1 minute and gradually decreases thereafter.[18] However, an adenoma may enhance earlier than pituitary tissue due to direct

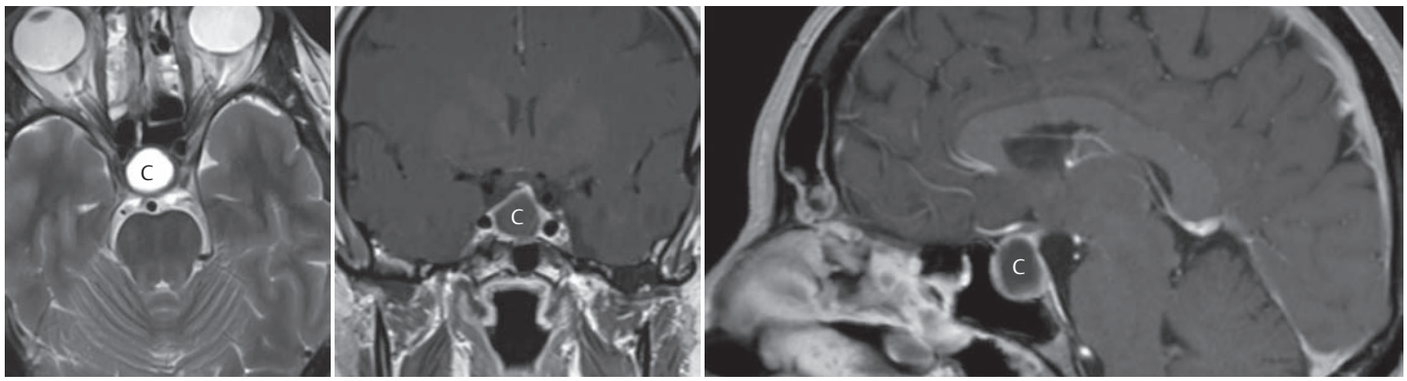

Fig. 3.17 T2 axial, postcontrast T1 coronal, and sagittal images show Rathke's cleft cyst appearing well-defined intrasellar CSF intense peripherally enhancing cystic lesion (C).

arterial supply.[17] While signal intensity on T2-weighted sequences is variable (particularly in large tumors) due to hemorrhage, cysts, or necrosis,[19] T2 hypointensity has been commonly reported in growth hormone–producing adenomas[20] (**Table 3.4**). Large adenomas usually infiltrate the gland; therefore, a displaced but otherwise normal-appearing pituitary gland may be helpful in ruling out an adenoma (**Figs. 3.18–3.36**).

Up to 10% of adenomas invade the cavernous sinuses.[8–10]

Imaging features that may be indicative or highly suggestive of cavernous sinus invasion are usually assessed on coronal pre- and postcontrast T1-weighted sequences.[10,21]

- Greater than 67% encasement of the internal carotid artery by tumor (about 240 degrees) yielded a 100% positive predictive value (PPV) for invasion as confirmed by surgery.[10]
- Obliteration of the carotid sulcus venous compartment (95% PPV).
- Tumor extension beyond the lateral intercarotid line (85% PPV).[10]

Features predicting absence of cavernous sinus invasion include:

- Less than 25% of carotid encasement.
- Presence of pituitary tissue between the tumor and carotid artery.
- Tumor not extending beyond the medial intercarotid line.[10]

Adenomas greater than 4 cm are classified as "giant."[14] Despite their benign histology, such tumors can infiltrate the skull base and, rarely, extend to the nasopharynx.[22] Large adenomas undergo spontaneous infarction at a greater rate than any other tumor of the central nervous

Table 3.4 MRI characteristics of pituitary microadenoma and macroadenoma

Pituitary pathology		Plain MRI		MRI with contrast
		T1	T2	
1	Microadenoma	Not clearly visualized		Early phase no enhancement compared to normal pituitary gland enhancement Delayed contrast enhancement
2	Macroadenoma			
	Without hemorrhage	Hypointense	Hyperintense Hypointense (in functioning GH-secreting tumor)	Early intense contrast enhancement
	With hemorrhage	Hyperintense	Depends on the stage of hemorrhage	Peripheral enhancement
	With necrosis	Hypointense	Hyperintense	Peripheral enhancement
	With cystic changes	Hypointense	Mixed signal intensity	Solid portions enhance

Abbreviations: GH, growth hormone; MRI, magnetic resonance imaging.

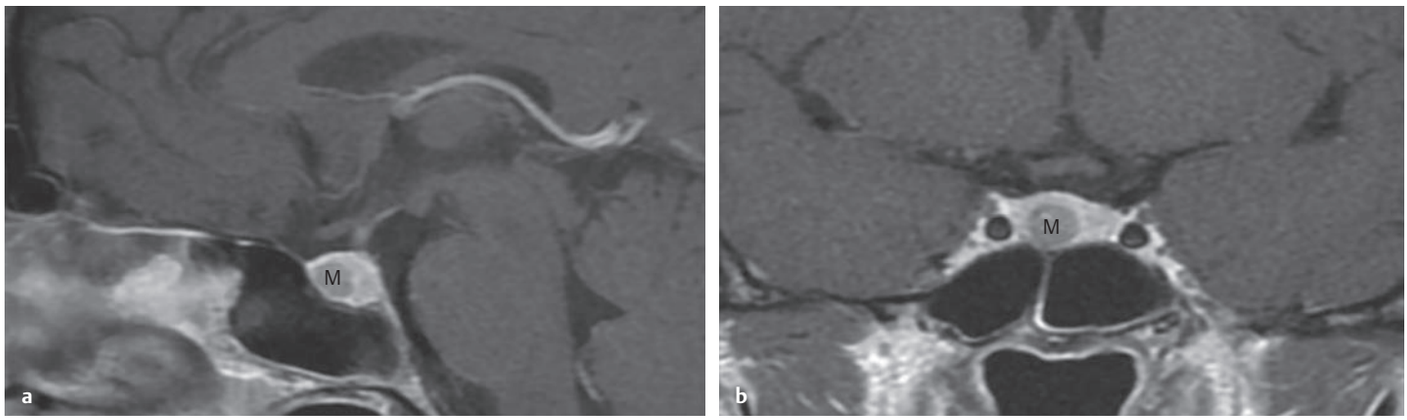

Fig. 3.18 **(a,b)** Postcontrast T1 fat-saturated sagittal and coronal images showing nonenhancing pituitary microadenoma (M) in comparison with enhancing background of normal pituitary gland.

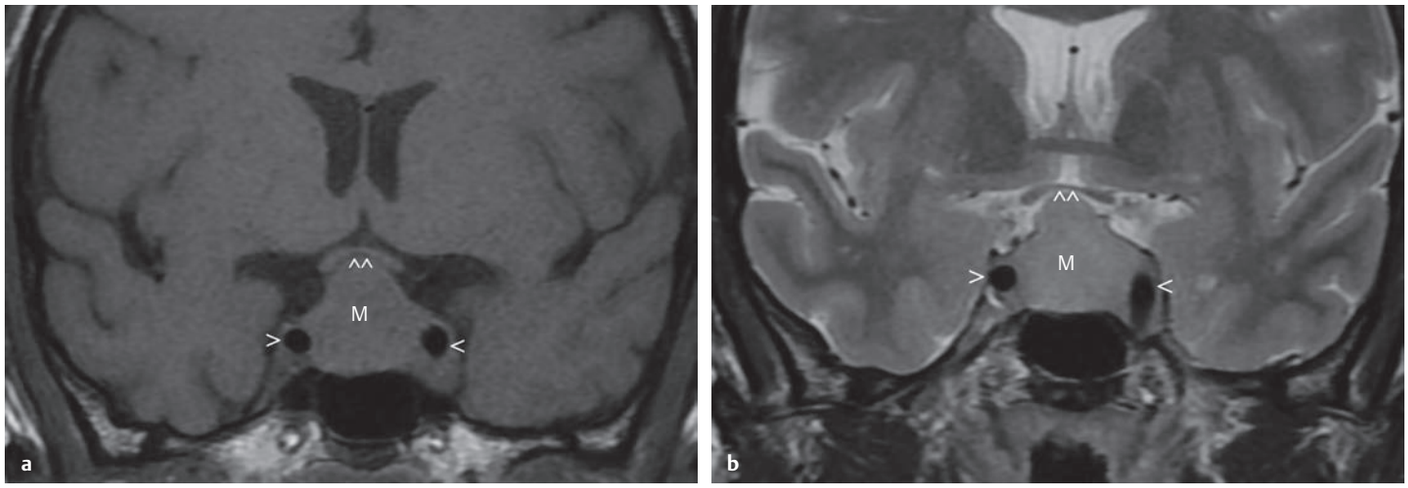

Fig. 3.19 **(a,b)** T1W and T2W coronal images showing sellar and suprasellar mass (M) appearing isointense to grey matter (figure of "8" appearance) indenting on the optic chiasm (*double white arrow*). Bilateral internal carotid artery (*single white arrow*).

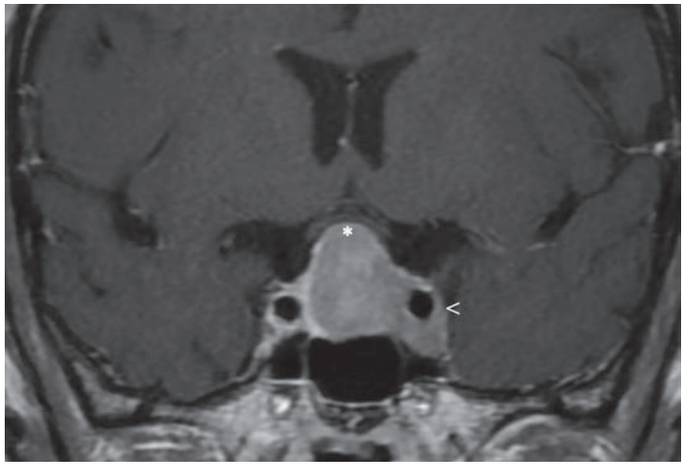

Fig. 3.20 Postcontrast T1W coronal image showing enhancing pituitary macroadenoma impinging on optic chiasm (*) and encasing the left internal carotid artery (*white arrow*). Normal pituitary gland not separately visualized.

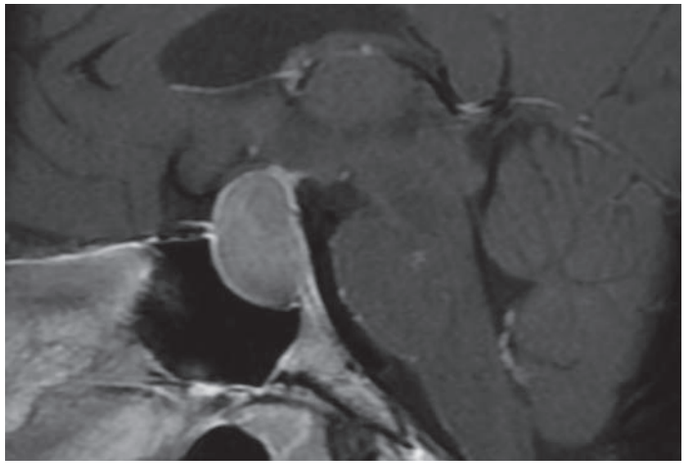

Fig. 3.21 Postcontrast T1W sagittal images showing enhancing pituitary macroadenoma.

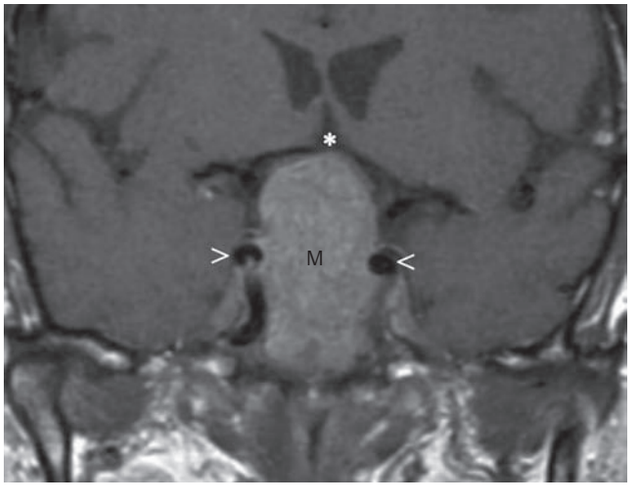

Fig. 3.22 Postcontrast T1W coronal images showing homogeneously enhancing pituitary macroadenoma with suprasellar extension compression on the optic chiasm. No evidence of parasellar extension. Pituitary macroadenoma (M); internal carotid artery (*white arrow*).

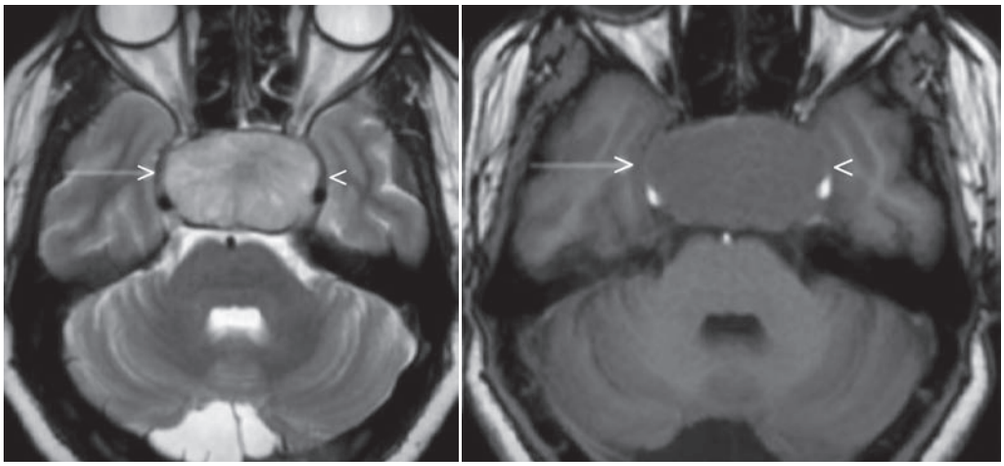

Fig. 3.23 Axial T2 and T1W images showing pituitary macroadenoma displacing both the internal carotid arteries (*white arrow*). No evidence of carotid encasement/parasellar extension.

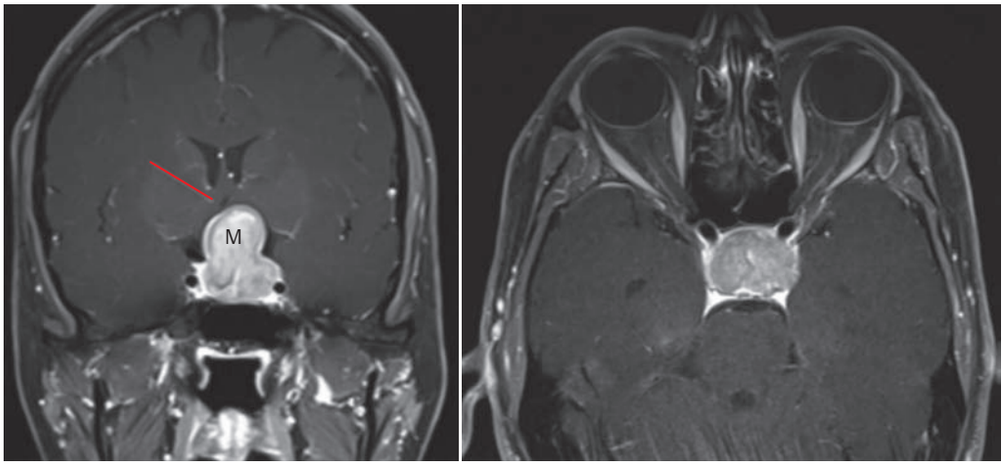

Fig. 3.24 Postcontrast T1 coronal and axial images showing homogeneously enhancing pituitary macroadenoma (M) with suprasellar extension (showing mass configuration) indenting on optic chiasm

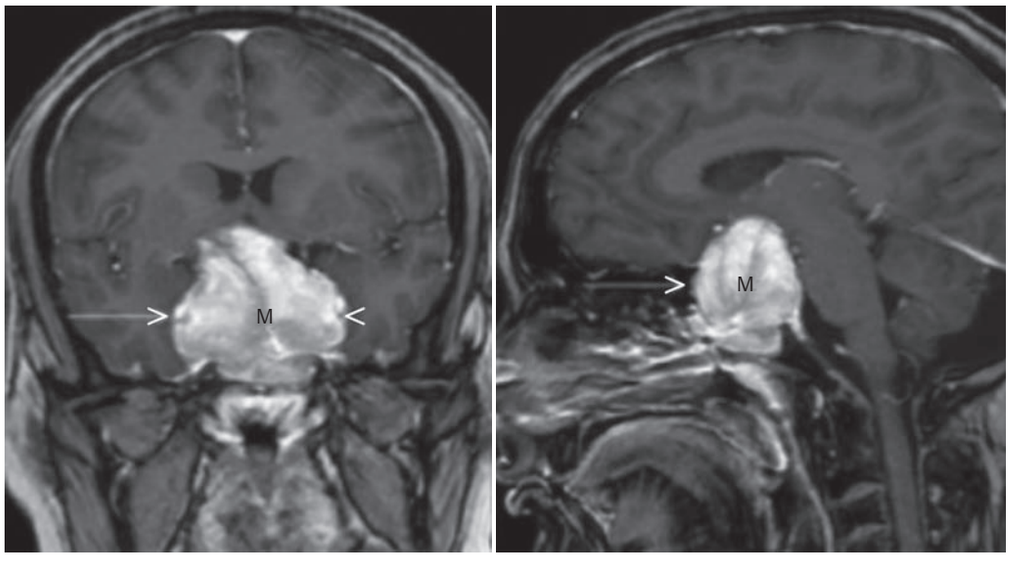

Fig. 3.25 Postcontrast T1W coronal and sagittal images showing homogeneously enhancing pituitary macroadenoma (M) with suprasellar extension encasing the bilateral internal carotid arteries (*arrow*).

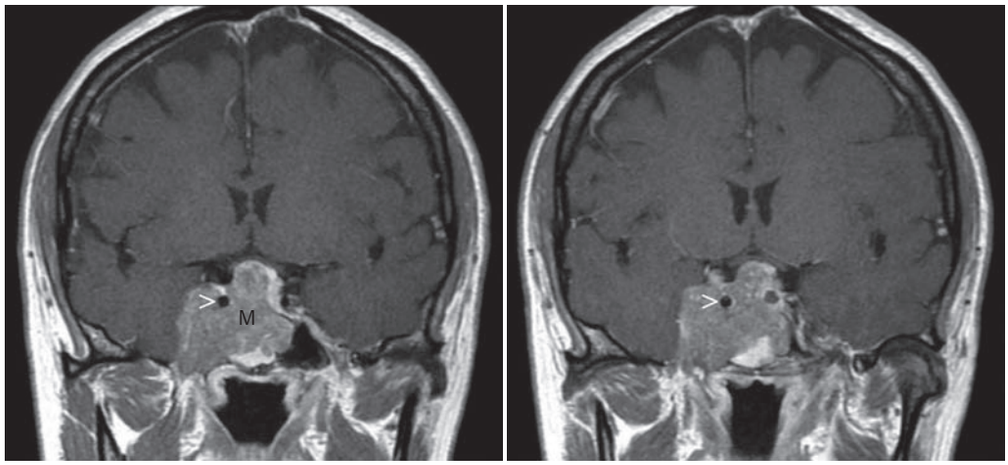

Fig. 3.26 Postcontrast T1W coronal images showing mildly enhancing pituitary macroadenoma (M) (fibrous content predominantly) completely encasing the right internal carotid artery (*arrow*) and invading the cavernous sinus.

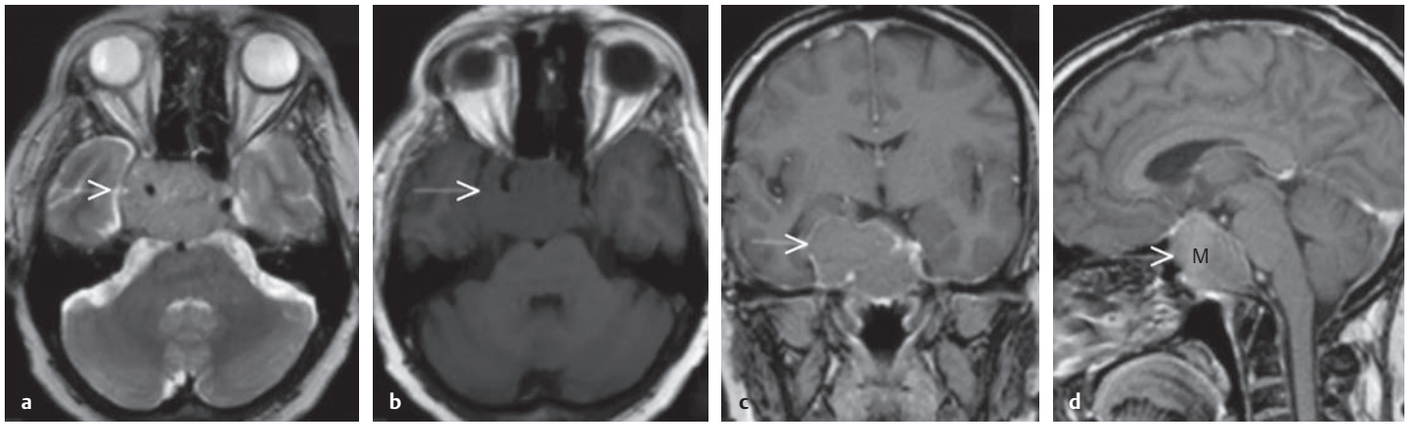

Fig. 3.27 **(a)** Axial T2W, **(b)** axial T1W, **(c)** postcontrast T1 coronal, **(d)** postcontrast T1 sagittal. Pituitary macroadenoma (M) encasing the right internal carotid artery with cavernous sinus invasion (*arrow*).

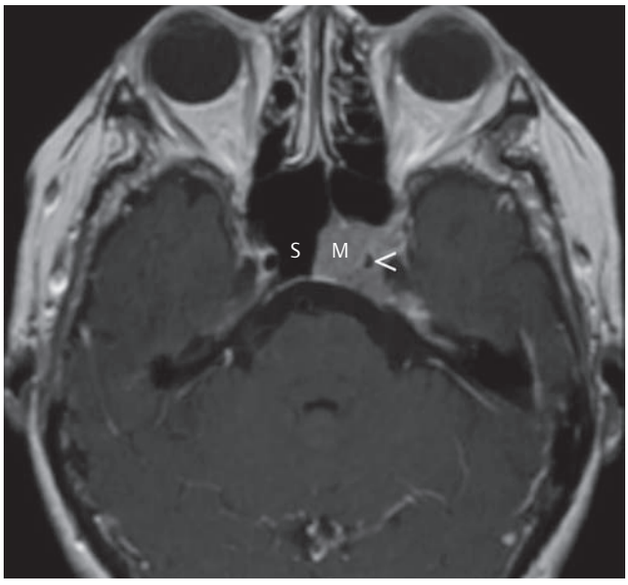

Fig. 3.28 Axial T1W postcontrast MRI showing pituitary macroadenoma (M) encasing the left internal carotid artery (*arrow*) with extension into sphenoid sinus (S).

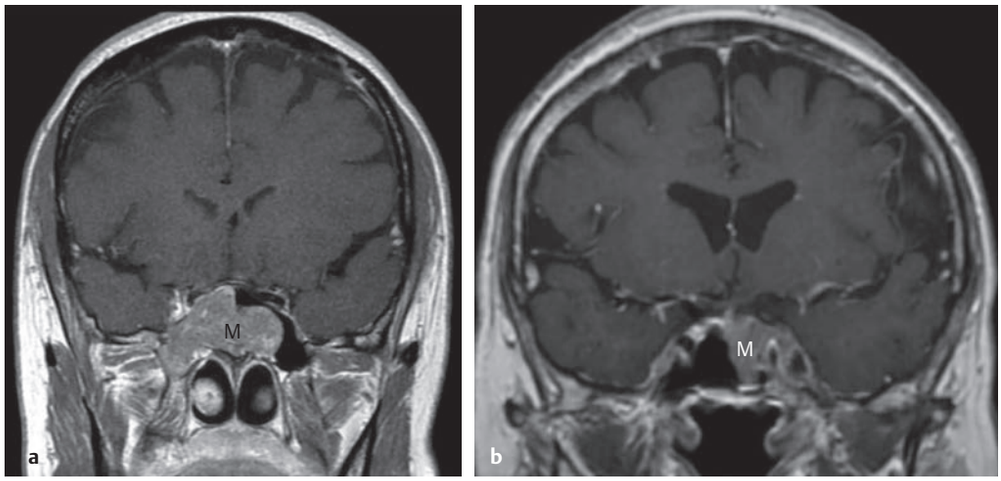

Fig. 3.29 **(a,b)** Postcontrast coronal T1W MRI showing sphenoid sinus extension of pituitary macroadenoma (M).

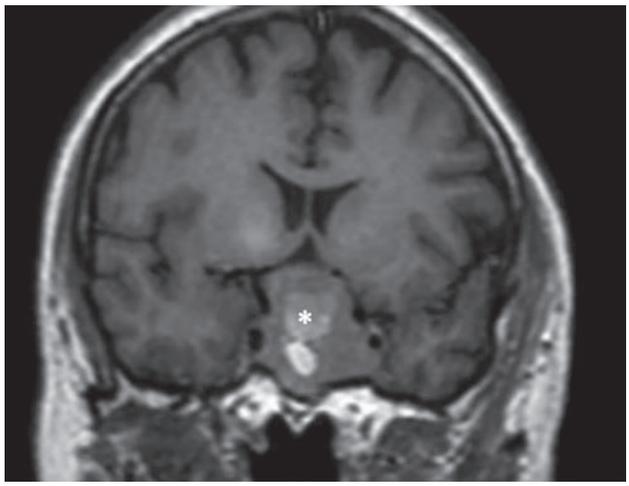

Fig. 3.30 T1W coronal images showing pituitary macroadenoma with acute hemorrhage (*) (pituitary apoplexy).

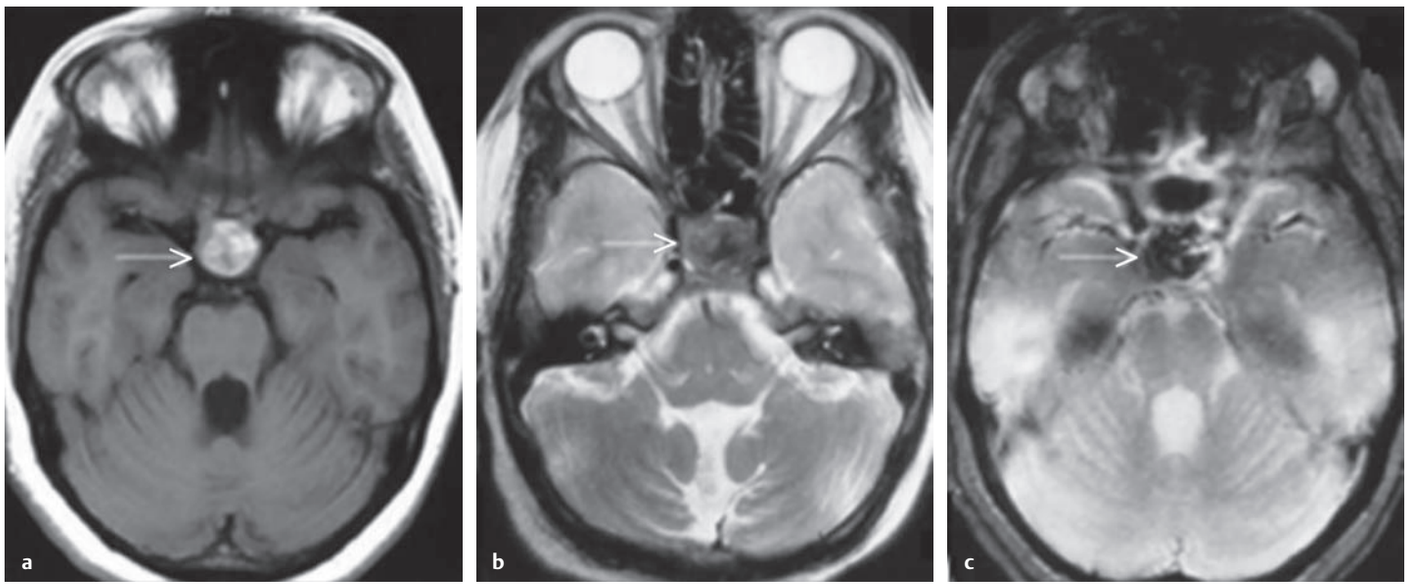

Fig. 3.31 **(a)** Axial T1 MRI, **(b)** T2 axial, **(c)** gradient MRI images showing pituitary apoplexy with hemorrhage (*arrow*) appearing hyperintense on T1, hypointense on T2 with gradient blooming.

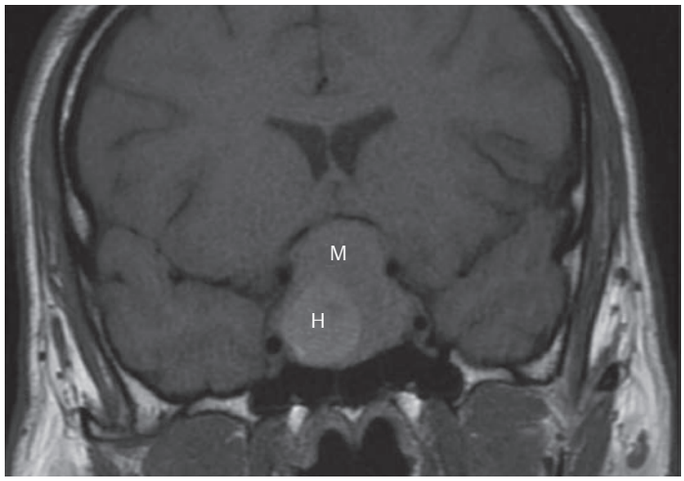

Fig. 3.32 T1W coronal images showing pituitary macroadenoma (M) with acute hemorrhage (H) (pituitary apoplexy).

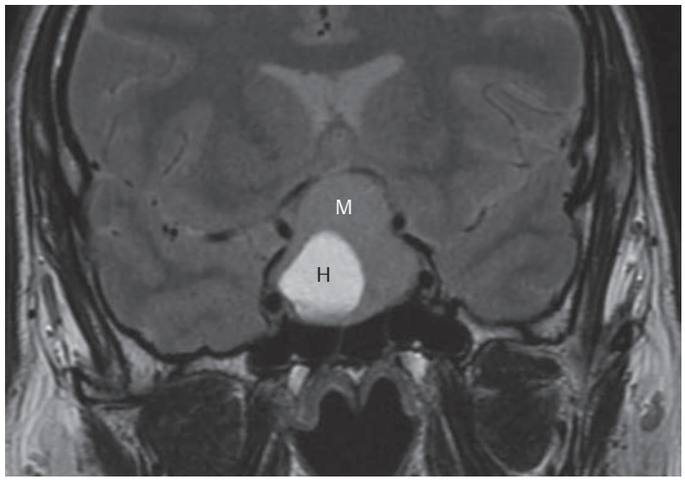

Fig. 3.33 Coronal T2W MRI showing pituitary adenoma (M) with T2 hyperintense hemorrhage (H).

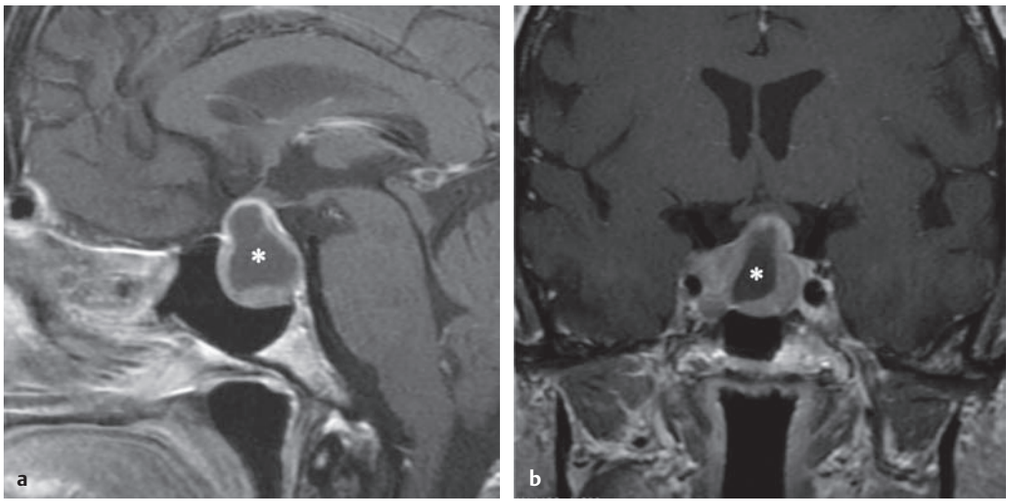

Fig. 3.34 (a,b) Postcontrast T1W sagittal and coronal images showing pituitary macroadenoma with nonenhancing central lesional necrosis (*).

system, probably due to outgrowth of their blood supply, vascular compression from expansion, or other intrinsic features.[23,24] This occurs with or without hemorrhage and may lead to pituitary apoplexy, which can rarely be complicated by retroclival hematomas.[23–25]

MRI plays an important role in differentiating between solid and cystic pituitary adenomas. It also helps in identifying hemorrhage in the gland or in a tumor involving the gland.

The surgical suckability of the tumor during surgery depends on the fibrous content of the tumor. This fibrotic component may appear hypo- or hyperintense on T2 but may not avidly take up contrast as a suckable nonfibrotic cellular tumor.

Craniopharyngioma

Craniopharyngiomas are nonglial epithelial tumors that arise from remnants of Rathke's pouch or the rests of Buccal mucosa along the path of the craniopharyngeal canal. Most involve both the intrasellar and suprasellar compartments (70%); 10% are intrasellar and 20% are suprasellar. They can be seen in children (peak at 5–10 years) and adults (fifth through seventh decades).

Craniopharyngiomas can cause symptoms such as visual disturbances, endocrine abnormalities, motor deficits, and increased intracranial pressure. The main histologic subtypes are adamantinomatous and squamous papillary (**Table 3.5**). Adamantinomatous subtypes are more often encountered in the suprasellar region in children. They are

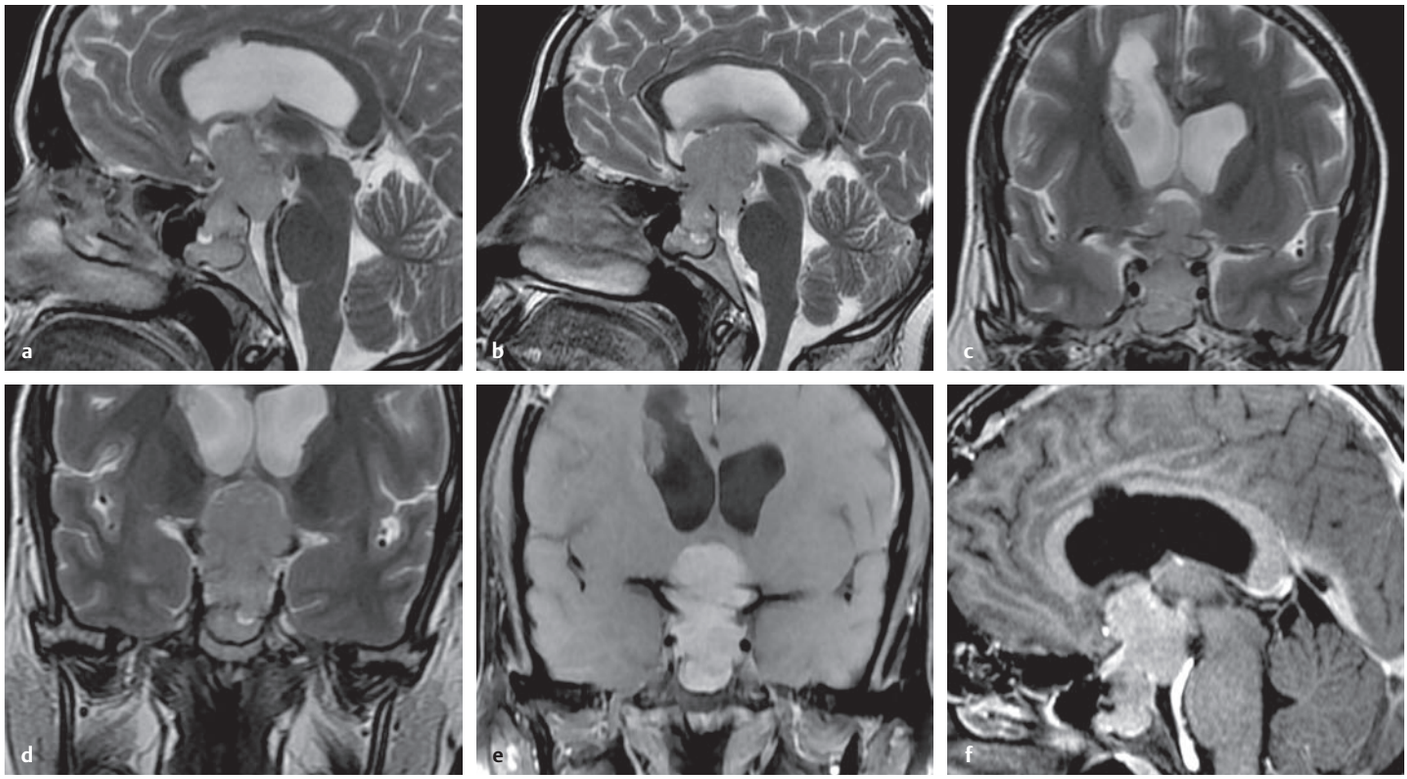

Fig. 3.35 Recurrent pituitary macroadenoma: with suprasellar extension up to the floor of third ventricle and extending into the sphenoid sinus. **(a,b)** T2 sagittal section showing an isointense mass. **(c,d)** T2 coronal section showing an isointense mass. **(e)** T1 coronal section showing postcontrast enhancement of the mass. **(f)** T1 sagittal section showing postcontrast enhancement of the mass.

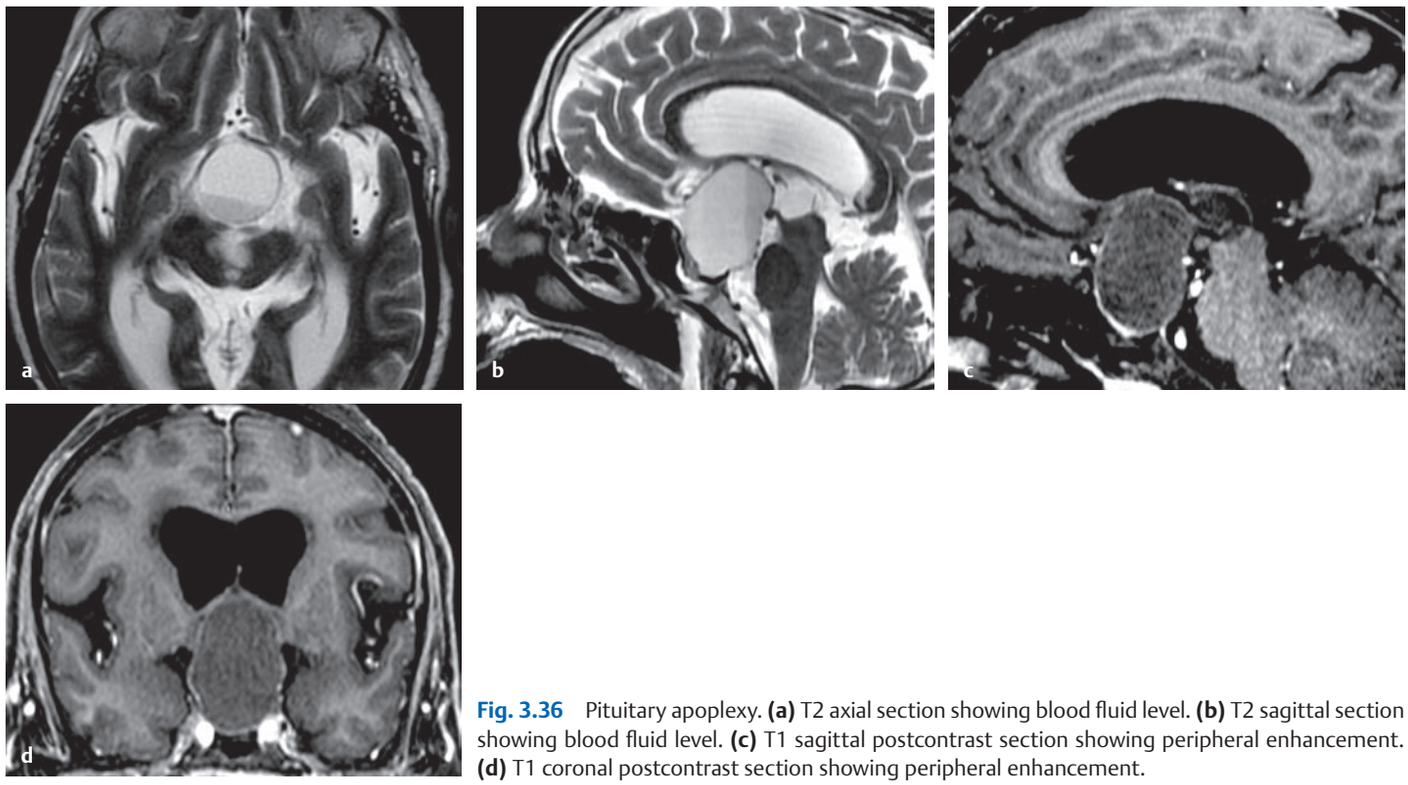

Fig. 3.36 Pituitary apoplexy. **(a)** T2 axial section showing blood fluid level. **(b)** T2 sagittal section showing blood fluid level. **(c)** T1 sagittal postcontrast section showing peripheral enhancement. **(d)** T1 coronal postcontrast section showing peripheral enhancement.

predominantly cystic and lobulated with calcifications, and tend to recur. The squamous papillary subtype presents more frequently in adults. These craniopharyngiomas are predominantly solid and spherical, and they occur in either the intrasellar or suprasellar regions.[26] Calcification is seen in 80% of lesions and is best delineated on CT. Cystic areas are observed in 85% of cases and can have a variable appearance on MRI depending on the degree of methemoglobin and/or high protein content. Enhancement can be solid or nodular (**Figs. 3.37–3.44**).

Table 3.5 Types of craniopharyngiomas

Type of craniopharyngioma	CT	MRI		Contrast enhancement	Other
		T1	T2		
Adamantinomatous type					
Cystic component	Follows CSF density	Isointense to hyperintense (depending on protein content)	Variable	Nil	Cyst shows lipid peak on MR spectroscopy
Solid component	Soft-tissue density	Hypointense	Variable	Present	
Calcification	Stippled calcification (90%)	Hypointense (in dense calcification)		Nil	
Papillary type (prominent solid content with very few cysts)					
Cystic component	Follows CSF density (if present are very small)	Variable (depending on protein content)		Nil	Cyst shows lipid peak on MR spectroscopy
Solid component (prominent solid content with very few cysts)	Soft-tissue density	Isointense to hypointense	Variable	Intense enhancement	
Calcification	Rare				

Abbreviations: CSF, cerebrospinal fluid; CT, computed tomography; MRI, magnetic resonance imaging.

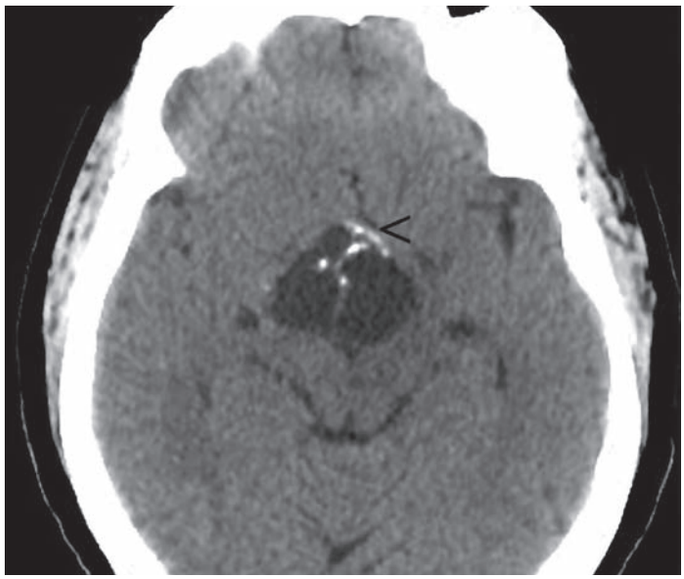

Fig. 3.37 Axial plain CT brain showing craniopharyngioma appearing as hypodense suprasellar lesion with peripheral calcifications (*arrow*).

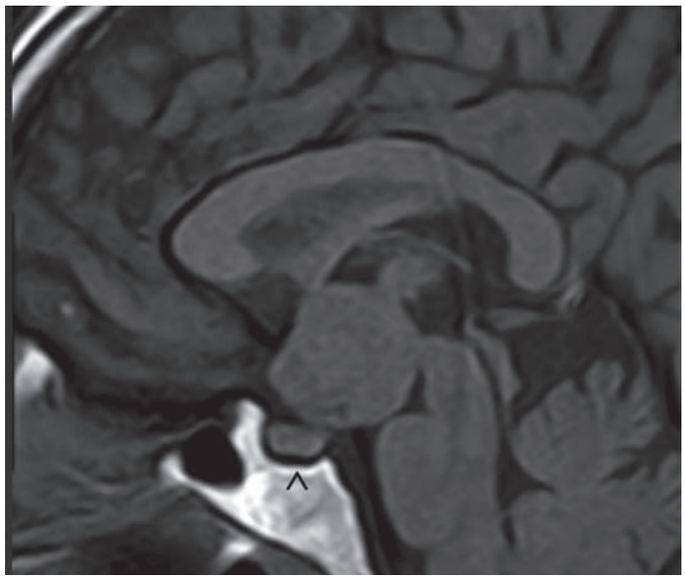

Fig. 3.38 Sagittal plain, T1W MRI; T1 hypointense suprasellar mass lesion (hypothalamic stalk type) extending into third ventricle. Note that the pituitary gland is separately visualized with depression of diaphragm sella (*arrow*).

Due to their preferred infundibular location, age at presentation, and solid appearance with lack of calcification or cystic changes, papillary craniopharyngiomas may be difficult to distinguish from germinomas. While they both usually show strong contrast enhancement, germinomas have lower ADC (apparent diffusion coefficient) values by virtue of their higher-grade histology and cellularity compared to papillary craniopharyngiomas.[27]

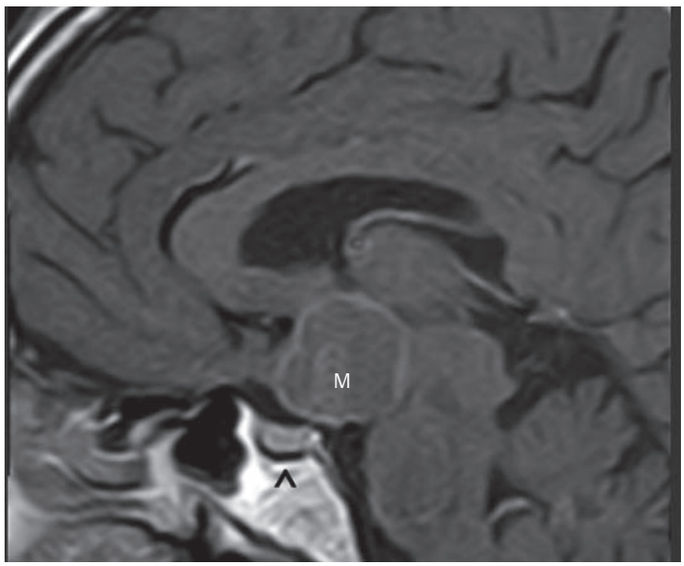

Fig. 3.39 Sagittal T1W postcontrast MRI image showing peripherally enhancing predominantly cystic suprasellar craniopharyngioma (M) enhancing normal pituitary gland (*arrow*).

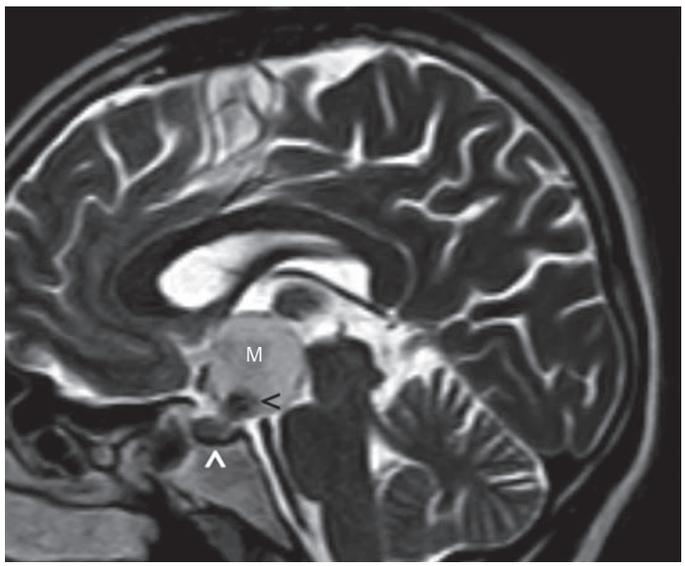

Fig. 3.40 Sagittal T2W MRI showing suprasellar craniopharyngioma (M), appearing hyperintense with hypointense calcification, displacing the stalk posteriorly (*black arrow*) (adamantinomatous). Normal pituitary (*white arrow*).

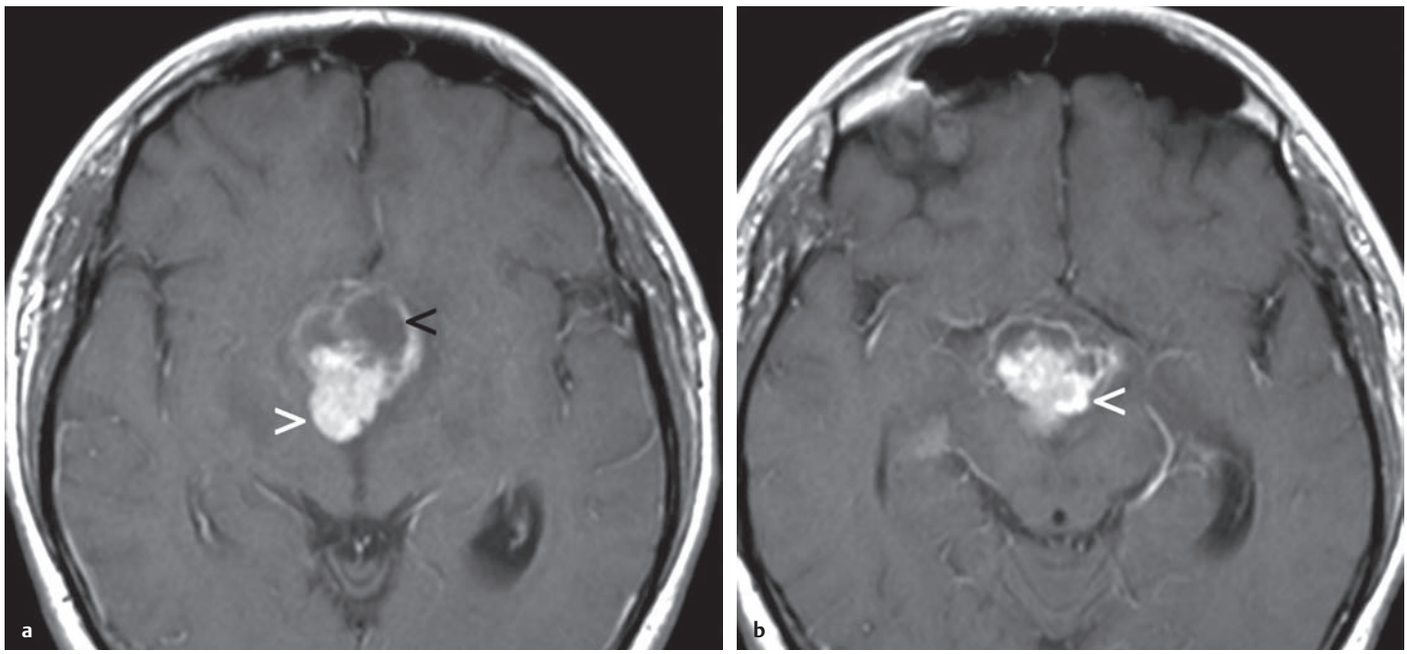

Fig. 3.41 **(a,b)** Postcontrast T1W axial images showing enhancing solid areas (*white arrow*) and nonenhancing cystic areas (*black arrow*) of suprasellar craniopharyngioma (adamantinomatous type).

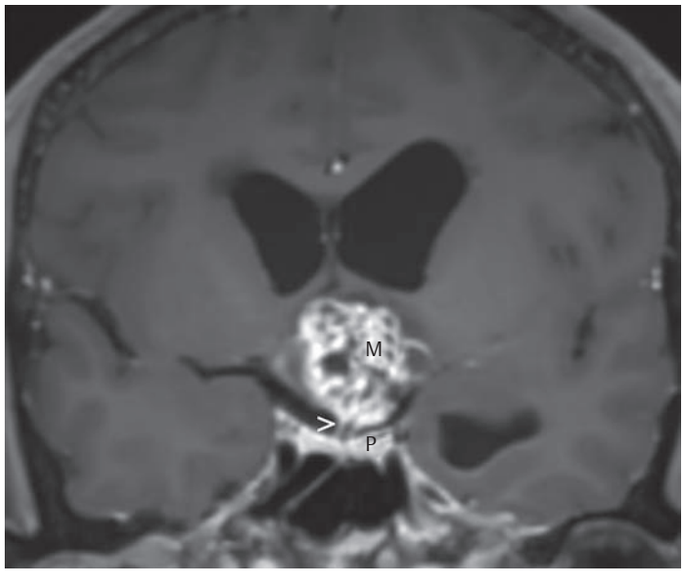

Fig. 3.42 Postcontrast T1W coronal MRI images showing heterogeneous enhancing multiloculated suprasellar mass (M) (papillary type). Pituitary gland (P) and stalk (*white arrow*) separately seen.

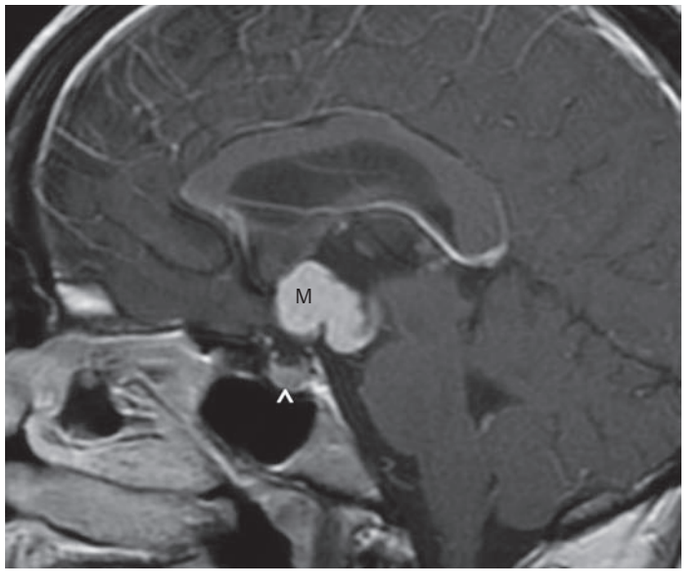

Fig. 3.43 Postcontrast T1W sagittal MRI images showing homogeneously enhancing solid suprasellar mass (M) (papillary type) displacing the stalk anteriorly. Normal pituitary (*white arrow*).

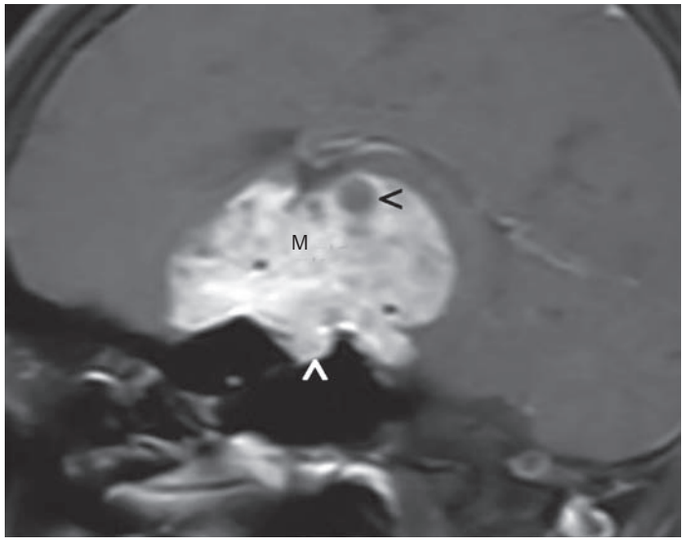

Fig. 3.44 Postcontrast T1W sagittal MRI images showing intensity-enhancing large suprasellar mass (papillary type) with peripheral small cysts (*black arrow*), with mass extending into the third ventricle (hypothalamic stalk type). Normal pituitary (*white arrow*).

Depending on the location of craniopharyngioma in relation to the pituitary stalk, it can be categorized as central and peripheral types:

- Central type:
  - Vertical growth pattern along the stalk encasing it in the midline.
  - There is no shift of the third ventricle.
  - As it is difficult to preserve the stalk during surgery, the surgeon should be careful in order to prevent injury to the hypothalamus.
- Peripheral type:
  - Vertical or horizontal growth pattern along the stalk or on either side of it.
  - It is usually a large volume tumor resulting in third ventricular shift.

Based on the location, it is subdivided as:

- Hypothalamic type:
  - Grows into the third ventricle.
  - In these cases, the hypothalamus is at risk of injury but the stalk is likely to be preserved.
- Suprasellar type:
  - Growth is seen between the sella and the hypothalamus.
  - It displaces the third ventricle superiorly.
  - In this subtype, both the hypothalamus and the stalk are likely to be preserved during surgery.
  - Displacement of the stalk depends on the site of tumor growth, i.e., tumor located posterosuperiorly displaces the stalk anteroinferiorly.
- Intrasellar type:
  - Frequently encountered in children.
  - Vertical growth pattern is seen along the stalk (**Table 3.6**).
  - Intrasellar stalk is prone to injury during surgery.

- Contrast study helps in differentiating normal pituitary from the lesion.

Meningioma

Meningiomas in this region originate from the tuberculum sella, anterior clinoid processes, diaphragma sellae, planum sphenoidale, and upper clivus. Meningiomas arise from arachnoid cap cells in the leptomeninges, which derive from the mesenchyme and neural crest.[28,29]

Half of anterior skull base meningiomas arise at the sphenoid wings and the remainder from the tuberculum sellae, limbus sphenoidale, and chiasmatic and olfactory grooves.[30] Therefore, extension frequently occurs into the optic canals, cavernous sinuses, or sella. Arterial encasement may be present, which can lead to stenosis.[31] Anterior skull base meningiomas can result in abnormal dilatation of an adjacent paranasal sinus (pneumosinus dilatans).[32]

On noncontrast CT, meningiomas tend to be iso- to hyperdense to cerebral cortex and are difficult to visualize unless they are large or calcified or there is hyperostosis, which appears to be more common in the skull base (occurring in 50% of patients) compared to convexity meningiomas.[33] They can cause osseous changes including hyperostosis and erosion. On MRI, they are isointense to slightly hypointense on T1-weighted imaging. They are isointense to slightly hyperintense on T2-weighted imaging and they enhance homogeneously and intensely with enhancing dural tail.[34] The vascular supply to these lesions is from the carotid meningeal and ophthalmic arteries (**Figs. 3.45–3.50**).

Table 3.6 Pituitary stalk positions in different pathologies

	Pathology	Pituitary stalk position
1	Pituitary adenoma	Superior
2	Planum sphenoidale meningioma (extending into the suprasellar cisterns)	Posterosuperior
3	Chordoma	Anterosuperior

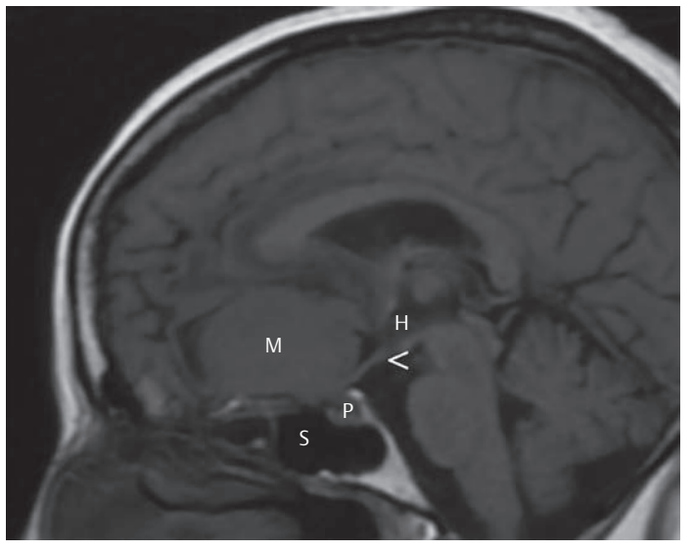

Fig. 3.45 Sagittal T1W MRI showing meningioma (M), appearing hypointense extra-axial mass in the basifrontal region with broad-based attachment to the planum. Normal pituitary gland and stalk are seen separately. Sphenoid (S), pituitary gland (P), stalk (S), hypothalamus (H).

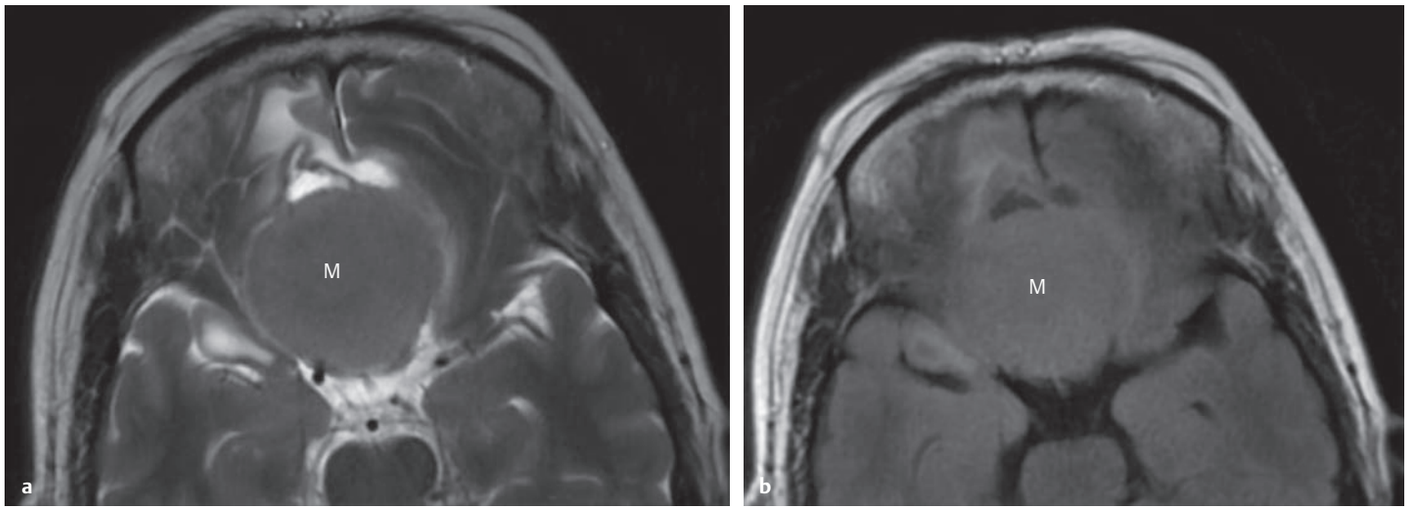

Fig. 3.46 **(a,b)** Axial T2 and T1 images of basifrontal region showing a hypointense extra-axial meningioma (M).

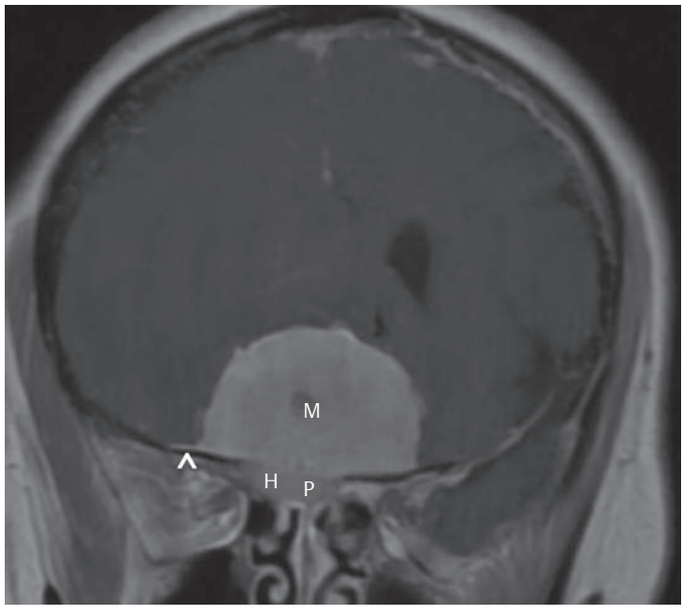

Fig. 3.47 Postcontrast T1W coronal images showing intensity-enhancing planum sphenoidale meningioma (M) with dural tail (*white arrow*) and hyperostosis.

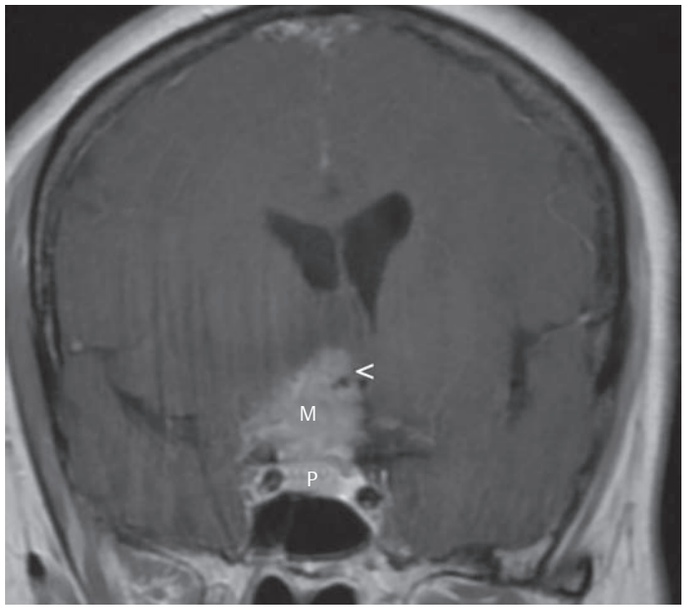

Fig. 3.48 Suprasellar extension of the meningioma partly encasing the right anterior cerebral artery (*white arrow*). Normal pituitary gland (P) is separately seen.

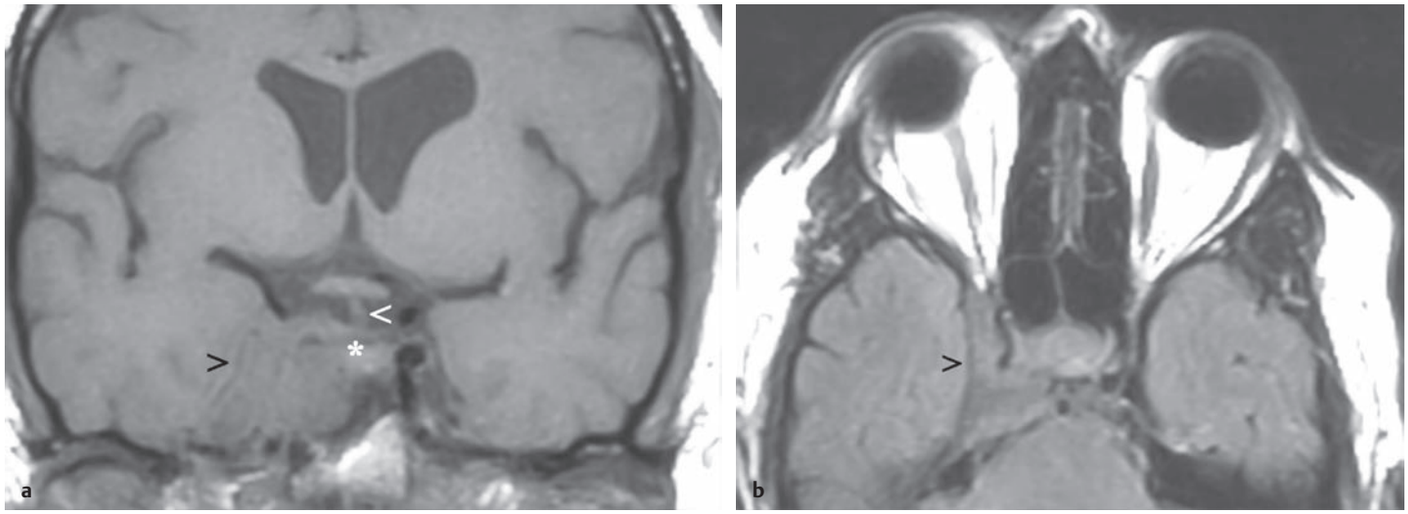

Fig. 3.49 **(a,b)** Coronal and axial T1W MRI images showing ill-defined hypointense to isointense right parasellar meningioma encasing the right internal carotid artery (*black arrow*). Pituitary gland (*) and stalk (*single white arrow*) are also seen.

Pituitary Stalk Lesions

The pituitary stalk is a funnel-like structure connecting the median eminence of the hypothalamus to the pituitary gland. A wide spectrum of neoplastic, inflammatory, and infectious disorders, such as germinoma, Langerhans cell histiocytosis (LCH), lymphocytic infundibuloneurohypophysitis, and sarcoidosis affect the pituitary stalk and cause stalk thickening.[35–39] These lesions often involve the hypothalamus and can result in diabetes insipidus. LCH is the most common pediatric infundibular tumor.[35,40] There may be meningeal involvement and choroid plexus lesions.[17] In nearly all cases of LCH, the normal T1 hyperintensity of the neurohypophysis is absent.[35]

Neoplastic processes that can enlarge the stalk include lymphoma, metastases, germinoma, and teratoma. Metastases have been reported in 3% of patients with carcinoma, particularly breast or primary bronchogenic.[41]

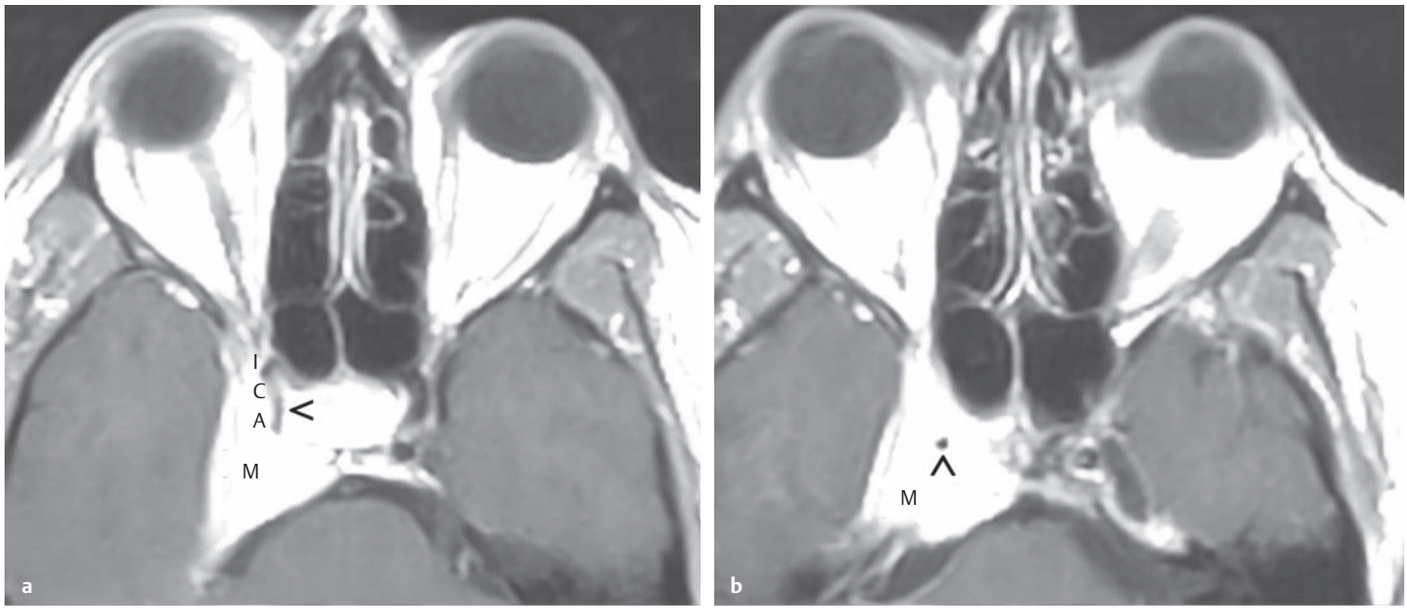

Fig. 3.50 **(a,b)** Postcontrast axial images showing intensity-enhancing right parasellar meningioma (M) encasing the right internal carotid artery (ICA, *black arrow*) involving the right cavernous sinus.

The hematogenous route is likely and additional intra-axial or extra-axial lesions may be a diagnostic clue. They may have a dumbbell morphology from invasion through the diaphragma sella.

Primary brain tumors such as medulloblastoma, pineoblastoma and germinoma, and lymphoma and leukemia may spread to the infundibular or suprasellar region via cerebrospinal fluid (CSF) seeding. Germinomas are more commonly seen in the pediatric population, presenting with diabetes insipidus, hypopituitarism, and optic chiasm compression. There may be coexistent pineal masses, and there may be subarachnoid spread.

Ectopic neurohypophysis can be caused by trauma or neoplastic processes, which disrupt the transport of hormones from the hypothalamus to the neurohypophysis. Congenital ectopic neurohypophysis is associated with other midline abnormalities such as septo-optic dysplasia. The normal posterior pituitary bright spot is frequently located in the suprasellar region. This can lead to growth hormone deficiency. In the extreme manifestation of this abnormality, i.e., pituitary stalk interruption syndrome, there is also an absence or hypoplastic infundibular stalk and adenohypophysis.[42]

Lymphocytic hypophysitis is an autoimmune disorder seen primarily in peripartum/postpartum females though it has also been reported in males and postmenopausal women.[43] On MRI, there is intense enhancement of a pituitary mass extending along the infundibulum to the floor of the hypothalamus. The posterior pituitary bright spot may be absent. The adenohypophysis and/or the neurohypophysis can be affected.[44] Dynamic MRI studies have shown that blood supply to the neurohypophysis is often compromised. Patients may present with visual field impairment and headache due to mass effect on adjacent structures. As the pituitary parenchyma is destroyed by the inflammatory process, partial or pan-hypopituitarism develops.[43] However, the condition is responsive to corticosteroid treatment and can spontaneously resolve.

Neurosarcoidosis is an inflammatory granulomatous process, which has a predilection for the leptomeninges.[45] There can be involvement of the optic chiasm, hypothalamus, pituitary gland, and infundibulum.

Chordoma

Most chordomas are histologically low-grade but locally aggressive tumors derived from embryonic remnants of the notochord.[46] Half of all chordomas are sacrococcygeal, one-third occur in the skull base, and a minority arise in the spine.[47] They are twice as common in males, have a peak incidence between 50 and 60 years of age, and are rare in children and adolescents.[48] These tumors most frequently occur midline at the spheno-occipital synchondrosis, although the chondroid subtype has a tendency to arise laterally at the petroclival junction.[46–48]

Chordomas are extradural and almost always originate in bone, which may lead to bony sequestra and the chondroid variant may have a true calcific matrix that can be demonstrated on CT.[48] On MRI, chordomas are well circumscribed with a pseudoencapsulated appearance and markedly bright on T2-weighted sequences, probably secondary to mucin and/or necrosis.[48,49] T2 signal in the chondroid variant may be relatively low due to cartilaginous tissue.[50] Interlobular septa are formed by epithelioid cells and appear hypointense on T2 with variable degrees of contrast enhancement.[48,49] Chordomas are soft tumors that tend to displace or encase blood vessels, but do not cause stenosis.[51] Dural transgression can be present, and tumor can extend into the subarachnoid space, increasing the risk of CSF leaks and infection.[52] Dural disruption may be identified on T2-weighted imaging but is best visualized on high-resolution SSFP-based sequences, where administration of contrast may aid in delineation of tumor against nonenhancing dura and depiction of its relationship to cranial nerves[53] (**Figs. 3.51–3.53**).

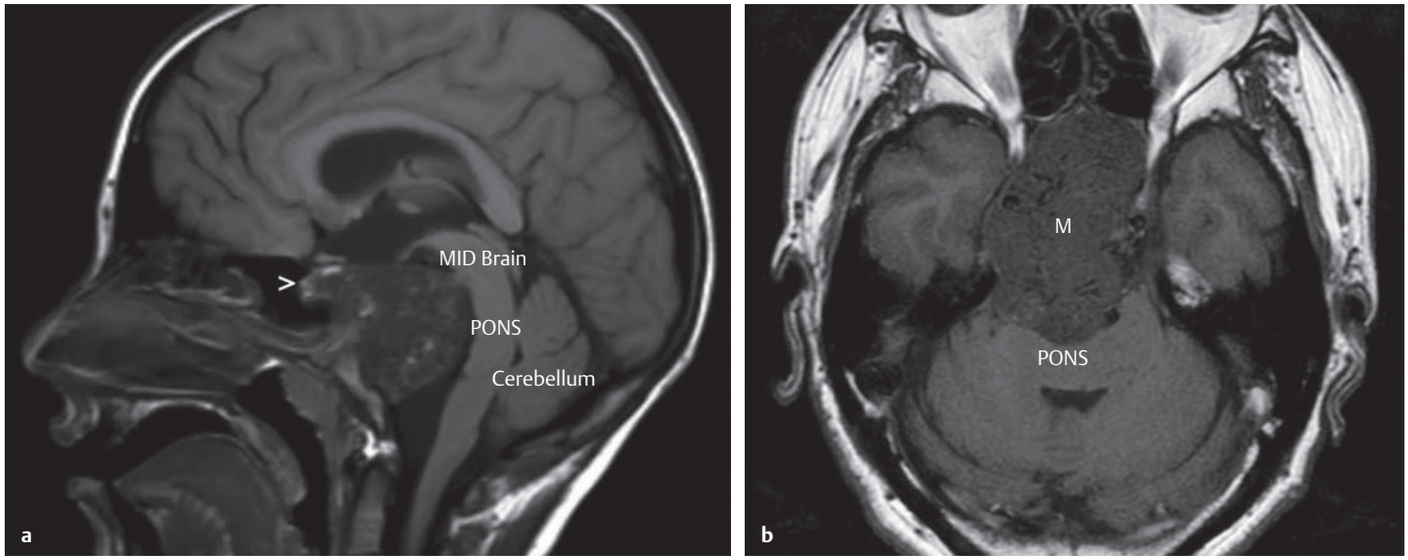

Fig. 3.51 **(a,b)** Sagittal and axial T1W plain MRI images showing chordoma appearing predominantly as hypointense mass which is seen in the skull base at the clivus, showing areas of hyperintensity due to mucus contents. The lesion is displacing the normal pituitary gland anteriorly (*white arrow*). Posteriorly, the lesion extending to prepontine cistern causing brainstem compression.

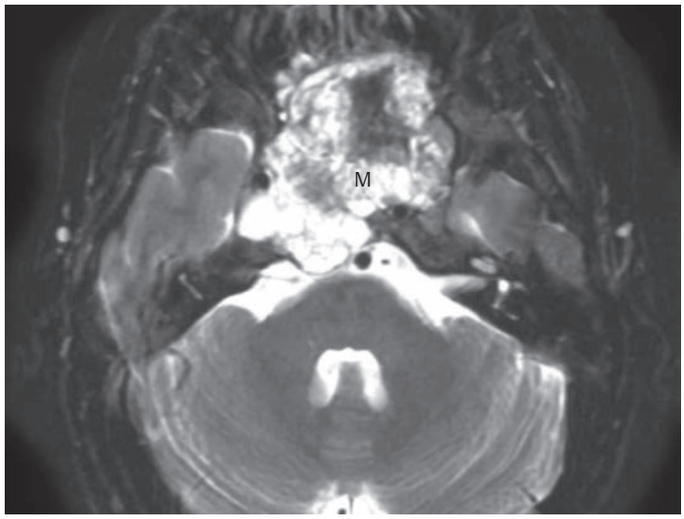

Fig. 3.52 Axial T2 fat-saturated MRI image showing a clival chordoma (M) appearing predominantly hyperintense with multiple septation.

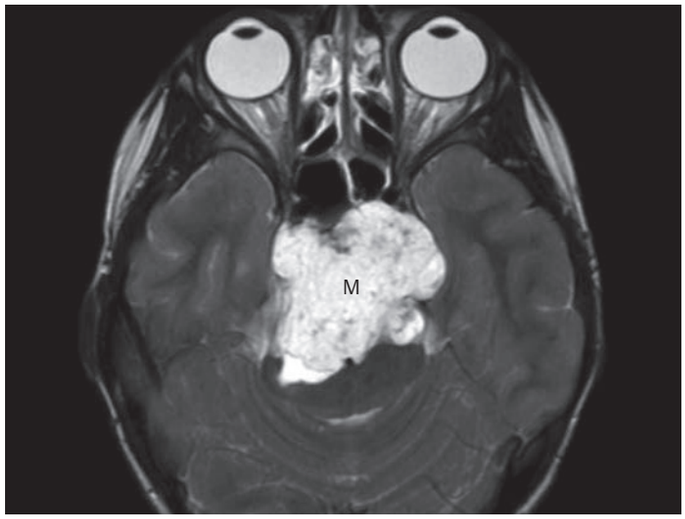

Fig. 3.53 Axial T2W MRI images showing hyperintense clival chordoma (M) with hypointense sepate showing extension into the prepontine cistern compressing on the basilar artery.

Miscellaneous Lesions

Hamartoma of the tuber cinereum (**Figs. 3.54 and 3.55**) is a developmental heterotopia, which presents in childhood as precocious puberty and gelastic seizures. Abnormalities of the corpus callosum and optic tracts can be associated. These suprasellar masses are isodense on CT, isotense on T1-weighted MRI, and hyperintense and nonenhancing on T2-weighted MRI.

Other lesions involving the suprasellar cistern include epidermoid, teratoma, and lipoma. Epidermoids can be differentiated from arachnoid cysts on fluid attenuated inversion recovery (FLAIR), in which epidermoids appear mildly hyperintense and hazy and show restriction (appears bright) on diffusion-weighted imaging.

Chiasmatic and hypothalamic gliomas (**Figs. 3.56–3.58**) are seen predominantly in the first decade of life and 20 to 50% of these patients have neurofibromatosis.[44] These lesions may be difficult to distinguish from hypothalamic astrocytomas or gangliogliomas. They demonstrate variable enhancement and appear T1 hypointense and

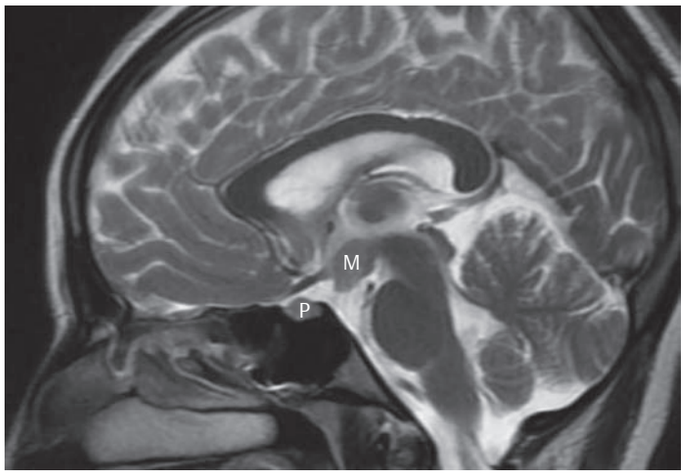

Fig. 3.54 T2W sagittal MRI images showing tuber cinereum hamartoma (M) appearing as well-defined T2 isointense to hypointense lesion in hypothalamus. Normal pituitary gland (P) is seen.

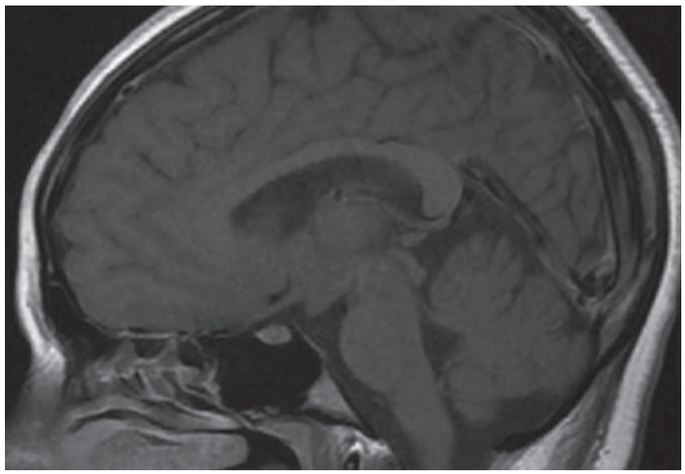

Fig. 3.55 Postcontrast T1W sagittal MRI showing no enhancement of tuber cinereum hamartoma (M). Normal pituitary gland (P) is seen.

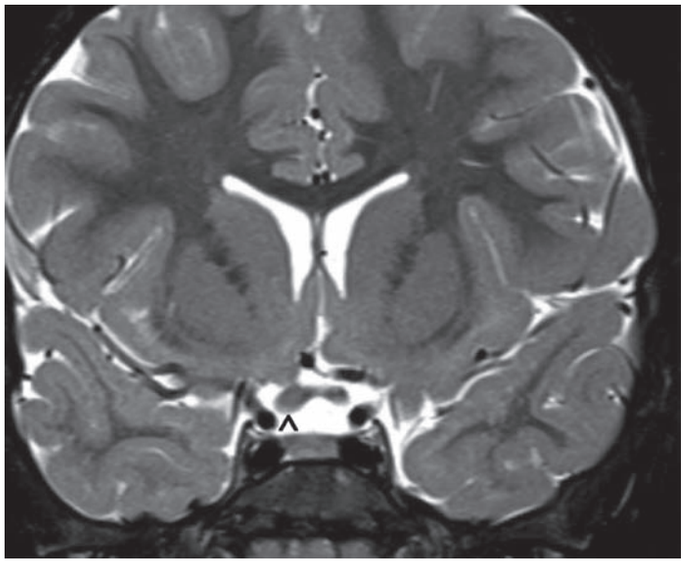

Fig. 3.56 T2 coronal images showing enlarged right optic nerve close to optic chiasm (optic pathway glioma) (*black arrow*).

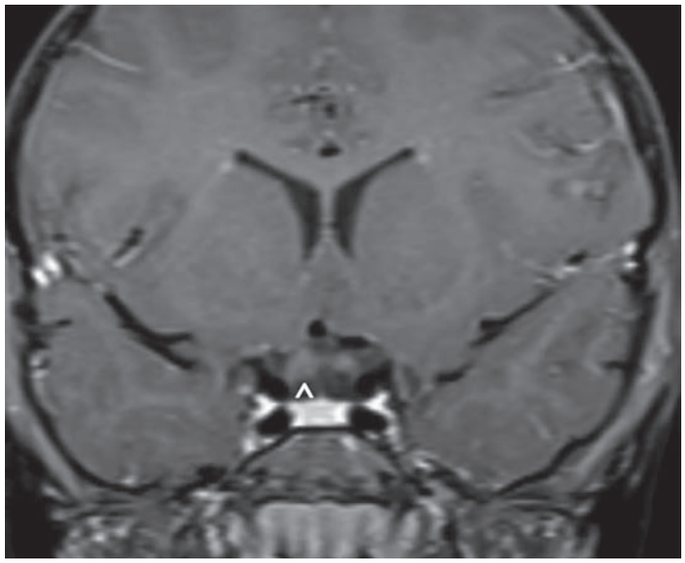

Fig. 3.57 Postcontrast T1W fat-saturated images showing enhancing mass in cisternal component of right optic nerve (optic glioma) (*white arrow*).

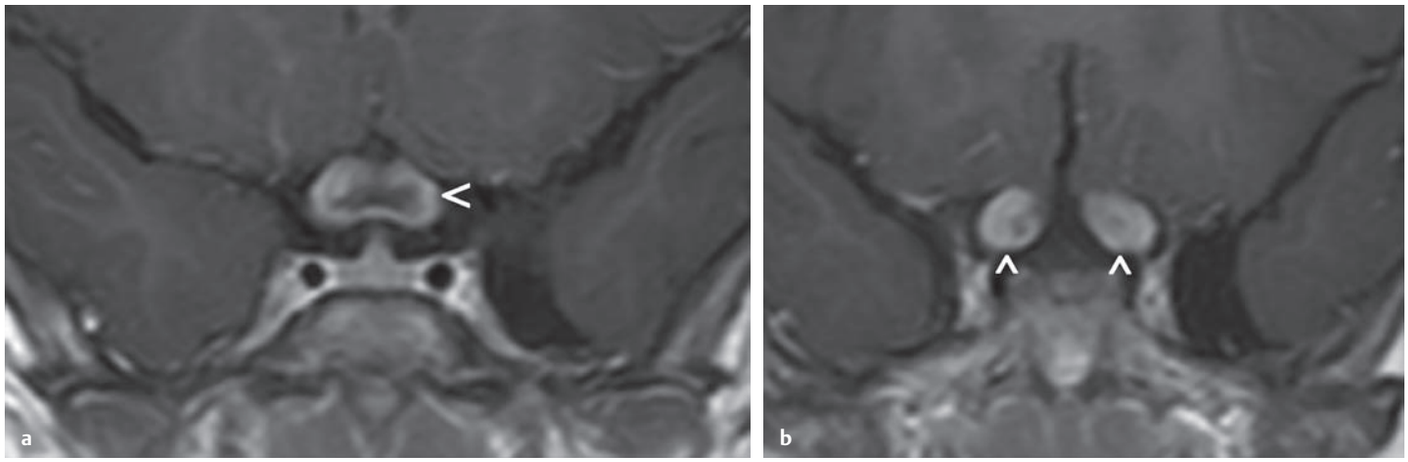

Fig. 3.58 **(a,b)** Postcontrast T1 fat-saturated MRI images showing enlarged homogeneously enhancing bilateral optic nerves (bilateral optic pathway glioma) (*white arrow*).

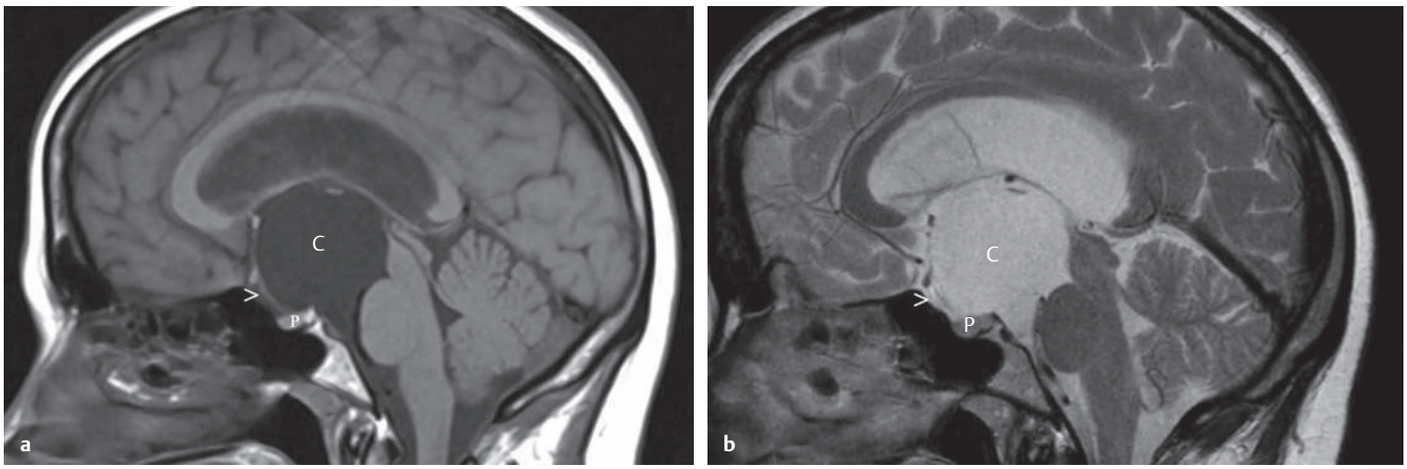

Fig. 3.59 **(a,b)** T1W and T2 sagittal MRI images of suprasellar arachnoid cyst **(c)** showing CSF signal intensity. Normal pituitary gland (P) is seen with displacing of stalk anteriorly (*white arrow*).

T2 hyperintense; this signal intensity can extend along the optic tracts.

Arachnoid cysts can occur in the suprasellar region, which appear smoothly marginated and they follow CSF imaging characteristics on CT and MRI. They may displace or compress the adjacent structures including the infundibulum, pituitary gland, and third ventricle (**Figs. 3.59 and 3.60**).

Mucocele of the sphenoid sinuses can extend into the suprasellar cisterns.

Vascular lesions such as aneurysms and cavernous carotid fistula and cavernous sinus thrombosis or thrombophlebitis can be seen in the cavernous sinus region. Aneurysms can produce mass effect on the intracavernous cranial nerves. Rupture of aneurysms of the cavernous

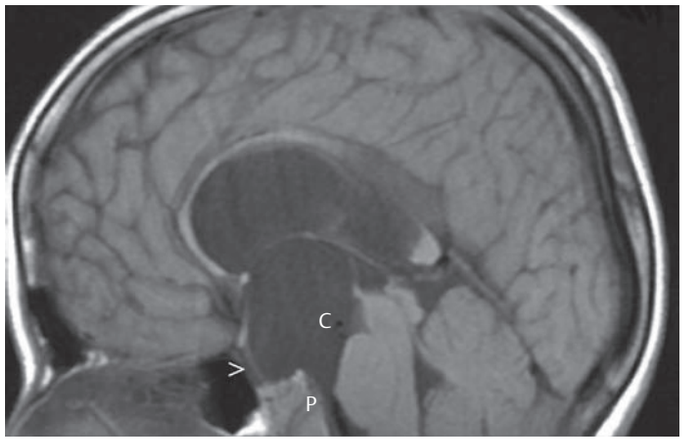

Fig. 3.60 Postcontrast T1W MRI showing nonenhancing suprasellar arachnoid cyst (c). Normal pituitary gland (P) is seen with displacing of stalk anteriorly (*white arrow*).

segment of the internal carotid arteries can result in carotico-cavernous fistulas (**Table 3.7**).

Postoperative Imaging

Ideal timing for postoperative imaging is the second or third postoperative day. Postoperative imaging modality of choice is MRI, as it picks up early hemorrhages and helps in differentiating residual tumor from surgical packing.

Plain MRI helps in identifying:

- Infarcts.
- Subtle subarachnoid or intraventricular hemorrhages.
- Contents of surgical packing such as fat, surgicel, or gel foam.

Contrast MRI helps in identifying (**Figs. 3.61 and 3.62**):

- Skull base flap integrity:
  - ➢ Uniform intensity and enhancement is seen in a viable flap.

Table 3.7 CT and MRI characteristics of various sellar and suprasellar lesions

Pathology		CT	MRI		
			T1	T2	Contrast enhancement
1	Rathke's cleft cyst	Follows CSF density (may be hyperintense)	Hyperintense Variable (depending on protein content)		Peripheral enhancement
2	Meningioma	Isodense or hyperdense to cerebral cortex Calcifications Hyperostosis Bone erosion	Hypointense to slightly hypointense	Hypointense to slightly hyperintense	Intense homogeneous enhancement with enhancing dural tail
3	Chordoma	Hypodense with calcification	Hypointense	Hyperintense with interlobular septae	Variable
4	Hamartoma	Isodense	Isointense	Hyperintense	Nil
5	Chiasmatic and hypothalamic glioma		Hypointense	Hyperintense	Variable
6	Arachnoid cyst	Follows CSF imaging characteristics			Nil
7	Mucocele	Isodense or hyperdense	Depends on protein content	Hyperintense	Nil
8	Epidermoid	Hypodense	Hypointense	Hyperintense	Mild or no enhancement
9	Teratoma	Fat and calcification	Hyperintense	Variable	Heterogeneous or no enhancement
10	Lipoma	Hypodense	Hyperintense	Hyperintense	Nil

Abbreviations: CSF, cerebrospinal fluid; CT, computed tomography; MRI, magnetic resonance imaging.

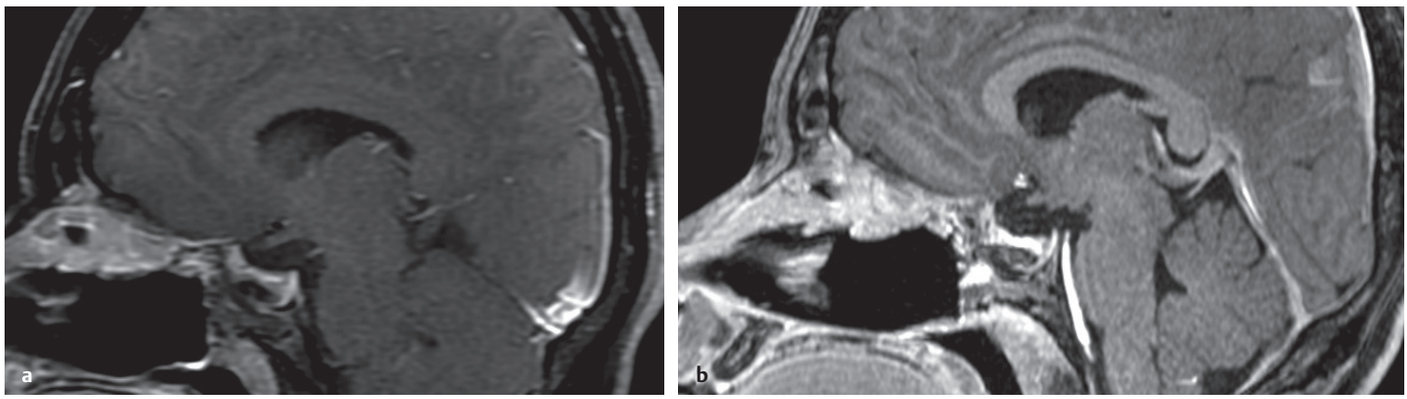

Fig. 3.61 **(a,b)** Sagittal postcontrast T1 showing enhancing postoperative Hadad flap with open cup configuration indicating a viable well-taken-up flap adherent to the skull base.

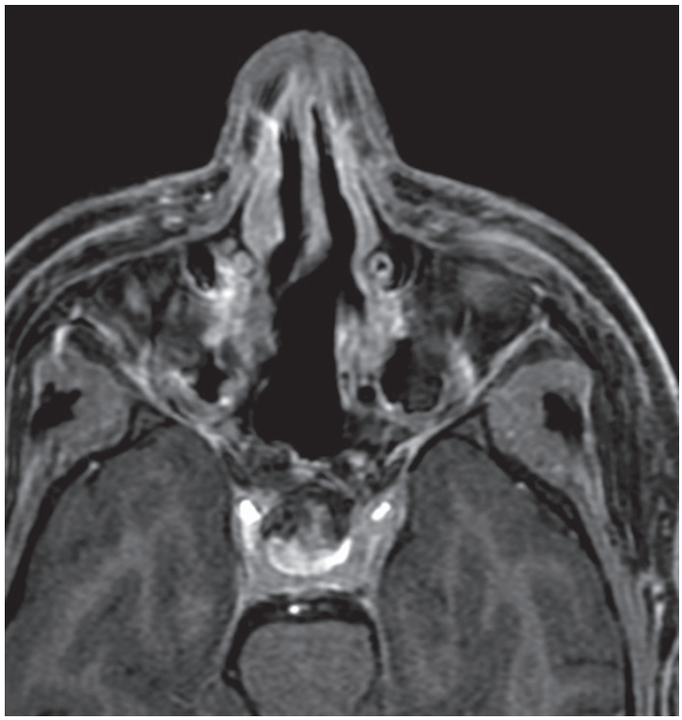

Fig. 3.62 Axial postcontrast T1 showing enhancing postoperative Hadad flap with open cup configuration indicating a viable well-taken-up flap adherent to the skull base.

  - Areas of nonenhancement suggest flap necrosis.
- Skull base flap displacement:
  - Open cup configuration suggests a nondisplaced flap.
  - Closed cup configuration suggests a displaced flap.

References

1. Carlos Zamora MD, Mauricio Castillo MD. Sellar and parasellar imaging. Neurosurgery 2017;80(1):17–38
2. Cheemum L, Walter K, Walter JM, Laurence EB. Magnetic Resonance Imaging of the Brain and Spine. Vol. 2. Philadelphia, PA: Lippincott Williams & Wilkins; 2002:1283–1362
3. Sakamoto Y, Takahashi M, Korogi Y, Bussaka H, Ushio Y. Normal and abnormal pituitary glands: gadopentetate dimeglumine-enhanced MR imaging. Radiology 1991;178(2):441–445
4. Dwyer AJ, Frank JA, Doppman JL, et al. Pituitary adenomas in patients with Cushing disease: initial experience with Gd-DTPA-enhanced MR imaging. Radiology 1987;163(2): 421–426
5. Yuh WT, Fisher DJ, Nguyen HD, et al. Sequential MR enhancement pattern in normal pituitary gland and in pituitary adenoma. AJNR Am J Neuroradiol 1994;15(1):101–108
6. Bonneville JF, Cattin F, Gorczyca W, Hardy J. Pituitary microadenomas: early enhancement with dynamic CT—implications of arterial blood supply and potential importance. Radiology 1993;187(3):857–861
7. Gao R, Isoda H, Tanaka T, et al. Dynamic gadolinium-enhanced MR imaging of pituitary adenomas: usefulness of sequential sagittal and coronal plane images. Eur J Radiol 2001;39(3): 139–146
8. Potorac I, Petrossians P, Daly AF, et al. Pituitary MRI characteristics in 297 acromegaly patients based on T2-weighted sequences. Endocr Relat Cancer 2015;22(2):169–177
9. Ahmadi J, North CM, Segall HD, Zee CS, Weiss MH. Cavernous sinus invasion by pituitary adenomas. AJR Am J Roentgenol 1986;146(2):257–262
10. Cottier JP, Destrieux C, Brunereau L, et al. Cavernous sinus invasion by pituitary adenoma: MR imaging. Radiology 2000; 215(2):463–469
11. Zagardo MT, Cail WS, Kelman SE, Rothman MI. Reversible empty sella in idiopathic intracranial hypertension: an indicator of successful therapy? AJNR Am J Neuroradiol 1996; 17(10):1953–1956
12. Swanson JA, Sherman BM, Van Gilder JC, Chapler FK. Coexistent empty sella and prolactin-secreting microadenoma. Obstet Gynecol 1979;53(2):258–263
13. Shimono T, Hatabu H, Kasagi K, et al. Rapid progression of pituitary hyperplasia in humans with primary hypothyroidism: demonstration with MR imaging. Radiology 1999;213(2):383–388
14. Chabot JD, Chakraborty S, Imbarrato G, Dehdashti AR. Evaluation of outcomes after endoscopic endonasal surgery for large and giant pituitary macroadenoma: a retrospective review of 39 consecutive patients. World Neurosurg 2015; 84(4):978–988
15. Agustsson TT, Baldvinsdottir T, Jonasson JG, et al. The epidemiology of pituitary adenomas in Iceland, 1955-2012: a nationwide population-based study. Eur J Endocrinol 2015;173(5):655–664
16. Ezzat S, Asa SL, Couldwell WT, et al. The prevalence of pituitary adenomas: a systematic review. Cancer 2004;101(3):613–619
17. Castillo M. Pituitary gland: development, normal appearances, and magnetic resonance imaging protocols. Top Magn Reson Imaging 2005;16(4):259–268
18. Miki Y, Matsuo M, Nishizawa S, et al. Pituitary adenomas and normal pituitary tissue: enhancement patterns on gadopentetate-enhanced MR imaging. Radiology 1990;177(1): 35–38
19. Bonneville JF, Bonneville F, Cattin F. Magnetic resonance imaging of pituitary adenomas. Eur Radiol 2005;15(3): 543–548
20. Hagiwara A, Inoue Y, Wakasa K, Haba T, Tashiro T, Miyamoto T. Comparison of growth hormone-producing and non-growth hormone-producing pituitary adenomas: imaging characteristics and pathologic correlation. Radiology 2003;228(2): 533–538
21. Vieira JO Jr, Cukiert A, Liberman B. Evaluation of magnetic resonance imaging criteria for cavernous sinus invasion in patients with pituitary adenomas: logistic regression

analysis and correlation with surgical findings. Surg Neurol 2006;65(2): 130–135, discussion 135
22. Inagawa H, Ishizawa K, Mitsuhashi T, et al. Giant invasive pituitary adenoma extending into the sphenoid sinus and nasopharynx: report of a case with intraoperative cytologic diagnosis. Acta Cytol 2005;49(4):452–456
23. Briet C, Salenave S, Chanson P. Pituitary apoplexy. Endocrinol Metab Clin North Am 2015;44(1):199–209
24. Oldfield EH, Merrill MJ. Apoplexy of pituitary adenomas: the perfect storm. J Neurosurg 2015;122(6):1444–1449
25. Azizyan A, Miller JM, Azzam RI, et al. Spontaneous retroclival hematoma in pituitary apoplexy: case series. J Neurosurg 2015;123(3):808–812
26. Sartoretti-Schefer S, Wichmann W, Aguzzi A, Valavanis A. MR differentiation of adamantinous and squamous-papillary craniopharyngiomas. AJNR Am J Neuroradiol 1997;18(1): 77–87
27. Lee HJ, Wu CC, Wu HM, et al. Pretreatment diagnosis of suprasellar papillary craniopharyngioma and germ cell tumors of adult patients. AJNR Am J Neuroradiol 2015;36(3):508–517
28. Fathi AR, Roelcke U. Meningioma. Curr Neurol Neurosci Rep 2013;13(4):337
29. Barshes N, Demopoulos A, Engelhard HH. Anatomy and physiology of the leptomeninges and CSF space. Cancer Treat Res 2005;125:1–16
30. DeMonte F. Surgical treatment of anterior basal meningiomas. J Neurooncol 1996;29(3):239–248
31. Nanda A, Konar SK, Maiti TK, Bir SC, Guthikonda B. Stratification of predictive factors to assess resectability and surgical outcome in clinoidal meningioma. Clin Neurol Neurosurg 2016;142:31–37
32. Parizel PM, Carpentier K, Van Marck V, et al. Pneumosinus dilatans in anterior skull base meningiomas. Neuroradiology 2013;55(3):307–311
33. Pieper DR, Al-Mefty O, Hanada Y, Buechner D. Hyperostosis associated with meningioma of the cranial base: secondary changes or tumor invasion. Neurosurgery 1999;44(4):742–746, discussion 746–747
34. Shah LM, Phillips CD. Imaging sellar and suprasellar pathology. Appl Radiol 2009; (September):24
35. Hamilton BE, Salzman KL, Osborn AG. Anatomic and pathologic spectrum of pituitary infundibulum lesions. AJR Am J Roentgenol 2007;188(3):W223-32
36. Kanagaki M, Miki Y, Takahashi JA, et al. MRI and CT findings of neurohypophyseal germinoma. Eur J Radiol 2004;49(3): 204–211
37. Tien RD, Newton TH, McDermott MW, Dillon WP, Kucharczyk J. Thickened pituitary stalk on MR images in patients with diabetes insipidus and Langerhans cell histiocytosis. AJNR Am J Neuroradiol 1990;11(4):703–708
38. Sato N, Sze G, Endo K. Hypophysitis: endocrinologic and dynamic MR findings. AJNR Am J Neuroradiol 1998;19(3):439–444
39. Bihan H, Christozova V, Dumas JL, et al. Sarcoidosis: clinical, hormonal, and magnetic resonance imaging (MRI) manifestations of hypothalamic-pituitary disease in 9 patients and review of the literature. Medicine (Baltimore) 2007;86(5):259–268
40. Prayer D, Grois N, Prosch H, Gadner H, Barkovich AJ. MR imaging presentation of intracranial disease associated with Langerhans cell histiocytosis. AJNR Am J Neuroradiol 2004;25(5):880–891
41. Schubiger O, Haller D. Metastases to the pituitary-hypothalamic axis: an MR study of 7 symptomatic patients. Neuroradiology 1992;34(2):131–134
42. Vijayanand P, Mahadevan S, So Shivbalan, Reddy N, Ramdoss N. Pituitary stalk interruption syndrome (PSIS). Indian J Pediatr 2007;74(9):874–875
43. Quencer RM. Lymphocytic adenohypophysitis: autoimmune disorder of the pituitary gland. AJNR Am J Neuroradiol 1980; 1(4):343–345
44. Osborn A, Blaser S, Salzman K. Sella and pituitary. In: Diagnostic Imaging: Brain. Salt Lake City, UT: Amirsys; 2004
45. Friedman TC, Zuckerbraun E, Lee ML, Kabil MS, Shahinian H. Dynamic pituitary MRI has high sensitivity and specificity for the diagnosis of mild Cushing's syndrome and should be part of the initial workup. Horm Metab Res 2007;39(6):451–456
46. Almefty K, Pravdenkova S, Colli BO, Al-Mefty O, Gokden M. Chordoma and chondrosarcoma: similar, but quite different, skull base tumors. Cancer 2007;110(11):2457–2467
47. Fernandez-Miranda JC, Gardner PA, Snyderman CH, et al. Clival chordomas: a pathological, surgical, and radiotherapeutic review. Head Neck 2014;36(6):892–906
48. Jahangiri A, Jian B, Miller L, El-Sayed IH, Aghi MK. Skull base chordomas: clinical features, prognostic factors, and therapeutics. Neurosurg Clin N Am 2013;24(1):79–88
49. Erdem E, Angtuaco EC, Van Hemert R, Park JS, Al-Mefty O. Comprehensive review of intracranial chordoma. Radiographics 2003;23(4):995–1009
50. Sze G, Uichanco LS III, Brant-Zawadzki MN, et al. Chordomas: MR imaging. Radiology 1988;166(1 Pt 1):187–191
51. Meyers SP, Hirsch WL Jr, Curtin HD, Barnes L, Sekhar LN, Sen C. Chordomas of the skull base: MR features. AJNR Am J Neuroradiol 1992;13(6):1627–1636
52. Choi D, Gleeson M. Surgery for chordomas of the craniocervical junction: lessons learned. Skull Base 2010;20(1):41–45
53. Blitz AM, Macedo LL, Chonka ZD, et al. High-resolution CISS MR imaging with and without contrast for evaluation of the upper cranial nerves: segmental anatomy and selected pathologic conditions of the cisternal through extraforaminal segments. Neuroimaging Clin N Am 2014;24(1):17–34

4 Perioperative Management for Anterior Skull Base Tumors

Vignesh G.

Introduction

Pituitary lesions are common in general population, which can present with varying clinical signs and symptoms.[1,2] Patient can present with either symptoms of hormonal hypo- or hypersecretion or tumor mass effects or both. Evaluation includes detailed clinical examination, hormonal workup, and pituitary imaging. Evaluation of pituitary hormonal function is essential in managing these tumors—both medical and surgical. Minimal set of preoperative endocrine investigations should include serum electrolytes, anterior pituitary hormones, and their target organ hormones. Assessment of pituitary function is essential at diagnosis, before surgery, and follow-up after surgery. Multidisciplinary team approach with endocrinologists, neurosurgeons/skull base surgeons, and neuroophthalmologists is essential for treatment planning.[3]

Preoperative Evaluation

All patients with pituitary lesion require a complete history of symptoms and detailed clinical examination including visual fields assessment. Formal visual field testing is essential if magnetic resonance imaging (MRI) shows sellar-suprasellar lesion abutting or compressing the optic chiasm. Endocrine hormonal evaluation should include serum electrolytes, free T4, thyroid-stimulating hormone (TSH), cortisol, prolactin (in dilution), testosterone, estradiol, follicle-stimulating hormone, luteinizing hormone, and insulin-like growth factor-1 (IGF-1). In patients with hyperprolactinemia and pituitary macroadenoma, tumoral hypersecretion of prolactin must be distinguished from hyperprolactinemia due to pituitary stalk compression.[4] Extremely high prolactin levels with macroprolactinomas may saturate the binding sites of prolactin antibody in immunoradiometric assays (IRMA).[4] This high-dose "hook effect" can artifactually lower prolactin values in assay. Sample dilution should always be done in patients with large adenomas with mildly elevated prolactin levels to rule out this "hook effect," thereby avoiding inappropriate surgery for macroprolactinomas. Medical management is the preferred initial modality of treatment for prolactin secreting adenomas.[4] Assessment of hypercortisolism should be done if there is clinical suspicion of Cushing's syndrome. Overnight dexamethasone suppression test is usually done for initial assessment of Cushing's syndrome.[5] Further assessment of endogenous hypercortisolism includes low-dose dexamethasone suppression test, 24-hour urinary-free cortisol levels, and midnight salivary cortisol. Measurement of IGF-1 or growth hormone suppression test should be done in patients with clinical suspicion of acromegaly.[6]

Assessment of pituitary hypofunction includes evaluation for central hypothyroidism, adrenal insufficiency, and hypogonadism. Pre- and perioperative replacement of deficient thyroxine and cortisol is essential for optimal surgical outcome. Replacement of sex steroids is usually deferred till long-term postoperative follow-up. Early morning cortisol should be measured for assessment of adrenal function. Basal cortisol less than 100 nmol/L (3 µg/dL) is suggestive of adrenal insufficiency. Basal cortisol greater than 450 nmol/L (18 µg/dL) rules out adrenal insufficiency. Stimulation testing may be required for intermediate values.[7] Secondary hypothyroidism is associated with low free-T4 levels and low, normal, or mildly elevated TSH levels. Central diabetes insipidus (DI) is rare with pituitary adenomas, though it commonly occurs with craniopharyngioma and hypothalamic lesions.[8] DI may by uncovered after glucocorticoid treatment for adrenal insufficiency. Acromegaly and Cushing's disease may be associated with diabetes mellitus, hypertension, or cardiac dysfunction. Evaluation of metabolic and cardiovascular function should be done in those patients.

Perioperative Management

There are several protocols for glucocorticoid management in peri- and postoperative periods. In steroid-sparing protocol, steroids would be withheld in patient with normal preoperative cortisol levels. Patient should be closely monitored for cortisol deficiency, and in the days following surgery, basal cortisol level is measured and glucocorticoid replacement is started if the value is suggestive of adrenal insufficiency.[7] A standard perioperative regimen comprises 50 to 100 mg of hydrocortisone at induction of anesthesia followed by 50 mg every 6 hourly or 10 mg/hour infusion for first day and tapered to regular replacement dose after 72 hours, depending on clinical progress.

Alterations in sodium and fluid balance are relatively common in early postoperative phase. DI may occur up to 30% of patients undergoing pituitary surgery.[8] DI presenting with polyuria and hypernatremia occurs more frequently than the syndrome of inappropriate antidiuretic hormone secretion (SIADH) manifesting with hyponatremia in the early postoperative period. Postoperative DI may be transient or permanent.[8] Transient DI usually occurs within 24 to 48 hours of surgery and usually resolves within few days. In a triphasic DI, first phase usually lasts for 5 to 7 days. Transition into second phase, i.e., antidiuretic phase of SIADH, is associated with decreased urine output and hyponatremia.[9] Duration of SIADH varies from 2 to 14 days after which the third chronic phase of DI occurs.[8] Diagnosis of DI is confirmed by continued hypotonic polyuria with serum hyperosmolality. If excess of fluid is administered intravenously during the perioperative period, which is then excreted appropriately in the postoperative period, incorrect diagnosis of DI may be made based on the resulting hypotonic polyuria. Therefore, diagnosis of DI should be made and treated only if the serum sodium is elevated concomitantly with the hypotonic polyuria. One study showed lower incidence of DI, when steroid-sparring protocol is followed. DI can be managed with desmopressin (DDAVP), as subcutaneous or intravenous (0.5–2 µg once daily) or intranasal (10 µg metered dose) or oral formulation (starting with 0.1–0.2 mg one to three times a day).[10] Intranasal DDAVP is usually deferred till improvement of nasal congestion after surgery. SIADH phase may also present with isolated hyponatremia. Mild hyponatremia (130–135 mmol/L) can be managed by fluid restriction and high salt diet. Vaptans, competitive vasopressin receptor antagonists, can be used in the setting of severe hyponatremia.

Long-Term Postoperative Management

It is recommended that all the patients should be evaluated for pituitary function at least 6 weeks after surgery.[11] Sometimes pituitary hormonal deficiency may recover postoperatively after the removal of adenoma compressing normal pituitary. Hence, all anterior pituitary hormonal axes are generally re-evaluated after surgery. If patient was treated with steroids perioperatively, long-term need of steroids should be evaluated. Basal cortisol level less than 100 nmol/L (3 µg/dL) is suggestive of adrenal insufficiency. Basal cortisol greater than 450 nmol/L (18 µg/dL) rules out adrenal insufficiency. Provocative testing of adrenocorticotropic hormone is reserved for intermediate values. Insulin tolerance test or cosyntropin stimulation test may be performed. Insulin tolerance test is not routinely performed due to risk of seizures or myocardial ischemia in susceptible individuals and need for close monitoring.[12] Cosyntropin stimulation test is commonly used because of ease of administration. Thyroxine replacement should be started along with or after steroid replacement. Low-normal fT4 may suggest mild central hypothyroidism. Thyroxine may be started in such patients if they have symptoms or the follow-up fT4 levels decreases by 20%.[13] Testosterone replacement in men with central hypogonadism should be initiated, if there is no contraindications.[14] Similarly, gonadal hormone replacement should be initiated in premenopausal women with central hypogonadism.

Postoperative MRI is usually performed at 12 weeks, when the surgical changes interfering with optimal interpretation resolves.[15,16] Periodic clinical assessment after 12 weeks of surgery is dictated by clinical condition of patient, need for titration of hormone replacement, and any persistent pituitary hormone hypersecretion. Pituitary imaging on follow-up depends on tumor type, residual tumor after surgery, and biochemical parameters. Many require individualized treatment based on their clinical and biochemical remission after surgery.

Conclusion

Multidisciplinary team approach with endocrinologists, skull base surgeon/neurosurgeon, and neuro-ophthalmologist is essential for evaluation and treatment of pituitary tumors. Treatment of pituitary hormonal hyper- or

hyposecretion and associated comorbidities is necessary to optimize the overall quality of life. All patients require lifelong observation for optimal hormonal management and monitoring for tumor recurrence (**Flowchart 4.1**).

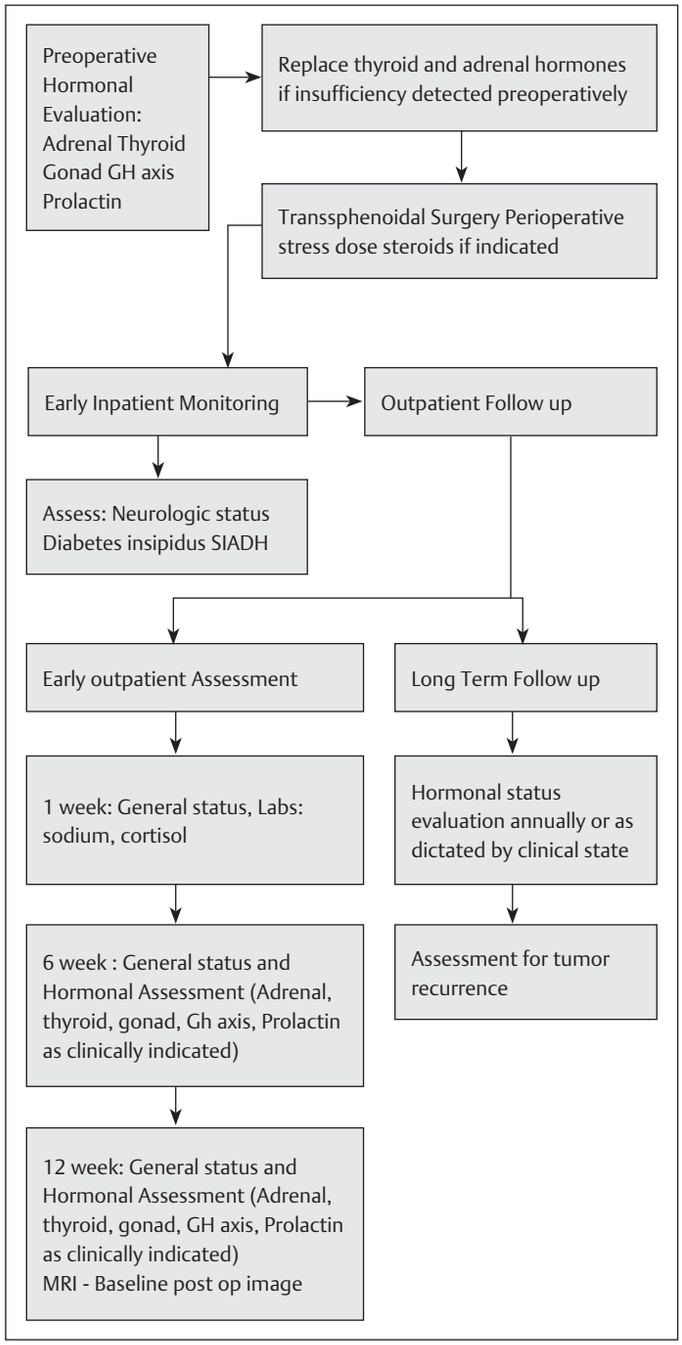
Preoperative Hormonal Evaluation: Adrenal Thyroid Gonad GH axis Prolactin
Replace thyroid and adrenal hormones if insufficiency detected preoperatively
Transsphenoidal Surgery Perioperative stress dose steroids if indicated
Early Inpatient Monitoring
Outpatient Follow up
Assess: Neurologic status Diabetes insipidus SIADH
Early outpatient Assessment
Long Term Follow up
1 week: General status, Labs: sodium, cortisol
Hormonal status evaluation annually or as dictated by clinical state
6 week : General status and Hormonal Assessment (Adrenal, thyroid, gonad, Gh axis, Prolactin as clinically indicated)
Assessment for tumor recurrence
12 week: General status and Hormonal Assessment (Adrenal, thyroid, gonad, GH axis, Prolactin as clinically indicated)
MRI - Baseline post op image

Flowchart. 4.1 Postoperative management following pituitary surgery. GH, growth hormone; SIADH, syndrome of inappropriate antidiuretic hormone. *(Source: American Association of Clinical Endocrinologists' perioperative management of pituitary tumors.)*

References

1. Ezzat S, Asa SL, Couldwell WT, et al. The prevalence of pituitary adenomas: a systematic review. Cancer 2004;101(3):613–619
2. Scangas GA, Laws ER Jr. Pituitary incidentalomas. Pituitary 2014;17(5):486–491
3. McLaughlin N, Laws ER, Oyesiku NM, Katznelson L, Kelly DF. Pituitary centers of excellence. Neurosurgery 2012;71(5):916–924, discussion 924–926
4. Melmed S, Casanueva FF, Hoffman AR, et al; Endocrine Society. Diagnosis and treatment of hyperprolactinemia: an Endocrine Society Clinical Practice guideli ne. J Clin Endocrinol Metab 2011;96(2):273–288
5. Nieman LK, Biller BM, Findling JW, et al. The diagnosis of Cushing's syndrome: an Endocrine Society Clinical Practice guideline. J Clin Endocrinol Metab 2008;93(5):1526–1540
6. Katznelson L, Atkinson JL, Cook DM, Ezzat SZ, Hamrahian AH, Miller KK; American Association of Clinical Endocrinologists. American Association of Clinical Endocrinologists medical guidelines for clinical practice for the diagnosis and treatment of acromegaly: 2011 update. Endocr Pract 2011;17(Suppl 4): 1–44
7. Inder WJ, Hunt PJ. Glucocorticoid replacement in pituitary surgery: guidelines for perioperative assessment and management. J Clin Endocrinol Metab 2002;87(6):2745–2750
8. Loh JA, Verbalis JG. Diabetes insipidus as a complication after pituitary surgery. Nat Clin Pract Endocrinol Metab 2007;3(6): 489–494
9. Kelly DF, Laws ER Jr, Fossett D. Delayed hyponatremia after transsphenoidal surgery for pituitary adenoma: report of nine cases. J Neurosurg 1995;83(2):363–367
10. Di Iorgi N, Napoli F, Allegri AE, et al. Diabetes insipidus: diagnosis and management. Horm Res Paediatr 2012;77(2):69–84
11. Fleseriu M, Hashim IA, Karavitaki N, et al. Hormonal replacement in hypopituitarism in adults: an Endocrine Society Clinical Practice guideline. J Clin Endocrinol Metab 2016; 101(11):3888–3921
12. Erturk E, Jaffe CA, Barkan AL. Evaluation of the integrity of the hypothalamic-pituitary-adrenal axis by insulin hypoglycemia test. J Clin Endocrinol Metab 1998;83(7):2350–2354
13. Alexopoulou O, Beguin C, De Nayer P, Maiter D. Clinical and hormonal characteristics of central hypothyroidism at diagnosis and during follow-up in adult patients. Eur J Endocrinol 2004; 150(1):1–8
14. Snyder PJ, Peachey H, Berlin JA, et al. Effects of testosterone replacement in hypogonadal men. J Clin Endocrinol Metab 2000;85(8):2670–2677
15. Dina TS, Feaster SH, Laws ER Jr, Davis DO. MR of the pituitary gland postsurgery: serial MR studies following transsphenoidal resection. AJNR Am J Neuroradiol 1993;14(3):763–769
16. Rajaraman V, Schulder M. Postoperative MRI appearance after transsphenoidal pituitary tumor resection. Surg Neurol 1999;52(6):592–598, discussion 598–599

5 Anesthetic Considerations in the Surgery for Sellar, Suprasellar, and Parasellar Lesions

Balamurugan Chinnasamy

Introduction

The perioperative anesthetic care of patients presenting for *sellar, suprasellar,* and *parasellar lesions* requires careful preoperative assessment and postoperative management. Problems in these patients are due to:

- Primary hormonal hypersecretion and its complications.
- Mass effects of the tumor.

This review intends to present the crucial issues for the safe anesthetic management of these challenging patients.

As the anatomical, physiological, and pathological disease considerations are already detailed in previous chapters, here we will discuss the clinical presentations that one has to consider for the anesthetic management.

Presentation

Pituitary lesions may present in as:

- Hormonal hypersecretion syndromes: hyperprolactinemia, acromegaly, and Cushing's disease.
- Mass effect: visual disturbance or raised intracranial pressure.
- Nonspecific: infertility, headache, epilepsy, etc.
- Incidental: those detected during imaging for other complaints.
- Rare: Pituitary apoplexy following hemorrhage into an adenoma, causing sudden endocrine alterations, presenting as headache, meningism, visual impairment, and other signs of space-occupying lesions.[1]

Preoperative Assessment

Preanesthetic assessment of a neurosurgical patient, which involves radiological studies and evaluation of hormone evaluation, should include an assessment of:

- Visual function: documentation of visual fields is mandatory.
- Signs and symptoms of raised intracranial pressure: to exclude lesions, like hydrocephalus, computed tomography or preferably magnetic resonance imaging should be performed.[2]
- The endocrine assessments.
- Hormonal hypersecretion effect.
  - (i) Acromegaly is recognized as one of the causes of difficult airway management and tracheal intubation. Careful airway assessment using conventional criteria and preoperative evaluation is indicated. Sleep apnea in acromegaly is associated with a high risk of perioperative airway compromise.[3] Cardiac evaluation is required to rule out hypertension, myocardial hypertrophy, and interstitial fibrosis. Glucose intolerance may occur in acromegalic patients.
  - (ii) Cushing's syndrome may present with hypertension, electrocardiographic (ECG) abnormalities (high voltage QRS complexes, and inverted T waves), left ventricular hypertrophy, and asymmetric septal hypertrophy. Other notable points to consider are glucose intolerance, obesity, gastroesophageal reflux, fragile skin, and easy bruising.[4]

Anesthetic Management

It is not the intention of this review to deal with all the aspects of neuroanesthesia; instead, we consider only the issues related to pituitary surgery. The general aims of anesthesia include hemodynamic stability, maintenance of cerebral oxygenation, provision of conditions to facilitate surgical exposure, prevention of intraoperative complications, and rapid emergence to facilitate early neurological assessment.

Hormone Replacement

Preoperative hormone replacement therapy should be continued into the operative period. In general, hydrocortisone 100 mg should be administered at the induction of anesthesia in all patients undergoing pituitary surgery.[5]

Airway Management

Careful preoperative assessment is done to diagnose the difficult.

- Four grades of airway involvement have been described in *acromegaly*:
  - Grade 1: no significant involvement.
  - Grade 2: nasal and pharyngeal mucosa hypertrophy but normal cords and glottis.
  - Grade 3: glottic involvement including glottic stenosis or vocal cord paresis.
  - Grade 4: combination of Grades 2 and 3, i.e., glottic and soft tissue abnormalities.

We perform fiberoptic intubation in patients with difficult airway management.[6] Equipment for tracheostomy should be available if airway changes are advanced.

Soon after intubation, the mouth and posterior pharynx should be packed before surgery. This will prevent bleeding into the glottic region during surgery, and entry of blood and secretions into the stomach, which may precipitate postoperative vomiting. The tracheal tube must be positioned to allow the neurosurgeon's access to the chosen incision site.

Preparation of the Nasal Mucosa

Most surgeons prefer to introduce a vasoconstriction agent into each nostril before transsphenoidal surgery. Xylometazoline, sympathomimetic amine acting at α adrenoreceptors, may be preferred. It produces rapid and prolonged vasoconstriction lasting up to 8 hours and, when combined with lidocaine, its effects are equivalent to traditional cocaine.[7,8]

Lumbar Drain

Few surgeons request insertion of a lumbar drain in patients with significant suprasellar tumor extension. This has two uses:

- Introduction of 10-mL aliquots of 0.9% saline, during transsphenoidal surgery, produce prolapse of the suprasellar portion of the tumor into the operative field.
- Besides, should the dura be breached during the procedure, the catheter can be left in place postoperatively to act as a cerebrospinal fluid (CSF) drain in an attempt to control any leak of CSF.

Position

Transsphenoidal surgery is performed with the patient in supine position with a moderate degree of head-up tilt. The head may be turned slightly to the side to facilitate surgical access. The surgeon may stand at the top of the table, behind the head, or to the right or left. The tracheal tube and the anesthetic circuit should be placed away from the surgical field. Care should be taken to ensure that the neck veins are not obstructed.

Induction and Maintenance of Anesthesia

All the patients should have large-bore intravenous access for rapid volume resuscitation. A reinforced orotracheal tube is recommended, positioned in the left corner of the mouth. A throat pack is inserted and ensured that it is removed before extubation.

While deciding the technique of anesthesia, the basic principles of neuroanesthesia should be followed.

Choice of anesthetic technique is usually determined by personal preference, tailor-made to suit the patient's requirements. The merits of inhalational and total intravenous techniques during neuroanesthesia are not discussed here, although neither is superior to the other under most circumstances.

In the presence of raised intracranial pressure, total intravenous anesthesia and the avoidance of nitrous oxide have been recommended.[9] Whichever technique is chosen, it is important that short-acting agents are used to allow rapid recovery at the end of surgery. Drugs such as propofol and sevoflurane are preferred. During transsphenoidal surgery, ventilation to normocapnia should be employed. Excessive hyperventilation will result in the loss of brain bulk and make any suprasellar extension of the tumor less accessible from below. There are periods of intense stimulation during transsphenoidal access to the pituitary fossa. The ultrashort-acting opioid, Remifentanil, allows maintenance of stable conditions in neurosurgical patients and is useful during transsphenoidal surgery.[10] Its short half-life ensures rapid offset of action when the infusion is discontinued and allows rapid emergence from anesthesia.

Monitoring

Monitoring during pituitary surgery will include ECG, SpO_2, end tidal carbon dioxide, and direct arterial blood pressure. In Cushing's syndrome, patients may require additional invasive cardiovascular monitoring. If cavernous sinus invasion is suspected, and the patient is positioned in a steep head-up tilt, monitoring for the possibility of venous air embolus should be considered. Visual evoked potential (VEP) recording has been recommended for tumor surgery in the region of the visual pathways. The sensitivity of VEPs to anesthetic agents has led some to suggest that, during anesthesia, the waveforms are too unstable to be of much practical use.[11]

Prophylactic Antibiotics

Some neurosurgeons do not use prophylaxis and claim no problems; most units have adopted a consensus policy that involves the administration of a cephalosporin, at the induction of anesthesia and every 3 hours thereafter during surgery. No further doses are given in the postoperative period, to minimize the development of resistant organisms.

Intraoperative Complications

Complications during transsphenoidal surgery are rare. Pituitary tumors are not usually vascular and the slight venous ooze that inevitably occurs can be controlled easily by gentle pressure.

If carotid injury occurs, it is controlled by packing. As there is a risk of a false aneurysm in the postoperative period, carotid angiography should be performed. If an aneurysm is confirmed, it should be treated by endovascular radiological techniques or by clipping to prevent later rupture. If the surgeon misses the fossa altogether, damage to the Pons may occur, which has serious consequences. The risk of these complications is minimized by frequent radiographic confirmation of the position during transsphenoidal surgery.

Emergence

Smooth and rapid emergence from anesthesia following neurosurgery is essential to allow early neurological assessment and maintenance of stable respiratory and cardiovascular variables. This is facilitated by the use of short-acting agents for the maintenance of anesthesia.

At the end of transsphenoidal surgery, extubation is performed after the return of spontaneous ventilation, pharyngeal suction under direct vision, removal of the throat pack, and return of laryngeal reflexes. Smooth emergence is facilitated by placing the patient in a semiseated position and ensuring that there is a response to verbal commands before extubation.

Care should be taken to ensure that nasal packs or stents, put in place at the end of the surgery, do not become dislodged during extubation.

Postoperative Care

It includes careful airway management, provision of adequate postoperative analgesia, appropriate fluid and hormone replacement, and careful monitoring for postoperative complications. After a brief observation in the recovery room, the patient may usually be returned to a general ward. After transcranial pituitary surgery, patients should be managed in a neurosurgical intensive care or high-dependency unit for at least 24 hours.

Airway Management

Maintenance of a clear airway is difficult and requires careful attention. All patients must be closely observed after

transsphenoidal surgery until fully awake. Airway management is particularly vital in acromegalic patients, especially in those with a history of sleep apnea. These patients are to be nursed in a high-dependency units during the first postoperative night when hypoventilation and respiratory obstruction may occur. Usual treatment options such as nasal continuous positive airway pressure (CPAP) cannot be applied after transsphenoidal surgery.

Postoperative Analgesia

Transsphenoidal surgery usually causes only moderate postoperative pain, but the feeling of nasal congestion from the presence of nasal packs is frequently distressing to patients. Craniotomy is more painful and stronger analgesia is required. Intravenous morphine administered via a patient-controlled analgesia has been used successfully in neurosurgical patients. The perioperative use of acetaminophen (or Paracetamol) is opioid-sparing and is recommended.[12]

Diabetes Insipidus

Diabetes insipidus usually develops within the first 24 hours. It should be suspected if the patient is producing >1 L of dilute urine in 12 hours, associated with a plasma Na^+ concentration of >143 mmol/L. Urine output and specific gravity should be measured routinely after pituitary surgery.

Modest polyuria in the early postoperative period may be due to delayed excretion of the fluid given during surgery or corticosteroid-induced hyperglycemia. Patients may feel thirsty after transsphenoidal surgery, but this can be due to mouth breathing because of nasal packs rather than diabetes insipidus. The diagnosis of diabetes insipidus must be confirmed biochemically before the treatment is started by the following criteria:

- Increased plasma osmolality (>295 mosmol/kg).
- Hypotonic urine (<300 mosmol/kg).
- A high urine output (>2 mL/kg/h). These are the criteria on which the diagnosis should be based.

Diabetes insipidus is easily treated with desmopressin acetate (DDAVP). If the patient is awake and has a normal thirst mechanism, it is safest to allow free access to fluid rather than attempt overzealous intravenous (IV) fluid and DDAVP replacement. Overenthusiastic use of DDAVP may lead to hyponatremia with its attendant problems of confusion, seizures, and coma. Most cases of diabetes insipidus resolve spontaneously over a few days, as posterior lobe function recovers. Comatose patients, those with no thirst response and the minority in whom urine volumes are excessively large, are at particular risk, both from underhydration as a consequence of the diabetes insipidus or of overhydration as a consequence of therapy. Careful treatment with DDAVP will usually be required under such circumstances. The recommended IV/intramuscular dose of DDAVP is 0.1 µg repeated as required. In the acute phase, a smaller dose of 0.04 µg IV provides an adequate response with a shorter duration of action. Plasma Na^+ concentration and osmolality should be closely monitored until normal water balance has been re-established. Long-term DDAVP therapy is required in only a minority of the cases.

Hyponatremia

- The usual cause of hyponatremia after pituitary surgery is overzealous use of DDAVP.
- It may occur because of the syndrome of inappropriate antidiuretic hormone secretion (SIADH) caused by nonspecific release of antidiuretic hormone from degenerating posterior pituitary neurosecretory terminals.[13] This results in water retention and secondary loss of urinary Na^+. It is usually transitory and rarely lasts for >7 to 10 days. It is managed by fluid restriction which should be carefully monitored by the regular measurement of plasma electrolytes.
- Rarely, hyponatremia after intracranial neurosurgery may be associated not only with natriuresis but also with a tendency to diuresis, leading to a significant contraction of circulating and extracellular volumes.[14] This phenomenon is known as cerebral salt wasting (CSW) syndrome and may be difficult to differentiate from SIADH. It is crucial that the diagnosis is made correctly because the treatment regimens of the two conditions are diametrically opposed. In SIADH, the problem is one of extracellular volume expansion caused by water retention, and the best approach is to limit the water intake from 500 to 1,000 mL/day depending upon the plasma Na^+ concentration.[15] In CSW, the fluid restriction will not correct the hyponatremia and be harmful because it will further reduce intravascular volume. Hypertonic saline is used to correct the hyponatremia of CSW. Correction of low

Na^+ concentrations should always take place over 24 to 48 hours, at a rate to increase the plasma Na^+ concentration by <1 mmol/h. Too rapid correction may result in the central pontine myelinolysis.

Pituitary Apoplexy

The term is defined as acute hemorrhagic infarction of a gland whose blood supply is earlier compromised by a tumor or pregnancy. Characteristic features are severe headache, nausea and vomiting, visual field defects, and cranial nerve palsies. It is managed by treating adrenocortical failure with intravenous fluids, urgent transsphenoidal decompression, and replacement of hydrocortisone.

Conclusion

Pituitary surgery involves a multidisciplinary approach consisting of an endocrinologist, the neurosurgeon, radiologist, and the anesthesiologist. Their teamwork and coordination is of immense importance. Preoperative optimization of systemic diseases due to pituitary involvement must be performed. Appropriate anesthetic management based on patient's disease and surgical procedure should be performed intraoperatively. Fast recovery from anesthesia is vital because early neurological assessment can disclose most serious surgical complications.

References

1. Molitch ME. Management of prolactinomas. Annu Rev Med 1989;40:225–232
2. Levy A, Lightman SL. Diagnosis and management of pituitary tumours. BMJ 1994;308(6936):1087–1091
3. Burn JM. Airway difficulties associated with anaesthesia in acromegaly. Br J Anaesth 1972;44(4):413–414
4. Crapo L. Cushing's syndrome: a review of diagnostic tests. Metabolism 1979;28(9):955–977
5. Bornstein SR, Allolio B, Arlt W, et al. Diagnosis and treatment of primary adrenal insufficiency: An Endocrine Society Clinical Practice Guideline. J Clin Endocrinol Metab. 2016 Feb;101(2):364-89
6. Ovassapian A. Fiberoptic Airway Endoscopy in Anesthesia and Critical Care. New York, NY: Raven Press;1990
7. Campbell JP, Campbell CD, Warren DW, Prazma TU, Pillsbury HC III. Comparison of the vasoconstrictive and anesthetic effects of intranasally applied cocaine vs. xylometazoline/lidocaine solution. Otolaryngol Head Neck Surg 1992;107(5):697–700
8. Chiu YC, Brecht K, DasGupta DS, Mhoon E. Myocardial infarction with topical cocaine anesthesia for nasal surgery. Arch Otolaryngol Head Neck Surg 1986;112(9):988–990
9. Ravussin P, de Tribolet N, Wilder-Smith OHG. Total intravenous anesthesia is best for neurological surgery. J Neurosurg Anesthesiol 1994;6(4):285–289
10. Guy J, Hindman BJ, Baker KZ, et al. Comparison of remifentanil and fentanyl in patients undergoing craniotomy for supratentorial space-occupying lesions. Anesthesiology 1997;86(3):514–524
11. Cedzich C, Schramm J, Mengedoht CF, Fahlbusch R. Factors that limit the use of flash visual evoked potentials for surgical monitoring. Electroencephalogr Clin Neurophysiol 1988;71(2):142–145
12. Powell M, Lightman SL. Post-operative management. In: Powell M, Lightman SL, eds. The Management of Pituitary Tumours: A Handbook. London: Churchill Livingstone 1996; 145–58
13. Cusick JF, Hagen TC, Findling JW. Inappropriate secretion of antidiuretic hormone after transsphenoidal surgery for pituitary tumors. N Engl J Med 1984;311(1):36–38
14. Kelly DF, Laws ER Jr, Fossett D. Delayed hyponatremia after transsphenoidal surgery for pituitary adenoma. Report of nine cases. J Neurosurg 1995;83(2):363–367
15. Lolin Y, Jackowski A. Hyponatraemia in neurosurgical patients: diagnosis using derived parameters of sodium and water homeostasis. Br J Neurosurg 1992;6(5):457–466

6 Reconstructive Options in the Surgery for Sellar, Suprasellar, and Parasellar Lesions

Joseph Nadakkavukaran, Shilpee Bhatia Sharma, Narayanan Janakiram

Introduction

Endoscopic skull base reconstructive (ESBR) techniques have been the rate-limiting step in endoscopic approaches to the skull base. Recent evolution seen in this field has led to a paradigm shift and has revolutionized endoscopic management of skull base lesions. Currently the expanded endoscopic endonasal approaches (EEAs) to the anterior, middle, and the posterior cranial fossa uses various endoscopic corridors such as transcribiform, transplanum, transtuberculum, transsellar, transclival, and transodontoid routes[1] (**Fig. 6.1**). Postoperative CSF leak is the most relevant primary outcome measure which reflects the success of ESBR. The use of vascularized pedicle flaps has dramatically reduced the incidence of postoperative CSF leaks to less than 5%.[2–5] In the authors' experience, the incidence of postoperative CSF leak is around 3 to 5% by using multilayer closure with vascularized pedicle flaps.

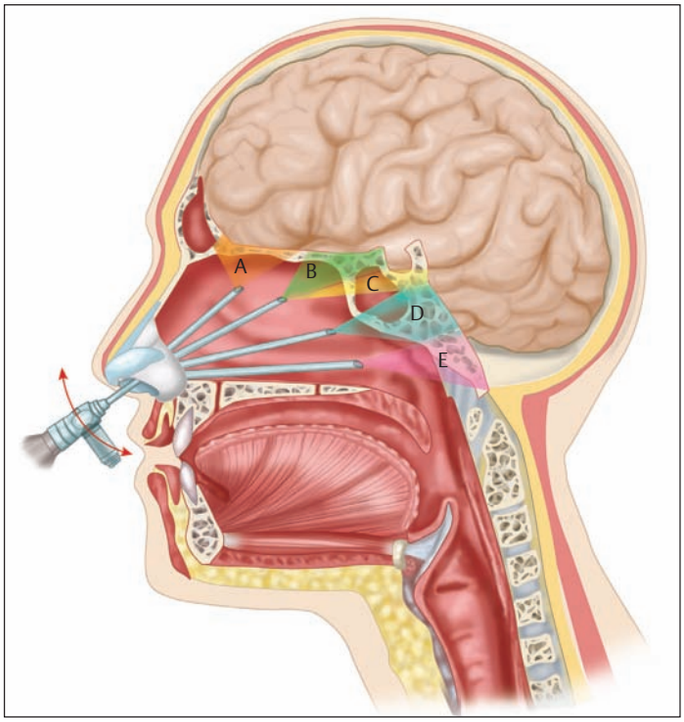

Fig. 6.1 Illustration showing various endoscopic skull base corridors: **(A)** transcribriform, **(B)** transplanar/transtubercular, **(C)** transsellar, **(D)** transclival, and **(E)** transodontoid.

Goals of Endoscopic Skull Base Reconstruction

- The primary goal is to create an effective watertight seal separating the cranial and the sinonasal cavity, preventing postoperative CSF leak and ascending intracranial infection such as meningitis, encephalitis, and intracranial abscess formation.[6–9] This can be achieved using multilayer closure techniques with onlay vascularized pedicle flap grafting, reestablishing the spatial integrity of the region.[10–15]
- Decrease dead space seen after tumor removal (**Fig. 6.2**).
- Reestablishing the lining and drainage of the sinonasal cavities.
- Promote faster wound healing.
- Providing adequate coverage and supporting exposed or prolapsing brain tissue, vital neurovascular structures, and orbital contents preserving neurovascular and ocular function[16] (**Fig. 6.3**).

Selection of Reconstructive Measures

Selection of appropriate reconstructive measure depends on the following factors:

- Patient-related factors
  - Age and sex.
  - Presence of comorbidities such as obesity, increased intracranial pressure (ICP),[17,18] Cushing's syndrome, and diabetes (poor wound healing).[9,10]

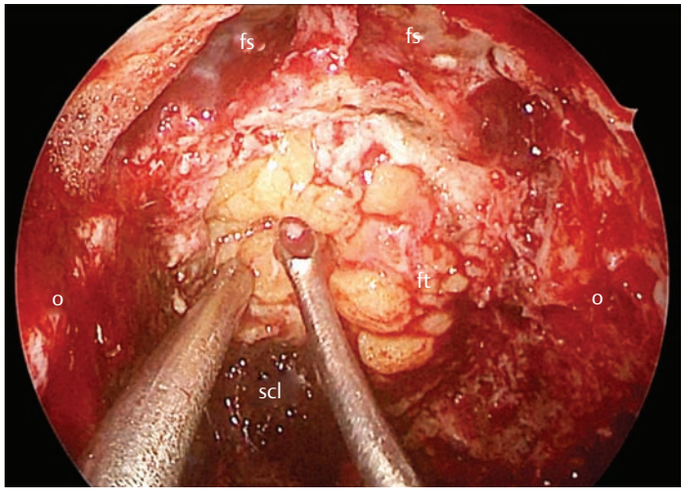

Fig. 6.2 Defect filled with autologous dumbbell fat.

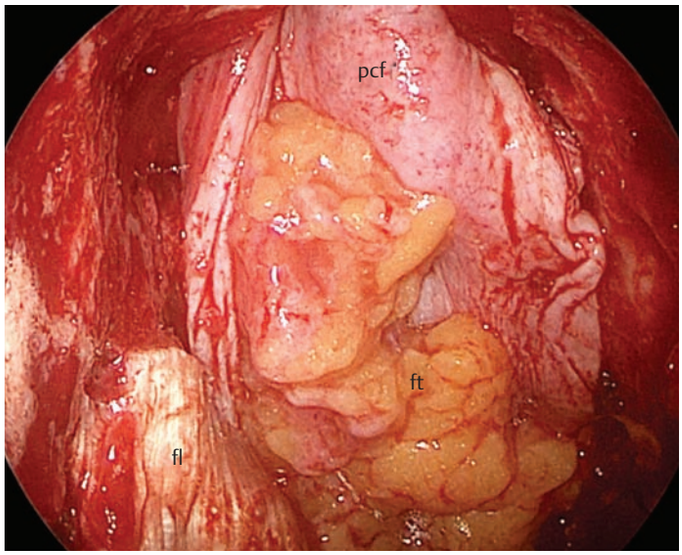

Fig. 6.3 Pericranial flap is positioned over the fascia lata and autologous fat is used to support the flap. Note: another layer of fascia lata is used to cover orbital contents on the right.

- Prior history of radiotherapy, leading to devascularization of the graft bed.[6,10,19,20]
- Prior history of nasal surgery and the availability of local pedicle flaps.

- Disease-related factors
  - Benign or malignant pathology dictating the extent of resection.
  - Need for postoperative chemotherapy or radiotherapy.
- Approach-related and intraoperative factors
  - Selected approach and the possibility of preserving a local pedicle flap.
  - Resultant skull base defect location and dimension.
    1. Defects <1 cm can be managed with free mucosal grafts,[21–23] fat, fascia, and other graft support materials.[21]
    2. Larger defects specially those >3 cm requires multilayer closure with the use of vascularized pedicle flaps as an onlay graft.[10–15]
  - Degree of dural resection and arachnoid dissection.[9]
  - Presence of intraoperative CSF leak.
    1. High-flow leak necessitates the use of a vascularized pedicle flap, CSF diversion procedures such as a lumbar drain, ventriculoperitoneal (VP) or thecoperitoneal (TP) shunt, and the use of acetazolamide to decrease CSF production.[9,10,22,24,25]
    2. Low-flow leaks generally require only vascularized pedicle flap reconstruction.
  - Potential for retention of a bony rim around the defect for graft support.[9]

General Principles

Surrounding dura and bone should be cleared of surgical debris to prepare the graft bed. Nasal mucosa that comes in contact with the flap should be denuded off the bone to prevent delayed mucocele formation.[9]

In this chapter, multilayer closure technique has been described, which is the preferred technique in most cases[10–15] (**Fig. 6.4**).

- **Intracranial inlay grafting:** Autologous tissue such as fat (**Fig. 6.2**),[20,22] cartilage, and/or synthetic materials (Surgicel, Duraform, or DuraGen) are used as inlay grafts[9] (**Figs. 6.5 and 6.6**). It is positioned as a subdural layer (between the dura and the arachnoid) or as an epidural layer (between the bone and the dura)[20] (**Figs. 6.7 and 6.8**). The grafting material should be at least 1 cm greater than the dimensions of the bony defect.[9] "Gasket seal" closure as described by Leng et al can be employed in select cases where a soft graft such as fascia lata is placed over the defect overlapping the surrounding bone. A harder graft such as cartilage or bone is fashioned to almost the same size as the defect and is placed over the fascia and gently pushed in to countersink into the defect[26] (**Fig. 6.9**). Cases where dural resection has been performed, care should be taken to juxtapose the graft with dural margins.
- **Extracranial onlay grafting:** The grafting material, fascia lata[8,27] with free mucosa or vascularized flap, is

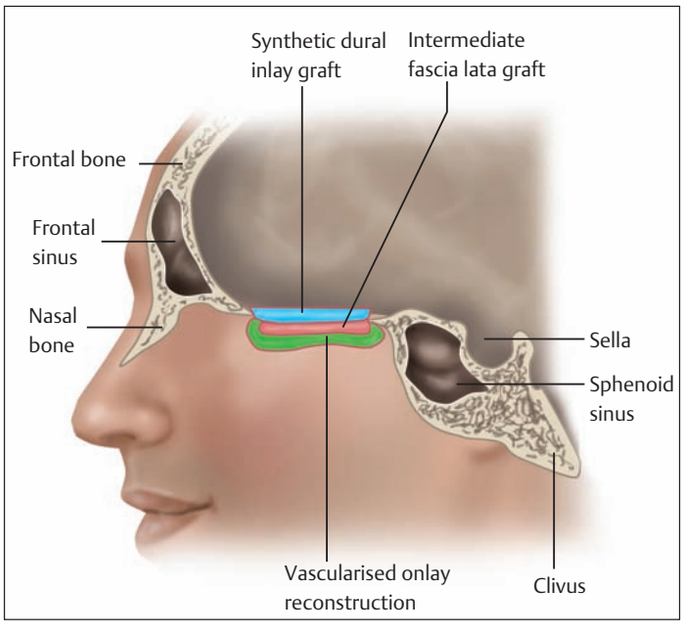

Fig. 6.4 Illustration showing multilayer closure technique using inlay and onlay grafting.

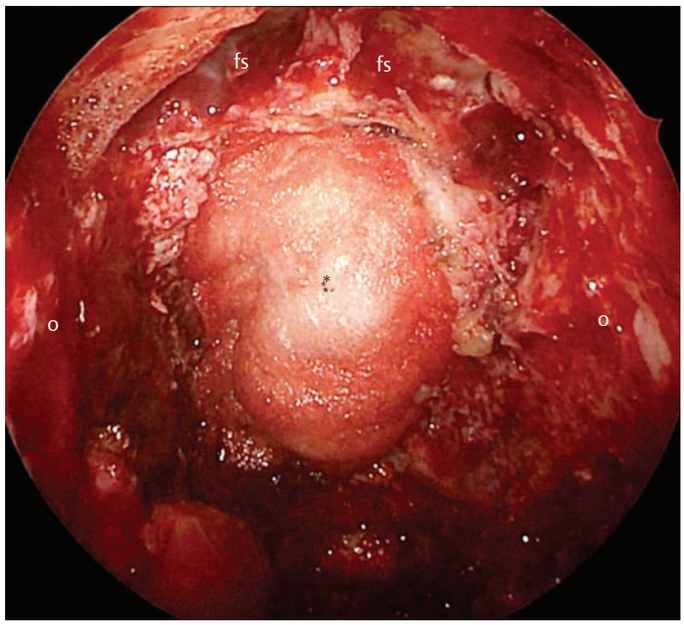

Fig. 6.5 Duraform (*) used as an extradural inlay layer.

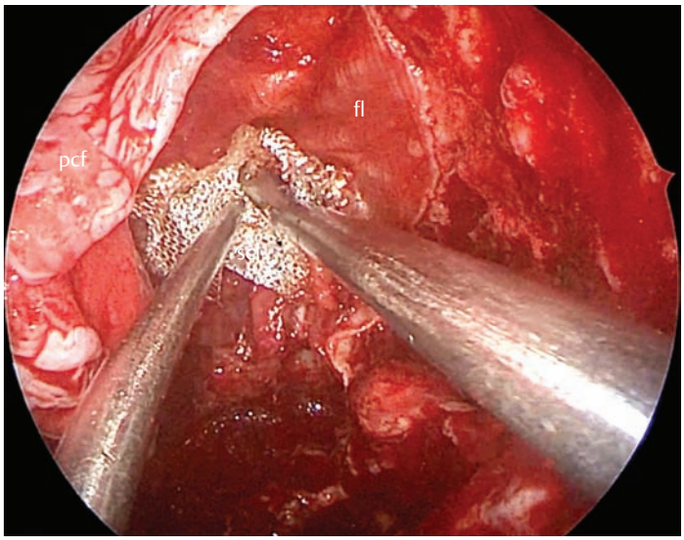

Fig. 6.6 Surgicel placed over fascia lata.

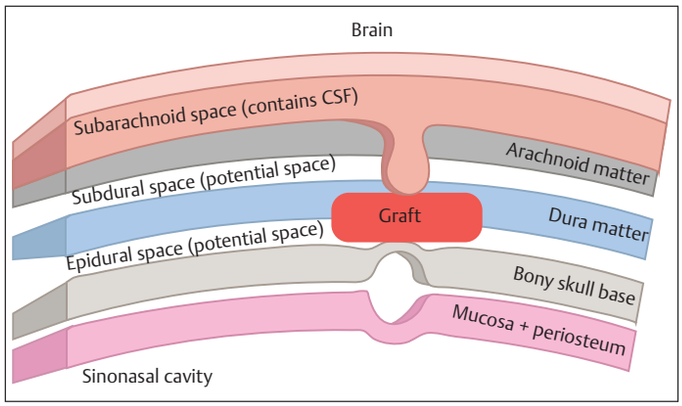

Fig. 6.7 Illustration showing extradural inlay grating between the bony skull base and the dura matter.

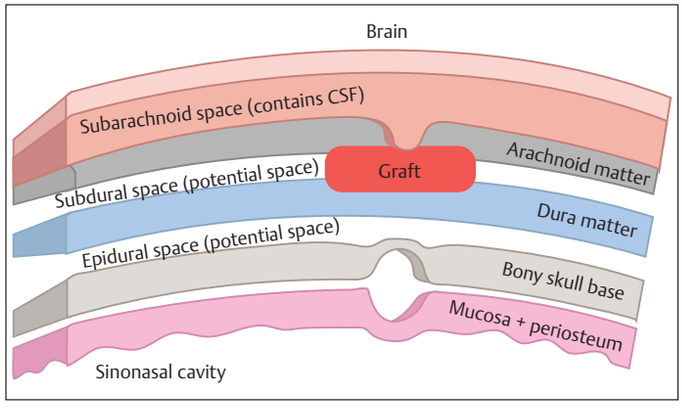

Fig. 6.8 Illustration showing intradural inlay grating between the dura and the arachnoid matter.

fashioned such that it is at least 1 cm greater than the dimensions of the bony defect and is directly placed on it (**Figs. 6.6 and 6.10**). Free mucosal graft or pedicle flap is then placed over the fascia lata again, overlapping the surrounding bone.

- **Free mucosal graft:** It is harvested from the turbinates, septum, or the nasal floor and is positioned over the defect and the surrounding bone such that the mucosal surface faces toward the nasal cavity.[18,28,29]

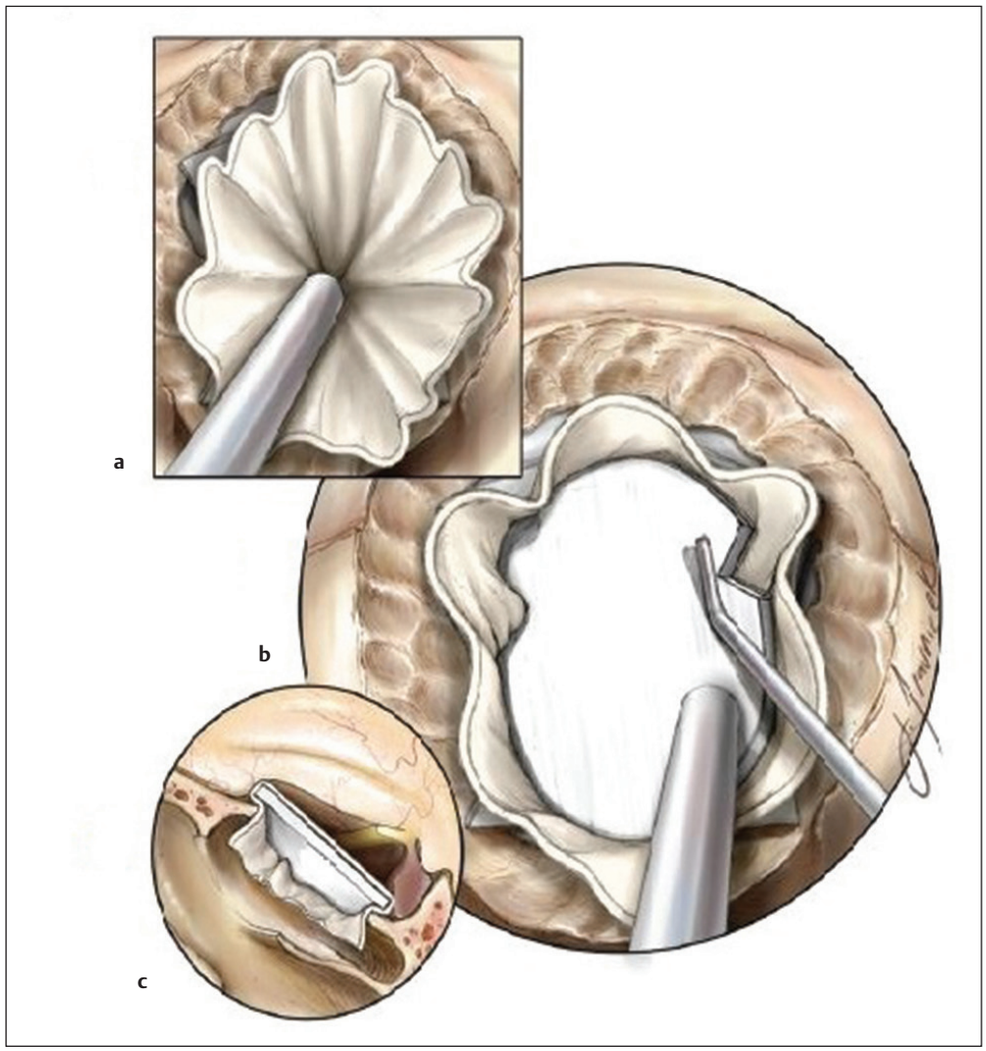

Fig. 6.9 Illustration showing **(a)** Gasket seal technique using dural substitute or fascia lata that is 1 cm larger than the dural opening. (**b, c**) Cartilage fashioned to be almost the same size of the bony defect, is placed over the dural substitute or fascia lata layer. Gentle pressure is applied over the cartilage to countersink it under the bony edges.

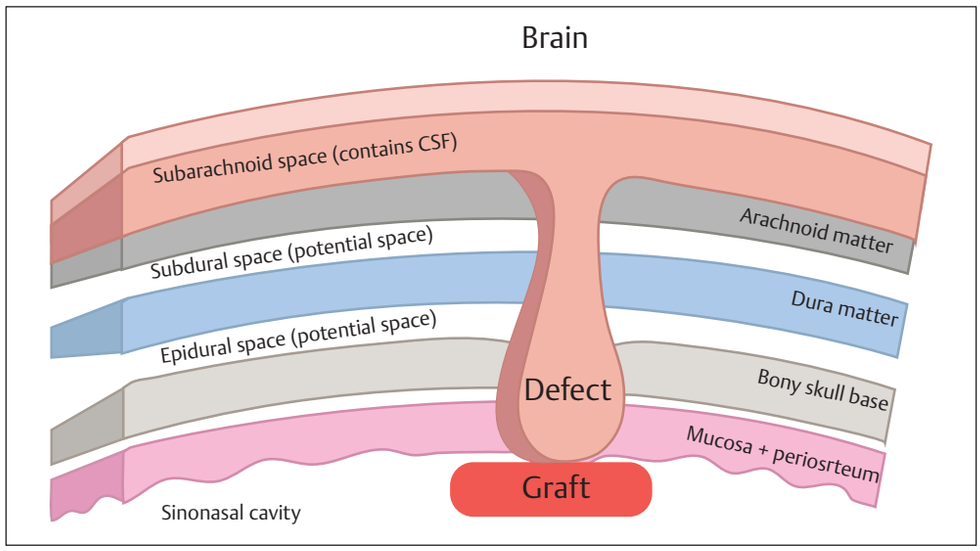

Fig. 6.10 Illustration showing extracranial onlay grafting that is 1 cm larger than the defect.

- Vascularized pedicle flap
  1. **Mobilizing and positioning flap over the defect:** Care should be taken to avoid flap tear, torsion, or twisting of the vascular pedicle. The periosteal side of the flap should lie against the skull base defect without any folds along its edges. The part of the flap that corresponds to the anterior-superior nasal septum is thicker and should be placed at the site of the dural defect.
  2. **Flap orientation:** In sellar and suprasellar reconstruction the flap is oriented vertically and can cover a defect that extends from the sellar region to the frontal sinus and from orbit to orbit. The sphenoid sinus is filled with fat after complete removal of mucosa to increase the reach of the flap. The vascular pedicle is supported on the medial wall of the orbit, the sphenoid floor, and the clival recess.
  3. **Pedicle care:** Periosteal surface should be in contact with tissue to prevent contracture postoperatively. Redundant flap pedicle can be folded to provide contact. Undue traction/torsion of the pedicle and the use of electrocautery in the vicinity should be avoided.
  4. **Ensuring complete coverage of the defect:** In case the flap has a tear or is not covering the defect completely it can be augmented with fat, fascia, or free mucosal grafts harvested from resected turbinates most commonly the middle turbinate. The most common cause of failure is an incomplete closure.

- **Supporting layer:** After proper positioning, graft bulldozing is done with the help of a lint to ensure tight seal between the graft and the skull base. Pieces of Surgicel (hemostatic agent made of an oxidized cellulose polymer, manufactured by the Ethicon subsidiary of Johnson & Johnson) are placed on the graft and along its margins to hold it in position and to prevent tissue glue from seeping under the flap. Fibrin glue (Tisseel, Baxter), a surgical formulation made up of fibrinogen (lyophilized pooled human concentrate) and thrombin (bovine, reconstituted with calcium chloride), is used as the next layer to create a fibrin clot for hemostasis and promoting faster wound healing. Pieces of Gelfoam (sterile compressed sponge that is prepared from purified porcine skin, gelatin granules and water for injection) is placed to ensure the position, contour and to provide a cushion between the glue and packing. Foley's balloon catheter inflated with air fits the shape of the cavity and is used to hold the different layers in place. Finally, Merocel (Medtronic, Standard Nasal Dressing) is used to pack the remaining nasal cavity and is left in situ for 5 to 7 days[9] (**Figs. 6.3, 6.11–6.13**).

Vascularized Flaps in Anterior Skull Base Reconstruction

There are two types of vascularized flaps; pedicled and free flaps. Important features of some of these flaps are discussed later in this chapter.

- Vascularized pedicled flap
  A) Local/Intranasal vascularized flaps
  - Posteriorly pedicled flaps
    1. Nasoseptal flap (Hadad-Bassagaisteguy or HB flap).[30,31]
    2. Inferior turbinate flap.
    3. Middle turbinate flap.
    4. Lateral nasal wall flap (Carrau-Hadad flap).
  - Anteriorly pedicled flaps
    1. Lateral nasal wall flap (Hadad-Bassagaisteguy 2 or HB2 flap).
    2. Inferior turbinate flap

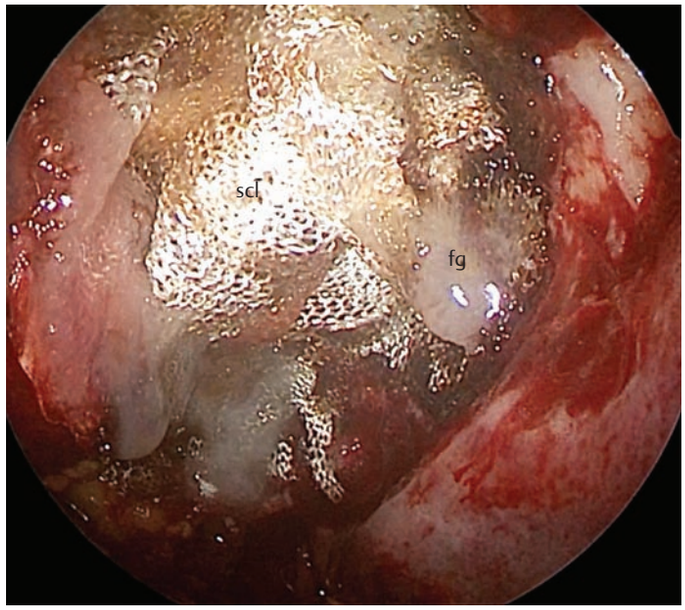

Fig. 6.11 A layer of Surgicel is placed over the flap and biosynthetic glue is used to anchor different layers.

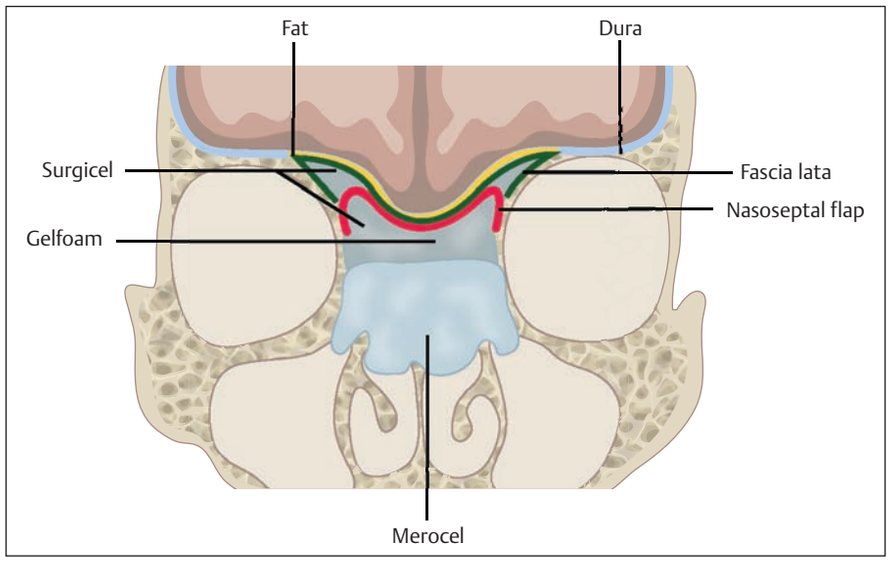

Fig. 6.12 Illustration showing multilayer closure with inlay fat and onlay nasoseptal flap. Graft support is given using material such as Surgicel, Gelfoam, and Merocel.

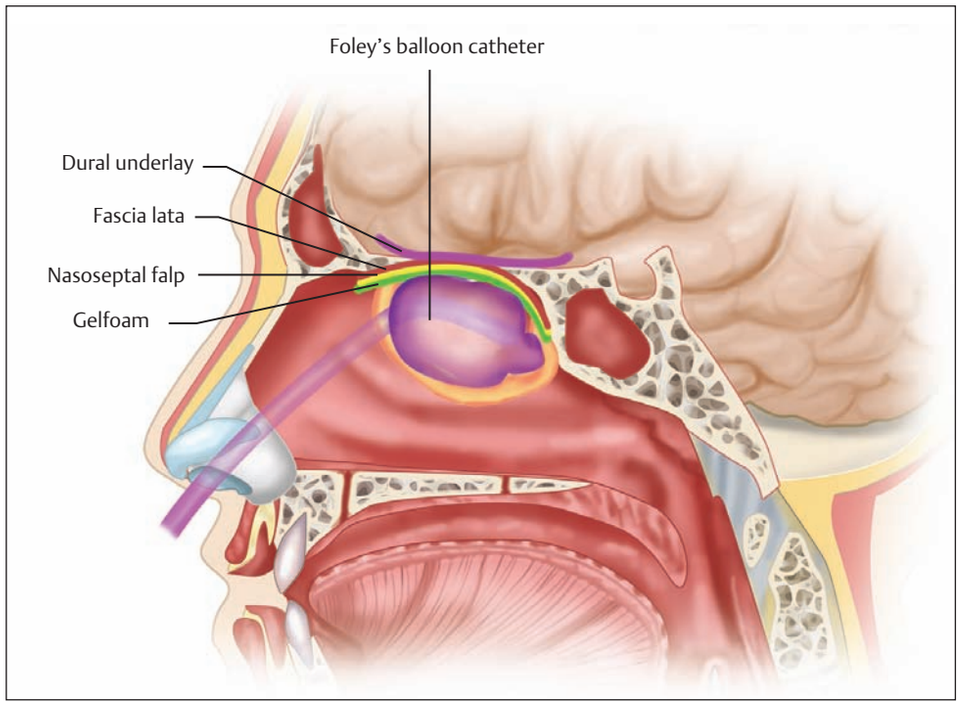

Fig. 6.13 Illustration showing multilayer closure with Foley's balloon catheter inflated with air supporting the various layers.

B) Regional/Extranasal vascularized flaps
   1. Pericranial flap (midline).
   2. Temporoparietal fascial flap (paramedian).
   3. Oliver palatal flap.
   4. Facial artery buccinator flap.

- Vascularized free flaps
  - ➢ Anterior lateral thigh (ALT) flaps.
  - ➢ Radial forearm flap (RFF).

■ Nasoseptal Flap

Nasoseptal flap (NSF) is often described as the workhorse for ESBR and is considered the first choice in most skull base reconstruction procedures.[20,30]

Vascular Anatomy

Vascular pedicle: Based on the posterior septal artery, the terminal posterior branch of the sphenopalatine artery

(SPA). It exits the sphenopalatine foramen (SPF) and ascends to traverse the anterior face of sphenoid sinus between the ostium and the superior margin of posterior choana to reach the septum (**Fig. 6.14**). Along this course, it divides into two branches shortly after origin in 40% of cases and at the level of the sphenoid ostium in 70% of cases.[30–33]

Advantages of Using Nasoseptal flap

- Reduces the incidence of postoperative CSF leaks to less than 5%, making NSF the first choice in most anterior skull base defect reconstruction.[2–5]
- Robust vascular supply effectively reduces healing time especially in cases requiring radiotherapy.
- Ability to design the flap with varying degrees of rotation, mobility, length, and width to tailor fit defects of various dimensions from the level of the frontal sinus to the clivus in suprasellar, sellar/parasellar, and infrasellar approaches.
- Lowers incidences of other postoperative complications such as meningitis, encephalitis, and pneumocephalus.
- Reusability in revision cases: In cases without recurrence of a malignant disease or if the flap is not directly involved in benign pathologies, it can be recycled.[9] Frozen section of flap margins should be used to rule out any involvement.[34] In most cases there is a good plane of dissection and the flap retains its contour (**Figs. 6.15–6.17**).

Limitations of Using NSF

- Inability to cover both suprasellar and infrasellar defects at the same time.
- Bilateral flap elevation leads to devascularization and necrosis of the septal cartilage.
- Local factors such as a deviated nasal septum, septal spur, nasal perforation, or previous surgeries may pose challenging situations during flap elevation but is not an absolute contraindication.[9]
- In pediatric age group (<14 years), the relative area of septum is less compared with that of the skull base.[35]
- In growing children, long-term effects on nasal growth is unknown.
- Donor-site crusting (can be prevented by using reverse flap to cover the exposed cartilage).[36,37]

Choice of Side

Side selection depends on multiple factors[9,38]:

- **Septal factors**
  - ➢ Septal deviation and spur: Flap elevation on the same side may lead to tear, hence contralateral side is preferred.

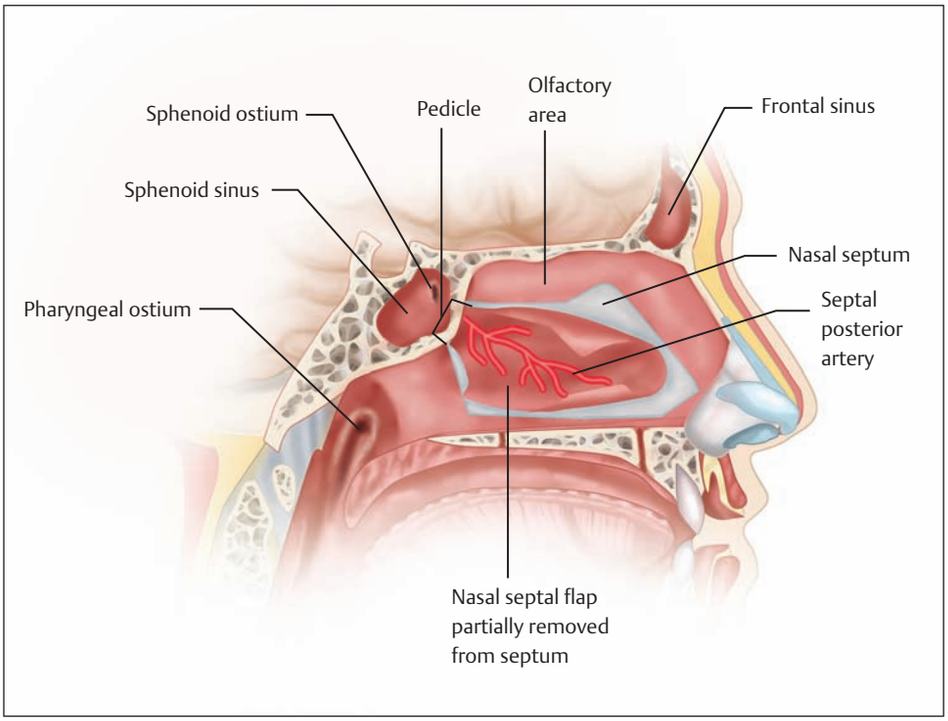

Fig. 6.14 Illustration showing partially elevated nasoseptal flap with its vascular pedicle.

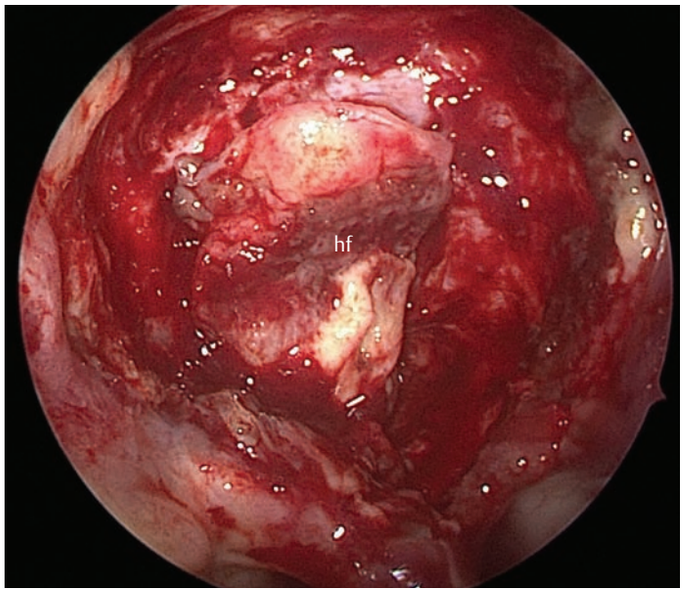

Fig. 6.15 Nasoseptal flap (NSF) recycling: NSF prior to dissection in revision surgery.

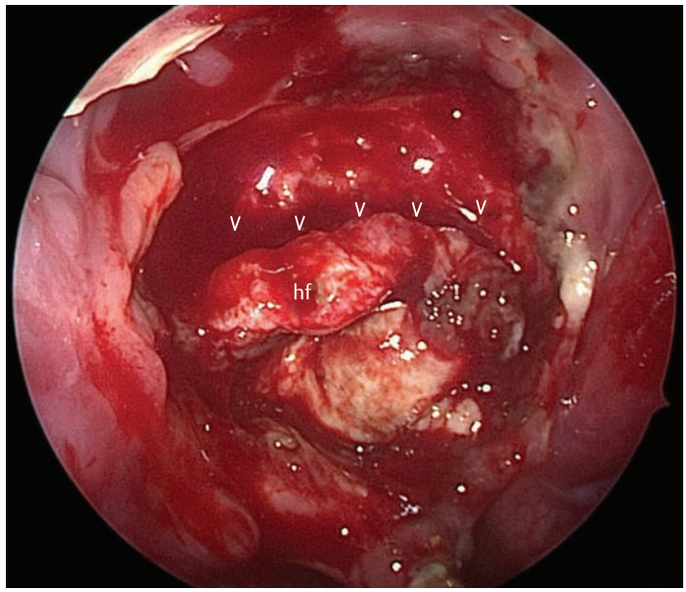

Fig. 6.16 Nasoseptal flap (NSF) recycling: Partially dissected NSF.

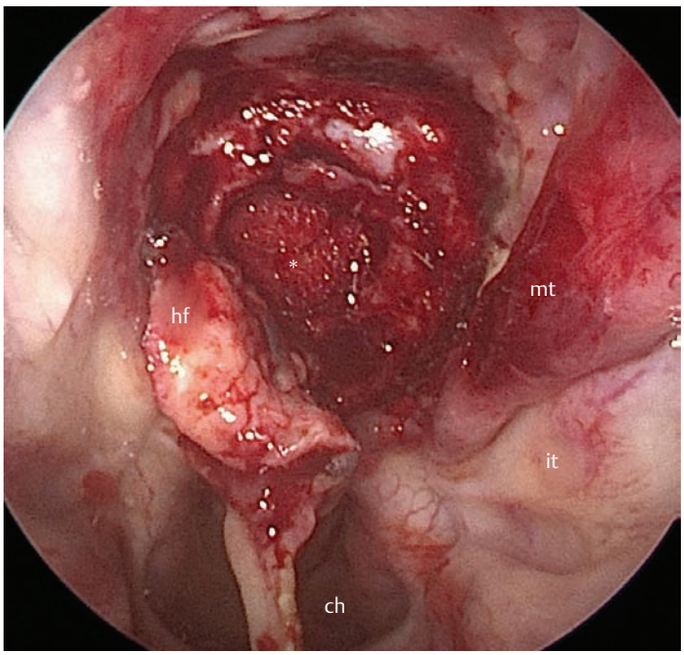

Fig. 6.17 Nasoseptal flap (NSF) recycling: NSF after complete dissection. *Showing the defect in the skull base.

- Perforation: In medium size perforations, the flap is prepared to avoid the region of the perforation, and in small perforations, flap is augmented with free mucosal grafts, fat, or fascia.
- Disease pathology involving the septal mucosa.
- Previous surgery: This is not an absolute contraindication in harvesting NSF. Careful blunt and sharp dissection is used to raise the flap.

- **Side of the tumor/defect:** If the approach poses danger to ipsilateral pedicle or if preservation of the ipsilateral pedicle compromises on the surgical exposure, maneuverability, and instrumentation, a contralateral flap is elevated. In other cases, ipsilateral flap is preferred as it increases the reach and reduces the length between the pedicle and the defect.
- **Preference of the surgeon:** For a right-handed surgeon right-sided flap elevation is easier.
- **Nasal corridor dimensions:** For visualization and instrumentation.

Surgical Technique[30,31]

Flap Harvesting

- **Mucosal decongestion:** It is done with topical adrenaline-soaked pledgets (**Fig. 6.18**).
- **Exposure of the sphenoethmoidal recess and the vascular pedicle:** Achieved by lateralization of the turbinates or partial middle turbinate resection (**Figs. 6.19–6.21**).
- **Confirming vascularity of the pedicle:** In cases with prior history of surgery, vascularity is confirmed with endoscopic Doppler probe.[39]

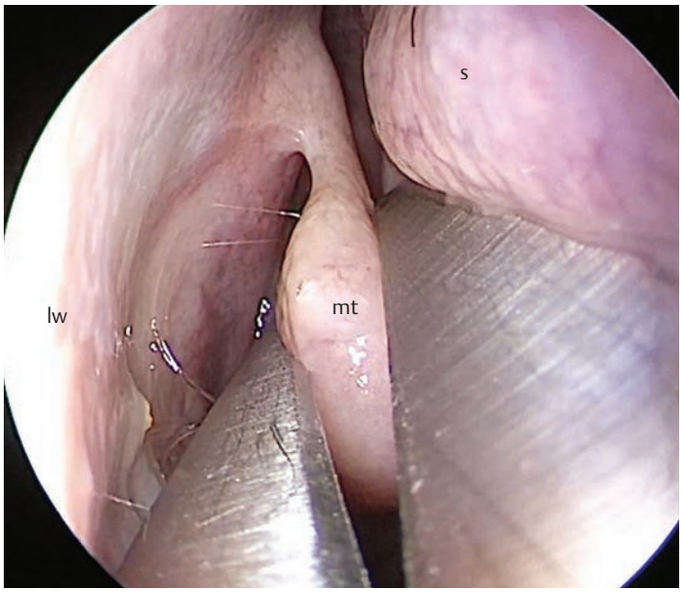

Fig. 6.18 Well-decongested nasal cavity immediately prior to partial middle turbinate (MT) resection.

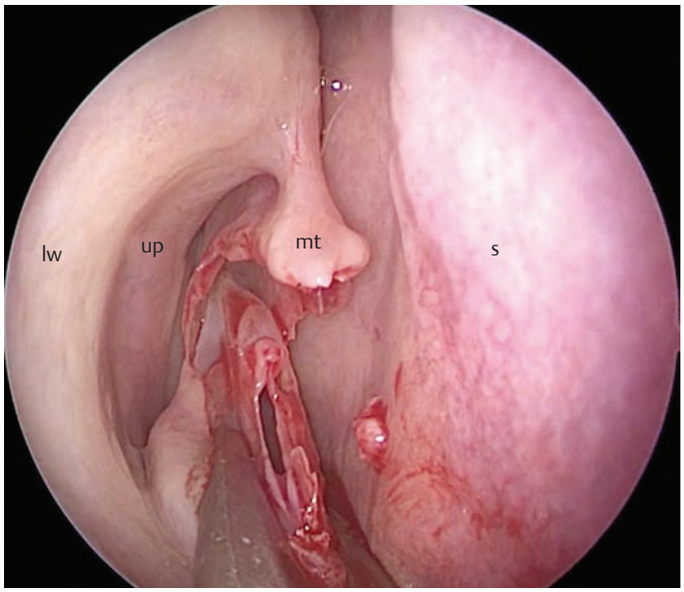

Fig. 6.19 Partial middle turbinate resection completed with the help of turbinectomy scissors.

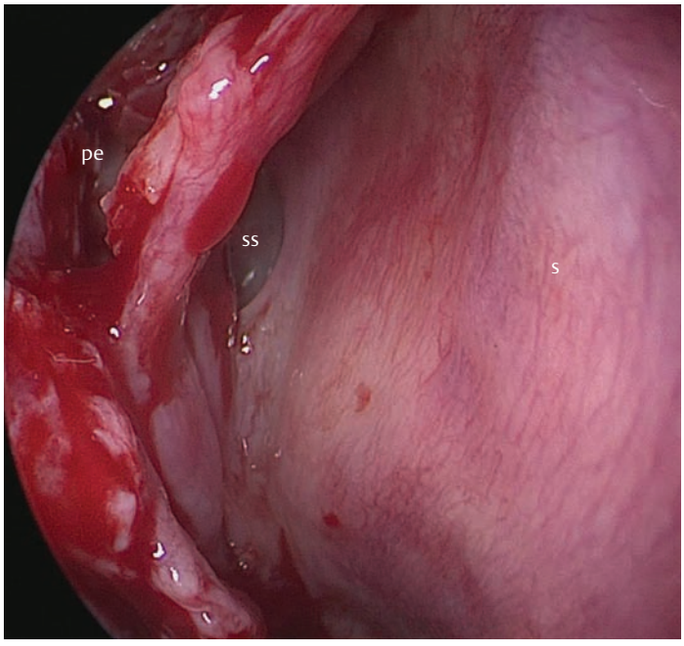

Fig. 6.20 Identification of sphenoid sinus ostium in the sphenoethmoidal recess.

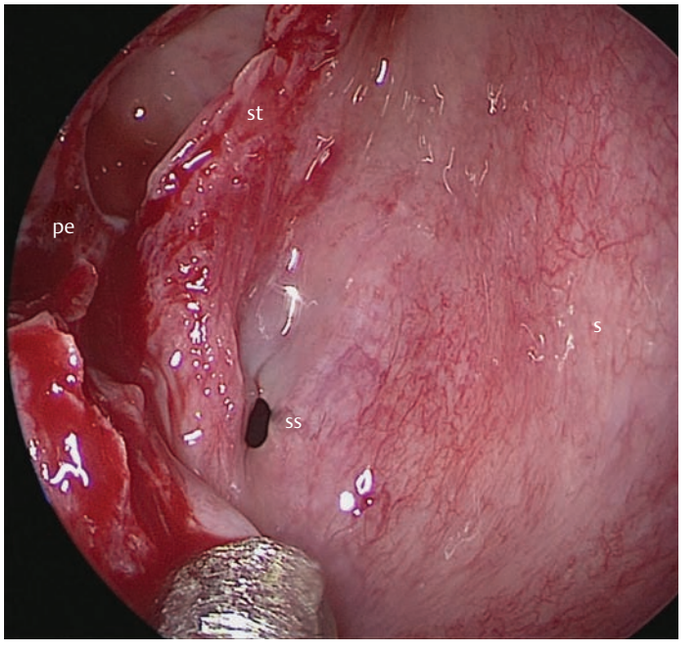

Fig. 6.21 Identification of sphenoid sinus ostium in the sphenoethmoidal recess.

- **Infiltration of nasal septal mucosa:** Normal saline infiltration at anterior end of ipsilateral septum is done for hydro dissection and ease of dissection.
- **Incision:** Performed with number 15 blade or a needle tip extended monopolar electrocautery device set at 15W. Harvesting of the flap entails three different incisions: (**Fig. 6.22**)
  - **Inferior incision:** Begins at the superior margin of posterior choana continued medially along the posterior margin of vomer toward the nasal floor.

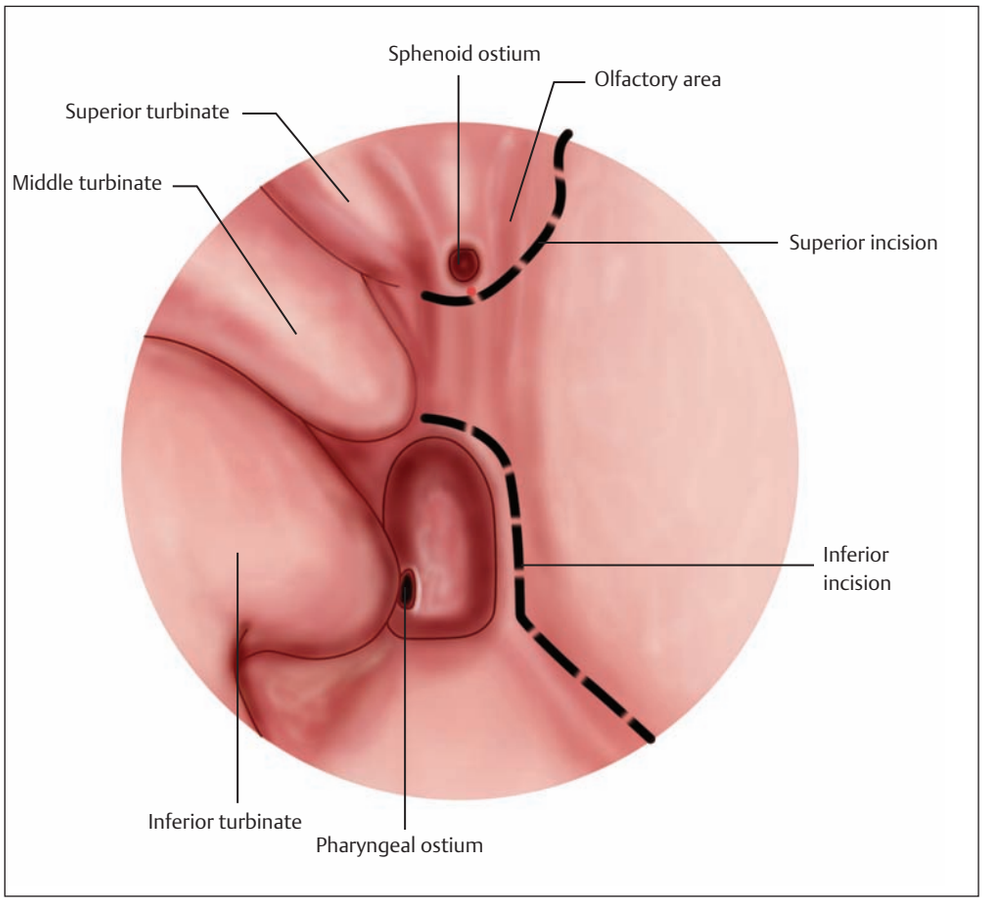

Fig. 6.22 Illustration showing superior and inferior incision lines prior to nasoseptal flap elevation.

It is further extended anteriorly along the junction of the septum and nasal floor up to the mucocutaneous junction (**Figs. 6.23 and 6.24**).

- **Superior incision:** Begins at sphenoid ostium and runs anteriorly parallel to the skull base 1 cm inferior to the nasal vault (olfactory sulcus). At the level of the anterior attachment of middle turbinate, the incision is directed superiorly toward the nasal dorsum to include the anterosuperior area (**Fig. 6.23**).
- **Anterior incision:** Placed at the mucocutaneous junction connecting both the superior and inferior incisions (**Figs. 6.24 and 6.25**).
- Modified incisions for additional mobility and width (**Figs. 6.26–6.30**).
  1. **Mobility:** Wide middle meatal antrostomy (MMA) is performed and the SPF is identified. The inferior incision is extended from posterior choana to lateral nasal wall between the SPF and the eustachian tube (ET). Pedicle flap is then elevated from the base of the pterygoid plates and mobilized to the pterygopalatine fossa (PPF), pterygoid canal being the lateral limit of elevation.
  2. **Width:** After medializing the inferior turbinate, the inferior incision is extended along the nasal floor posteriorly into the inferior meatus and continued anteriorly. The anterior incision extends across the nasal floor anteriorly from the inferior meatus to the caudal edge of the septum.

- **Elevation of the flap:** Care should be taken while elevating flaps at sites where it is tightly adherent to underlying periosteum such as in the region of pre maxilla, maxillary crest, and along the junction of septum and the nasal floor (**Figs. 6.31–6.34**).
- **Securing the flap:** Flap is secured in the nasopharynx (for sellar/ suprasellar approaches) or in the maxillary sinus (for transclival approaches) (**Figs. 6.35 and 6.36**).

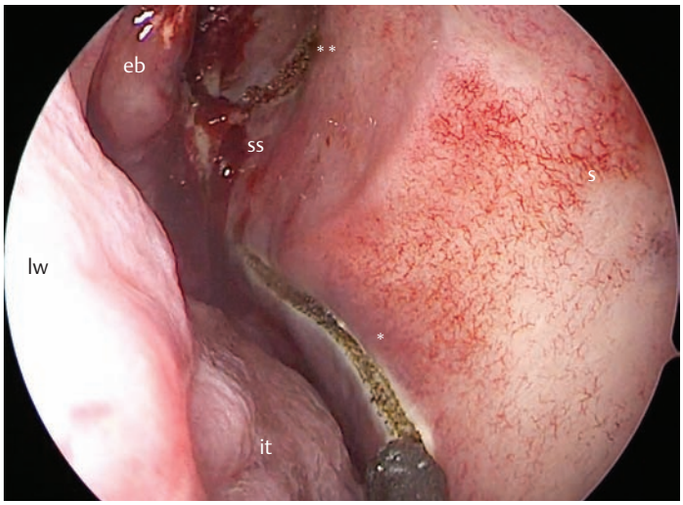

Fig. 6.23 Incision: Performed with an extended tip monopolar electrocautery device set at 15W. *Inferior incision **Superior incision.

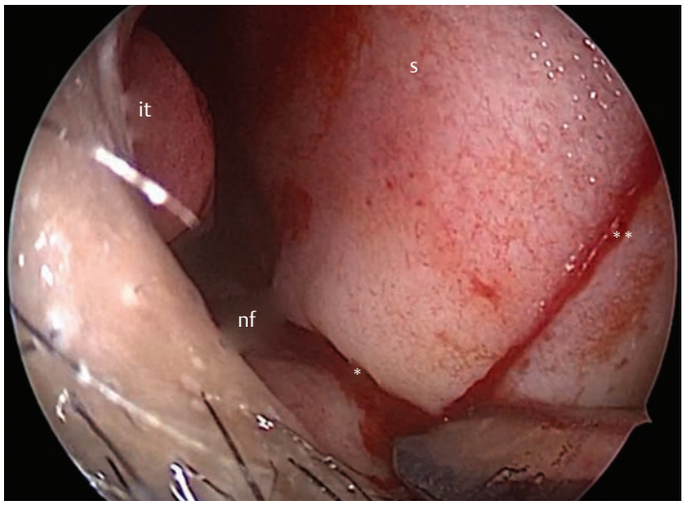

Fig. 6.24 Incision: Performed with a number 15 blade. **Anterior incision: Placed at the mucocutaneous junction connecting both the superior and inferior incisions. *Inferior incision.

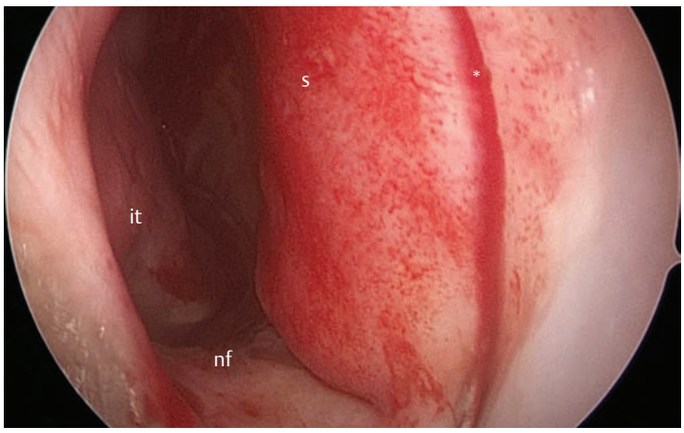

Fig. 6.25 Incision: Performed with a number 15 blade. *Anterior incision: Placed at the mucocutaneous junction.

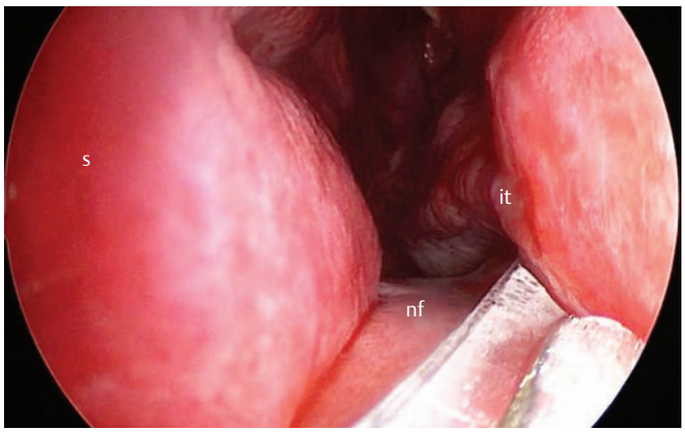

Fig. 6.26 Incision made in the inferior meatus for extended hadad flap.

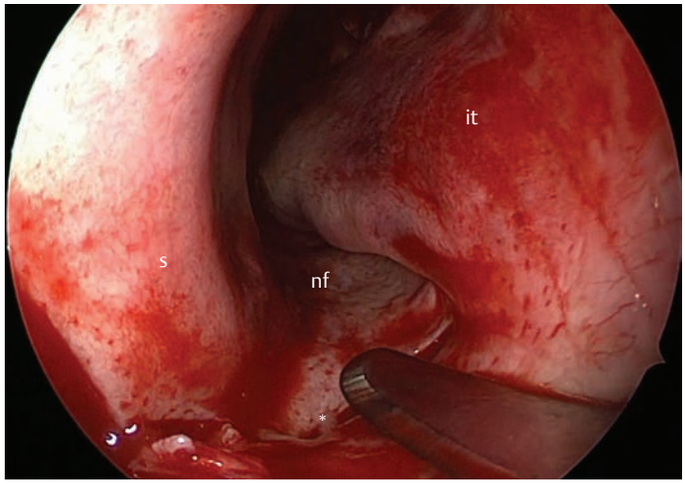

Fig. 6.27 The anterior incision extends across the nasal floor anteriorly from the inferior meatus to the anterior septum.

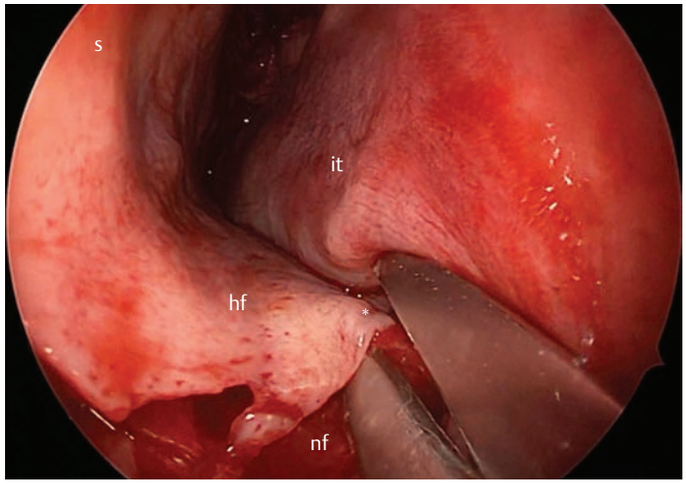

Fig. 6.28 Flap elevated partially from the septum, nasal floor, and the inferior meatus. *Release incision given anteriorly to facilitate posterior flap elevation.

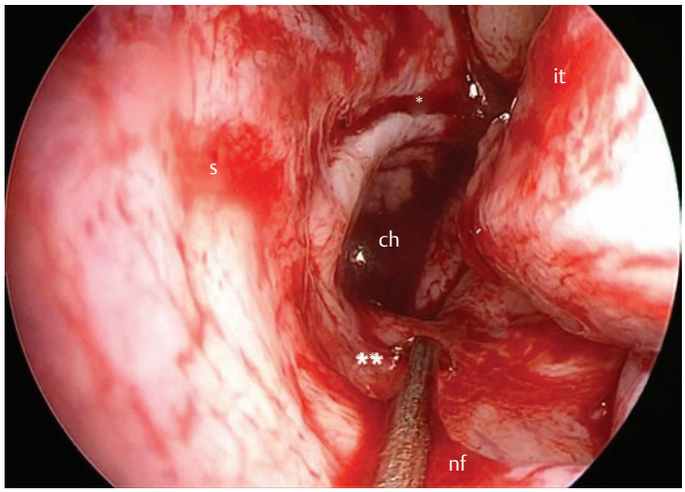

Fig. 6.29 Inferior incision is extended along the nasal floor posteriorly into the inferior meatus. (*) Inferior incision. (**) Incision along the nasal floor posteriorly to the inferior meatus.

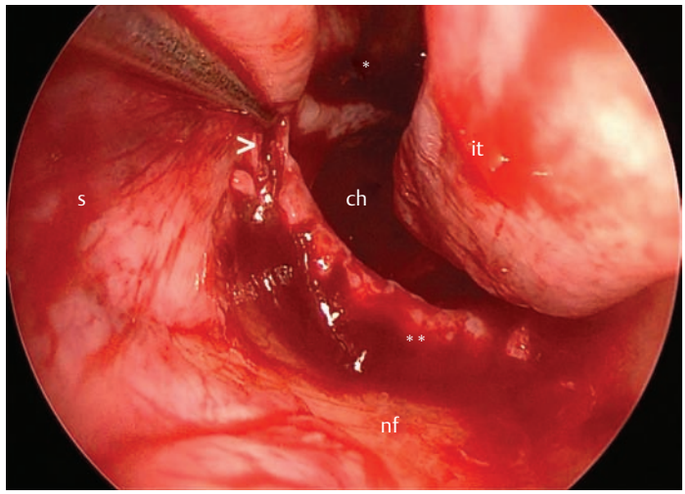

Fig. 6.30 Flap elevation using circular knife (open arrow). (*) Inferior incision. (**) Incision along the nasal floor posteriorly to the inferior meatus.

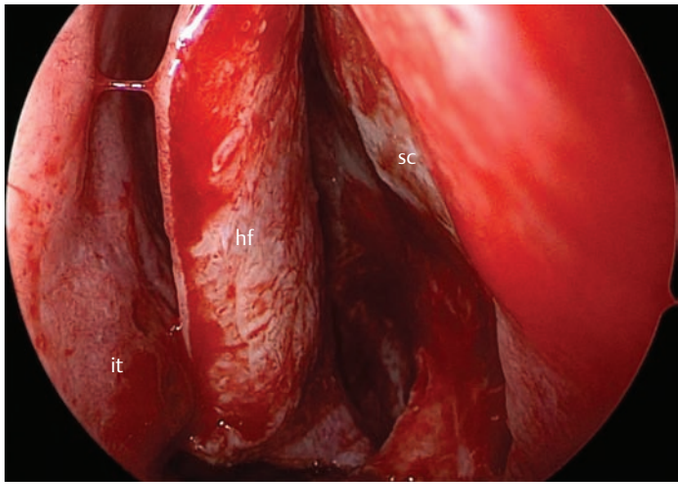

Fig. 6.31 Submucoperichondrial flap elevation.

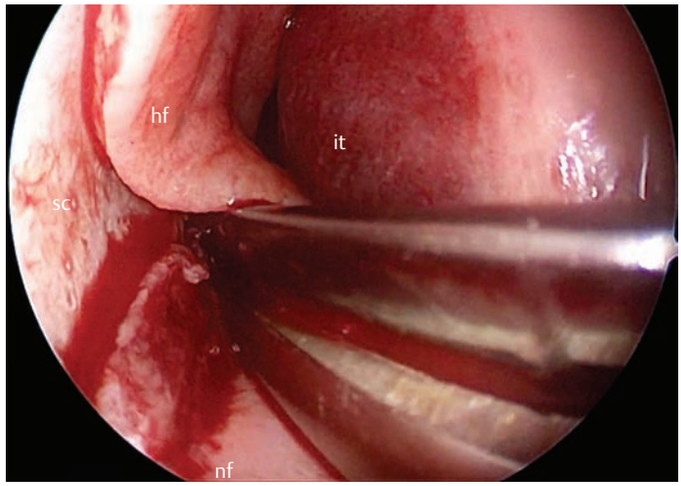

Fig. 6.32 Elevation of the flap along the junction of septum and the nasal floor.

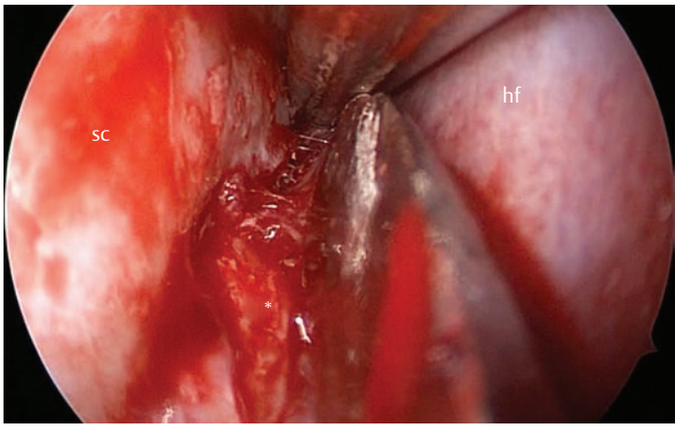

Fig. 6.33 Elevation of the flap: Care should be taken while elevating flaps at sites where they tightly adherent to underlying periosteum such as in the region of premaxilla and maxillary crest.

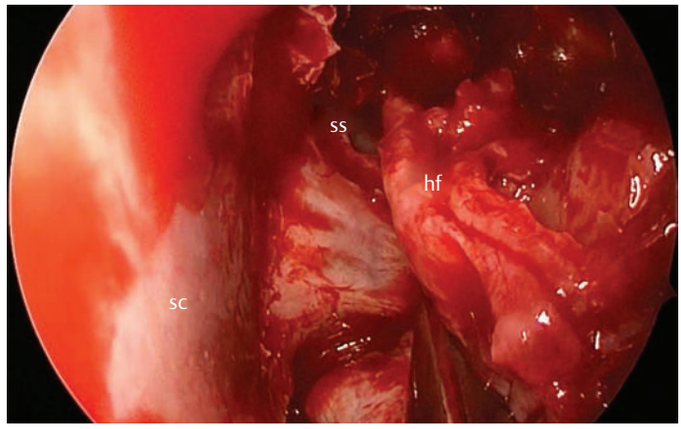

Fig. 6.34 Securing the flap**:** Flap is secured in the nasopharynx.

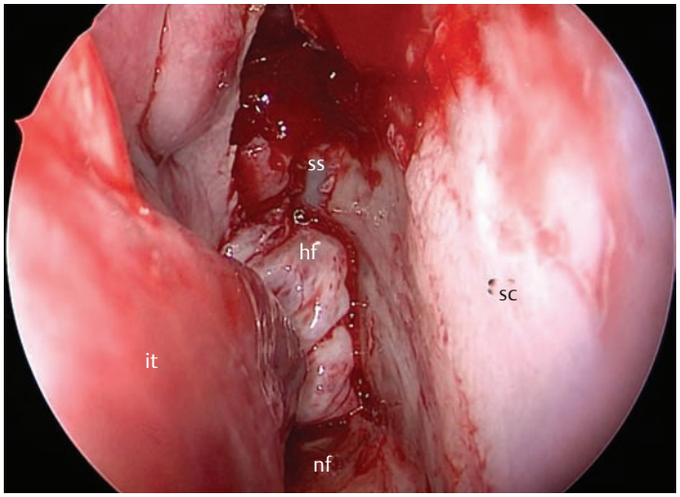

Fig. 6.35 Securing the flap**:** Flap is secured in the nasopharynx.

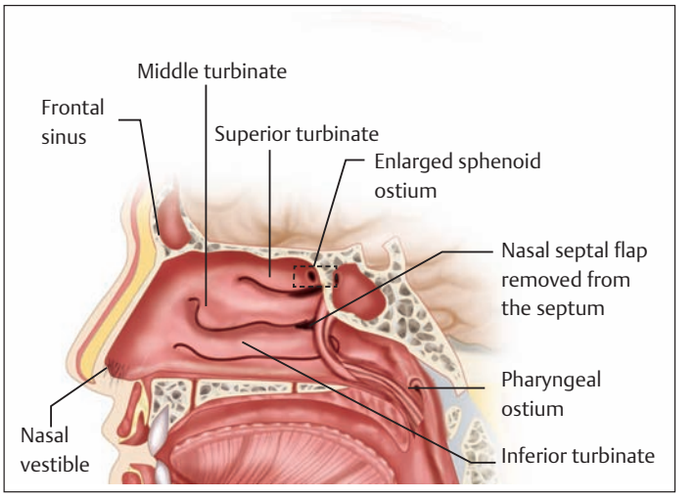

Fig. 6.36 Illustration showing nasoseptal flap being parked in the nasopharynx after complete elevation.

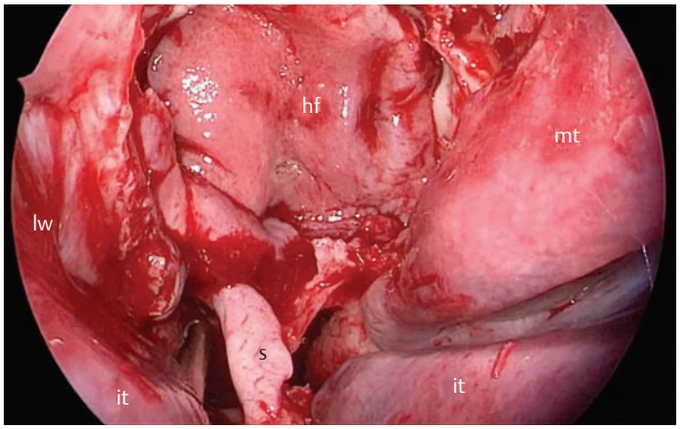

Fig. 6.37 Flap mobilization and defect coverage: The flap is rotated from a sagittal orientation to cover the defect without any folds.

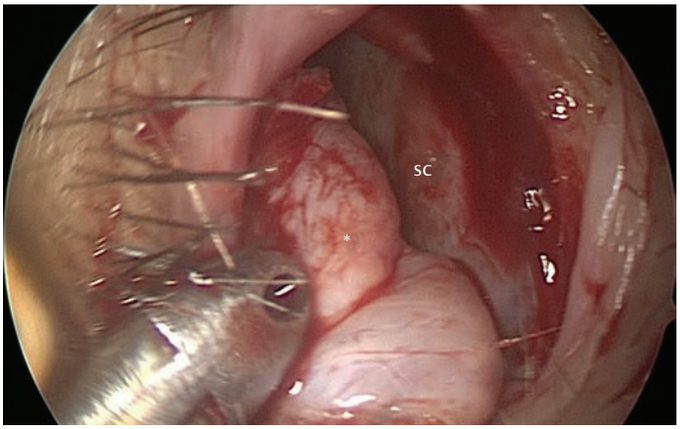

Fig. 6.38 Flap transposition: Once the incisions free the reverse flap, it is transposed to the opposite nasal cavity by rotating it by 180 degrees.

- **Flap mobilization and defect coverage:** The flap is rotated from a sagittal orientation to an axial plane to cover the defect without any folds (**Fig. 6.37**).
- **Donor site care:** A free mucosal graft or a reverse flap is sutured to the anterior septum to cover the flap donor site (**Figs. 6.38 and 6.39**).[36,37] This speeds up mucosalization of the exposed cartilage and helps minimize long-term postoperative crusting (**Fig. 6.40**). In cases where the use of the flap is not required, it can be sutured back to the septum.

"Rescue" Nasoseptal Flap

In cases where CSF leak is not anticipated but is a possibility, a conventional NSF is not harvested at the onset of surgery, instead only the vascular pedicle is mobilized and protected throughout the approach. In case a CSF leak ensues, a traditional NSF may be harvested toward the end of surgery for reconstruction of the defect. Care should be taken to avoid trauma to septal mucosa on the nonendoscopic side while passing instruments. This approach avoids nasal comorbidities associated with the donor site of the NSF in cases where it is not indicated.[9,38,40]

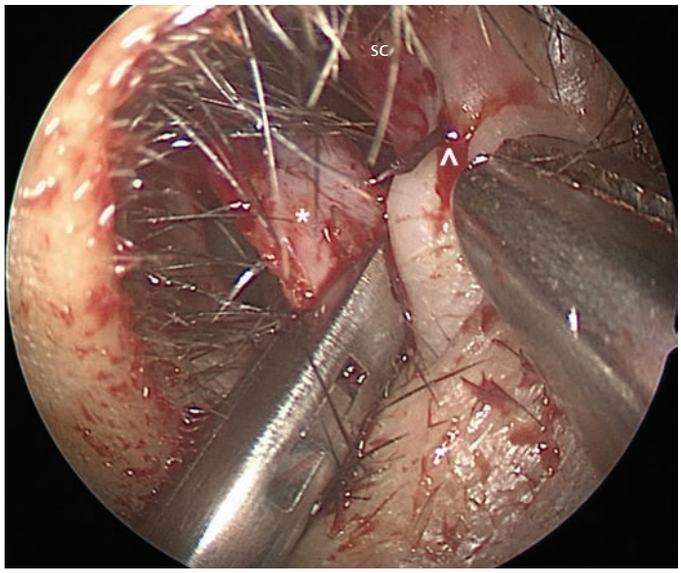

Fig. 6.39 Securing the flap: The free edge of the reverse flap is now sutured to the columella with 4–0 absorbable sutures and to the septal cartilage using 3–0 absorbable sutures.

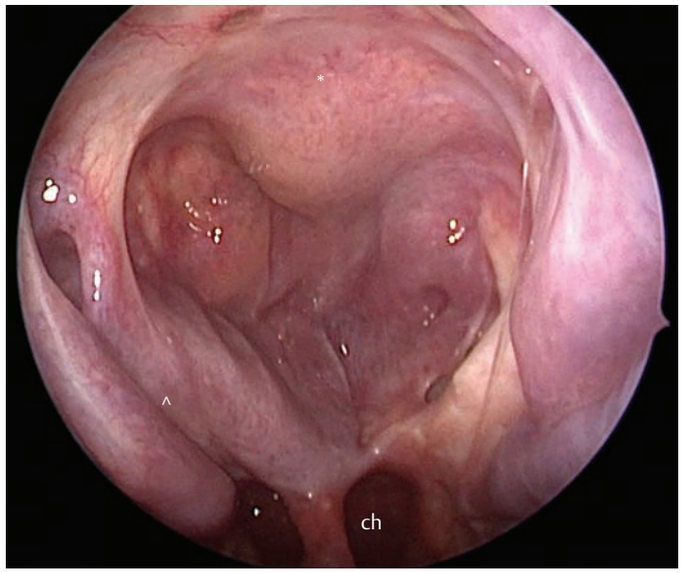

Fig. 6.40 Postoperative endoscopic view of a well taken up nasoseptal flap.

Vascular Anatomy

Vascular pedicle: As for the NSF, it is based on the posterior septal artery, the terminal posterior branch of the SPA.[38]

Surgical Technique[38,40]

- **Mucosal decongestion:** Done with topical adrenaline-soaked pledgets.
- **Incision:** It is performed bilaterally with a number 15 blade or a needle tip extended monopolar electrocautery device set at 15W, to mobilize the strip of mucoperiosteum containing the pedicle.
  - **Inferior incision:** Along the superior margin of posterior choana continued medially along the posterior margin of vomer (**Fig. 6.41**).
  - **Superior incision:** Beginning at sphenoid ostium similar to that of the NSF is placed toward the superior part of the septum up to the anterior attachment of the middle turbinate (**Fig. 6.41**).
- **Submucoperiosteal elevation:** It is performed bilaterally using a Freer's elevator to free the pedicle from the anterior face of the sphenoid sinus, exposing the posterior part of the septum and the sphenoid rostrum (**Fig. 6.42**).
- **Pedicle mobilization:** The vascular pedicle is then displaced inferiorly on both sides (**Fig. 6.43**).
- **Posterior septectomy and bilateral wide sphenoidotomy:** It is done by working above and below the pedicle taking care not to cause trauma to it.
- **CSF leak:**
  - If present, the incisions and steps described for raising the NSF are completed to close the defect.
  - If absent, the pedicle is mobilized back to cover the anterior face of the sphenoid sinus.

Reverse Nasoseptal Rotation Flap (Caicedo Flap)

The reverse nasoseptal rotation flap also known as the Caicedo reverse flap was designed to deal with the nasal comorbidities associated with the donor site of the NSF. The denuded septal cartilage and bone takes about 3 to 6 months for complete remucosalization, leading to prolonged periods of nasal crusting requiring repeated debridement. The reverse NSF hastens healing by covering the donor site and promoting remucosalization within 2 weeks' time.[36–38]

Vascular Anatomy

The reverse NSF is essentially an anteriorly pedicled septal flap vascularized by the branches of the anterior ethmoidal artery and the facial artery.[36–38]

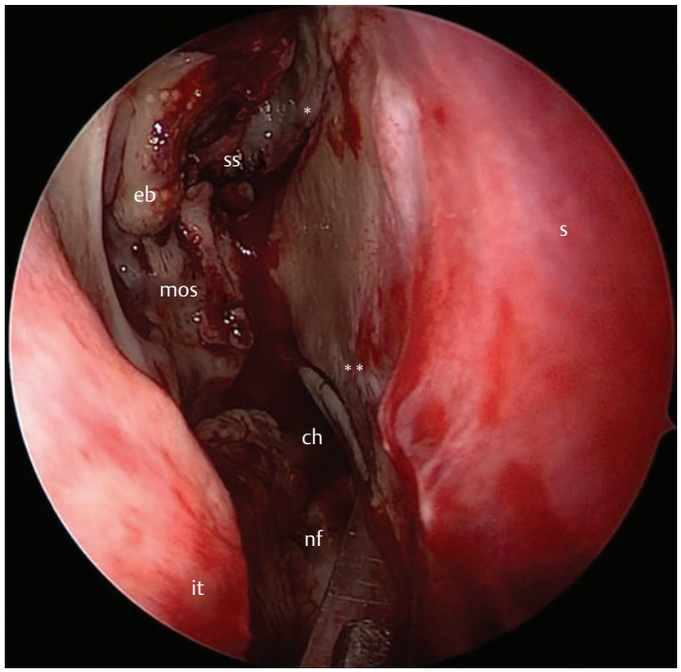

Fig. 6.41 **(*)** Inferior incision: along the superior margin of Posterior choana continued medially along the posterior margin of vomer. **(**)** Superior incision: starting at sphenoid ostium and continued toward the superior part of the septum.

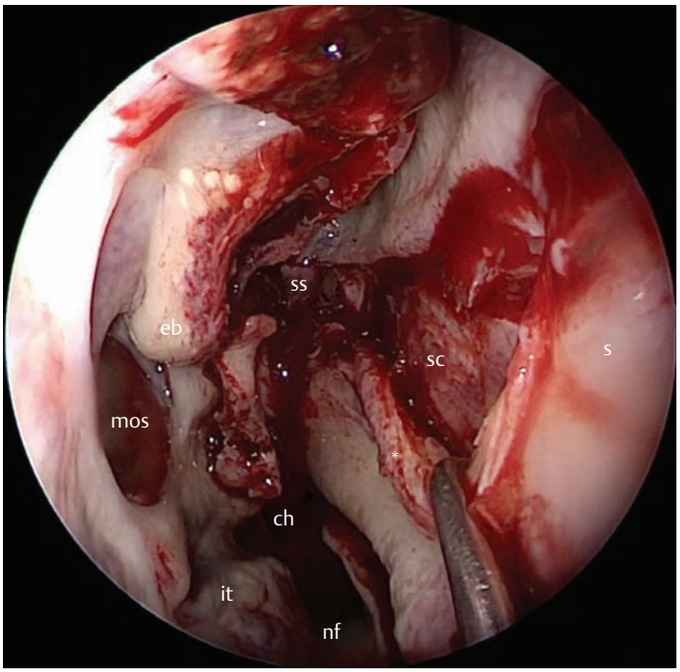

Fig. 6.42 Submucoperiosteal elevation is performed bilaterally using a Freer's elevator to free the pedicle from the anterior face of the sphenoid sinus. It also exposes the posterior part of the septum and the sphenoid rostrum.

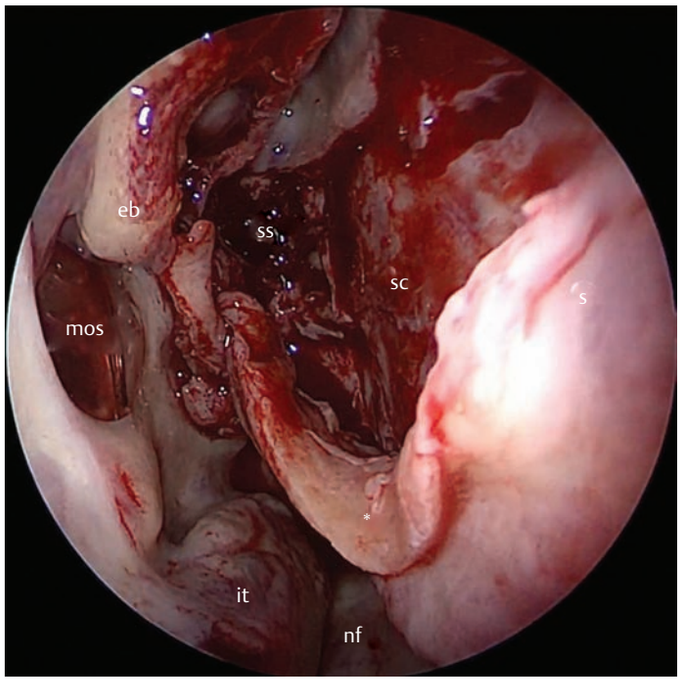

Fig. 6.43 Pedicle mobilization: The vascular pedicle is then displaced inferiorly on both sides.

Surgical Technique[36–38]

- **Mucosal decongestion:** Done with topical adrenaline-soaked pledgets.
- Harvesting of the NSF.
- **Posterior septectomy:** The septal bony cartilaginous junction is dislocated ipsilaterally to remove the vomer and perpendicular plate of the ethmoid exposing contralateral septal mucoperiosteum.
- **Submucoperiosteal dissection:** Submucoperiosteal dissection of the contralateral side is performed ipsilaterally using a Freer's elevator up to the sphenoid rostrum (**Fig. 6.44**).
- **Incisions:** Coming to the contralateral nasal cavity, septal mucoperiosteal incisions is made with a number 15 blade or a needle tip extended monopolar electrocautery device set at 15W. Mobilizing the flap entails three different incisions:
  - **Inferior horizontal incision:** Begins at the posteroinferior margin of vomer and continues anteriorly along the nasal floor up to the posterior free edge of the remaining nasal septum.

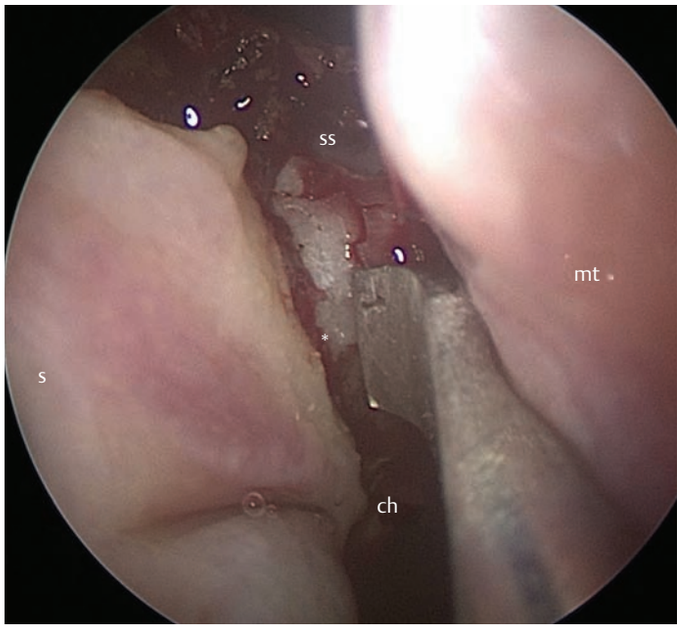

Fig. 6.44 Flap elevation from the anterior face of the sphenoid sinus.

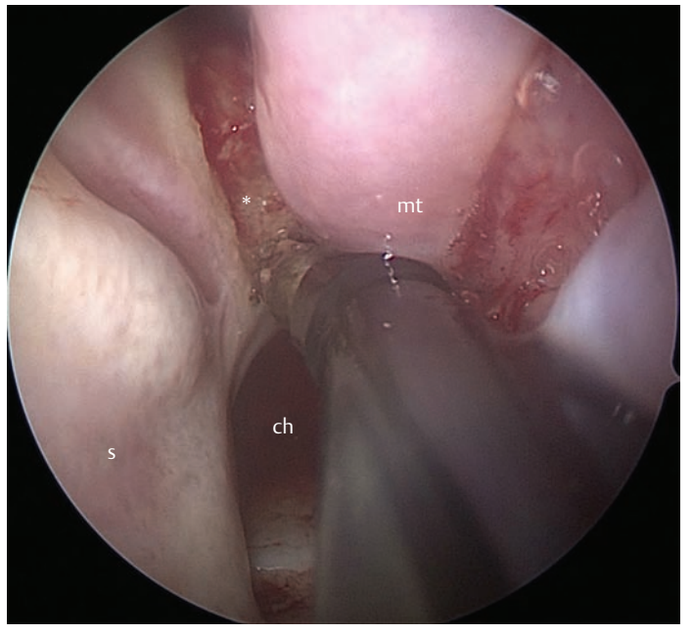

Fig. 6.45 **(*)** Posterior vertical incision: Placed at the rostrum of sphenoid connecting both the superior and inferior incisions.

- **Superior horizontal incision:** Begins at sphenoid ostium and runs anteriorly parallel to the skull base 1 cm inferior to the nasal vault (olfactory sulcus) up to the posterior free edge of the remaining nasal septum.
- **Posterior vertical incision:** Placed at the pterygo spheno synchondrosis along the anterior face of sphenoid connecting both the superior and inferior incisions (**Fig. 6.45**).

- **Flap transposition:** Once the incision frees the reverse flap, it is transposed to the opposite nasal cavity by rotating it by 180 degrees (**Figs. 6.38 and 6.46**).
- **Securing the flap:** The free edge of the reverse flap is now sutured to the remnant mucoperiosteum with 4–0 absorbable sutures. Tight nasal packing together with the sutures help preventing septal hematoma formation (**Fig. 6.39**).

Inferior Turbinate Flap

In 2007, Fortes-Carrau et al first described the posteriorly pedicled inferior turbinate flap (PPITF).[41] It is most commonly employed in small clival and sellar defect reconstructions.

Recently, an anteriorly pedicled inferior turbinate flap (APITF) has also been described by Gil Z et al in 2012, for reconstruction of defects in the posterior table of frontal sinus, cribriform plate, and the ethmoid roof.[42]

Vascular Anatomy

- **PPITF:** It is based on the inferior turbinate artery, a terminal branch of the posterolateral nasal artery (nasolateral artery) which in turn is a branch of the SPA.[41]

  At a distance of 10 to 15 mm from the posterior choana, the nasolateral artery courses onto the posterosuperior aspect of the inferior turbinates' lateral attachment. It courses 12 mm anteriorly before entering the bone and soft tissue of the inferior turbinate.[43,44]
- **APITF:** It is based on anterolateral branch of the anterior ethmoidal artery and the lateral nasal branch of the facial artery.[42]

Surgical Technique

Surgical technique for PPITF[41] is described in stepwise manner.

- **Mucosal decongestion:** Done with topical adrenaline-soaked pledgets.
- Medialization of the inferior turbinate.
- Uncinectomy, bullectomy, and middle meatal antrostomy are done.

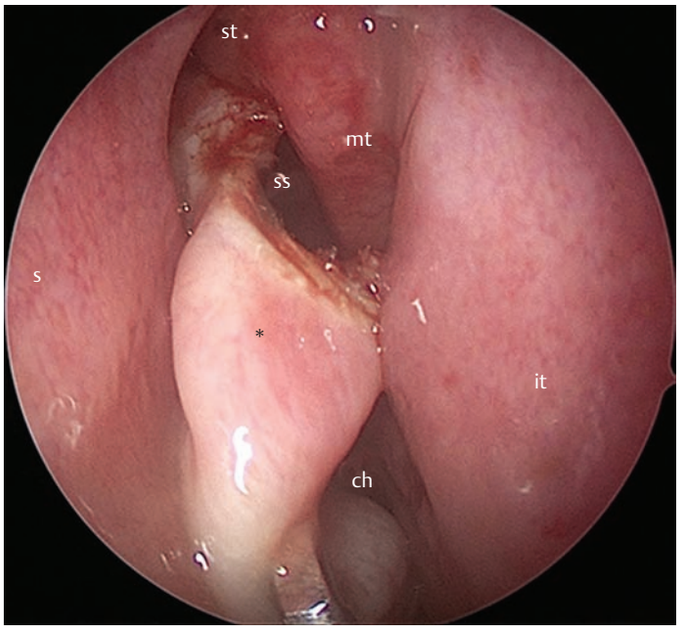

Fig. 6.46 **(*)** Flap elevation completed in a posterior to anterior direction up to the level of posterior septectomy.

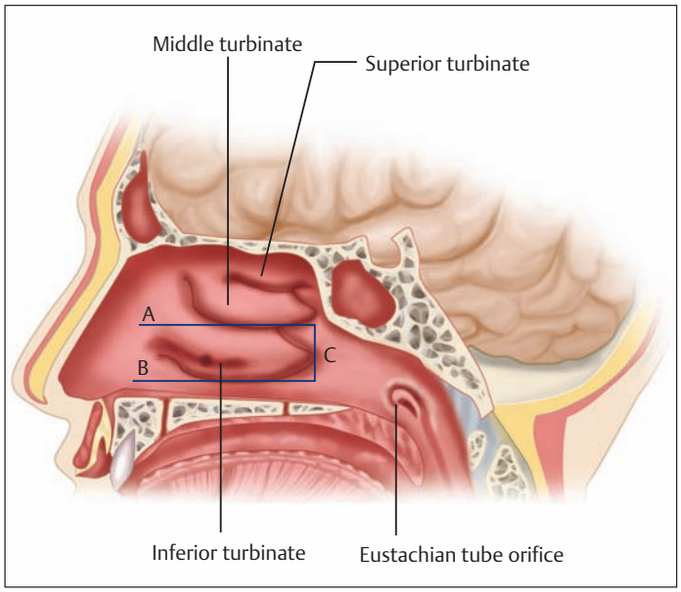

Fig. 6.48 Illustration showing various incisions employed in harvesting an anterior pedicle inferior turbinate flap. **(A)** Superior incision along the superior border of the inferior turbinate. **(B)** Inferior incision along the Inferior border of the inferior turbinate. **(C)** Posterior vertical incision along the head of inferior turbinate.

- **Identification of the sphenopalatine and nasolateral artery at the sphenopalatine foramen:** Subperiosteal dissection is performed posteriorly over the ascending process of palatine bone to identify the crista ethmoidalis. The crista ethmoidalis is removed with rongeurs to identify the SPA and its branches. In some cases the nasolateral artery may be seen anterior to the posterior maxillary sinus, so care should be taken not to injure it during maxillary antrostomy.

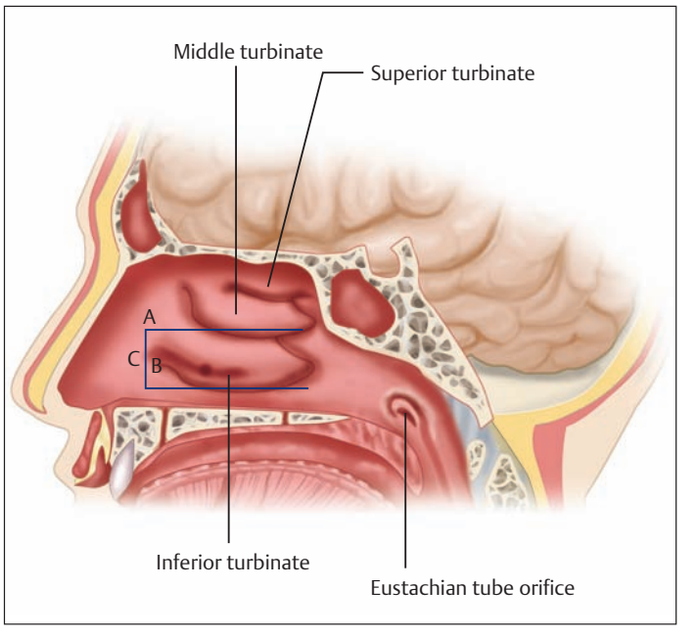

Fig. 6.47 Illustration showing various incisions employed in harvesting a posterior pedicle inferior turbinate flap. **(A)** Superior incision along the superior border of the inferior turbinate. **(B)** Inferior incision along the Inferior border of the inferior turbinate. **(C)** Anterior vertical incision along the head of the inferior turbinate.

- **Incisions (Figs 6.47 and 6.48):**
  - ➢ Two parallel superior and inferior horizontal incisions are made using electrocautery or a scalpel.
    1. **Superior incision:** Begins along superior margin of the inferior turbinate at the level of the maxillary sinus fontanelle. Can be modified to a higher level, to include the lateral nasal wall for a wider flap.
    2. **Inferior incision:** Begins along the inferior margin of the inferior turbinate posterior limit being the eustachian tube. Can be modified to include the nasal floor/inferior meatus for a wider flap.
  - ➢ Anterior vertical incision: Begins at the head of the inferior turbinate connecting the parallel incisions.
- **Flap elevation:** Using a Freer's elevator in the subperiosteal plane in an anteroposterior and medial to lateral direction.
- Flap mobilization and defect coverage (**Fig. 6.49**).[42]

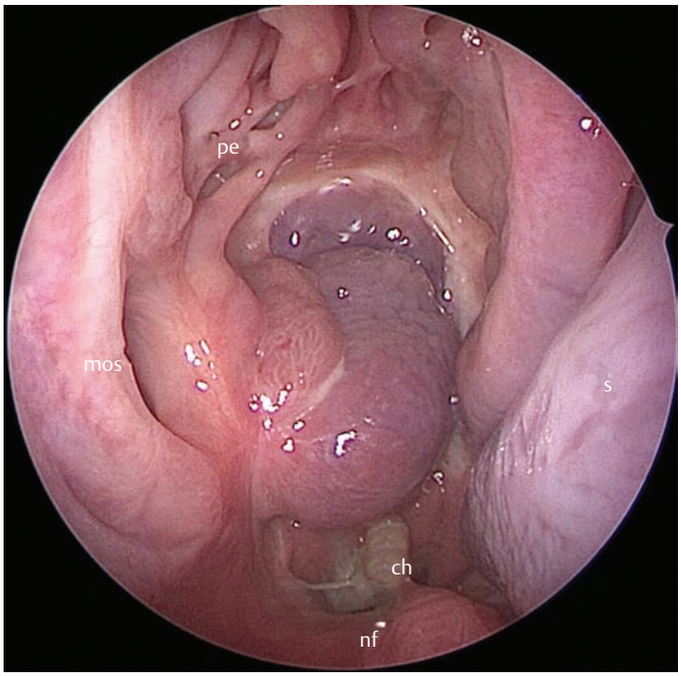

Fig. 6.49 Postoperative view of a well taken up inferior turbinate flap.

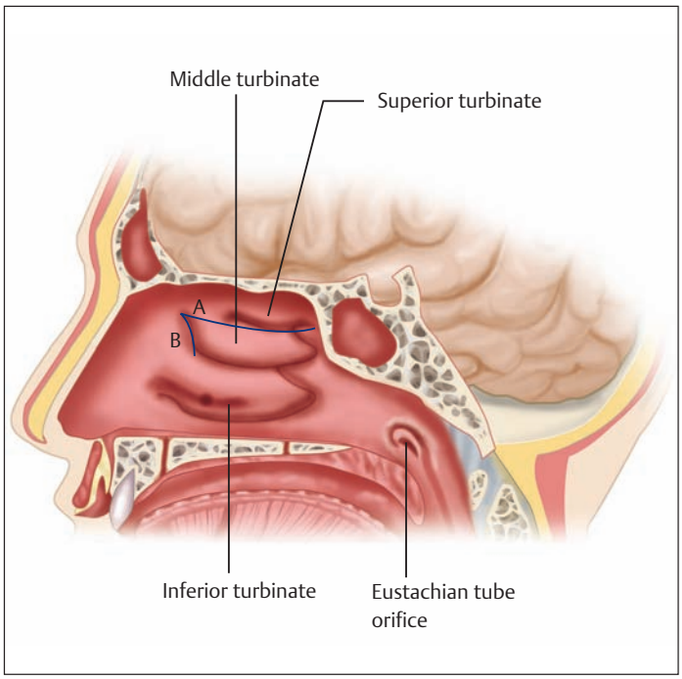

Fig. 6.50 Illustration showing various incisions employed in harvesting a middle turbinate flap. **(A)** Two parallel incisions along the medial and lateral aspect of the middle turbinate at the level of the axilla. **(B)** One anterior vertical incision: on the face of the middle turbinate head.

Middle Turbinate Flap

A posteriorly pedicled flap was first described by Prevedello et al and Simal et al. It has limited use in reconstruction of small defects in the anterior cranial fossa, cribriform plate, fovea ethmoidalis, planum sphenoidale, and the sellar region.[10,38,45–47]

Vascular Anatomy

Pedicle based on the anterior branch of SPA.[38,45]

Disadvantages of Using Middle Turbinate Flap[10,38,45,46]

- Difficult to elevate due to thick mucoperiosteum tightly adherent to the irregularly shaped middle turbinate.
- Potential to destabilize the middle turbinate and its attachment to the cribriform plate leading to CSF leaks.
- Previous SPA ligation precludes its use and is a contraindication for middle turbinate flap.
- Middle turbinate variations such as concha bullosa, paradoxically curved middle turbinate, and turbinate sinus may pose challenging situations.

Surgical Techniques[10,38,45–47]

- **Mucosal decongestion:** Done with topical adrenaline-soaked pledgets.
- **Incision:** Performed with a number 15 blade or a needle tip extended monopolar electrocautery device set at 15W (**Fig. 6.50**).
  - ➢ Two parallel incisions in anterior to posterior direction are made.
    1. Lateral incision: Begins along the lateral aspect of the axilla extending posteriorly up to the level of SPF.
    2. Medial incision: Begins on the medial aspect of the middle turbinate along its vertical attachment below the skull base.
  - ➢ One anterior vertical incision: Begins on the face of the middle turbinate head.
- **Flap elevation:** Done in submucoperiosteal plane in a superior to inferior direction, around the middle turbinate bone to the level of the pedicle.
- **Middle turbinate bone removal:** The vertical attachment as well as the basal lamella of the middle turbinate is removed to mobilize the flap and its pedicle.
- Flap mobilization and defect coverage.

Posterior Pedicled Lateral Nasal Wall Flap (Carrau-Hadad Flap)

This flap has been designed to include the mucoperiosteum of the lateral nasal wall and the floor of the nasal cavity. It can be employed to cover defects from the planum sphenoidale to the nasopharynx between the two orbits.[38,48]

Vascular Anatomy

Posteriorly based pedicle, based on the branches of the SPAs.[38,48]

Surgical Technique[38,48]

- **Mucosal decongestion:** Done with topical adrenaline-soaked pledgets.
- **Incision:** Performed with a number 15 blade or a needle tip extended monopolar electrocautery device set at 15W. Incisions are listed in a stepwise manner (**Fig. 6.51**).
  - **Anterior incision:** Begins along the anterior border of ascending maxillary process and the inferior turbinate head to the nasal floor (**Fig. 6.52**).
  - **Posterior incision:** Begins along the uncinate process extending posteriorly along the superior margin of the inferior turbinate until its posterior end (**Fig. 6.53**). Posterior to the uncinate process this incision can be taken superiorly to include the maxillary fontanelle region into the flap (**Fig. 6.54**).
  - **Anteroposterior incision:** Begins along the junction of the lateral nasal wall and the nasal floor. This incision can be made on the nasal floor, at the nasoseptal junction, or higher above on the septum for a wider flap (**Fig. 6.55**).
  - **Anterior horizontal incision:** Begins anteriorly on the lateral nasal wall connecting the anterior and posterior incisions (**Fig. 6.56**).
- **Mucoperiosteal elevation:** From the lateral nasal wall, medial and lateral side of the inferior turbinate and lastly the nasal floor is done using a Freer's elevator (**Figs. 6.54, 6.57, and 6.58**).
- Inferior turbinate fracturing and bone removal.
- **Flap mobilization and defect coverage:** The flap is rotated from a sagittal orientation to an axial plane to cover the defect without any folds (**Fig. 6.59**).
- **Flap support:** As mentioned in general principles.

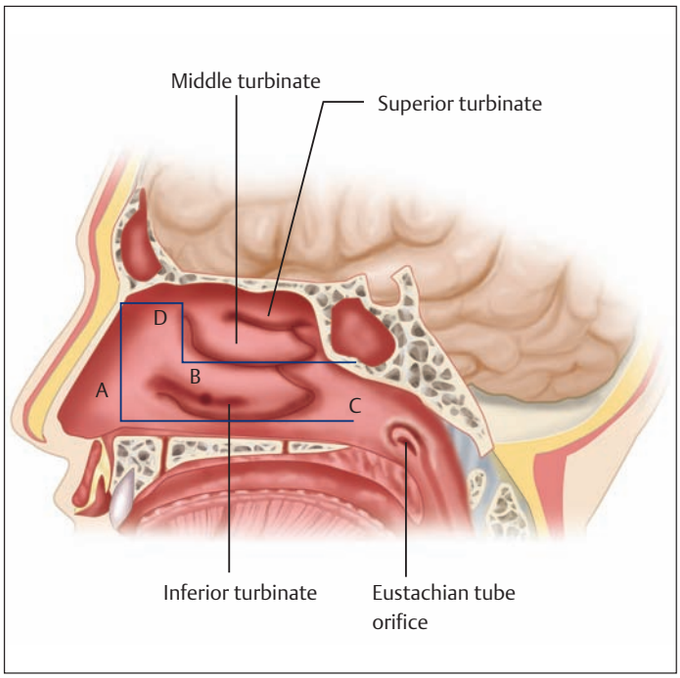

Fig. 6.51 Illustration showing various incisions employed in harvesting a posterior pedicled lateral nasal wall flap. **(A)** Anterior incision. **(B)** Posterior incision. **(C)** Anteroposterior incision. **(D)** Anterior horizontal incision.

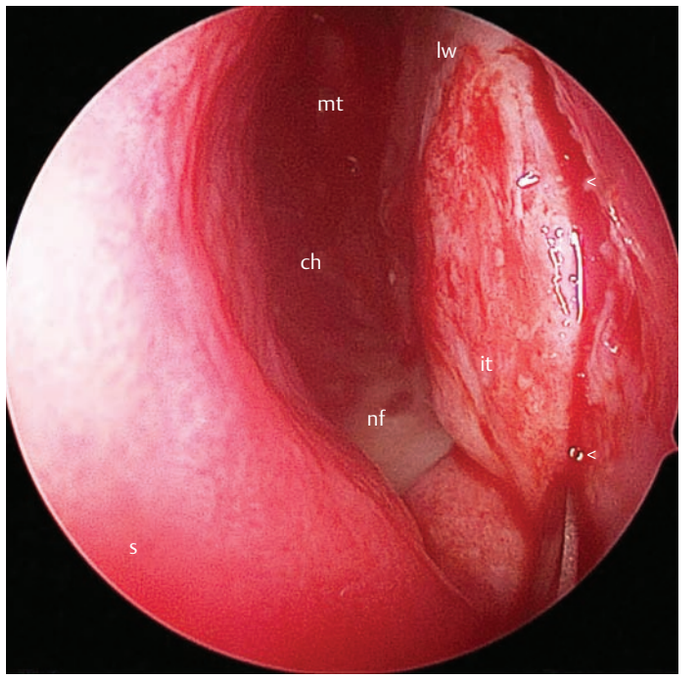

Fig. 6.52 The anterior incision: Along the anterior border of ascending maxillary process and the inferior turbinate head to the nasal floor.

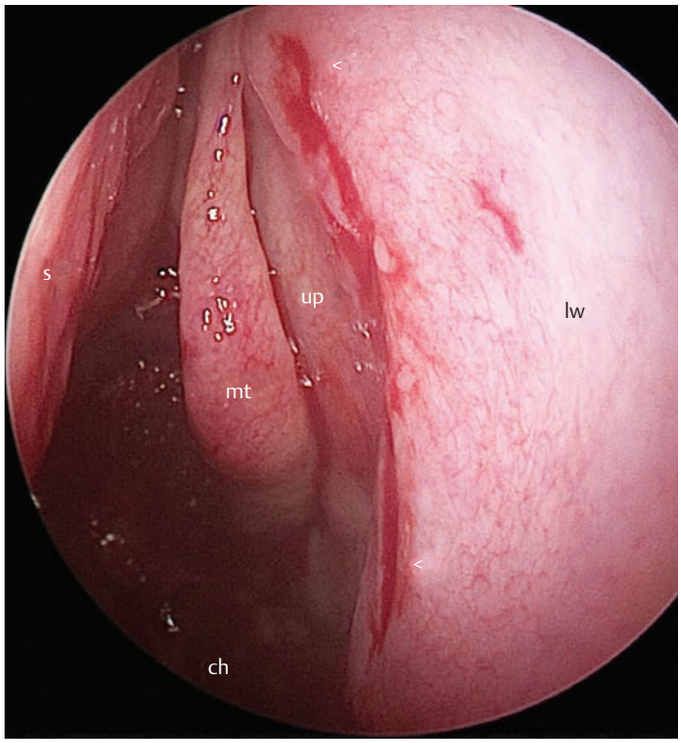

Fig. 6.53 The posterior incision: Immediately anterior to the uncinate process (white arrowhead).

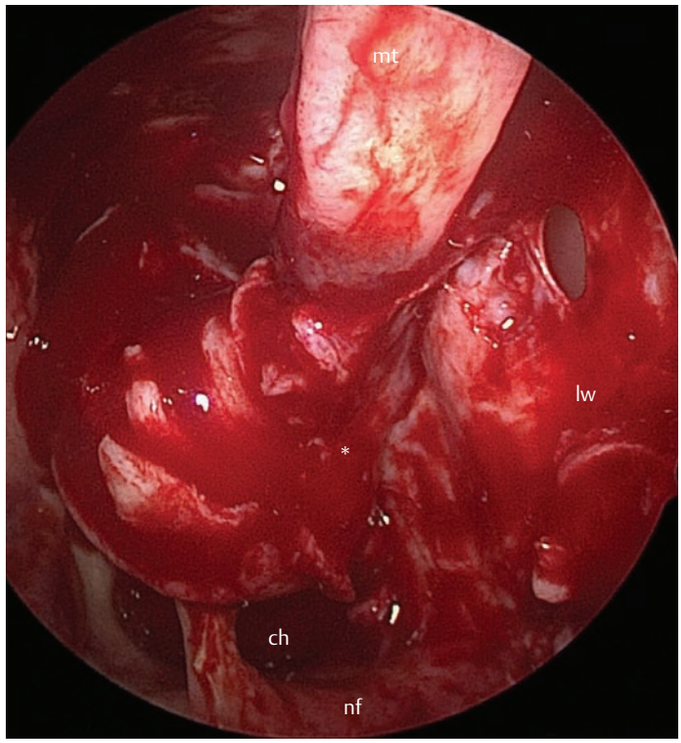

Fig. 6.54 Flap mobilization and defect coverage: The flap is rotated from a sagittal orientation to an axial plane to cover the defect without any folds. The accessory maxillary sinus ostium (white arrowhead) *Flap pedicle.

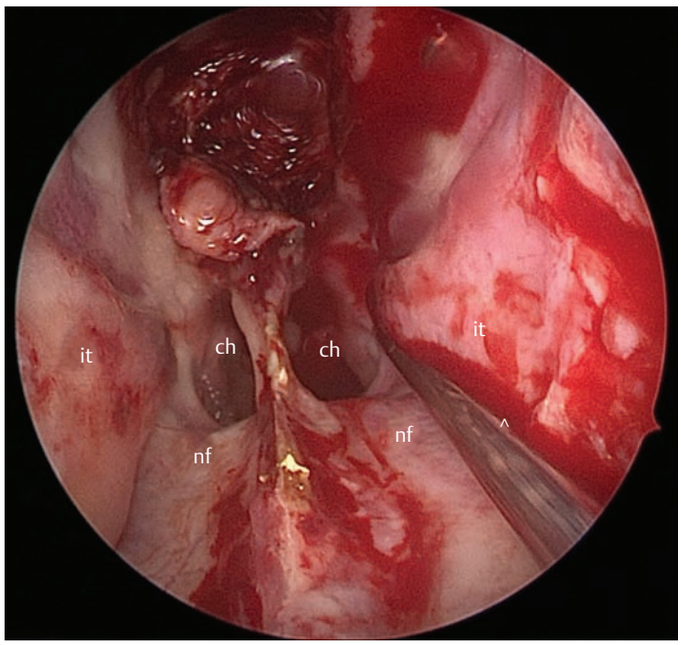

Fig. 6.55 The antero posterior incision: Along the junction of the lateral nasal wall and the nasal floor.

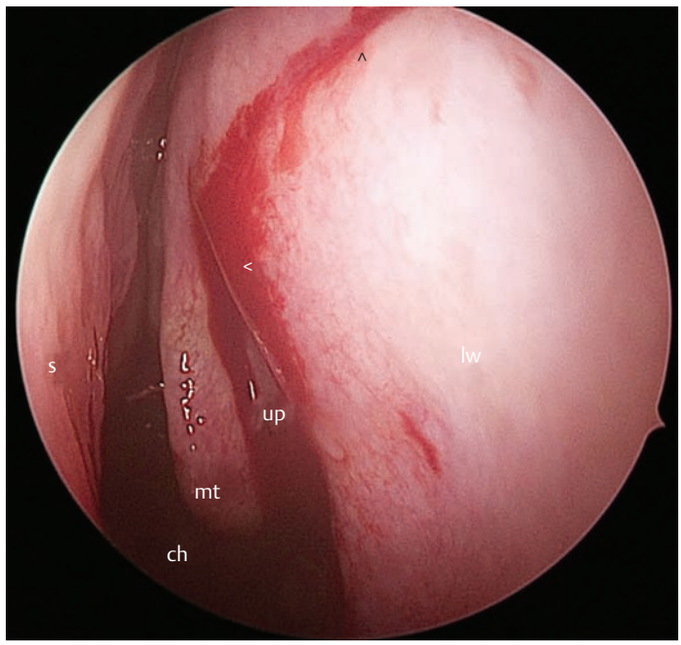

Fig. 6.56 The anterior horizontal incision: Anteriorly on the lateral nasal wall connecting the anterior and posterior incisions (black arrowhead); The posterior incision (White arrowhead).

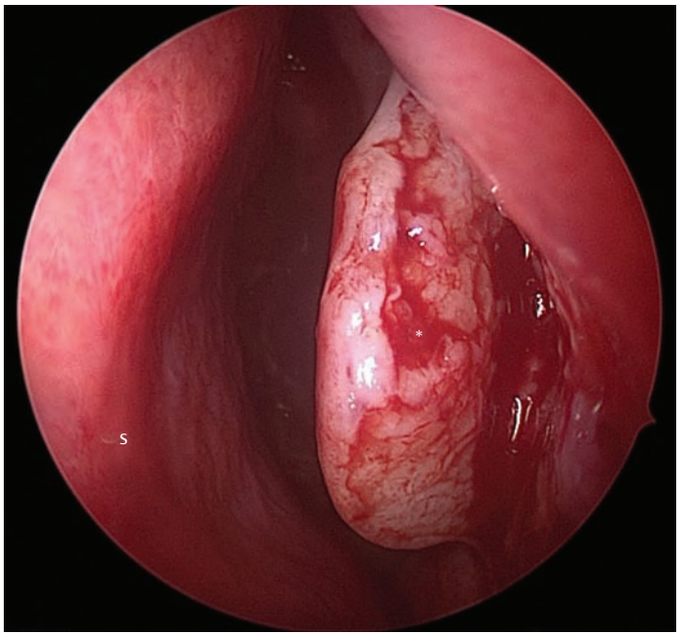

Fig. 6.57 Submucoperiosteal flap elevation.

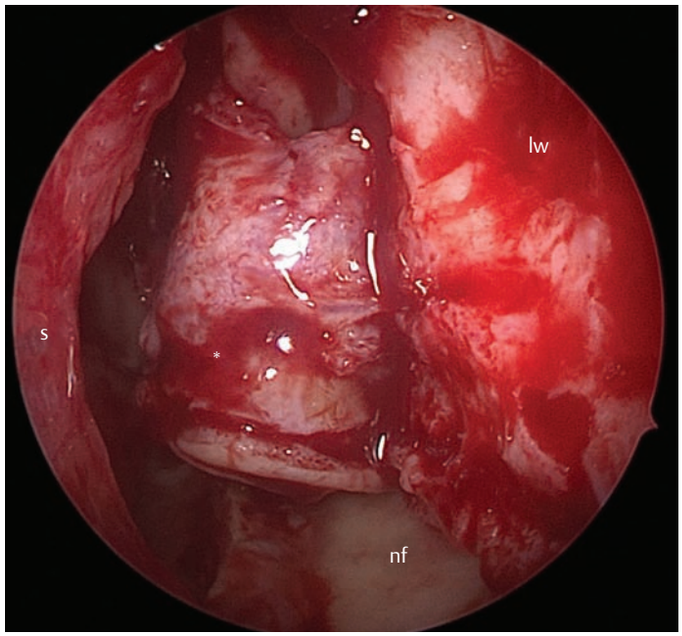

Fig. 6.58 Submucoperiosteal flap elevation.

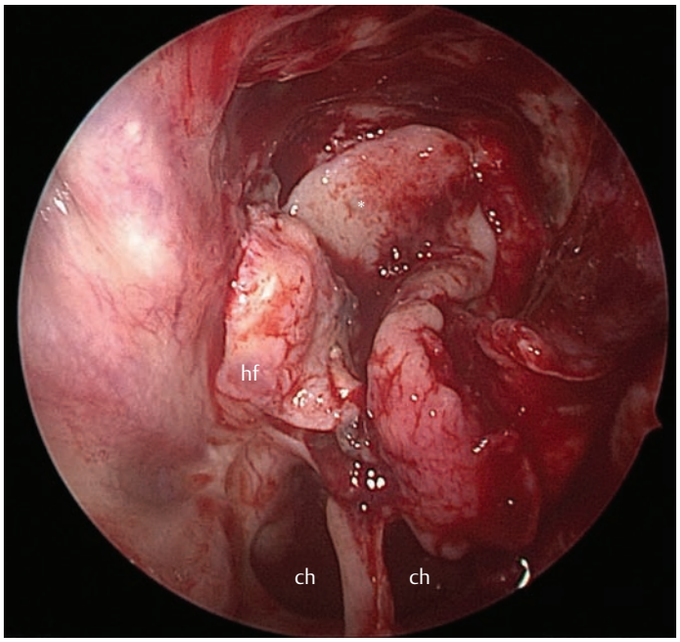

Fig. 6.59 Flap mobilization and defect coverage: The flap is rotated from a sagittal orientation to an axial plane to cover the defect without any folds. The recycled nasoseptal flap (hf) is augmented with lateral nasal wall flap.

Anterior Pedicle Lateral Nasal Wall Flap (Hadad-Bassagaisteguy 2 or HB2 Flap)

In 2011, Hadad et al described the anterior pedicle lateral nasal wall flap as an alternative to the Hadad flap when it's not feasible or the defect demands the use of multiple flaps. It has the adequate length and width to cover defects from the crista galli anteriorly to the tuberculum sella posteriorly between the two orbits.[38,49]

Vascular Anatomy

Anterior pedicle based on the branches of the facial and the anterior ethmoidal arteries. The pedicle is oriented vertically on the lateral nasal wall. It extends from the area anterior to the middle turbinate up to the head of the inferior turbinate.[38,49]

Surgical Technique[38,49]

- **Mucosal decongestion:** Done with topical adrenaline-soaked pledgets.

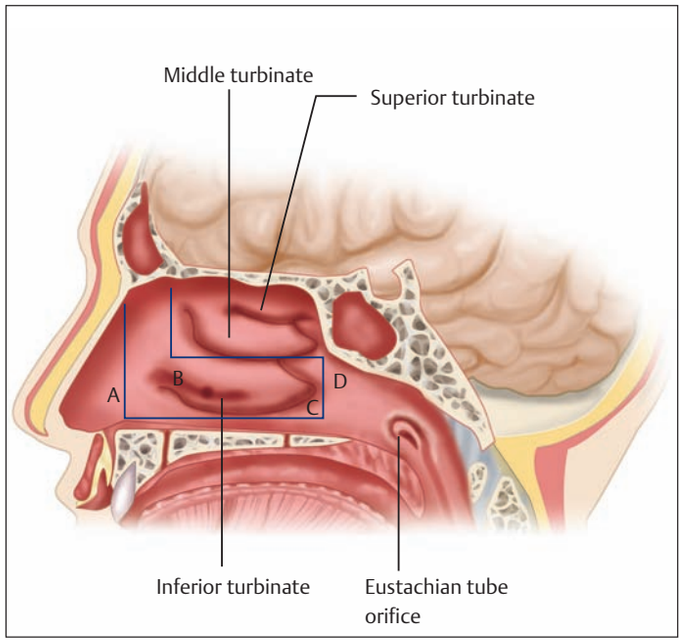

Fig. 6.60 Illustration showing various incisions employed in harvesting an anterior pedicled lateral nasal wall flap. **(A)** Anterior incision. **(B)** Posterior incision. **(C)** Anteroposterior incision. **(D)** Posterior vertical incision.

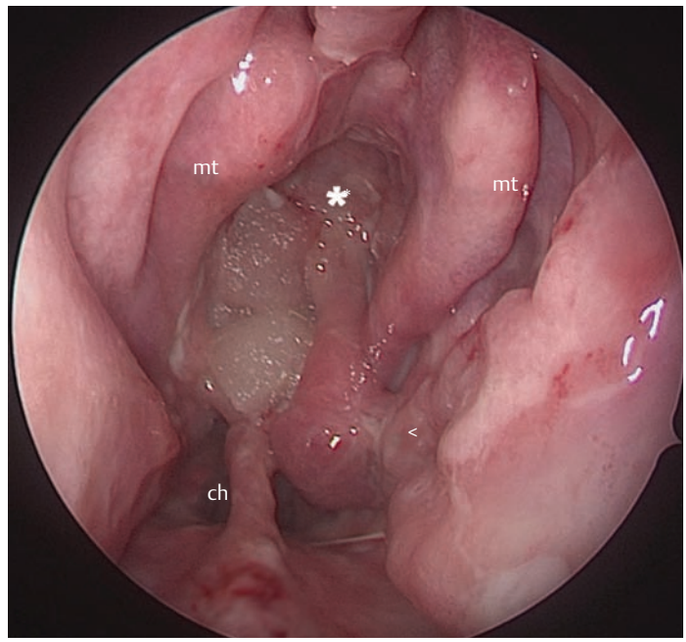

Fig. 6.61 Postoperative view of a well taken up lateral nasal wall flap.

- **Incision:** It is performed with a number 15 blade or a needle tip extended monopolar electrocautery device set at 15W. Incisions are listed in a stepwise manner (**Fig. 6.60**).
  - **Anterior incision:** Begins along the anterior border of ascending maxillary process and the inferior turbinate head to the nasal floor.
  - **Posterior incision:** Begins along the uncinate process extending posteriorly along the superior margin of the inferior turbinate until its posterior end. Posterior to the uncinate process this incision can be taken superiorly to include the maxillary fontanelle region into the flap.
  - **Anteroposterior incision:** Begins along the junction of the lateral nasal wall and the nasal floor. This incision can be made on the nasal floor, at the nasoseptal junction, or higher above on the septum for a wider flap.
  - **Posterior vertical incision:** Begins posteriorly on the lateral nasal wall connecting the anteroposterior and posterior incisions.
- **Mucoperiosteal elevation:** From the lateral nasal wall, medial and lateral side of the inferior turbinate and lastly the nasal floor is done using a Freer's elevator.
- Inferior turbinate fracturing and bone removal.
- **Flap mobilization and defect coverage:** The flap is rotated from a sagittal orientation to an axial plane to cover the defect without any folds (**Fig. 6.61**).
- **Flap support:** As mentioned in general principles.

Pericranial Flap

It is the vascularized flap of choice for large anterior skull base defects in cases were NSF is either unavailable or is insufficient to completely cover the defect necessitating the use of multiple flaps. This flap was first described by Wolfe in 1978 for craniofacial reconstruction[50] and was initially used in open skull base reconstruction procedures. Currently, pericranial flap (PCF) is considered the second choice in endoscopic skull base reconstruction for large defects.[10,51] Even though minimally invasive endoscopic harvestation techniques have been described, the author prefers conventional technique using the classical bicoronal incision[38,52–54]

Advantages of classical technique:

- Decreased operative time hence cost-effective.
- More degree of freedom and bimanual dexterity allows better dissection of flap and pedicle care.

- Excellent exposure to effectively design the flap to the desired dimensions, thus avoiding a smaller flap.
- More cosmetic as the incision is well hidden in the hair line and it avoids a separate glabellar incision.

Vascular Anatomy

Pedicled by the supraorbital and the supratrochlear arteries, branches of the ophthalmic artery which in turn is the branch of the supraclinoid internal carotid artery (ICA).[16] They exit via the supraorbital and the supratrochlear notches/foramina located ~1 cm above the superior orbital rim. These arteries course in the galea frontalis muscular layer giving off branches to the pericranium[38,52–55] (**Figs. 6.62 and 6.63**).

Surgical Technique[38,52–54,56]

- **Incison:** Bicoronal scalp incision placed at the vertex extending into the preauricular region bilaterally. Incision is deepened to the level of pericranium from one superior temporal line to the other. Care is taken not to incise the pericranium (**Fig. 6.64**).
- **Flap dissection:** Scalp layers are dissected off the pericranium in a posterior to anterior direction up to the level of the superior orbital rim.
- **Fashioning PCF:** Incision over the pericranium not crossing the midline is designed such that flap of desired dimension can be obtained. For additional length, this incision can be made further posterior to the bicoronal scalp incision.
- **PCF elevation:** Pericranial flap is elevated from the cranium using blunt dissection until the level of the superior orbital rim anteriorly (**Fig. 6.65**).
- **The pedicle:** The supraorbital and supratrochlear neurovascular bundles are identified as they exit their respective foramina. Care is taken not to cause trauma or undue traction to the pedicle (**Fig. 6.63**).
- **Nasinectomy window:** A 2-cm osteotomy is created at the nasion using a 5-mm cutting burr and micro drill (**Fig. 6.66**).
- **Flap delivery:** Flap is slowly delivered via the osteotomy into the nasofrontal area and is received endoscopically (**Fig. 6.67**).
- **Flap positioning:** Flap is positioned without any folds and bulldozed onto the defect using a lint to snuggly cover it.
- **Flap support:** As mentioned in general principles (**Figs. 6.3, 6.6, 6.11, and 6.68**).

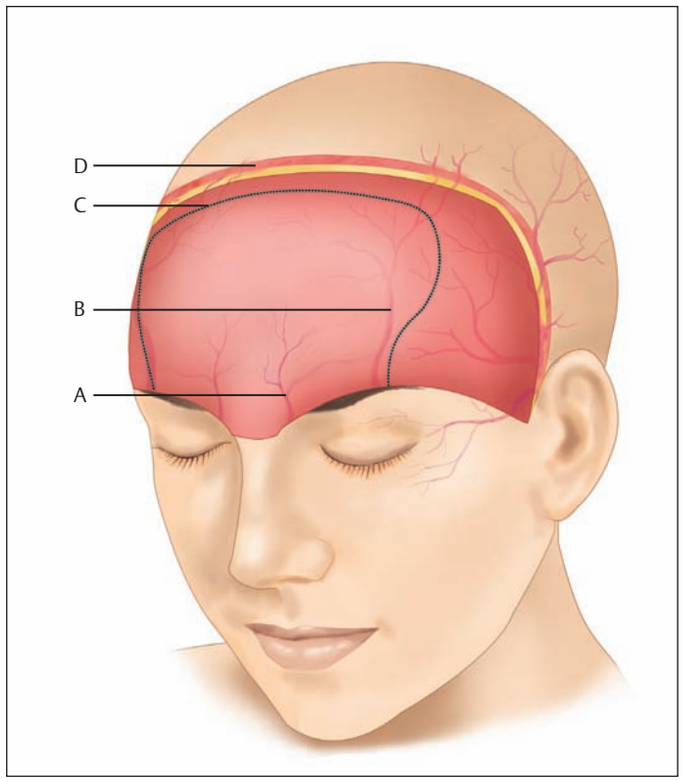

Fig. 6.62 Illustration showing. **(A)** Supratrochlear artery. **(B)** Supraorbital artery. **(C)** Pericranial incision. **(D)** Bicoronal scalp incision.

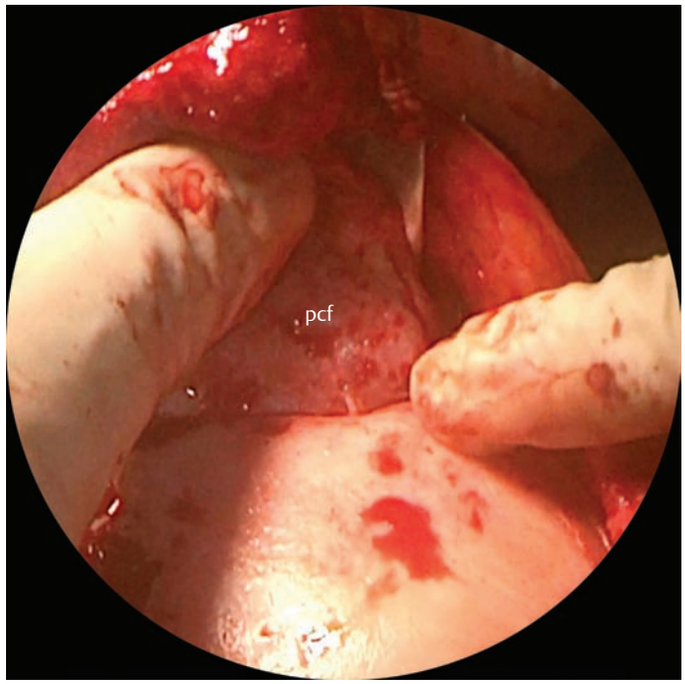

Fig. 6.63 The pedicle: the supraorbital and supratrochlear neurovascular bundles are identified as they exit their respective foramina.

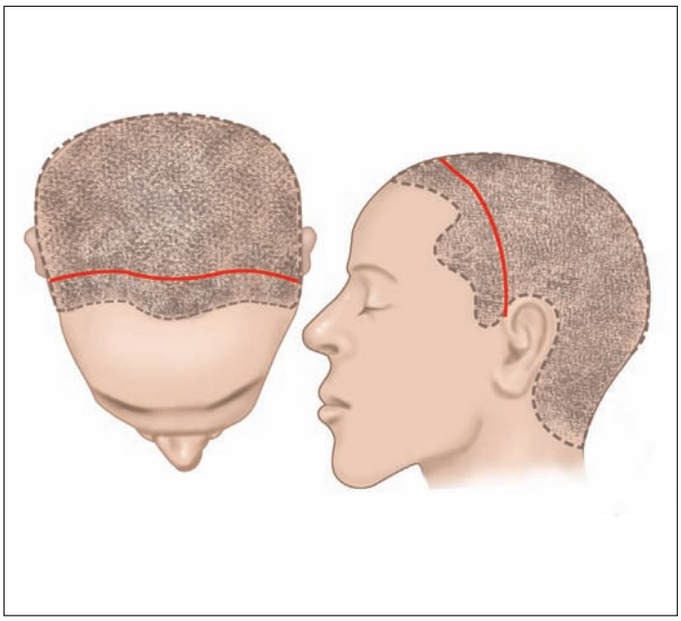

Fig. 6.64 Illustration showing the extend of bicoronal incision.

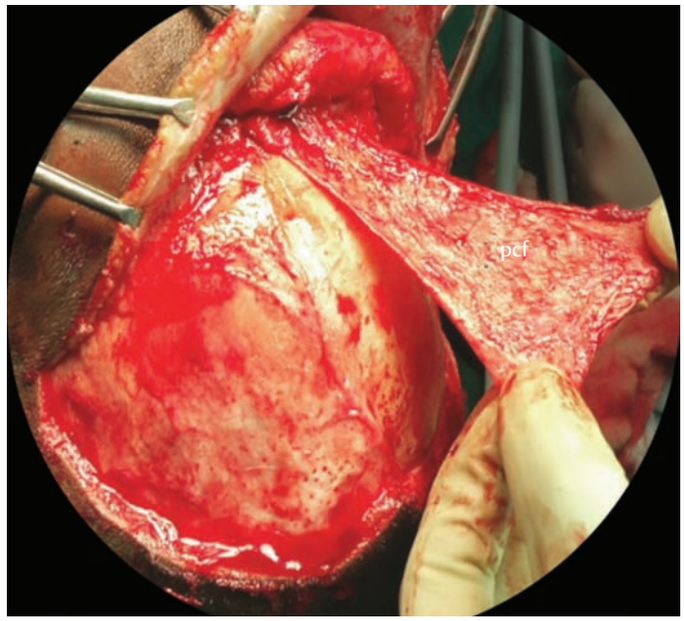

Fig. 6.65 Pericranial flap upon complete dissection.

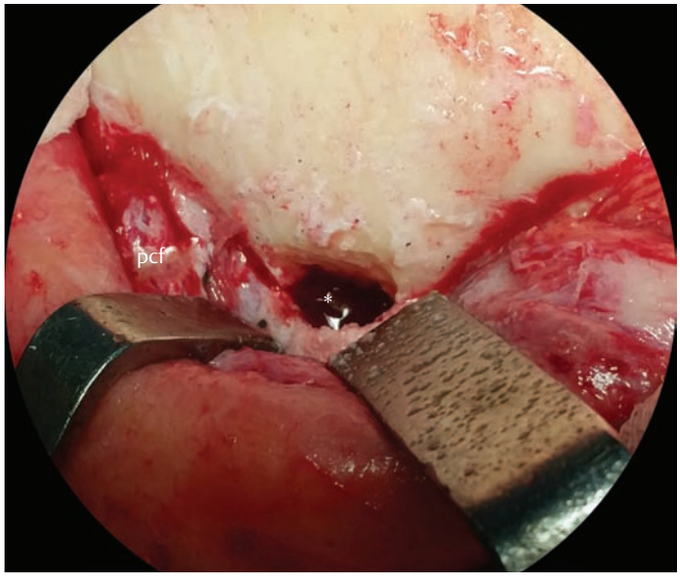

Fig. 6.66 *Nasinectomy window: A 2-cm osteotomy is created at the nasion using a 5-mm cutting burr and micro drill.

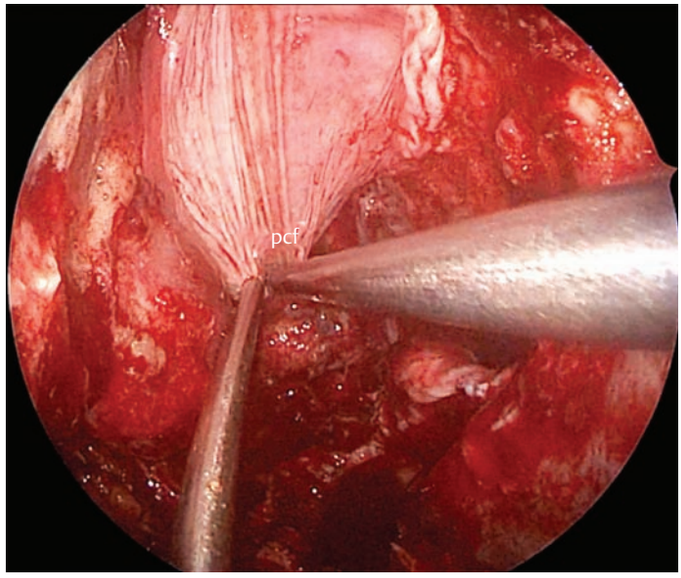

Fig. 6.67 Flap delivery: Flap is slowly delivered via the osteotomy into the nasofrontal area and is received endoscopically.

Temporoparietal Fascial Flap

The temporoparietal fascial flap was first described in1898, in the reconstruction of the external ear and the lower eyelid. Thereafter it was used in various head and neck reconstructive procedures. In skull base reconstruction, it is used as an alternative to the NSF, when it is not available or the defect demands the use of multiple flaps. It is a 2- to 3-mm thick, fan-shaped fascial flap from the temporoparietal region of the scalp. It is pedicled at the preauricular region and has a surface area of 17 × 14 cm. It is employed in reconstruction of large defects in the posterior and middle skull base. A transpterygoid tunnel has to be created to deliver the flap into the nasal cavity.[10,13,38,46,57–59]

Vascular Anatomy

Its pedicle is based on the branches of the superficial temporal artery along with its accompanying veins[13,38,57,58] (**Fig. 6.69**).

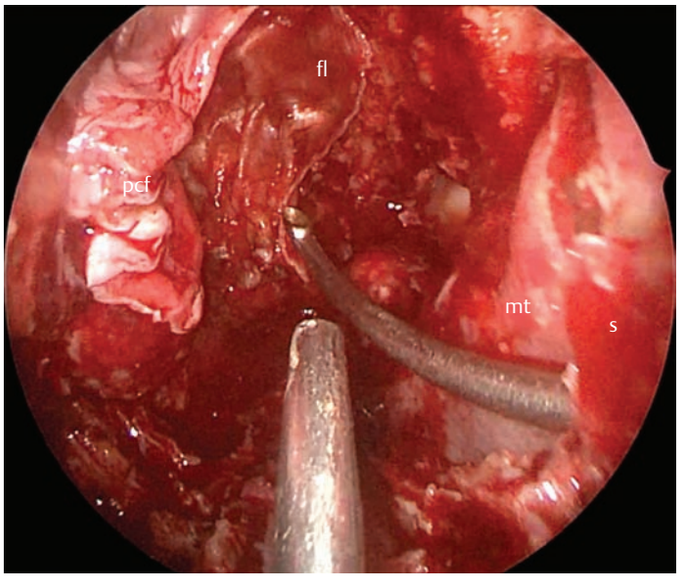

Fig. 6.68 Fascia lata placed over Duraform.

Surgical Technique[10,13,38,46,57–59]

- **Hemicoronal scalp incision:** An incision at the level of the hair follicles is made (**Fig. 6.69**).
- **Temporoparietal fascial flap dissection:** Begins from the superficial subcutaneous tissue to create a flap of adequate dimension. Inferiorly the dissection extends up to the level of the pedicle. Care is taken not to injure the frontal branch of the facial nerve while dissection. This is ensured by staying behind the hairline and an imaginary line connecting the tragus and the lateral eyebrow (**Fig. 6.70**).
- **Temporoparietal fascial flap elevation:** This is done after deepening the incision along the edges of the flap, down to the pericranium above, and the deep temporal fascia below the superficial temporal line (**Fig. 6.71**).
- **Transpterygoid tunnel creation:**
  - **Endonasal component of the transpterygoid tunnel:**
    1. Ipsilateral anterior and posterior ethmoidectomies, followed by a wide maxillary antrostomy and removal of the posterior wall of maxillary sinus is done. The SPA is identified and ligated.

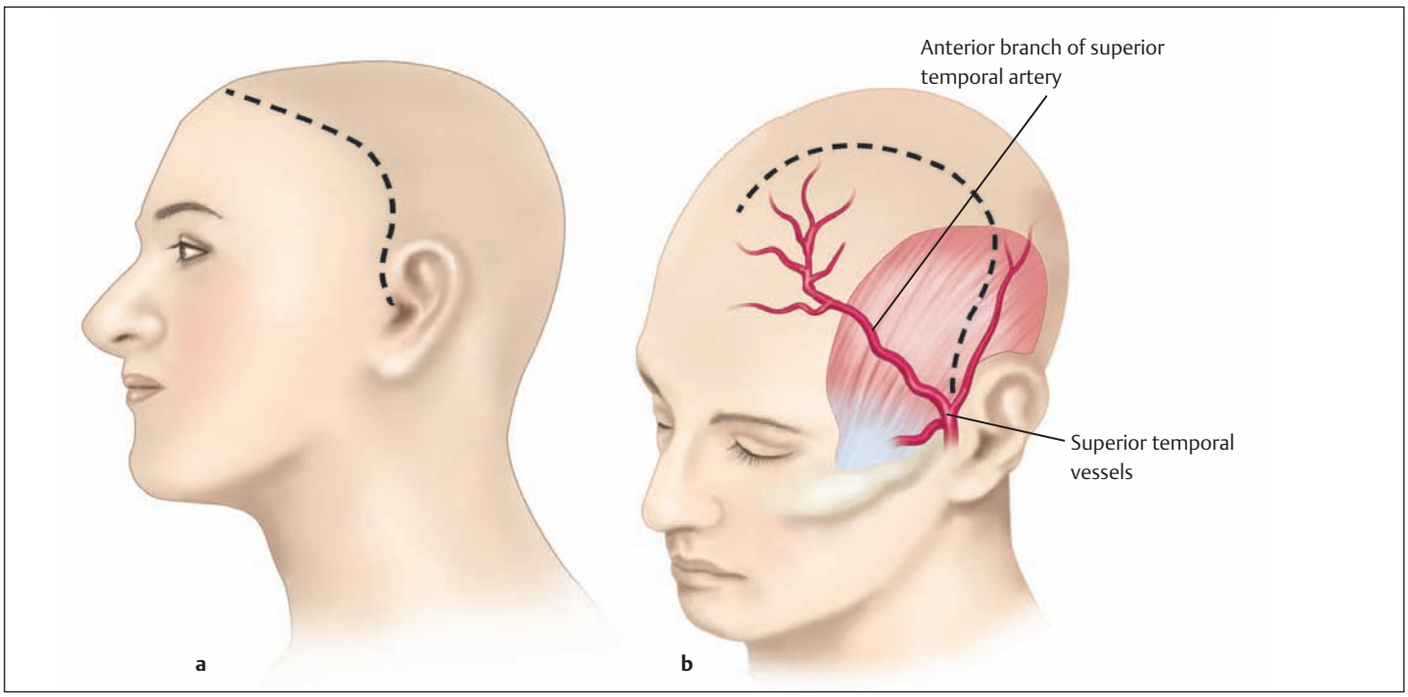

Fig. 6.69 Illustration showing. **(a)** Extend of hemicoronal incision. **(b)** Vascular pedicle of temporoparietal fascial flap (TPFF), the anterior branch of superficial temporal artery.

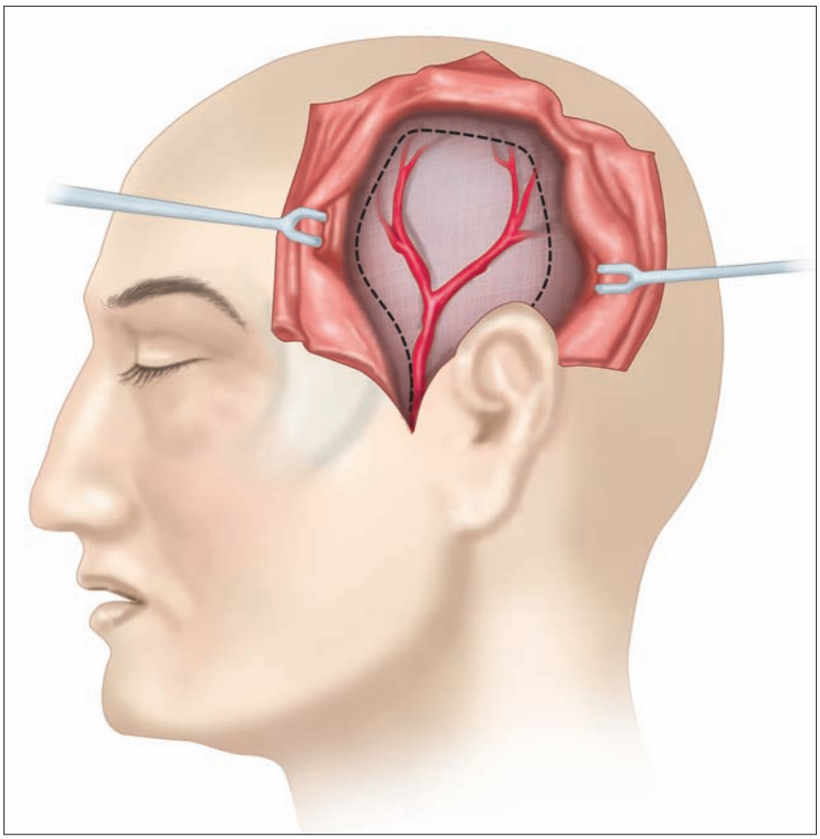

Fig. 6.70 Illustration showing temporoparietal fascial flap (TPFF) incision line and its vascular pedicle.

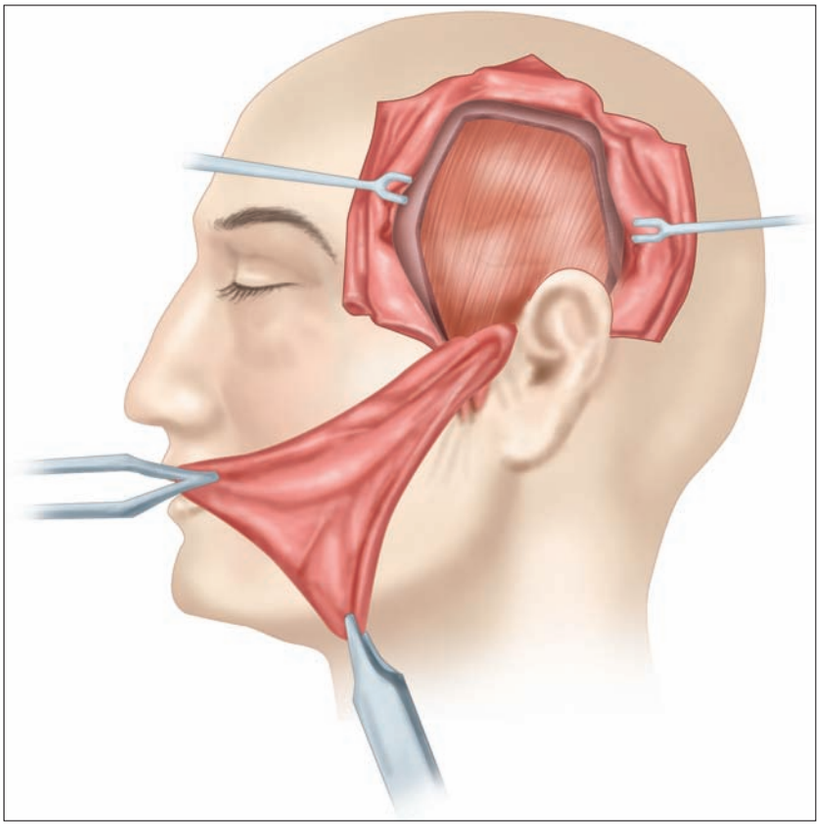

Fig. 6.71 Illustration showing temporoparietal fascial flap (TPFF) upon complete elevation.

Contents of the pterygopalatine fossa are lateralized to expose the lateral pterygoid plate, which is then reduced by drilling.

- **External component of the transpterygoid tunnel:**
  1. **Lateral canthotomy incision:** It is given to expose and separate the temporalis muscle from the lateral orbital wall and the pterygomaxillary fissure; thus creating a soft tissue tunnel connecting the temporal, infratemporal, and the pterygopalatine fossa.
  2. **Dilatation of the soft tissue canal:** This is done by passing a guide wire and dilator through it into the nasal cavity.

- **Transposition of the flap into the nasal cavity:** The external end of the guide wire is tied to the distal part of the flap. The guide wire is then pulled out of the nostril to deliver the flap into the nasal cavity via the transpterygoid canal.
- **Flap positioning:** Flap is positioned without any folds and bulldozed onto the defect using a lint to snuggly cover it.
- **Flap support:** As mentioned in general principles.

Palatal Flap

Palatal flap, as described in cadaveric studies, comprises the mucoperiosteal tissue of the hard palate and is supplied by the greater palatine vessels. It is raised by subperiosteal dissection and is delivered intranasally via the greater palatine foramen. Palatal flaps are not favored due to lack of clinical experience and due to donor site morbidity.[10,46]

Facial Buccinator Flap

Buccinator flap has been recently described in cadaveric studies by Rivera Serrano et al in 2010. It has a pedicle based on the facial artery and comprises the buccal soft tissue along with the surrounding muscle (facial artery musculobuccinator flap) and mucosa (facial artery musculomucosal buccinator flap). The flap is delivered intranasally through a maxillary window.[60]

Conclusion

Endoscopic skull base reconstruction has evolved to address defects involving the entire anterior craniosacral fossa floor with the use of multilayer closure techniques and pedicled flaps. Preoperative planning and perioperative care is crucial in successfully repairing the cranial fossa floor. In the authors' experience the use of aforementioned ESBR techniques has drastically reduced the incidence of postoperative CSF leaks to 3 to 5%. Before embarking on endoscopic anterior skull base tumor resections, one must master the art of skull base reconstruction to keep at bay untoward postoperative sequelae.

References

1. Kassam A, Thomas AJ, Snyderman C, et al. Fully endoscopic expanded endonasal approach treating skull base lesions in pediatric patients. J Neurosurg 2007;106(2, Suppl)75–86
2. Eloy JA, Kuperan AB, Choudhry OJ, Harirchian S, Liu JK. Efficacy of the pedicled nasoseptal flap without cerebrospinal fluid (CSF) diversion for repair of skull base defects: incidence of postoperative CSF leaks. Int Forum Allergy Rhinol 2012;2(5): 397–401
3. Martín-Martín C, Martínez-Capoccioni G, Serramito-García R, Espinosa-Restrepo F. Surgical challenge: endoscopic repair of cerebrospinal fluid leak. BMC Res Notes 2012;5:459
4. Shin M, Kondo K, Saito N. Current status of endoscopic endonasal surgery for skull base meningiomas: review of the literature. Neurol Med Chir (Tokyo) 2015;55(9):735–743
5. Kassam A, Carrau RL, Snyderman CH, Gardner P, Mintz A. Evolution of reconstructive techniques following endoscopic expanded endonasal approaches. Neurosurg Focus 2005; 19(1):E8
6. Harvey RJ, Smith JE, Wise SK, Patel SJ, Frankel BM, Schlosser RJ. Intracranial complications before and after endoscopic skull base reconstruction. Am J Rhinol 2008;22(5):516–521
7. Bernal-Sprekelsen M, Bleda-Vázquez C, Carrau RL. Ascending meningitis secondary to traumatic cerebrospinal fluid leaks. Am J Rhinol 2000;14(4):257–259
8. Bernal-Sprekelsen M, Alobid I, Mullol J, Trobat F, Tomás-Barberán M. Closure of cerebrospinal fluid leaks prevents ascending bacterial meningitis. Rhinology 2005;43(4): 277–281
9. Bleier BS, ed. Comprehensive Techniques in CSF Leak Repair and Skull Base Reconstruction. Adv Otorhinolaryngol. Basel, Karger, 2013; 74: 104–118

10. Zanation AM, Thorp BD, Parmar P, Harvey RJ. Reconstructive options for endoscopic skull base surgery. Otolaryngol Clin North Am 2011;44(5):1201–1222
11. Liu JK, Schmidt RF, Choudhry OJ, Shukla PA, Eloy JA. Surgical nuances for nasoseptal flap reconstruction of cranial base defects with high-flow cerebrospinal fluid leaks after endoscopic skull base surgery. Neurosurg Focus 2012;32(6):E7
12. Chin D, Harvey RJ. Endoscopic reconstruction of frontal, cribiform and ethmoid skull base defects. Adv Otorhinolaryngol 2013;74:104–118
13. Kim GG, Hang AX, Mitchell CA, Zanation AM. Pedicled extranasal flaps in skull base reconstruction. Adv Otorhinolaryngol 2013; 74:71–80
14. Soudry E, Turner JH, Nayak JV, Hwang PH. Endoscopic reconstruction of surgically created skull base defects: a systematic review. Otolaryngol Head Neck Surg 2014;150(5):730–738
15. Pinheiro-Neto CD, Snyderman CH. Nasoseptal flap. Adv Otorhinolaryngol 2013;74:42–55
16. Snyderman CH, Janecka IP, Sekhar LN, Sen CN, Eibling DE. Anterior cranial base reconstruction: role of galeal and pericranial flaps. Laryngoscope 1990;100(6):607–614
17. Schlosser RJ, Wilensky EM, Grady MS, Palmer JN, Kennedy DW, Bolger WE. Cerebrospinal fluid pressure monitoring after repair of cerebrospinal fluid leaks. Otolaryngol Head Neck Surg 2004;130(4):443–448
18. Schlosser RJ, Bolger WE. Nasal cerebrospinal fluid leaks: critical review and surgical considerations. Laryngoscope 2004;114(2): 255–265
19. Zanation AM, Carrau RL, Snyderman CH, et al. Nasoseptal flap reconstruction of high flow intraoperative cerebral spinal fluid leaks during endoscopic skull base surgery. Am J Rhinol Allergy 2009;23(5):518–521
20. Snyderman CH, Kassam AB, Carrau R, Mintz A. Endoscopic reconstruction of cranial base defects following endonasal skull base surgery. Skull Base 2007;17(1):73–78
21. Harvey RJ, Nogueira JF, Schlosser RJ, Patel SJ, Vellutini E, Stamm AC. Closure of large skull base defects after endoscopic transnasal craniotomy. Clinical article. J Neurosurg 2009;111(2): 371–379
22. Leong JL, Citardi MJ, Batra PS. Reconstruction of skull base defects after minimally invasive endoscopic resection of anterior skull base neoplasms. Am J Rhinol 2006;20(5):476–482
23. El-Banhawy OA, Halaka AN, Altuwaijri MA, Ayad H, El-Sharnoby MM. Long-term outcome of endonasal endoscopic skull base reconstruction with nasal turbinate graft. Skull Base 2008; 18(5):297–308
24. Carrau RL, Snyderman CH, Kassam AB. The management of cerebrospinal fluid leaks in patients at risk for high-pressure hydrocephalus. Laryngoscope 2005;115(2):205–212
25. Seth R, Rajasekaran K III, Luong A, Benninger MS, Batra PS. Spontaneous CSF leaks: factors predictive of additional interventions. Laryngoscope 2010;120(11):2141–2146
26. Leng LZ, Brown S, Anand VK, Schwartz TH. "Gasket-seal" watertight closure in minimal-access endoscopic cranial base surgery. Neurosurgery 2008;62(5, Suppl 2)E342–E343, discussion E343
27. Gil Z, Abergel A, Leider-Trejo L, et al. A comprehensive algorithm for anterior skull base reconstruction after oncological resections. Skull Base 2007;17(1):25–37
28. Mattox DE, Kennedy DW. Endoscopic management of cerebrospinal fluid leaks and cephaloceles. Laryngoscope 1990; 100(8):857–862
29. Lee TJ, Huang CC, Chuang CC, Huang SF. Transnasal endoscopic repair of cerebrospinal fluid rhinorrhea and skull base defect: ten-year experience. Laryngoscope 2004;114(8):1475–1481
30. Hadad G, Bassagasteguy L, Carrau RL, et al. A novel reconstructive technique after endoscopic expanded endonasal approaches: vascular pedicle nasoseptal flap. Laryngoscope 2006;116(10):1882–1886
31. Kassam AB, Thomas A, Carrau RL, et al. Endoscopic reconstruction of the cranial base using a pedicled nasoseptal flap. Neurosurgery 2008;63(1, Suppl 1)ONS44–ONS52, discussion ONS52–ONS53
32. Babin E, Moreau S, de Rugy MG, Delmas P, Valdazo A, Bequignon A. Anatomic variations of the arteries of the nasal fossa. Otolaryngol Head Neck Surg 2003;128(2):236–239
33. Pinheiro-Neto CD, Ramos HF, Peris-Celda M, et al. Study of the nasoseptal flap for endoscopic anterior cranial base reconstruction. Laryngoscope 2011;121(12):2514–2520
34. Snyderman CH, Carrau RL, Kassam AB, et al. Endoscopic skull base surgery: principles of endonasal oncological surgery. J Surg Oncol 2008;97(8):658–664
35. Shah RN, Surowitz JB, Patel MR, et al. Endoscopic pedicled nasoseptal flap reconstruction for pediatric skull base defects. Laryngoscope 2009;119(6):1067–1075
36. Caicedo-Granados E, Carrau R, Snyderman CH, et al. Reverse rotation flap for reconstruction of donor site after vascular pedicled nasoseptal flap in skull base surgery. Laryngoscope 2010;120(8):1550–1552
37. Kasemsiri P, Carrau RL, Otto BA, et al. Reconstruction of the pedicled nasoseptal flap donor site with a contralateral reverse rotation flap: technical modifications and outcomes. Laryngoscope 2013;123(11):2601–2604
38. Tang IP, Carrau RL, Otto BA, et al. Technical nuances of commonly used vascularised flaps for skull base reconstruction. J Laryngol Otol 2015;129(8):752–761
39. Pinheiro-Neto CD, Carrau RL, Prevedello DM, et al. Use of acoustic Doppler sonography to ascertain the feasibility of the pedicled nasoseptal flap after prior bilateral sphenoidotomy. Laryngoscope 2010;120(9):1798–1801
40. Rivera-Serrano CM, Snyderman CH, Gardner P, et al. Nasoseptal "rescue" flap: a novel modification of the nasoseptal flap technique for pituitary surgery. Laryngoscope 2011;121(5):990–993

41. Fortes FS, Carrau RL, Snyderman CH, et al. The posterior pedicle inferior turbinate flap: a new vascularized flap for skull base reconstruction. Laryngoscope 2007;117(8):1329–1332
42. Gil Z, Margalit N. Anteriorly based inferior turbinate flap for endoscopic skull base reconstruction. Otolaryngol Head Neck Surg 2012;146(5):842–847
43. Hadar T, Ophir D, Yaniv E, Berger G. Inferior turbinate arterial supply: histologic analysis and clinical implications. J Otolaryngol 2005;34(1):46–50
44. Padgham N, Vaughan-Jones R. Cadaver studies of the anatomy of arterial supply to the inferior turbinates. J R Soc Med 1991; 84(12):728–730
45. Prevedello DM, Barges-Coll J, Fernandez-Miranda JC, et al. Middle turbinate flap for skull base reconstruction: cadaveric feasibility study. Laryngoscope 2009;119(11):2094–2098
46. Patel MR, Stadler ME, Snyderman CH, et al. How to choose? Endoscopic skull base reconstructive options and limitations. Skull Base 2010;20(6):397–404
47. Simal Julián JA, Miranda Lloret P, Cárdenas Ruiz-Valdepeñas E, Barges Coll J, Beltrán Giner A, Botella Asunción C. Middle turbinate vascularized flap for skull base reconstruction after an expanded endonasal approach. Acta Neurochir (Wien) 2011; 153(9):1827–1832
48. Rivera-Serrano CM, Bassagaisteguy LH, Hadad G, et al. Posterior pedicle lateral nasal wall flap: new reconstructive technique for large defects of the skull base. Am J Rhinol Allergy 2011;25(6):e212–e216
49. Hadad G, Rivera-Serrano CM, Bassagaisteguy LH, et al. Anterior pedicle lateral nasal wall flap: a novel technique for the reconstruction of anterior skull base defects. Laryngoscope 2011;121(8):1606–1610
50. Wolfe SA. The utility of pericranial flaps. Ann Plast Surg 1978;1(2):147–153
51. Zanation AM, Snyderman CH, Carrau RL, Kassam AB, Gardner PA, Prevedello DM. Minimally invasive endoscopic pericranial flap: a new method for endonasal skull base reconstruction. Laryngoscope 2009;119(1):13–18
52. Yoshioka N, Rhoton AL Jr. Vascular anatomy of the anteriorly based pericranial flap. Neurosurgery 2005;57(1, Suppl)11–16, discussion 11–16
53. Price JC, Loury M, Carson B, Johns ME. The pericranial flap for reconstruction of anterior skull base defects. Laryngoscope 1988;98(11):1159–1164
54. Smith JE, Ducic Y. The versatile extended pericranial flap for closure of skull base defects. Otolaryngol Head Neck Surg 2004;130(6):704–711
55. Yoshioka N, Kishimoto S. Anteriorly based pericranial flap: an anatomic study of feeding arteries. Skull Base Surg 1991; 1(3):161–164
56. Patel MR, Shah RN, Snyderman CH, et al. Pericranial flap for endoscopic anterior skull-base reconstruction: clinical outcomes and radioanatomic analysis of preoperative planning. Neurosurgery 2010;66(3):506–512, discussion 512
57. David SK, Cheney ML. An anatomic study of the temporoparietal fascial flap. Arch Otolaryngol Head Neck Surg 1995; 121(10):1153–1156
58. Fortes FS, Carrau RL, Snyderman CH, et al. Transpterygoid transposition of a temporoparietal fascia flap: a new method for skull base reconstruction after endoscopic expanded endonasal approaches. Laryngoscope 2007;117(6):970–976
59. Harvey RJ, Parmar P, Sacks R, Zanation AM. Endoscopic skull base reconstruction of large dural defects: a systematic review of published evidence. Laryngoscope 2012;122(2):452–459
60. Rivera-Serrano CM, Oliver CL, Sok J, et al. Pedicled facial buccinator (FAB) flap: a new flap for reconstruction of skull base defects. Laryngoscope 2010;120(10):1922–1930

6A Temporoparietal Fascial Flap for Skull Base Reconstruction

Alberto Schreiber, Puya Dehgani-Mobaraki

The nasoseptal flap, by virtue of its safety, reliability, and versatility, is now being considered as the first option for skull base reconstruction after transnasal endoscopic procedures. However, skull base surgeons should be familiar with alternative options, whenever intranasal local flaps are unavailable or inadequate. Regional extranasal vascularized flaps, such as pericranial or temporoparietal fascial flap (TPFF), are preferable in the following critical circumstances: wide areas of bared bone, exposure of the internal carotid artery, previous treatments, osteomyelitis, or need for (re-)irradiation.[1–3] The TPFF has a thickness, pliability, long pedicle, and wide arch of rotation that confer a high versatility for complex defect of the middle and posterior skull base.[4] It has been recently described as a valuable option for the reconstruction of the anterior skull base.[5]

Ipsilateral nasal fossa must be prepared by performing a medial maxillectomy, to dominate the posterior wall of the maxillary sinus. Starting from the sphenopalatine foramen, all the bone of the posterior maxillary wall should be removed to expose the underlying periosteum. The periosteum should be opened to expose the fat of the infratemporal fossa that has to be partially removed to identify the coronoid insertion of the temporal muscle and the maxillary artery. Ligation of the maxillary artery can be avoided but, in this scenario, it is mandatory to proceed with a careful manipulation of the artery during the flap transposition.

A "question mark" shaped coronal incision from the pretragal area to the vertex is performed and the subcutaneous layer of the skin is carefully dissected from the temporoparietal fascia and galea aponeurotica along a virtual plane below the hair follicles (**Fig. 6A.1a**). The superficial temporal bundle and its branches are identified and preserved (**Fig. 6A.1b**). Care should be taken to avoid injury of the frontal branch of the facial nerve during the anterior subcutaneous dissection. TPFF is harvested centered on the main branch of the superficial temporal artery (commonly the parietal branch) and elevated including the pericranium (**Fig. 6A.1c, d**). An incision is made in the deep temporal fascia along the free margin of the zygomatic arch and the anterior border of the temporal muscle is displaced posteriorly (**Fig. 6A.1e, f**). The corridor through the temporal and infratemporal fossae is then completed by sliding a finger along the anterior border of the muscle and medial to the coronoid process to reach the posterior maxillary wall that is already open (**Fig. 6A.2a**). Using dilatators provided by Ciaglia percutaneous tracheostomy set (Cook Percutaneous Tracheostomy Introducer set, Cook Critical Care, Bloomington, IN), the corridor is enlarged (**Fig. 6A.2a, b**) and the distal portion of the TPFF is fixed to the guide wire of the set by a stitch to finally transpose it into the nasal cavity (**Fig. 6A.2c, d**).

References

1. Kim GG, Hang AX, Mitchell CA, Zanation AM. Pedicled extranasal flaps in skull base reconstruction. Adv Otorhinolaryngol 2013;74:71–80
2. Tang IP, Carrau RL, Otto BA, et al. Technical nuances of commonly used vascularised flaps for skull base reconstruction. J Laryngol Otol 2015;129(8):752–761
3. Bolzoni Villaret A, Nicolai P, Schreiber A, Bizzoni A, Farina D, Tschabitscher M. The temporo-parietal fascial flap in extended transnasal endoscopic procedures: cadaver dissection and personal clinical experience. Eur Arch Otorhinolaryngol 2013;270(4):1473–1479
4. Fortes FS, Carrau RL, Snyderman CH, et al. Transpterygoid transposition of a temporoparietal fascia flap: a new method for skull base reconstruction after endoscopic expanded endonasal approaches. Laryngoscope 2007;117(6):970–976
5. Ferrari M, Vural A, Schreiber A, et al. Side-door temporoparietal fascia flap: a novel strategy for anterior skull base reconstruction. World Neurosurg 2019

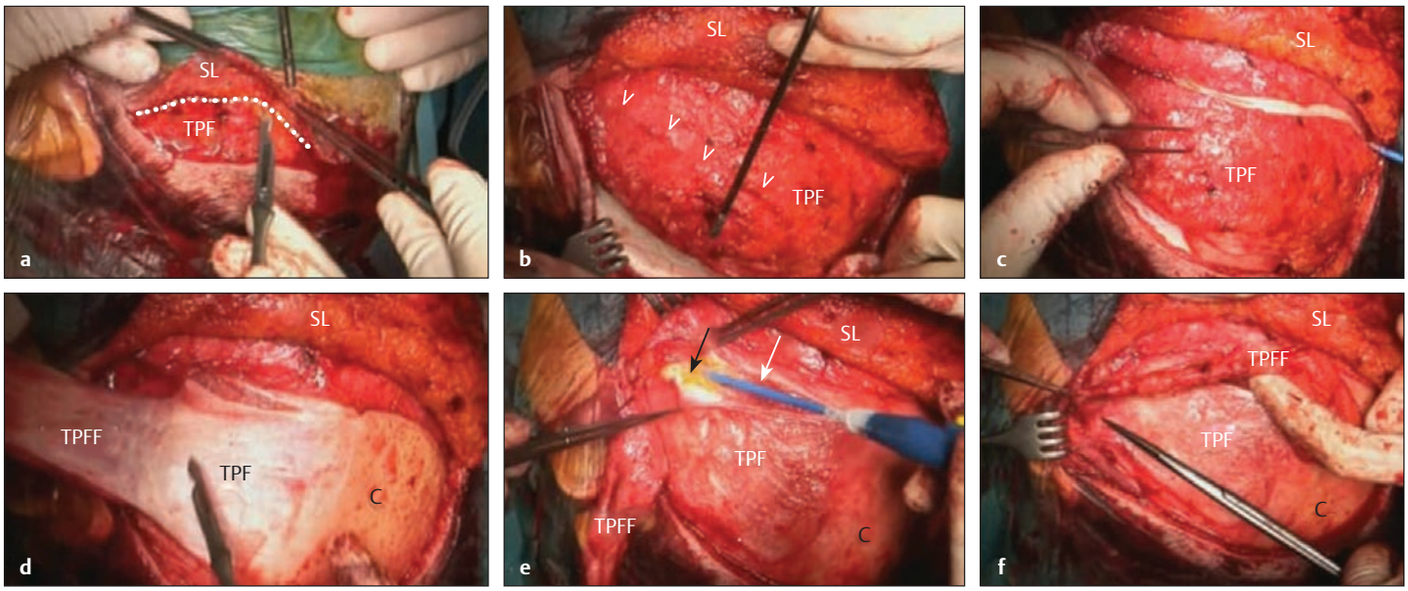

Fig. 6A.1 Temporoparietal fascial flap (TPFF) harvesting. **(a)** Dissection along the virtual plane deep to the hair follicles and superficial to the temporoparietal fascia and galea aponeurotica. **(b)** Identification of the superficial temporal bundle. Care should be taken to avoid injury of the frontal branch of the facial nerve during the anterior subcutaneous dissection. (**c, d**) Elevation of the TPFF including the pericranium. **(e)** Incision of the deep temporal fascia and fat pad along the free margin of the zygomatic arch and dissection of the temporal muscle anterior border. **(f)** Posterior dissection of the TPFF pedicle to increase the arch of rotation. C, calvaria; SL, subcutaneous layer; TF, deep temporal fascia; TPF, temporoparietal fascia; TPFF, temporoparietal fascial flap; *dotted line*: virtual plane deep to the hair follicles; *white arrowheads*: parietal branch of the superficial temporal artery; *black arrow*: fat pad; *white arrow*; anterior border of the temporal muscle.

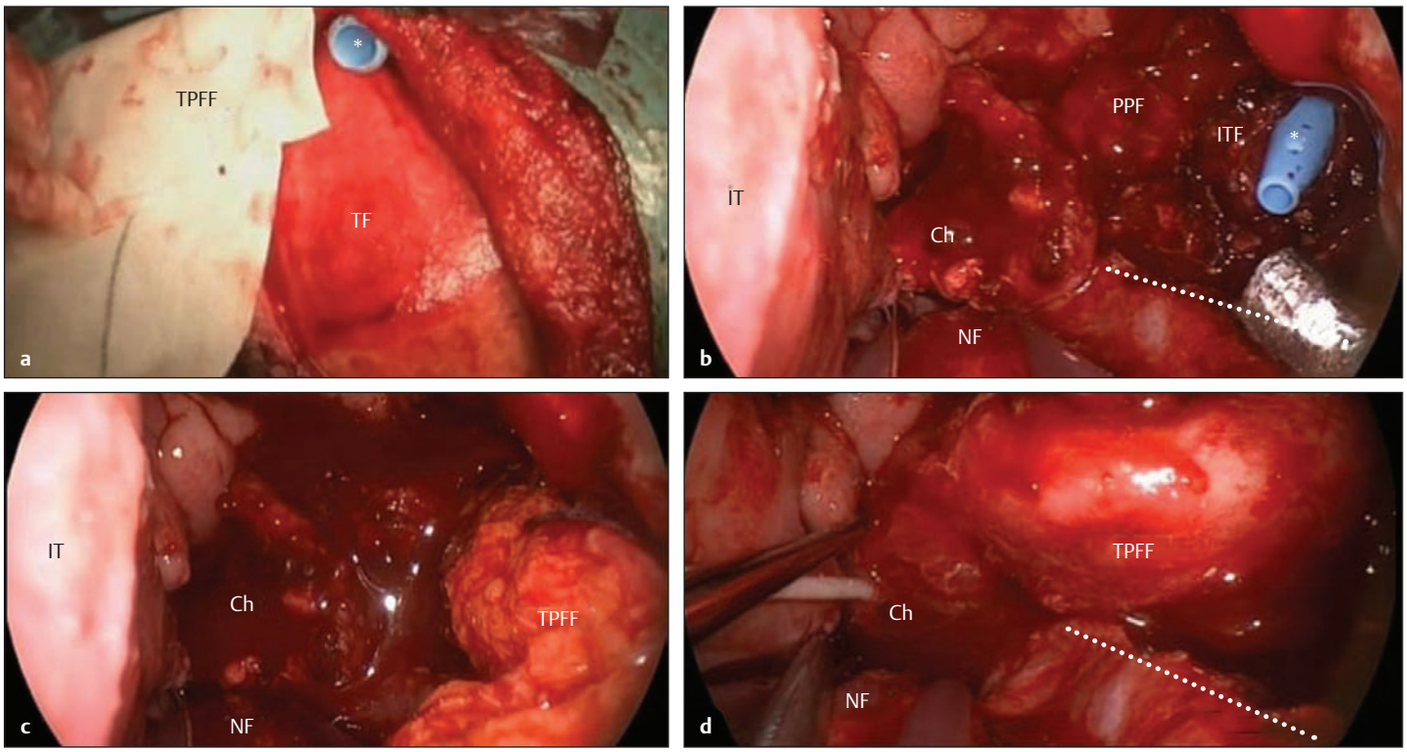

Fig. 6A.2 Temporoparietal fascial flap (TPFF) transposition. (**a, b**) Widening of the corridor through the temporal and infratemporal fossae with Ciaglia dilatators. **(c)** Transposition of the TPFF into the nose. **(d)** Positioning of the TPFF to reconstruct the middle/posterior skull base. Ch, choana; IT, inferior turbinate; ITF, infratemporal fossa; NF, nasal floor; PPF, pterygopalatine fossa; TF, deep temporal fascia; TPFF, temporoparietal fascial flap; *white dotted line*: inferior extension of the medial maxillectomy.

7 Endoscopic Approach to Sellar Lesions

Nisha Shrivastava, Shilpee Bhatia Sharma, Narayanan Janakiram

Introduction

Approximately 10 to 15% of all intracranial neoplasms involve the pituitary gland and sellar region.[1,2] Nearly 9% of them are pituitary adenomas, rest being neoplastic, inflammatory, vascular, or developmental lesions.[2]

With the evolution of endoscopes and high-quality camera systems capturing enhanced resolution and high-definition images, the technique of pituitary surgery has crossed the edges in the past few decades. Endoscopes have widened the field of visualization, being especially beneficial for larger tumors, limiting the complications and reducing the health care cost. The endonasal endoscopic transsphenoidal, transsellar, transtubercular, and transplanar approaches are now being practiced as purely endoscopic maneuver.

The refined interpretation of the anatomy of skull base along with the formulation of appropriately designed instruments and advanced navigation systems has added to the serenity of this approach.

The advantages of transsphenoidal route leading to versatility of the approach are: (1) it is the least traumatic approach to the sella; (2) brain retraction and external scars are avoided; (3) it provides direct visualization of the pituitary gland and other tumors of the region and eases the dissection of the tumor interface with the optic apparatus or the pituitary stalk, with a panoramic and close-up view; (4) in comparison to transcranial approach, the morbidity and mortality rates are lower.

Classification of Pituitary Adenoma

1. Classification on the basis of size

Based on the radiological findings, pituitary adenomas are classified on the basis of their size as:

- Pituitary microadenomas (size less than 10 mm).
- Pituitary macroadenomas (size more than 10 mm).

2. Histological classification by WHO[3]

WHO (2007) has histologically classified adenohypophyseal tumors as:

- Typical adenoma.
- Atypical adenoma.
- Carcinoma.

As per the 2004 WHO classification of central nervous system (CNS) tumors, the criteria to diagnose the atypical adenomas are: excessive p53 immunoreactivity, elevated MIB-1 proliferative index (>3%), increased mitotic activity, and atypical morphological features.[4]

Pituitary masses with cerebrospinal and/or systemic metastasis are classified as carcinoma.[4]

3. Hardy's classification of pituitary adenomas[5]

This classification is based on radiological parameters of pituitary adenomas, i.e., size, invasion, and surgical expansion of the tumors.

- Grades I and II are enclosed within the sella.
- Grades III and IV are invasive.

Extrasellar Classifications

- A, B, and C are increasing amounts of direct suprasellar adenomas.
- D is asymmetric extension.
- E is lateral extension into the cavernous sinus.

Indications for Transsphenoidal Transsellar Approach

A wide range of tumors present in the sellar region, and these can be developmental, infectious, inflammatory, vascular, benign, or neoplastic. Pituitary lesions initially involve the sella and might further extend to suprasellar or parasellar regions.

- Benign pituitary adenoma comprises 85% of the pathologies of sella.[3]
- Pituitary carcinoma and pituicytoma are the neoplastic lesions involving the sella.

- Nonpituitary benign tumors such as craniopharyngioma, meningioma, lipoma, gangliocytoma, schwannoma, and hemangioblastoma are sellar lesions.
- Malignant nonpituitary lesions occupying the sellar region are gliomas, germ cell tumors, chordoma, chondrosarcoma, solitary fibrous tumors, granular cell tumor of neurohypophysis, pituitary metastasis, and other rare lesions.
- Developmental lesions like Rathke's cleft cyst, epidermoid/dermoid cysts, and arachnoid cysts are sellar lesions.
- Infectious conditions like pituitary abscess, tuberculosis, or mycoses might extend to this area.
- Granulomatous lesions have also been reported such as sarcoidosis, Wegener granulomatosis, and hypophysitis.
- Vascular lesions such as aneurysms, cavernous sinus thrombosis, and caroticocavernous fistulas are other lesions occupying the sella.

Of the wide differential diagnosis of sellar lesions, the most commonly encountered ones requiring a surgical treatment are[3]:

- Pituitary adenoma (85%).
- Craniopharyngioma (3%).
- Rathke's cleft cyst (2%).
- Meningioma (1%).
- Metastasis (0.5%) and others (hypophysitis, pituicytoma, spindle cell oncocytoma, granular cell tumor of neurohypophysis) if not cured by medical treatment or producing compression symptoms.

Limitations of Transsphenoidal Transsellar Approach

- Tumor-related factors:
  - Tumors extending laterally beyond medial wall of cavernous sinus and internal carotid artery cannot be accessed completely by this approach.[6]
  - Tumors extending superiorly beyond diaphragm sellae are difficult to reach by this approach alone and usually require a combined approach.
- Patient-related factors:
  - General condition of the patient and fitness for general anesthesia is the prime factor to be considered for any surgical procedure.
  - Presence of sinonasal infection is an absolute contraindication for this surgery.
  - Patients who are extremely obese have higher chances of developing complications postoperatively, as they might not be able to tolerate nasal packing (critical need of continuous positive airway pressure) or there might be an increased risk of cerebrospinal fluid (CSF) leak.[7]
- Surgeon-related factors[7]:
  - Absence of a multidisciplinary team.
  - Lack of advanced equipment.
  - Requirement of extensive training of the surgeon, in terms of detailed anatomical knowledge, preoperative planning, and advanced microdissection techniques, makes this approach have a long learning curve. Lack of these abilities raises the risks involved.

Preoperative Preparation

Routine blood tests along with complete hormone profile should be inspected and endocrinologist's opinion should be taken. The requirement of an ophthalmologist's or neurologist's opinion and any other opinion depends on the extent of the tumor and clinical findings. Thus, the surgery requires a multidisciplinary approach by well-trained doctors in respective subspecialties.

MRI brain (high-resolution, noncontrast, and contrast-enhanced T1 and T2 weighted) and CT paranasal sinuses in coronal, sagittal, and axial views are done preoperatively for the extension of the tumor, anatomy, bone erosions (if any), tumor calcification, etc., supplementing the preoperative formulation of a sequence of steps to be implemented in the operation.

Proper endoscopic examination of the nasal cavities of the patient is done. At this first step itself, the surgeon must foresee the framework of the surgical procedure from the anatomy, septal deviation, if any, and remaining anatomical landmarks in case of revision surgeries.

Disinfection of nasal cavities is done before surgery by nasal douching with 3% saline and mupirocin.

Steps of Surgery

- *Step 1: Preoperative nasal decongestion*. The author uses 5% chlorhexidine gluconate and adrenaline with 1:5,000 dilution-soaked neuropatties to decongest the nasal cavities prior to induction.

- *Step 2: General anesthesia and intubation*. Infusion of hydrocortisone, 250 mg in 50 mL normal saline, is started at the rate of 2 mL/h. Oral endotracheal intubation is preferred at authors' center. For the monitoring of the urinary output, both intraoperatively and postoperatively, a Foley's urinary catheter is routinely inserted after intubation. A central venous catheter is inserted in the right subclavian vein to avoid repeated peripheral line blockage and multiple venous punctures. The proposed reconstruction site (thigh or abdomen) must always be painted and draped before initiating the surgery to facilitate access when required. The image guidance system is positioned and the registration process is completed and checked.
- *Step 3: Positioning of patient*. The patient's head is placed in neutral position with a horseshoe pad below the vertex or in pin immobilization to make the head stable. In authors' standard practice, they position the patient in reverse Trendelenburg pose without pin immobilization. The head is minimally flexed for sellar dissection, while minimally hyperextended for suprasellar or planum dissection.
- *Step 4: Intraoperative nasal packing*. Nasal cavities are further decongested using neuropatties soaked in adrenaline with 1:1,000 dilution under endoscopic guidance.

Nasal Phase

The camera and light are connected to a 4-mm 0° rigid endoscope, and nasal endoscopy is performed. The landmarks in the nasal cavities and the anatomic variations are identified. All attempts are taken to widen the surgical corridor, and any septal deviation or spur seen is corrected.

- *Step 5: Lateralization of inferior turbinates*. The right inferior turbinate is lateralized to achieve extra space to operate.
- *Step 6: Partial resection of middle turbinate*. The right nasal corridor is further expanded by a partial middle turbinectomy.
- *Step 7: Principle of "cavity-and-a-half."* Right-sided posterior ethmoidectomy facilitates the four-handed technique, broadening the track to the sphenoid. The principle of cavity-and-a-half implies opening of the sphenoid, which represents the "cavity," and posterior ethmoids, which represent the "half." Proper tissue handling with avoidance of pulling or plucking the tissues has extreme importance in this delicate procedure, and in minimizing injury to the olfactory epithelium.
- *Step 8: Identification and widening of the sphenoid ostium*. The superior turbinate is then lateralized to expose the sphenoid os. The ostium lies about 1.2 to 1.5 cm above the superior edge of choana, in the sphenoethmoid recess and at the inferior third of the superior turbinate. It might be covered by a supreme turbinate, which can be resected or gently retracted laterally as per the comfort of the surgeon. Throughout these steps, the surgeon must be gentle in dissection and make sure not to disrupt the septal branch of the sphenopalatine artery, because this will be the base vessel of the reconstructive nasoseptal flap by the end of the surgery.
- *Step 9: Lateralization of turbinates in left nasal cavity*. The left inferior, middle, and superior turbinates are lateralized to expose the posterior ethmoids and the sphenoid os.
- *Step 10: Principle of "cavity-and-a-half."* Left posterior ethmoids and sphenoid sinuses are dissected in line with the principle of "cavity-and-a-half" described above.
- *Step 11: Harvesting of the nasoseptal flap and rescue flap*. In all authors' cases of transsellar approach, the nasoseptal flap is harvested from the right side. Overestimation of the flap size is always better. Sharp instruments must be used to place the incisions. Hadad flap or a rescue flap might be harvested and positioned in choana to avoid interference during drilling.
- *Step 12: Posterior septectomy*. Posterior part of septum, i.e., the bony septum, is disarticulated from the rostrum of the sphenoid. To assist the binostril four-handed technique, the septum is excised posteriorly 1 to 2 cm using back biter instrument or debrider, thus increasing the space available for manipulation of the instruments. The two sphenoid os with the rostrum of sphenoid in between give the **appearance of an owl's eye**.
- *Step 13: Shifting to "two-surgeon four-handed" technique*. It is in this step that the author shifts to two-surgeon four-handed technique wherein the assistant holds the endoscope without a holder and also passes instruments, and the main surgeon holds an instrument in one hand and suction in the other.

It enhances the three-dimensional perspective of the surgery.

Sphenoid Phase

- *Step 14: Triple osteotomies*. The planar osteotomy is drilling the bone just below the planum sphenoidale and shoulder osteotomies are at the level of pterygosphenoid synchondrosis. A high-speed drill or a rongeur is used horizontally for planar osteotomy and in the inferomedial direction for shoulder osteotomies.
- *Step 15: Removal of the rostrum of sphenoid*. The rostrum of sphenoid is then resected out of the nasal cavity exposing the sella.
- *Step 16: Exposure*. The lateral wall of sphenoid sinus and the medial pterygoid plate are the lateral limit of wide sphenoidotomy, with the superior limit being planum sphenoidale and inferior being the point, two suction tips below the sellar bulge. The bleeding from the planar mucosa might cause fogging of endoscope, which can be avoided using coblation, and the use of monopolar cautery at and after this step is to be avoided for the risk of thermal injury. The sphenoid septations are removed using tru-cut forceps or by drilling using a diamond burr. A smooth surface is to be prepared along the posterior wall of sphenoid sinus, for placement of the nasoseptal flap. The sphenoid sinus mucosa is removed to prevent postoperative formation of sphenoid mucocele, with the venous bleeding encountered in the process being controlled by warm saline irrigations.
- *Step 17: Identification of landmarks*. The posterior wall of sphenoid sinus is demarcated and the sellar prominence, medial and lateral opticocarotid recess, parasellar carotid prominences, and clival recess are delineated. For the presellar and conchal type of pneumatization of sphenoid sinus, it becomes difficult for the surgeon to maintain his orientation due to the absence of these landmarks. It is then advised to stay in the midline while proceeding toward sella and employ neuronavigation along with microvascular Doppler to avoid unintended injury to vital structures, making a note here that it's not safe to totally rely on these tools and that detailed anatomical knowledge is the key to safety.

Sellar Phase

- *Step 18: Drilling of the floor of sella*. The bony covering of sella is drilled using a high-speed diamond drill with a 4-mm diamond burr and detached from the dura behind using a Rosen's elevator. The authors use the Karl Storz S3 neurodrill with a 4-mm diamond burr for this phase. Constant irrigation with normal saline is important at this point. The sellar bone is cleared laterally, from the right cavernous sinus till the left, and superiorly from the superior intercavernous sinus till the inferior intercavernous sinus, thus exposing the "four blues." The navigation or the microvascular Doppler is employed for accurate identification of both the internal carotid arteries. The bone in proximity to the neurovascular structures is removed with a Rosen's elevator with swift movements to avoid injury, and the use of Kerrison punch is avoided.
- *Step 19: Incision of the dura*. Once the internal carotid arteries and the intercavernous sinuses are delineated, dural incisions are made. Various shapes of incision have been described in literature, but the authors prefer a horizontal incision inferiorly, in the center, with the Cappabianca knife, and then extending it superiorly on its both sides using rotatable scissors, staying medial to the carotid vessels. A superior-based U-shaped flap of the endosteal layer of dura is raised using a Rosen's elevator.
- *Step 20: Tumor dissection*. The tumors with soft consistency are internally debulked, starting inferiorly with the help of two suctions. In this way the early descent of the diaphragm can be avoided. Further, the tumor is cleared from the medial walls of the cavernous sinuses, proceeding posteriorly and superolaterally to completely excise the tumor.

  The *Q-tip technique*, wherein a cotton swab or a gauze piece is used to manipulate the corners of the space and inspect thoroughly the field, is employed, to avoid overlooking any residual tumor, especially concentrating on the area around the pituitary stalk. Once the normal gland comes in view, it is retracted and preserved.

  The tumors which are firm in consistency are excised by extracapsular dissection along with the pseudocapsule, making sure that the normal gland is

identified and preserved. The fibrous bands are separated endoscopically by fine blunt dissection.

- *Step 21: Reconstruction*. Cases where no CSF leak is encountered, the sellar cavity and the sphenoid sinus are filled with fat till the anterior wall of the sinus, the endosteal layer of dura, is repositioned and further covered with Surgicel, Gelfoam, and fibrin glue.

  Cases where CSF leak is present during the surgery, an onlay graft or a nasoseptal flap is placed, with fibrin glue over it, and packed in multiple layers.

  The details of all reconstruction methods have been explained in a separate section of the book.

Conclusion

Endonasal endoscopic approach is being adopted worldwide by skull base surgeons owing to its results which are superior to open transcranial approaches and its minimal invasiveness. Although the approach has certain limitations and an increased risk of CSF leak compared with transcranial approach, a step-wise preoperative planning with in-depth anatomical knowledge and use of appropriate instruments makes the scenario comfortable for the surgeon. Further, accomplishment of higher rates of remission along with minimal scar is particularly attractive for the patients. With time, more efficacious procedures and instruments are expected to evolve, improvising the approach and taking it to newer heights.

Acknowledgment

We acknowledge the contributions of our neurosurgeons in the intraoperative and postoperative management of the patients.

Case 1: Pituitary Macroadenoma

A 56-year-old male presented with headache. He was treated symptomatically for many days. After a long duration of treatment with no improvement in another center, an MRI scan was done which showed a sellar lesion (**Fig. 7.1**). It was diagnosed as pituitary macroadenoma. The case was referred to the authors and was taken up for surgery under general anesthesia. Bilateral nasal cavities were decongested. Right inferior turbinate was lateralized, and middle turbinate resected (**Fig. 7.2**). In accordance with the "cavity-and-a-half" technique, both posterior ethmoid sinus and sphenoid sinus were opened (**Fig. 7.3**). Left sphenoid sinus opening was exposed by lateralizing the inferior and middle turbinates. Incisions for nasoseptal flap were placed on the right side of the septum (**Fig. 7.4**) and the flap was elevated and pushed into the nasopharynx to keep it protected from any injury during the surgery. Posterior septectomy was done (**Fig. 7.5**) exposing the rostrum of sphenoid (**Fig. 7.6**). At this point authors shifted to four-handed technique as described previously. This was followed by triple osteotomies, i.e., the planar osteotomy (**Fig. 7.7**), and right (**Fig. 7.8**) and left shoulder osteotomies (**Fig. 7.9**), and the rostrum of sphenoid was removed. A wide exposure of the sphenoid sinus was obtained and the sellar bone was drilled using the Storz S3 neurodrill (**Fig. 7.10**). After drilling the bone, a Rosen's elevator was used to raise the bone flap (**Fig. 7.11**). The exposure was widened by removing the bone over tuberculum sella (**Fig. 7.12**). Micro-Doppler was used to locate the internal carotid arteries (**Fig. 7.13**). A Cappabianca knife was used to incise the endosteal layer of dura horizontally (**Fig. 7.14**), and was extended vertically on both sides by rotatable Kassam scissors to obtain a superior-based U-shaped dural flap (**Fig. 7.15**). The tumor was exposed and biopsy was taken. Then the authors shifted to two-suction technique (**Fig. 7.16**); starting first at 6 o' clock position, the tumor was sucked out. Tumors in the 3 o' clock and 9 o' clock regions were cleared using two-suction tip technique. The Q-tip technique was used to remove the residual tumor in the suprasellar compartment (**Fig. 7.17**). All of it was done under vision till the normal pituitary gland was exposed (**Fig. 7.18**). The final cavity was packed using Surgicel. The dural flap was repositioned (**Fig. 7.19**) and reconstruction done using the nasoseptal flap (**Fig. 7.20**). See **Video 7.1**.

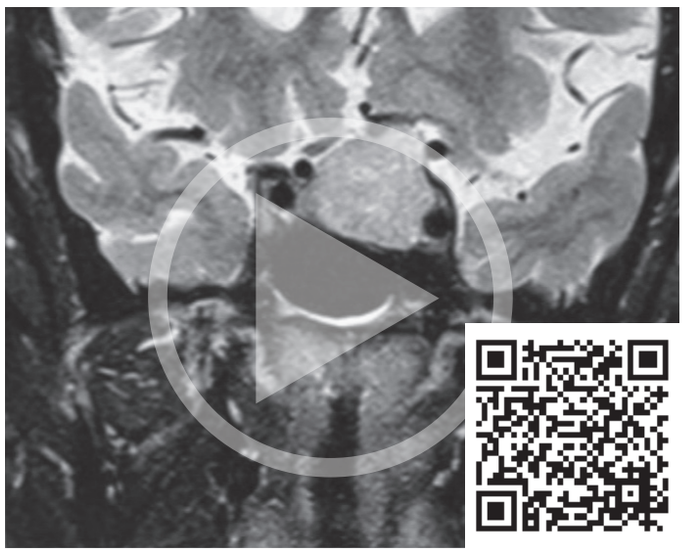

Video 7.1 Pituitary macroadenoma. https://www.thieme.de/de/q.htm?p=opn/cs/19/9/10104320-c36436b2

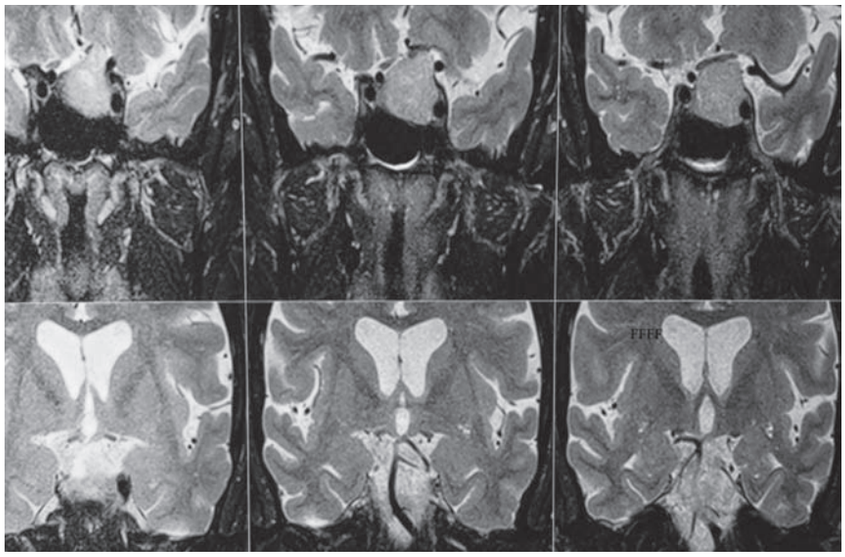

Fig. 7.1 MRI coronal view showing sellar lesion.

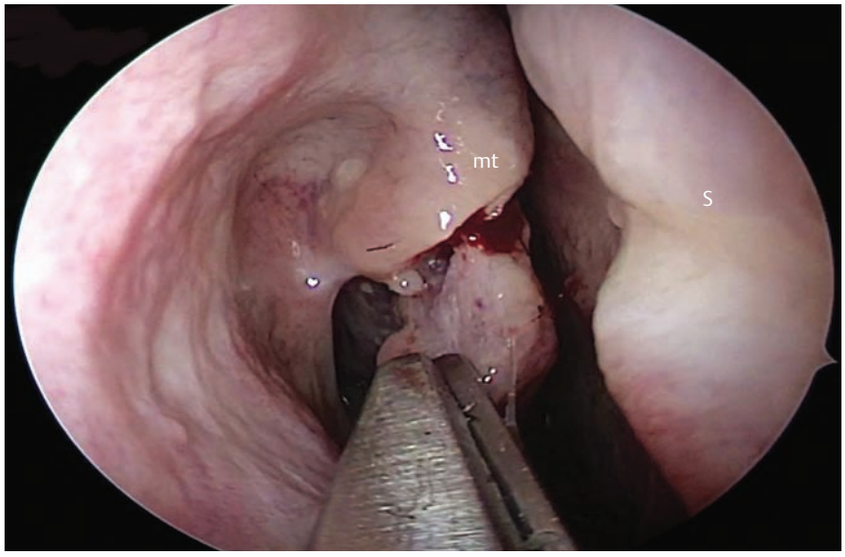

Fig. 7.2 Middle turbinate resection. mt: Middle turbinate; S: nasal septum.

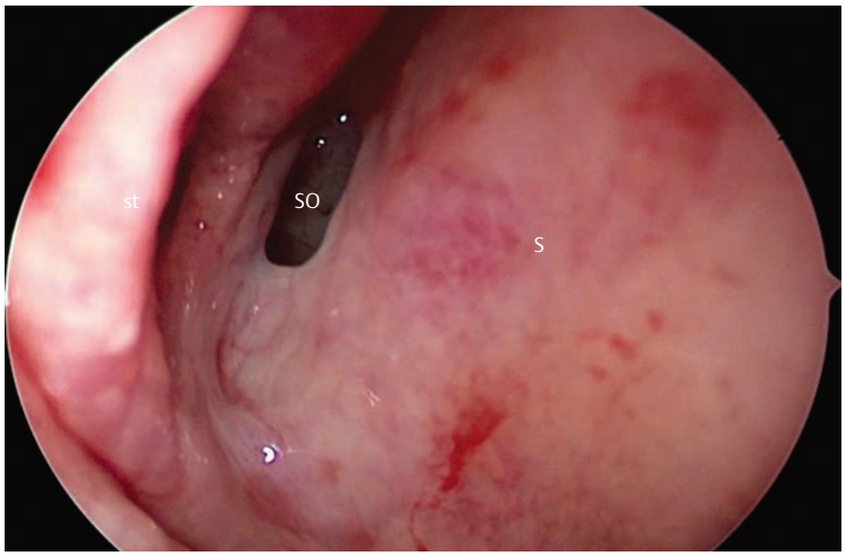

Fig. 7.3 Exposure of right sphenoid os. so: Sphenoid os; S: nasal septum.

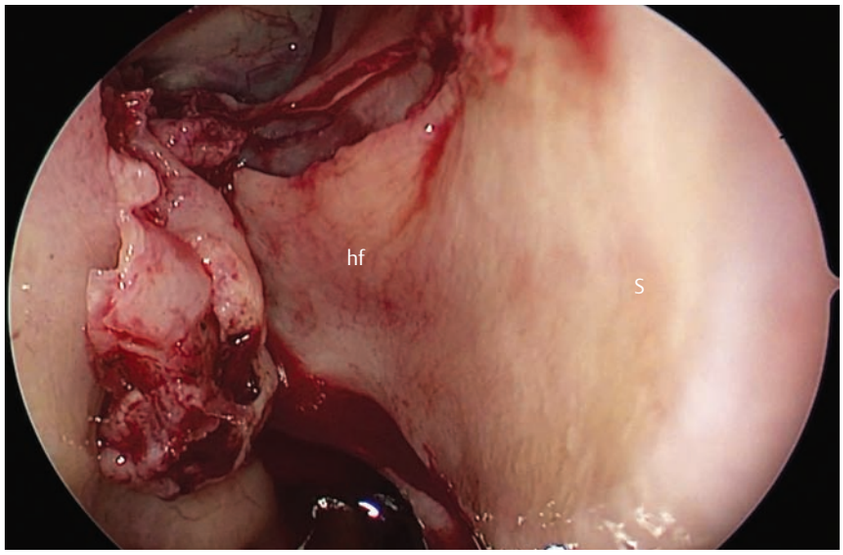

Fig. 7.4 Incision for nasoseptal flap. hf: nasoseptal flap; S: nasal septum.

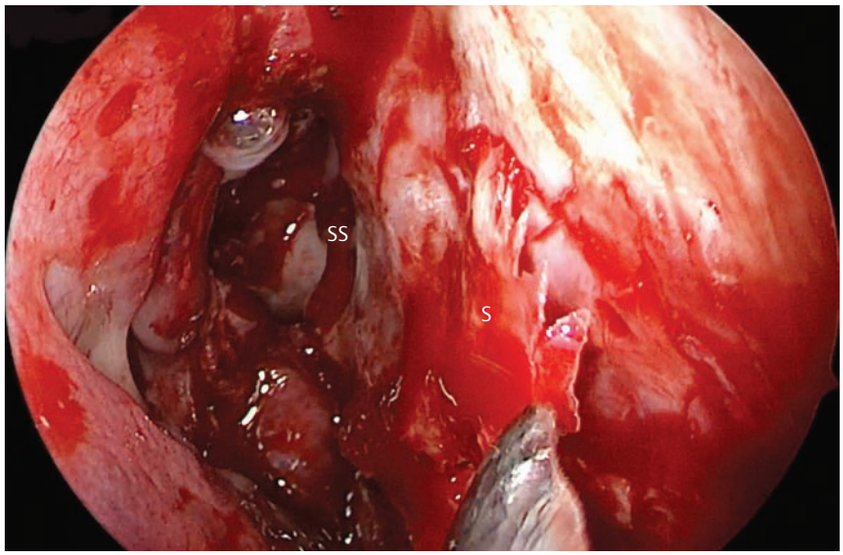

Fig. 7.5 Posterior septectomy. S: Nasal septum; ss: sphenoid sinus.

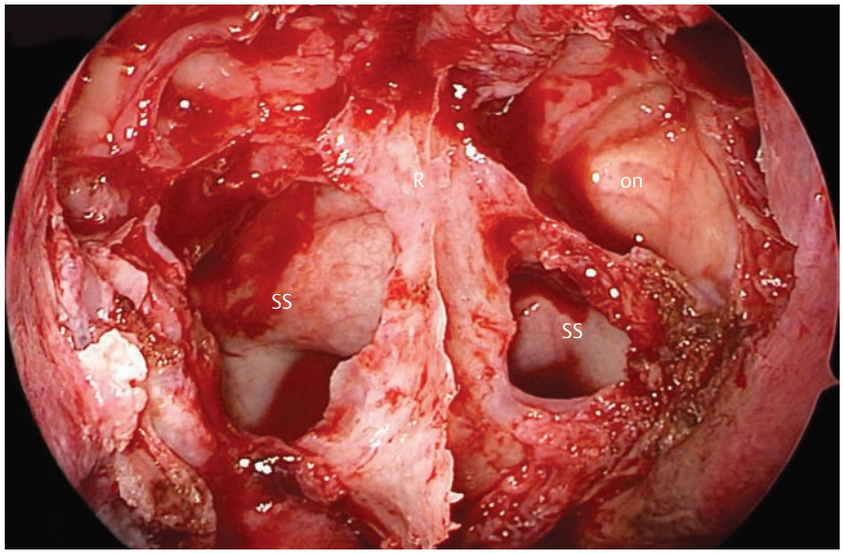

Fig. 7.6 Rostrum of sphenoid exposed. on: Optic nerve; R: rostrum of sphenoid; ss: sphenoid sinus.

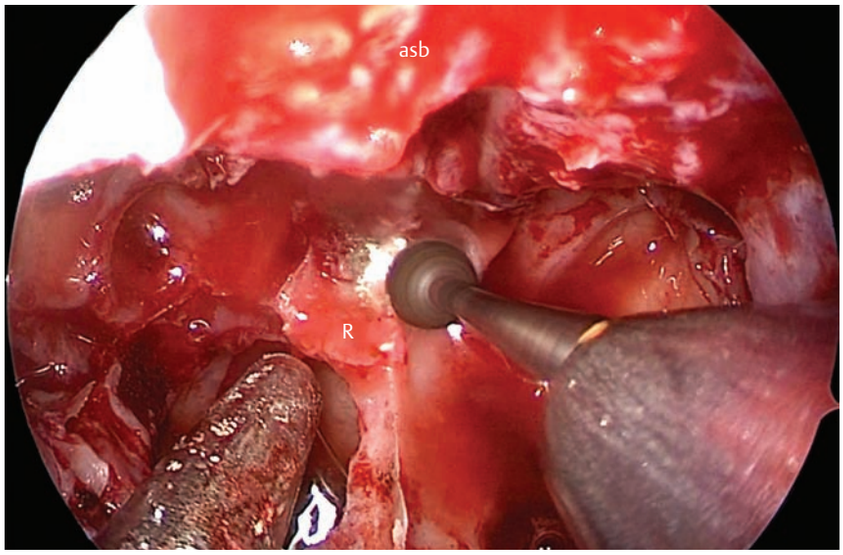

Fig. 7.7 Planar osteotomy. acb: Anterior cranial base; R: rostrum of sphenoid.

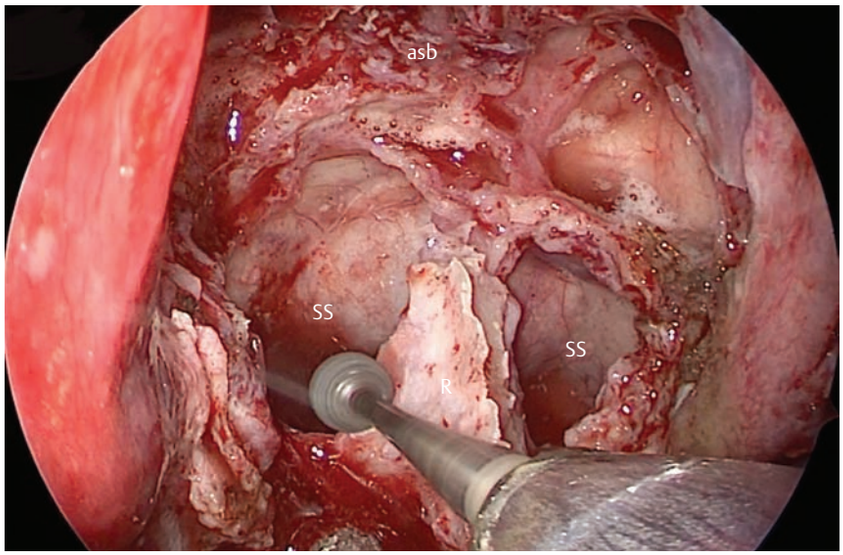

Fig. 7.8 Right shoulder osteotomy at right pterygosphenoid synchondrosis. acb: Anterior cranial base; R: rostrum of sphenoid; ss: sphenoid sinus.

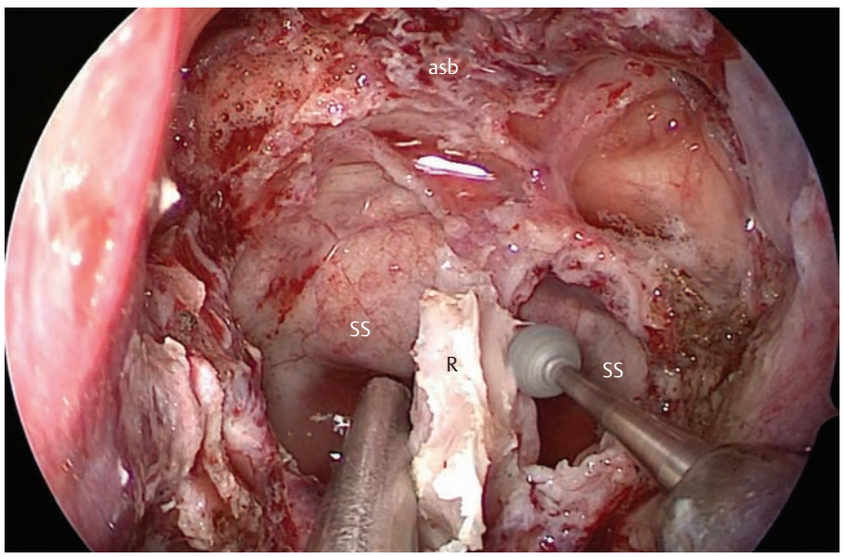

Fig. 7.9 Left shoulder osteotomy at left pterygosphenoid synchondrosis. acb: anterior cranial base; R: rostrum of sphenoid; ss: sphenoid sinus.

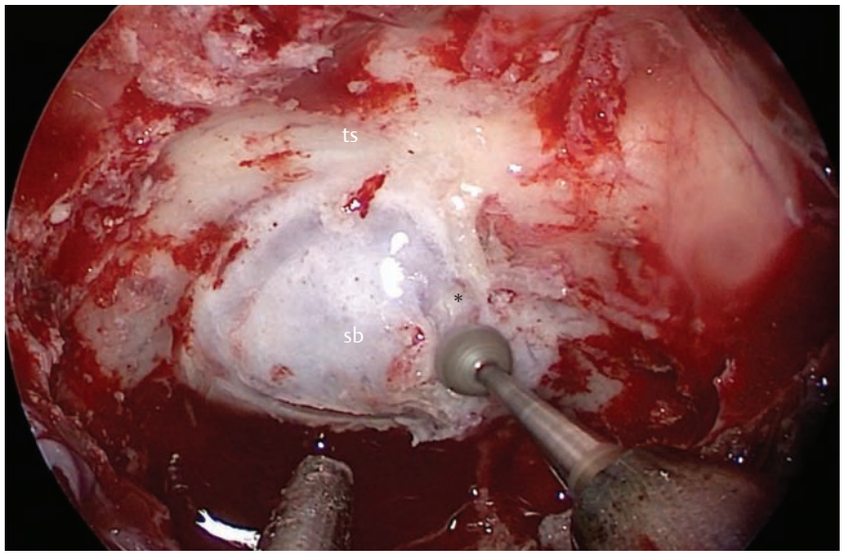

Fig. 7.10 Sellar bone drilling. sb: Sellar bone; ts: bone over tuberculum sellae; *: drilling of sellar bone.

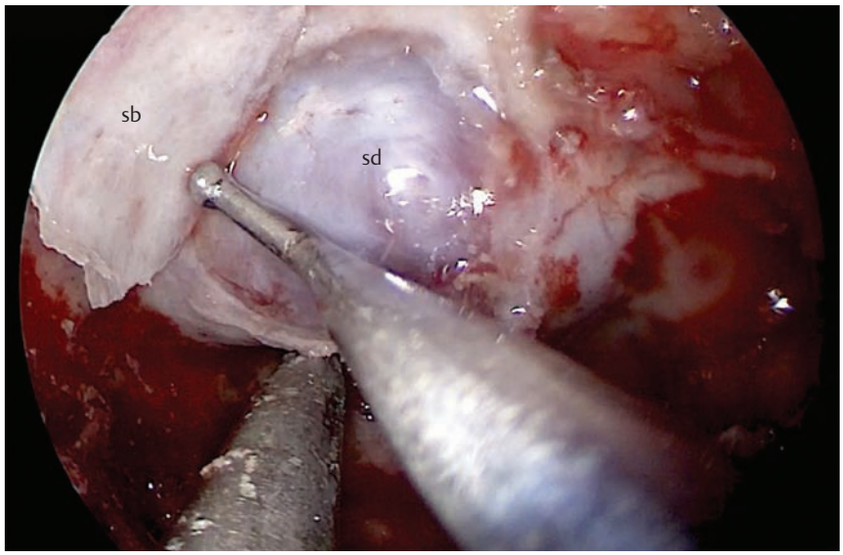

Fig. 7.11 Elevation of bone flap. sb: Sellar bone; sd: endosteal layer of dura.

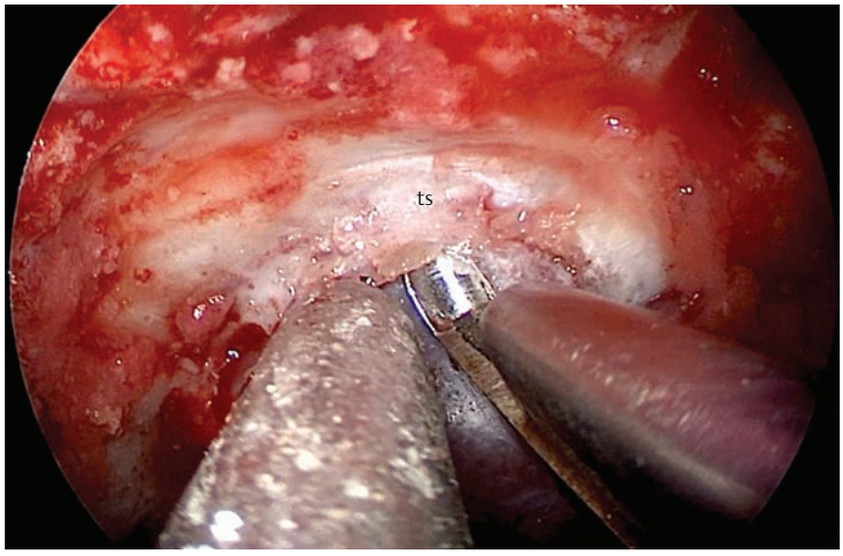

Fig. 7.12 Widening of exposure by removal of bone over tuberculum sella. ts: Bone over tuberculum sella.

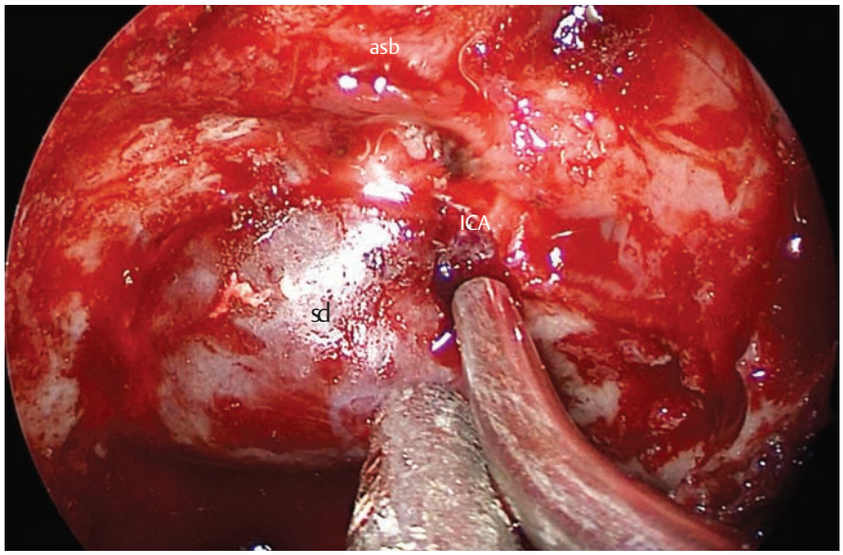

Fig. 7.13 Use of doppler to locate the ICA. acb: anterior cranial base; ICA: internal carotid artery; sd: endosteal layer of dura.

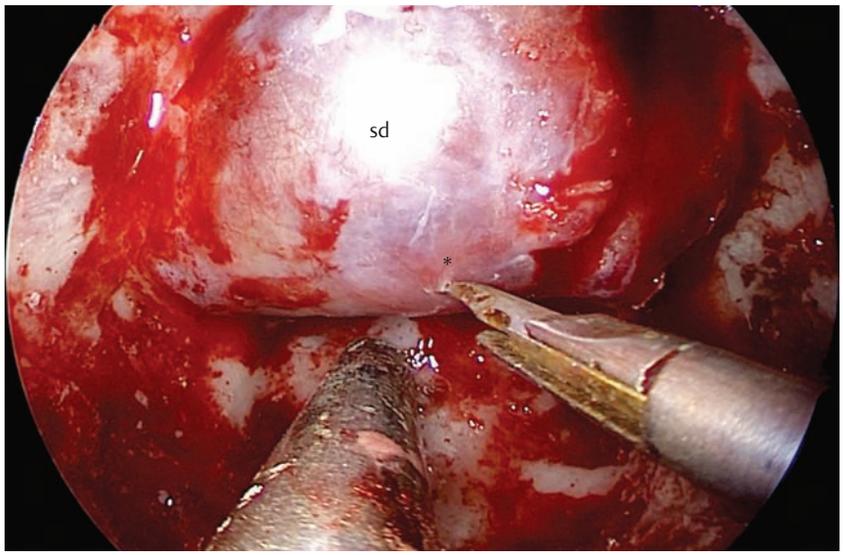

Fig. 7.14 Incision over endosteal layer of dura using Cappabianca knife. sd: Endosteal layer of dura; *: incision line.

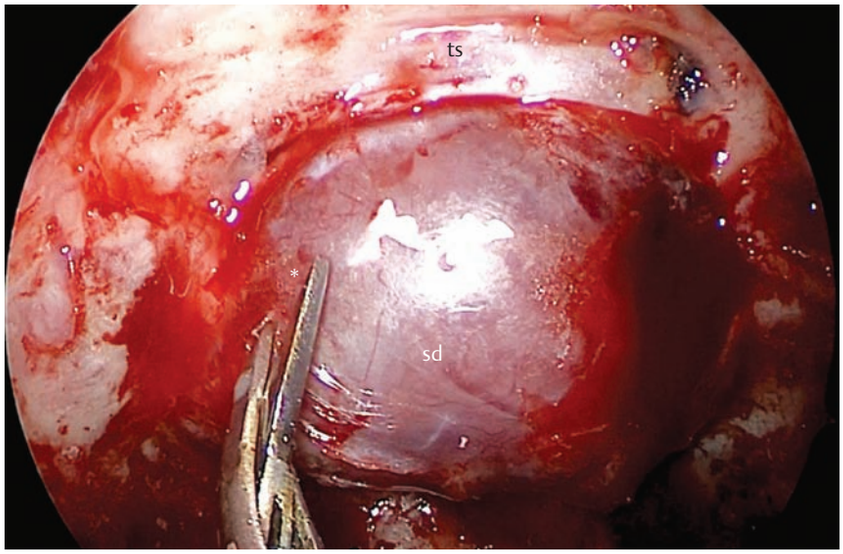

Fig. 7.15 Extension of dural incision using Kassam rotatable scissors. sd: Endosteal layer of dura; ts: bone over tuberculum sella; *: line of extension of incision over endosteal layer of dura.

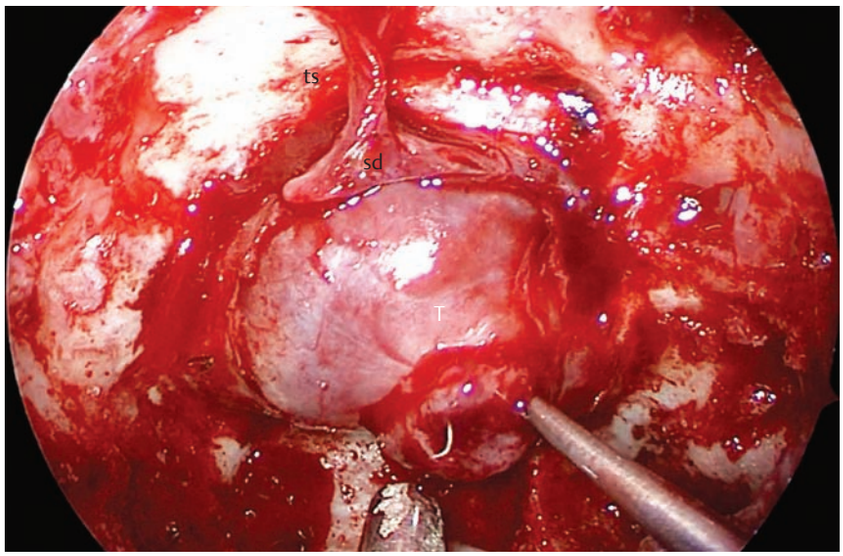

Fig. 7.16 Exposure of tumor and the two-suction technique for excision of tumor. sd: Endosteal layer of dura; ts: bone over tuberculum sella; T: tumor.

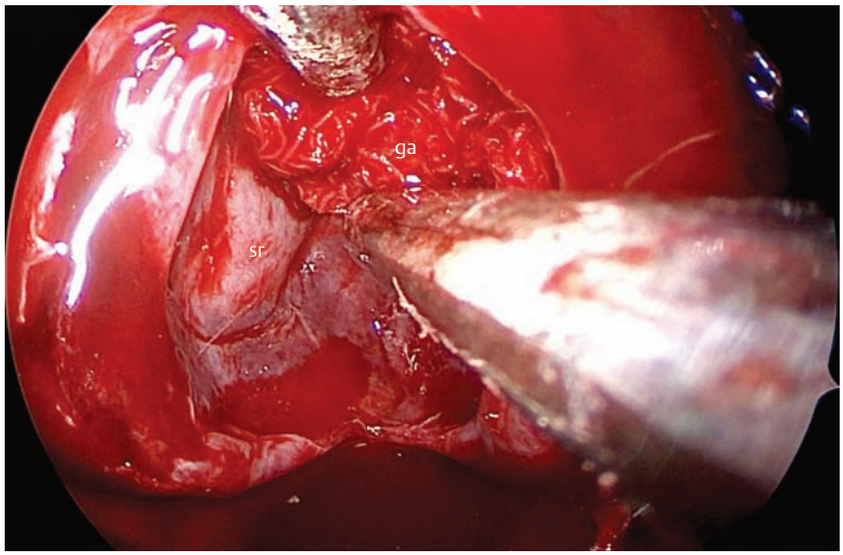

Fig. 7.17 Q-tip technique for exposure of any residual tumor. ga: Gauze; sr: sellar region.

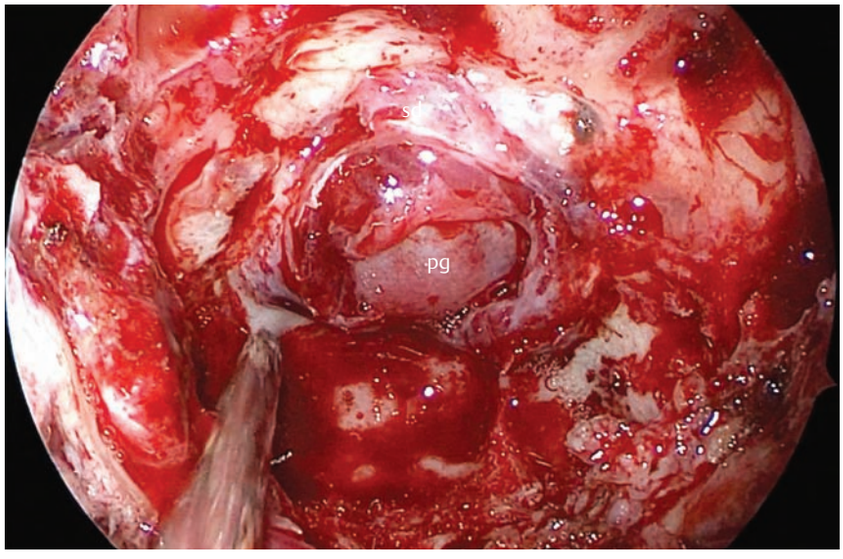

Fig. 7.18 Normal pituitary gland exposed after excision of tumor. pg: Pituitary gland; sd: endosteal layer of dura.

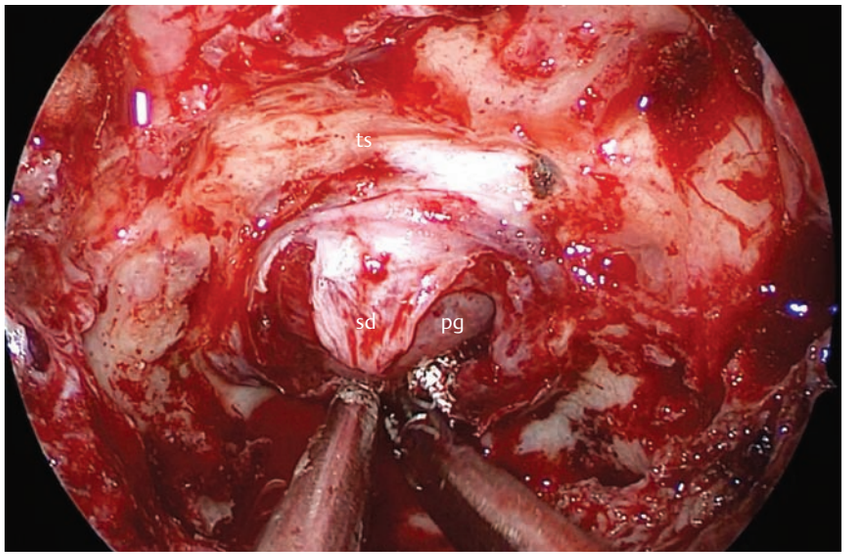

Fig. 7.19 Reposition of U-shaped dural flap. pg: Pituitary gland; sd: endosteal layer of dura; ts: bone over tuberculum sella.

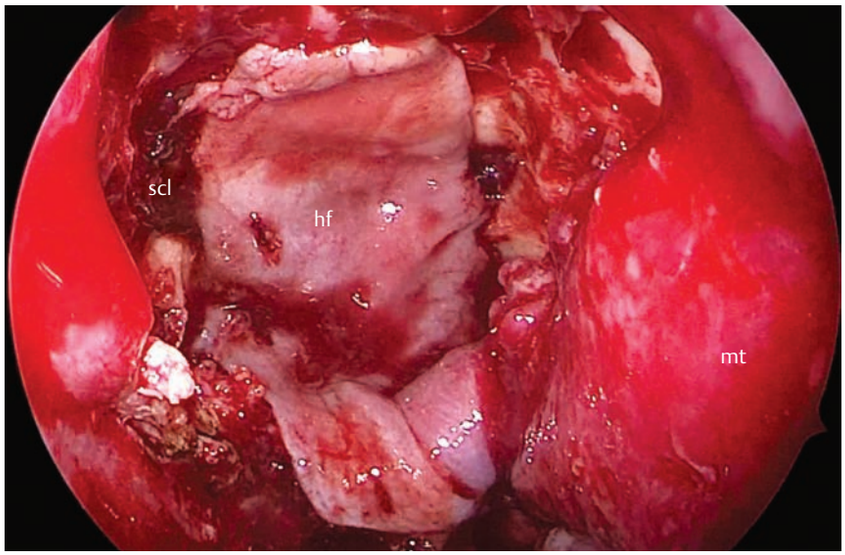

Fig. 7.20 Placement of nasoseptal flap for reconstruction of defect. hf: Nasoseptal flap; mt: middle turbinate; scl: Surgicel.

Case 2: Pituitary Apoplexy

A 34-year-old male presented with headache and diminished vision. The MRI showed a cystic lesion inside the pituitary involving the sellar region (**Fig. 7.21**). After intubation bilateral nasal cavities were decongested. Right inferior turbinate was lateralized and middle turbinate resected partially. Following the principle of cavity-and-a-half, bilateral posterior ethmoidectomies were done (**Fig. 7.22**) and sphenoid sinus was opened. Bilateral rescue flaps were taken (**Fig. 7.23**). This was followed by posterior septectomy, and the rostrum of sphenoid was exposed (**Fig. 7.24**). Triple osteotomies were done and sella exposed (**Fig. 7.25**). The sellar bone was drilled (**Fig. 7.26**) and the bone flap was elevated using a Rosen's elevator (**Figs. 7.27 and 7.28**). The endosteal layer of dura was exposed (**Fig. 7.29**). A Cappabianca knife was used to place an incision over the endosteal layer of dura (**Fig. 7.30**) and extended on both sides using a rotatable Kassam scissors (**Fig. 7.31**). Biopsy of the tumor was taken, the lesion was removed completely (**Fig. 7.32**). The cavity was obliterated with fat and Surgicel, and the dural flap was repositioned (**Fig. 7.33**) and covered with Surgicel and Gelfoam (**Fig. 7.34**).

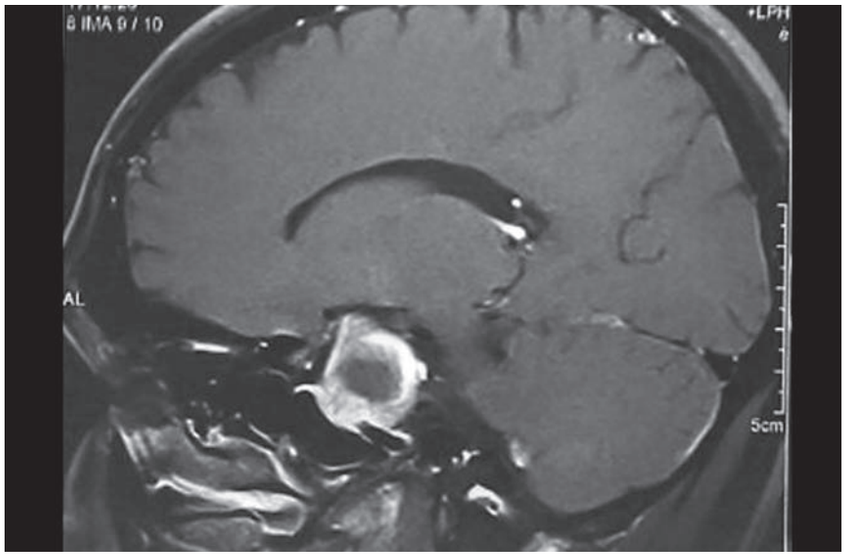

Fig. 7.21 MRI sagittal view showing sellar lesion.

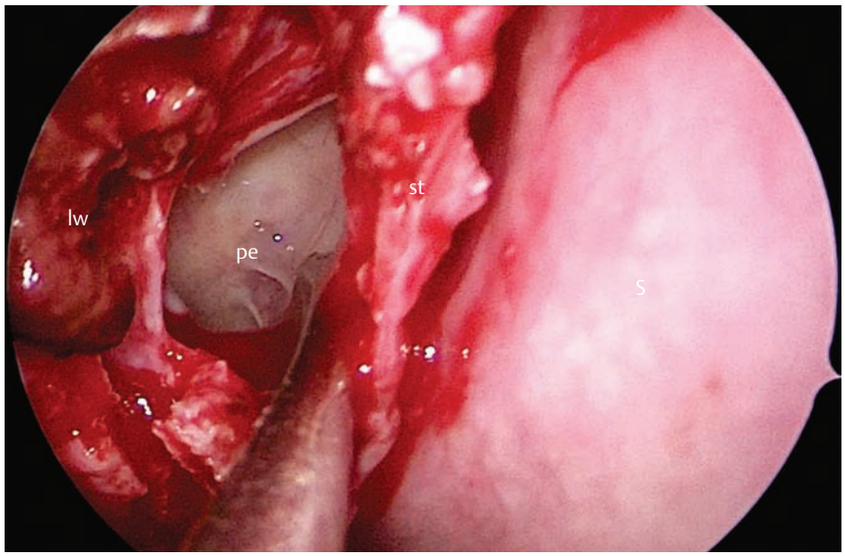

Fig. 7.22 Right posterior ethmoidectomy. lw: lateral nasal wall, pe: posterior ethmoids, S: nasal septum, st: superior turbinate.

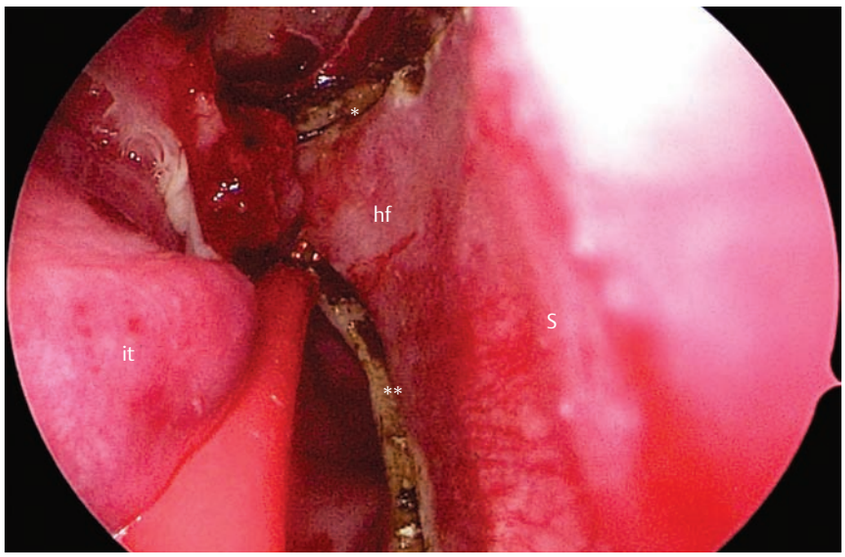

Fig. 7.23 Harvesting the rescue flap. Hf: Nasoseptal flap; it: inferior turbinate; S: nasal septum.

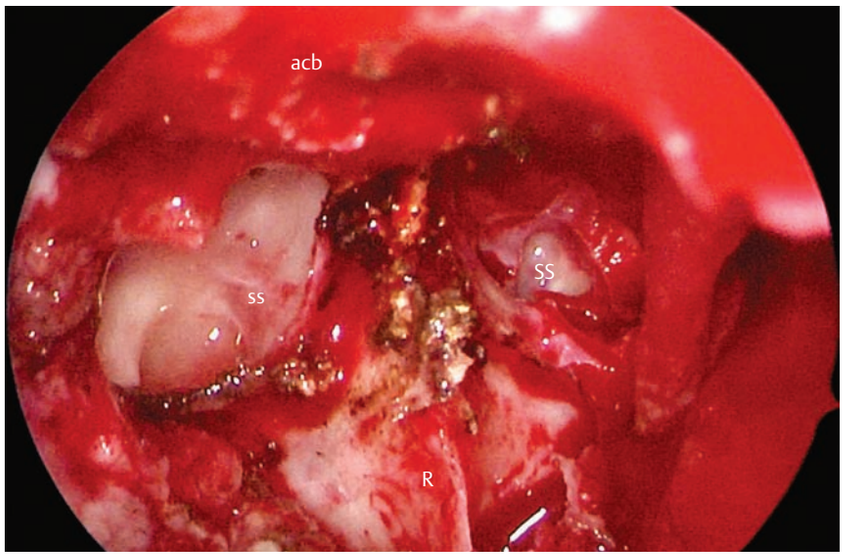

Fig. 7.24 Owl eye appearance. acb: Anterior cranial base; R: rostrum of sphenoid; ss: sphenoid sinus.

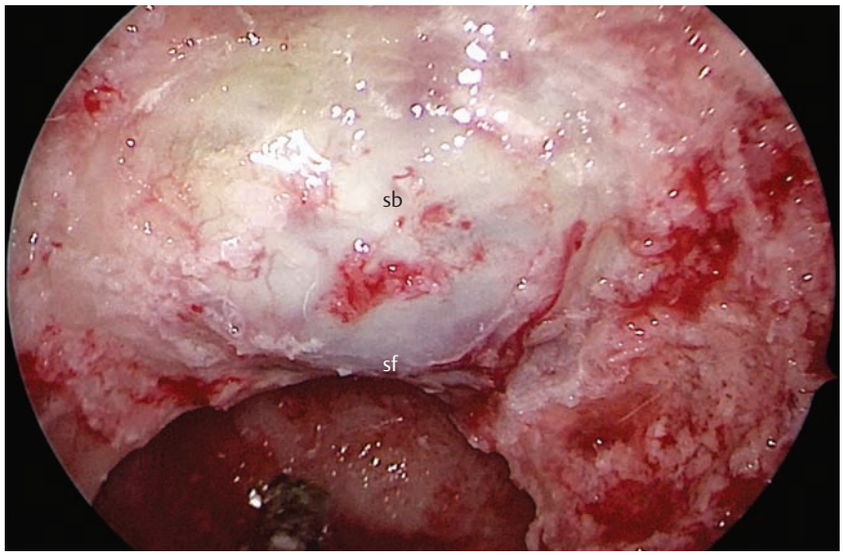

Fig. 7.25 Exposure of sella. sb: Sellar bone; sf: sellar floor.

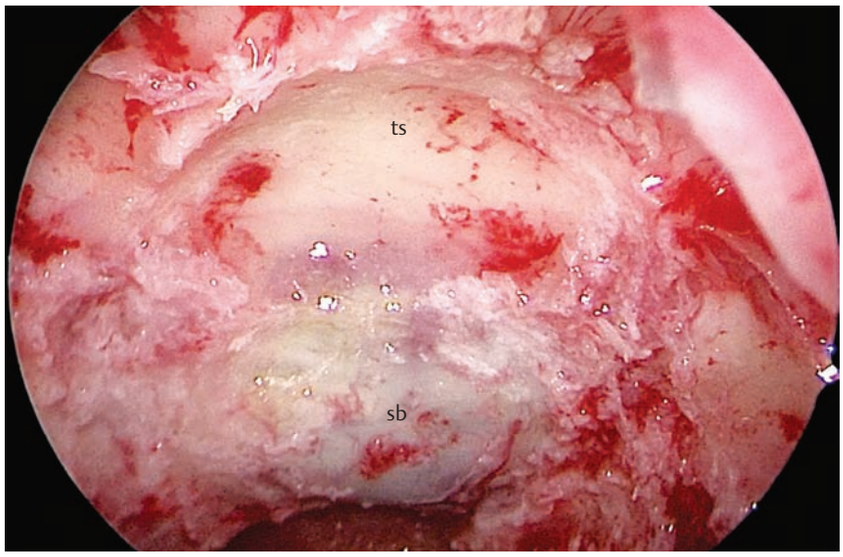

Fig. 7.26 Exposure after drilling of sellar bone. sb: Sellar bone; ts: tuberculum sella.

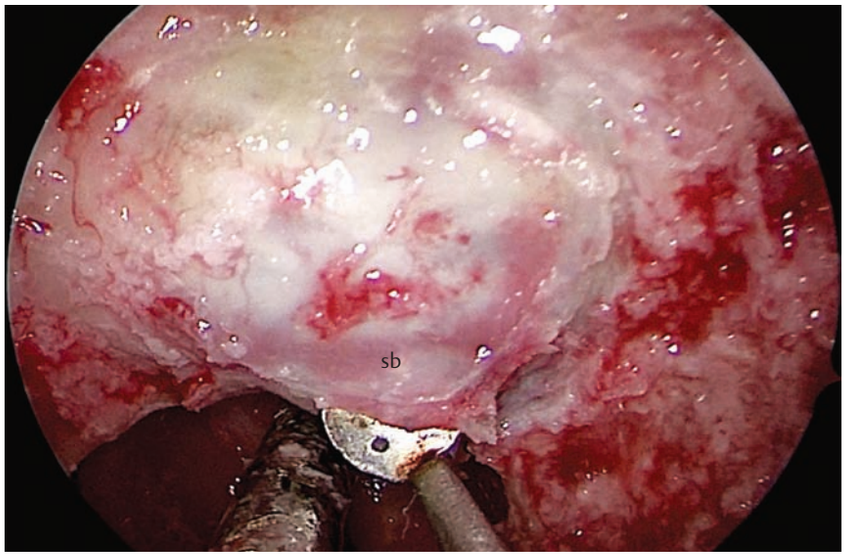

Fig. 7.27 Elevation of sellar bone flap using Rosen's elevator. sb: Sellar bone.

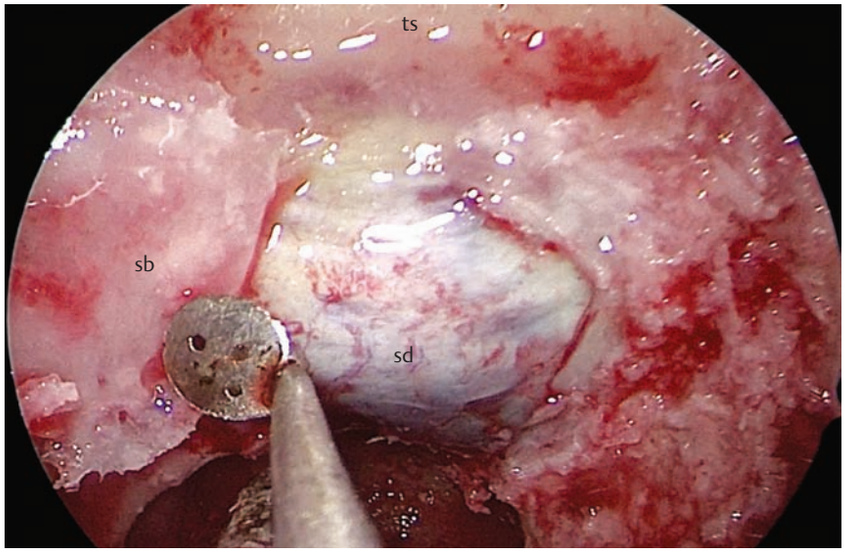

Fig. 7.28 Exposure of endosteal layer of dura after elevation of bone flap. sb: Sellar bone; sd: endosteal layer of dura; ts: tuberculum sella.

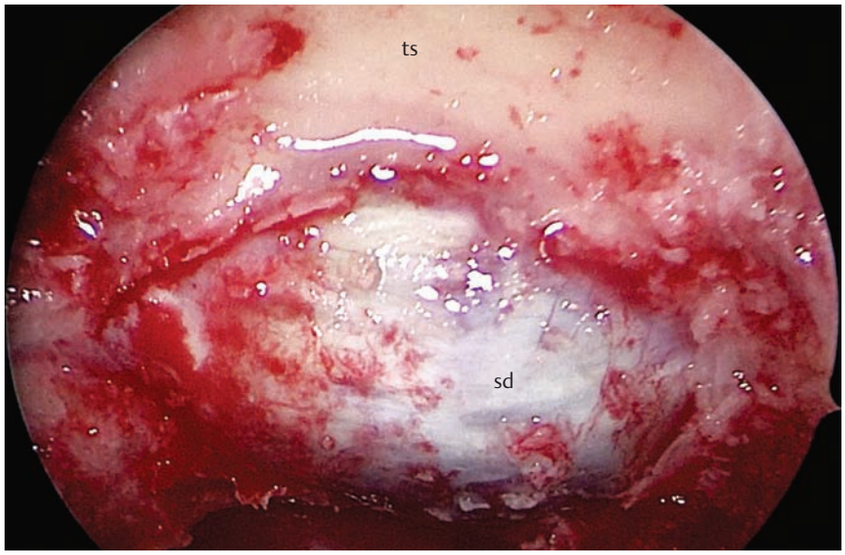

Fig. 7.29 Widening of exposure by drilling of bone over carotids. sd: Endosteal layer of dura; ts: tuberculum sella.

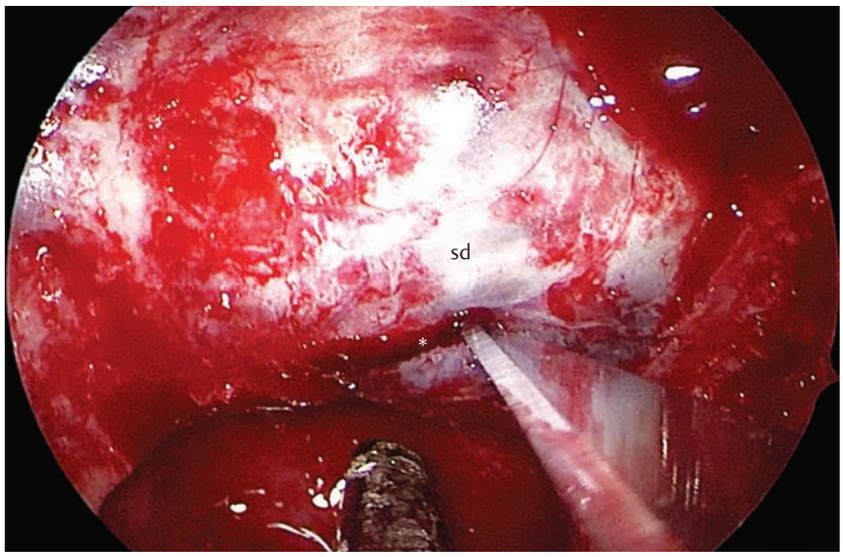

Fig. 7.30 Incision over the endosteal layer of dura using a Cappabianca knife. sd: endosteal layer of dura; *: incision over endosteal layer of dura.

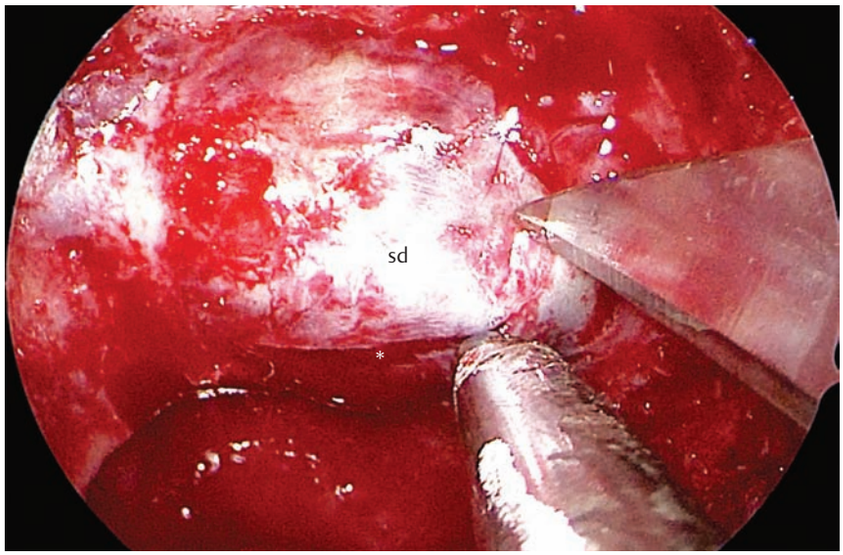

Fig. 7.31 Extension of the incision over endosteal layer of dura. sd: Endosteal layer of dura.

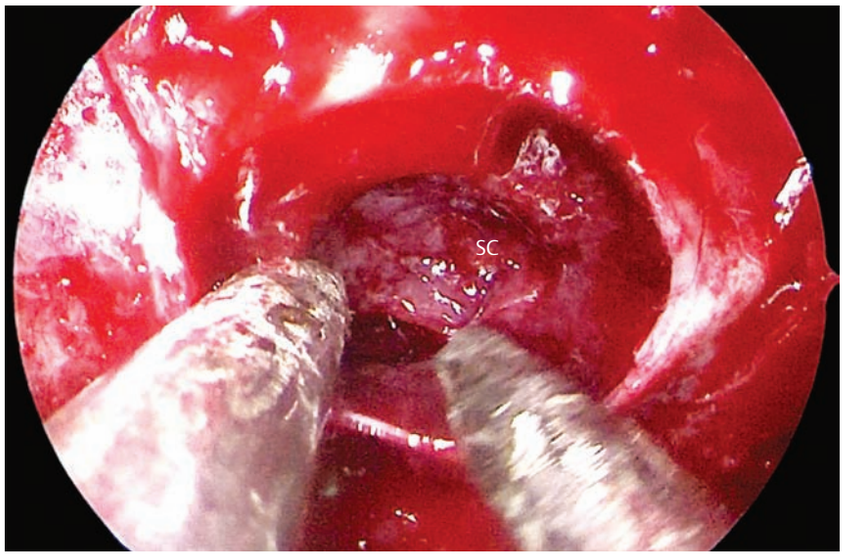

Fig. 7.32 The two-suction technique for tumor excision. sc: Sellar cavity.

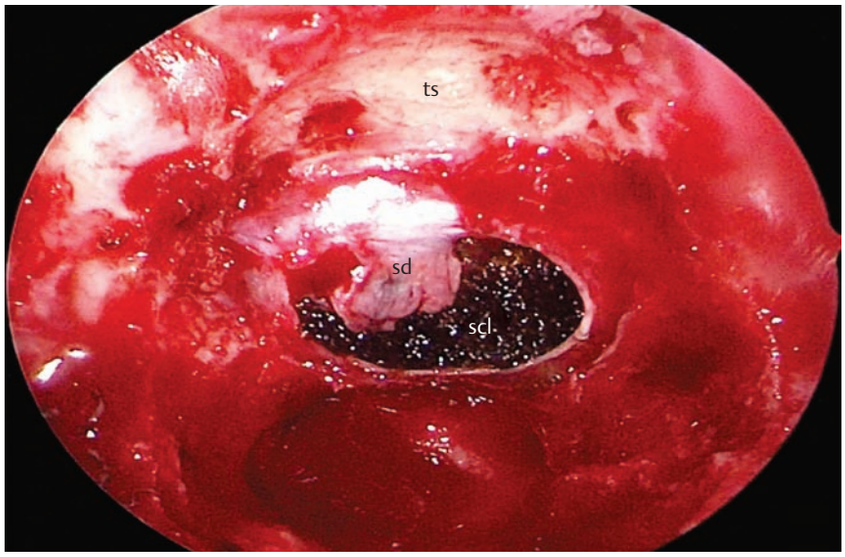

Fig. 7.33 Sellar cavity reconstituted with Surgicel and repositioning of dural flap. scl: Surgicel; sd: endosteal layer of dura; ts: tuberculum sella.

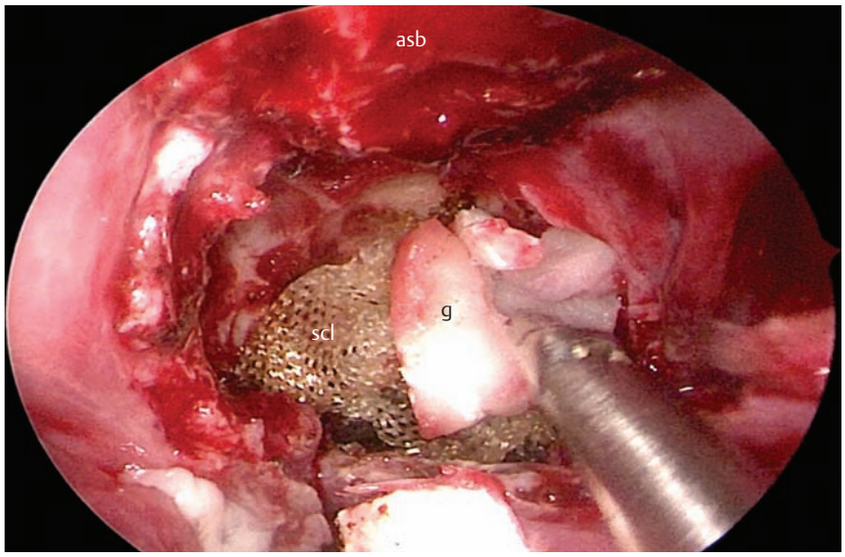

Fig. 7.34 Reconstruction using surgicel and gelfoam. asb: anterior skullbase, g: gelfoam, scl: surgicel.

Case 3: Pituitary Macroadenoma

A 48-year-old female presented with headache and bilateral hemianopia. The MRI showed a sellar lesion which was diagnosed as pituitary macroadenoma (**Fig. 7.35**). The patient was taken under general anesthesia and after partial resection of right middle turbinate, bilateral posterior ethmoids and sphenoid sinuses were opened widely. Bilateral rescue flaps were taken. After posterior septectomy, the rostrum of sphenoid was exposed and triple osteotomies were done (**Fig. 7.36**) to resect the rostrum of sphenoid (**Fig. 7.37**). The sellar bone exposed (**Fig. 7.38**) was drilled (**Fig. 7.39**) using a Karl Storz neurodrill and a 4-mm diamond burr and the bone flap was elevated using a Rosen's elevator (**Fig. 7.40**). The endosteal layer of dura was incised using a Cappabianca knife (**Fig. 7.41**) and extended on both sides using a rotatable Kassam scissors (**Fig. 7.42**). The U-shaped dural flap was elevated and tumor exposed (**Fig. 7.43**). Biopsy of the tumor was taken (**Fig. 7.44**). The two-suction technique was applied for resection of the tumor completely from the cavity (**Fig. 7.45**). After complete tumor removal (**Fig. 7.46**), the cavity was reconstituted with fat and Surgicel, and the dural flap was repositioned (**Fig. 7.47**) and covered with Surgicel and Gelfoam (**Fig. 7.48**). Since there was minimal CSF leak the rescue flap was converted to nasoseptal flap and used for reconstruction (**Fig. 7.49**), followed by Surgicel, Gelfoam, and tissue glue. The nasal cavities were packed with Merocel and the patient was extubated.

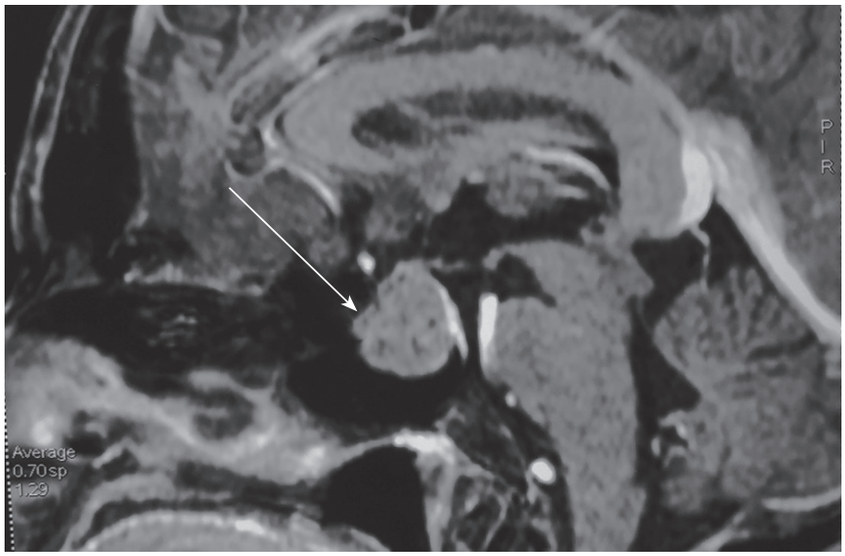

Fig. 7.35 MRI sagittal view showing sellar mass, diagnosed as pituitary macroadenoma.

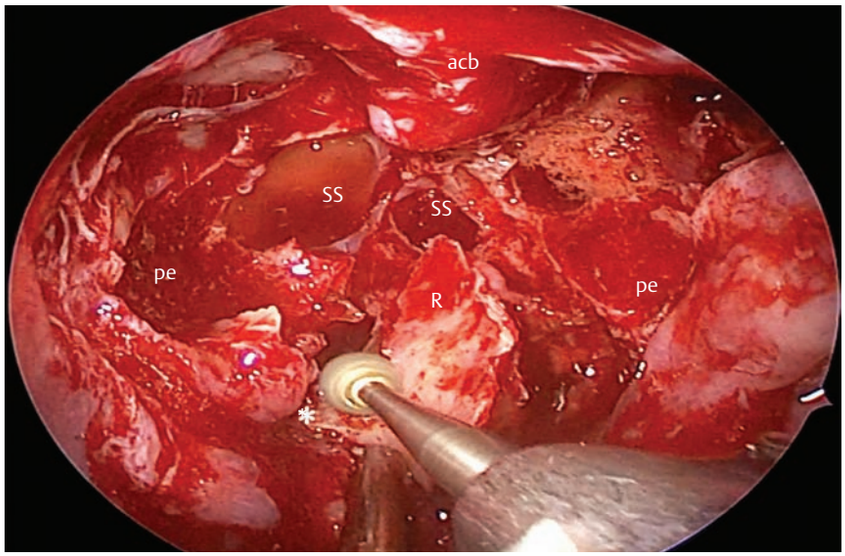

Fig. 7.36 Right shoulder osteotomy at pterygosphenoidsynchondrosis. acb: anterior cranial base, pe: posterior ethmoids, R: rostrum of sphenoid, ss: sphenoid sinus, *: Drilling at right pterygosphenoid synchodrsis.

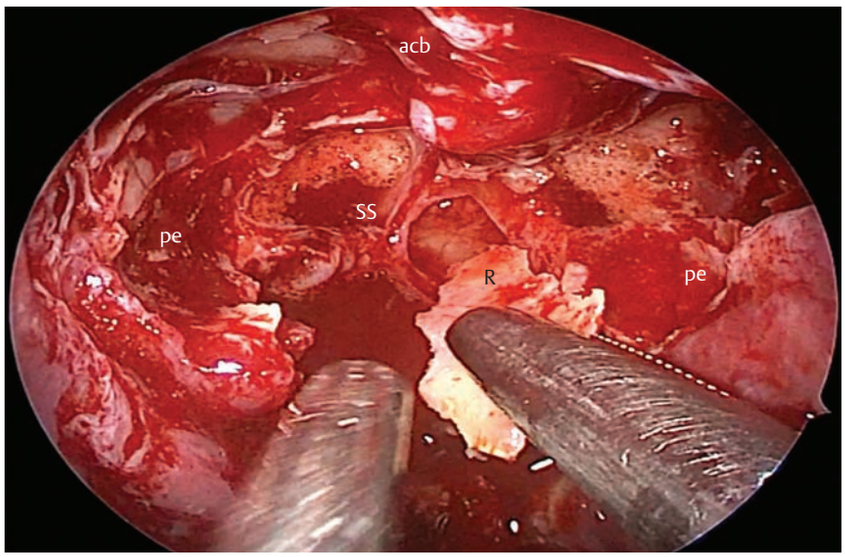

Fig. 7.37 Removal of rostrum of sphenoid after triple osteotomy. acb: Anterior cranial base; pe: posterior ethmoids; R: rostrum of sphenoid; ss: sphenoid sinus.

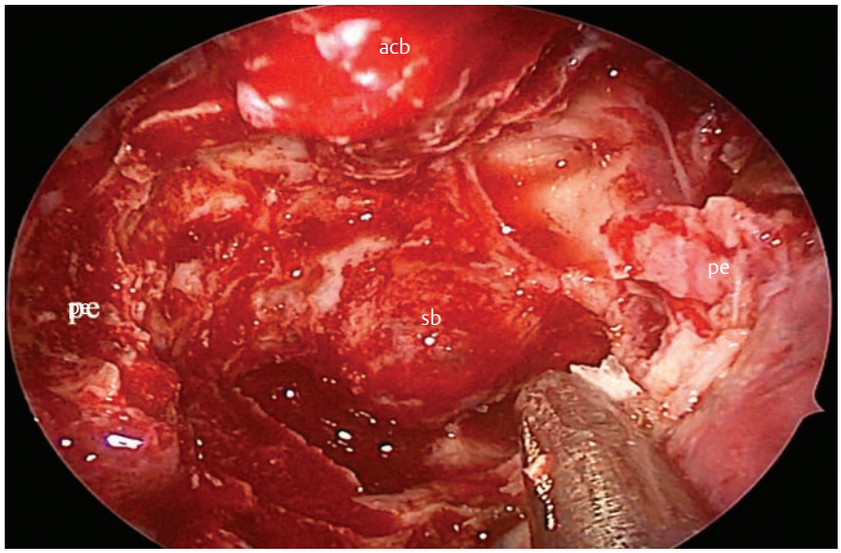

Fig. 7.38 Exposure of sellar floor. acb: Anterior cranial base; pe: posterior ethmoids; sb: sellar bone.

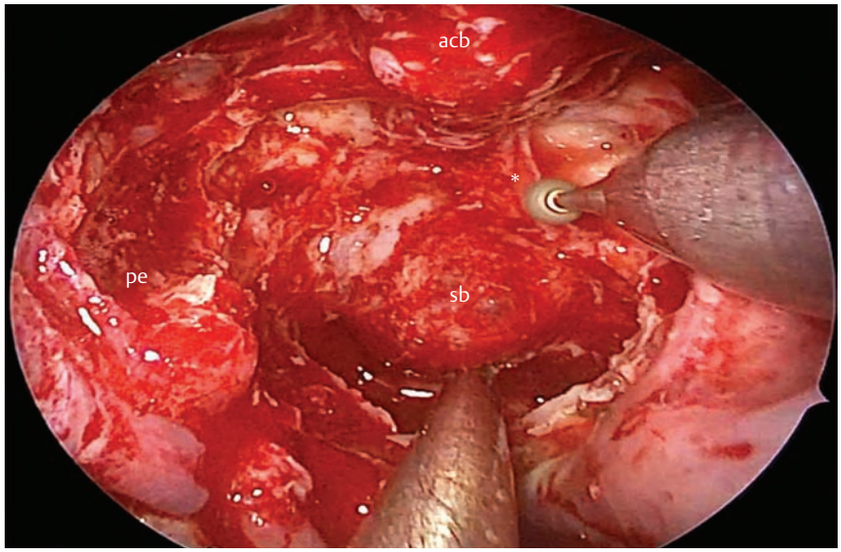

Fig. 7.39 Drilling of the sellar bone. acb: Anterior cranial base; pe: posterior ethmoids; sb: sellar bone; *: drilling of sellar bone.

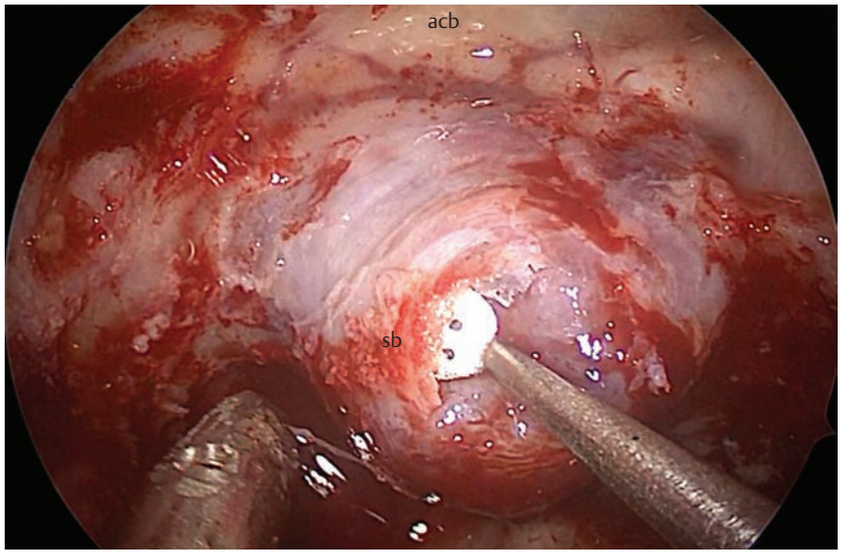

Fig. 7.40 Removal of sellar bone flap using Rosen's elevator to expose the endosteal layer of dura. acb: Anterior cranial base; sb: sellar bone.

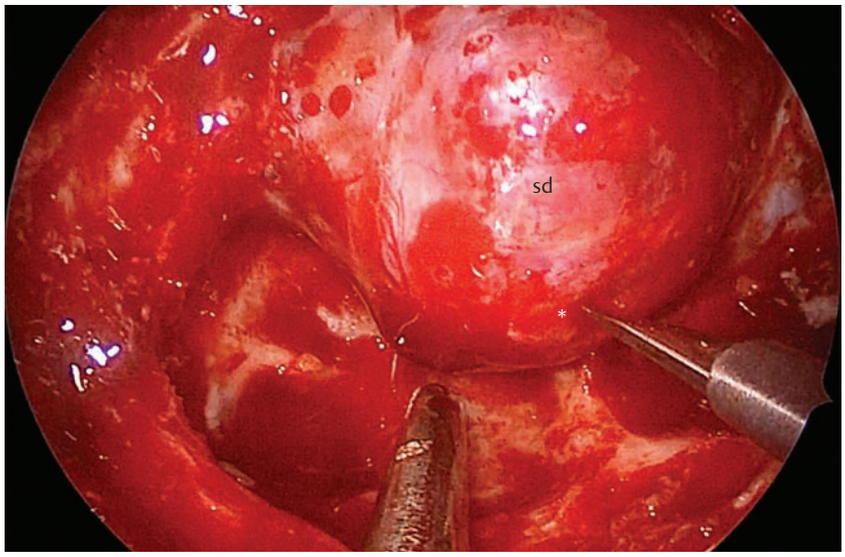

Fig. 7.41 Incision over the endosteal layer of dura using Cappabianca knife. sd: Endosteal layer of dura; *: site of incision over endosteal layer of dura.

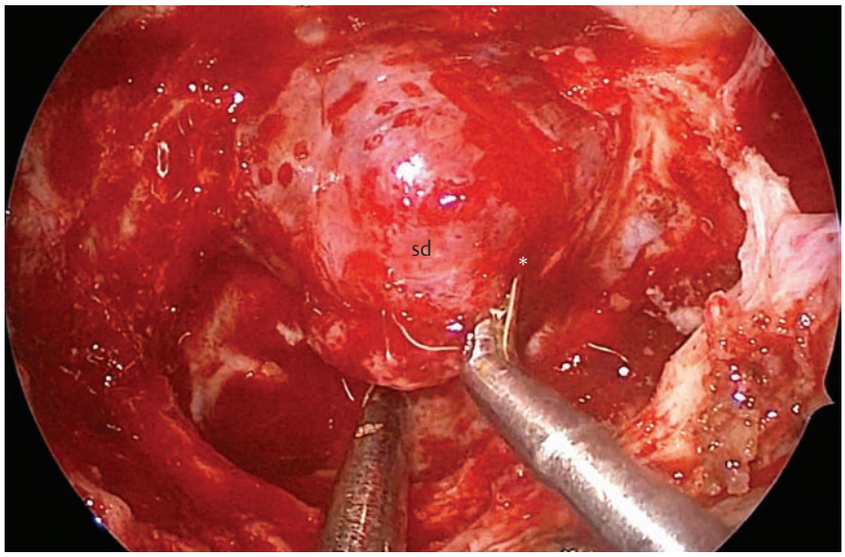

Fig. 7.42 Extension of incision over endosteal layer of dura using rotatable Kassam scissors. sd: Sellar dura; *: site of extension of incision over dura.

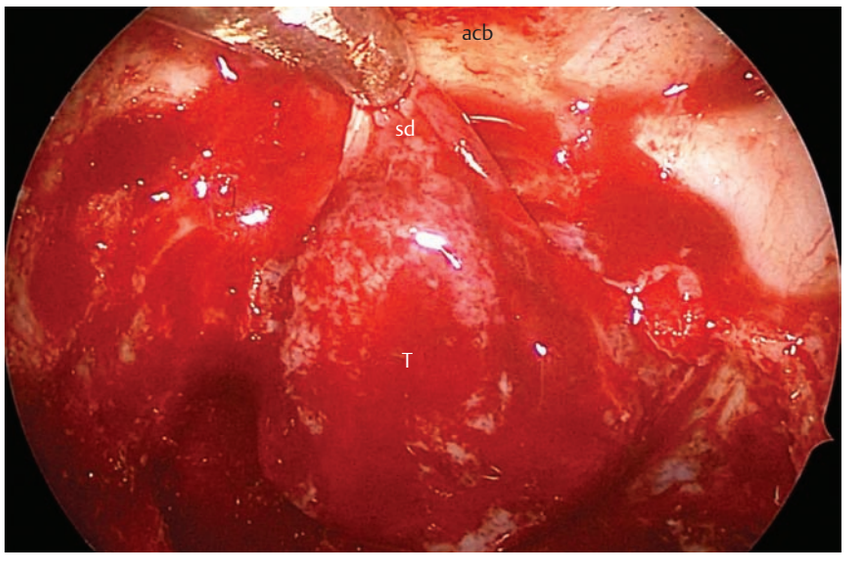

Fig. 7.43 Exposure of tumor after elevation of the endosteal layer of dura as a U-shaped flap. acb: Anterior cranial base; sd: sellar dura; T: tumor.

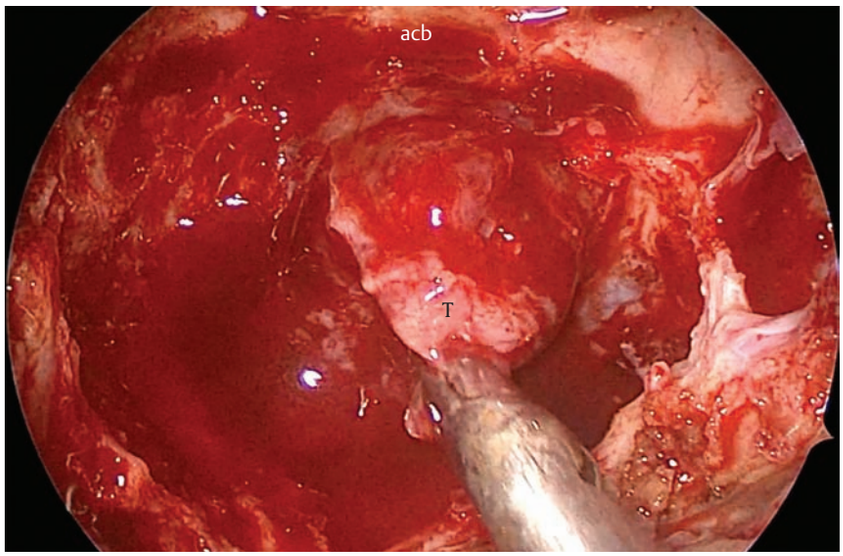

Fig. 7.44 Biopsy of the tumor. acb: Anterior cranial base; T: tumor.

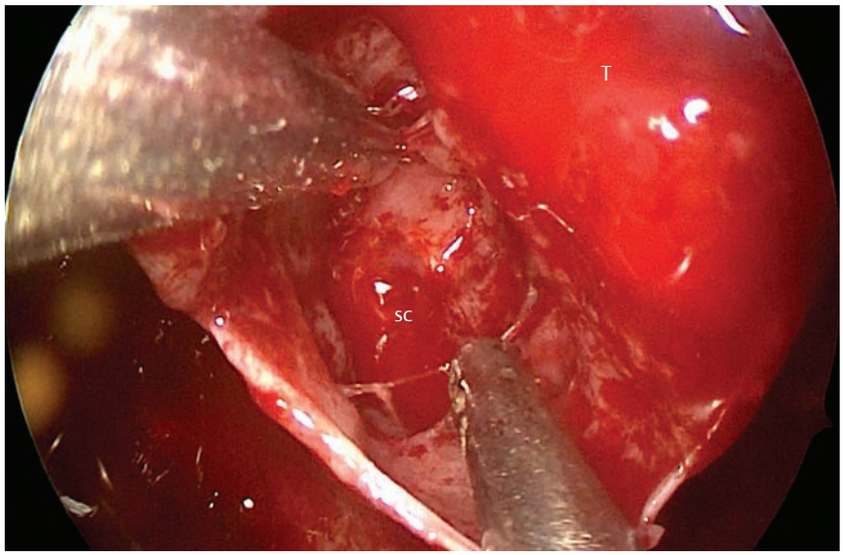

Fig. 7.45 The two-suction technique for tumor resection. sc: Sellar cavity.

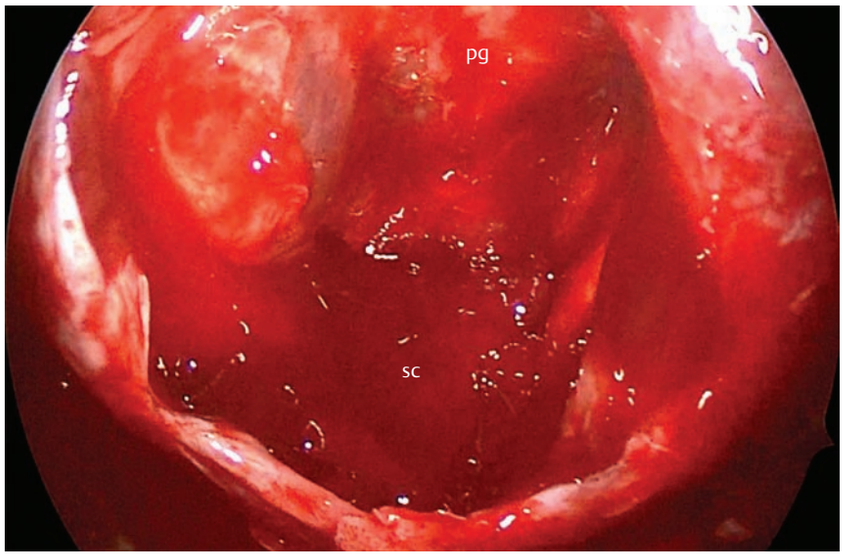

Fig. 7.46 Cavity after complete removal of tumor and exposure of normal pituitary gland. pg: Normal pituitary gland; sc: sellar cavity.

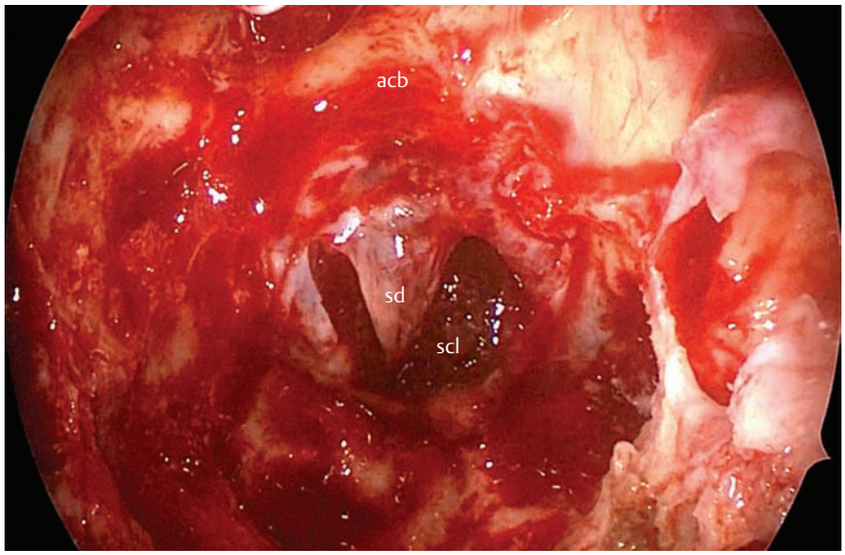

Fig. 7.47 Repositioning of endosteal layer of dura after cavity obliteration with Surgicel. acb: Anterior cranial base; scl: Surgicel; sd: endosteal layer of dura.

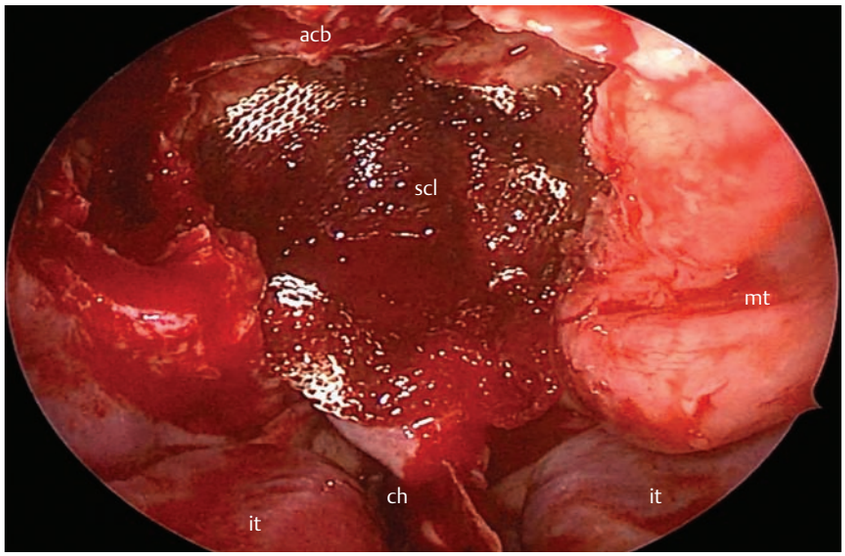

Fig. 7.48 Placement of Surgicel over the endosteal layer of dura for reconstruction. acb: Anterior cranial base; ch: choana; it: inferior turbinate; mt: middle turbinate; scl: Surgicel.

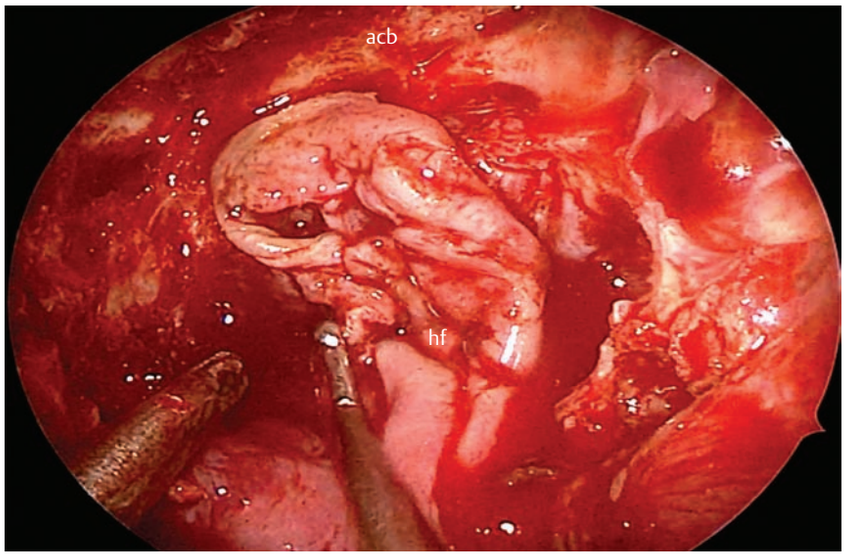

Fig. 7.49 Placement of nasoseptal flap over Surgicel for reconstruction. acb: Anterior cranial base; hf: nasoseptal flap.

Case 4: Pituitary Abscess

A 34-year-old female presented with severe headache. Blood test reports revealed raised serum prolactin levels. MRI of the brain was done and showed a cystic lesion surrounded by normal pituitary gland (**Figs. 7.50 and 7.51**). Since it did not respond to medical treatment the case was planned for transnasal endoscopic transsellar approach under general anesthesia. Bilateral nasal cavities were decongested. Right inferior turbinate was lateralized, and partial resection of middle turbinate was done. In accordance with the "cavity-and-a-half" technique, the right posterior ethmoidectomy was done, to enter into the sphenoid sinus. Left sphenoid sinus opening was exposed by lateralizing the inferior and middle turbinates. Incisions for rescue flap were placed on right side of the septum and the flap was elevated using a ball-point probe (**Fig. 7.52**). Posterior septectomy was done, and bony septum was removed (**Fig. 7.53**), exposing the rostrum of sphenoid (**Fig. 7.54**). Using the two-surgeon, four-handed technique, the planar (**Fig. 7.55**) and shoulder osteotomies (**Fig. 7.56**) were done, and a wide exposure of the posterior wall of sphenoid sinus was obtained (**Fig. 7.57**). The sphenoid mucosa and the intrasphenoidal septae were removed. The sellar bone was drilled using the Storz S3 neurodrill with a 4-mm diamond burr (**Fig. 7.58**). After drilling the bone, a Rosen's elevator was used to raise the bone flap (**Fig. 7.59**). A Cappabianca knife was used to incise the endosteal layer of dura horizontally (**Fig. 7.60**), and vertical extensions were placed by rotatable Kassam scissors to obtain a superior-based U-shaped dural flap (**Figs. 7.61 and 7.62**). This exposed the yellowish normal pituitary gland (**Fig. 7.62**). Incision was placed over the normal gland (**Fig. 7.63**) and pus was seen oozing out of it (**Fig. 7.64**). The pus obtained was sent for gram staining, fungal culture, and AFB; tests were negative. The two-suction technique (**Fig. 7.65**) was used to clear the cavity of all the pus completely (**Fig. 7.66**). The final cavity was packed using Surgicel, and the dural flap was repositioned (**Fig. 7.67**) and reconstruction done using the Surgicel and Gelfoam (**Fig. 7.68**). Postoperative scan showed complete clearance of cystic lesion with reconstruction material (**Fig. 7.69**). See **Video 7.2**.

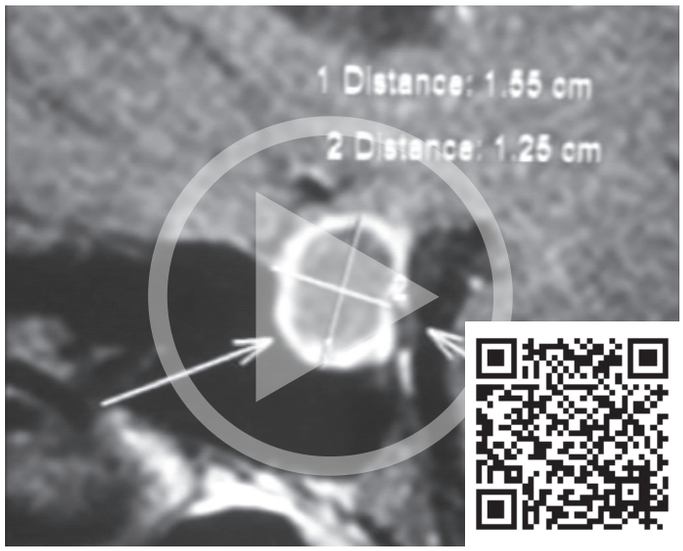

Video 7.2 Pituitary abscess. https://www.thieme.de/de/q.htm?p=opn/cs/19/9/10104321-98f24639

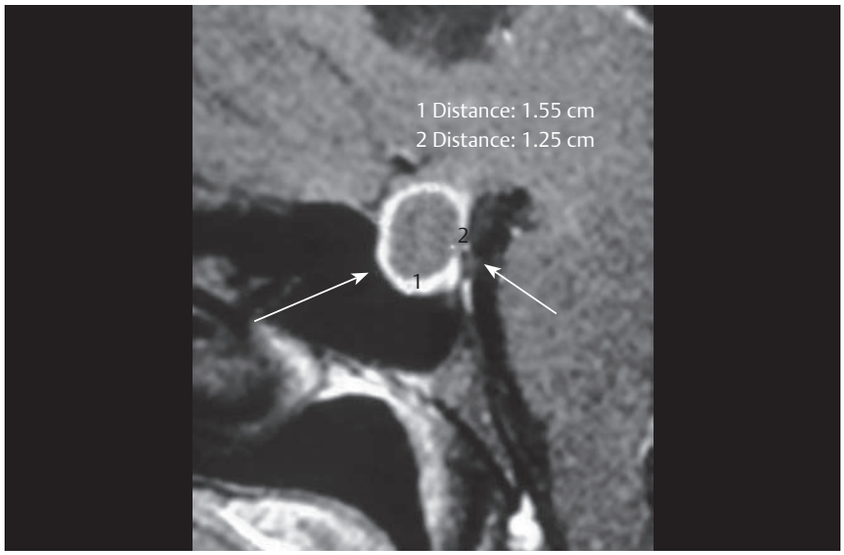

Fig. 7.50 MRI sagittal view showing cystic lesion inside pituitary gland.

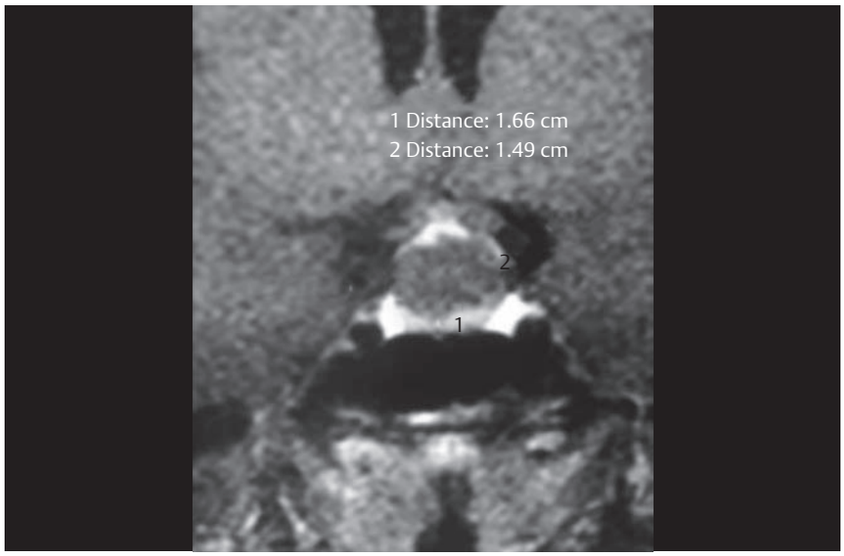

Fig. 7.51 MRI coronal view showing cystic lesion inside pituitary gland.

Fig. 7.52 Incisions for rescue flap. lw: lateral nasal wall, S: nasal septum, *: Incision lines for nasoseptal flap.

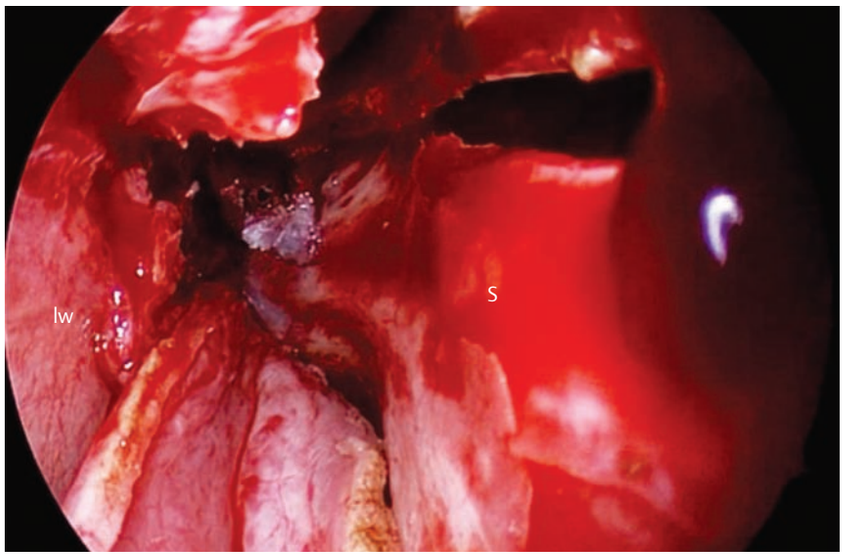

Fig. 7.53 Posterior septectomy. S: Nasal septum; lw: lateral nasal wall.

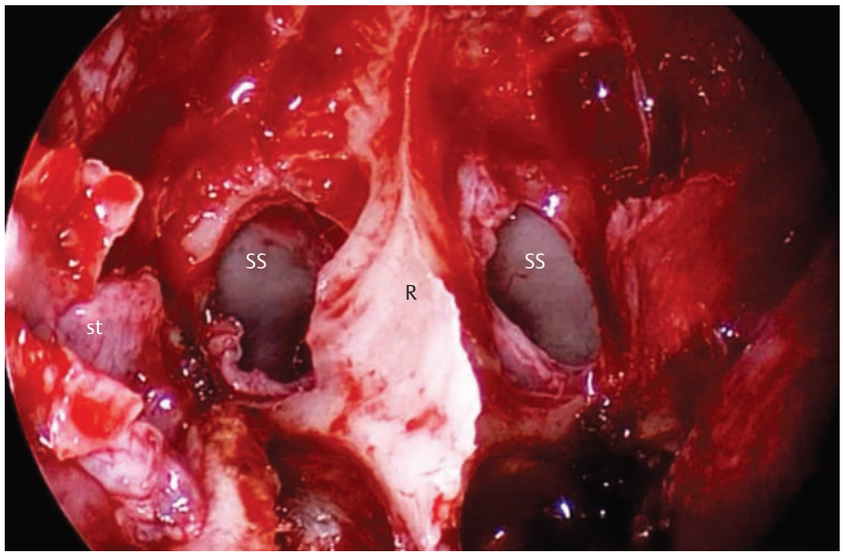

Fig. 7.54 Exposure of rostrum of sphenoid. R: Rostrum of sphenoid; ss: sphenoid sinus; st: superior turbinate.

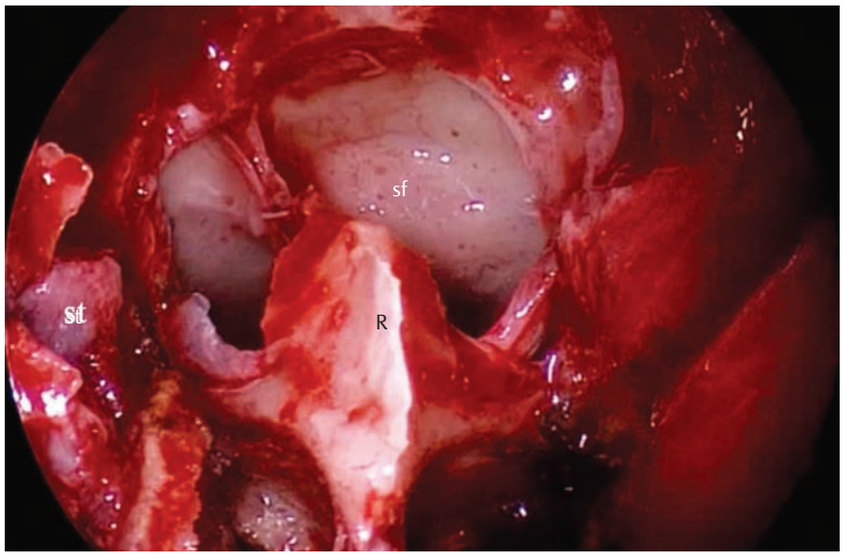

Fig. 7.55 Exposure obtained after planar osteotomy. R: Rostrum of sphenoid; sf: sellar floor; st: superior turbinate.

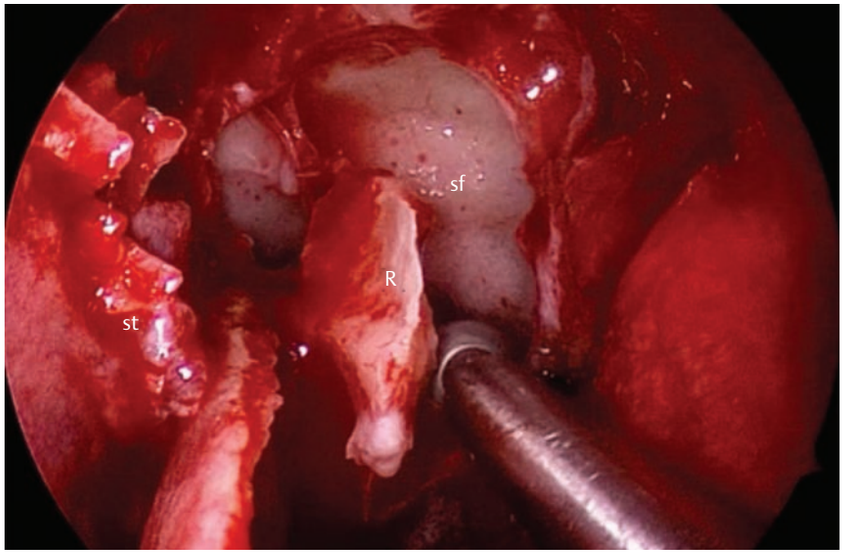

Fig. 7.56 Left shoulder osteotomy at pterygosphenoid synchondrosis. R: Rostrum of sphenoid; sf: sellar floor; st: superior turbinate.

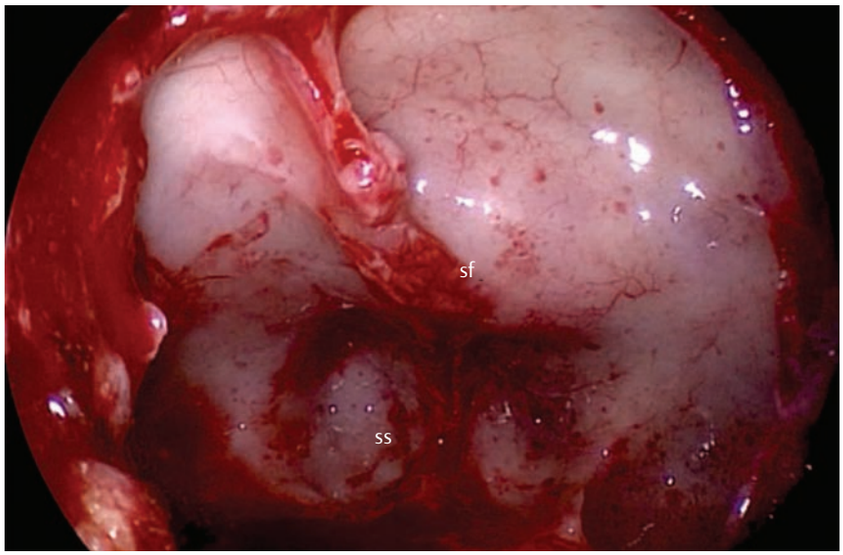

Fig. 7.57 Sellar exposure. sf: Sellar floor; ss: sphenoid sinus.

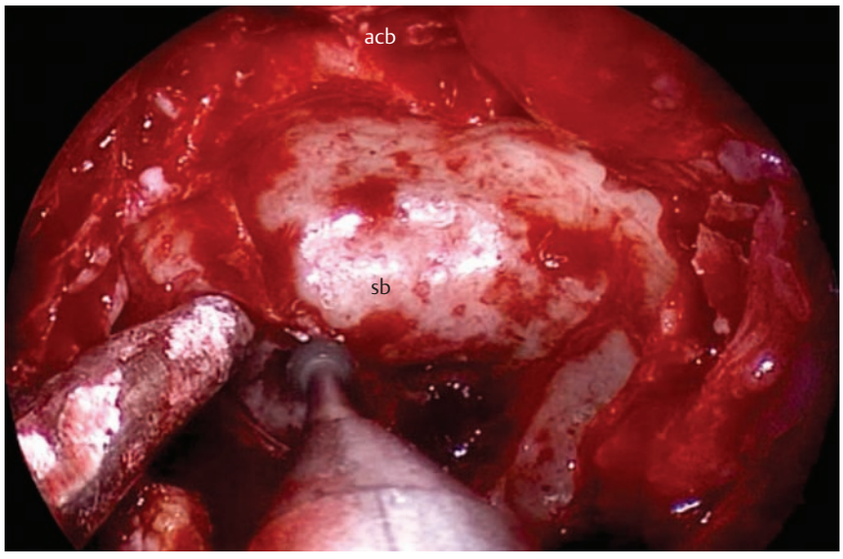

Fig. 7.58 Drilling of sellar bone. acb: Anterior cranial base; sb: sellar bone.

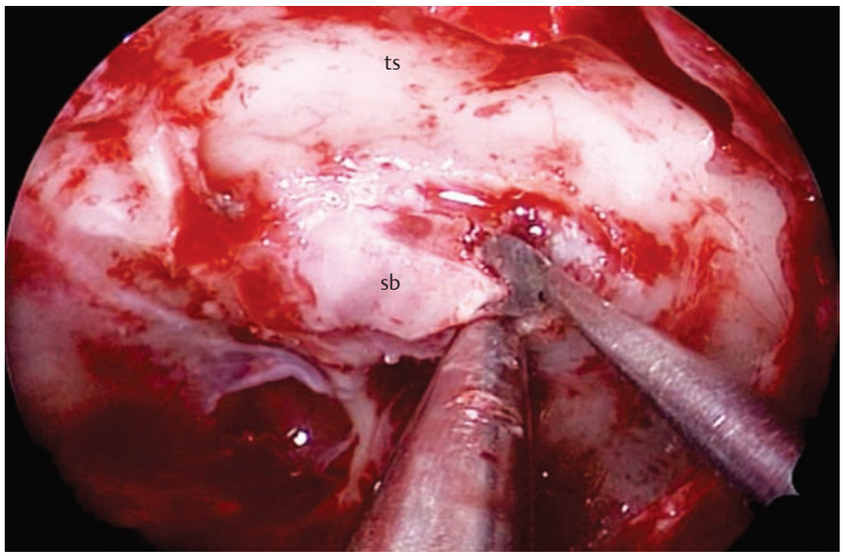

Fig. 7.59 Elevation of sellar bone flap using Rosen's elevator. sb: Sellar bone; ts: tuberculum sella.

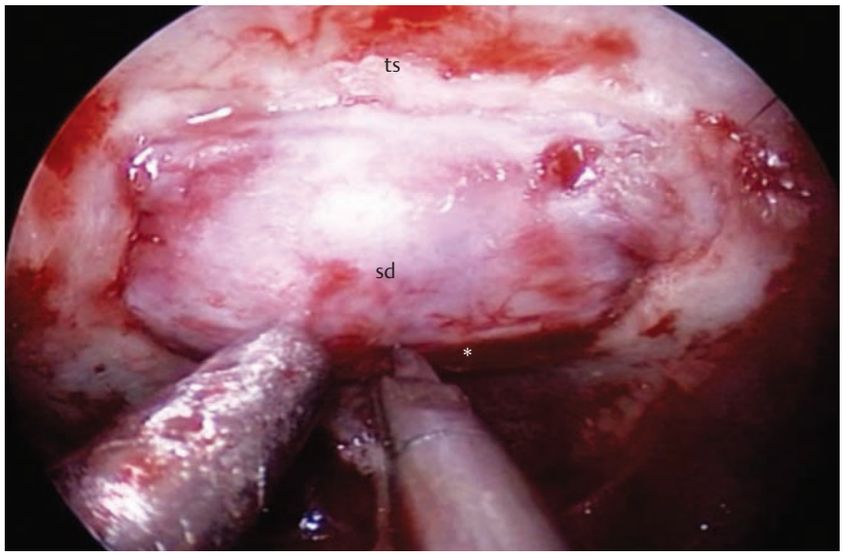

Fig. 7.60 Exposure of endosteal layer of dura and dural incision using Cappabianca knife. sd: Endosteal layer of dura; ts: tuberculum sella; *: incision line.

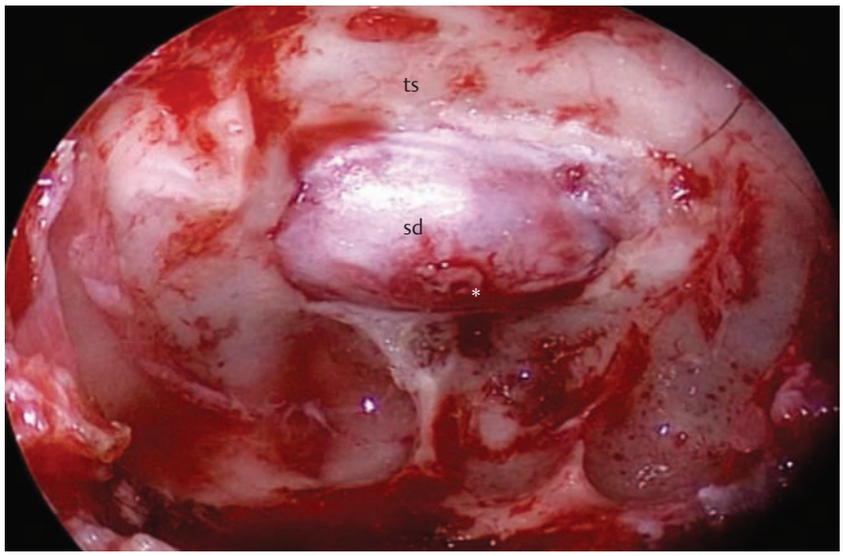

Fig. 7.61 Pituitary gland bulging out from the incision. sd: Endosteal layer of dura; ts: tuberculum sella; *: pituitary gland bulging out.

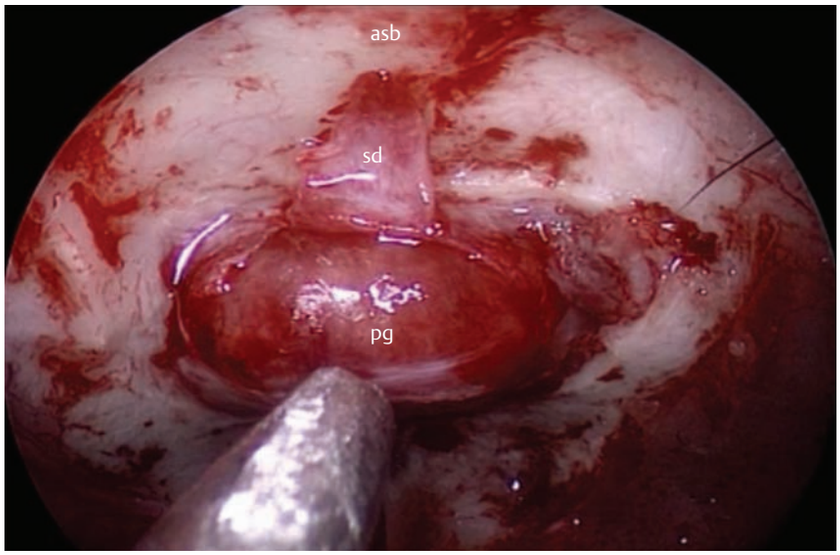

Fig. 7.62 Exposure of pituitary gland after elevation of dural flap. acb: Anterior cranial base; pg: pituitary gland; sd: sellar dura.

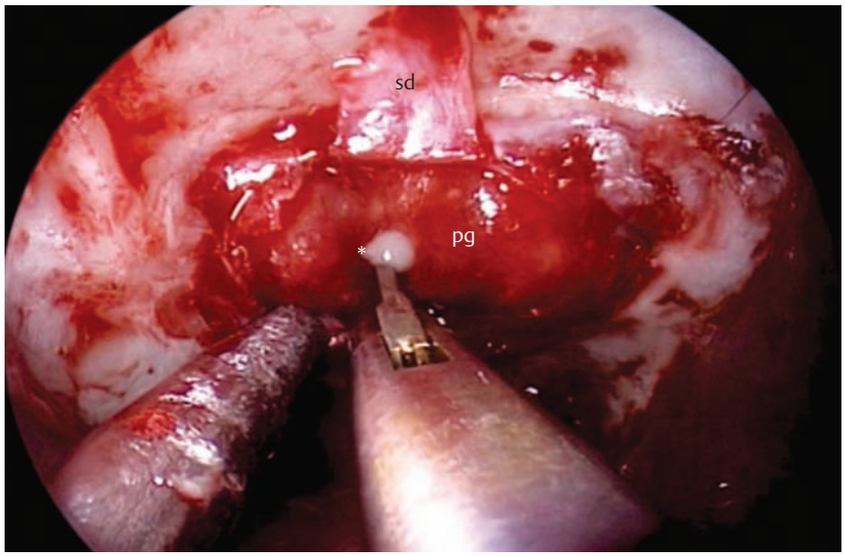

Fig. 7.63 Incision over pituitary gland. pg: Pituitary gland; sd: endosteal layer of dura; *: pus from incision.

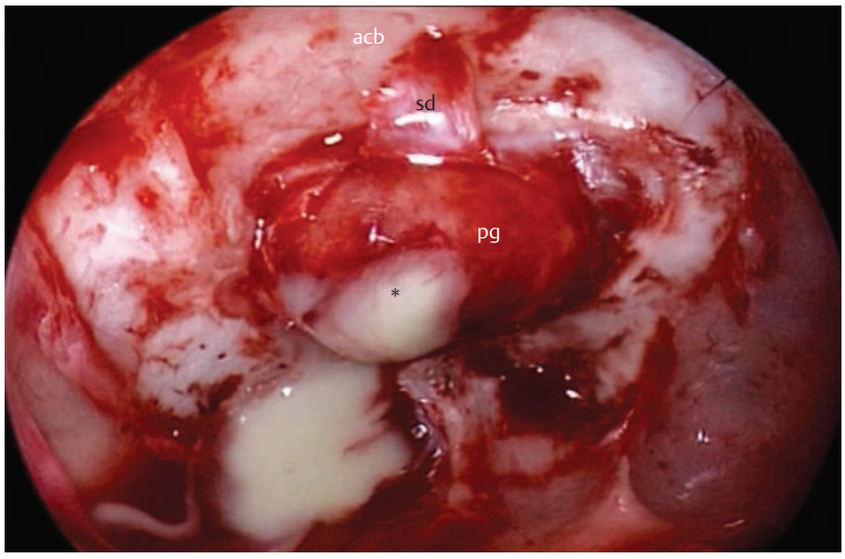

Fig. 7.64 Pus oozing out from the incision over pituitary gland. acb: Anterior cranial base; pg: pituitary gland; sd: endosteal layer of dura; *: pus from the cavity.

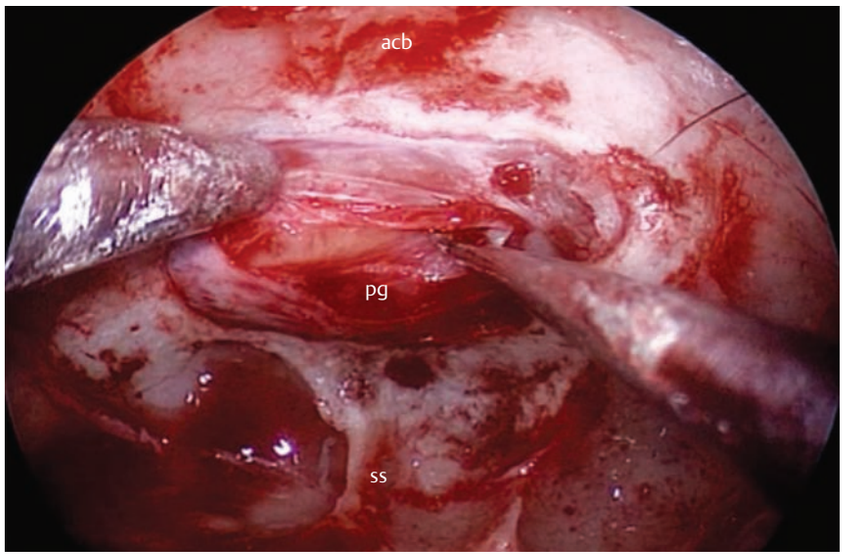

Fig. 7.65 Cavity of cystic lesion exposed. acb: Anterior cranial base; pg: pituitary gland; ss: sphenoid sinus.

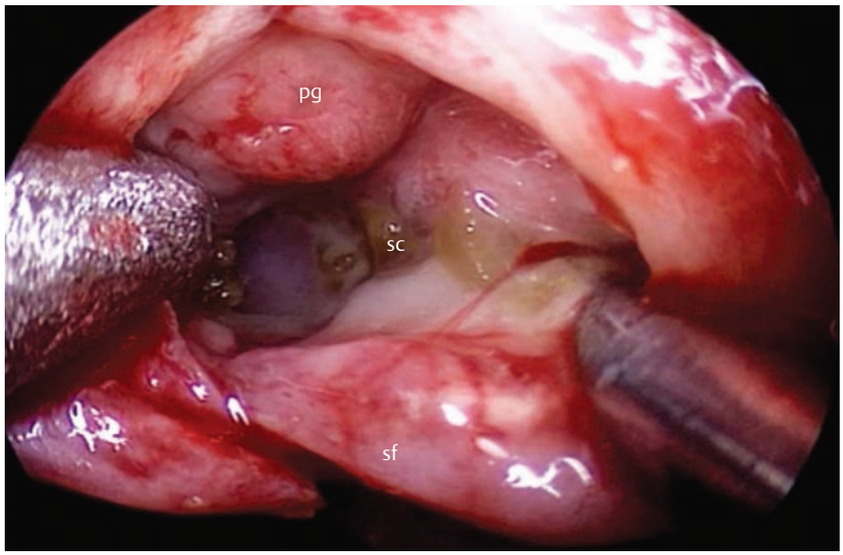

Fig. 7.66 Clearance of cystic cavity obtained. pg: Pituitary gland; sc: sellar cystic cavity.

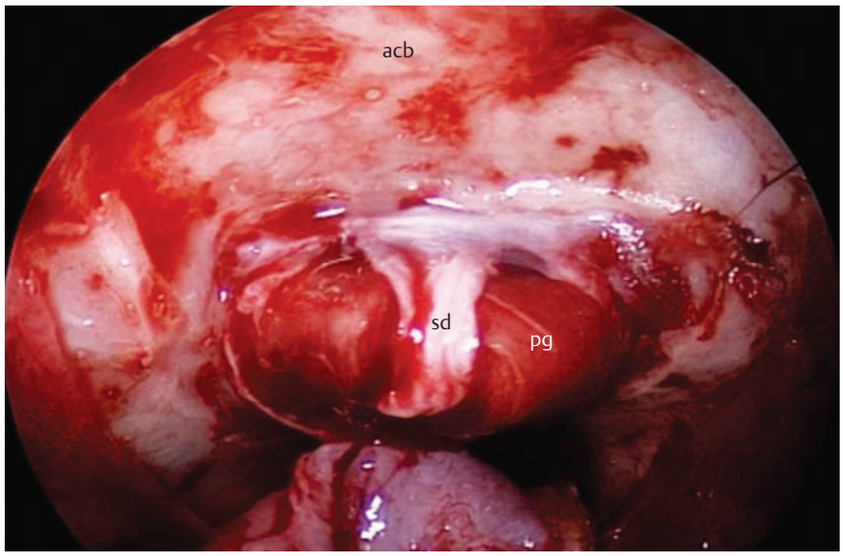

Fig. 7.67 Endosteal layer of dura repositioned. acb: Anterior cranial base; pg: pituitary gland; sd: endosteal layer of dura.

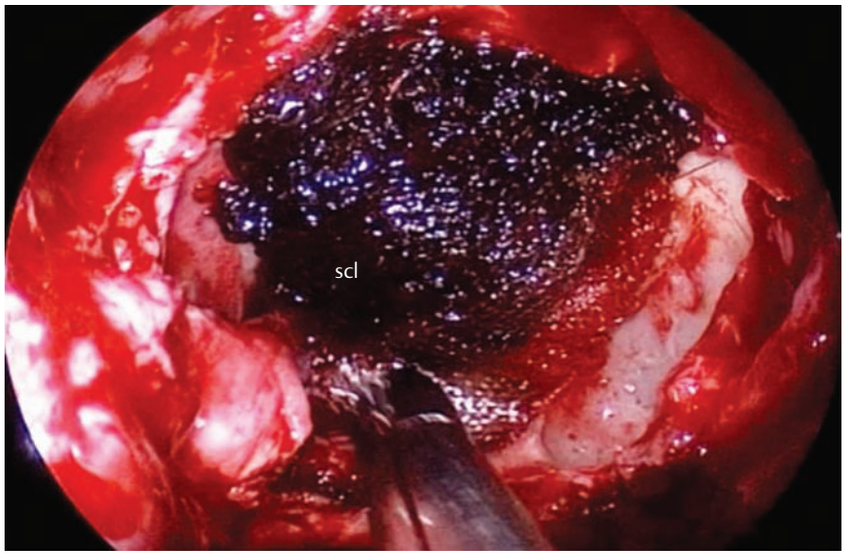

Fig. 7.68 Reconstruction using Surgicel. scl: Surgicel.

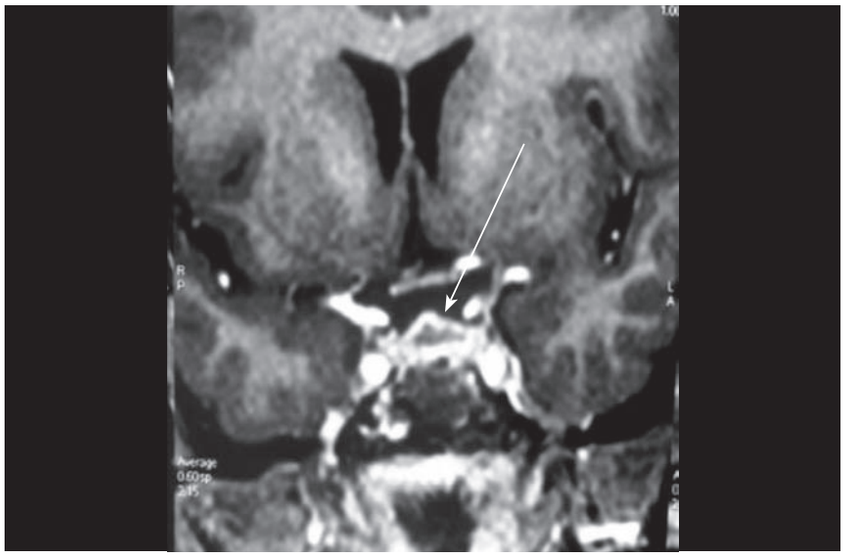

Fig. 7.69 Postoperative MRI showing reconstruction material and normal pituitary gland.

Case 5: Pituitary Macroadenoma with Acromegaly

A 56-year-old female presented with features of acromegaly, i.e., coarseness of facial features (**Fig. 7.70**) and enlargement of extremities (**Fig. 7.71**). MRI scan showed a sellar and parasellar lesion, diagnosed as pituitary macroadenoma (**Figs. 7.72 and 7.73**). The case was taken up for surgery under general anesthesia. Bilateral nasal cavities were decongested. Right inferior turbinate was lateralized, and middle turbinate resected. In accordance with the "cavity-and-a-half" technique, right posterior ethmoidectomy was done to enter into the sphenoid sinus. Left sphenoid sinus opening was exposed by lateralizing the inferior and middle turbinates. Incisions for Hadad flap were placed on the right side of the septum and the flap was elevated and pushed into the nasopharynx to keep it protected from any injury during the surgery. Posterior septectomy was done, and the bony septum was removed, exposing the rostrum of sphenoid. At this point authors shifted to four-handed technique as described previously. This was followed by triple osteotomies, i.e., the planar and shoulder osteotomies, and the rostrum of sphenoid was extracted. A wide exposure of the posterior wall of sphenoid sinus was obtained and the sellar bone was drilled using the Storz S3 neurodrill, which provides a good tactile feedback (**Fig. 7.74**). After drilling the bone, a Rosen's elevator was used to raise the bone flap (**Fig. 7.75**). Widening of exposure was done (**Fig. 7.76**) and Doppler was used to locate the internal carotid arteries (**Fig. 7.77**). A Cappabianca knife was used to incise the endosteal layer of dura horizontally, and vertical extensions of the incision were placed by rotatable Kassam scissors to obtain a superior-based U-shaped dural flap (**Figs. 7.78 and 7.79**). The dural flap was elevated using a Rosen's knife (**Fig. 7.80**). Biopsy of the tissue was taken (**Fig. 7.81**). Then authors shifted to two-suction technique; starting first at 6 o' clock position, the tumor was sucked out (**Figs. 7.82, 7.83, and 7.84**). Calcifications in the tumor are more or less a constant feature found in cases with acromegaly; the calcifications in this case were removed completely. Tumor in the 3 o' clock and 6 o'clock positions were cleared (first right cavernous and left cavernous sinus, **Figs. 7.85 and 7.86**). The strokes of suction tips should resemble to that of a paint brush. All of it was done under vision till the normal pituitary was exposed (**Fig. 7.87**). The final cavity (**Fig. 7.88**) was packed using Surgicel and reconstruction done using the nasoseptal flap.

Fig. 7.70 Facial features of acromegaly.

Fig. 7.71 Features of hand.

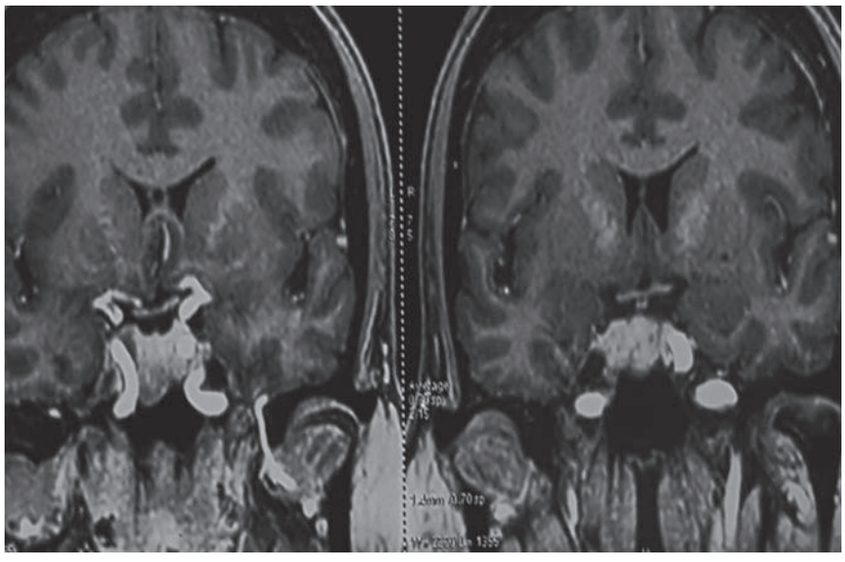

Fig. 7.72 MRI coronal view showing sellar pituitary macroadenoma.

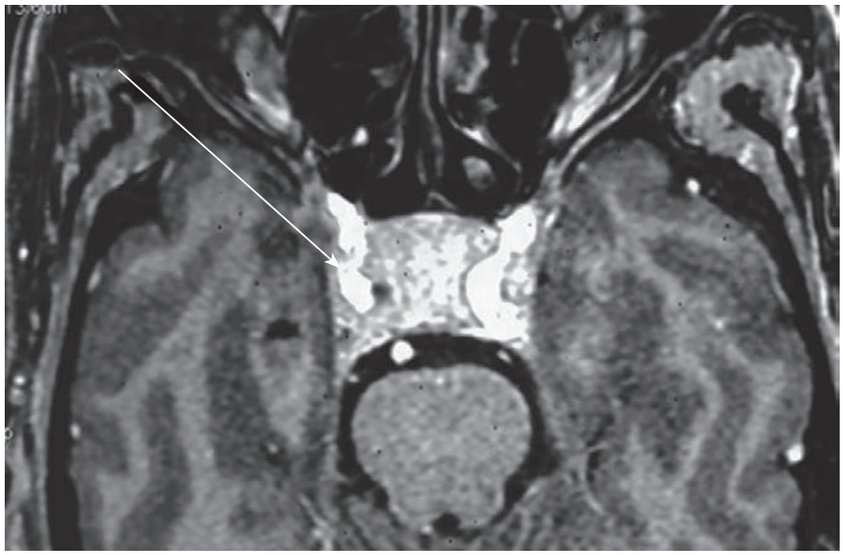

Fig. 7.73 MRI axial view showing sellar lesion.

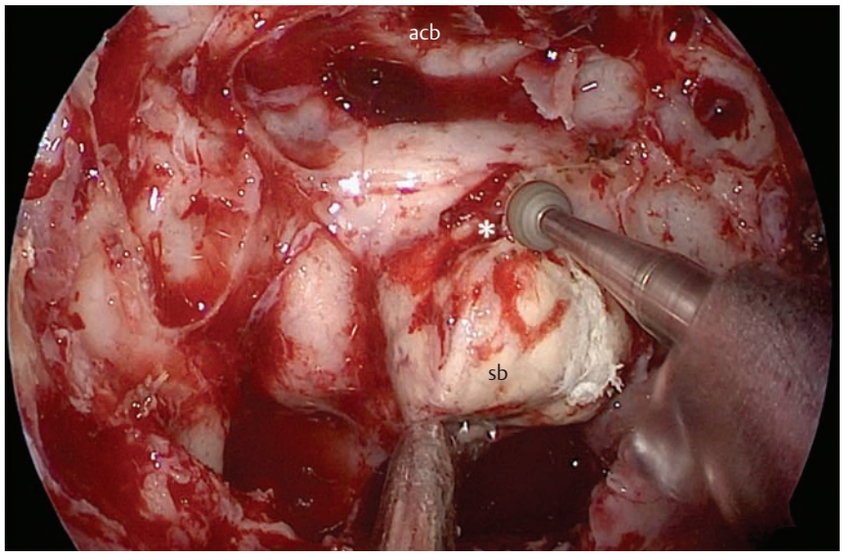

Fig. 7.74 Drilling of the bone over floor of sella. acb: Anterior cranial base; sb: sellar bone; *: site of drilling of bone.

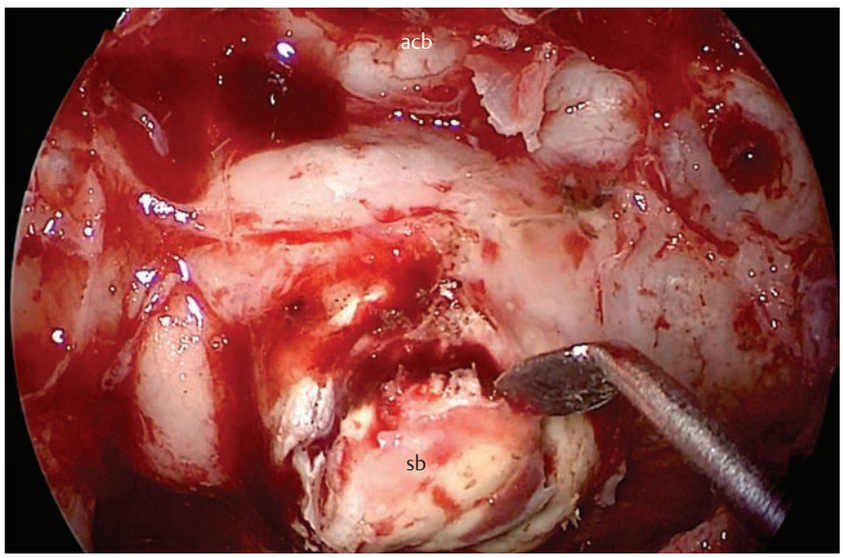

Fig. 7.75 Elevation of bone flap after completion of drilling. acb: Anterior cranial base; sb: sellar bone.

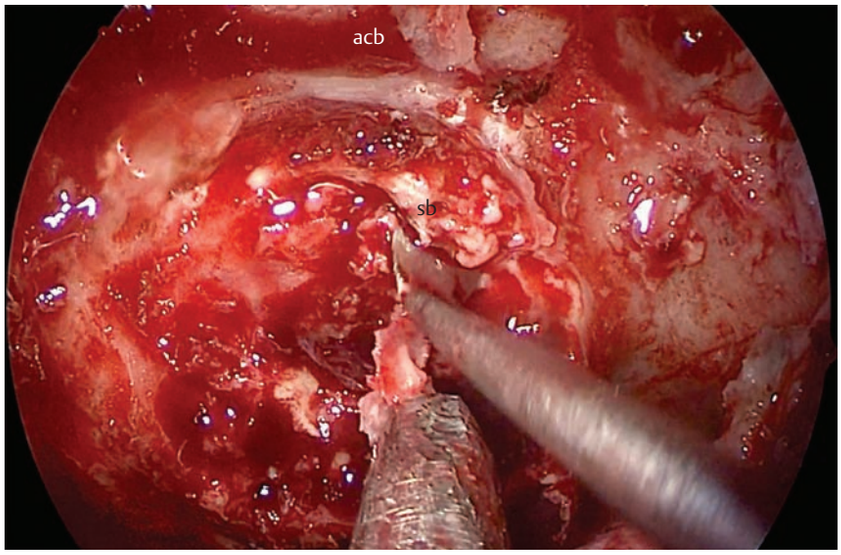

Fig. 7.76 Widening of exposure of endosteal layer of dura. acb: Anterior cranial base; sb: sellar bone.

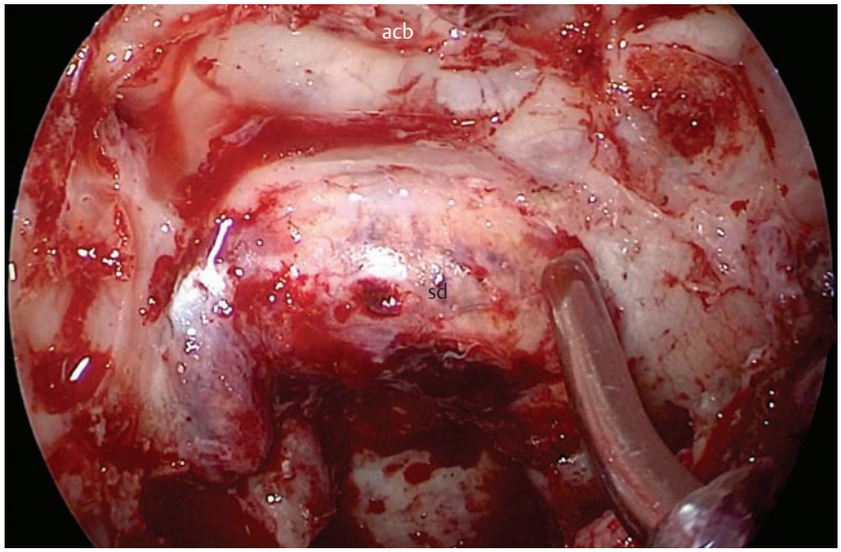

Fig. 7.77 Use of Doppler to locate the cavernous internal carotid artery. acb: Anterior cranial base; sd: endosteal layer of dura.

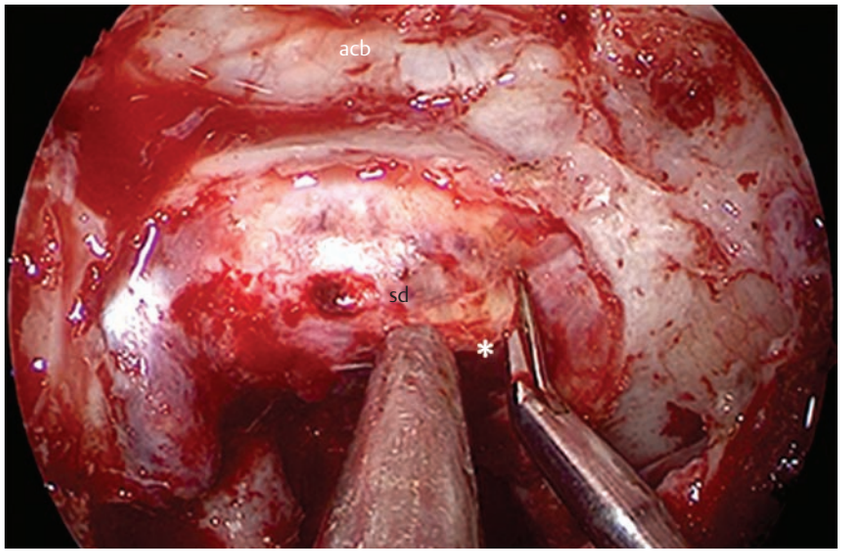

Fig. 7.78 Incision over endosteal layer of dura. acb: Anterior cranial base; sd: endosteal layer of dura; *: incision line.

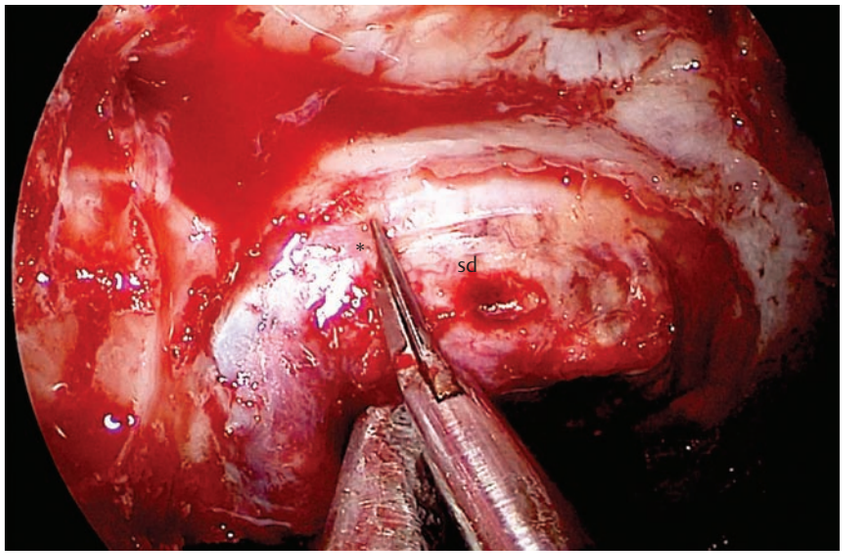

Fig. 7.79 Extension of U-shaped incision over endosteal layer of dura. sd: Endosteal layer of dura; *: incision line.

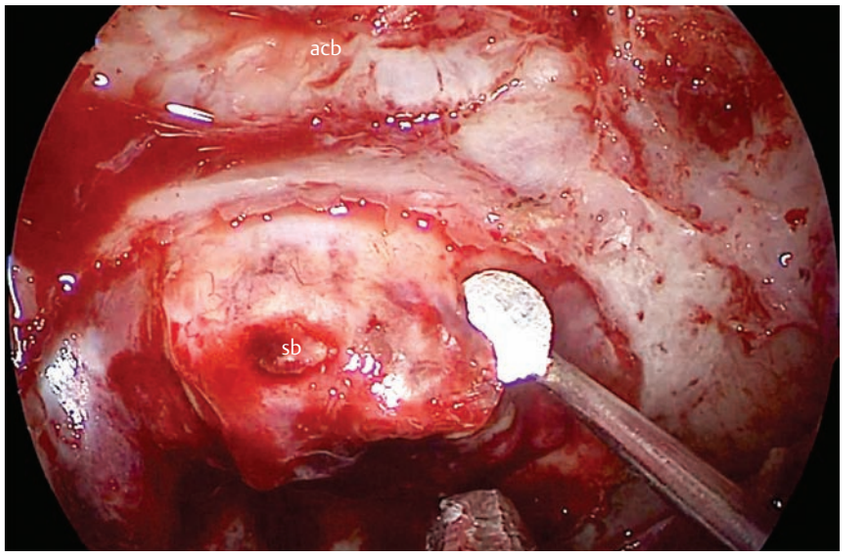

Fig. 7.80 Elevation of endosteal layer of dura using Rosen's elevator. acb: Anterior cranial base; sb: sellar bone.

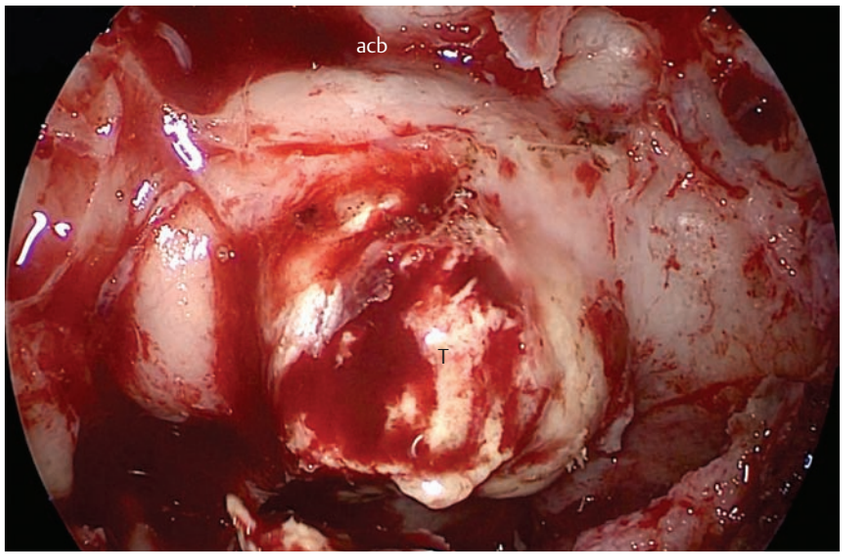

Fig. 7.81 Exposure of the tumor in sellar cavity. acb: Anterior cranial base; T: tumor.

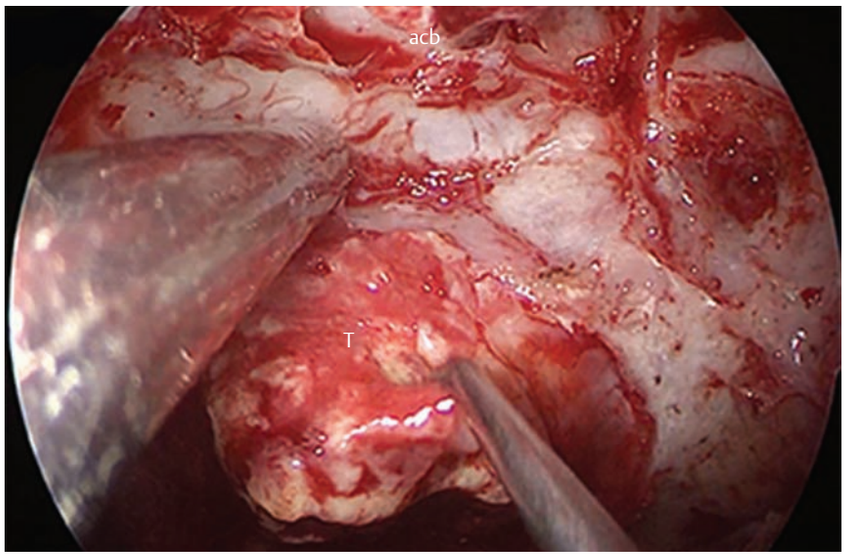

Fig. 7.82 The two-suction technique for tumor excision. acb: Anterior cranial base; T: tumor.

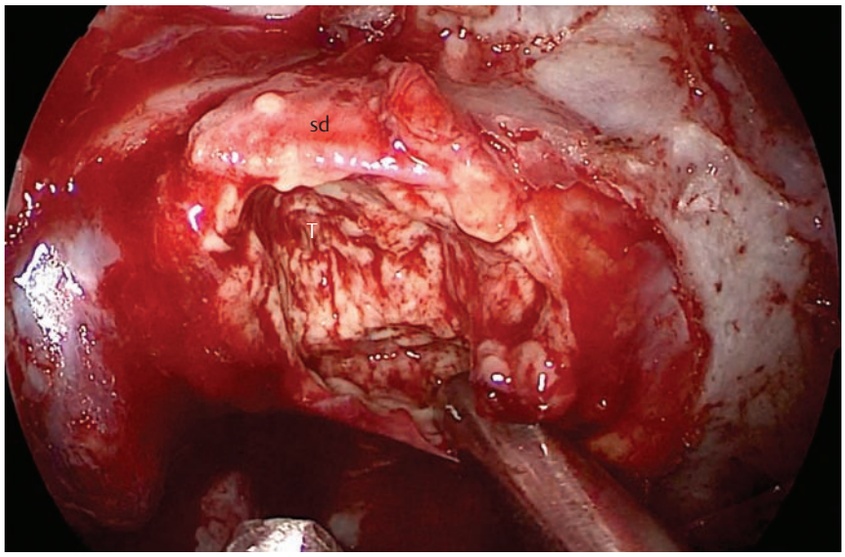

Fig. 7.83 Use of suction to remove inferior part of the tumor. sd: flap of endosteal layer of dura, T: tumor.

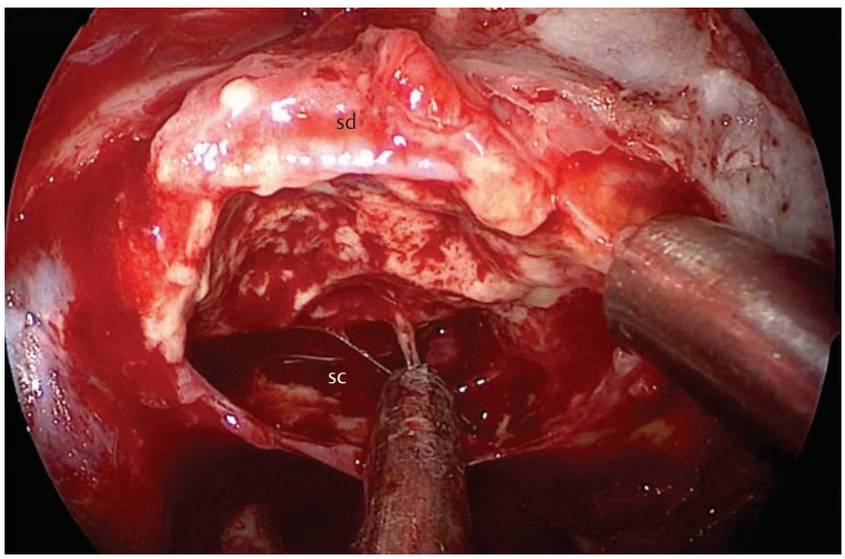

Fig. 7.84 Inferior part of tumor excised. sc: Sellar cavity; sd: endosteal layer of dura.

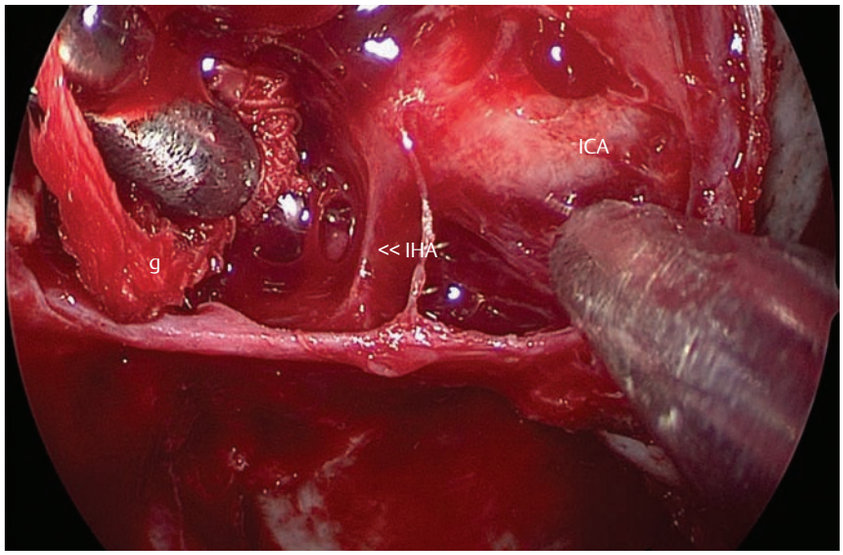

Fig. 7.85 Clearance of sellar cavity of tumor. g: Gauze; IHA: inferior hypophyseal artery; ICA: cavernous part of left internal carotid artery.

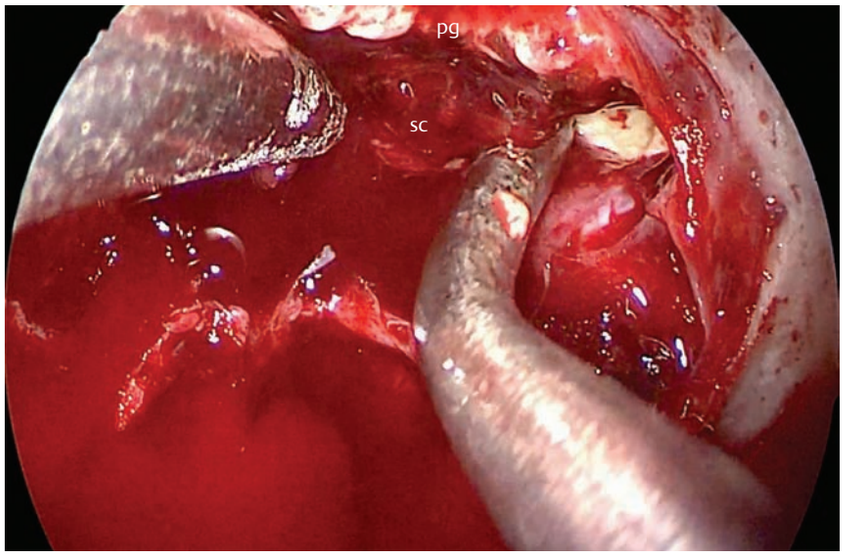

Fig. 7.86 Clearance of left cavernous sinus. pg: Normal pituitary gland; sc: sellar cavity.

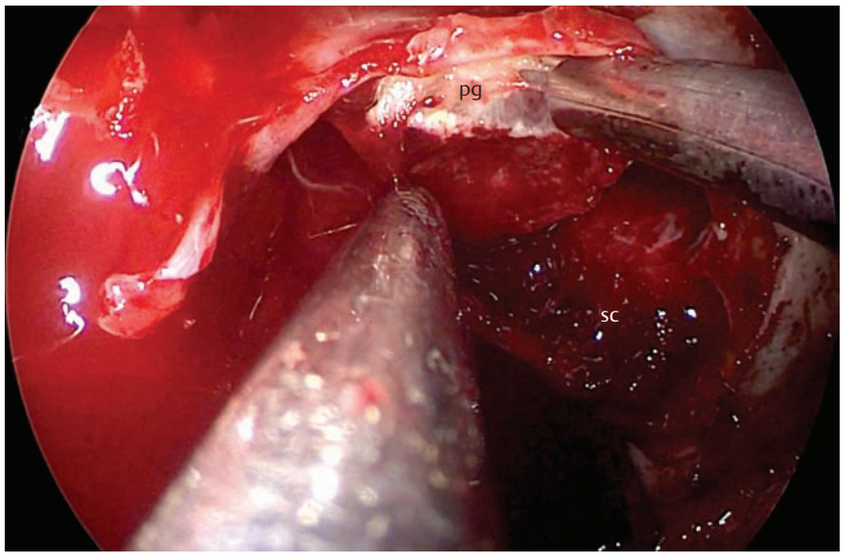

Fig. 7.87 Normal pituitary gland exposed. pg: Normal pituitary gland.

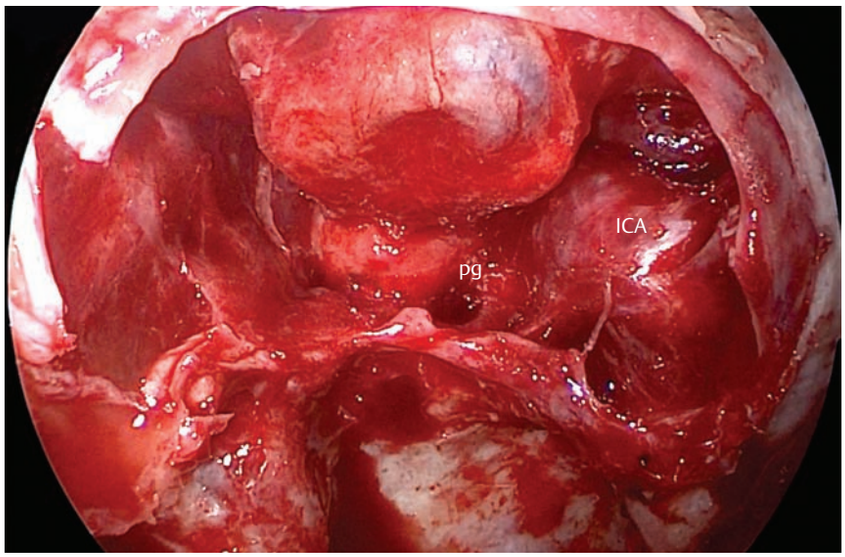

Fig. 7.88 Sellar cavity after complete clearance of tumor. ICA: Left cavernous internal carotid artery; pg: normal pituitary gland.

Case 6: Fibrous Pituitary Lesion

A 35-year-old female presented with complaints of headache. She had raised serum prolactin levels. MRI of the brain was suggestive of pituitary macroadenoma (**Figs. 7.89 and 7.90**). She did not respond to medications so authors had to plan for a transnasal, transsellar approach for excision of the adenoma. The right inferior turbinate was lateralized and middle turbinate resected. Right posterior ethmoidectomy was done and the sphenoid os exposed was widened. Left sphenoid sinus opening was exposed by lateralizing the inferior and middle turbinates. Incisions for rescue flap were placed bilaterally to be harvested later as per requirement. Posterior septectomy was done, and the rostrum of sphenoid was exposed. This was followed by triple osteotomies, i.e., the planar (**Fig. 7.91**) and shoulder osteotomies (**Fig. 7.92**), and the rostrum of sphenoid was removed. A wide exposure of the posterior wall of sphenoid sinus was obtained (**Fig. 7.93**) and the sellar mucosa was removed completely (**Fig. 7.94**). The sellar floor was drilled using the Storz S3 neurodrill with a 4-mm diamond burr (**Fig. 7.95**). After drilling the bone, a Rosen's elevator was used to raise the bone flap (**Fig. 7.96**) to expose the endosteal dura (**Fig. 7.97**). A Cappabianca knife was used to incise the dura horizontally and the incision was vertical, extended on both sides by rotatable Kassam scissors to obtain a superior-based U-shaped dural flap. The flap was raised to expose the lesion (**Fig. 7.98**). Using a suction tip and an elevator, extracapsular dissection was carried out starting from the 3 o' clock position, 6 o' clock. 9 o' clock, and finally the 12 o' clock position. The tumor was delivered in a single piece (**Figs. 7.99, 7.100, 7.101, and 7.102**). The final cavity was packed using fat and Surgicel (**Fig. 7.103**), and dura was repositioned and sutured to anchor the fat inside the cavity (**Fig. 7.104**). The final reconstruction was done using the nasoseptal flap, followed by Surgicel, Gelfoam, and tissue glue. See **Video 7.3**.

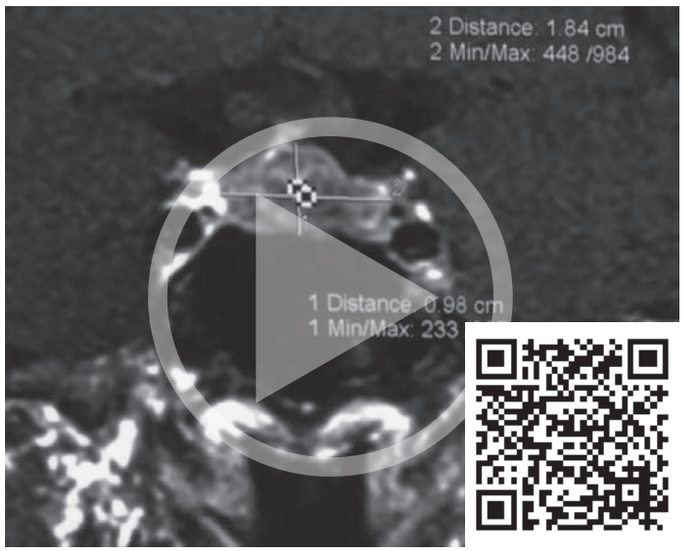

Video 7.3 Fibrous pituitary macroadenoma: Fibrous lesion. https://www.thieme.de/de/q.htm?p=opn/cs/19/9/10104322-35cad7c6

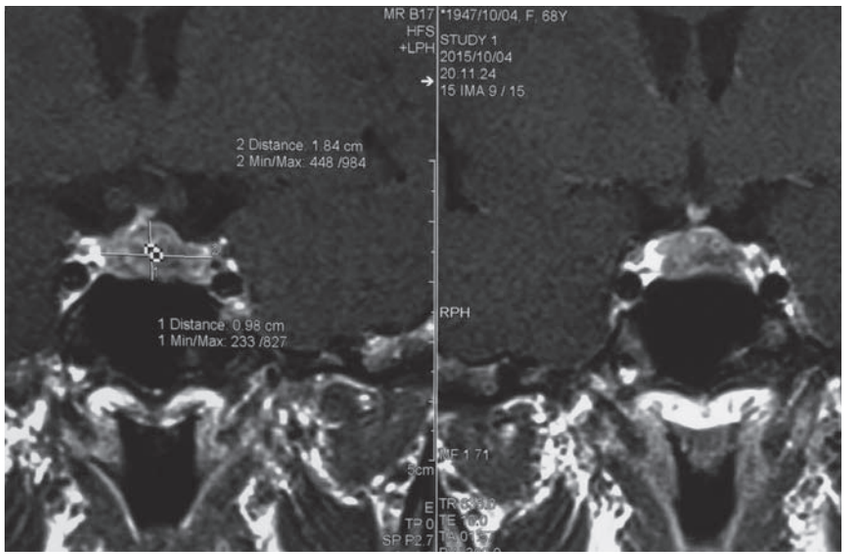

Fig. 7.89 MRI coronal view showing sellar lesion.

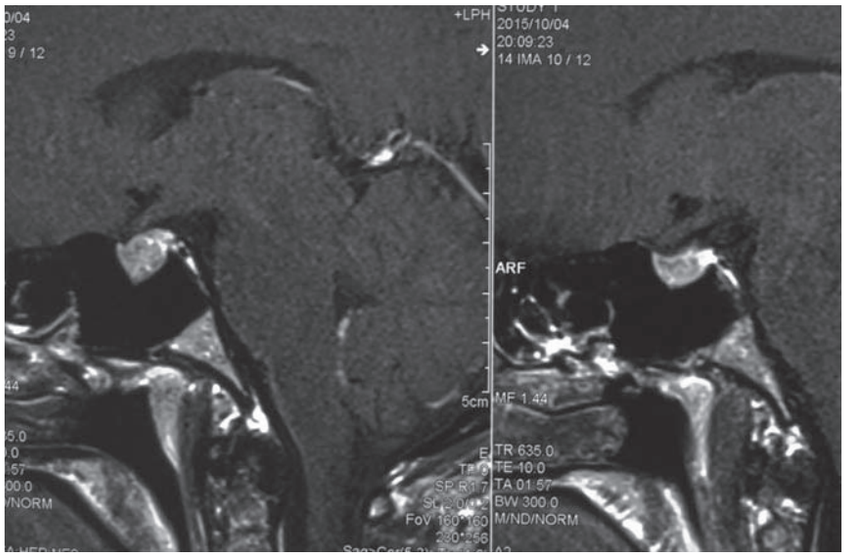

Fig. 7.90 MRI sagittal view showing sellar pituitary macroadenoma.

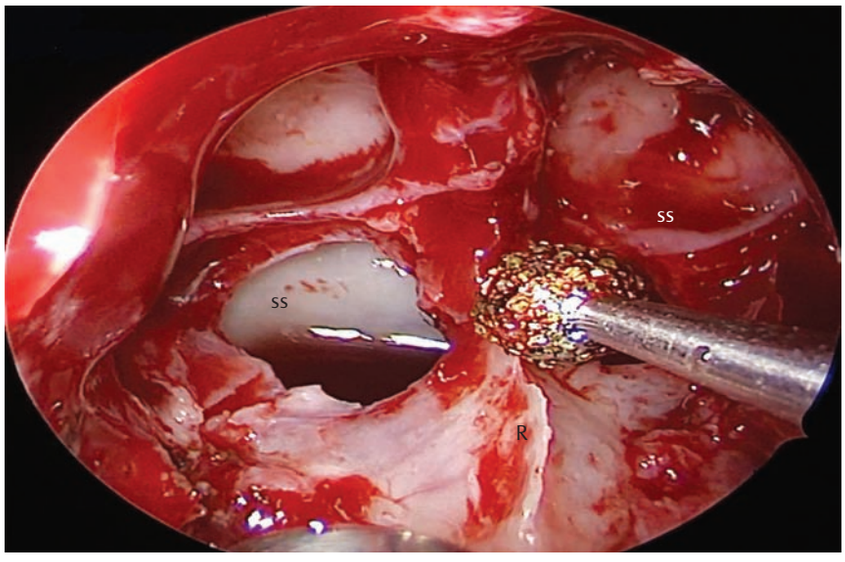

Fig. 7.91 Planar osteotomy. R: Rostrum of sphenoid; ss: sphenoid sinus.

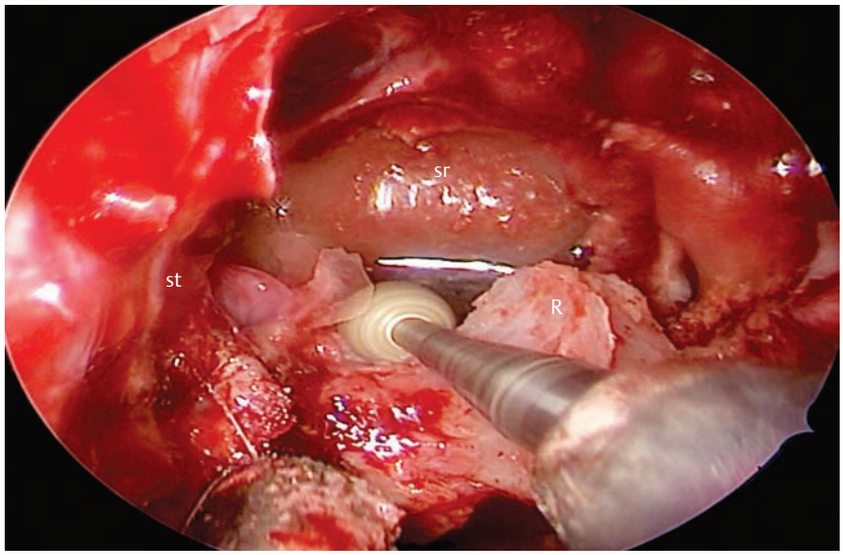

Fig. 7.92 Right shoulder osteotomy at pterygosphenoid synchondrosis. R: Rostrum of sphenoid; sr: sellar region.

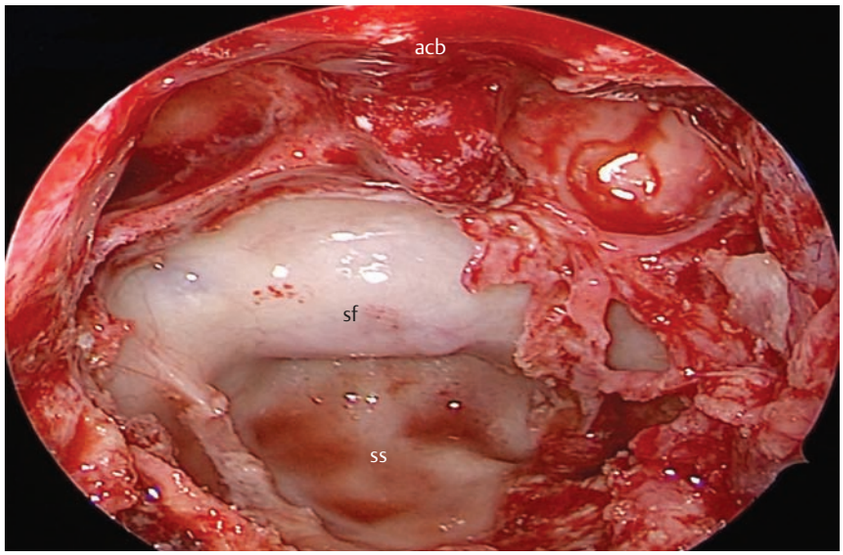

Fig. 7.93 Sellar exposure obtained. acb: Anterior cranial base; sf: sellar floor; ss: sphenoid sinus.

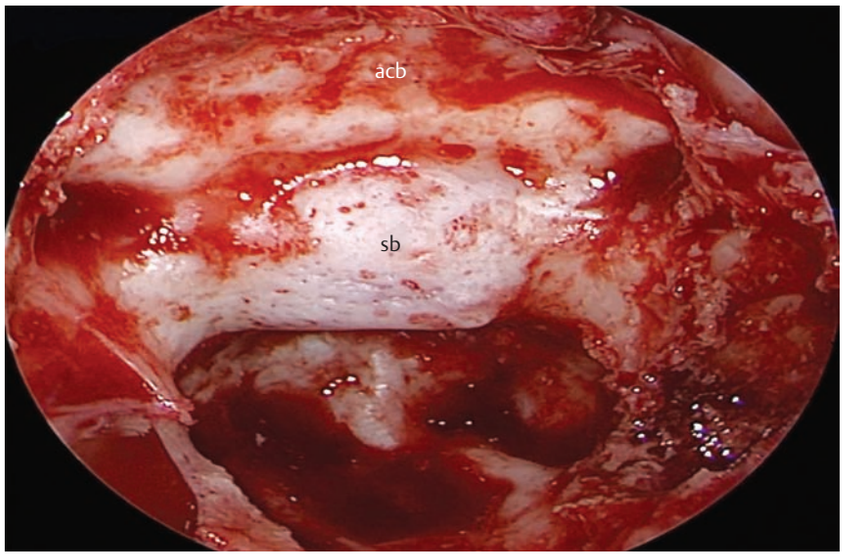

Fig. 7.94 Exposure after removal of sphenoid mucosa. acb: Anterior cranial base; sb: sellar bone.

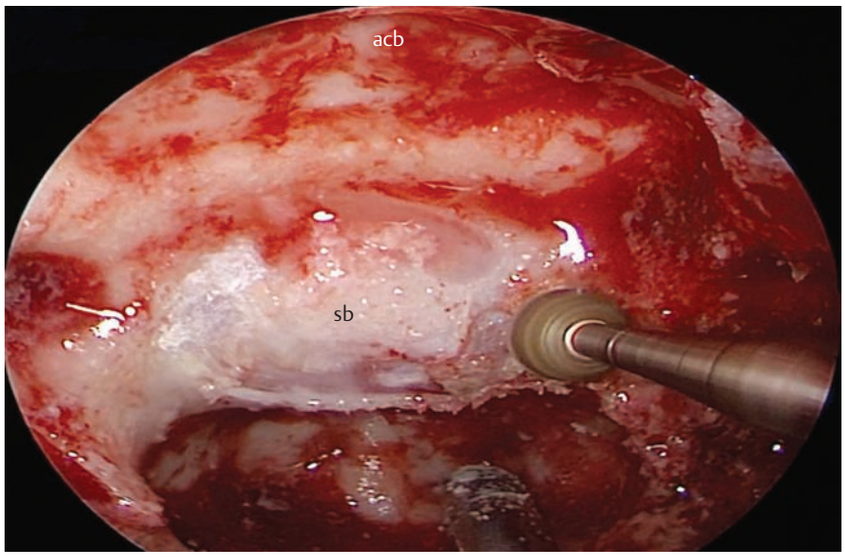

Fig. 7.95 Drilling of sellar bone. acb: Anterior cranial base; sb: sellar bone.

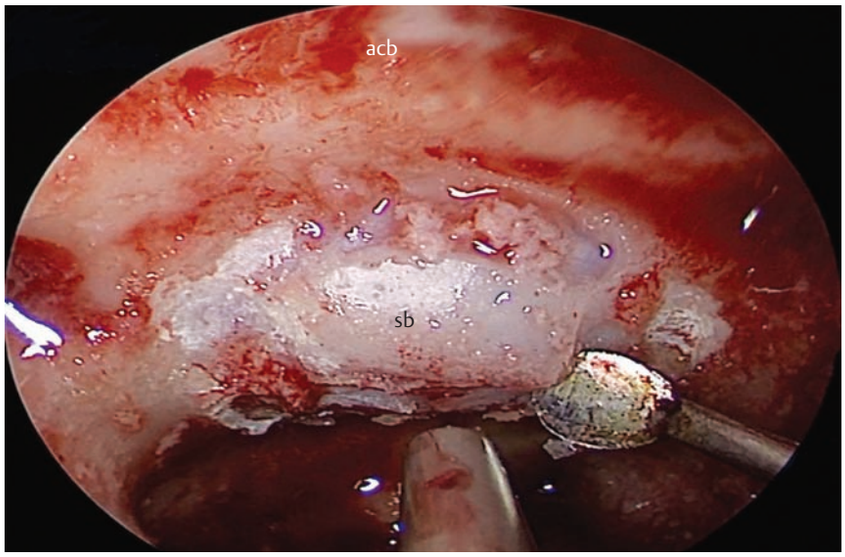

Fig. 7.96 Elevation of bone flap using Rosen's elevator. acb: Anterior cranial base; sb: sellar bone.

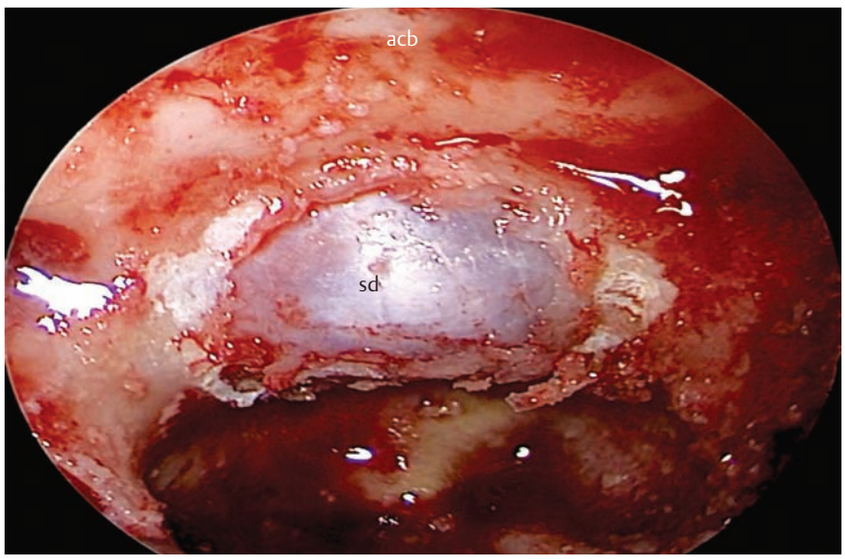

Fig. 7.97 Exposure of endosteal layer of dura. acb: Anterior cranial base; sd: endosteal layer of dura.

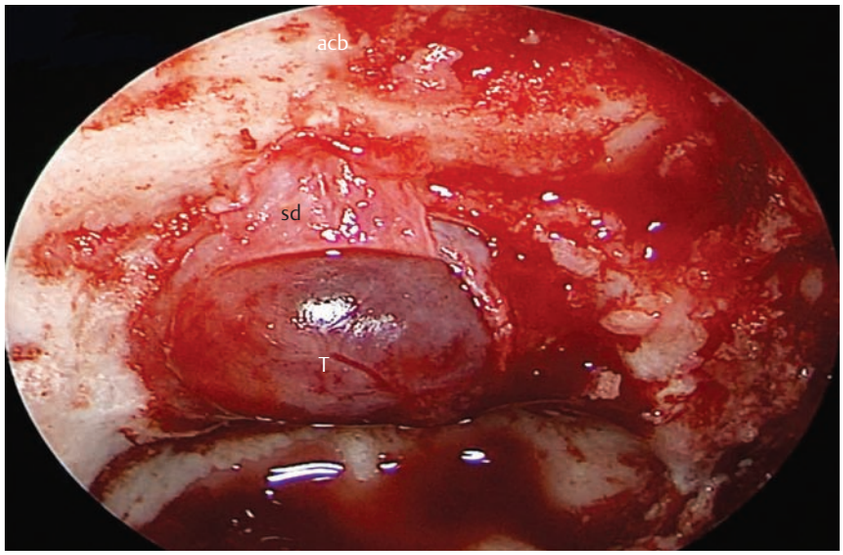

Fig. 7.98 Tumor exposed after elevation of U-shaped dural flap. acb: Anterior cranial base; sd: dural flap; T: tumor.

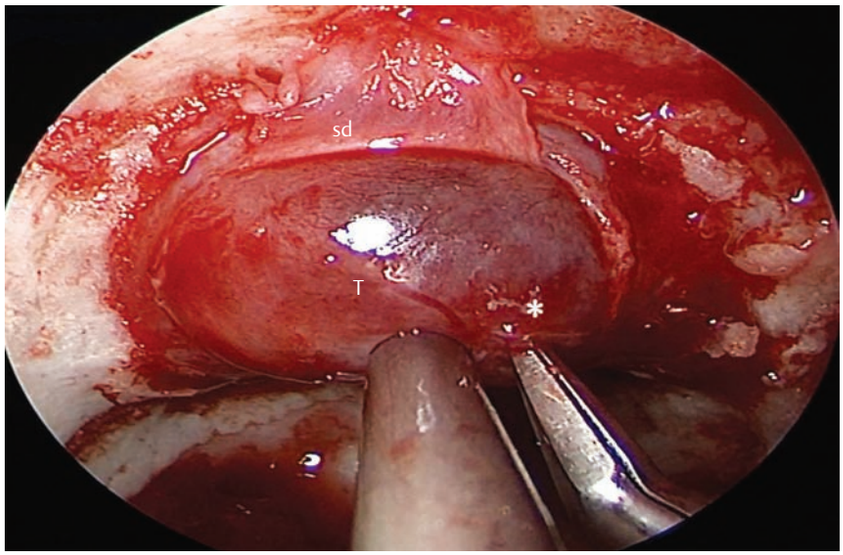

Fig. 7.99 Incision over tumor capsule using rotatable Kassam scissors. sd: Endosteal layer of dura; T: tumor; *: line of incision.

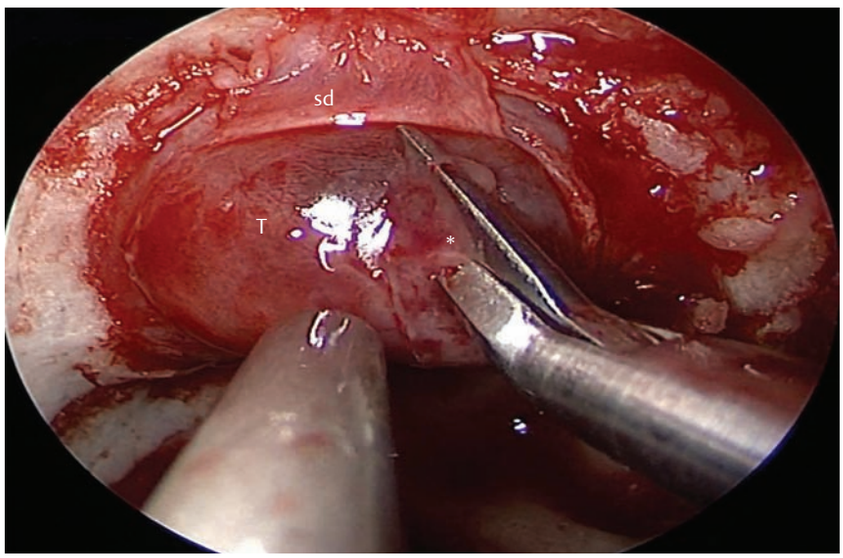

Fig. 7.100 Extension of incision over capsule of tumor. sd: Endosteal layer of dura; T: tumor; *: incision line.

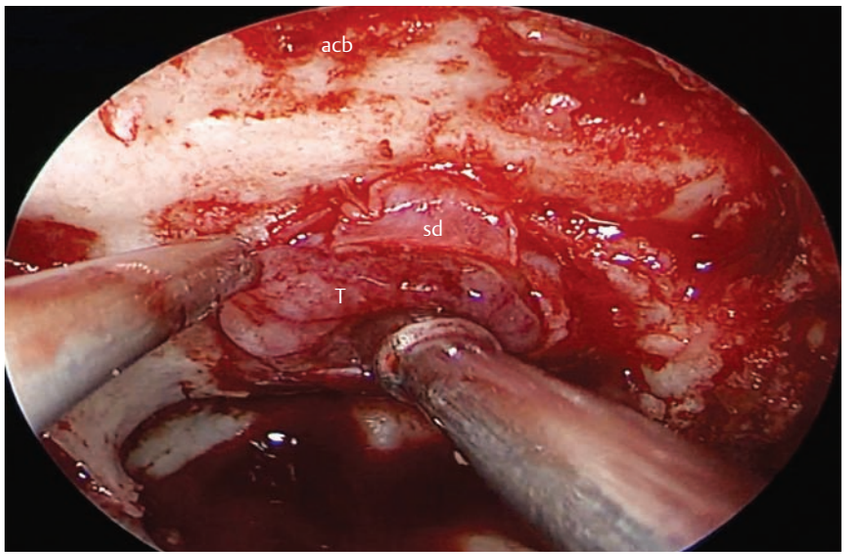

Fig. 7.101 The two-suction technique for tumor removal. acb: Anterior cranial base; sd: dural flap; T: tumor.

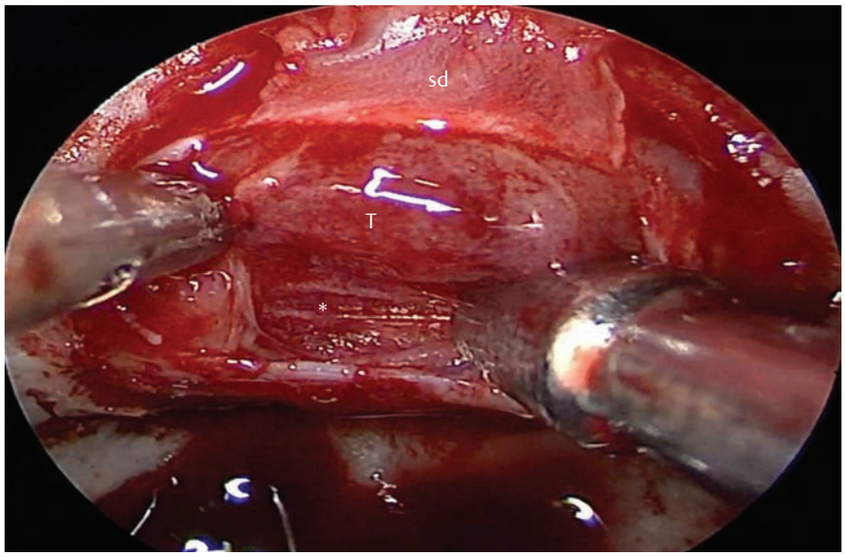

Fig. 7.102 Clearance of inferior part of tumor using suction. sd: Dural flap; *: inferior part of sellar cavity cleared of tumor.

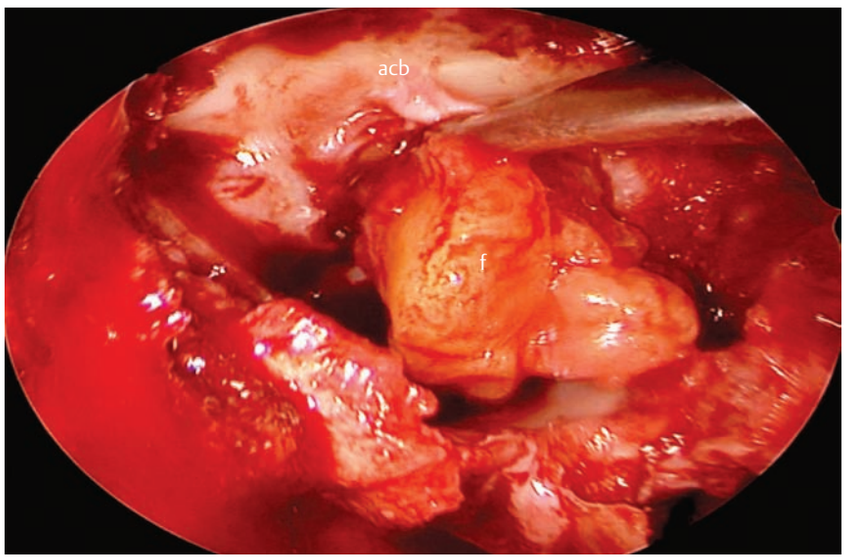

Fig. 7.103 Reconstitution sellar cavity with fat. acb: Anterior cranial base; f: fat.

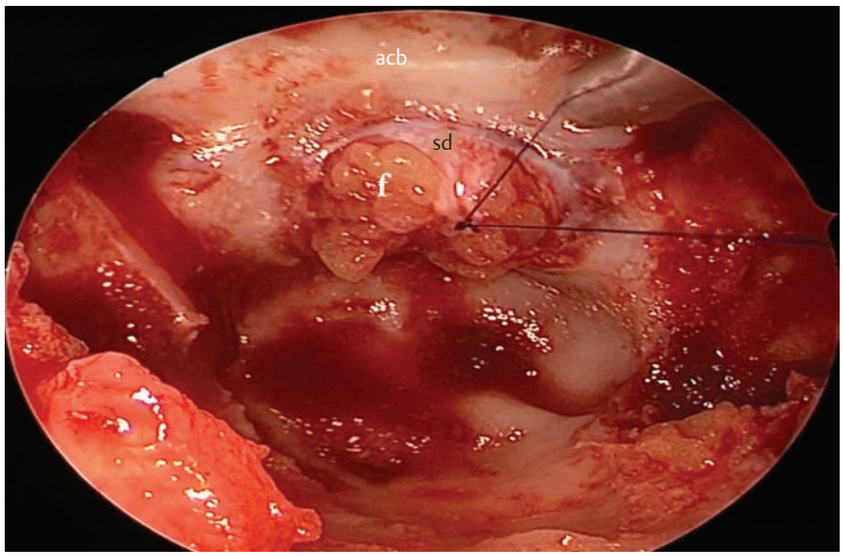

Fig. 7.104 Suturing of dural flap over fat in sellar cavity. acb: Anterior cranial base; *: suturing.

Case 7: Pituitary Macroadenoma Extending to Left Sphenoid Sinus

A 56-year-old female presented with headache. After symptomatic treatment with no relief, she was advised for MRI of the brain. The MRI showed a mass lesion in sella, extending to left sphenoid sinus (**Figs. 7.105 and 7.106**). After intubation bilateral nasal cavities were decongested (**Fig. 7.107**). Right inferior turbinate was lateralized and middle turbinate resected partially (**Fig. 7.108**). A wide corridor was obtained (**Fig. 7.109**) which was further widened by posterior ethmoidectomy. Superior turbinate was lateralized to expose the right sphenoid os (**Fig. 7.110**). The sphenoid os was widened (**Fig. 7.111**) and sphenoid sinus was opened. Nasoseptal flap was elevated (**Fig. 7.112**). In accordance with a cavity-and-a-half, left posterior ethmoidectomy was done and sphenoid sinus opened. This was followed by posterior septectomy (**Fig. 7.113**) and the rostrum of sphenoid was exposed (**Fig. 7.114**). Planar osteotomy was done (**Fig. 7.115**) followed by shoulder osteotomy (**Figs. 7.116 and 7.117**). This exposed the tumor in left sphenoid (**Fig. 7.118**). A Cappabianca knife was used to place an incision over the endosteal layer of dura (**Fig. 7.119**) and extended on both sides using a rotatable Kassam scissors (**Fig. 7.120**). Biopsy of the tumor was taken (**Fig. 7.121**). The two-suction technique was used to first resect the inferior part of tumor (**Fig. 7.122**) and complete tumor was removed till exposure of normal pituitary gland (**Fig. 7.123**). The normal pituitary gland appears yellowish and has vascularity over it. Diaphragma appears bluish in color. The cavity was reconstituted with fat and Surgicel, dural flap was repositioned, and nasoseptal flap was placed (**Fig. 7.124**). See **Video 7.4**.

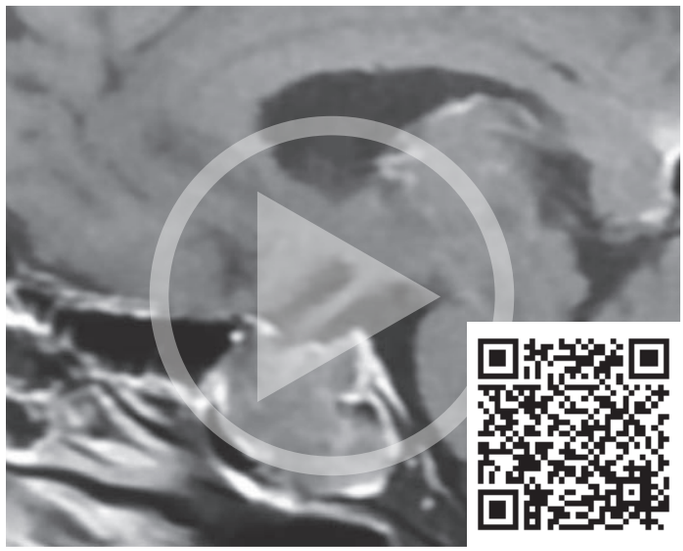

Video 7.4 Pituitary macroadenoma extending to left sphenoid sinus. https://www.thieme.de/de/q.htm?p=opn/cs/19/9/10104323-4f6374a9

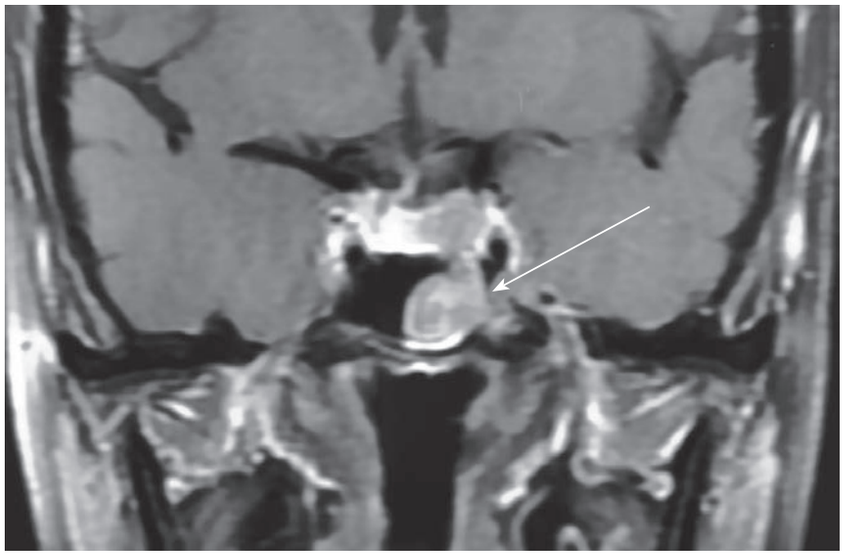

Fig. 7.105 MRI coronal view showing sellar lesion extending to left sphenoid sinus.

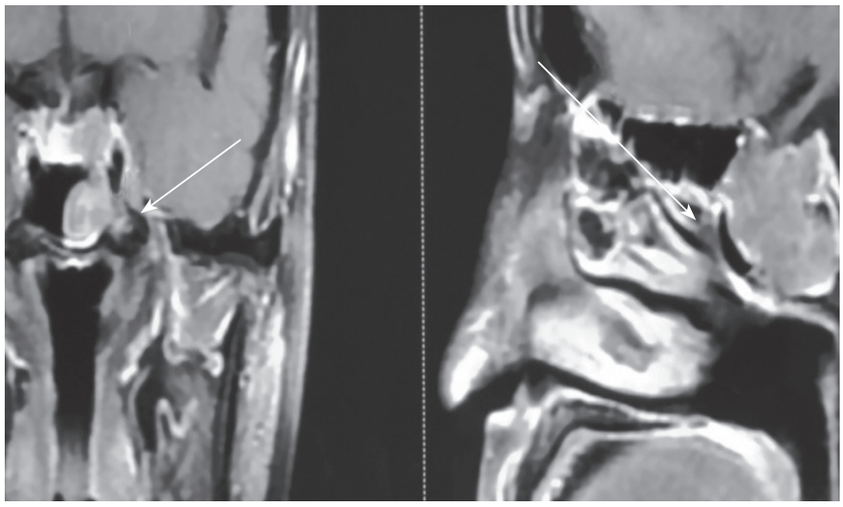

Fig. 7.106 MRI sagittal view showing lesion involving sella.

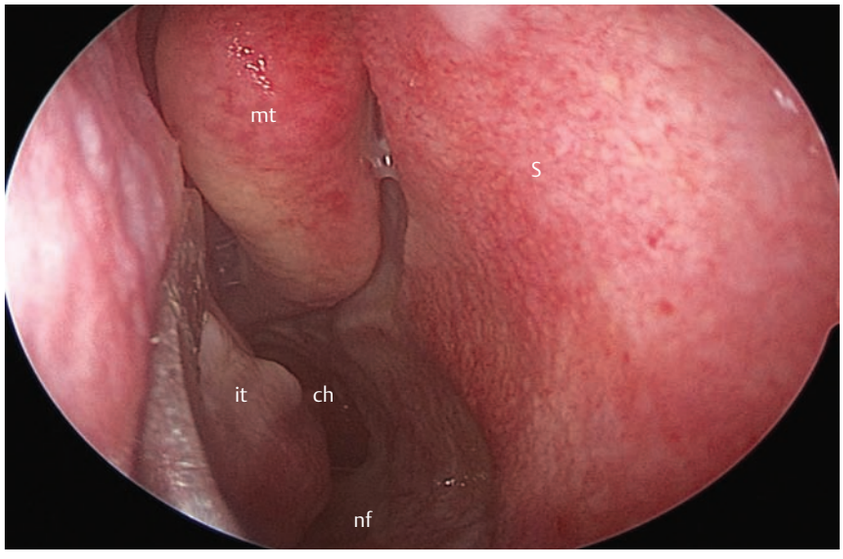

Fig. 7.107 Right middle turbinate. ch: Right choana; it: inferior turbinate; mt: middle turbinate; nf: floor of nasal cavity; mt: middle turbinate.

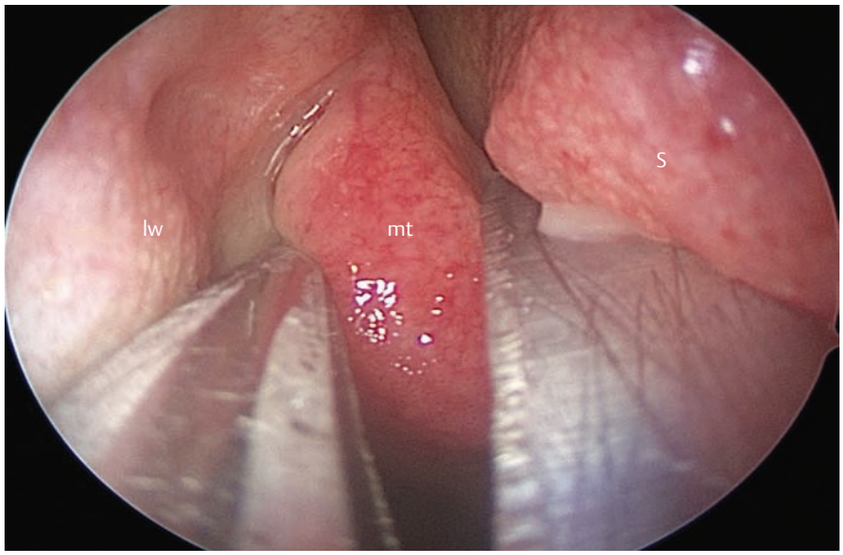

Fig. 7.108 Resection of middle turbinate. lw: Lateral nasal wall; mt: middle turbinate; S: nasal septum.

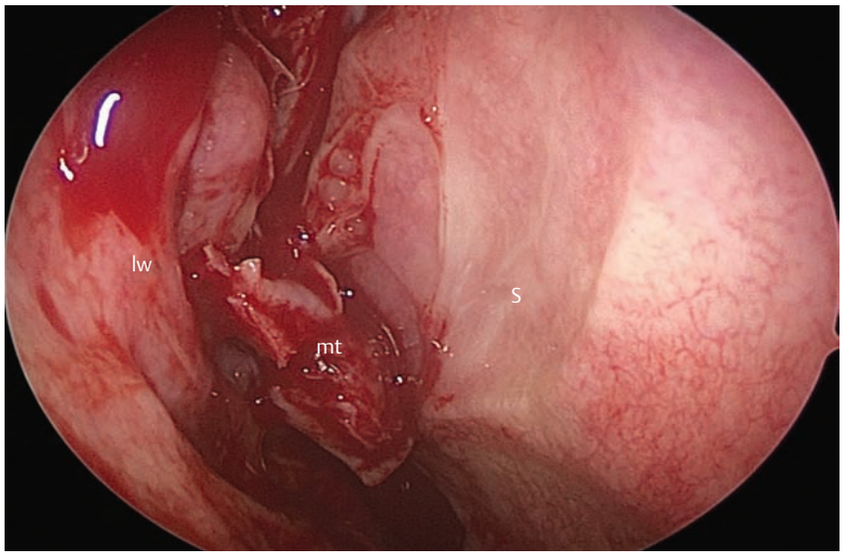

Fig. 7.109 After resection of middle turbinate. lw: Lateral nasal wall; mt: middle turbinate; S: nasal septum.

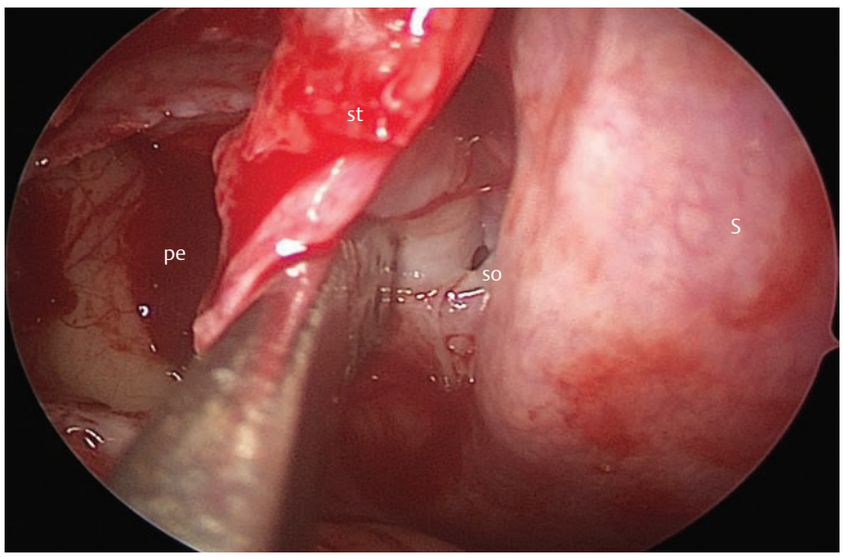

Fig. 7.110 Exposure of right sphenoid ostium. pe: Posterior ethmoids; S: nasal septum; so: sphenoid ostium; st: superior turbinate.

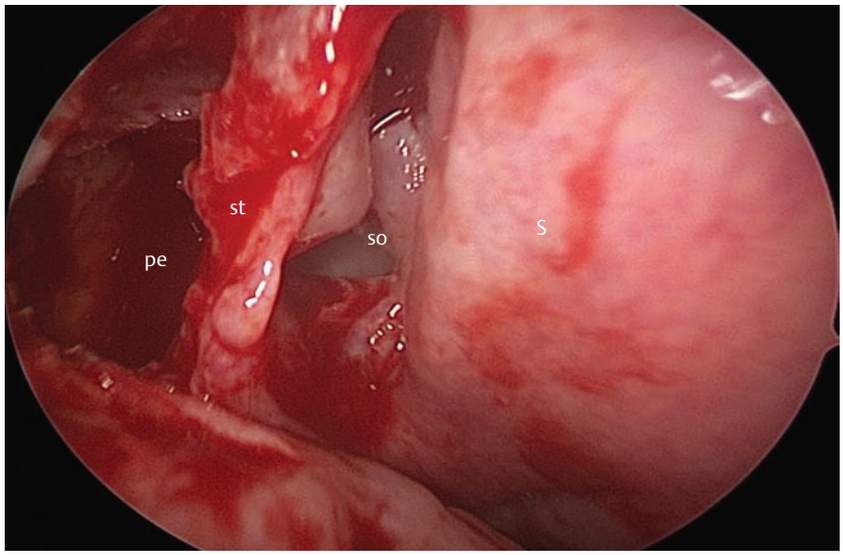

Fig. 7.111 Widening of right sphenoid sinus. pe: Posterior ethmoids; S: nasal septum; so: sphenoid ostium.

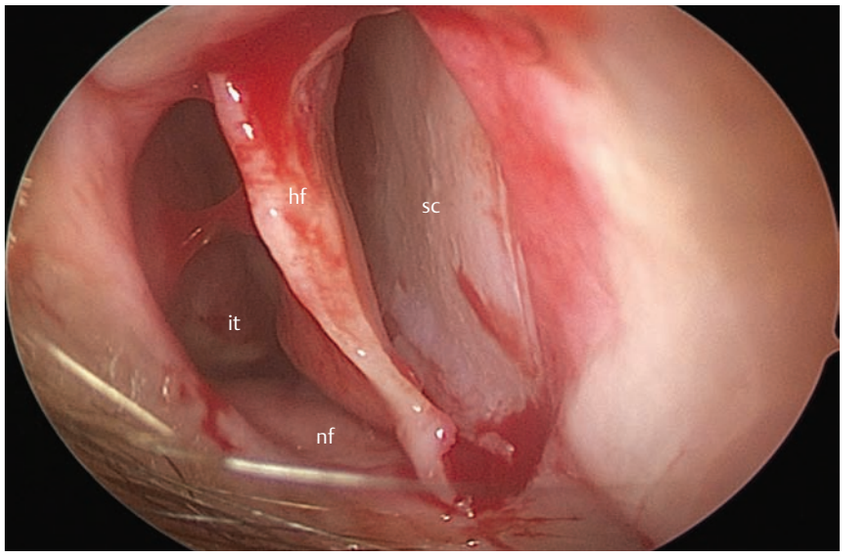

Fig. 7.112 Anterior incision for nasoseptal flap. it: Inferior turbinate; nf: floor of nasal cavity; SC: septal cartilage.

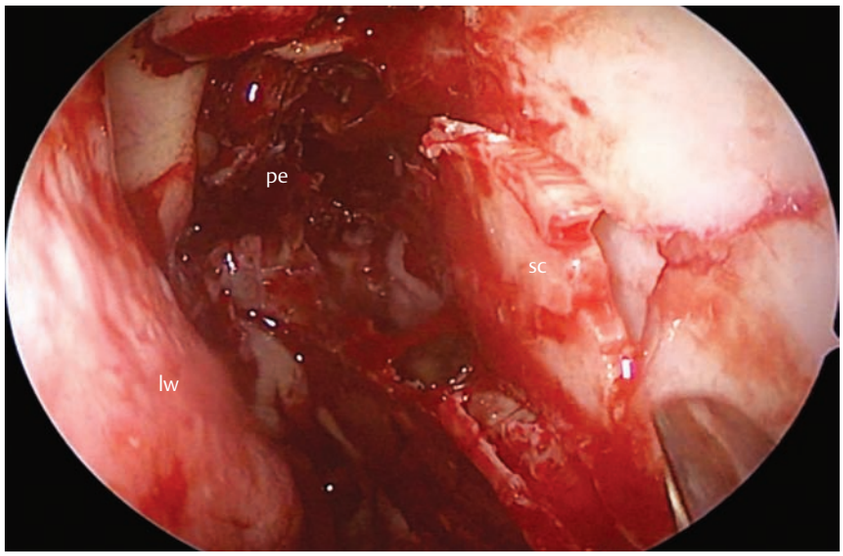

Fig. 7.113 Posterior septectomy. lw: Lateral nasal wall; pe: posterior ethmoids; SC: septal cartilage.

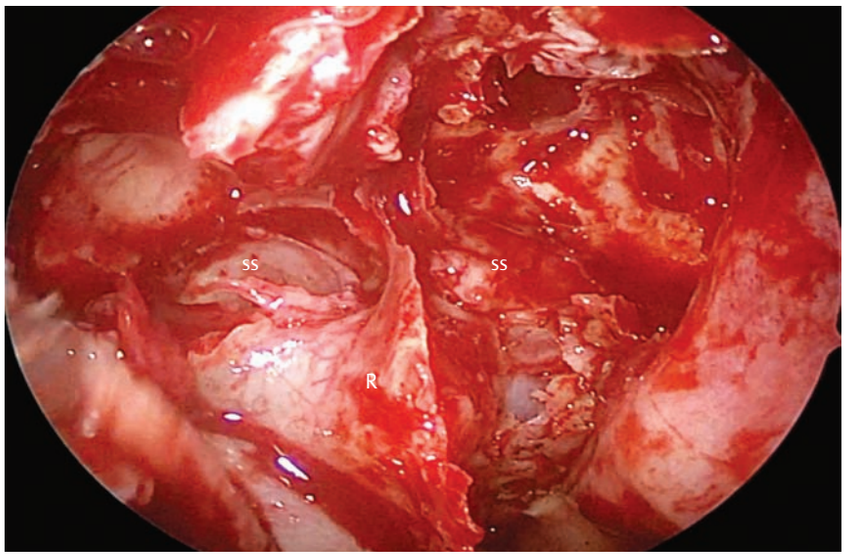

Fig. 7.114 Exposure of rostrum of sphenoid. R: Rostrum of sphenoid; ss: sphenoid sinus.

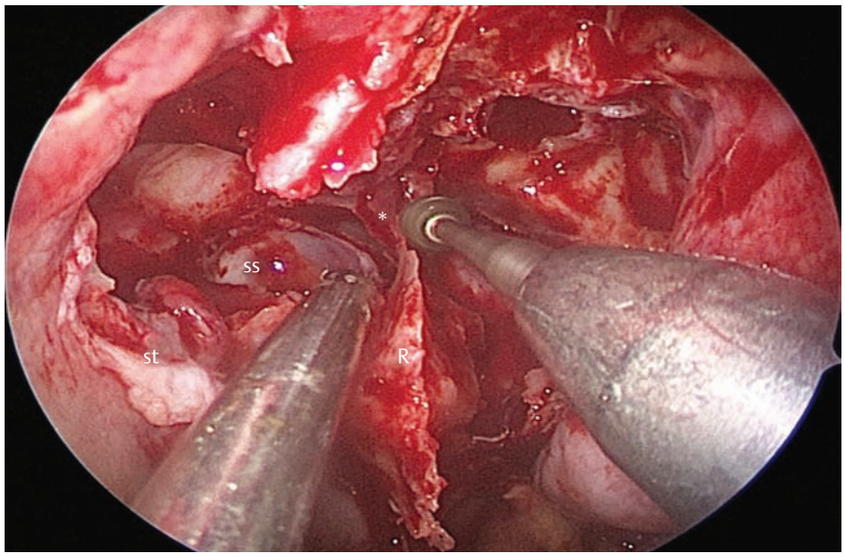

Fig. 7.115 Planar osteotomy. R: Rostrum of sphenoid; *: site of drilling for planar osteotomy.

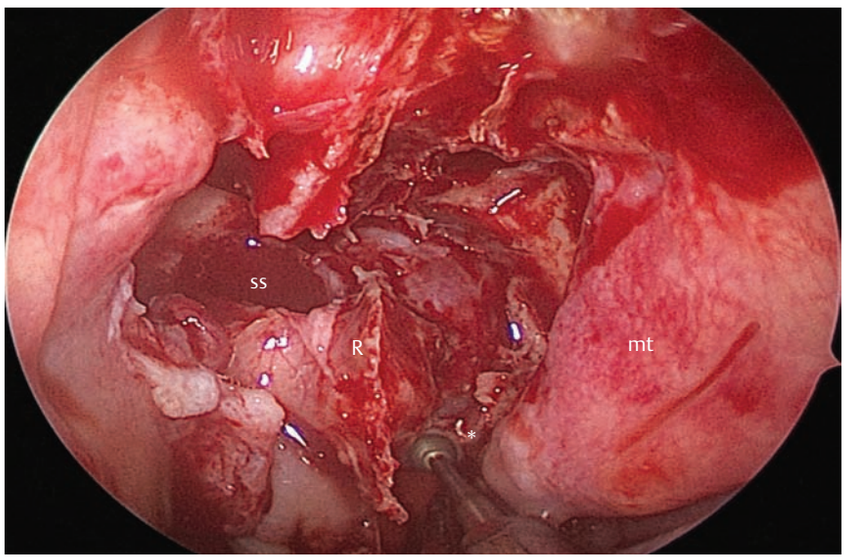

Fig. 7.116 Left shoulder osteotomy at pterygosphenoid synchondrosis. mt: Middle turbinate; R: rostrum of sphenoid; ss: sphenoid sinus.

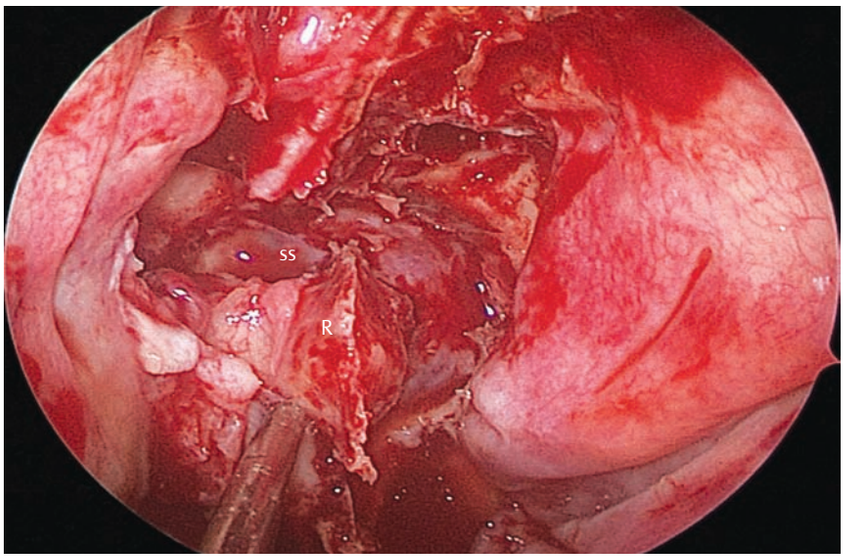

Fig. 7.117 Exposure after left shoulder osteotomy. mt: Middle turbinate; R: rostrum of sphenoid; ss: sphenoid sinus.

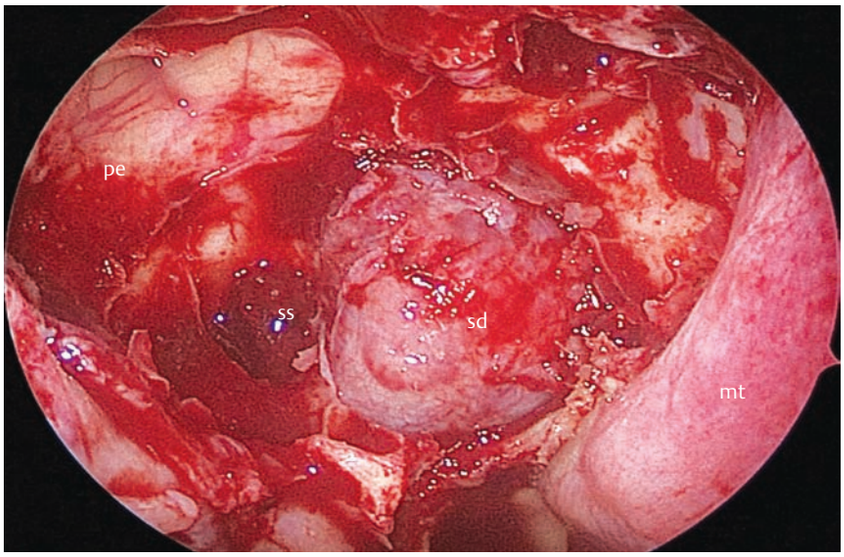

Fig. 7.118 Exposure after resection of rostrum of sphenoid. pe: Posterior ethmoids; mt: middle turbinate; sd: endosteal layer of dura; ss: sphenoid sinus.

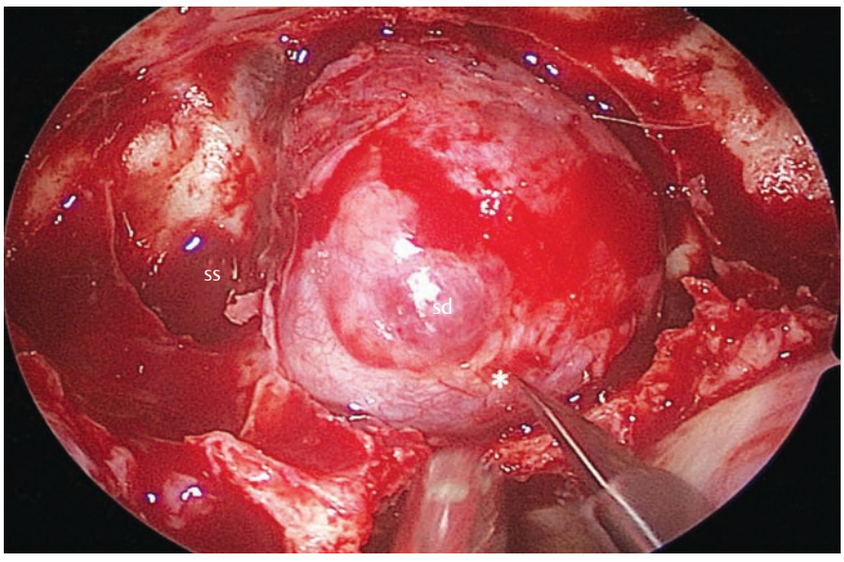

Fig. 7.119 Incision over endosteal layer of dura using Cappabianca knife. sd: Endosteal layer of dura; ss: sphenoid sinus; *: incision line.

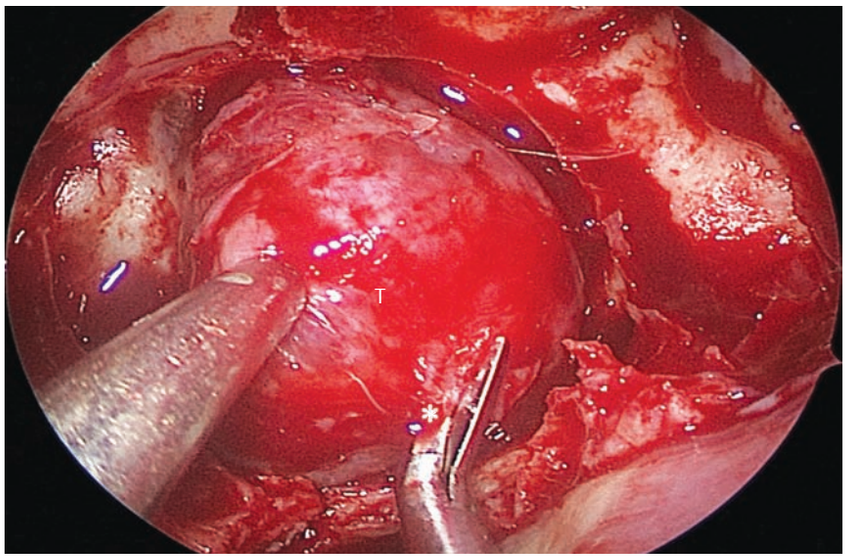

Fig. 7.120 Extension of incision over endosteal layer of dura. sd: Endosteal layer of dura; *: incision line.

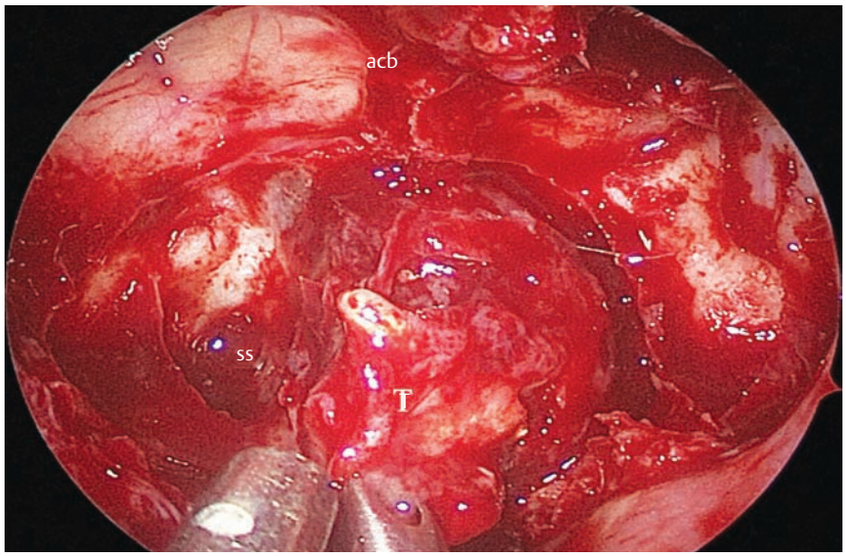

Fig. 7.121 Biopsy of tumor. acb: Anterior cranial base; ss: sphenoid sinus; T: tumor.

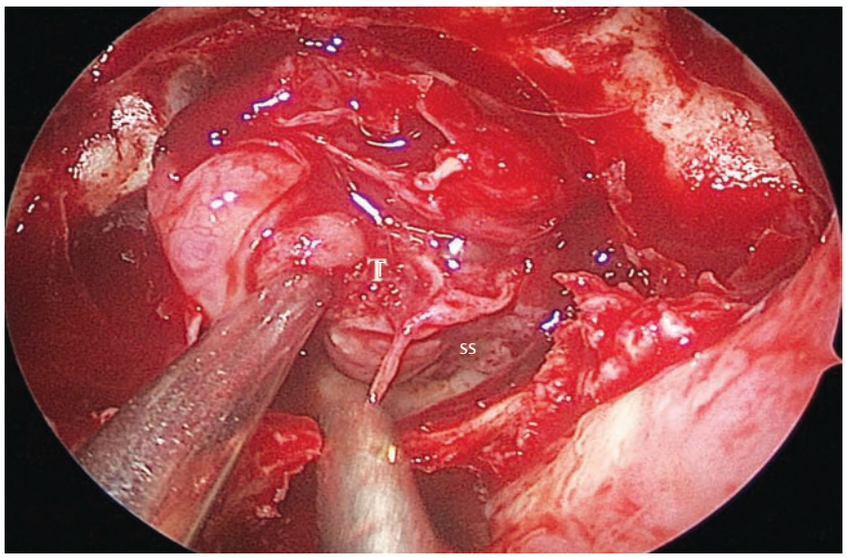

Fig. 7.122 The two-suction technique for tumor excision. sc: Sellar cavity; T: tumor.

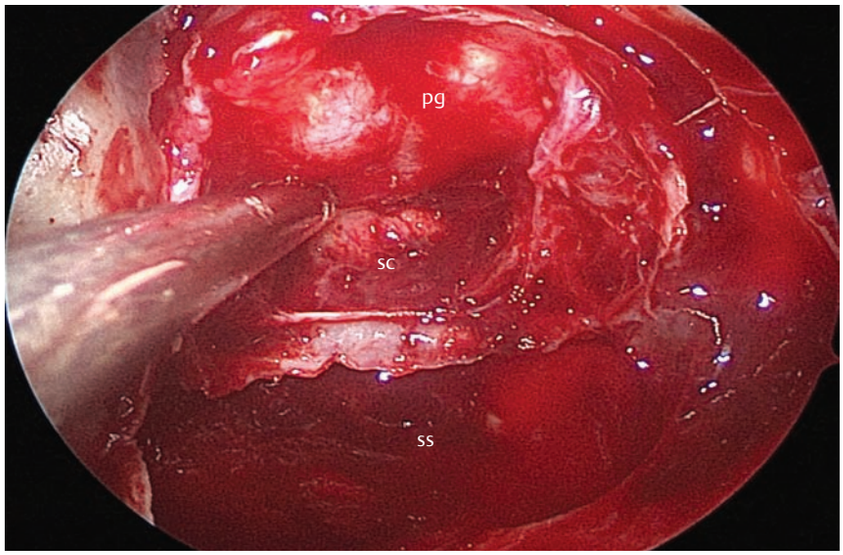

Fig. 7.123 Exposure of normal pituitary gland after tumor removal. pg: Normal pituitary gland; sc: sellar cavity; ss: sphenoid sinus.

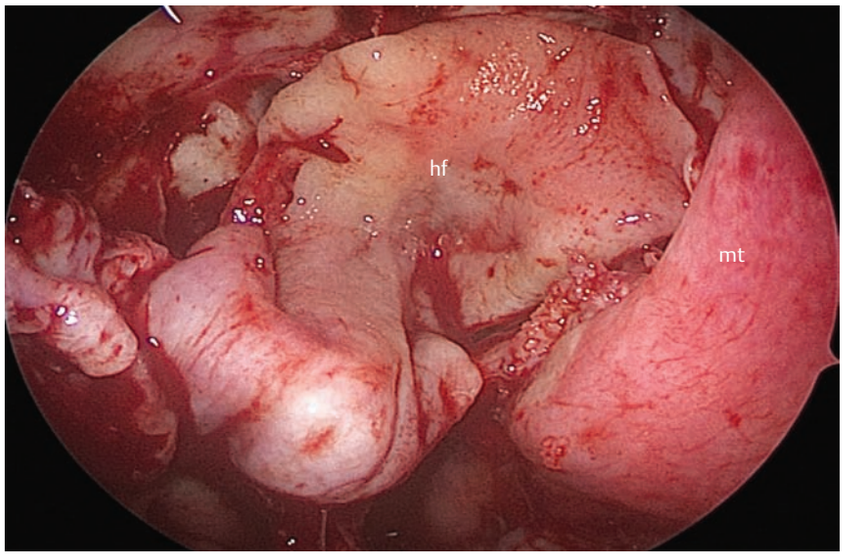

Fig. 7.124 Reconstruction with nasoseptal flap. acb: Anterior cranial base; hf: nasoseptal flap; mt: middle turbinate.

Case 8: Pituitary Tuberculosis

A 22-year-old female presented with headache and visual disturbances, with episodes of low-grade fever. The MRI showed a sellar space-occupying lesion and the patient was taken for surgery under general anesthesia. After partial resection of right middle turbinate, bilateral posterior ethmoids and sphenoid sinuses were opened widely. Right-sided nasoseptal flap was harvested. Posterior septectomy was done to expose the rostrum of sphenoid (**Fig. 7.125**), which was resected and removed (**Fig. 7.126**) after triple osteotomies. The sellar bone was drilled (**Fig. 7.127**) using a Karl Storz neurodrill and a 4-mm diamond burr, and the bone flap was elevated using a Rosen's elevator (**Fig. 7.128**). The endosteal layer of dura was incised and incisions extended on both sides using a rotatable Kassam scissors (**Fig. 7.129**). The U-shaped dural flap was elevated and tumor exposed (**Fig. 7.130**). Biopsy of the tumor was taken (**Fig. 7.131**). Extracapsular dissection was performed and the tumor was removed in one piece and sent for biopsy (**Figs. 7.132, 7.133, and 7.134**). The cavity was obliterated with fat (**Fig. 7.135**) and Surgicel (**Fig. 7.136**), and the dural flap was repositioned and covered with nasoseptal flap (**Fig. 7.137**), Surgicel (**Fig. 7.138**), Gelfoam, and tissue glue for multilayered reconstruction (**Fig. 7.139**). See **Video 7.5**.

Video 7.5 Pituitary tuberculosis. https://www.thieme.de/de/q.htm?p=opn/cs/19/9/10104249-4672b41d

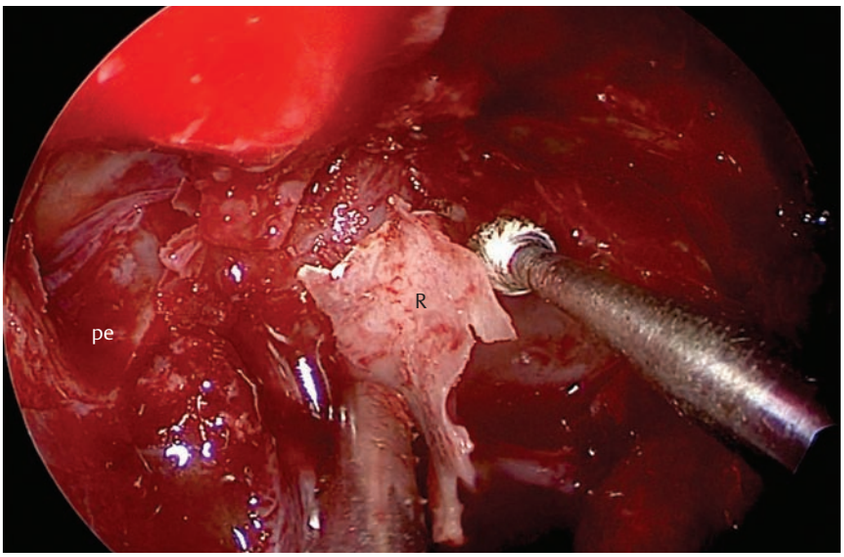

Fig. 7.125 Exposure of rostrum of sphenoid and triple osteotomy. pe: Posterior ethmoids; R: rostrum of sphenoid.

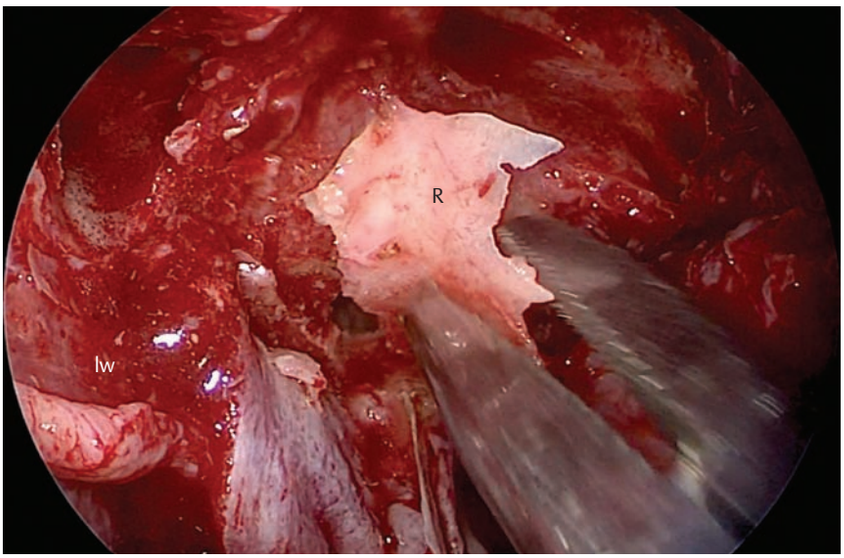

Fig. 7.126 Resection of rostrum of sphenoid after triple osteotomy. R: Rostrum of sphenoid.

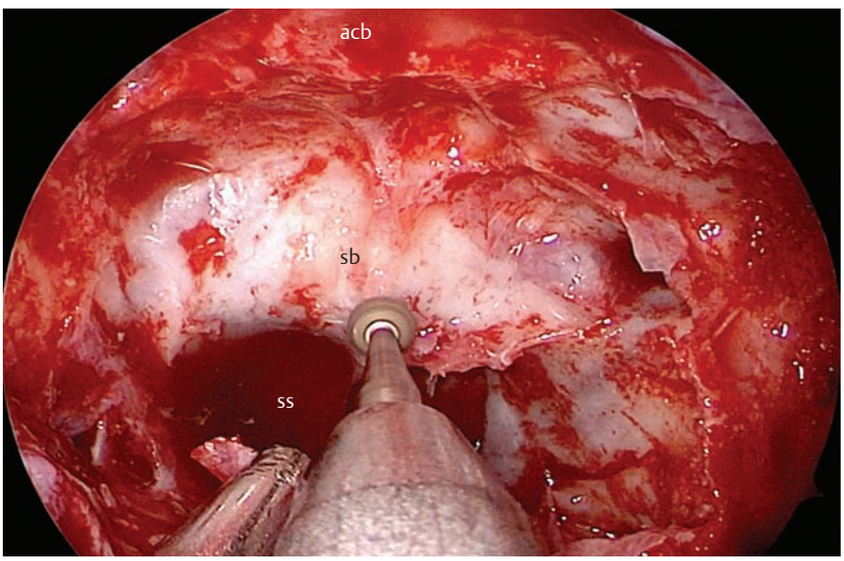

Fig. 7.127 Drilling of sellar bone. acb: Anterior cranial base; sb: sellar bone; ss: sphenoid sinus.

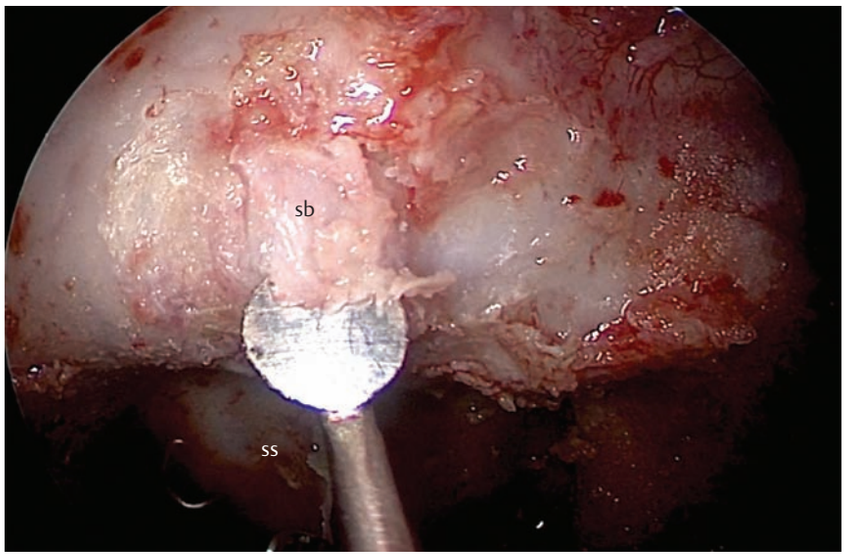

Fig. 7.128 Elevation of sellar bone flap using Rosen's elevator. sb: Sellar bone; ss: sphenoid sinus.

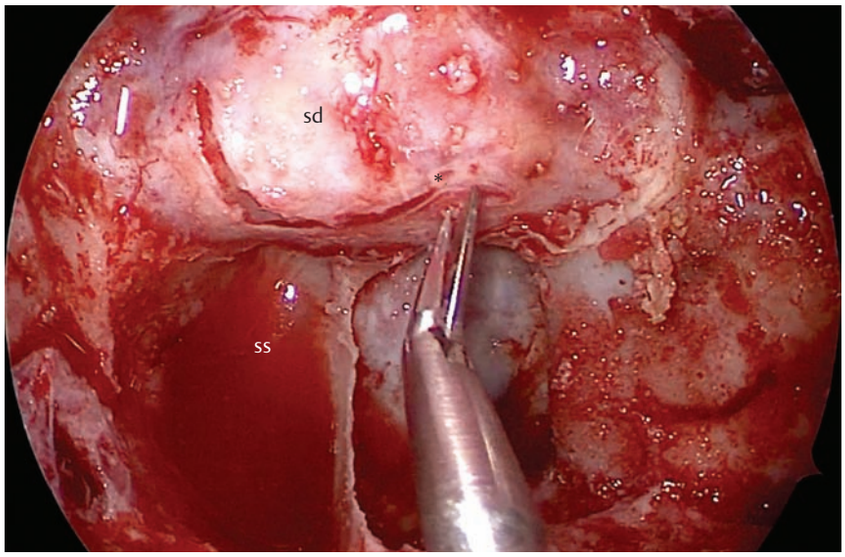

Fig. 7.129 Incision of endosteal layer of dura using rotatable Kassam scissors. sd: Endosteal layer of dura; ss: sphenoid sinus; *: incision line.

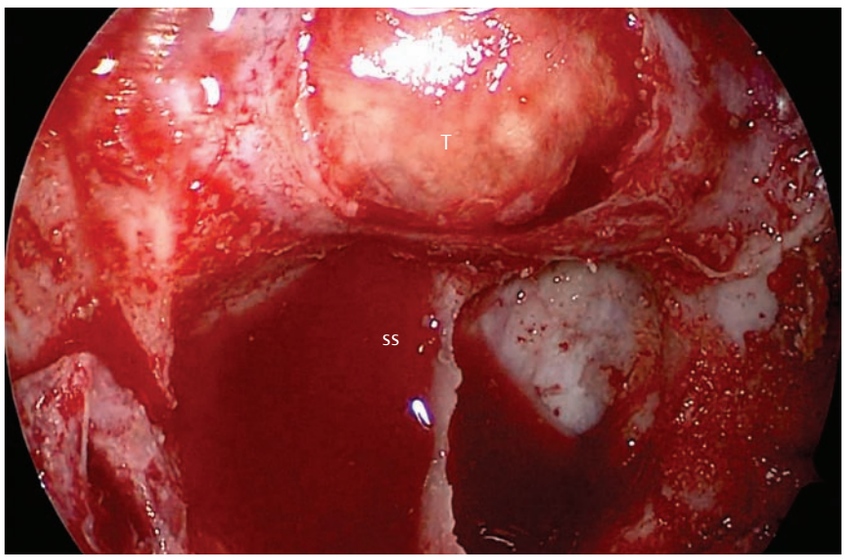

Fig. 7.130 Exposure after elevation of U-shaped dural flap. ss: Sphenoid sinus; T: tumor.

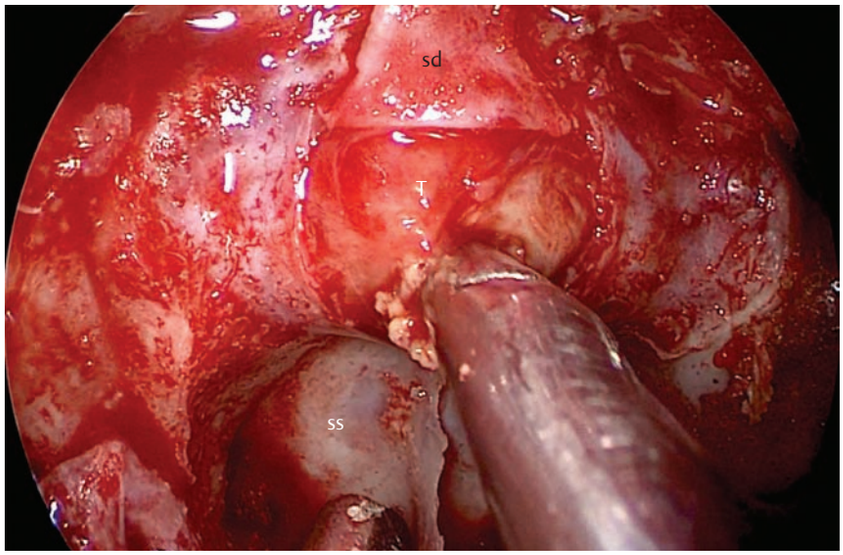

Fig. 7.131 Biopsy of tumor. sd: Endosteal layer of dura; ss: sphenoid sinus; T: tumor.

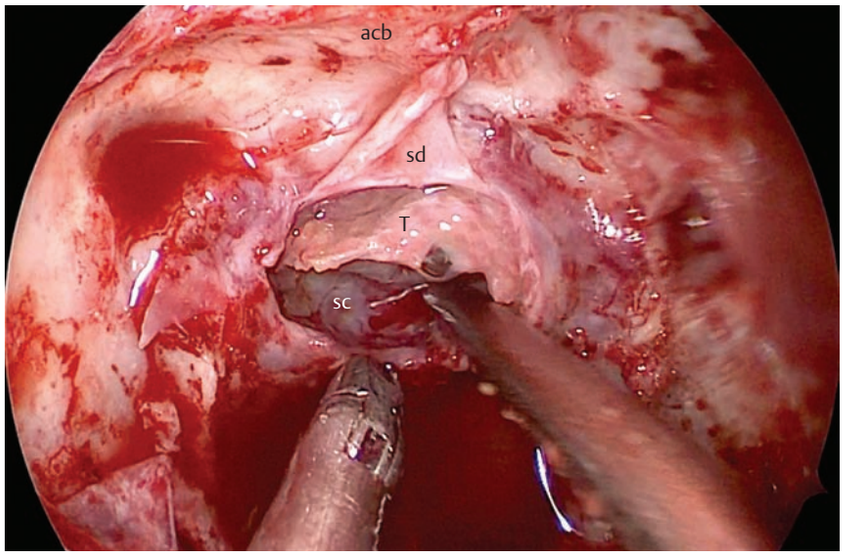

Fig. 7.132 The two-suction technique for excision of inferior part of tumor. acb: Anterior cranial base; sc: sellar cavity; sd: endosteal layer of dura; T: tumor.

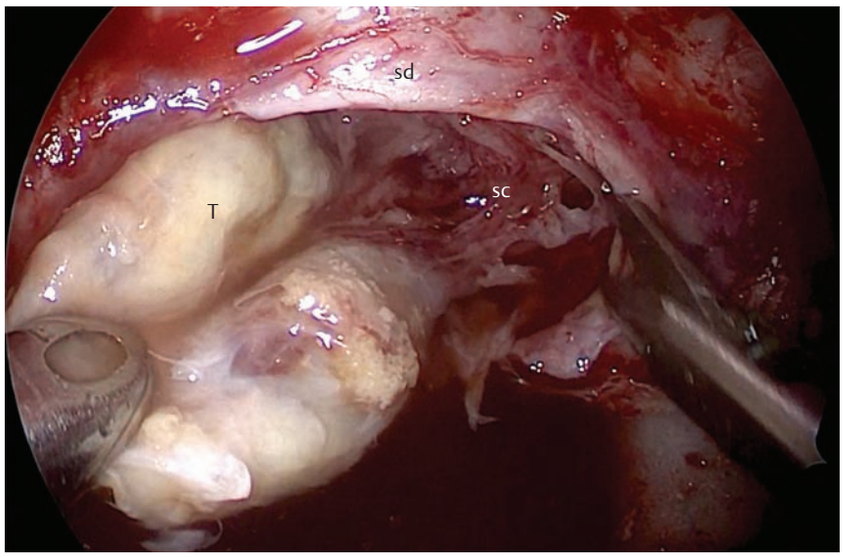

Fig. 7.133 Removal of lateral part of tumor. sc: Sellar cavity; sd: endosteal layer of dura; T: tumor.

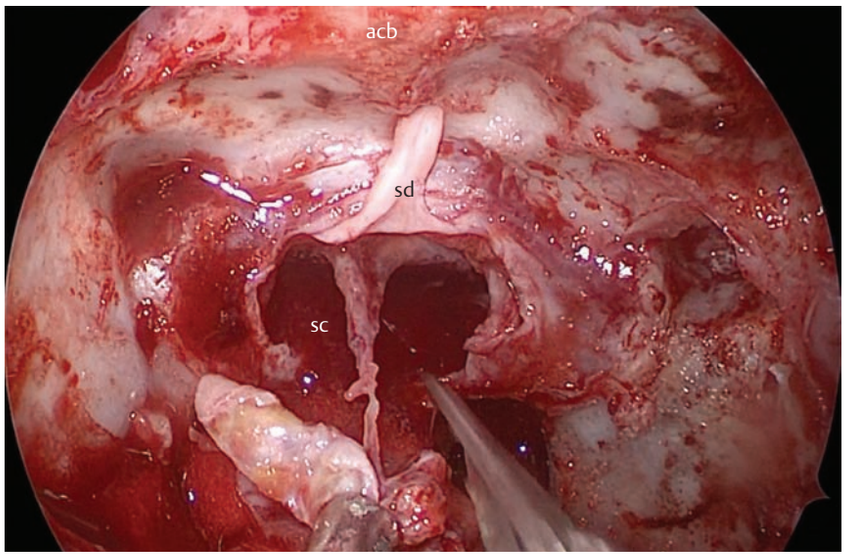

Fig. 7.134 Complete clearance of tumor. acb: Anterior cranial base; sc: sellar cavity; sd: endosteal layer of dura.

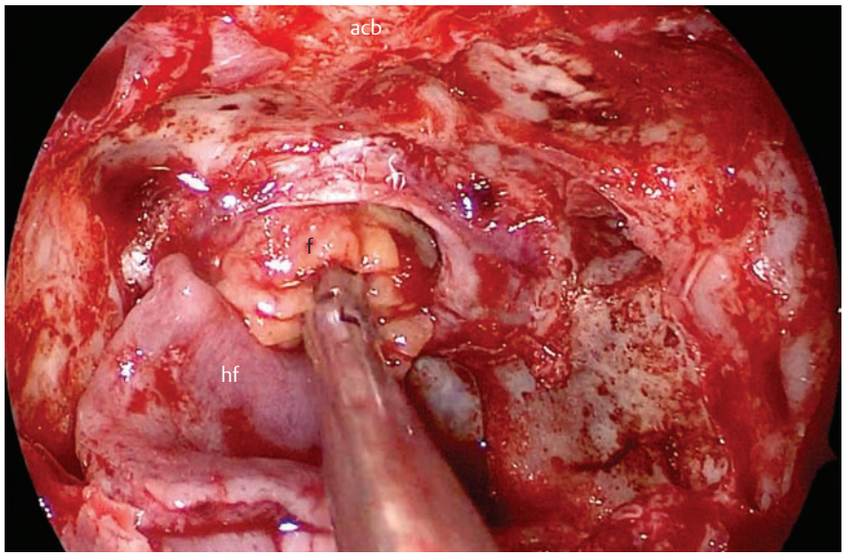

Fig. 7.135 Reconstitution of sellar cavity with fat. acb: Anterior cranial base; f: fat; hf: nasoseptal flap.

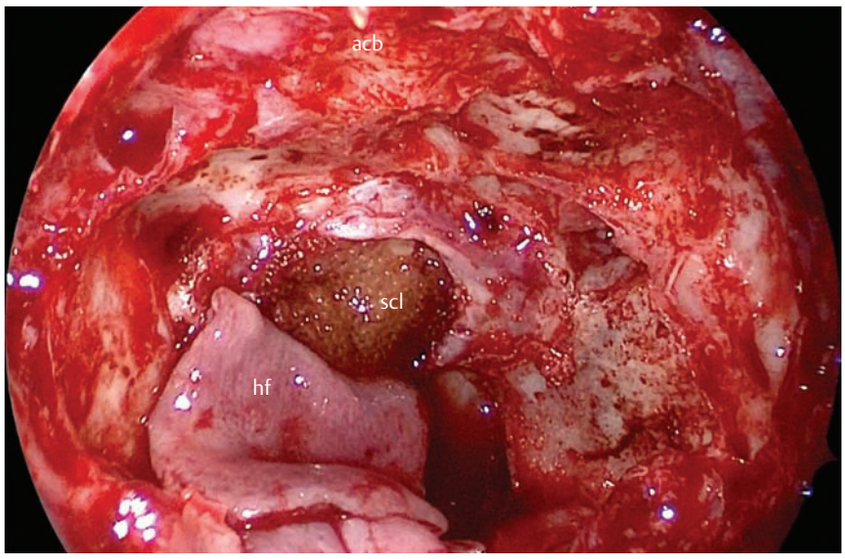

Fig. 7.136 Surgicel placed over fat. hf: Nasoseptal flap; scl: Surgicel.

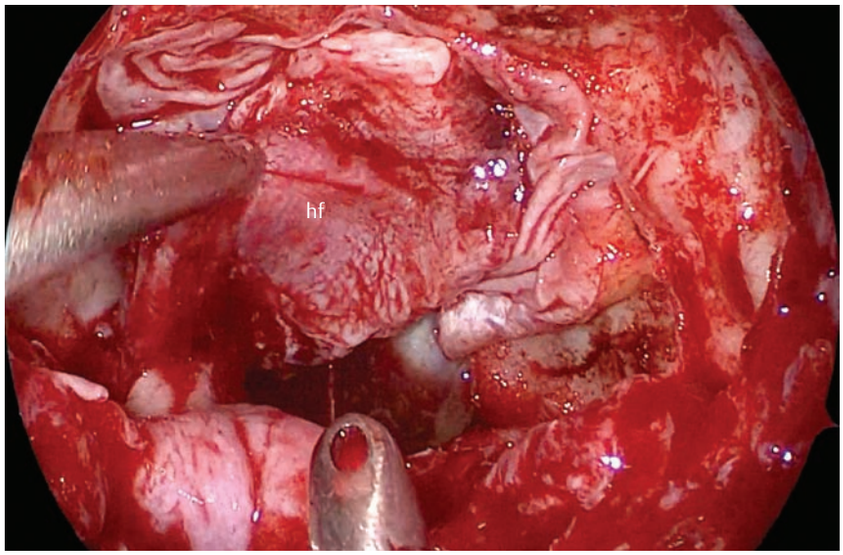

Fig. 7.137 Nasoseptal flap placed over Surgicel. hf: Nasoseptal flap.

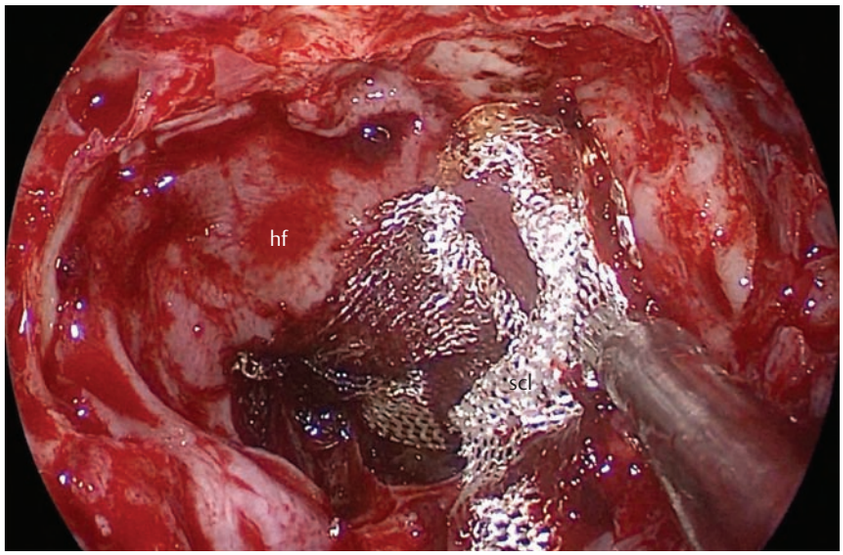

Fig. 7.138 Reconstruction with Surgicel placed over nasoseptal flap. hf: Nasoseptal flap; scl: Surgicel.

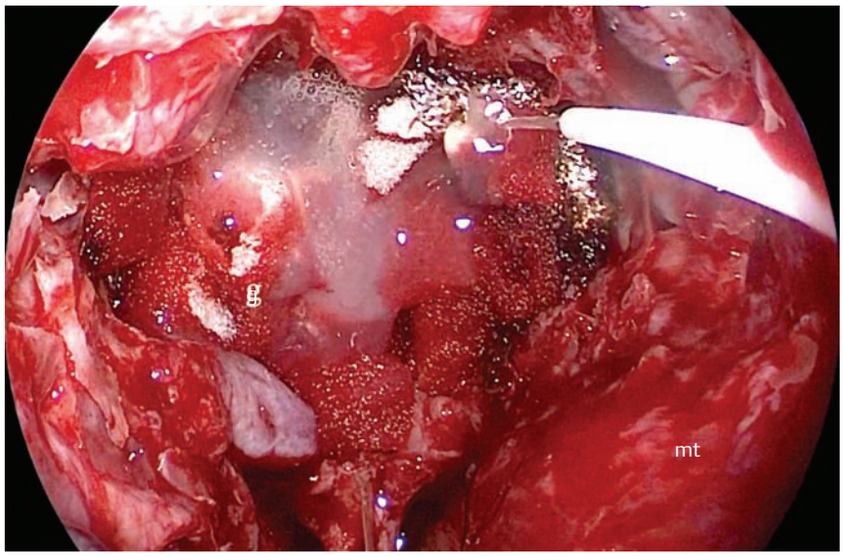

Fig. 7.139 Reconstruction completed with tissue glue. g: Gelfoam; mt: middle turbinate.

Case 9: Rathke's Cleft Cyst

A 12-year-old female presented with complaint of headache. MRI of the brain (**Figs. 7.140, 7.141, and 7.142**) revealed a well-defined nonenhancing cystic lesion in the sella with a thin rim of normal gland all around it. After right-sided partial middle turbinectomy, bilateral rescue flaps were raised. This was followed by posterior septectomy and triple osteotomies, and a wide exposure of the sphenoid sinus was obtained. The sphenoid sinus was found to be of presellar type; hence, the bone was drilled (**Fig. 7.143**) to identify the anatomical landmarks, i.e., the internal carotid artery and optic nerve. Drilling of the sellar floor was done and bone removed after thinning it off. The endosteal layer of dura was incised using a Cappabianca knife (**Fig. 7.144**) and Kassam rotatable scissors (**Figs. 7.145 and 7.146**). The dural layer was elevated as a "U"-shaped flap (**Fig. 7.147**). Normal pituitary gland was exposed after elevation of the flap (**Fig. 7.148**). Incision was made on the pituitary gland with a knife (**Fig. 7.149**). Cystic fluid was aspirated (**Fig. 7.150**) after retracting the normal pituitary gland. Contents of the cyst were sucked out. Some solid part was also present (**Fig. 7.151**) in the cyst which was removed with suction and irrigation with ringer lactate. A clear cavity was then obtained (**Fig. 7.152**). Reconstruction was done with multilayer technique with the help of fat, Surgicel, and nasoseptal flap. See **Video 7.6**.

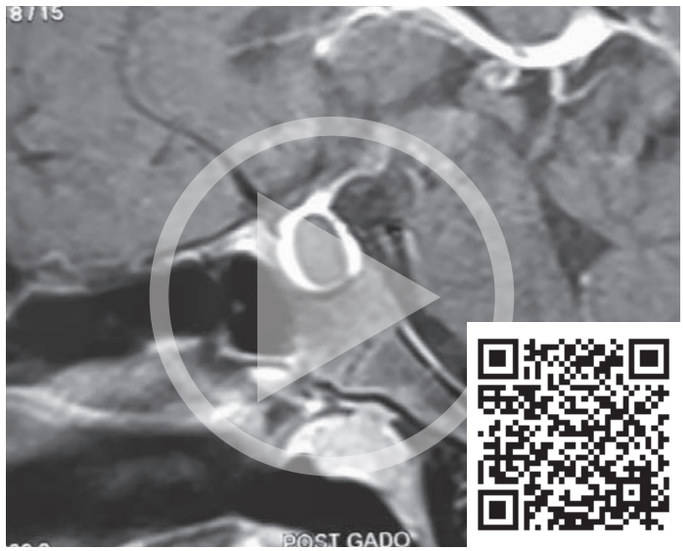

Video 7.6 Rathke's cleft cyst 1. https://www.thieme.de/de/q.htm?p=opn/cs/19/9/10104250-c478e211

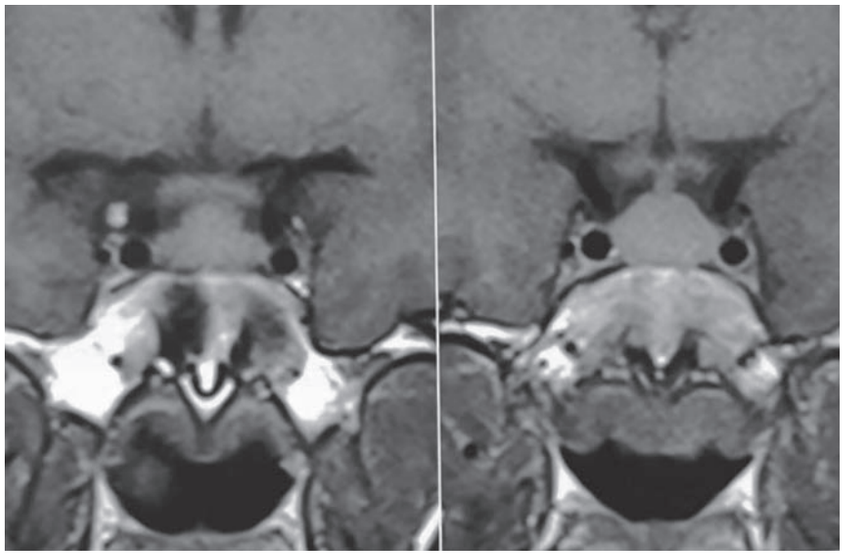

Fig. 7.140 MRI coronal view showing cystic lesion inside pituitary gland.

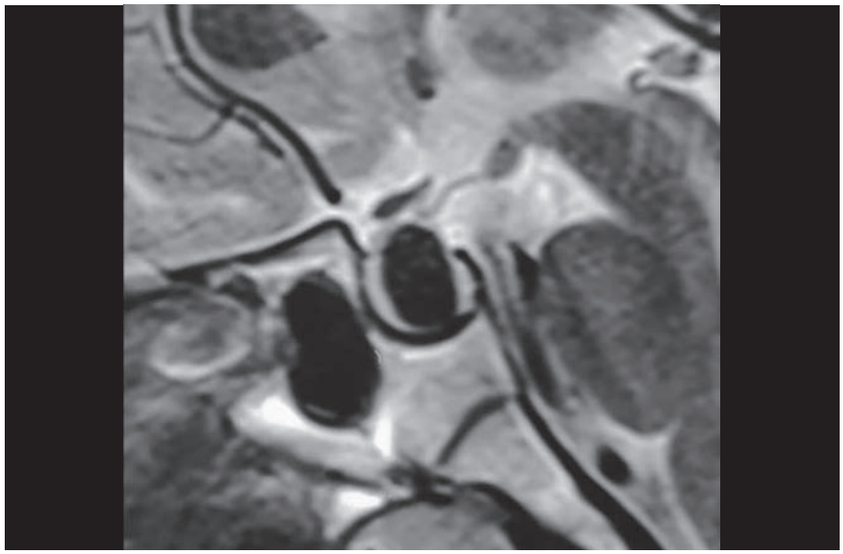

Fig. 7.141 T1 MRI sagittal view showing cystic lesion inside pituitary gland.

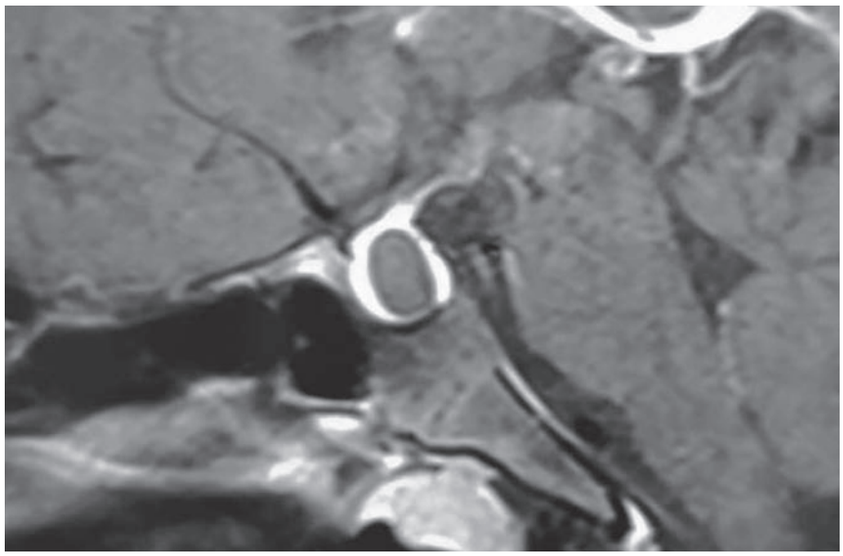

Fig. 7.142 T2 MRI sagittal view showing cystic lesion inside pituitary gland.

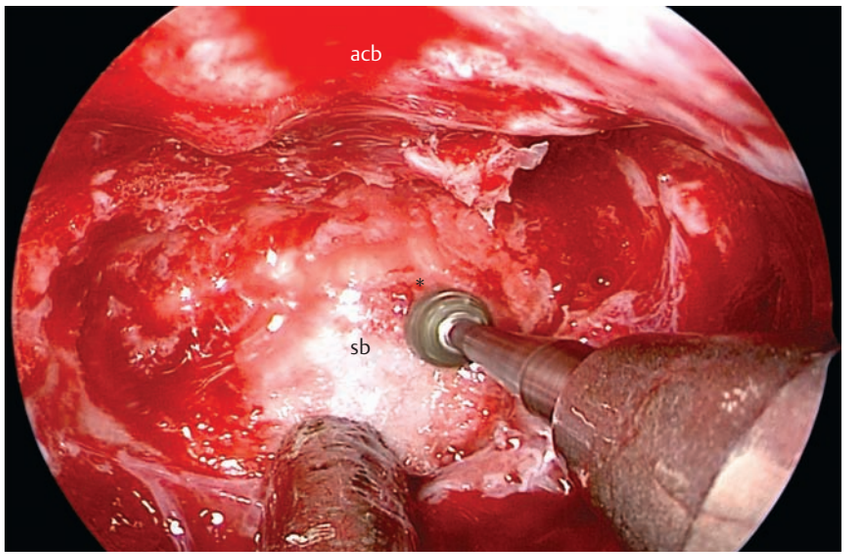

Fig. 7.143 Drilling of sellar bone. acb: Anterior cranial base; sb: sellar bone; *: site of drilling.

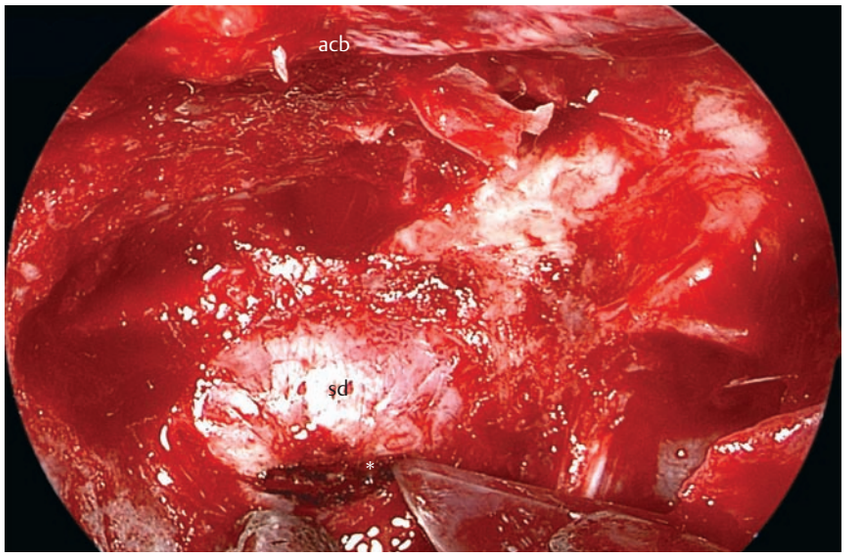

Fig. 7.144 Incision over endosteal layer of dura using Cappabianca knife. acb: Anterior cranial base; sd: endosteal layer of dura; *: line of incision.

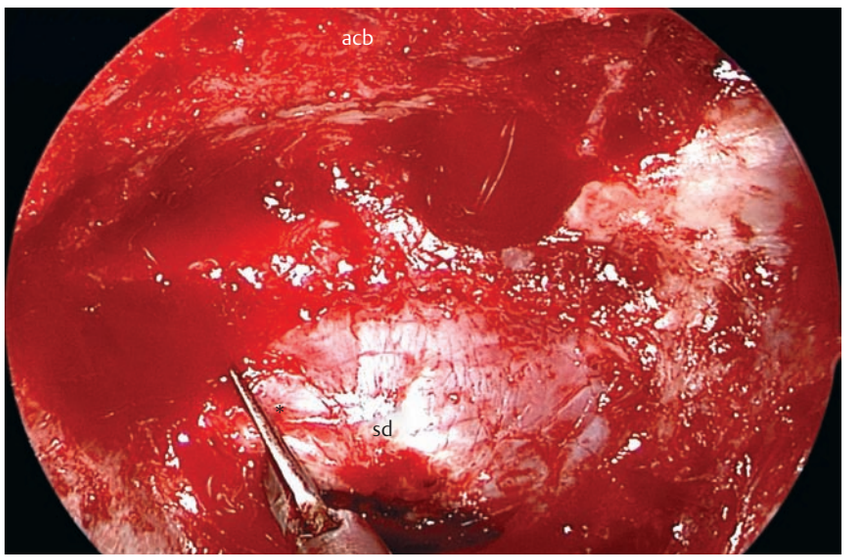

Fig. 7.145 Extension of incision over endosteal layer of dura to right. acb: Anterior cranial base; sd: endosteal layer of dura; *: line of incision.

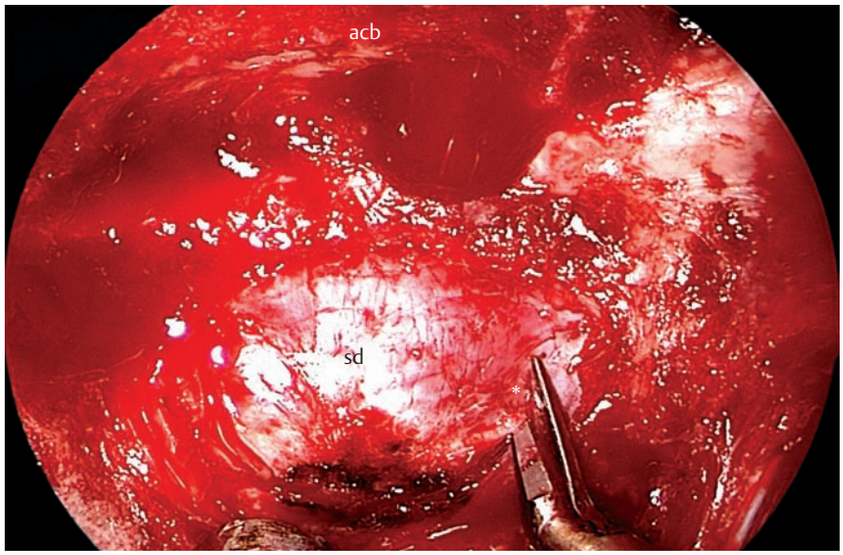

Fig. 7.146 Extension of incision over endosteal layer of dura to left. acb: Anterior cranial base; sd: endosteal layer of dura; *: incision line.

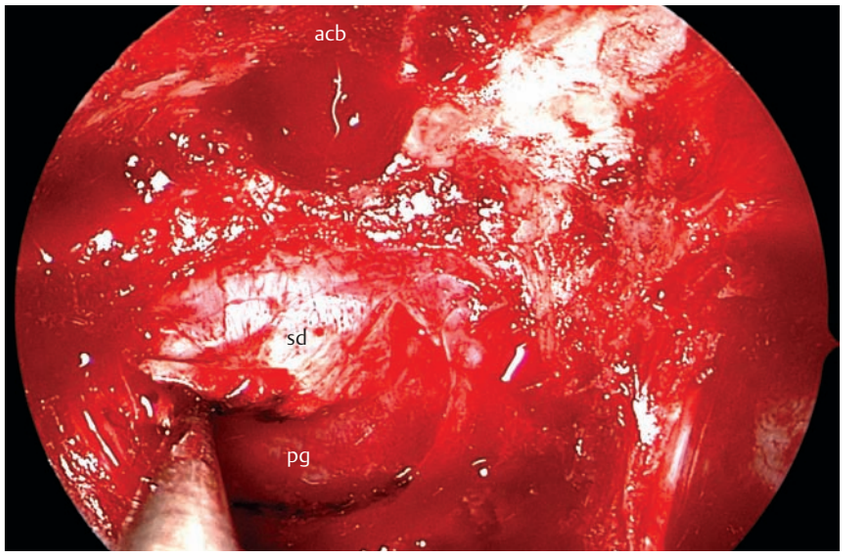

Fig. 7.147 Elevation of U-shaped dural flap. acb: Anterior cranial base; pg: pituitary gland; sd: endosteal layer of dura.

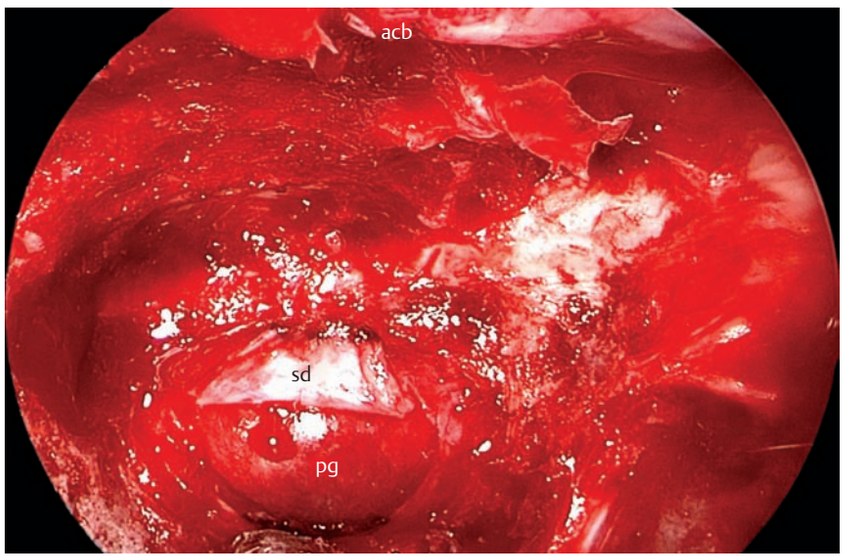

Fig. 7.148 Exposure of pituitary gland. acb: Anterior cranial base; pg: normal pituitary gland; sd: endosteal layer of dura.

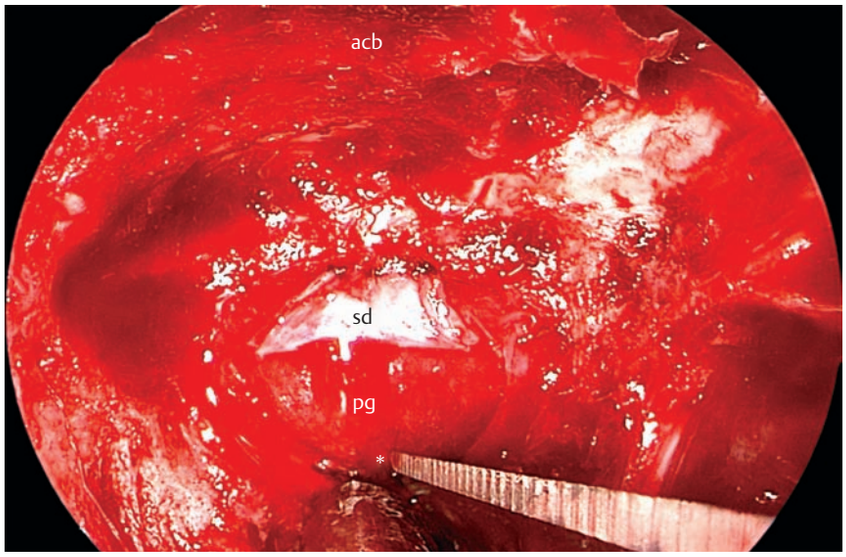

Fig. 7.149 Incision over pituitary gland. acb: Anterior cranial base; pg: pituitary gland; sd: endosteal layer of dura; *: site of incision over pituitary gland.

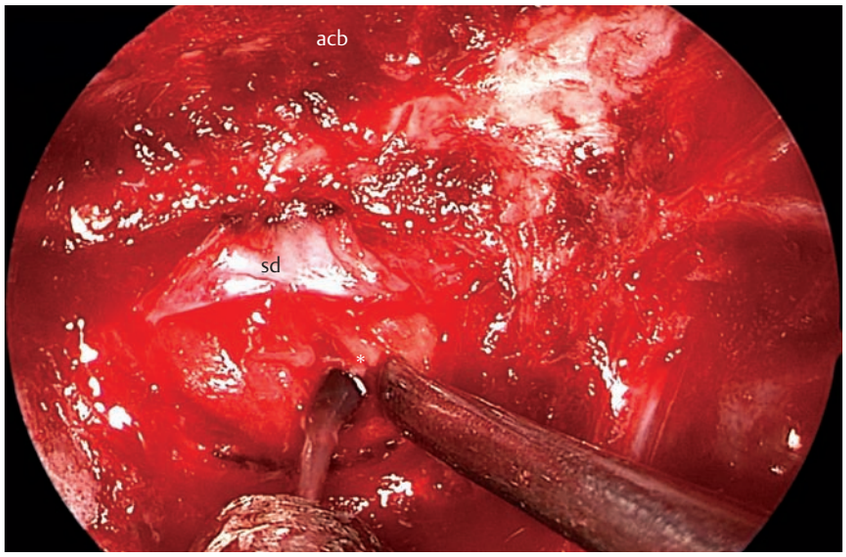

Fig. 7.150 Aspiration of cystic content. acb: Anterior cranial base; pg: pituitary gland; sd: endosteal layer of dura; *: site of incision over pituitary gland.

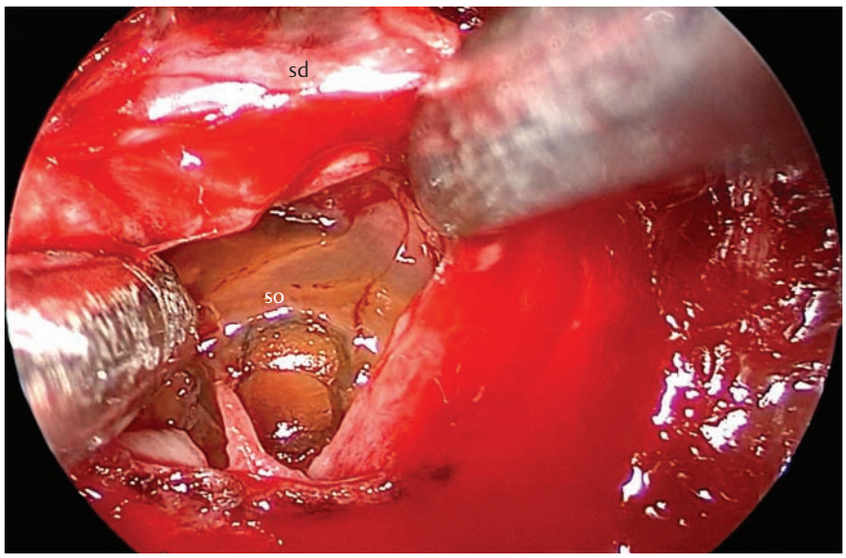

Fig. 7.151 Aspiration of solid content of lesion. sc: Sellar cavity; sd: endosteal layer of dura.

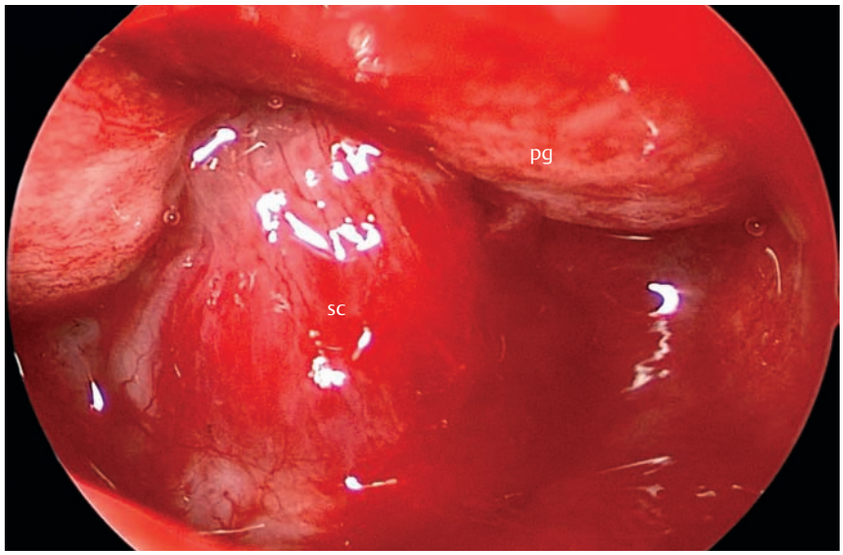

Fig. 7.152 Clearance of the lesion inside pituitary gland. sc: Sellar cavity.

Case 10: Rathke's Cyst

A 32-year-old female presented with complaint of diminished vision and hemianopia. MRI of the brain (**Fig. 7.153**) revealed a well-defined lesion in the sella within the pituitary gland, which was cystic and nonenhancing. A right-sided partial middle turbinectomy was done and rescue flaps were raised on both sides. Then a posterior septectomy was done and the rostrum of sphenoid was exposed (**Fig. 7.154**). After triple osteotomies, a wide exposure of the sphenoid sinus was obtained. The mucosa was removed and sellar bone exposed (**Fig. 7.155**). Drilling of the sellar floor was done (**Fig. 7.156**) and bone flap was removed using a Rosen's elevator (**Fig. 7.157**). This exposed the endosteal layer of dura (**Fig. 7.158**). Incision was placed over the endosteal layer of the dura (**Fig. 7.159**) using a Cappabianca knife and Kassam rotatable scissors (**Figs. 7.160 and 7.161**). The dural layer was elevated as a "U"-shaped flap (**Fig. 7.162**), to expose the normal pituitary gland (**Fig. 7.163**). Incision was placed on the pituitary gland with a knife and after retracting the normal pituitary gland biopsy of the tumor was taken (**Fig. 7.164**). Contents of the cyst were sucked out. Tumor was removed using the two-suction technique and irrigated with ringer lactate (**Figs 7.165 and 7.166**). The tumor was finally delivered out of the cavity (**Fig. 7.167**) and a clear cavity was then obtained (**Fig. 7.168**). Multilayered reconstruction was done with fat, Surgicel, and nasoseptal flap. See **Video 7.7**.

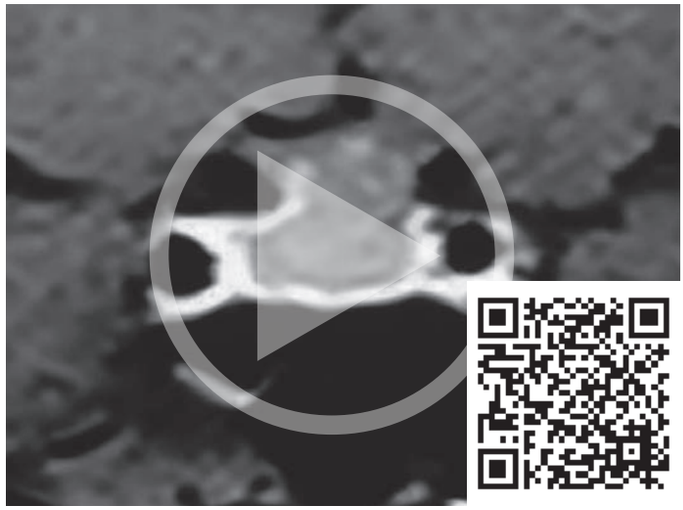

Video 7.7 Rathke's cleft cyst 2. https://www.thieme.de/de/q.htm?p=opn/cs/19/9/10104301-9bc53895

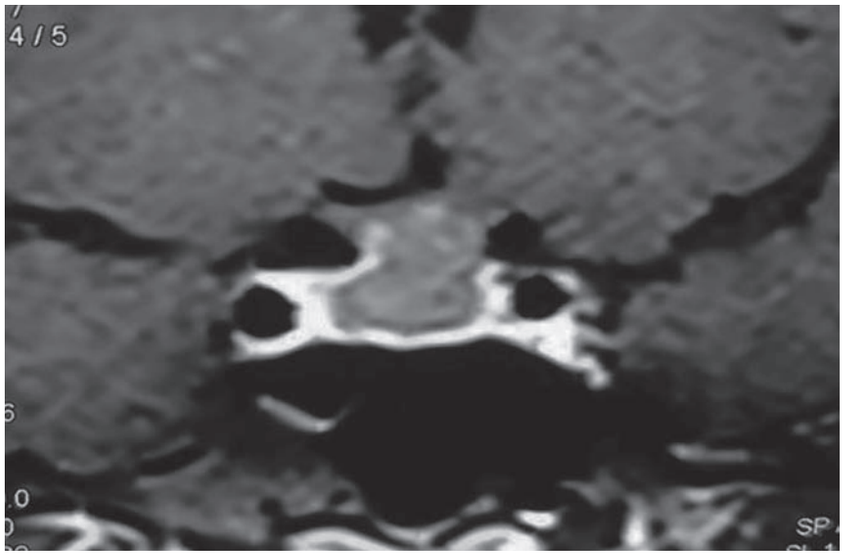

Fig. 7.153 MRI coronal view showing sellar lesion inside pituitary gland.

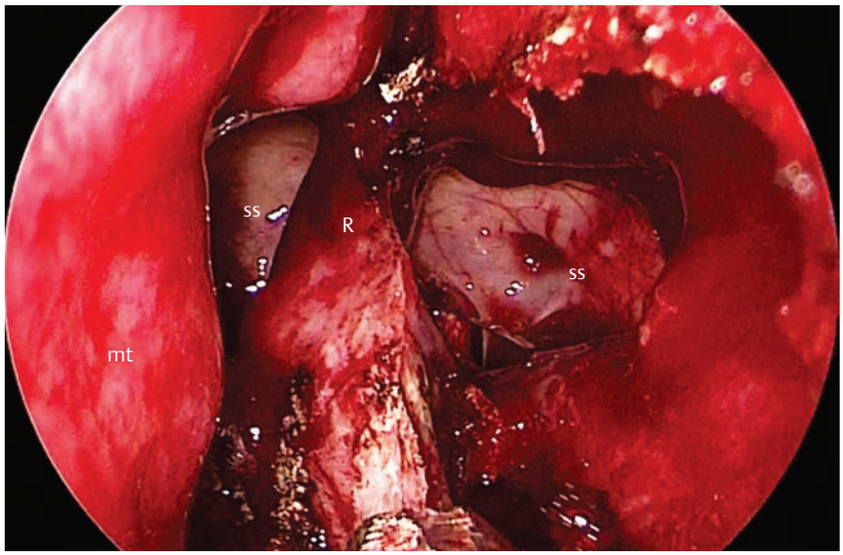

Fig. 7.154 Exposure of rostrum of sphenoid: Owl's eye appearance. mt: Middle turbinate; R: rostrum of sphenoid; ss: sphenoid sinus.

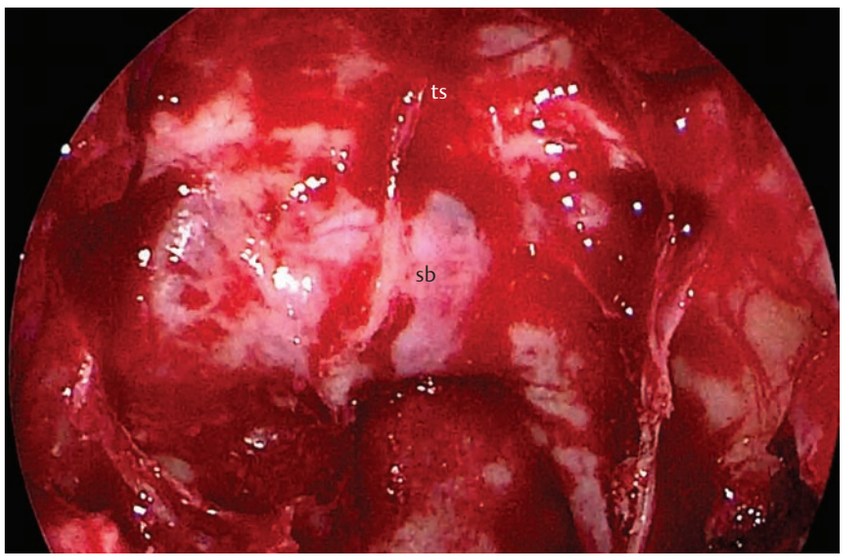

Fig. 7.155 Sellar exposure. sb: Sellar bone; ts: tuberculum sella.

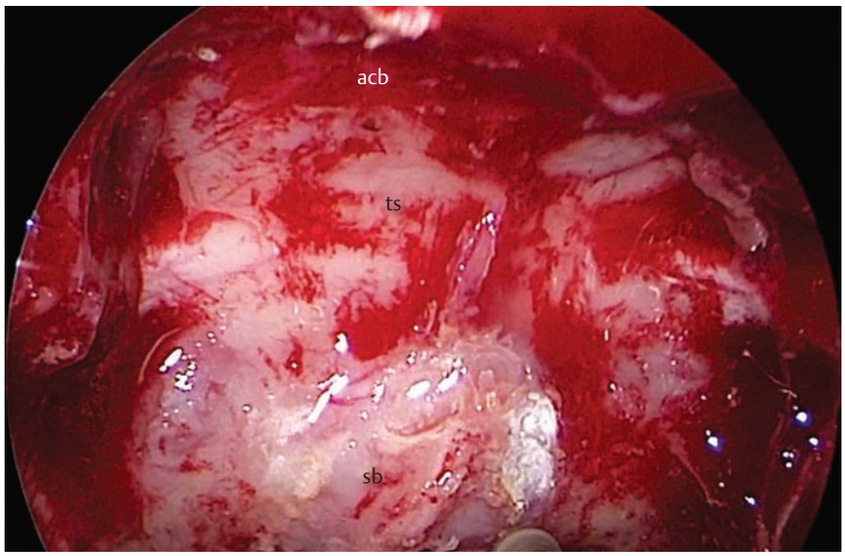

Fig. 7.156 Drilling of sellar bone. acb: Anterior cranial base; sb: sellar bone; ts: tuberculum sella.

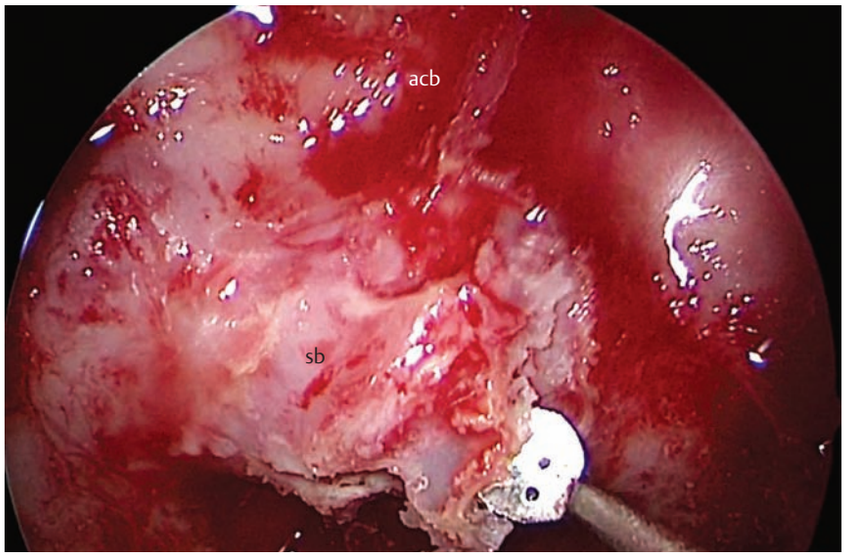

Fig. 7.157 Elevation of sellar bone flap using Rosen's elevator. acb: Anterior cranial base; sb: sellar bone.

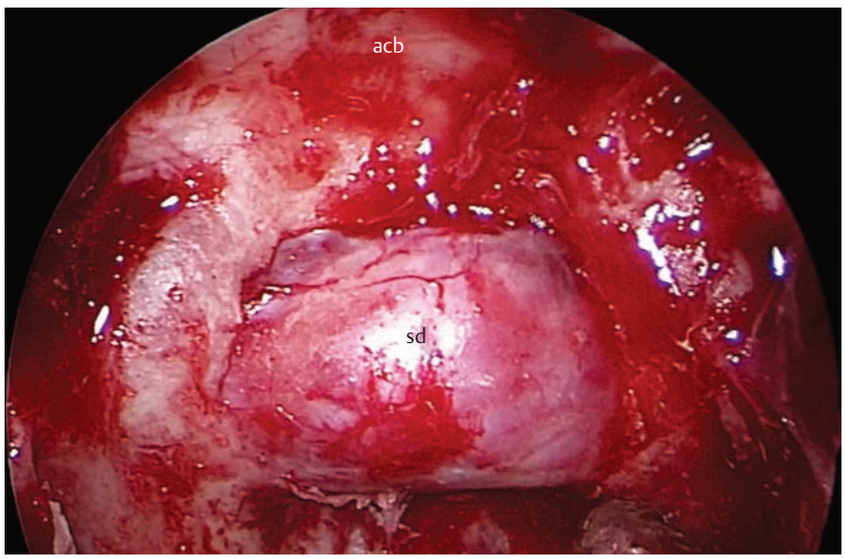

Fig. 7.158 Exposure of endosteal layer of dura. acb: Anterior cranial base; sd: endosteal layer of dura.

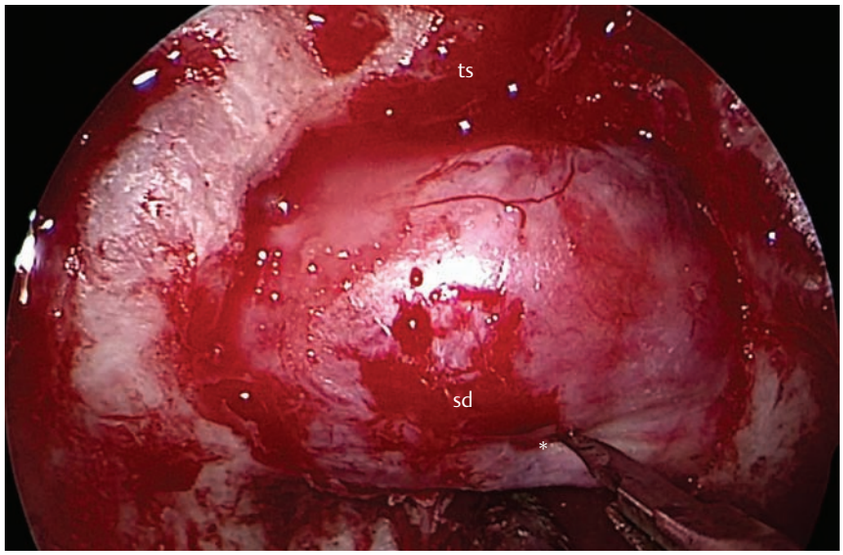

Fig. 7.159 Incision over endosteal layer of dura. sd: Endosteal layer of dura; ts: tuberculum sella; *: incision line.

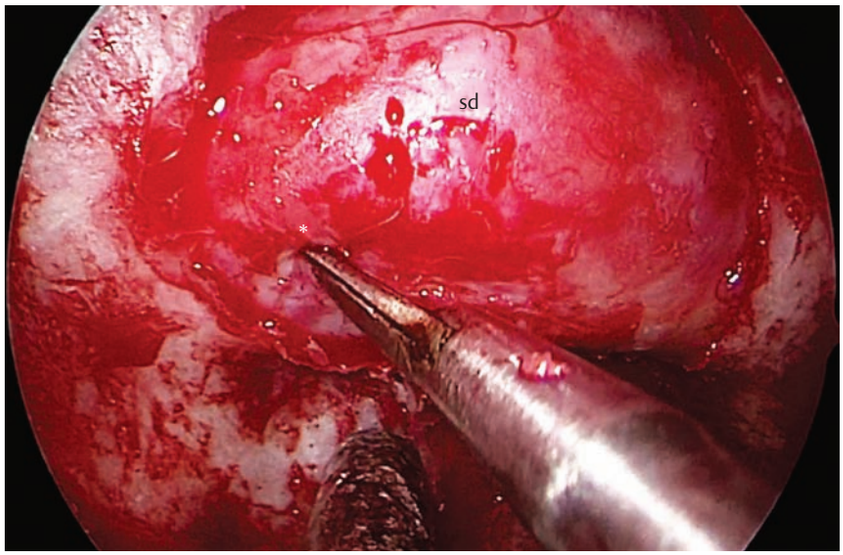

Fig. 7.160 Extension of incision line on right using rotatable scissors. sd: Endosteal layer of dura; *: incision line.

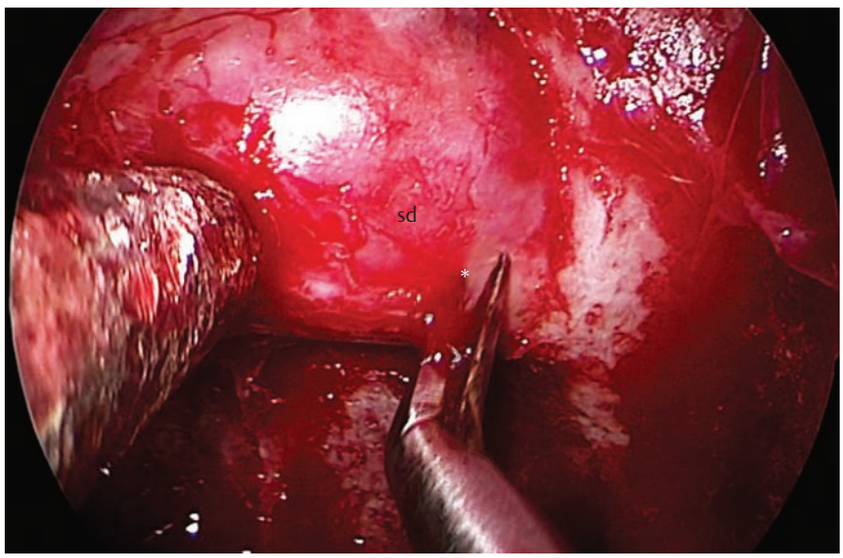

Fig. 7.161 Extension of incision on left over endosteal layer of dura using rotatable scissors. sd: Endosteal layer of dura; *: incision line.

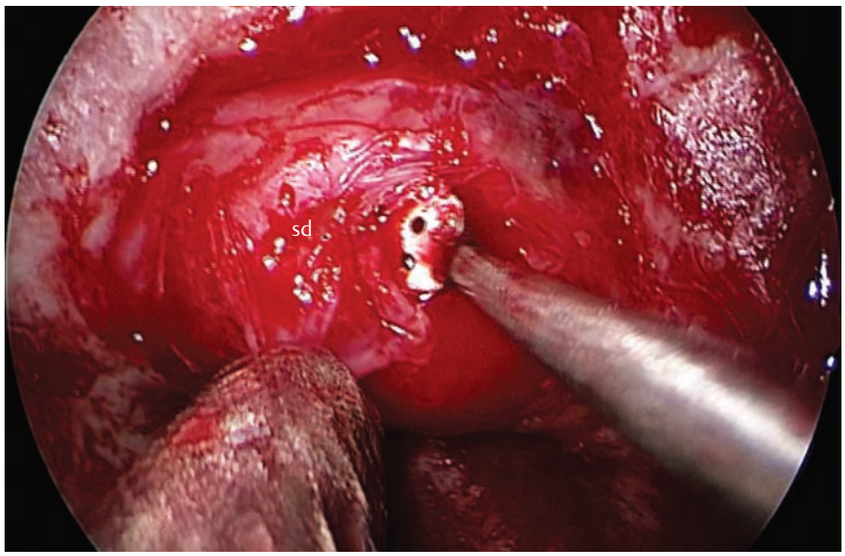

Fig. 7.162 Elevation of endosteal layer of dura as a U-shaped flap using Rosen's elevator. sd: Endosteal layer of dura.

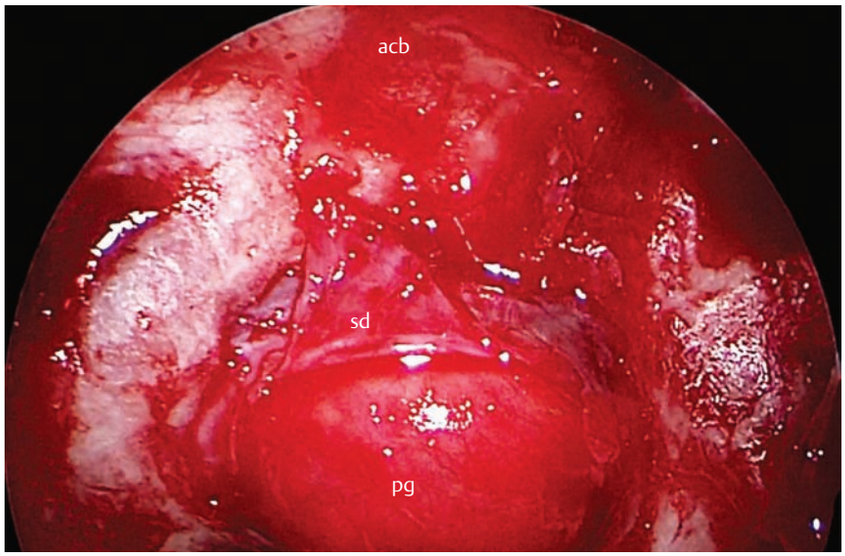

Fig. 7.163 Exposure of pituitary gland. acb: Anterior cranial base; pg: pituitary gland; sd: endosteal layer of dura.

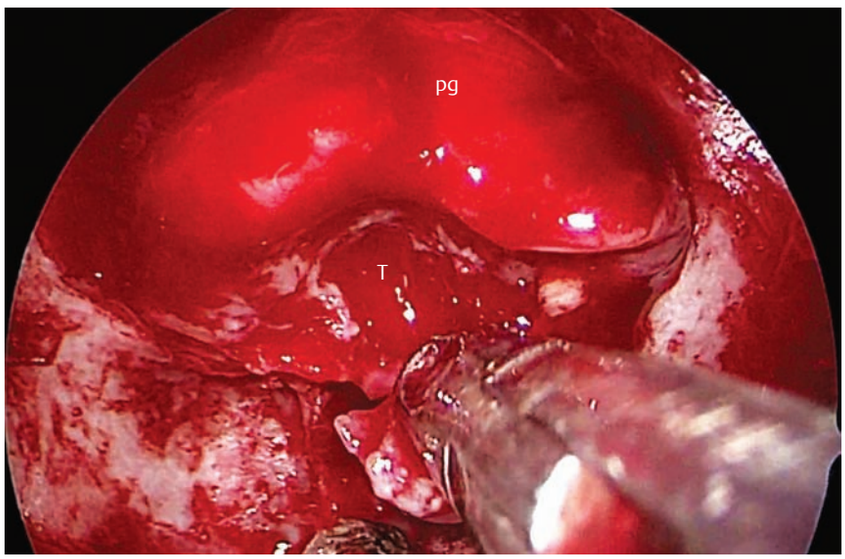

Fig. 7.164 Biopsy of lesion for histopathological examination. pg: Pituitary gland; T: tumor.

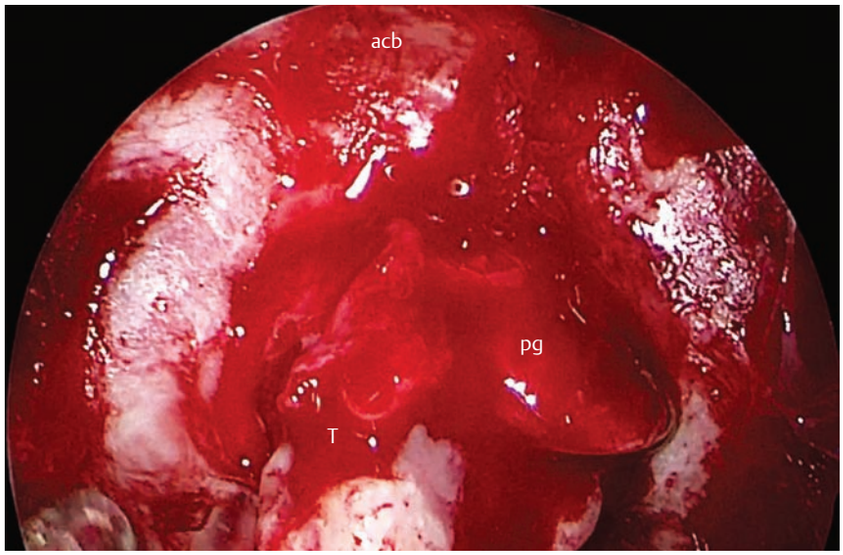

Fig. 7.165 Extracapsular dissection of tumor. acb: Anterior cranial base; pg: pituitary gland; T: tumor.

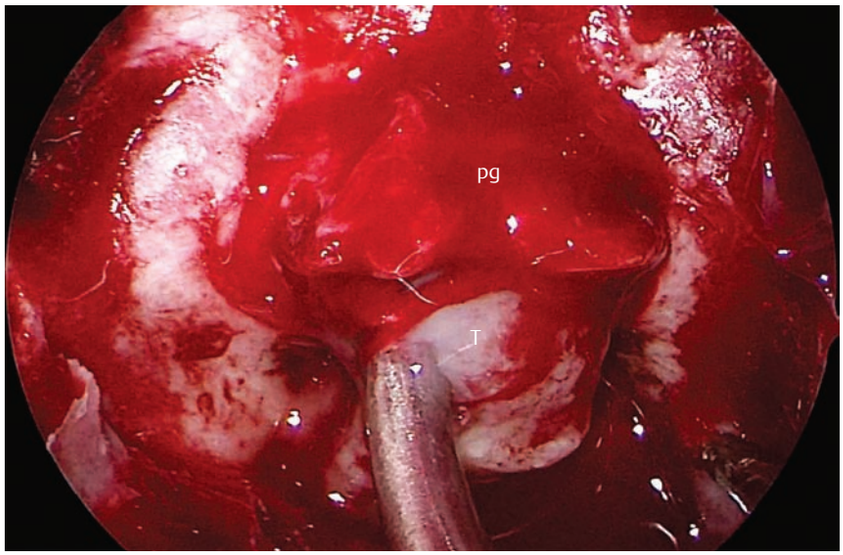

Fig. 7.166 Hydrodissection of tumor using Ringer Lactate. pg: Pituitary gland; T: tumor.

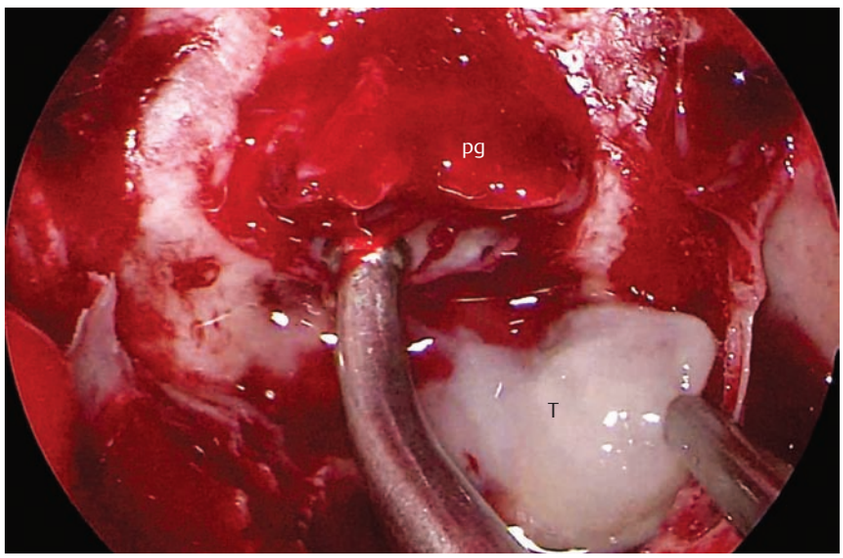

Fig. 7.167 Delivery of tumor from cavity. pg: Pituitary gland; T: tumor.

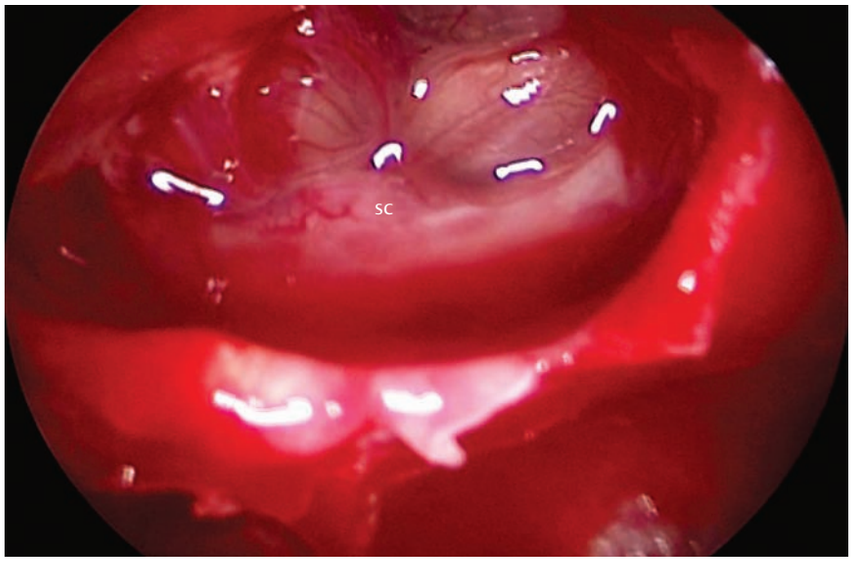

Fig. 7.168 Cavity after complete clearance of tumor. sc: Sellar cavity.

Case 11: Sellar–Suprasellar Craniopharyngioma

A 7-year-old male presented with complaints of headache. MRI of the brain (**Figs. 7.169 and 7.170**) revealed a well-defined lesion in the sella, extending suprasellar. A right-sided partial middle turbinectomy was done and the nasoseptal flap was harvested right. Then a posterior septectomy was done and the rostrum of sphenoid was excised after triple osteotomies, to obtain a wide exposure of the sella (**Fig. 7.171**). It was a conchal type of pneumatization of sphenoid sinus. Drilling of the sellar floor was done (**Fig. 7.172**) and bone flap was removed. The planum–tuberculum angle in this case was almost 90° (**Fig. 7.173**). This exposed the endosteal layer of dura (**Fig. 7.174**). The dura over the cavernous sinuses was exposed and Doppler was used to identify the position of the internal carotid arteries (**Figs. 7.175 and 7.176**).The endosteal layer of dura was incised using a Cappabianca knife and extended on both sides using Kassam rotatable scissors (**Figs. 7.177 and 7.178**). The tumor was seen behind the normal gland. The normal gland was incised and elevated (**Fig. 7.179**). Biopsy was taken from the capsule of the tumor (**Fig. 7.180**). This revealed the fluid content of the tumor with motor-oil appearance. The tumor was first cleared from 6 o' clock position, then 3 o' clock and 9 o' clock positions. The calcified part of the tumor was seen toward the medial walls of cavernous sinuses, which was cleared using suction and extracapsular dissection was done (**Fig. 7.181**). A small suprasellar extension of the tumor was present. It was pulled out through a small perforation in the diaphragma sella (**Fig. 7.182**). The capsule of the tumor was excised and completely separated from the diaphragma (**Fig. 7.183**). A 0° endoscope was used to visualize the floor of the third and the mammillary bodies (**Fig. 7.184**), and the basilar artery with bilateral P1 segments (**Fig. 7.185**). Finally, the clearance of the cavity was obtained and the cavity was reconstituted with fat and Surgicel, and multilayered reconstruction was done using nasoseptal flap (**Fig. 7.186**), Surgicel, Gelfoam, and tissue glue. See **Video 7.8**.

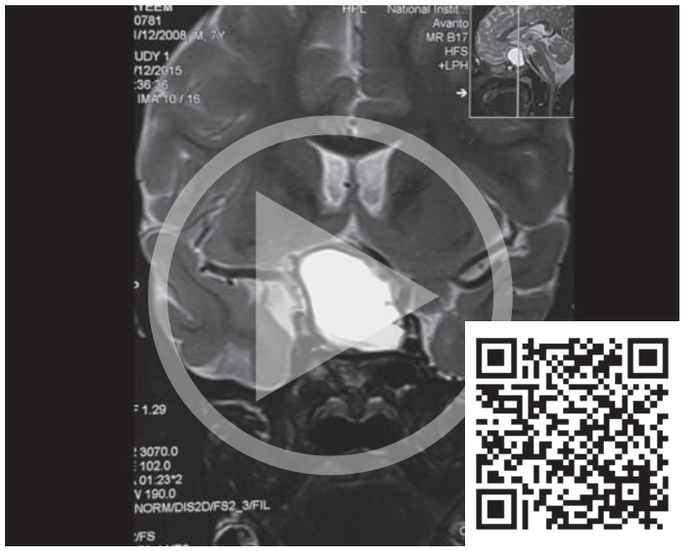

Video 7.8 Sellar craniopharyngioma. https://www.thieme.de/de/q.htm?p=opn/cs/19/9/10104302-db697f22

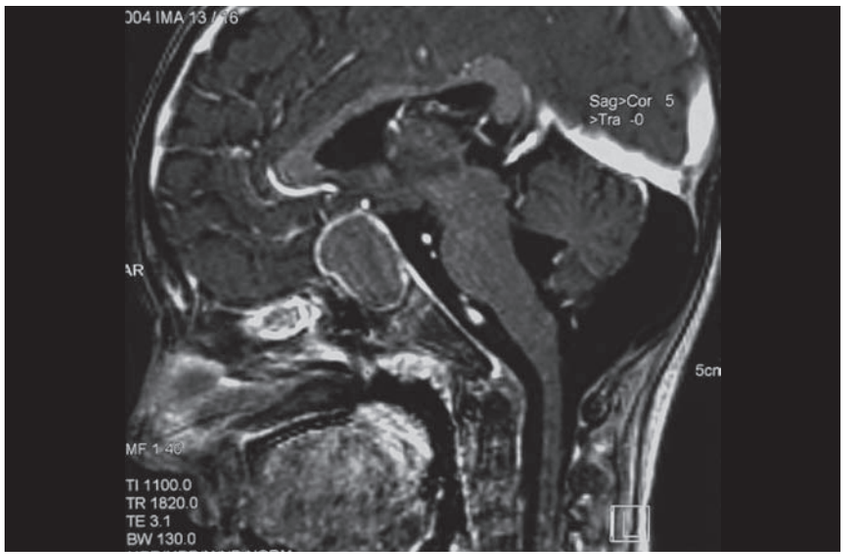

Fig. 7.169 T1 MRI coronal view showing sellar–suprasellar lesion.

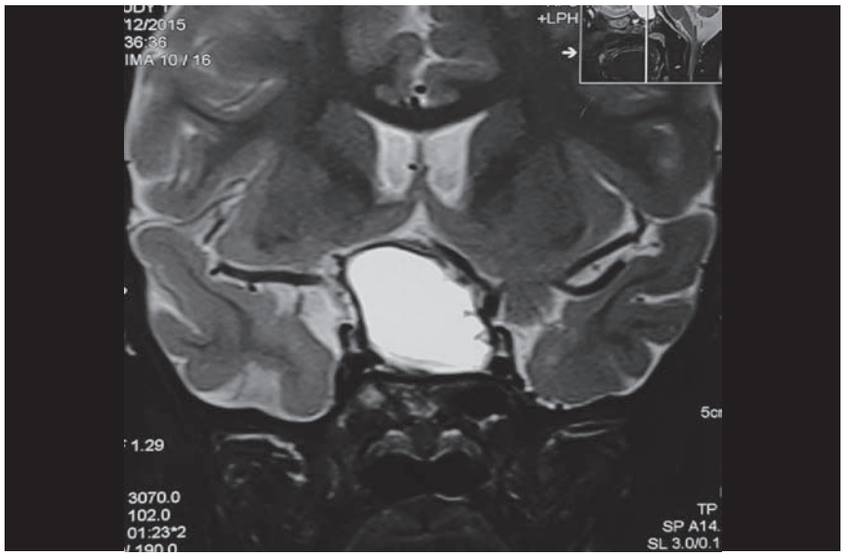

Fig. 7.170 T2 MRI sagittal view showing sellar–suprasellar lesion.

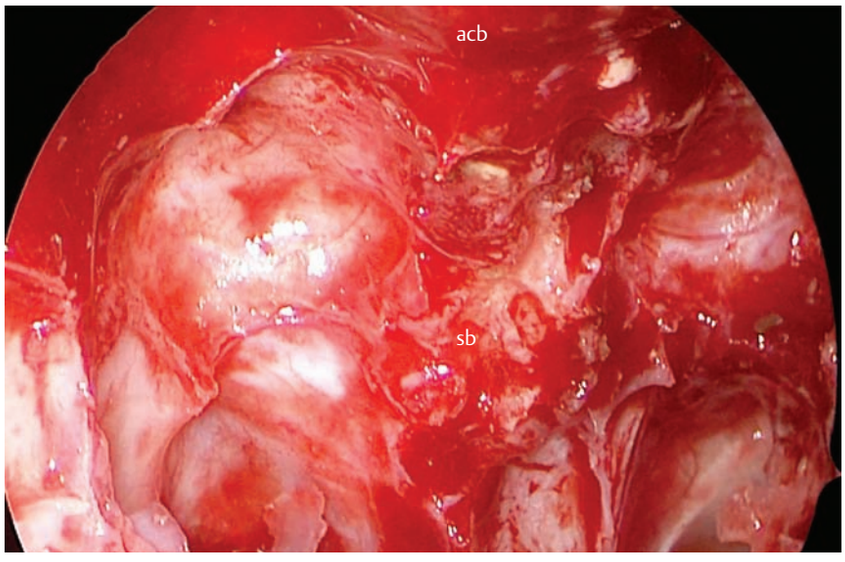

Fig. 7.171 Exposure of sella after resection of rostrum of sphenoid. acb: anterior cranial base, sb: sellar bone.

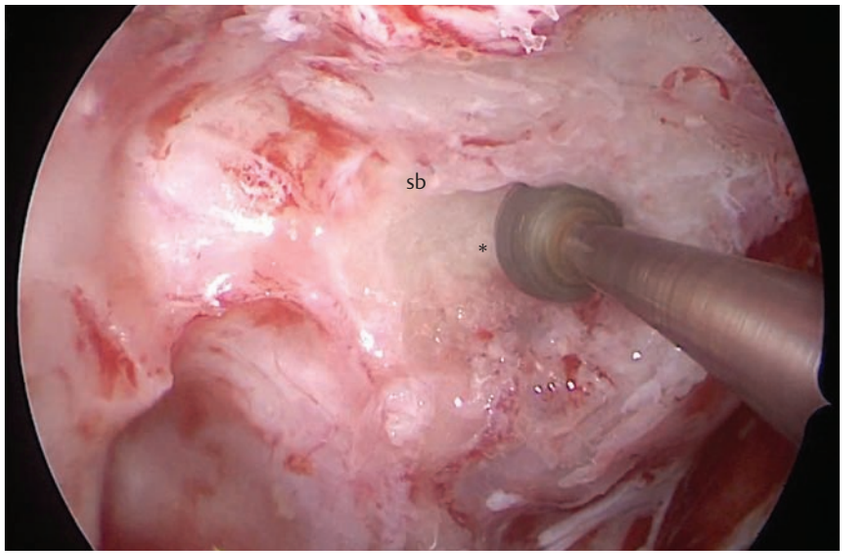

Fig. 7.172 Drilling of sellar bone. sb: Sellar bone; *: site of drilling of sellar bone.

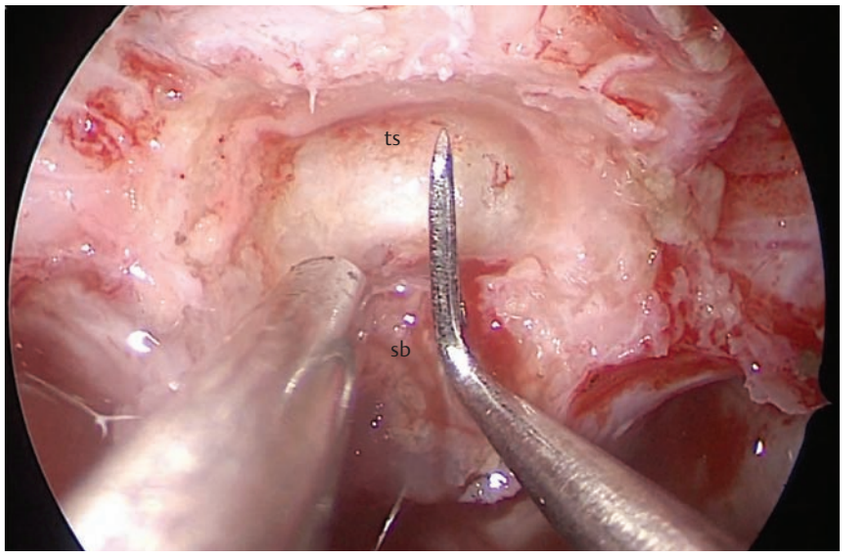

Fig. 7.173 Planum–tuberculum angle. sb: Sellar bone; ts: tuberculum sella.

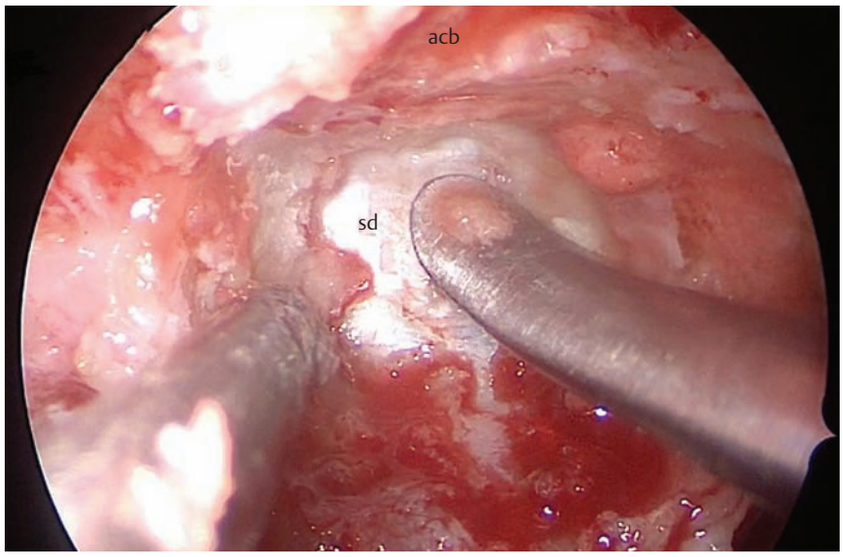

Fig. 7.174 Elevation of bone and exposure of endosteal layer of dura. acb: Anterior cranial base; sd: endosteal layer of dura.

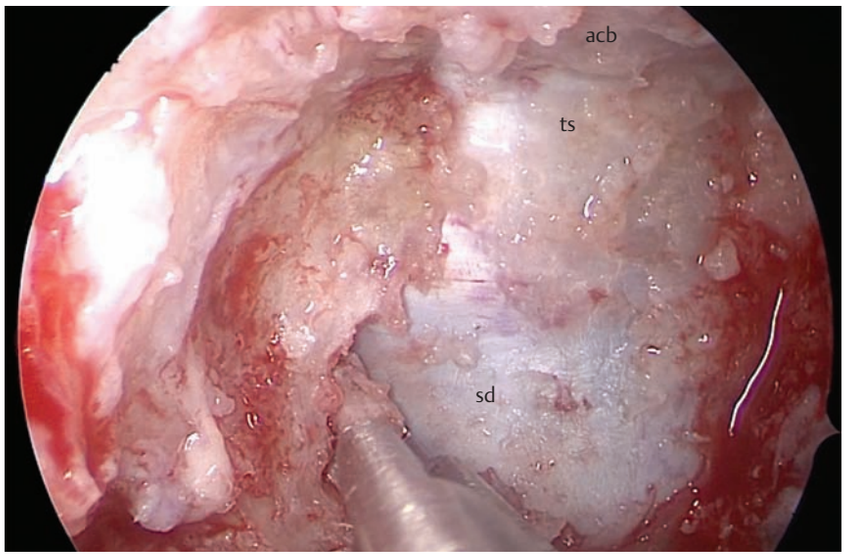

Fig. 7.175 Removal of bone over cavernous sinus dura. acb: Anterior cranial base; sd: endosteal layer of dura; ts: tuberculum sella.

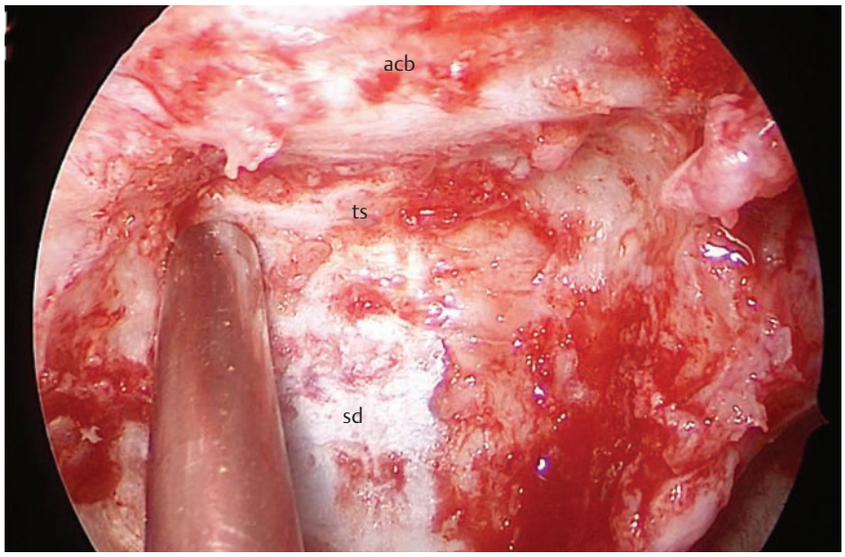

Fig. 7.176 Use of Doppler to locate the right cavernous internal carotid artery. acb: Anterior cranial base; sd: endosteal layer of dura; ts: tuberculum sella.

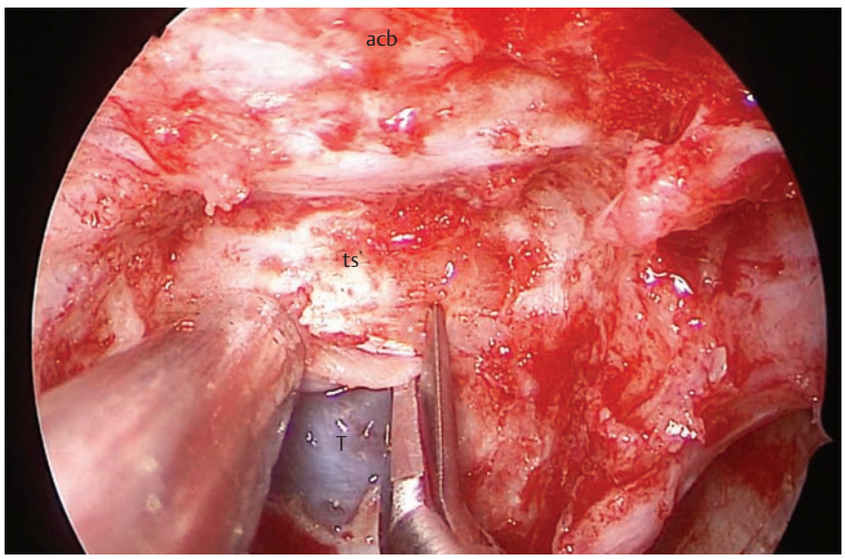

Fig. 7.177 Incision over endosteal layer of dura using rotatable Kassam scissors. acb: Anterior cranial base; T: tumor; ts: tuberculum sella; *: incision line.

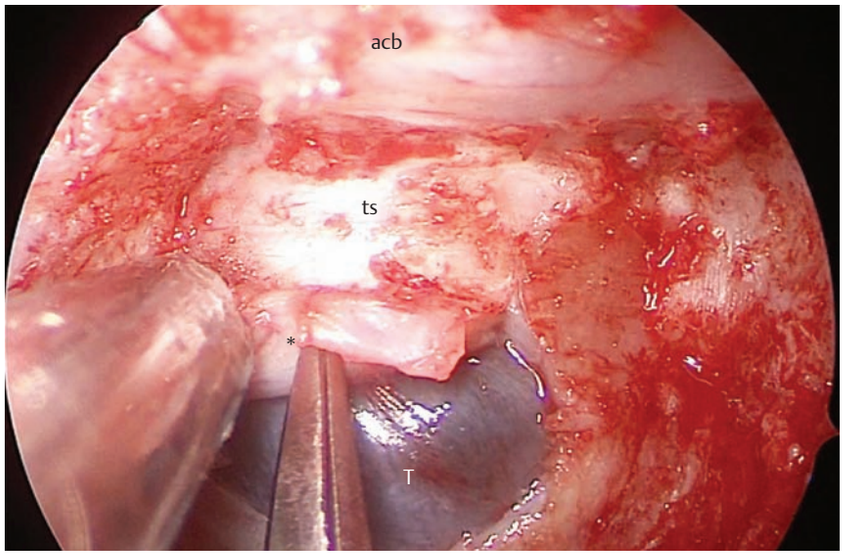

Fig. 7.178 Extension of incision using rotatable Kassam scissors. acb: Anterior cranial base; T: tumor; ts: tuberculum sella; *: incision line.

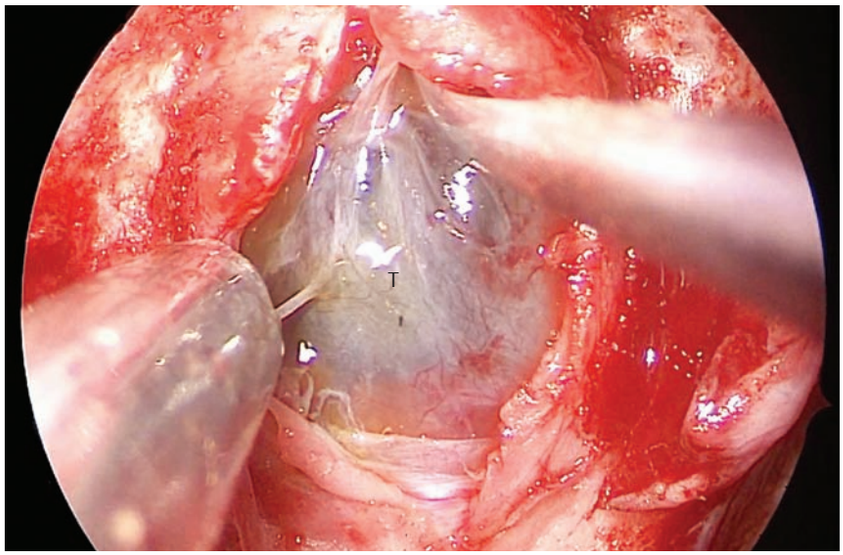

Fig. 7.179 Elevation of dura to expose the tumor. T: tumor.

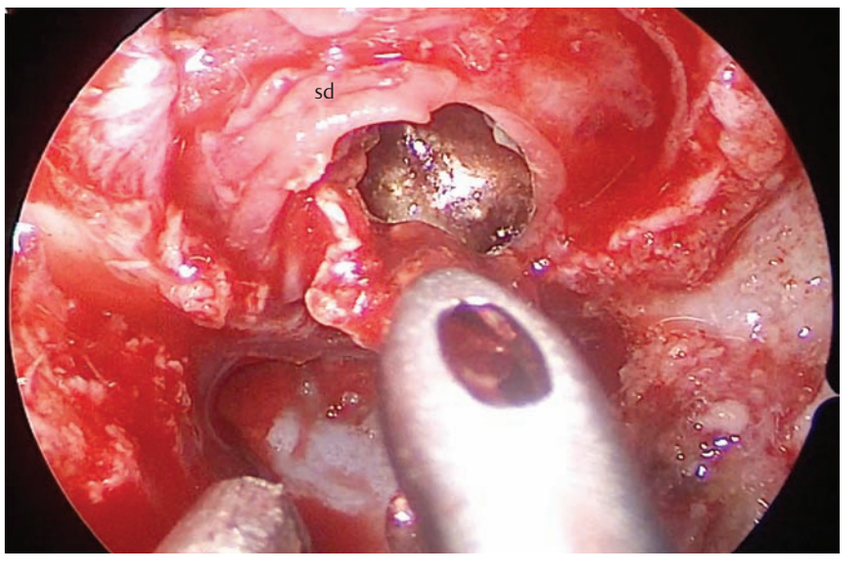

Fig. 7.180 Biopsy taken from capsule of tumor for histopathological examination. sd: Endosteal layer of dura.

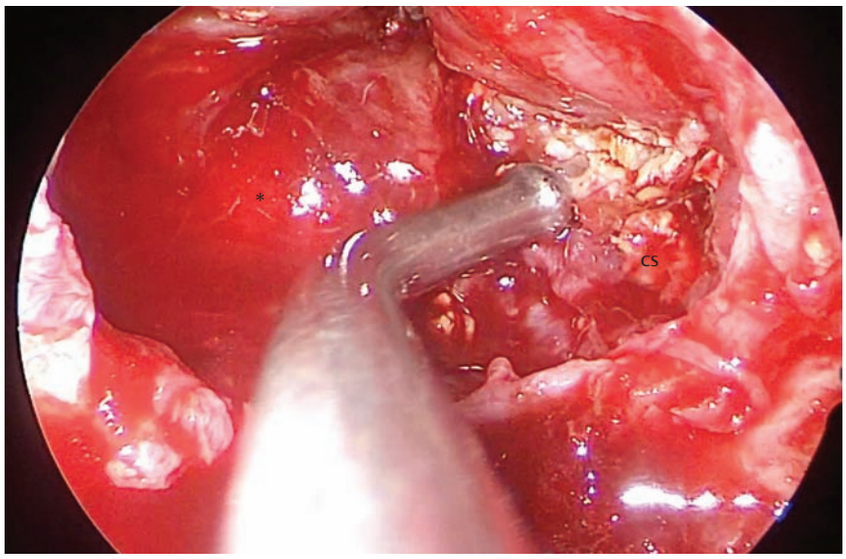

Fig. 7.181 Clearance of calcified component of tumor from left cavernous sinus. cs: Cavernous sinus of left side; *: cavity of tumor.

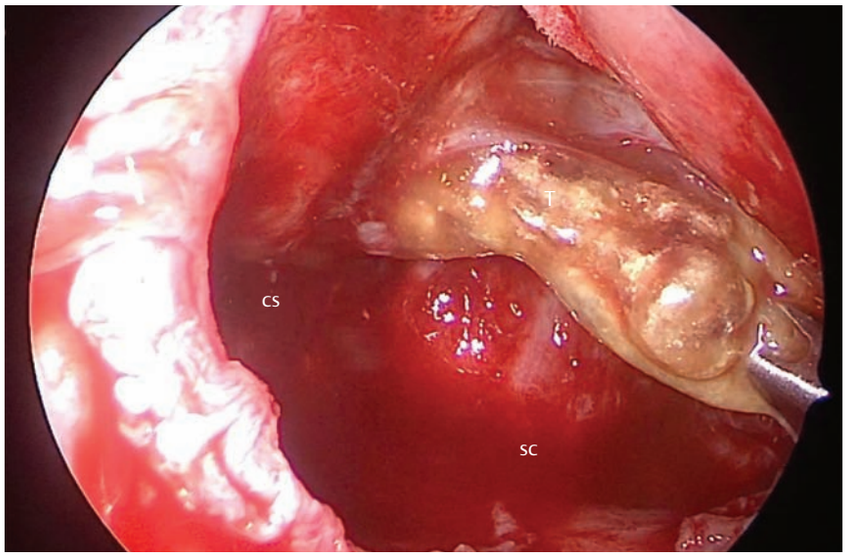

Fig. 7.182 Excision of suprasellar part of tumor. cs: Cavernous sinus of right side; sc: sellar cavity; T: tumor.

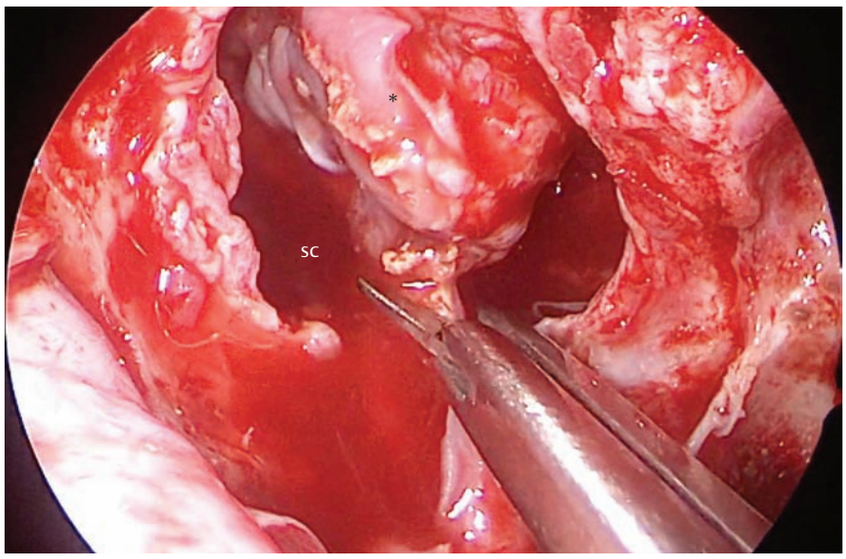

Fig. 7.183 Clearance of cavity obtained. sc: Sellar cavity; *: diaphragma sella.

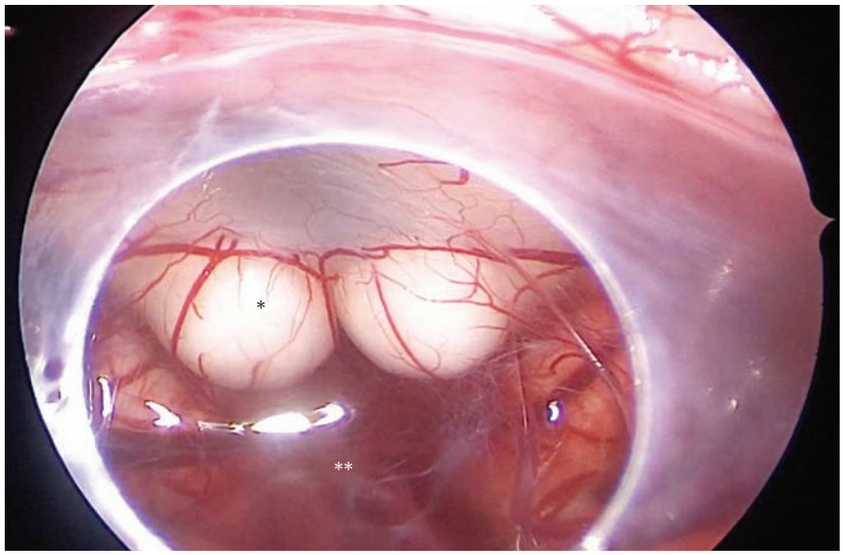

Fig. 7.184 Mammillary bodies exposed. *: mammillary bodies.

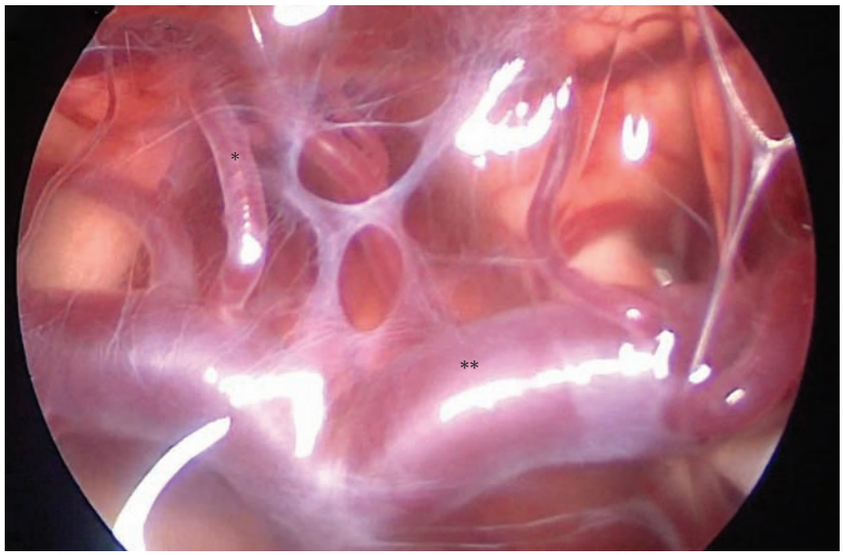

Fig. 7.185 Basilar artery and P1 segments exposed. *: P1 segment; **: left posterior cerebral artery.

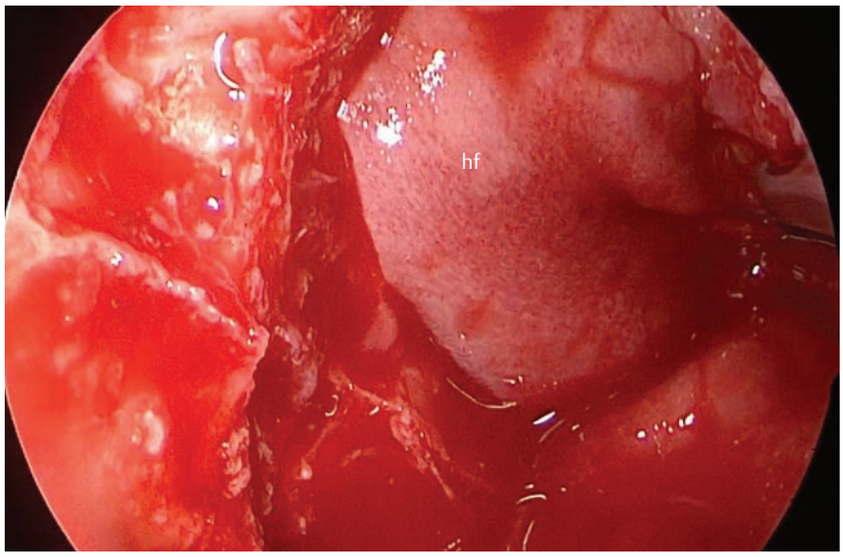

Fig. 7.186 Reconstruction done with nasoseptal flap. hf: Nasoseptal flap.

References

1. Ezzat S, Asa SL, Couldwell WT, et al. The prevalence of pituitary adenomas: a systematic review. Cancer 2004;101(3):613–619
2. Freda PU, Post KD. Differential diagnosis of sellar masses. Endocrinol Metab Clin North Am 1999;28(1):81–117, vi
3. Louis DN, Ohgaki H, Wiestler OD, et al. The 2007 WHO classification of tumours of the central nervous system. Acta Neuropathol 2007;114(2):97–109
4. DeLellis RA, Lloyd RV, Heitz PU, Eng C, eds. World Health Organization Classification of Tumors: Pathology and Genetics of Tumors of Endocrine Organs. Lyon: IARC Press; 2004:10–35
5. Hardy J, Somma M. Acromegaly: surgical treatment by transsphenoidal microsurgical removal of the pituitary adenoma. In: Collins WF, Tindall GT, eds. Clinical Management of Pituitary Disorders. New York, NY: Raven Press;1979: 209–217
6. Muto J, Carrau RL, Prevedello DM, et al. Endoscopic Endonasal Approaches to the Skull Base - A Review. Austin J Otolaryngol 2015;2(7):1055
7. Koutourousiou M, Fernandez-Miranda JC, Wang EW, Snyderman CH, Gardner PA. The limits of transsellar/transtuberculum surgery for craniopharyngioma. J Neurosurg Sci 2018;62(3):301–309

8 Endoscopic Approach to Suprasellar Lesions

Dipen Thakkar, Shilpee Bhatia Sharma, Narayanan Janakiram

Introduction

In 1987, Weiss first detailed the careful administration of suprasellar lesions using a modified transsphenoidal approach that required extra bone removal from the ventral cranial base. Based on this experience, others started to broaden the standard methodology and apply it to the pituitary fossa, tuberculum sellae, and posterior segment of the sphenoidal planum. This transsphenoidal transtubercular approach enables direct access to the supradiaphragmatic space.[1]

Endoscopic endonasal transsphenoidal approach has more advantages over other approaches for suprasellar lesions such as avoidance of brain retraction, absence of scars, less blood loss, no blind spot from carotid to carotid, more direct access to tumor and its bony attachment, better visualization of arachnoid planes, less chance of optic chiasmal injury, preservation of superior hypophysial artery, easy removal of hyperostotic bone, and less recovery time.[2]

Suprasellar lesions include tumors such as pituitary adenomas, craniopharyngioma, meningioma, glioma/astrocytoma, hamartoma, lipoma, dermoid epidermoid dysgerminoma/germinoma (ectopic pinealoma), congenital cholesteatoma, choristoma, infundibuloma, lymphoma, and metastases; inflammatory diseases such as sarcoidosis, tuberculosis, and collagenosis; and miscellaneous lesions such as arachnoid cyst, aneurysm, Rathke's cleft cyst, and histiocytosis X.[3]

Suprasellar tumors can give a wide range of manifestations, from visual disturbance to behavioral changes from secondary hydrocephalus and pituitary hormonal variations.[1,3]

Indications of Endoscopic Endonasal Transsphenoidal Approach

- Pituitary adenomas with a huge suprasellar expansion.[4] Tumors that stretch out over the planum sphenoidale (PS) and anterior to the tuberculum sellae may benefit from removal of the tuberculum sellae and a part of the PS. This will permit an extracapsular dissection of the tumor and guarantee a total resection.
- Rathke's cyst[5] that arises from the stalk and mostly extend toward suprasellar area; some can descend in sella.
- Extended transtubercular transplanum approach is pragmatic for craniopharyngioma that are midline and do not cross carotids laterally.[6]
- Tuberculum and PS meningiomas[7] are amenable to extended endonasal transtubercular transplanum approach. Tumors extending laterally to carotids are usually not suitable for this approach.
- Transplanum approach may supplement transclival approach for chordomas which extends in suprasellar area.
- Expansive tumors that can't be totally resected using an endonasal approach are not generally a contraindication. Depending upon the age of the patient and the surgical priorities, inner decompression or staged resection with secondary transcranial or cranioendoscopic approach can be performed.
- Suprasellar and third ventricle arachnoid cysts.
- Intraventricular tumors (colloid cysts, choroid plexus papillomas, and ependymomas).

Contraindications of Endoscopic Endonasal Transsphenoidal Approach

- This approach requires a careful case selection. Pathology extending lateral and posterior to carotids and orbit are difficult to deal with this minimal invasive endonasal endoscopic approach.[2,7]
- Encasement of A2 segment of anterior cerebral artery is no absolute contraindication for this approach

but depends on experience and ability of surgeon to do fine microdissection. A surgeon should also keep in mind possibilities of postoperative radiosurgery and fractionated radiation to decrease growth of residual mass.

- Hypothalamic hamartomas, large intracranial aneurysms, and germ cell tumors are examples of differential diagnosis of the large macroadenoma which are not suitable for this approach. Proper preoperative evaluation should be done to differentiate these tumors that require different methods for workup and approach.
- Sinonasal infection is the relative contraindication.
- For patients whose general condition does not allow for general anesthesia.
- This approach is absolutely contraindicated for surgeons with a lack of appropriate experience and instruments.

Preoperative Planning

Teamwork between neurosurgeon and otolaryngologist is needed to deal with the pathology of suprasellar region for optimum results. The patient is analyzed from both neurosurgeon and otolaryngologist perspective for planning approach and closure. Patients with visual symptoms are referred for neuro-ophthalmologic examination and visual field testing. Preoperative comprehensive endocrinological assessment is advisable to know baseline endocrine function as well as deficiency if present. Watchful examination of the preoperative imaging is fundamental. Both computed tomography (CT) and magnetic resonance imaging (MRI) scans should be performed. They are useful to examine preoperative paranasal sinus and skull base surgical anatomy. Vascular encasement and brain invasion can be judged by MRI.

Patient Positioning and Preparation

Most surgeons use 1:5,000 adrenaline soaked three patties on each side to decongest nasal mucosa preoperatively. After oral endotracheal intubation, a Foley's urinary catheter is inserted to monitor urinary output intraoperatively and postoperatively. In selected post operated cases a lumbar drain can be placed prior to surgery. The patient's head is placed on a horseshoe pad slightly extended and to the right or in pin immobilization. It is authors' standard practice to place patient in slight reverse Trendelenburg without pin immobilization. The position of the head while doing sellar dissection is flexed, whereas in suprasellar or planum dissection the head is placed in slight hyperextension. In expected large skull base defect authors prepare thigh or abdomen for access of fat and fascia. The image guidance system is positioned and registration process is completed and checked. Preoperative antibiotics and a stress dose of methylprednisolone are administered.

Surgical Technique

Exposure

The wide surgical corridor is provided by right partial middle turbinectomy (**Figs. 8.1 and 8.2**) and posterior ethmoidectomy done as author uses principal of cavity and half (**Figs. 8.3 and 8.4**). Posterior ethmoid cavity is used to position endoscope in four-handed technique. A nasoseptal flap is created as wide as possible and placed in nasopharynx (**Figs. 8.5 and 8.6**). The middle, inferior, and superior turbinates of the contralateral side are lateralized and bilateral sphenoidotomy is performed (**Fig. 8.7**). The posterior septectomy is performed to expose the rostrum of sphenoid (**Fig. 8.8**). Triple osteotomy is done to remove the rostrum of the sphenoid (**Figs. 8.9 and 8.10**). The floor of sphenoid is thinned and all intrasphenoidal septations are reduced. Adequate exposure ensures avoiding collision of instruments during dissection (**Fig. 8.11**). The bleeding from the mucosa of the planum and superior part of the posterior septectomy is coagulated and controlled using a coblator. The identification of anatomical landmarks is essential for orientation during surgery. Sellar bone is removed with an elevator after drilling it to eggshell thin (**Fig. 8.12**). The medial opticocarotid recess marks the lateral most limit of the tuberculum.

Transtubercular Approach

The bone over the tuberculum between the medial clinoid is drilled using Karl Storz S III neurodrill with 4-mm diamond burr (**Figs. 8.13 and 8.14**). After the bone is drilled eggshell thin, it is removed using Cottle's or Rosen's elevator. Inferior bone removal continues halfway up to sellae. Superior bone removal continues in the planum up to the

Fig. 8.1 Endoscopic view of right nasal cavity showing partial resection of middle turbinate. Mt, middle turbinate; s, nasal septum.

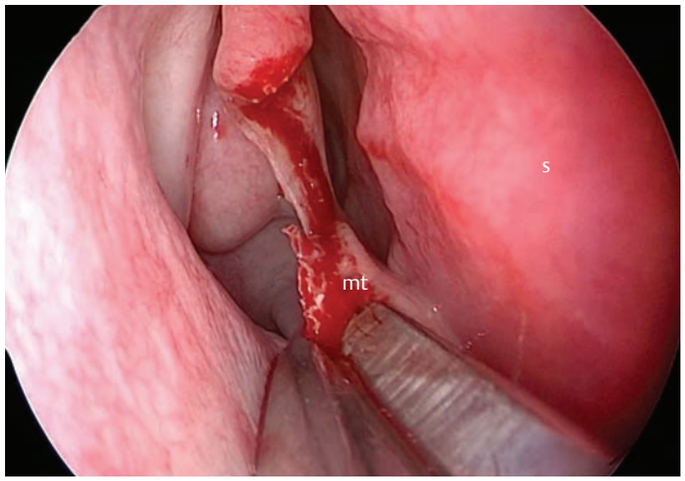

Fig. 8.2 Partially resected middle turbinate. Mt, middle turbinate; s, nasal septum.

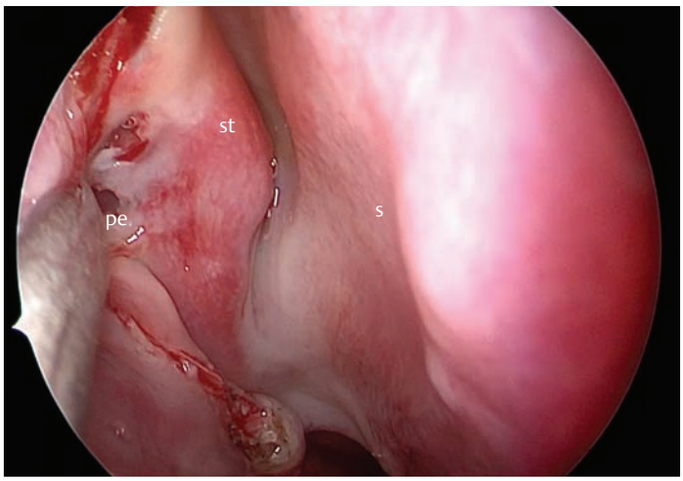

Fig. 8.3 Posterior ethmoidectomy performed and sphenoid OSS is widened. St, superior turbinate; pe, posterior ethmoid; s, nasal septum.

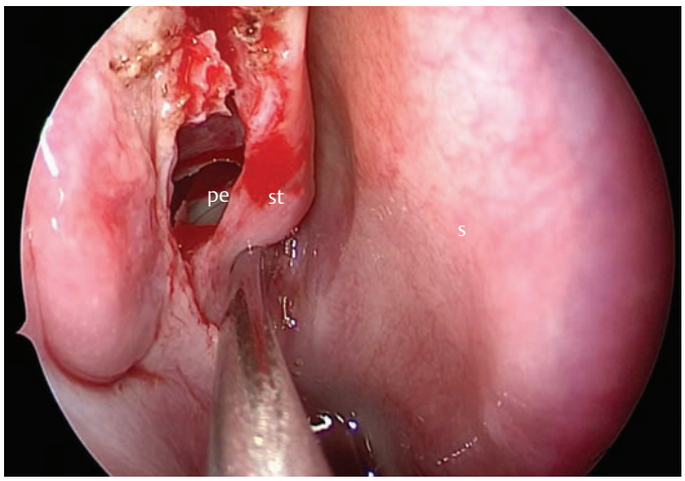

Fig. 8.4 Superior turbinate is lateralized to widen sphenoid ostium.

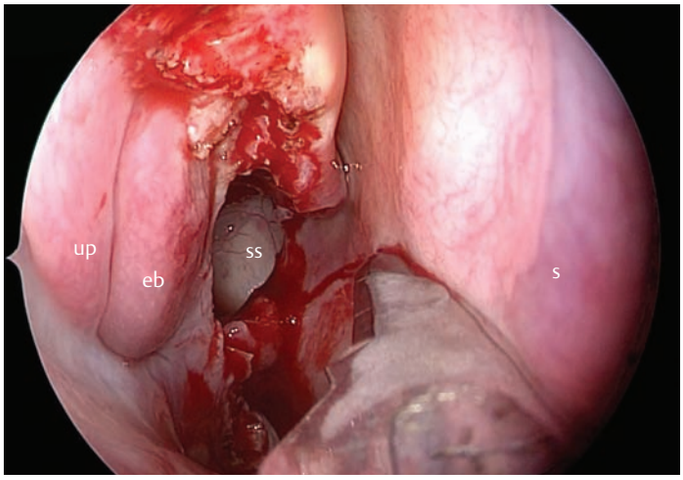

Fig. 8.5 Making superior incision for nasoseptal flap. Up, uncinate process; eb, ethmoidal bulla; ss, sphenoid sinus.

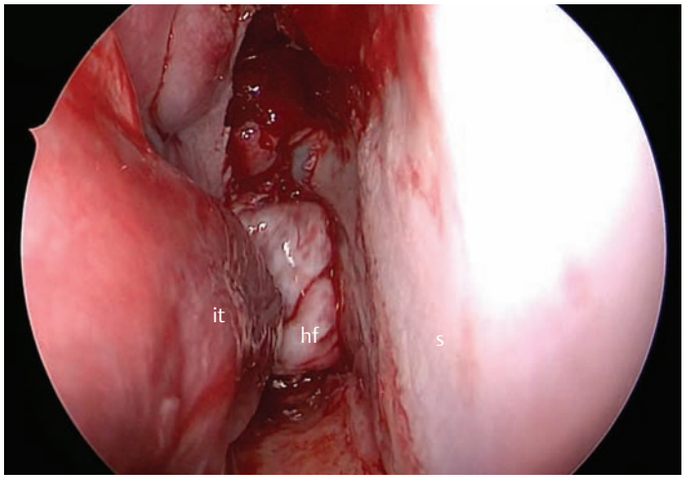

Fig. 8.6 Harvested nasoseptal flap is placed in nasopharynx. It, inferior turbinate; hf, Hadad flap.

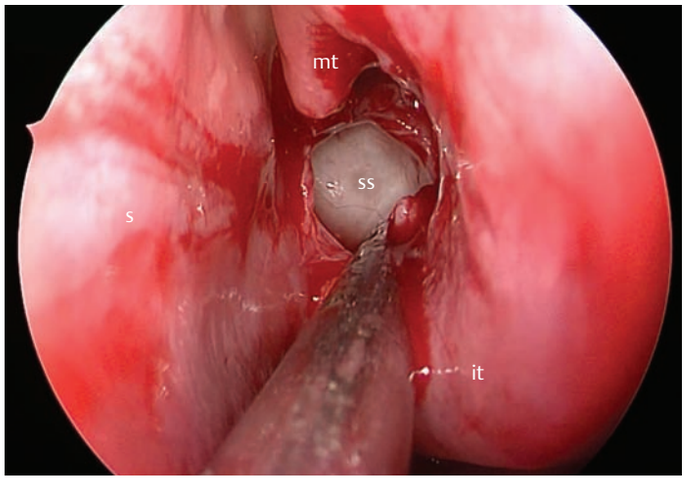

Fig. 8.7 Left side posterior ethmoidectomy and sphenoidotomy performed. Mt, middle turbinate; ss, sphenoid sinus; it: inferior turbinate.

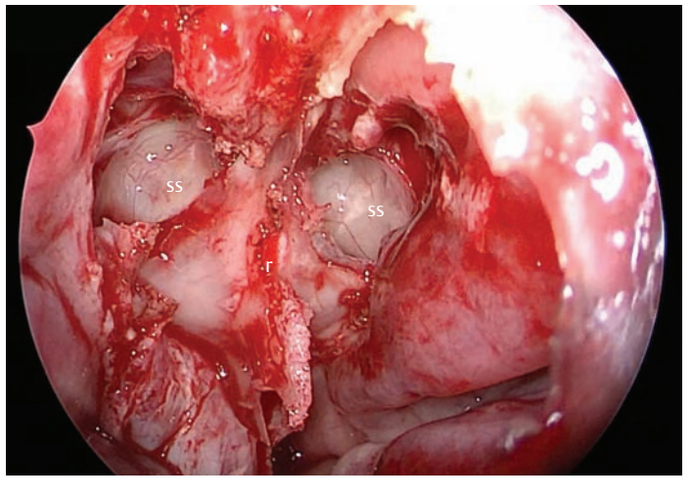

Fig. 8.8 Owl's eye appearance after performing the posterior septectomy. Ss, sphenoid sinus; r, sphenoid rostrum.

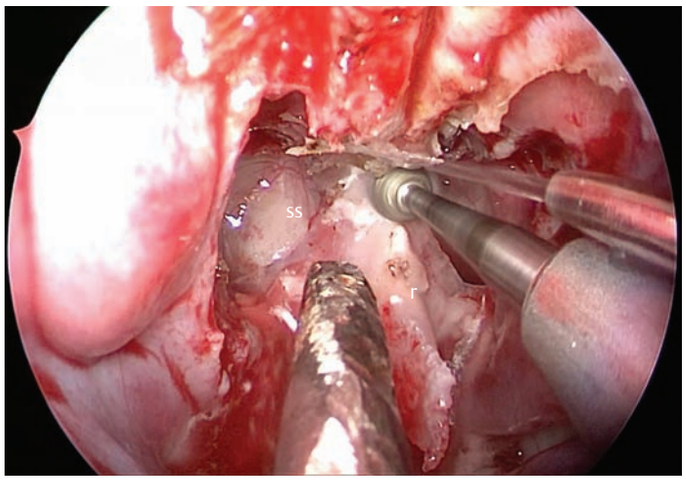

Fig. 8.9 Performing planner osteotomy. Ss, sphenoid sinus; r, sphenoid rostrum.

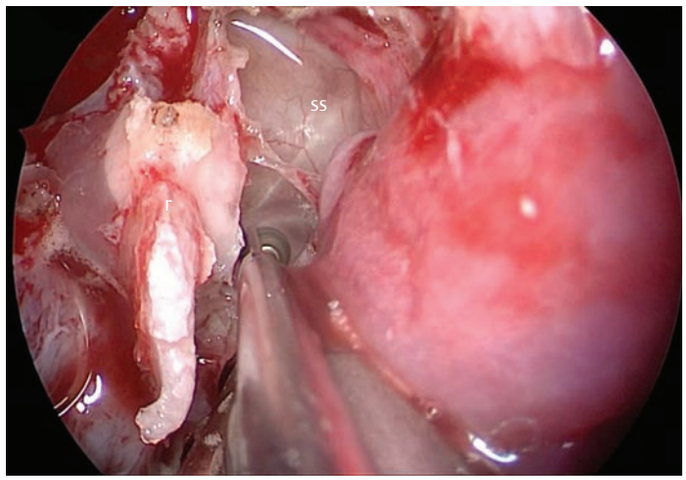

Fig. 8.10 Performing shoulder osteotomy. Ss, sphenoid sinus; r, sphenoid rostrum.

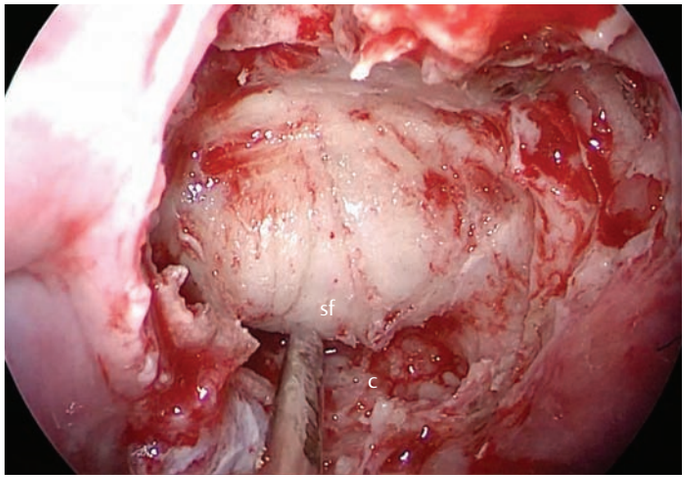

Fig. 8.11 Endoscopic view showing wide exposure of cavity and half. Sf, sellar floor; c, clinoid.

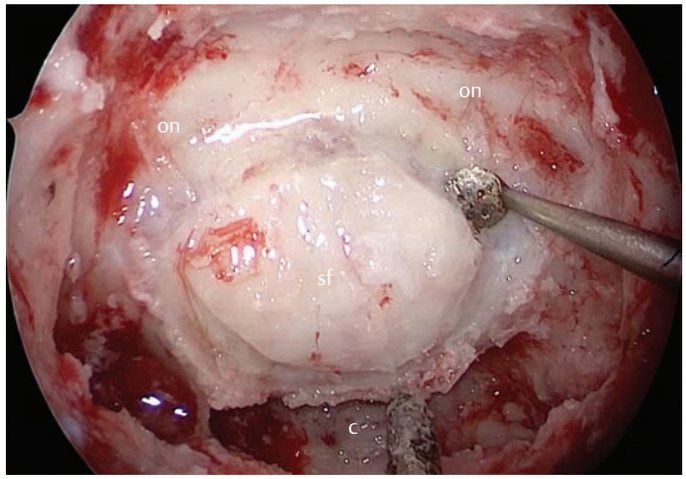

Fig. 8.12 Removing sellar floor bone after drilling it to eggshell thin. Sf, sellar floor; on, optic nerve; c, clinoid.

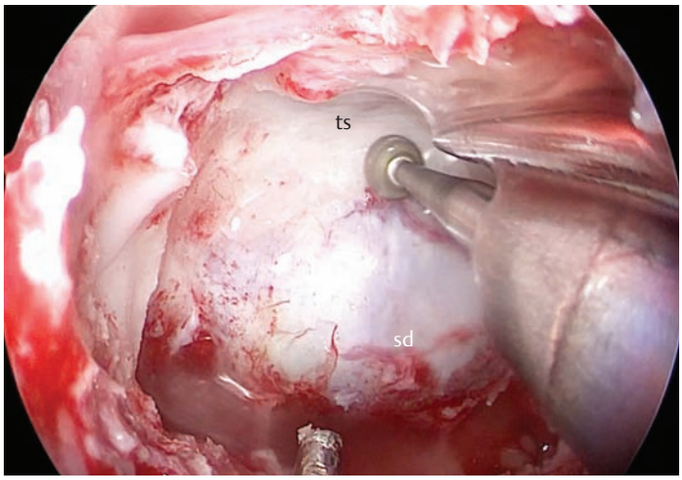

Fig. 8.13 Endoscopic view showing drilling of tubercular areatus. ts, tubercular sellae; sd, sellar dura.

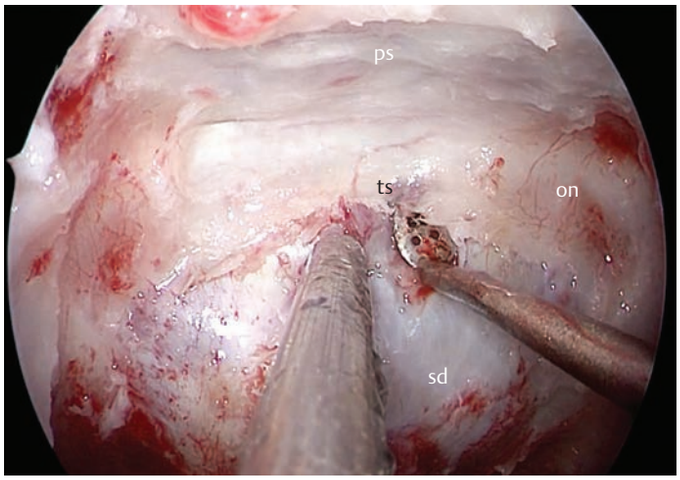

Fig. 8.14 Removing tubercular bone after drilling it to eggshell thin. PS, planum sphenoidale; ts, tubercular sellae.

tumor extent. Suprasellar notch or tuberculum sellae is described endoscopically as bounded superiorly by a line joining the two lateral opticocarotid recesses (LOCR), inferiorly just above superior margin of sella and lateral by parasellar internal carotid artery (ICA). LOCR is a triangular-shaped bony depression formed superiorly by the floor of optic canal, inferiorly by superior orbital fissure, and medially by lateral part of carotid eminence. Medial opticocarotid recess (MOCR) is important landmark in endoscopic approach to sella, parasellar, and suprasellar surgery.[8] Two horizontal incisions are made in the dura: one above and other below the superior intercavernous sinus (SICS) using Cappabianca knife. The SICS is then isolated; it can be clipped or cauterized and transected.

This region can be divided into four areas namely the suprachiasmatic region, the subchiasmatic region, the retrosellar area, and the ventricular region by two ideal planes, one passing along the inferior surface of the optic chiasm and the mammillary bodies and another passing via the posterior margin of chiasm and the dorsum sellae.[1,2]

Transplanum Approach

Posterior ethmoidal artery anteriorly and optic nerve laterally are boundaries of planum.

The osteotomies are made in planum in a triangular fashion using Karl Storz S III neurodrill with 4-mm diamond burr. First osteotomy is made at the base of the triangle just posterior to posterior ethmoidal artery and the two edges of the osteotomies above optic canal (**Fig. 8.15**). The triangular bone over the planum is then removed using Cottle's

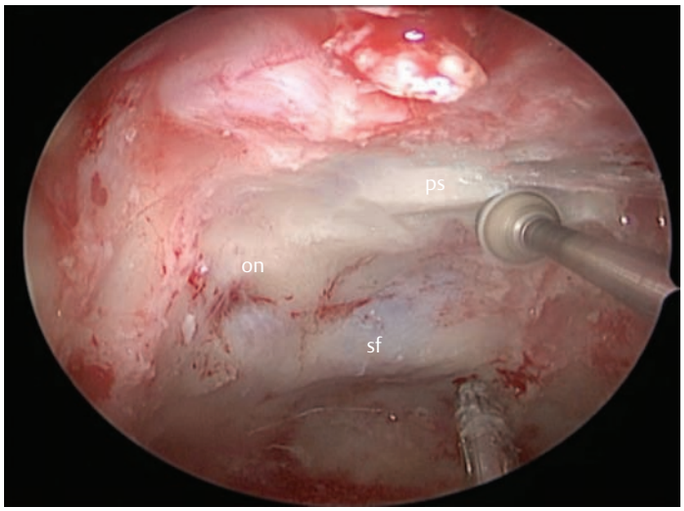

Fig. 8.15 Drilling planum sphenoidale. On, optic nerve, sf, sellar floor; PS, planum sphenoidale; white line triangle, area of drilling.

elevator. In combined transsellar transtubercular/transplanar approach, bone over the tuberculum and sella is also drilled (**Figs. 8.16 and 8.17**). The dura is incised with a Cappabianca knife with two horizontal incisions: one in the frontal dura and one in the sellar dura. The vertical incision is made over the SICS joining the two horizontal incisions. The SICS is clipped or coagulated before making the vertical incision, and the dura is retracted laterally. The optic nerve and optic chiasm are seen in the upper portion, the pituitary stalk is seen in the midline, and ICA can be visualized on both sides.

The downward slope of the PS and cribriform plate makes this approach difficult with a 0 degree scope. It can be difficult to advance straight instruments in this situation without

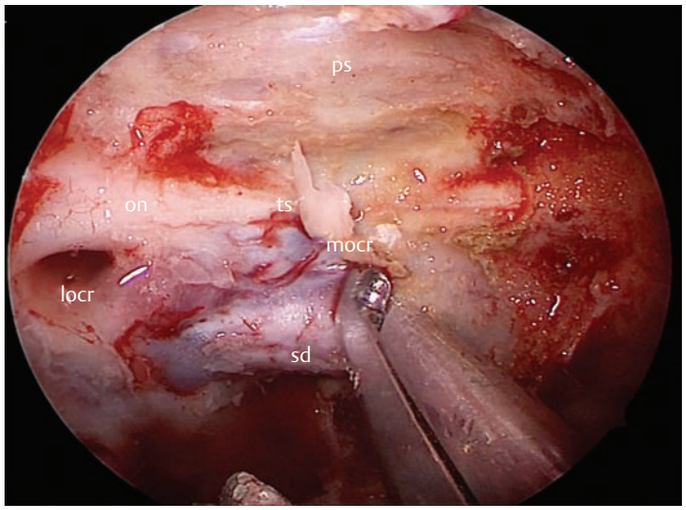

Fig. 8.16 Removing left medial opticocarotid recess (MOCR).

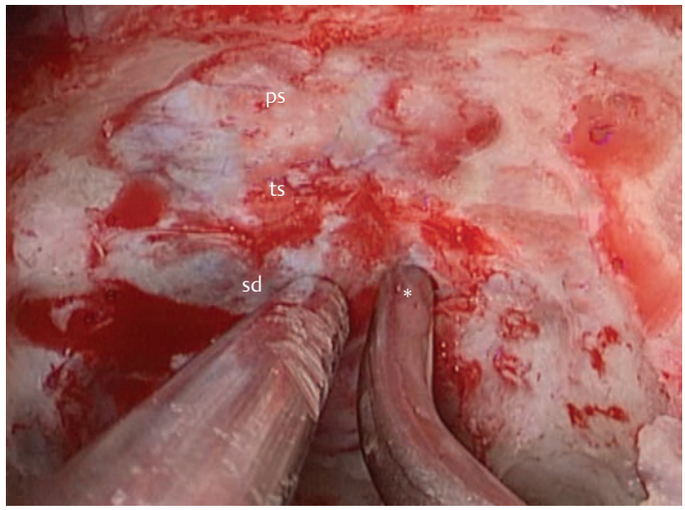

Fig. 8.17 Mapping of carotid after complete exposure of sellar suprasellar dura. Sd, sellar dura; PS, planum sphenoidale; ts, tubercular sellae; *, microvascular Doppler.

significant drilling of the cribriform plate or an angled drill can be used to drill planum. Visualization can be facilitated by performing bilateral posterior ethmoidectomies.

Pituitary Tumors

Pituitary adenomas comprise 10 to 15% of all intracranial tumors. Patients have characteristic endocrinological features of either hypopituitarism or hypersecretion of certain hormones.[9] The most definitive treatment for pituitary macroadenomas are surgical removal. Surgery can be performed via transsphenoidal or transcranial route.[10]

In this technologically advanced era, transsphenoidal approach is preferred over transcranial approach due to fewer surgical complications, pituitary gland injury, and early recovery from endocrinological as well as visual impairments.

Anatomical classification for pituitary macroadenomas is given by Hardy. Suprasellar extension of tumor is classified as follows[11]:

- **Type 0:** The tumor is entirely confined within the sella turcica.
- **Type A:** The suprasellar expansion bulges into the chiasmatic cistern but does not reach the floor of the anterior third ventricle.
- **Type B:** The tumor reaches the floor of the third ventricle, giving the image of an inverse cupula of the anterior recesses of the third ventricle.
- **Type C:** A voluminous suprasellar expansion bulges largely into the third ventricle up to the foramen of Monro.
- **Type D:** Rare aberrant expansions occur in temporal or frontal fossa.

Step-by-Step Approach to Sellar and Suprasellar Pituitary Tumors

Case 1: Pituitary Macroadenoma with Suprasellar Extension

A 45-year-old male who presented with complaints of diminishing vision. MRI depicted sellar and suprasellar tumor (**Fig. 8.18a, b**). Wide exposure of the sphenoid sinuses was done (**Fig. 8.18c**). Drilling was started over the tubercular area. Transsellar, transtubercular approach was done (**Fig. 8.18d**). Sellar dura was exposed (**Fig. 8.18e**). The endosteal layer of dura was incised using a Cappabianca knife and incision was extended with rotatable scissors (**Fig. 8.18f**). Endosteal layer was elevated in a "U"-shaped manner. Biopsy from the tumor part was taken. Tumor was removed with the two-suction tip technique (**Fig. 8.18g–i**). A tumor near cavernous part and suprasellar part was removed with curved suction tip with reduced power suction (**Fig. 8.18j, k**). No leak was identified in the diaphragmatic sellae region. (**Fig. 8.18**). Reconstruction in multilayer was carried out. See **Video 8.1**.

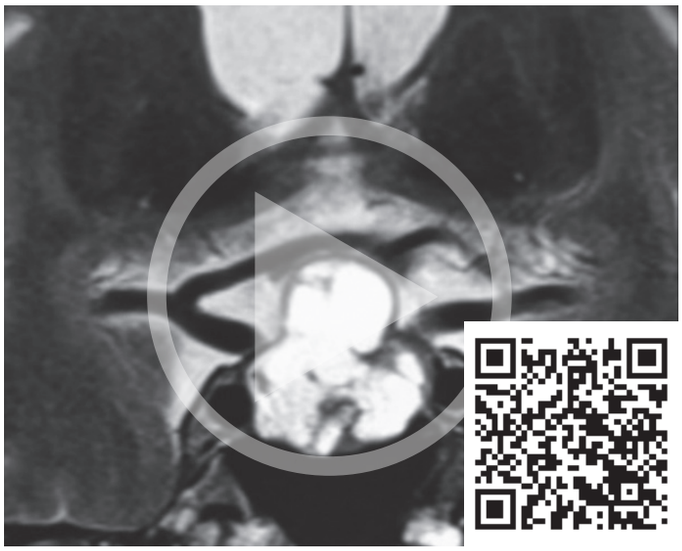

Video 8.1 Pituitary macroadenoma with suprasellar extension. https://www.thieme.de/de/q.htm?p=opn/cs/19/9/10104303-451d0d82

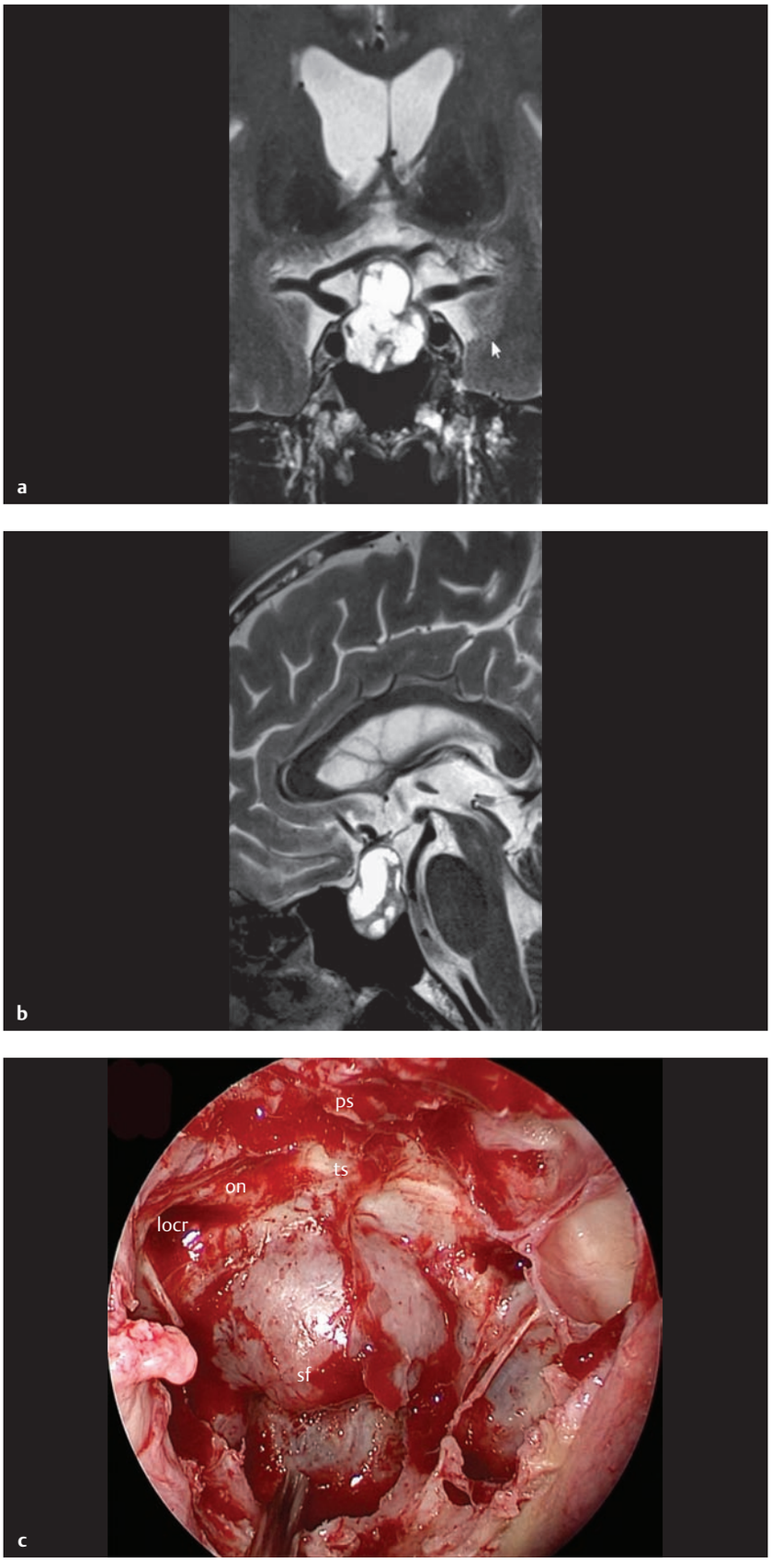

Fig. 8.18 **(a)** MRI coronal scan showing mass lesion in sellar and suprasellar parts. **(b)** MRI scan sagittal view showing sellar and suprasellar mass lesion. **(c)** Endoscopic view showing complete exposure of the sphenoid sinuses. Sf, sellar floor; on, optic nerve; ts, tubercular sellae; PS, planum sphenoidale; LOCR, lateral opticocarotid recess; c, clinoid.

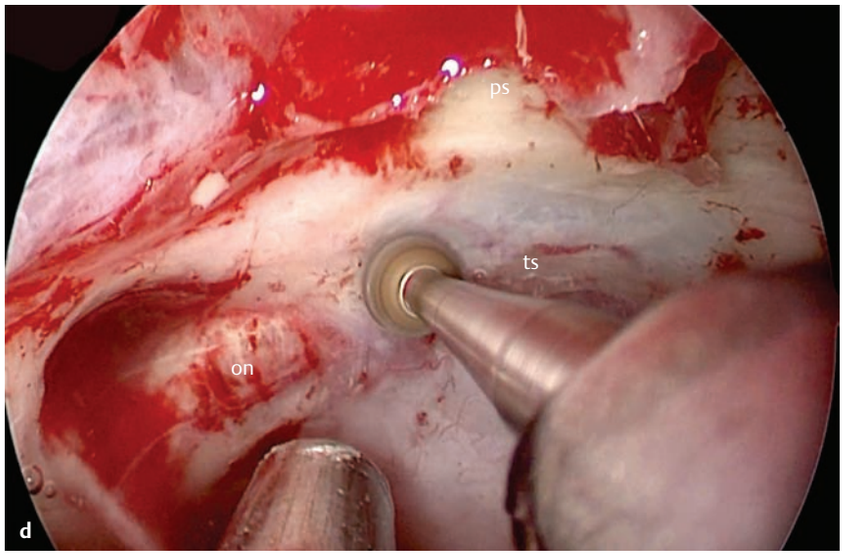

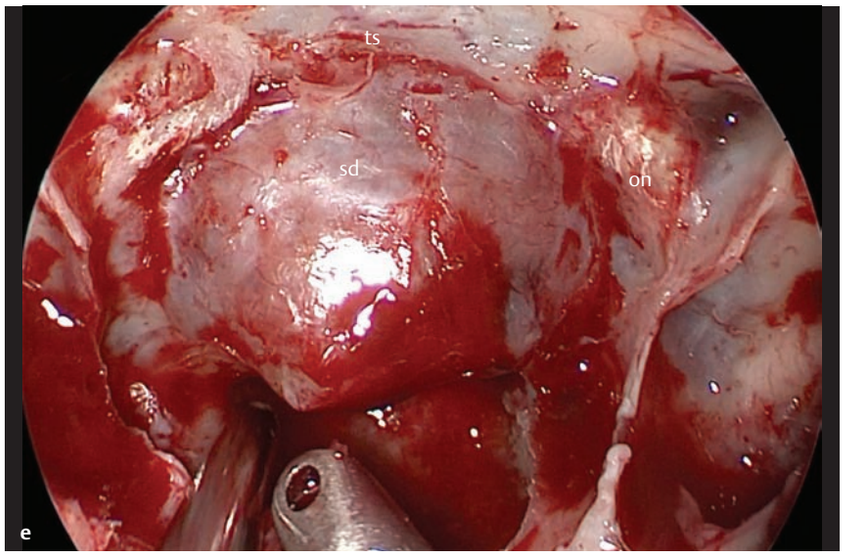

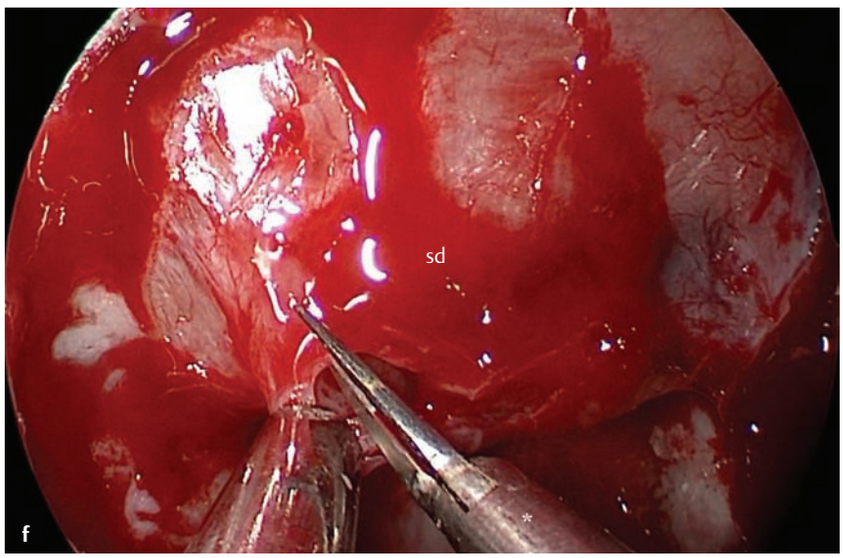

Fig. 8.18 **(d)** Endoscopic view showing drilling of the tubercular area. On, optic nerve; ts, tubercular sellae; PS, planum sphenoidale. **(e)** Endoscopic view showing exposure of the sellar dura after removal of sellar floor bone. On, optic nerve; ts, tubercular sellae; sd, sellar dura; c, clinoid. **(f)** Endoscopic view showing putting incision over sellar dura. Sd, sellar dura.

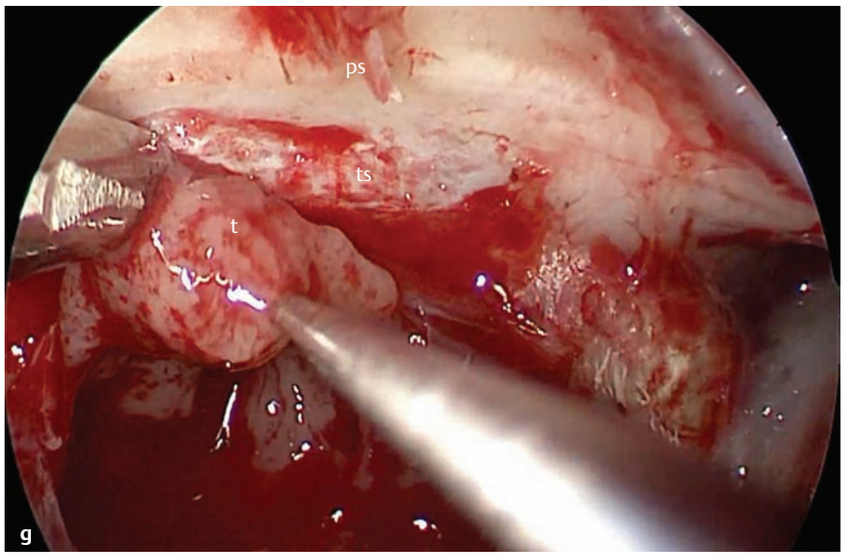

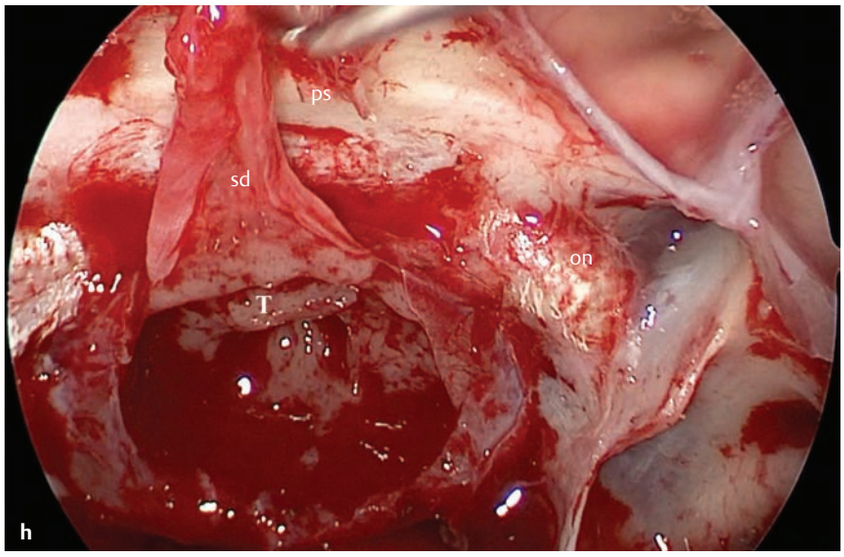

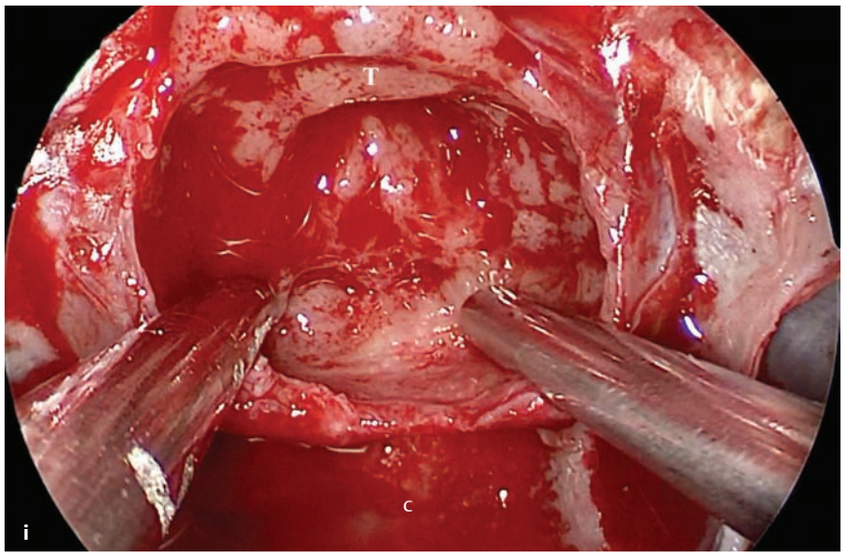

Fig. 8.18 **(g)** Endoscopic view showing removal of the sellar part of the tumor with two-suction tips. T, tumor; ts, tubercular sellae; PS, planum sphenoidale. **(h)** Endoscopic view showing remaining part of tumor in suprasellar part and near cavernous sinus. T, tumor; sd, sellar dura; PS, planum sphenoidale; on, optic nerve. **(i)** Endoscopic view showing sellar cavity after tumor removal, suprasellar part of the tumor can be seen. c, clinoid.

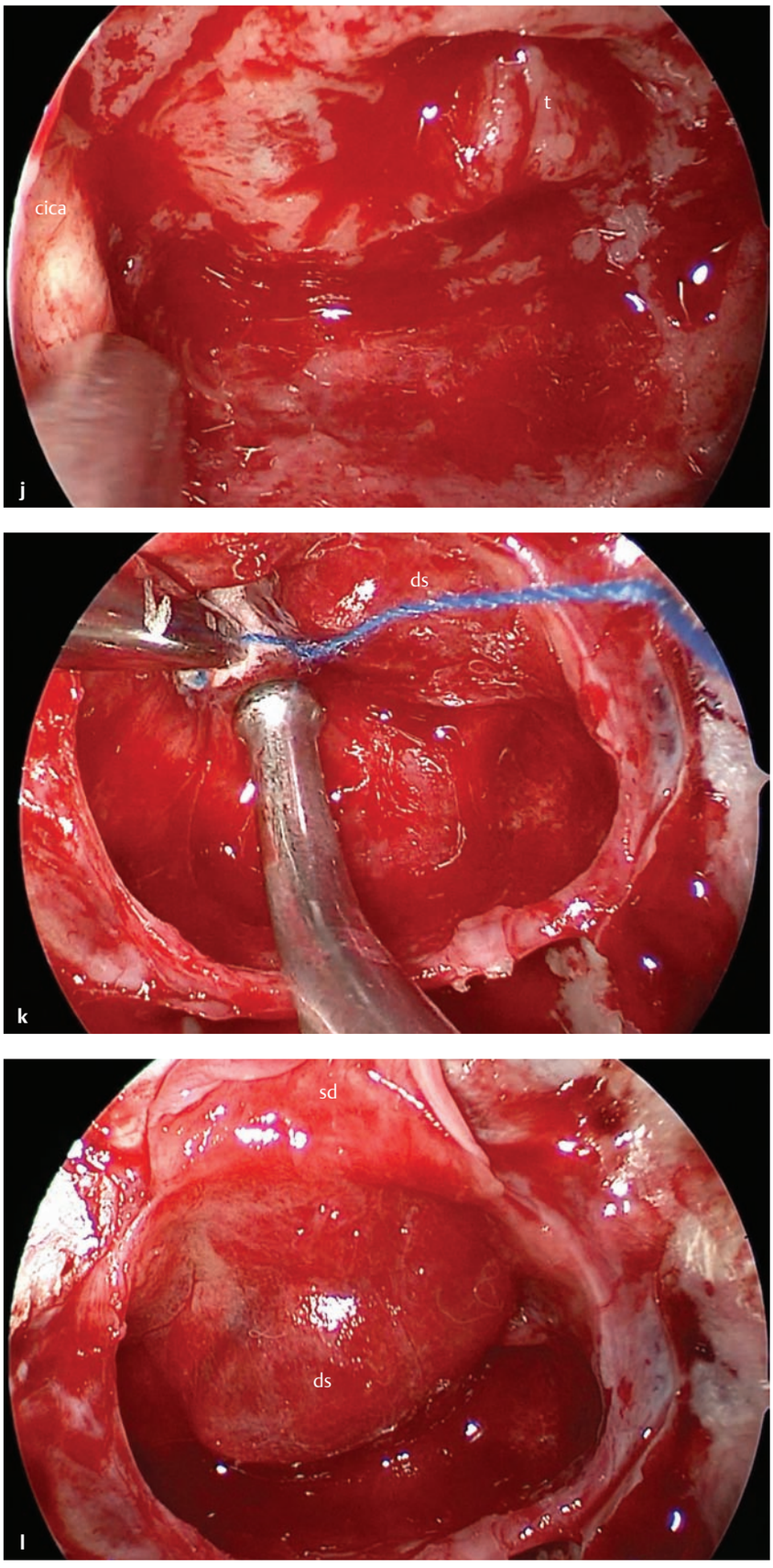

Fig. 8.18 **(j)** Endoscopic view showing right cavernous internal carotid artery after tumor removal from the right cavernous sinus. T, tumor; cica, cavernous internal carotid artery. **(k)** Endoscopic view showing removal of the tumor from the suprasellar part with curved suction tip. T, tumor; ds, diaphragma sellae. **(l)** After complete removal of tumor sellar cavity. Ds, diaphragma sellae; mwcs-l, medial wall of left cavernous sinus.

Case 2: Pituitary Macroadenoma Fibrous Type

A 35-year-old woman presented with complaints of headache and bitemporal hemianopia. MRI brain showed a huge sellar, suprasellar mass with compression of bilateral optic nerve (**Fig. 8.19a**). Wide exposure of sphenoid sinuses was done and intersphenoidal septum was removed (**Fig. 8.19b**). Sellar dura was exposed after removing the sellar floor bone (**Fig. 8.19c**). Tubercular sellae bone was removed after drilling it to eggshell thin and bilateral MOCR were removed (**Fig. 8.19d**). Tumor was visualized in sellar region after elevating sellar dura flap (**Fig. 8.19e**). Suckable tumor was removed with two-suction technique (**Fig. 8.19f**). Tumor from right cavernous sinus was removed with curved suction tip (**Fig. 8.19g**). The fibrous part of tumor was dissected from right cavernous sinus (**Fig. 8.19h**). The tumor over left cavernous sinus was dissected with the help of dissection plane between cavernous sinus, cavernous ICA, and tumor (**Fig. 8.19i**). Dissection of the suprasellar part of tumor was carried out with micro elevator (**Fig. 8.19j**). Huge suprasellar part of tumor was removed with good dissection plane (**Figs. 8.19k and 8.19l**). Last piece of tumor was removed after lifting the diaphragma sellae (**Fig. 8.19m**). After complete removal of tumor, bulged out diaphragma sellae can be seen but there was no leak (**Fig. 8.19n**). Reconstruction was carried out with fat, Surgicel, and nasoseptal flap (**Fig. 8.19o**). See **Video 8.2**.

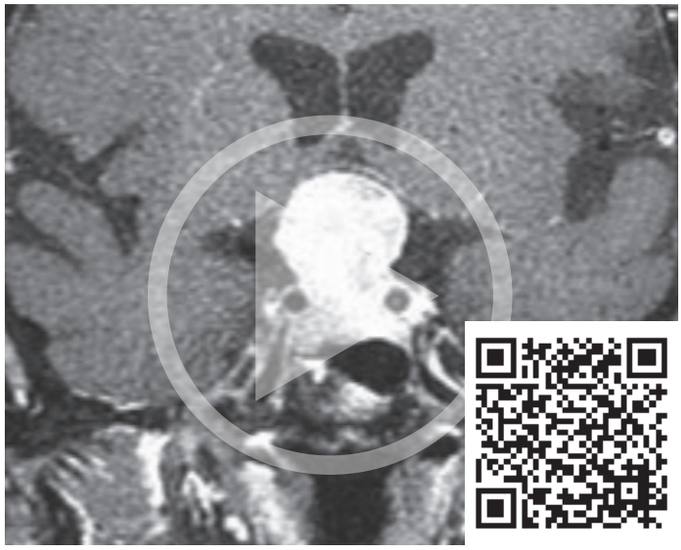

Video 8.2 Pituitary adenoma: Fibrous type. https://www.thieme.de/de/q.htm?p=opn/cs/19/9/10104304-8c61d171

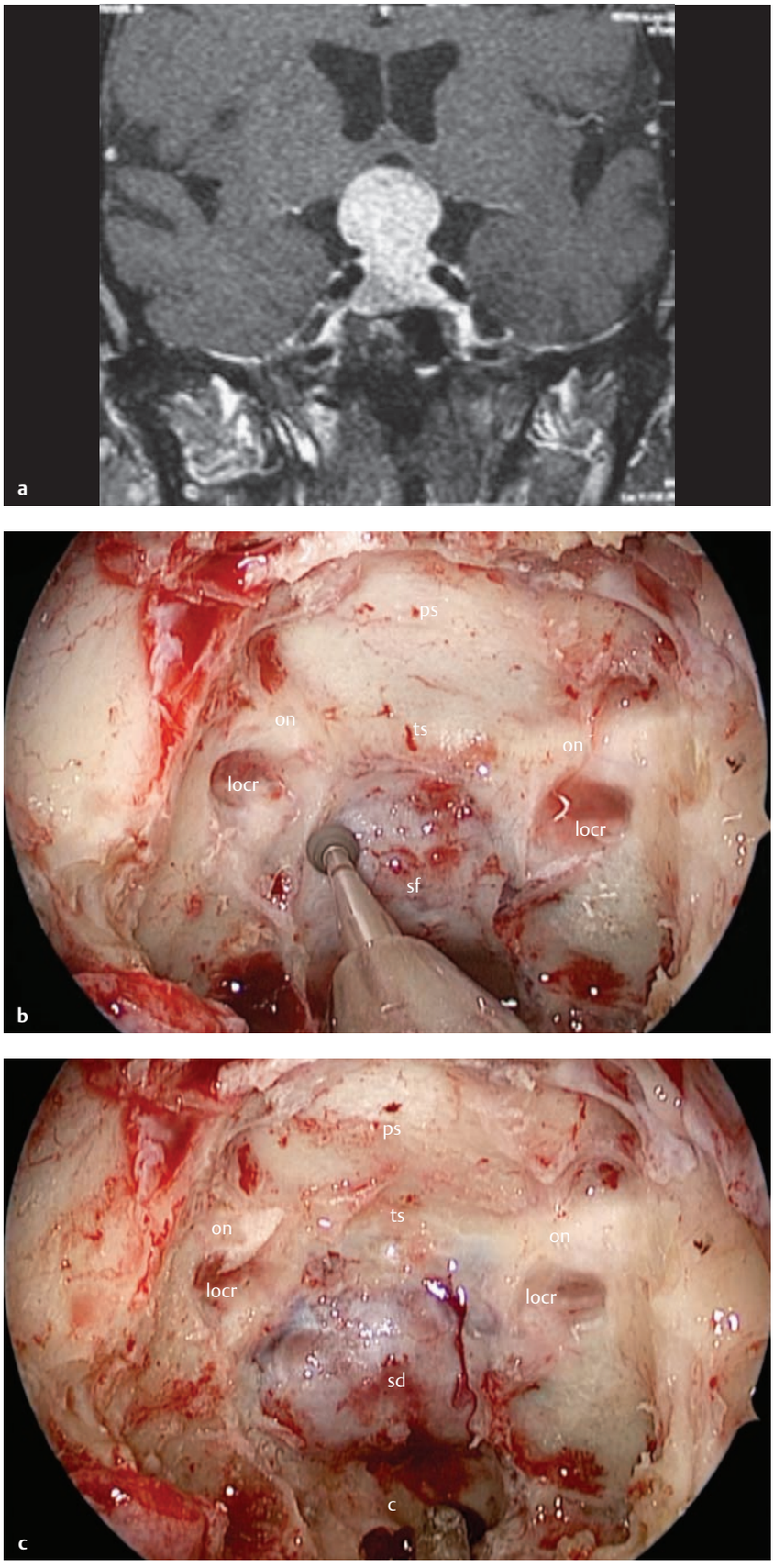

Fig. 8.19 **(a)** MRI coronal cut showing sellar suprasellar mass lesion. **(b)** Endoscopic view showing wide exposure of sphenoid sinus and drilling of sellar floor bone. PS, planum sphenoidale; sf, sellar floor; ts, tubercular sellae; on, optic nerve; LOCR, lateral opticocarotid recess. **(c)** Endoscopic view showing exposure of sellar dura after removal of sellar floor bone. C, clinoid; ts, tubercular sellae; sd, sellar dura; on, optic nerve; PS, planum sphenoidale; LOCR, lateral opticocarotid recess.

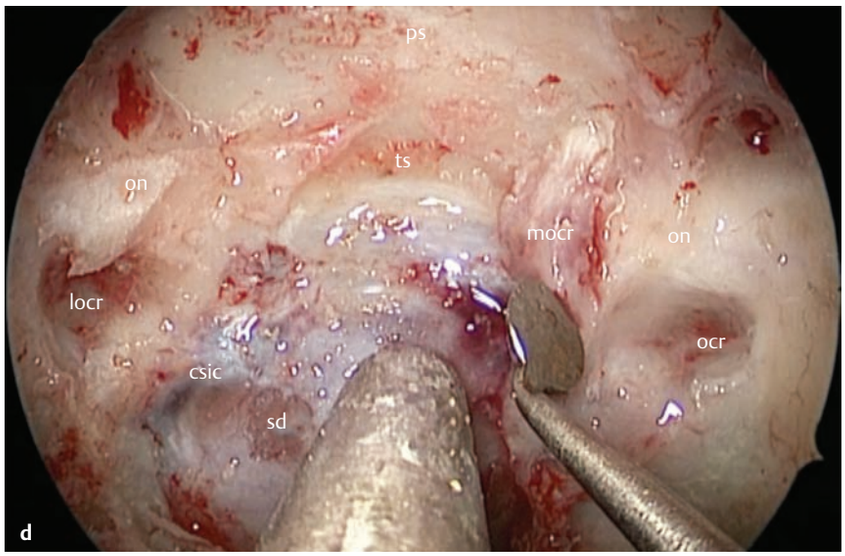

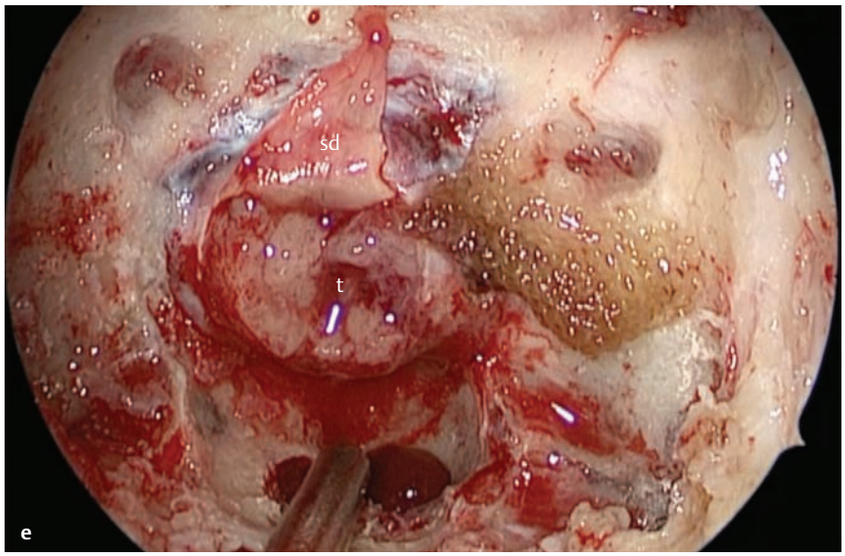

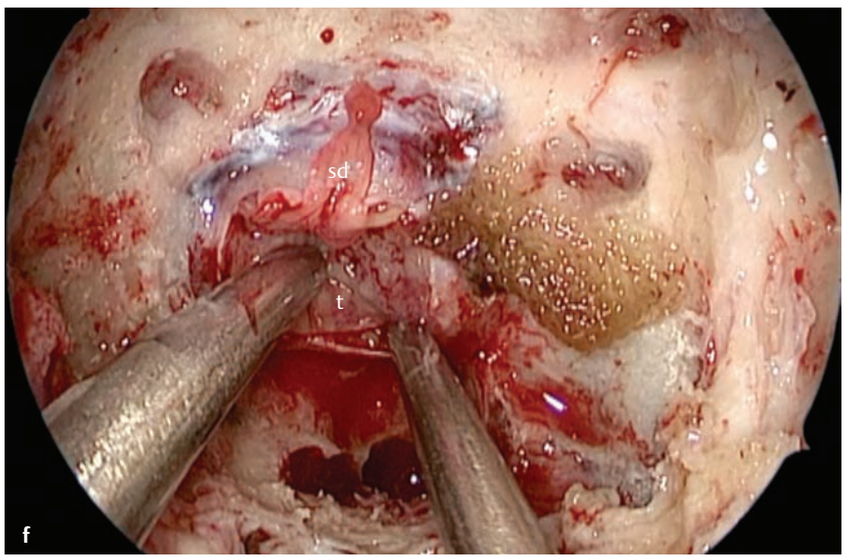

Fig. 8.19 **(d)** Endoscopic view showing removal of left MOCR. Ts, tubercular sellae; sd, sellar dura; on, optic nerve; PS, planum sphenoidale; LOCR, lateral opticocarotid recess; CSIC, cavernous sinus internal carotid artery. **(e)** Endoscopic view showing elevation of sellar dura. Sd, sellar dura; t, tumor. **(f)** Endoscopic view showing removal of suckable tumor with two-suction technique. Sd, sellar dura; t, tumor.

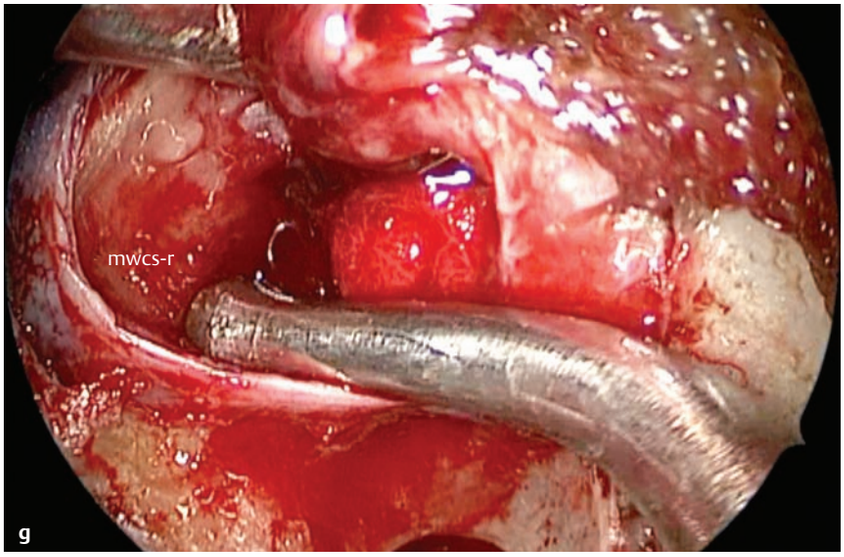

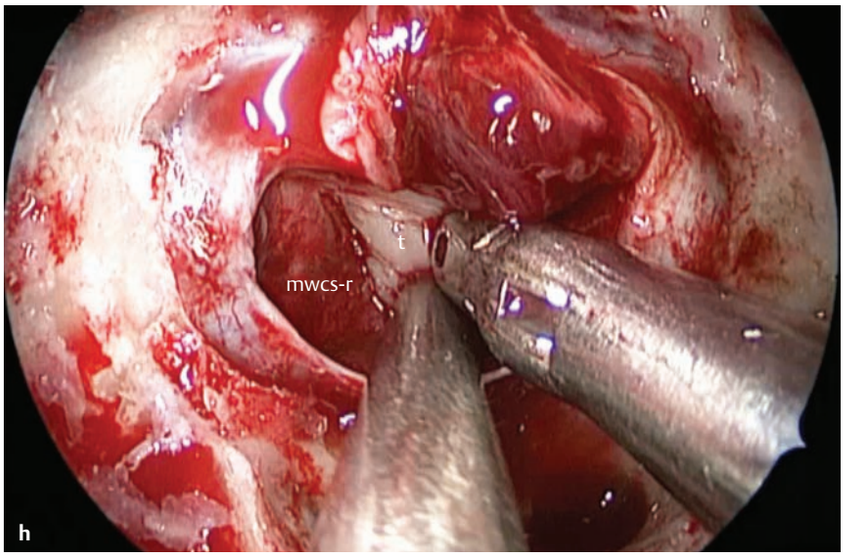

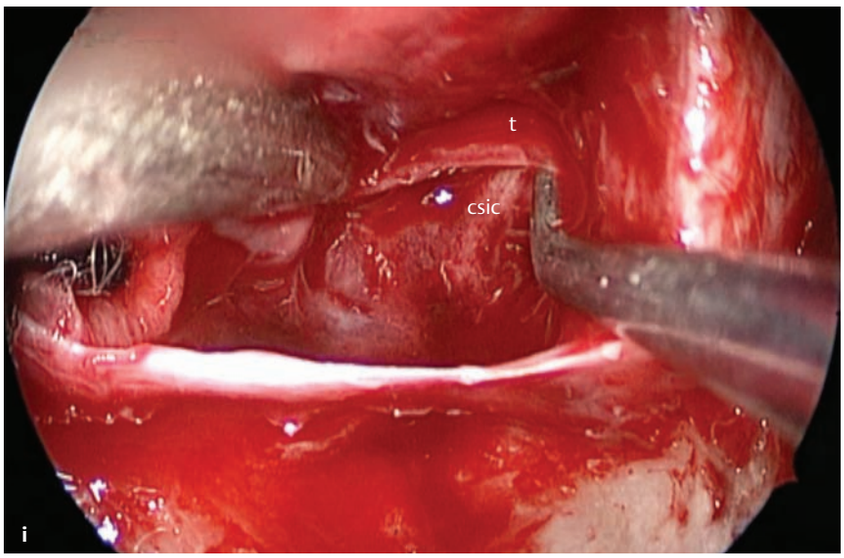

Fig. 8.19 **(g)** Endoscopic view showing removal of tumor from the right cavernous sinus. Mwcs-r, medial wall of right cavernous sinus. **(h)** Endoscopic view showing removing fibrous part of tumor after getting good plane. T, tumor; mwcs-r, medial wall of right cavernous sinus. **(i)** Endoscopic view showing dissection of tumor from the left cavernous sinus. T, tumor; CSIC, cavernous sinus internal carotid artery.

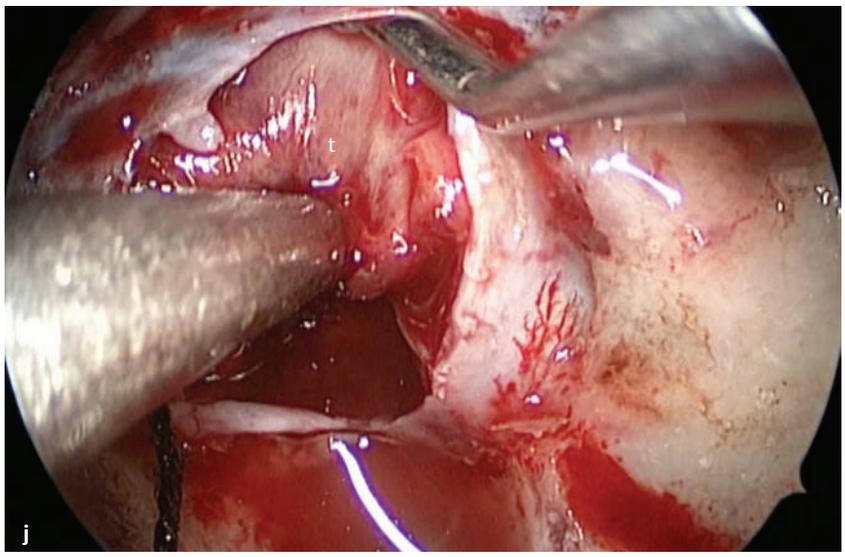

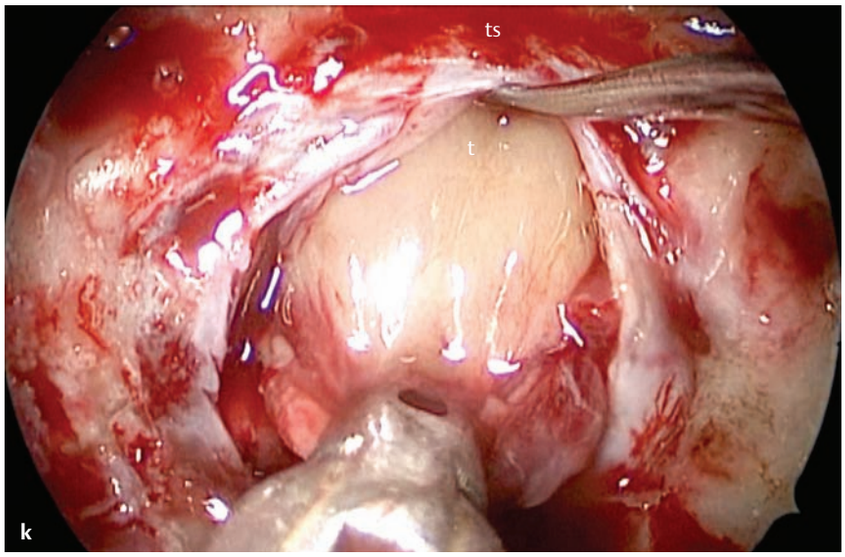

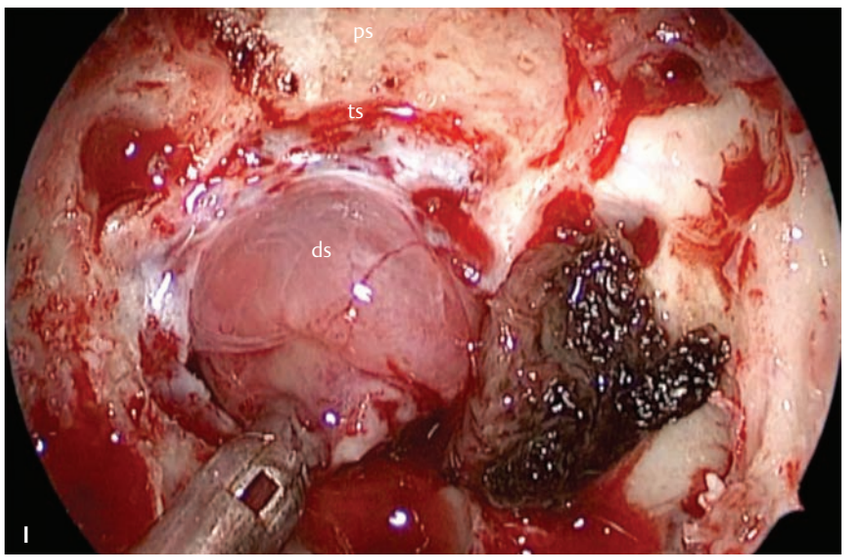

Fig. 8.19 **(j)** Endoscopic view showing dissection of the tumor from the suprasellar region. T, tumor. **(k)** Endoscopic view showing dissection of suprasellar fibrous part of the tumor after getting good plane. T, tumor; ts, tubercular sellae. **(l)** Endoscopic view showing dissection of last bit of tumor from the diaphragma sellae. Ds, diaphragma sellae; ts, tubercular sellae; PS, planum sphenoidale.

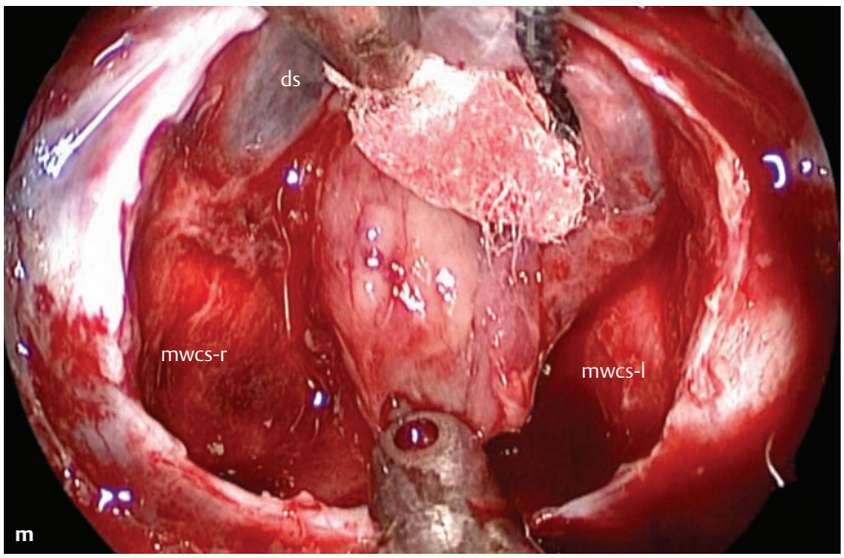

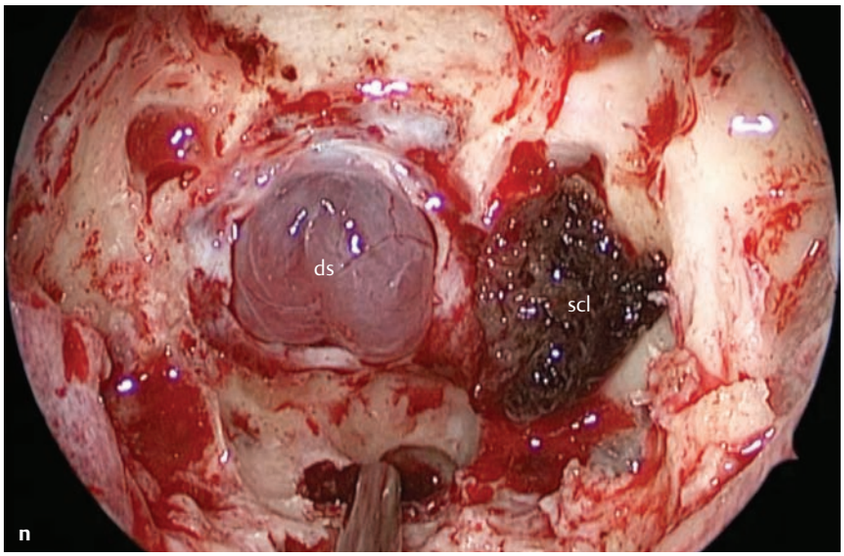

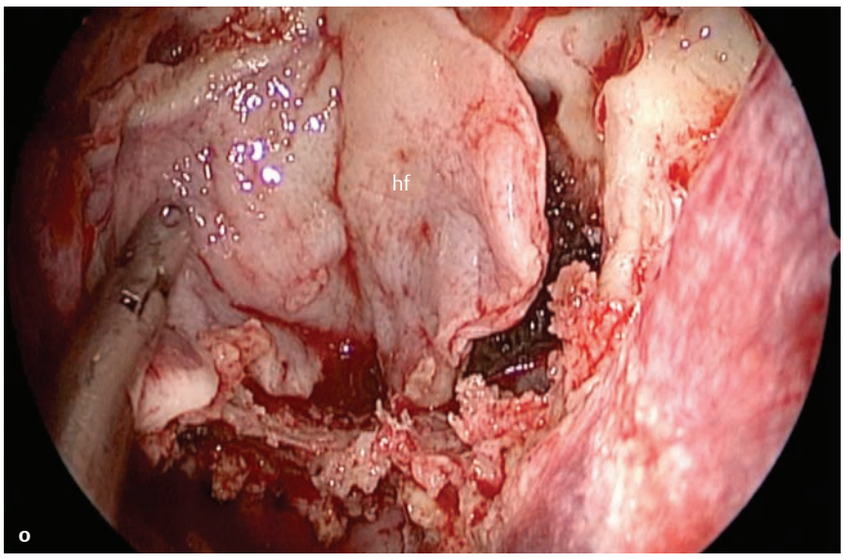

Fig. 8.19 **(m)** Endoscopic view showing tumor removal after elevating diaphragma sellae. Ds, diaphragma sellae; t, tumor; mwcs-r, medial wall of right cavernous sinus; mwcs-l, medial wall of left cavernous sinus. **(n)** Endoscopic view showing diaphragma sellae bulge out and no csf leak. Ds, diaphragma sellae; scl, Surgicel. **(o)** Endoscopic view showing reconstruction with naso septal flap. Hf, Hadad flap.

Case 3: Pituitary Macroadenoma with Suprasellar Extension

A 28-year-old male patient presented with bitemporal hemianopia. MRI scan of brain shows a huge sellar suprasellar mass compressing bilateral optic nerve (**Fig. 8.20a, b**). Wide exposure of sphenoid sinuses was done for cavity and a half approach and drilling of sellar bone was initiated (**Fig. 8.20c**). Sellar floor bone was removed (**Fig. 8.20d**). Bone over bilateral cavernous carotid artery was removed (**Fig. 8.20e**). Bone over tubercular sellae and PS was removed and extended exposure of sellar, tubercular, and PS dura was done (**Fig. 8.20f**). Bilateral MOCR was removed after drilling it to eggshell thin (**Fig. 8.20g**). Horizontal incision over PS dura was kept just above SICS (**Fig. 8.20h**). Dural flap of planar dura was elevated after making two vertical incisions (**Fig. 8.20i**). The sellar dura flap was also elevated after making an incision with Cappabianca knife and Kassam's rotatable scissors (**Fig. 8.20j**). Sellar part of tumor was removed with two-suction technique (**Fig. 8.20k**). Tumor from bilateral cavernous sinuses was removed with curved suction tip (**Fig. 8.20l**). Suprasellar part of tumor was seen with help of angled telescope (**Fig. 8.20m**). Sellar and suprasellar exposure was combined after coagulating SICS with Kassam's bipolar cautery (**Fig. 8.20n**). Suprasellar part of tumor dissection was carried out with with two-suction technique. (**Fig. 8.20o**). Anterior cerebral circulation, ICA, and optic nerve were visualized in suprasellar cistern (**Fig. 8.20p**). Last piece of suprasellar tumor was removed with curved suction tip (**Fig. 8.20q**). After complete removal of tumor, sellar cavity and suprachiasmatic cistern were seen (**Fig. 8.20r**). Reconstruction was done in multilayer with fat, Surgicel, and nasoseptal flap (**Fig. 8.20s**). See **Video 8.3**.

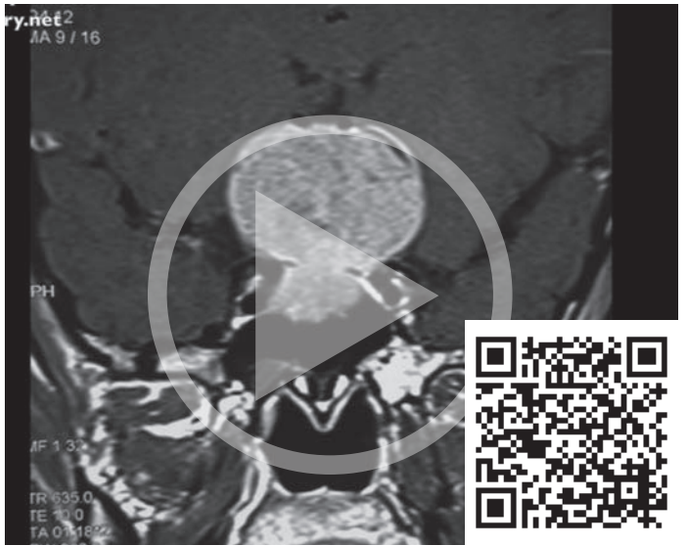

Video 8.3 Pituitary macroadenoma with suprasellar extension. https://www.thieme.de/de/q.htm?p=opn/cs/19/9/10104305-b6a6377c

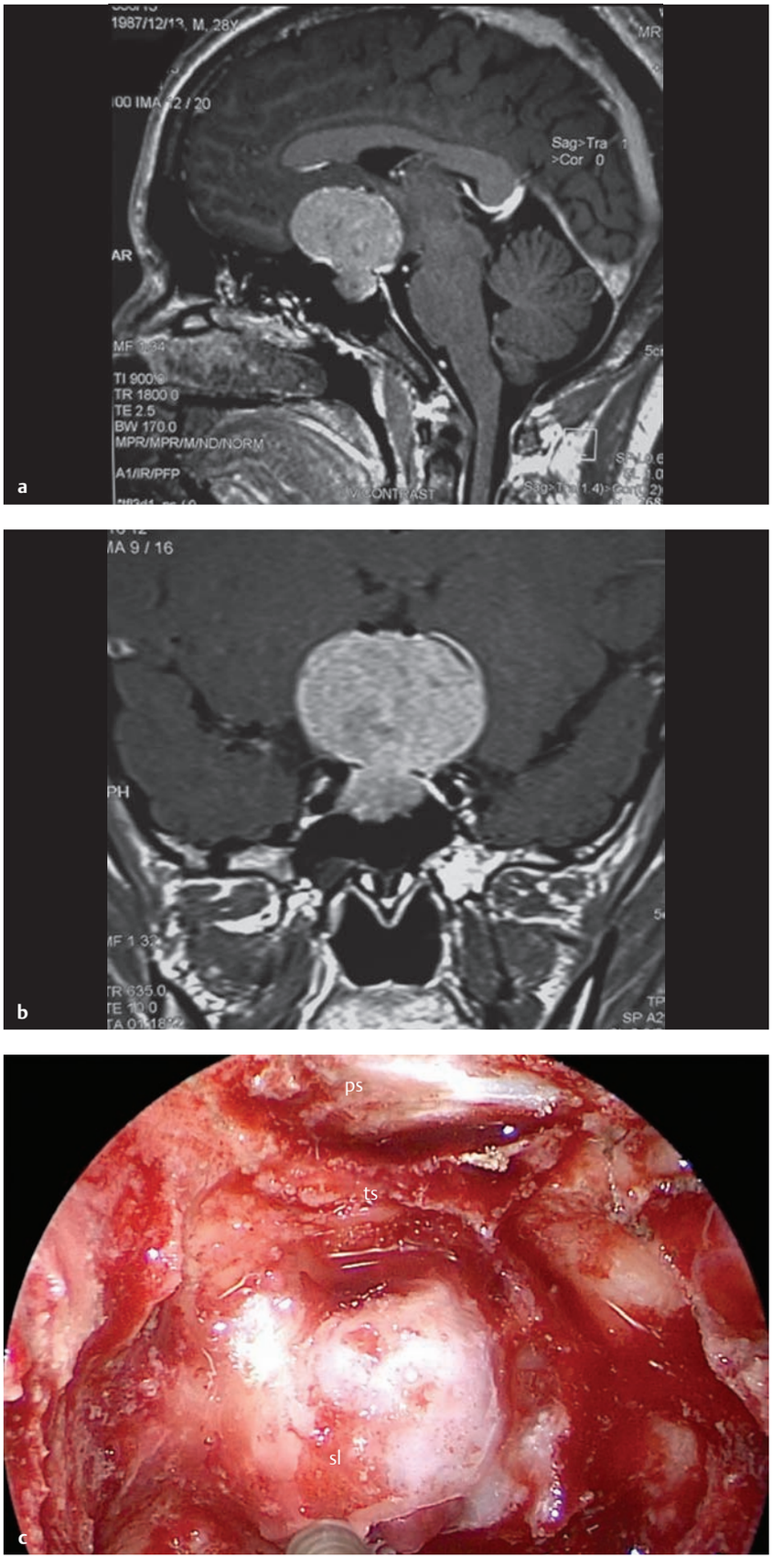

Fig. 8.20 **(a)** MRI sagittal cut showing huge mass lesion in sellar- suprasellar region. **(b)** MRI coronal cut showing huge mass lesion in sellar and suprasellar region compressing optic nerve. **(c)** Endoscopic view showing drilling of sellar floor bone after complete exposure of sphenoid sinuses. Sf, sellar floor; PS, planum sphenoidale; ts, tubercular sellae.

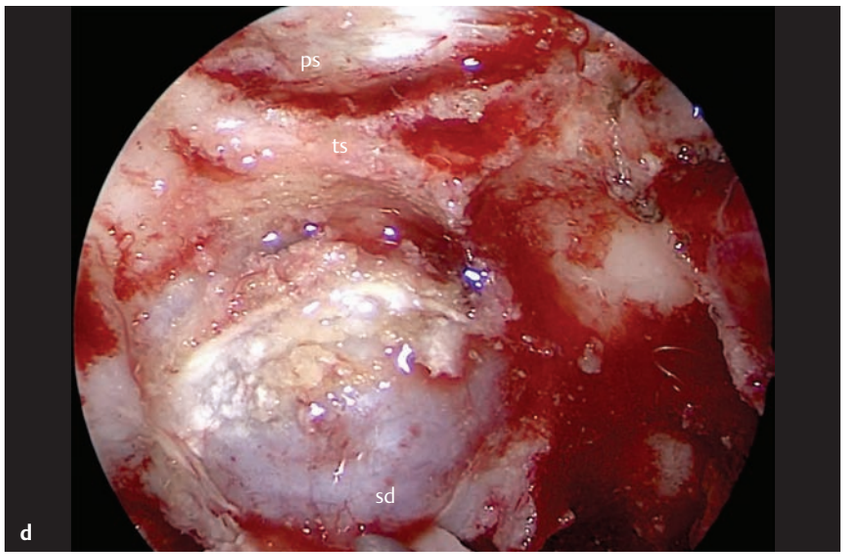

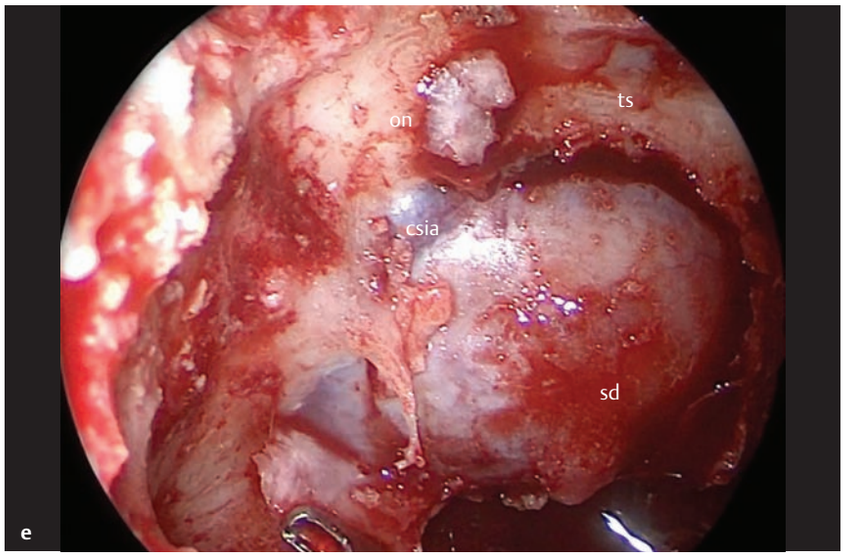

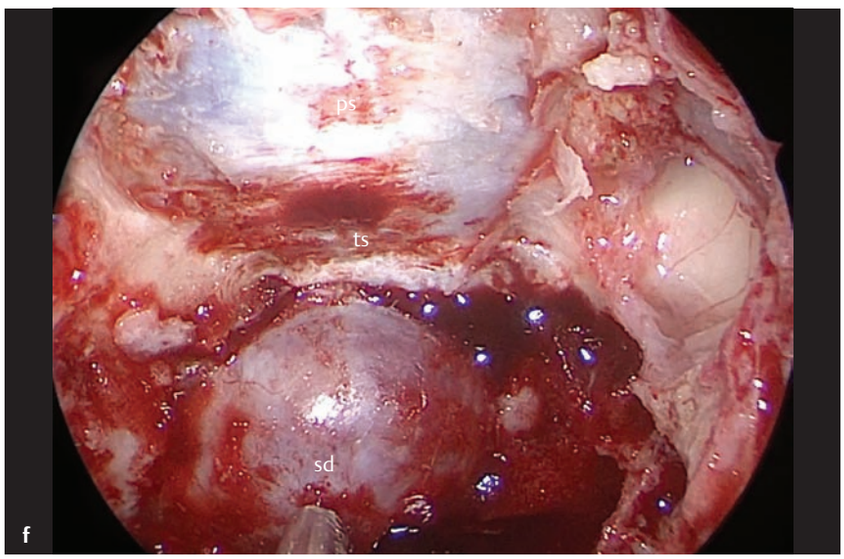

Fig. 8.20 **(d)** Endoscopic view showing elevating sellar floor bone after drilling it to eggshell thin. Sd, sellar dura; ts, tubercular sellae; PS, planum sphenoidale. **(e)** Removing bove over right cavernous internal carotid artery. Sd, sellar dura; on, optic nerve; CICA, cavernous internal carotid artery; ts, tubercular sellae. **(f)** Endoscopic view showing complete exposure of sellar and supra-sellar dura. PS, planum sphenoidale; ts, tubercular sellae; sd, sellar dura.

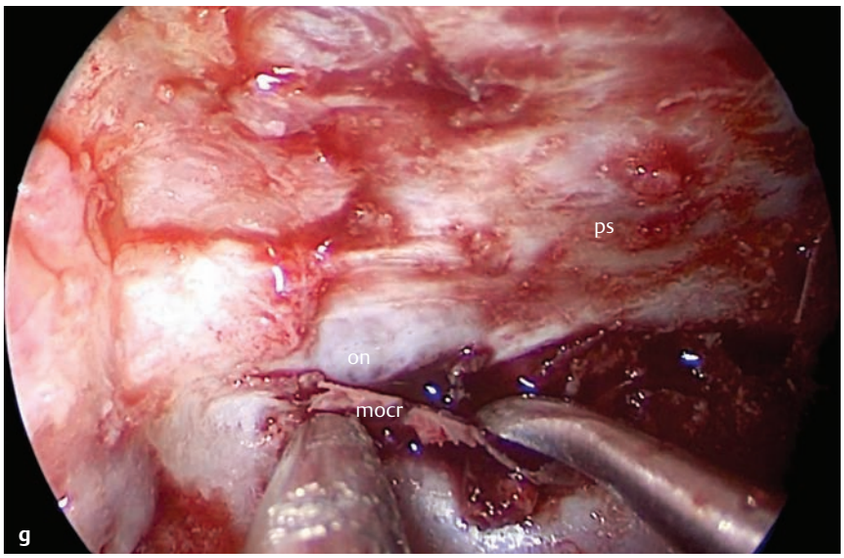

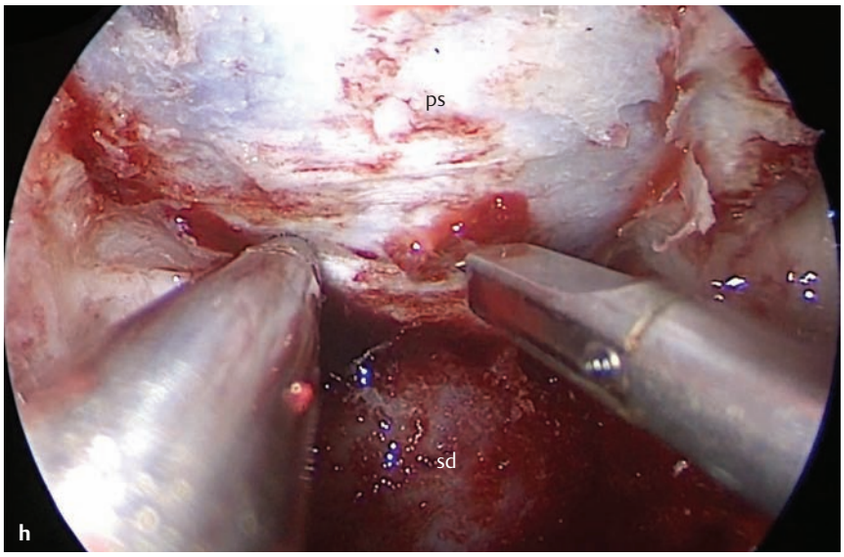

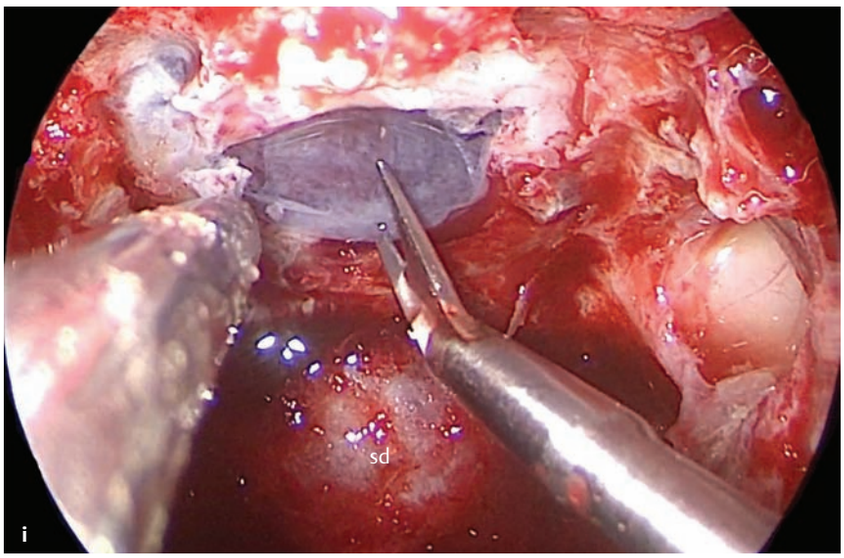

Fig. 8.20 **(g)** Endoscopic view showing removal of right MOCR. Sd, sellar dura; PS, planum sphenoidale; on, optic nerve; MOCR, medial opticocarotid recess. **(h)** Endoscopic view showing keeping incision over planum dura just above superior intersphenoidal sinus. Sd, sellar dura; PS, planum sphenoidale. **(i)** Elevation of U-shapped planum dura flap. Sd, sellar dura; *, dural flap.

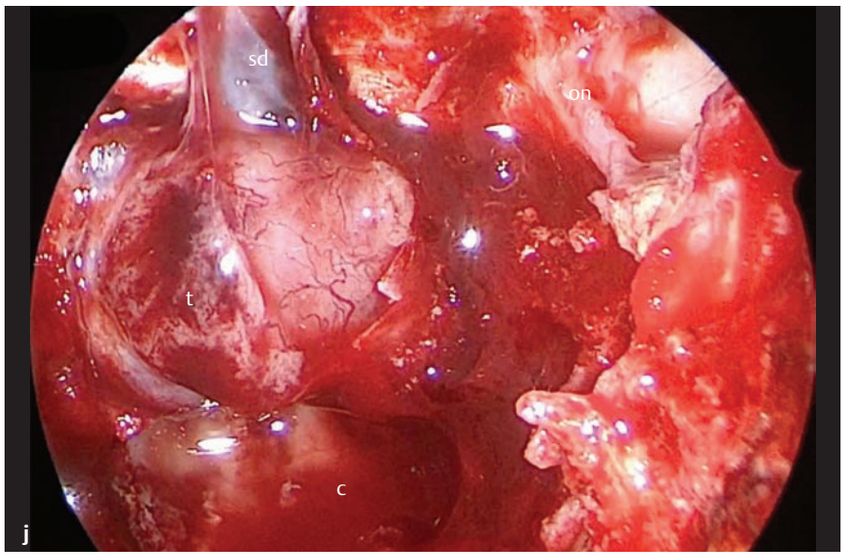

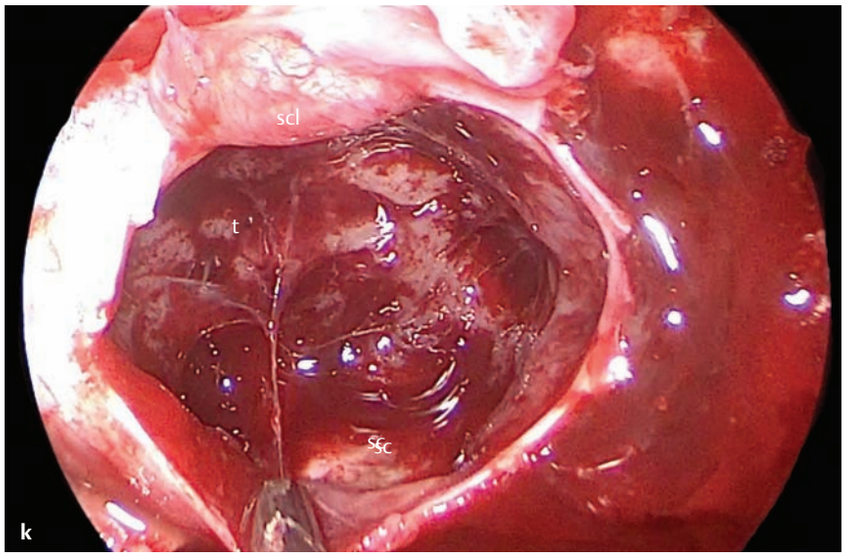

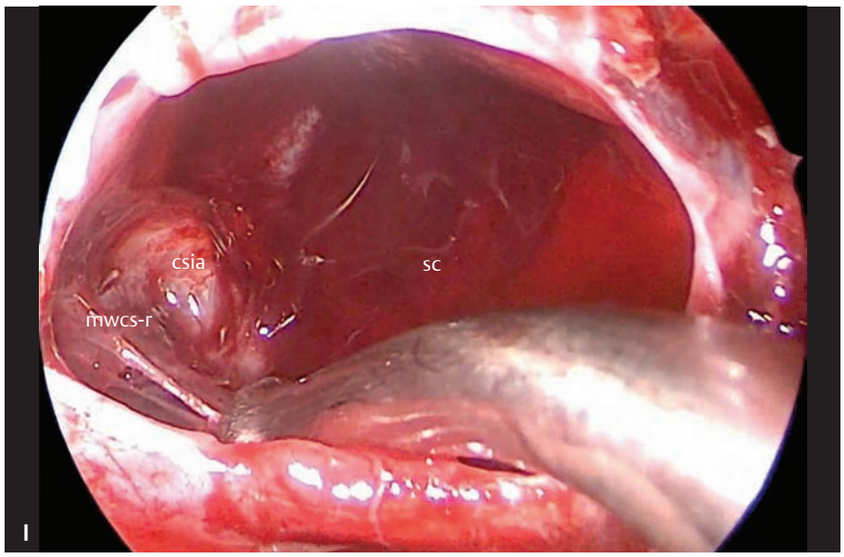

Fig. 8.20 **(j)** Endoscopic view showing elevation of sellar dural flap. Sd, sellar dura; t, tumor; c, clinoid; on, optic nerve. **(k)** Endoscopic view showing removal of sellar part of tumor with two-suction technique. Sc, sellar cavity; sd, sellar dura; t, tumor. **(l)** Endoscopic view showing removal of tumor from right cavernous sinus. Sc, sellar cavity; mwcs-r, medial wall of right cavernous sinus; CICA, cavernous internal carotid artery.

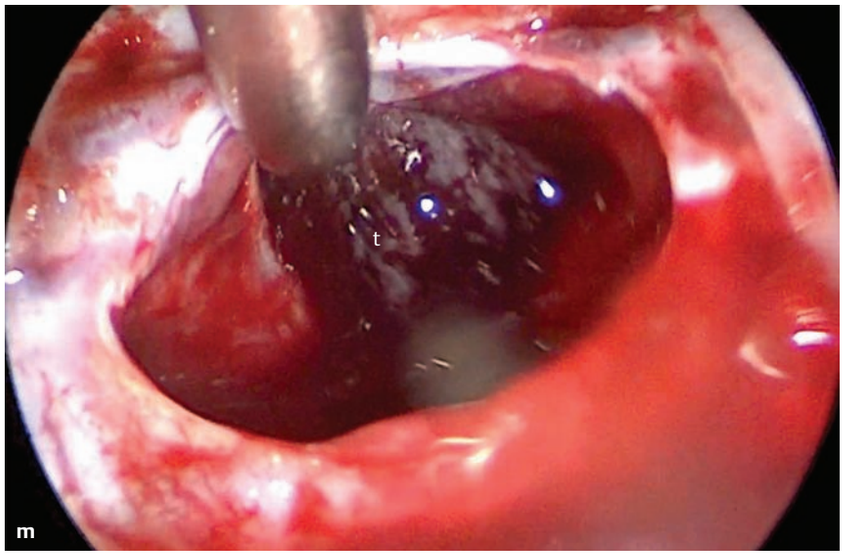

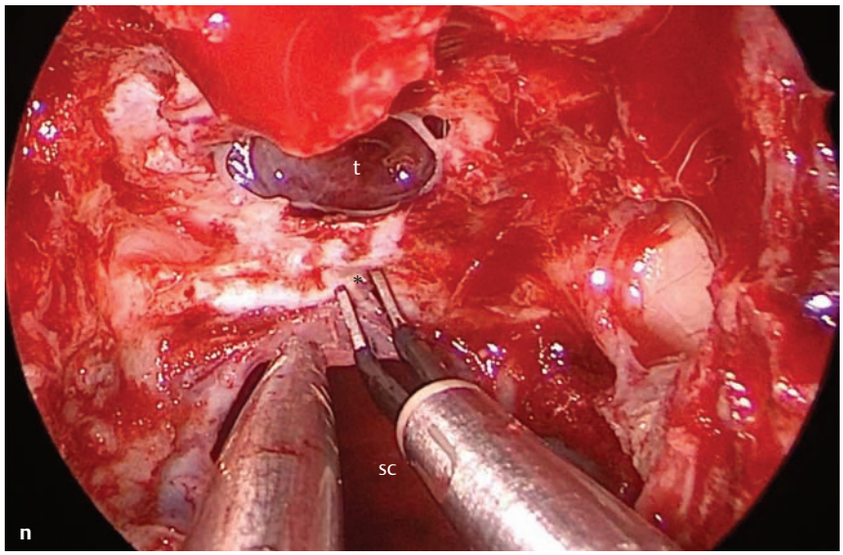

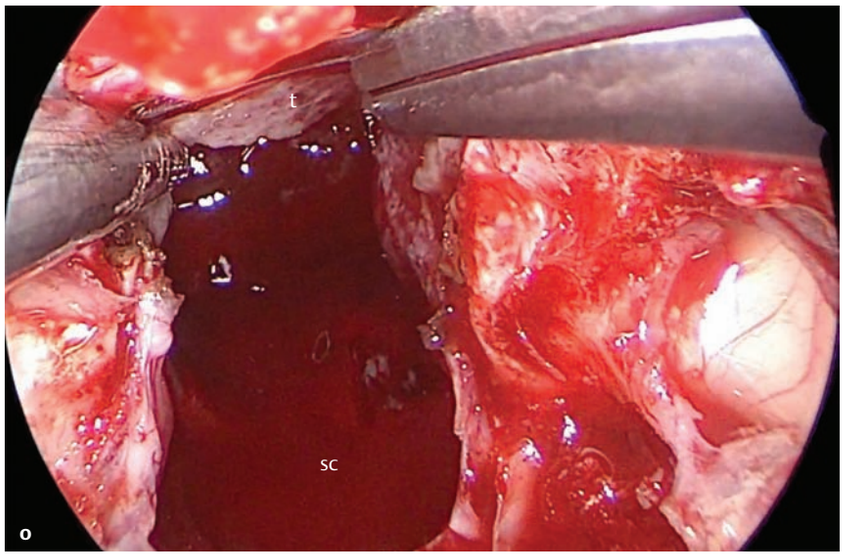

Fig. 8.20 **(m)** endoscopic view with 45 degree angled telescope showing tumor in the suprasellar region. T, tumor. **(n)** Endoscopic view showing cauterization of superior intercavernous sinus to extend the exposure. T, tumor; sc, sellar cavity. **(o)** Endoscopic view showing exposure is exposed to suprasellar part. Sc, sellar cavity; t, tumor.

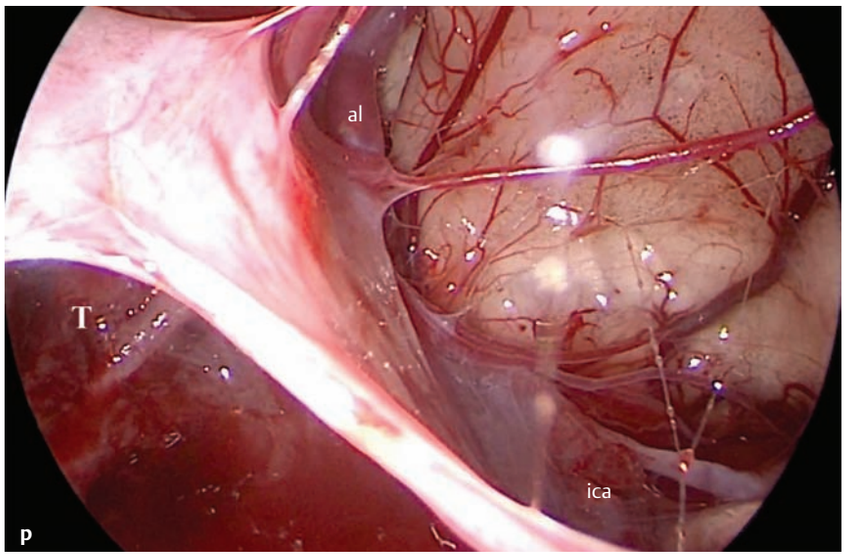

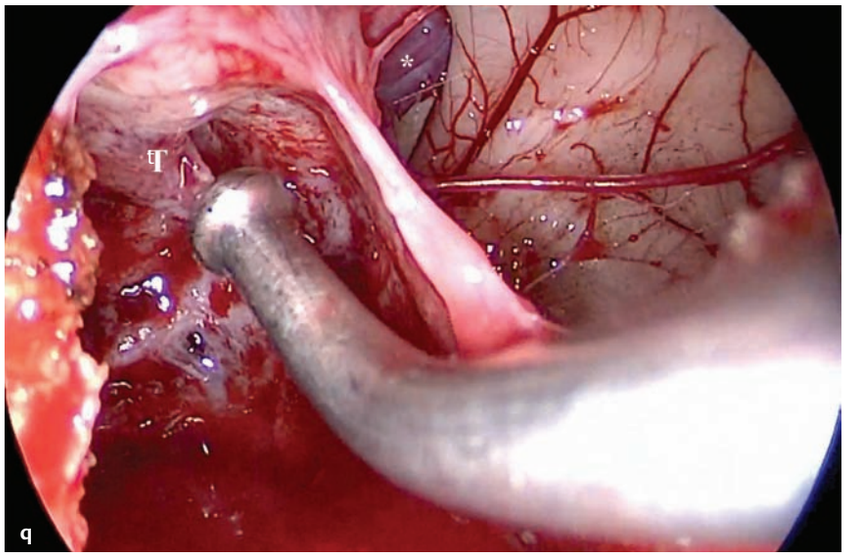

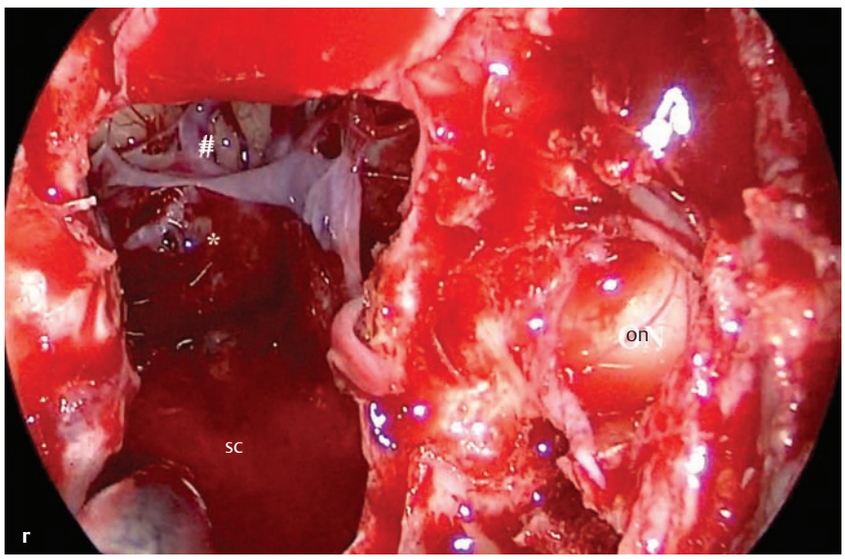

Fig. 8.20 **(p)** Endoscopic view showing left anterior cerebral artery, left ICA and left optic nerve. ICA, internal carotid artery; a1, a1 segment of left anterior cerebral artery. **(q)** Endoscopic view showing removal of tumor from the suprasellar region. T, tumor. **(r)** Endoscopic view showing sellar cavity and suprasellar cistern after complete removal of tumor. Sc, sellar cavity. #, anterior cerebral artery.

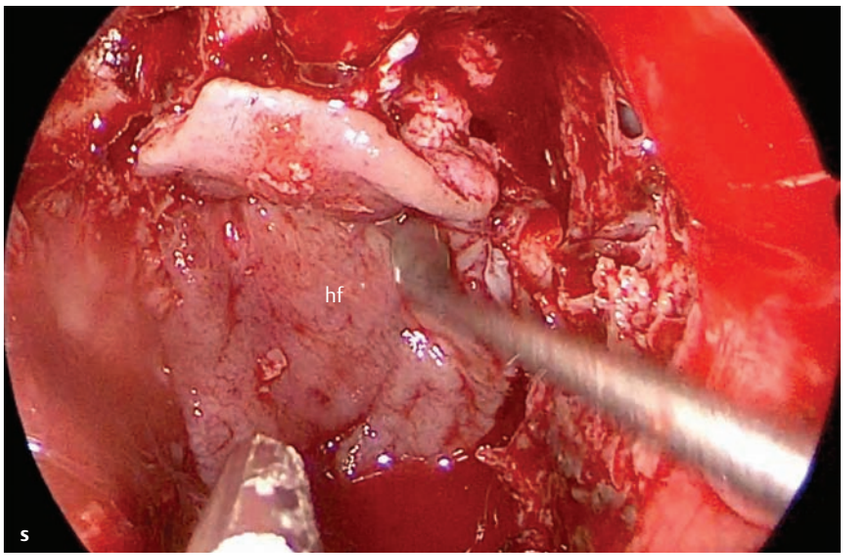

Fig. 8.20 **(s)** Endoscopic view showing reconstruction with nasoseptal flap. Hf, Hadad flap.

Case 4: Revision Pituitary Macroadenoma with Suprasellar Extension

A 37-year-old man presented with bitemporal hemianopia and headache. He was operated twice before, once transcranially and the other endoscopically. MRI showed a huge sellar and suprasellar mass (**Fig. 8.21a**). After adequate exposure of both sphenoid sinuses (**Fig. 8.21b**) drilling of sellar floor was carried out (**Fig. 8.21c**). Thinned-out sellar bone was removed with Rosen's elevator (**Fig. 8.21d**). Bone over the carotids were removed with Kerrison's punch. Planectomy was done and planum dura was exposed. Drilling over tubercular strut was started (**Fig. 8.21e, f**). Thinned-out bone of tubercular strut was removed with Rosen's elevator and bilateral carotids were mapped with microvascular Doppler (**Fig. 8.21g**). Endosteal layer of sellar dura was incised with Cappabianca knife and incision was extended with the rotatable scissors (**Fig. 8.21h**). A "U"-shaped flap was elevated (**Fig. 8.21i**). Some reconstructive materials which were kept during the previous surgery were found and removed. Sellar part of the tumor was removed with two-suction tip technique (**Fig. 8.21j, k**) and tumor near medial walls of cavernous sinus was removed with curved suction tip. Suprasellar part of the tumor was viewed with help of 45-degree angled telescope SICS was cauterized (**Fig. 8.21l**). Tumor from the suprasellar region was sucked out. After tumor removal anterior circulation could be visualized (**Fig. 8.21m**). The last part of the suprasellar tumor was removed with curved suction tip. Left optic nerve A1, A2, and dural perforators were identified and saved (**Fig. 8.21n**). Reconstruction was done with fat, fascia, and nasoseptal flap (**Fig. 8.21o**). See **Video 8.4**.

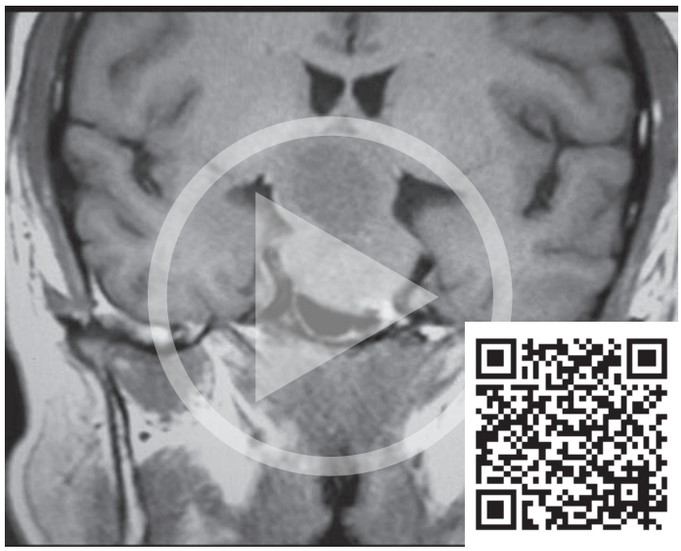

Video 8.4 Revision pituitary macroadenoma with suprasellar extension.
https://www.thieme.de/de/q.htm?p=opn/cs/19/9/10104306-047e874e

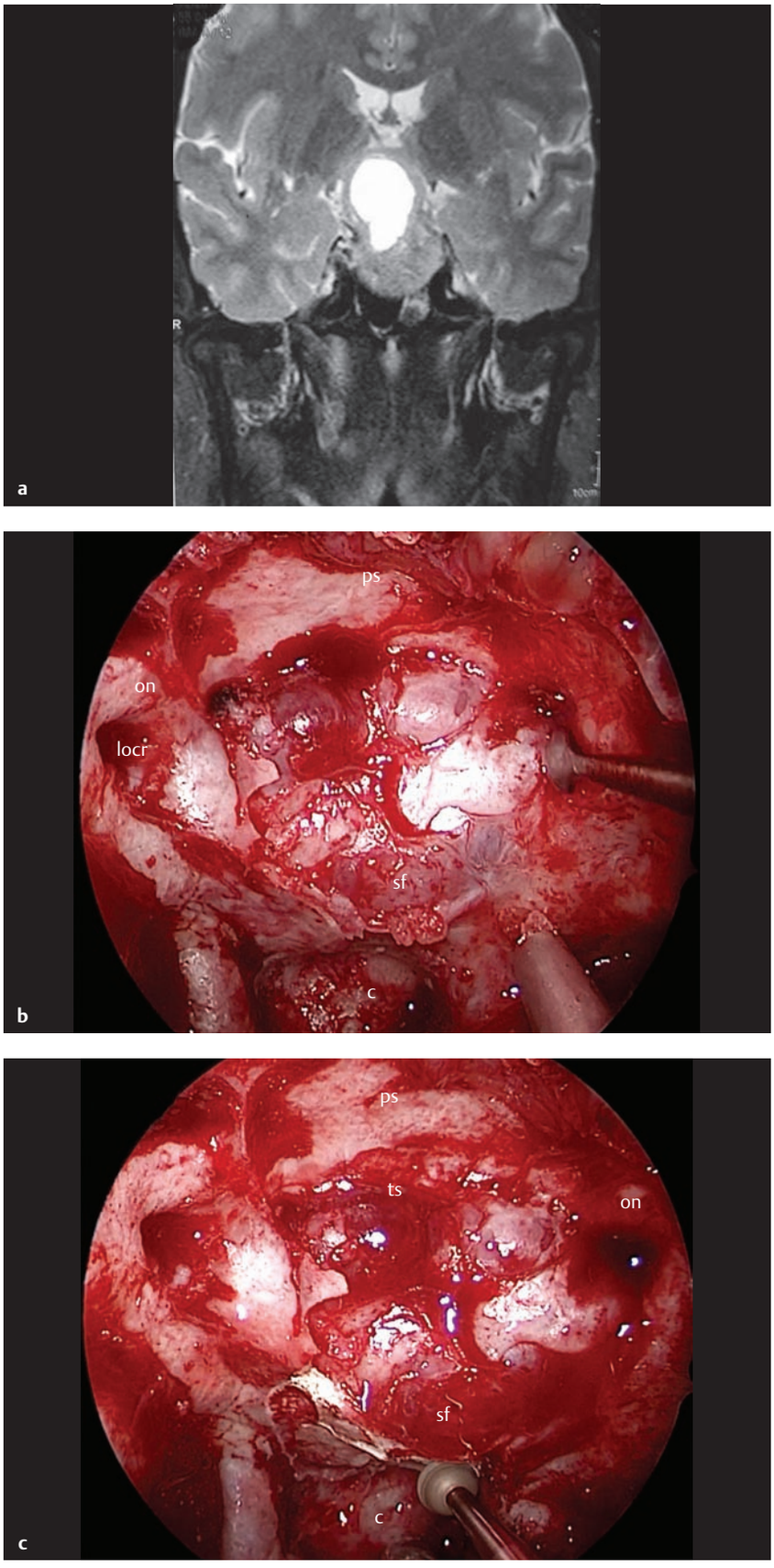

Fig. 8.21 **(a)** MRI coronal cut showing mass lesion in the sellar suprasellar region. **(b)** Endoscopic view showing wide exposure of the sphenoid sinuses. Sf, sellar floor; on, optic nerve; PS, planum sphenoidale; on, optic nerve; LOCR, lateral opticocarotid recess. **(c)** Endoscopic view showing drilling of the sellar floor. Sf, sellar floor; ts, tuberculum sellae; PS, planum sphenoidale; on, optic nerve; c, clinoid.

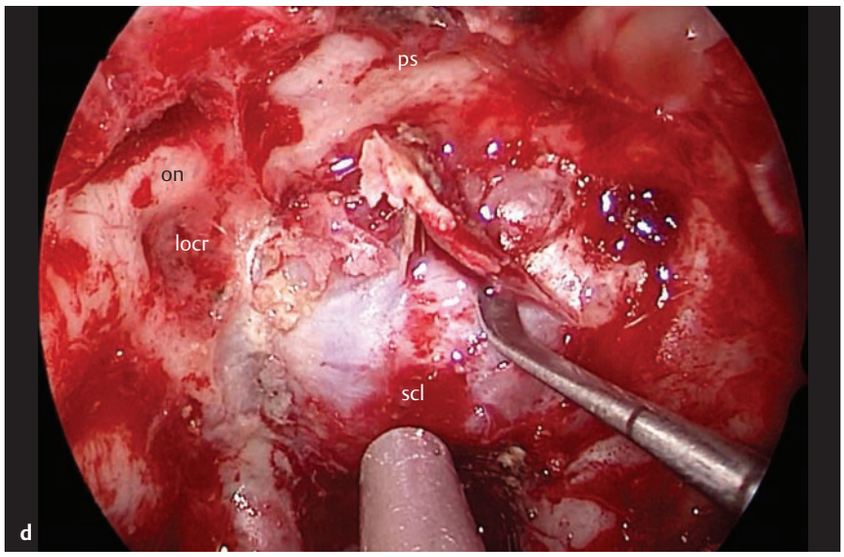

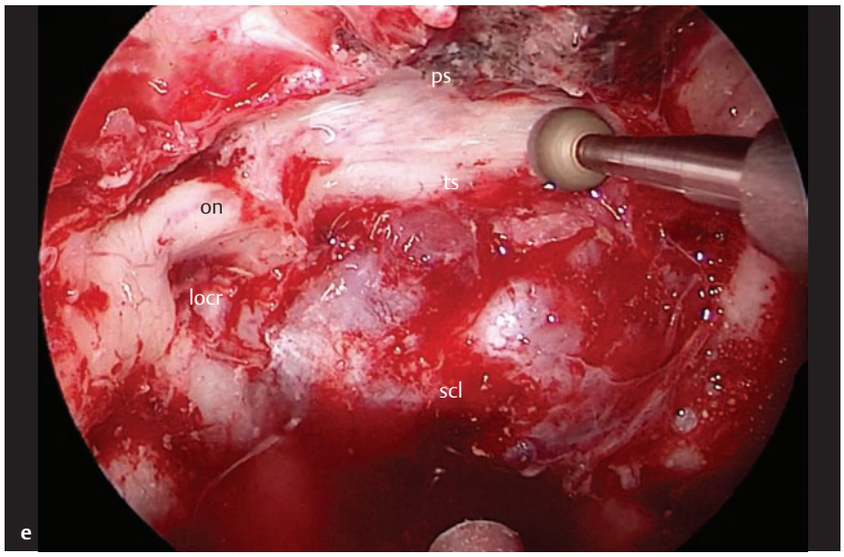

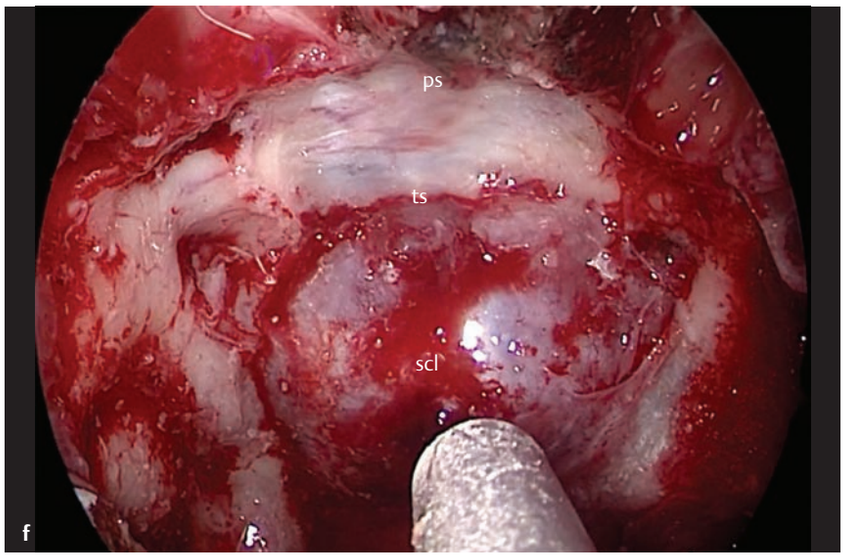

Fig. 8.21 **(d)** Removing sellar floor bone after drilling it to eggshell. Sd, sellar dura; PS, planum sphenoidale; on, optic nerve; LOCR, lateral opticocarotid recess. **(e)** Endoscopic view showing drilling of the planum bone. Sd, sellar dura; on, optic nerve; LOCR, lateral opticocarotid recess; Ts, tuberculum sellae. **(f)** Endoscopic view showing complete exposure for sellar suprasellar approach. PS, planum sphenoidale; sd, sellar dura; ts, tuberculum sphenoidale.

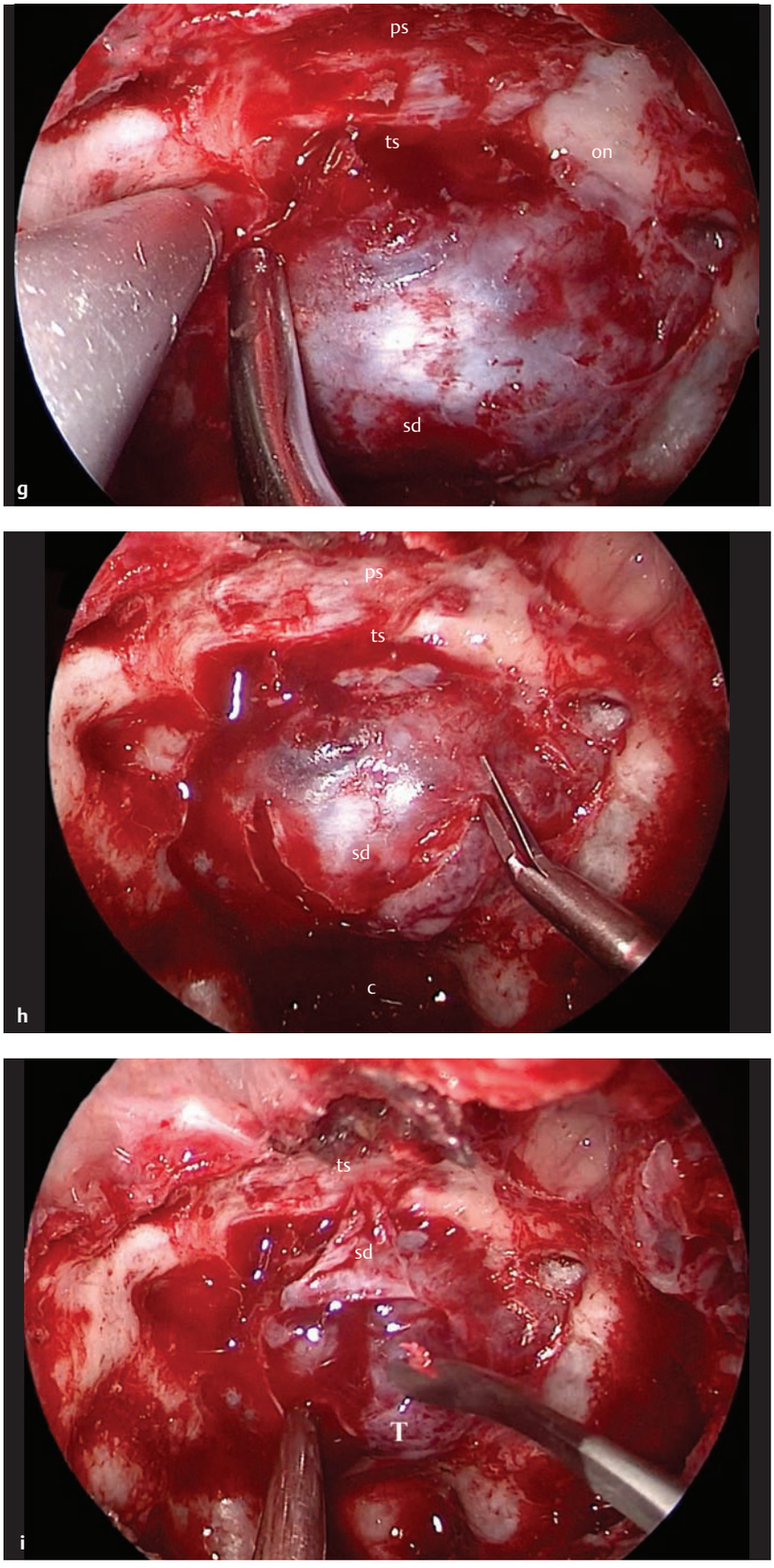

Fig. 8.21 **(g)** Mapping carotid artery after complete exposure with carotid microvascular doppler. PS, planum sphenoidale; ts, tuberculum sphenoidale; on, optic nerve; *, micro vascular Doppler. **(h)** Endoscopic view showing giving incision on the sellar dura. PS, planum sphenoidale; sd, sellar dura; ts, tuberculum sphenoidale; c, clinoid. **(i)** Endoscopic view showing after elevation of the sellar dural flap tumor can be visualized. T, tumor; ts, tuberculum sellae; sd, sellar dura.

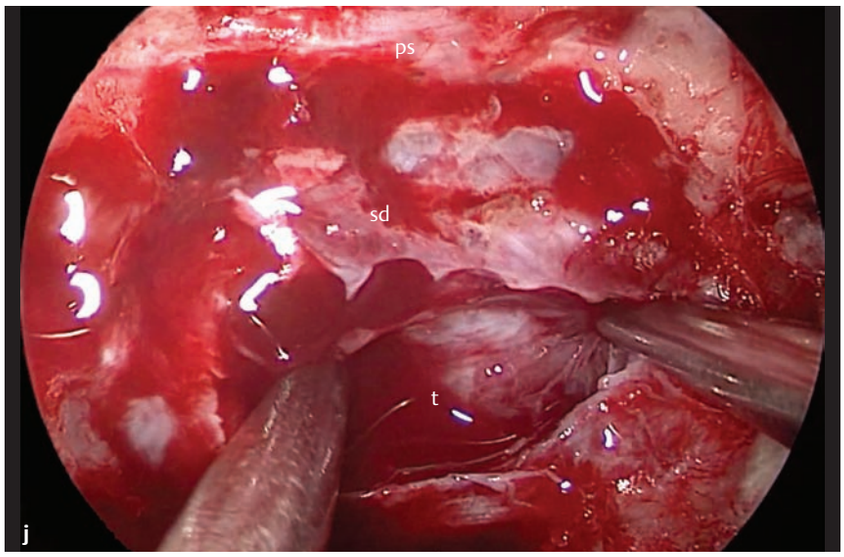

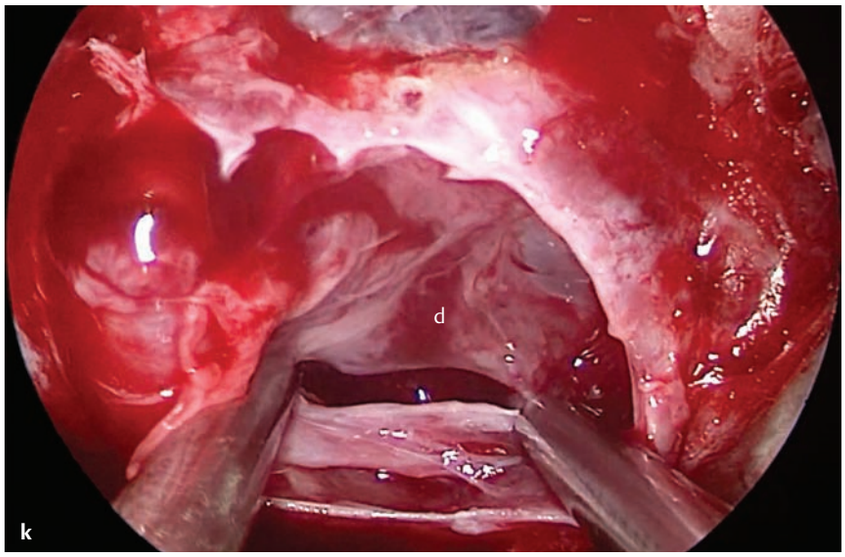

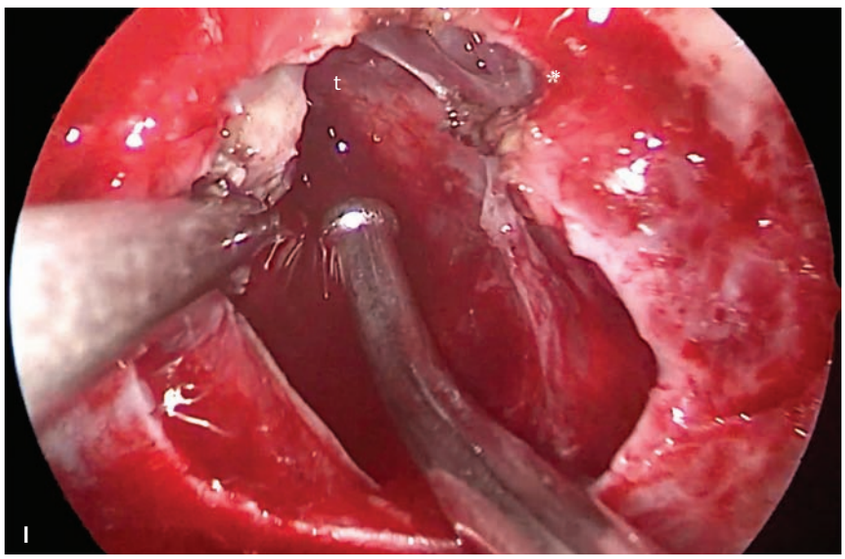

Fig. 8.21 **(j)** Endoscopic view showing removal of the tumor with two-suction technique. Sd, sellar dura; PS, planum sphenoidale; t, tumor. **(k)** endoscopic view showing removal of tumor from the diaphragma sellae. D, diaphragma sellae. **(l)** Endoscopic view showing sucking out tumor from suprasellar region with curved suction tip. T, tumor.

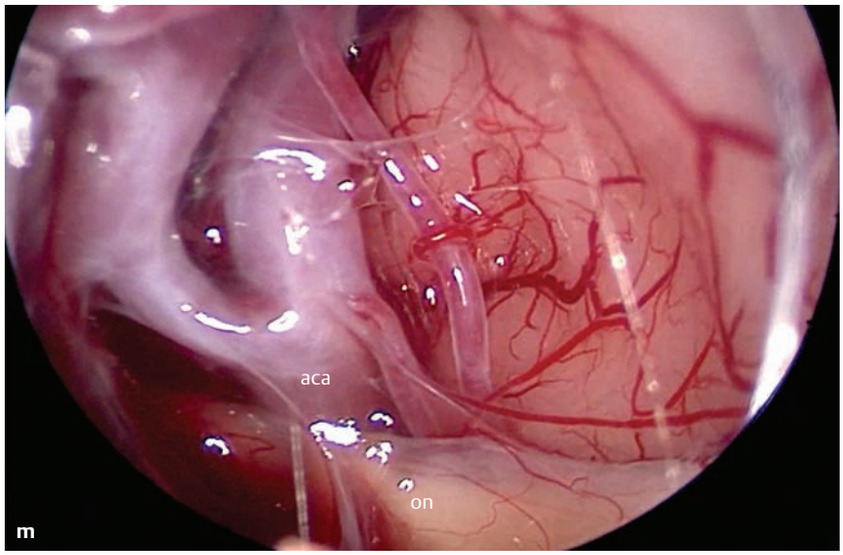

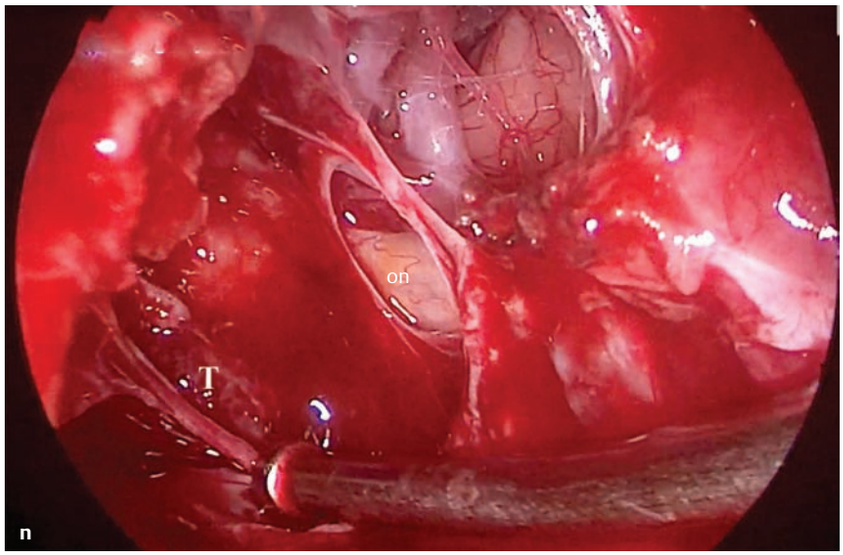

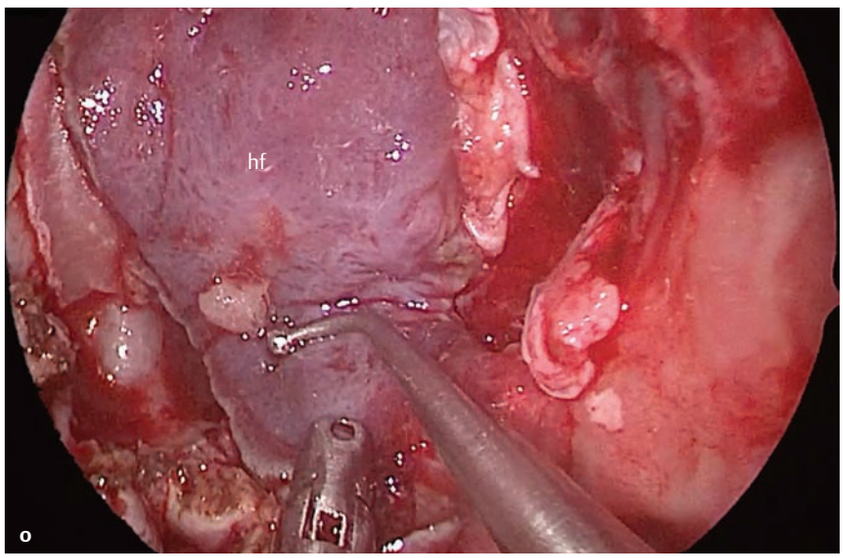

Fig. 8.21 **(m)** Endoscopic view showing suprasellar cistern after tumor removal. On, optic nerve; ACA, anterior cerebral artery. **(n)** Endoscopic view showing removal of the suckable tumor from the suprasellar region optic nerve and anterior cerebral circulation can be seen. On, optic nerve; A1, A1 segment of anterior cerebral artery; t, tumor. **(o)** Reconstruction with nasoseptal flap; Hf, Hadad flap.

Case 5: Revision Pituitary Macroadenoma with Suprasellar Extension

A 40-year-old man presented with bilateral diminishing of vision, he was operated previously twice for pituitary macroadenoma. MRI brain showed mass lesion in sellar and suprasellar region (**Fig. 8.22a**). As right-side nasoseptal flap was used previously author decided to go for left side nasoseptal flap. After wide exposure of sphenoid sinus it was clear that the keel was not drilled completely during previous surgeries (**Fig. 8.22b**). Complete exposure of the sellar dura was done up to bilateral cavernous carotid arteries. Bilateral carotid arteries were mapped with carotid Doppler (**Fig. 8.22c**). PS and tubercular sellae area were drilled (**Fig. 8.22d**) and thinned out bone was removed with Kerrison's punch to expose (**Fig. 8.22e**) tubercular sellae dura. Sellar and tubercular sellae area dura were exposed (**Fig. 8.22f**). The endosteal layer of dura was incised using a Cappabianca knife and sellar dural flap was elevated. The fibrous part of tumor was dissected from sellar region with micro elevator by extracapsular dissection technique (**Fig. 8.22g**). Authors found that tumor was left near cavernous region and suprasellar part (**Fig. 8.22h**). Cavernous and suprasellar part of tumor was removed with low-power suction tip after gently elevating the diaphragma sellae (**Fig. 8.22i**). After complete removal of tumor, cavity was examined by gently elevating diaphragma sellae (**Fig. 8.22j**) and no leaks were found (**Fig. 8.22k**). Reconstruction was done with fat, Surgicel, and nasoseptal flap.

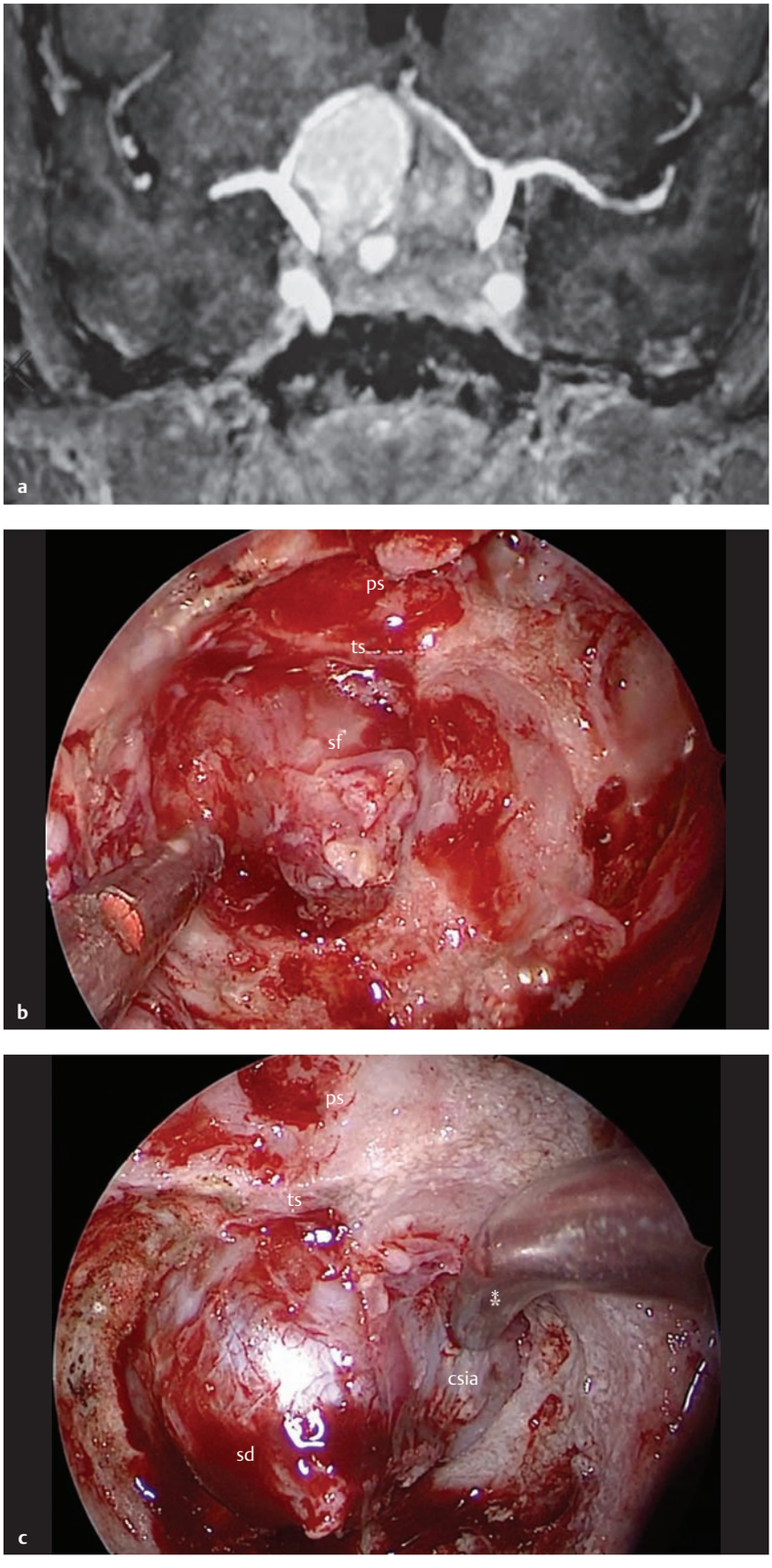

Fig. 8.22 **(a)** MRI coronal cut showing mass lesion in sellar and suprasellar region. **(b)** Endoscopic view showing wide exposure of sphenoid sinuses. Sf, sellar floor; ts, tubercular sellae; PS, planum sphenoidale. **(c)** Endoscopic view showing mapping of cavernous internal carotid artery after exposure of sellar dura. Sd, sellar dura; ts, tubercular sellae; CICA, cavernous internal carotid artery; PS, planum sphenoidale; *, microvascular Doppler.

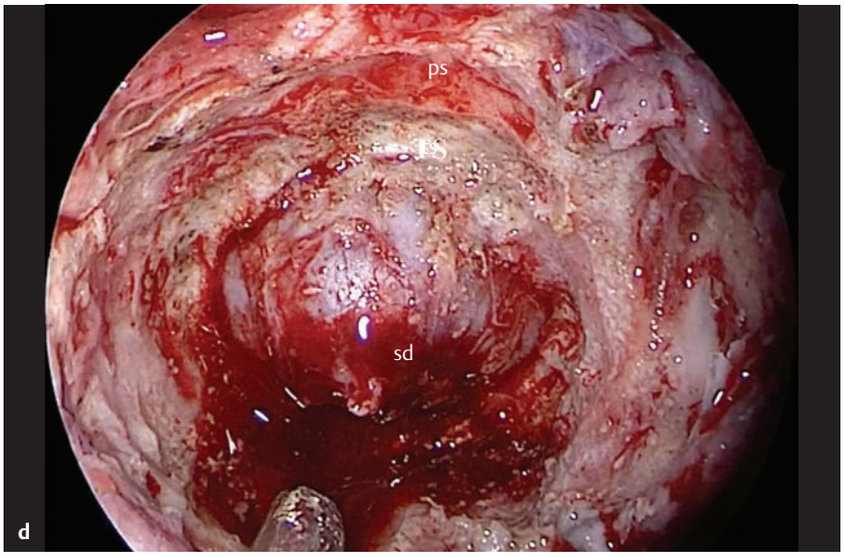

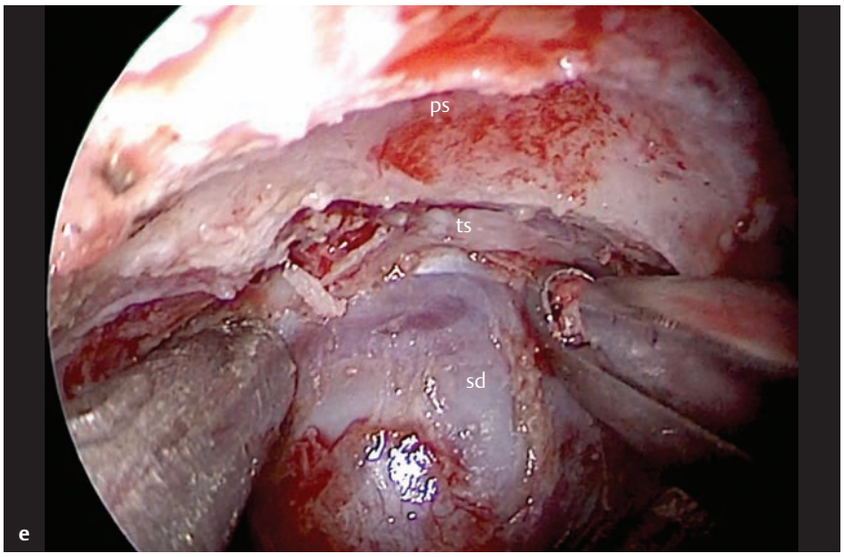

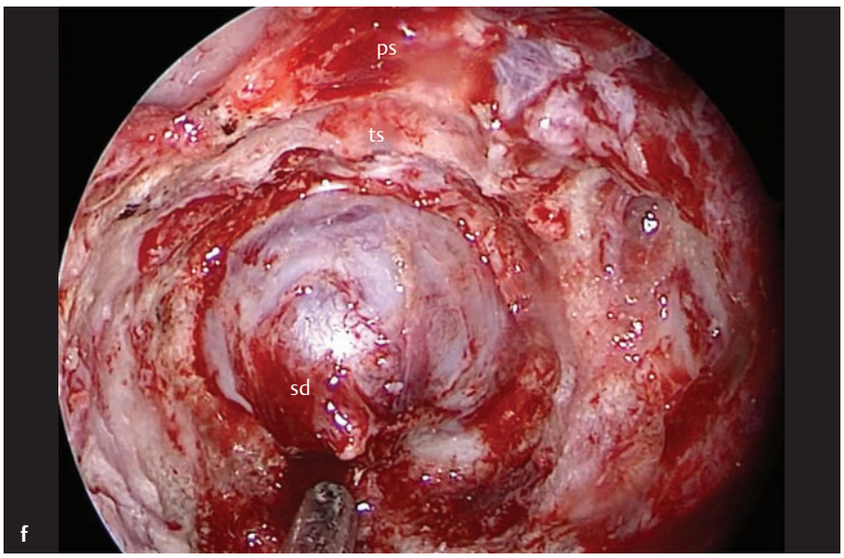

Fig. 8.22 **(d)** Endoscopic view showing complete exposure of sellar dura and suprasellar exposure. Sd, sellar dura; ts, tubercular sellae; PS, planum sphenoidale. **(e)** Endoscopic view showing removal of the tubercular bone after drilling it to eggshell thin. Sd, sellar dura; PS, planum sphenoidale; ts, tubercular sellae. **(f)** Endoscopic view showing sellar suprasellar exposure. Sd, sellar dura; ts, tubercular sellae; PS, planum sphenoidale.

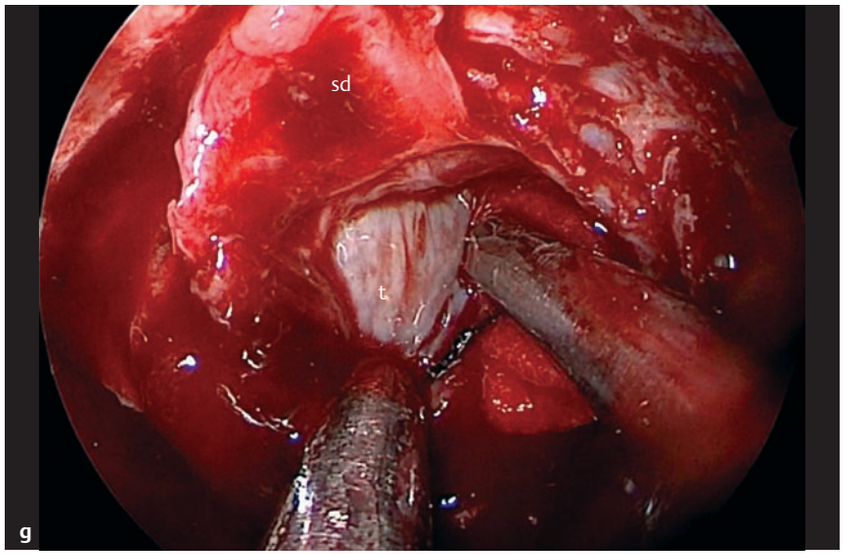

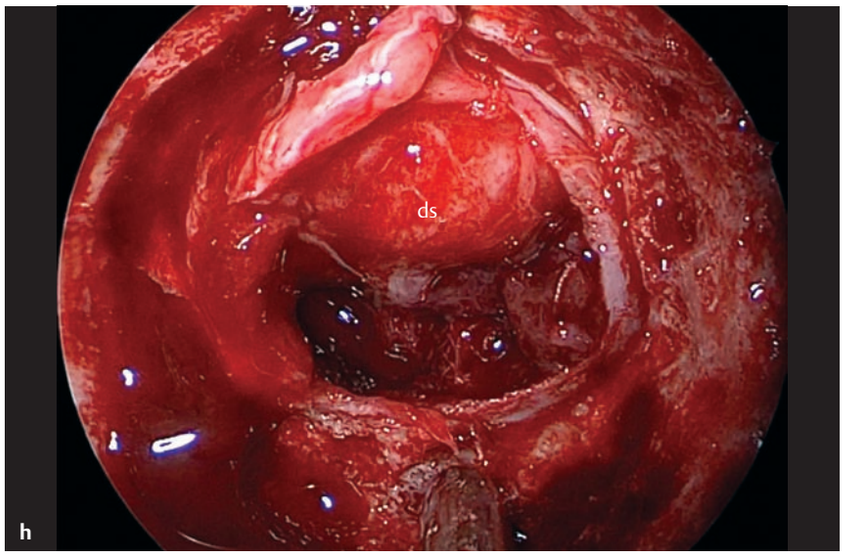

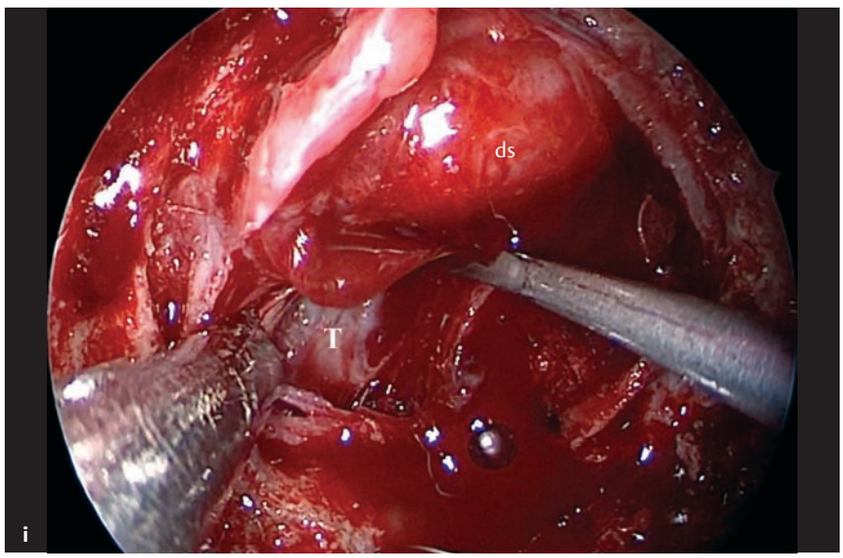

Fig. 8.22 **(g)** Endoscopic view showing sellar dural flap and extracapsular dissection of tumor. Sd, sellar dura; t, tumor. **(h)** Endoscopic view showing bulge out diaphragma sellae after tumor removal. Ds, diaphragma sellae. **(i)** Endoscopic view showing gentle elevation of diaphragma to visualize tumor in right cavernous sinus. Ds, diaphragma sellae; t, tumor.

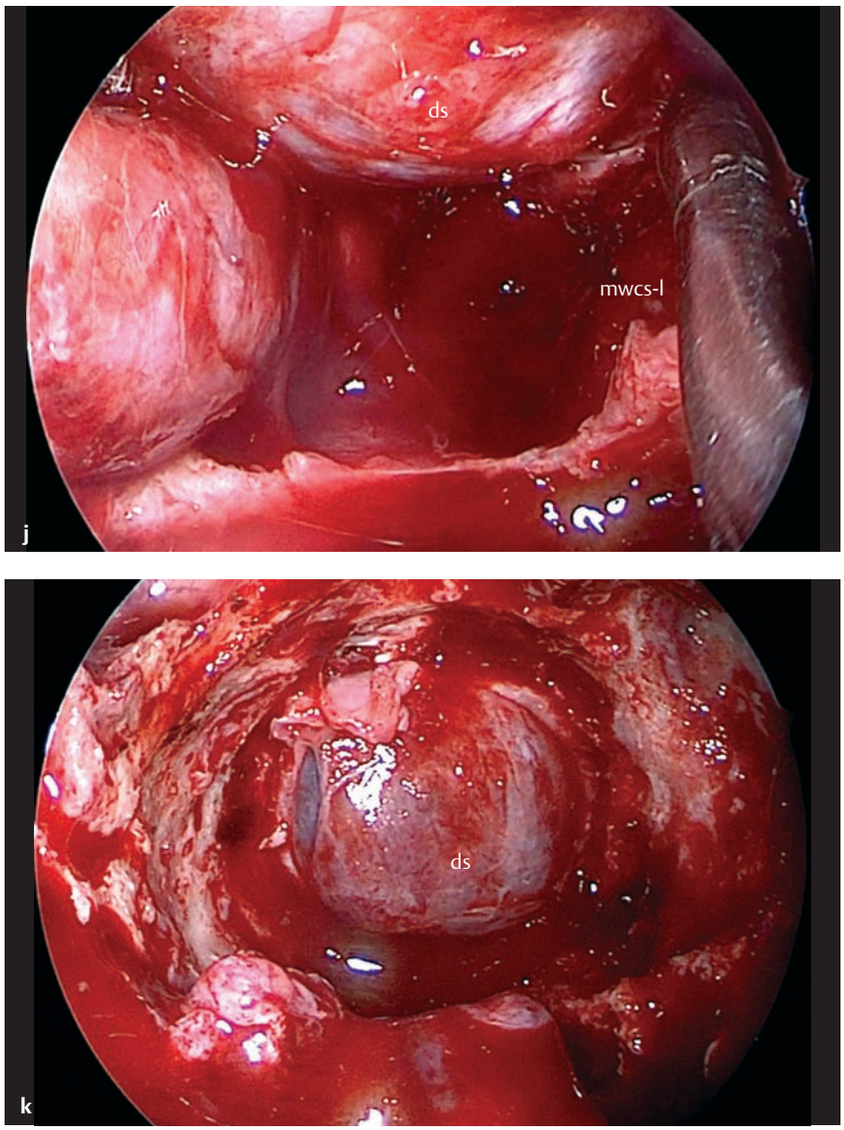

Fig. 8.22 **(j)** Endoscopic view showing gentle elevation of diaphragma sellae to inspect left cavernous sinus. Ds, diaphragma sellae; mwcs-l, medial wall of left cavernous sinus. *, interclinoid ligament. **(k)** Endoscopic view showing bulge out diaphragma sellae after complete tumor removal without any csf leak. Ds, diaphragma sellae.

Case 6: Pituitary Macroadenoma with Suprasellar and Right Parasellar Extension

A 35-year-old woman presented with history of headaches and diminishing vision. MRI scan showed a pituitary macroadenoma with suprasellar and right parasellar extension (**Fig. 8.23a**). After harvesting left nasoseptal flap wide exposure of sphenoid sinus was done. Drilling of sellar floor bone was started (**Fig. 8.23b**). As tumor had right parasellar extension right trans pterygoid approach was performed and right vidian nerve was identified (**Fig. 8.23c**). The vidian canal and bone over right cavernous sinus was dissected (**Fig. 8.23d**). Sellar floor bone and bone over right cavernous carotid were removed after drilling it to eggshell thin (**Fig. 8.23e**). Tubercullum sellae was drilled and tubercular strut was removed with Rosen's elevator after thinning it (**Fig. 8.23f**). Bilateral MOCR was removed after drilling it to eggshell thin (**Fig. 8.23g**). Incision was placed over endosteal layer of dura with Cappabianca knife and sellar dura flap was elevated from the tumor (**Fig. 8.23h**). Extracapsular dissection was carried out for the fibrous part of the tumor (**Fig. 8.23i**). Deeper part of the tumor found was suckable so after taking biopsy (**Fig. 8.23j**) dissection was carried out with two-suction technique (**Fig. 8.23k**). A tumor near left cavernous sinus was removed with cavernous sinus suction tip (**Fig. 8.23l**). Dural layer anterior to right cavernous carotid artery was incised (**Fig. 8.23m**). Tumor posterior to cavernous carotid artery was removed gently with keyhole suction tip by gently transposing the ICA laterally (**Fig. 8.23n**). After complete dissection of tumor from both cavernous sinuses, dissection of suprasellar part of tumor was carried out (**Fig. 8.23o**). After complete removal of tumor, cavity was examined after lifting diaphragma sellae gently and no leak was found (**Fig. 8.23p**) the cavity filled was with fat and Surgicel.

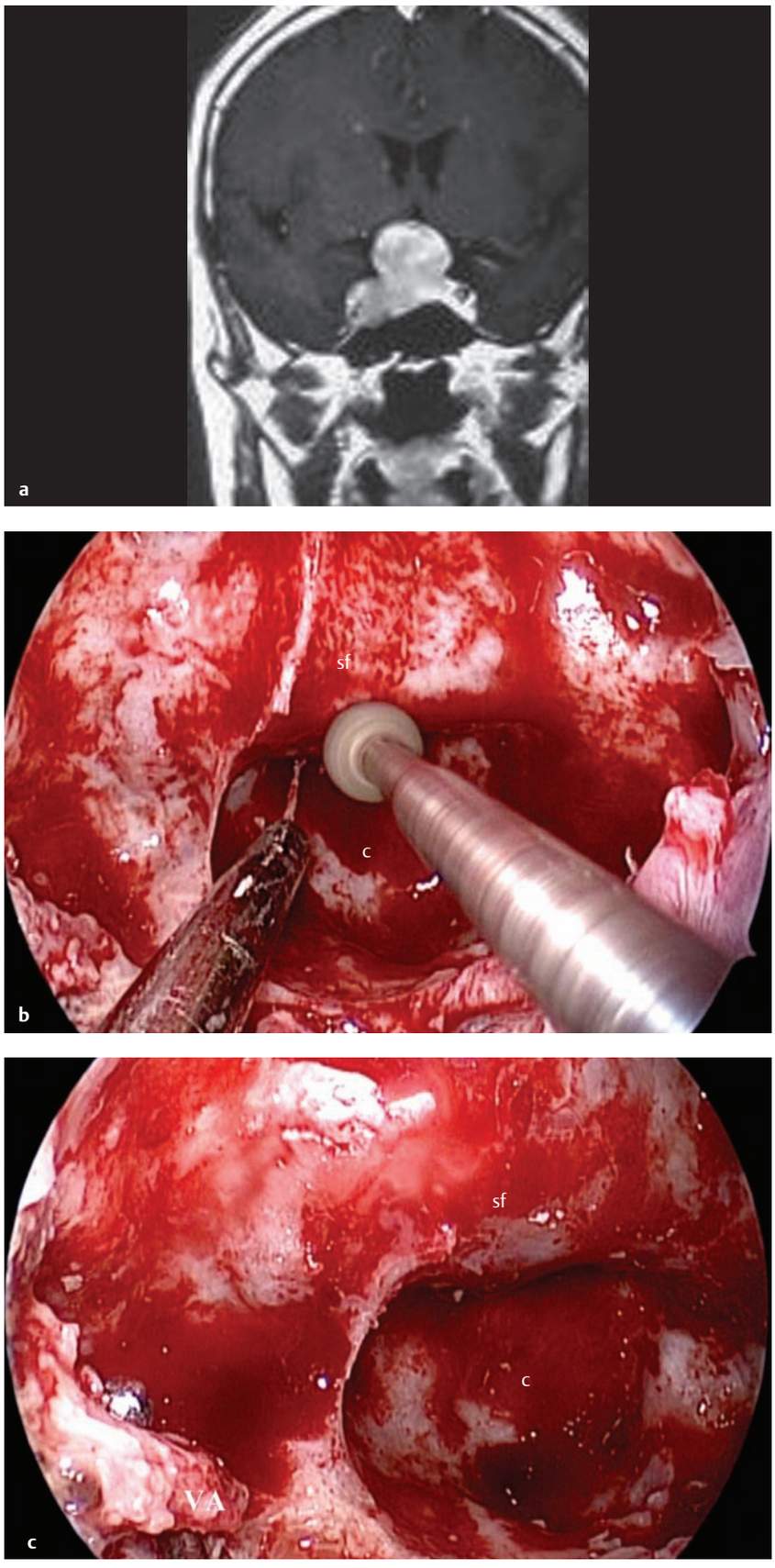

Fig. 8.23 **(a)** MRI coronal cut showing sellar, suprasellar and right parasellar mass lesion. **(b)** Endoscopic view showing drilling of sellar floor bone after wide exposure of sphenoid sinuses. Sf, sellar floor; c, clinoid. **(c)** Endoscopic view showing right trans pterygoid approach and dissection of right vidian nerve. Right vidian nerve is hooked with ball point tip. Sf, sellar floor; c, clinoid; va, vidian nerve.

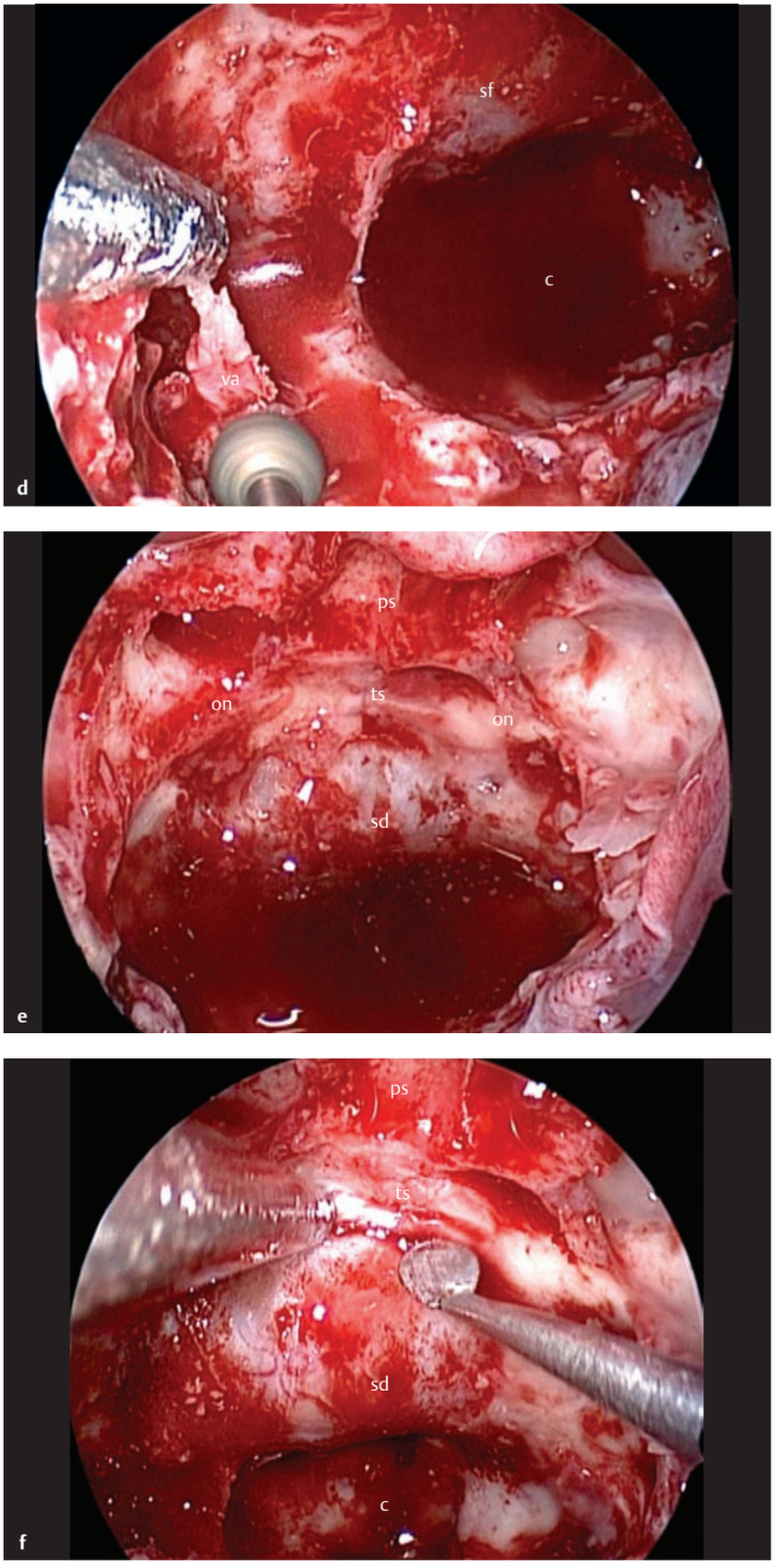

Fig. 8.23 **(d)** Endoscopic view showing drilling of the right vidian nerve. Sf, sellar floor; c, clinoid; va, vidian nerve. **(e)** Endoscopic view showing exposure of sellar dura and right cavernous sinus. Sd, sellar dura; ts, tubercular sellae; PS, planum sphenoidale; on, optic nerve. **(f)** Endoscopic view showing elevation of tubercular sellae bone. C, clinoid; sd, sellar dura; on, optic nerve; PS, planum sphenoidale; ts, tubercular sellae.

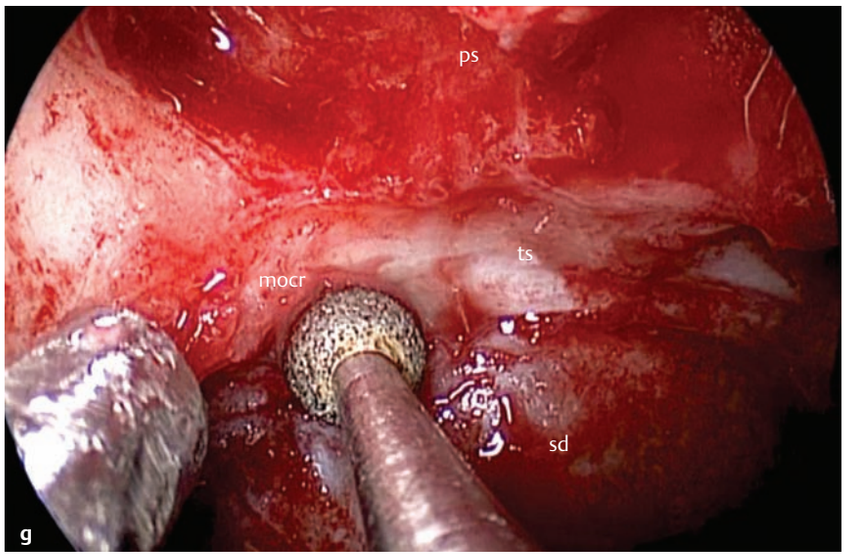

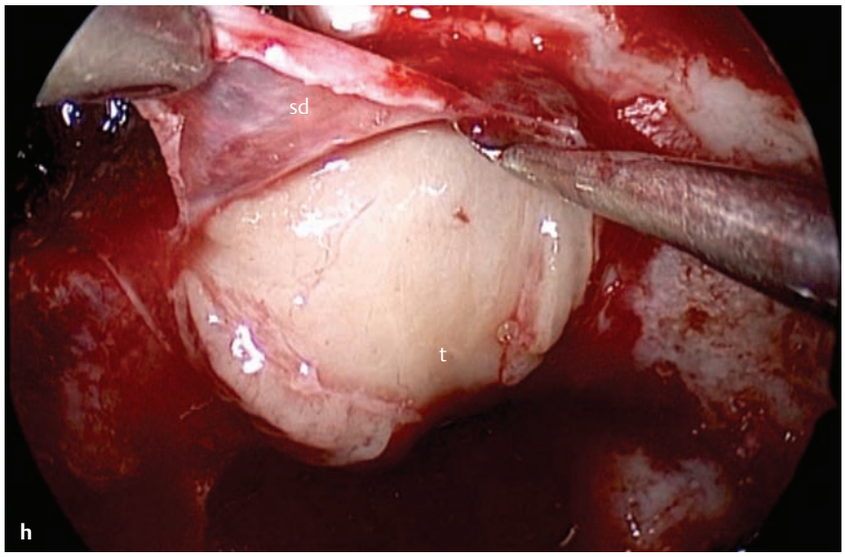

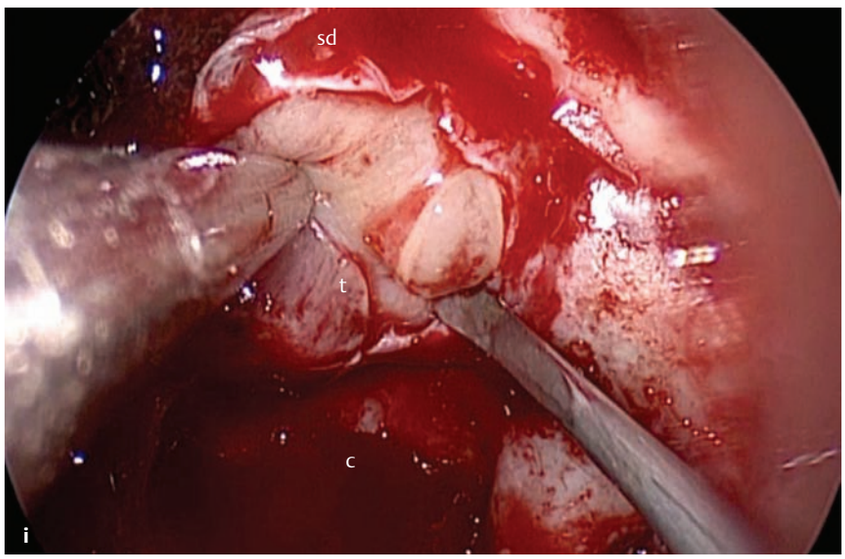

Fig. 8.23 **(g)** Endoscopic view showing drilling of right medial opticocarotid recess. Ps, planum sphenoidale; ts, tubercular sellae; sd, sellar dura; MOCR, medial opticocarotid recess. **(h)** Endoscopic view showing elevation of sellar dura flap and tumor is seen. Sd, sellar dura; t, tumor. **(i)** Dissection of tumor with microelevator. C, clinoid; t, tumor; sd, sellar dura.

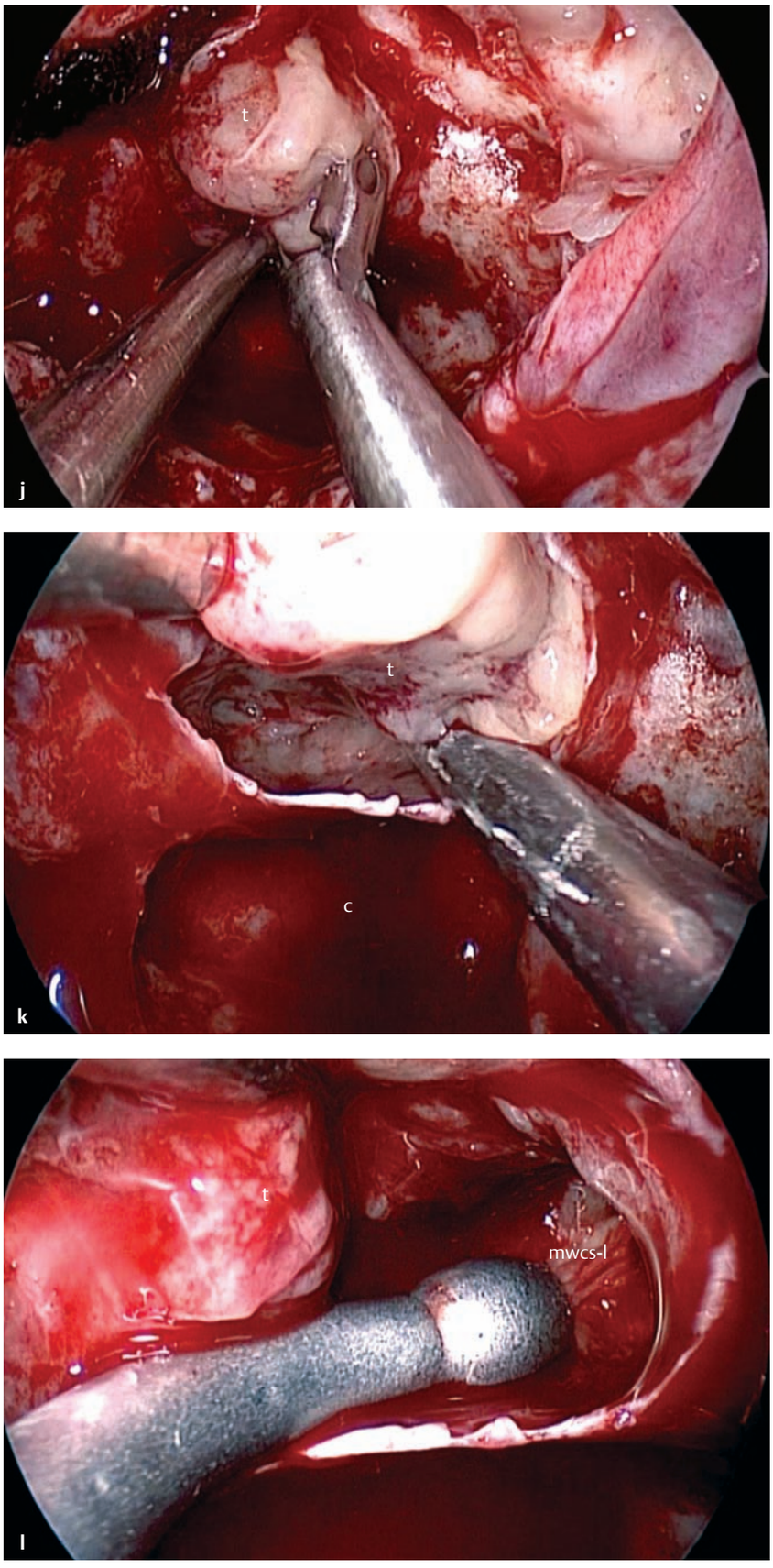

Fig. 8.23 **(j)** Taking biopsy from tumor. T, tumor. **(k)** Endoscopic view showing removal of suckable tumor with two-suction technique. T, tumor; c, clinoid. **(l)** Endoscopic view showing dissection of tumor from the left cavernous sinus. T, tumor; mwcs-l, medial wall of left cavernous sinus.

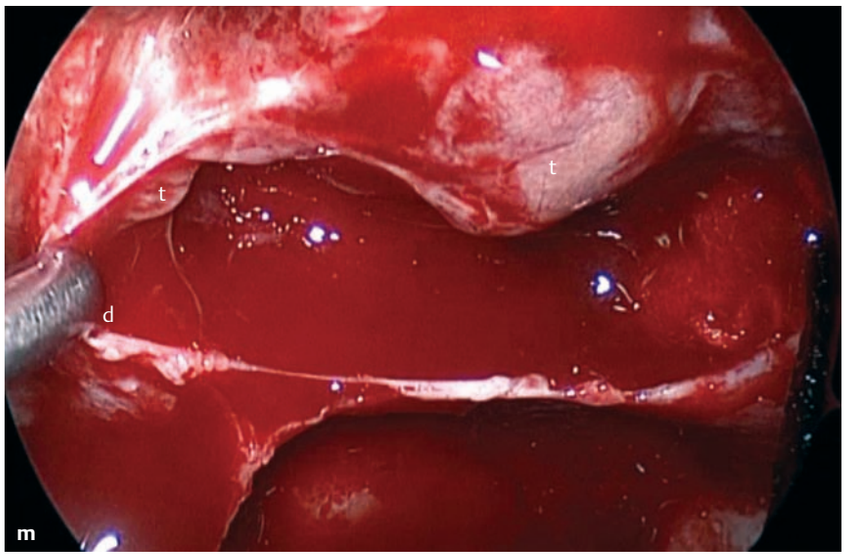

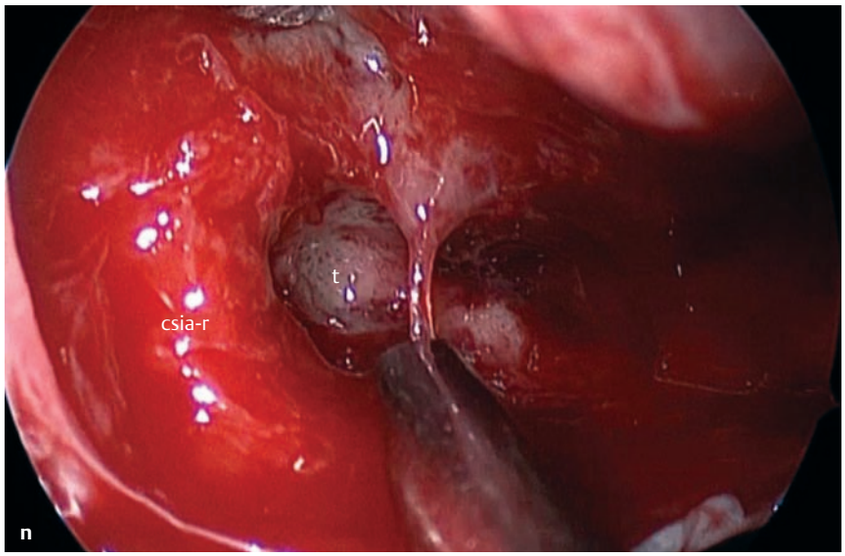

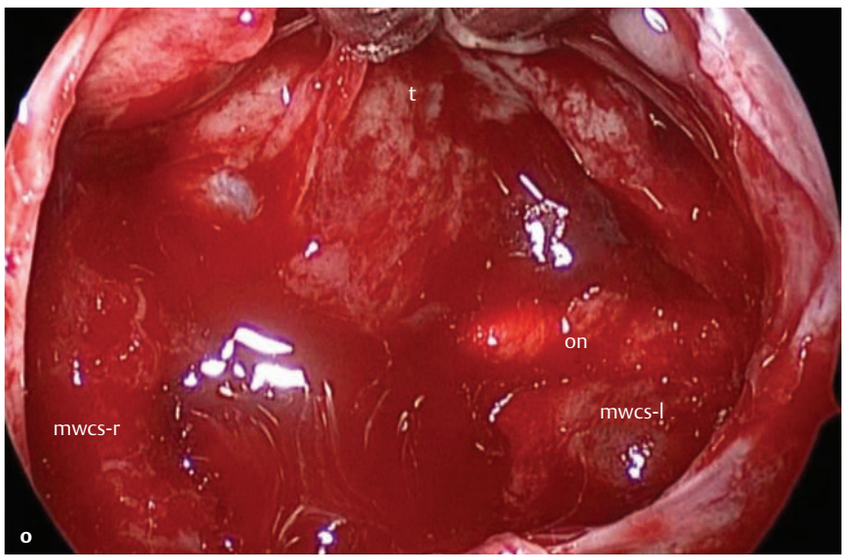

Fig. 8.23 **(m)** Endoscopic view showing retraction of dura to visualize tumor in right cavernous sinus. T, tumor; d, dura. **(n)** Endoscopic view showing removal of tumor posterior to right cavernous internal carotid artery. T, tumor; cica-r, cavernous internal carotid artery. **(o)** Removing suprasellar part of tumor after complete removal of tumor from sellar and parasellar region. T, tumor; on, optic nerve; mwcs-r, medial wall of right cavernous sinus; mwcs-l, medial wall of left cavernous sinus.

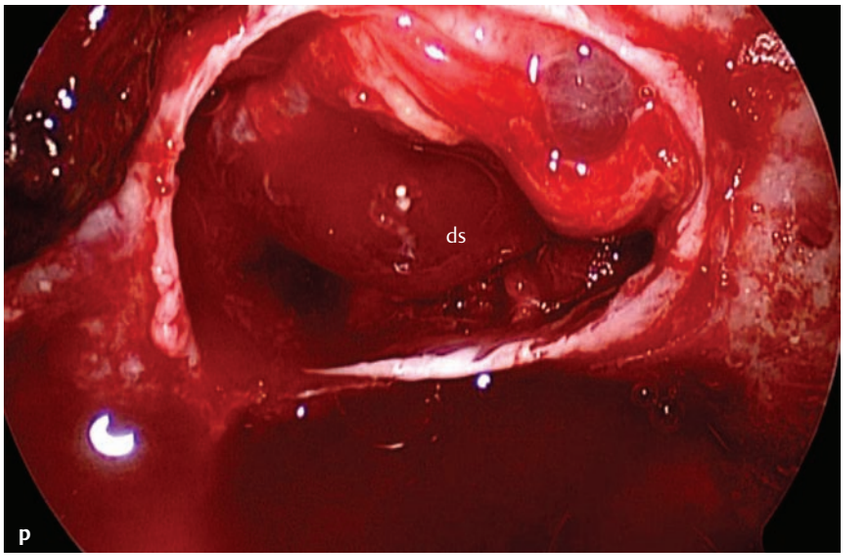

Fig. 8.23 **(p)** After complete removal of tumor diaphragma sellae is seen. Ds, diaphragma sellae.

Case 7: Pituitary Macroadenoma with Suprasellar Extension

A 47-year-old woman presented with bitemporal hemianopia and headache. MRI scan showed a huge sellar suprasellar macroadenoma (**Fig. 8.24a**). Wide exposure of sphenoid sinuses was performed after harvesting nasoseptal flap (**Fig. 8.24b**). Sellar floor bone drilled out (**Fig. 8.24c**) and sellar dura flap was elevated. Biopsy sample was taken from sellar part of tumor (**Fig. 8.24d**). Sellar part of tumor was removed after debulking it (**Fig. 8.24e**). Extracapsular dissection of tumor was started from right cavernous sinus (**Fig. 8.24f**) and same way tumor was removed from suprasellar part (**Fig. 8.24g**). After complete removal of tumor, diaphragma sellae was found bulging into the sellar cavity (**Fig. 8.24h**). Sellar cavity was examined after gently elevating diaphragma sellae (**Fig. 8.24i**). Reconstruction was carried out in multilayer with fat, Surgicel, Gelfoam, and nasoseptal flap (**Fig. 8.24j**).

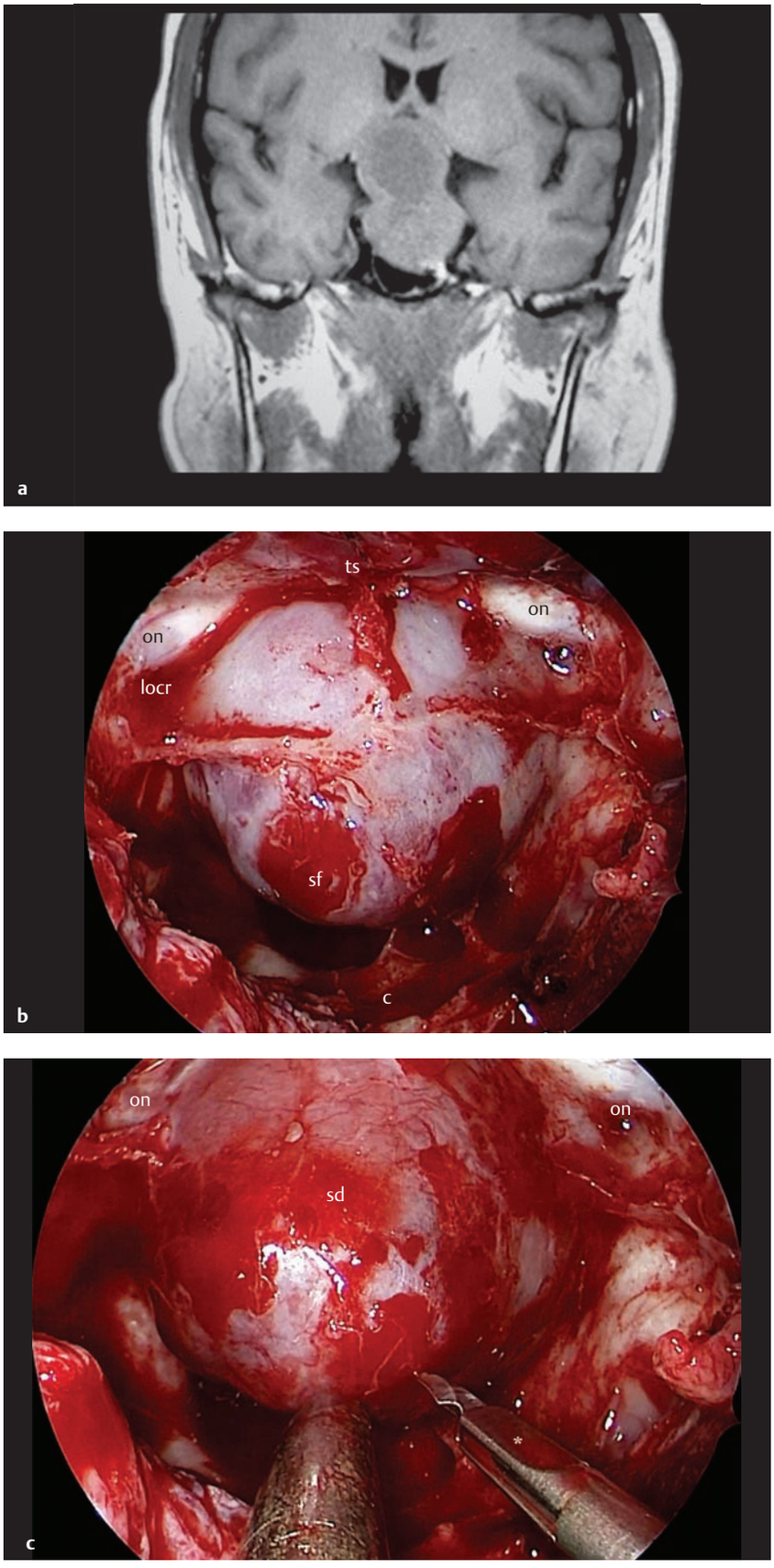

Fig. 8.24 **(a)** MRI coronal cut showing mass lesion in sellar suprasellar region compressing bilateral optic nerve. **(b)** Endoscopic view showing wide exposure of the sphenoid sinuses. Sf, sellar floor; c, clinoid; on, optic nerve; ts, tubercular sellae; LOCR, lateral opticocarotid recess. **(c)** Endoscopic view showing keeping incision over the sellar dura with Cappabianca knife. Sd, sellar dura; on, optic nerve; *, Cappabianca knife.

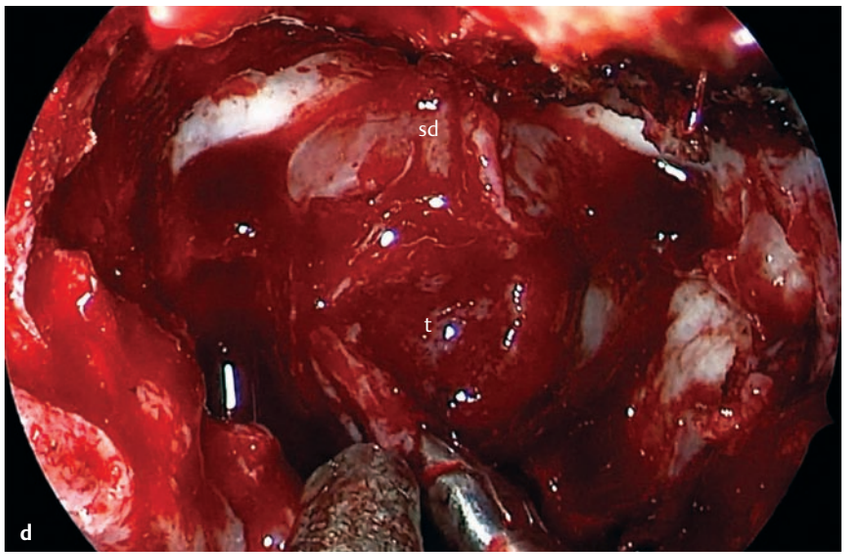

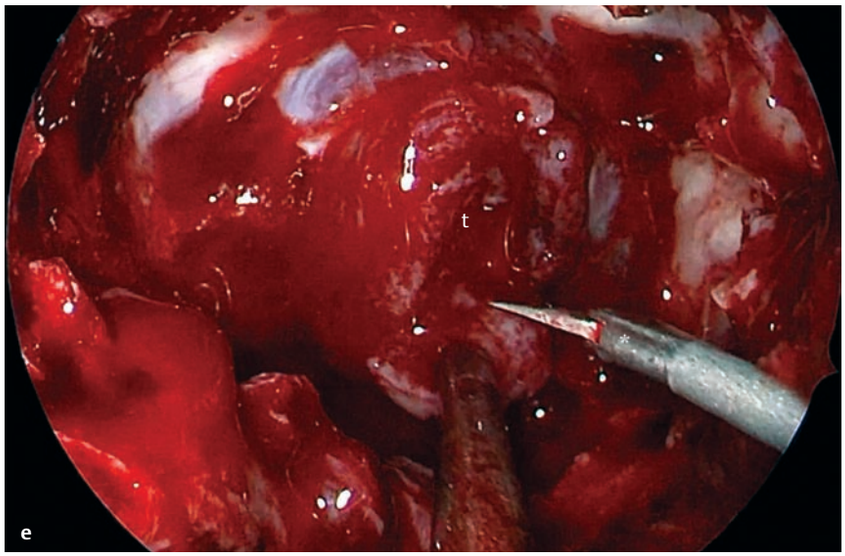

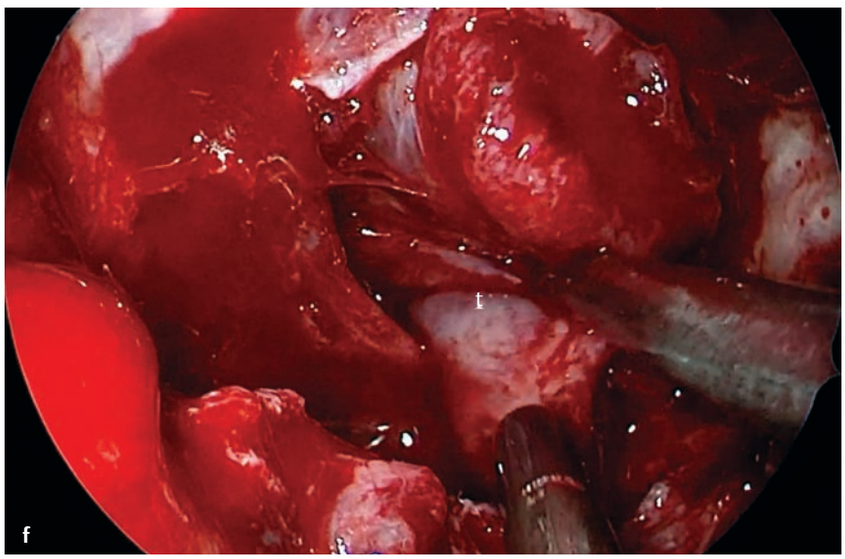

Fig. 8.24 **(d)** Endoscopic view showing taking biopsy from the sellar tumor after elevating sellar dural flaps. **(e)** Doing debulking of tumor with microdissection technique. T, tumor. **(f)** Endoscopic view showing extracapsular dissection of the fibrous component of the tumor. T, tumor.

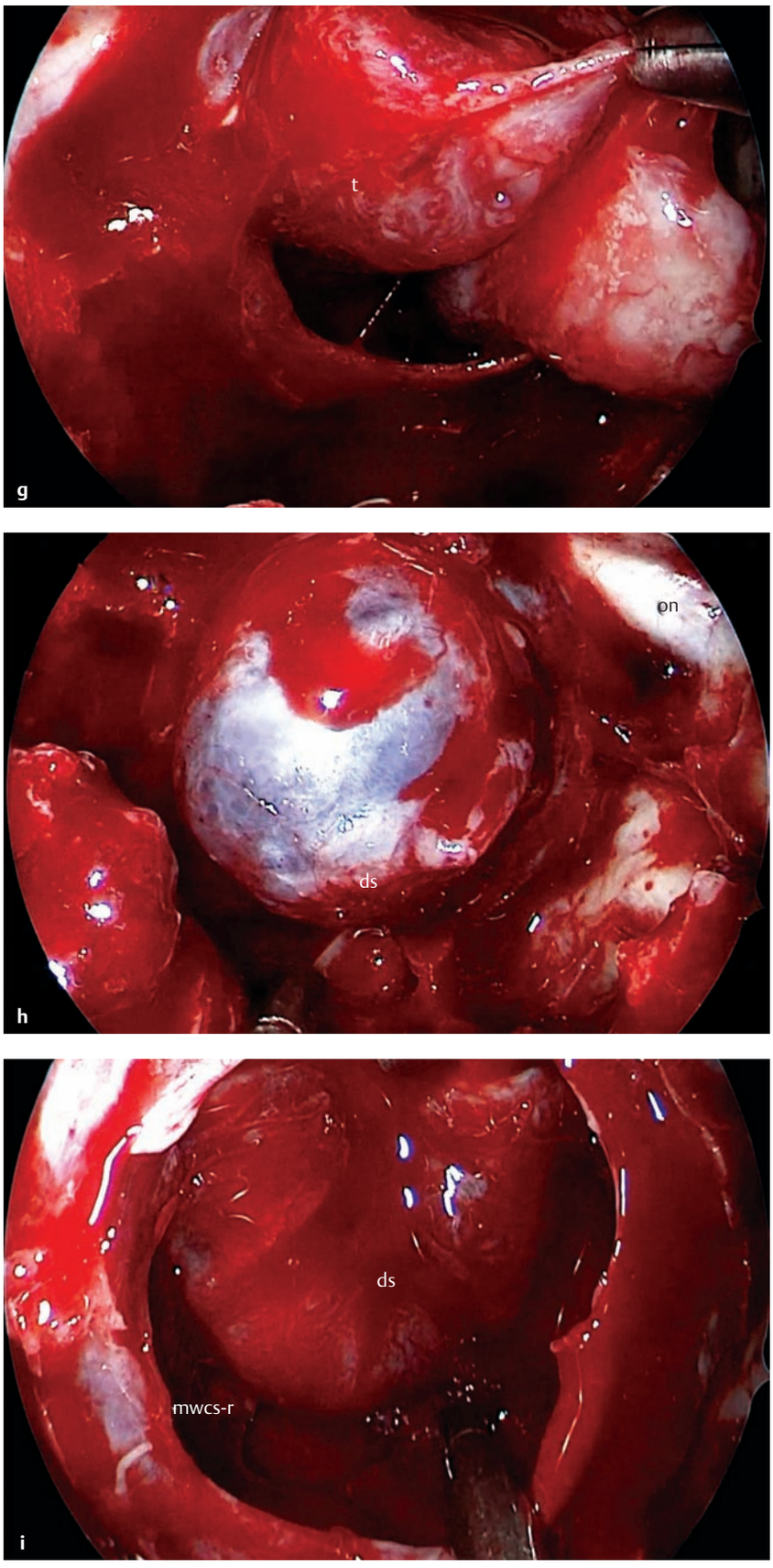

Fig. 8.24 **(g)** Extracapsular dissection of tumor from last attachment. T, tumor. **(h)** After complete removal of the tumor bulged out diaphragma sellae can be seen. Ds, diaphragma sellae; on, optic nerve. **(i)** Endoscopic view showing examination of sellar cavity after lifting diaphragmatic sellae. Ds, diaphragmatic sellae; mwcs-r, medial wall of right cavernous sinus.

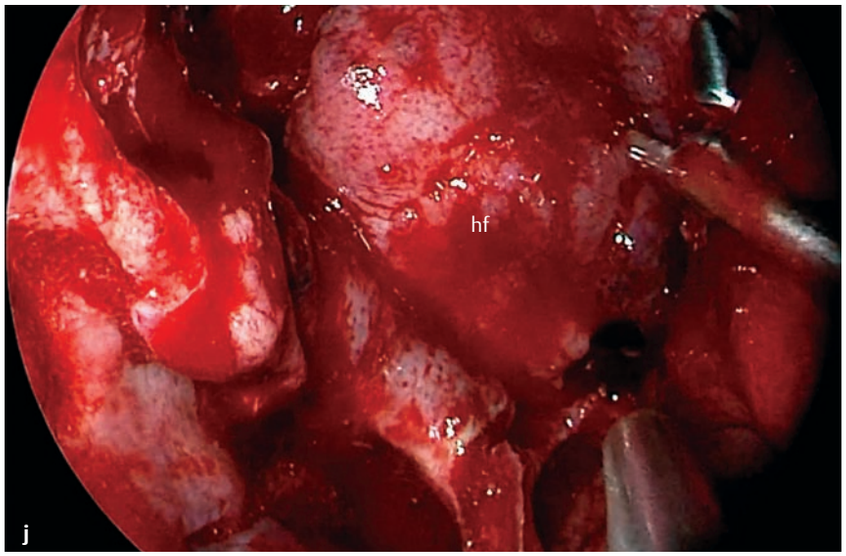

Fig. 8.24 **(j)** Endoscopic view showing reconstruction with nasoseptal flap. Hf, Hadad flap.

Case 8: Pituitary Macroadenoma with Suprasellar Extension

A 57-year-old male patient presented with complaints of bitemporal hemianopia and headache. MRI brain showed a huge mass in sellar suprasellar part (**Fig. 8.25a**). Wide exposure of sphenoid sinus were done (**Fig. 8.25b**). After drilling sellar bone to eggshell thin it was removed with Rosen's elevator (**Fig. 8.25c**). Drilling over tuberculum and planum area was done (**Fig. 8.25d**). Thin bone over tuberculum was removed with Rosen's elevator (**Fig. 8.25e**). Bone over bilateral carotid as well as MOCR was removed (**Fig. 8.25f**) and bilateral carotids were mapped with carotid Doppler (**Fig. 8.25g**). The endosteal layer of dura was incised using a Cappabianca knife and incision was extended with scissors (**Fig. 8.25h**). Dural flap was elevated with Rosen's elevator (**Fig. 8.25i**). Biopsy from the tumor was taken (**Fig. 8.25j**). Suckable part of tumor was removed with suction (**Fig. 8.25k**). Fibrous part of the tumor was dissected with the elevator and forceps (extracapsular dissection) (**Fig. 8.25l**). After complete removal of tumor diaphragma descended and filled up sellar cavity, no CSF leak was identified (**Fig. 8.25m**). The closure was done with Surgicel, fat, fascia, and nasoseptal flap (**Fig. 8.25n**).

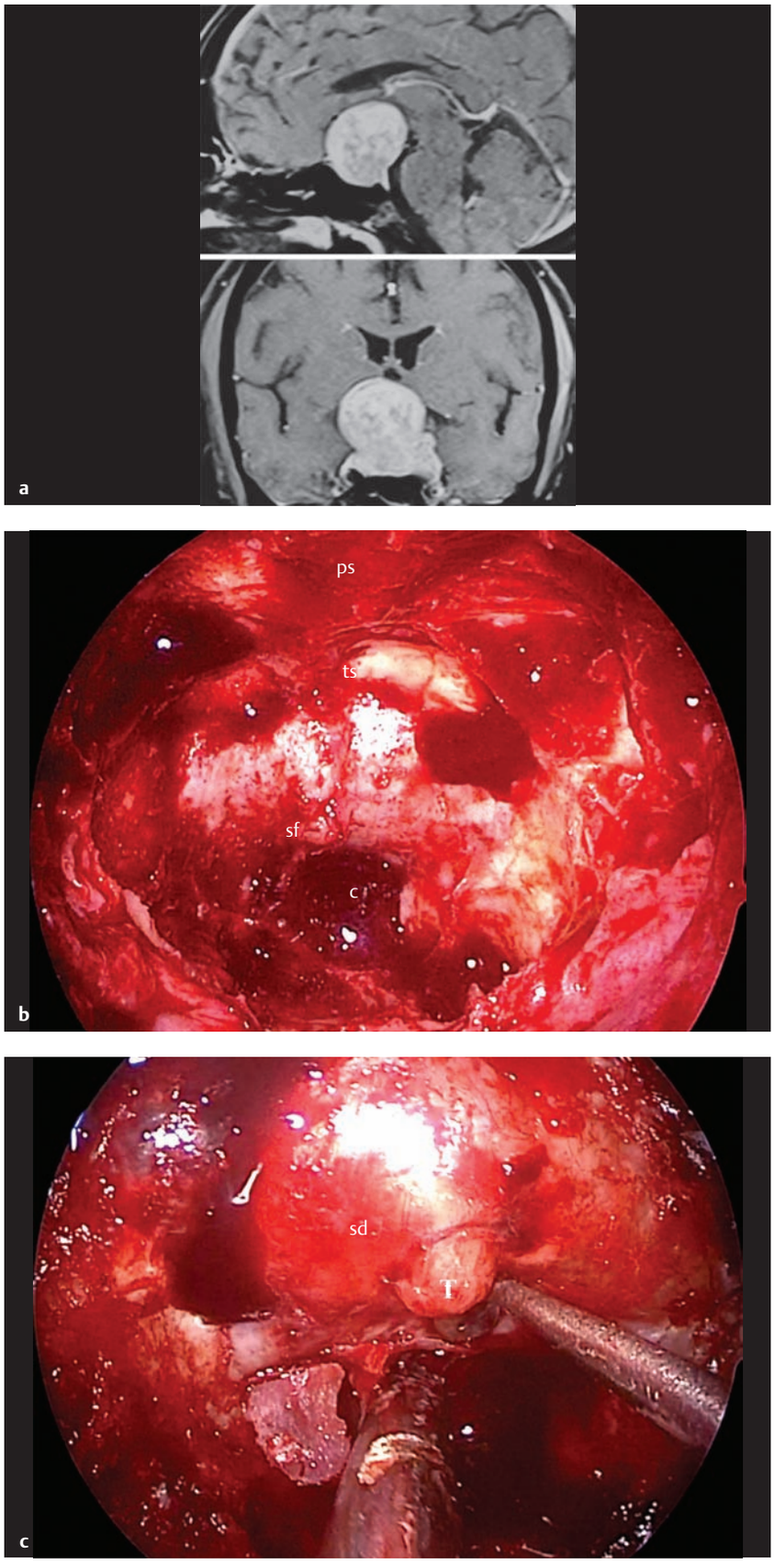

Fig. 8.25 **(a)** MRI scan showing solid cystic mass in sellar suprasellar region and compressing bilateral optic nerve. **(b)** Endoscopic view showing wide exposure of the sphenoid sinuses. Sf, sellar floor; c, clinoid; ts, tubercular sellae; PS, planum sphenoidale. **(c)** Endoscopic view showing elevation of the sellar floor bone after thinning it to egg shell. Sd, sellar dura; t, tumor.

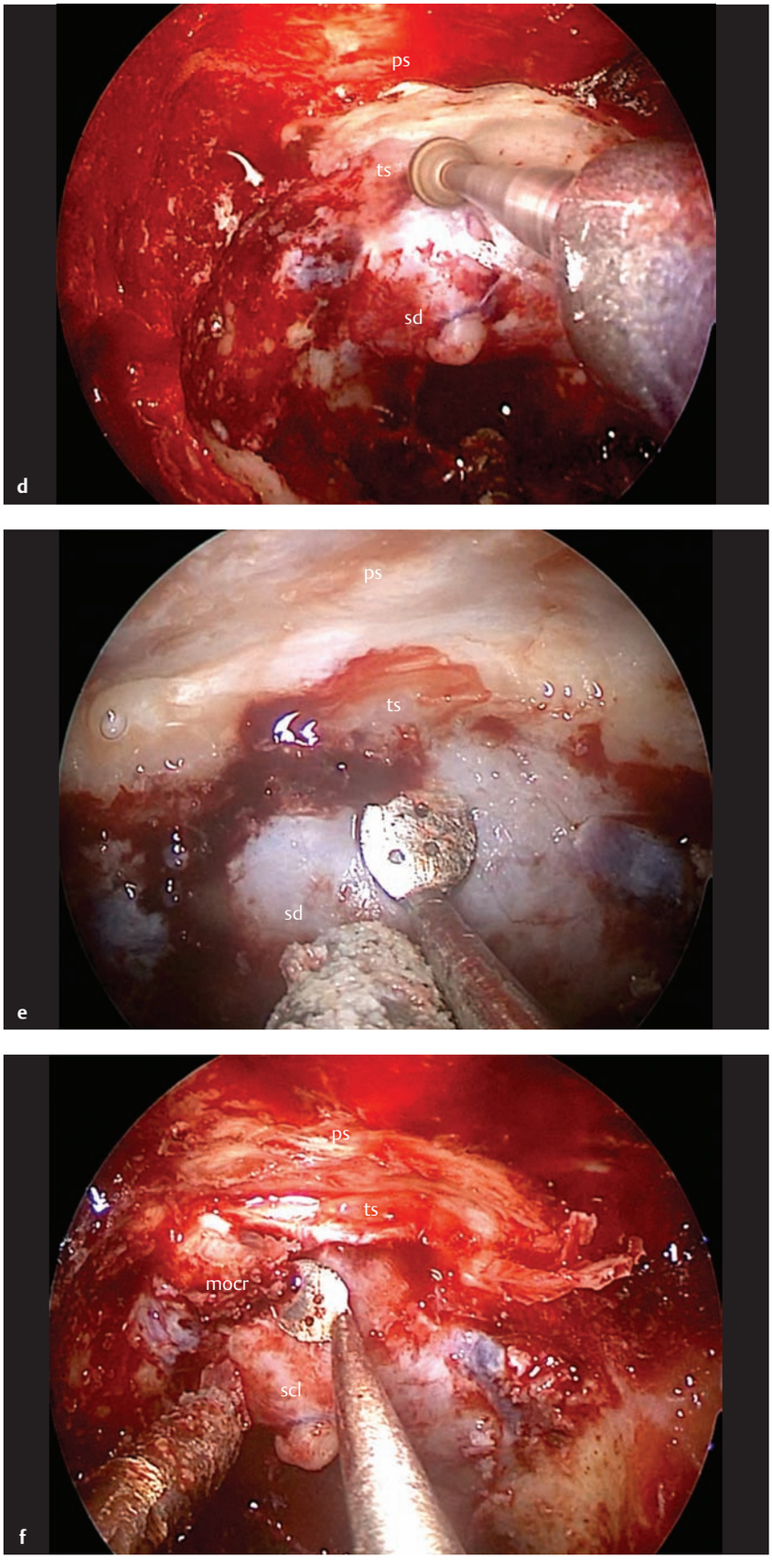

Fig. 8.25 **(d)** Endoscopic view showing drilling of the tubercular area. Sd, sellar dura; ts, tubercular sellae; PS, planum sphenoidale. **(e)** Endoscopic view showing removal of the tubercular sellae bone. Sd, sellar dura; ts, tubercular sellae; PS, planum sphenoidale. **(f)** Endoscopic view showing removal of right MOCR. Sd, sellar dura; ts, tubercular sellae; PS, planum sphenoidale; MOCR, medial opticocarotid recess.

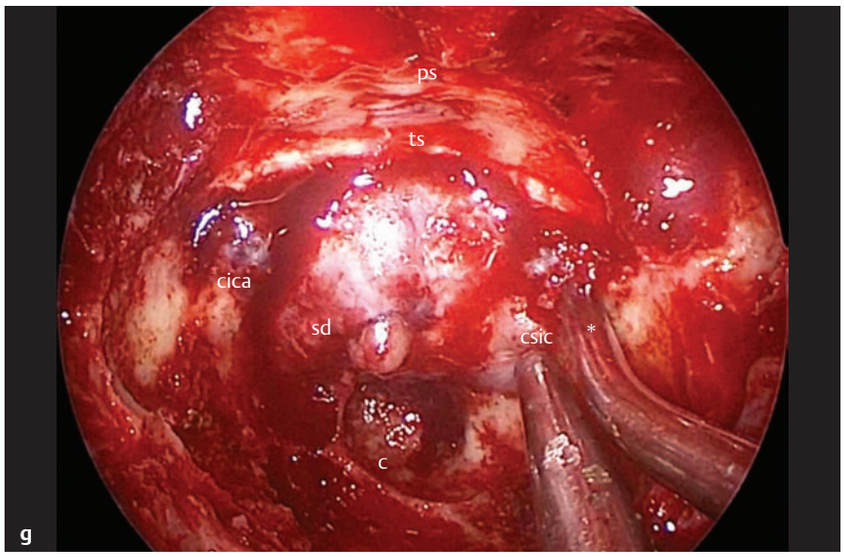

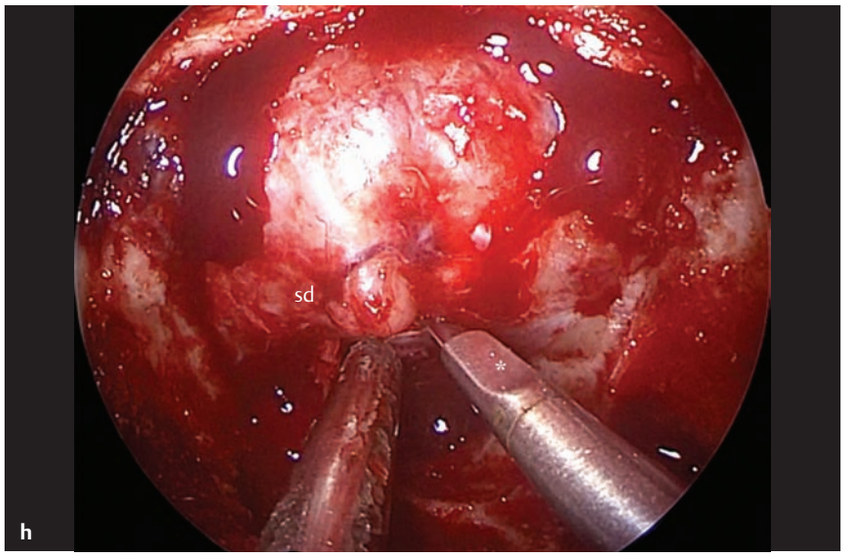

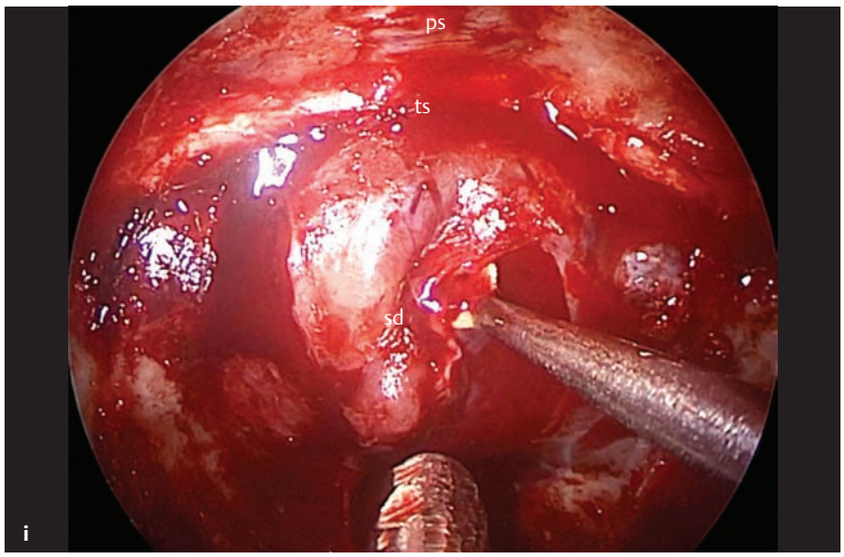

Fig. 8.25 **(g)** Endoscopic view showing mapping of carotids after complete exposure. Sd, sellar dura; ts, tubercular sellae; Ps, planum sphenoidale; CICA, cavernous internal carotid artery; c, clinoid; *, microcarotid Doppler. **(h)** Endoscopic view showing giving incision over sellar dura with Cappabianca knife. Sd, sellar dura. **(i)** Endoscopic view showing elevation of the sellar dura flap. Sd, sellar dura; ts, tubercular sellae; PS, planum sphenoidale.

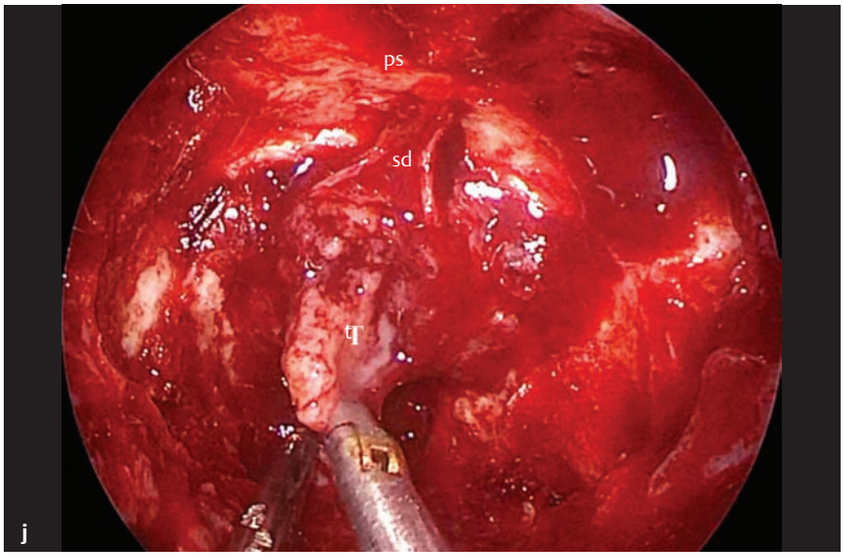

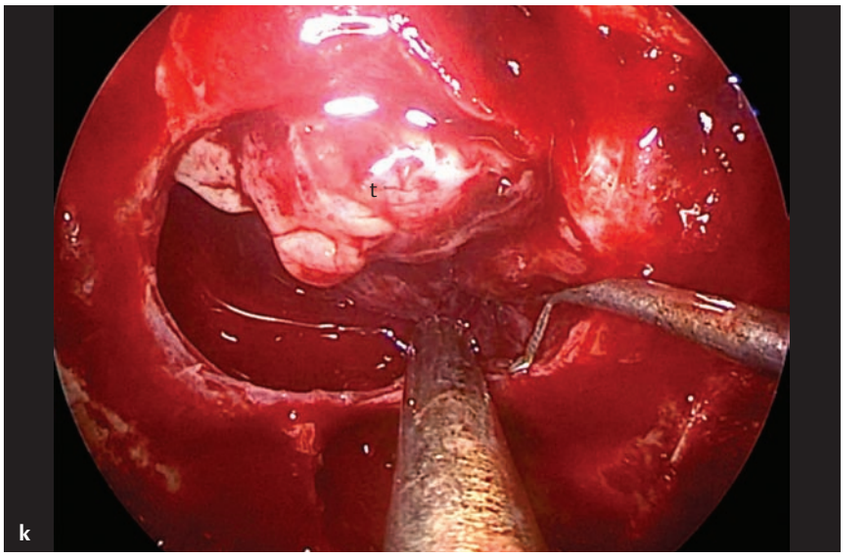

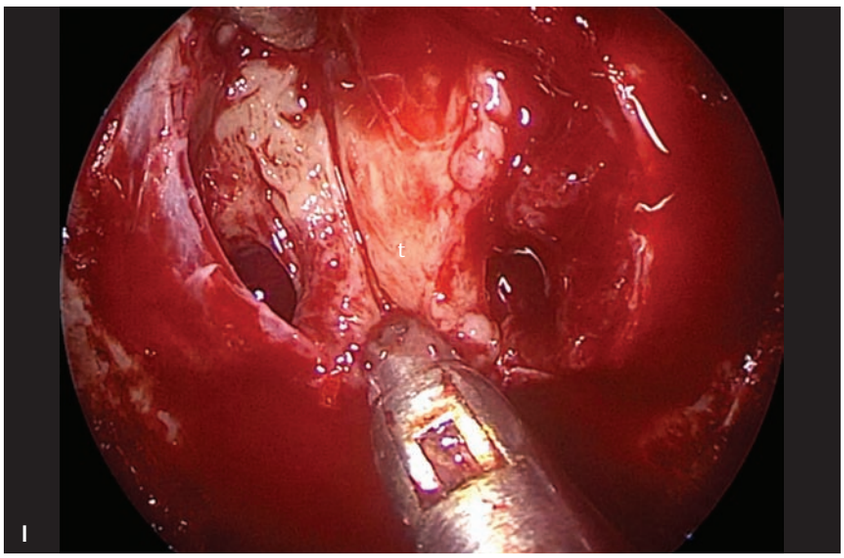

Fig. 8.25 **(j)** Taking biopsy from the tumor. PS, planum sphenoidale; T, tumor; ts, tubercular sellae. **(k)** Endoscopic view showing removal of tumor from the left cavernous sinus. T, tumor. **(l)** Endoscopic view showing removal of fibrous part of the tumor from the suprasellar region. T, tumor.

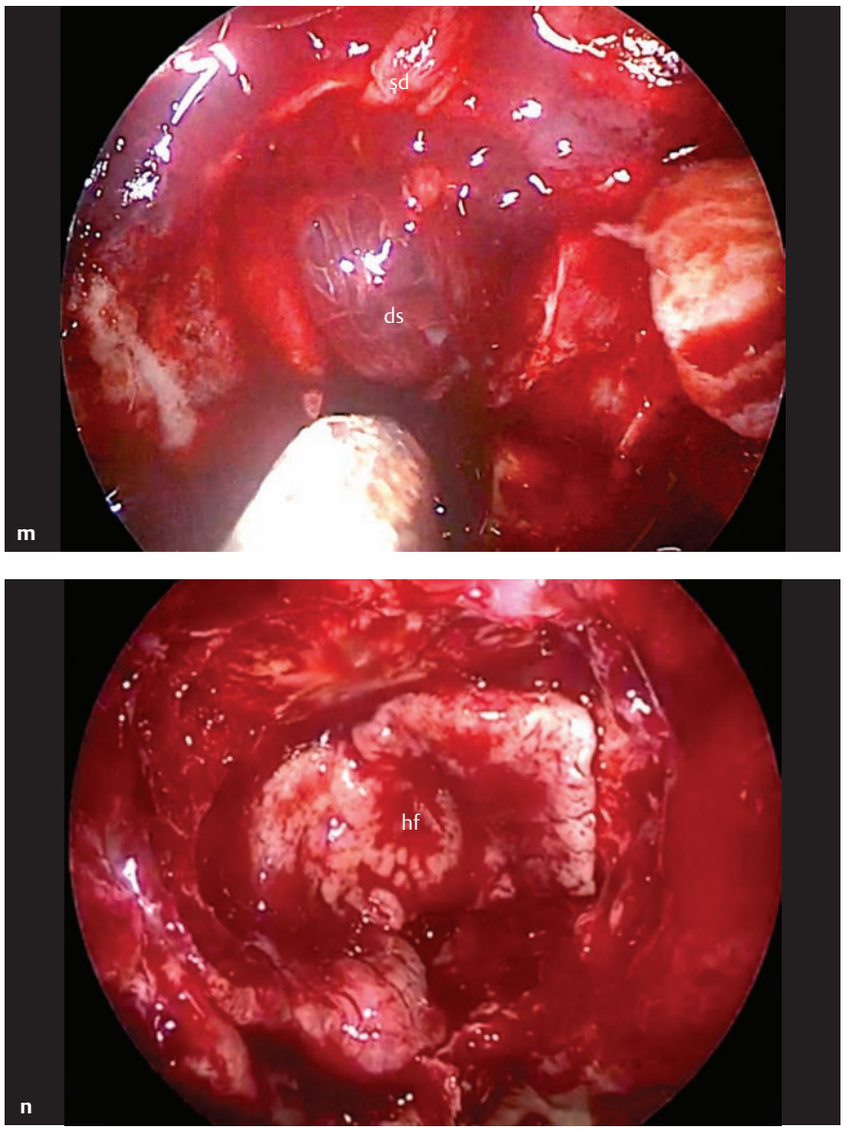

Fig. 8.25 **(m)** Endoscopic view showing sellar cavity after total removal of the tumor. Sd, sellar dura; ds, diaphragma sellae. **(n)** Endoscopic view showing reconstruction with nasoseptal flap. Hf, Hadad flap.

Case 9: Pituitary Macroadenoma with Suprasellar Extension

This patient was presented with bitemporal hemianopia. MRI showed sellar and suprasellar pituitary macroadenoma (**Fig. 8.26a**). After wide exposure of bilateral sphenoid sinuses and elevation of nasoseptal flap, drilling of floor of sella was carried out (**Fig. 8.26b**). Sellar bone was removed with Rosen's elevator after thinning it (**Fig. 8.26c**). Bone over carotids was drilled and removed (**Fig. 8.26d**). Tuberculum area bone was drilled out and removed (**Fig. 8.26e**). Bilateral MOCR was drilled out, thinnned, and removed with Kerrison's rongeurs. Bilateral carotids were mapped with carotid Doppler (**Fig. 8.26f**). Then incision was made on the endosteal layer of dura with Cappabianca knife (**Fig. 8.26g**) and Kassam's rotatable scissors and "U"-shaped flap of endosteal dura was raised (**Fig. 8.26h**). Tumor removal was initiated at 6 o'clock position with two-suction tip techniques (**Fig. 8.26i**). Then at 3 o'clock and 6 o'clock positions tumor was removed. Tumor from the medial wall of the cavernous sinus was removed with curved suction tip (**Fig. 8.26j**). After this, 12 o'clock dissection was carried out and the suprasellar part of the tumor was identified (**Fig. 8.26k**). Suprasellar part of the tumor was removed with low power curved tip suction from the diaphragm (**Fig. 8.26l**). With the help of small neuro patty, diaphragma sellae was gently elevated to confirm total removal of tumor (Q-tip technique) (**Fig. 8.26m**). No CSF leak was found (**Fig. 8.26n**), reconstruction was carried out in multilayer fashion using fat, fascia, and nasoseptal flap (**Fig. 8.26o**).

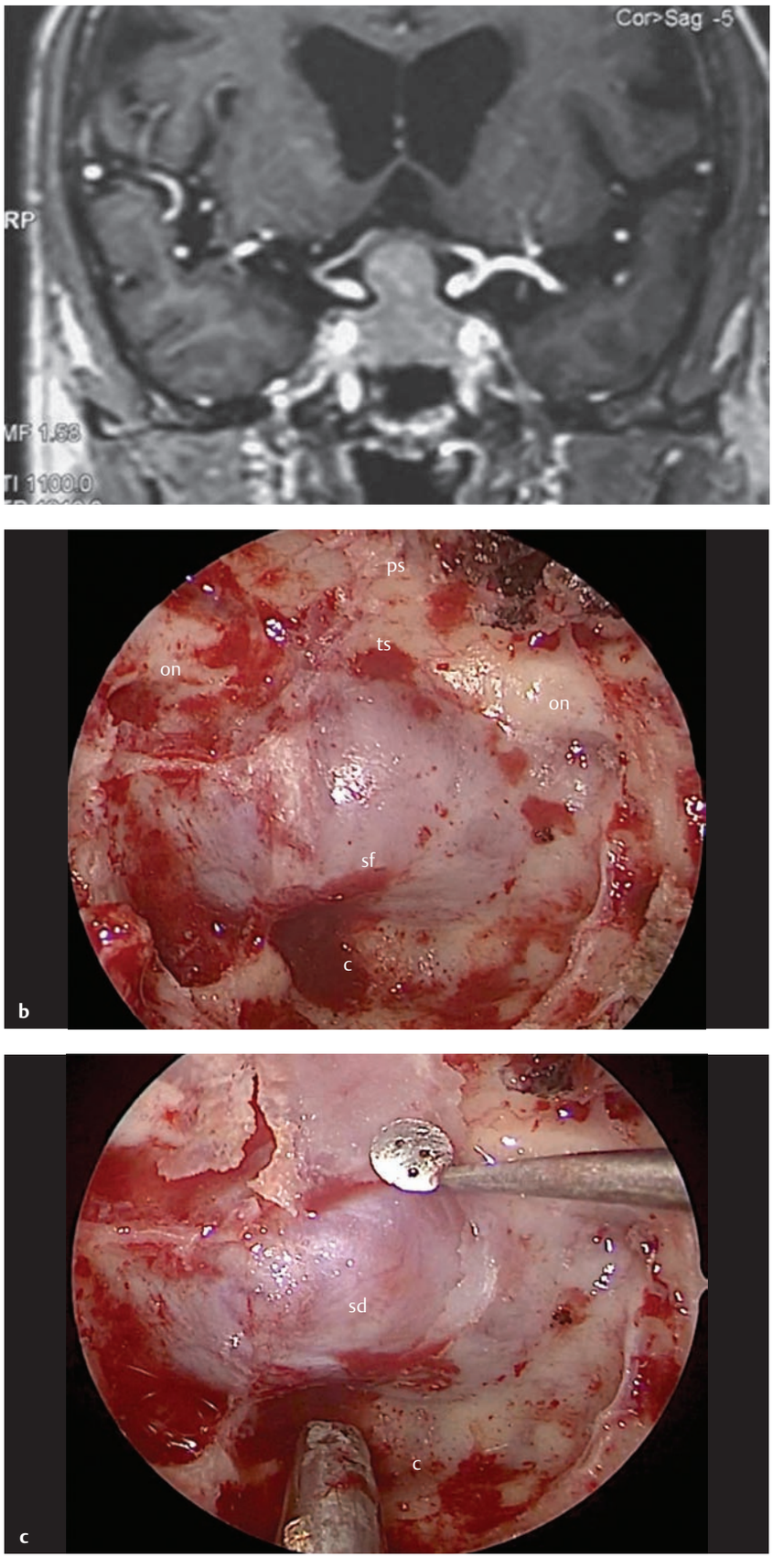

Fig. 8.26 **(a)** MRI coronal section showing mass lesion in sellar region extending to suprasellar region. **(b)** Endoscopic view showing wide exposure of sphenoid sinuses. C, clinoid; PS, planum sphenoidale; Sf, sellar floor; on, optic nerve; ts, tuberculum sellae. **(c)** Endoscopic view showing elevation of the sellar floor bone after drilling it to eggshell. C, clinoid; sd, sellar dura.

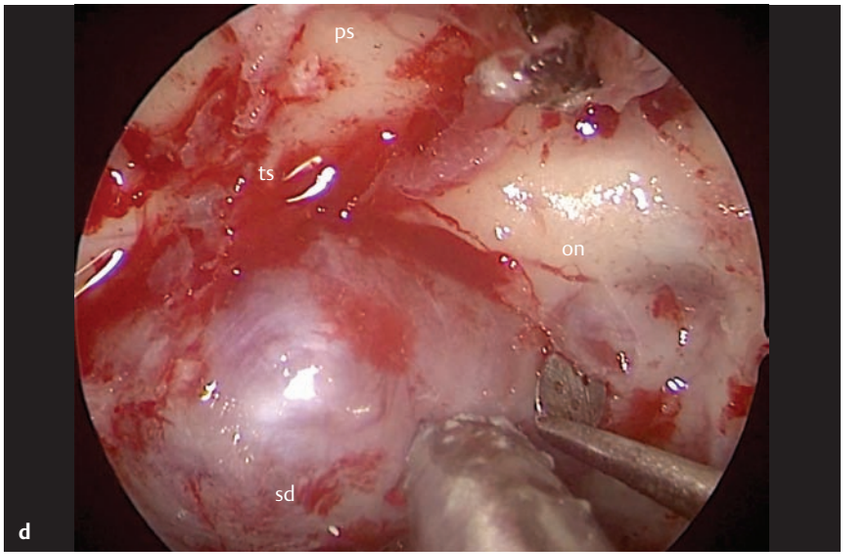

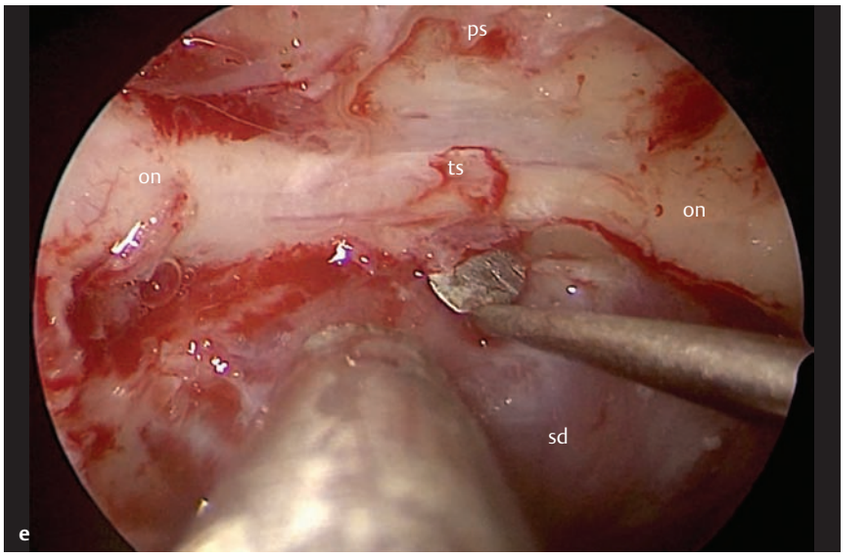

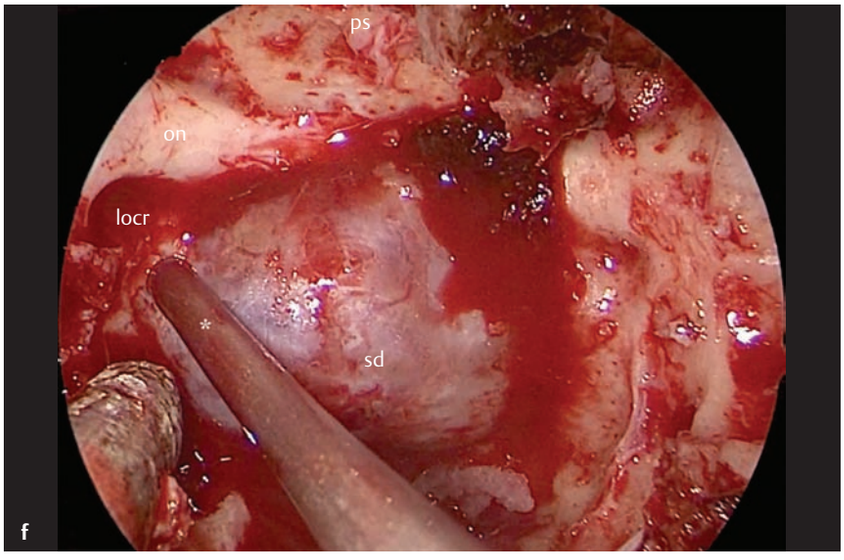

Fig. 8.26 **(d)** Endoscopic view showing removing of left medial opticocarotid recess. PS, planum sphenoidale; sd, sellar dura; ts, tuberculum sphenoidale; on, optic nerve. **(e)** Endoscopic view showing removal of the tuberculum sphenoidale bone. On, optic nerve; ps, planum sphenoidale; sd, sellar dura; ts, tuberculum sphenoidale. **(f)** Endoscopic view showing mapping of internal carotid artery with micro doppler. On, optic nerve; ps, planum sphenoidale; ts, tuberculum sphenoidale; sd, sellar dura; *, carotid micro Doppler.

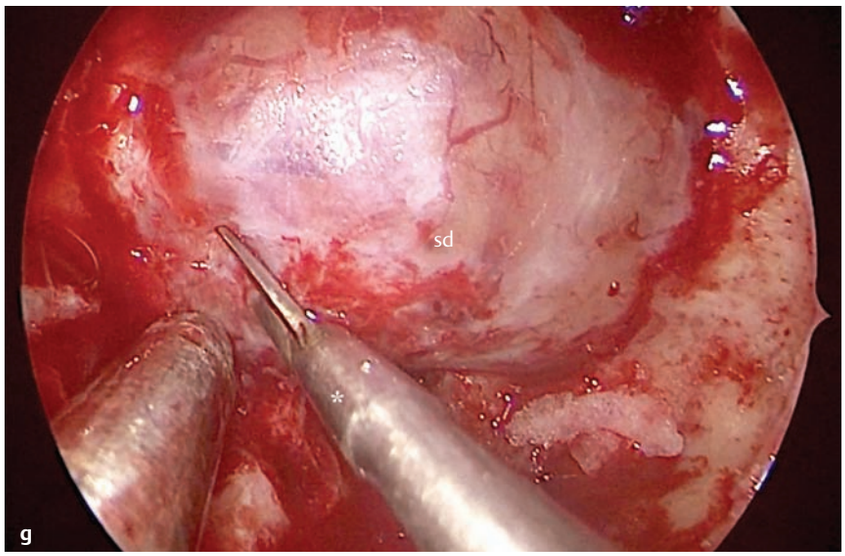

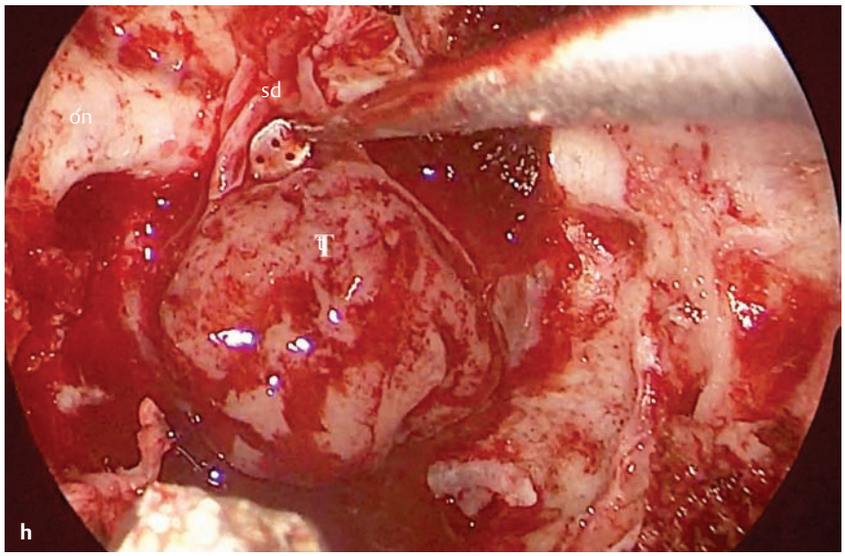

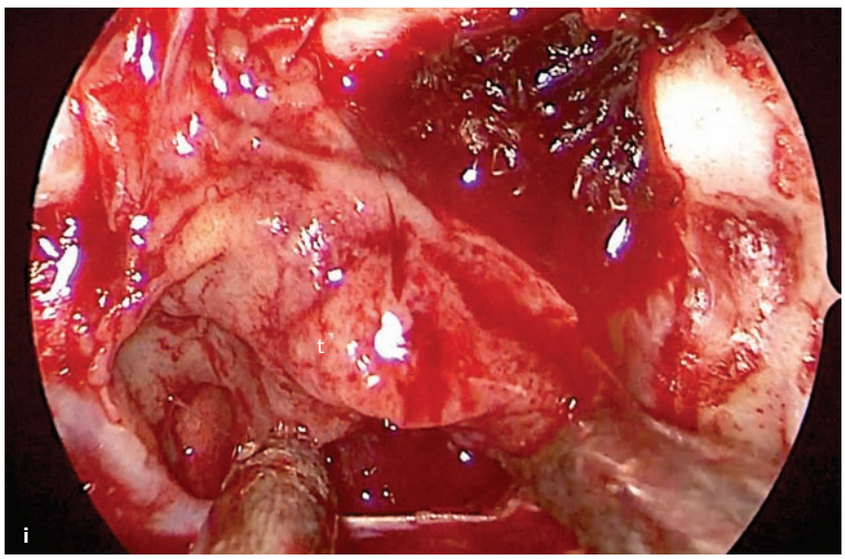

Fig. 8.26 **(g)** Endoscopic view showing giving incision over sellar dura. Sd, sellar dura. **(h)** Endoscopic view showing tumor in sellar region after elevation of the dural flap. On, optic nerve; sd, sellar dura; t, tumor. **(i)** Endoscopic view showing dissection of the tumor with two-suction technique. T, tumor.

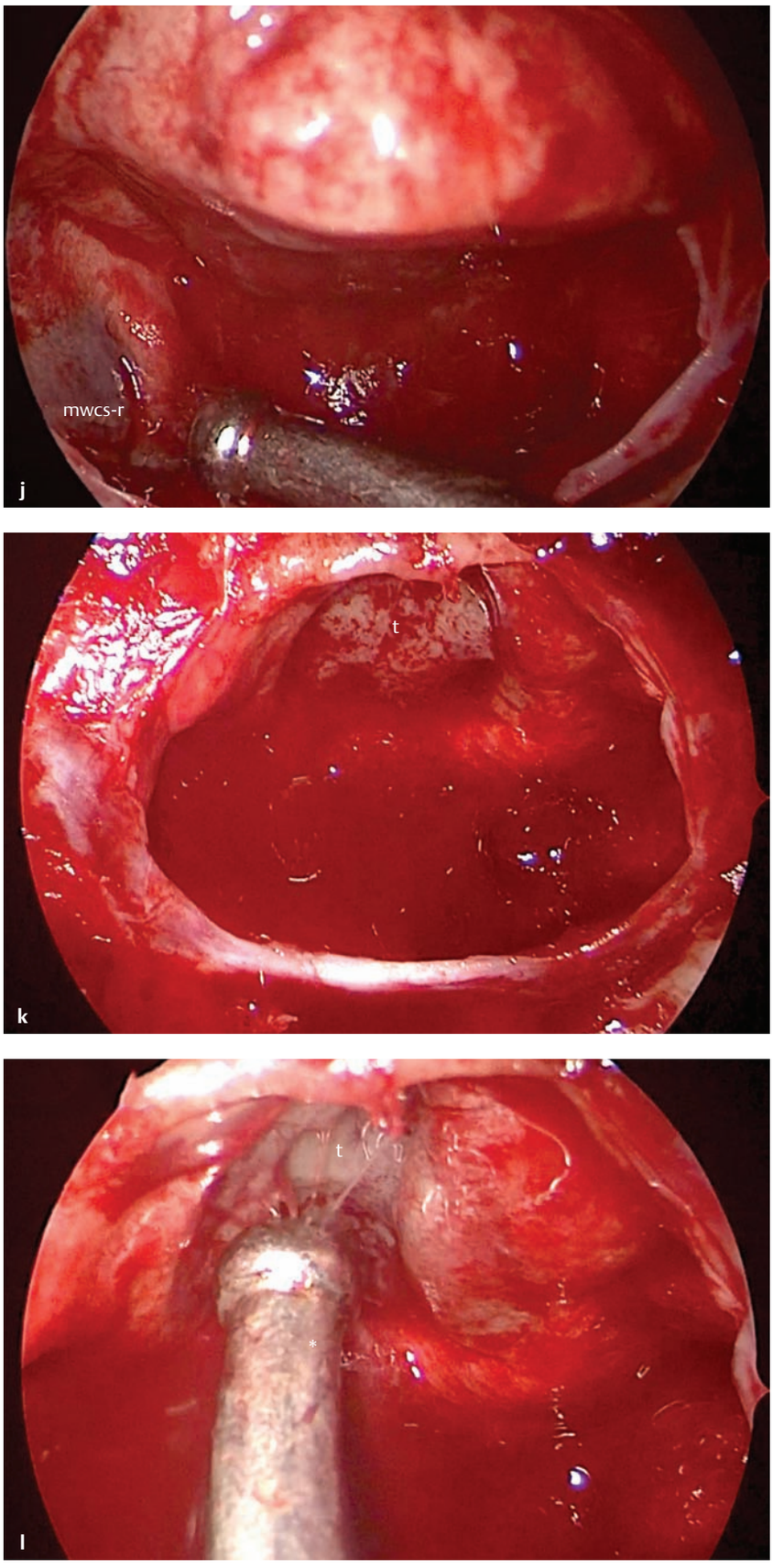

Fig. 8.26 **(j)** Endoscopic view showing clearance of tumor from the medial wall of right cavernous sinus. Mwcs-r, medial wall of right cavernous sinus. **(k)** Endoscopic view showing sellar cavity after clearance of sellar part of tumor. Suprasellar part of tumor can be seen. Sd, sellar dura; t, tumor. **(l)** Endoscopic view showing removal of tumor from the suprasellar area. T, tumor; *, cavernous sinus suction tip.

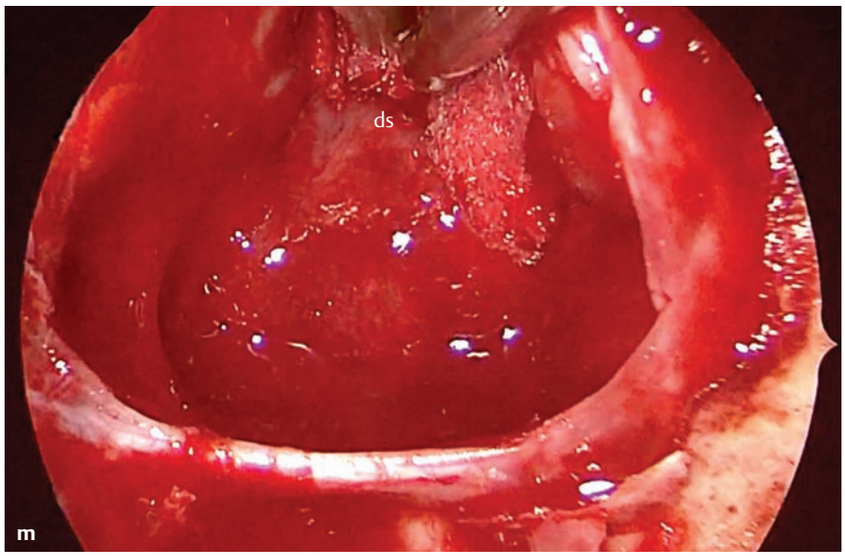

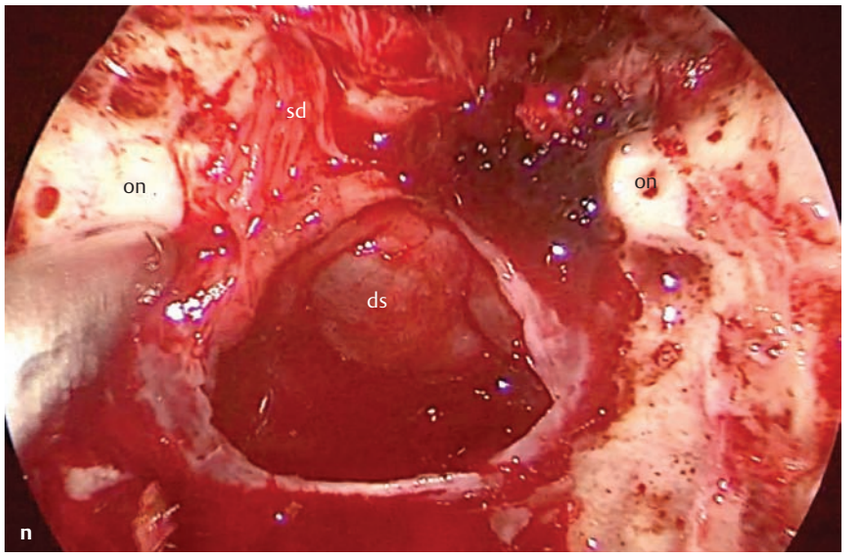

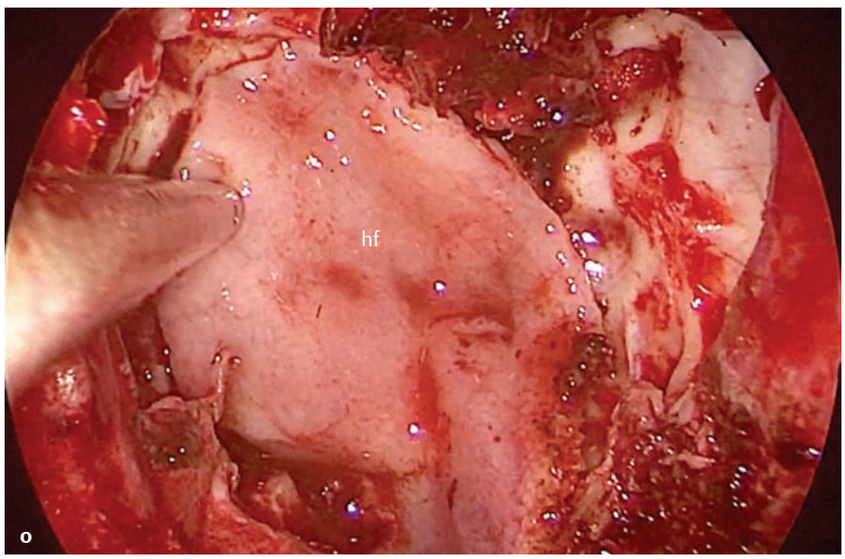

Fig. 8.26 **(m)** Endoscopic view showing examination of cavity with q tip technique. Ds, diaphragma sellae. **(n)** Endoscopic view showing sellar cavity after tumor removal. Ds, diaphragma sellae; on, optic nerve; sd, sellar dura. **(o)** Reconstruction with nasoseptal flap. Hf, Hadad flap.

Pearls and Tips

- In soft consistency tumors, internal debulking can be done using two suctions inferiorly to prevent early descent of the diaphragm.
- The Q-tip technique is used to inspect the corners for any residue of tumor, especially around the pituitary stalk. The normal gland should be identified and preserved.
- In case of the firm tumor with pseudocapsule, extracapsular dissection is performed with identification and preservation of the normal pituitary gland. Fine blunt endoscopic dissection is performed to separate fibrous bands and remove tumor in toto.

Meningiomas

PS and tuberculum sphenoidale meningiomas require precise surgical attention due to their close proximity to important neurovascular and endocrine structure. Tuberculum sellae meningiomas comprise 3 to 10% of all intracranial meningiomas. They arise from chiasmatic sulcus, tuberculum sellae, and limbus sphenoidale. PS meningiomas, account for 8 to 18% of intracranial meningiomas. PS meningiomas are diagnosed at later stages with symptoms of frontal lobe compression such as apraxia and behavioral changes.[12]

Case 10: Planum Tuberculum Meningioma

A 55-year-old woman presented with complaints of headache and bilateral diminishing vision. MRI showed mass lesion in the suprasellar region compressing bilateral optic nerves and the anterior circulation (**Fig. 8.27a, b**). After wide exposure of sphenoid sinuses (**Fig. 8.27c**) sellar floor was drilled with s3 neurodrill and removed with gentle elevation with Rosen's elevator (**Fig. 8.27d**). Bone of planum sphenoidale was drilled up to the exposure of the dura (**Fig. 8.27e**). Bilateral optic canals were also drilled because there was an invasion by the tumor (**Fig. 8.27f**). Microdissection of the tumor was started. Internal debulking of the tumor was done with microdissection technique. Inferiorly tumor was dissected from the optics along the arachnoid plane and decompression of the left optic nerve up to the optic chiasma was done (**Fig. 8.27g**). Tumor from the right optic nerve was dissected and decompression of the right optic nerve was done (**Fig. 8.27h**). Anterior circulation could be visualized. Superior limit of the tumor was dissected with the help of neuro patties and tumor was rolled downward and again debulked. A small part of the tumor over the anterior communicating artery (ACOM) was left behind. Multilayered reconstruction of defect was performed using Surgicel, fascia lata, vascularized pedicled nasoseptal flap (**Fig. 8.27i**).

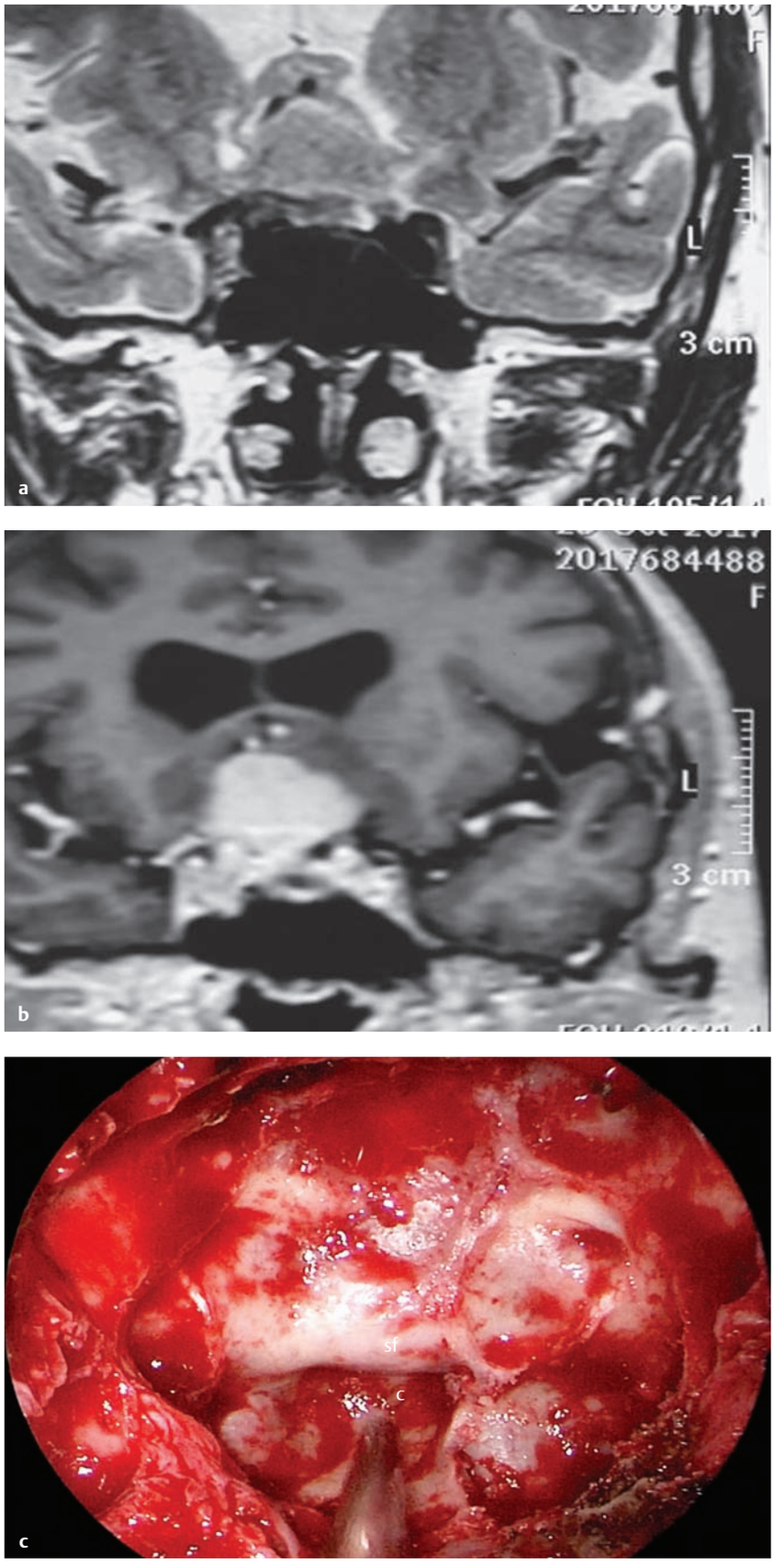

Fig. 8.27 (a and b) MRI coronal cut showing mass lesion in the suprasellar region. **(c)** Endoscopic view showing wide exposure of the sphenoid sinuses. C, clinoid; sf, sellar floor.

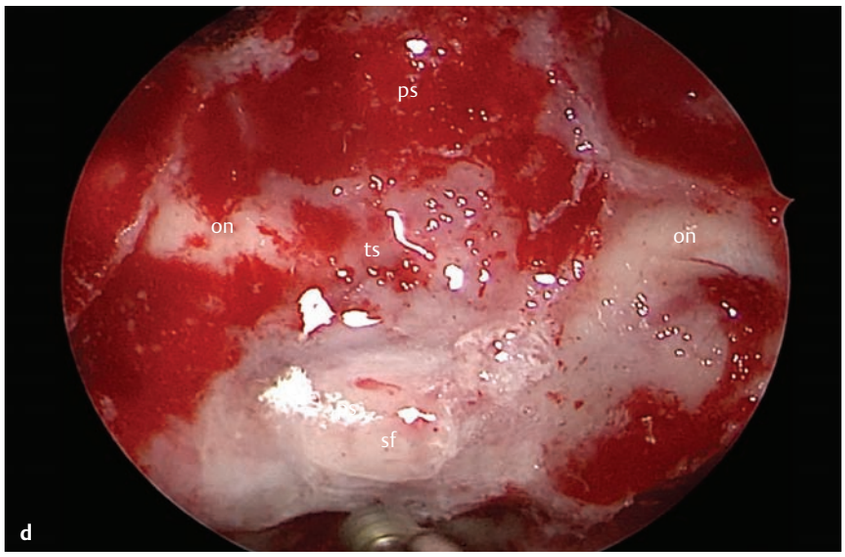

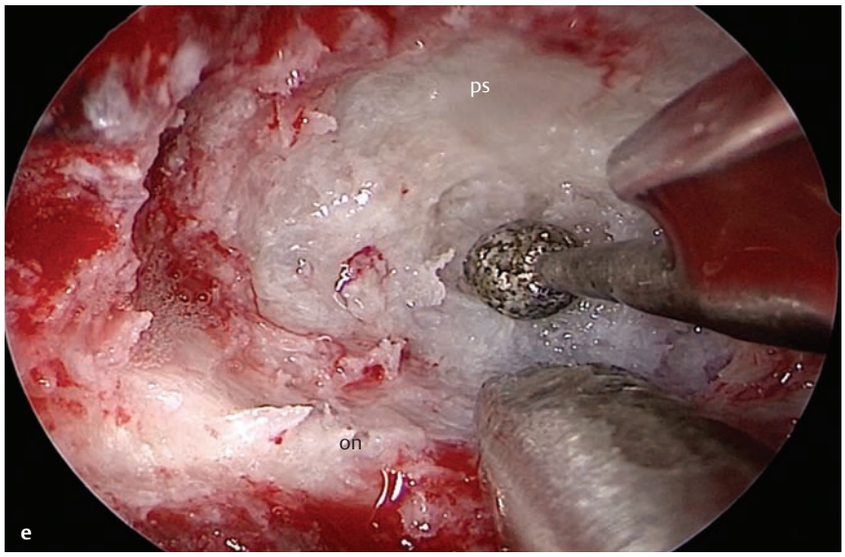

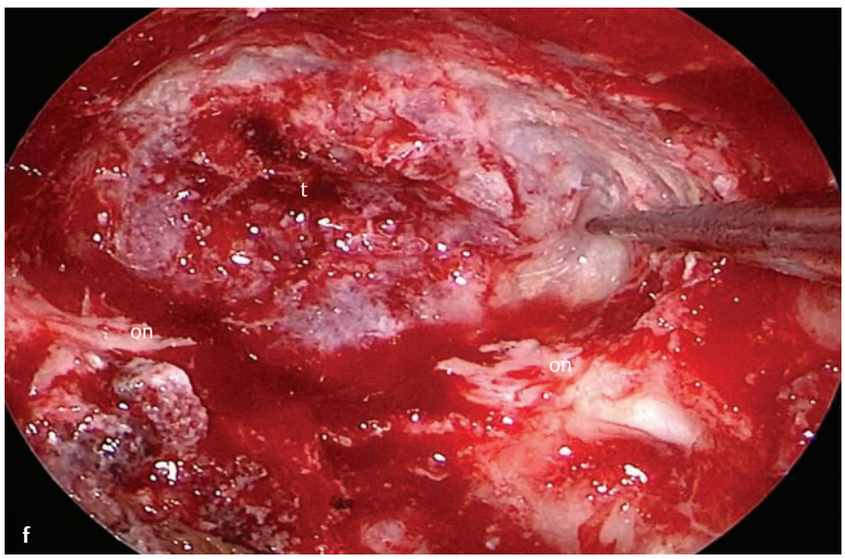

Fig. 8.27 **(d)** Endoscopic view showing drilling of the sellar floor. On, optic nerve; ps, planum sphenoidale; ts, tuberculum sphenoidale. **(e)** Endoscopic view showing drilling of the right optic canal and planum area. On, optic nerve; ps, planum sphenoidale. **(f)** Endoscopic view showing wide exposure of the tumor after removal of the planum sphenoidale bone. On, optic nerve; t, tumor.

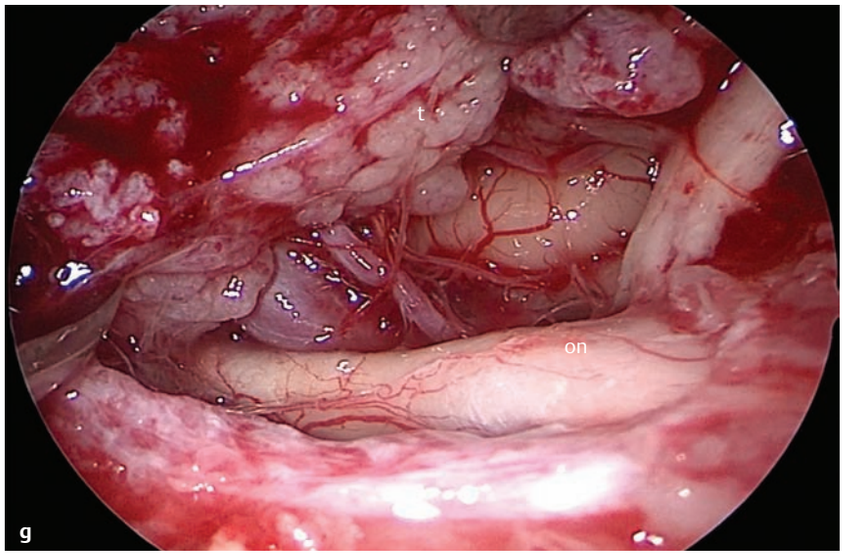

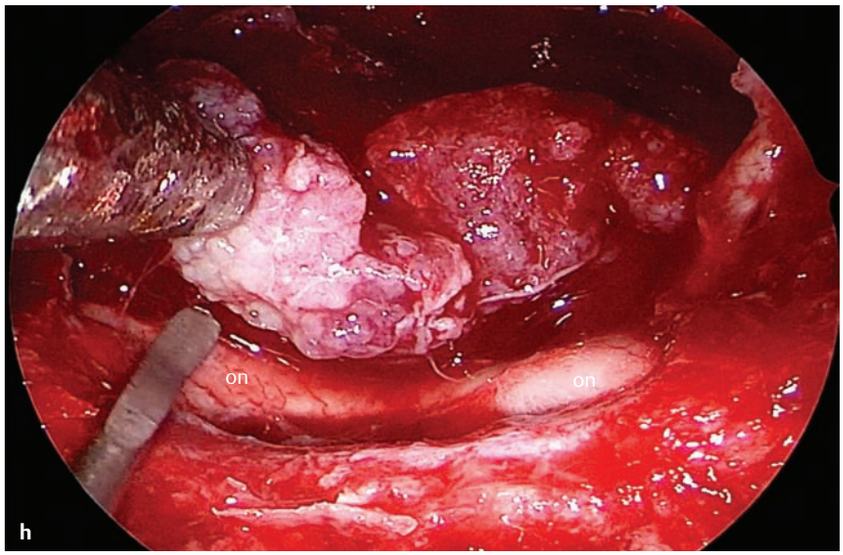

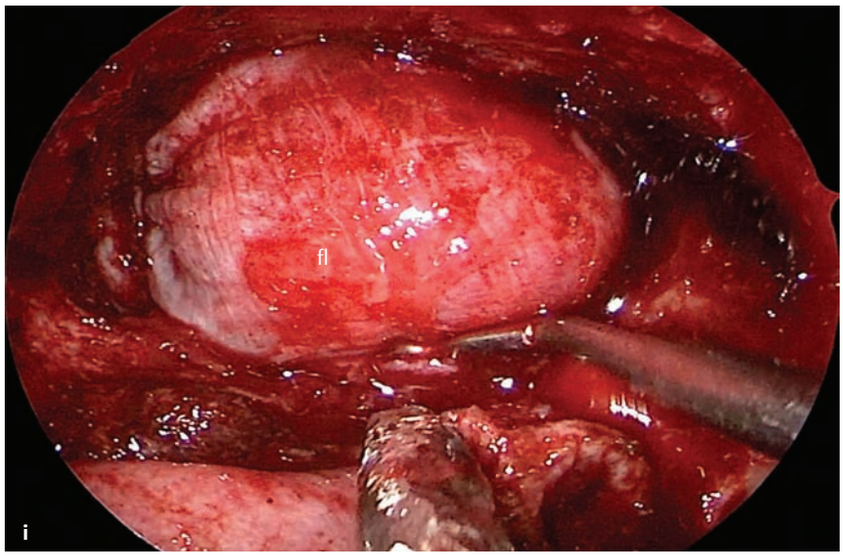

Fig. 8.27 **(g)** Endoscopic view showing dissection of tumor from the left optic nerve. On, optic nerve. **(h)** Endoscopic view showing dissection of tumor from the right optic nerve. On, optic nerve. **(i)** Endoscopic view showing reconstruction using fat and fascia lata graft. Fl, fascia lata.

Case 11: Planum Tuberculum Meningioma

A 35-year-old woman presented with persistent headache. MRI showed a mass lesion in suprasellar region, which was diagnosed as a planum/tuberculum meningioma (**Fig. 8.28a, b**). Wide exposure of the sphenoid sinus was done (**Fig. 8.28c**). Bone over the PS and tubercular area was drilled to eggshell thin (**Fig. 8.28d**) and removed with the help of Rosen's elevator (**Fig. 8.28e**). Bone over supraoptic recess was drilled. Dura over the planum was incised with Cappabianca knife and a flap was raised with Kassam's rotatable scissors (**Fig. 8.28f**). Tumor was identified. Biopsy sample from the tumor was taken and debulking of tumor was carried out (**Fig. 8.28g**). Extracapsular dissection of the tumor was carried out (**Fig. 8.28h**). Tumor was gently dissected from the left side optic nerve and ICA (**Fig. 8.28i**). Anterior circulation was visualized. Tumor was found adherent to ACOM. Authors dissected tumor out from the ACOM without damaging it (**Fig. 8.28j**). A perforator was seen on the right side of tumor which was cauterized with Kassam's bipolar cautery (**Fig. 8.28k**). Tumor was dissected from the right side optic nerve and pituitary chiasm. Panoramic view of suprachiasmatic cistern can be seen. Anterior circulation, optic nerves, optic chiasm were identified (**Fig. 8.28l**). Reconstruction was carried out in a multilayer fashion with Surgicel, DuraGen, fascia lata, nasoseptal flap, and Gelfoams (**Fig. 8.28m**). Endoscopic examination after 1 year shows nasoseptal flap in situ (**Fig. 8.28n**). See **Video 8.5**.

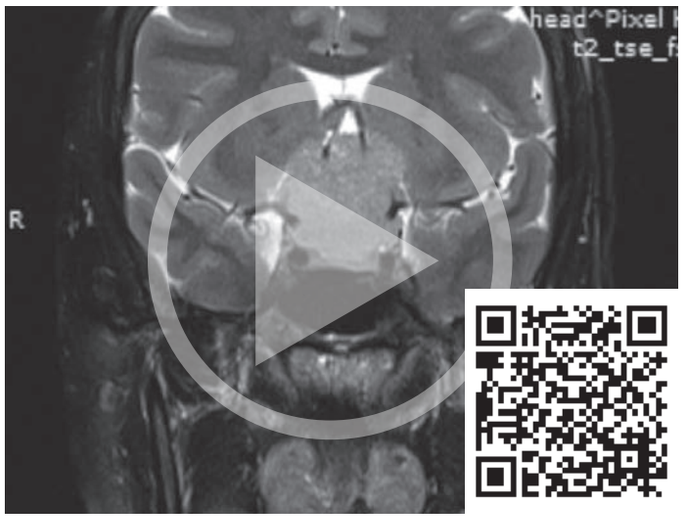

Video 8.5 Planum/ Tuberculum meningioma – 1. https://www.thieme.de/de/q.htm?p=opn/cs/19/9/10104307-e00c26f7

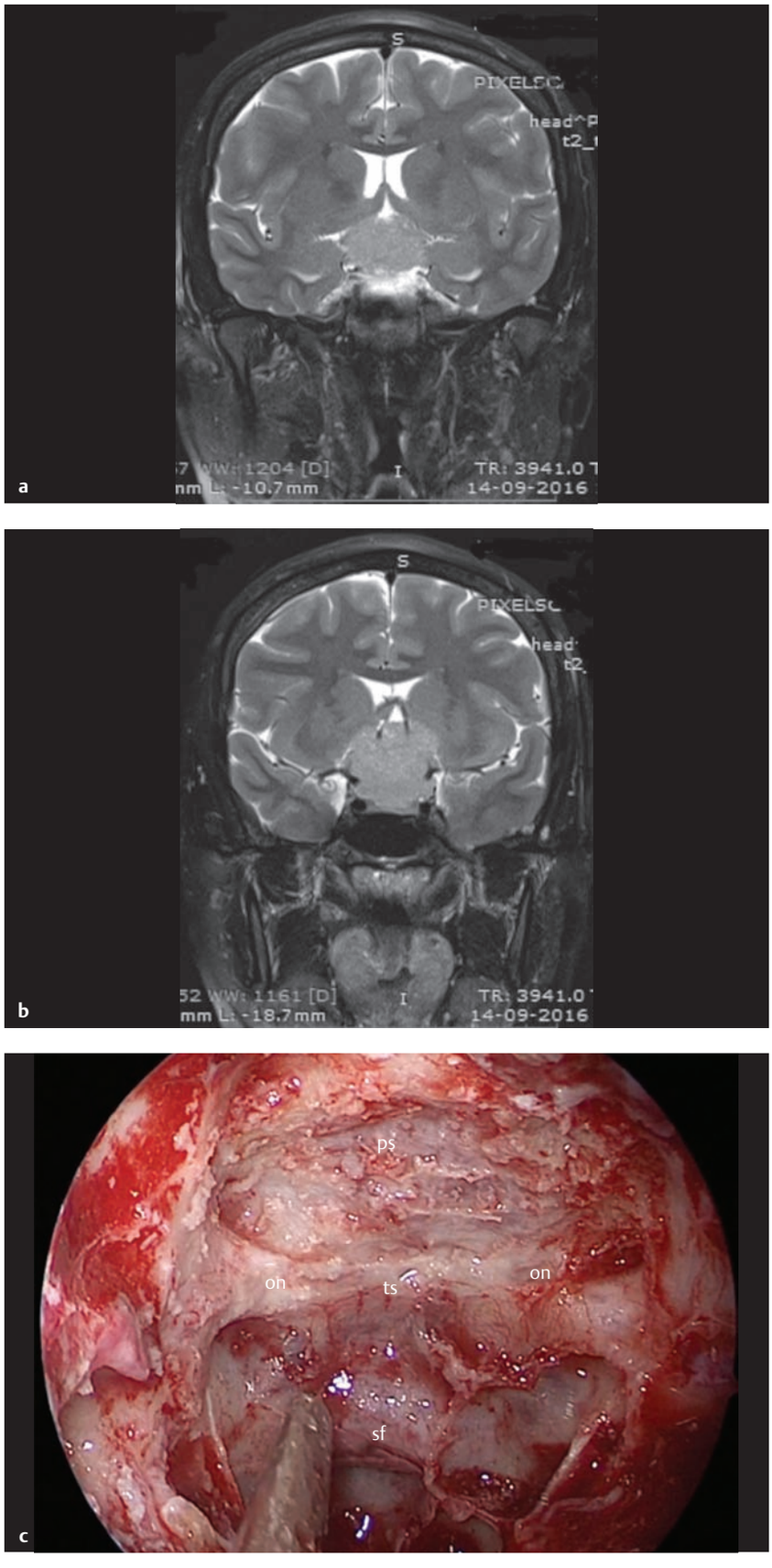

Fig. 8.28 **(a)** MRI coronal cut showing mass lesion in the suprasellar region. **(b)** MRI coronal cut showing mass lesion in suprasellar region and it is closely related to optic nerves and carotid arteries. **(c)** Endoscopic view showing wide exposure of the bilateral sphenoid sinuses. On, optic nerve; PS, planum sphenoidale; sf, sellar floor; ts, tuberculum.

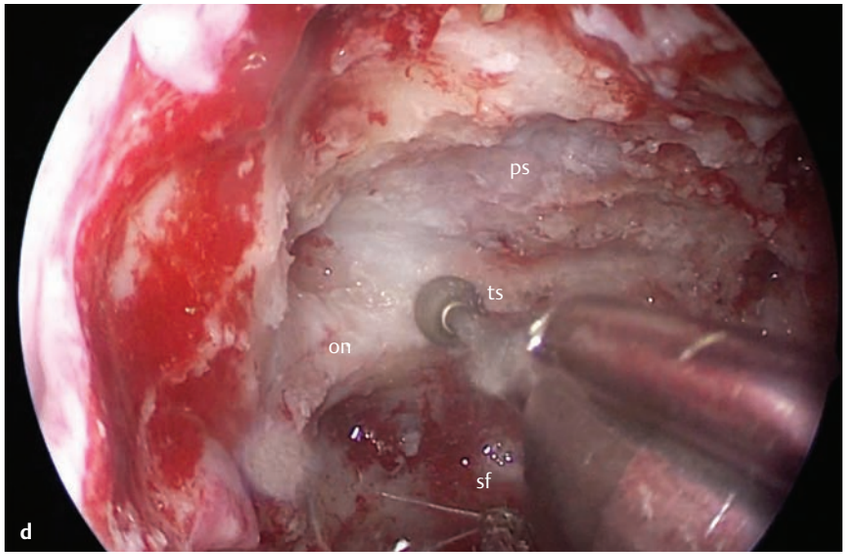

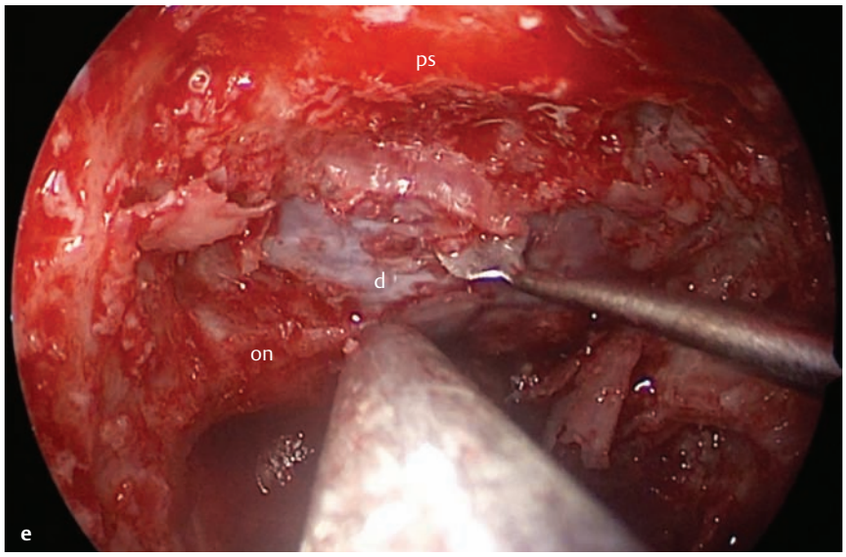

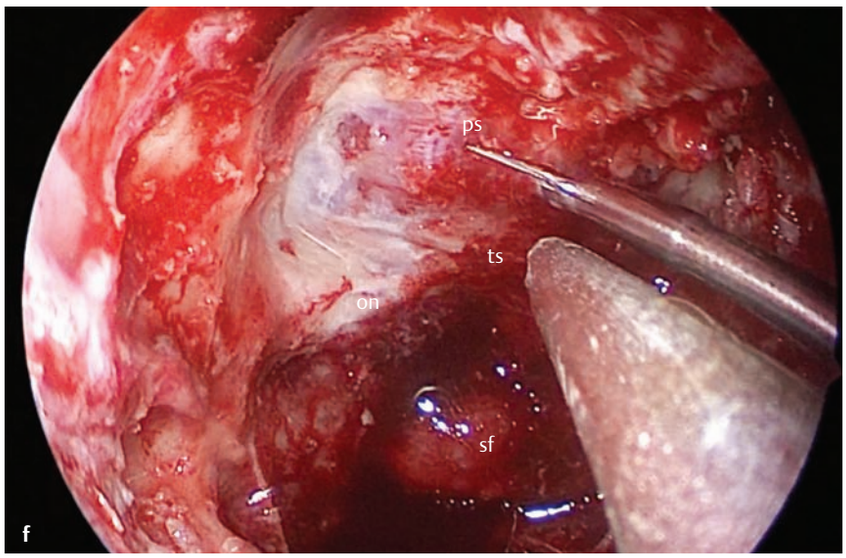

Fig. 8.28 **(d)** Endoscopic view showing drilling of the right optic canal. On, optic nerve; PS, planum sphenoidale; sf, sellar floor; ts, tuberculum. **(e)** Endoscopic view showing elevation of the planum sphenoidale bone after drilling it to eggshell. D, dura; on, optic nerve; ps, planum sphenoidale. **(f)** Endoscopic view showing giving incision over planum dura. On, optic nerve; ps, planum sphenoidale; ts, tuberculum.

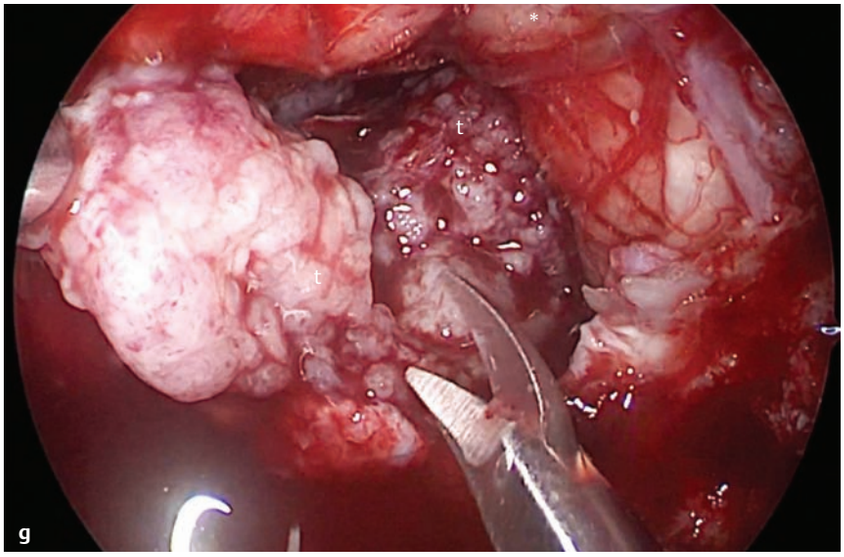

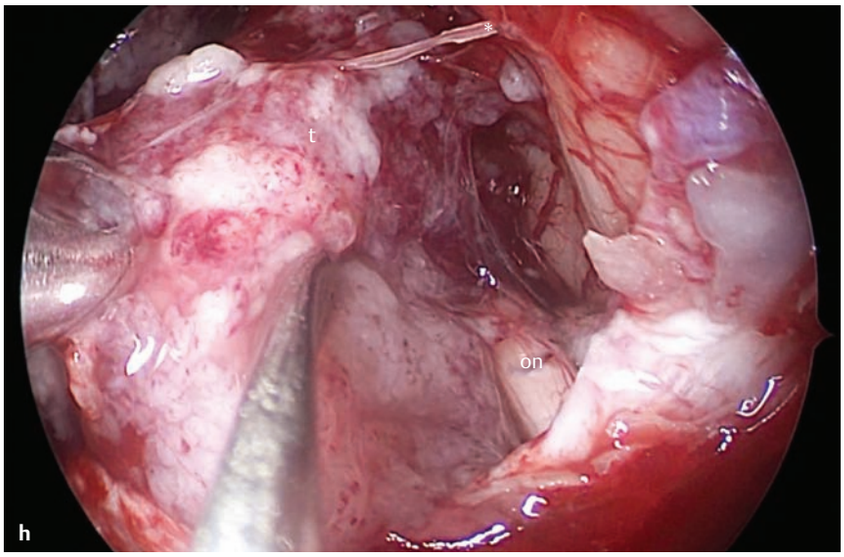

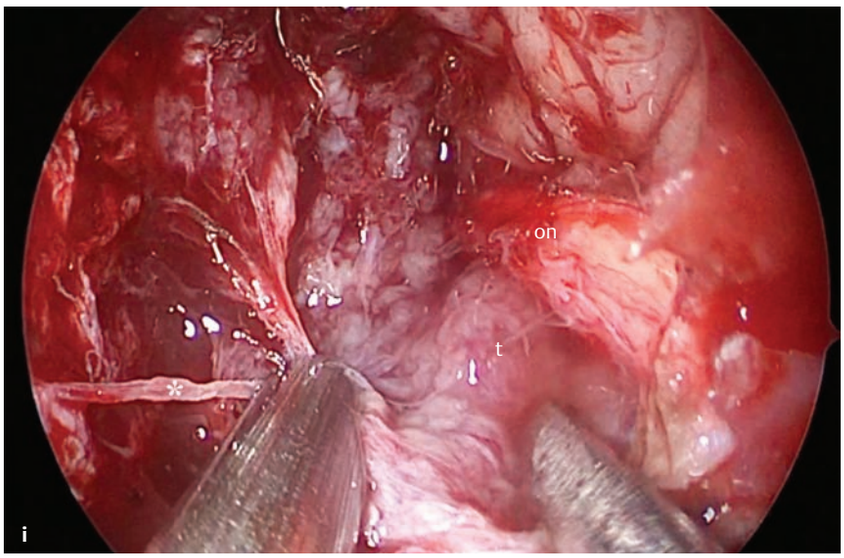

Fig. 8.28 **(g)** Endoscopic view showing debulking of tumor. T, tumor. **(h)** Endoscopic view showing dissection of the tumor from the left optic nerve. On, optic nerve; t, tumor. **(i)** Endoscopic view showing dissection of the tumor from the left optic nerve and frontal lobe. On, optic nerve; t, tumor.

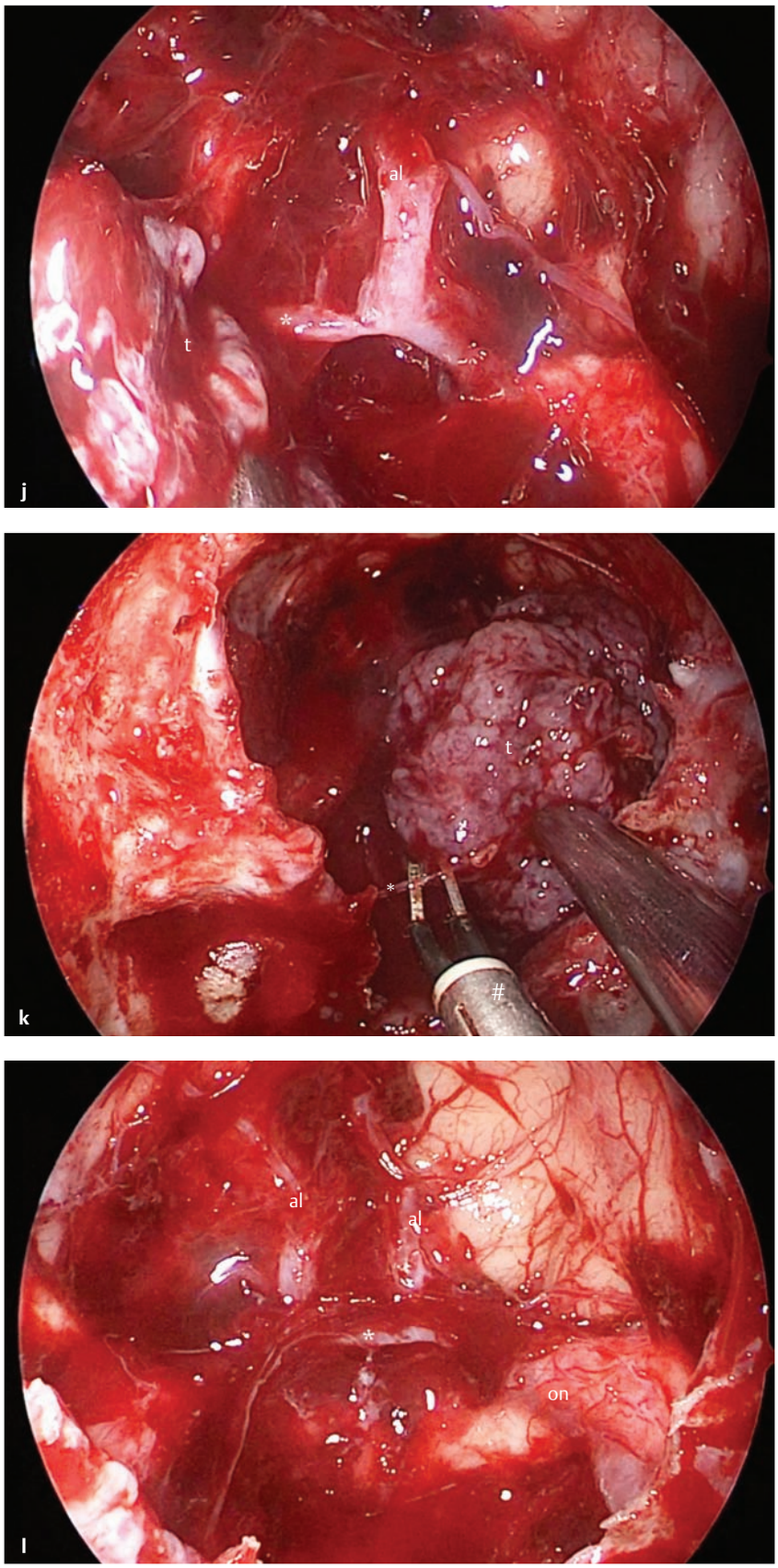

Fig. 8.28 **(j)** Endoscopic view showing dissection of tumor from the anterior circulation; *, anterior communicating artery; a1, a1 segment of anterior cerebral artery. **(k)** Endoscopic view showing dissection of tumor from right optic nerve and cauterization of dural blood vessel suppling tumor. T, tumor; *, dural blood vessel. **(l)** After complete removal of tumor view of the suprachiasmatic cistern. a1, a1 segment of anterior cerebral artery; on, optic nerve; *, anterior communicating artery.

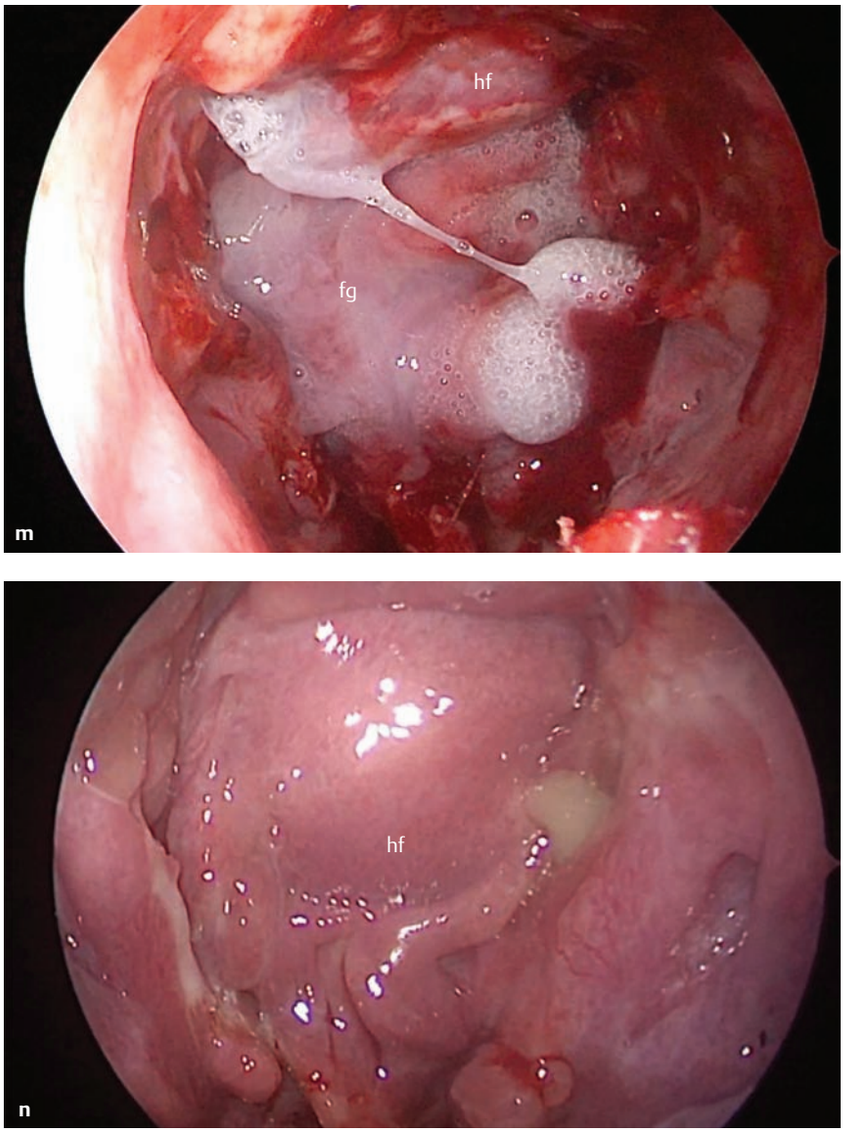

Fig. 8.28 **(m)** Endoscopic view showing reconstruction with nasoseptal flap. Fg, fibrin glue; Hf, Hadad flap. **(n)** 1-year postop endoscopic image showing well vascularized Hadad flap. Hf, Hadad flap.

Case 12: Planum Tuberculum Meningioma

A 45-year-old patient presented with bilateral diminishing vision. CT and MRI were suggestive of mass lesion in suprasellar region compressing the optic nerve bilaterally. A diagnosis of planum/tuberculum meningioma was made (**Fig. 8.29a**). Wide exposure of the sphenoid sinus was done (**Fig. 8.29b**). Important anatomical landmarks such as bilateral LOCR, carotids, anterior most level of the tumor (**Fig. 8.29c**), and level of the normal pituitary gland (**Fig. 8.29d, e**) were identified and verified with help of the navigation. Drilling over the sellar floor, bilateral cavernous carotids, tubercular strut, PS, and bilateral optic canals with bilateral superior optic recesses were done (**Fig. 8.29g**). After exposure, limits were confirmed with the navigation. Horizontal dural incision at the level of planum was made (**Fig. 8.29h**). Incision enlarged inferiorly up to the sellar level vertically. SICS was cauterized with the help of bipolar cautery (**Fig. 8.29i**). Superior border of normal pituitary gland was identified. Tumor was visualized after opening the dura. Dissection of the tumor was carried out (**Fig. 8.29j**). Left side of tumor was dissected from the optic nerve and decompression of left optic nerve was completed (**Fig. 8.29k**). Left side carotid artery is visualized. With microdissection technique debulking of tumor was performed. Tumor was adherent to the right side A1 artery. Very careful dissection of the tumor from A1 segment was done with help of pituitary elevator without damaging it. Complete removal of the tumor was done (**Fig. 8.29l**). Cavity was irrigated with the ringer lactate solution. Suprachiasmatic cistern was examined thoroughly. Bilateral optic nerve, optic chiasm, pituitary gland, pituitary stalk, A1, A2, and anterior communicating arteries were identified. Multilayer reconstruction was carried out with Surgicel, fat, fascia lata, nasoseptal flap, fibrin tissue glue, and Gelfoams (**Fig. 8.29m**). See **Video 8.6**.

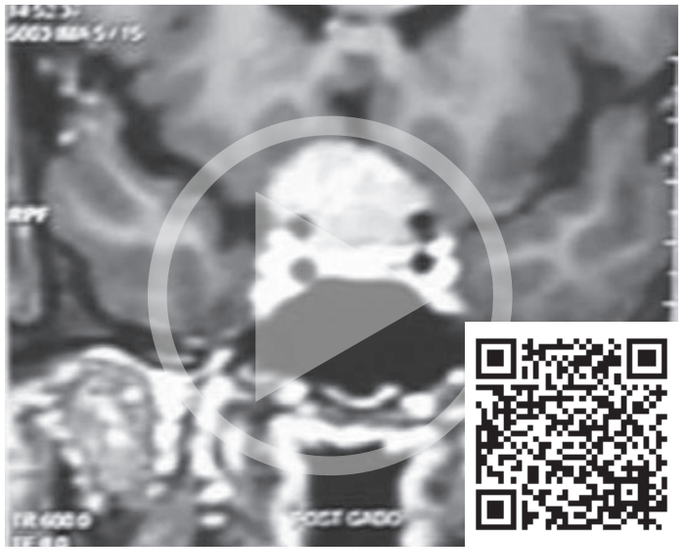

Video 8.6 Planum/ Tuberculum meningioma – 2. https://www.thieme.de/de/q.htm?p=opn/cs/19/9/10104308-39c6c647

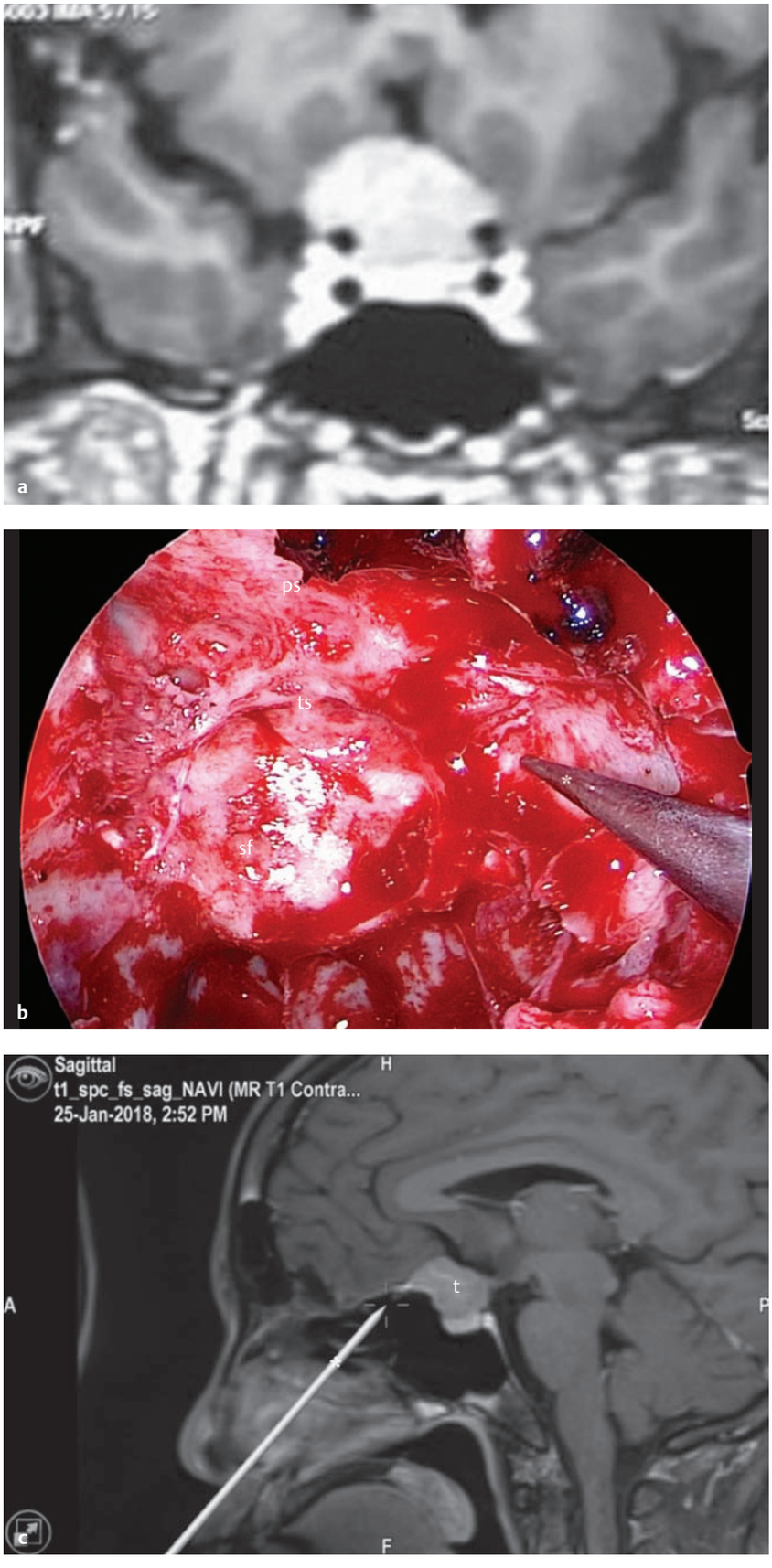

Fig. 8.29 **(a)** Showing MRI coronal cut mass lesion at suprasellar region. **(b)** Endoscopic view showing wide exposure of sphenoid sinuses and locating optic nerve with navigation probe. Ps, planum sphenoidale; sf, sellar floor; ts, tuberculum sellae. **(c)** Sagittal view on navigation probe locating anterior border of tumor.

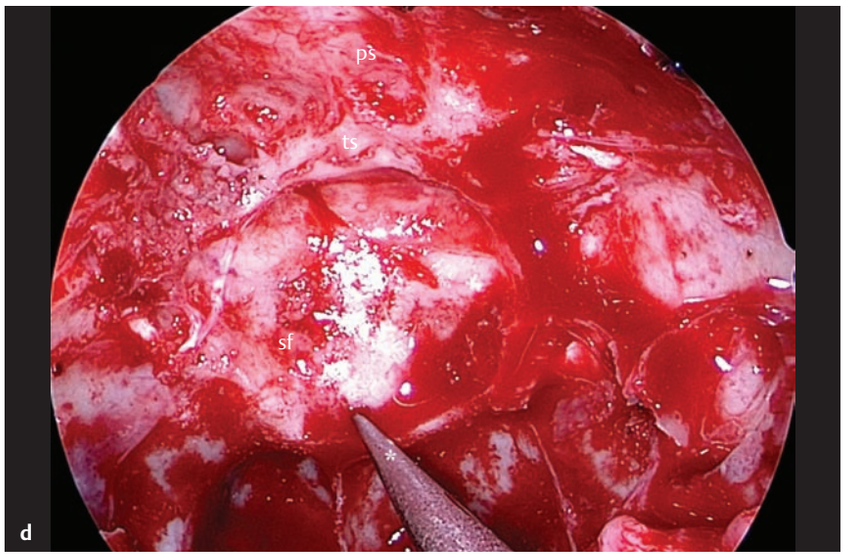

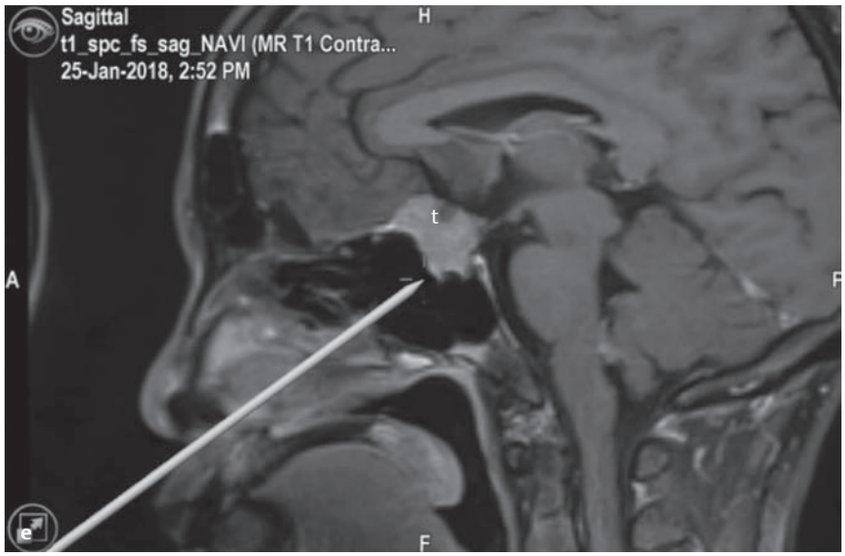

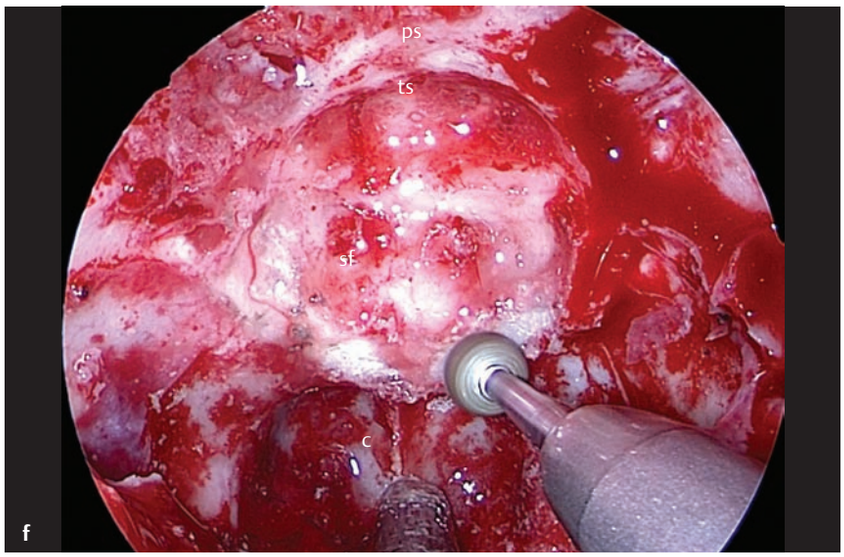

Fig. 8.29 **(d)** Endoscopic view showing locating normal pituitary gland with navigation probe. PS, planum sphenoidale; sf, sellar floor; ts, tuberculum sellae; *, navigation probe. **(e)** Sagittal view on navigation locating normal pituitary gland. Pg, pituitary gland; t, tumor. **(f)** Endoscopic view showing drilling of sellar floor. C, clinoidps; ps, planum sphenoidale; sf, sellar floor; ts, tuberculum.

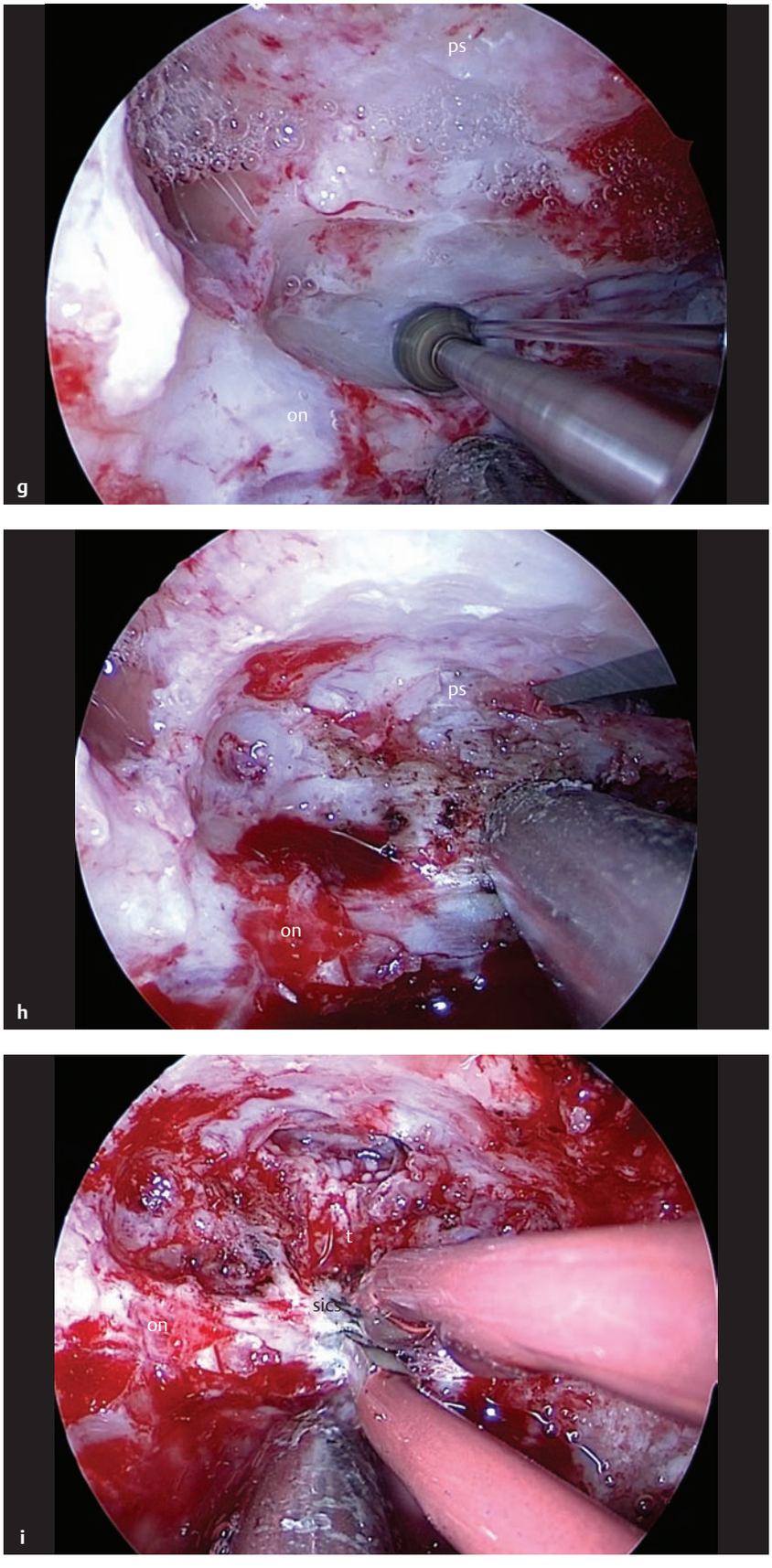

Fig. 8.29 **(g)** Endoscopic view showing drilling of optic canal. On, optic nerve; ps, planum sphenoidale. **(h)** Endoscopic view showing dural incision over planum dura. On, optic nerve; ps, planum sphenoidale. **(i)** Endoscopic view showing cauterizing superior intercavernous sinus with bipolar cautery. SICS, superior intercavernous sinus; on, optic nerve; t, tumor.

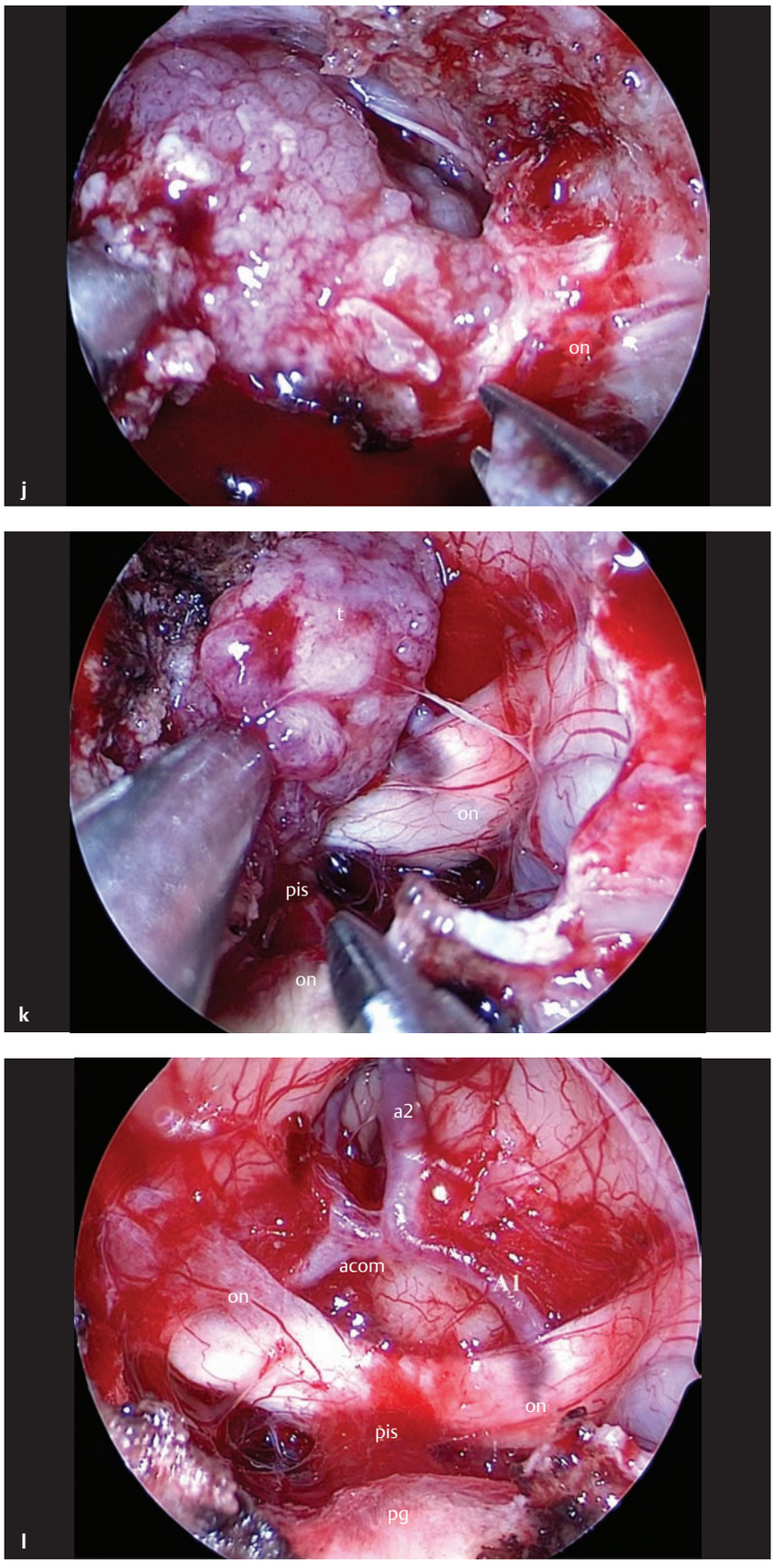

Fig. 8.29 **(j)** Endoscopic view showing dissection of tumor from the left optic nerve. On, optic nerve; t, tumor. **(k)** Endoscopic view showing dissection of tumor from the left optic nerve and pituitary stalk. On, optic nerve; pg, pituitary gland; pis, pituitary stalk; t, tumor. **(l)** Endoscopic view showing suprasellar cistern after tumor removal. A1, a1 segment of anterior cerebral artery; a2, a2 segment of anterior cerebral artery; acom, anterior communicating artery; on, optic nerve; Pg, pituitary gland; pis, pituitary stalk.

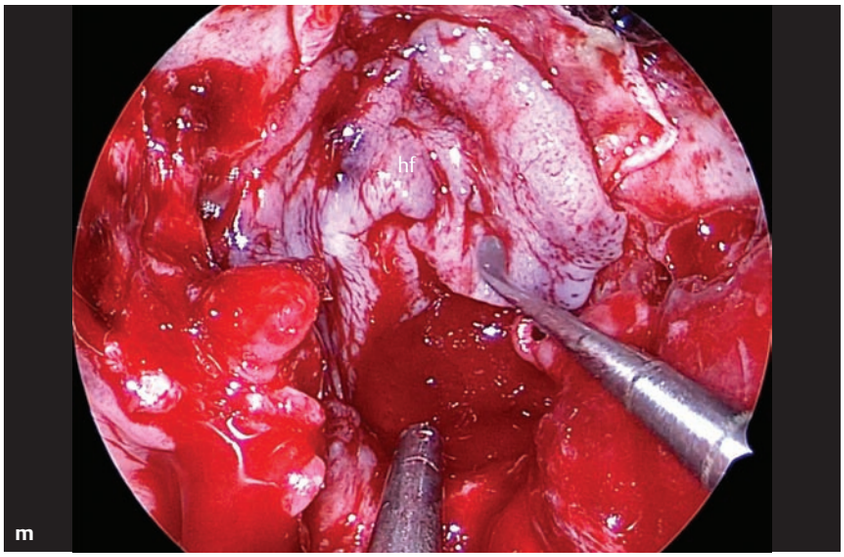

Fig. 8.29 **(m)** Endoscopic view showing reconstruction with nasoseptal flap. Hf, Hadad flap.

Case 13: Planum Tubercular Meningioma

A 58-year-old woman presented with loss of vision on left side and diminishing vision on right side. MRI scan showed a mass lesion in suprasellar region which was compressing the optic nerve bilaterally and the anterior cerebral circulation (**Fig. 8.30a, b**). After wide exposure of sphenoid sinuses PS bone was removed after drilling it to eggshell thin (**Fig. 8.30c**). Bone over tubercular sellae and sellar floor was removed (**Fig. 8.30d**). Bilateral optic canal was drilled (**Fig. 8.30e**). Dura of the tubercular area and sellar area was exposed after removing bone over it (**Fig. 8.30f**). The course of the carotid artery was mapped with carotid Doppler (**Fig. 8.30g**). Planum dura was incised and extended inferiorly after cauterizing SICS (**Fig. 8.30h**). Tumor dissection was started from the right side of the optic nerve (**Fig. 8.30i**). In the same way left optic nerve was decompressed after dissection of tumor over it (**Fig. 8.30j**). Right side of tumor was dissected from A1 segment of anterior cerebral artery (**Fig. 8.30k**). Tumor was dissected then from ACOM (**Fig. 8.30l**). After complete removal of tumor, bilateral optic nerve and anterior circulation was visualized (**Fig. 8.30m**). Reconstruction was carried out in multilayer with fat, Surgicel, and nasoseptal flap.

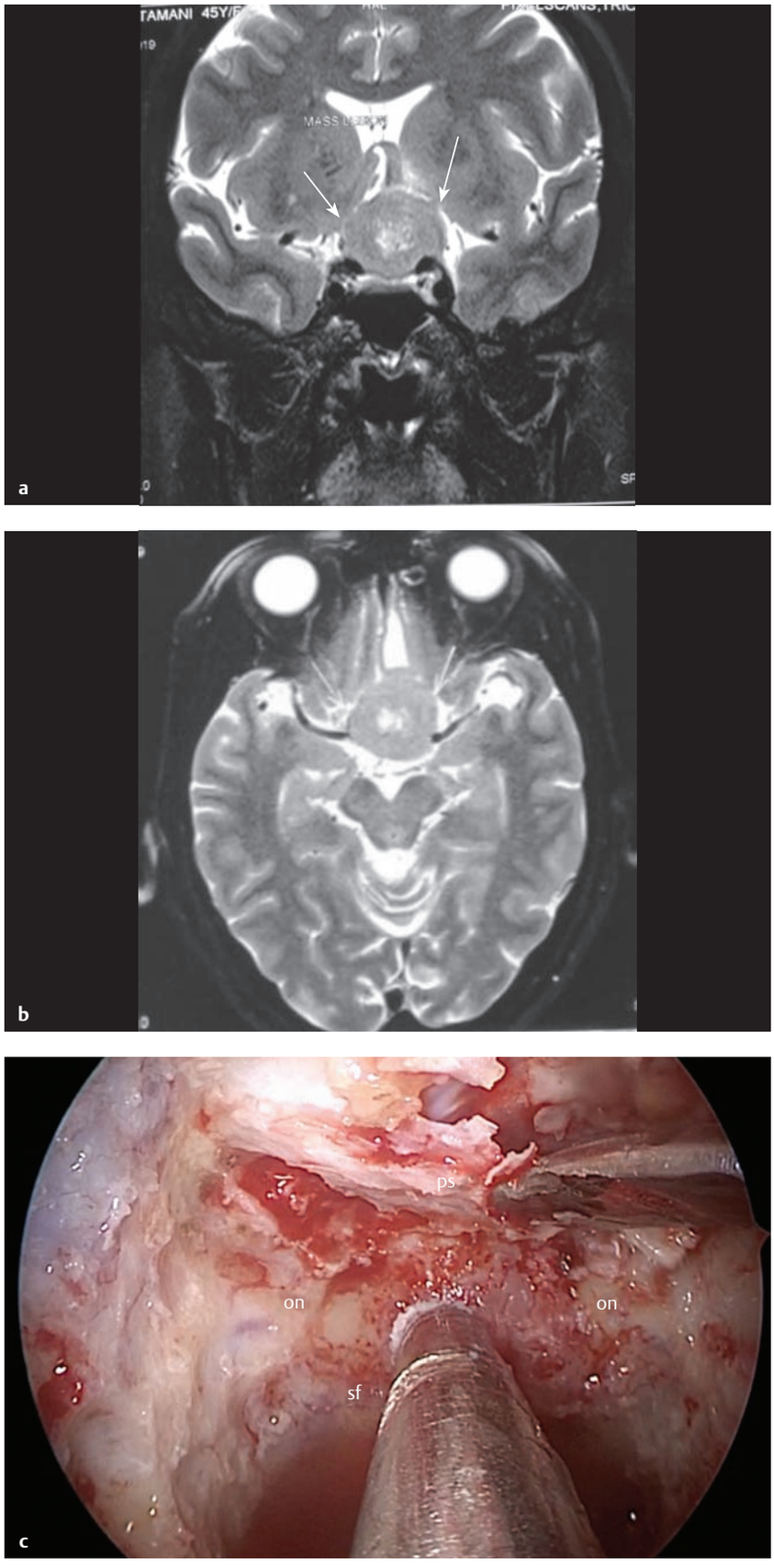

Fig. 8.30 **(a)** MRI coronal cut showing mass lesion in suprasellar area compressing bilateral optic nerve and optic chiasma and bilateral anterior cerebral artery. **(b)** MRI scan axial cut showing mass lesion in suprasellar area compressing bilateral optic nerve and optic chiasma. **(c)** Endoscopic view showing elevation of planum bone after drilling it to eggshell. On, optic nerve; ps, planum sphenoidale; sf, sellar floor.

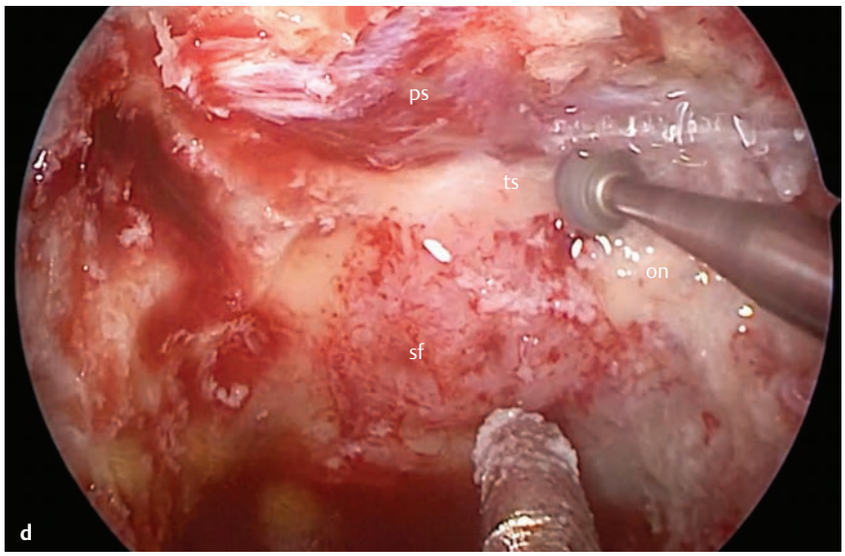

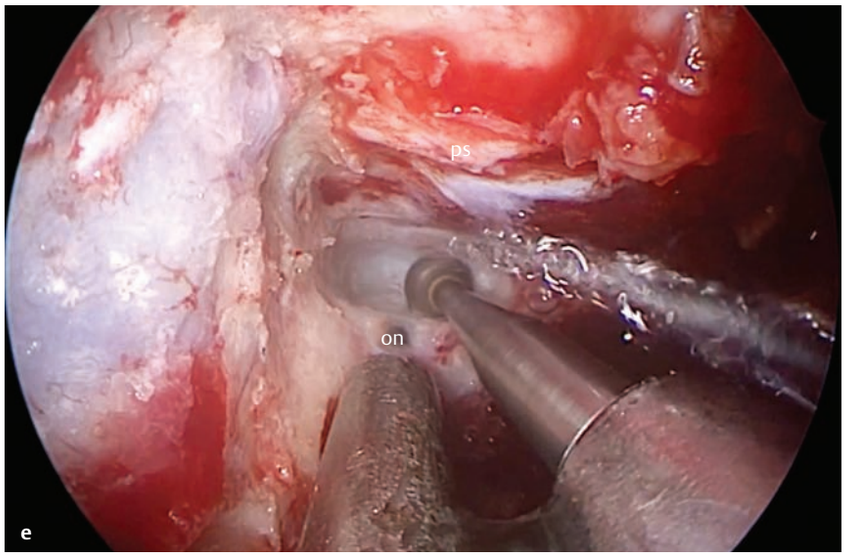

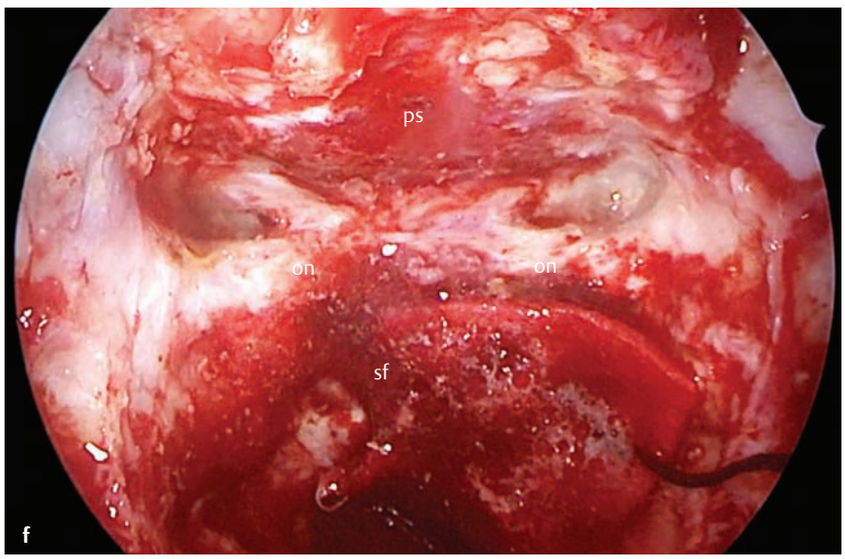

Fig. 8.30 **(d)** Endoscopic view showing drilling of tubercular sellae. On, optic nerve; ps, planum sphenoidale; sf, sellar floor; ts, tubercular sellae. **(e)** Endoscopic view showing drilling of right optic canal. On, optic nerve; ps, planum sphenoidale. **(f)** Endoscopic view showing sellar- suprasellar exposure and drilled out bilateral optic nerve. On, optic nerve; ps, planum sphenoidale; sf, sellar floor.

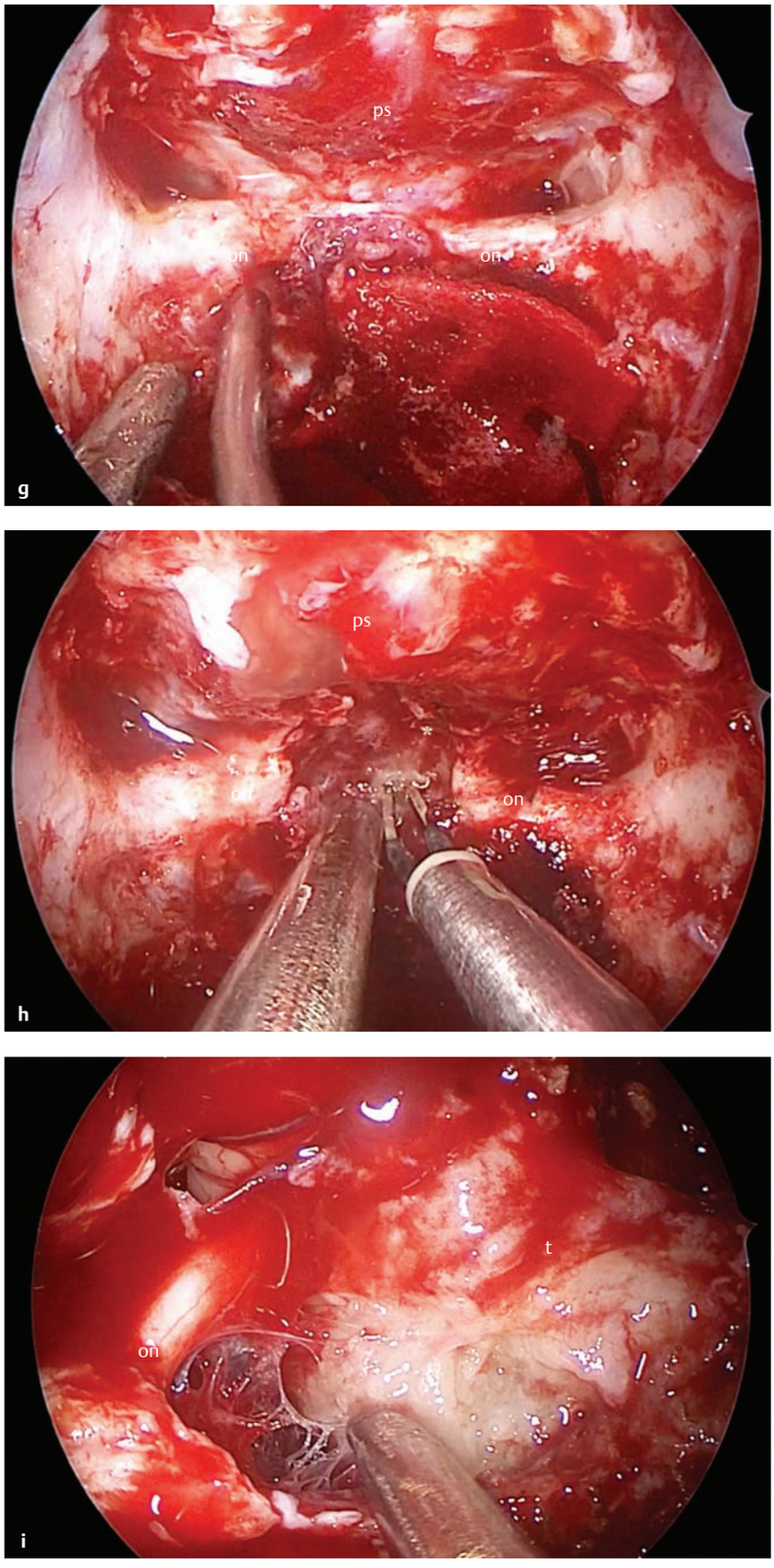

Fig. 8.30 **(g)** Endoscopic view showing mapping of internal carotid artery after complete exposure. On, optic nerve; PS, planum sphenoidale. **(h)** Endoscopic view showing cauterization of superior inter cavernous sinus with Kassam's bipolar. On, optic nerve; ps, planum sphenoidale. **(i)** Dissection of the tumor from the right optic nerve. On, optic nerve; t, tumor.

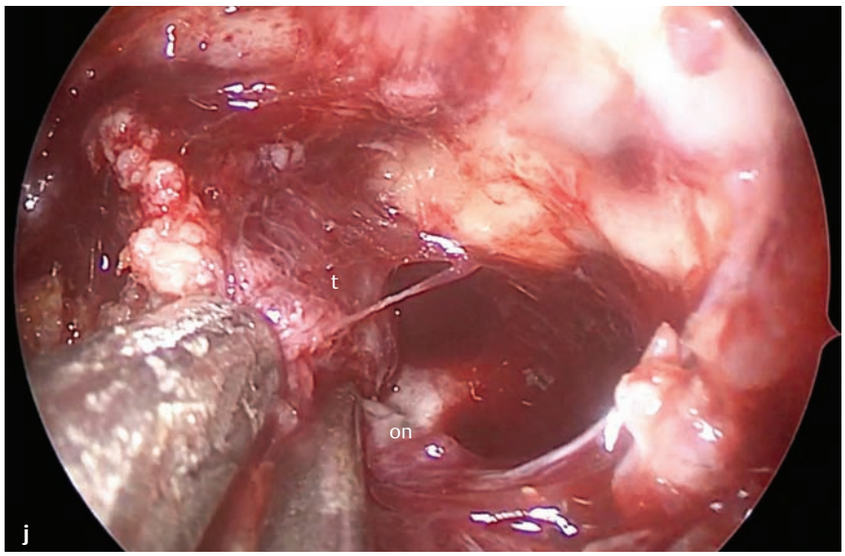

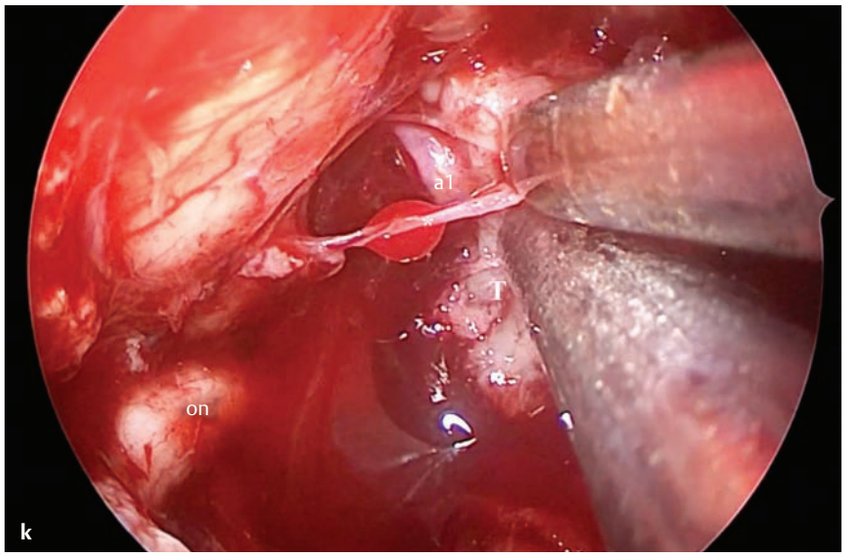

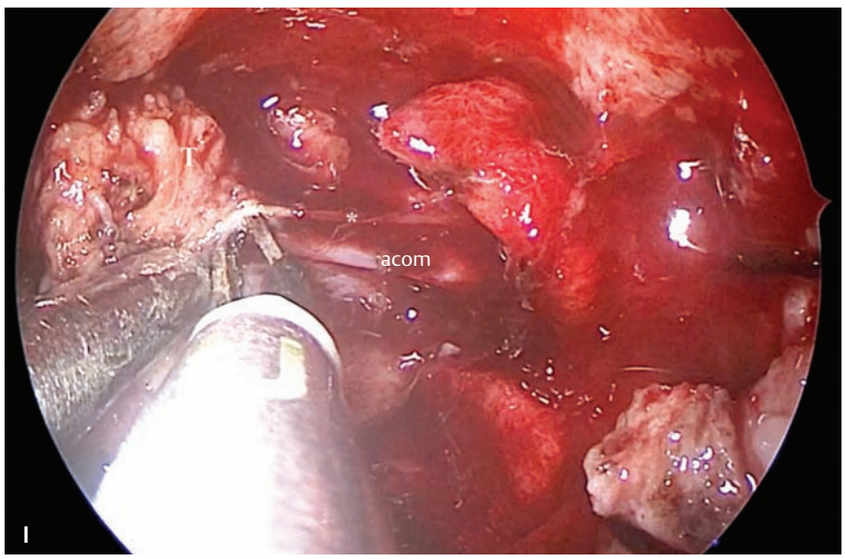

Fig. 8.30 **(j)** dissection of the tumor from the left optic nerve. On, optic nerve; t, tumor. **(k)** Endoscopic view showing dissection of the tumor from the anterior cerebral circulation, dural blood supply of the tumor can be seen. A1, a1 segment of anterior cerebral artery; on, optic nerve; t, tumor. **(l)** Endoscopic view showing cauterization of dural blood supply of tumor and dissection from the anterior communicating artery. Acom,anterior communicating artery; t, tumor.

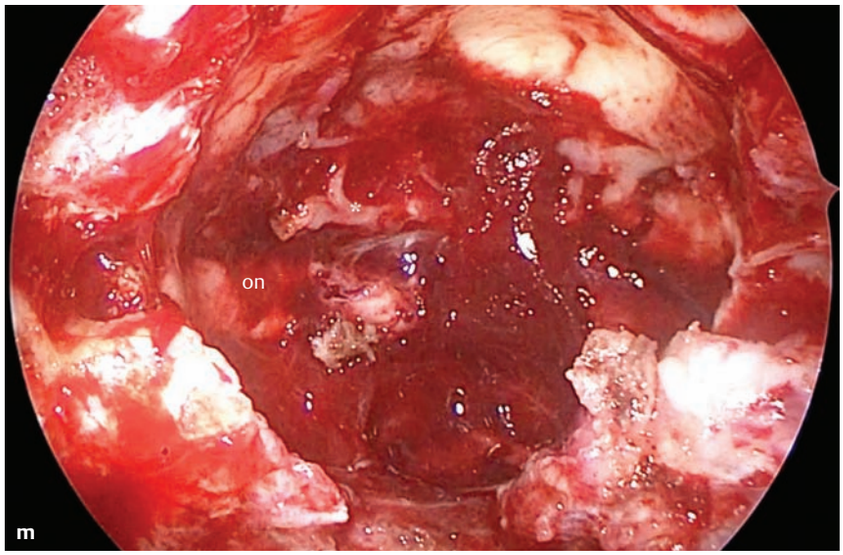

Fig. 8.30 **(m)** Endoscopic view showing suprasellar cistern after tumor removal. On, optic nerve; *, anterior cerebral artery.

Pearls and Tips

- If optic canal invasion was identified on scans preoperatively then medial optic canals should be drilled away to dissect out tumor completely.
- Coagulation of the dural attachment is advisable for early devascularization of the tumor.
- Involved dura and involved bone should be removed.
- Optic nerve decompression is indicated in cases with optic nerve involvement.
- The dura is excised superiorly, and Doppler can be used to identify the ophthalmic artery. Drilling of MOCR facilitates early identification of the ophthalmic artery avoiding injury to it.
- Gentle traction should be applied to the tumor to identify the plane avoiding any manipulation of optic nerve. In case of adhesions to the optic nerve, cautious dissection is advised preserving the arachnoid sheet covering the blood supply of the optic pathway. In case adhesions are firm to optic nerve it is recommended to leave the adhered portion to preserve functionality. The perforators should be preserved to avoid visual complications.

Table 8.1 Classification of craniopharyngioma

Type	Name	Anatomy
1	Preinfundibular	They are bounded laterally by the carotid arteries, inferiorly by the diaphragma sella, posteriorly by the infundibulum, and superiorly by the displaced chiasm.
2	Transinfundibular	The anatomical boundaries are as described for the preinfundibular type, but because of their growth along the stalk, they grow along the ventral side of the chiasm, through the tuber cinereum and into the third ventricle. As a result, the rostral extent of the tumor is bounded by the anterior portion of the hypothalamus.
3	Post- or retroinfundibular	They are bounded anteriorly by the stalk and posteriorly by the mammillary bodies and basilar apex. Usually, the tumor penetrates the membrane of Liljenquist and encroaches on the PCAs and the P1 perforating vessels. In addition, the tumor can extend caudally to spill into the interpeduncular fossa and toward the SCA. The origin of the oculomotor nerve between the SCA and PCA also can be involved.
4	Isolated third ventricular	They are not well accessed via endonasal routes.

Abbreviations: PCAs, posterior cerebral artery; SCA, superior cerebellar artery.

Craniopharyngioma

The resection of craniopharyngioma has high morbidity due to relationship with optic chiasm, pituitary stalk, hypothalamus, carotid artery, and anterior cerebral circulation. The consistency of tumor (cystic or solid), tumor size, calcifications, and extension to the ventricles are to be taken into consideration. The selection of surgical approach is controversial and based on surgeon's preference. Many classification systems have been described to help selection of surgical corridor for craniopharyngioma excision. Kassam et al and Kassam et al have classified craniopharyngioma to guide surgical approach selection (**Table 8.1**).[13].

Case 14: Craniopharyngioma

A 21-year-old woman presented with the history of headache and diminishing vision. CT/MRI scan shows cystic lesion with calcification in suprasellar region (**Fig. 8.31a, b**). After wide exposure of the sphenoid sinuses (**Fig. 8.31c**) authors planned for a transtubercular transplanar approach. Bone over the tuberculum strut, PS, and sellar area were drilled and removed with Rosen's elevator (**Fig. 8.31d**). Bone over bilateral carotids was removed with Rosen's elevator very gently and MOCR was removed with Kerrison's punch (**Fig. 8.31e**). Sellar suprasellar dura was exposed (**Fig. 8.31f**) and bilateral carotid artery was mapped with carotid Doppler (**Fig. 8.31g**). Sellar and suprasellar dura was opened by giving vertical incision (**Fig. 8.31h, i**). Bleeding from the SICS was controlled by FloSeal hemostatic matrix. After opening the dura, tumor was identified superior hypophyseal artery was then identified (**Fig. 8.31j**). Superior hypophyseal artery was dissected free from the tumor (**Fig. 8.31k**). Cyst was decompressed after opening the cyst and the material sucked out (**Fig. 8.31l**). Debulking of the solid part of the tumor was carried out with microdissection technique. Tumor mass was reduced by precise dissection with the help of ultrasonic suction aspirator (**Fig. 8.31m**). Tumor was dissected from the optic chiasm and posterior circulation (**Fig. 8.31n**). Tumor attached to floor of the third ventricle was dissected. Third ventricle cavity was visualized; foramen Monro and choroid plexus were seen (**Fig. 8.31o**). Anterior circulation and optic chiasm were seen very clearly without evidence of tumor (**Fig. 8.31p, r**); third ventricle cavity was examined again and no evidence of tumor found (**Fig. 8.31q**). Reconstruction was carried out in multilayered fashion with fat, Surgicel, nasoseptal flap, and tissue fibrin glue (**Fig. 8.31s**). See **Video 8.7**.

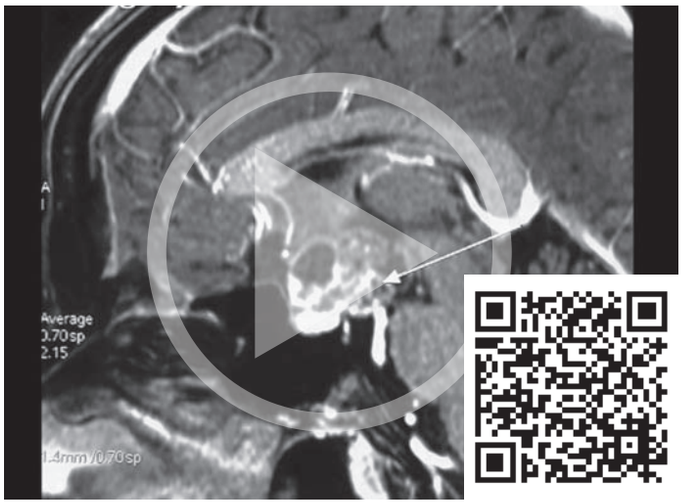

Video 8.7 Craniopharyngioma. https://www.thieme.de/de/q.htm?p=opn/cs/19/9/10104309-3107e214

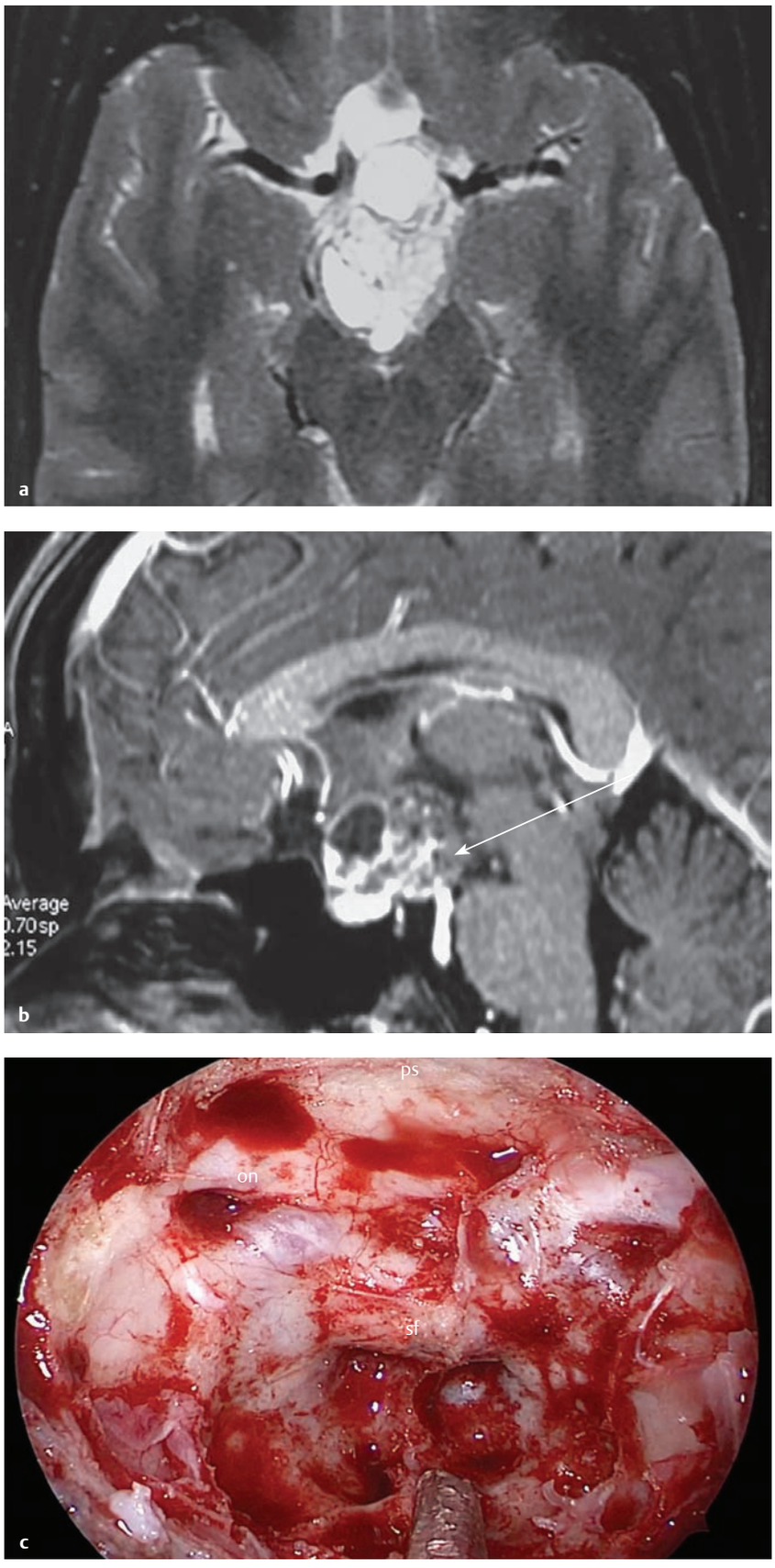

Fig. 8.31 **(a)** MRI axial cut showing tumor in suprasellar region. **(b)** Sagittal cut showing suprasellar lesion. **(c)** Endoscopic view showing wide exposure of sphenoid sinuses. On, optic nerve; ps, planum spenoidale; sf, sellar floor.

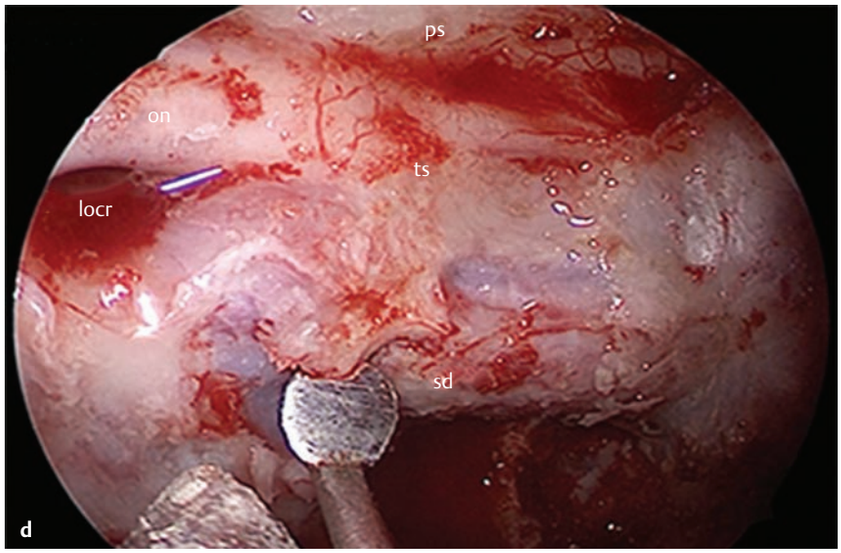

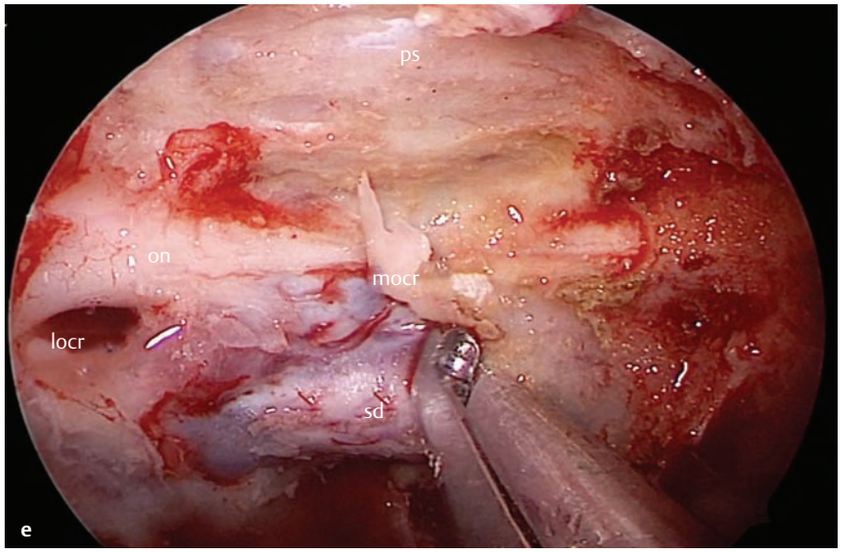

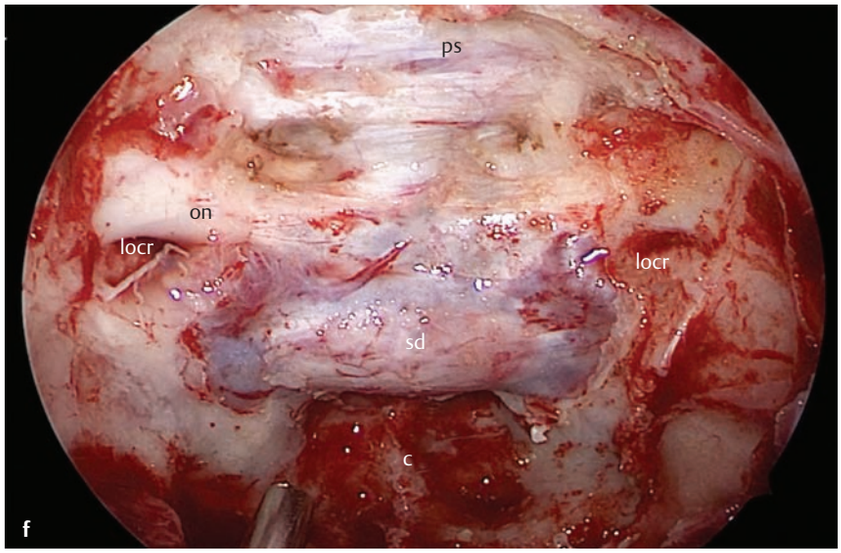

Fig. 8.31 **(d)** Endoscopic view showing removal of thinned out tuberculum bone. Locr, lateral opticocarotid recess; on, optic nerve; ps, planum sphenoidale; sd, sellar dura; ts, tuberculum sellae. **(e)** Endoscopic view showing removal of the left MOCR with Rongen. Locr, lateral opticocarotid recess; mocr, medial opticocarotid recess; on, optic nerve; ps, planum sphenoidale; sd, sellar dura. **(f)** Endoscopic view showing wide sellar suprasellar exposure. Locr, lateral opticocarotid recess; on, optic nerve; ps, planum sphenoidale; sd, sellar dura; ts, tuberculum sellae.

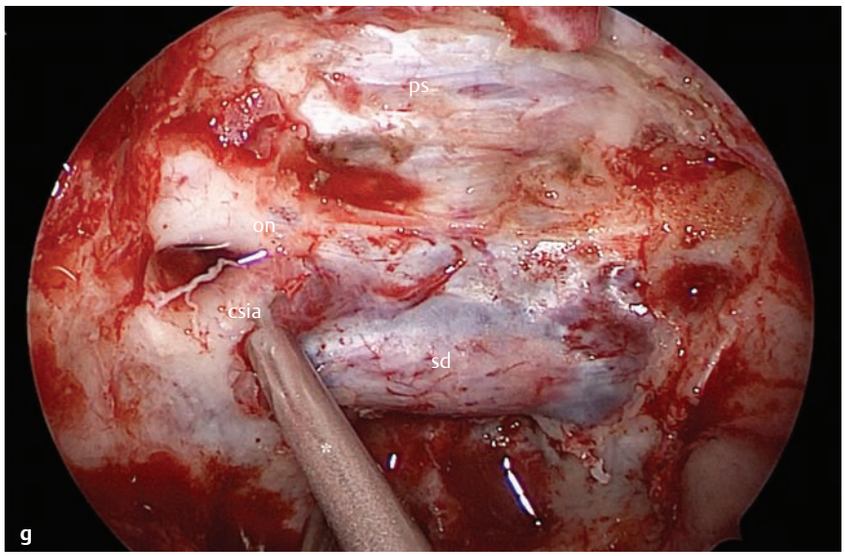

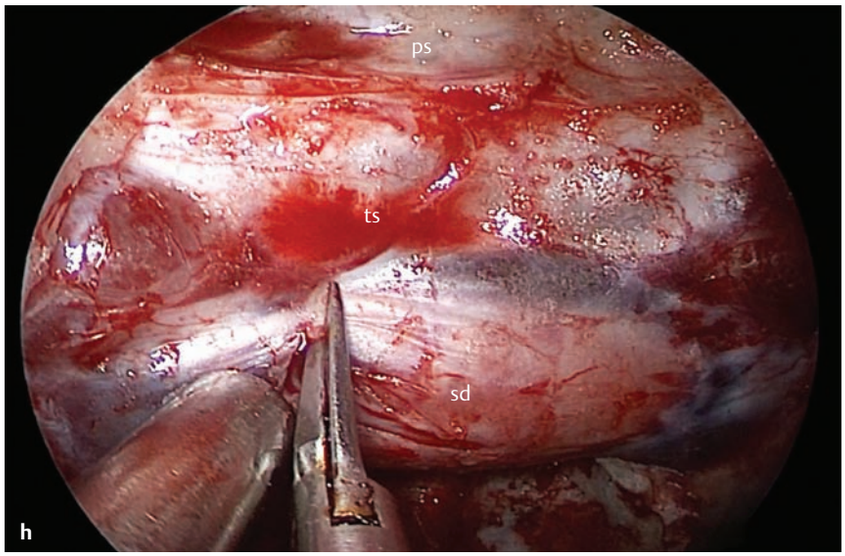

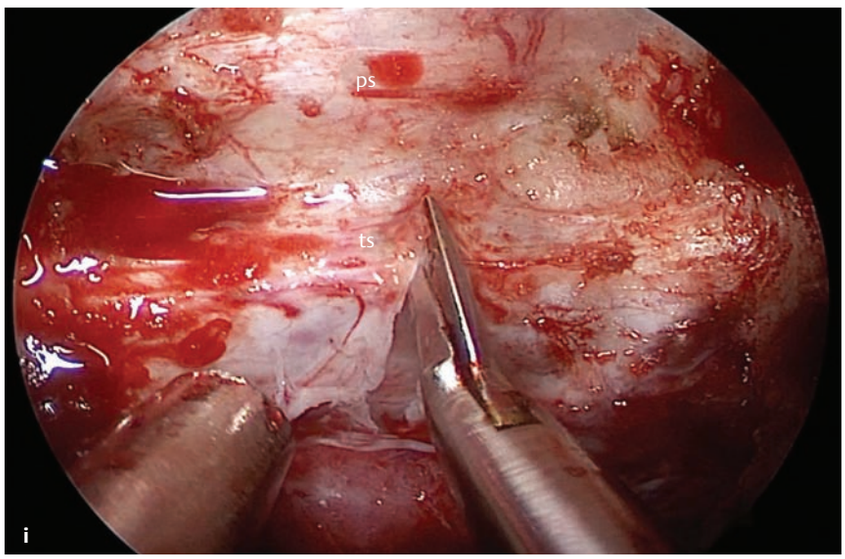

Fig. 8.31 **(g)** Endoscopic view showing after wide sellar suprasellar exposure mapping of carotid artery. Cica, cavernous internal carotid artery; on: optic nerve; ps, planum sphenoidale; sd, sellar dura; *, carotid doppler. **(h)** Giving incision over the sellar dura with scissors. Ps, planum sphenoidale; sd, sellar dura; ts, tuberculum sellae. **(i)** Endoscopic view showing extension of incision over tuberculum sellae dura. Ps, planum sphenoidale; ts, tuberculum sellae.

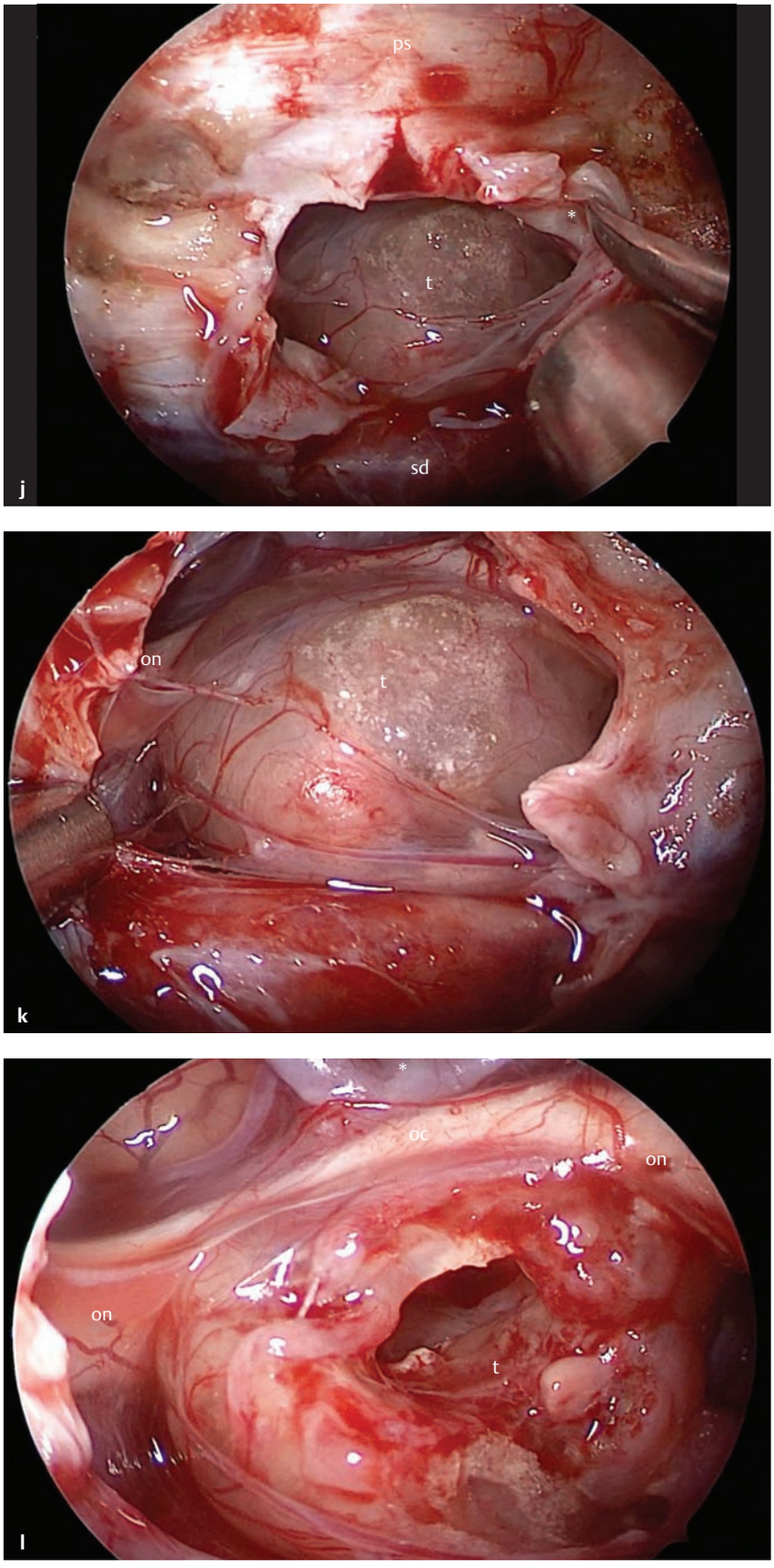

Fig. 8.31 **(j)** Endoscopic view showing dural flaps after giving incision. Tumor is visible. T, tumor; *, dural flaps. **(k)** Endoscopic view showing exposure of the tumor. On, optic nerve; t, tumor; *, anterior circulation. **(l)** Endoscopic view showing debulking of the tumor started. Bilateral optic nerve and anterior circulation is visualized. Oc, optic chiasm; on, optic nerve; t, tumor; *, anterior circulation.

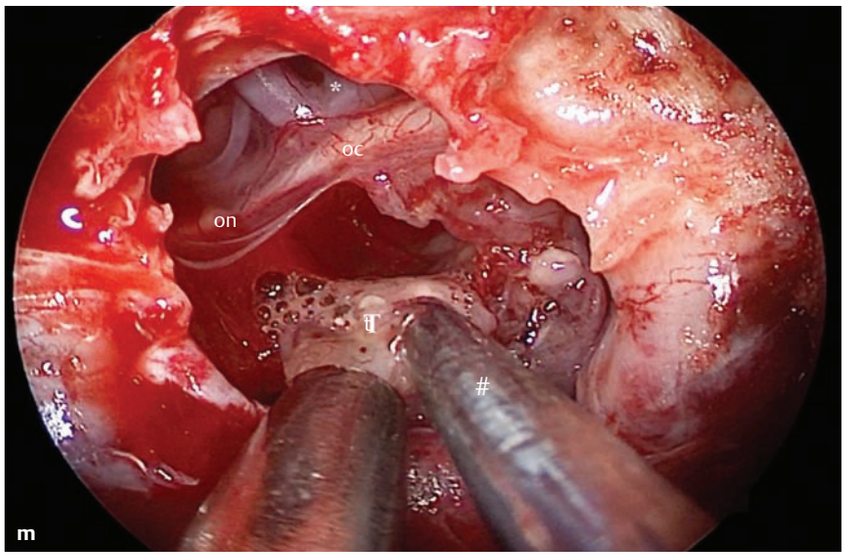

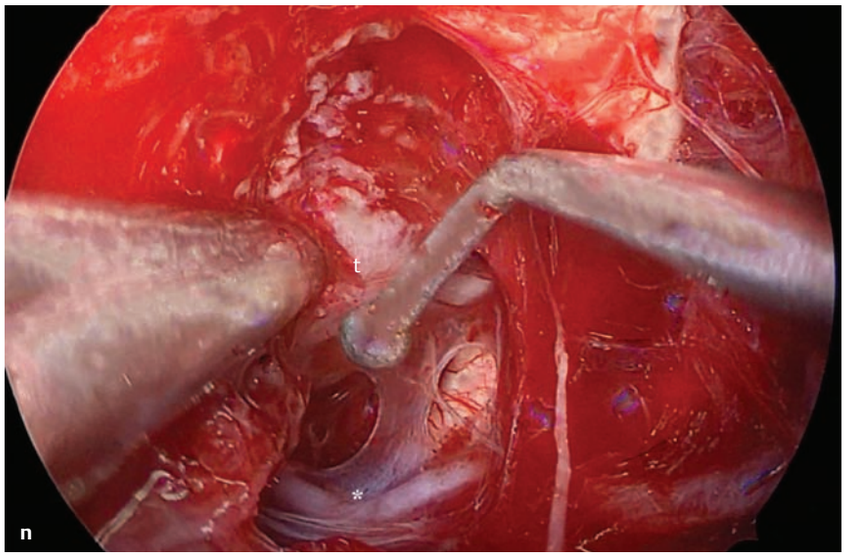

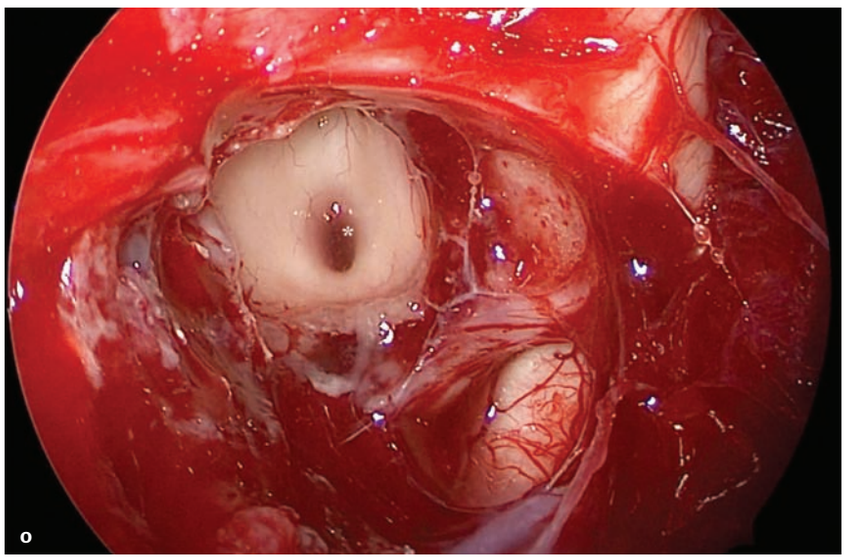

Fig. 8.31 **(m)** Endoscopic view showing debulking of the tumor with ultrasonic aspirator. Oc, optic chiasm; on, optic nerve; t, tumor; *, anterior circulation; #, ultrasonic aspirator. **(n)** Endoscopic view showing elevation of the tumor from the posterior circulation. T, tumor; *, posterior circulation. **(o)** Endoscopic view showing aqueduct of Sylvius after tumor removal. *, aqueduct of Sylvius.

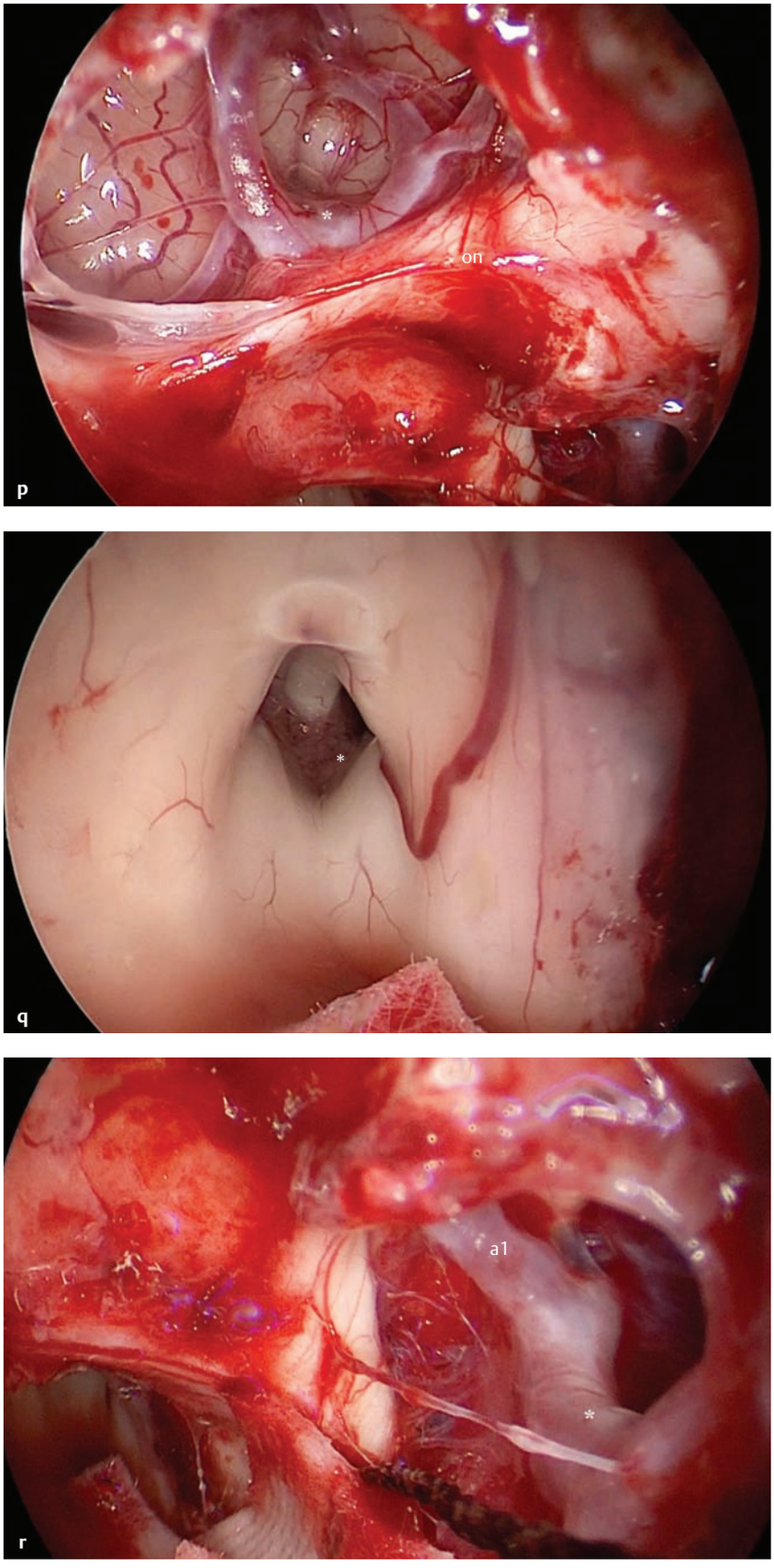

Fig. 8.31 **(p)** Endoscopic view showing anterior circulation and optic nerve after tumor removal. On, optic nerve, * anterior circulation. **(q)** Endoscopic view showing after opening of the floor of the third ventricle foramen of Munro seen. *, foramen of Munro. **(r)** Endoscopic view showing left side internal carotid artery and A1. *, left internal carotid artery; A1, A1 branch.

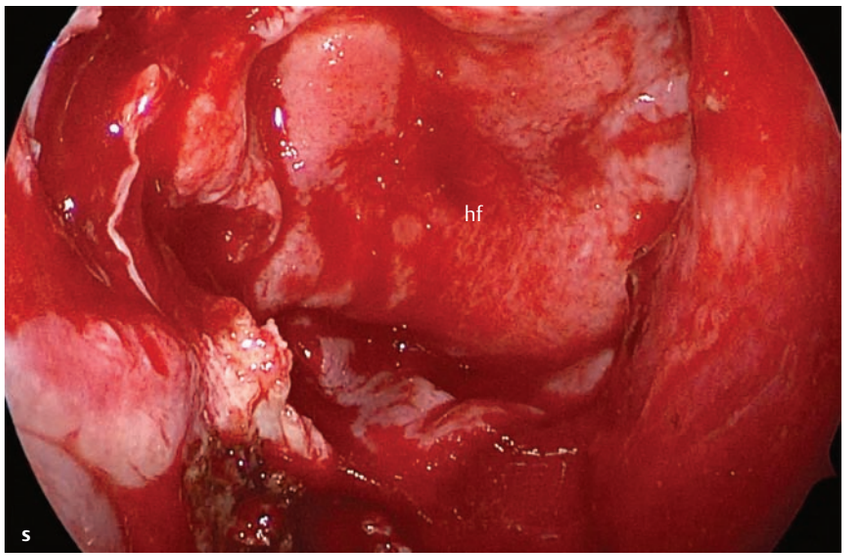

Fig. 8.31 **(s)** Endoscopic view showing reconstruction with naso septal flap. Hf, Hadad flap.

Case 15: Craniopharyngioma

A 17-year-old woman presented with headache and diminishing vision. CT scan showed a well pneumatized sphenoid sinus. MRI showed suprasellar mass with both cystic and solid component which was found extending up to the third ventricle (**Fig. 8.32a**). Wide exposure of the sphenoid sinuses was done (**Fig. 8.32b**). Planectomy was done in a triangular shape with base facing anteriorly and sides facing posteriorly just above optic canals (**Fig. 8.32c, d**). Sellar bone was drilled and removed after thinning it (**Fig. 8.32e**). Cavernous carotids and MOCR were exposed and carotids mapped using Doppler (**Fig. 8.32f**). After exposure, dural incision was made and subchiasmatic cistern opened and the first structure identified was the superior hypophyseal artery (**Fig. 8.32g, h**). Tumor was then gently dissected from both the sides of superior hypophyseal artery (**Fig. 8.32i**). Internal debulking of tumor was carried out, following which extracapsular dissection was carried out. Tumor attached with the pituitary stalk was dissected very gently (**Fig. 8.32j**). Small part of the tumor which was attached to the stalk was left behind (**Fig. 8.32k**). Structures in the interpeduncular fossa were identified such as a basilar artery, P1 and P2 segments, and P1 perforators, and third nerve. Finally the superior part was dissected by extracapsular dissection and the third ventricle was opened up. Foramen of Monro was identified (**Fig. 8.32l**). After complete dissection, gentle irrigation with ringer lactate was given. Reconstruction was carried out with fat, fascia, and nasoseptal flaps (**Fig. 8.32m, n**). See **Video 8.8**.

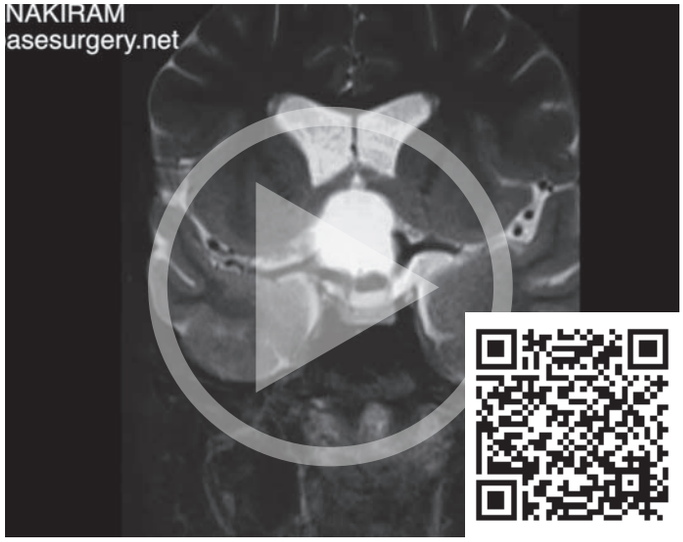

Video 8.8 Craniopharyngioma. https://www.thieme.de/de/q.htm?p=opn/cs/19/9/10104310-fa9c34fe

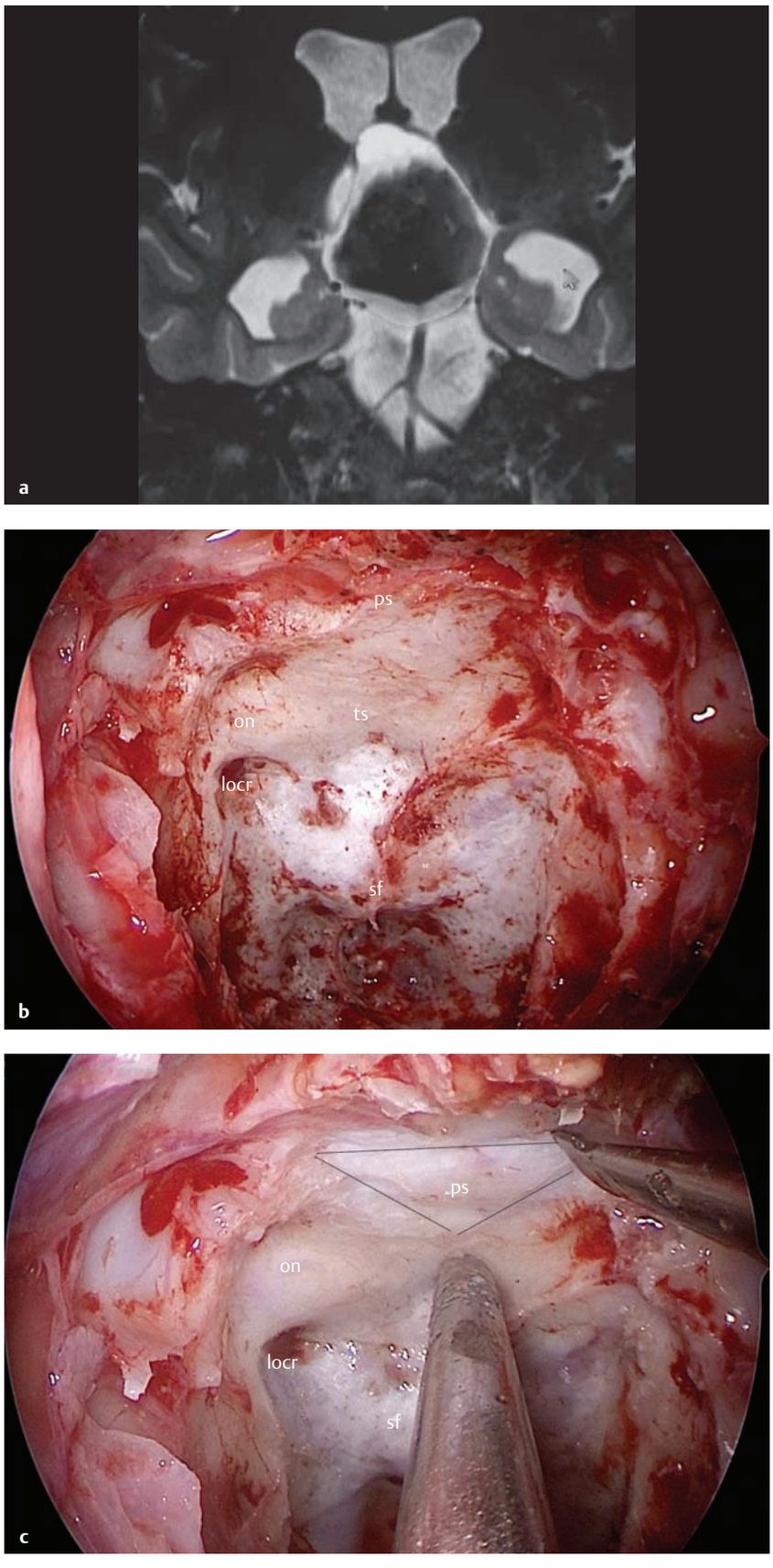

Fig. 8.32 **(a)** MRI showing solid cytic lesion in suprasellar region extending up to third ventricular cavity. **(b)** Endoscopic view showing wide exposure of cavity and half. Locr, lateral opticocarotid recess; on, optic nerve; ps, planum sphenoidale; sf, sellar floor; ts, tuberculum sphenoidale. **(c)** Endoscopic view showing elevation of planum sphenoidale bone after drilling it to eggshell. Locr, lateral opticocarotid recess; on, optic nerve; ps, planum sphenoidale; sf, sellar floor. Black line triangle showing area of drilling for planum sphenoidale.

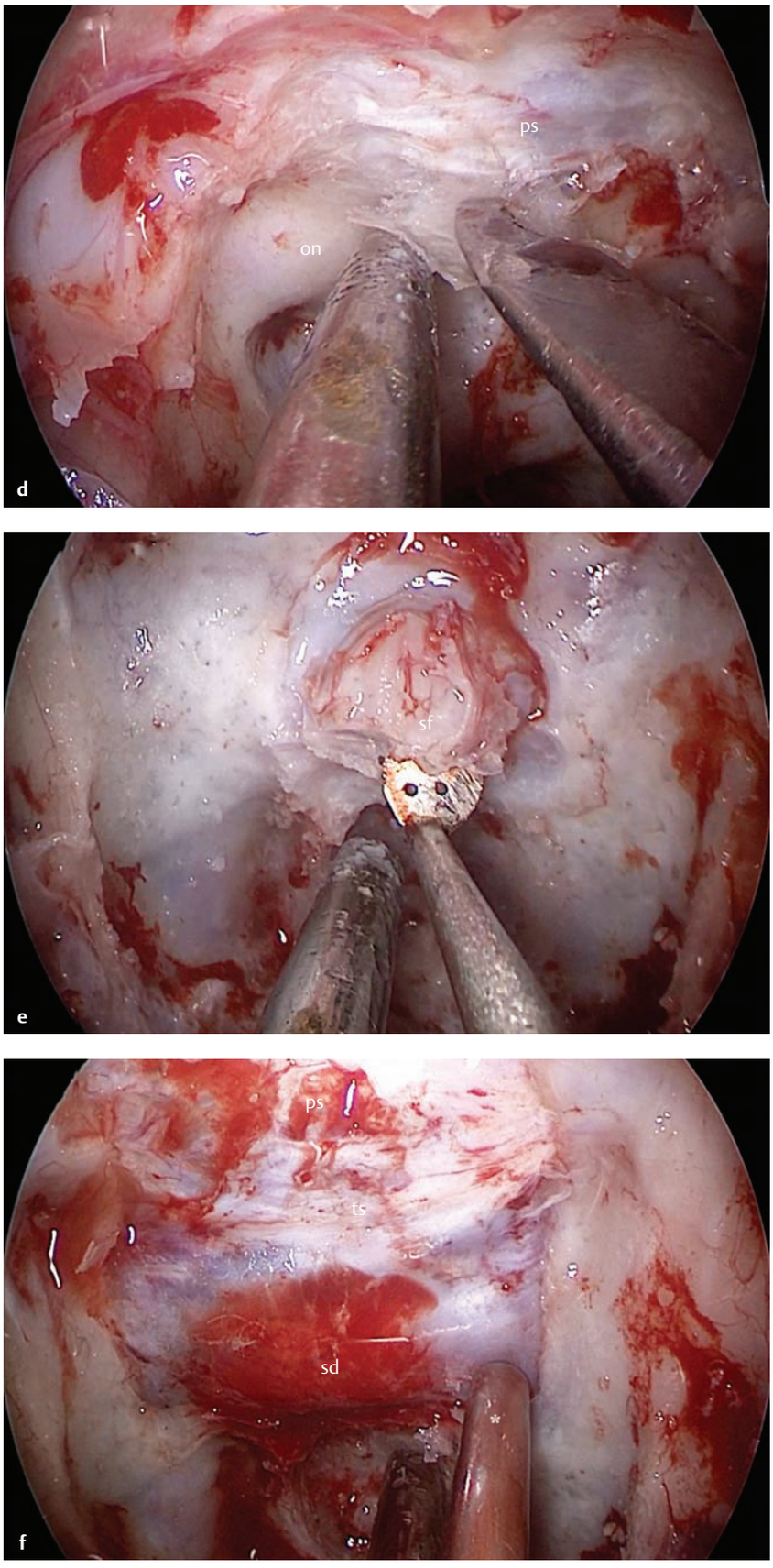

Fig. 8.32 **(d)** Elevation of the planum bone. On, optic nerve; ps, planum sphenoidale. **(e)** Endoscopic view showing elevation of sellar floor bone. Sf, sellar floor. **(f)** Endoscopic view showing sellar and suprasellar exposure and mapping of carotid with micro Doppler. Ps, planum sphenoidale; sd, sellar dura; ts, tuberculum sellae; *, micro doppler.

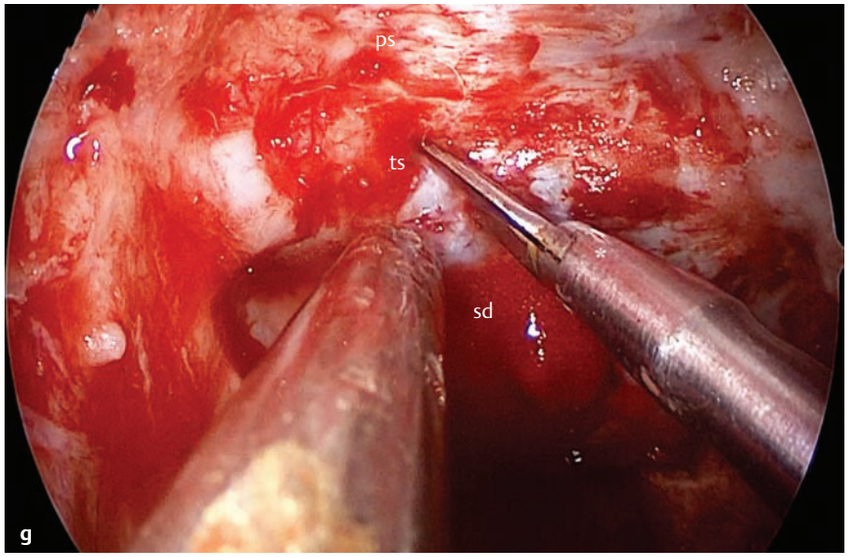

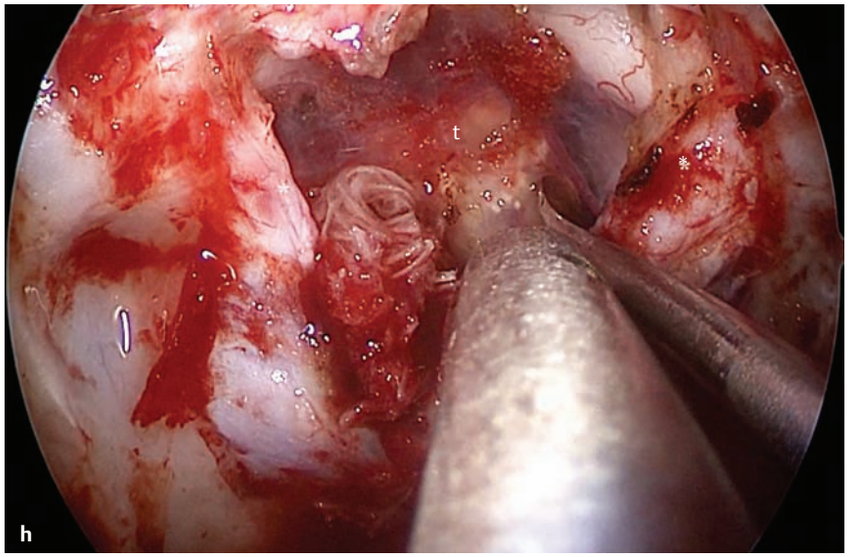

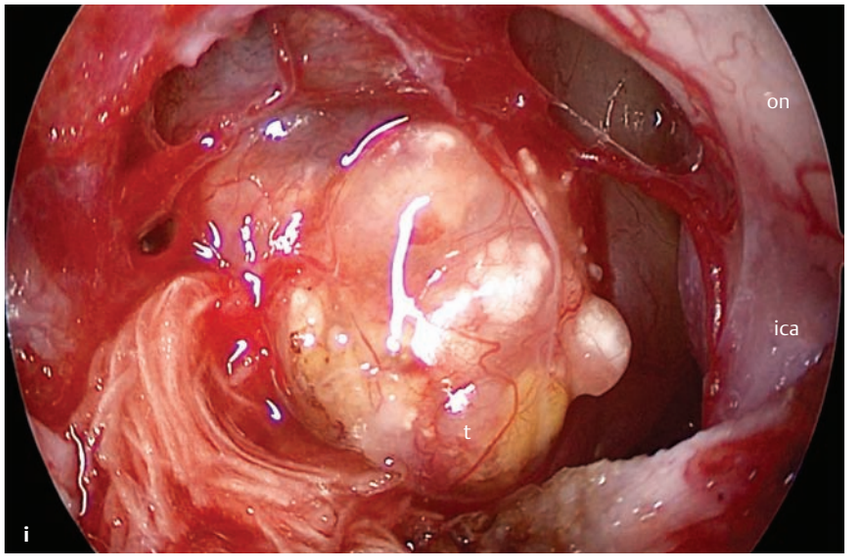

Fig. 8.32 **(g)** Endoscopic view showing putting incision over suprasellar dura with Kassam's scissors. Ps, planum sphenoidale; sd, sellar dura; ts, tuberculum sellae. **(h)** Endoscopic view showing elevation of the dural flaps and tumor is exposed. T, tumor. **(i)** Endoscopic view showing relation of tumor with optic nerve and internal carotid arteries. Ica, internal carotid artery; on, optic nerve.

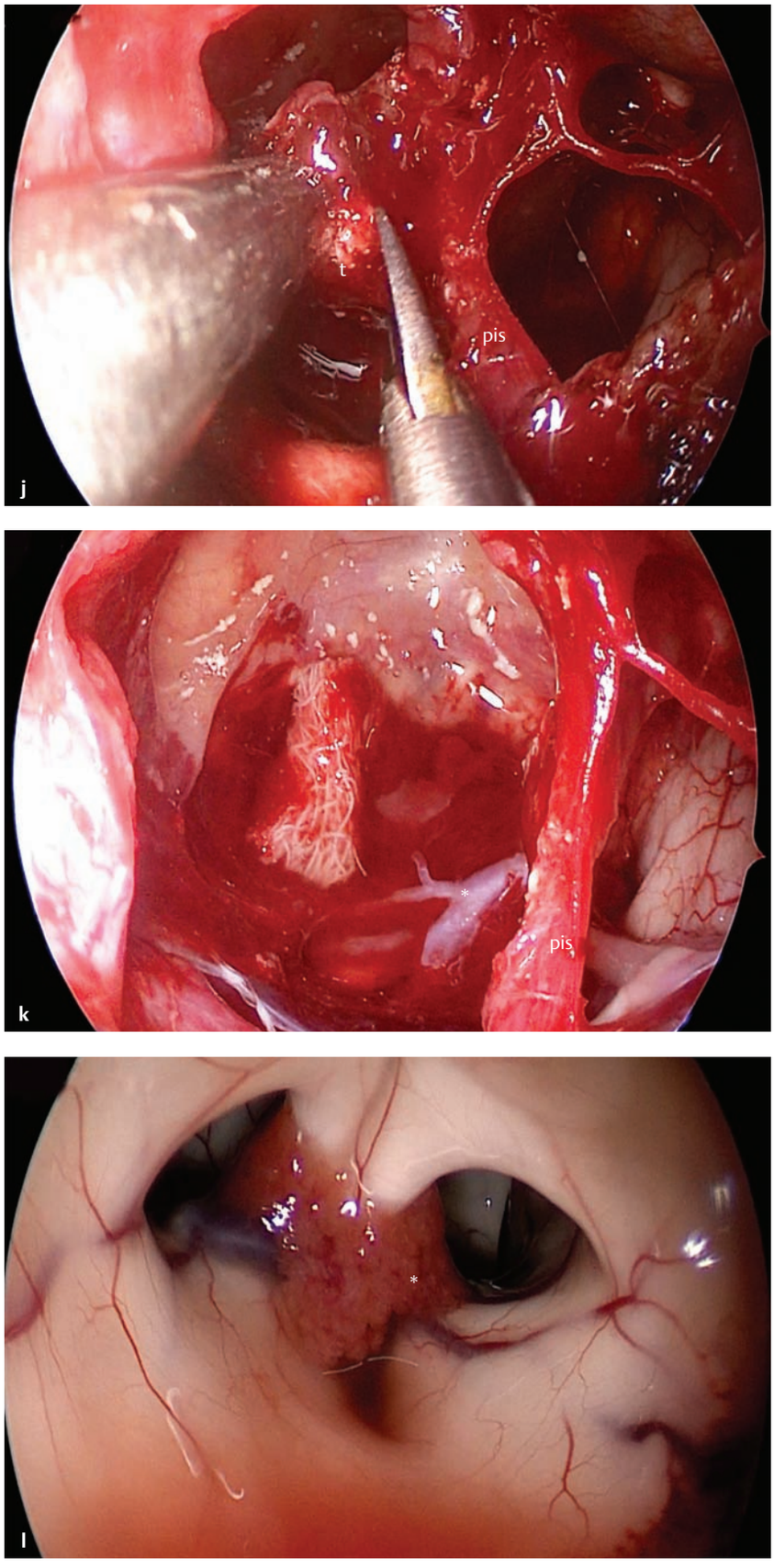

Fig. 8.32 **(j)** Endoscopic view showing microdissection of tumor from the pituitary stalk. Pis, pituitary stalk. **(k)** Endoscopic view after total removal of tumor. Pis, pituitary stalk. **(l)** Endoscopic view showing foramen Monro. *, foramen of Monro.

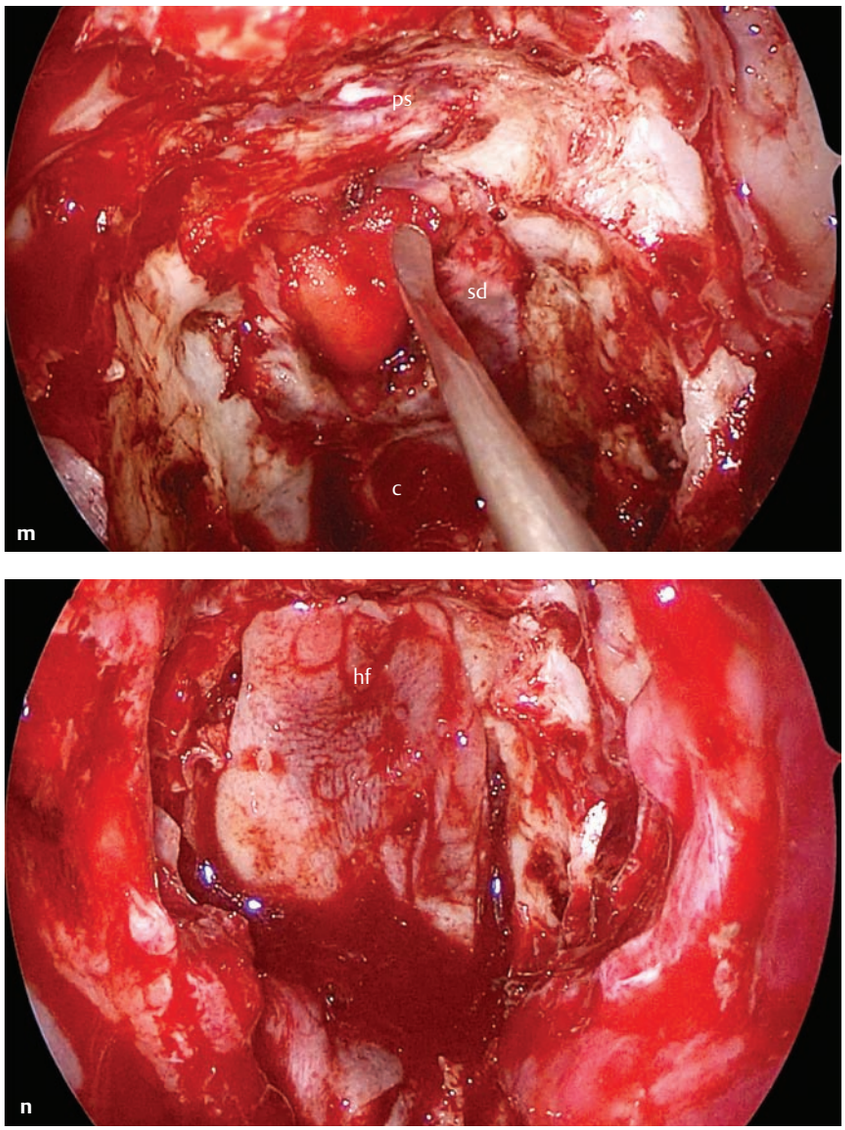

Fig. 8.32 **(m)** Reconstruction with DuraGen. C, clinoid; ps, planum sphenoidale; sd, sellar dura. **(n)** Endoscopic view showing reconstruction with nasoseptal flap. Hf, Hadad flap.

Case 16: Craniopharyngioma

A 20-year-old woman presented with headache, diabetes insipidus, and diminished vision. CT and MRI scans showed a huge suprasellar cystic mass lesion with calcification (**Fig. 8.33a, b**). The sphenoid sinus was exposed from optic to optic and carotid to carotid. Anatomical landmarks such as LOCR, MOCR, optic canal, optic strut, maxillary strut, and PS were identified (**Fig. 8.33c**). Osteotomy of planum was carried out in a triangular fashion. The base of the triangular area is just posterior to the posterior ethmoidal artery and sides are superior to the optic canals on both sides (**Fig. 8.33d**). Osteotomy over the sella and tubercular area were completed (**Fig. 8.33e**). Thinned bone over the sella, tuberculum, and planum area was removed with help of the Rosen's elevator. Bone over bilateral carotid arteries was also removed. Bilateral carotids were mapped with help of carotid Doppler (**Fig. 8.33f**). Vertical incision over the dura was kept with Cappabianca knife and rotatable Kassam's scissors (**Fig. 8.33g**). SICS was cauterized with Kassam's bipolar cautery (**Fig. 8.33h**). The superior hypophyseal artery was identified on both sides (**Fig. 8.33i**). Internal debulking of the tumor was done (**Fig. 8.33j**). The tumor was separated from the optic chiasm and posterior circulation (**Fig. 8.33k**). Microdissection of tumor was done from floor of the third ventricle (**Fig. 8.33l, m**). Examination of the third ventricle cavity and optic chiasm was done after opening the floor with a 30 degree scope (**Fig. 8.33n**). Foramen of Monro, thalamus, choroid plexus can be visualized (**Fig. 8.33o**). The tumor was snuggly adherent to pituitary stalk (**Fig. 8.33p**) and as the patient was already having pan hypopituirism, the authors decided to cut the pituitary stalk (**Fig. 8.33q**). Tumor near to right PCOM was separated with microdissection. Small bit of the tumor adherent to hypothalamus was left behind (**Fig. 8.33r**). Endoscopic anatomy of interpeduncular fossa with contents such as basilar artery, bilateral posterior communicating artery, bilateral oculomotor nerve, bilateral P2, optic chiasm, bilateral A1, anterior communicating artery were seen (**Fig. 8.33s**). Reconstruction was done in multilayers with the use of Surgicel, fat, nasoseptal flap, and tissue fibrin glue (**Fig. 8.33t**). Postoperative scan showed a small bit of tumor attached to the thalamus (**Fig. 8.33u**). See **Video 8.9**.

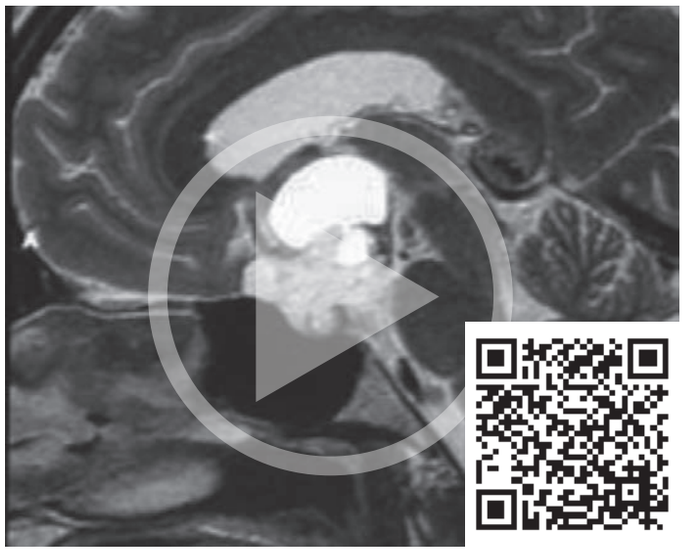

Video 8.9 Craniopharyngioma. https://www.thieme.de/de/q.htm?p=opn/cs/19/9/10104311-1d21a901

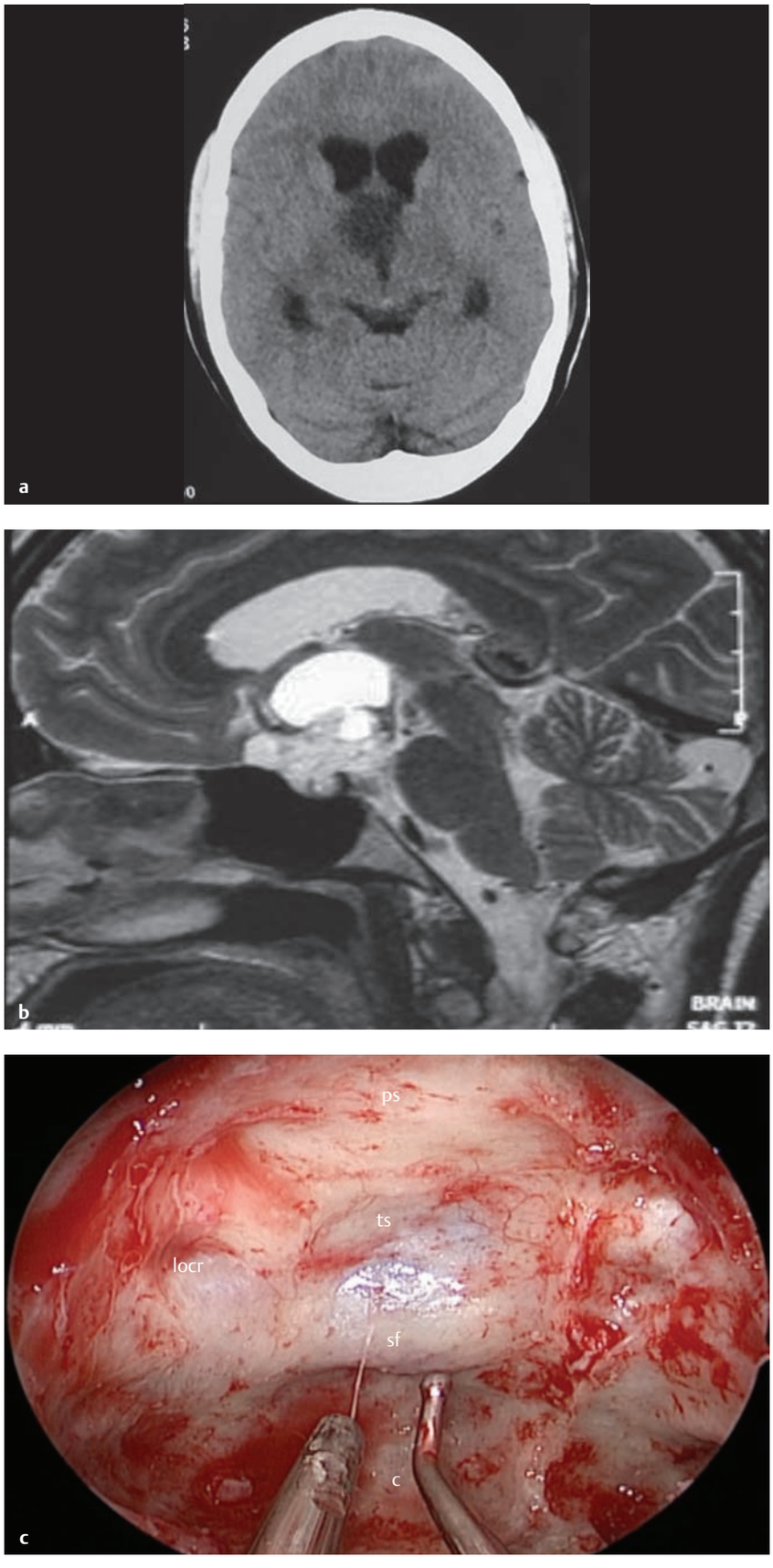

Fig. 8.33 **(a)** MRI axial cut showing mass in suprasellar region reaching up to ventricles. **(b)** MRI sagittal cut showing solid cystic mass in suprasellar region extending in ventricular cavities. **(c)** Endoscopic view after complete exposure of sphenoid sinuses. C, clinoid; locr, lateral opticocarotid recess; PS, planum sphenoidale; sf, sellar-floor; ts, tuberculum sellae.

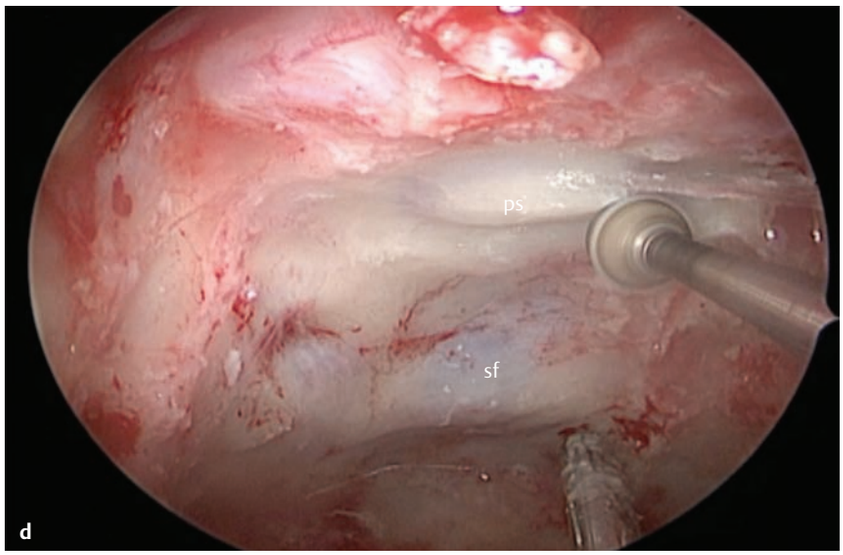

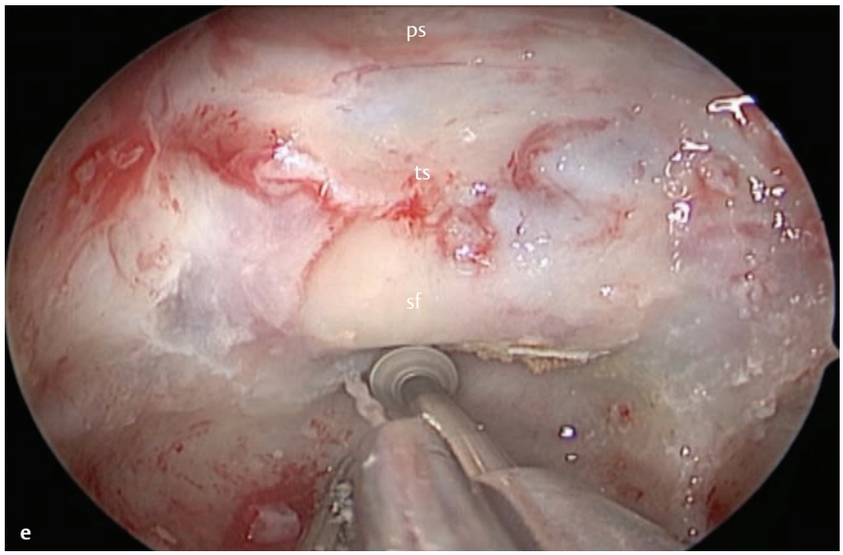

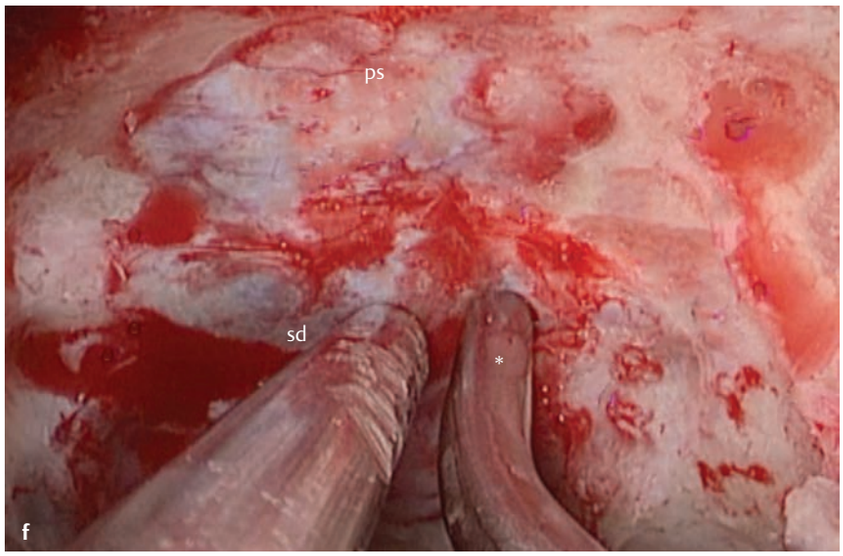

Fig. 8.33 **(d)** Endoscopic view showing drilling of the planum sphenoidale. PS, planum sphenoidale; sf, sellar floor. **(e)** Drilling of the sellar floor. Ps, planum sphenoidale; sf, sellar floor; ts, tuberculum sellae. **(f)** Endoscopic view showing mapping of carotids after complete exposure of the sella and suprasellar dura. Ps, planum sphenoidale; Sd, sellar dura.

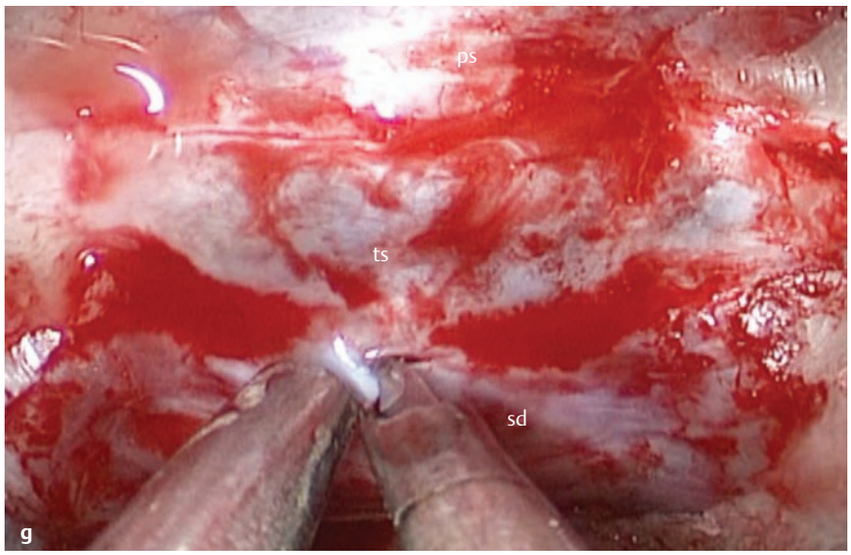

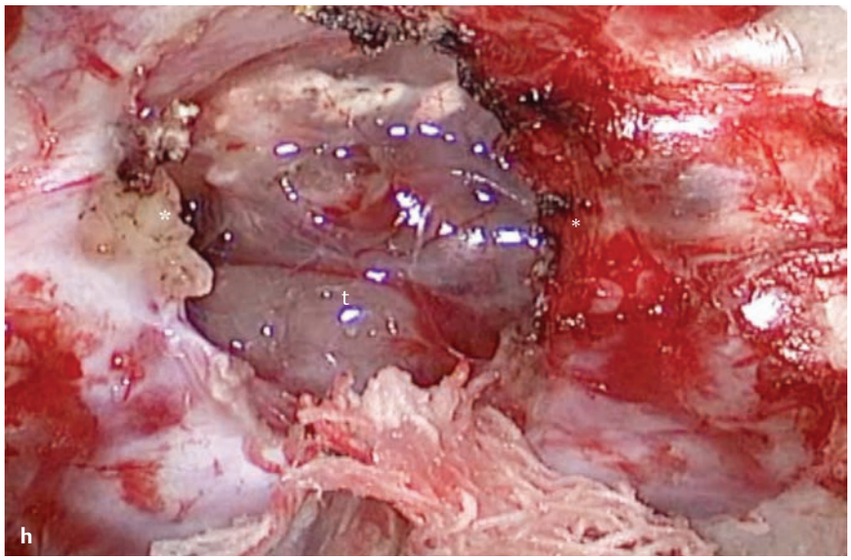

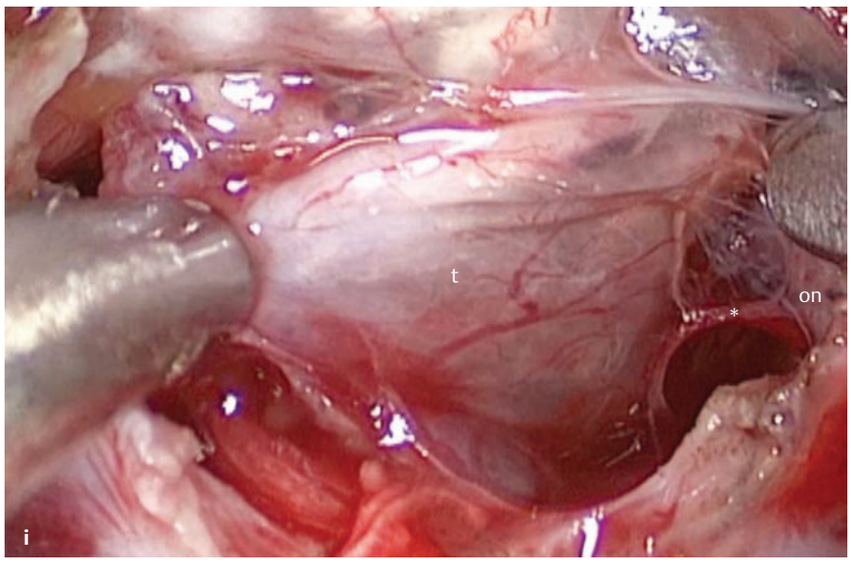

Fig. 8.33 **(g)** Endoscopic view showing incision over the suprasellar dura. Sd, sellar dura; ts, tuberculum sellae. **(h)** Endoscopic view showing tumor after complete elevation of dural flaps. T, tumor; *, dural flaps. **(i)** Endoscopic view showing relation of tumor with optic nerve and superior hypophyseal artery. On, optic nerve; t, tumor; *, superior hypophyseal artery.

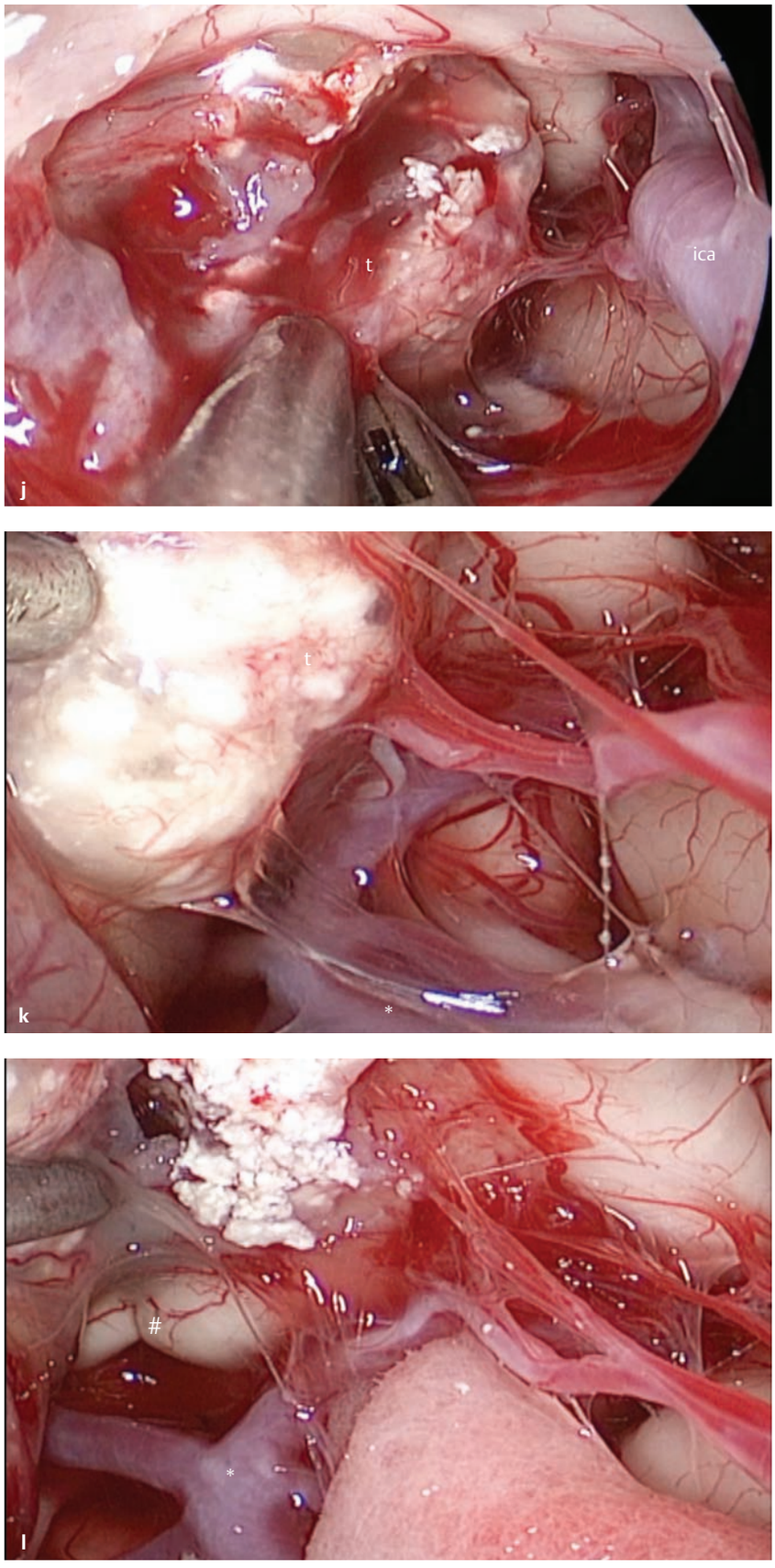

Fig. 8.33 **(j)** Endoscopic view showing careful dissection of superior hypophyseal artery from the tumor. ICA, internal carotid artery; t, tumor. **(k)** Endoscopic view showing dissection of tumor from the posterior circulation. T, tumor; *, basilar artery. **(l)** Endoscopic view showing mamillary bodies and posterior circulation. T, tumor; *, basilar artery; #, mamillary body.

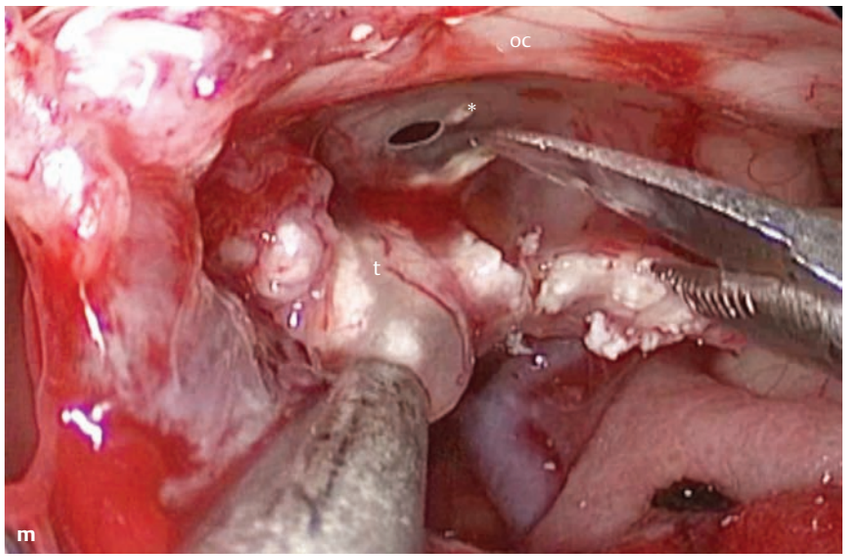

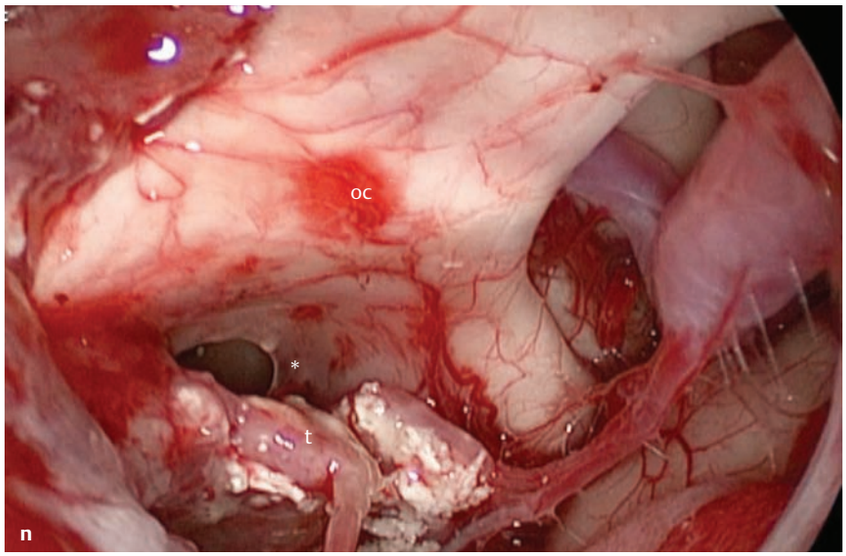

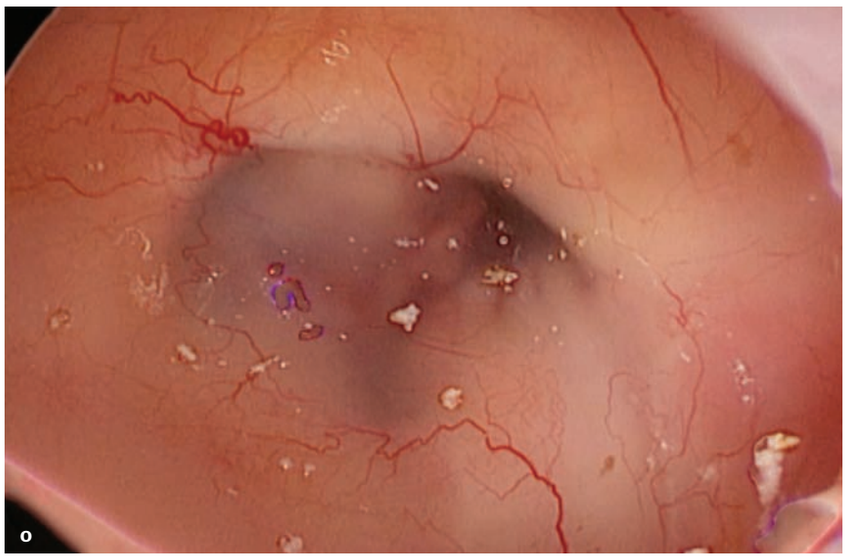

Fig. 8.33 **(m)** Endoscopic view showing microdissection of the tumor from the floor of the third ventricle. Oc, optic chiasm; t, tumor; *, floor of the third ventricle. **(n)** Endoscopic view with the 45 degree angled telescope after partial removal of tumor. ICA, internal carotid artery; oc, optic chiasm; t, tumor; *, floor of the third ventricle. **(o)** Endoscopic view of the foramen of Munro. *, foramen of Munro.

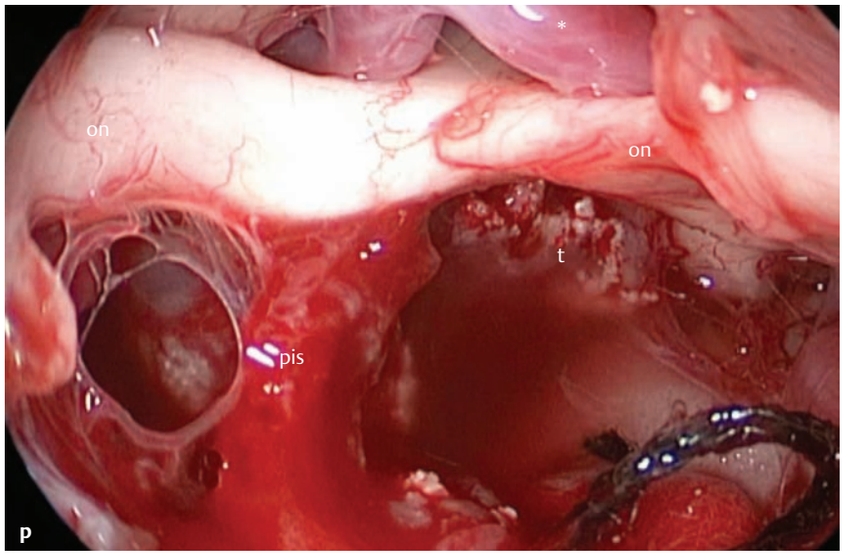

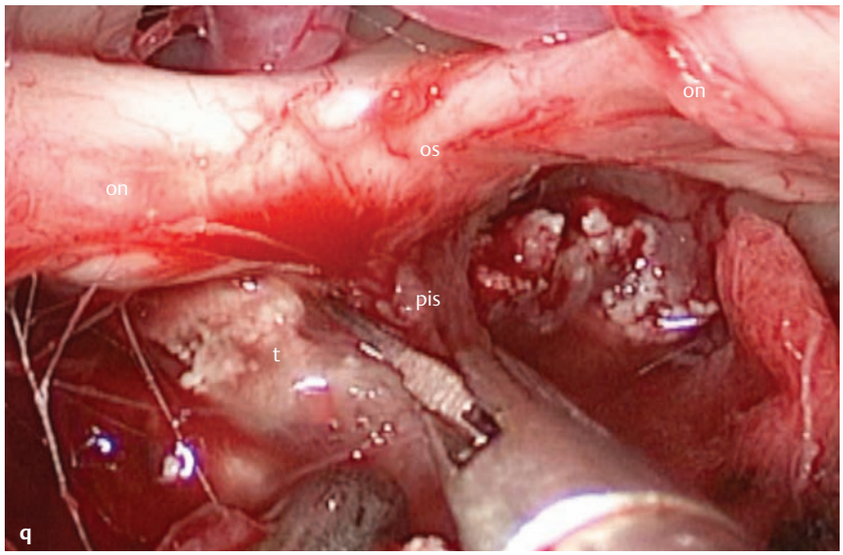

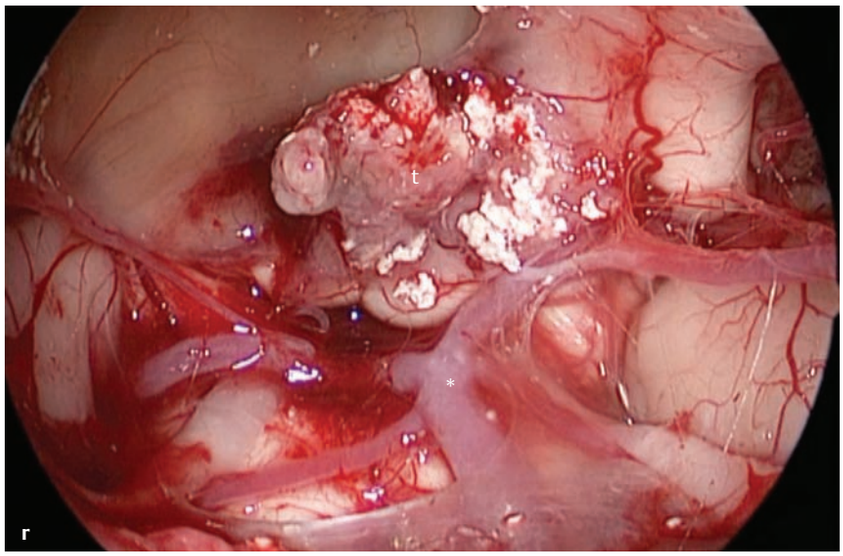

Fig. 8.33 **(p)** Endoscopic view showing bits of tumor attached to pituitary stalk. On, optic nerve; pis, pituitary stalk; t, tumor; *, anterior cerebral artery. **(q)** Endoscopic view showing dissection of tumor along with pituitary stalk. On, optic nerve; pis, pituitary stalk; t, tumor; *, anterior cerebral artery. **(r)** Endoscopic view showing bits of tumor attached near posterior circulation and mamillary body. T, tumor; *, basilar artery.

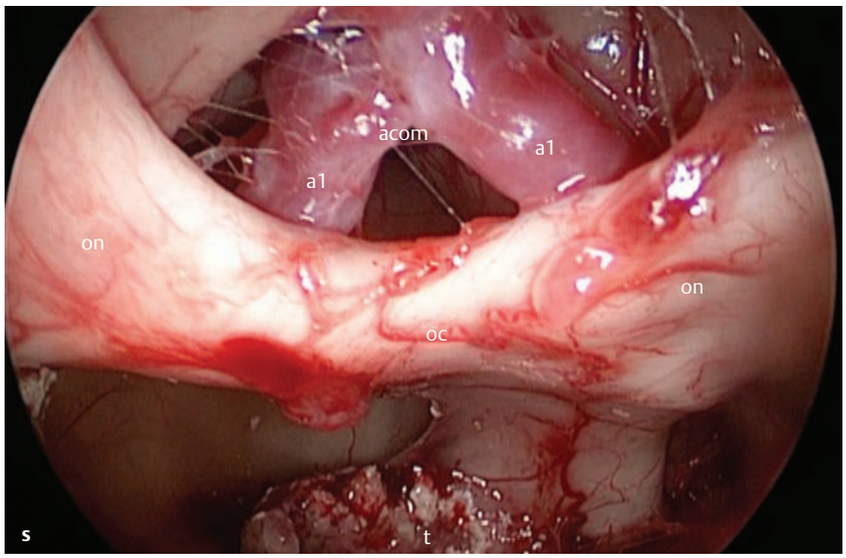

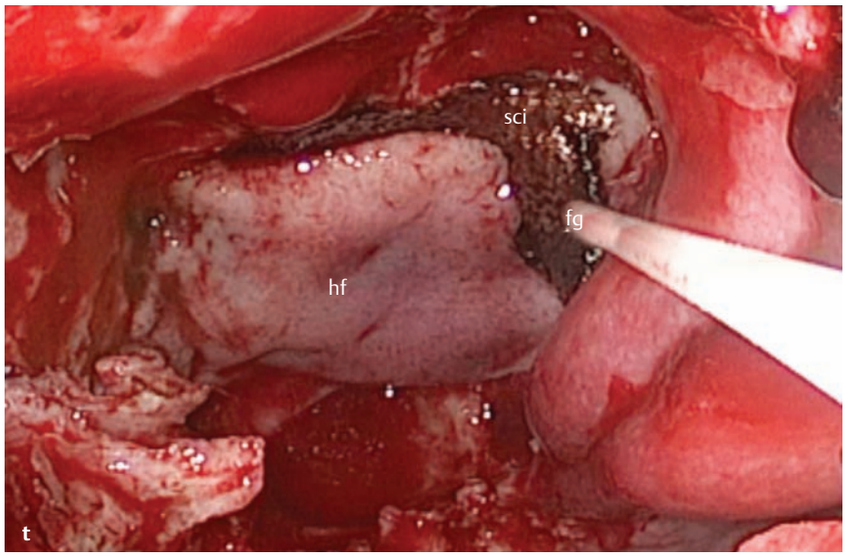

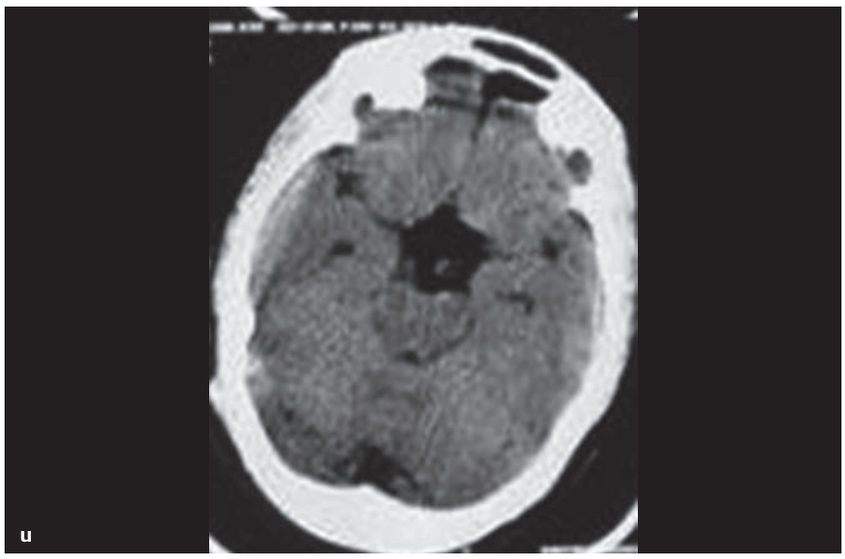

Fig. 8.33 **(s)** Endoscopic view of suprasellar cistern after tumor removal. A1, a1 segment of anterior cerebral artery; acom, anterior communicating artery; oc, optic chiasm; on, optic nerve; t, tumor. **(t)** Endoscopic view showing reconstruction. Fg, fibrin glue; hf, Hadad flap; scl, Surgicel. **(u)** Postoperative MRI showing complete removal of tumor except small part attached to thalamus.

Case 17: Craniopharyngioma

An 11-year-old boy presented with diminishing vision. MRI scan shows infundibular type of craniopharyngioma (**Fig. 8.34a**). After wide exposure of sphenoid sinuses the bone over the sellar floor, tubercular sellae, and PS were removed and sellar and suprasellar dura was exposed (**Fig. 8.34b**). PS dura was opened like a flap after giving vertical and horizontal incisions and tumor was visualized (**Fig. 8.34c**). Tumor was seen in close proximity to bilateral optic nerve (**Fig. 8.34d**). Cystic part of the tumor was opened and internal debulking done (**Fig. 8.34e**). Wall of the tumor was removed with a microdissection technique from an anterior cerebral artery (**Fig. 8.34f**). Reconstruction of cavity was done in multilayers with fat, Surgicel, Gelfoam, and nasoseptal flap (**Fig. 8.34g**).

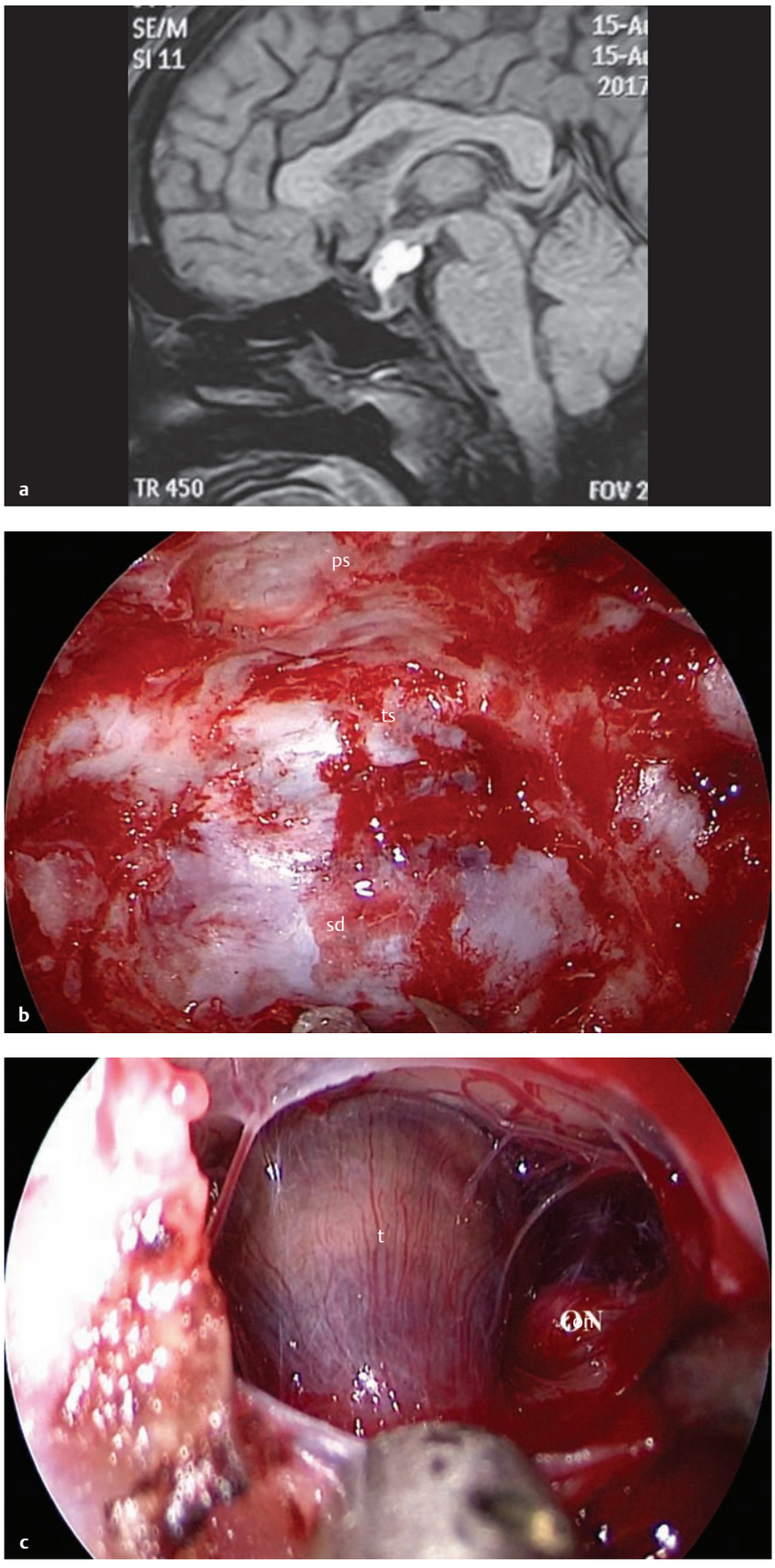

Fig. 8.34 **(a)** MRI sagittal cut showing cystic lesion in suprasellar region extending up to the third ventricle. **(b)** Wide exposure of sellar and suprasellar dura. Ps, planum sphenoidale; sd, sellar dura; ts, tubercular sellae. **(c)** Endoscopic view showing tumor in suprasellar region after opening up planum dura. On, optic nerve; t, tumor.

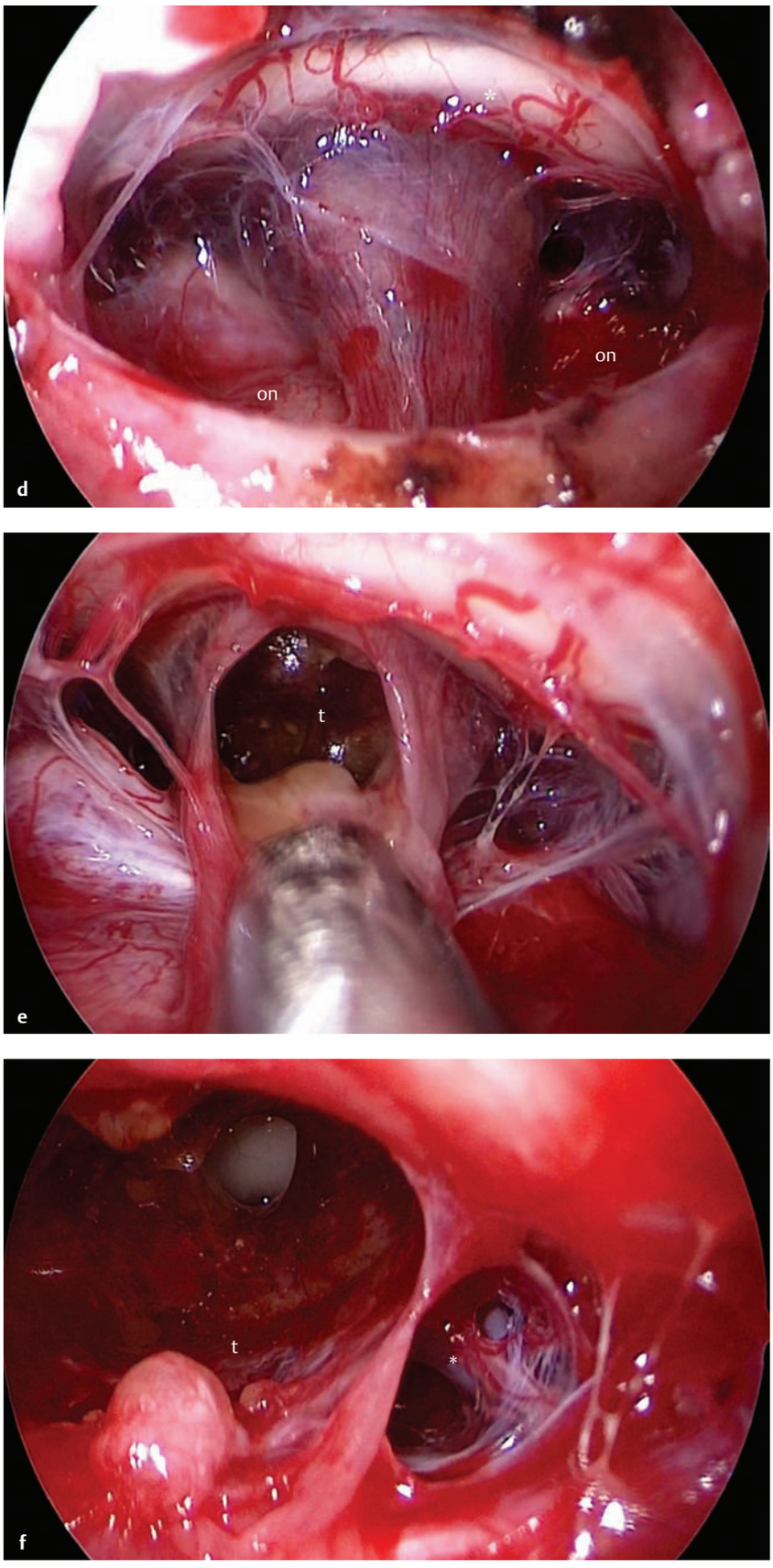

Fig. 8.34 **(d)** Endoscopic view showing tumor in close relation with bilateral optic nerve in suprasellar region. On, optic nerve; t, tumor. **(e)** Endoscopic view showing debulking of tumor. T, tumor. **(f)** Endoscopic view showing tumor wall after internal debulking and close proximity of tumor to anterior cerebral artery. T, tumor; *, anterior cerebral artery.

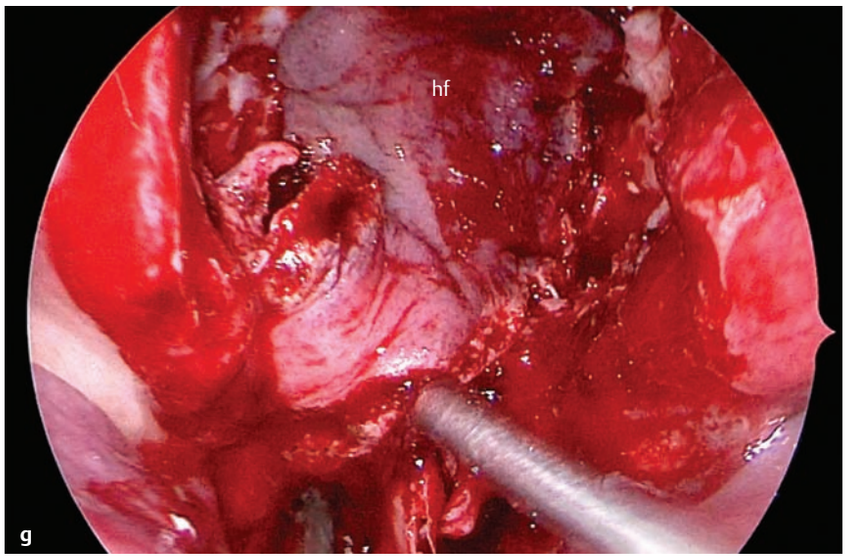

Fig. 8.34 **(g)** Endoscopic view showing reconstruction with nasoseptal flap. Hf, Hadad flap.

Case 18: Craniopharyngioma

A 7-year-old male child presented with headache and diminishing vision. CT/MRI showed cystic lesion in the suprasellar part with internal calcification (**Fig. 8.35a, b**). It was a conchal type of pneumatization of sphenoid sinus. Drilling was started in the midline at the level of PS followed by tuberculum. Sellar floor drilling was carried out till the level of carotids laterally (**Fig. 8.35c**). Bone over the sellar floor, tubercular sellae, and PS was removed after drilling it to eggshell thin and dura was exposed. Bilateral carotids were mapped with carotid Doppler (**Fig. 8.35d**). A dural incision with Cappabianca knife and Kassam's rotatable scissors was carried out (**Fig. 8.35e, f**). After elevating dural flaps, tumor was seen (**Fig. 8.35g**). Incision over tumor wall was kept and content of cyst drained out. Extracapsular dissection of tumor was carried out from the right optic nerve (**Fig. 8.35h**) and floor of the third ventricle. Foramen of Monro, choroid plexus was visualized after tumor removal (**Fig. 8.35i**). Reconstruction was carried out with fat, Surgicel, and nasoseptal flap (**Fig. 8.35j, k**).

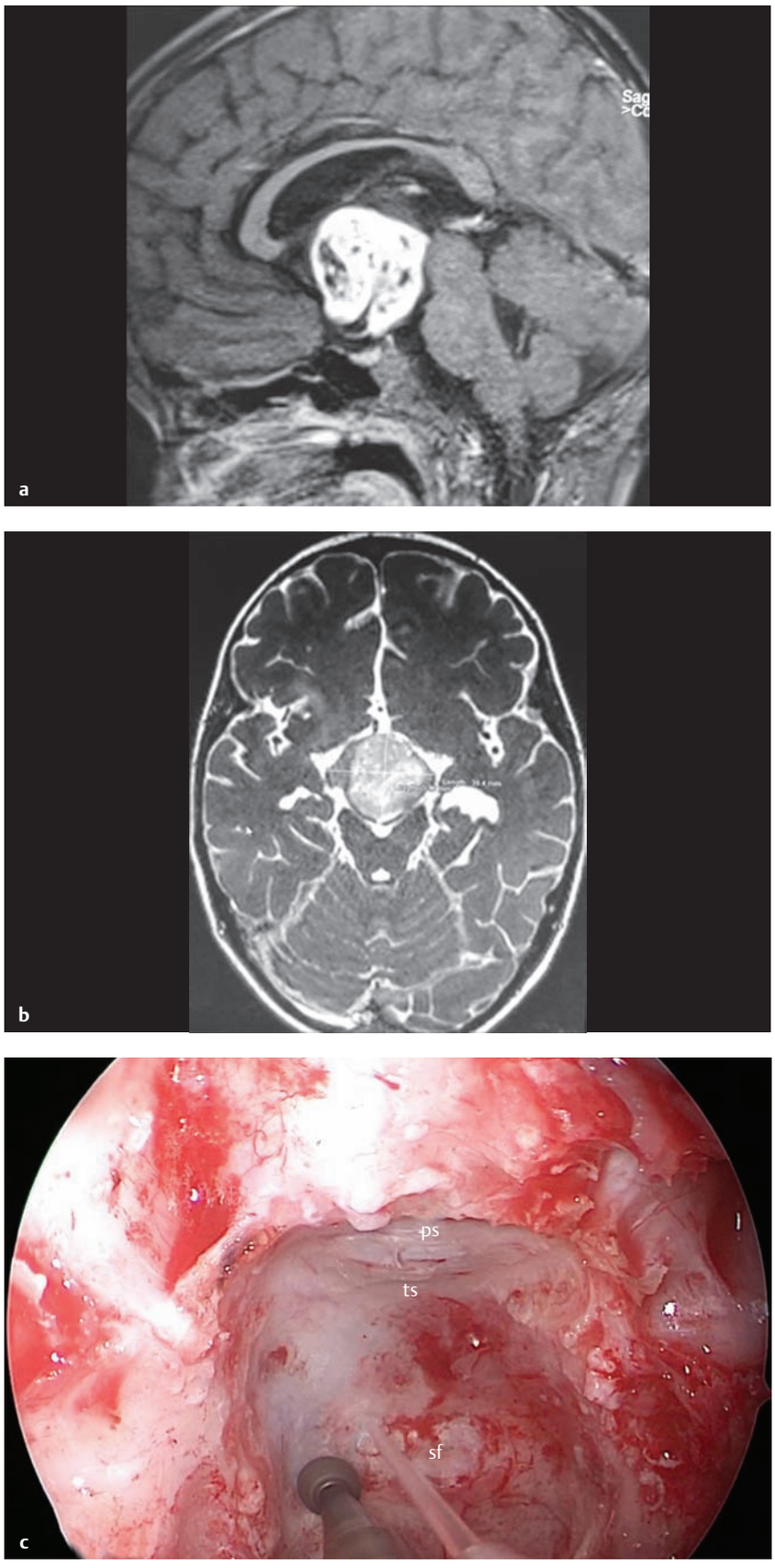

Fig. 8.35 **(a)** MRI sagittal cut showing mass lesion in suprasellar region. **(b)** MRI scan axial cut showing mass lesion in suprasellar region. **(c)** Endoscopic view showing drilling of sellar floor after complete exposure of sphenoid sinuses. Ps, planum sphenoidale; sf, sellar floor; ts, tuberculum sphenoidale.

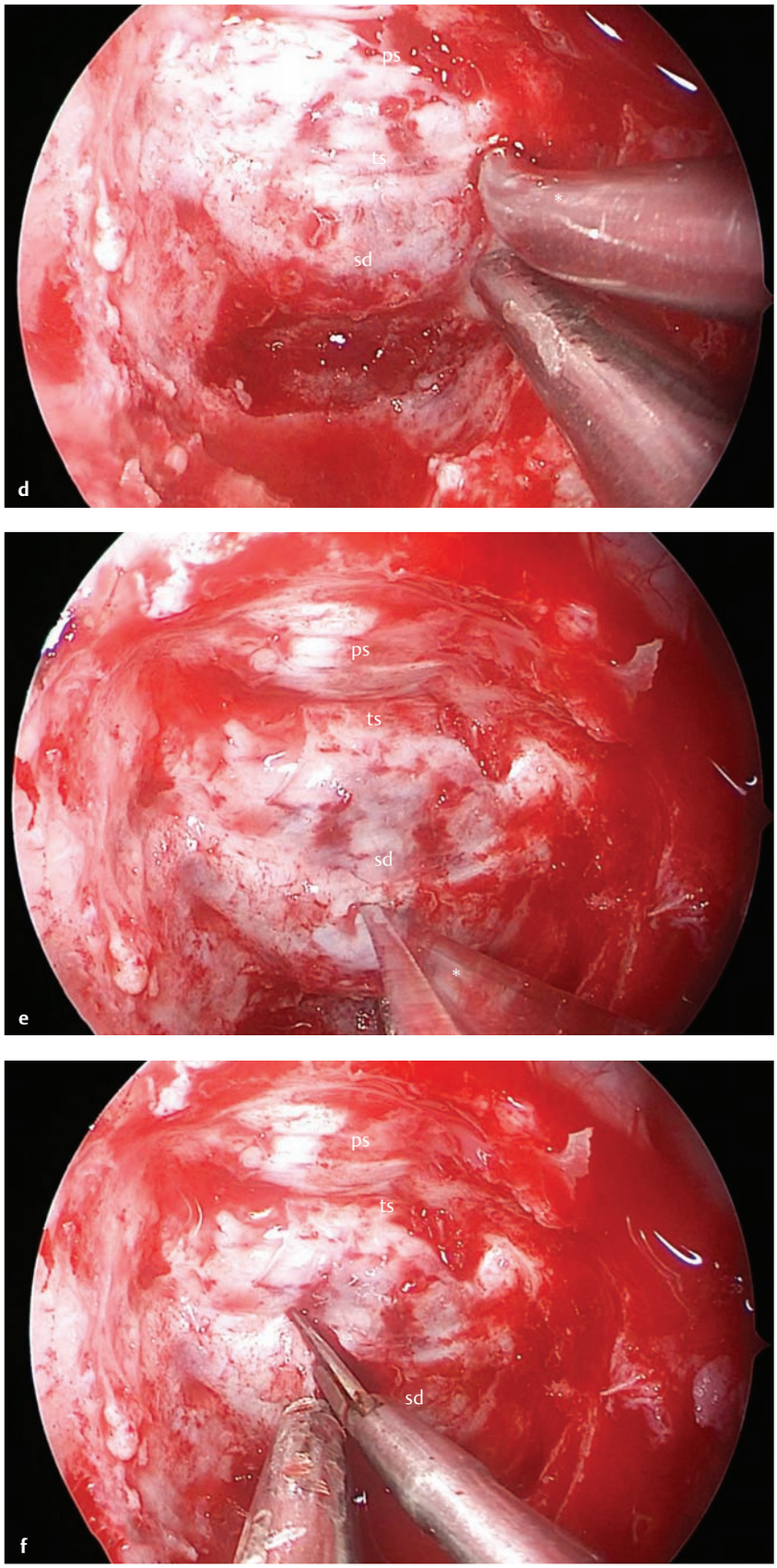

Fig. 8.35 **(d)** Endoscopic view showing mapping of carotid artery after complete exposure of sellar and suprasellar dura. Ps, planum sphenoidale; sd, sellar dura; ts, tuberculum sphenoidale. **(e)** Endoscopic view showing putting incision over sellar dura. Ps, planum sphenoidale; sd, sellar dura; ts, tuberculum sphenoidale; *, knife. **(f)** Extension of dural incision with Kassam's scissors. Ps, planum sphenoidale; sd, sellar dura; ts, tuberculum sphenoidale.

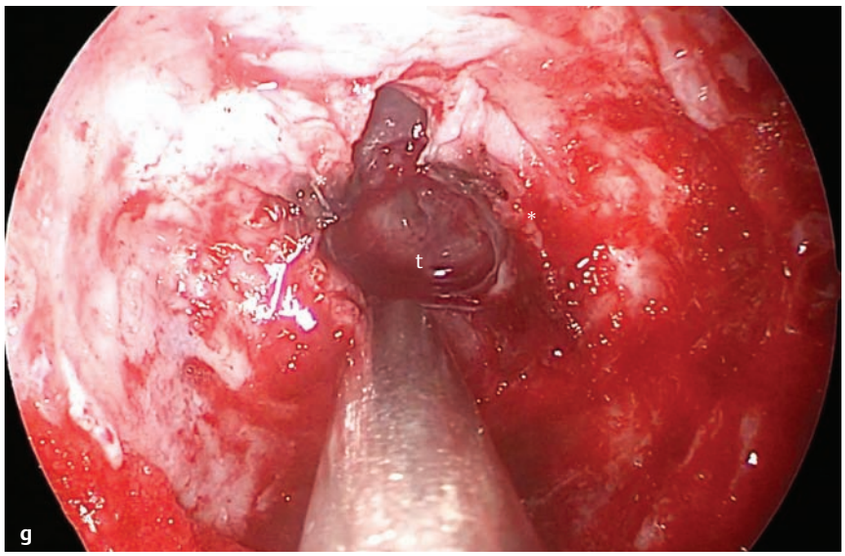

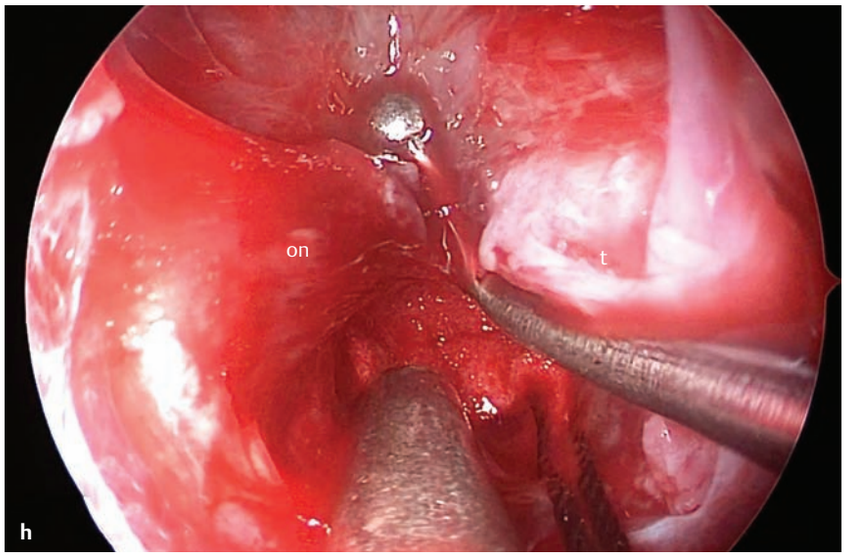

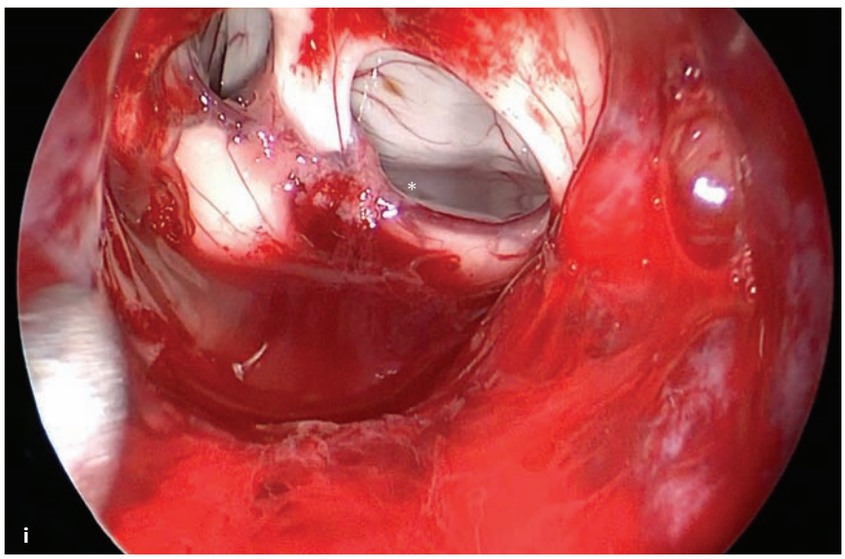

Fig. 8.35 **(g)** After elevation of dural flaps tumor can be visualized. T, tumor. **(h)** Endoscopic view showing dissection of tumor from right optic nerve. On, optic nerve; t, tumor. **(i)** Endoscopic view showing foramen of Munro after removal of tumor. *, foramen of Munro.

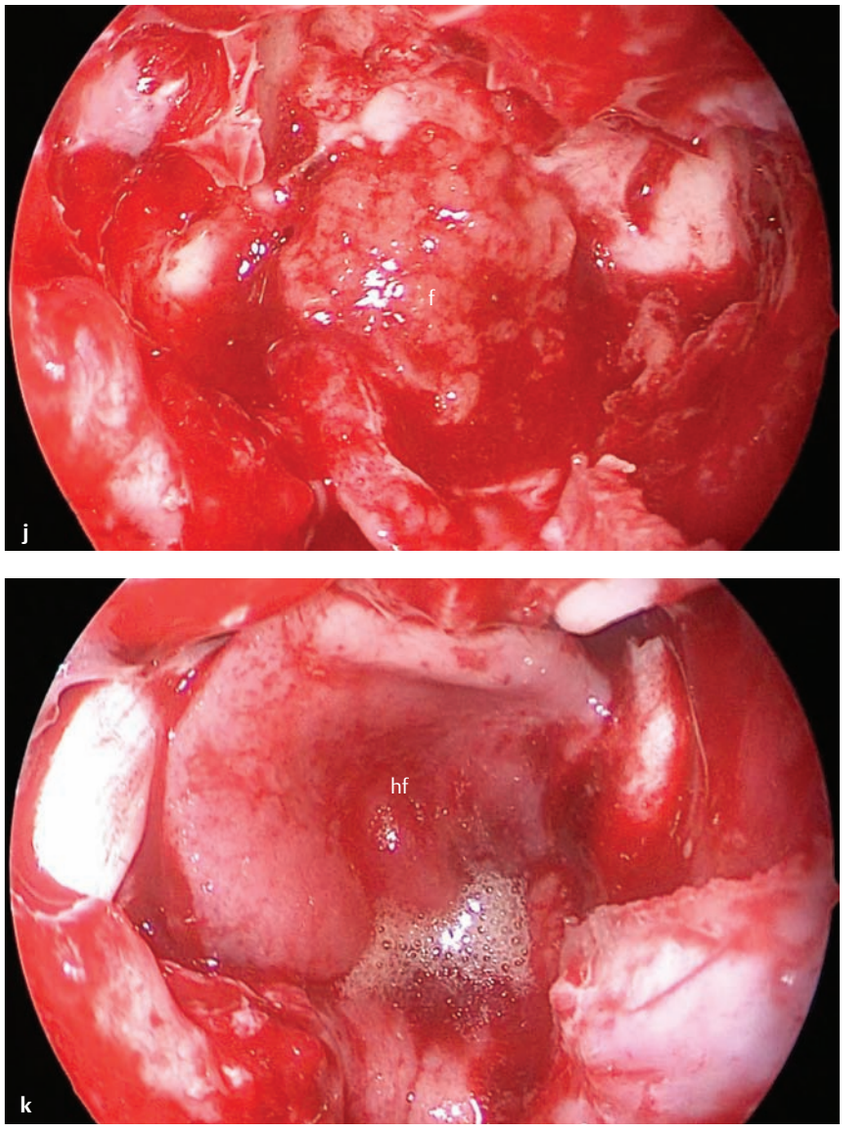

Fig. 8.35 **(j)** Endoscopic view showing reconstruction of cavity with fat. F, fat. **(k)** Reconstruction with nasoseptal flap. Hf, Hadad flap.

Case 19: Craniopharyngioma

A 14-year-old male patient presented with stunted growth and hypogonadism. CT/MRI scan showed cystic lesion with calcified component seen in the sellar and suprasellar region (**Fig. 8.36a, b**). After harvesting right-side nasoseptal flap exposure of the sphenoid sinus, drilling of the floor of sellar bone was done. Sellar floor bone was drilled to eggshell thin and removed with the Rosen's elevator (**Fig. 8.36c**). Tuberculum and MOCR were drilled (**Fig. 8.36d**). Thinned MOCR was removed with the help of the Rosen's elevator (**Fig. 8.36e**). With the help of the Kerrison's sphenoid punch planum bone was removed and sellar, tubercular, and planar dura were exposed (**Fig. 8.36f**). Bilateral ICAs were mapped with the help of carotid artery Doppler (**Fig. 8.36g**). Dural flap was developed with help of Cappabianca knife and Kassam's rotatable scissors (**Fig. 8.36h–j**). The cystic part of the tumor was decompressed by putting incision over the wall (**Fig. 8.36k**). Classical "motor oil" content was drained out (**Fig. 8.36l**). Internal debulking of the solid part of the tumor was done with help of two-suction technique (**Fig. 8.36m**). Extracapsular dissection was carried out with the help of pituitary holding forceps and elevator (**Fig. 8.36n**). Lateral part of the capsule was first dissected and debulked (**Fig. 8.36o**). Superior part of the capsule was dissected (**Fig. 8.36p**). A small piece of tumor was found adherent to right cavernous sinus. Gentle dissection of the last part of the tumor was done (**Fig. 8.36q**). No leak from the diaphragma was seen (**Fig. 8.36r**). Cavity was filled with free fat graft and piece of cartilage and diaphragma was pushed inside (**Fig. 8.36s**). Defect was closed in multilayers with nasoseptal flap, Surgicel, Gelfoams, and fibrin tissue glue (**Fig. 8.36t**).

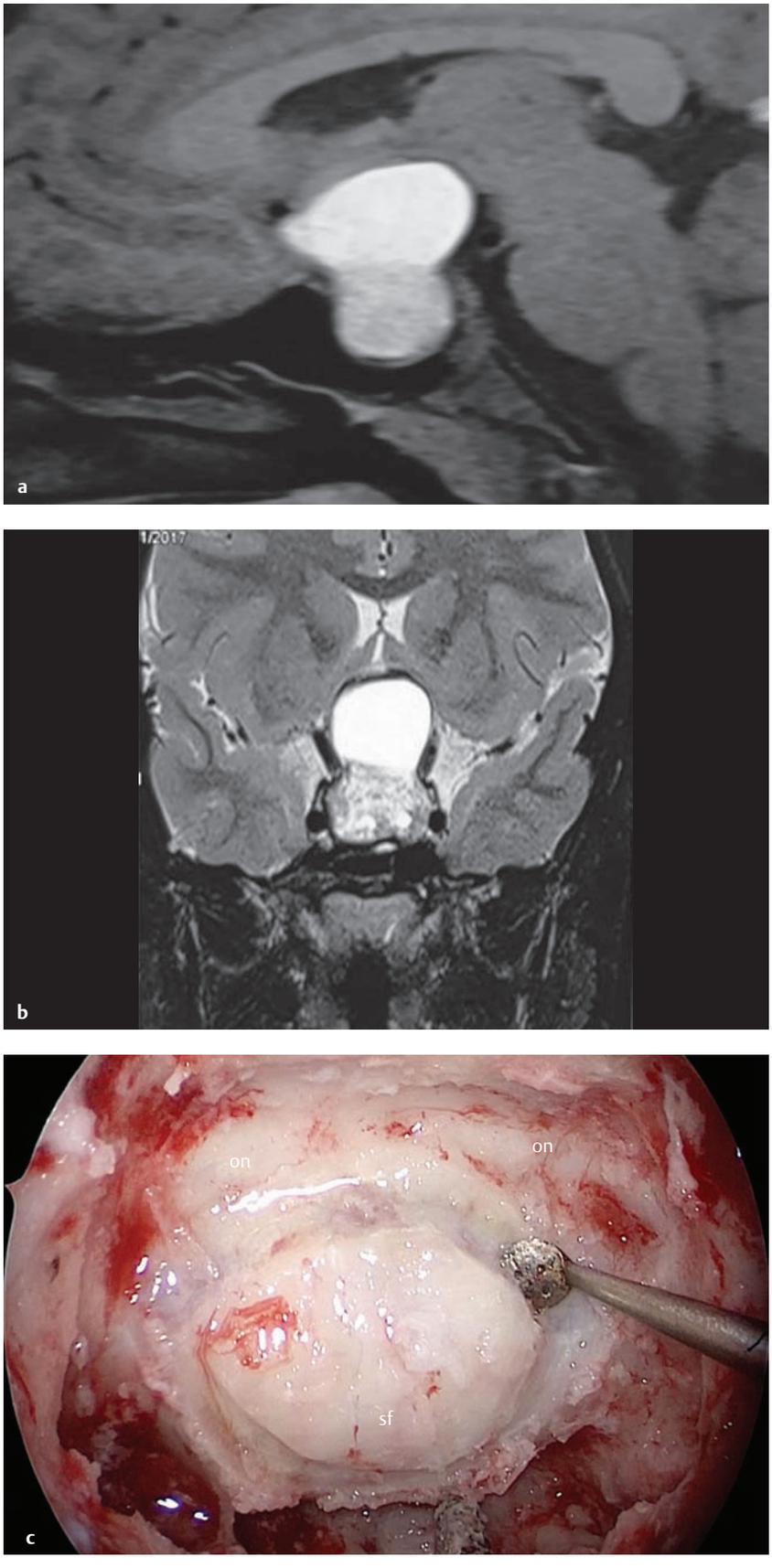

Fig. 8.36 **(a)** Sagittal cut in MRI scan showing solid cystic lesion in sellar and suprasellar region. **(b)** Coronal cut of MRI scan showing cystic as well as calcified lesion in sellar and suprasellar region. **(c)** Endoscopic view showing wide exposure of sphenoid sinuses and elevation of the sellar floor bone with elevator. On, optic nerve; sf, sellar floor.

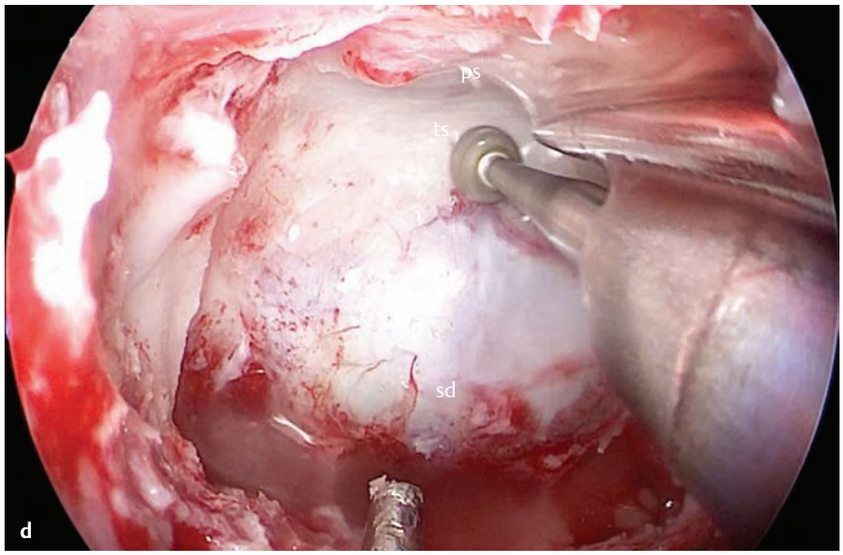

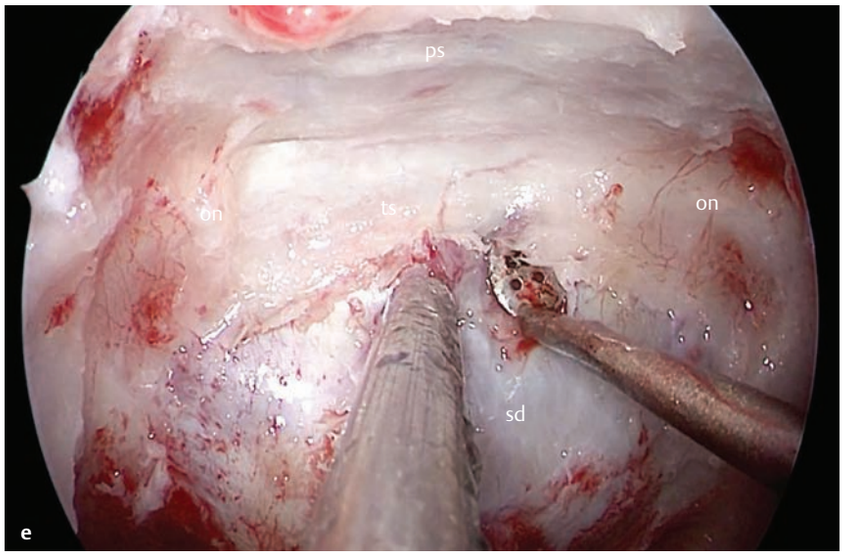

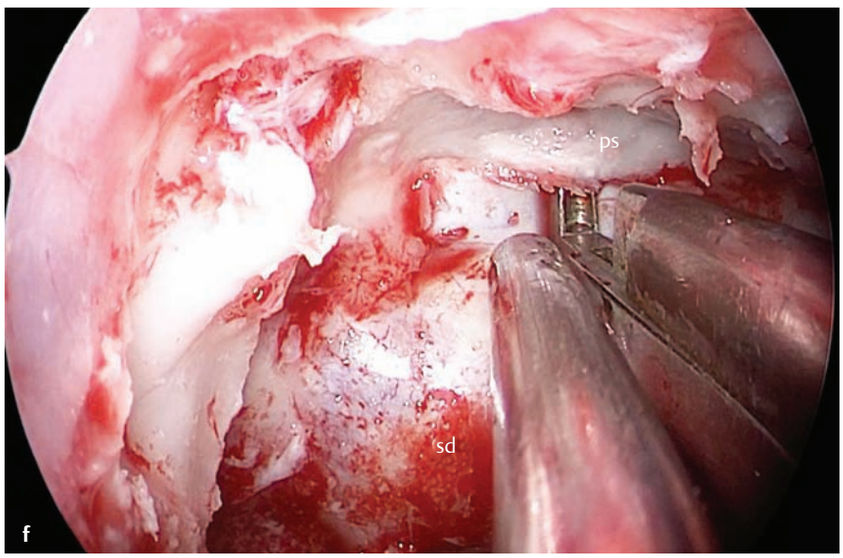

Fig. 8.36 **(d)** Endoscopic view showing drilling of the tuberculum sella. Ps, planum sphenoidale.sd, sellar dura; ts, tuberculum sella; **(e)** Endoscopic view showing elevation of the thinned-out tuberculum sella bone. On, optic nerve; ps, planum sphenoidale; sd, sellar dura; ts, tuberculum sella. **(f)** Endoscopic view showing elevation of the thinned-out planum sphenoidale bone. Ps, planum sphenoidale; sd, sellar dura.

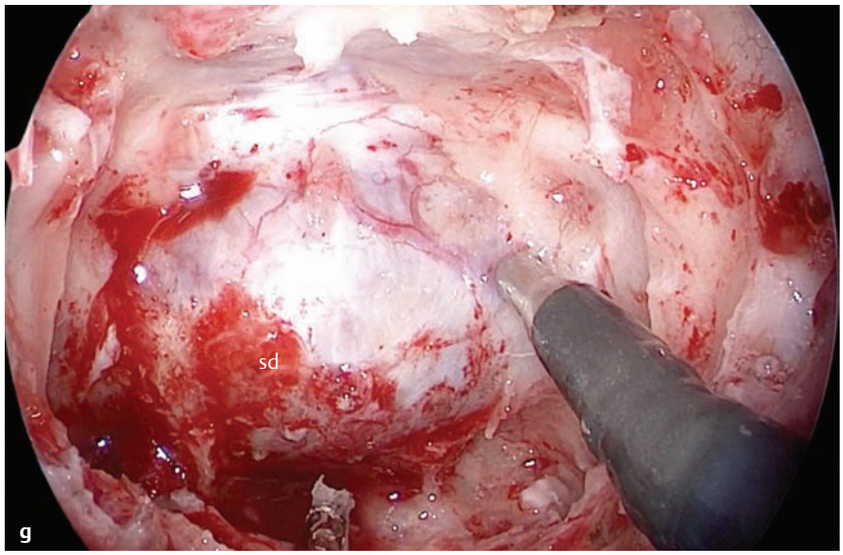

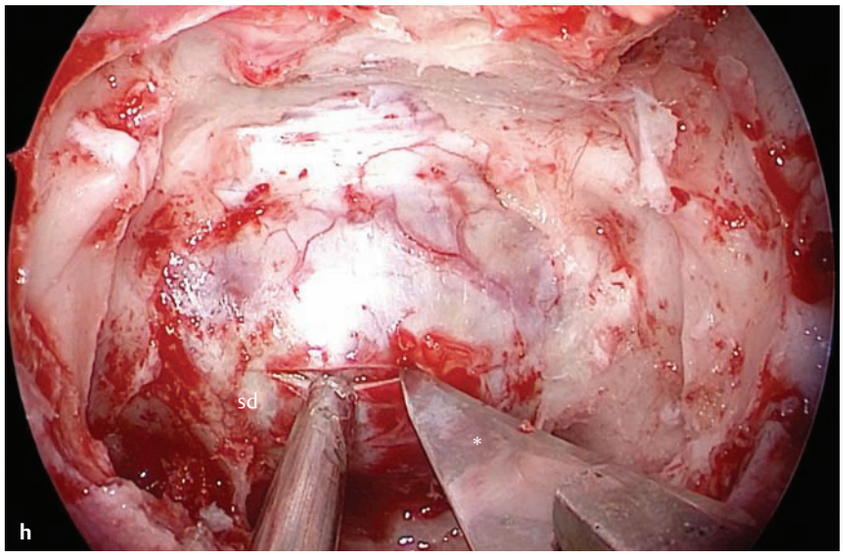

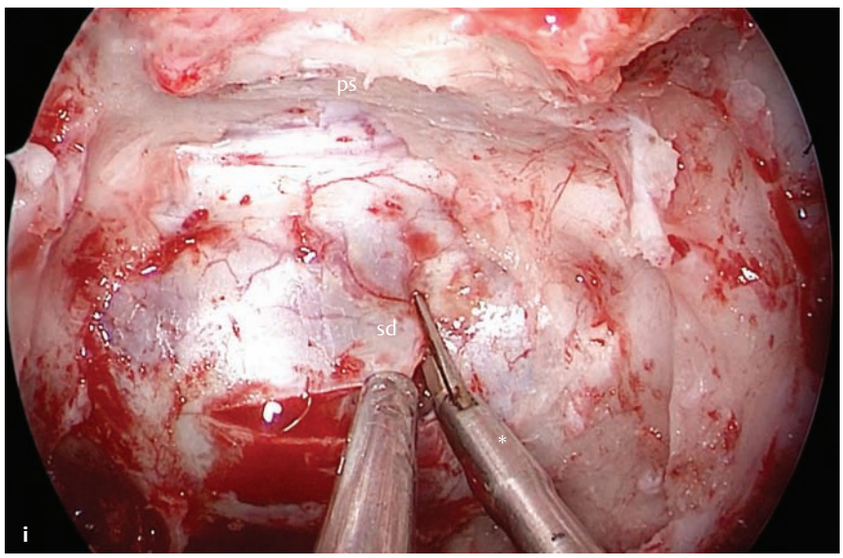

Fig. 8.36 **(g)** Endoscopic view mapping of carotid artery with carotid Doppler after sellar suprasellar exposure. Sd, sellar dura; *, carotid Doppler. **(h)** Endoscopic view showing giving incision over sellar dura. Sd, sellar dura; *, knife. **(i)** Extension of dural incision with Kassam's scissors. Ps, planum sphenoidale; sd, sellar dura; ts, tuberculum sella; *, Kassam's rotatable scissors.

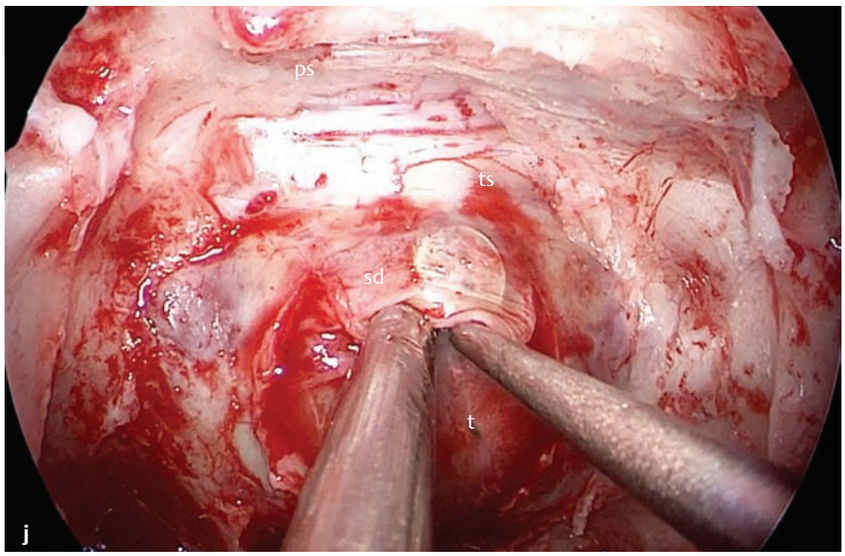

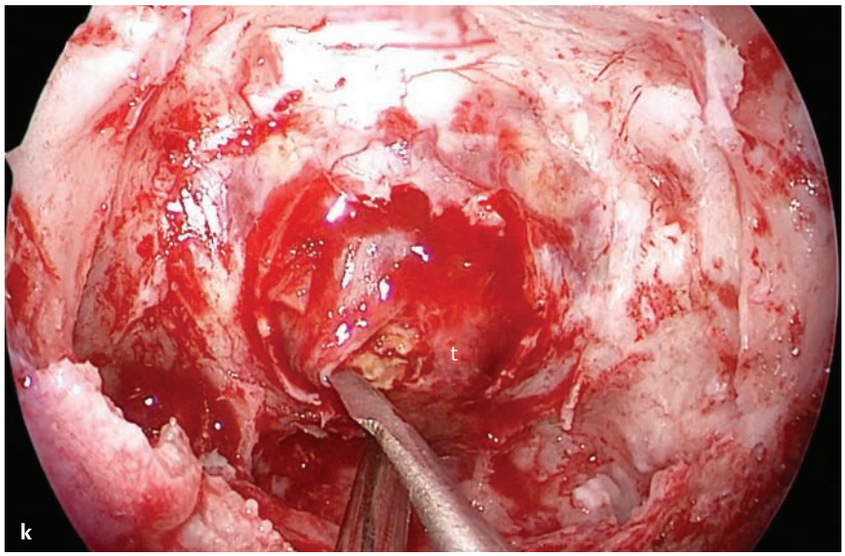

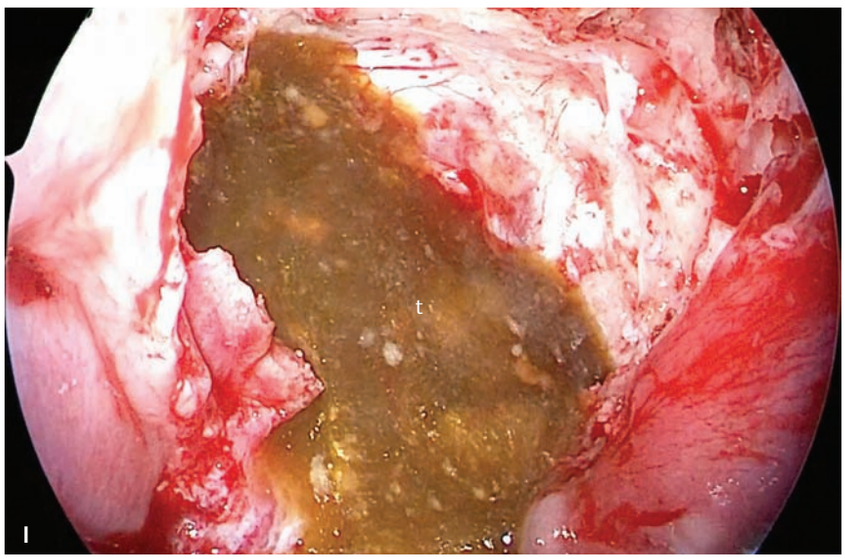

Fig. 8.36 **(j)** Endoscopic view showing elevation of endosteal layer of sellar dura. Ps, planum sphenoidale; sd, sellar dura; t, tumor; ts, tuberculum sella. **(k)** Endoscopic view showing incision is given on the cystic tumor wall. T, tumor. **(l)** Endoscopic view showing typical "motor oil" content of the cyst. *, content of the cystic part of tumor.

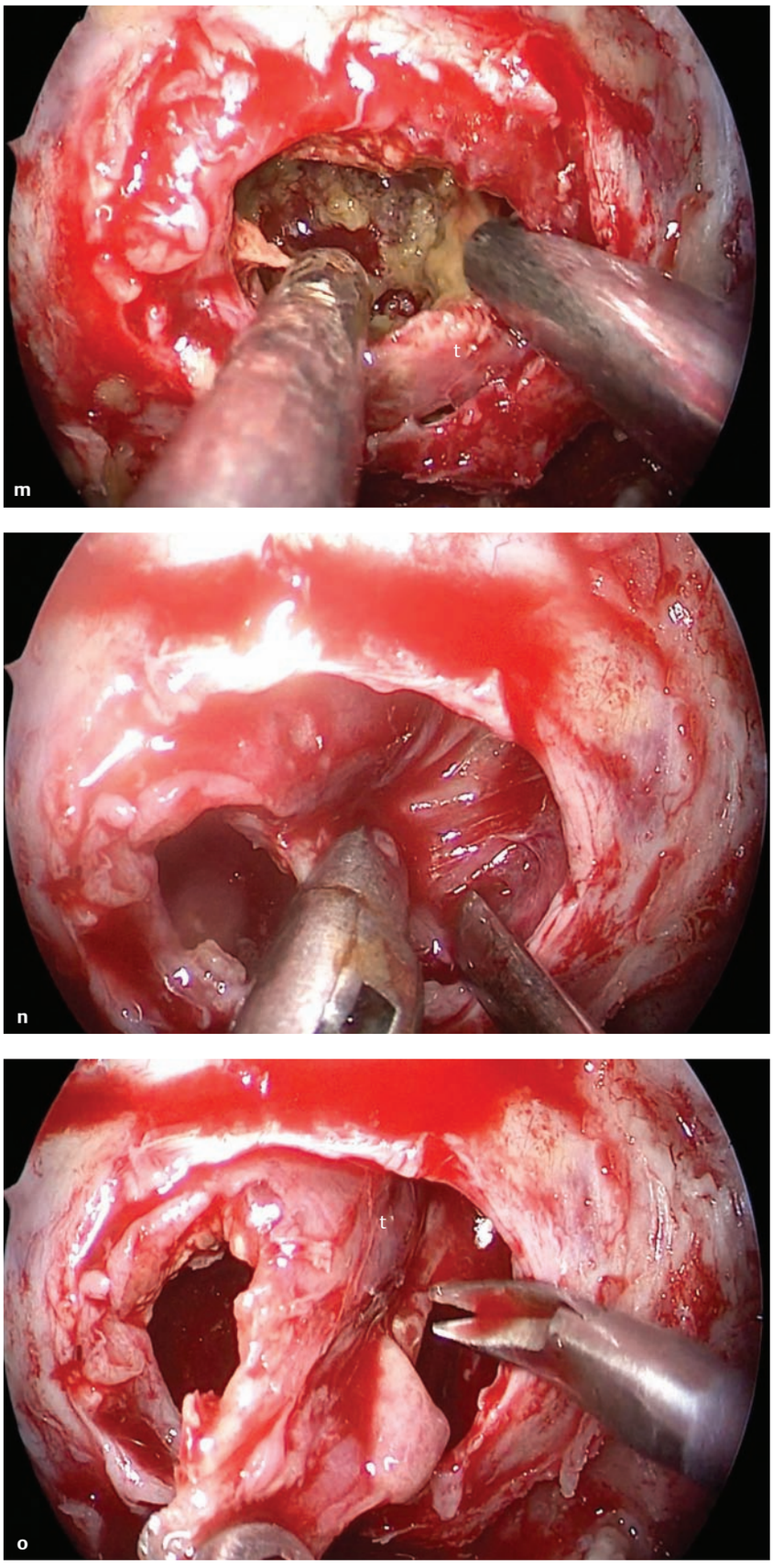

Fig. 8.36 **(m)** Endoscopic view showing debulking of the tumor by two suction method. T, tumor. **(n)** Endoscopic view showing extracapsular dissection of the tumor by elevator. T, tumor. **(o)** Endoscopic view showing debulking of tumor with microdissection. T, tumor.

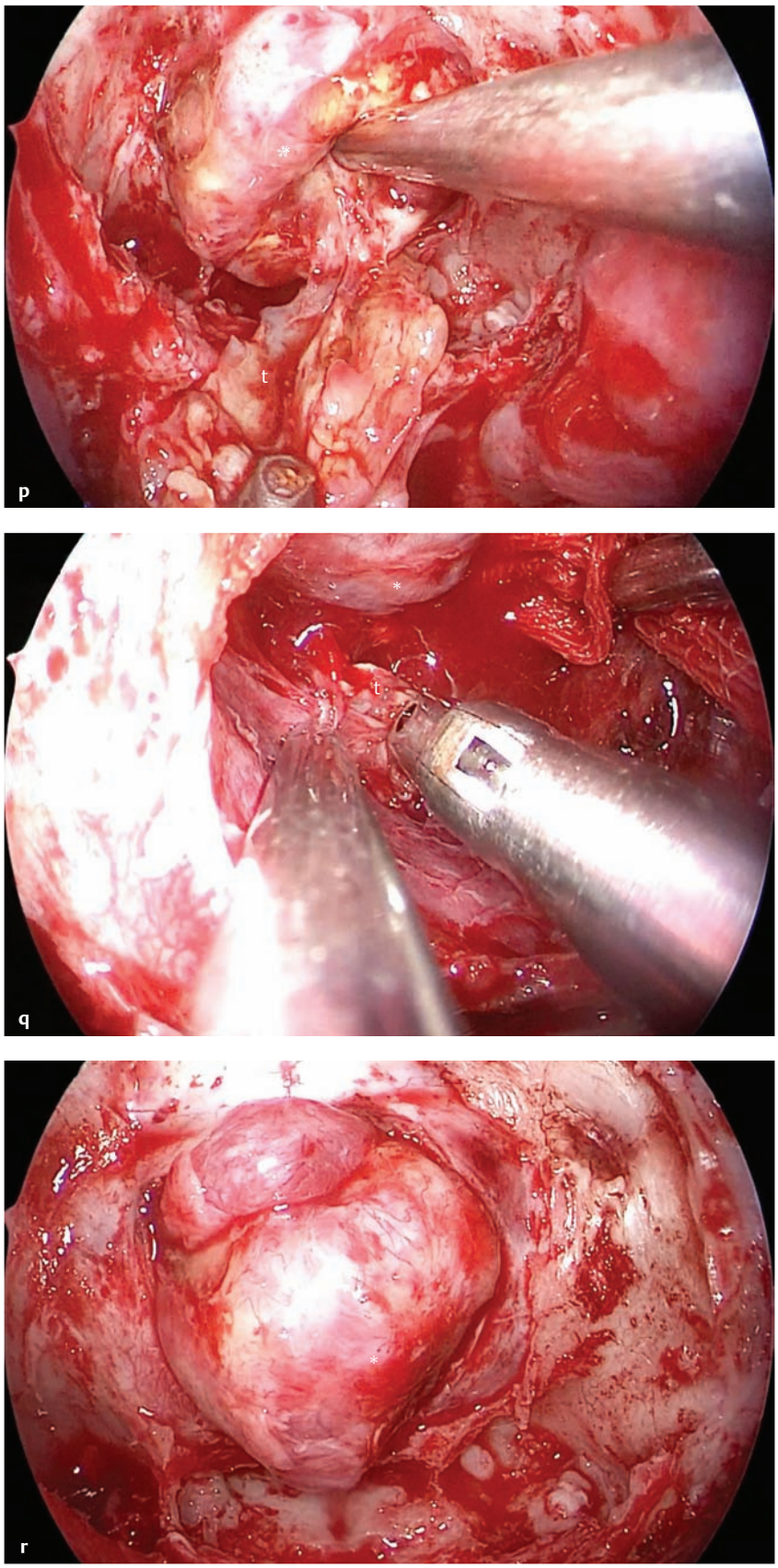

Fig. 8.36 **(p)** Endoscopic view showing removal of tumor from the diaphragma. T, tumor; *, diaphragma. **(q)** Removing last bit of tumor near right optic nerve after elevating diaphragma. T, tumor; *, diaphragma. **(r)** Endoscopic view of the diaphragma after complete removal of tumor. *, diaphragma.

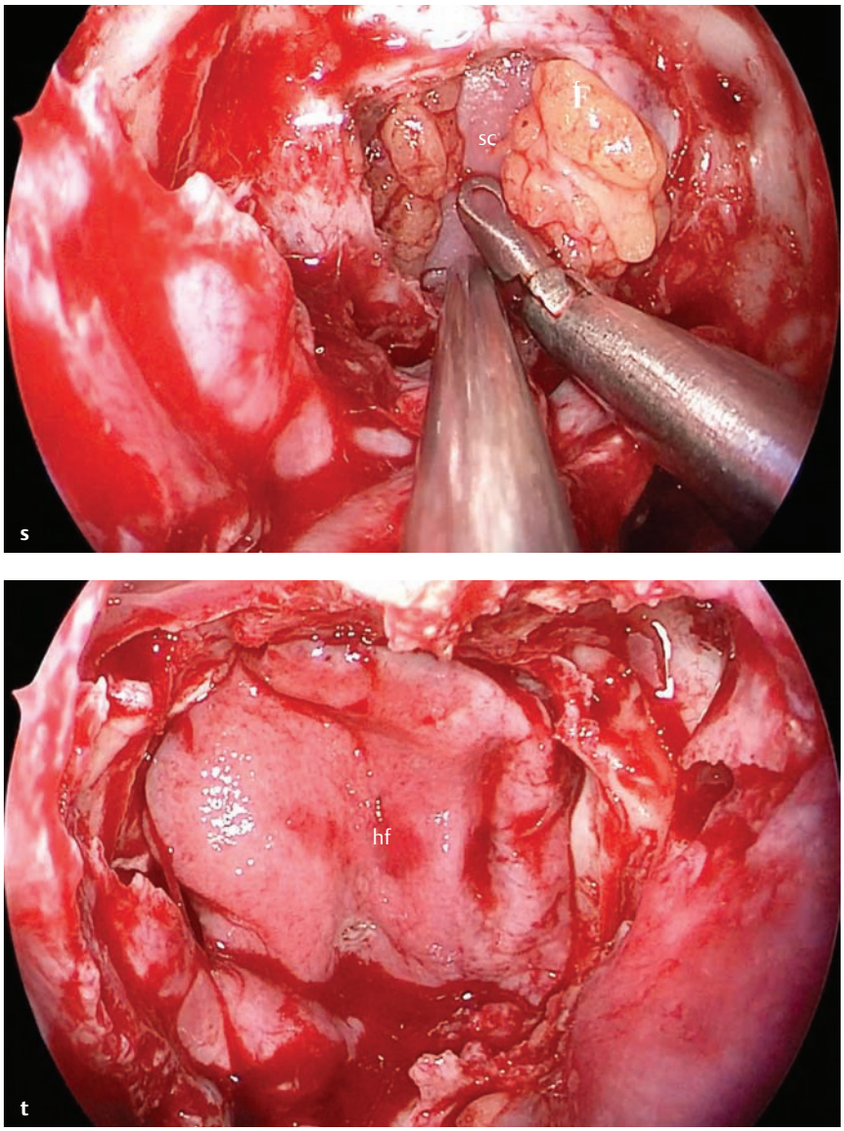

Fig. 8.36 **(s)** Closure with fat and septal cartilage. F, fat; sc, septal cartilage. **(t)** Endoscopic view showing placement of nasoseptal flap. Hf, Hadad flap.

Pearls and Tips

- Adequate surgical exposure includes exposure of the posterior part of cribriform plate, PS, tuberculum, sella, clinoid, parasellar carotid protuberance, and the optic canal to allow binostril instrumentation and proper exposure of the tumor.
- MOCR should be removed as it allows identification of paraclinoid carotid and optic nerve. Most important, complete removal of this bone is mandatory to isolate the opticocarotid cistern without having to significantly retract the tumor medially and risk arterial or nerve injury. It will also help isolate the subchiasmatic perforating vessels that have been displaced over the lateral dome of the tumor, thus preventing devascularization of the optic nerves, chiasm, and infundibulum.
- While drilling MOCR copious irrigation is required to avoid thermal damage to underlying vessels and nerve.
- After removal of the MOCR the site may bleed because at this site SICS drain into the cavernous sinus. This bleeding can be controlled by placing Surgicel or applying Surgiflo.
- It is advisable not to overexpose dura mater anteriorly as excess removal of the bone may lead to brain herniation obscuring the vision.
- In most cases superior hypophysial artery is the first structure to be identified and preserved.
- Decompression of the cystic part followed by debulking of the solid part is done by microdissection or using an ultrasonic aspirator. After adequate debulking of the tumor, extra capsular dissection is carried out using keyhole suction in left hand and micro elevator in the right hand of the surgeon.
- In cases where stalk is infiltrated and panhypopituitarism is present preoperatively, stalk can be resected.
- It is advisable to leave small part adherent to vital structures and think for secondary gamma knife radiosurgery.

Conclusion

Endoscopic endonasal surgery is less invasive and more direct route to suprasellar area. It is best method for midline ventral skull base lesions such as craniopharyngiomas, PS and tubercular meningiomas, pituitary macroadenomas with suprasellar extension, and Rathke's cyst.

This route provides direct access to tumor, involved bone removal, early devascularization of tumor, less damage to optic nerves, and less retraction to brain compared to craniotomies.

Due to the availability of vascularized flaps, such as nasoseptal flap, lateral nasal wall flaps, inferior turbinate flaps, there is less possibilities of CSF leak nowadays.

Endoscopic endonasal suprasellar approach requires more expertise, specific instruments, and multidisciplinary team approach to perform it.

References

1. Cavallo LM, de Divitiis O, Aydin S, et al. Extended endoscopic endonasal transsphenoidal approach to the suprasellar area: anatomic considerations—part 1. Neurosurgery 2008;62(6, Suppl 3)1202–1212
2. Bowers CA, Altay T, Couldwell WT. Surgical decision-making strategies in tuberculum sellae meningioma resection. Neurosurg Focus 2011;30(5):E1
3. Reul J. Differential diagnosis of truly suprasellar space-occupying masses: synopsis of clinical findings, CT, and MRI. Eur Radiol 1995;5:224–237
4. Sharma BS, Sawarkar DP, Suri A. Endoscopic pituitary surgery: techniques, tips and tricks, nuances, and complication avoidance. Neurol India 2016;64(4):724–736
5. Madhok R, Prevedello DM, Gardner P, Carrau RL, Snyderman CH, Kassam AB. Endoscopic endonasal resection of Rathke's cleft cysts: clinical outcomes and surgical nuances. J Neurosurg 2010;112(6):1333–1339
6. Jeswani S, Nuño M. Comparative analysis of outcomes following craniotomy and expanded endoscopic endonasal transsphenoidal resection of craniopharyngioma and related tumors: a single-institution. J Neurosurg 2016;124:627–638
7. Bardeesi AM, Alsaleh S, Ajlan AM. Endoscopic transnasal suprasellar approach for anterior clinoidal meningioma: a case report and review of the literature. Surg Neurol Int 2017;8:194
8. Labib MA, Prevedello DM, Fernandez-Miranda JC, et al. The medial opticocarotid recess: an anatomic study of an endoscopic "key landmark" for the ventral cranial base. Neurosurgery 2013;72(1, Suppl Operative):66–76, discussion 76
9. Black PM, Zervas NT, Candia G. Management of large pituitary adenomas by transsphenoidal surgery. Surg Neurol 1988;29(6):443–447
10. Mortini P, Barzaghi R, Losa M, Boari N, Giovanelli M. Surgical treatment of giant pituitary adenomas: strategies and results in a series of 95 consecutive patients. Neurosurgery 2007;60(6): 993–1002, discussion 1003–1004
11. Hardy J, Vezina JL. Transsphenoidal neurosurgery of intracranial neoplasm. Adv Neurol 1976;15:261–273
12. Komotar RJ, Starke RM, Raper DM, Anand VK, Schwartz TH. Endoscopic endonasal versus open transcranial resection of anterior midline skull base meningiomas. World Neurosurg 2012;77(5-6):713–724
13. Kassam AB, Gardner PA, Snyderman CH, Carrau RL, Mintz AH, Prevedello DM. Expanded endonasal approach, a fully endoscopic transnasal approach for the resection of midline suprasellar craniopharyngiomas: a new classification based on the infundibulum. J Neurosurg 2008;108(4):715–728

9 Endoscopic Approach to Parasellar Lesions

Chaithra B. G., Shilpee Bhatia Sharma, Narayanan Janakiram

Parasellar Area

The parasellar region is a part of the middle cranial base situated between the sella and the temporal fossa. It is considered the smallest part and the most critical part of the skull base with the highest concentration of neurovascular structures as it houses the cavernous sinuses.

Cavernous sinus (CS) surgery represents a surgical challenge due to the anatomical complexity and high functional value of the structures contained in it. It was considered no man's land. There is no single gold standard approach to the parasellar area and CS. Selection of the appropriate approach solely depends upon the extent and behavior of the tumor.[1]

Extended endoscopic approach and the transcranial approach are complementary, aiming to deliver the best possible result with minimal surgical morbidity.

Distinct advantages of extended endoscopic approach (extradural approach) over the transcranial approach are:

- Being extracerebral, it avoids brain retraction and manipulation.
- Enters the CS through the medial wall, which is devoid of any vital neurovascular structure.

The emergence of the endoscope on the neurosurgical landscape has introduced the possibility of wide peripheral and endocavitary vision through a limited surgical channel. Expanded endoscopic endonasal approach has opened new venues in CS surgery: the wider view provided by the endoscope allows the surgeon to see inside the CS either through medial–lateral trajectory or anterior–posterior trajectory.[2] The trajectory has the potential of providing a direct route into the lesion, minimizing the need to manipulate structures located circumferentially along the perimeter.[3]

Lesions Affecting the Parasellar Area

- Primary lesions of the CS are rare. Other lesions include:
  - Vascular lesions: hemangioma, A-V malformation.
  - Neoplastic: lymphoma, hemangiopericytoma, chondrosarcoma.
- Secondary tumors invading CS: more common.

Pituitary adenoma is the most common tumor invading the CS that has been extensively studied. Other tumors like chordomas, meningioma, chondrosarcoma, juvenile nasopharyngeal angiofibroma are comparatively less common.

The area most likely to be involved is the endosteal layer of the sellar floor.

The degree/extent of invasion of pituitary macroadenoma to the parasellar region/CS is graded based on the preoperative coronal magnetic resonance imaging (MRI). Micko et al[4] proposed the modified Knosp–Steiner classification for the parasellar extension.

According to this classification, three lines connecting the cross-sections of the intracavernous and supracavernous ICAs distinguish four grades of parasellar adenoma extension: a medial tangent, a line through the cross-sectional centers, and a lateral tangent (**Table 9.1**).

Indications of Surgery

Surgery is influenced by tumor factors such as its biologic behavior, extension, and consistency.

- CS tumors with an extradural location (more frequently adenomas, chordomas, and chondrosarcomas).
- Minimal intradural extension: it is of great importance to have good instrumentation and a skilled surgical team, to plan an appropriate approach according to the CS compartment involved by the tumor.[1]

Limitations of Surgery

Anatomical Limitations

- Difficulty in the management of internal carotid artery (ICA) injury.

Table 9.1 Knosp–Steiner classification for parasellar extension (Fig. 9.1)

Grades	Extension of the tumor
Grade 0	The adenoma does not encroach on the CS space.
Grade 1	The medial tangent is passed, but the extension does not go beyond a line drawn between the cross-sectional centers of the intracavernous and supracavernous ICAs (the intercarotid line).
Grade 2	The tumor extends beyond the intercarotid line but not past the tangent on the lateral aspects of the intracavernous and supracavernous ICAs.
Grade 3A	The tumor extends lateral to the lateral tangent of the intracavernous and supracavernous ICAs into the superior CS compartment.
Grade 3B	The tumor extends lateral to the lateral tangent of the intracavernous and supracavernous ICAs into the inferior CS compartment.
Grade 4	Total encasement of the intracavernous carotid artery.

Abbreviations: CS, cavernous sinus; ICA, internal carotid artery.

- Tumors involving the vessel wall-like meningioma, increase the risk of carotid artery injury.
- Significant posterior fossa extension with the tumor located behind the ICA (not protruding into the sphenoid sinus).
- Significant intradural involvement (temporal lobe involvement), displacing the CS and trigeminal ganglion medially.

Patient and Institution Factors

- Patients without any neurological deficits.
- Institutional limitations—institutions lacking facilities of transnasal-Doppler, neuronavigation, endobipolars, etc.
- CS surgery requires in-depth anatomical knowledge, experience gained by cadaver dissection because of the concentrated neurovascular structure present there.[5]

Rationale of Surgery

- Gross total resection or near-total resection.
- Debulking of the tumor.
- Confirming CS invasion by surgical inspection.
- Pathological diagnosis.
- Improving the compression effect.
- Increasing the safety and efficacy of medical and radiation treatment.

Instrumentation and Technical Adjuncts

Neuronavigation and micro-Doppler (**Figs. 9.2–9.5**) help to accurately delineate the ICA before the incision of the CS wall and during tumor debulking. Modern navigation systems using a magnetic field to localize the pointer are used during the procedure.

Real-time intraoperative MRI or CT are also extremely useful.

Preoperative Planning

Different surgical corridors are proposed for CS or parasellar area. The appropriate approach selection is based on the compartments involved by the tumor. The various approaches employed are:

- Midline transsphenoidal endoscopic approach: it is performed when the tumor involves medial and posterosuperior compartment.
- Ethmoid–pterygoid–sphenoidal endoscopic approach: it is selected in cases where tumor involves the lateral and anteroinferior compartment.
- Transmaxilla pterygoid endoscopic approach: it is also considered a far lateral approach for tumors extending from lateral compartment, through the foramen rotundum to pterygopalatine fossa.[1]

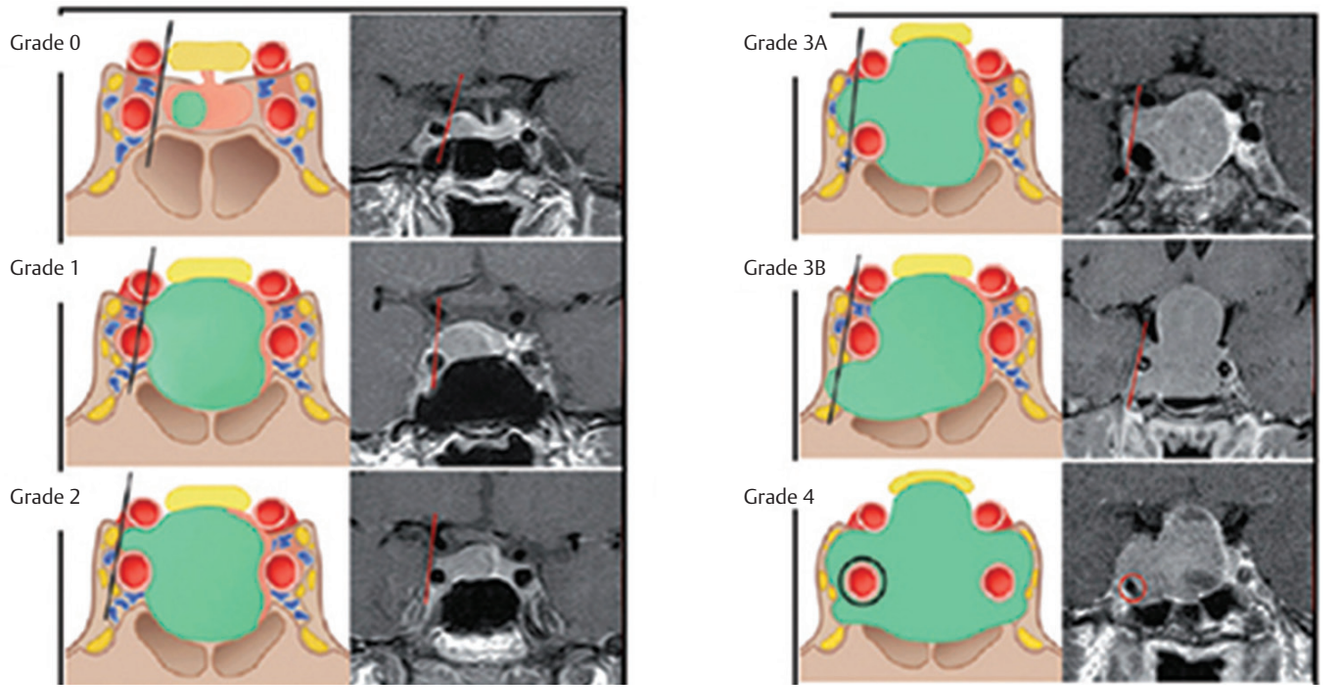

Fig. 9.1 Modified Knosp classification of pituitary macroadenoma.

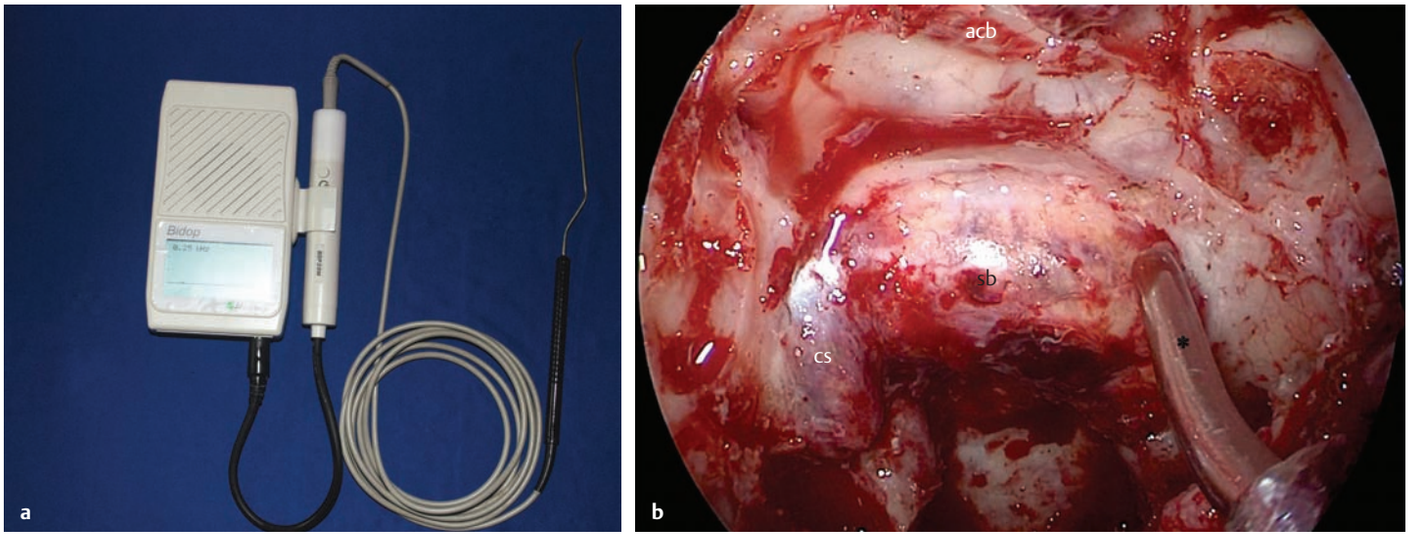

Fig. 9.2 **(a)** Micro-Doppler to map the course of internal carotid artery. **(b)** Image showing the use of micro-Doppler.

Surgical Technique

Surgery is carried out under general anesthesia with orotracheal intubation.

Position: Patient is placed in reverse Trendelenburg position with horse pad placed beneath the head. Complete head immobilization in pin holder is also practiced. Head is placed in neutral position. The nose area is cleaned with betadine aqueous solution.

Nasal decongestion is achieved by placing gauze soaked in 2% xylocaine and epinephrine. Thigh is routinely prepared as eventual site for harvesting free fat and fascia graft for reconstruction.

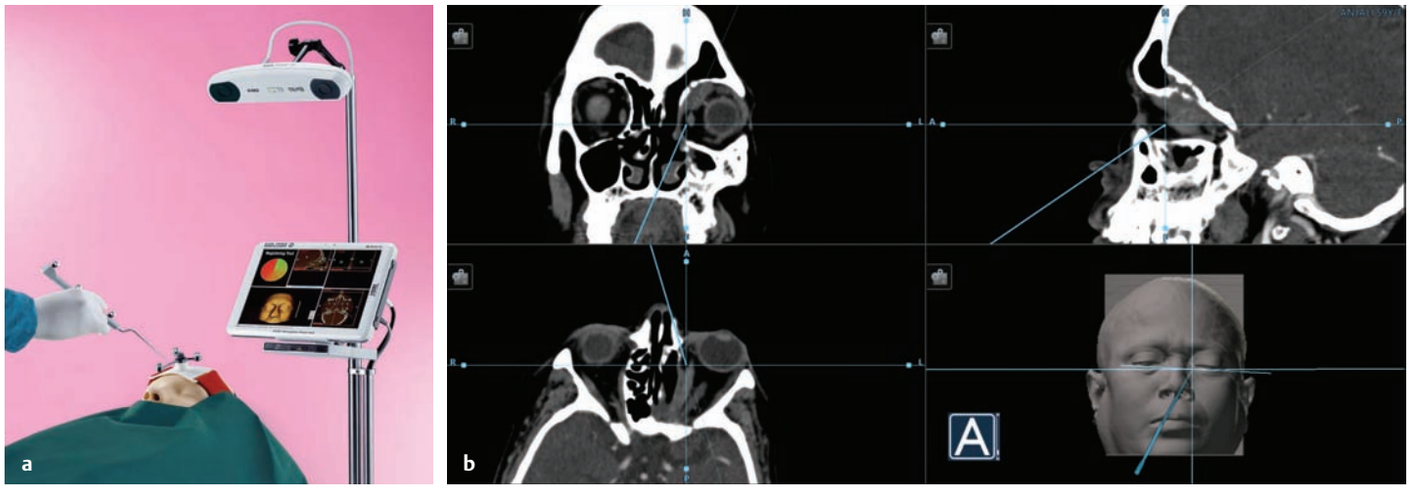

Fig. 9.3 **(a, b)** Neuronavigation to determine the anatomical landmarks.

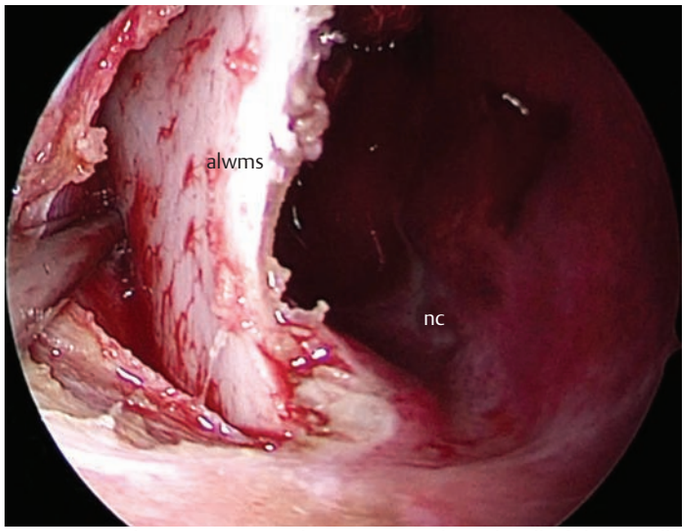

Fig. 9.4 Endoscopic picture showing anterolateral wall of the maxilla exposed during modified endoscopic Denker's procedure. awms, anterior wall of maxillary sinus.

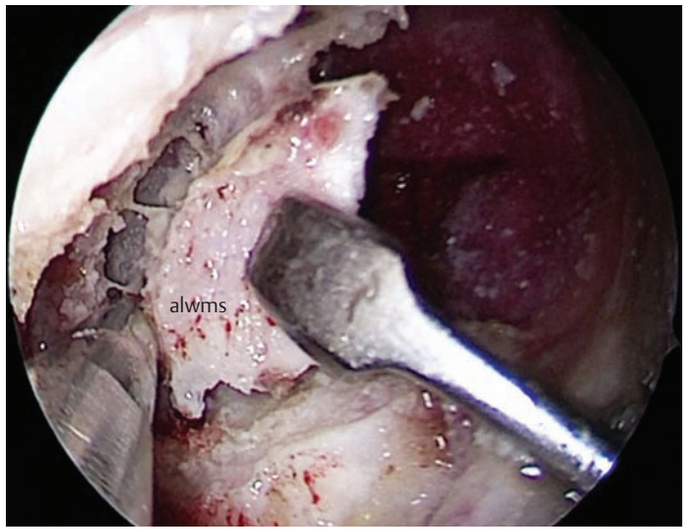

Fig. 9.5 Anterolateral wall of the maxillary sinus is drilled out. Awms, anterior wall of the maxillary sinus.

Midline Transsphenoidal Endoscopic Approach

Nasal and sphenoid phases are same as explained in Chapter 7 titled "Endoscopic Approach to Sellar Lesion" in this atlas.

Sellar Phase

- The bony covering of sella is drilled using a high-speed diamond drill of 4-mm size and detached from the dura behind. Constant irrigation with normal saline is important at this point. The sellar bone is cleared laterally, from the right CS to the left, and superiorly from the superior intercavernous sinus to the inferior intercavernous sinus. The microvascular Doppler is now employed for precise identification of both the ICAs. The bone in proximity to the neurovascular structures is removed using a Rosen's elevator with swift movements to avoid injury, use of Kerrison's punch being avoided.
- The bone overlying the invaded CS must be carefully removed from the optic–carotid recess to the

paraclival carotid protuberance vertically and 1 cm laterally to the sella, exposing the main bulge of the parasellar carotid artery. This bone removal later increases the capacity of inspection of the CS content by gently displacing the anterior membranous CS wall laterally.

- Dural incision: The dural opening starts in the sellar area. A horizontal incision is placed inferiorly, in the center, with a retractable knife, and then extending it superiorly on its both sides using Kassam rotatable scissors, staying within the confines of the carotid vessels. The dura is then raised and detached from the tumor as a superior based **U**-shaped flap.

Tumor Dissection

After debulking the tumor in the sella, the medial compartment of the CS is entered, by either enlarging the opening of the medial wall created by the tumor itself or (more rarely) making an incision into the medial wall in a safe area (normally located in the posterior two-thirds of the medial wall of the CS). Recognition of this "safe" area requires identification of the bulging of the tumor and an accurate mapping of the ICA course (using direct vision, micro-Doppler and neuronavigation).

Removal of the tumor inside the medial and posterosuperior compartments of the CS is performed under direct view and has no risk of neural damage due to the absence of cranial nerves in this location. Usually, a 0-degree endoscope is adequate for the procedure.

Tumors with a soft and suckable consistency are internally debulked inferiorly from the 6 o'clock position with the help of two suctions. Tumors which are firm in consistency are excised by extracapsular dissection along with the pseudocapsule. The fibrous bands are separated endoscopically by fine blunt dissection.

At the end, gentle displacement of the anterior wall of CS, aids in the better visualization of these compartments. Surgical exploration of the cavity is performed using angled 30- or 45-degree endoscope.

Reconstruction

Hemostasis is obtained by packing with Cottonoid, warm saline irrigation, and Surgiflo.

Cases where no cerebrospinal fluid (CSF) leak is encountered, the sellar cavity and the sphenoid sinus are filled with fat, up to the anterior wall of the sinus, and further with fibrin glue.

Cases where intra-operative leak is noted, an onlay graft or a nasoseptal flap is placed, with fibrin glue over it, and packed in multiple layers.

Ethmoid-Pterygoid-Sphenoidal Approach

This corridor is the most versatile approach allowing total exposure of the CS with simultaneous direct control of all compartments of CS. It provides excellent exposure to the tumors invading the lateral and anteroinferior compartments. Normally 0-degree endoscope gives good visualization.[1]

Ethmoid Phase

- Ipsilateral middle turbinate is resected sparing its superior third, and a wide middle meatal antrostomy, the posterior wall of the maxillary sinus is exposed, and infraorbital nerve is identified. The posterior wall of the maxillary sinus is removed to expose the pterygopalatine fossa.
- This is followed by removal of the anterior and posterior ethmoidal air cells. Complete ethmoidectomy provides a wide surgical corridor for instrument maneuverability.
- A nasoseptal flap is raised on the contralateral side.

Pterygoid Phase

Removal of the orbital process and perpendicular plate of the palatine bone allows access to the medial aspect of the pterygopalatine fossa.

Dissecting backward in the subperiosteal plane, a bony crest is exposed that serves as a landmark for the palatine artery. Sphenopalatine artery is the first vascular structure to be encountered. It is the terminal branch of internal maxillary artery emerging from the sphenopalatine foramen. The artery is cauterized using bipolar or coblation. Ligaclips may also be utilized for vascular control. Dissection of contents of the pterygopalatine fossa permits the identification of vidian nerve and pterygopalatine ganglion.

Medial and inferior to the foramen rotundum lies the vidian canal, which is a critical landmark for safe identification of the second genu of the petrous segment of the ICA. The author subsequently, identifies the vidian nerve by drilling the vidian canal. Once the ICA position is corroborated, vidian nerve is transected. A lateral transposition of the vidian nerve is practiced by some other authors. The pterygoid

wedge is drilled out. This permits the exposition of the inferolateral portion of the CS.[6]

Sphenoid Phase

This step involves the removal of the basisphenoid. The floor of the sphenoid is drilled using an intranasal diamond burr beginning from the choana to its insertion into the clivus working in an anteroposterior and mediolateral direction medial to the vidian canal.

For complete exposure, bone of the posterolateral wall of the sphenoid sinus is drilled out. The bone to be removed is a quadrilateral-shaped structure located between the optic–carotid recess, and the paraclival carotid protuberance medially and the orbital apex, and the trigeminal nerve protuberance laterally.

Intracavernous Phase

Opening the dura: The precise site of dural incision over inferior wall of CS (sphenoidal part of medial wall) is dictated by the displacement of the ICA caused by the tumor. Routinely the incision is given over the safe area away from the artery. Depending upon the bulk of the tumor either in the medial or the lateral compartment, it may displace ICA either laterally or medially, respectively. In addition to the displacement of ICA in coronal plane, displacement in the sagittal plane should also be considered. If the tumor bulk is present in the anteroinferior compartment, it pushes the ICA posteriorly, with tumor in between, rendering the anterior cavernous dura safe for incision. In the similar manner, if the tumor is present in posterosuperior venous space, the ICA is pushed forward and in direct contact with the dura. In the latter circumstances, the accurate position of ICA is confirmed by using microdropper or neuronavigation before incising the dura.

Except for a tumor exclusively located in the lateral compartment of the CS, two separate dural incisions are given, first over the sellar dura and the second cavernous sinus dura over the cavernous sinus dura on the lateral compartment. The incision is then progressively enlarged in lateral to medial direction. For tumors present in the CS, dural incision is given over the CS, extended medially if required after confirming the position of the ICA with micro-Doppler. As mentioned earlier, maximal care is taken while incising the dura in front of the carotid artery to avoid injury to the vessel, and the abducens nerve which, in the inferior portion of the CS, runs close to the dura in an inferolateral direction toward the superior orbital fissure.[1,7]

Tumor Dissection

After dural incision, the tumor is mobilized by using curette; suction tips and fragments are removed using aspirator and forceps.

The author has vast experience in dealing with anterior skull base tumor resection with special emphasis on juvenile nasopharyngeal angiofibroma with extensive spread wherein the principle of segmental resection of the tumor is employed after good vascular control. Instances where the tumor is engulfing the ICA (medial displacement, lateral displacement, or 360-degree engulfment), ICA embolization by coiling is carried out if the patient successfully passes the balloon occlusion test.

Transmaxilla-Pterygoid Endoscopic Approach

This procedure is indicated for rare tumors from the CS extending through the foramen rotundum to the pterygomaxillary fossa (mainly neuromas and meningiomas). This approach is the combination of an EPSEA and an endoscopic medial maxillectomy or modified Denker's procedure (**Figs. 9.6–9.9**).[1,7]

The procedure commences with an ipsilateral sphenoethmoidectomy to the involved CS. Then, the inferior turbinate is outfractured and resected using either coblater or cold steel instruments.

Next the vertical portion of the maxillary bone is drilled out and the medial wall of the maxillary sinus is removed. In this way, wide exposition of the lateral and posterior wall of the maxillary sinus is achieved.

The nasolacrimal duct is transected immediately below the lacrimal sac in order to maintain its patency using a sharp instrument.

The next step is characterized by the identification of the vidian canal after the resection of both the vertical process of the palatine bone and the medial pterygoid process. The terminal branches of internal maxillary artery are cauterized.

The posterior bone of the maxillary sinus is removed up to the course of the infraorbital nerve, and the periosteum of the pterygomaxillary fossa is exposed. The exposure is tailor-made to tumor extension into the pterygomaxillary fossa.

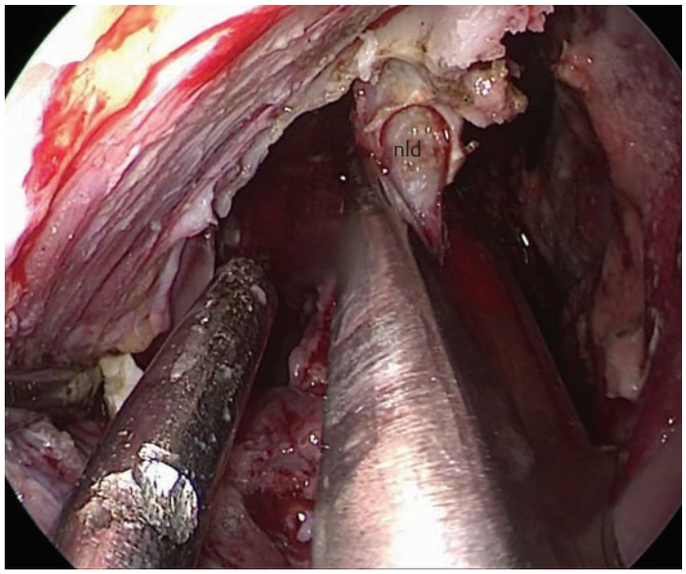

Fig. 9.6 Endoscopic image showing nasolacrimal duct transection. nld, nasolacrimal duct.

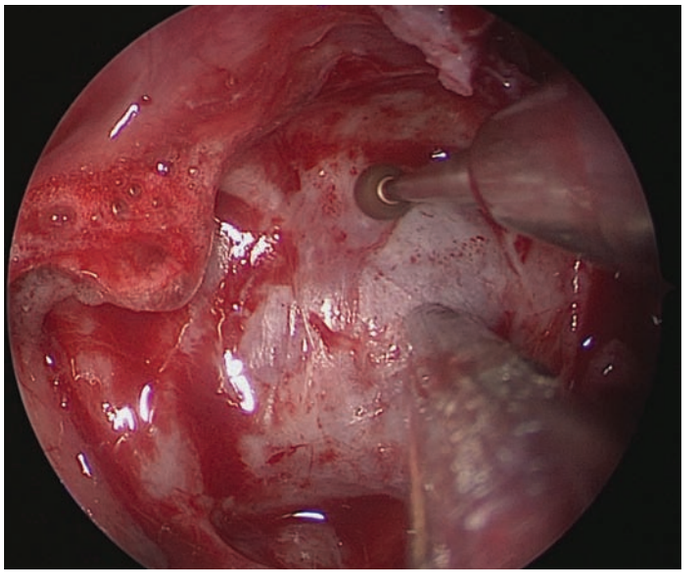

Fig. 9.7 Exposure of posterior wall of maxillary sinus wall.

The landmarks are: medially, the vidian canal with the vidian nerve to localize the paraclival portion of the ICA; laterally and inferiorly, the maxillary artery and the pterygoid muscles; and superiorly, the infraorbital nerve and V2 following which, bypassing through the foramen rotundum, makes it possible to arrive in the inferolateral compartment of the CS.[1,8]

Intracavernous phase is as mentioned earlier.

Case illustrations:

Case 1: Pituitary Macroadenoma

This is a case of pituitary macroadenoma (secretory) involving the medial compartment of the CS.

A 45-year-old lady presented with the history of headache and features suggestive of acromegaly. Endocrinological investigations suggested acromegaly (**Fig. 9.8**). The MRI showed pituitary macroadenoma involving the medial compartment of the CS and tumor medial to the ICA (**Fig. 9.9**). The wide exposure to the sella was attained after the completion of the nasal and the sphenoid phase (**Fig. 9.10**). The sellar phase is described for exposure of the tumor (**Figs. 9.11–9.15**). The soft suckable tumor in the sellar cavity was removed using extracapsular dissection technique (**Figs. 9.16 and 9.17**). The penetration of the tumor through the medial wall CS dura was clearly (**Fig. 9.18**). The tumor from the medial compartment of the CS was completely removed (**Fig. 9.19**). The sellar cavity was closed using multilayered reconstruction with fat, Surgicel, and nasoseptal flap (**Fig. 9.20**). See **Video 9.1**.

Video 9.1 Pituitary macroadenoma with acromegaly. https://www.thieme.de/de/q.htm?p=opn/cs/19/9/10104312-b117b669

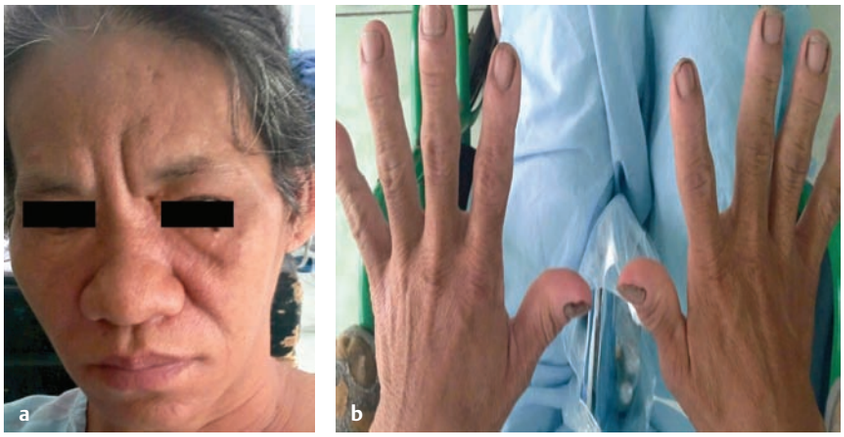

Fig. 9.8 **(a)** A clinical photograph of the patient showing features of acromegaly. **(b)** A clinical photograph of the hand of the patient depicting enlarged size, thickened, and roughened skin.

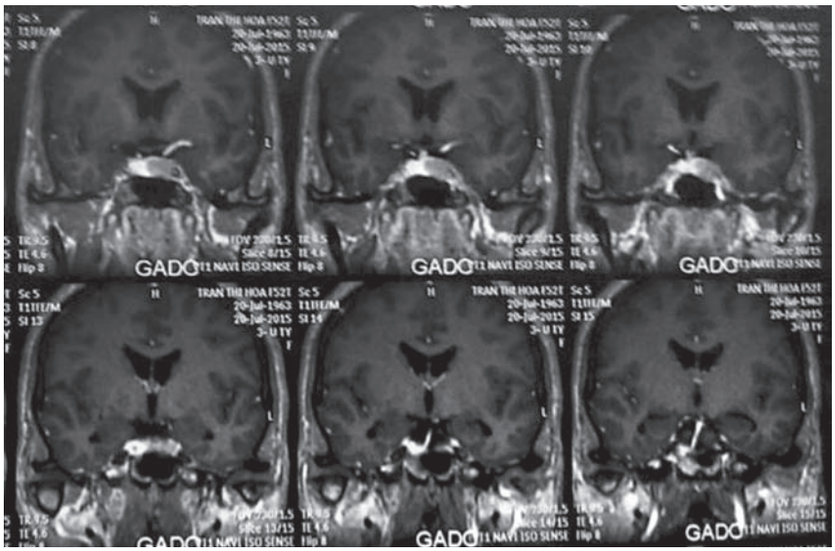

Fig. 9.9a MRI post contrast T1 image suggesting pituitary macroadenoma involving the medial compartment of the cavernous sinus.

Fig. 9.9b MRI post contrast T1 image suggesting pituitary macroadenoma involving the medial compartment of the cavernous sinus.

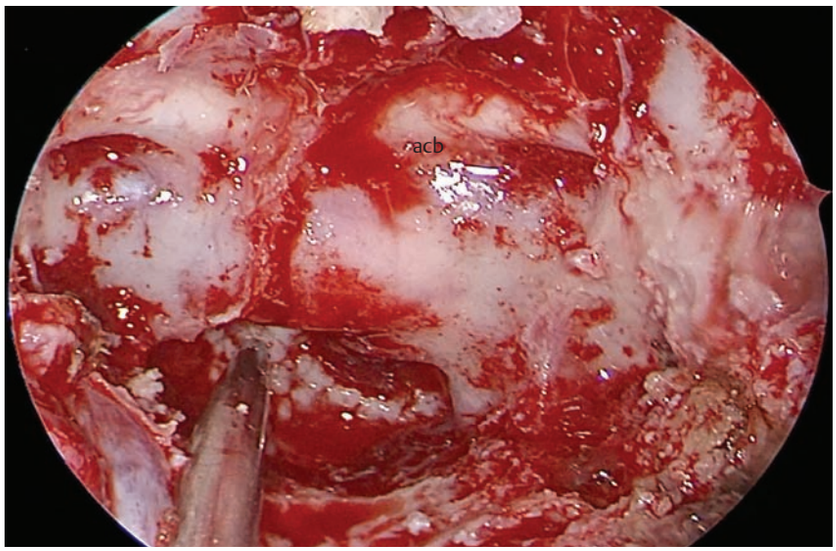

Fig. 9.10 Wide bony exposure after the nasal and sphenoid phase. acb, anterior cranial base.

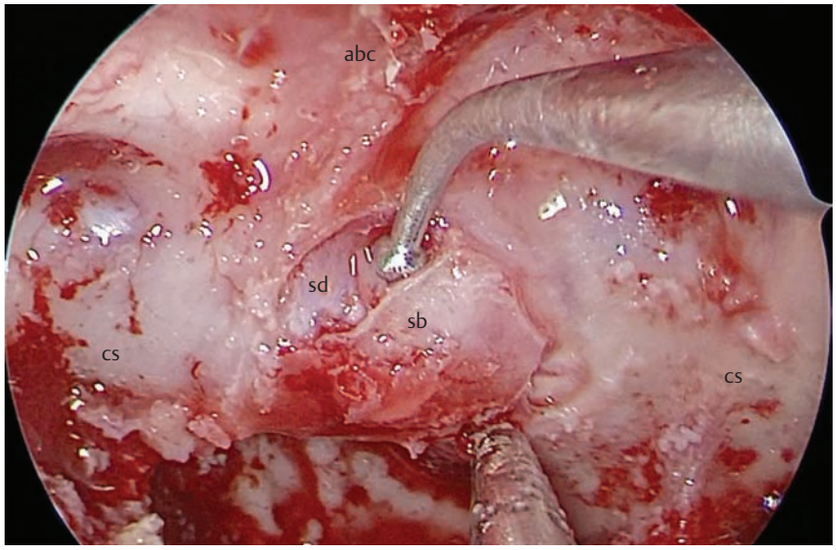

Fig. 9.11 Elevating the thinned-out sellar bone. acb, anterior cranial base; cs, cavernous sinus; sb, sellar bone; sd, sellar dura.

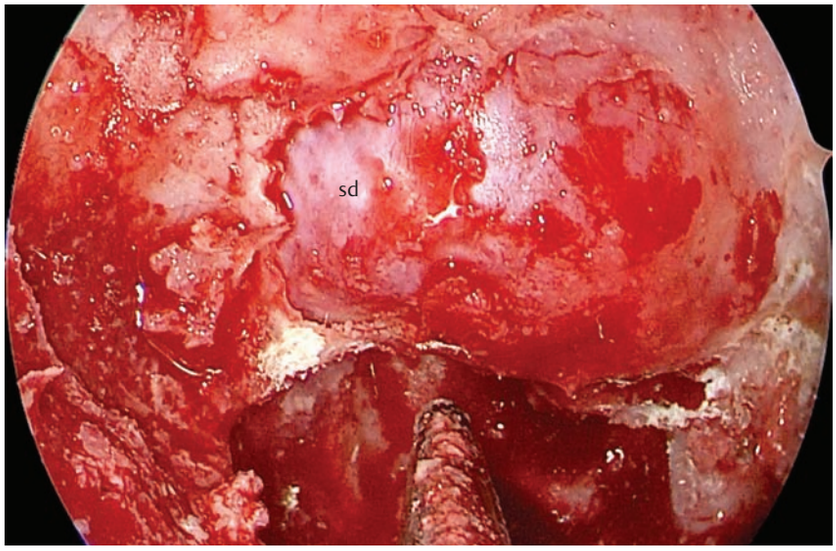

Fig. 9.12 Complete exposure of the sellar dura. sd, sellar dura.

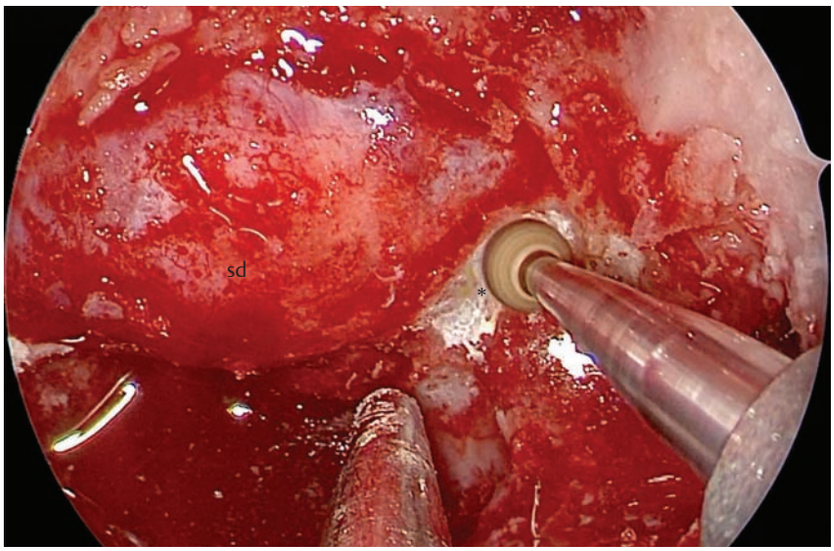

Fig. 9.13 Drilling along the lateral wall of the sphenoid sinus for the cavernous sinus exposure. sd, sellar dura; *, drilling using s3 neurodrill.

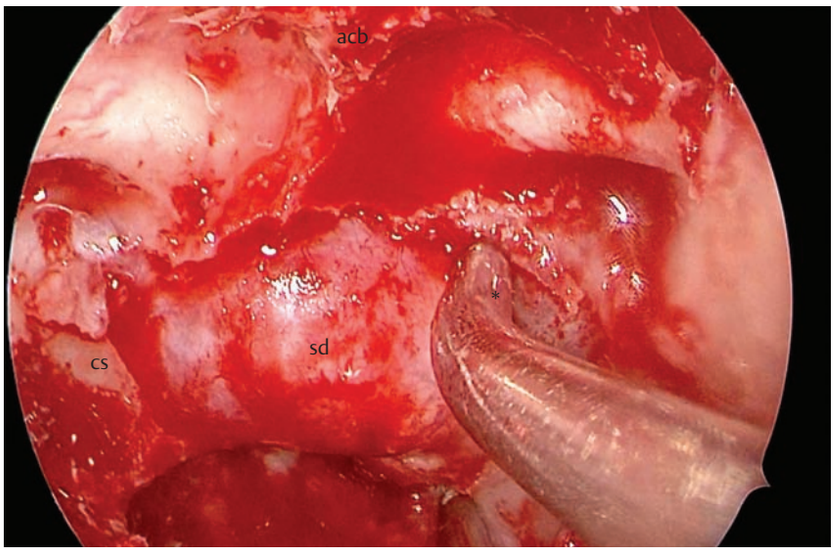

Fig. 9.14 Endoscopic picture showing micro-Doppler used to map the course of the carotid artery. acb, anterior cranial base; cs, cavernous sinus; sd, sellar dura; *, micro-Doppler.

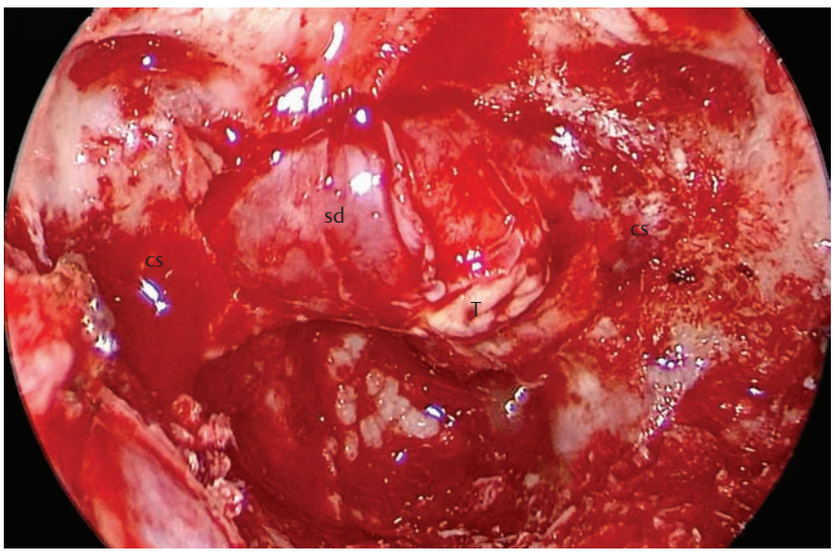

Fig. 9.15 **U**-shaped dural flap is elevated. cs, cavernous sinus; sd, sellar dura; T, tumor.

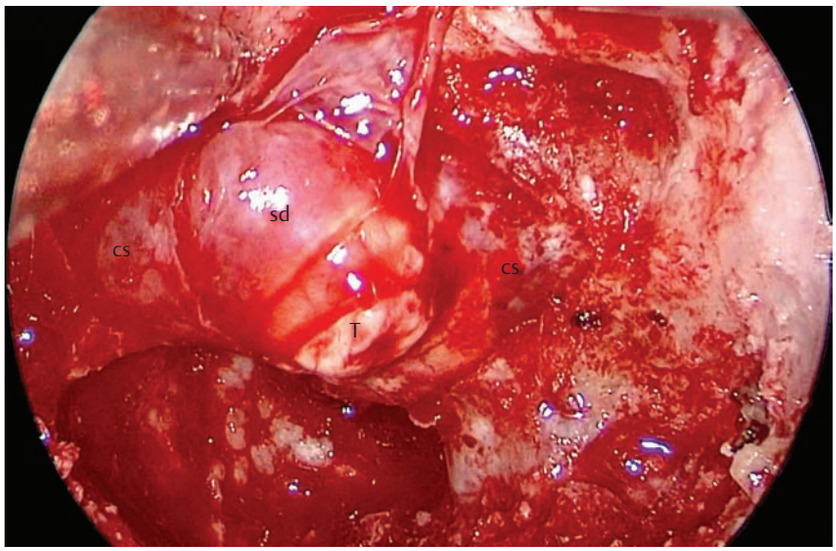

Fig. 9.16 Endoscopic view showing the exposed tumor. cs, cavernous sinus; sd, sellar dura; T, tumor.

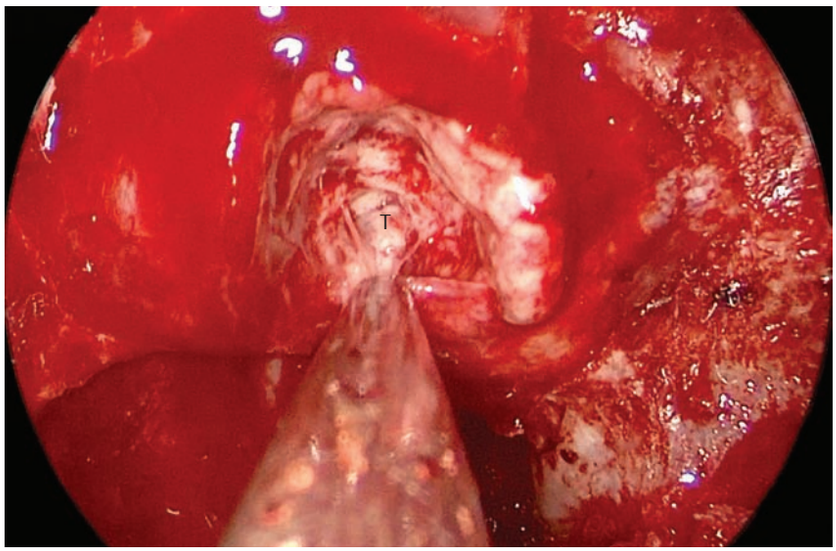

Fig. 9.17 Removal of the liquid tumor using suction from the sellar region. T, tumor.

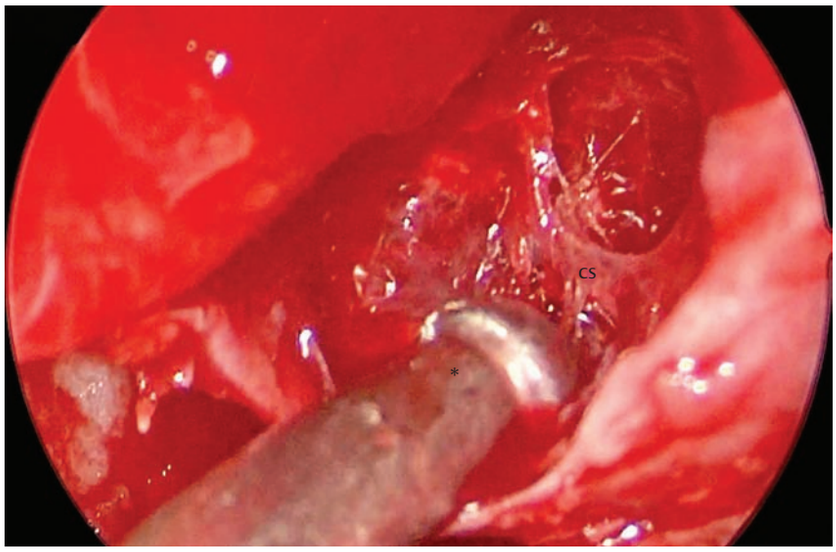

Fig. 9.18 Exposure of the medial wall of the cavernous sinus. CS, cavernous sinus; *, suction.

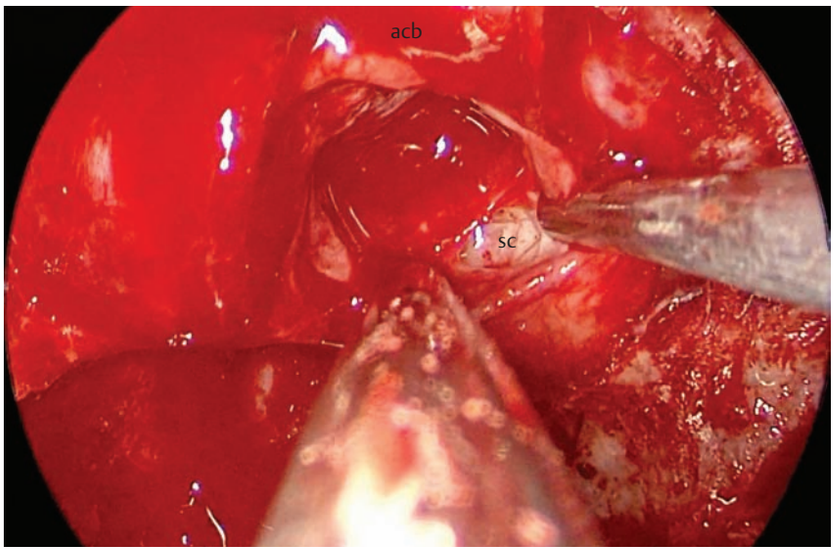

Fig. 9.19a Tumor clearance from the medial compartment of the cavernous sinus. acb, anterior cranial base; CS, cavernous sinus; SC, sellar cavity.

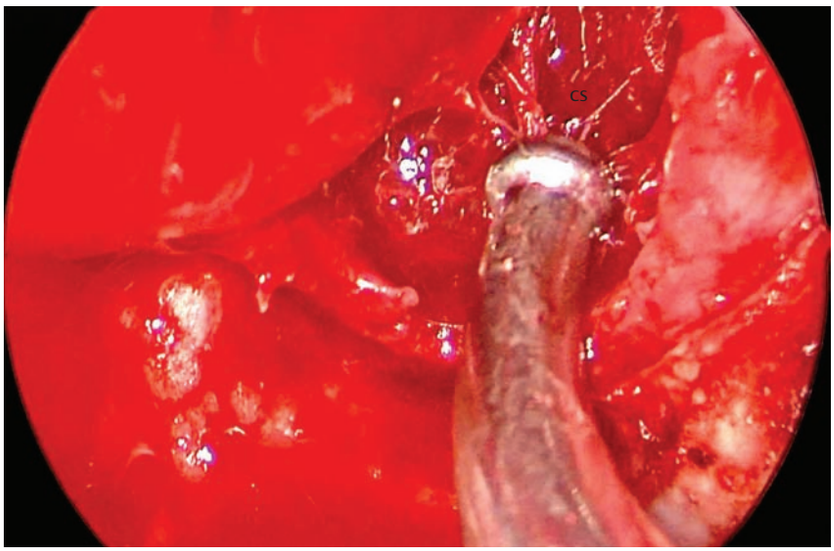

Fig. 9.19b Tumor clearance from the medial compartment of the cavernous sinus. CS, cavernous sinus; SC, sellar cavity.

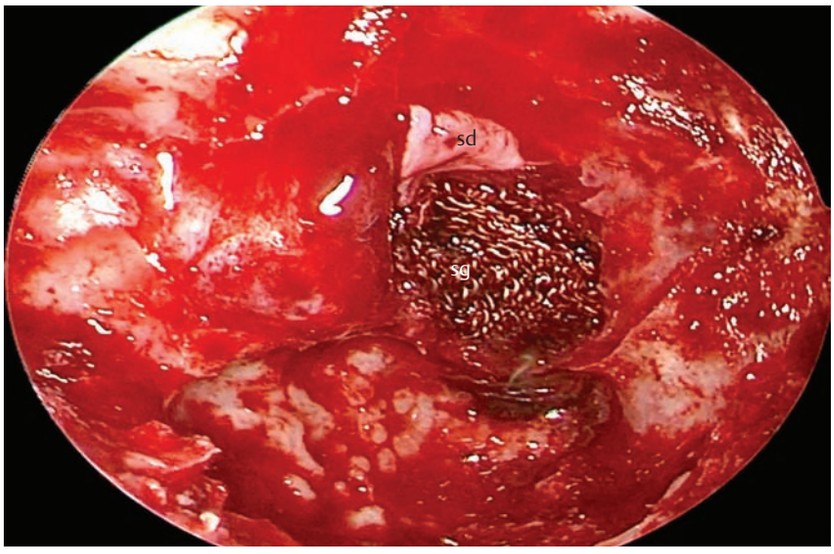

Fig. 9.20a Closure of the defect using the Surgicel and vascularized nasoseptal flap. acb, anterior cranial base; sd, sellar dura; sgl, Surgicel.

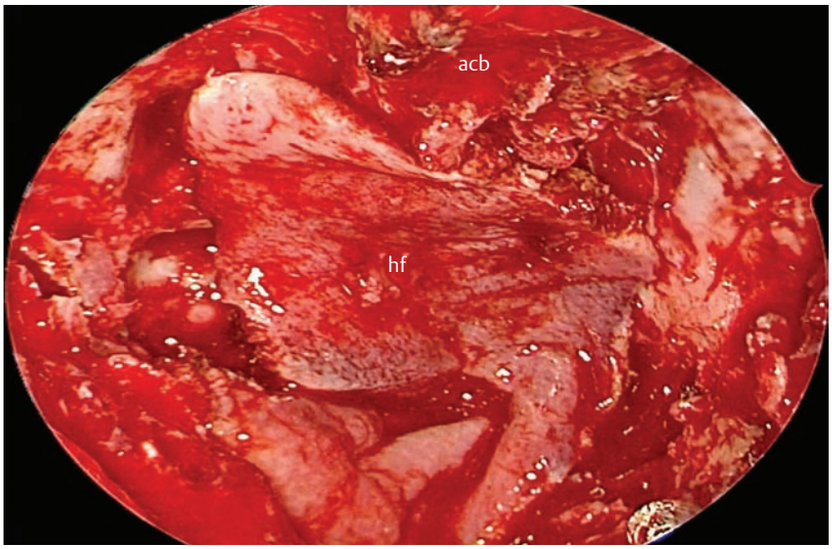

Fig. 9.20b Closure of the defect using the Surgicel and vascularized nasoseptal flap. acb, anterior cranial base; hf, Hadad flap.

Case 2: Inferomedial Compartment Involvement of the Cavernous Sinus

A 36-year-old female presented with headache and progressive decline of vision. Imaging showed pituitary macroadenoma and endocrinology reports suggested a secretory tumor. Complete bone exposure was achieved thus obtaining classically described as owl's eye appearance (**Fig. 9.21**). Bone over CS was thinned out using S3 neurodrill (**Fig. 9.22**). Dural flap was elevated using Rosen's elevator (**Fig. 9.23**). After exposure of the tumor, biopsy was taken using Blakesley forceps (**Fig. 9.24**). The medial wall of the CS was exposed (**Fig. 9.25**). Dural incision was extended over the CS (**Fig. 9.26**). The medial compartment of the CS (**Fig. 9.27**) and the right ICA were exposed (**Fig. 9.28**). Tumor in the inferomedial compartment was completely cleared by transposing the ICA laterally. Complete clearance of the parasellar tumor was achieved (**Fig. 9.29**). See **Video 9.2**.

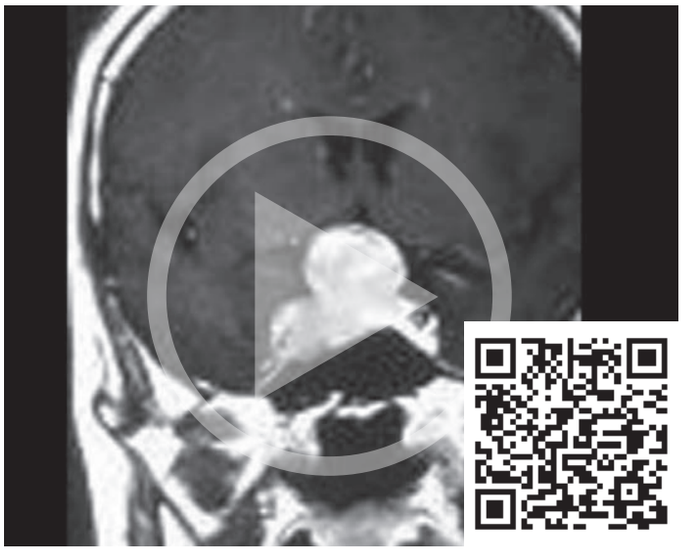

Video 9.2 Pituitary macroadenoma with inferomedial compartment involvement of the cavernous sinus. https://www.thieme.de/de/q.htm?p=opn/cs/19/9/10104313-aee2c9c4

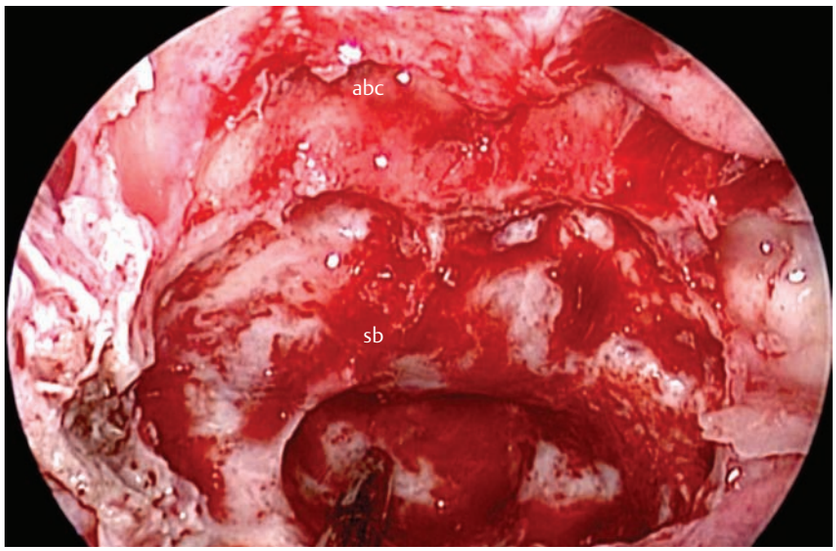

Fig. 9.21 Endoscopic picture showing complete bone exposure classically described as owl's eye appearance. acb, anterior cranial base; sb, sellar bone.

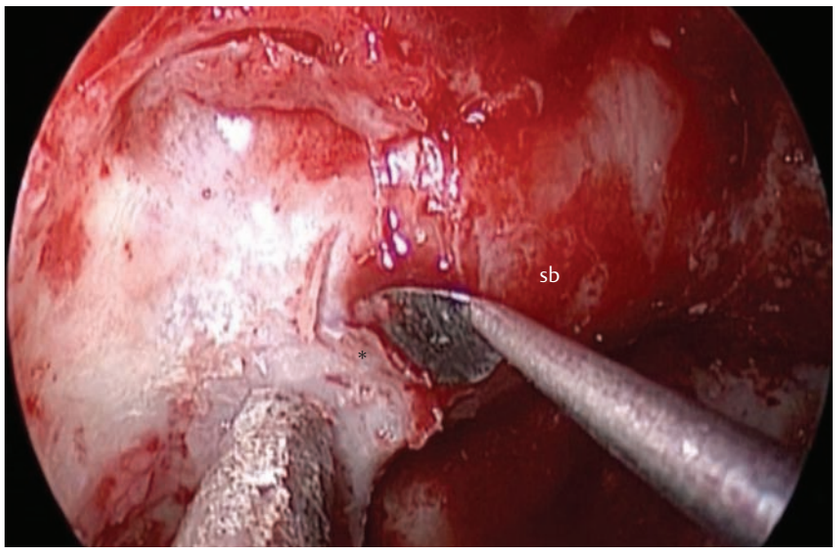

Fig. 9.22 Bone over cavernous sinus is thinned out using S3 neurodrill. sb, sellar bone; *, bone elevation.

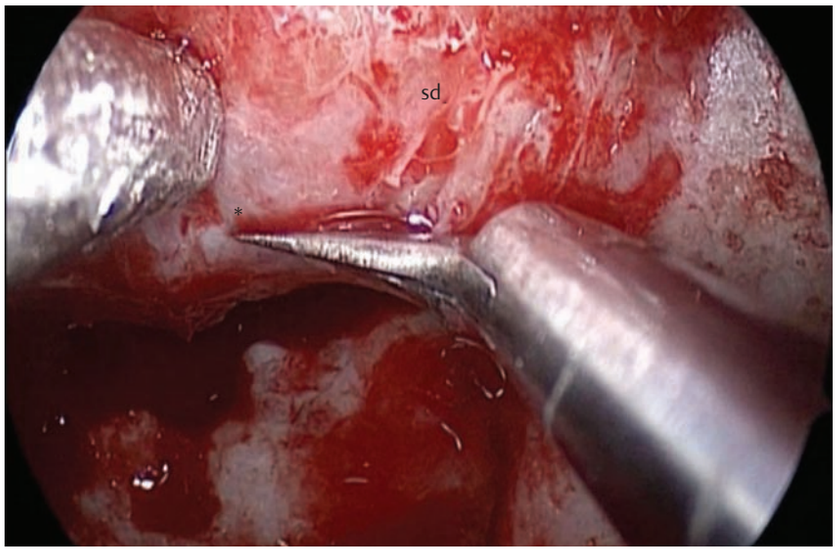

Fig. 9.23 Dural flap elevated using Rosen's elevator. sd, sellar dura.

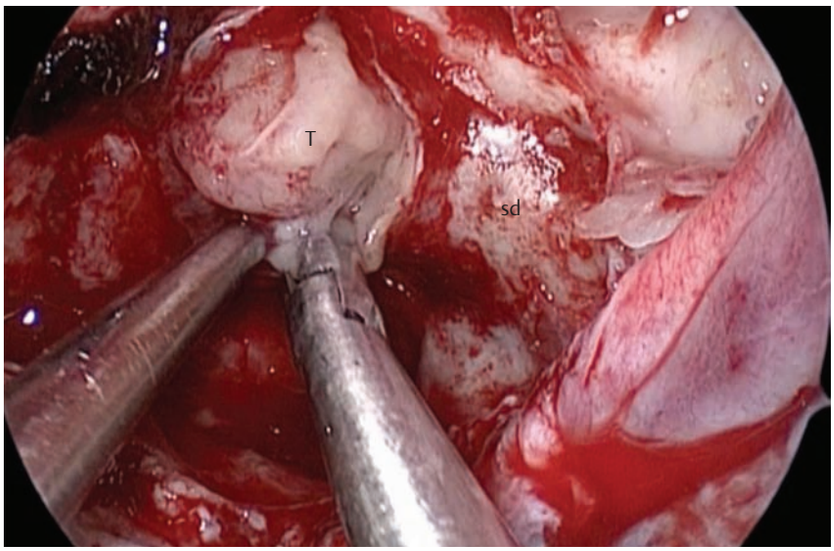

Fig. 9.24 Tumor exposed, biopsy taken using Blakesley forceps. sd, sellar dura; T, tumor.

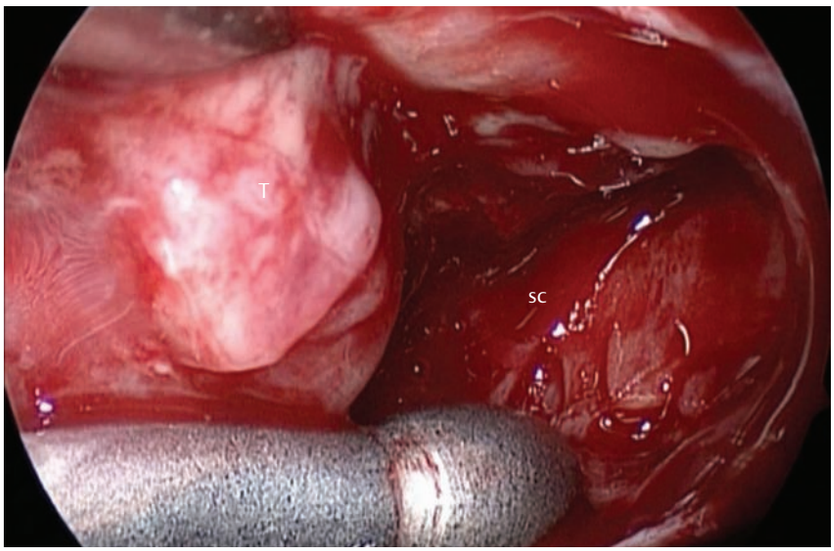

Fig. 9.25 Medial wall of the cavernous sinus exposed. sc, sellar cavity.

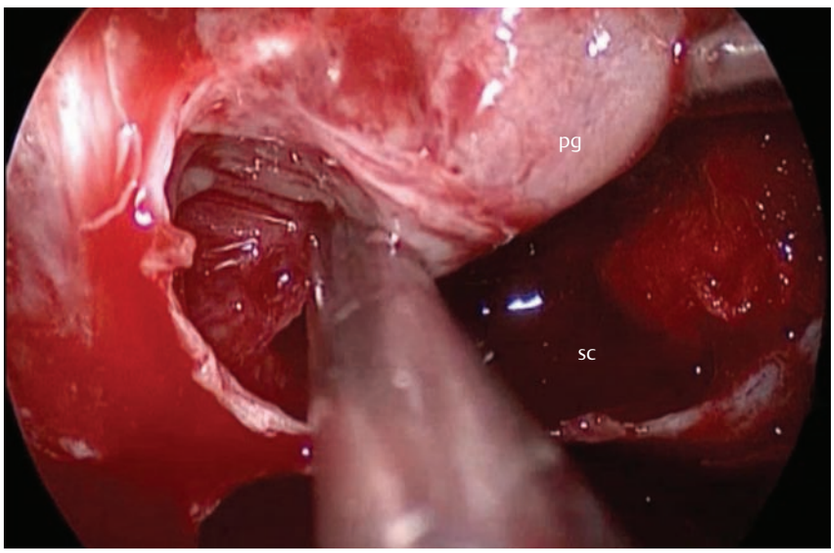

Fig. 9.26 Dural incision extended over the cavernous sinus. cs, cavernous sinus; pg, pituitary gland; sc, sellar cavity.

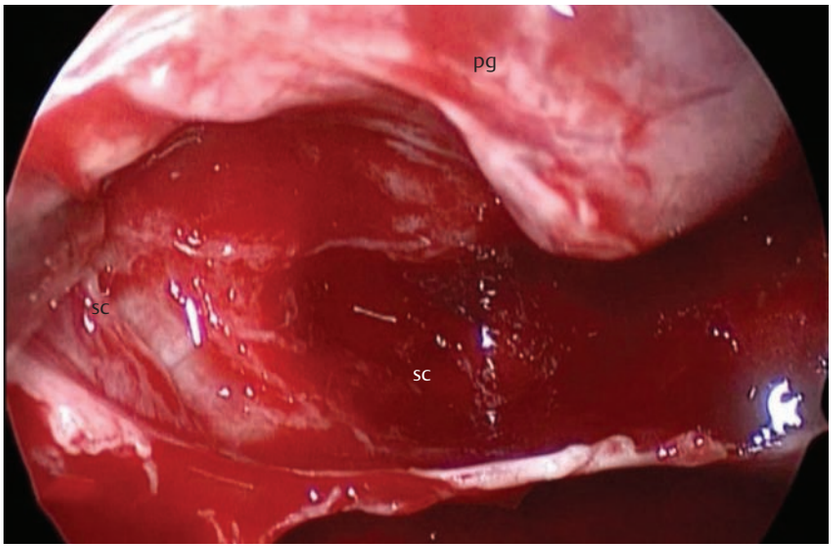

Fig. 9.27 Exposure of the medial compartment of the cavernous sinus. cs, cavernous sinus; pg, pituitary gland; sc, sellar cavity.

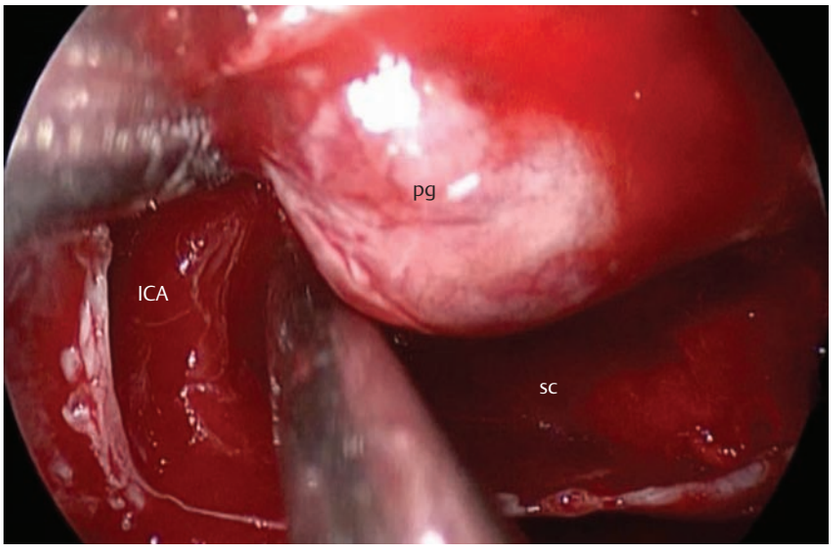

Fig. 9.28 Right internal carotid artery exposed. ICA, internal carotid artery; pg, pituitary gland; sc, sellar cavity.

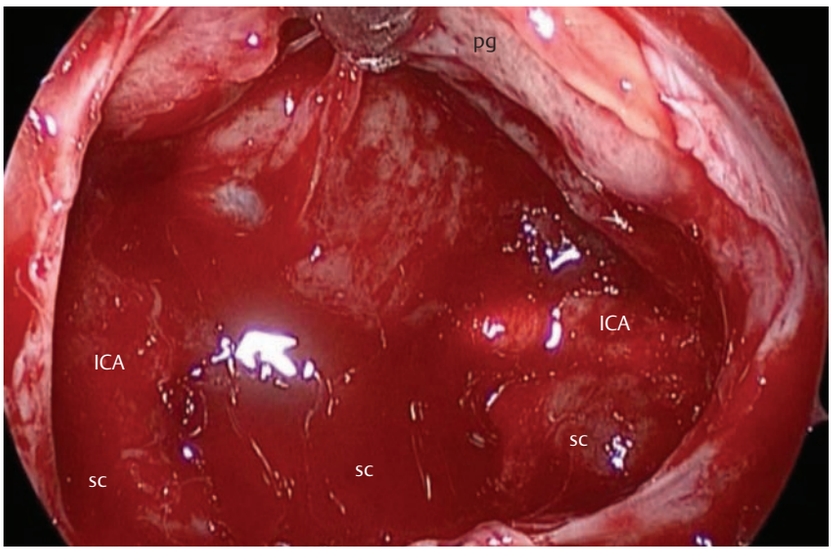

Fig. 9.29 Complete clearance of the parasellar tumor done. ICA, internal carotid artery; cs, cavernous sinus; pg, pituitary gland.

Case 3: Superomedial Compartment of the Cavernous Sinus

A 38-year-old lady presented with headache, and 3rd nerve paresis. Endocrinological examination revealed secretory growth hormone tumor (acromegaly). Imaging showed pituitary macroadenoma involving the CS region on both sides (**Fig. 9.30**). During the sellar phase of the surgery, wide exposure was obtained (**Fig. 9.31**). The bone over the sella was thinned out using the diamond burr and removed using a Rosen's elevator (**Fig. 9.32**). The precise course of the ICA was mapped with the micro-Doppler (**Fig. 9.33**). Sellar dura was incised and a superiorly based dural flap was elevated (**Fig. 9.34**). The extracapsular dissection of the tumor is carried out (**Fig. 9.35**). Tumor dissection was started from the 6 o'clock position (**Fig. 9.36**). Since the tumor was soft, two suction tips were used to dissect the tumor. The medial wall of the CS was exposed on the left side (**Fig. 9.37**). A dural incision was placed anterior to ICA on the right side since the tumor is in the superomedial compartment of CS (**Fig. 9.38**). Left CS dissection in the Perneczky's triangle was performed (**Fig. 9.39**). The oculomotor triangle is delineated (**Fig. 9.40**). The panoramic view of both the CS is seen (**Fig. 9.41**). See **Video 9.3**.

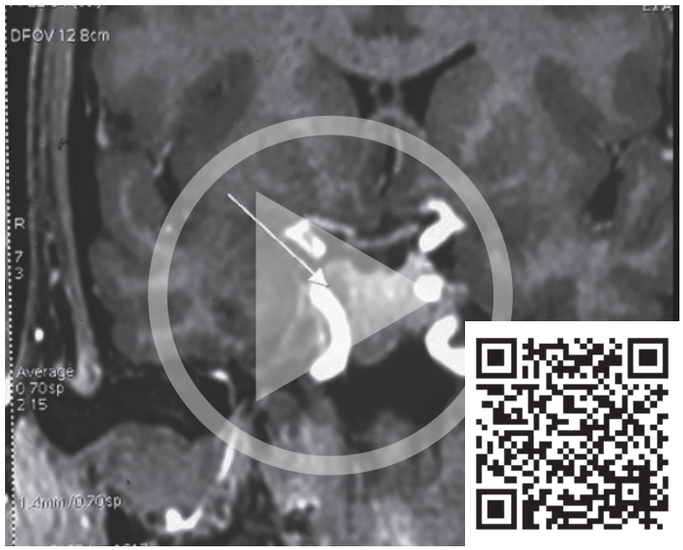

Video 9.3 Pituitary macroadenoma with superomedial compartment involvement of the cavernous sinus. https://www.thieme.de/de/q.htm?p=opn/cs/19/9/10104314-f2530668

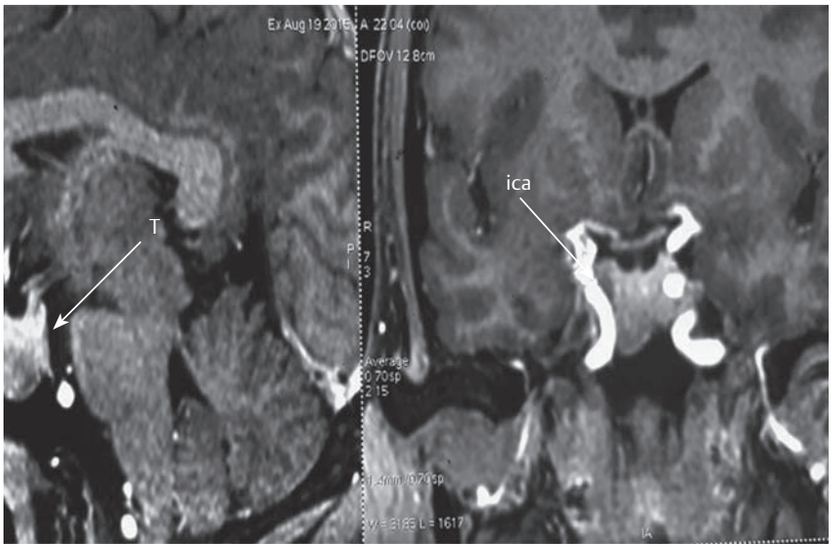

Fig. 9.30 MRI post contrast T1 image showed pituitary macroadenoma involving the parasellar area. ICA, internal carotid artery; T, tumor.

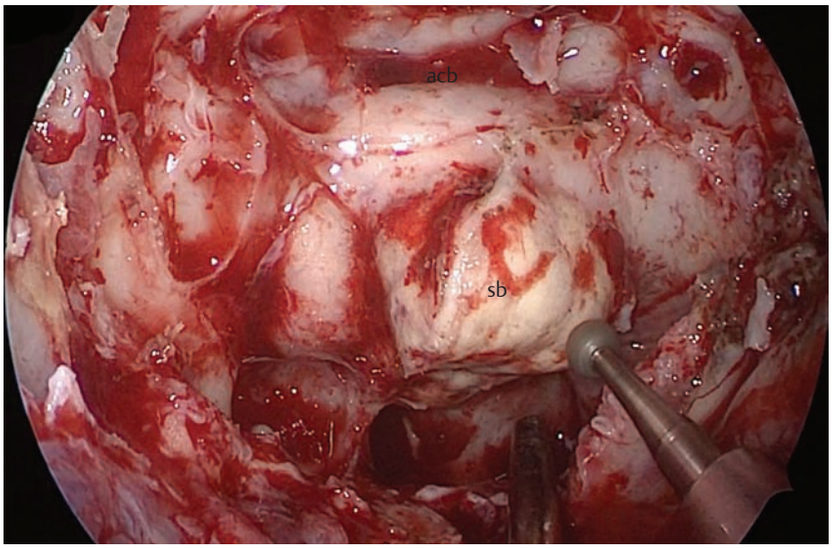

Fig. 9.31 Wide bony exposure from one carotid to another (owl's eye appearance). acb, anterior cranial base; sb, sellar bone.

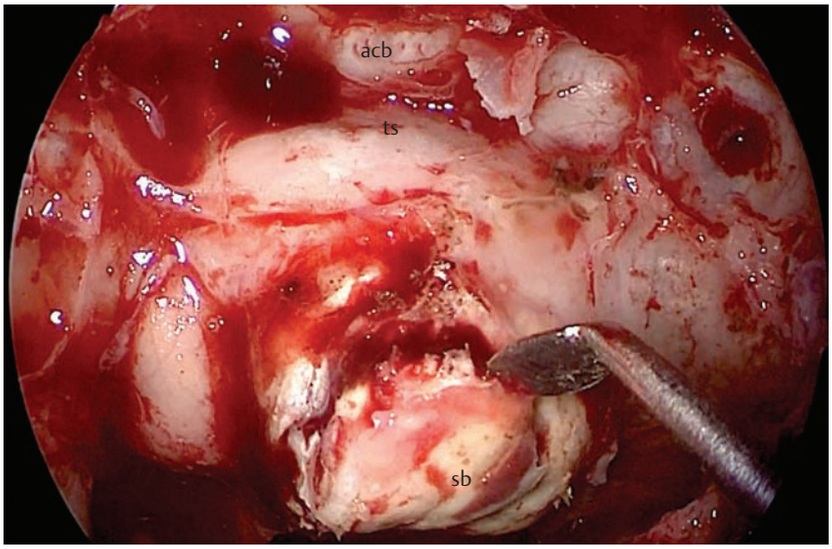

Fig. 9.32 Sellar exposure and bone elevated over the sella. acb, anterior cranial base; sb, sellar bone; ts, tuberculum sellae.

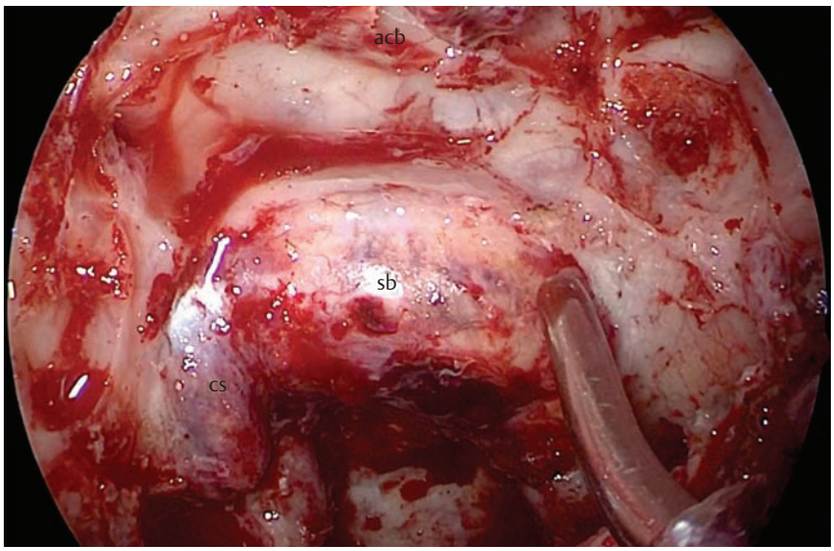

Fig. 9.33 Micro-Doppler in use to map the position of the carotids. acb, anterior cranial base; cs, cavernous sinus; sd, sellar dura; *, micro-Doppler.

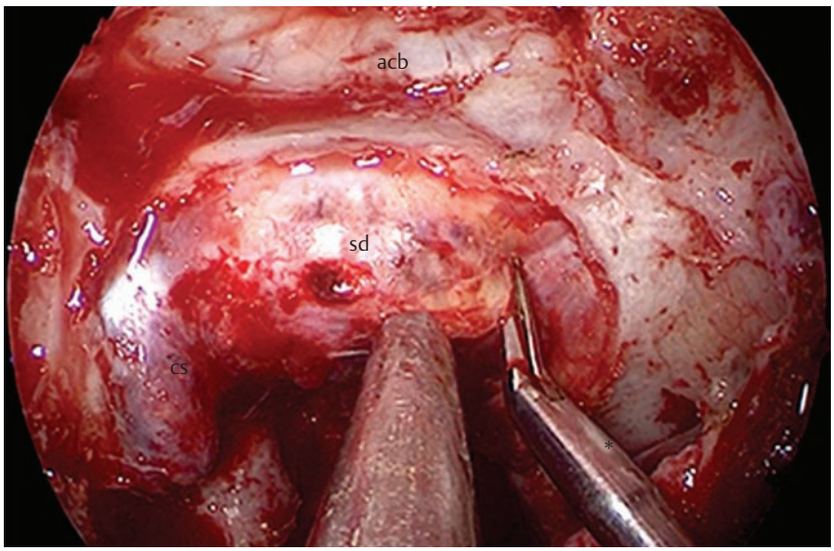

Fig. 9.34 Dural incision placed using the Cappabianca knife and extracapsular dissection is done. acb, anterior cranial base; cs, cavernous sinus; sd, sellar dura; *, micro-Doppler.

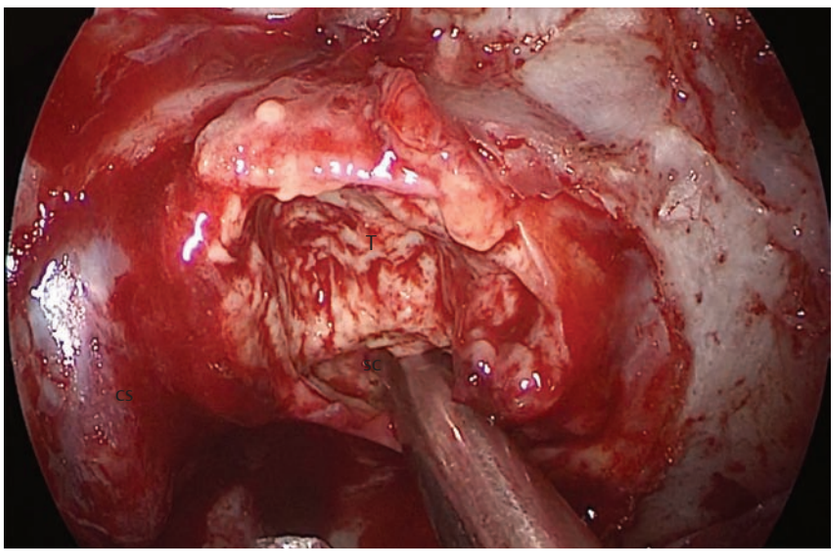

Fig. 9.35 The sellar cavity is exposed and tumor dissection is commenced. cs, cavernous sinus; sc, sellar cavity; T, tumor.

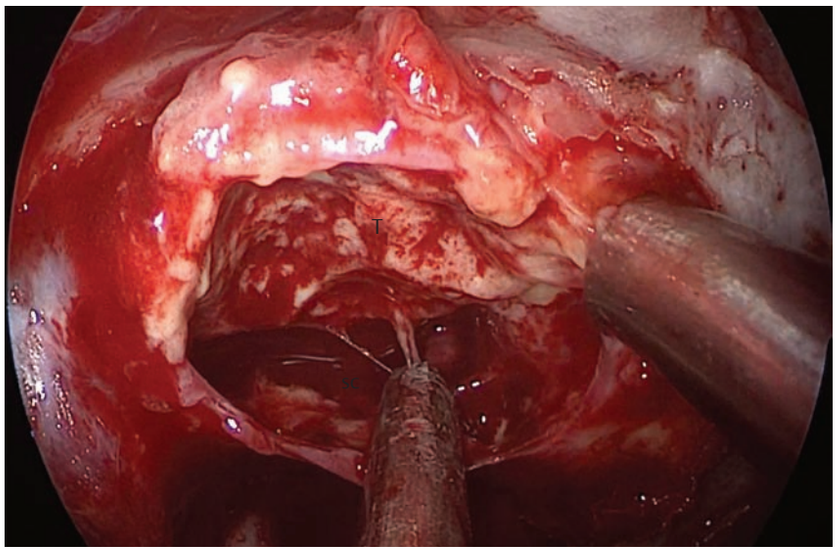

Fig. 9.36 Tumor dissection is commenced from 6 o'clock position. sc, sellar cavity; T, tumor dissection.

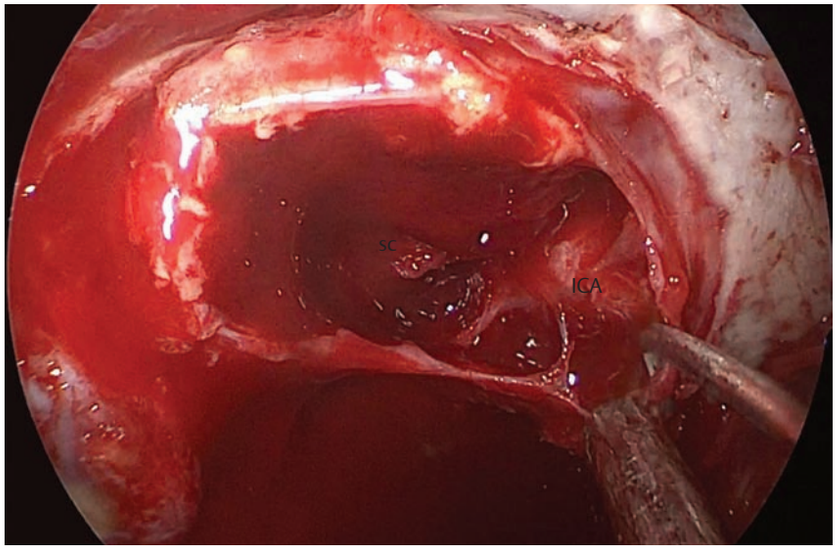

Fig. 9.37 Dissection extending to left cavernous sinus for tumor clearance. ICA, internal carotid artery; sc, sellar cavity.

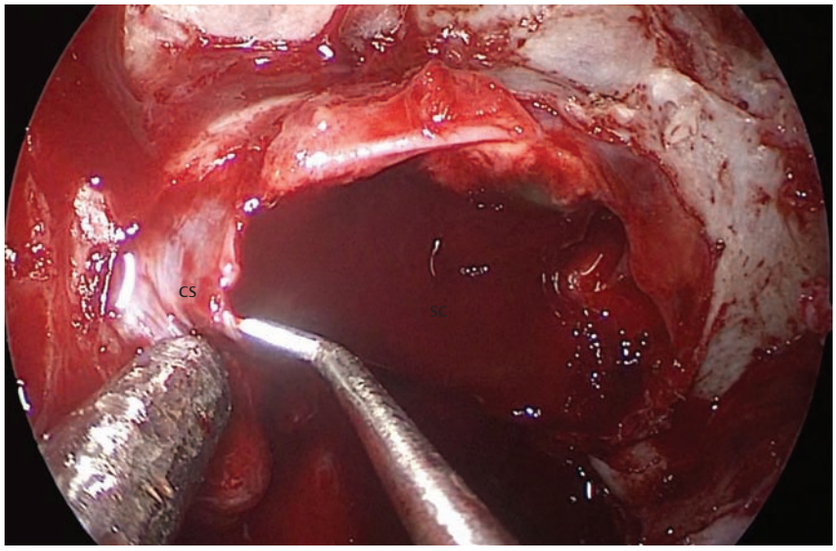

Fig. 9.38 On the right side, dural incision placed anterior to the internal carotid artery and tumor cleared from the right cavernous sinus. CS, cavernous sinus; SC, sellar cavity.

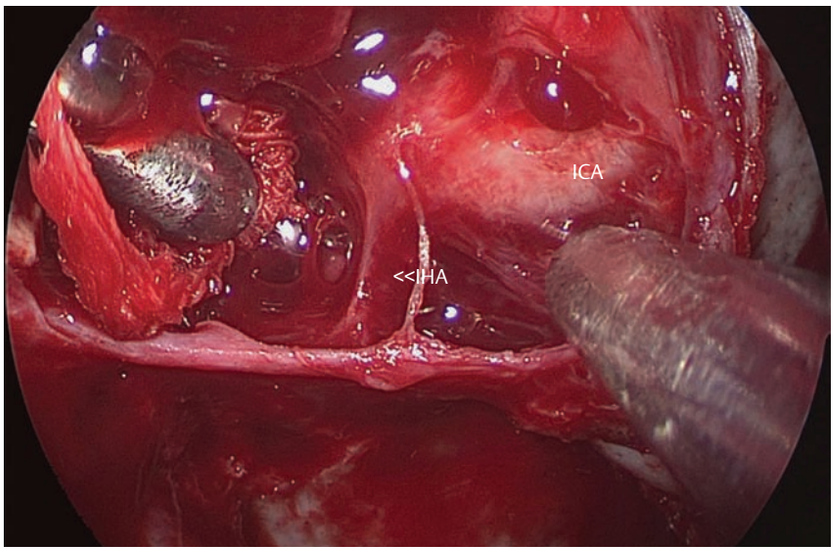

Fig. 9.39 Left cavernous sinus after dissection. ICA, internal carotid artery; IHA, inferior hypophyseal artery.

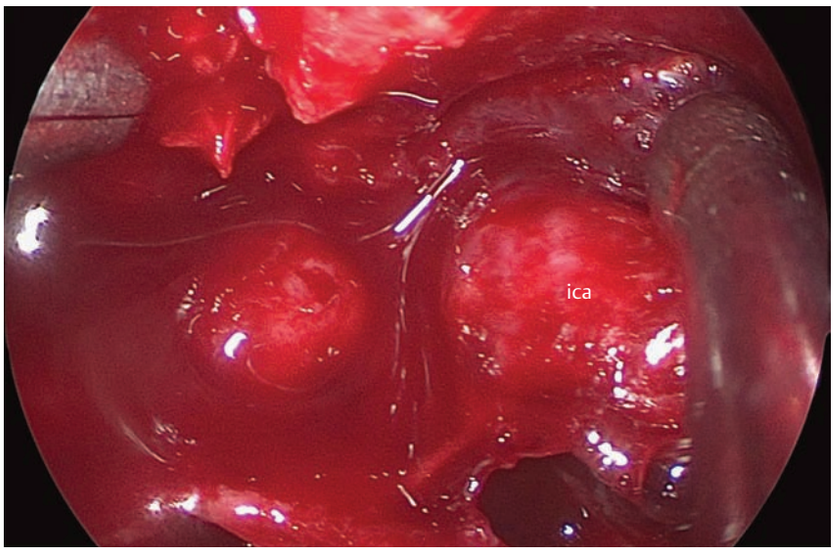

Fig. 9.40 Left oculomotor triangle exposed after complete tumor clearance. ICA, internal carotid artery.

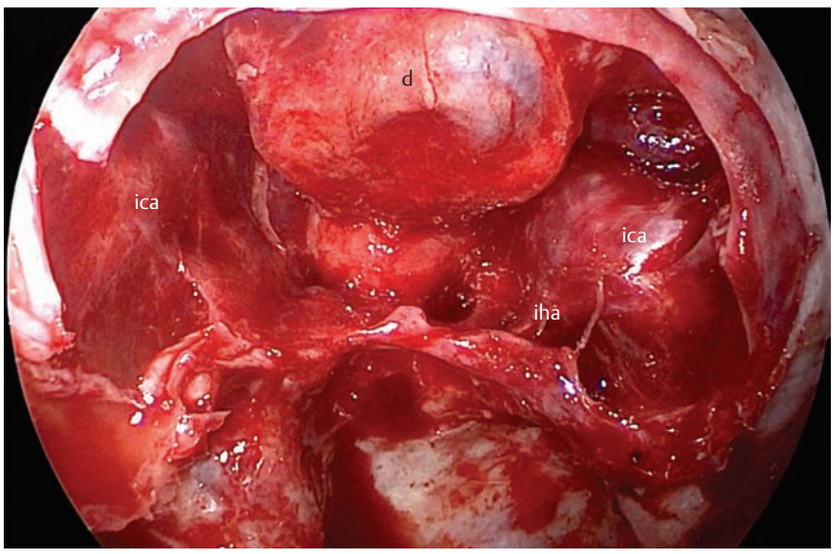

Fig. 9.41 Panoramic view after complete tumor clearance. D, diaphragma; ICA, internal carotid artery; IHA, inferior hypophyseal artery.

Case 4: Pituitary Macroadenoma: Fibrous Type

This is a case of fibrous type of pituitary macroadenoma. Fibrous consistency of the tumor is encountered in around 10% of all the adenomas due to an increased amount of collagen in them. They are technically more challenging compared to the soft adenomas. The clinical photograph shows the patient who was suffering from a secretory (growth hormone) type of adenoma with right sixth nerve palsy (**Fig. 9.42**). Imaging characteristics showed high uniform signal intensity on T1 contrast MRI scan images (**Fig. 9.43**). Transsphenoidal and transpterygoid approaches were employed to achieve the exposure of the sella and the CS (**Figs. 9.44–9.47**). Intraoperative navigation system and micro-Doppler were used to map the ICA (**Figs. 9.48 and 9.49**). Complete dural exposure was achieved (**Fig. 9.50**). Dural incision was placed over the CS and extended medially to join the sellar incision (**Figs. 9.51 and 9.52**). U-shaped superiorly placed dural flap was elevated (**Fig. 9.53**). Tumor was cleared from the sellar cavity and and the right CS was exposed (**Fig. 9.54**). Right CS dissection was carried out with complete tumor clearance by extracapsular dissection of the fibrous lesion (**Figs. 9.55 and 9.56**). No CSF leak was encountered. The defect is closed with the nasoseptal flap (**Fig. 9.57**). See **Video 9.4**.

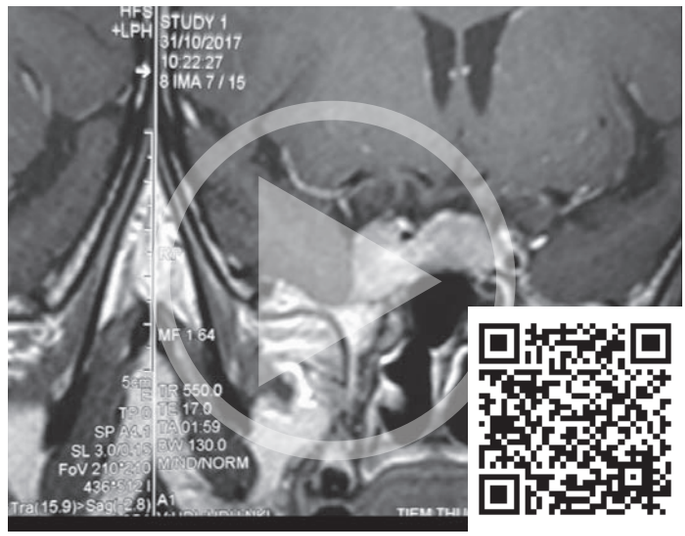

Video 9.4 Revision pituitary macroadenoma: Fibrous type with parasellar extension. https://www.thieme.de/de/q.htm?p=opn/cs/19/9/10104315-e68b37eb

Fig. 9.42 Patient photograph showing features of acromegaly.

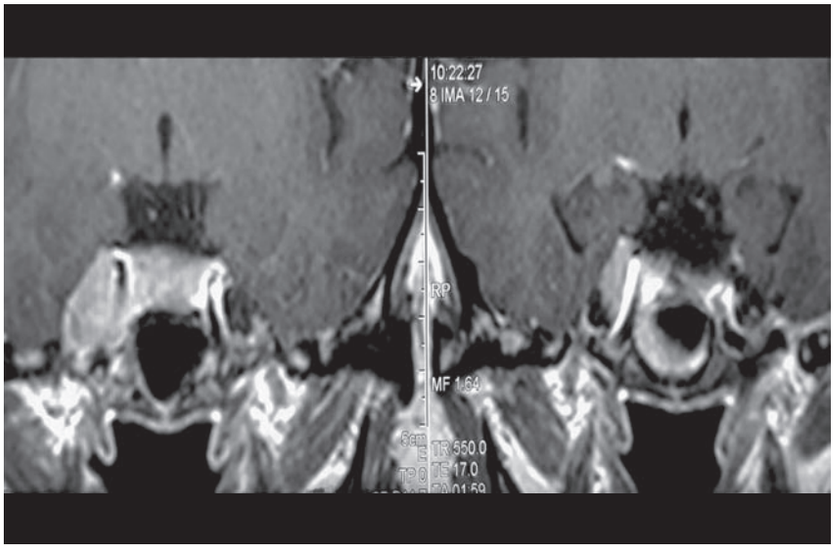

Fig. 9.43a MRI T1 post contrast image showing pituitary macroadenoma with right parasellar extension.

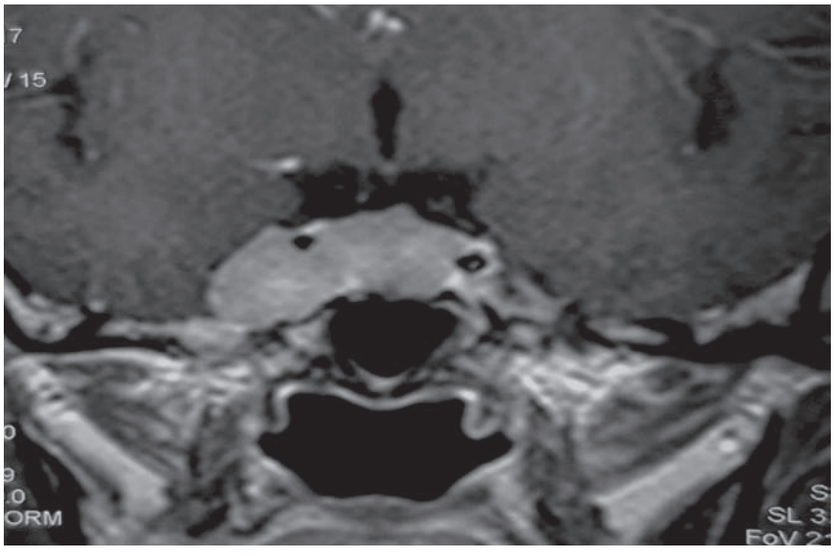

Fig. 9.43b MRI T1 post contrast image showing pituitary macroadenoma with right parasellar extension.

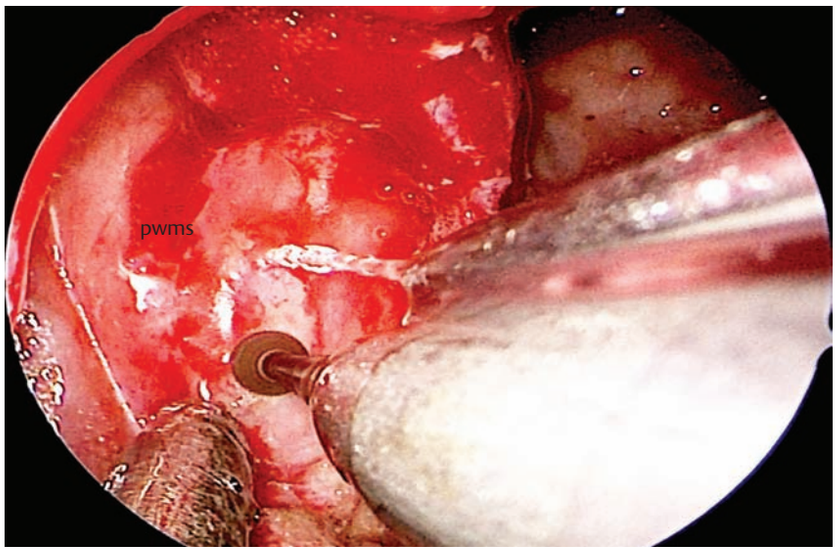

Fig. 9.44 Transpterygoid approach showing the posterior wall of the maxillary sinus (pwms).

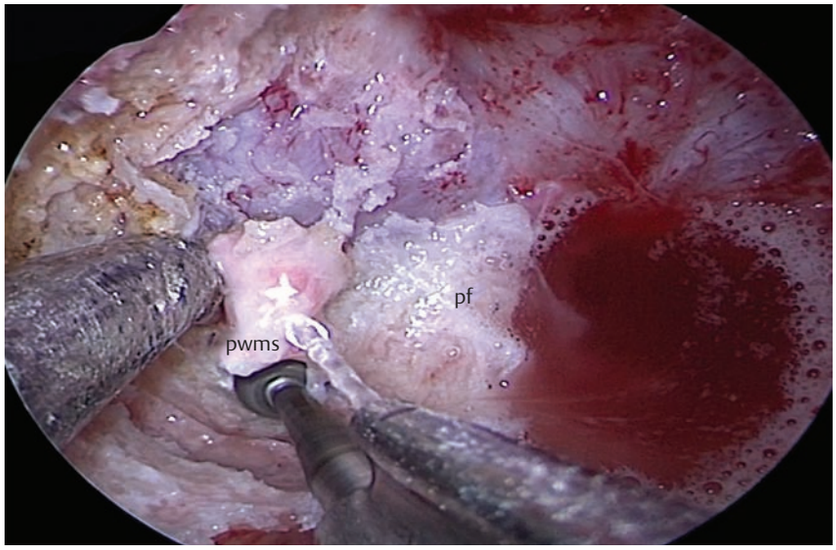

Fig. 9.45 Drilling of the pterygopalatine fossa. pf, pterygoid fossa; pwms, the posterior wall of the maxillary sinus.

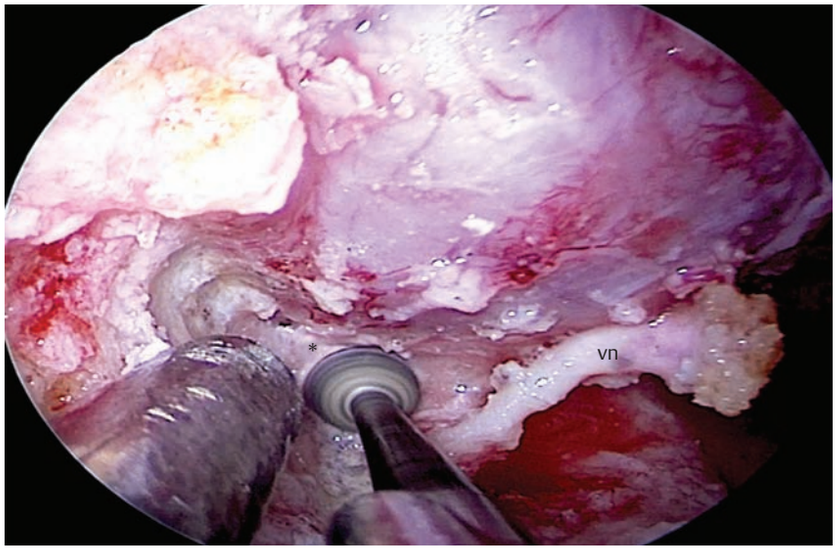

Fig. 9.46 Transected vidian nerve. vn, vidian nerve; *, S3 neuro drill.

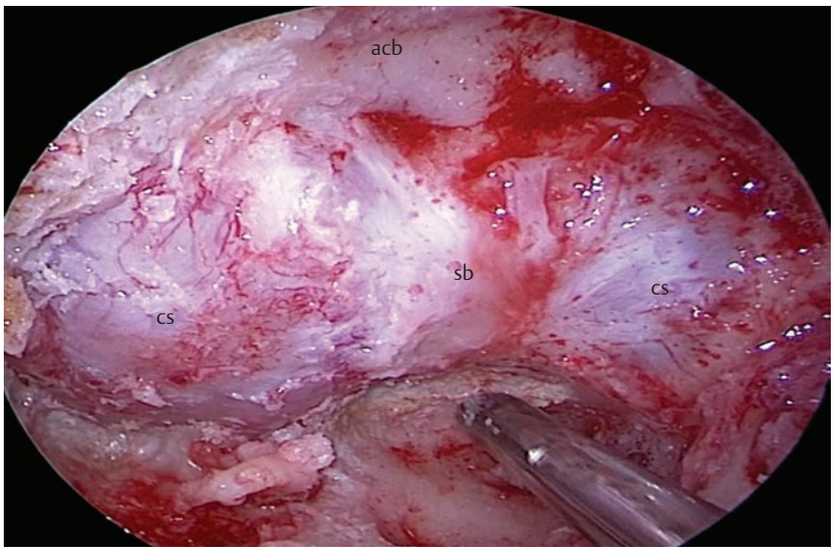

Fig. 9.47 Complete bony exposure. acb, anterior cranial base; cs, cavernous sinus; sb, sellar bone.

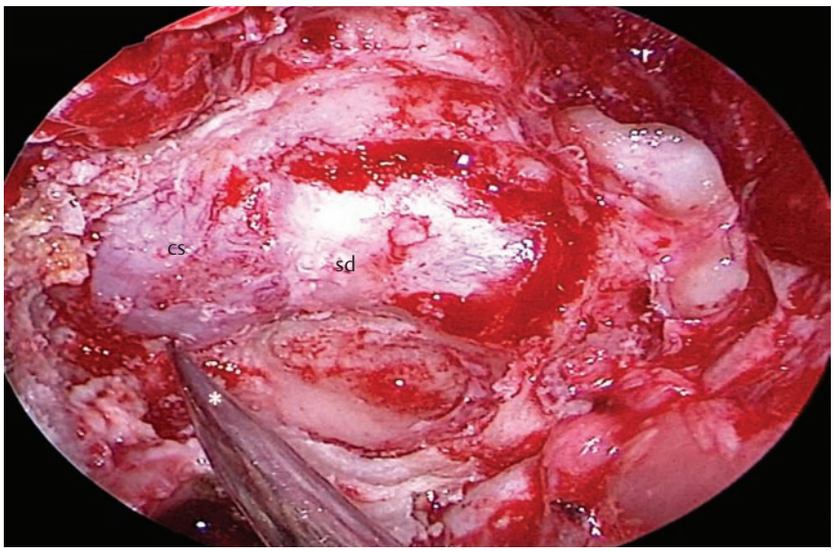

Fig. 9.48 Use of navigation to map the structures. sb, sellar bone.

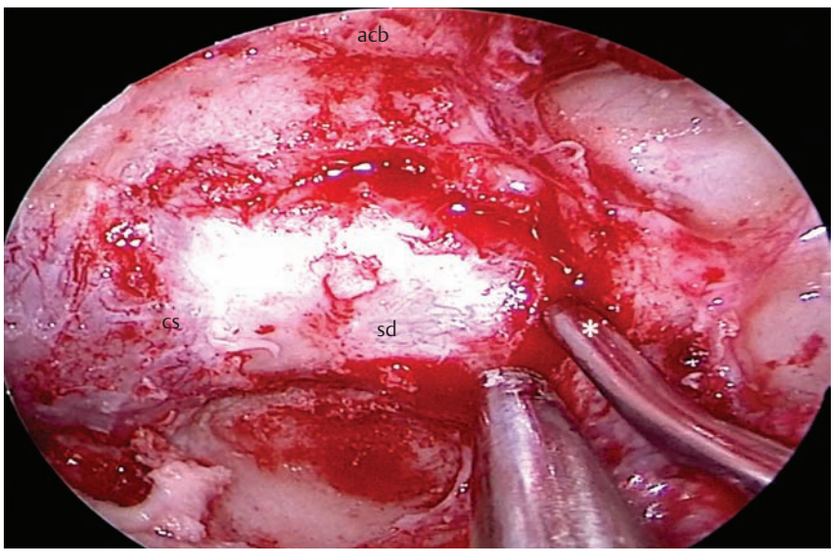

Fig. 9.49a Use of micro-Doppler to map bilateral carotids. sd, sellar dura; abc, anterior cranial base.

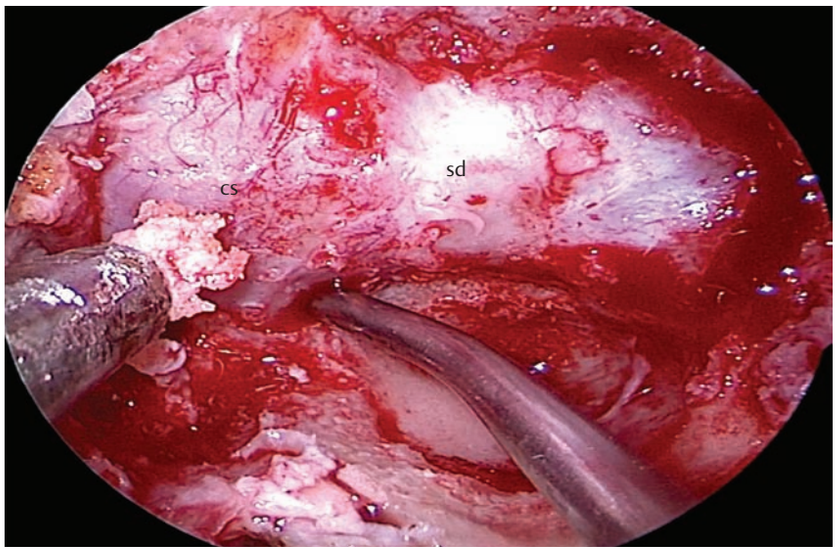

Fig. 9.49b Use of micro-Doppler to map bilateral carotids. sd, sellar dura; cs, cavernous sinus.

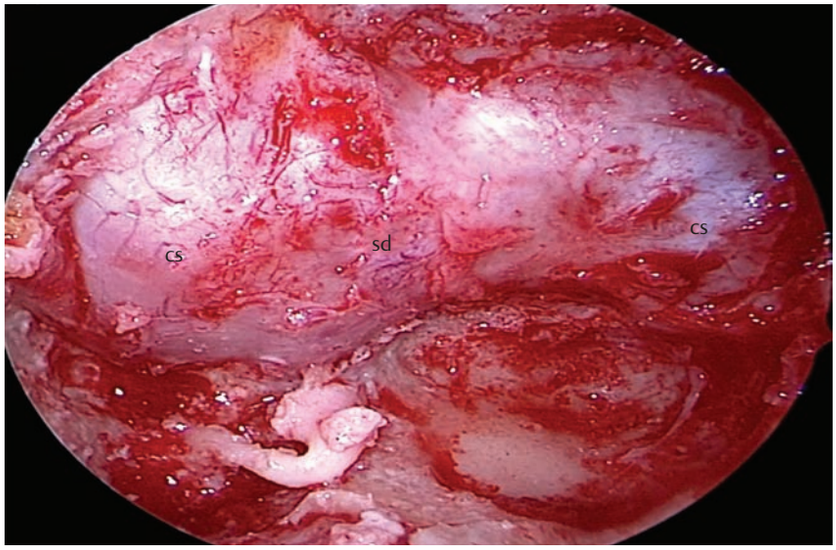

Fig. 9.50 Complete dural exposure of the sella and cavernous sinus. cs, cavernous sinus; sd, sellar dura.

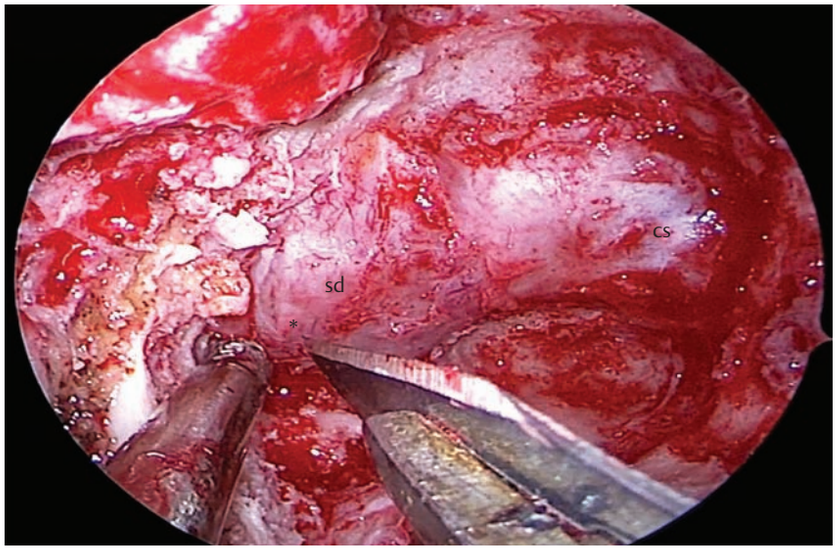

Fig. 9.51 Dural incision given over cavernous sinus lateral to the vidian nerve. cs, cavernous sinus; *, dural incision.

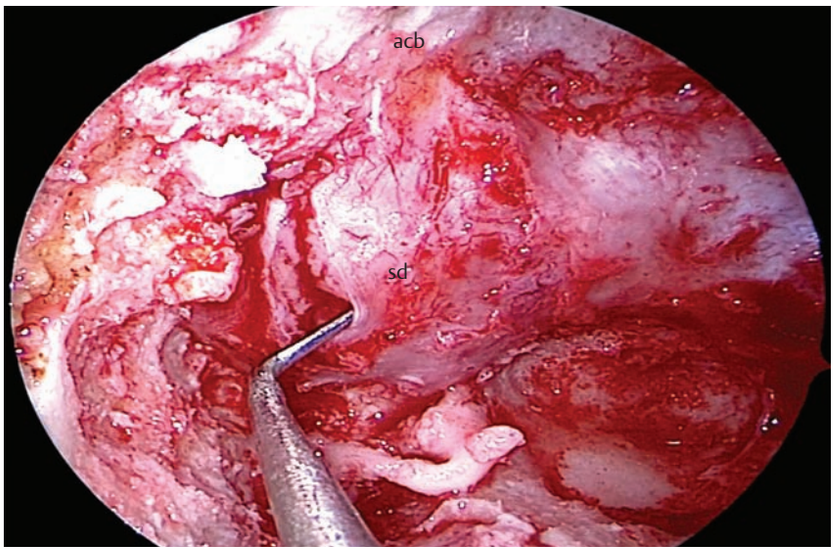

Fig. 9.52 Extension of the dural incision from lateral to medial. acb, anterior cranial base; sd, sellar dura.

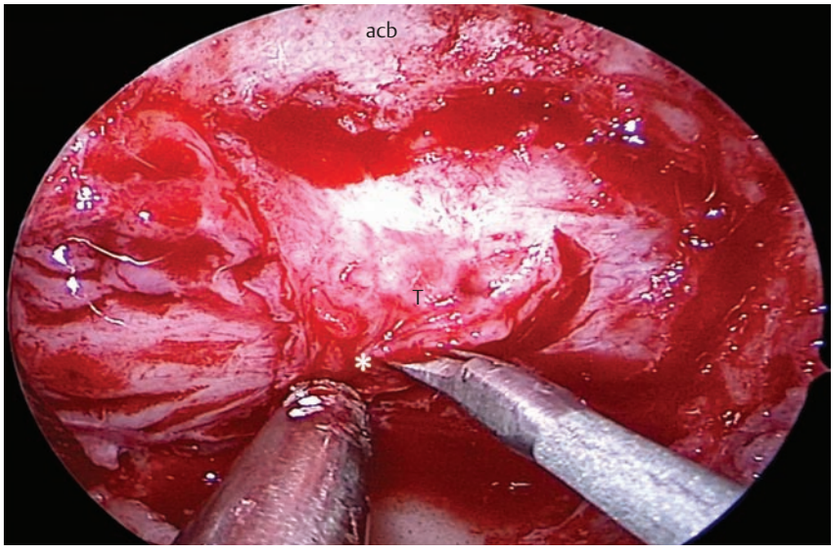

Fig. 9.53 Raised **U**-shaped dural flap. cs, cavernous sinus; sc, sella cavity; sd, sella dura; T, tumor.

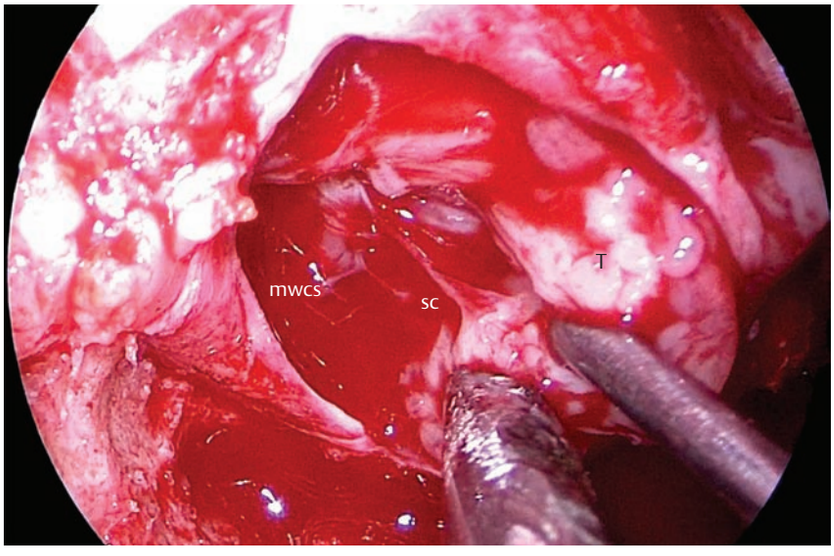

Fig. 9.54 Exposure of the tumor in the right cavernous sinus. mwcs, medial wall of the cavernous sinus; sc, sellar cavity.

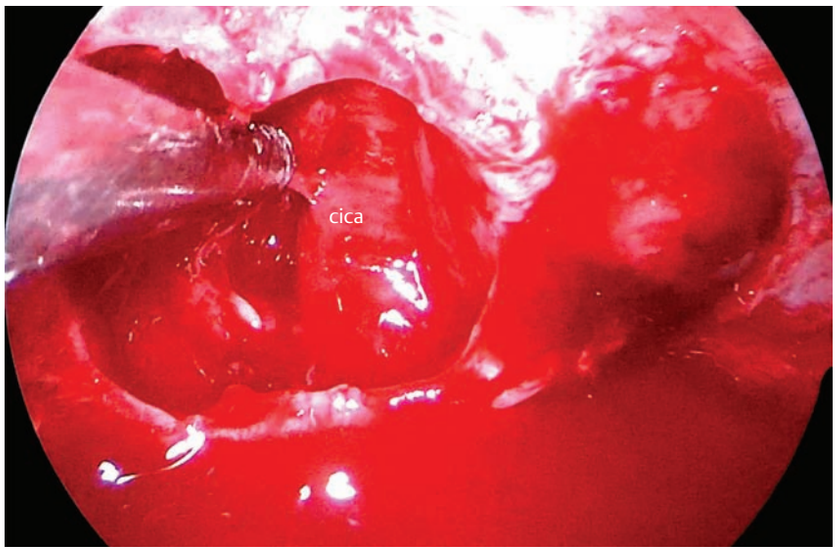

Fig. 9.55a Tumor dissection in the right cavernous sinus using the ring curette. cs, cavernous sinus; ica, internal carotid artery.

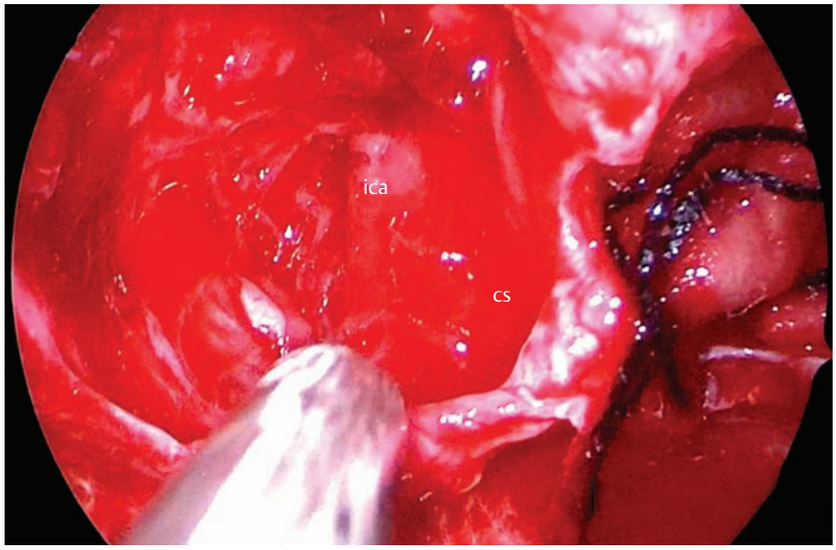

Fig. 9.55b Tumor dissection in the right cavernous sinus using the ring curette. cs, cavernous sinus; ica, internal carotid artery.

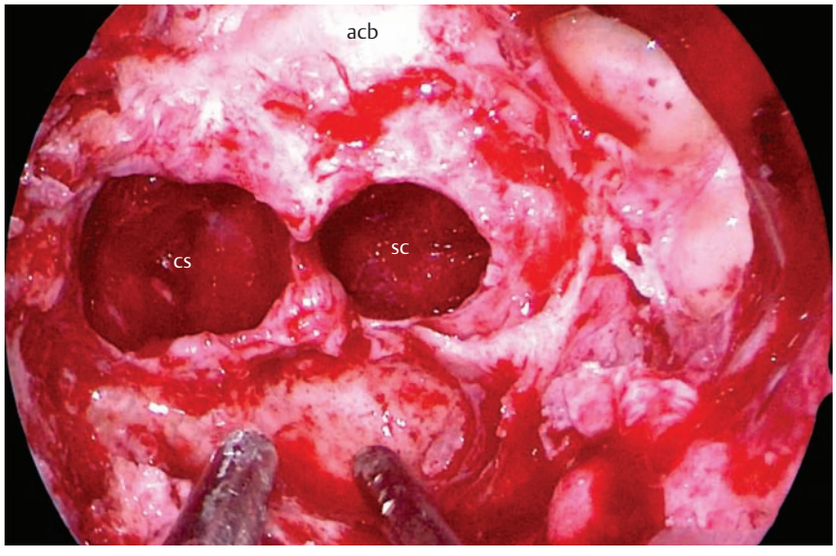

Fig. 9.56 Exposure of the right internal carotid artery and complete tumor removal. acb, anterior cranial base; cs, cavernous sinus; sc, sellar cavity.

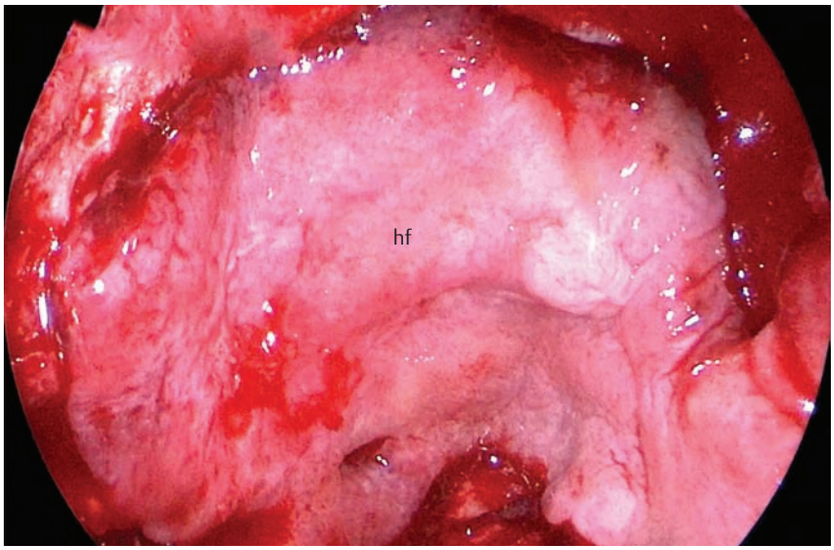

Fig. 9.57 Closure of the defect using nasoseptal flap. hf, Hadad flap.

Case 5: Revision Pituitary Macroadenoma (Acromegaly)

A 34-year-old male presented with chronic headache and features suggestive of acromegaly and sixth nerve palsy. Past history of multiple pituitary surgeries is present (**Fig. 9.58**).

MRI showed pituitary macroadenoma with parasellar extension completely encasing the cavernous carotid (**Fig. 9.59**).

Transmaxillary-transpterygoid approach was employed (**Figs. 9.60–9.62**). First, the tumor was dissected from the sellar region (**Figs. 9.63–9.67**), following which the dural opening was made lateral to the vidian nerve. Carotid artery course was mapped using the micro-Doppler (**Fig. 9.68**). Sellar dura and cavernous sinus dural incisions were joined together using the dural knife (**Figs. 9.69 and 9.70**). The tumor present anterior to the carotid artery was gently dissected out (**Fig. 9.71**). Transposition of the carotid artery was done and the tumor was dissected all around the ICA (**Figs. 9.72–9.75**). The postoperative MRI revealed complete removal of the tumor. See **Video 9.5**.

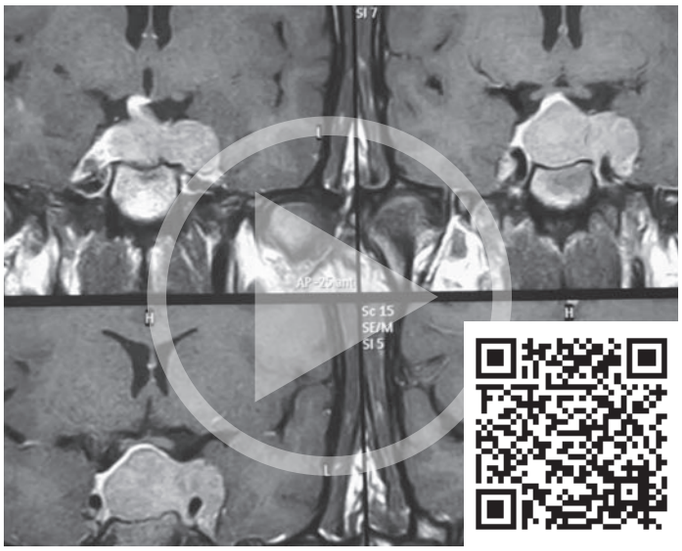

Video 9.5 Revision pituitary macroadenoma with acromegaly. https://www.thieme.de/de/q.htm?p=opn/cs/19/9/10104316-92c1758e

Fig. 9.58 **(a, b)** Pictures show the clinical presentation of acromegaly.

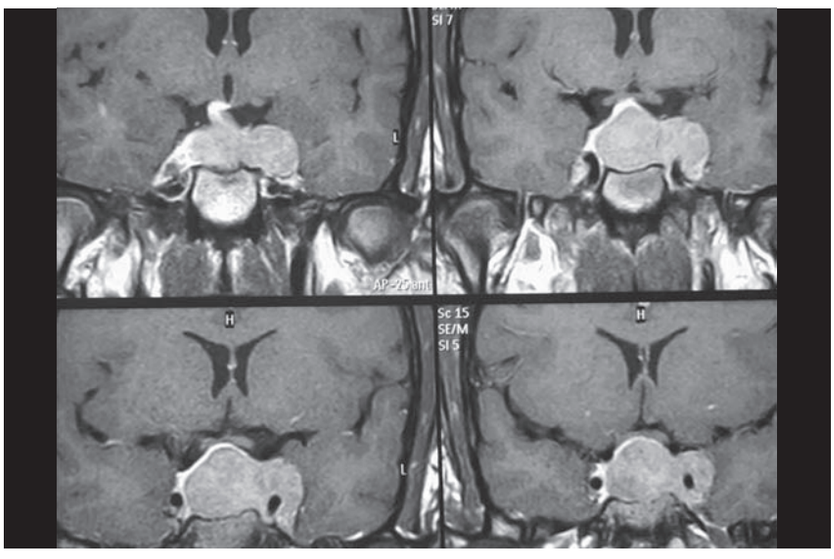

Fig. 9.59 MRI T1 post contrast image of the coronal section showing pituitary macroadenoma with parasellar extension.

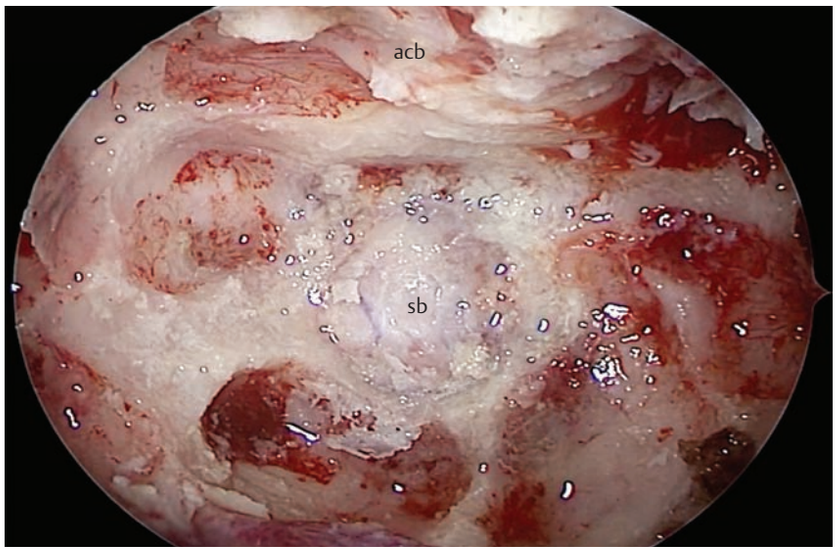

Fig. 9.60 Sellar exposure. acb, anterior cranial base; sb, sellar bone.

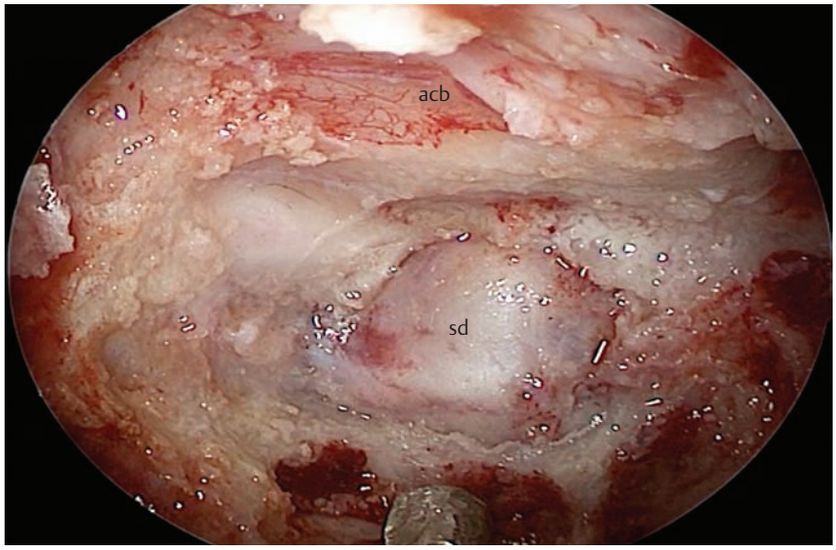

Fig. 9.61 Sellar bone is drilled out exposing the dura. acb, anterior cranial base dural incision; sd, sellar dura.

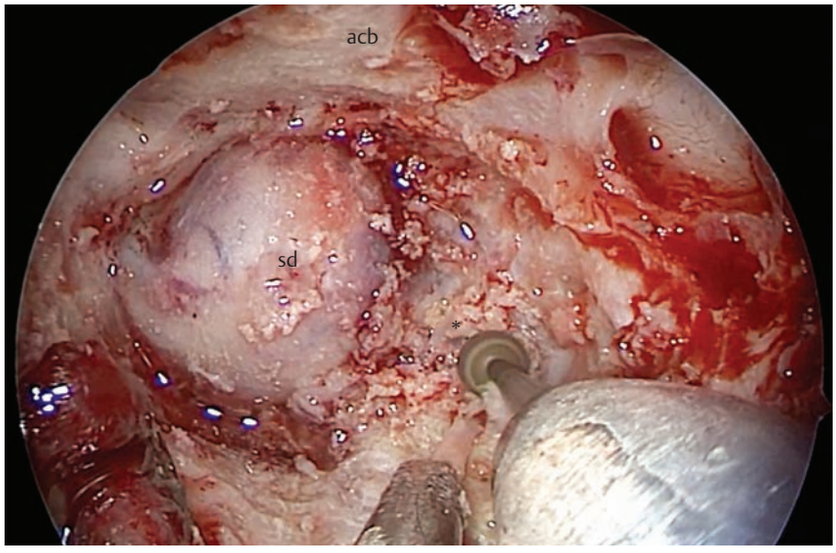

Fig. 9.62 Transpterygoid approach to the cavernous sinus. Drilling of the bone over the cavernous sinus. acb, anterior cranial base; sd, sellar dura.

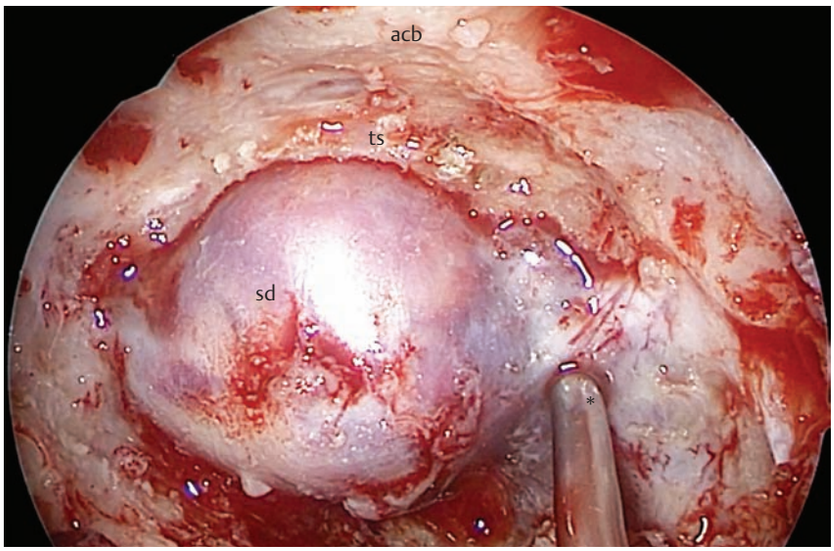

Fig. 9.63 The incision is given over the sellar dura. sd, sellar dura; *, Cappabianca knife.

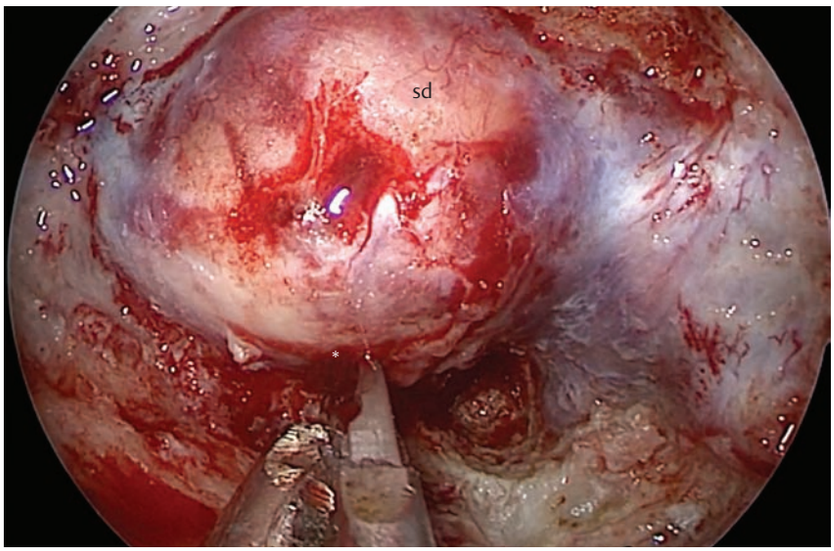

Fig. 9.64 **U**-shaped dural flap is raised. acb, anterior cranial base; sd, sellar dura; *, Kassam scissors.

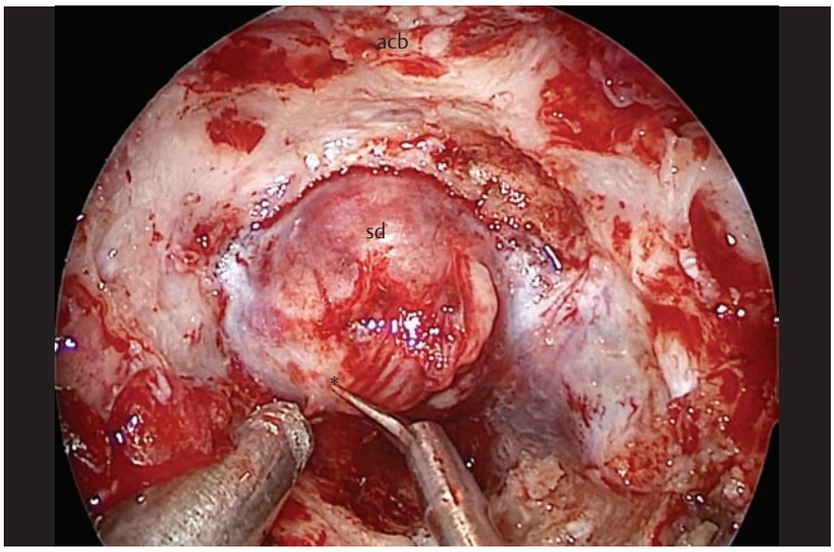

Fig. 9.65 Tumor exposed in the sellar cavity. acb, anterior cranial base; T, tumor.

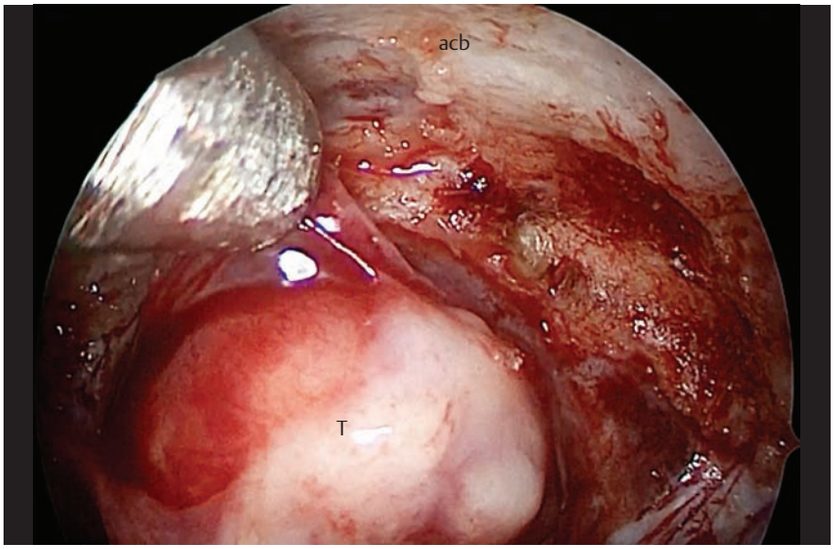

Fig. 9.66 Tumor cleared from the sellar cavity. acb, anterior cranial base; T, tumor.

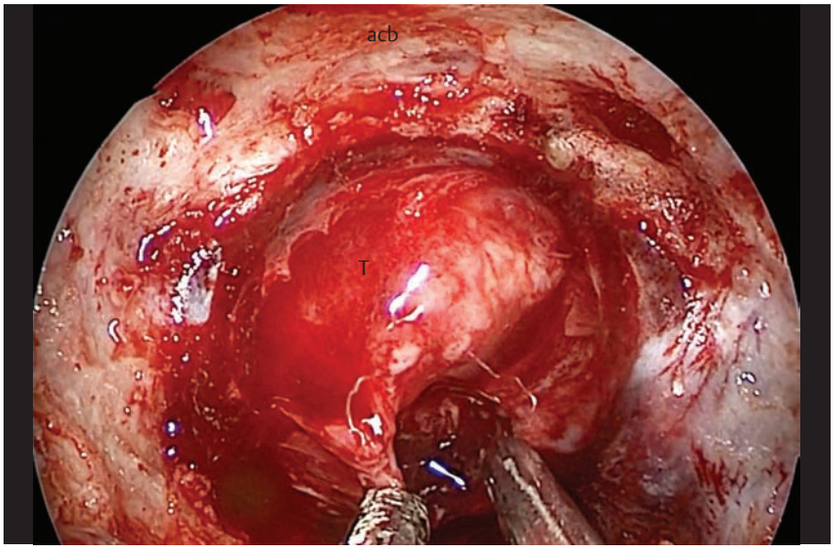

Fig. 9.67 Complete tumor clearance from the sellar cavity. sc, sellar cavity; T, tumor.

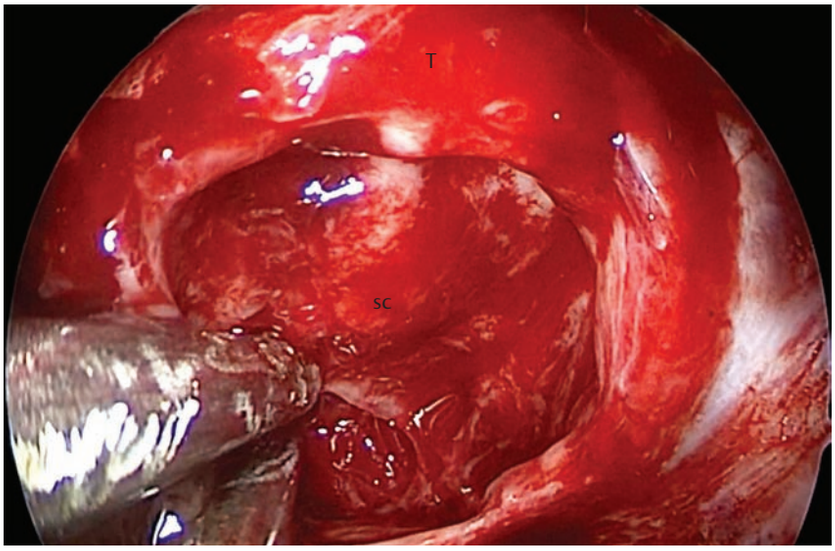

Fig. 9.68 Micro-Doppler used to map the course of the internal carotid artery. acb, anterior cranial base; sd, sellar dura; ts, tuberculum sellae.

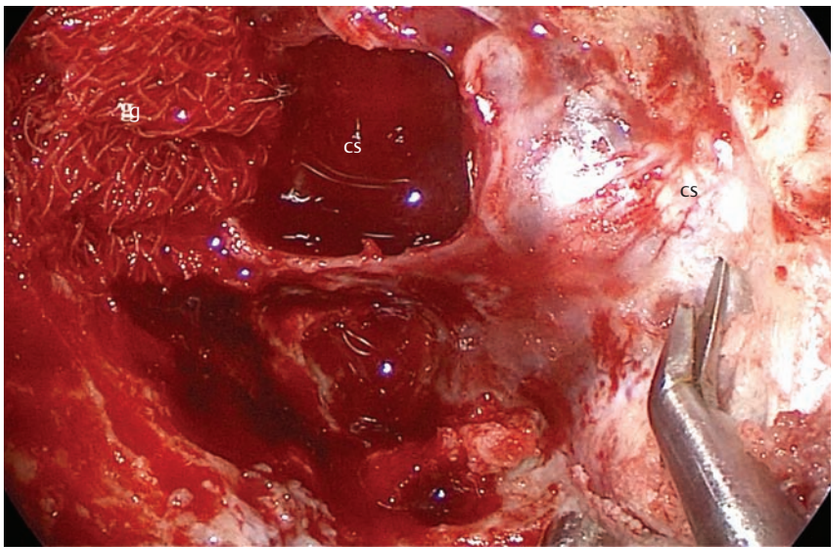

Fig. 9.69 Left cavernous sinus dura incision is given. cs, cavernous sinus; sc, sellar cavity.

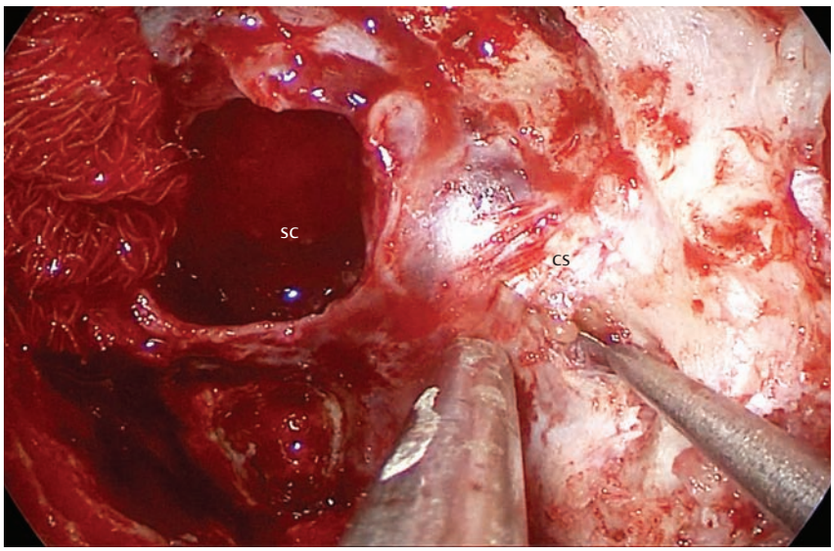

Fig. 9.70a Dural incision extended toward the sellar incision. cs, cavernous sinus; sc, sellar cavity.

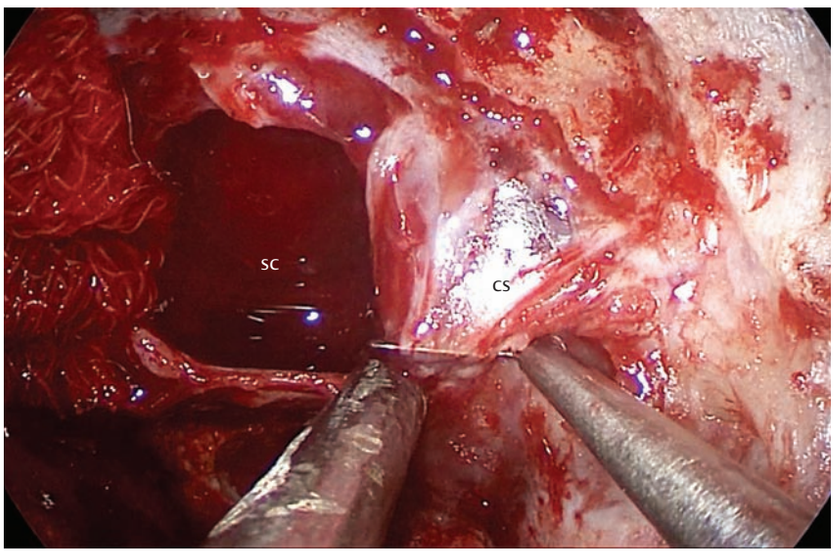

Fig. 9.70b Dural incision extended toward the sellar incision. cs, cavernous sinus; sc, sellar cavity.

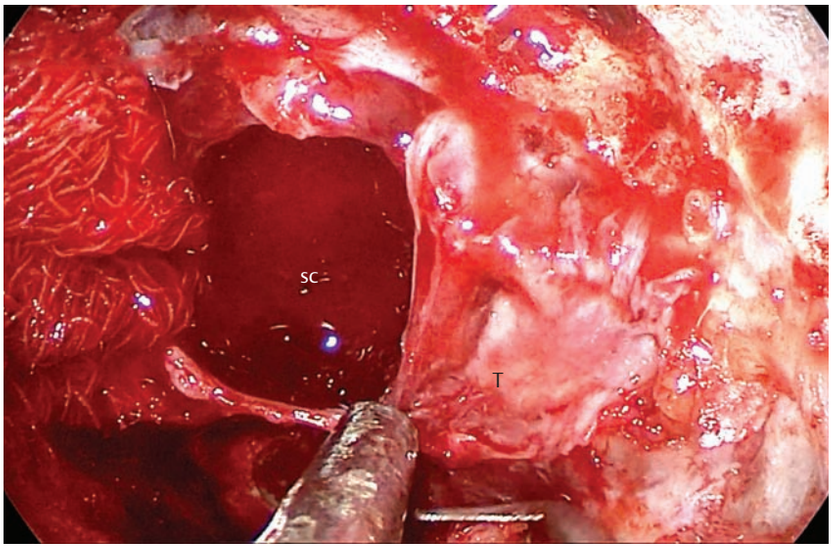

Fig. 9.71 Tumor exposed in the left cavernous sinus. T, tumor.

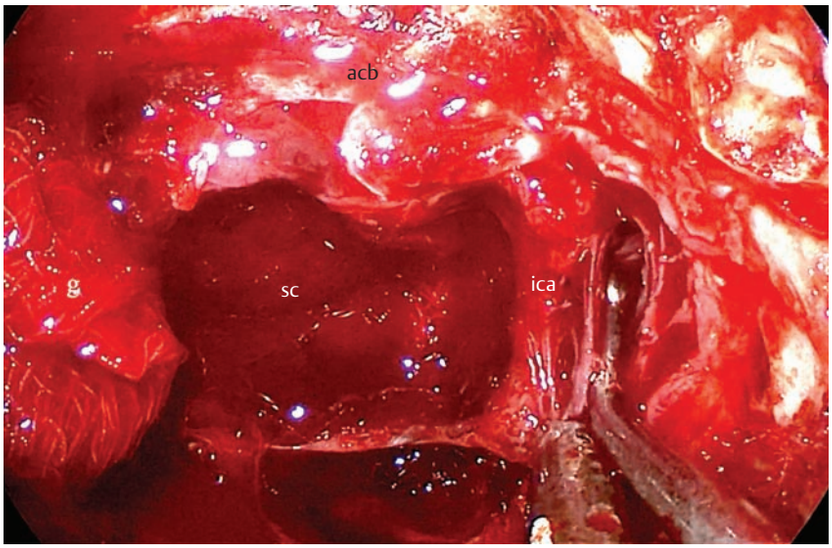

Fig. 9.72 Left internal carotid artery exposed in the cavernous sinus. acb, anterior cranial base; ica, internal carotid artery. Tumor clearance from the inferomedial compartment of the cavernous sinus.

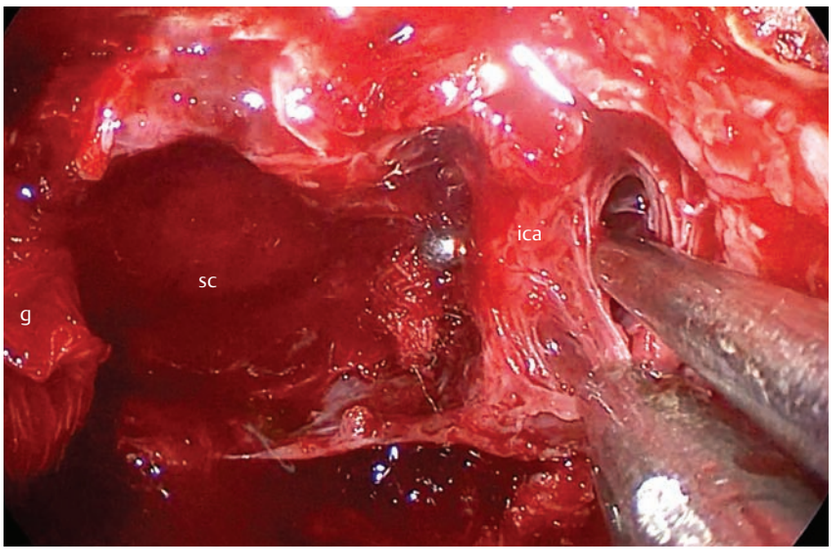

Fig. 9.73 Carotid transposition. cica, cavernous internal carotid artery. g, lint.

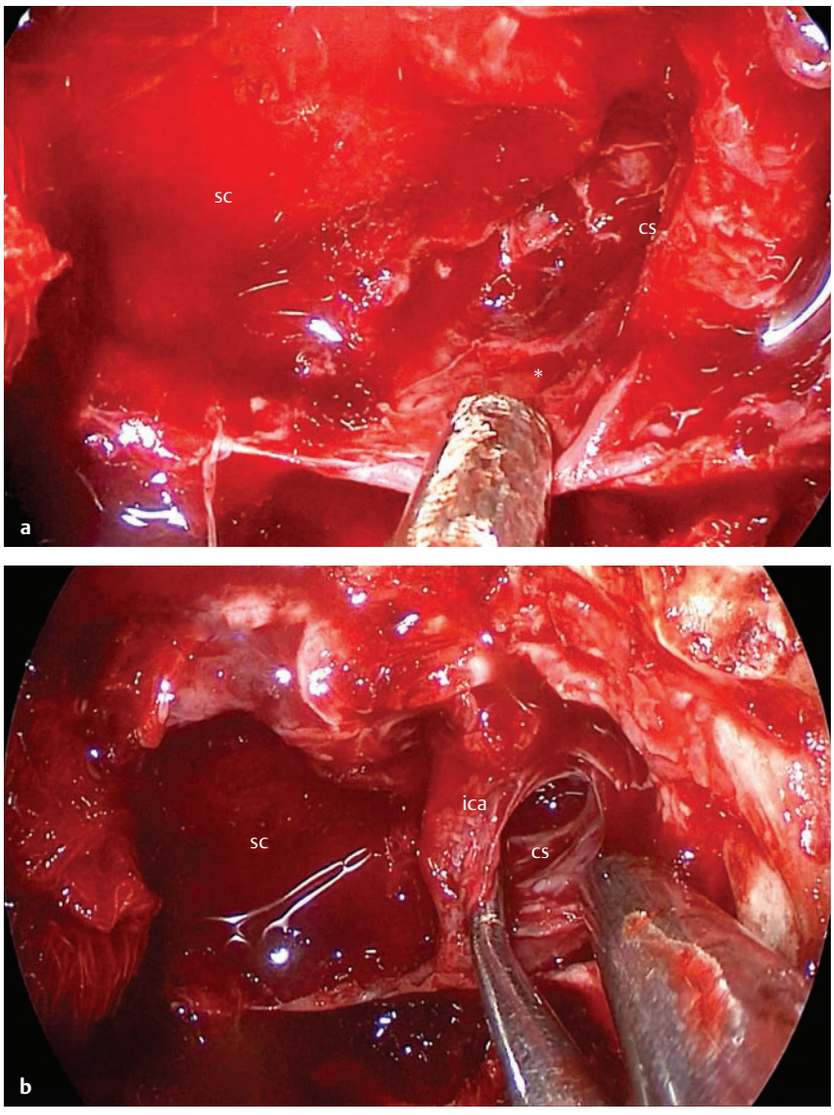

Fig. 9.74 **(a, b)** Left cavernous sinus dissection. cs, cavernous sinus; ica, internal carotid artery; sc, sellar cavity.

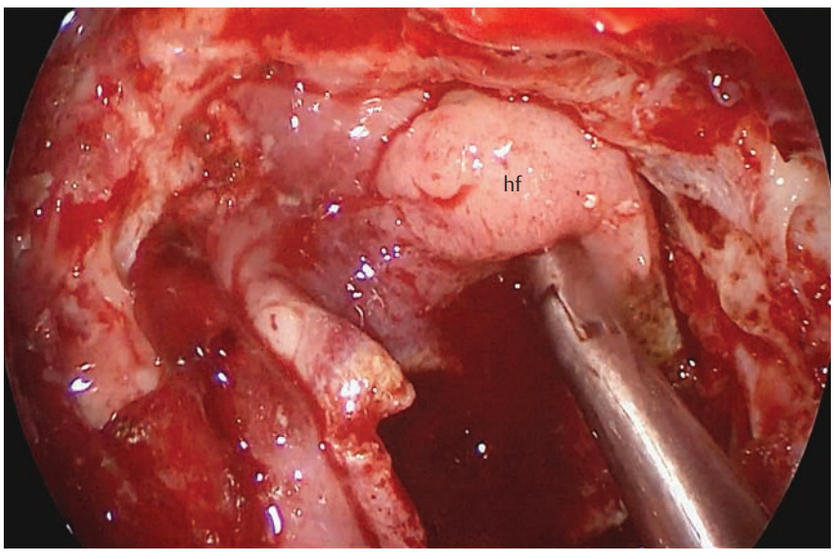

Fig. 9.75 Closure with Hadad flap. hf, Hadad flap.

Case 6: Pituitary Macroadenoma: Parasellar Extension

This is a case of pituitary macroadenoma with parasellar extension. The patient presented with headache and progressive diplopia for 1 year.

The imaging study showed pituitary macroadenoma with CS extension on the right side (**Fig. 9.76**). Transpterygoid approach was employed. The sphenoid sinus was widely exposed at the completion of the nasal phase (**Fig. 9.77**). Transpterygoid approach to the CS was employed (**Figs. 9.78–9.82**). Micro-Doppler and navigation were used to locate the course of the carotid artery. The dural incision was placed and the tumor cleared from the sellar cavity (**Figs. 9.83 and 9.84**). Tumor clearance from the right CS wasstarted (**Fig. 9.85**). Right CS dissection was continued with the identification of the ICA (**Fig. 9.86**). Tumor lateral to ICA was dissected (**Fig. 9.87**). A complete view of the right CS was seen (**Fig. 9.88**). No active CSF leak was observed. The defect was closed with Hadad flap (**Fig. 9.89**).

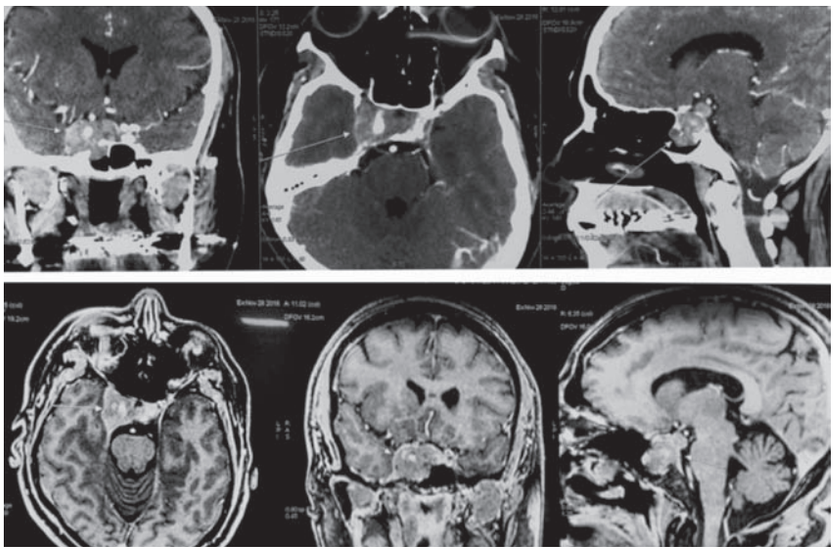

Fig. 9.76 MRI sequence showing pituitary macroadenoma with parasellar extension.

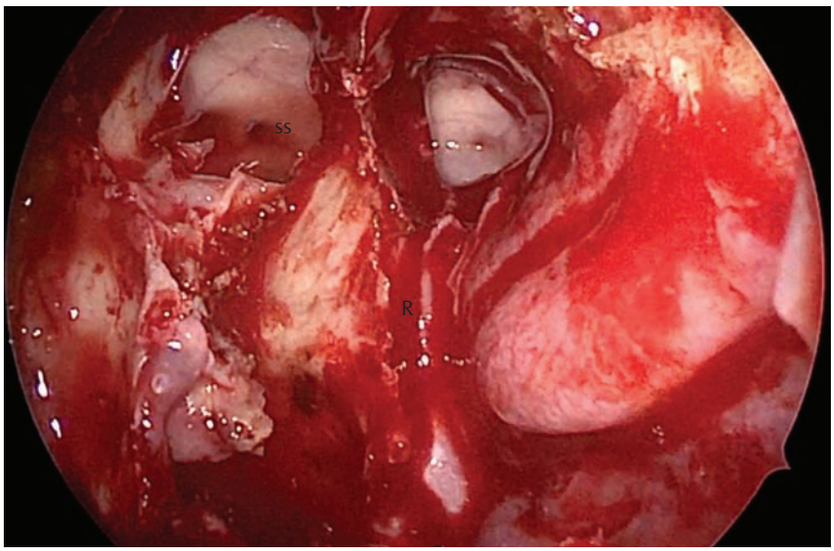

Fig. 9.77 Endoscopic picture showing exposure of the sphenoid sinus. R, rostrum of the sphenoid; ss, sphenoid sinus.

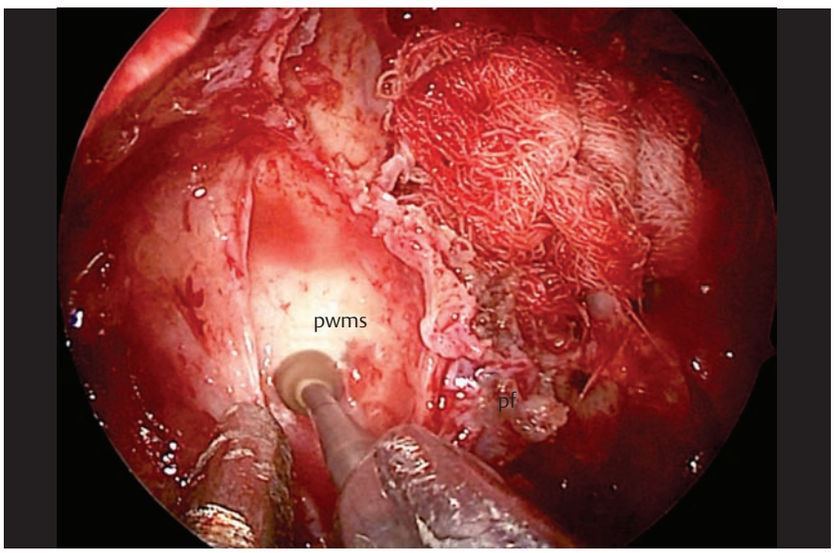

Fig. 9.78 Endoscopic image of the transpterygoid approach showing the posterior maxillary wall and pterygopalatine fossa. pf, pterygopalatine fossa; pwms, the posterior wall of the maxillary sinus.

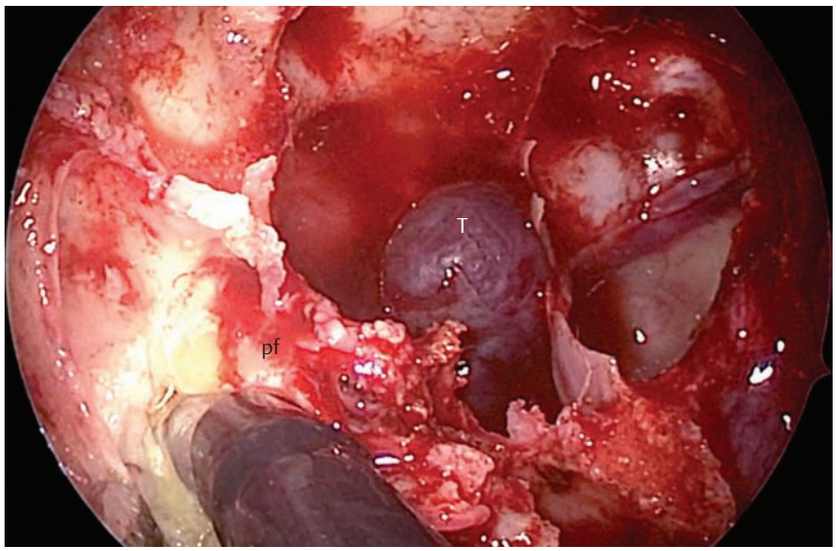

Fig. 9.79 Coblation used to coagulate the contents of the pterygopalatine fossa. pf, pterygoid fossa; T, tumor.

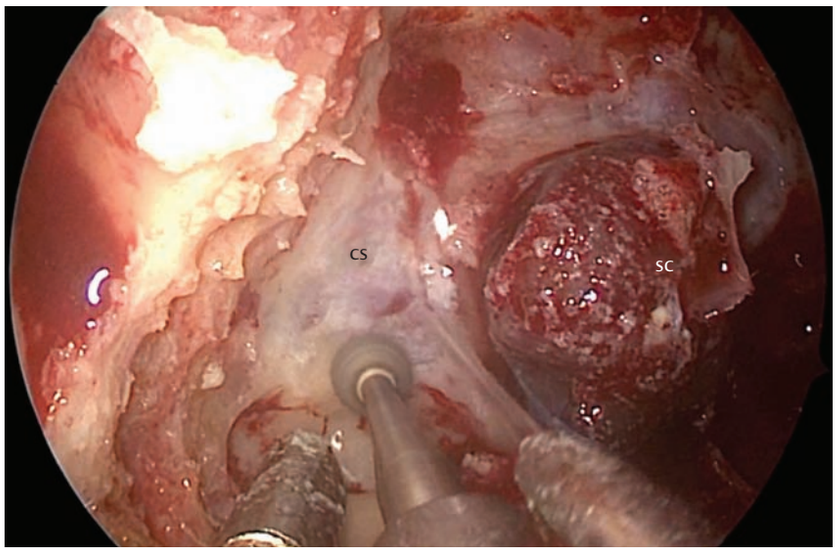

Fig. 9.80 Bone exposed over the cavernous sinus using a diamond drill. cs, cavernous sinus; sc, sellar cavity.

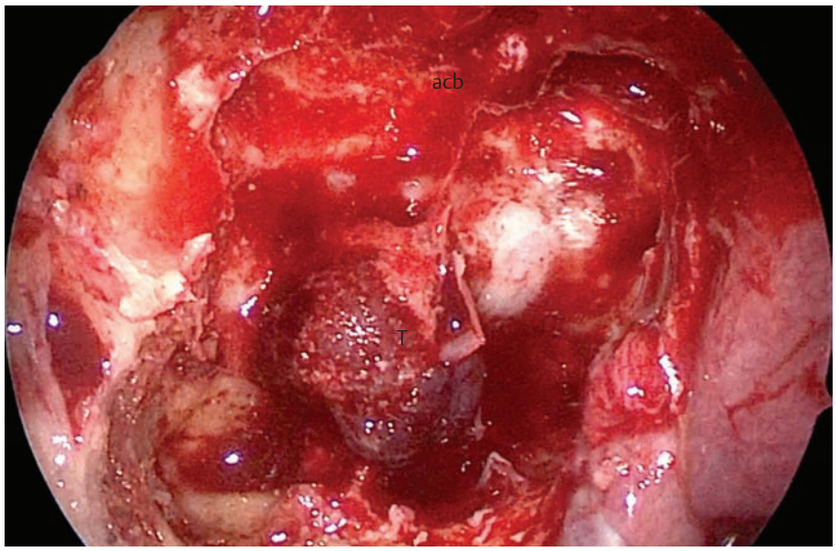

Fig. 9.81 Exposure of sella with the tumor. acb, anterior cranial base; T, tumor.

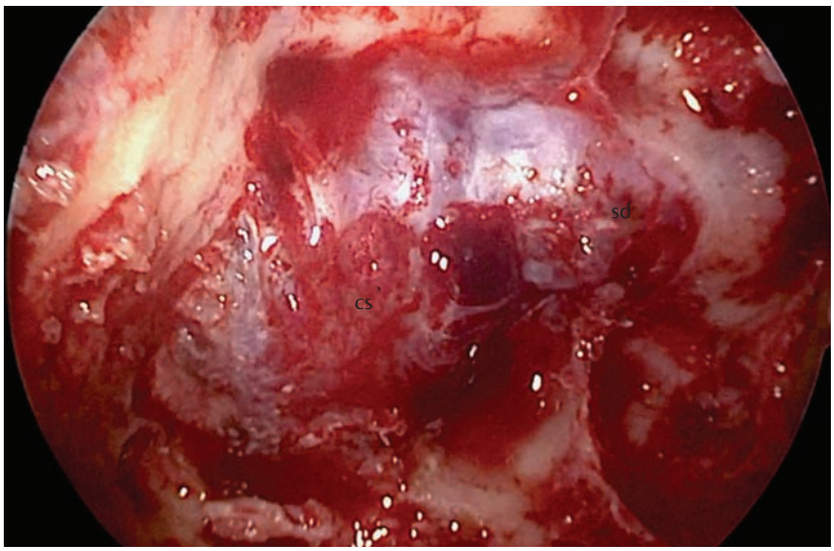

Fig. 9.82 Completed transpterygoid approach showing wide exposure of the sella and cavernous sinus dura. cs, cavernous sinus; sd, sella dura.

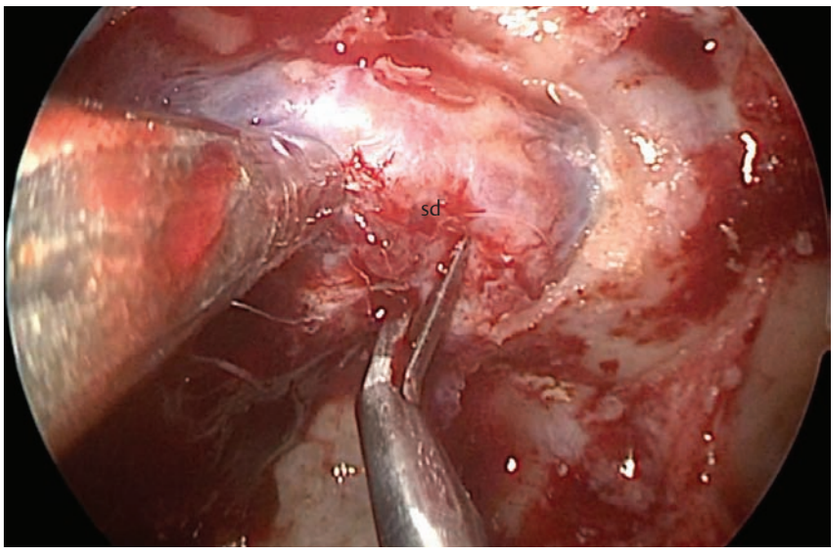

Fig. 9.83 Dural incision given over the sella dura. sd, sella dura.

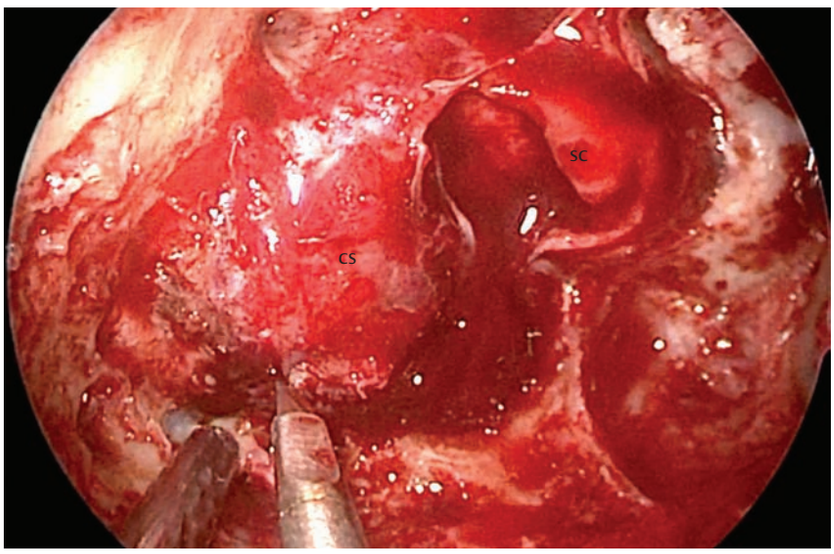

Fig. 9.84 Dural incision given over the cavernous sinus dura after tumor clearance from the sellar cavity. cs, cavernous sinus; sc, sellar cavity.

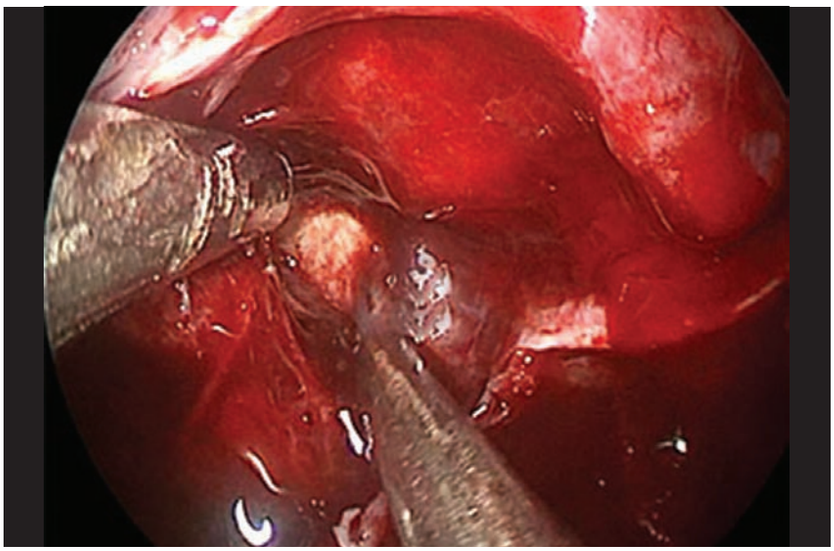

Fig. 9.85 Tumor clearance from the right cavernous sinus. cs, cavernous sinus; T, tumor.

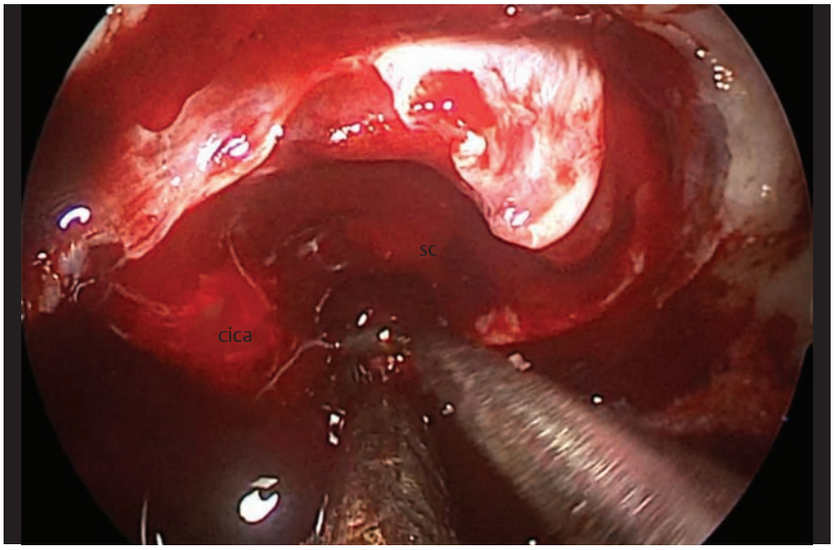

Fig. 9.86 Right internal carotid artery exposed in the cavernous sinus. ica, internal carotid artery; sc, sellar cavity.

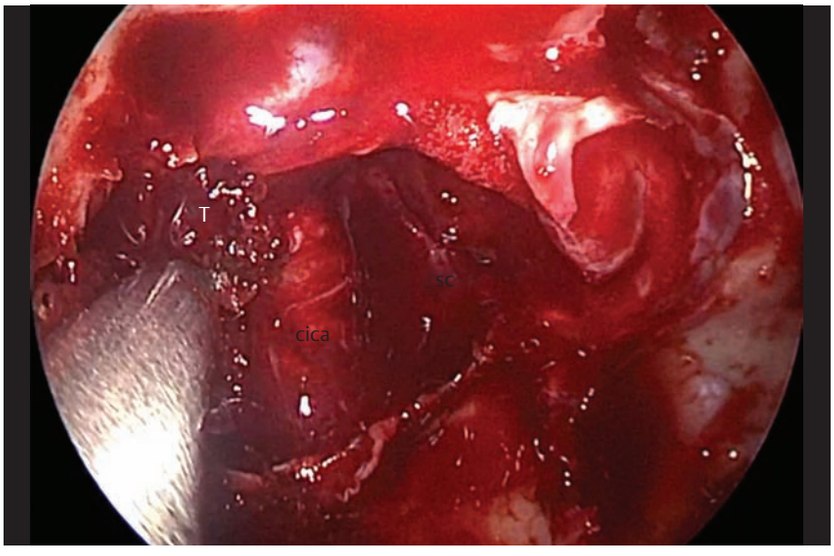

Fig. 9.87 Tumor cleared from the retrogenu area and lateral to the Internal carotid artery. cica, cavernous internal carotid artery; sc, sellar cavity.

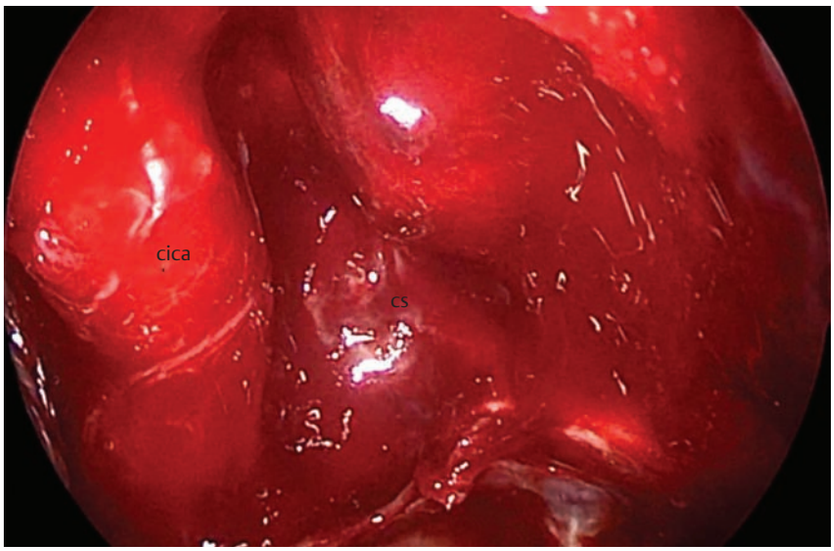

Fig. 9.88 Endoscopic picture depicting right cavernous sinus dissection. cica, cavernous internal carotid artery; cs, cavernous sinus.

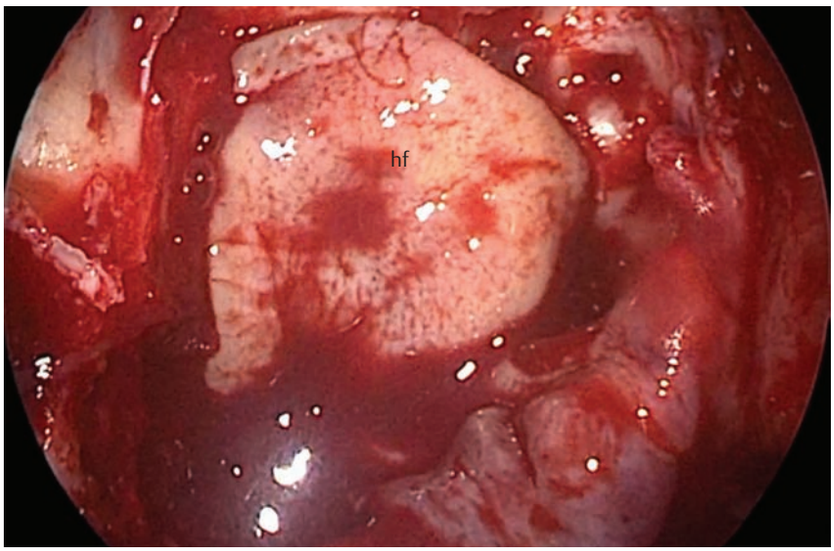

Fig. 9.89 Closure with Hadad flap. hf, Hadad flap.

Case 7: Pituitary Macroadenoma (Invasive)

This is a case of invasive pituitary macroadenoma. An invasive macroadenoma is defined as the one which is infiltrating the dura and the bone. It is one of the aggressive forms of pituitary adenoma. MRI in this patient suggested pituitary macroadenoma with invasive features with complete ICA encasement (**Fig. 9.90**). Transsphenoidal-transpterygoid approach was planned. Wide exposure of the sella and CS was achieved (**Figs. 9.91 and 9.92**). Micro-Doppler was used to navigate the course of the ICA. Dural incision was placed over the sellar dura, as seen in the figures (**Figs. 9.93–9.95**). The tumor was cleared from the sellar cavity (**Figs. 9.96 and 9.97**). The CS dura was cut using a Cappabianca knife lateral to the vidian nerve and was continued medially (**Figs. 9.98 and 9.99**). Left CS dissection was carried out with the clearance of the tumor (**Figs. 9.100 and 9.101**). Sixth nerve is seen in the figure (**Figs. 9.102 and 9.103**). As the right CS dissection was carried out, inferior hypophyseal artery was visualised (**Fig. 9.104**). CS dissection with the suprasellar extension was shown in **Fig. 9.105**. Closure of the defect with nasoseptal flap wasshown in **Fig. 9.106**.

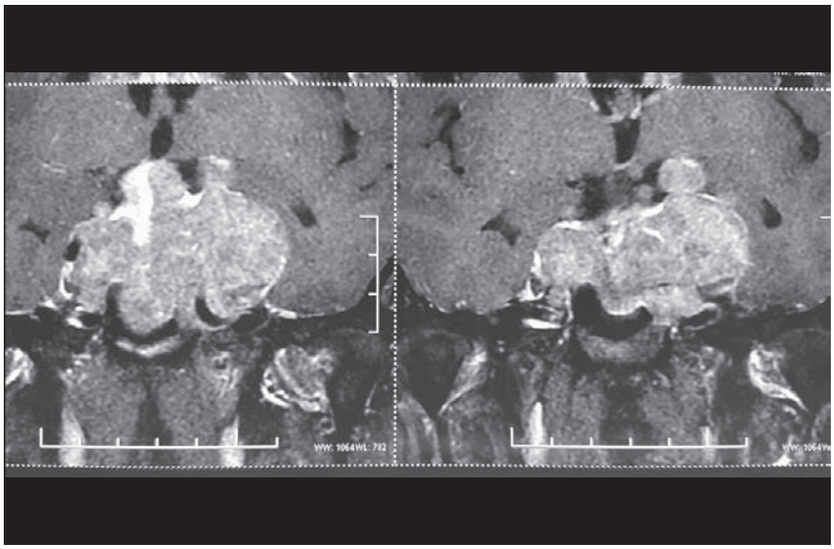

Fig. 9.90 MRI coronal imaging shows pituitary macroadenoma with extensive parasellar and suprasellar extension.

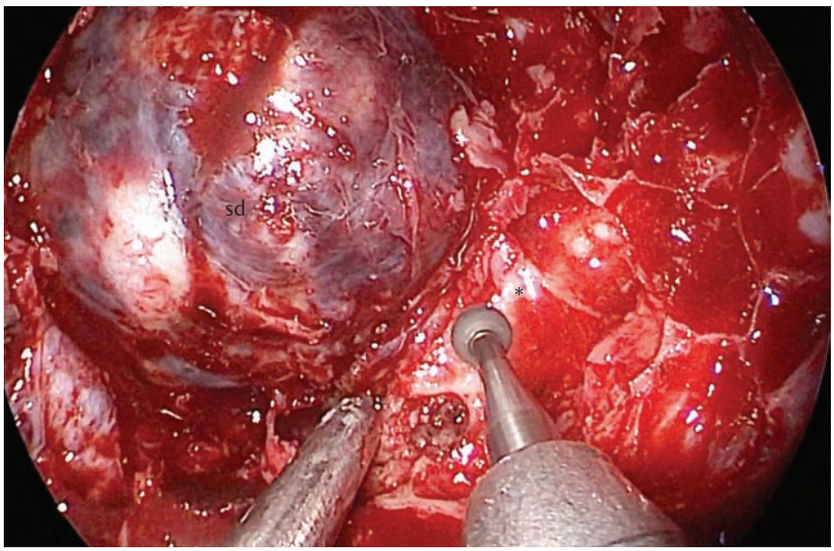

Fig. 9.91 Sellar exposure. sd, sellar dura; *, drilling of the bone over the cavernous sinus.

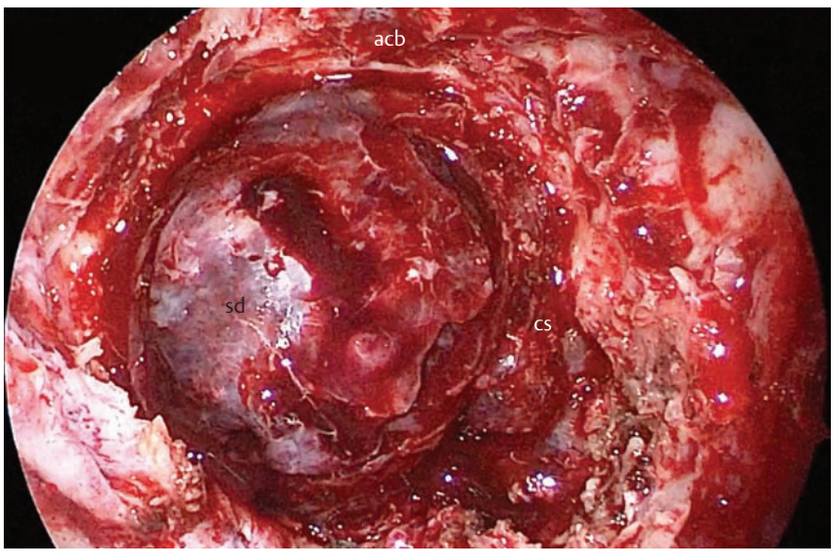

Fig. 9.92 Exposure of the cavernous sinus. acb, anterior cranial base; cs, cavernous sinus; sd, sellar dura.

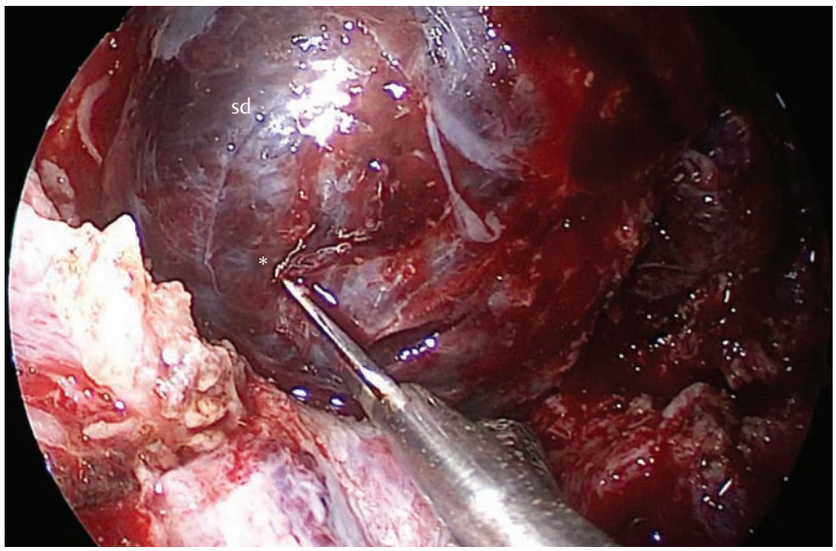

Fig. 9.93 Dural incision placed. sd, sella dura; *, incision given with Cappabianca knife.

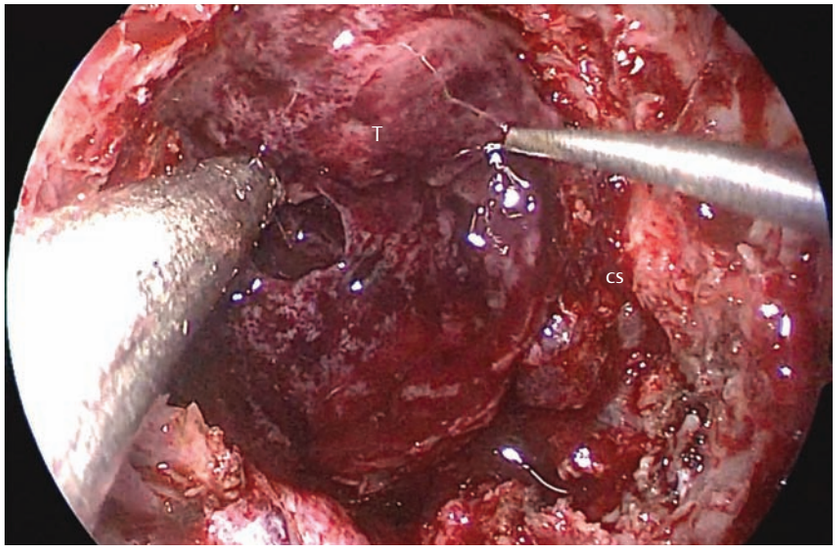

Fig. 9.94 Tumor seen infiltrating the dura. cs, cavernous sinus; T, tumor.

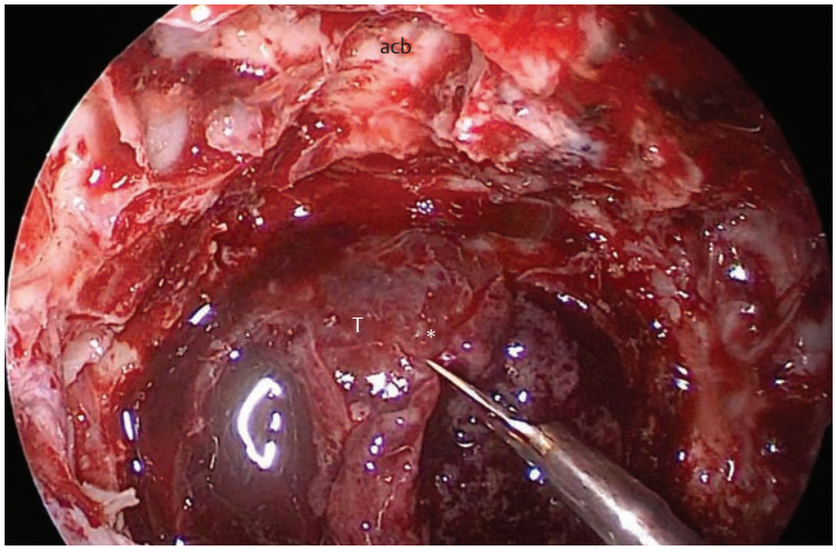

Fig. 9.95 **U**-shaped dural flap is incised due to tumor infiltration. acb, anterior cranial base; T, tumor.

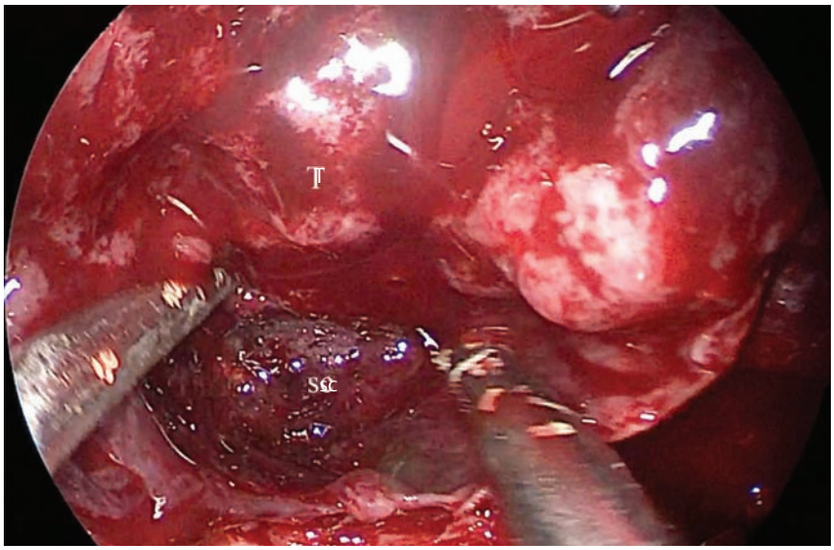

Fig. 9.96 Tumor clearance from the sellar cavity starting from the 6 o'clock position. T, tumor.

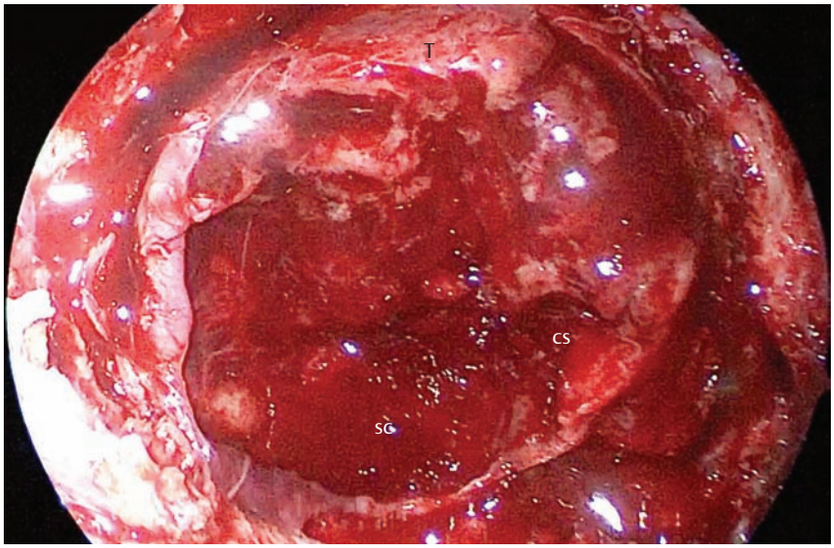

Fig. 9.97 Tumor cleared from the sellar region. cs, cavernous sinus; sc, sellar cavity; T, tumor.

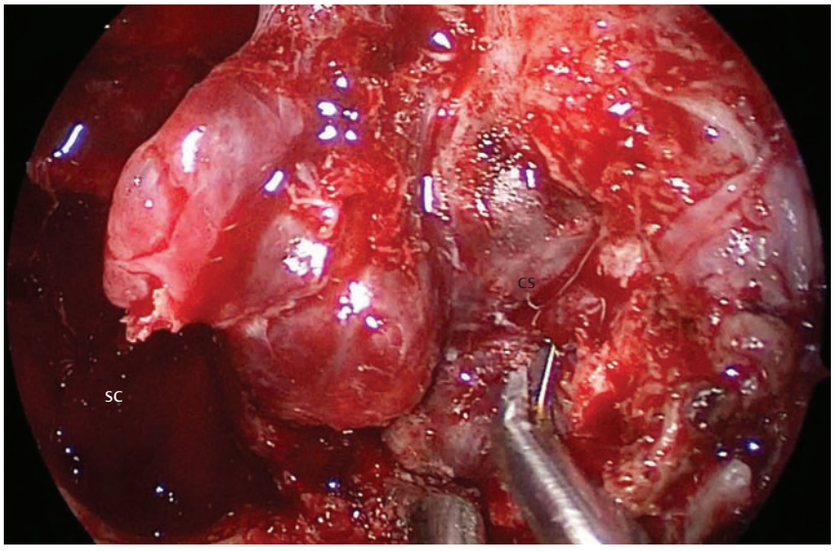

Fig. 9.98 Dural incision over the cavernous sinus region. cs, cavernous sinus.

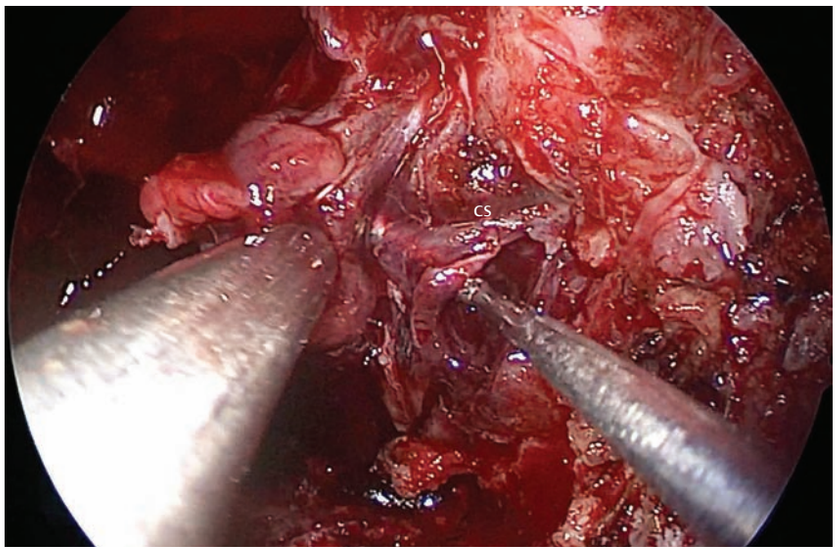

Fig. 9.99 Extension of the incision to join the sellar one. cs, cavernous sinus.

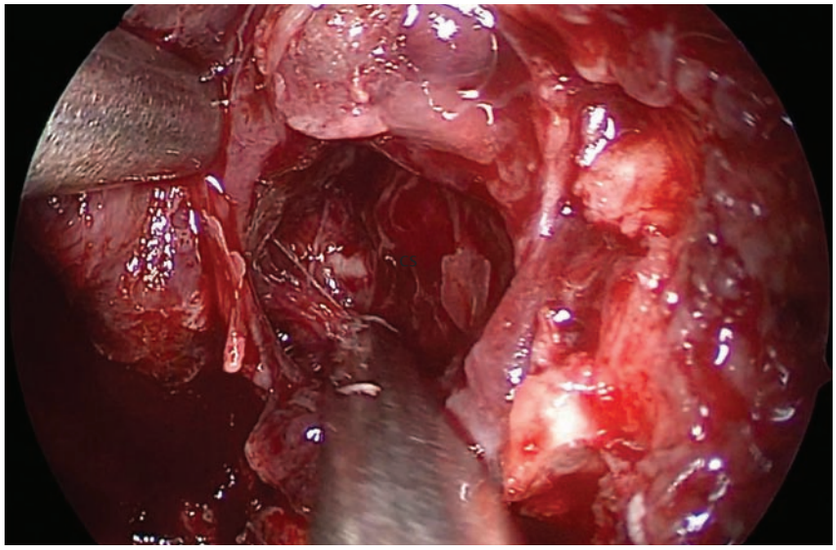

Fig. 9.100 Clearance of the tumor from the left cavernous sinus. cs, cavernous sinus.

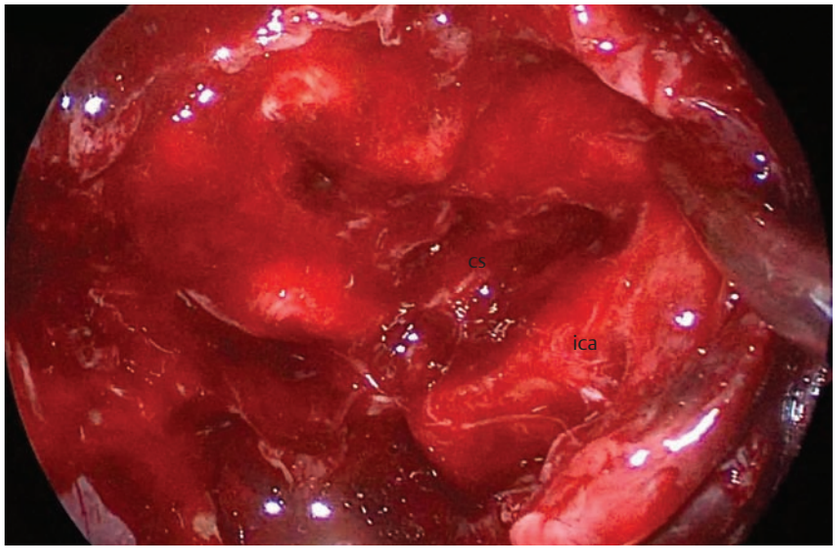

Fig. 9.101 Tumor cleared from left cavernous sinus. cs, cavernous sinus; ica, internal carotid artery.

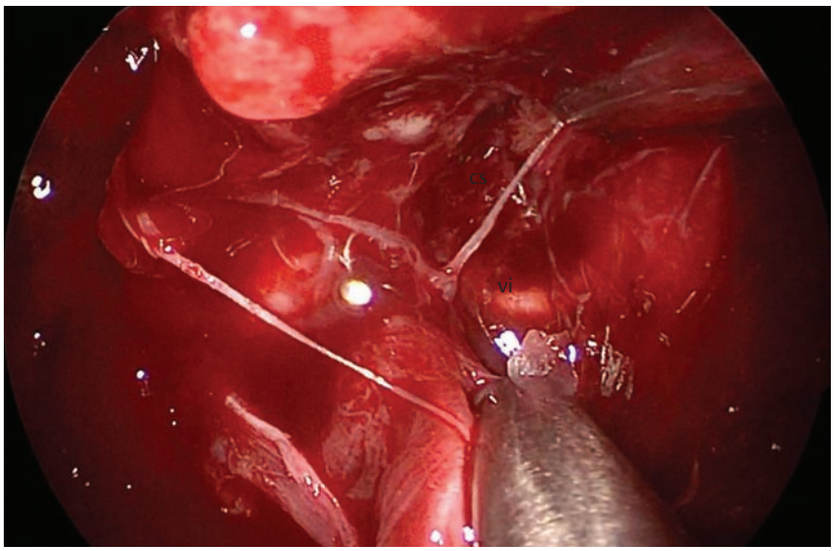

Fig. 9.102 Left internal carotid artery and VI nerve visualized in the cavernous sinus. cs, cavernous sinus.

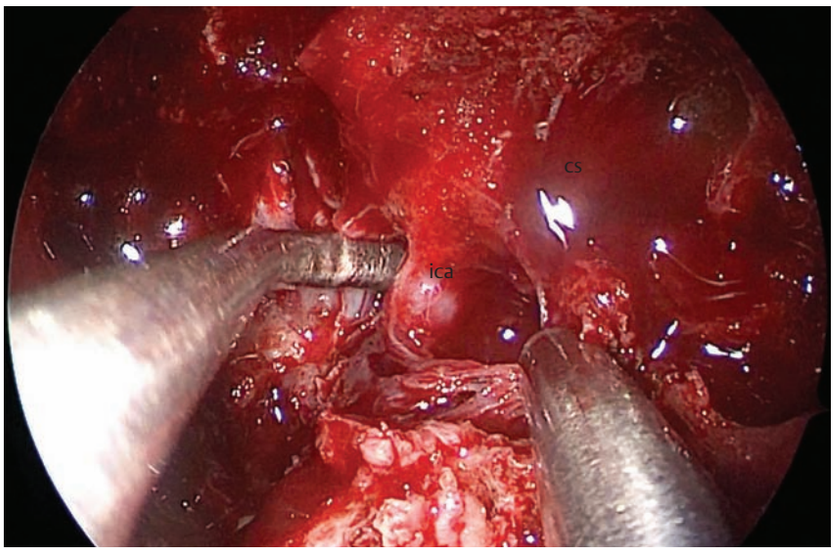

Fig. 9.103 Ball probe passed around the internal carotid artery. cs, cavernous sinus; ica, internal carotid artery.

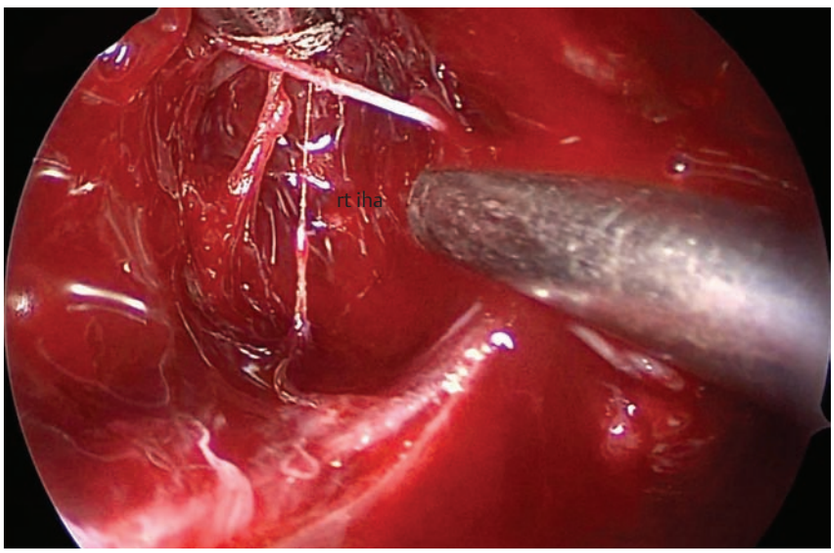

Fig. 9.104 Right cavernous sinus dissection. rt iha, inferior hypophyseal artery.

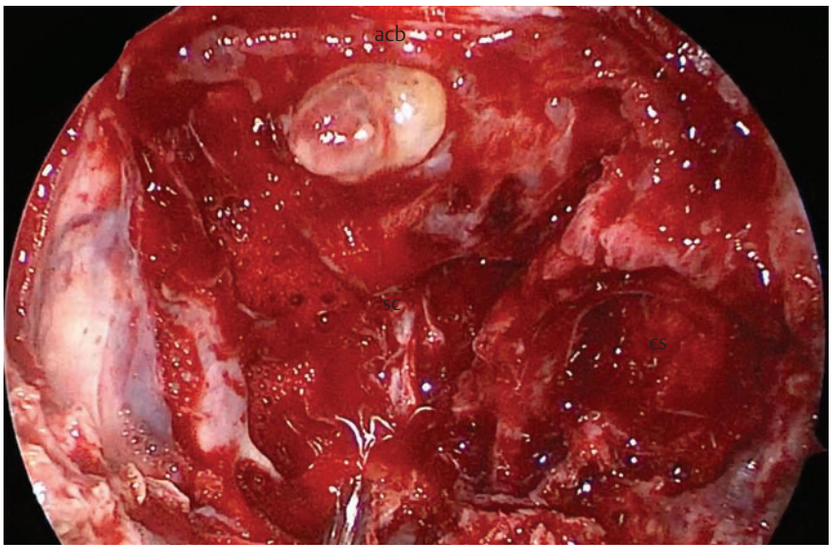

Fig. 9.105 Complete tumor clearance from the parasellar region with tumor seen extending to the suprasellar region. acb, anterior cranial base; cs, cavernous sinus; sc, sellar cavity.

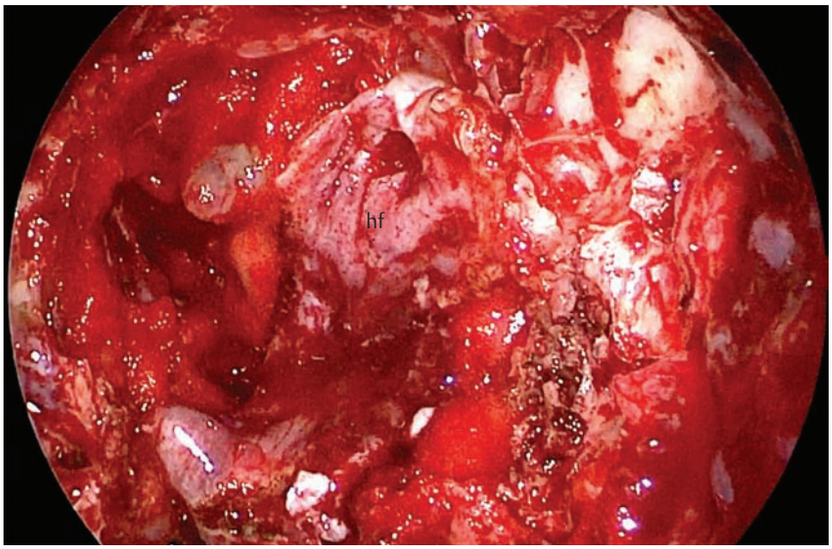

Fig. 9.106 Closure of the defect with nasoseptal flap. hf, Hadad flap.

Case 8: Pituitary Macroadenoma

A 60-year-old female patient presented with headache and progressive decline of vision in the right eye for 6 months. MRI revealed pituitary macroadenoma with extensive parasellar extension involving the right CS (**Fig. 9.107**). Transmaxillary-transpterygoid approach was used to expose the tumor. At the conclusion of the nasal and sphenoid phase, wide exposure to the sellar region was achieved (**Figs. 9.108 and 9.109**). Diamond burr was used to drill the pterygoid wedge to identify the vidian nerve which is an important landmark to ascertain the position of the ICA and provide a wide view of the CS (**Fig. 9.110**). Bone over the cavernous and sellar region was removed to expose the dura (**Fig. 9.111**). Micro-Doppler was used to map the accurate position of the ICA (**Fig. 9.112**). The dural incision was made using Cappabianca knife and extended to create a superiorly based **U**-shaped flap (**Figs. 9.113 and 9.114**). The tumor was cleared from the sellar cavity starting from 6 o'clock position (**Fig. 9.115**). The incision over the CS dura was placed in a lateral to medial fashion staying lateral to the vidian nerve (**Fig. 9.116**). Right CS dissection was carried out and the tumor is cleared from the medial and anteroinferior compartments (**Fig. 9.117**). Micro-Doppler was used to confirm the position of the ICA. The tumor lateral and behind the ICA was carefully dissected out by transposing the ICA (**Fig. 9.118**). Complete tumor removal was accomplished and reconstruction of the defect is done by using the nasoseptal flap (**Figs. 9.119 and 9.120**).

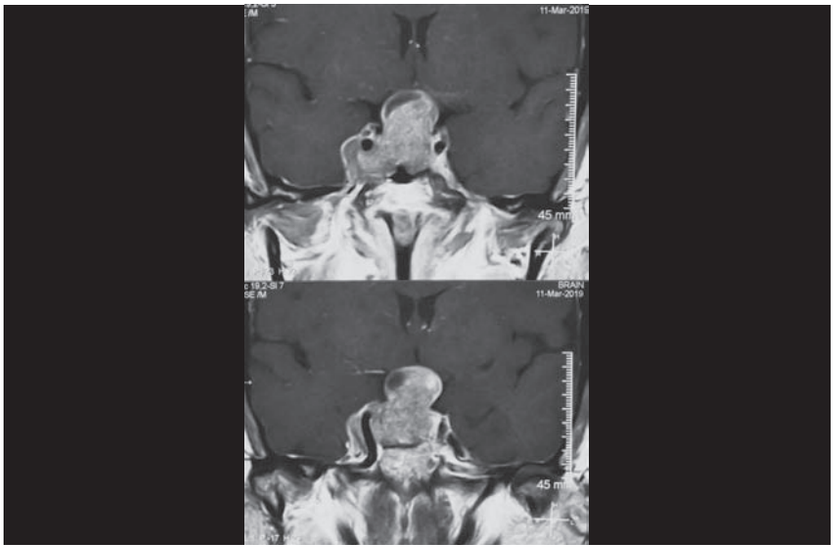

Fig. 9.107 MRI T1 post contrast image sequence showing pituitary macroadenoma with parasellar extension.

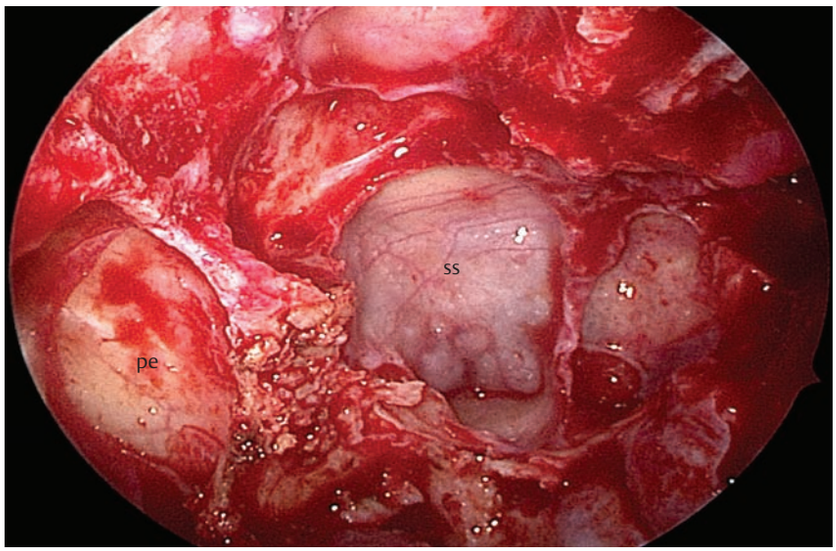

Fig. 9.108 Endoscopic image showing sellar exposure. sb, sellar bone.

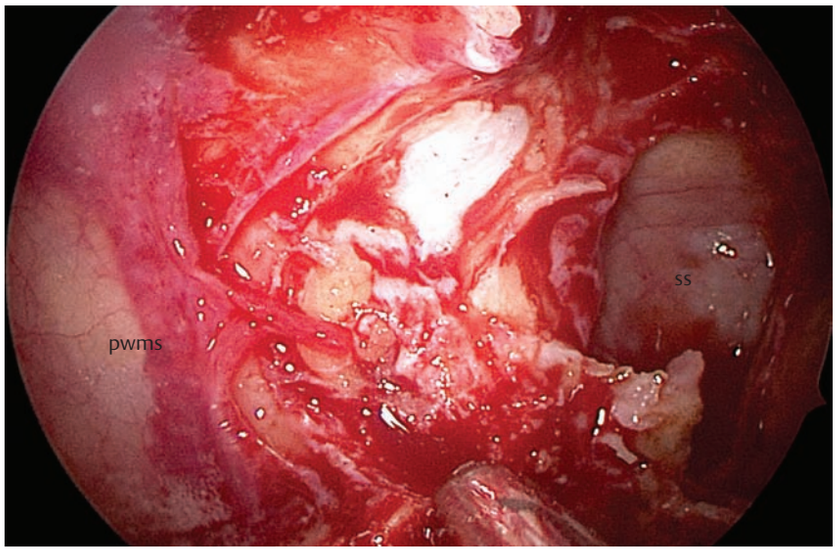

Fig. 9.109 Transpterygoid approach: drilling over the posterior maxillary wall and pterygoid process. pwms, the posterior wall of the maxillary sinus; ss, sphenoid sinus.

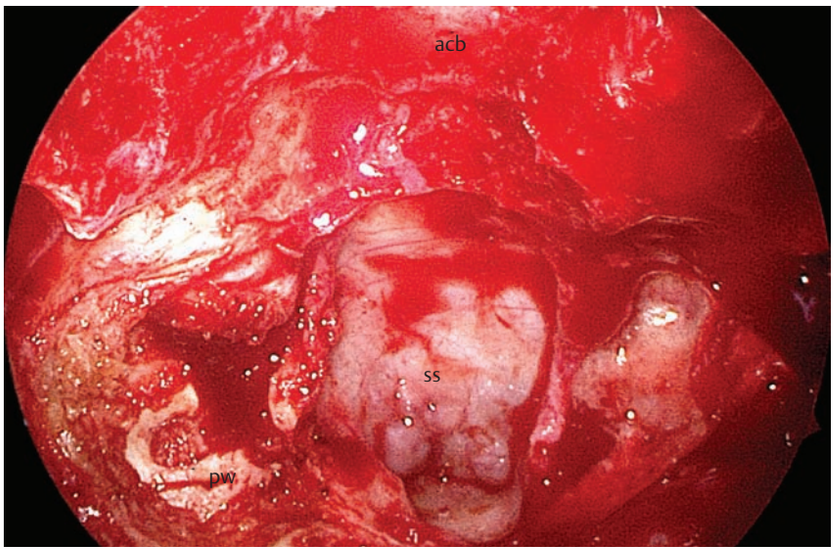

Fig. 9.110 Complete exposure over the cavernous sinus on the right side. acb, anterior cranial base; pw, pterygoid wedge; ss, sphenoid sinus.

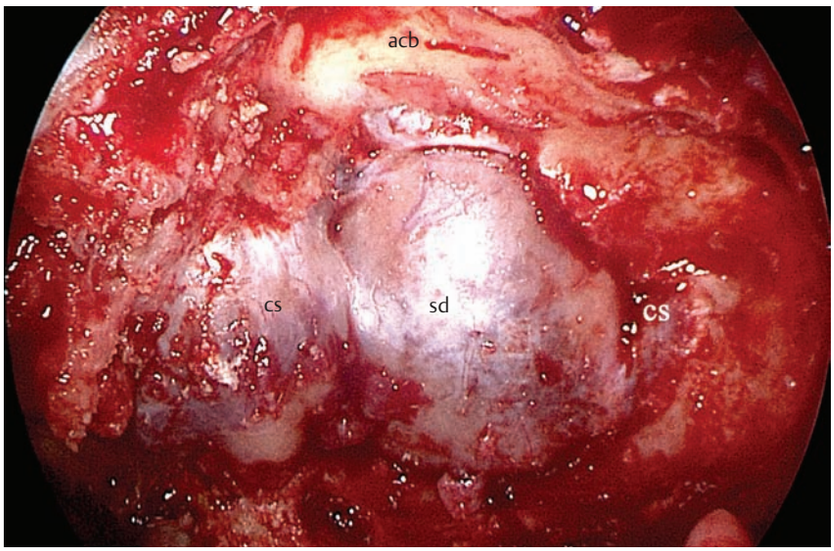

Fig. 9.111 Exposure of the dura over the sellar and cavernous region. acb, anterior cranial base; cs, cavernous sinus; sd, sella dura.

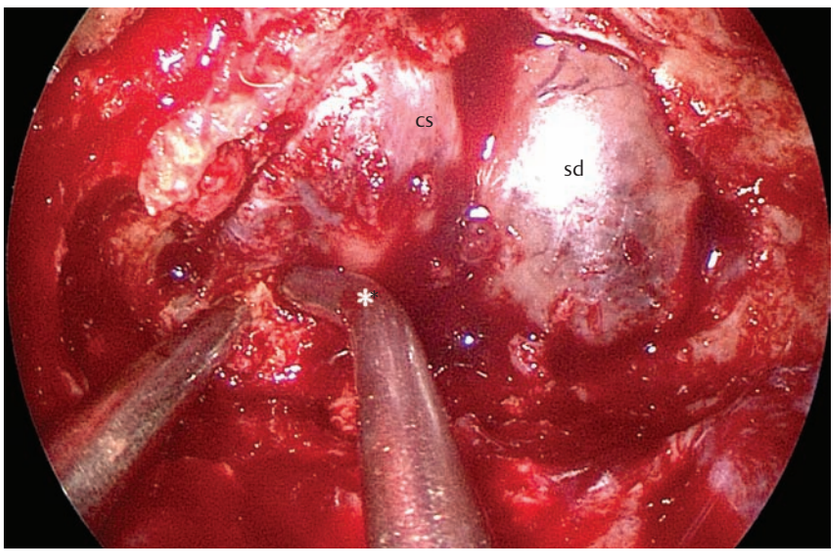

Fig. 9.112 Micro-Doppler is used to ascertain the course of the internal carotid artery. acb, anterior cranial base; cs, cavernous sinus; sd, sella dura.

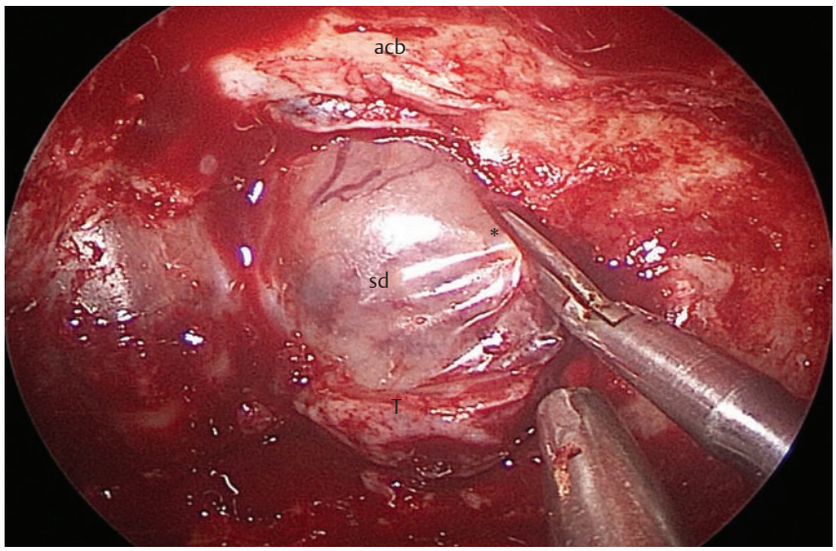

Fig. 9.113 Dural incision given. acb, anterior cranial base; T, tumor; sd, sella dura.

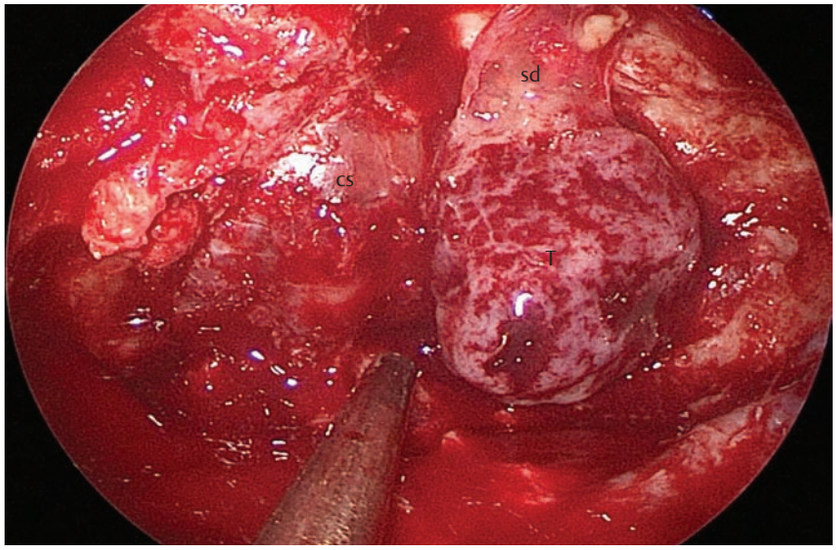

Fig. 9.114 **U**-shaped dural flap elevated and tumor exposed in the sellar cavity. cs, cavernous sinus; sd, sellar dura; T, tumor.

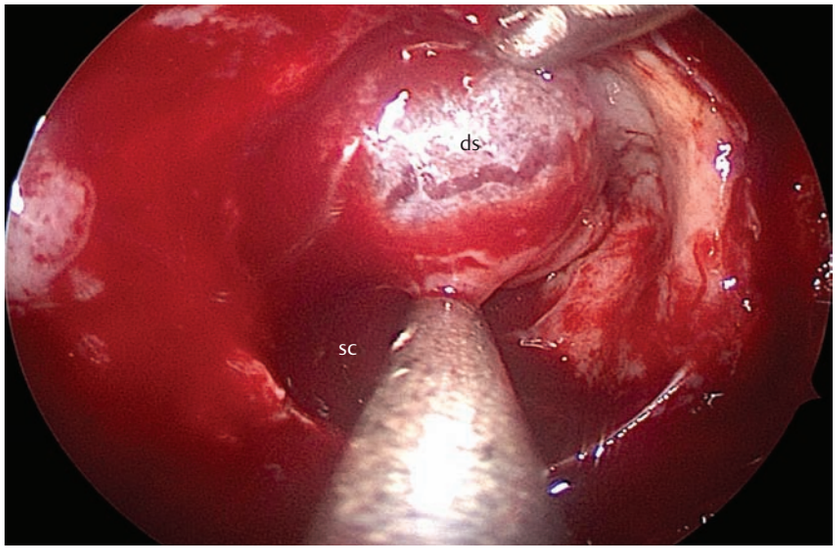

Fig. 9.115 Tumor clearance from the sellar cavity. ds, diaphragm sella; sc, sellar cavity.

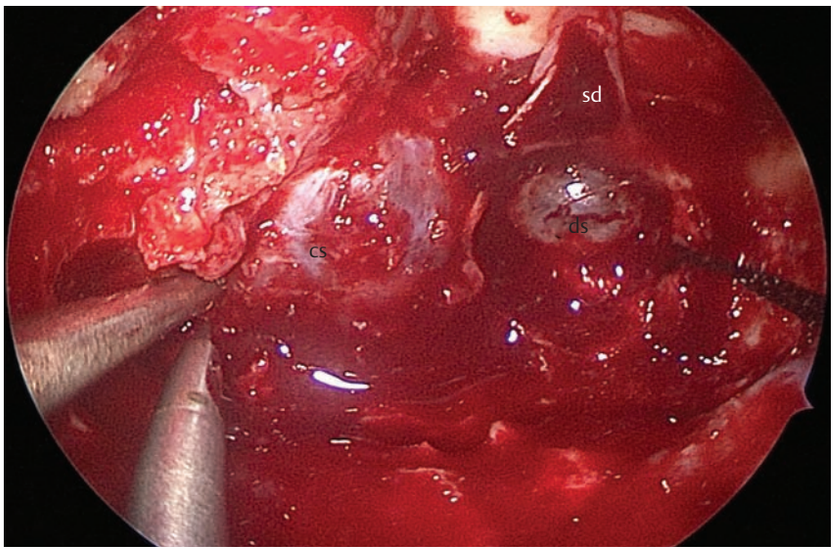

Fig. 9.116 Incision over cavernous sinus dura. cs, cavernous sinus; ds, diaphragm sella; sd, sellar dura.

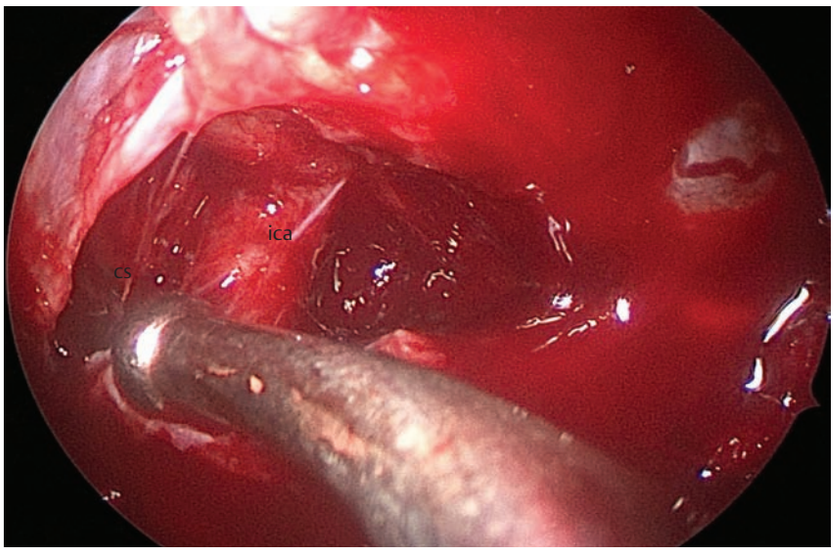

Fig. 9.117 RT cavernous sinus exposed and the tumor is dissected medial and anterior to the internal carotid artery. cs, cavernous sinus; ica, internal carotid artery.

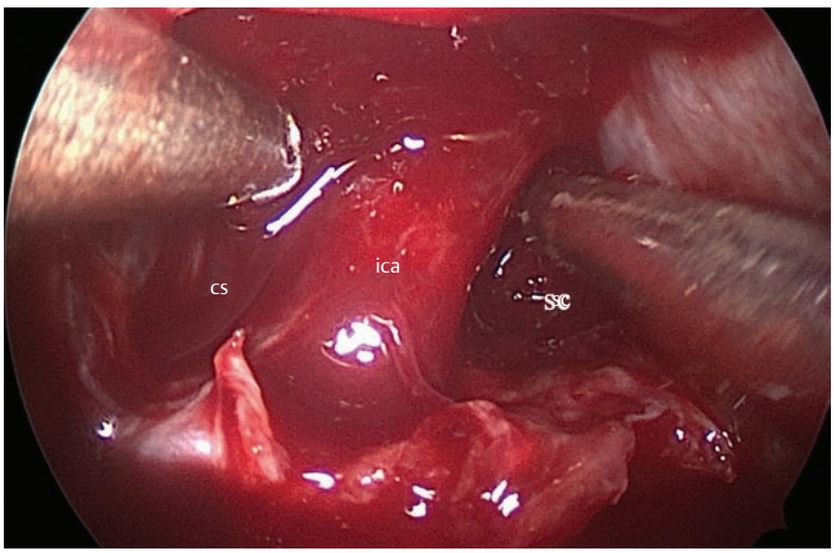

Fig. 9.118 Tumor cleared lateral and in the retrogenu area to internal carotid artery. cs, cavernous sinus; ica, internal carotid artery; sc, sellar cavity.

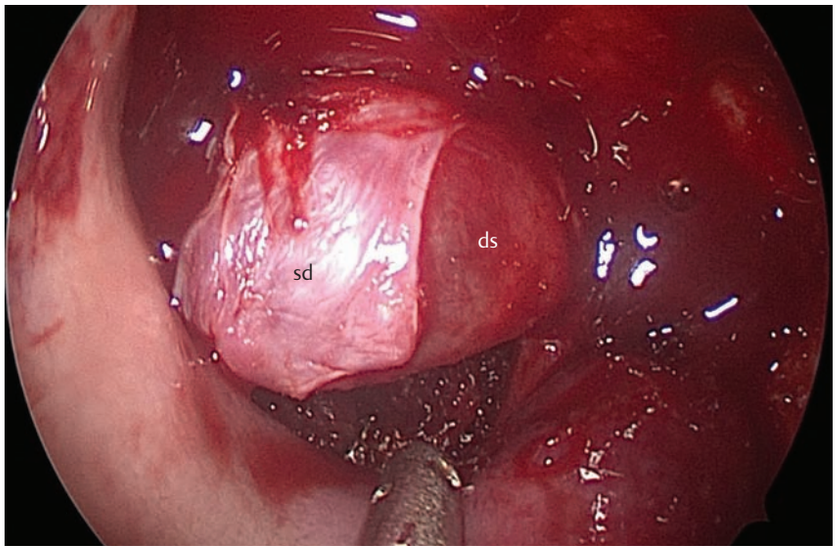

Fig. 9.119 Complete tumor removal. ds, diaphragm sella; sd, sellar dura.

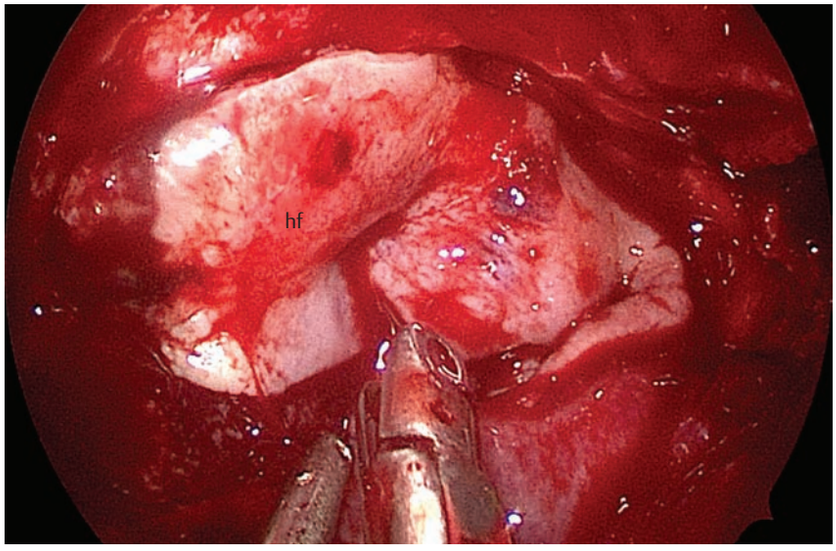

Fig. 9.120 Closure with nasoseptal flap. hf, Hadad flap.

Case 9: Pituitary Macroadenoma (Suprasellar and Parasellar Extension)

A 50-year-old woman presented with a history of headache, progressive loss of vision and sixth nerve paresis on the left side since 6 months. Further evaluation with the MRI showed pituitary lesion extending into the parasellar region (Grade 4 on modified Knosp classification) with suprasellar extension (**Fig. 9.121**). Transsphenoidal and transpterygoid approaches were planned. **Fig. 9.122** shows the sphenoid sinus exposure after the nasal phase. A wide pituitary exposure was achieved and sphenoid mucosa removed (**Fig. 9.123**), after which, wide middle meatal antrostomy was carried out to expose the posterior wall of the maxillary sinus. S3 neurodrill was used to thin out the posterior wall of the maxillary sinus and removed using an elevator. The internal maxillary artery was identified and clipped (**Fig. 9.124**). The pterygoid fossa contents were exposed and coagulated. The pterygoid wedge was drilled out to identify the vidian nerve and V2 and this provided a wide exposure to CS (**Figs. 9.125 and 9.126**). Sellar bone was eggshell thinned out and removed exposing the sellar dura. Extracapsular dissection was commenced (**Fig. 9.127**). With meticulous dissection, tumor was cleared from the sellar cavity and the CS (**Fig. 9.128**). The tumor clearance from the CS triangle is seen (**Fig. 9.129**). The tumor was seen engulfing the carotid; transposition of the ICA was performed to clear the tumor from the retrogene area and medial petrous part (**Fig. 9.130**). Postoperative MRI taken 72-hours postprocedure showed total tumor removal (**Fig. 9.131**).

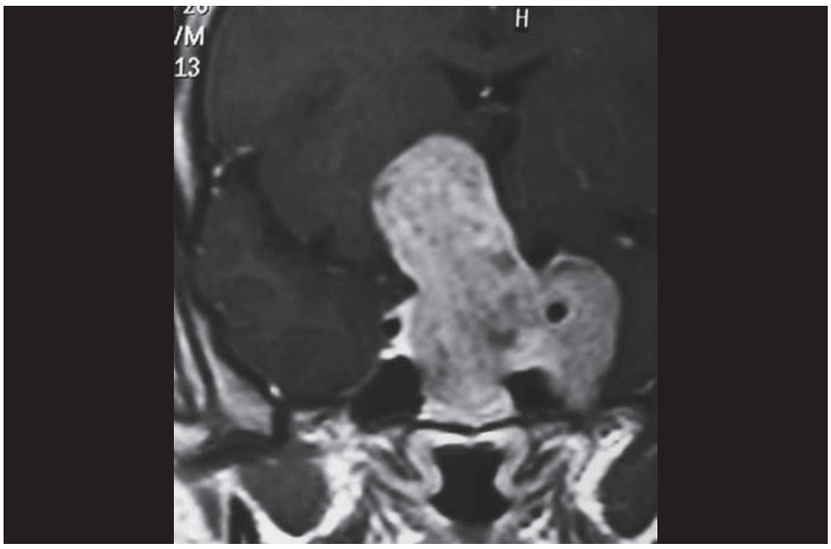

Fig. 9.121a MRI post contrast T1 image sequence showing pituitary macroadenoma with giant parasellar and suprasellar extension with encasing carotid artery.

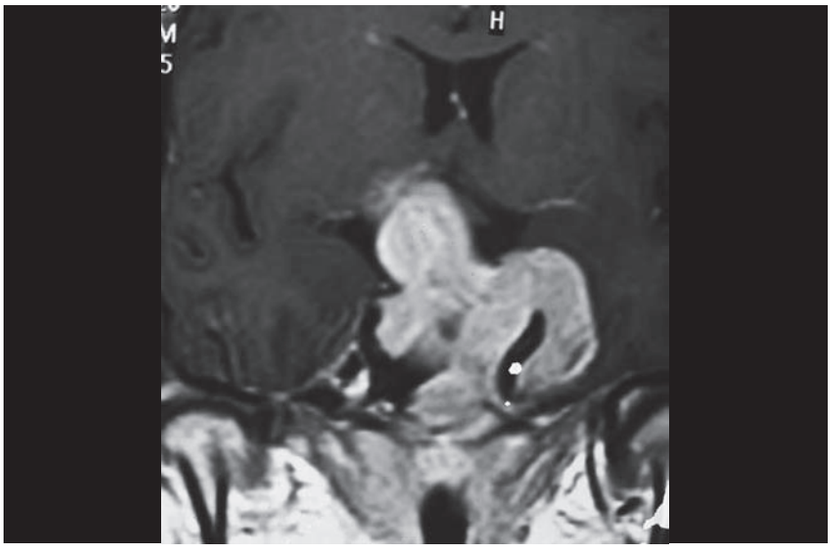

Fig. 9.121b MRI post contrast T1 image sequence showing pituitary macroadenoma with giant parasellar and suprasellar extension with encasing carotid artery.

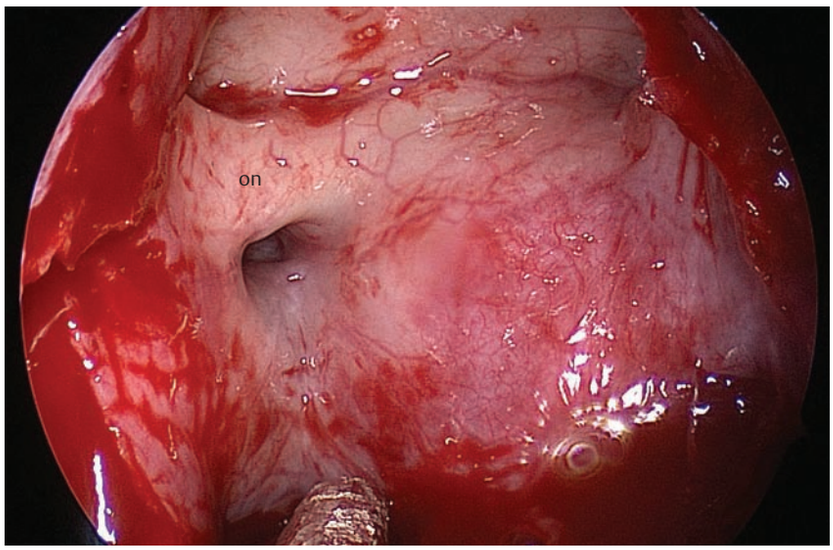

Fig. 9.122 Sphenoid sinus exposure. ON, optic nerve; ss, sphenoid sinus.

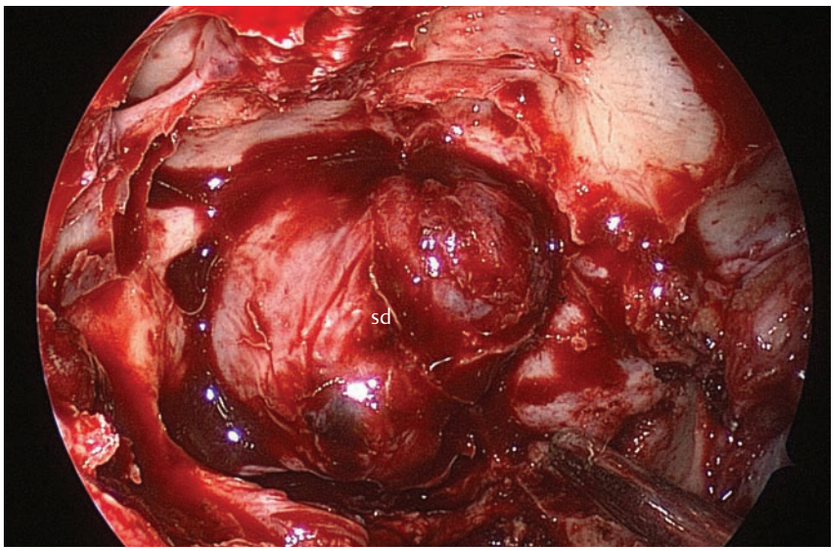

Fig. 9.123 Endoscopic image shows wide sellar exposure. sd, sellar dura.

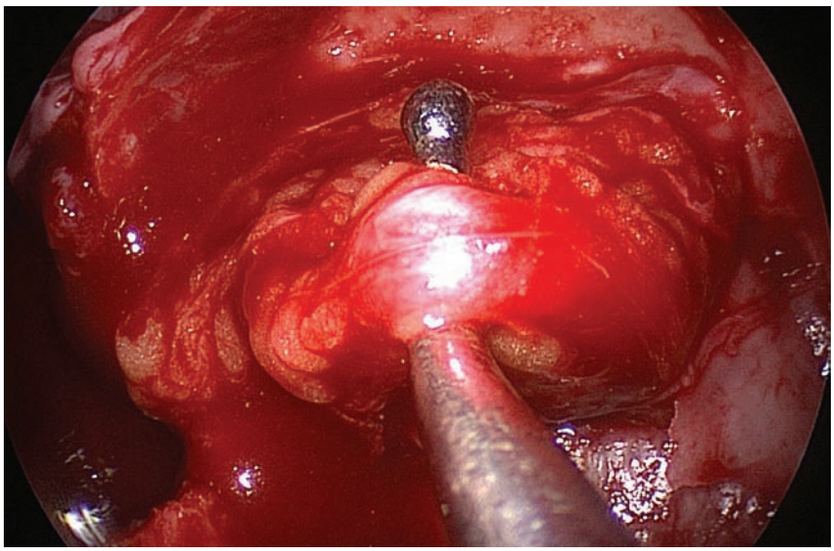

Fig. 9.124 Transpterygoid approach, posterior wall of maxillary is removed, showing clipping of internal maxillary artery.

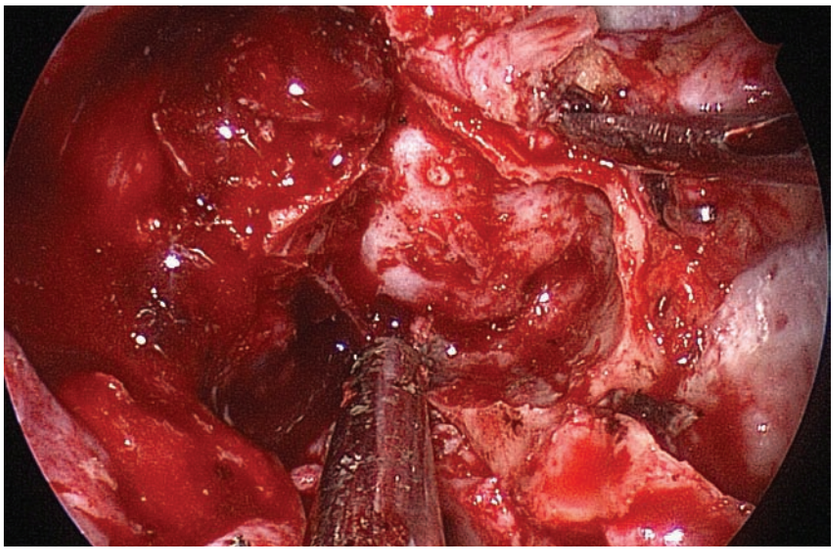

Fig. 9.125 Exposure of the vidian and V2. The suction tip and elevator show the position of the vidian nerve and V2.

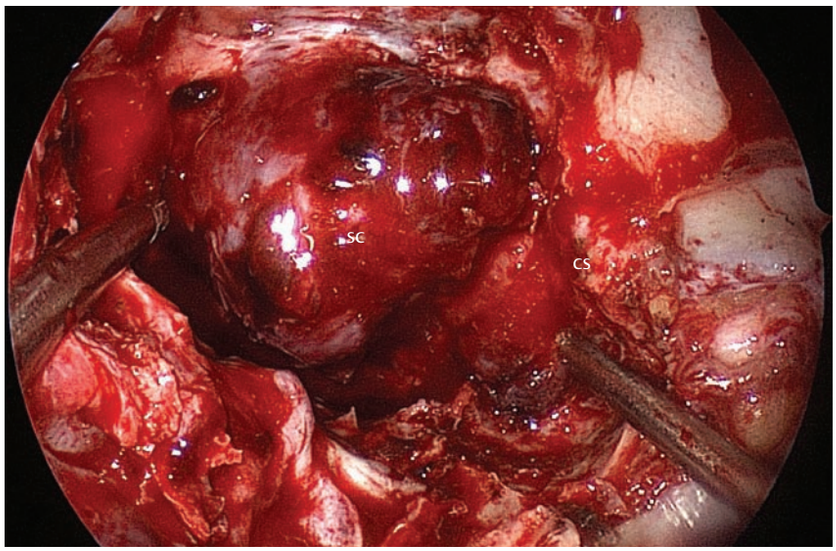

Fig. 9.126 Exposure beyond cavernous sinus. cs, cavernous sinus; sc, sellar cavity.

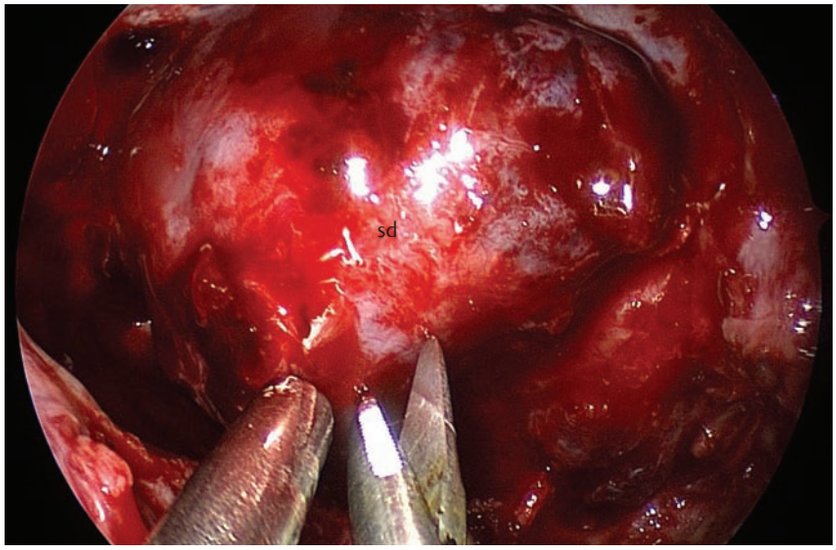

Fig. 9.127 Extracapsular dissection of the pituitary tumor. sd, sellar dura.

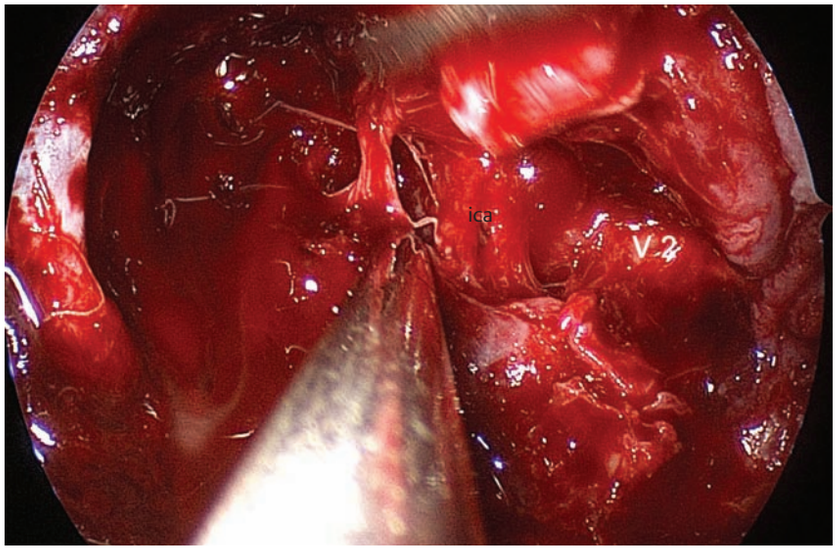

Fig. 9.128 Cavernous sinus dissection. ica, internal carotid artery; V2, maxillary nerve.

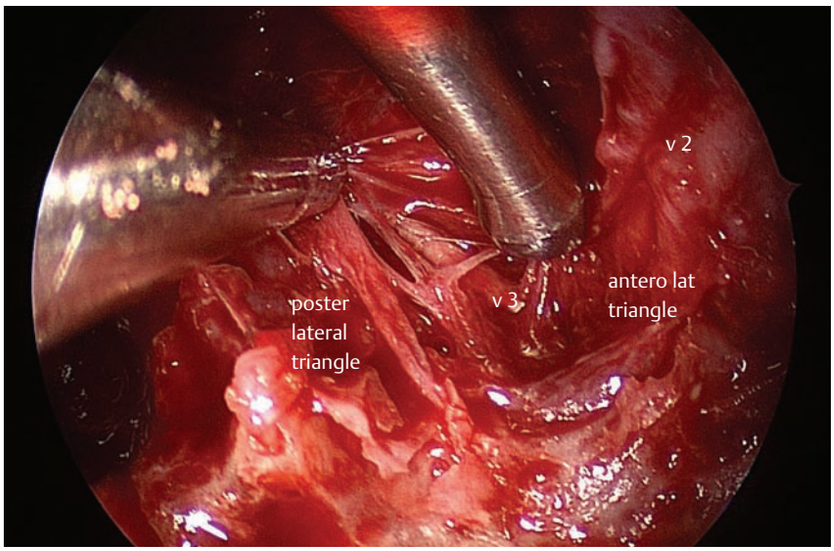

Fig. 9.129 Cavernous sinus triangle clearance. ica, internal carotid artery.

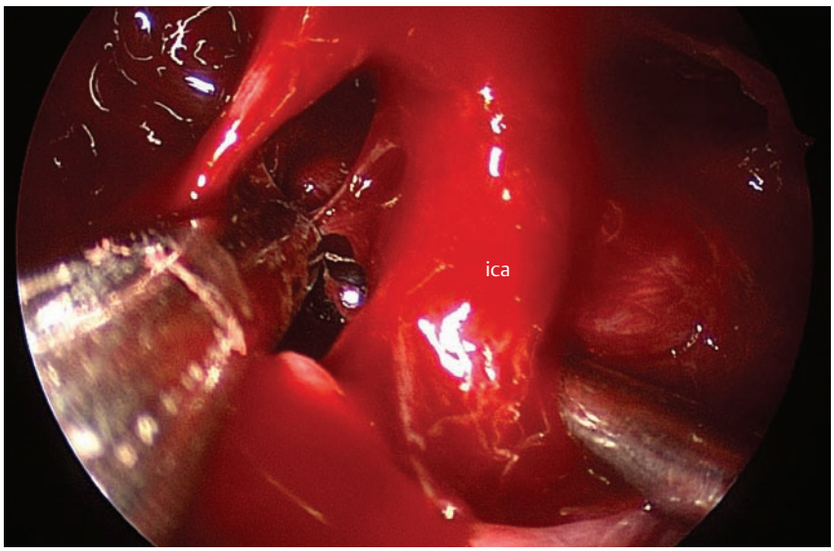

Fig. 9.130 Transposition of the internal carotid artery to clear the tumor from the medial petrous part. ica, internal carotid artery.

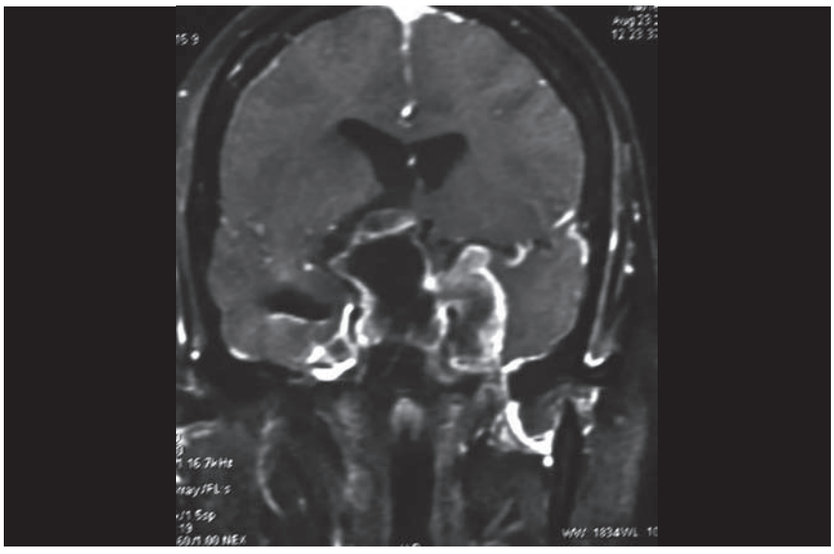

Fig. 9.131 Postoperative MRI showing complete removal of the tumor.

Case 10: Acinic Cell Carcinoma of the Cavernous Sinus

It is one of the rare tumors of the CS, usually, caused by metastatic spread from minor salivary glands tumors.

A 43-year-old patient presented with complaints of double vision due to the involvement of the sixth nerve in the CS. The MRI T2 sequence showed the tumor involving the CS on the left side (**Fig. 9.132**). The extended endonasal approach was planned. **Fig. 9.133** showing the wide exposure was attained after completing the nasal and sphenoid phase, following which, exposure of the sellar dura was done (**Figs. 9.134 and 9.135**). The course of the ICA was mapped using the micro-Doppler (**Fig. 9.136**). The dural incision was given where maximum bulge of the tumor was felt. In this case, tumor had pushed the ICA posteriorly (**Fig. 9.137**). Once the dural flap was elevated, the tumor biopsy is taken (**Fig. 9.138**). Careful and meticulous dissection of the left CS was performed and complete tumor clearance was achieved (**Figs. 9.139–9.141**).

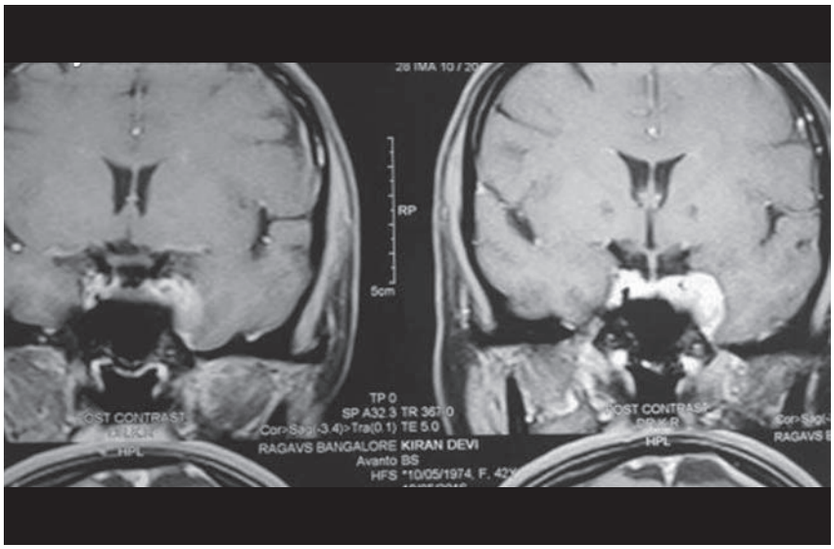

Fig. 9.132 MRI postcontrast showing enhanced hyperintense lesion in the left cavernous sinus.

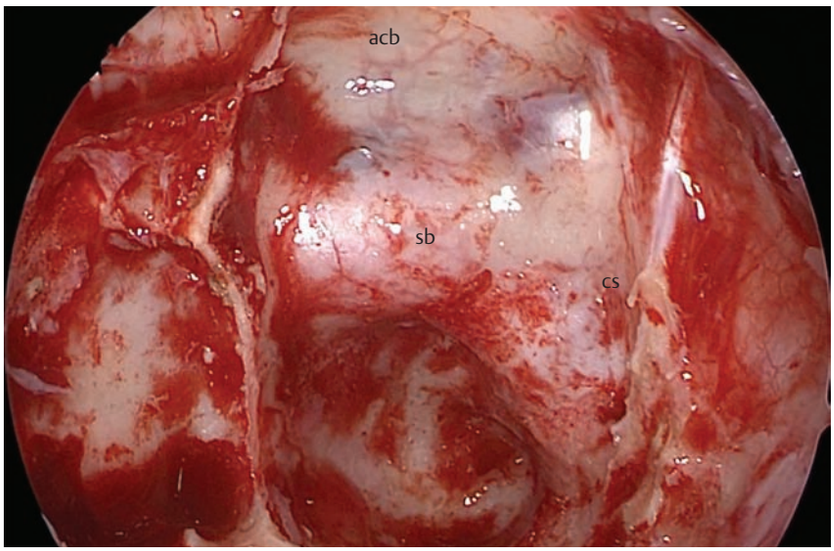

Fig. 9.133 Wide exposure postsphenoid phase. acb, anterior cranial base; cs, cavernous sinus; sb, sellar bone.

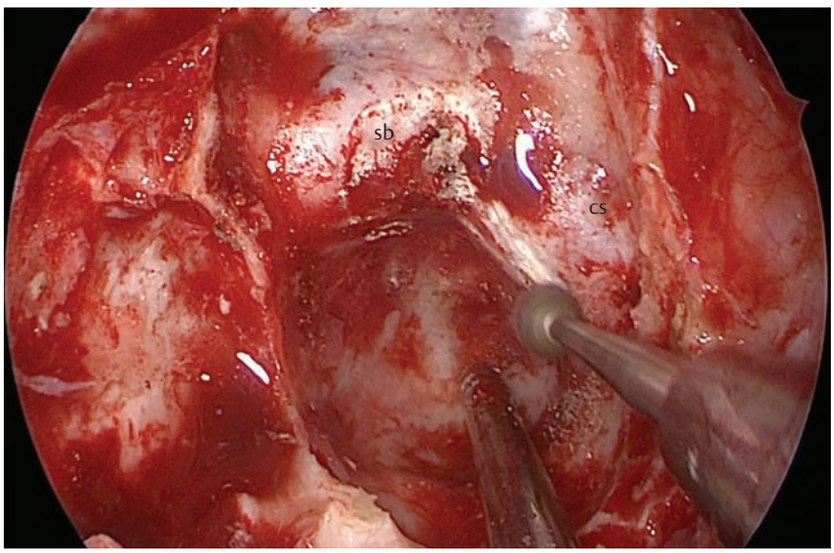

Fig. 9.134 Drilling the sellar bone and the bone covering left cavernous sinus. cs, cavernous sinus; sb, sellar bone.

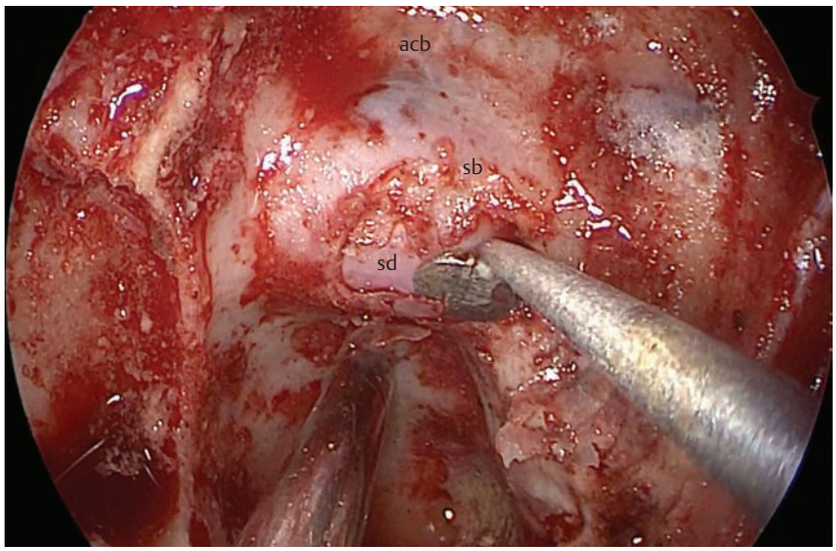

Fig. 9.135 Sellar bone removal to expose sellar dura using Rosen's elevator. acb, anterior cranial base; sb, sellar bone; sd, sellar dura.

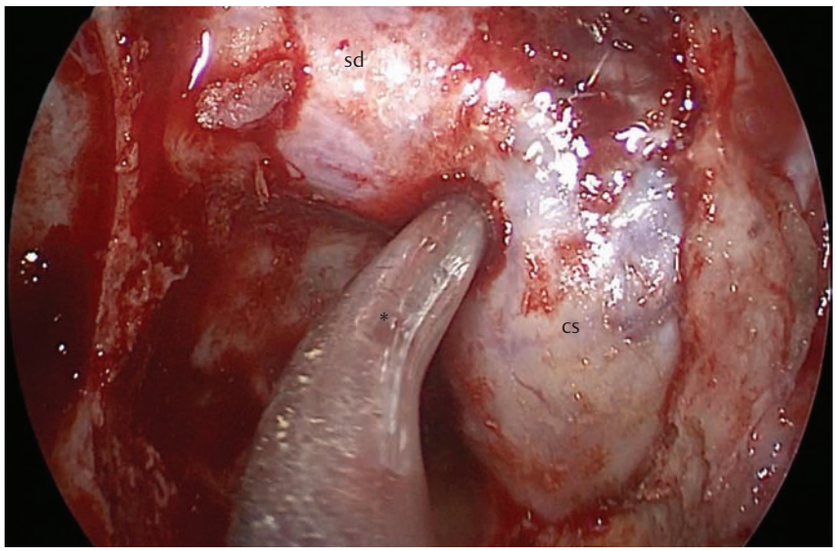

Fig. 9.136 Mapping the course of the cavernous internal carotid artery. cs, cavernous sinus; sd, sellar dura; *, micro-Doppler.

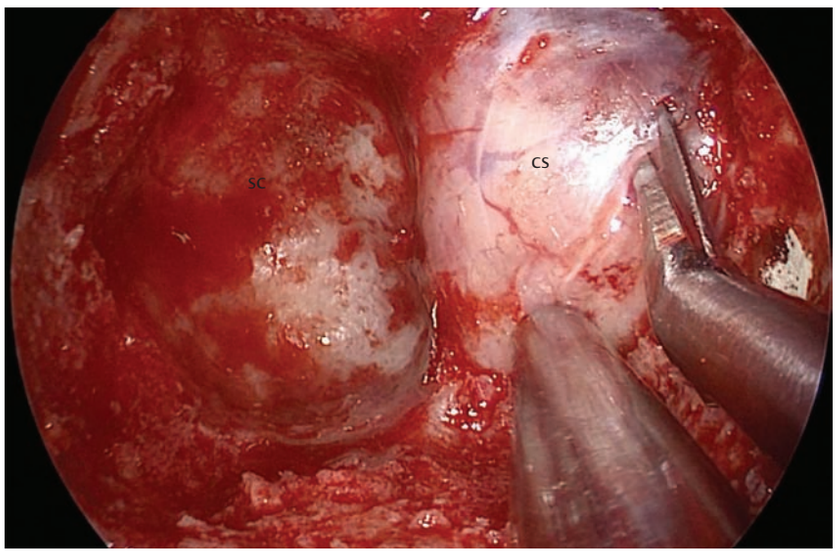

Fig. 9.137 Dural incision over the left cavernous sinus using Cappabianca knife. cs, cavernous sinus; sc, sellar cavity.

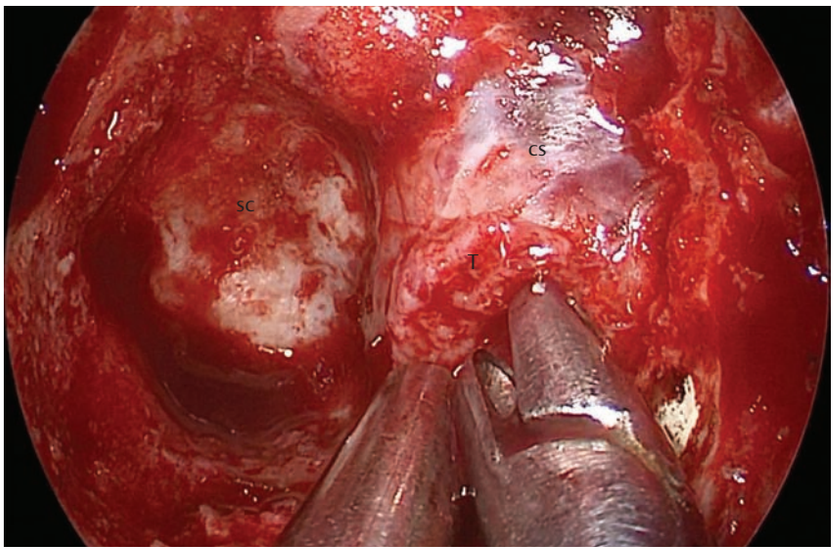

Fig. 9.138 Dural flap elevated, tumor exposed, and a biopsy taken. cs, cavernous sinus; sc, sellar cavity; T, tumor.

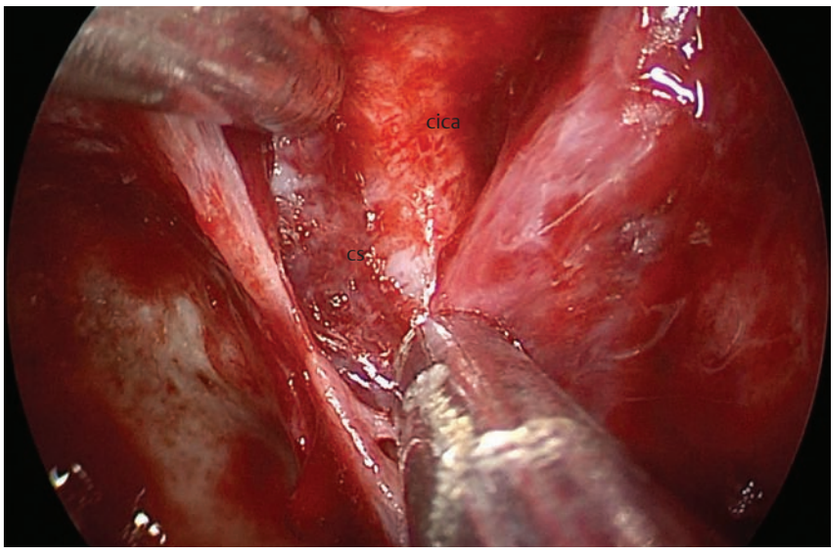

Fig. 9.139 Left cavernous sinus exposed; cica, cavernous internal carotid artery. cs, cavernous sinus.

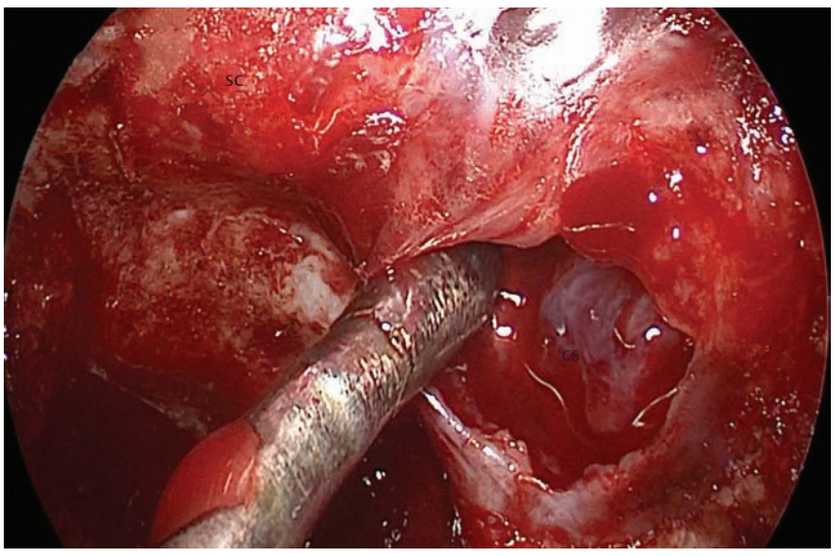

Fig. 9.140 Left cavernous sinus dissection. cs, cavernous sinus; sc, sellar cavity.

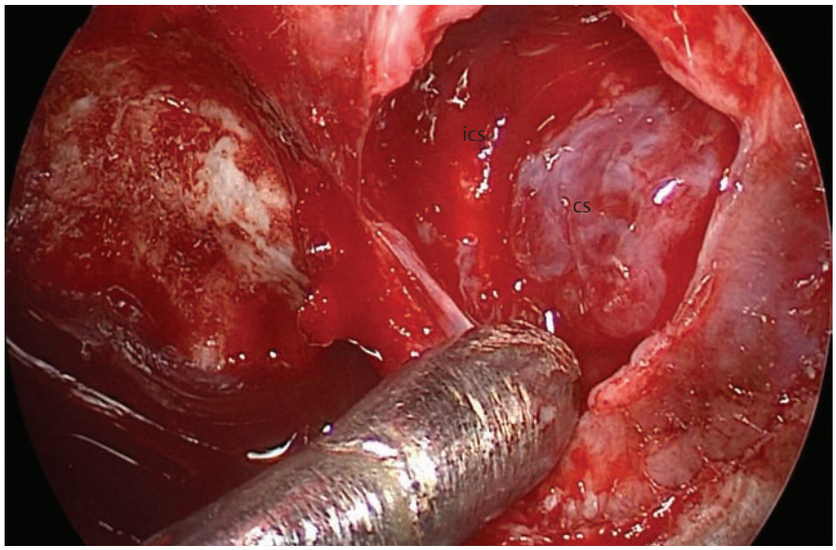

Fig. 9.141 Tumor cleared from the left cavernous sinus. cs, cavernous sinus; ica, internal carotid artery.

Case 11: Cavernous Hemangioma

Cavernous sinus hemangiomas (CSHs) are rare, vascular, extra-axial tumors. They encase the cavernous segment of the ICA, making surgical resection challenging. CSH causes local mass effect within the CS, leading to cranial nerve deficits. In this case, MRI scan of the brain demonstrated an extra-axial right parasellar mass. The lesion was iso- to hyperintense on T2-weighted imaging with heterogeneous enhancement after contrast administration (**Fig. 9.142**). The nasal phase was concluded at the end of medial maxillectomy to expose the posterior wall of the maxilla (**Fig. 9.143**). Following exposure of pterygopalatine fossa and lateral wall of the sphenoid sinus, DPA and SPA were identified and coblated (**Figs. 9.143 and 9.144**). This was followed by drilling of the pterygoid wedge and exposure of its contents along with the identification of vidian nerve. Drilling the bone over the anterior wall of CS and the removal of eggshell-thinned bone using the Rosen's elevator was done to expose the tumor (**Fig. 9.144**). Navigation and micro-Doppler were used to map the course of the ICA. In this instance, the tumor was present in the anteroinferior triangle pushing the carotid artery posteriorly. The cranial nerves were pushed laterally (**Fig. 9.145**). The dural incision was placed lateral to the vidian nerve, which is the safe zone. The endosteal layer of the dura reflected upward and **U**-shaped flap was raised (**Fig. 9.146**). Careful and gentle dissection of the tumor was carried out using suction and elevator. Fibrous attachment to the surrounding tissues was dissected by sharp dissection (**Fig. 9.147**). The tumor was separated from the cavernous and clinoidal ICA (**Figs. 9.148 and 9.149**). The tumor was removed in toto, and the defect was closed using Hadad flap (**Fig. 9.150**). See **Video 9.6**.

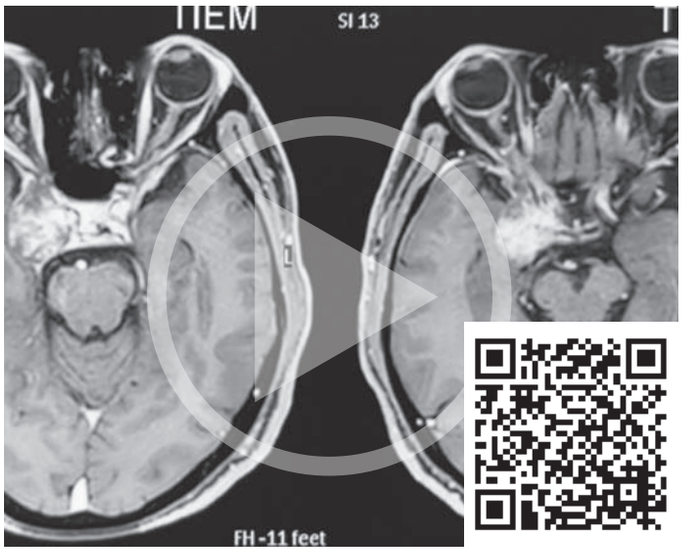

Video 9.6 Cavernous hemangioma: Cavernous sinus. https://www.thieme.de/de/q.htm?p=opn/cs/19/9/10104317-ac939ed0

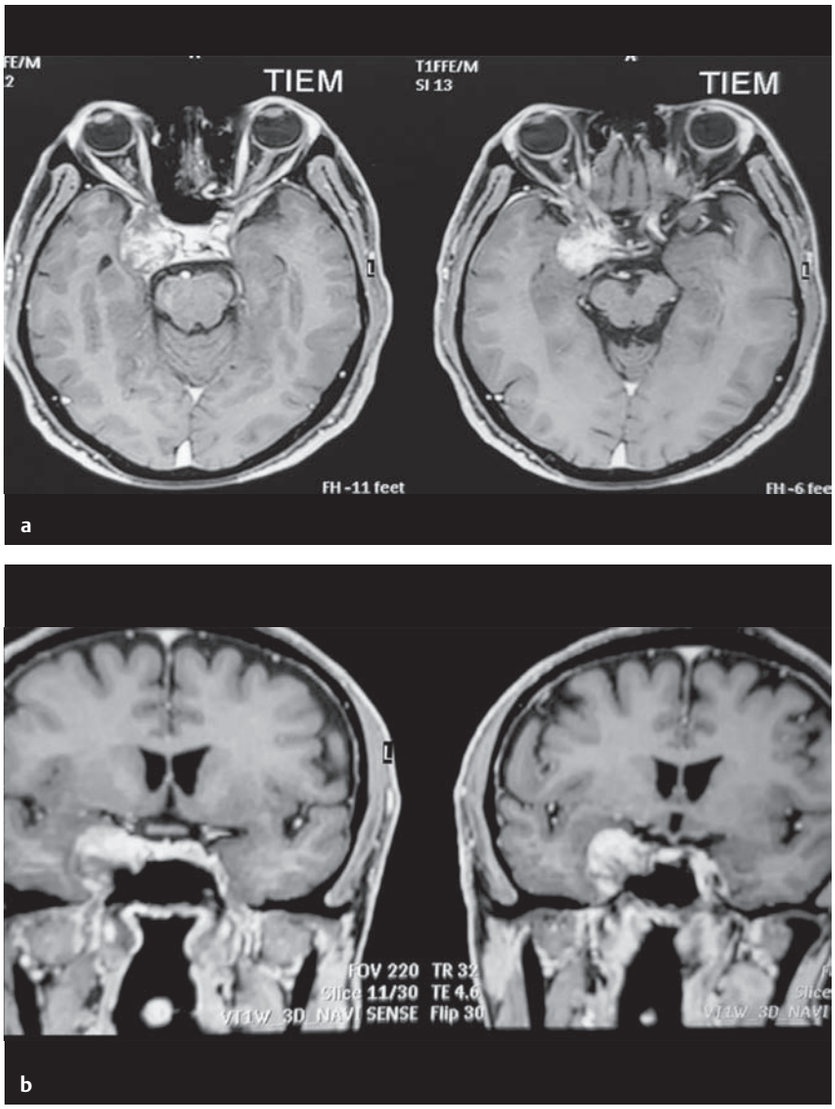

Fig. 9.142 **(a, b)** MRI sequence showing the tumor in the cavernous sinus on the right side.

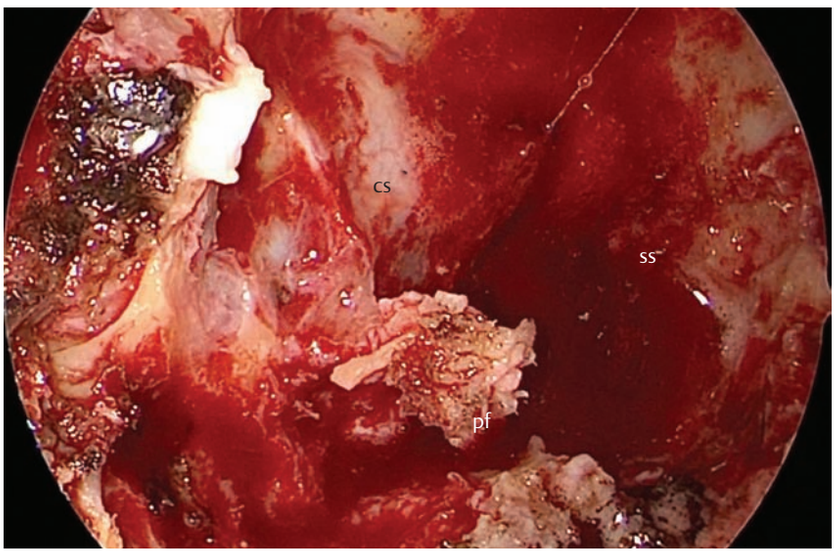

Fig. 9.143 Endoscopic picture showing the transpterygoid approach to the cavernous sinus. cs, cavernous sinus; pf, pterygoid fossa; ss, sphenoid sinus.

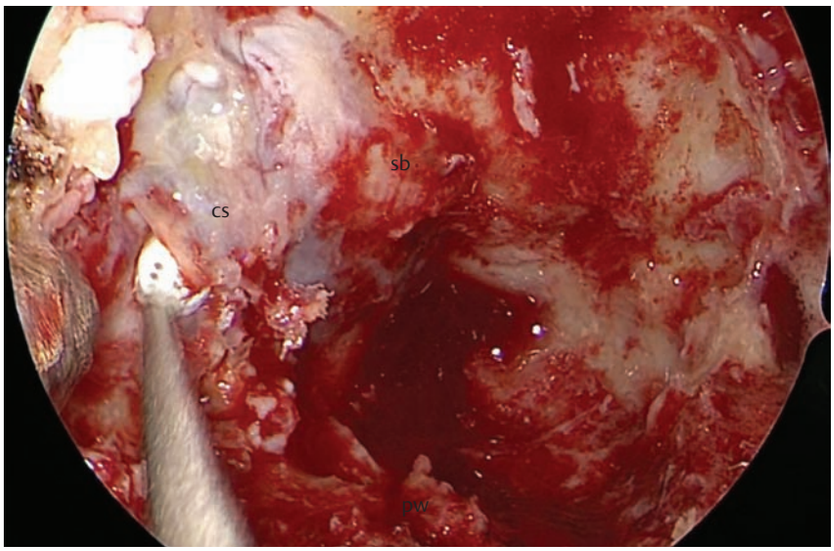

Fig. 9.144 Wide exposure of the right cavernous sinus and gentle elevation of the bone. cs, cavernous sinus; pw, pterygoid wedge; sb, sellar bone.

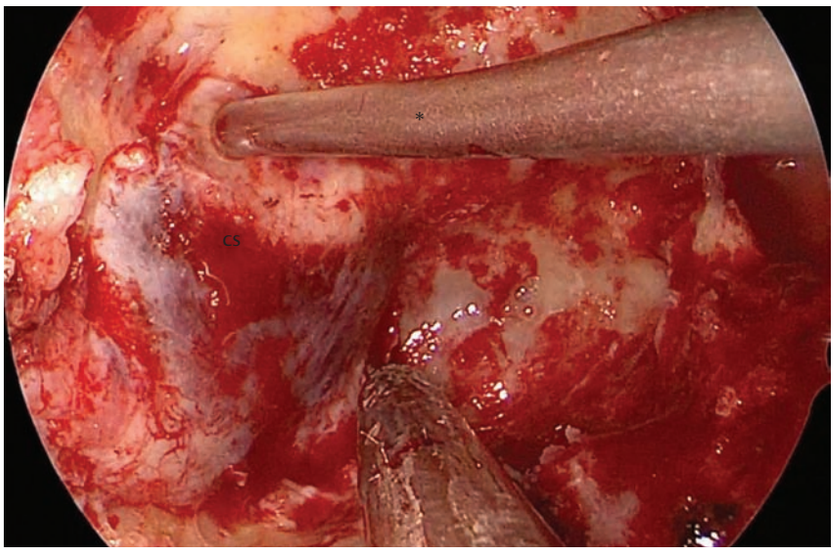

Fig. 9.145a Endoscopic picture showing the precise location of internal carotid artery. cs, cavernous sinus; *, micro-Doppler.

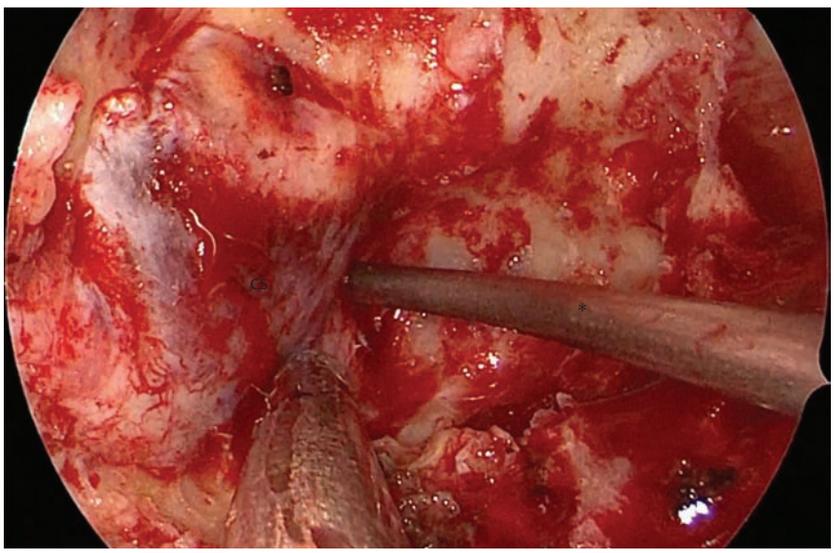

Fig. 9.145b Endoscopic picture showing the precise location of internal carotid artery. cs, cavernous sinus; *, micro-Doppler.

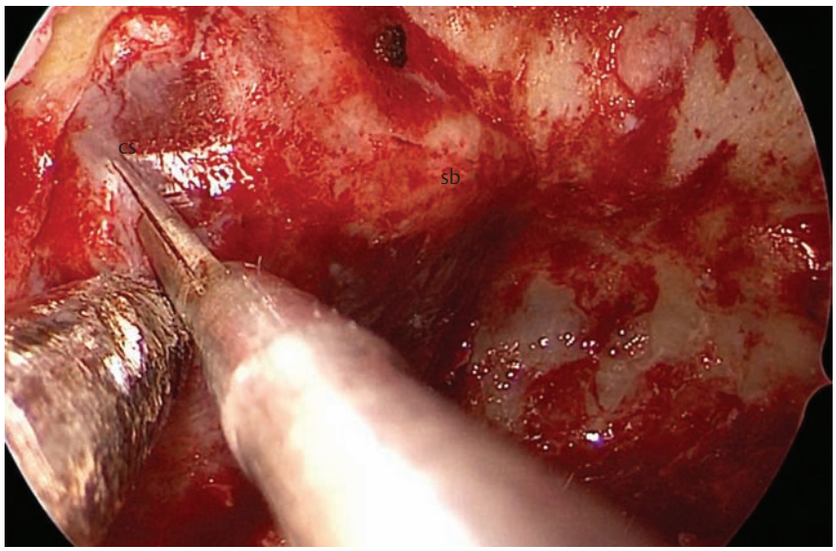

Fig. 9.146 Dural incision is been given using Cappabianca knife. cs, cavernous sinus; sb, sellar bone.

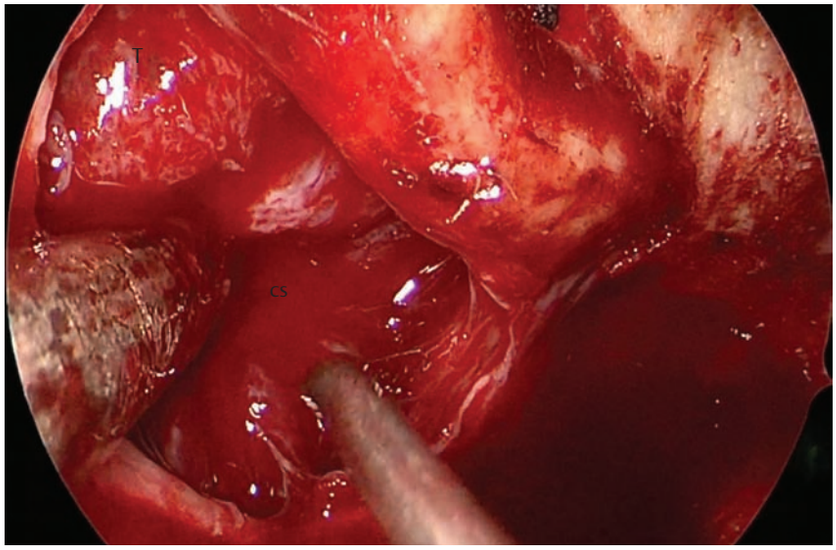

Fig. 9.147 Endoscopic picture showing meticulous dissection of the tumor in the right cavernous sinus. cs, cavernous sinus; T, tumor.

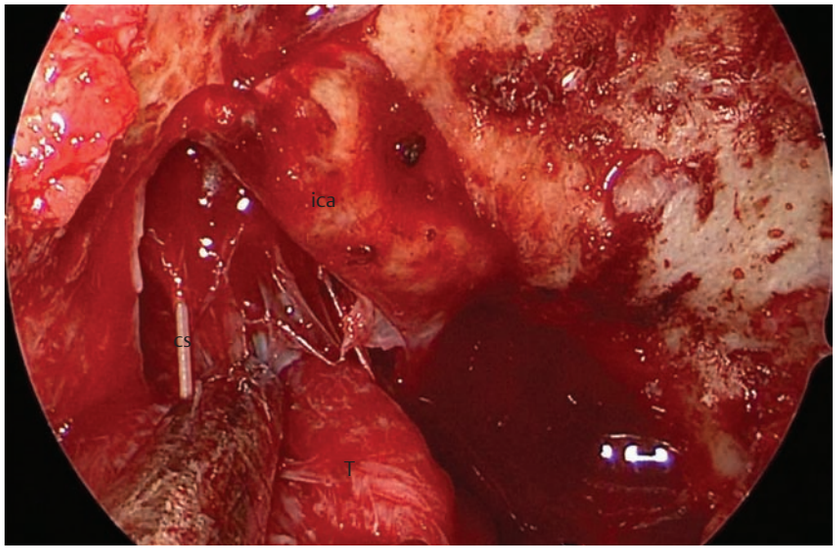

Fig. 9.148 Dissection of the tumor from the suspensory ligaments of cavernous sinus. cs, cavernous sinus; ica, internal carotid artery; T, tumor.

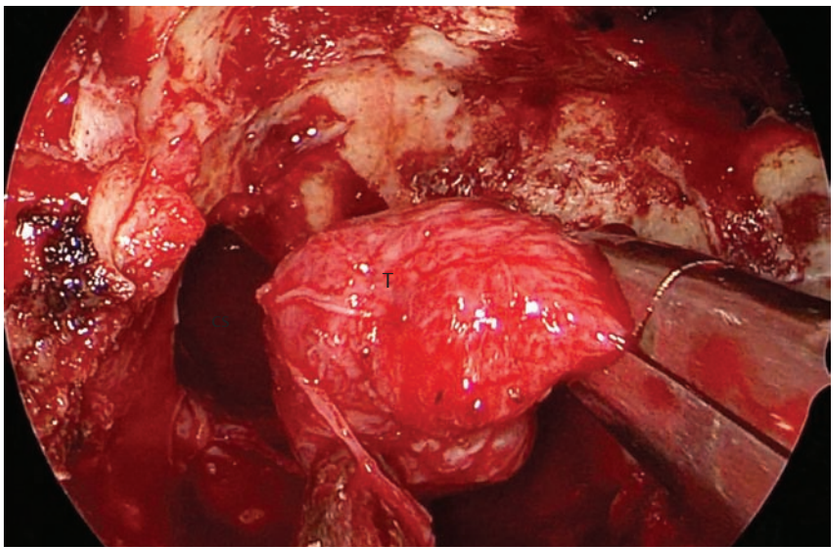

Fig. 9.149 Endoscopic picture showing dissected tumor. cs, cavernous sinus; T, tumor.

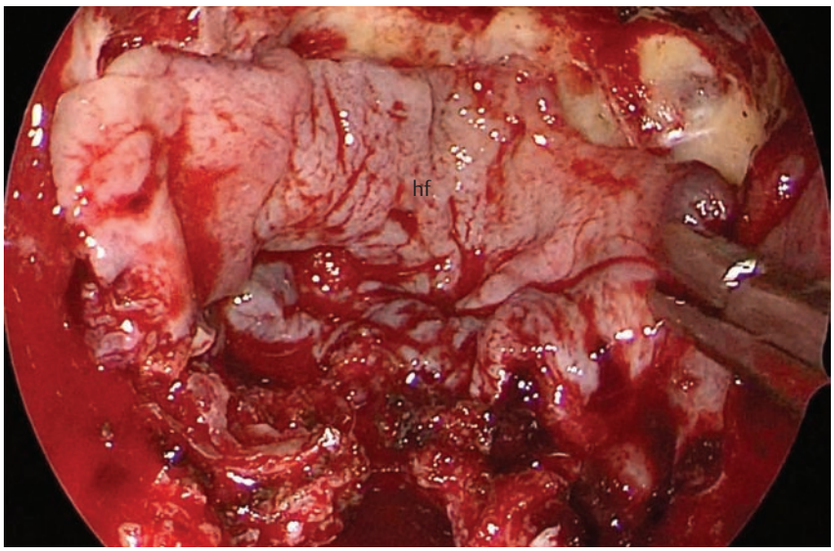

Fig. 9.150 Reconstruction of the skull base defect by a vascularized pedicle flap. Hf, Hadad flap.

Case 12: Cavernous Sinus Meningioma

Parasellar and CS meningiomas require an aggressive surgical approach for cranial nerve decompression either by bony decompression or dural decompression. The main goal of the surgery was tumor debulking and reduce the overall size of the tumor, which will be amenable to radiotherapy. The main steps followed in the endoscopic approach are as described below.

Fig. 9.151 describes the imaging study of the tumor showing involvement of the CS and parasellar area.

The nasal, sphenoid, and pterygoid phase was performed to give wide exposure of the sella and CS (**Fig. 9.152**).

Sellar bone was eggshell-thinned out using the S3 neurodrill system, bone elevated using Rosen's elevator to expose the dura (**Figs. 9.153 and 9.154**). Once the exposure was attained, the course of the carotids was mapped using micro-Doppler (**Fig. 9.155**). Dural incision was placed lateral to the vidian nerve (**Fig. 9.156**). Tumor was exposed and meticulous dissection was carried out in the CS. Tumor was cleared from the CS (**Figs. 9.157 and 9.158**). CS dissection after tumor removal is shown (**Fig. 9.159**).

JNA with Cavernous Extension

In author's experience, the common secondary pathologies involving the parasellar area are either of infective origin like invasive fungal sinusitis or tumors like juvenile nasopharyngeal angiofibroma. The following case illustrations are of JNA involving the CS classified as stage III (Janakiram staging).

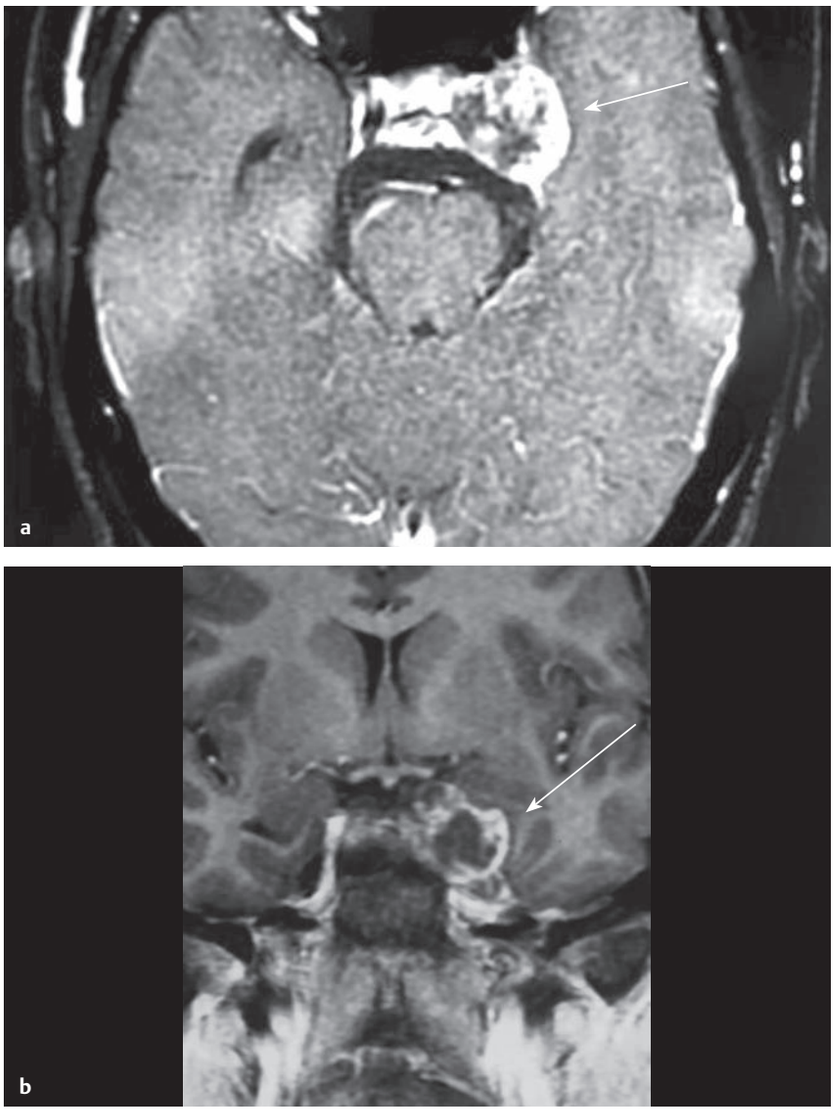

Fig. 9.151 **(a, b)** MRI sequence showing meningioma in the cavernous sinus.

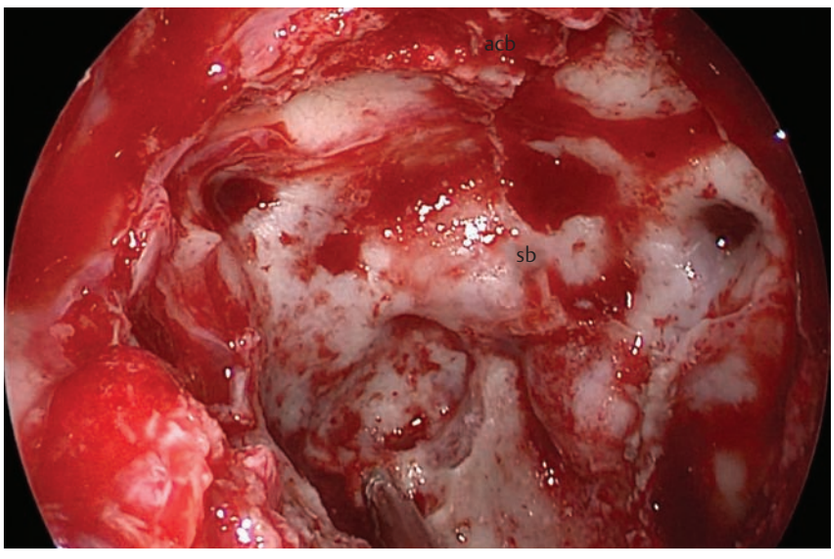

Fig. 9.152 Endoscopic view showing wide sellar exposure. acb, anterior cranial base; sb, sellar bone.

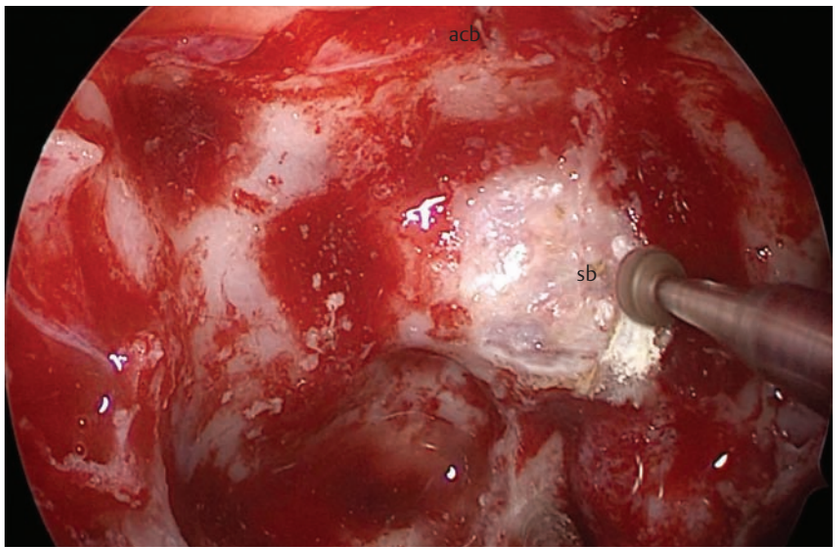

Fig. 9.153 Drilling of the sellar bone using S3 neuro drill. acb, anterior cranial base; sb, sellar bone.

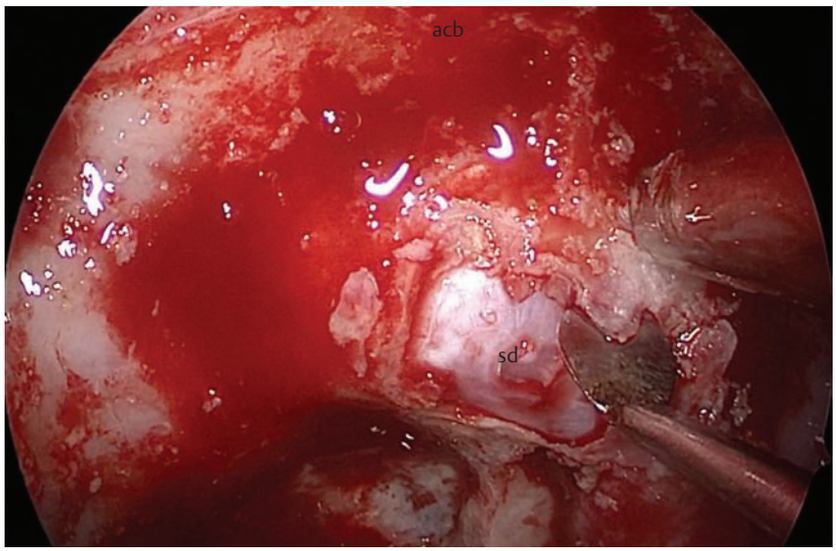

Fig. 9.154 Thinned-out sellar bone elevated using the Rosen's knife. acb, anterior cranial base; sd, sellar dura.

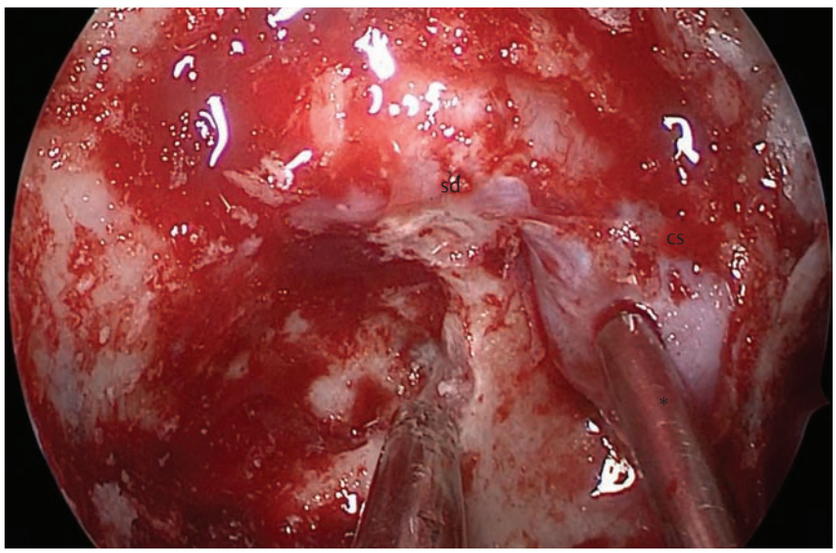

Fig. 9.155 Internal carotid artery course is mapped using the micro-Doppler. cs, cavernous sinus; sd, sellar dura; *, micro-Doppler.

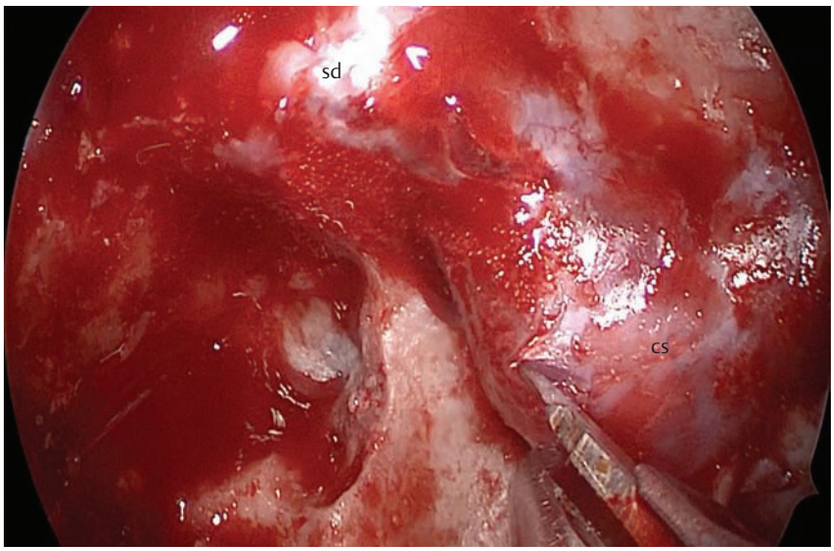

Fig. 9.156 Dural incision given over the cavernous sinus dura from lateral to medial. cs, cavernous sinus; sd, sellar dura.

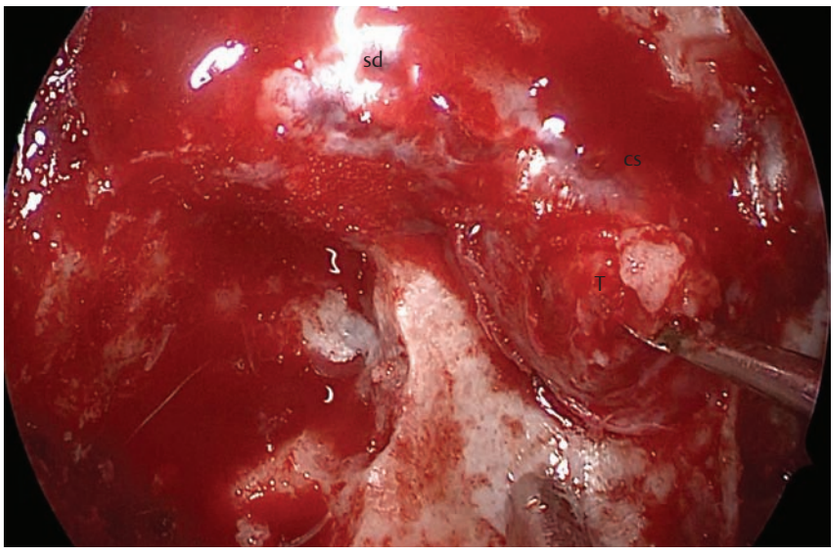

Fig. 9.157 **U**-shaped dural flap elevated exposing the tumor. cs, cavernous sinus; sd, sellar dura; T, tumor.

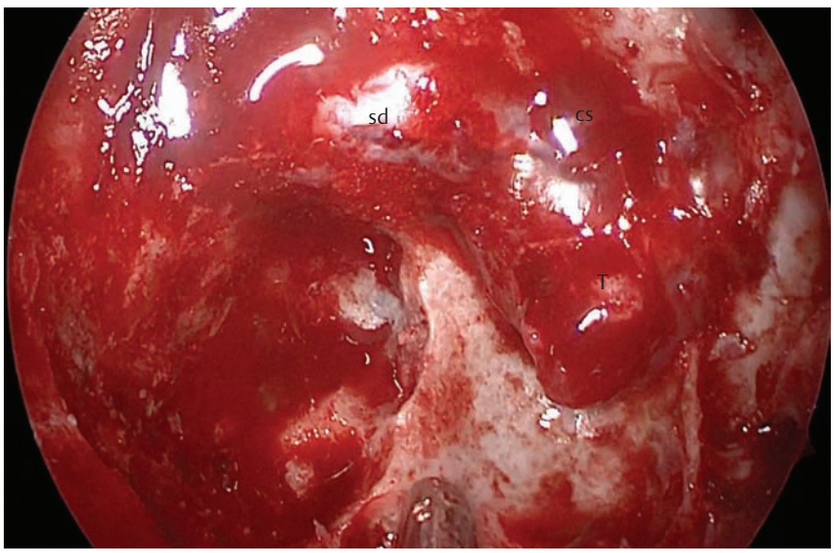

Fig. 9.158 Tumor dissection in the cavernous sinus. cs, cavernous sinus; sd, sellar dura; T, tumor.

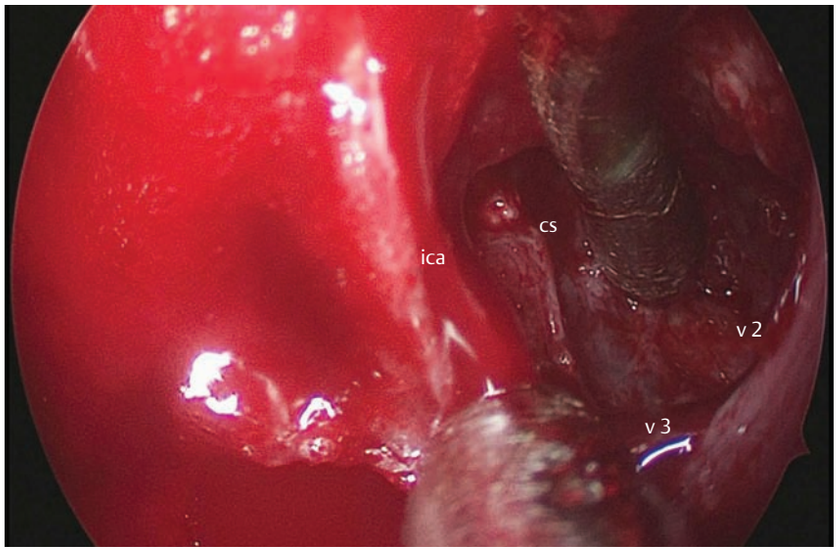

Fig. 9.159 Cavernous sinus after tumor removal. cs, cavernous sinus; ica, internal carotid artery; V2, maxillary nerve; V3, mandibular nerve.

Case 13: Involving Medial Cavernous Sinus

In this scenario, the preoperative scan showed the involvement of the CS. The principle of the segmental resection is followed and tumor anterior to the left CS is resected (**Fig. 9.160**). JNA is seen involving the left CS (**Fig. 9.161**). Tumor is separated from the suspensory ligaments of the pituitary gland and the carotid artery is seen in the CS (**Figs. 9.162 and 9.163**). The course of the ICA is mapped using the micro-Doppler. The tumor is gently dissected out of the medial compartment of the CS. After the removal, the ICA is visualized. Bleeding in the CS is controlled using Surgiflo and other hemostatic agents (**Figs. 9.164 and 9.165**).

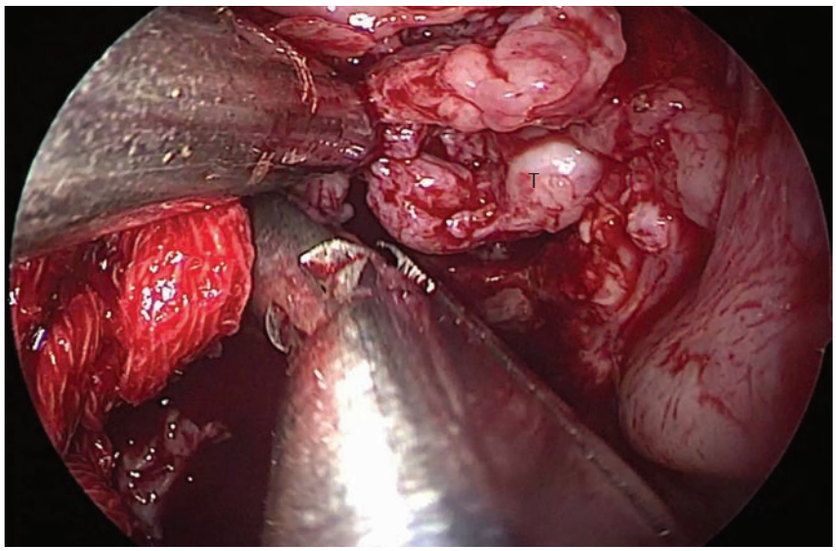

Fig. 9.160 Endoscopic image showing the principle of segmental resection.

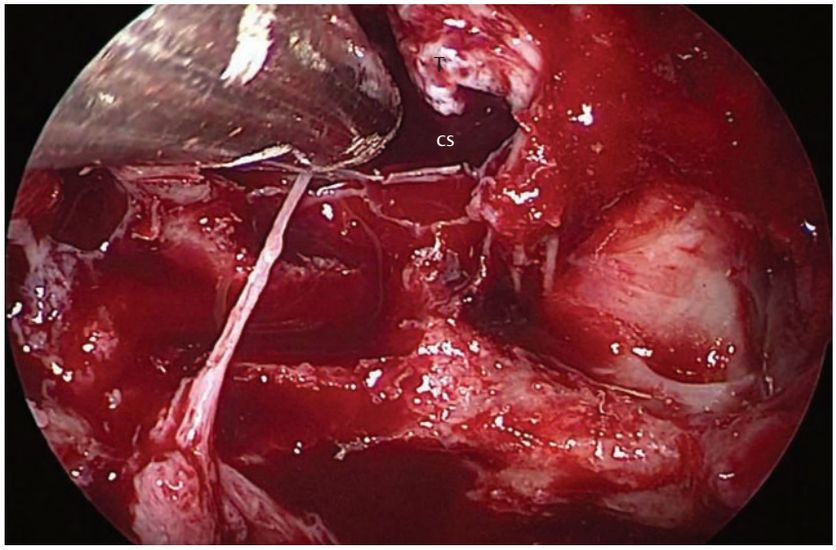

Fig. 9.161 JNA has seen involving the left cavernous sinus. cs, cavernous sinus.

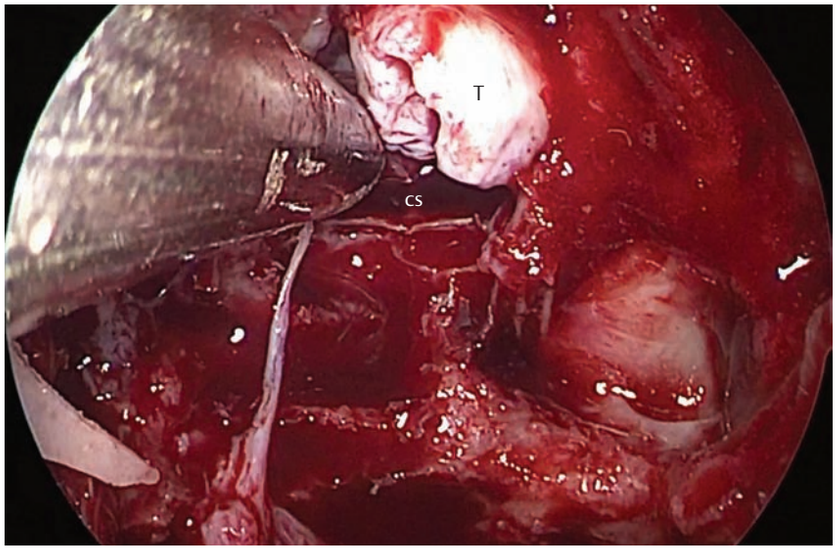

Fig. 9.162 Segmental resection of tumor from the cavernous sinus. cs, cavernous sinus; T, tumor.

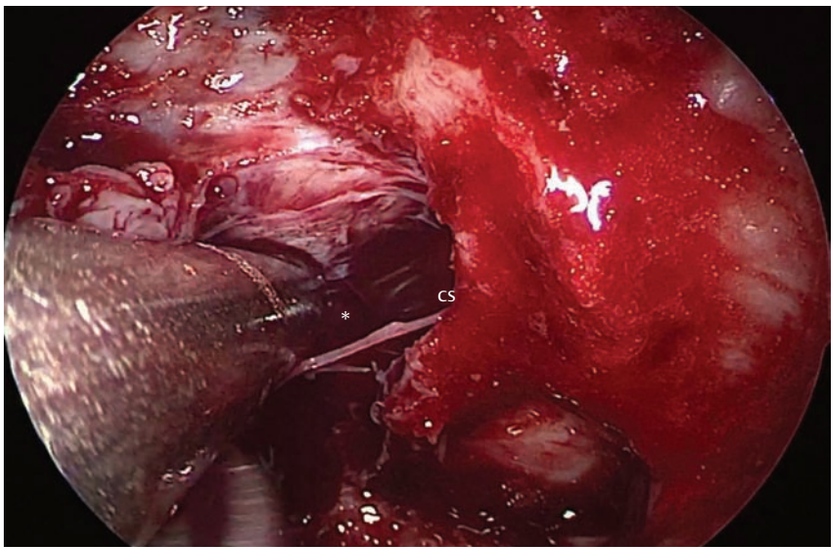

Fig. 9.163 Tumor being separated from the suspensory ligaments. cs, cavernous sinus.

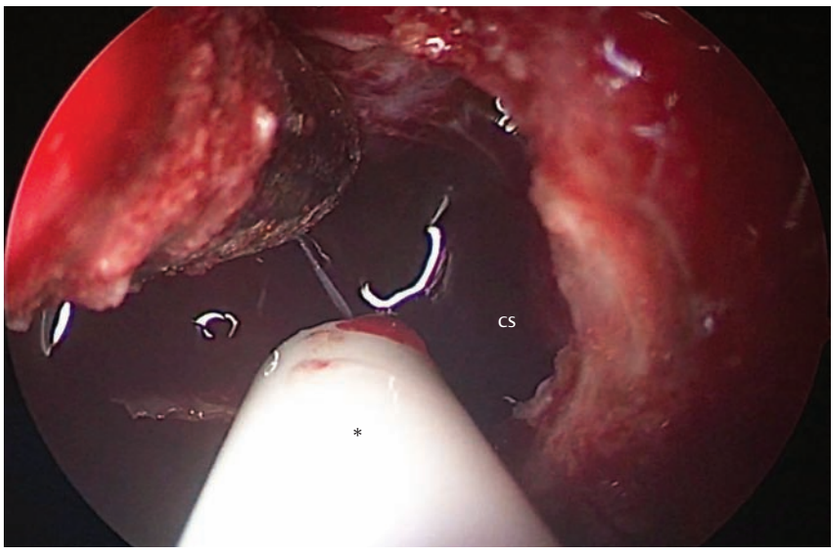

Fig. 9.164 Endoscopic image showing the hemostatic agent used to control the bleeding in the cavernous sinus. cs, cavernous sinus; *, Surgiflo.

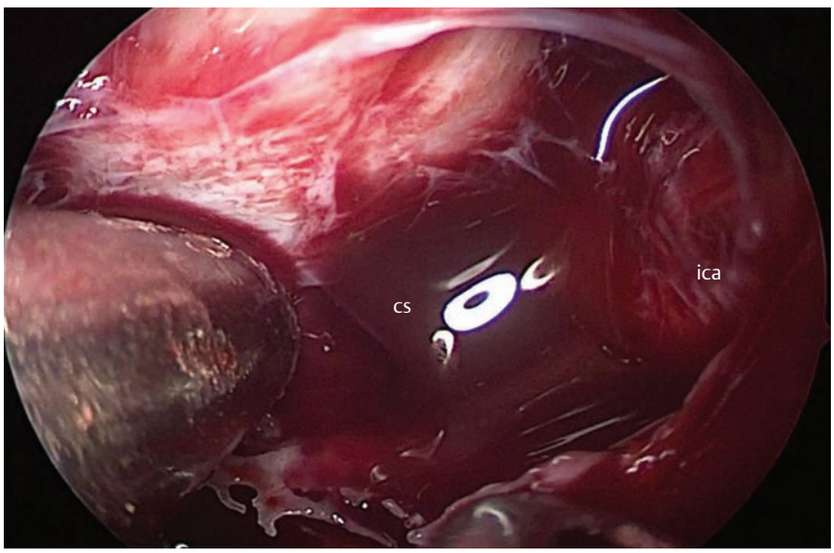

Fig. 9.165 Medial compartment of the left cavernous sinus seen. ica, internal carotid artery; sc, sellar cavity.

Case 14: Displacing the Carotid Laterally/Lateral Cavernous Sinus

In this case, the tumor is seen involving the lateral compartment of the CS.

The principle of segmental resection is followed. The tumor in the petrous apex is now no visualized (**Fig. 9.166**). The tumor is removed from the petrous apex. The bone is drilled over the paraclival ICA and its course is delineated (**Figs. 9.167 and 9.168**). A small bit of tumor present on the paraclival carotid is gently removed (**Fig. 9.169**). A small bleeder from the carotid is seen (**Fig. 9.170**) and controlled. The cavity is packed with Surgicel (**Fig. 9.171**).

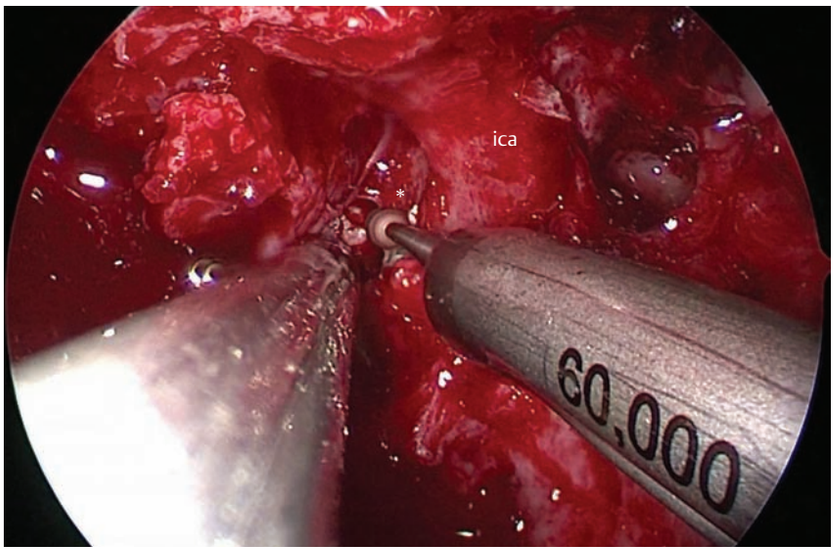

Fig. 9.166 Endoscopic view drilling of the petrous apex. *, area of the petrous apex.

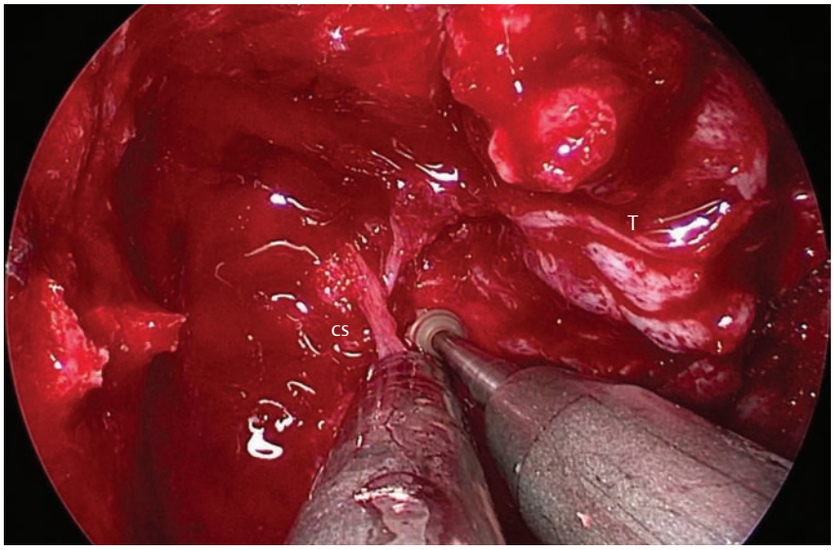

Fig. 9.167 Drilling the proximal internal carotid artery (ICD), the tumor is adherent to the ICD.

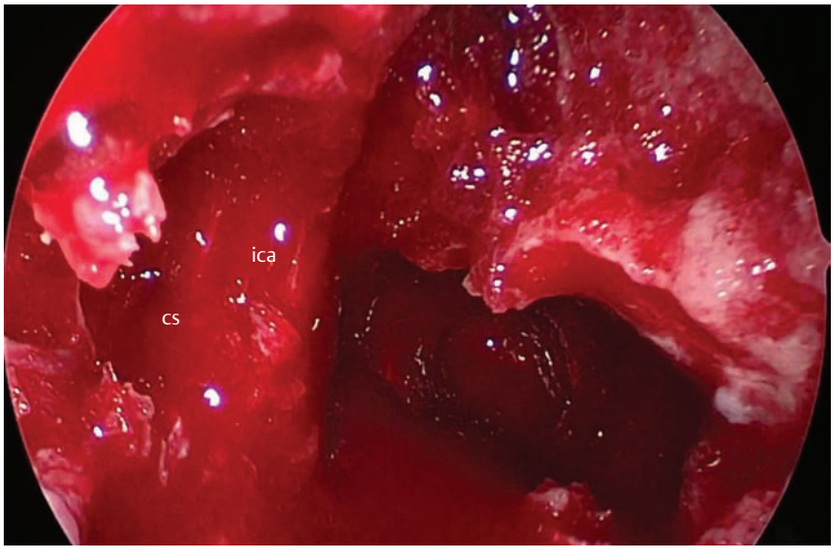

Fig. 9.168 Exposed paraclival internal carotid artery.

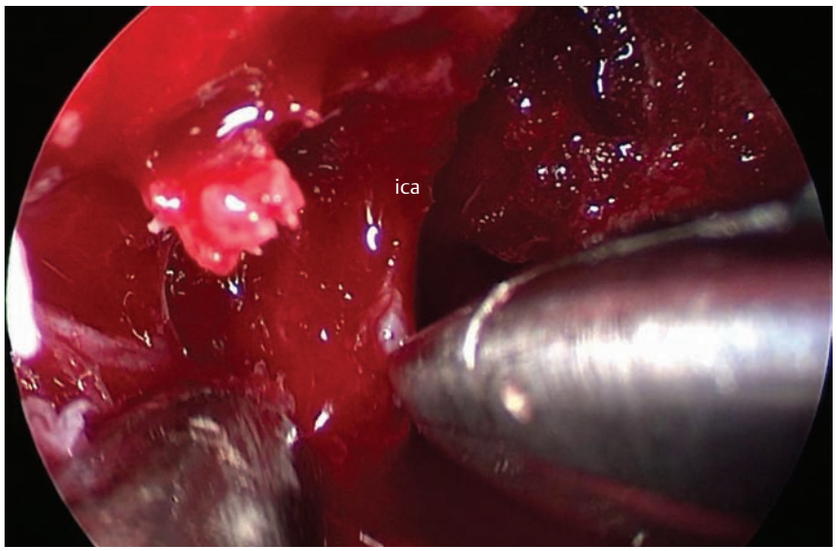

Fig. 9.169 Tumor removal from the endosteal layer of the internal carotid artery. ica, internal carotid artery.

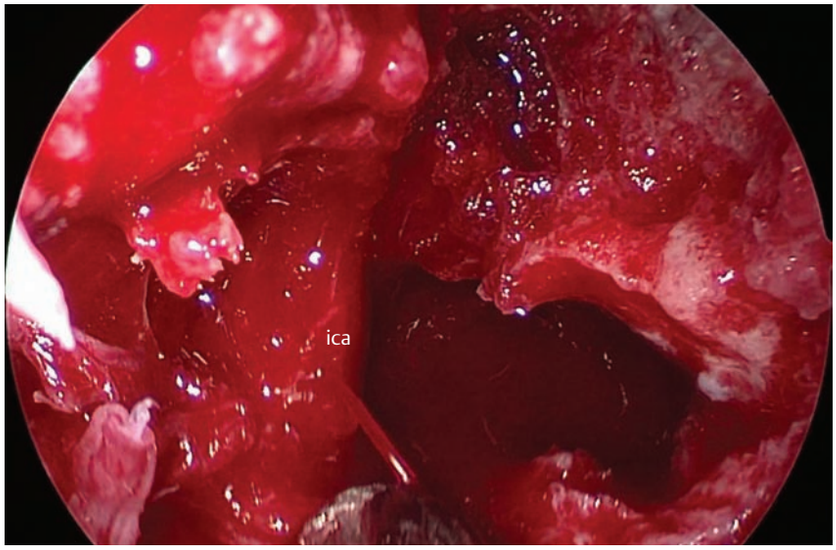

Fig. 9.170 Tumor dissected from the internal carotid artery, note a small bleeder.

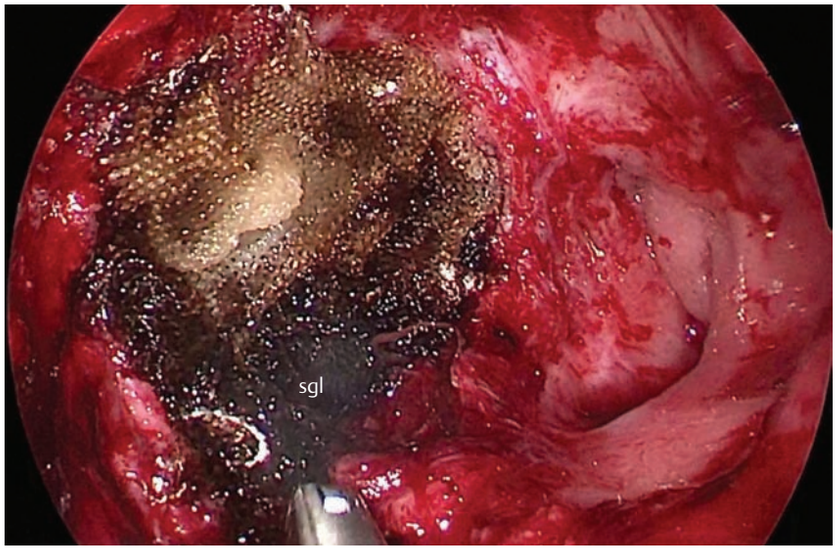

Fig. 9.171 Hemostasis achieved using the surgical. sgl, Surgiflo.

Case 15: Internal Carotid Artery Engulfment (360-Degree Engulfment)

In this case illustration, tumor is seen completely engulfing the cavernous part of the ICA as appreciated in the endoscopic image (**Fig. 9.172**).

By following the method of segmental resection, the tumor anterior to pterygoid fossa is resected. Piecemeal resection is done with intermittent use of the micro-Doppler to map the course of the carotid artery. Any displacement from the normal course is ascertained.

Initially, meticulous tumor dissection medial to cavernous ICA is carried out. Tumor is resected using a sharp cutting instrument like scissors to avoid pulling (**Fig. 9.173**), after which, a ball probe is introduced to hook the ICA and transposition is done (**Fig. 9.174**). Dissection lateral to ICA is performed (**Figs. 9.175 and 9.176**). The cranial nerves present in the lateral wall of the CS are identified.

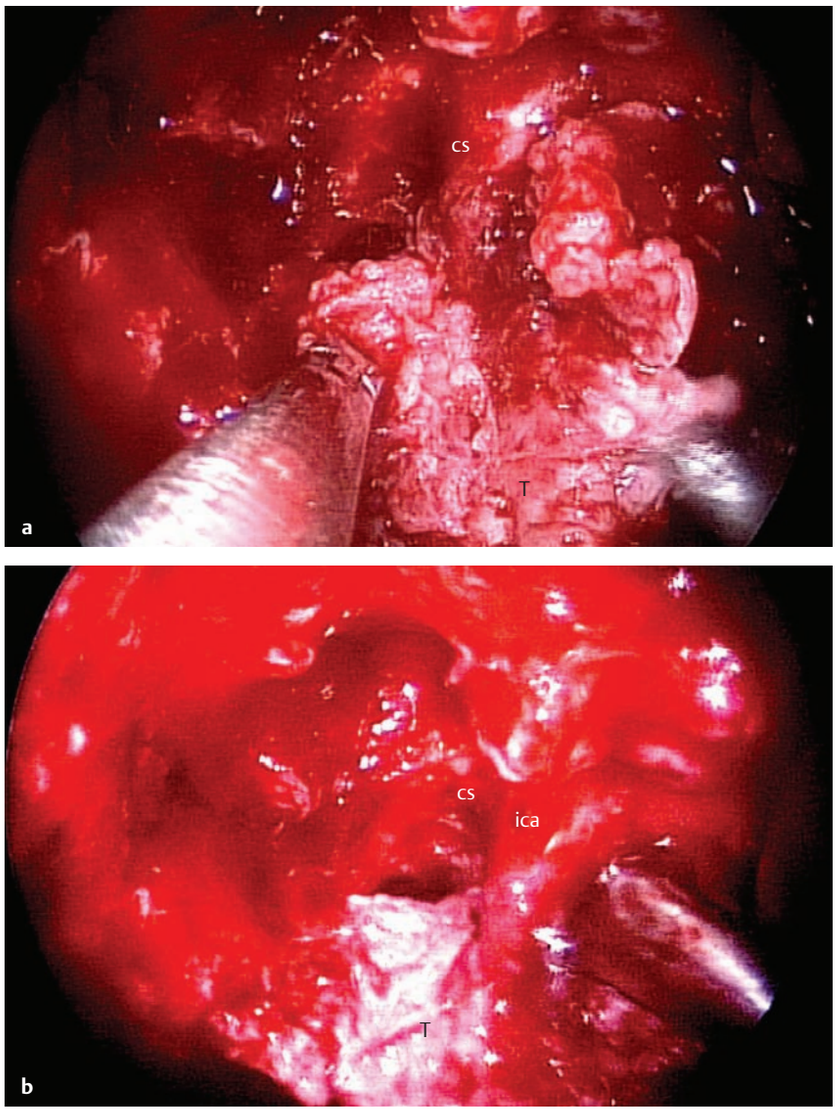

Fig. 9.172 **(a, b)** Endoscopic image showing the complete encasement of the internal carotid artery by the tumor. cs, cavernous sinus; ica, internal carotid artery; T, tumor.

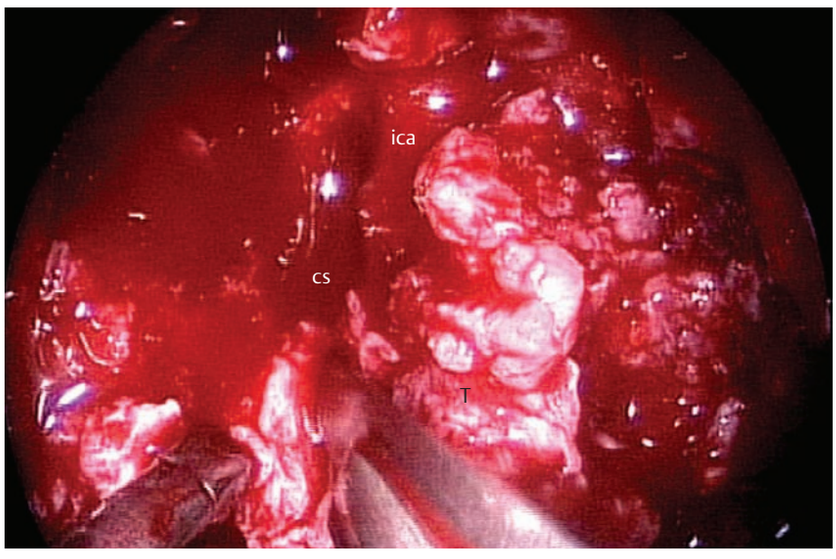

Fig. 9.173 Tumor dissected medially to the internal carotid artery. cs, cavernous sinus; ica, internal carotid artery; T, tumor.

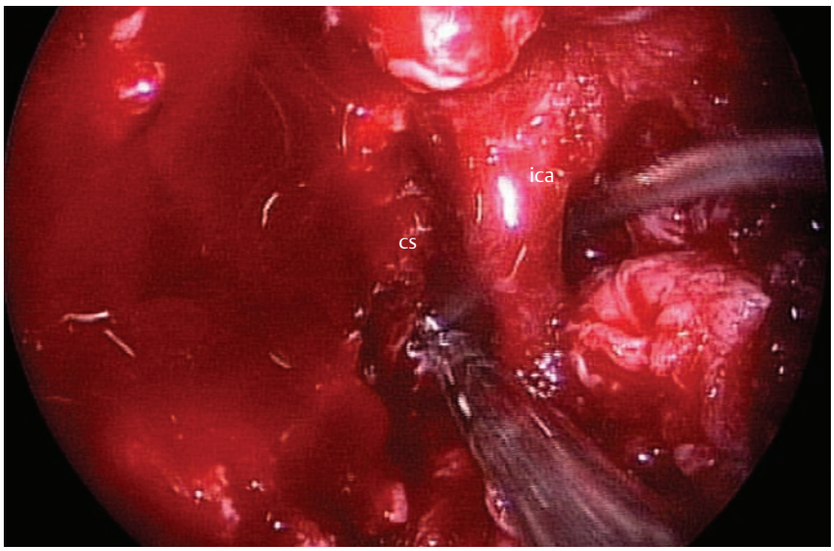

Fig. 9.174 Note the ball probe is passed around the internal carotid artery. cs, cavernous sinus; ica, internal carotid artery.

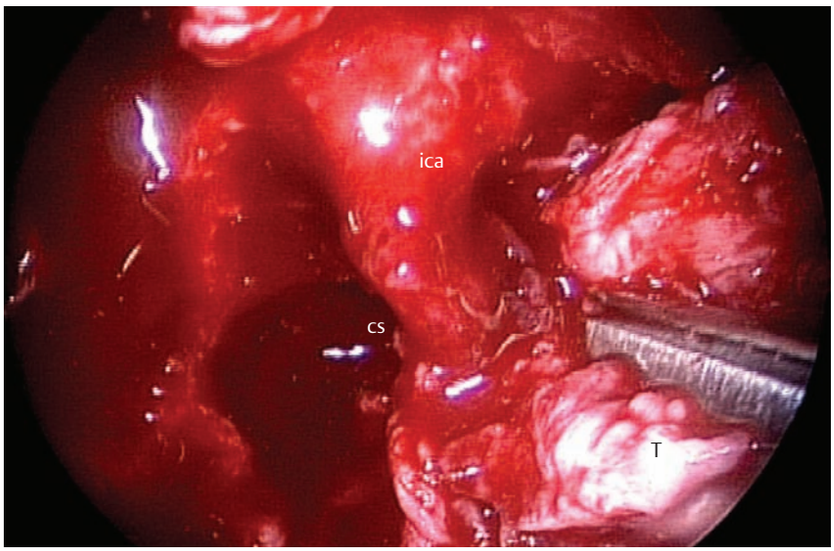

Fig. 9.175 Tumor dissected laterally to the internal carotid artery. cs, cavernous sinus; ica, internal carotid artery.

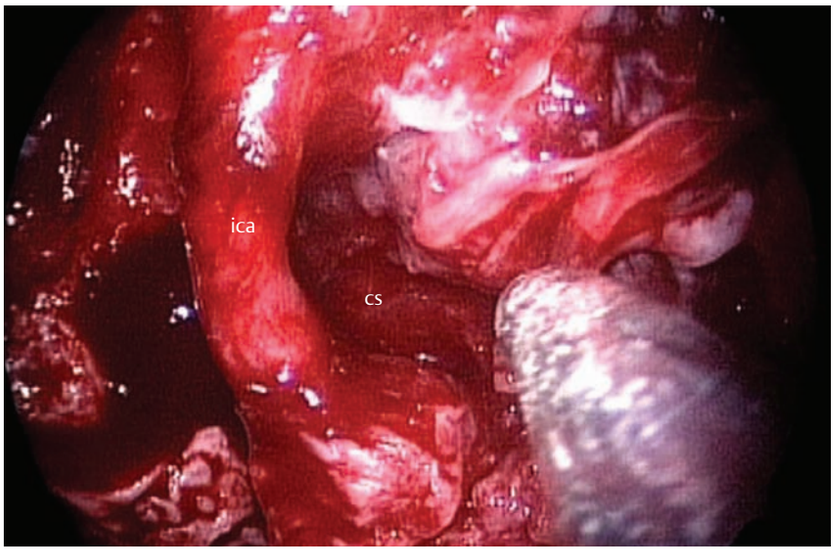

Fig. 9.176 Endoscopic view after complete dissection of the cavernous internal carotid artery. cs, cavernous sinus; ica, internal carotid artery.

Conclusion

For a long time, the parasellar area was considered as no man's land due to its complex anatomy and the presence of various vital neurovascular structures. With the advent of technical advances in the last decades in terms of angled endoscopes, camera system, micro-Doppler, and neuronavigation, the expanded endonasal approach is regarded as the mainstay for various lesions of the anterior skull base with special emphasis on the tumors involving the CS. The extended endonasal approaches have advantages such as minimal mortality, morbidity, functional and cosmetic disability compared to extracranial approaches.

References

1. Frank G, Pasquini E. Cavernous sinus: endoscopic endonasal approaches. In: Kassam AB, Gardner PA, eds. Endoscopic Approaches to the Skull Base. Basel: Karger; 2012:119–139
2. Koutourousiou M, Vaz Guimaraes Filho F, Fernandez-Miranda JC, et al. Endoscopic endonasal surgery for tumors of the cavernous sinus: a series of 234 patients. World Neurosurg 2017;103:713–732
3. Kassam AB, Gardner PA. Endoscopic Approaches to the Skull Base. Progress in Neurological Surgery. Basel: Karger; 2012
4. Micko ASG, Wöhrer A, Wolfsberger S, Knosp E. Invasion of the cavernous sinus space in pituitary adenomas: endoscopic verification and its correlation with an MRI-based classification. J Neurosurg 2015;122(4):803–811
5. Hardesty DA, Montaser AS, Carrau RL, Prevedello DM. Limits of endoscopic endonasal transpterygoid approach to cavernous sinus and Meckel's cave. J Neurosurg Sci 2018;62(3):332–338
6. Kassam AB, Vescan AD, Carrau RL, et al. Expanded endonasal approach: vidian canal as a landmark to the petrous internal carotid artery. J Neurosurg 2008;108(1):177–183
7. Kasemsiri P, Solares CA, Carrau RL, et al. Endoscopic endonasal transpterygoid approaches: anatomical landmarks for planning the surgical corridor. Laryngoscope 2013;123(4):811–815
8. Dolci RLL, Upadhyay S, Ditzel Filho LFS, et al. Endoscopic endonasal study of the cavernous sinus and quadrangular space: anatomic relationships. Head Neck 2016;38(Suppl 1): E1680–E1687

10 Intraoperative Magnetic Resonance Imaging in Endonasal Surgery for Pituitary Adenoma

Beng-Ti Ang, Dharambir S. Sethi

Pituitary adenomas, although benign, are responsible for significant morbidity due to vision compromise and endocrine dysfunction. Compression of the optic chiasm leads to the classic presentation of bitemporal hemianopia, with prolonged compression leading to progressive optic nerve atrophy and attendant poor vision. Complete surgical decompression of the optic apparatus can salvage vision in early cases and prevent further worsening of visual loss in cases where optic neuropathy is already permanent. The issue of vision salvage forms the primary aim of surgery for nonfunctioning pituitary adenomas. Cranial nerve neuropathies from cavernous sinus extension or invasion are a less common indication for surgery, but again demand effective removal of the adenoma from the cavernous sinus to obtain clinical relief. Reversal of hypopituitarism is not reliably achieved following surgery for nonfunctioning adenomas; however, achieving endocrine cure in situations of hormone overproduction, such as in Cushing's syndrome and acromegaly is a key aim of surgery in such tumors and is critically linked to completeness of resection.

The endoscopic transsphenoidal approach to expose the sella for the resection of pituitary adenomas is now a widely accepted surgical technique. Previously, pituitary tumors with irregular shape and significant extension in an anterior direction along the planum sphenoidale, significant suprasellar extension toward the third ventricle, and posterior extension toward the interpeduncular fossa of the midbrain and extension toward the pons were immediately managed with transcranial approaches. With the advent of the expanded endonasal technique, the addition of transplanum and transclival exposures to the core transsphenoidal module has allowed for the resection of the vast majority of pituitary tumors via the endonasal route. The application of the coronal plane-expanded techniques has also led to the ability to approach tumor extension in a lateral direction, leading to more complete removal.

While the above-mentioned techniques have improved the extent of adenoma resection, improving the visibility of small lesions and the margins and extensions of large lesions can further enhance rates of complete resection to obviate repeat surgery and radiation therapy and to achieve endocrine cure. Attempts to improve visibility in such a fashion have led to the development of intraoperative magnetic resonance imaging (iMRI). Excellent reviews of the evolution of iMRI have been published,[1–7] and in this chapter, authors have highlighted their local experience at the Singapore General Hospital. They employ the use of a 1.5T high-field iMRI system in the conventional horizontal bore configuration. Preliminary imaging is carried out following induction of anesthesia to obtain baseline preoperative imaging information to enable neuronavigation and stereotaxy. Following the initial surgical approach and maximal possible resection as ascertained by direct endoscopic visualization, the imaging is repeated and integrated with neuronavigation again, to allow for continued stereotactically guided resection of remnant tumor, as is necessary.

Endonasal endoscopic surgery has a significant learning curve, especially for the novice neurosurgeon more accustomed to a cranial practice. The iMRI allowed for the visualization of unexpected remnants and hence additional surgery to be carried out to effect maximal safe removal. This obviously leads to improved rates of gross total resection for nonfunctioning adenomas[8] and facilitates biochemical cure of the functioning adenomas.[9,10] We notice in our early experience of surgery for large pituitary tumors that early descent of the diaphragm in a nonsymmetric fashion as resection proceeded, led to close apposition of folds of the diaphragm and arachnoid to mask pockets of residual

tumor. Termination of surgery at this stage would have led to a suboptimal resection. With this knowledge, authors then developed a systematic fashion of sectorial inspection of the walls of the resection cavity. They used suction apparatus and Rhoton microdissectors to retract and expose sections of the walls and floor; the loose and pulsating diaphragm was everted gently using neurosurgical patties rolled up in a cylindrical fashion/folded in an accordion-like fashion to progressively allow for the visualization of different regions of the collapsed diaphragm, separating its leaves which may be opposed due to its redundancy following removal of a large adenoma. It has been reported that the use of iMRI becomes valuable only when actionable remnants are visualized—this refers to the scenario where the surgeon is able to effectively remove the remnant seen, leading to a more complete resection. Over the years of practice, the numbers of cases of actionable remnants has actually fallen remarkably, attesting to the ability of the iMRI in facilitating the adoption of improved surgical techniques following a reflection and analysis of prior surgical outcomes. The integration of neuronavigation with iMRI has also contributed to an improved appreciation of skull base anatomy and importantly, the critical relationships of the tumor to important vascular and neural structures (**Fig. 10.1**).

In an elderly individual, a patient with significant medical comorbidity or one who is highly risk averse, the preoperative decision may be one to effect complete decompression of the chiasm but not to pursue complete resection to reduce the risk profile of the surgery. The iMRI helps confirm that the operative plan has indeed been carried out. If the surgeon deems that further safe debulking surgery can be achieved, then further resection should be carried out (**Fig. 10.2**).

With irregularly shaped lesions, an expanded endonasal approach may be used to effect complete removal. The iMRI together with neuronavigation helps confirm this (**Fig. 10.3**).

Another scenario where authors have found the use of iMRI to be particularly useful is in the surgery for recurrent tumors. The iMRI helps confirm completeness of resection/optimal resection in a setting where the patient may get distressed at having to undergo repeated surgery. If there is remnant which is deemed unresectable, a discussion on subsequent surgical plans, be it a transcranial approach or radiation therapy, may immediately be carried out in the postoperative period (**Fig. 10.4**).

The implementation of iMRI can also help in the detection of postoperative complications such as hematoma in the surgical cavity or bed. The hematoma may not be

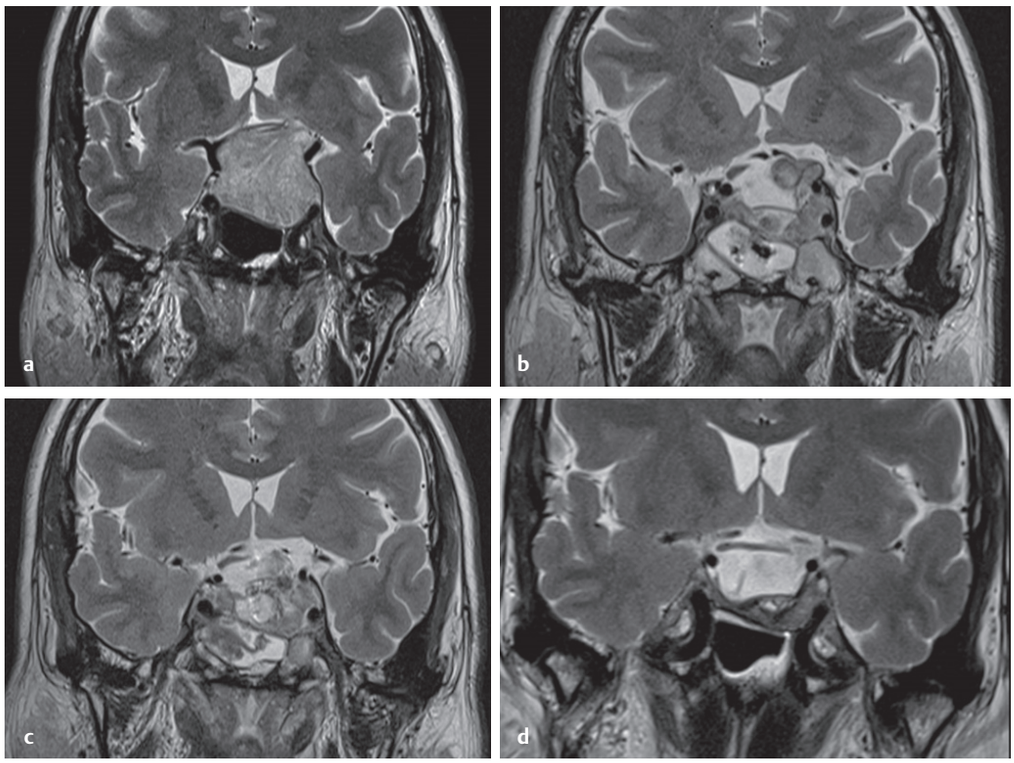

Fig. 10.1 A case of large pituitary macroadenoma **(a)** where the loose redundant diaphragmatic descent following tumor resection led to close apposition of the diaphragmatic leaves, obscuring the presence of a pocket of tumor **(b)** on the initial intraoperative magnetic resonance (MR) scan. **(c)** Intraoperative image confirming removal of the remnant. **(d)** Postoperative scan obtained 2 months after surgery.

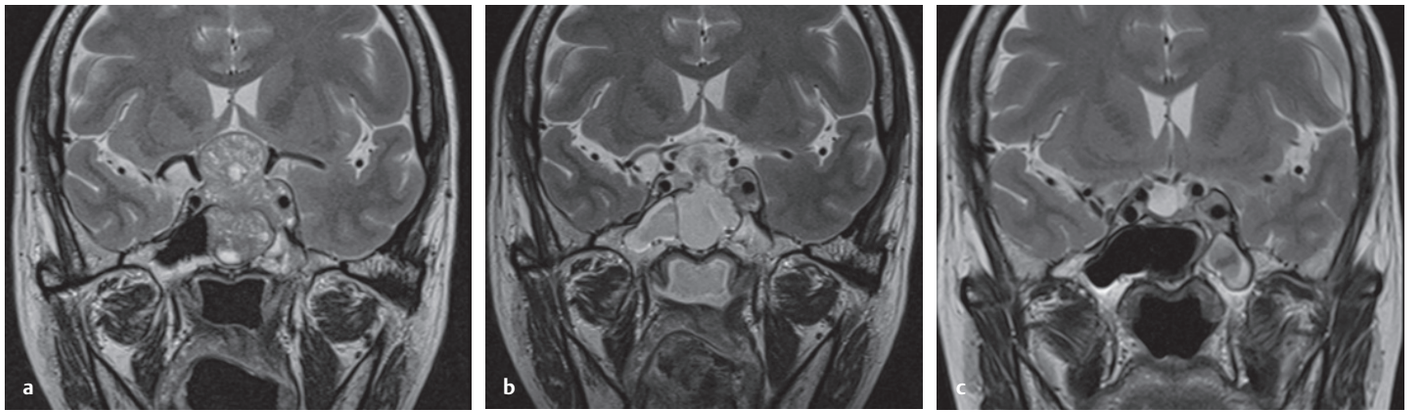

Fig. 10.2 In this case, the preoperative plan for this macroadenoma **(a)** was to effect chiasmal decompression but to leave the cavernous sinus portion in situ. **(b)** Intraoperative scan and **(c)** the postoperative scan at 2 months. This elderly patient expressed a desire to avoid additional risk from extensive surgery and was comfortable with radiation therapy, if subsequent imaging showed enlargement of the remnant in the cavernous sinus.

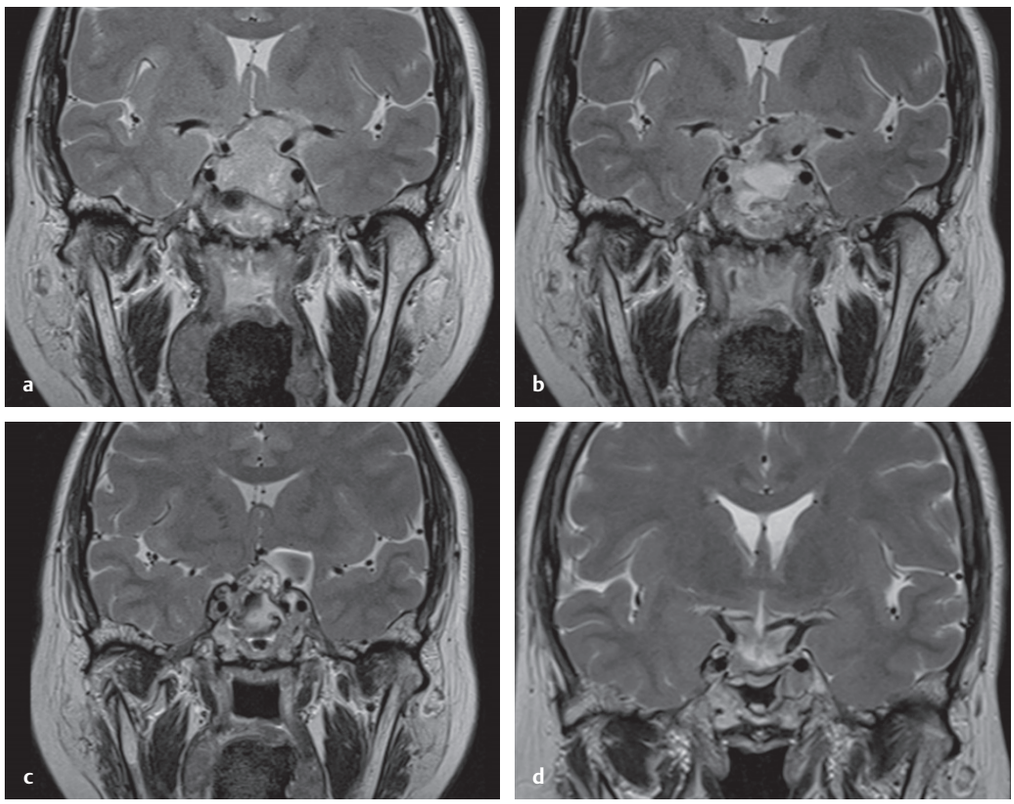

Fig. 10.3 This case of macroadenoma exhibited an eccentric morphology with suprasellar extension of tumor to the left, adjacent to and abutting the left internal carotid artery bifurcation **(a)**. The intraoperative scan following resection of the majority of the lesion **(b)** was carried out to reobtain neuronavigation parameters to guide resection of the suprasellar segment via a transplanum approach. The intraoperative scan **(c)** following satisfactory resection as ascertained endoscopically. **(d)** Postoperative scan at 2 months.

directly visualized as it may lie outside the tumor capsule or external to the diaphragm in the subarachnoid space. It may also not be seen if a pedicled nasoseptal flap repair had been carried out, thus obscuring the direct view of the resection cavity.

Admittedly, the use of iMRI has indeed led to an increase in operating theatre time. The institution of protocols for the preparation and positioning of the patient often contribute an additional 1 to 2 hours. The authors have, however, not experienced any additional complications from the use of iMRI in pituitary tumor surgery. Their use of high-quality T2-weighted imaging in the iMRI for pre- and intraoperative scanning, rather than contrast-enhanced T1-weighted images, has led to accurate assessment of tumor residuals with little false-positives. Admittedly, the construction and implementation of an iMRI operating room is expensive and requires significant infrastructure modification. A shared-room strategy or two-room solution can allow for

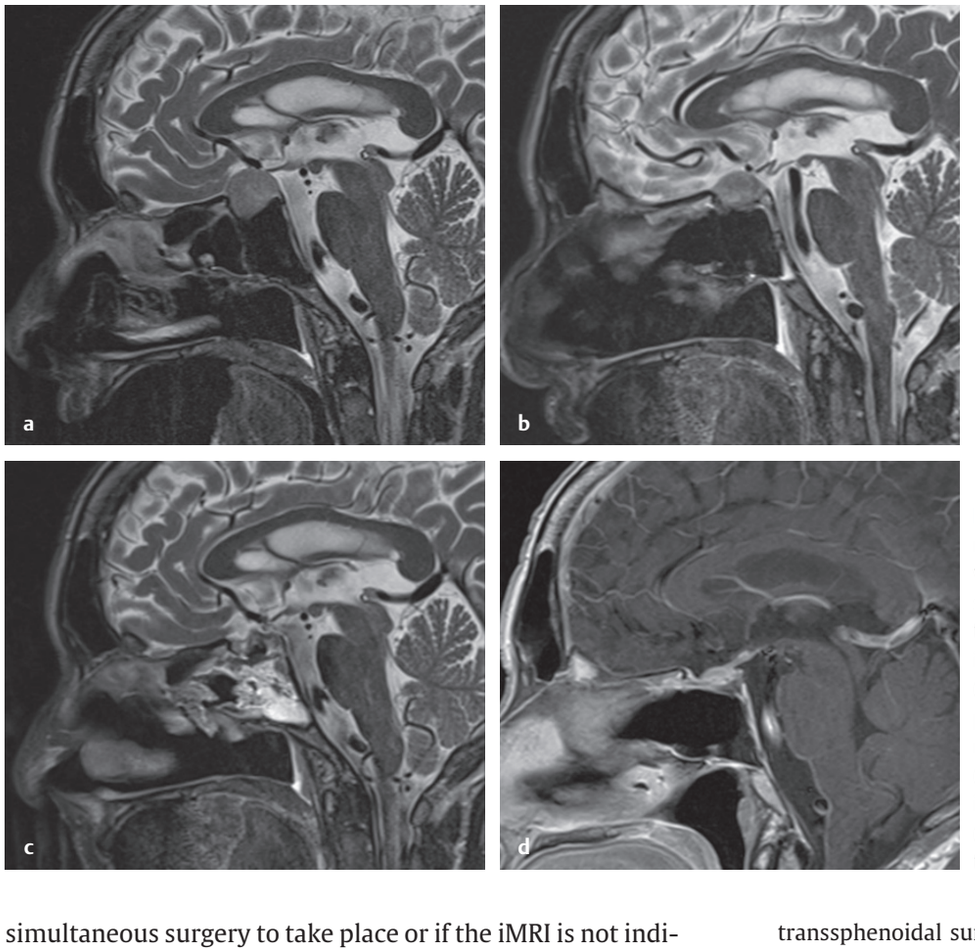

Fig. 10.4 This is a case of recurrent adenoma referred from a separate institution with significant scarring at the operative site **(a)**. Initial resection was carried out of this firm lesion till it showed good pulsatility and descent and an intraoperative scan **(b)** was done to ascertain neuronavigation parameters before proceeding with an extracapsular dissection of the remaining lesion. **(c)** Represents the intraoperative scan following resection showing satisfactory removal. **(d)** Postoperative scan at 2 months following the surgery.

simultaneous surgery to take place or if the iMRI is not indicated/used, diagnostic imaging can be carried out. Despite these shortcomings, authors' experience with the iMRI has been positive with definite benefit in terms of patient outcome, by improving the extent of resection, and, correspondingly, the outcome, for both nonfunctioning and functioning pituitary macroadenomas.

References

1. Buchfelder M, Schlaffer SM. Intraoperative magnetic resonance imaging for pituitary adenomas. Front Horm Res 2016;45: 121–132
2. Buchfelder M, Schlaffer SM. Intraoperative magnetic resonance imaging during surgery for pituitary adenomas: pros and cons. Endocrine 2012;42(3):483–495
3. Jones J, Ruge J. Intraoperative magnetic resonance imaging in pituitary macroadenoma surgery: an assessment of visual outcome. Neurosurg Focus 2007;23(5):E12
4. Chittiboina P. iMRI during transsphenoidal surgery. Neurosurg Clin N Am 2017;28(4):499–512
5. Zaidi HA, De Los Reyes K, Barkhoudarian G, et al. The utility of high-resolution intraoperative MRI in endoscopic transsphenoidal surgery for pituitary macroadenomas: early experience in the advanced multimodality image guided operating suite. Neurosurg Focus 2016;40(3):E18
6. Boellis A, Espagnet MC, Romano A, et al. Dynamic intraoperative MRI in transsphenoidal resection of pituitary macroadenomas: a quantitative analysis. J Magn Reson Imaging 2014;40(3):668–673
7. Anand VK, Schwartz TH, Hiltzik DH, Kacker A. Endoscopic transphenoidal pituitary surgery with real-time intraoperative magnetic resonance imaging. Am J Rhinol 2006;20(4): 401–405
8. Nimsky C, von Keller B, Ganslandt O, Fahlbusch R. Intraoperative high-field magnetic resonance imaging in transsphenoidal surgery of hormonally inactive pituitary macroadenomas. Neurosurgery 2006;59(1):105–114
9. Mastorakos P, Taylor DG, Chen C, Buell T, Donahue JH, Jane JA. Prediction of cavernous sinus invasion in patients with Cushing's disease by magnetic resonance imaging. J Neurosurg 2018;(1):1-6
10. Netuka D, Májovský M, Masopust V, et al. Intraoperative magnetic resonance imaging during endoscopic transsphenoidal surgery of growth hormone-secreting pituitary adenomas. World Neurosurg 2016;91:490–496

11 Endoscopic Surgery for Sellar and Parasellar Lesions: A Tailored Approach

Michel Roethlisberger, Vicknes Waran, Prepageran Narayanan

Mononostril Transseptal Transsphenoidal Resection of a Pituitary Macroadenoma

Pituitary macroadenomas are the most frequent lesions encountered when performing endonasal endoscopic surgery. A systematic approach in resecting these lesions leads to a higher routine for the surgeon and therefore better results in the extent of resection. Described surgical corridors to the sphenoid sinus include the transseptal, transnasal, and transethmoidal approach. In the authors' institution, the preferred surgical route is a **transseptal transsphenoidal approach** with removal of the superior and preservation of the middle turbinates. This technique was initially used with the assistance of a modified speculum.[1–3]

Case History

A 45-year-old patient presented with slowly decreasing libido, impotence, and a generally reduced level of energy for daily activities. Endocrinological examination revealed a deficient gonadotropic axis (follicular-stimulating hormone, luteinizing hormone) and low-normal thyroid-stimulating hormone levels. Consecutive ophthalmological examination further detected a bitemporal visual field defect.

Neurocranial imaging confirmed the presence of a sellar mass extending into the suprasellar space with compression of the optic chiasm and extension into the sphenoid cavity, being suspicious for a pituitary macroadenoma (**Fig. 11.1**).

A single nostril endoscopic transseptal transsphenoidal excision of the tumor was planned.

Presurgical Steps

- General anesthesia with orotracheal intubation and throat pack in situ.
- A prophylactic antibiotic should be given at induction of anesthesia.
- Bladder catheterization is recommended and should be kept postoperative to monitor urine output in the first days.
- The patient's head is placed neutrally with a supine neck in a slightly extended position. In the authors' institution, the head is fixed within a NORAS frame for intraoperative MRI (iMRI) (**Fig. 11.2**).

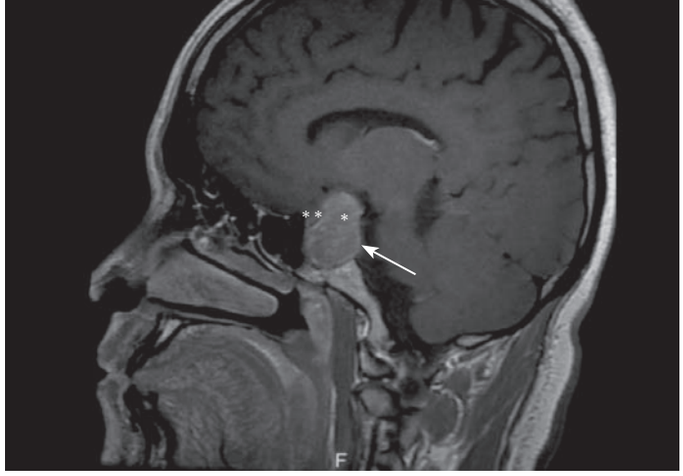

Fig. 11.1 Preoperative T1-weighted gadolinium contrast-enhanced sagittal MRI sections showing an isointense intra- and suprasellar mass and moderate homogenous enhancement, along with areas of signal shortening suggestive for micro-hemorrhage or necrosis (*). The pituitary gland (*arrow*) presents with slightly more enhancement and is displaced posteriorly. There is compression of the optic chiasm (**) and both optic nerves.

Fig. 11.2 Patient head fixation for intraoperative MRI control (iMRI).

Fig. 11.3 For the two-surgeon four-hand technique, each surgeon stands on his side of the patient's head. The ENT surgeon (on the patient's left side) holds the endoscope and assists the neurosurgeon with a third hand in more complex maneuvers.

- To allow a more flexible handling of instruments for mononostril and binostril endonasal approaches, the two surgeons stand on either side of the patient (**Fig. 11.3**).
- The nose is sprayed with co-phenylcaine (lignocaine 5% and phenylephrine 0.5% spray).
- The nasal packing is performed with cottonoids soaked with adrenaline 1:1,000. Packing is done along the floor of the nose and in between septum and middle turbinate.
- The abdomen is routinely prepared for fat graft harvest in a later step (if required).

Surgical Steps

- The preliminary packing is removed and the nose is inspected with a 0-degree nasal endoscope.
- Both sphenoethmoidal recesses are packed with cottonoids soaked in adrenaline 1:1,000.
- The osteocartilaginous junction is infiltrated with mepivacaine and adrenaline 1:100,000 on both sides of the septum (**Figs. 11.4 and 11.5**).
- Bipolar diathermy is used to cauterize the site of incision, followed by a vertical incision at the osteocartilaginous junction (**Fig. 11.6**).
- A mucoperiosteal flap is elevated on one side of the septum (**Fig. 11.7**).
- The bony cartilaginous junction is dislocated using a Freer's elevator (**Fig. 11.8**). This gives access for the flap elevation on the contralateral side (**Fig. 11.9**).

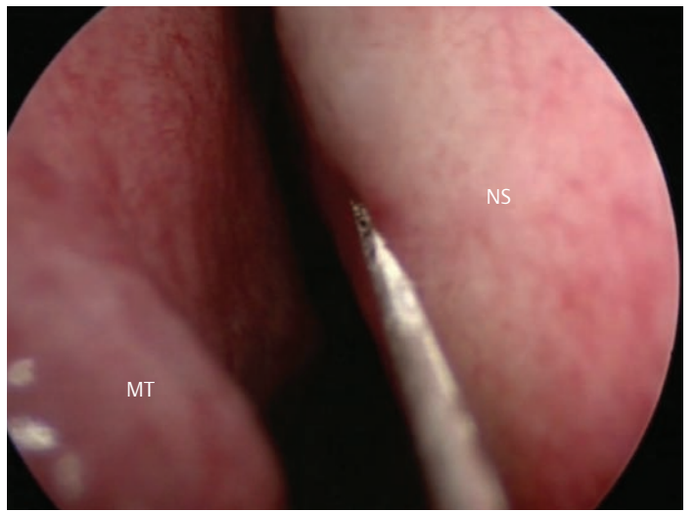

Fig. 11.4 Infiltration of the right osteocartilaginous junction. Nasal septum (NS), middle turbinate (MT).

- The posterior bony septum is then removed.
- Mucoperiosteal elevation is continued bilaterally to the sphenovomerine suture.
- The sphenoid ostia are exposed when the mucoperiosteal elevation is continued laterally. The surgeon has to take care not to damage the posterior septal branch of the sphenopalatine artery (SPA) (**Fig. 11.10**).
- A Kerrison's punch is used to remove the keel of sphenoid and the anterior wall of sphenoid sinus to give a wide exposure of the sphenoid cavity (**Fig. 11.11**).

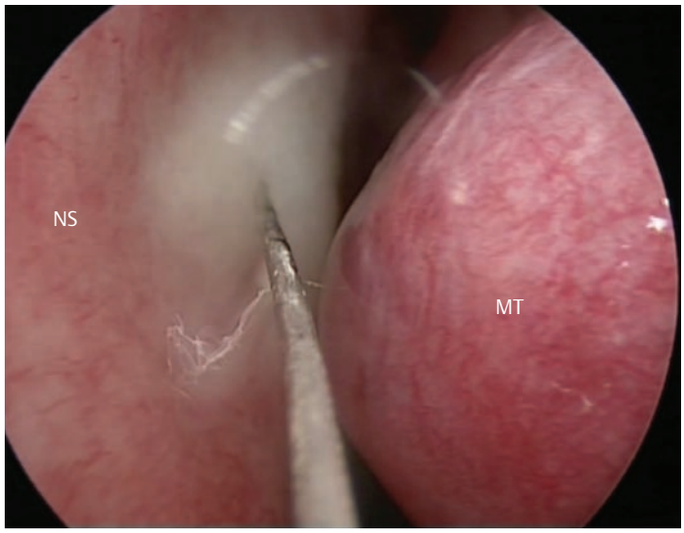

Fig. 11.5 Infiltration of the left osteocartilaginous junction. Nasal septum (NS), middle turbinate (MT).

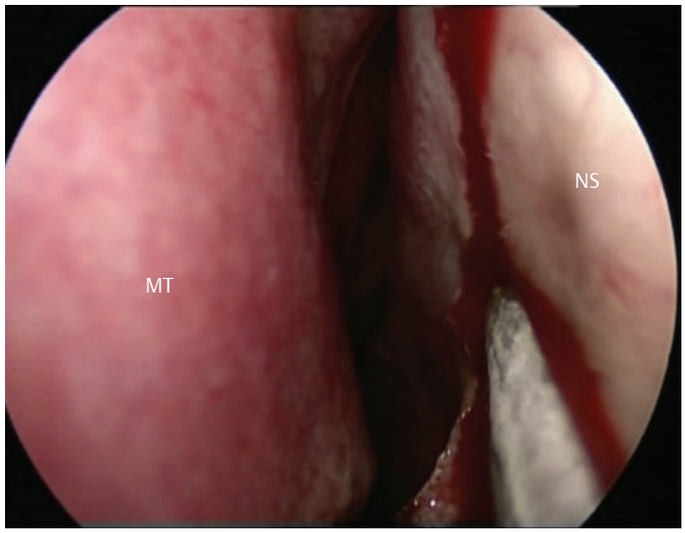

Fig. 11.6 Incision on the right nasal septum (NS) opposite to the anterior part of middle turbinate (MT).

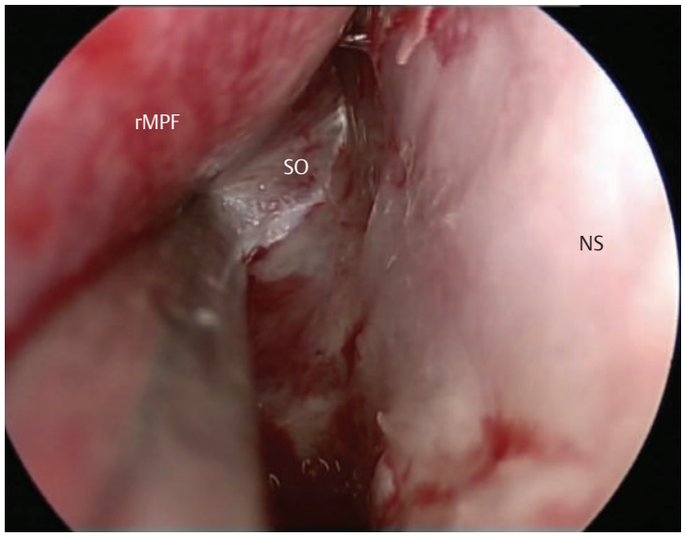

Fig. 11.7 Elevation of the right mucoperichondrial flap (rMPF) along the nasal septum (NS). Sphenoid ostium (SO).

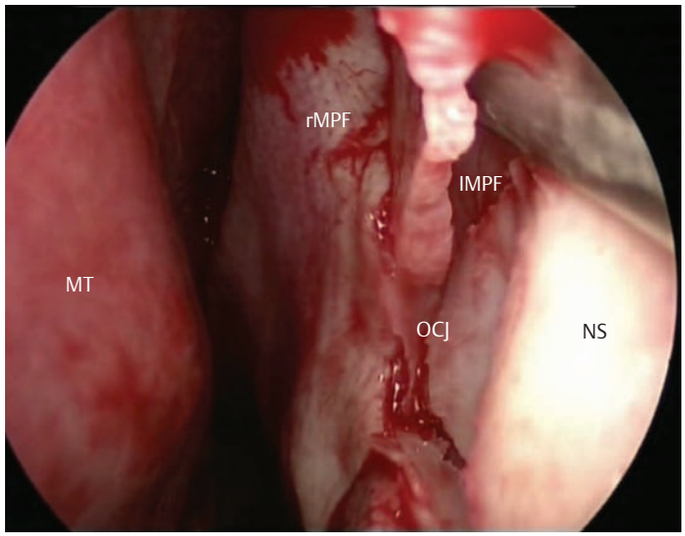

Fig. 11.8 Fracturing of the nasal septum (NS) at the osteocartilaginous junction (OCJ). Middle turbinate (MT), right mucoperichondrial flap (rMPF), left mucoperichondrial flap (lMPF).

- Septations in the sphenoid sinus are carefully removed, paying particular attention to the septations inserting at the paraclival and cavernous internal carotid artery (ICA).
- The critical landmarks of the skull base should be identified visually and confirmed with image-guided surgery (planum sphenoidale, tuberculum sellae, sella turcica, paraclival carotid, clivus, cavernous internal carotid artery, optic nerves, and opticocarotid recess).
- In the present case, the pituitary adenoma extends into the sphenoid cavity and has distorted the bony anatomy of the base of skull. In these cases, image-guided surgery is of great importance to identify the critical neurovascular structures (**Fig. 11.12**).
- Sphenoid mucosa covering the dura mater is removed carefully beginning in the midline and moving laterally. Dehiscent neurovascular structures should be anticipated and preoperative imaging should be studied accordingly (**Fig. 11.12**).
- A plane between the dura mater and the bony cover of the sella turcica is dissected (**Fig. 11.13**).

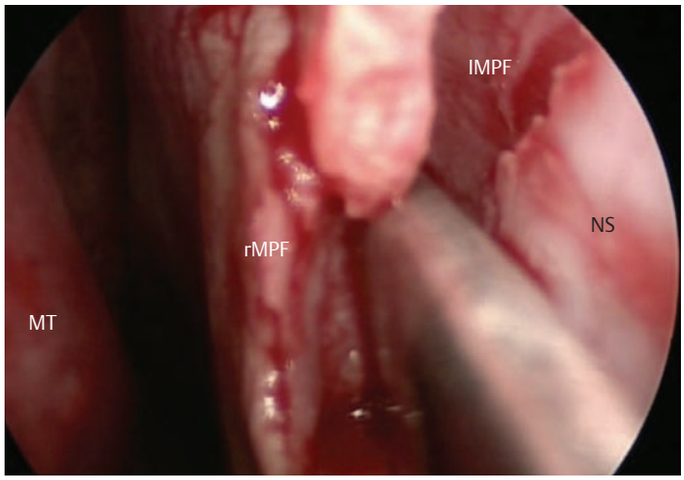

Fig. 11.9 Raising of left mucoperichondrial flap (lMPF) along the contralateral nasal septum (NS). Middle turbinate (MT), right mucoperichondrial flap (rMPF).

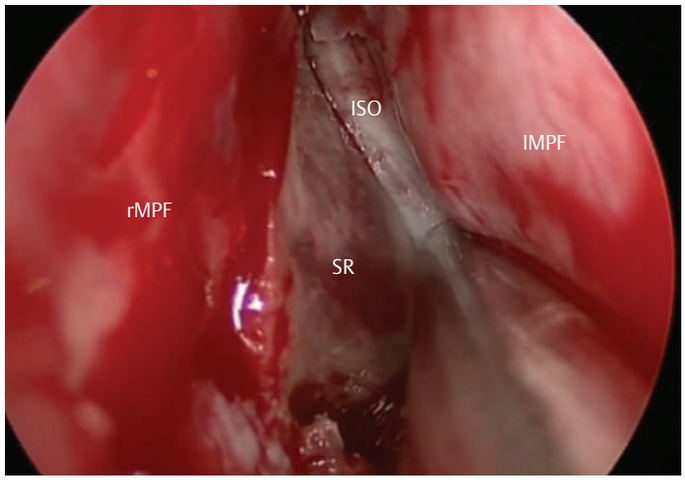

Fig. 11.10 Raising of left mucoperichondrial flap (lMPF) and removal of cartilaginous and bony septum. Sphenoid rostrum (SR), left sphenoid ostium (lSO), right mucoperichondrial flap (rMPF).

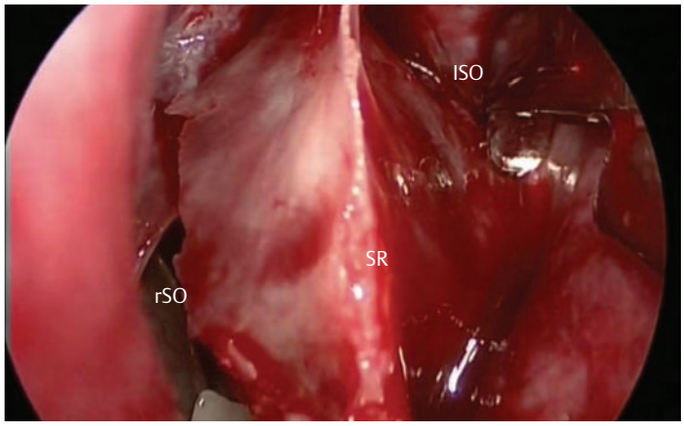

Fig. 11.11 Osteotomy of the left sphenoid ostium (lSO) with a Kerrison's punch. The right sphenoid ostium (rSO) has been opened from laterally to inferomedially. Sphenoid rostrum (SR).

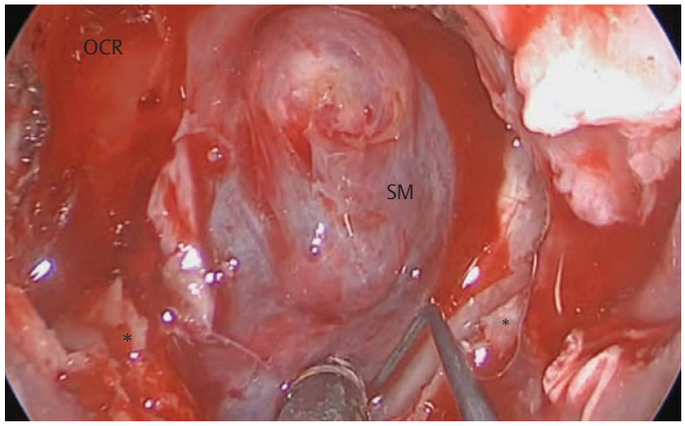

Fig. 11.12 After removal of the anterior wall of the sphenoid sinus (*), the eroded anterior wall of the sella covered by sphenoid mucosa (SM) is seen with the sellar dura shining through. Opticocarotid recess (OCR).

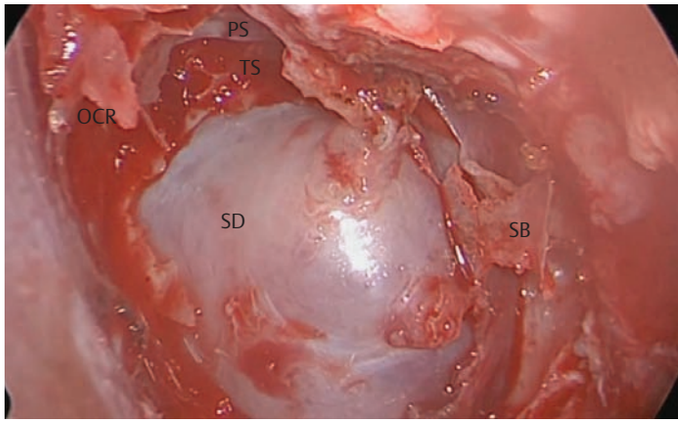

Fig. 11.13 Opening after removal of the sphenoid mucosa and the thinned out bony covering of the sella turcica. Sellar dura (SD), flicked sellar bone (SB), tuberculum sellae (TS), planum sphenoidale (PS), opticocarotid recess (OCR).

- If necessary, the bony opening of the sella turcica can be widened using a Kerrison's punch and by flicking the bony covering laterally (**Fig. 11.14**).
- The dura is open in a cross-shaped manner and typical pituitary adenoma tissue is exposed (**Fig. 11.15**).
- Tumor tissue should be preserved for histological examination using a grasping instrument (**Fig. 11.16**).
- Tumor removal should be performed systemically from inferior to lateral and then superiorly. Inferior tumor debulking should be started in the midline along the sellar floor (central pillar) (**Fig. 11.17**) and then extended laterally on each side (lateral pillars) (**Figs. 11.18 and 11.19**).

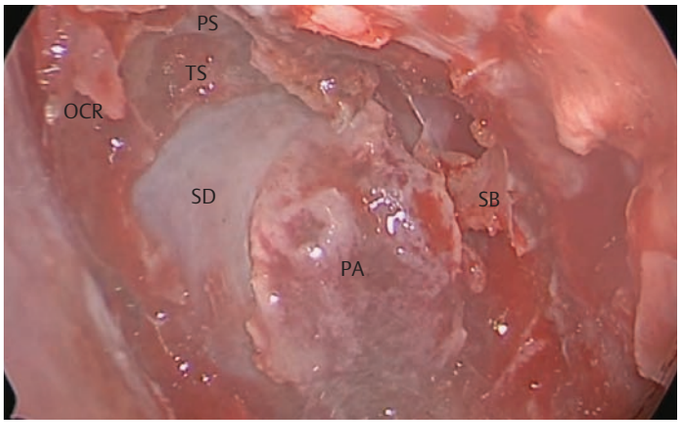

Fig. 11.14 After incision of the sellar dura (SD), tumor tissue evacuates under pressure. Sellar bone (SB), tuberculum sellae (TS), planum sphenoidale (PS), opticocarotid recess (OCR), pituitary macroadenoma (PMA).

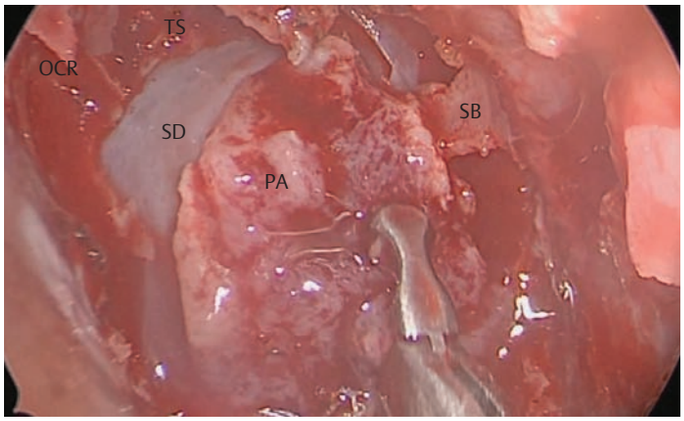

Fig. 11.15 Preservation of specimen. Sellar dura (SD), sellar bone (SB), tuberculum sellae (TS), planum sphenoidale (PS), opticocarotid recess (OCR), pituitary macroadenoma (PMA).

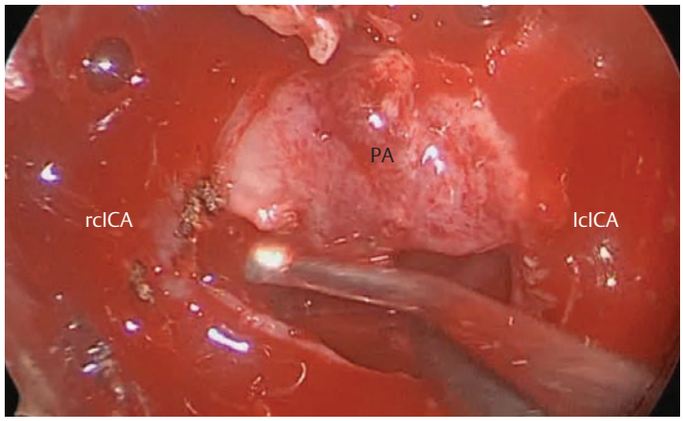

Fig. 11.16 Removal of the inferior anterior tumor compartment using a blunt ring curette. Pituitary adenoma (PA), right cavernous ICA (rcICA), left cavernous ICA (lcICA).

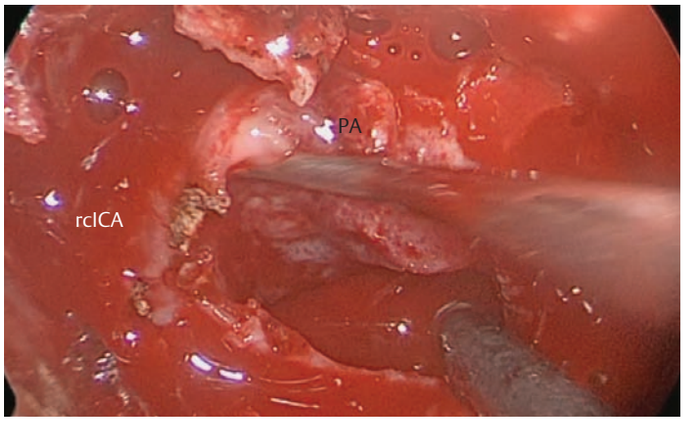

Fig. 11.17 Removal of the inferior lateral tumor compartment using a blunt ring curette. Pituitary adenoma (PA), right cavernous ICA (rcICA), left cavernous ICA (lcICA).

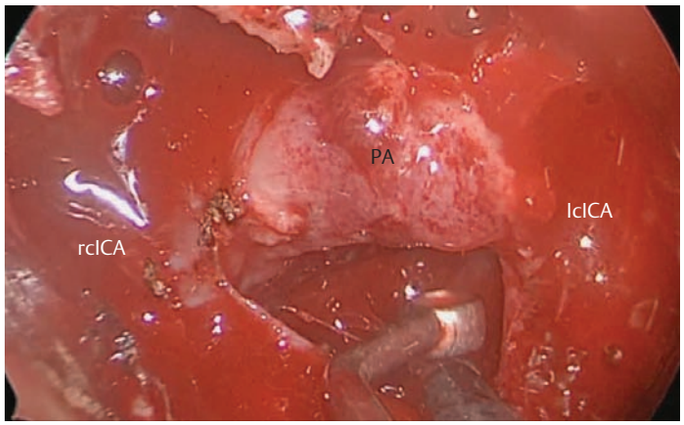

Fig. 11.18 Removal of the inferior posterior tumor compartment using a blunt ring curette. The clival dura (C) covering the posterior wall of the sella turcica is the posterior limitation. Pituitary macroadenoma (PMA), right cavernous ICA (rcICA), left cavernous ICA (lcICA).

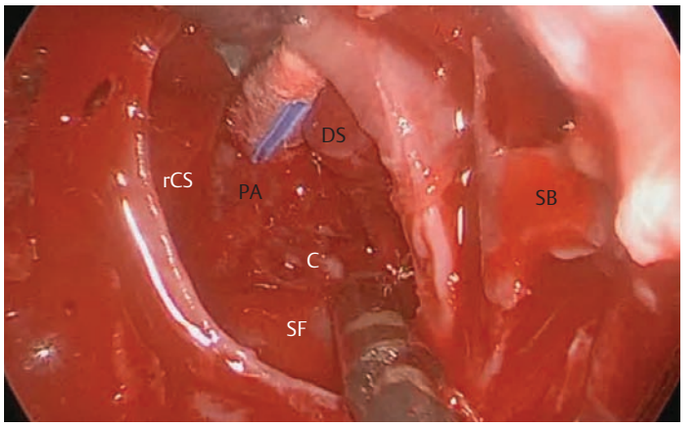

Fig. 11.19 Removal of the superior posterior tumor compartment. The diaphragma sellae (DS) is protected with a cottonoid to prevent prolapse and obstruction of the surgical field. Right cavernous sinus (rCS), clivus (C), sellar floor (SF), sellar bone (SB), pituitary adenoma (PA).

- Posterior limitation is the dura covering the clivus forming the posterior wall of the sella turcica (**Fig. 11.20**).
- Superior tumor debulking should be started posteriorly to avoid diaphragmal dura to bulge into the field and block the surgeon's view (**Fig. 11.21**).
- The anterior superior part should be approached as a last step. The likelihood for cerebrospinal fluid leaks is higher while resecting these parts of the tumor near the planum sphenoidale (**Figs. 11.22 and 11.23**).
- The small skull base defect is closed with Surgicel (oxidized cellulose polymer) and the sphenoid sinus is filled with Gelfoam (absorbable gelatin sponge).
- Both septal flaps are approximated in the midline and the septal incision is covered with NasoPore (synthetic biodegradable foam) while making sure to provide adequate airway along the nasal floor.

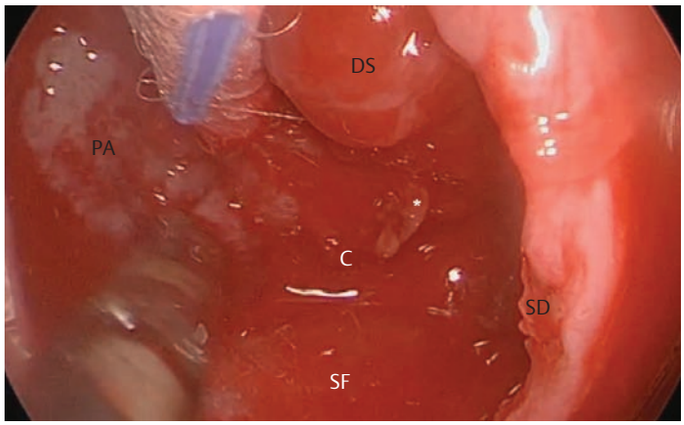

Fig. 11.20 Removal of the superior posterior tumor compartment. The diaphragma sellae (DS) is protected with a cottonoid to prevent prolapse and obstruction of the surgical field. Clivus (C), compressed pituitary gland (*), sellar floor (SF), sellar dura (SD), pituitary adenoma (PA).

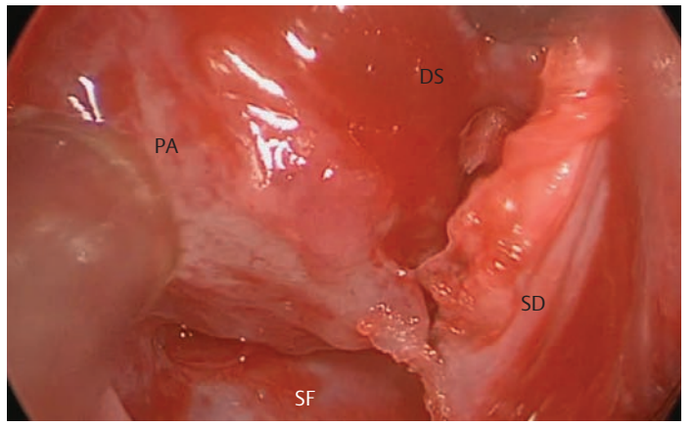

Fig. 11.21 Removal of the superior anterior tumor compartment from the compressed pituitary gland (*) along the diaphragma sellae (DS). Sellar floor (SF), sellar dura (SD), pituitary adenoma (PA).

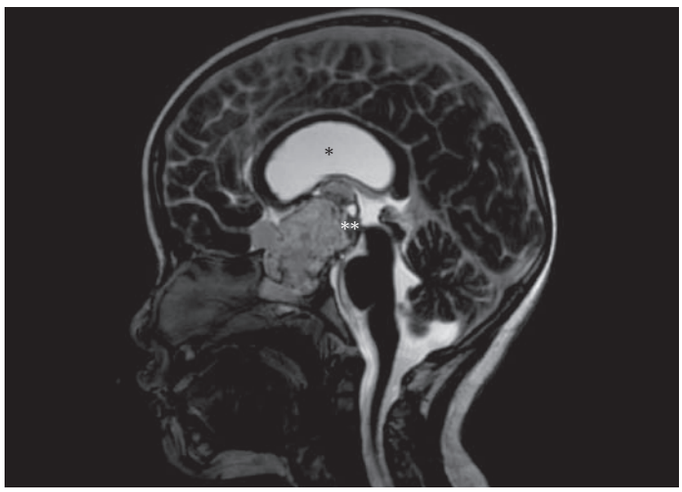

Fig. 11.22 Preoperative T2-weighted sagittal MRI section showing a hyperintense intra- and suprasellar mass involving the third ventricle and causing an obstructive hydrocephalus (*). Hypointense signals are suggestive of calcifications (**). No cortical cuff is distinguishable.

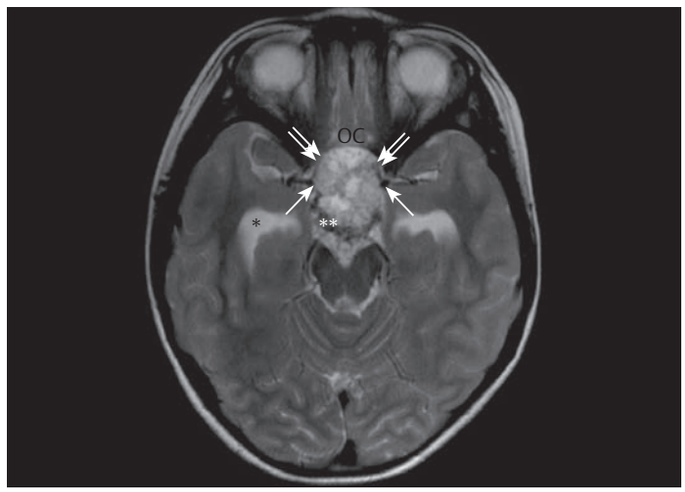

Fig. 11.23 Preoperative T2-weighted axial MRI section showing a hyperintense suprasellar mass causing an obstructive hydrocephalus (*). Hypointense signals are suggestive of calcifications (**). No cortical cuff is distinguishable. The tumor seems to be adherent to the internal carotid artery bifurcations (*arrow*) and anterior cerebral arteries (*double arrow*). Optic chiasm (OC).

Binostril Transseptal Transsphenoidal Approach for a Large Solid Pediatric Adamantinomatous Craniopharyngioma Involving the Third Ventricle

Tailoring the nasal approach using both narises for the surgical resection of larger sellar lesions allows a broader range of maneuvers. The binostril approach provides a higher flexibility for the ENT surgeon in terms of positioning of the endoscope and allows a two-surgeon four-hand technique.[4,5] The possibility for the neurosurgeon to bimanually dissect using microsurgical instruments are of particular importance when addressing suprasellar lesion like craniopharyngioma that, when compared with pituitary adenoma, tend to adhere and be in close relationship with critical neurovascular structures and might even extend into the third ventricle.[6]

Case History

A 6-year-old child was presented with progressive headaches and loss of vision, as well as occasional vomiting. Endocrinological examination revealed a growth hormone deficiency. Neurocranial imaging confirmed a mainly solid sellar and suprasellar lesion involving third ventricle with compression and dislocation of the optic nerves, being suspicious for a craniopharyngioma (**Figs. 11.24 and 11.25**).

A binostril endonasal endoscopic transsphenoidal resection of the lesion was recommended.

Surgical Steps

- Local anesthesia is infiltrated into the septum to raise the mucoperichondrial flaps bilaterally in preparation for creation of the pedicled nasoseptal flaps.
- An incision is made with a size 15 blade anterior to the middle turbinate down to the cartilaginous septum.
- The nasoseptal flap is raised off the septum with a Freer's elevator posteriorly until the sphenoid ostia and posterior choana are visible. Superiorly, the flap maybe taken up to ~0.5 to 1 cm below the skull base to preserve the olfactory function. Inferiorly, the flap can be taken as far as half the nasal floor if a large skull base defect is expected.
- The nasoseptal flap is then freed with microscissors superiorly and inferiorly aiming for the sphenoid ostia and posterior choana, respectively (Hadad–Bassagasteguy flap).[7,8]

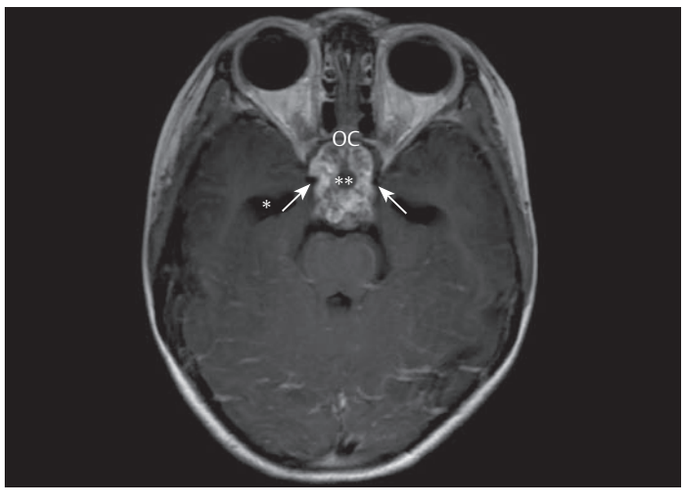

Fig. 11.24 Preoperative T1-weighted gadolinium contrast-enhanced axial MRI section showing a hyperintense contrast-enhancing suprasellar mass causing an obstructive hydrocephalus (*). Hypointense non-enhancing areas are present and are suggestive of calcifications (**). Internal carotid artery bifurcations (*arrow*), optic chiasm (OC).

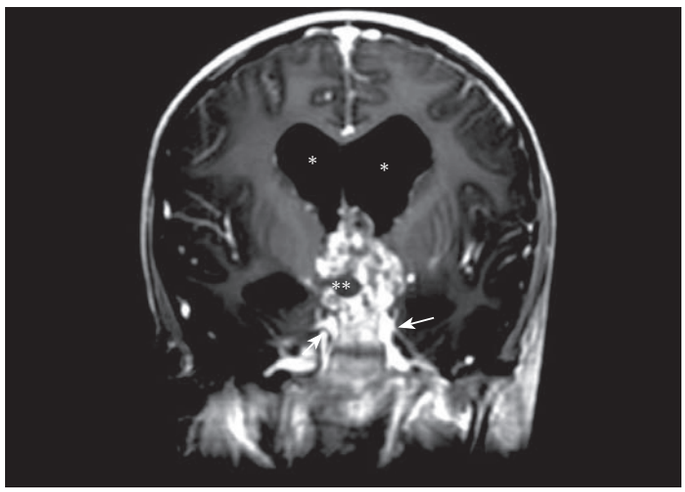

Fig. 11.25 Preoperative T1-weighted gadolinium contrast-enhanced coronal MRI section showing a hyperintense contrast-enhancing suprasellar mass causing an obstructive hydrocephalus (*). Hypointense non-enhancing areas are present and are suggestive of calcifications (**). Internal carotid artery bifurcations (*arrow*).

- The exposed cartilaginous septum is fractured through to the contralateral side and removed by piecemeal, all the while freeing it from the overlying contralateral septal mucoperichondrium (**Fig. 11.26**).
- This step is continued until the sphenoid keel is exposed with both sphenoid ostia visible. The pedicled flap can then be stored in the nasopharynx until reconstruction is required (**Fig. 11.27**).
- At this point, the contralateral nasoseptal flap can be created in the same manner as previously described.
- Once the sphenoid keel is fully exposed, the ostia are widened inferomedially using a Kerrison's punch in a V shape toward the midline (**Figs. 11.28 and 11.29**).
- The sphenoid keel is removed with a pituitary rongeur forceps.
- Remnant sphenoid keel, posterior ethmoid cells and mucosa, as well as sphenoid sinus septations are removed to allow an unobstructed view.
- The posterior wall of the sphenoid sinus is demucosalized with a monopolar cautery tipped aspirator.

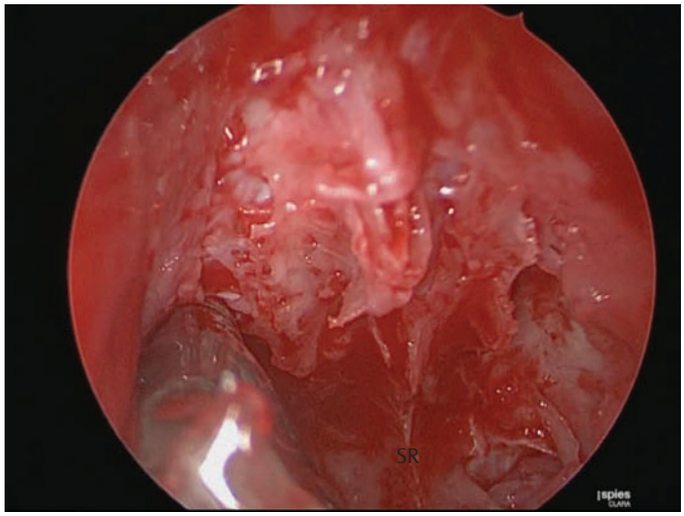

Fig. 11.26 View of the superior sphenoid rostrum (SR) after posterior ethmoidectomy and removal of the posterior bony septum.

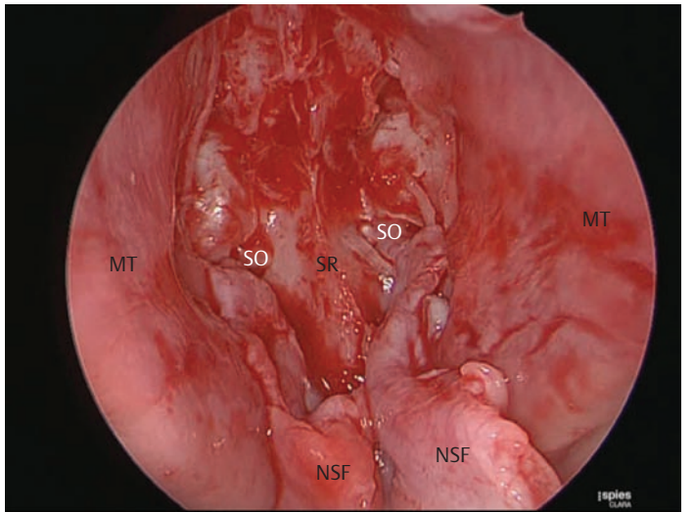

Fig. 11.27 View of the sphenoid rostrum (SR), the sphenoid ostia (SO) as well as the bilateral harvested nasoseptal flaps (NSF). Middle turbinates (MT).

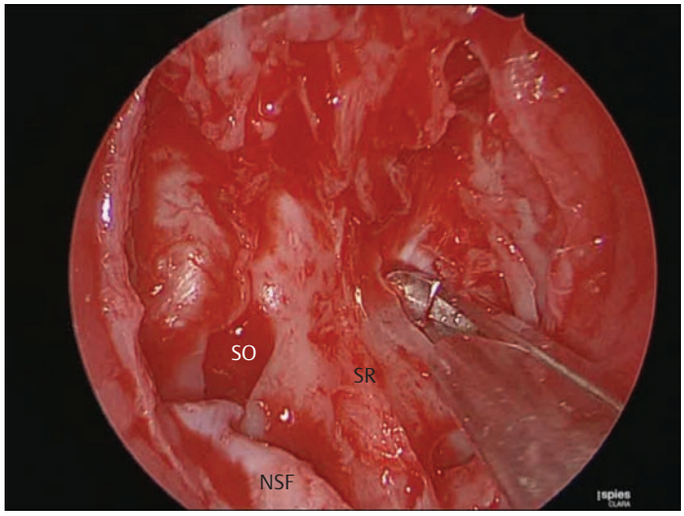

Fig. 11.28 Sphenoid osteotomy (SO) using a Kerrison's punch. Nasoseptal flaps (NSF). Sphenoid rostrum (SR).

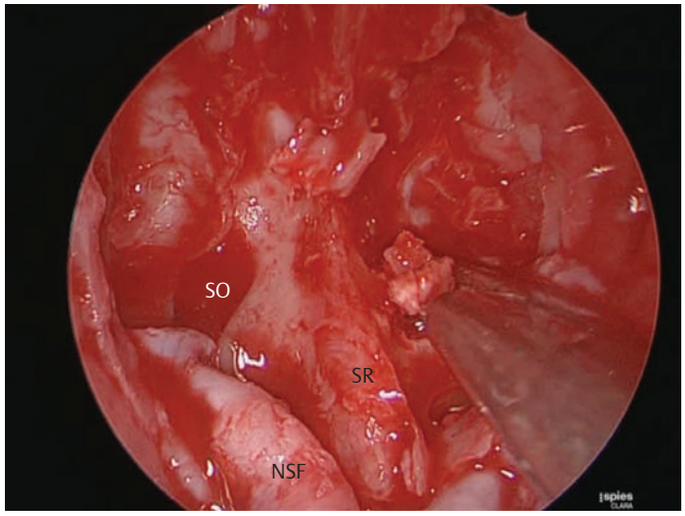

Fig. 11.29 Sphenoid osteotomy (SO) using a Kerrison's punch. Nasoseptal flaps (NSF). Sphenoid rostrum (SR).

This maneuver faciliates drilling of the sella and tuberculum and prevents oozing from mucosal edges.

- Drilling is then commenced with a high speed diamond burr to thin out the bone overlying the sella and tuberculum. An aspirator is kept within the nasal cavity to allow bone dust and smoke to be cleared to give an unobstructed view.
- Once the bone has been sufficiently thinned out, a right angle dissector can be insinuated between the bone and the dura, and the bone is flaked off.
- After enough bone has been removed, exposure can be completed with a Kerrison's punch. The superior and inferior extent of osteodural exposure is dictated by the size of the lesion and can be confirmed with neuronavigation (**Fig. 11.30**).
- Dura overlying the lesion is incised vertically (**Fig. 11.31**).
- The underlying tissue is separated from the incision using a blunt hooked instrument and the opening is completed in a cross-shaped manner (**Figs. 11.32 and 11.33**).
- Excision is then started at the central component of the lesion with a combination of suction, dissection, and ultrasonic aspirator (**Fig. 11.34**).

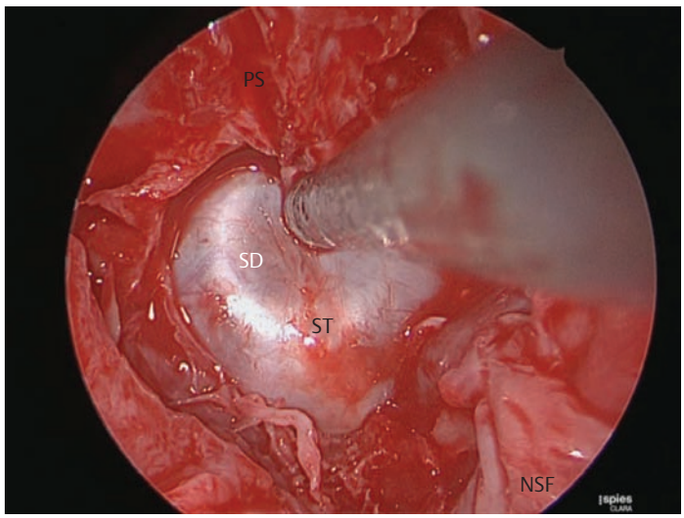

Fig. 11.30 The view of the sellar dura (SD) after removal of the sphenoid keel and opening of the bone covering the sella turcica (ST). Pedicle of the left nasoseptal flap (NSF). Planum sphenoidale (PS).

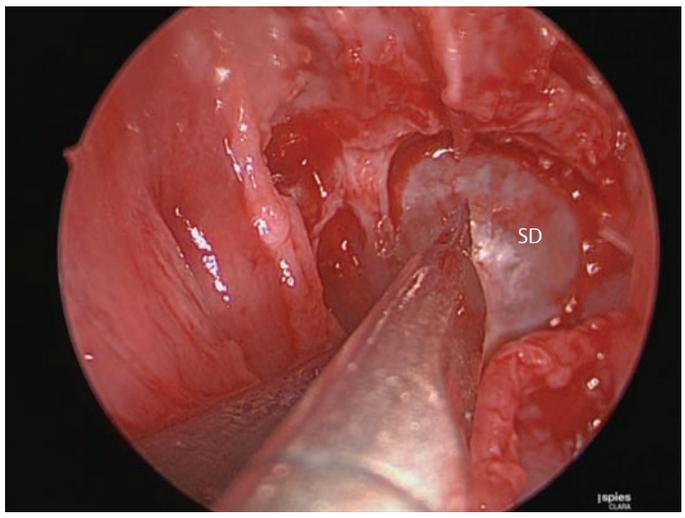

Fig. 11.31 Vertical incision of the sellar dura (SD).

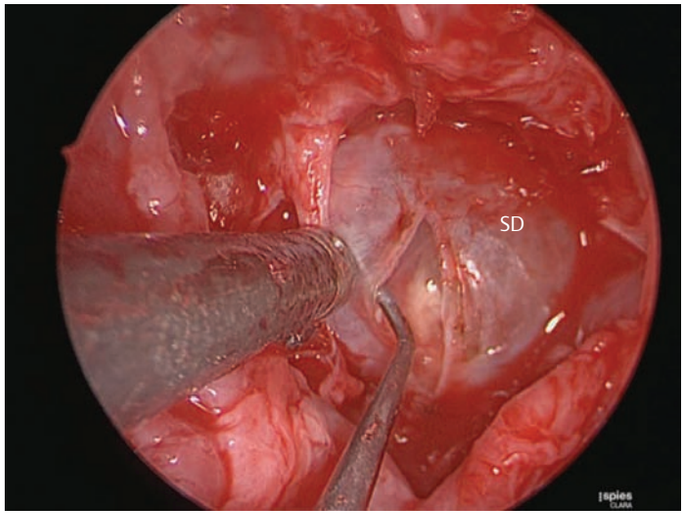

Fig. 11.32 Definition of the dissection plane between the sellar dura (SD) and the intrasellar lesion using a blunt hooked instrument.

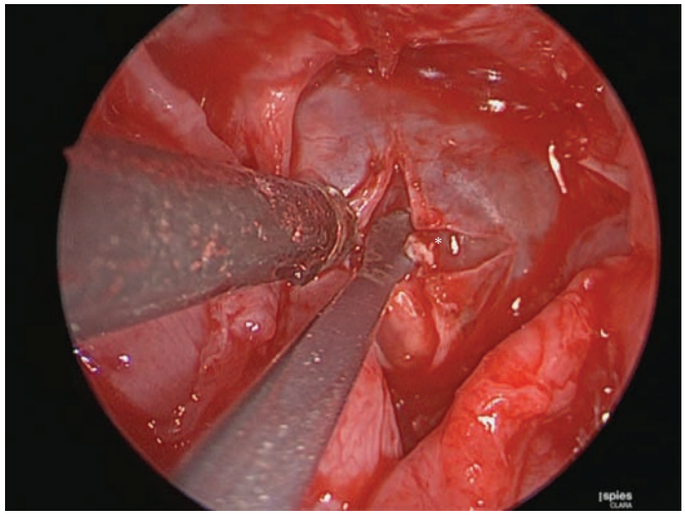

Fig. 11.33 Cruciate incision and definition of a dissection plane (*).

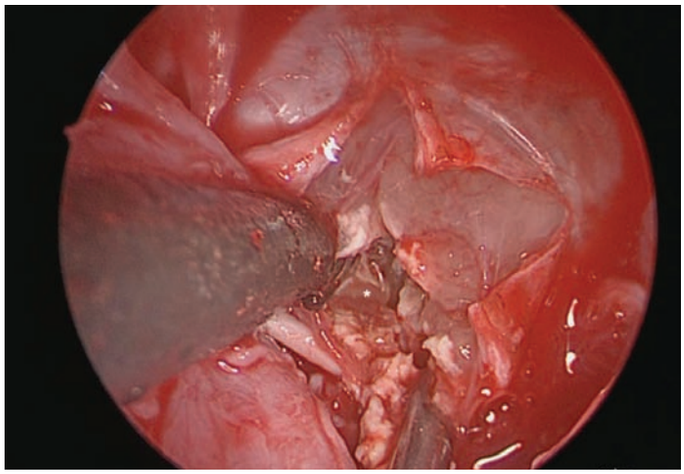

Fig. 11.34 Central tumor debulking. The lesion is fleshy with occasional calcifications (*). The superior edge can be seen gradually falling into view.

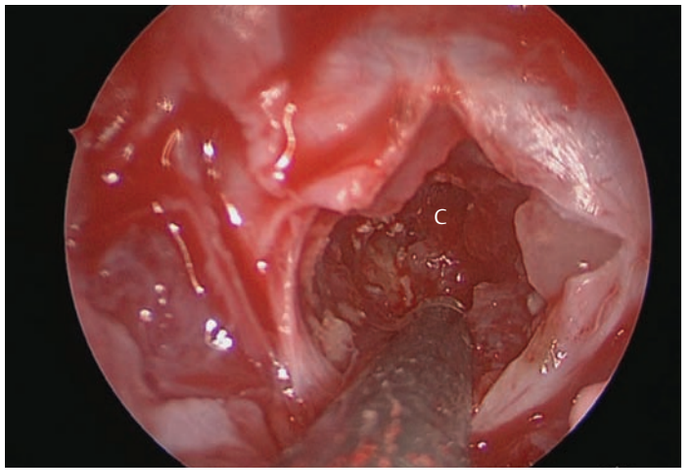

Fig. 11.35 Removal of the more posterior inferior solid tumor compartments until the clival dura is reached (C) defining the posterior wall of the sella turcica.

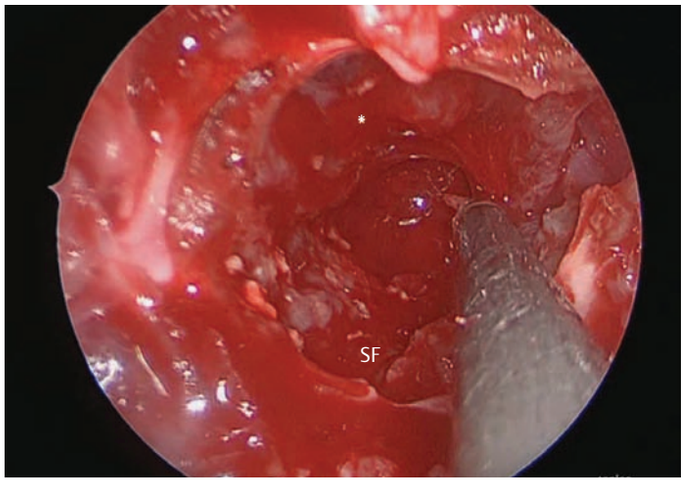

Fig. 11.36 More lateral inferior tumor debulking along the sellar floor (SF) allows the superior tumor compartment (*) to collapse.

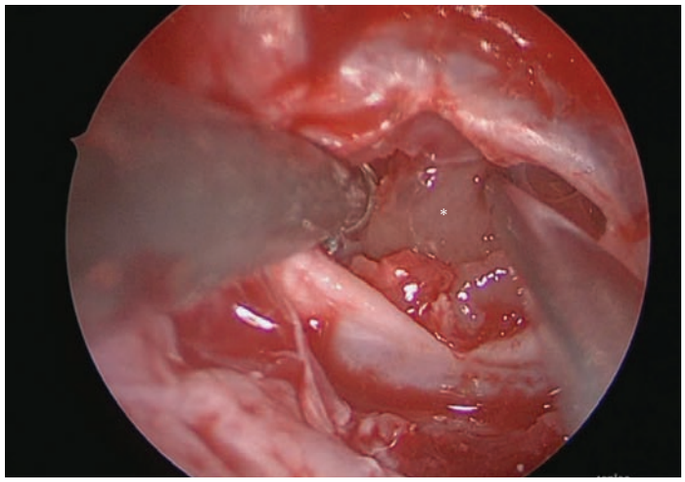

Fig. 11.37 The superior tumor compartment (*) is delivered centrally.

- As the central component is debulked, the weight of the surrounding soft tissue will cause the tumor edges to collapse into the central zone. This allows the periphery of the lesion and the edges to be delivered through a smaller opening rather than having to expand the exposure along the skull base (**Figs. 11.35 and 11.36**).
- The central debulking should be continued as far as safely visualized. Localization should be confirmed with image-guided surgery regularly. Dissection should not be continued when a depth reference is lacking (**Fig. 11.37**).
- The superior edge of the tumor is then delivered into view. This step should be performed gently so as not to put too much traction on the optic chiasm superiorly (**Fig. 11.38**).
- Calcified tumor compartments might be adherent to the intracranial and adjacent perforating vessels and have to be dissected from the optic chiasm (**Fig. 11.39**).
- As the tumor is delivered centrally, it may be debulked further to allow the edges to fall in. However, the capsule should be maintained as not to lose the dissection plane (**Fig. 11.40**).

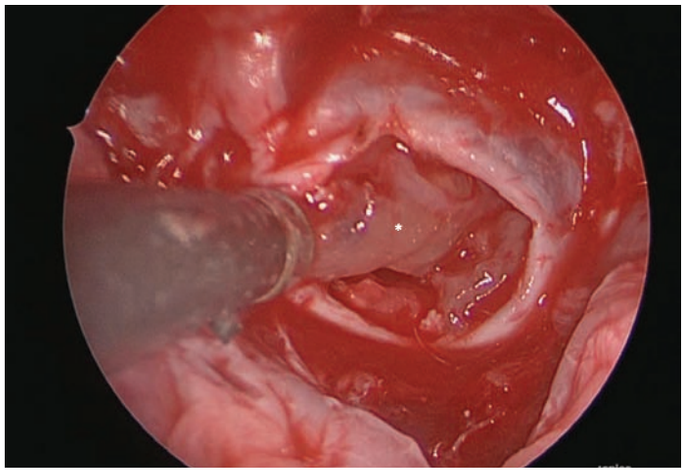

Fig. 11.38 The superior tumor compartment (*) is removed carefully with inspection of the adherent tissue and dissection along anatomical planes leading to relevant neurovascular structures.

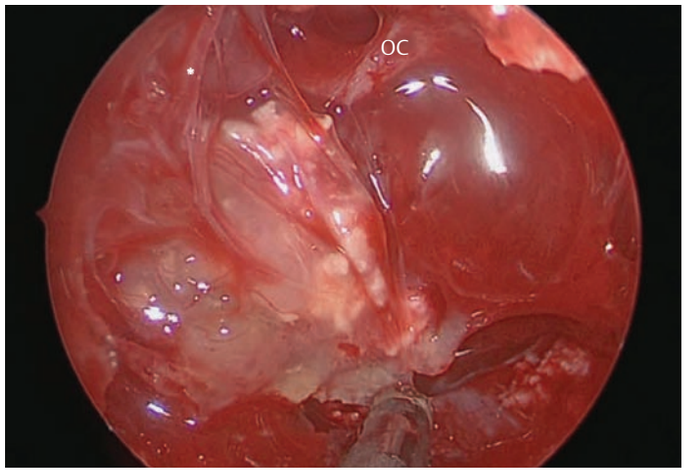

Fig. 11.39 Solid tumor component with calcifications show adherences to perforating vessels arising from the anterior H-complex (*) and the optic chiasm (OC).

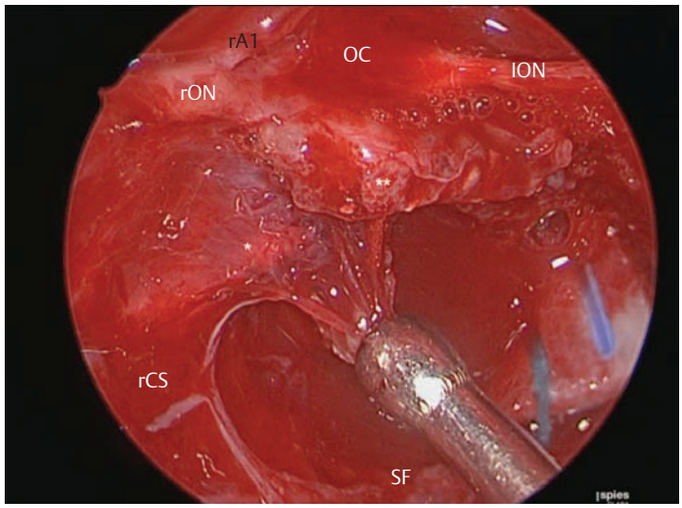

Fig. 11.40 The preservation of capsular planes and careful dissection in case of adherences allows identification and protection of critical neurovascular structures. Tumor capsule (*), solid tumor (**), left optic nerve (ION), right optic nerve (rON), right proximal anterior cerebral artery (rA1), right cavernous sinus (rCS), sellar floor (SF).

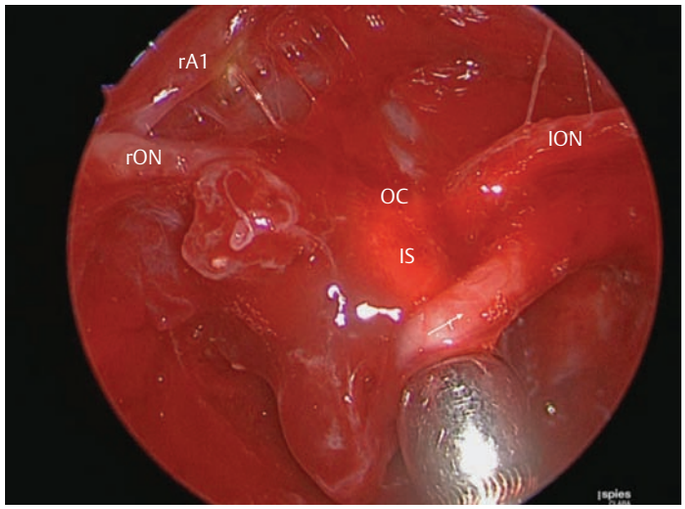

Fig. 11.41 Careful removal of the adherent tumor capsule (*arrow*) from the optic chiasm (OC), left optic nerve (ION), infundibular stalk (IS). Right optic nerve (rON), right proximal anterior cerebral artery (A1), anterior perforating vessels (*).

- The dissection plane and careful removal of solid tumor pieces, as well as the adherent tumor capsule, allows to identify and preserve crucial structures including the vessels of the anterior H-complex, the optic chiasm, the optic nerves, and the infundibular stalk (**Fig. 11.41**).
- After removal of the anterior tumor compartments, the anatomical structures of the suprasellar cistern are identified, resection of the more posterior and superior tumor compartments leading to the third ventricle is performed (**Fig. 11.42**).
- Craniopharyngiomas involving the third ventricle can be very adherent to the walls of the hypothalamus and removal should only be considered if a dissection plane or spontaneous collapse of the tumor capsule allows non-traumatic removal (**Fig. 11.43**).
- After removal of the intraventricular part, the choroid plexus of the third ventricle and the foramina of

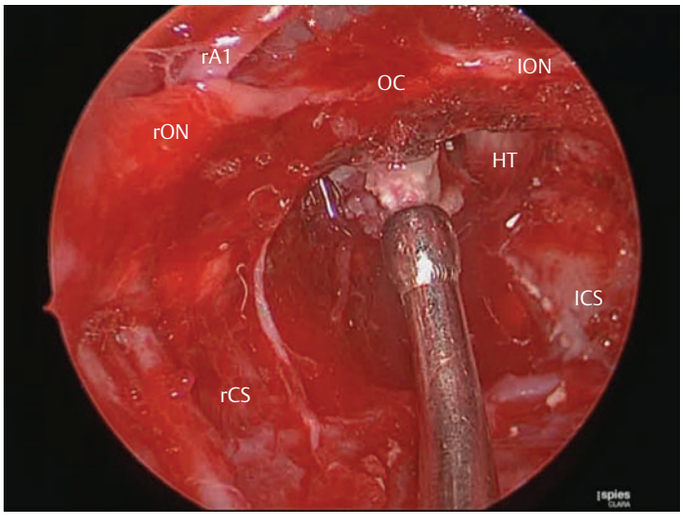

Fig. 11.42 Resection of the intraventricular solid tumor compartment from the third ventricular wall formed by the hypothalamus (HT). Optic chiasm (OC), left optic nerve (lON), right optic nerve (rON), right proximal anterior cerebral artery (A1), anterior perforating vessels (*), right cavernous sinus (rCS), left cavernous sinus (lCS).

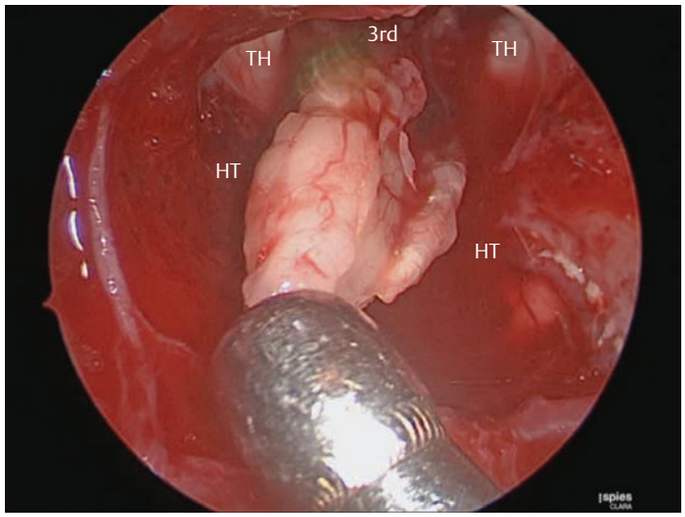

Fig. 11.43 Resection of the intraventricular solid tumor compartment from the third ventricular (3rd) wall formed by the hypothalamus (HT) and thalamus (TH).

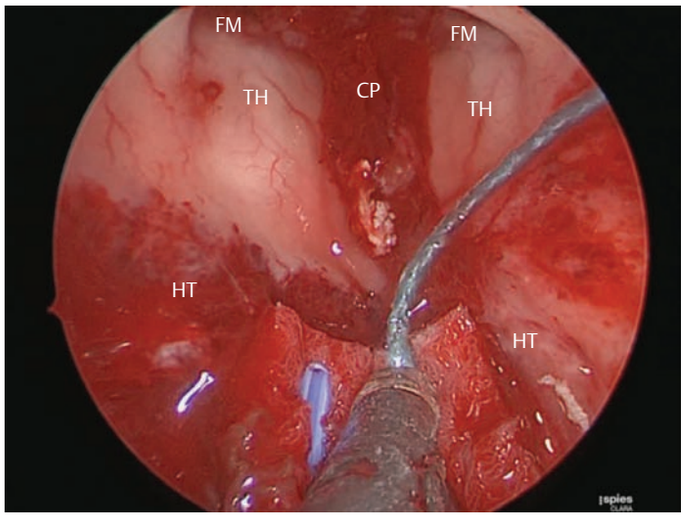

Fig. 11.44 Endoscopic endonasal view into the third ventricle, with no remnant tumor identified. The interventricular foramina of Monro (FM) are visible superiorly leading to the lateral ventricles and the choroid plexus (CP) is seen at the bottom of the picture. Bilaterally, the hypothalamus (HT) and thalamus (TH) are visible.

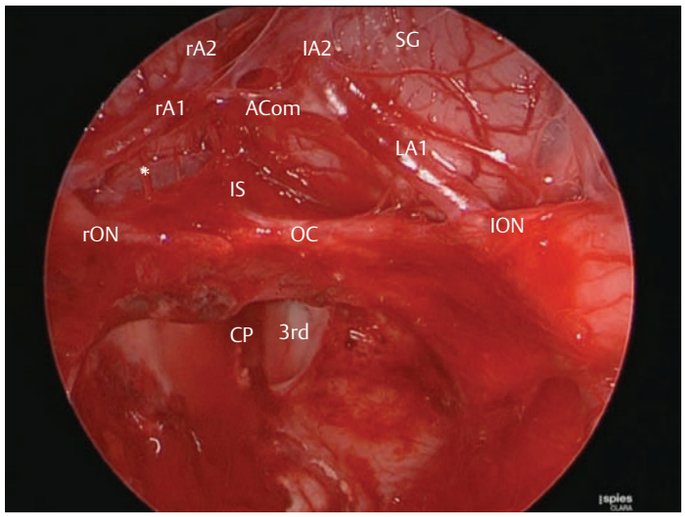

Fig. 11.45 Final view after tumor resection. Optic chiasm (OC), left optic nerve (lON), right optic nerve (rON), right proximal anterior cerebral artery (rA1), left proximal anterior cerebral artery (lA1), anterior communicating artery (ACom), anterior perforating vessels (*), right distal anterior cerebral artery (rA2), left distal anterior cerebral artery (lA2), infundibular stalk (IS), straight gyrus (SG), third ventricle (3rd), choroid plexus (CP).

Monro are important anatomical landmarks to identify (**Figs. 11.44–11.46**).

- The dural defect is then plugged with a harvested fat graft from the right thigh. The edges are tucked under the defect for a watertight closure (**Fig. 11.47**).
- A layer of harvested fascia lata graft from the right thigh is then placed over the fat (**Fig. 11.48**).
- The construct is sealed with an artificial dural sealant (**Fig. 11.49**), and reinforced with a further layer of absorbable hemostat.

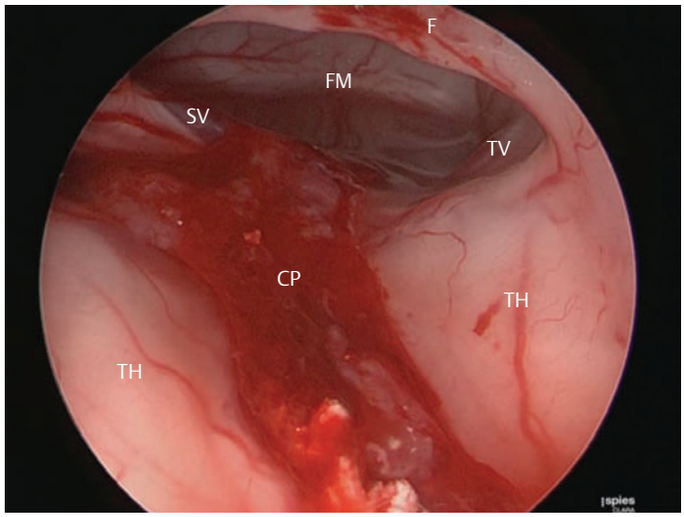

Fig. 11.46 Endoscopic endonasal view into the third ventricle. The fornix (F) forms the roof of the left interventricular foramina of Monro (lFM) leading to the left lateral ventricle (lLV). The choroid plexus (CP), the septal vein (SV), and the thalamic vein (TV) are visible. The thalamus is visible on both sides (TH) at the bottom of the picture. Bilaterally, the hypothalamus (HT) and thalamus (TH) are visible.

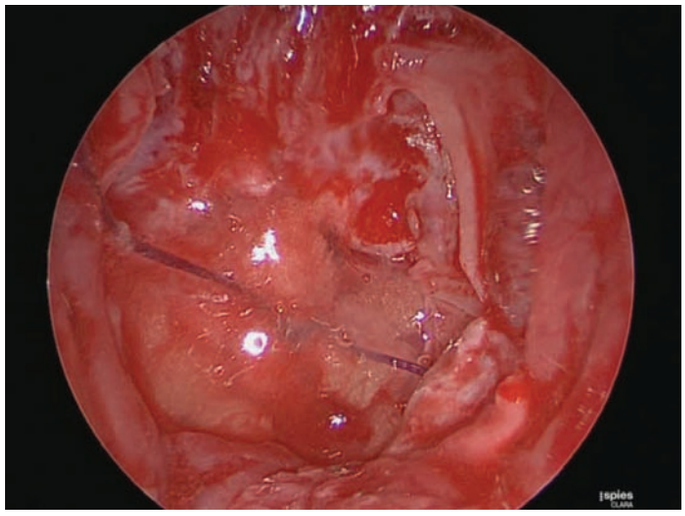

Fig. 11.47 Autologous fat graft being tucked under the defect edges.

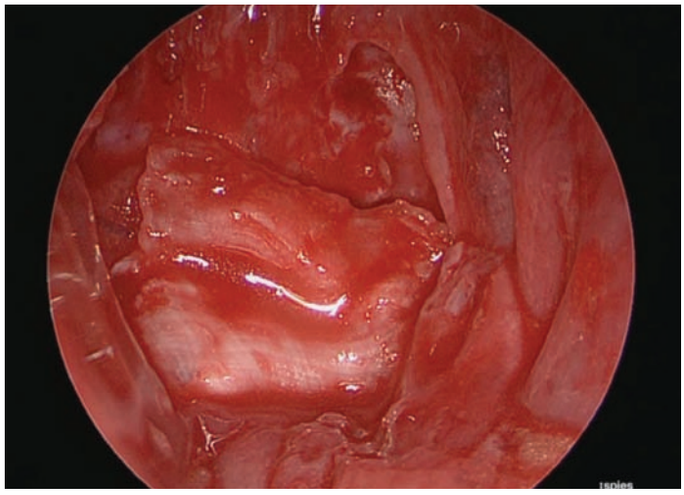

Fig. 11.48 Autologous fascia lata graft covering the construct.

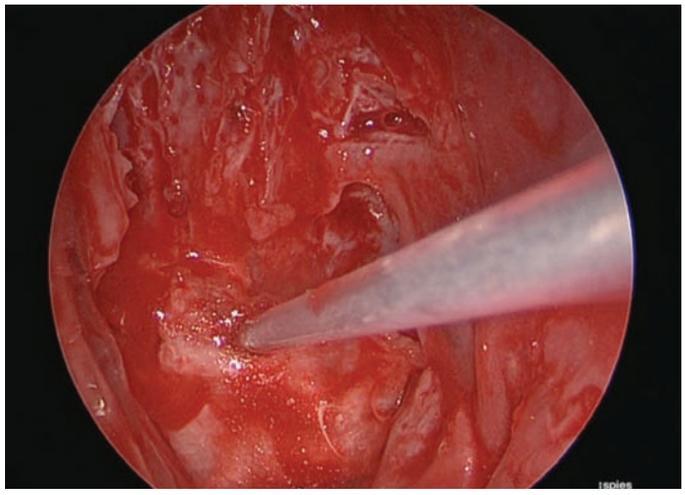

Fig. 11.49 Application of artificial dural sealant.

- Finally, the pedicled nasoseptal flaps are rotated over the repair as a final layer.
- The nasoseptal flaps are then held in place with absorbable gelatin sponges. No nasal packing is required.

Expanded Endonasal Endoscopic Transplanum Transtuberculum Approach for a Tuberculum Sellae Meningioma

Extending the zonal dissection of the skull base beyond the sellar opening has been extensively described in the literature.[6,9–13] Possible extensions that can be applied when

addressing larger lesions of the skull base include transcribriform, transplanum, transtuberculum, and transclivus extensions.[14,15] These extensions of the surgical route depend on the size and firmness of the treated lesion: zonal dissection of the base of skull.[16,17] In the modern era of endonasal endoscopic surgeries, suprasellar meningiomas have been more and more amenable for pure endoscopic endonasal resection. The proximity to critical surrounding neurovascular structures remains a challenging feature of these tumors.[18] Many groups around the world report the extension of the classic midline corridor to the tuberculum sellae and planum sphenoidale.[19,20] The correct indication and assessment of factors that predict non-successful or incomplete resection of skull base meningioma previous to surgery are of great importance.[21,22] Transcranial approaches are well described and have to be considered when resection of these lesions is necessary.[23–26]

Case History

A 36-year-old woman was assessed due to occasional headaches and slowly progressive loss of vision. Ophthalmological examination revealed a typical unilateral temporal field defect with a contralateral quadrantanopia. Endocrinological examination depicted normal pituitary gland function. Neurocranial imaging confirmed the presence of a large suprasellar lesion involving the tuberculum sellae and the planum sphenoidale with dislocation of the carotid bifurcations and in close contact with the anterior cerebral artery complex. Dislocation of the chiasma opticum and the optic nerves was found to be related to the ophthalmological symptoms (**Figs. 11.50–11.53**).

The lesion was considered amenable for binostril endonasal endoscopic transsphenoidal resection.

Surgical Steps

- A binostril transseptal transsphenoidal approach with harvesting of bilateral pedicled nasoseptal flaps (Hadad–Bassagasteguy) allows exposure of the sella turcica, tuberculum sellae, and planum sphenoidale.
- The planum sphenoidale has to be exposed sufficiently prior to starting the osteodural exposure of the meningioma (**Fig. 11.54**).
- The most anterior and lateral extension of the anterior lesion can be defined using intraoperative neuronavigation.
- For the transplanum approach, the bony covering of the planum sphenoidale is thinned out using a high-speed diamond burr (**Fig. 11.55**).
- The thinned out bone should be dissected away from the dura and a circumferential widening of the osteodural exposure can be continued.
- For the transsellar and transtuberculum approach, the bone of the tuberculum sellae and the bony coverage

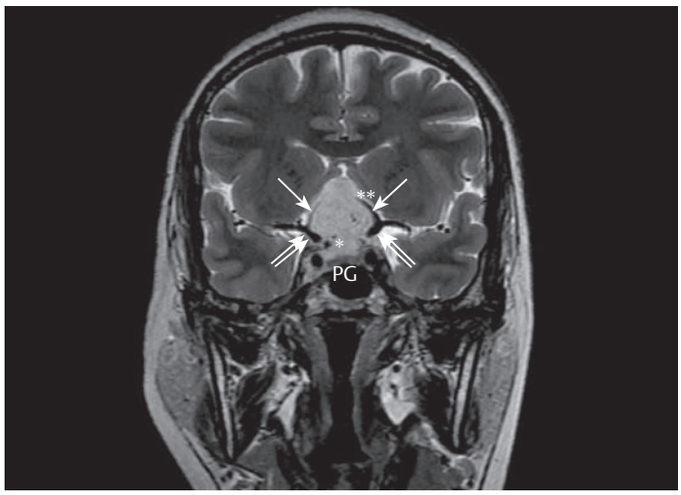

Fig. 11.50 Preoperative T2-weighted coronal MRI section showing a T2-isointense extra-axial solid mass on the tuberculum sella. The apex is in contact with the precommunicating segments of the anterior cerebral arteries (*arrow*) and dislocates the carotid bifurcations laterally on each side (*double arrow*). Hypointense signals are suggestive for calcifications (*). A cortical cuff sign can be appreciated (**).

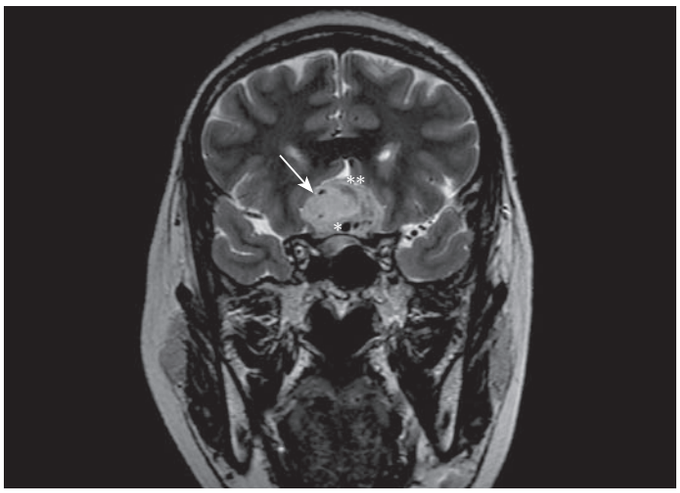

Fig. 11.51 Preoperative T2-weighted coronal MRI section showing the T2-isointense extra-axial solid mass extending along the planum sphenoidale. The apex is in contact with the postcommunicating segment of the anterior cerebral arteries (*arrow*). Hypointense signals are suggestive for calcifications (*). A cortical cuff sign can be appreciated (**).

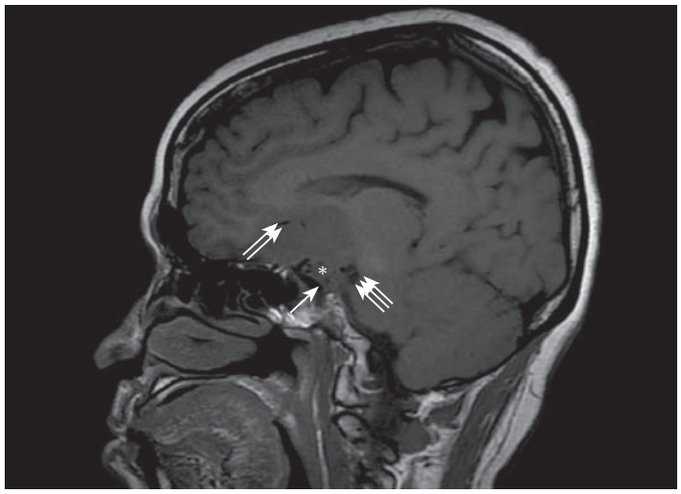

Fig. 11.52 Preoperative T1-weighted non-enhanced sagittal MRI section showing the suprasellar mass extending from the tuberculum sellae to the planum sphenoidale. Hypointense non-enhancing areas are present and are suggestive for calcifications (*). Internal carotid artery bifurcations (*arrow*), postcommunicating segment of the anterior cerebral arteries (*double arrow*), basilar artery (*triple arrow*).

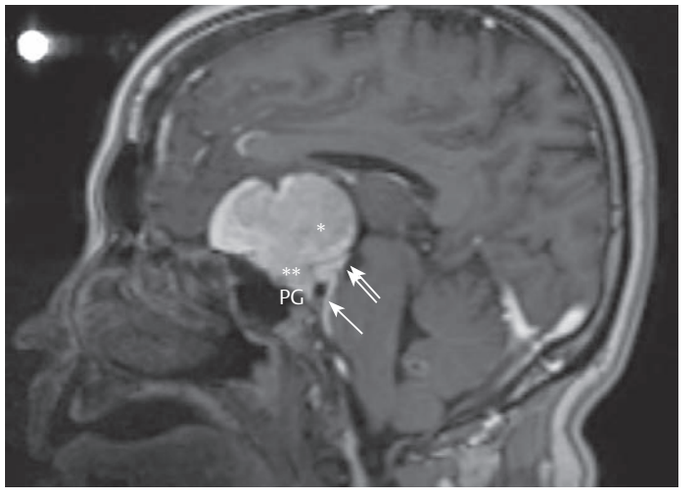

Fig. 11.53 Preoperative T1-weighted gadolinium contrast-enhanced sagittal MRI section showing the suprasellar mass extending from the tuberculum sellae to the planum sphenoidale. Hypointense non-enhancing areas are present and are suggestive of calcifications (*). The pituitary gland (PG) is separated by a hypointense arachnoid cleft (**) from the lesion. Basilar artery (*arrow*), posterior cerebral artery (*double arrow*).

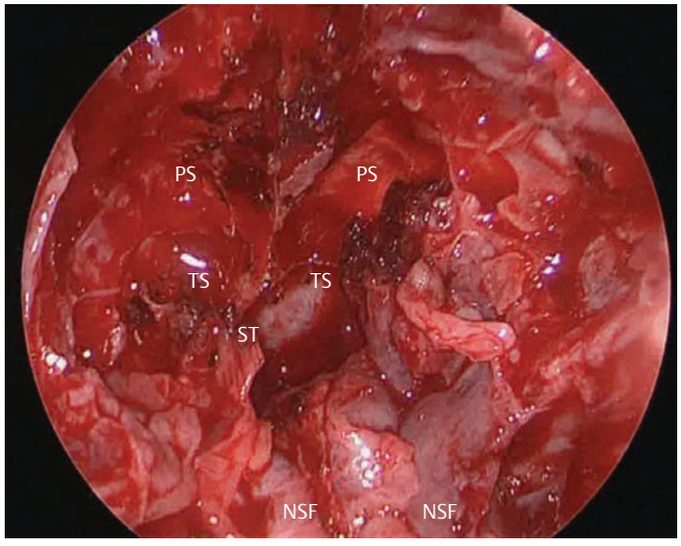

Fig. 11.54 Exposure of the sphenoid cavity with direct visualization of the planum sphenoidale (PS), tuberculum sellae (TS), and the sella turcica (ST), verified by image-guided surgery. Pedicle of nasoseptal flap (NSF).

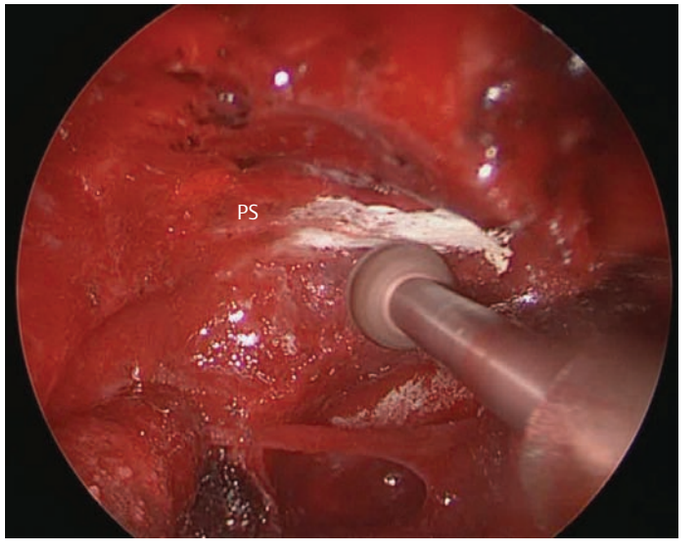

Fig. 11.55 Drilling of the planum sphenoidale (PS).

of the anterior intercavernous sinus are thinned out (**Fig. 11.56**). The drilling can be continued to the bone covering the sella turcica, when a relevant bone thickness is expected (**Fig. 11.57**).

- Removal of the lateral aspects of the tuberculum sellae allows a sufficient osteodural exposure and "release" of the meningioma in the posterior aspects. This will facilitate internal debulking of the posterior portion and facilitate extracapsular dissection along the brain–tumor interface (**Fig. 11.58**).
- Dural opening is started at the planum sphenoidale in a T-shaped manner. Using a dissecting instrument

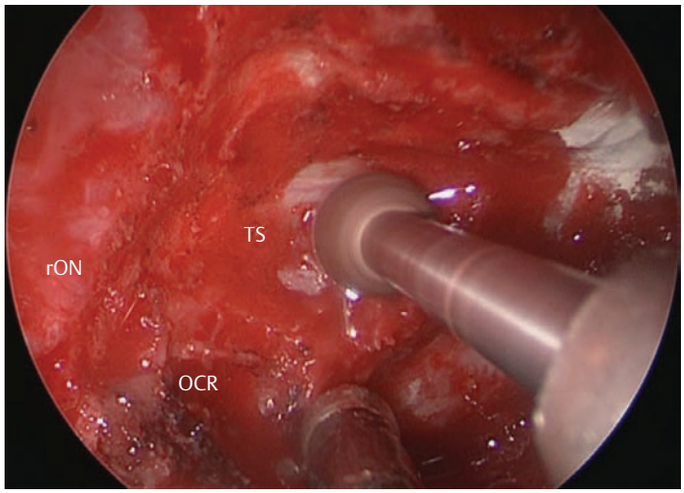

Fig. 11.56 Drilling of the tuberculum sellae (TS). Opticocarotid recess (OCR), right optic nerve (rON).

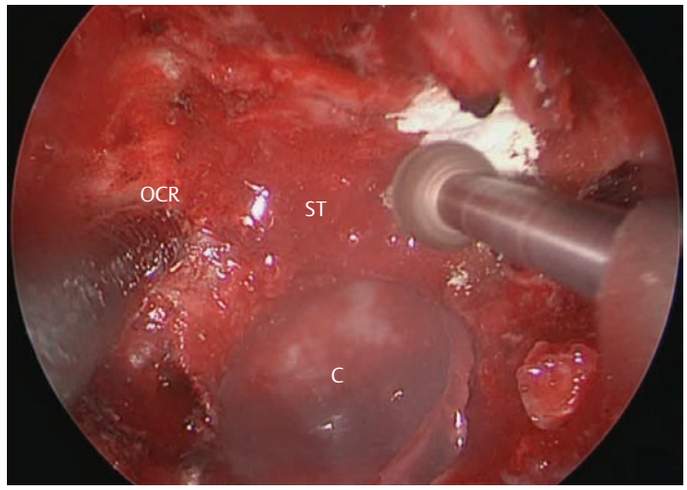

Fig. 11.57 Drilling of the sella turcica (ST). Opticocarotid recess (OCR), clivus (C).

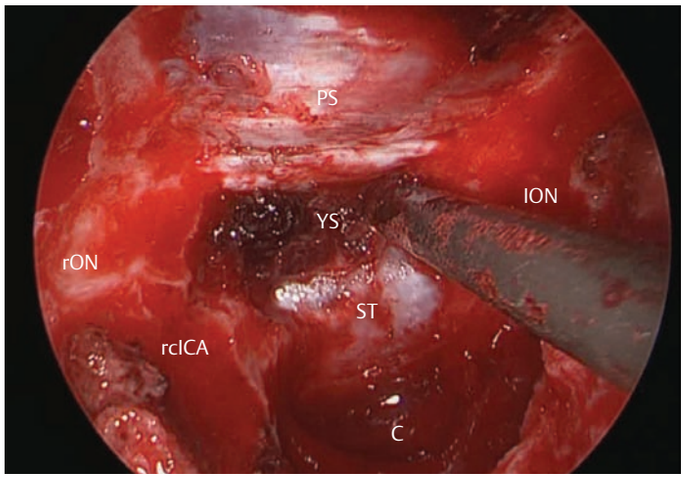

Fig. 11.58 Completed zonal dissection and osteodural exposure of the tuberculum sellae meningioma. Planum sphenoidale (PS), tuberculum sellae (TS), sella turcica (ST), clivus (C), right optic nerve (rON), left optic nerve (lON), right cavernous internal carotid artery (rcICA).

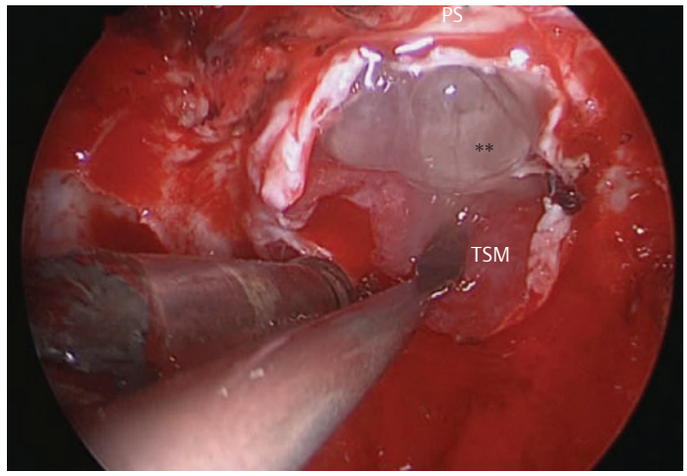

Fig. 11.59 Definition of the anterior brain–tumor interface (*) using the arachnoid layer (**). Planum sphenoidale (PS), tuberculum sellae meningioma (TSM).

and microscissors, the most anterior extension of the tumor has to be identified, and an arachnoid layer has to be visible (**Fig. 11.59**).

- Initial internal tumor debulking using suction or an ultrasonic aspirator is started in the anterior portion of the tumor (**Fig. 11.60**).
- The anterior extracapsular dissection is started from the most anterior point sideways bilaterally and continued posteriorly (**Fig. 11.61**).
- The dura of the sella turcica is then opened using a reversed T-shaped cut. This maneuver brings the pituitary gland and infundibular stalk into view.
- Meticulous coagulation and division of the anterior intercavernous sinus is necessary to connect the planum sphenoidale with the sellar region.
- Interior debulking of the posterior and tubercular portion of the tumor is then continued (**Fig. 11.62**).
- The extracapsular dissection using the arachnoid layer along the brain–tumor interface is continued posterioly on each side (**Figs. 11.63 and 11.64**).

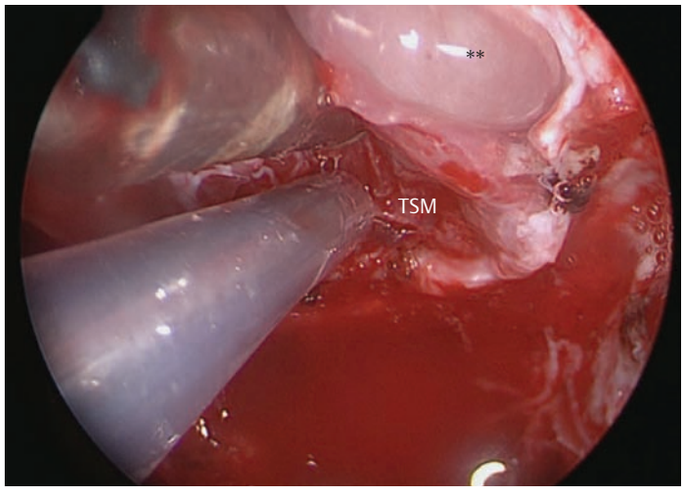

Fig. 11.60 Internal tumor debulking with an ultrasonic aspirator. The arachnoid layer (*) and the brain tumor interface (**) should be respected when removing the tuberculum sellae meningioma (TSM).

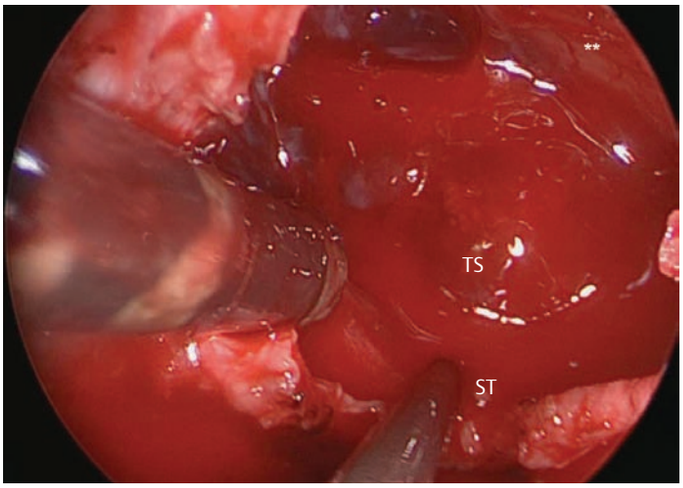

Fig. 11.61 Debulked tuberculum sellae (TS) and superior to the sella turcica (ST) portion of the meningioma.

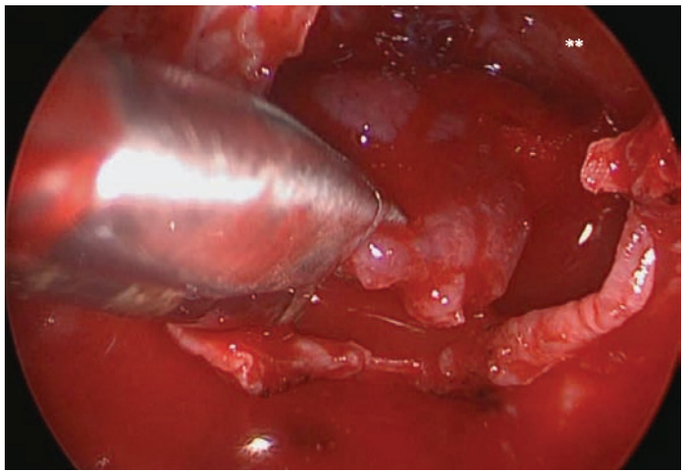

Fig. 11.62 Removal of the superior tuberculum sellae portion (*) of the meningioma from the brain surface (**).

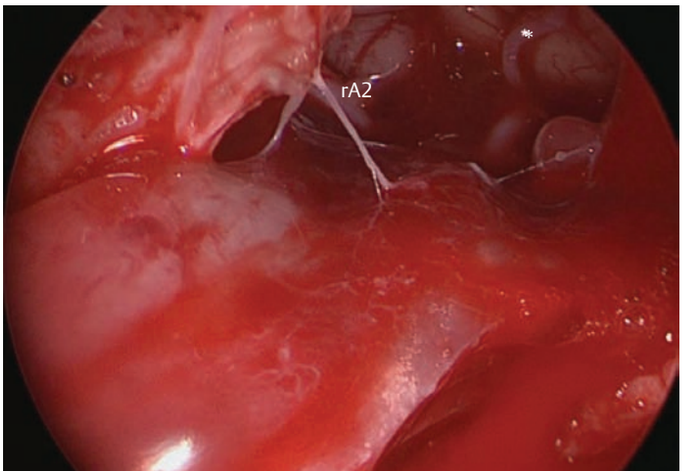

Fig. 11.63 The right distal anterior cerebral artery (rA2) and a small branch from the frontoporal artery (*) can be appreciated while removing the superior tuberculum sellae portion of the meningioma.

- The lateral tumor aspects of the tubercular portion are in anatomical relation with the optic nerve and the clinoidal portion of the carotid artery.
- The optic nerves, the optic chiasm, the pre- and post-communicating segments of both anterior cerebral arteries, the anterior communicating artery, and both recurrent arteries of Heubner have to be considered and identified (**Fig. 11.65**).
- Hemostasis is done with an absorbable hemostat (**Fig. 11.66**).
- The defect is plugged with an autologous fat graft from the thigh, and the edges of the fat are brought intracranially to create a watertight seal. Care is taken not to pack too much fat tightly into the cavity. The construct is sealed with an autologous fascia lata graft from the thigh (**Fig. 11.67**).
- A second autologous fat graft is used and the construct is stabilized with a synthetic dural sealant (**Fig. 11.68**).
- The bilateral vascularized nasoseptal flaps are then rotated over the defect to complete the repair and reinforced with gelatin sponges to keep the flaps in position. No other nasal packing is required.

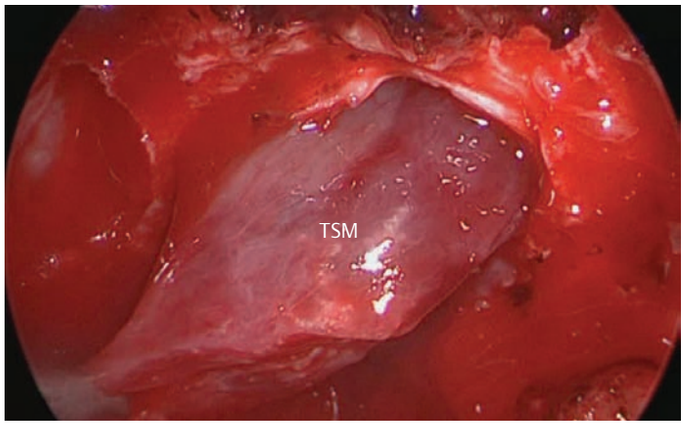

Fig. 11.64 When adequately liberated from the surrounding arachnoid layer, large pieces of meningioma can be removed. This maneuver has to be done carefully and only, if circumferential inspection of the dissection plane was possible, to not tear and injure adherent surrounding neurovascular structures.

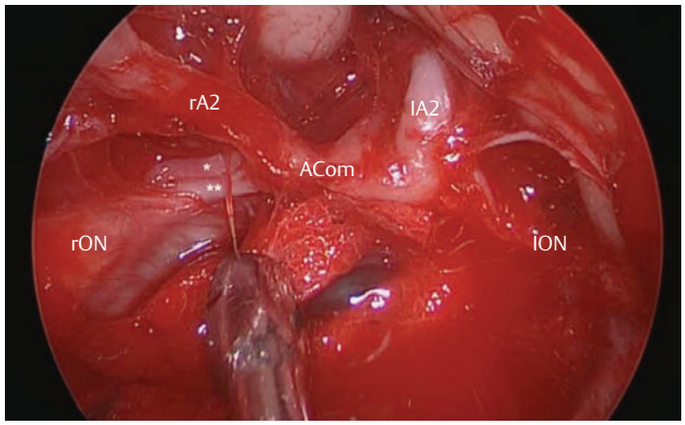

Fig. 11.65 Tumor resection cavity after removal of a tuberculum sellae meningioma. The optic chiasm is covered by a cottonoid. Right optic nerve (rON), left optic nerve (lON), anterior communicating artery (ACom), right distal anterior artery (rA2), left distal anterior artery (lA2), right recurrent artery of Heubner (*), perforating artery (**).

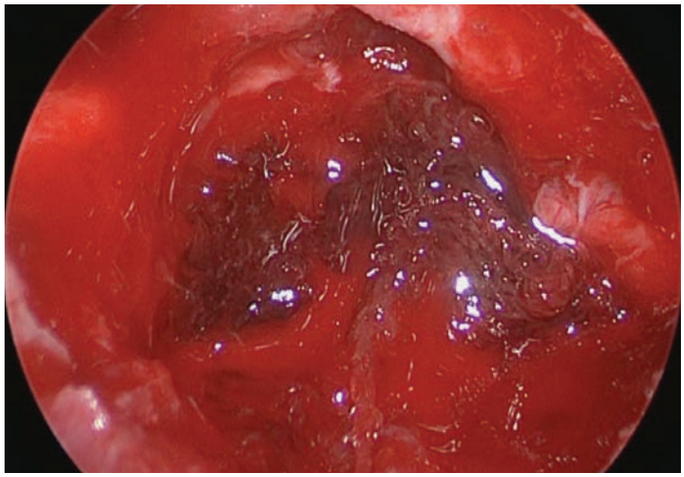

Fig. 11.66 Hemostasis with resorbable hemostat.

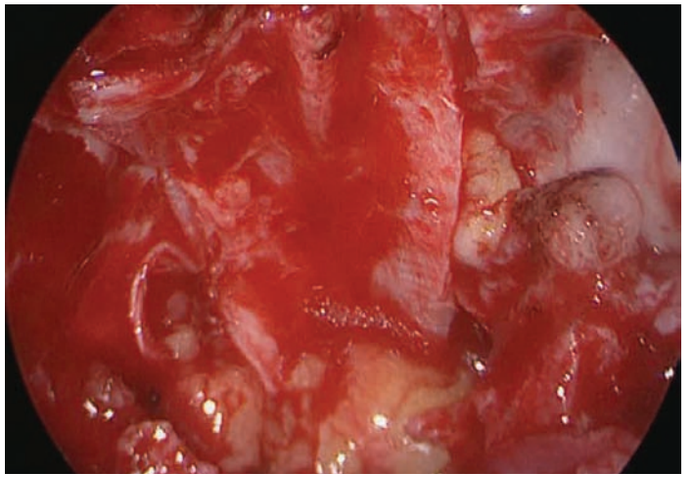

Fig. 11.67 Intradural autologous fat graft covered by autologous fascia lata graft.

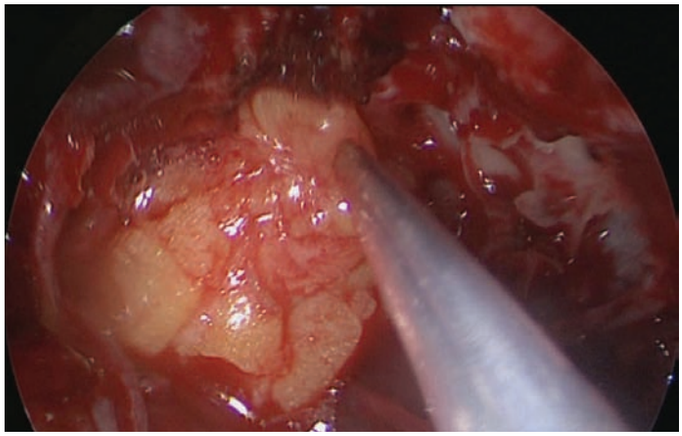

Fig. 11.68 Sealing of the reconstructed skull base defect with an artificial dural sealant.

References

1. Waran V, Tang IP, Karuppiah R, et al. A new modified speculum guided single nostril technique for endoscopic transnasal transsphenoidal surgery: an analysis of nasal complications. Br J Neurosurg 2013;27(6):742–746
2. Wen G, Tang C, Zhong C, et al. Mononostril versus binostril endoscopic transsphenoidal approach for pituitary adenomas: a systematic review and meta-analysis. PLoS One 2016;11(4): e0153397
3. Conrad J, Ayyad A, Wüster C, et al. Binostril versus mononostril approaches in endoscopic transsphenoidal pituitary surgery: clinical evaluation and cadaver study. J Neurosurg 2016; 125(2): 334–345

4. Gao Y, Zhong C, Wang Y, et al. Endoscopic versus microscopic transsphenoidal pituitary adenoma surgery: a meta-analysis. World J Surg Oncol 2014;12:94
5. Little AS, Kelly DF, Milligan J, et al. Comparison of sinonasal quality of life and health status in patients undergoing microscopic and endoscopic transsphenoidal surgery for pituitary lesions: a prospective cohort study. J Neurosurg 2015;123(3): 799–807
6. de Divitiis E, Cappabianca P, Cavallo LM. Endoscopic transsphenoidal approach: adaptability of the procedure to different sellar lesions. Neurosurgery 2002;51(3):699–705, discussion 705–707
7. Hadad G, Bassagasteguy L, Carrau RL, et al. A novel reconstructive technique after endoscopic expanded endonasal approaches: vascular pedicle nasoseptal flap. Laryngoscope 2006;116(10):1882–1886
8. Kassam AB, Thomas A, Carrau RL, et al. Endoscopic reconstruction of the cranial base using a pedicled nasoseptal flap. Neurosurgery 2008; 63(1, Suppl 1)ONS44–ONS52, discussion ONS52–ONS53
9. Dehdashti AR, Ganna A, Witterick I, Gentili F. Expanded endoscopic endonasal approach for anterior cranial base and suprasellar lesions: indications and limitations. Neurosurgery 2009;64(4):677–687, discussion 687–689
10. de Divitiis E, Cavallo LM, Cappabianca P, Esposito F. Extended endoscopic endonasal transsphenoidal approach for the removal of suprasellar tumors: Part 2. Neurosurgery 2007;60(1):46–58, discussion 58–59
11. Lee SC, Senior BA. Endoscopic skull base surgery. Clin Exp Otorhinolaryngol 2008;1(2):53–62
12. Lobo B, Heng A, Barkhoudarian G, Griffiths CF, Kelly DF. The expanding role of the endonasal endoscopic approach in pituitary and skull base surgery: a 2014 perspective. Surg Neurol Int 2015;6:82
13. Paluzzi A, Gardner P, Fernandez-Miranda JC, Snyderman C. The expanding role of endoscopic skull base surgery. Br J Neurosurg 2012;26(5):649–661
14. Solari D, Chiaramonte C, Di Somma A, et al. Endoscopic anatomy of the skull base explored through the nose. World Neurosurg 2014; 82(6, Suppl)S164–S170
15. Solari D, Villa A, De Angelis M, Esposito F, Cavallo LM, Cappabianca P. Anatomy and surgery of the endoscopic endonasal approach to the skull base. Transl Med UniSa 2012;2:36–46
16. Couldwell WT, Weiss MH, Rabb C, Liu JK, Apfelbaum RI, Fukushima T. Variations on the standard transsphenoidal approach to the sellar region, with emphasis on the extended approaches and parasellar approaches: surgical experience in 105 cases. Neurosurgery 2004;55(3):539–547, discussion 547–550
17. Couldwell WT. Transsphenoidal and transcranial surgery for pituitary adenomas. J Neurooncol 2004;69(1-3):237–256
18. Jallo GI, Benjamin V. Tuberculum sellae meningiomas: microsurgical anatomy and surgical technique. Neurosurgery 2002; 51(6):1432–1439, discussion 1439–1440
19. Lu VM, Goyal A, Rovin RA. Olfactory groove and tuberculum sellae meningioma resection by endoscopic endonasal approach versus transcranial approach: A systematic review and meta-analysis of comparative studies. Clin Neurol Neurosurg 2018; 174:13–20
20. Raza S, Effendi S, DeMonte F, Tuberculum sellae meningiomas: evolving surgical strategies. Curr Surg Rep 2014;2(11):73
21. Mascarella MA, Tewfik MA, Aldosari M, Sirhan D, Zeitouni A, Di Maio S. A simple scoring system to predict the resectability of skull base meningiomas via an endoscopic endonasal approach. World Neurosurg 2016;91:582–591.e1
22. Kong D, Hong C, Hong S, et al. Selection of endoscopic or transcranial surgery for tuberculum sellae meningiomas according to specific anatomical features: a retrospective multicenter analysis (KOSEN-002). J Neurosurg 2018;130(3): 838-847
23. de Divitiis E, Esposito F, Cappabianca P, Cavallo LM, de Divitiis O. Tuberculum sellae meningiomas: high route or low route? A series of 51 consecutive cases. Neurosurgery 2008;62(3):556–563, discussion 556–563
24. Muskens IS, Briceno V, Ouwehand TL, et al. The endoscopic endonasal approach is not superior to the microscopic transcranial approach for anterior skull base meningiomas: a meta-analysis. Acta Neurochir (Wien) 2018;160(1):59–75
25. Song SW, Kim YH, Kim JW, et al. Outcomes after transcranial and endoscopic endonasal approach for tuberculum meningiomas: a retrospective comparison. World Neurosurg 2018;109:e434–e445
26. Bohman LE, Stein SC, Newman JG, et al. Endoscopic versus open resection of tuberculum sellae meningiomas: a decision analysis. ORL J Otorhinolaryngol Relat Spec 2012;74(5): 255–263

12 Skull Base Approaches to the Lesions of Sellar and Parasellar Regions: Anatomy, Techniques, and Insights

Iype Cherian, Hira Burhan

Overview

Lesions of the sellar, parasellar, and suprasellar regions are common and account for up to 20% of all intracranial neoplasms. Of these, pituitary adenomas are the most common in adults, accounting for over 50% of all lesions in this region.[1] However, rare lesions involving vascular structures can arise in this region.[2] Magnetic resonance imaging has been a modality of choice to identify the type, location, and extension of the lesions, which determines the surgical planning and prognosis in sellar and parasellar pathologies.

With the use of endoscope as a routine surgical practice for sellar lesions, it is quite uncommon for sellar and suprasellar lesion to require complex intracranial approaches. However, the frontotemporal transcavernous approach can be used for tumors with extensive invasion. This approach defines the most intricate and advanced cranial base approach,[3] requiring elite surgical skills, and providing a maximal surgical corridor to adequately access the lesions.

The anatomy of the sellar region and its contents is important to understand the concept of skull base approach in surgical management of the lesions in these areas.

Anatomy

Located in the sphenoid bone, the sella turcica lies behind the chiasmatic groove and the tuberculum sellae, forming a part of the middle cranial fossa. The sella turcica houses the pituitary gland that rests on the hypophyseal fossa (the seat of the sella). Posteriorly, the bony sella is continuous with the clivus, which terminates laterally to form the posterior clinoid process.

These bony structures are valuable anatomical landmarks for surgical approaches to the lesions arising in these regions and also direct the course of the internal carotid artery (ICA) as it takes a torturous course during its extradural ascend from the parapharyngeal recess to the clinoid process.

Given the complex anatomy of the sellar region and the adjacent cavernous sinuses, bounded closely by the bony structures and the optic nerve pose a challenge in obtaining access while operating on lesions in the region. In this chapter, the approach to sellar lesions using a transcavernous frontotemporal modification of the conventional Dolenc's approach, for a bloodless, extradural surgical corridor has been discussed. See **Videos 12.1 and 12.2**.

Video 12.1 Modified Dolenc's Approach, Part 1. https://www.thieme.de/de/q.htm?p=opn/cs/19/9/10104318-94339f3f

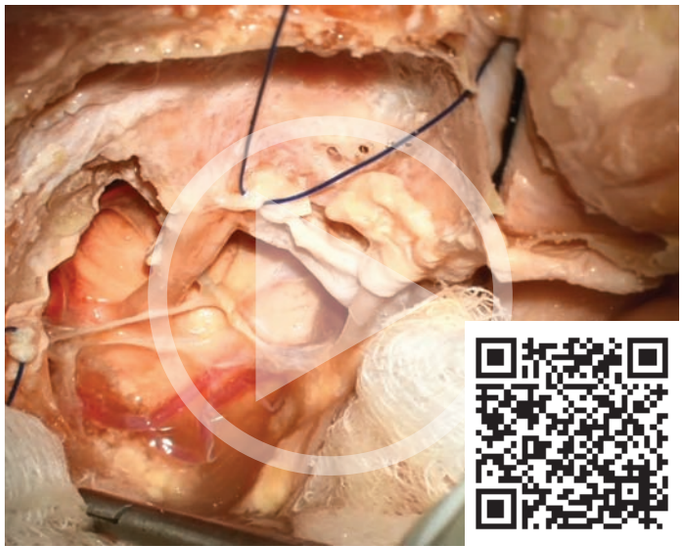

Video 12.2 Modified Dolenc's Approach, Part 2. https://www.thieme.de/de/q.htm?p=opn/cs/19/9/10104319-eaf37bc0

Surgical Techniques

Extended Skin Incision and Craniotomy

Lesions of the sellar and suprasellar regions are ideally approached using an extended skin incision to expose the frontotemporal, orbitobasal, and middle fossa. This skin excision is an extension of the routine pterional approach (**Fig. 12.1a**). A layer-by-layer dissection allows removal of subcutaneous tissue and the temporalis muscle is retracted to expose the bony structures underneath (**Fig. 12.1b, c**). The pterion and the keyhole serve as important landmarks for a craniotomy; the lateral margin of the sphenoid is drilled off as close to frontal bone as possible (**Fig. 12.1d**) and craniotomy is performed to prevent any interference with the retracted temporalis muscle (**Fig. 12.2**).

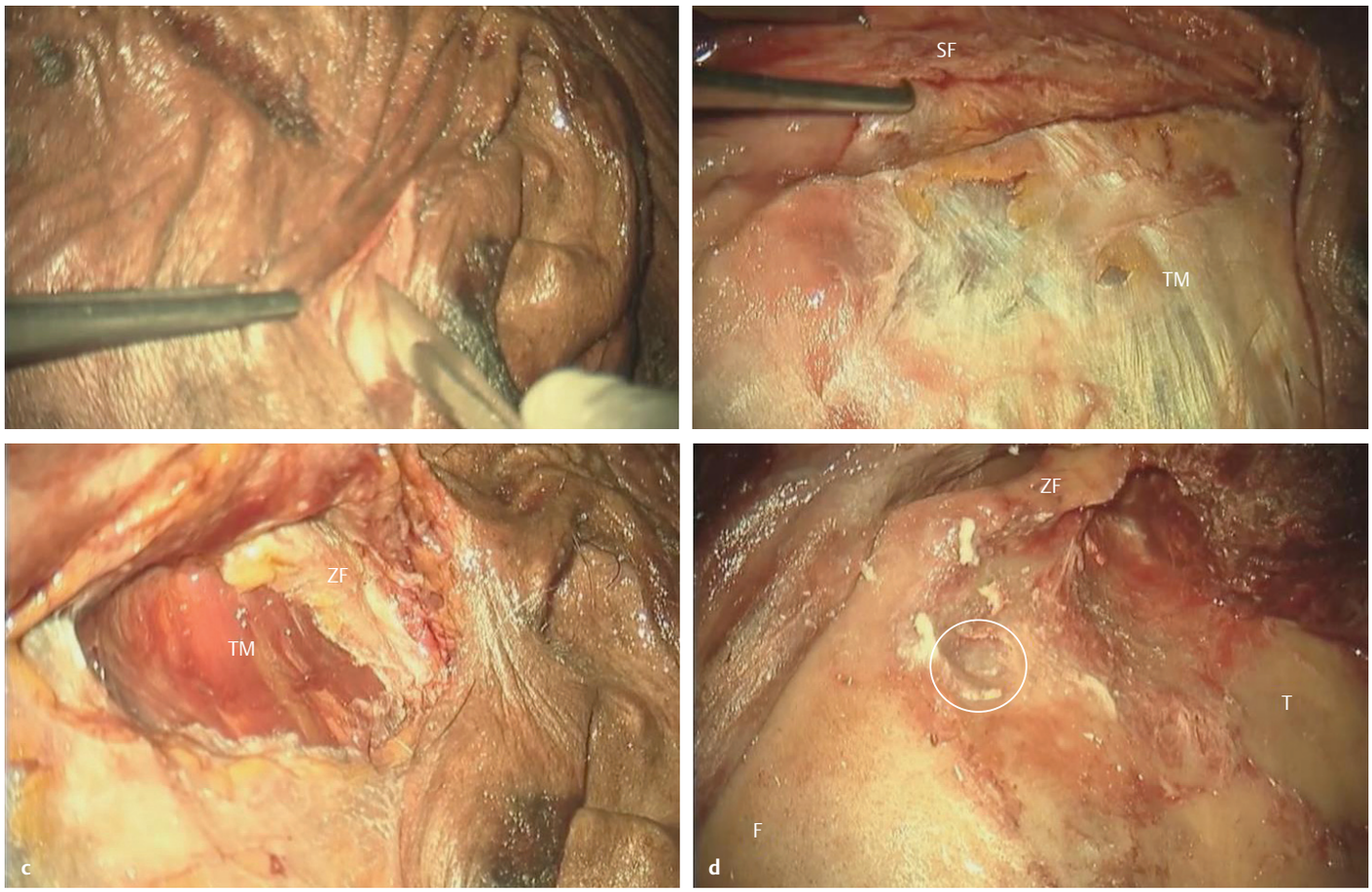

Fig. 12.1 Skin incision. **(a)** Extended incision for frontotemporal, orbitobasal, and middle fossa exposure; must be an extension of the incision in the routine pterional approach. Dissection is performed in layers. **(b)** Subcutaneous fat dissection of the tempoparietal muscle layer. **(c)** Separation of temporal muscle fascia from muscle fibers in the zygomatic arch before its exposure. **(d)** Exposure of the zygomatic arch (ZF), temporal bone (T), and frontal bone (F); the circle indicates the point where the keyhole for the craniotomy is made. Drilling should be done across the lateral surface of the greater wing of the sphenoid bone as close to the frontal process as possible.

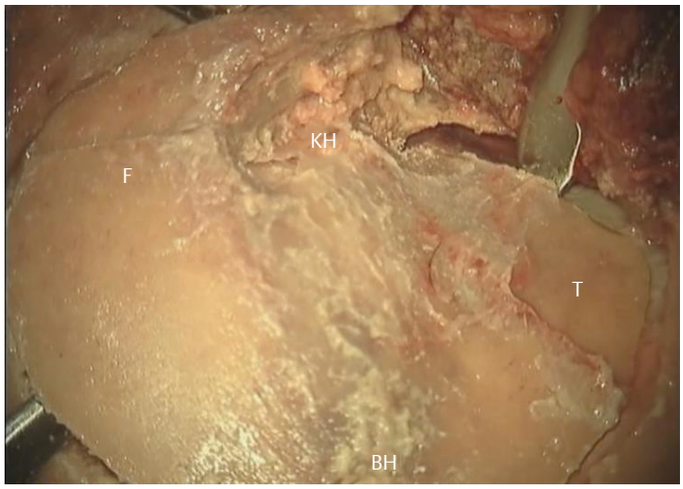

Fig. 12.2 Craniotomy. For exposure of the floor or the temporal base, groove is drilled to prevent interference with retracted temporal muscle. After drilling, a craniotomy is done.

Brain Unlocking in Axial and Sagittal Planes

Extradural maneuvers to "unlock" the frontotemporal folds of the brain allow for a wider surgical corridor to the sellar and suprasellar region. The frontal and temporal lobes are "unlocked" from each other in the **sagittal** and **axial** fashion, by drilling off the sphenoid and dissecting the orbitomeningeal band (OMB), respectively. Adding a sylvian dissection (**oblique intradural** unlocking) to the above-said maneuvers, greatly improves the basal exposure by opening up the brain in a lateral oblique fashion.[4]

Orbitomeningeal Band Dissection

Once the dura is exposed, the sphenoid ridge and the temporal bone are drilled to unfold the frontal lobe from the temporal lobe in a sagittal manner, providing a major view of skull base (**Fig. 12.3**). The OMB is located at the junction of basifrontal and temporal lobe and is the lateral aspect of superior orbital fissure (**Fig. 12.4**). Once the OMB is dissected under high magnification, the surgeon can clearly see a plane where the frontal lobe dura can be dissected off the anterior clinoid and the temporal dura can be dissected off the true cavernous membrane of the cavernous sinus. This uncovers the clinoid for easier anterior clinoidectomy and displaces the temporal lobe laterally in an extradural fashion, thus enabling axial unlocking.[5]

Pericavernous Dissection Techniques

Once the true cavernous membrane plane is reached by accurate dissection of the OMB, the surgeon can follow sharp dissection to maintain a pericavernous plane. At the level of V2 and below, this plane is absent, but the interdural plane may be maintained, thereby decreasing the bleeding. In cases of bleeding, fibrin glue and Surgicel is useful. Using this technique, once the dissection is extended behind V3, and the middle meningeal artery is coagulated and divided, the greater superior petrosal nerve (GSPN) can be seen as a dural band rather than a nerve. To prevent bleeding that usually occurs as a result of transcavernous technique, a

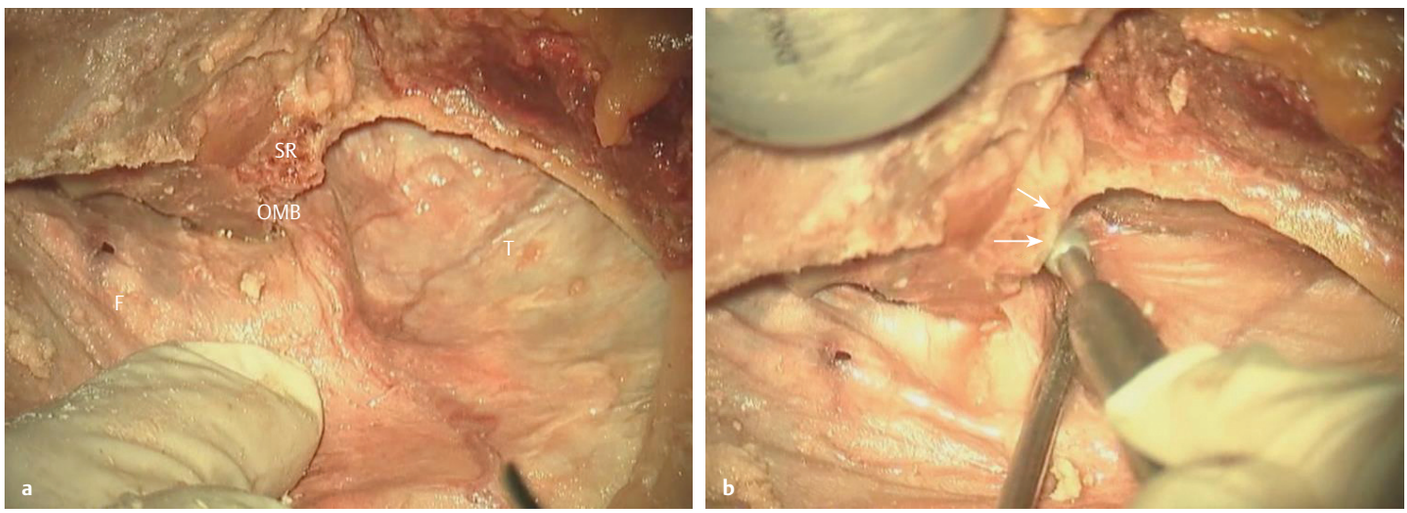

Fig. 12.3 Sagittal unlocking. **(a)** Exposure of the dura. The temporal lobe (T), frontal lobe (F), orbitomeningeal band (OMB), and sphenoid ridge (SR) can be seen. **(b)** The sphenoid ridge and temporal bone are drilled for one major view of the skull base.

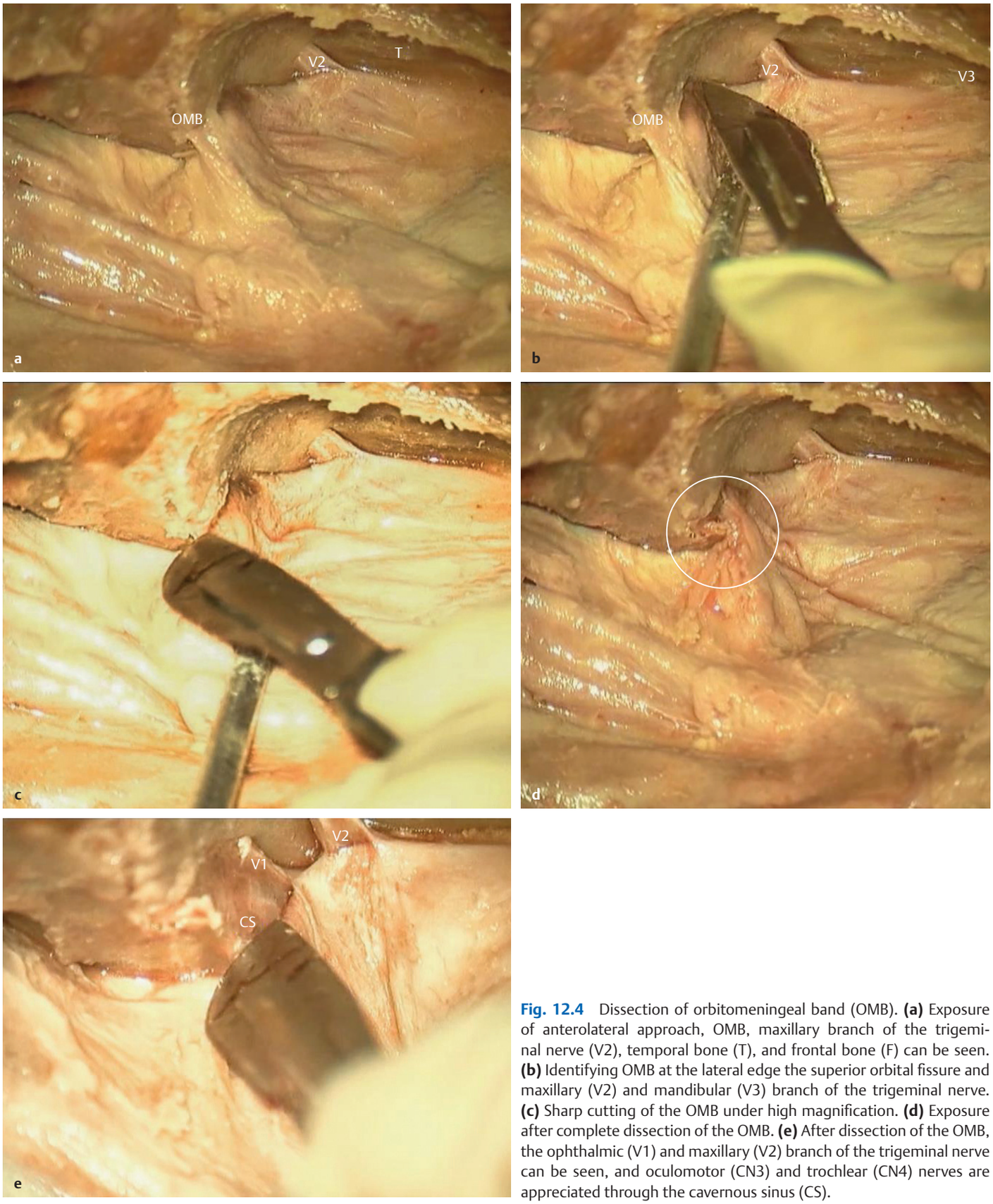

Fig. 12.4 Dissection of orbitomeningeal band (OMB). **(a)** Exposure of anterolateral approach, OMB, maxillary branch of the trigeminal nerve (V2), temporal bone (T), and frontal bone (F) can be seen. **(b)** Identifying OMB at the lateral edge the superior orbital fissure and maxillary (V2) and mandibular (V3) branch of the trigeminal nerve. **(c)** Sharp cutting of the OMB under high magnification. **(d)** Exposure after complete dissection of the OMB. **(e)** After dissection of the OMB, the ophthalmic (V1) and maxillary (V2) branch of the trigeminal nerve can be seen, and oculomotor (CN3) and trochlear (CN4) nerves are appreciated through the cavernous sinus (CS).

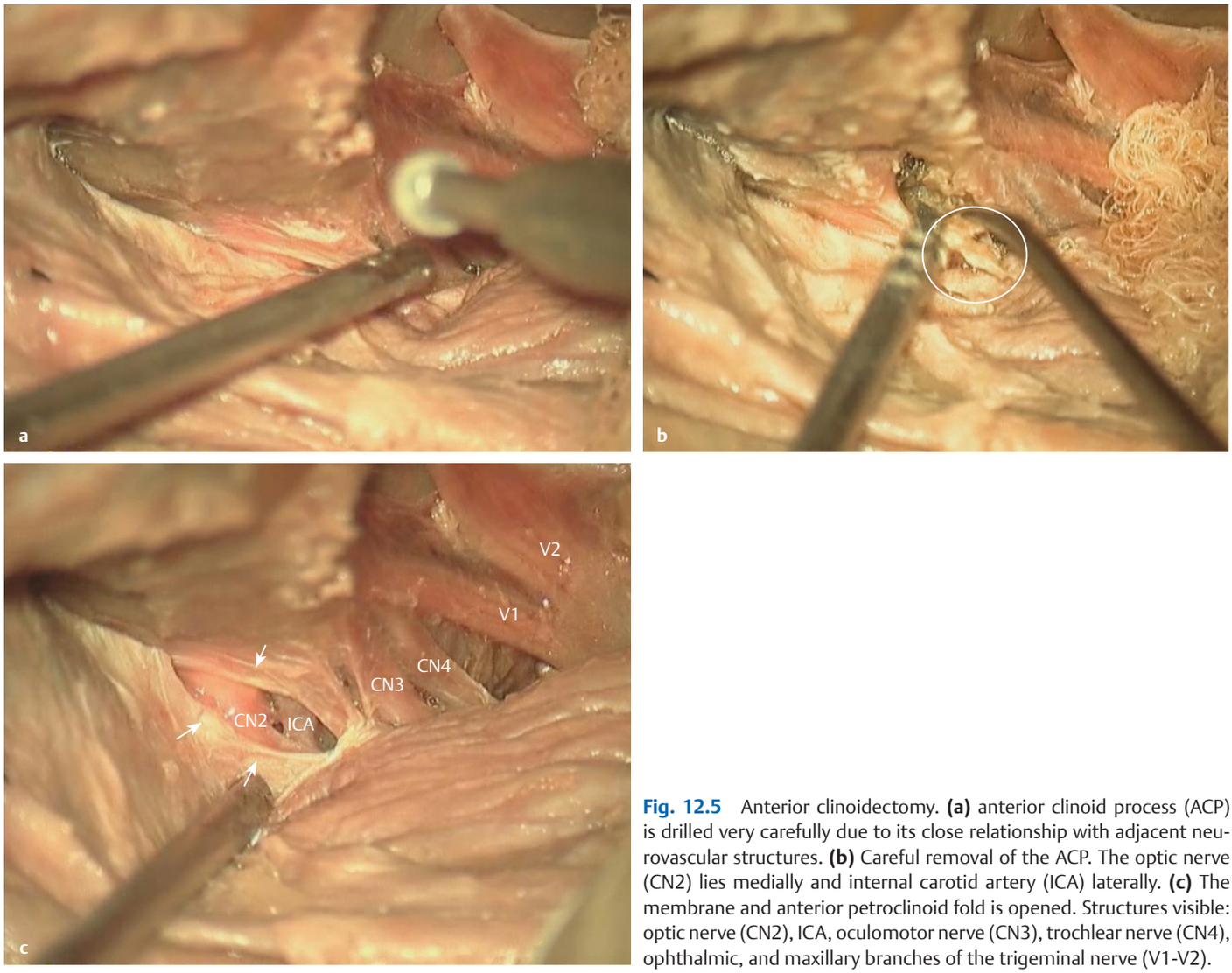

Fig. 12.5 Anterior clinoidectomy. **(a)** anterior clinoid process (ACP) is drilled very carefully due to its close relationship with adjacent neurovascular structures. **(b)** Careful removal of the ACP. The optic nerve (CN2) lies medially and internal carotid artery (ICA) laterally. **(c)** The membrane and anterior petroclinoid fold is opened. Structures visible: optic nerve (CN2), ICA, oculomotor nerve (CN3), trochlear nerve (CN4), ophthalmic, and maxillary branches of the trigeminal nerve (V1-V2).

modification in the conventional Dolenc's approach can be used to preserve the true cavernous membrane (TCM). This modification is the sharp dissection in a pericavernous plane such that the nerves of the cavernous sinuses remain covered by the TCM.

Anterior Clinoidectomy

The dissection of the OMB exposes the anterior clinoid process (ACP) that is covered laterally by the frontal and temporal dural folds. The basifrontal dura can be sharply dissected off the anterior clinoid to completely uncover it (**Fig. 12.5, Fig. 12.6**). This makes anterior clinoidectomy easier and safe. Orbital roof removal to uncover the extradural optic nerve can also be combined along with the

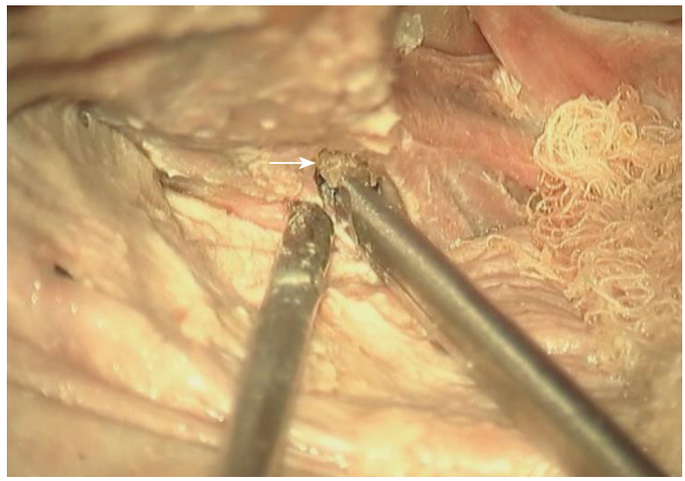

Fig. 12.6 Removal of the optic strut. After anterior clinoid process is dissected, optic strut is removed.

dural cutting and sectioning the distal dural band. This allows the mobilization of the carotid muscle and increase space while dealing with aneurysms of this region.[6] By complete removal of the ACP followed by careful extraction of the optic strut, one can visualize both, the extra and intra dural boundaries of the opticocarotid window and reach the interoptic or the suprasellar cisterns. This is the place where the entire skull base is centered, and this approach can allow for access to all sellar and suprasellar lesions.

Posterior Clinoidectomy

This maneuver is best done intradurally and requires understanding of microsurgical anatomy of the posterior clinoid process. The posterior clinoid may be drilled or removed using a Bone CUSA between the optic nerve, anterior cerebral artery, and carotid window or the window between the carotid and the oculomotor nerve (whichever is larger) (**Fig. 12.7**). This provides ample space to the posterior fossa and can be valuable in posterior circulation aneurysms as well as petroclival meningiomas. The key to safe drilling is that the drilling of the posterior clinoid needs to be performed in a "touch and back" manner (rather than clockwise or counterclockwise motion) to break the cortex.[7]

Petrous Anatomy and Anterior Petrosectomy

Once the dissection behind V3 is carried out, the surgeon must identify GSPN as a dural band thus protecting the nerve in the plane below. The middle meningeal artery is coagulated and cut to attain this plane.[8] The petrous ridges can be reached with continuous dissection and the arcuate eminence may be identified. The V3 may be drilled into the infratemporal fossa and this will help in mobilizing the Gasserian ganglion anteriorly so that petrous apex can be drilled more. Posteriorly, the surgeon can unroof the internal auditory meatus (IAM) and even do some drilling posterior to IAM. As the petrous bone is removed, the petrous carotid can be found in the lateral boundary and the cochlea that is anterolateral to IAM is avoided. The posterior fossa dura is exposed till the surgeon reaches the inferior petrosal sinus and the jugular tubercle is visualized (**Fig. 12.8**). Dural opening is a combination of temporal and posterior fossa durotomies after which the superior petrosal sinus is bipolarized off and the tent is cut to the incisura posterior to the entrance of the fourth nerve.

Opening the Membrane of Liliequist

The membrane of Liliequist can be cut using the window that can be seen between the optic nerve and the carotid artery. A sharp dissection is made using bayoneted side curve microscissors (working length 90 mm). The basilar quad comprising the superior cerebellar artery, the P1 segment, and the basilar artery is exposed. Tumors of the sellar and suprasellar lesions can be surgically removed using this surgical field.

Internal Carotid Artery in Relation to the Skull Base

The ICA is the most important vascular structure of the central nervous system providing two-thirds of the cerebral irrigation. It is important to understand the course of the ICA in the cranial base. The carotid artery follows a torturous course with sharp turns and relations to the adjacent bony structures. Knowing the anatomy of the carotid is crucial to all skull base surgeries involving the sellar region, and care needs to be taken to prevent any damage to the vessel.

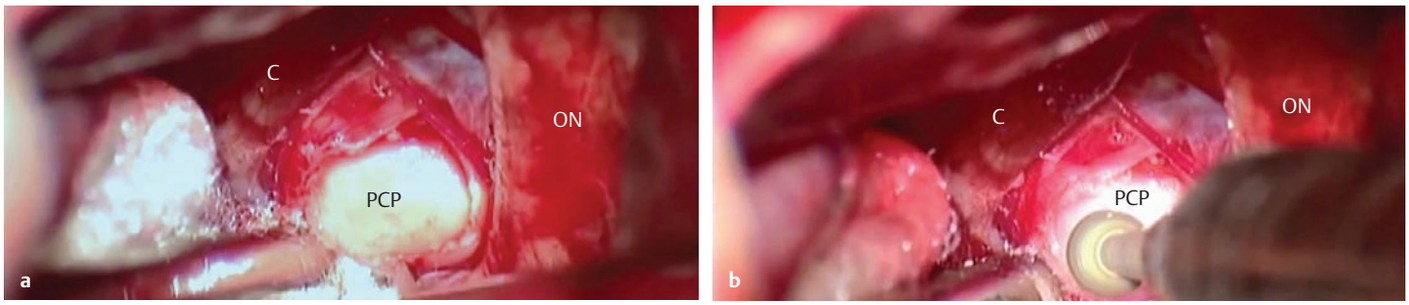

Fig. 12.7 Posterior clinoid process (PCP) drilling. **(a)** The dura covering the PCP is excised carefully between the optic nerve (ON) and the internal carotid artery **(C)**. **(b)** The PCP is drilled using a bone CUSA between the opticocarotid window.

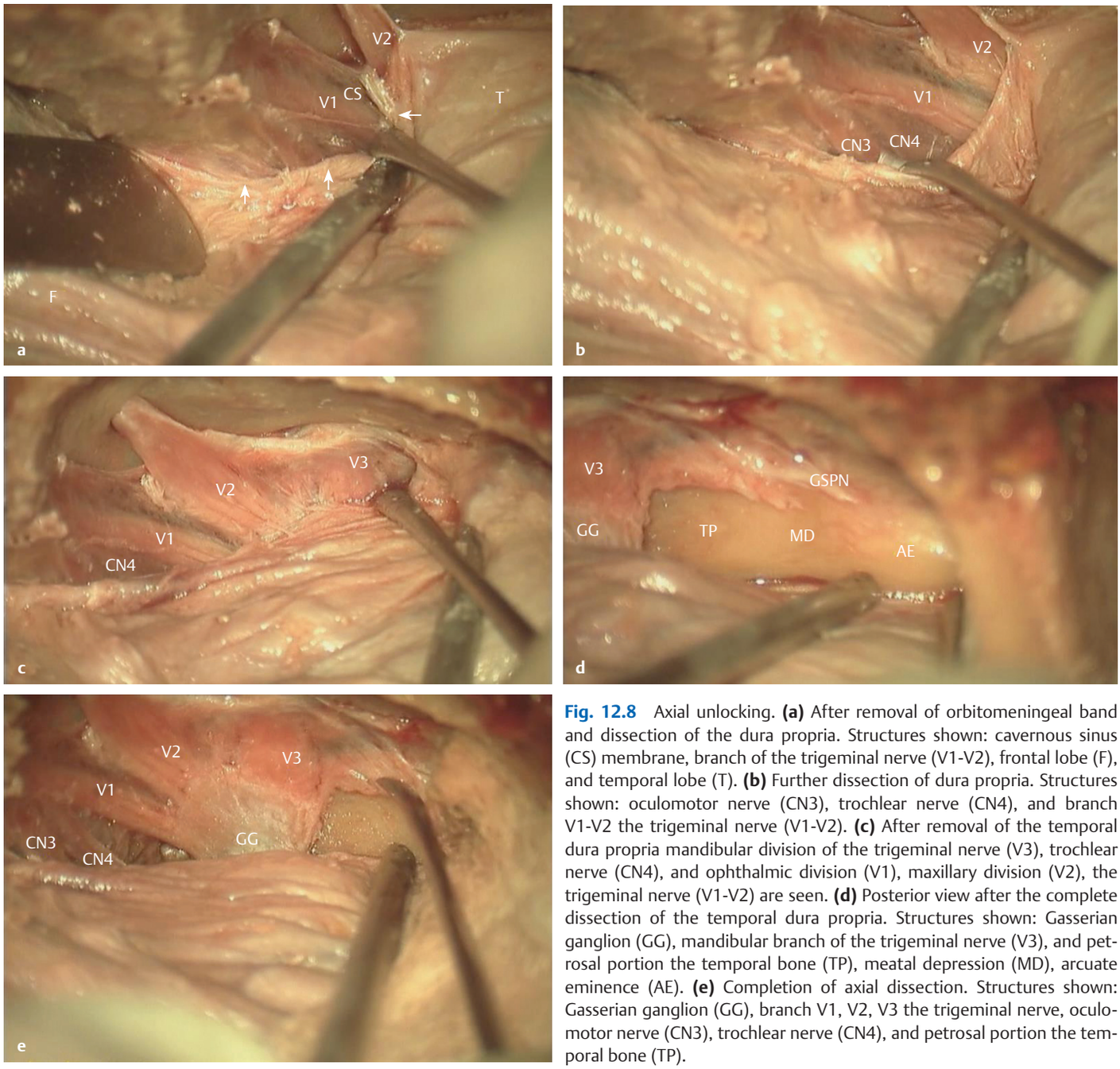

Fig. 12.8 Axial unlocking. **(a)** After removal of orbitomeningeal band and dissection of the dura propria. Structures shown: cavernous sinus (CS) membrane, branch of the trigeminal nerve (V1-V2), frontal lobe (F), and temporal lobe (T). **(b)** Further dissection of dura propria. Structures shown: oculomotor nerve (CN3), trochlear nerve (CN4), and branch V1-V2 the trigeminal nerve (V1-V2). **(c)** After removal of the temporal dura propria mandibular division of the trigeminal nerve (V3), trochlear nerve (CN4), and ophthalmic division (V1), maxillary division (V2), the trigeminal nerve (V1-V2) are seen. **(d)** Posterior view after the complete dissection of the temporal dura propria. Structures shown: Gasserian ganglion (GG), mandibular branch of the trigeminal nerve (V3), and petrosal portion the temporal bone (TP), meatal depression (MD), arcuate eminence (AE). **(e)** Completion of axial dissection. Structures shown: Gasserian ganglion (GG), branch V1, V2, V3 the trigeminal nerve, oculomotor nerve (CN3), trochlear nerve (CN4), and petrosal portion the temporal bone (TP).

An easier classification of the carotid artery can be used to understand the skull base anatomy. In a coronal plane, the carotid segments can be divided into horizontal and vertical, each responding to even and odd segments, respectively, in accordance to their adjacent bony, ligamentary, vascular, and nerve relationships. These anatomical landmarks help identify each segment, as well as its spatial position in the skull base. Over the years, many classifications have been proposed by dividing the carotid in segments, some simpler than others depending on the utility they pursue.[9–11] In this chapter, authors have decided to use a classification similar to the one proposed by Professor Fukushima,[12] yet much more simplified model based on the spatial guidance of each segment (**Fig. 12.9**).

Each segment is named in accordance to its relationship with an adjacent structure. Therefore, the C7 segment is "cervical," C6 "petrosal" segment, C5 "paraclival" segment, C4 "cavernous" segment, C3 "paraclinoid or parasellar"

segment, and C2 "ophthalmic" segment. Throughout its course, the carotid is in close relationship with the following bony structures: the petrosal bone, clivus, and posterior and anterior clinoid process, as shown in **Fig. 12.10**.

The majority of C7 is extracranial and only the distal part is in the petrosal bone. The entire C6 segment is intraosseous, within the petrosal bone. The small proximal part of C5 segment is within the petrosal bone (more specifically in the foramen lacerum); however, it lies in a close relationship with the clivus and the dorsum sellae. The proximal part of C4 is related to the posterior clinoid process, and parts of C3 and C2 are in relation to the anterior clinoid process.

Starting from the inferior, the parapharyngeal (C7 segment) enters the cranium most posterior-laterally. This segment is the first vertical segment, hence corresponding to the C7 (odd) part or the ICA. The distal end of the C7 reaches the petrosal bone, where it sharply takes a medial turn to follow the course of the petrosal bone horizontally. This segment is the petrosal part of the carotid, and is the first horizontal segment, C6 (even). The greater superior petrosal nerve lies lateral to the C6 carotid segment and can predict the course of the ICA at this level.

The petro-lingual ligament lies anteromedial to petrous bone and is an important landmark where the carotid again takes a sharp ascend vertically, and through the foramen lacerum, ascends along the clivus to form the second vertical segment, the paraclival or the C5 (odd) part of the carotid (**Fig. 12.11**). This segment is in close relationship to the trigeminal ganglion laterally and is an important structure in clival lesions.

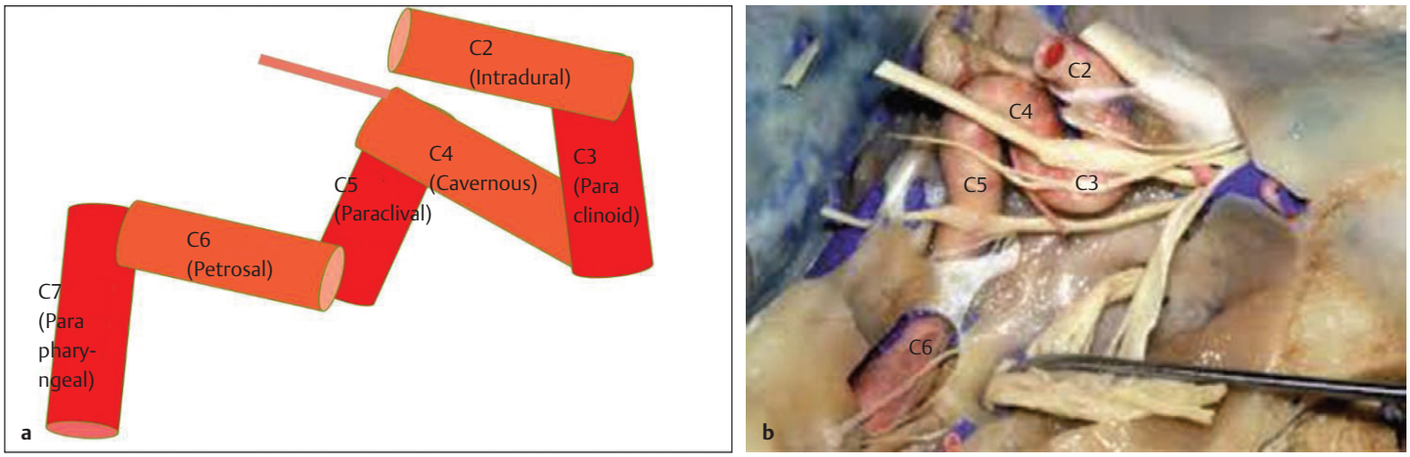

Fig. 12.9 **(a)** Schematic; **(b)** Cadaver: The carotid segments: two-dimensional orientation of horizontal and vertical segments. Note the sequence of odd and even numbers. (Dissection Image Courtesy: Rhoton Collection.)

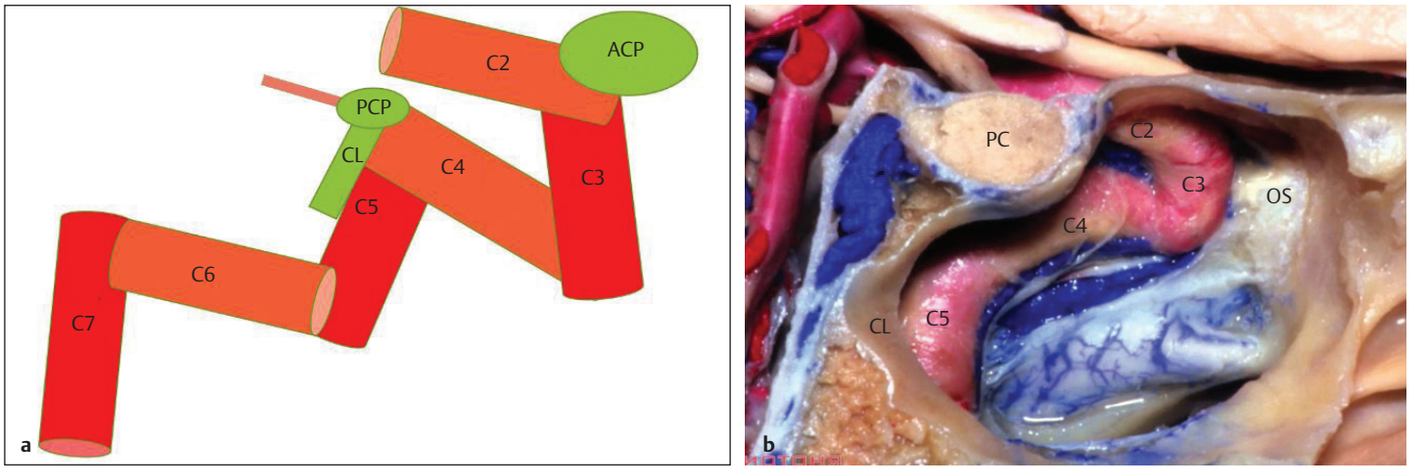

Fig. 12.10 The carotid segments **(a)** and bone relations **(b)**. (C2) Ophthalmic segment, (C3) paraclinoid or parasellar segment, (C4) cavernous segment, (C5) paraclival segment, (C6) petrosal segment, and (C7) cervical segment. ACP, anterior clinoid process; CL, clivus; OS, optic strut; PCP, posterior clinoid process.

The clivus ends at the posterior clinoid process where the C5 carotid continues horizontally to form the cavernous or the C4 (even) segment of the carotid. This segment spans the cavernous sinus and supplies the pituitary gland and the chiasma through the hypophyseal branches. The cavernous sinus completely covers the C4 segment, the distal part of C5 segment, and the proximal part of C3 segment (**Fig. 12.12**). Likewise, the cavernous sinus covers part of the cranial nerves III, IV, V1, V2, and part of the Gasserian ganglion.[13]

Some other important relationships of the carotid artery that the authors have identified are seen in **Fig. 12.13**. The proximal and distal dural rings practically delimit the C3 segment. The cochlea serves as an important structure to predict the location of the carotid curve from C7 to C6 (it is posterior and lateral to this curve). However, care must be taken while exposing the cochlea during petrosectomy to avoid hearing loss.[14]

While removing lesions of the pituitary gland, one needs to preserve the superior hypophyseal branches to prevent infarction of the optic chiasma. The C4 carotid runs inferomedially and then forms the clinoid segment or the C3 (odd), which ascends vertically in a close relationship with the optic nerve. This segment is the last extradural part of the ICA, which, on reaching the ACP anteriorly, can be exposed after ACP removal. Exiting from the distal dural ring, the C3 carotid enters the dura to form the horizontal C2 (even) segment, terminating the extradural course of the ICA.

From view of endoscope, the vertical segments can be seen as shown in **Fig. 12.14**.

It must be noted, however, that the ICA has three planes and each segment has an orientation in each of these three planes. Moreover, there are anatomical variants between one patient and another. Step-by-step transcavernous frontotemporal approach in craniopharyngioma is shown in **Fig. 12.15**.

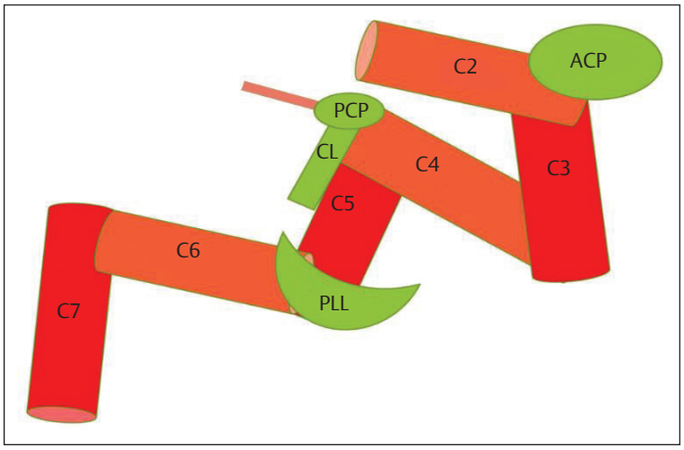

Fig. 12.11 The C5 segment crossing the petrolingual ligament (PLL) at the foramen lacerum.

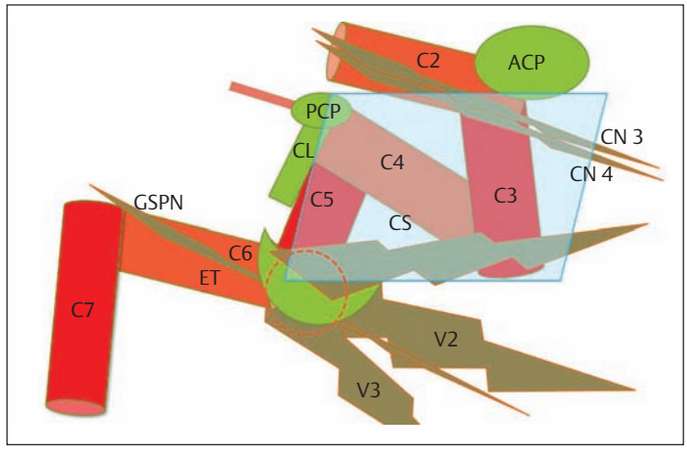

Fig. 12.12 Cavernous sinus (CS) in relation to carotid segments. The CS is covering a segment completely and part of two segments, as shown.

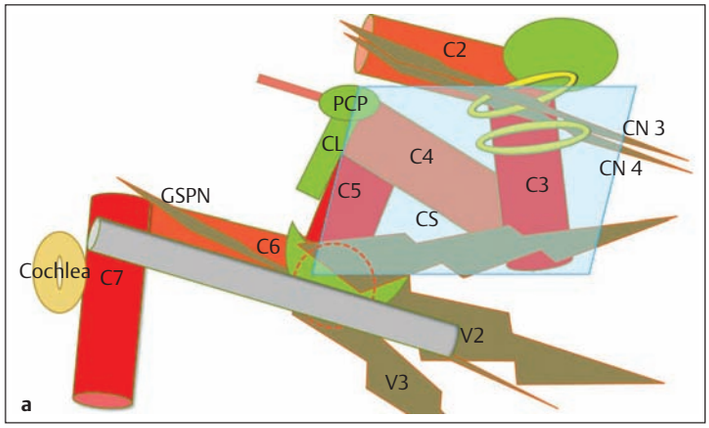

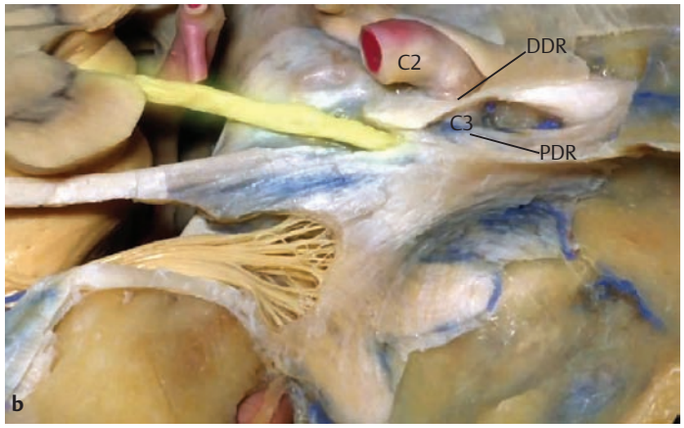

Fig. 12.13 **(a)** Schematic and **(b)** cadaver: Carotid segments, dural rings, and the cochlea. C2 (intradural segment); C3, clinoid; DDR, distal dural ring; PDR, proximal dural ring.

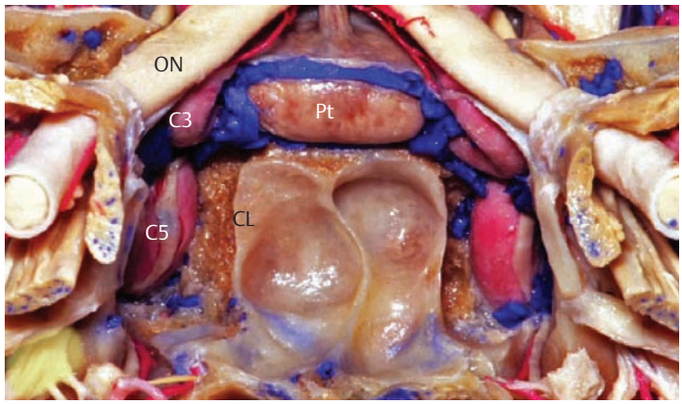

Fig. 12.14 Endoscopic view of carotid in relation to the clivus and cavernous sinus. C3, paraclinoid or parasellar segment; C5, paraclival segment; CL, clivus; ON, optic nerve; Pt: pituitary gland. (Image Courtesy: Rhoton Collection).

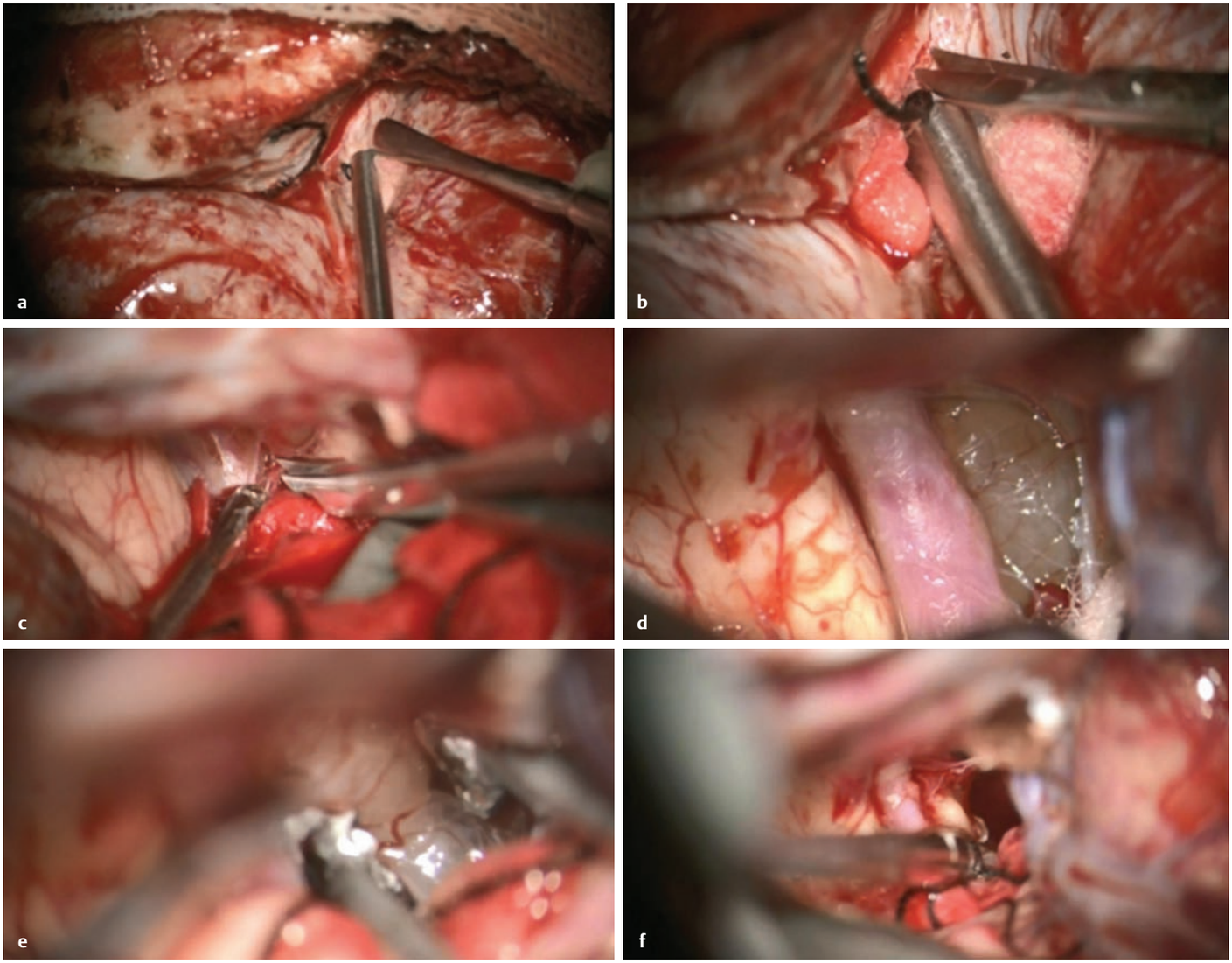

Fig. 12.15 Surgical Steps in a Craniopharyngioma using transcavernous frontotemporal approach. **(a)** Sagittal unlocking to expose the opticocarotid and the lateral carotid window. **(b)** Axial unlocking with sharp dissection of the orbitomeningeal band (OMB), followed by the dissection of the temporal dura from the true cavernous membrane. **(c)** Basal cisternal opening. **(d)** Tumor exposed in the lateral carotid window usually attached to the anterior choroidal and posterior communicating artery. **(e)** Tumor decompressed and dissected off anterior choroidal, posterior communicating and basilar artery. **(f)** Tumor dissected from the hypothalamus, mamillary bodies, and the inter-peduncular cisterns by displacing the tumor down.

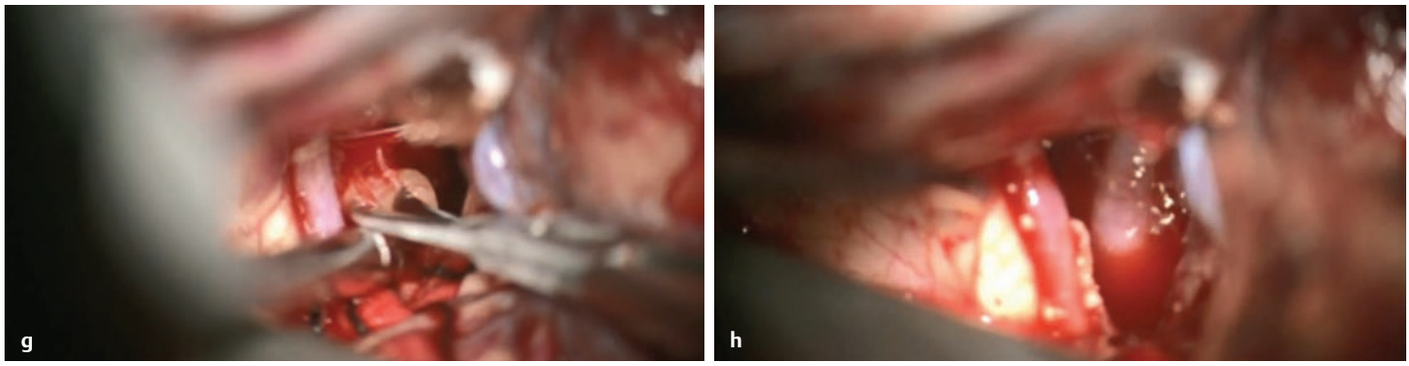

Fig. 12.15 *(Continued)* **(g)** Tumor further decompressed by dividing the capsule and removing the tumors. **(h)** Final removal of the tumor, the basilar artery, carotid artery, and the third nerve can be seen.

References

1. Bourekas EC, Solnes LB, Slone HW. Pituitary and sellar region lesions. In: Newton HB, ed. Handbook of Neuro-Oncology Neuroimaging. 2nd ed. Academic Press, 2016:Chapter 42: 483–501
2. Glezer A, Paraiba DB, Bronstein MD. Rare sellar lesions. Endocrinol Metab Clin North Am 2008;37(1):195–211
3. Day JD. Surgical approaches to suprasellar and parasellar tumors. Neurosurg Clin N Am 2003;14(1):109–122
4. Nathal E, Gomez-Amador JL. Anatomic and surgical basis of the sphenoid ridge keyhole approach for cerebral aneurysms. Neurosurgery 2005;56(1, Suppl)178–185, discussion 178–185
5. Cherian I, Kasper EM, Agarwal A. The orbitomeningeal band as a way to bloodless transcavernous dissection and anterior clinoidectomy. Asian J Neurosurg 2018;13(3):943–945
6. Mishra S, Leão B, Rosito DM. Extradural anterior clinoidectomy: Technical nuances from a learner's perspective. Asian J Neurosurg 2017;12(2):189–193
7. Cherian I, Kasper EM, Agarwal A. Technique of posterior clinoidectomy and its applications. Asian J Neurosurg 2018; 13(3):777–778
8. Shibao S, Borghei-Razavi H, Yoshida K. Intraspinosum middle meningeal artery ligation: a simple technique to control bleeding in the middle fossa during the anterior transpetrosal approach. Oper Neurosurg (Hagerstown) 2017;13(2):163–172
9. Bouthillier A, van Loveren HR, Keller JT. Segments of the internal carotid artery: a new classification. Neurosurgery 1996;38(3): 425–432, discussion 432–433
10. Ziyal IM, Ozgen T, Sekhar LN, Ozcan OE, Cekirge S. Proposed classification of segments of the internal carotid artery: anatomical study with angiographical interpretation. Neurol Med Chir (Tokyo) 2005;45(4):184–190, discussion 190–191
11. Abdulrauf SI, Ashour AM, Marvin E, et al. Proposed clinical internal carotid artery classification system. J Craniovertebr Junction Spine 2016;7(3):161–170
12. Sameshima T, Mastronardi L, Friedman A, Fukushima T, eds. Middle fossa dissection for extended middle fossa and anterior petrosectomy approach. Fukushima's microanatomy and dissection of the temporal bone for surgery of acoustic neuroma, and petroclival meningioma, 2nd ed. AF Neurovideo, Raleigh; 2007:51–83
13. Harris FS, Rhoton AL. Anatomy of the cavernous sinus. A microsurgical study. J Neurosurg 1976;45(2):169–180
14. Guo X, Tabani H, Griswold D, et al. Hearing preservation during anterior petrosectomy: the "cochlear safety line." World Neurosurg 2016;99:618–622

13 Surgery on Sellar and Parasellar Lesions

Atul Goel

Introduction

Surgery on pituitary tumors is usually safe and is highly result-oriented. Perfect understanding of nuances of pituitary tumor surgery is essential to achieve satisfactory results. Pituitary tumors range widely in their size. While microadenomas are generally associated with hormonally active tumors, large and giant sized tumors are usually hormonally nonfunctional. Surgical issues are unique for all sizes of pituitary tumors. All pituitary tumors require radical resection. In microadenomas associated with Cushing's disease and acromegaly or growth hormone tumors, radical and total resection is mandatory to achieve "cure." In such cases, while a successful surgery can lead to cure from hormonal dysfunction and immediate postoperative relief from symptoms, failures are associated with prolonged misery for the patient and even early or quick death. Larger tumors are usually associated with visual dysfunction. Timely radical resection can be associated with immediate postoperative recovery in vision.

Giant pituitary tumors are among the more complex neurosurgical challenges. Despite the histological benign nature, some of these tumors grow to a massive size. Due to the invasiveness and size of such tumors, surgical resection is difficult and, on some occasions, dangerous.[1-5] Inadequate resection can lead to postoperative complications and even death. As the results of radiation therapy are inconsistent, surgery forms the mainstay of treatment.

Revolutionary Concepts Regarding Dura and Its Relationship with Pituitary Tumors

Understanding the anatomy of the tumor extensions and their relationships with the dural layers of sella, diaphragma sellae, and walls of the cavernous sinus is crucially important for surgery, particularly when the tumors are large or giant in size. The author first described that the pituitary tumors elevate the diaphragma sellae and seldom transgress it.[2] The concept that the diaphragma sellae is elevated and not transgressed had significant implications in the development of surgical concepts of these tumors. This understanding that the cranial component of the tumor is covered by the "dural" layer of diaphragma sellae and is infradiaphragmatic in location revolutionized surgical approach to pituitary tumors. Earlier, dumbbell-shaped tumors were considered to be in the sella in its inferior aspect and in the intracranial subarachnoid compartment in its rostral component, the waist being formed by the edge of the defect in the diaphragma sellae. Transcranial surgery was the favored option in cases where the cranial component was significantly large. However, understanding of the fact that the dura of diaphragma sellae was elevated by the tumor and formed a barrier between the tumor and the brain permitted safe resection and allowed transnasal surgery for such tumors.

Cavernous Sinus Dural Walls: Relevance to Pituitary Surgery

The author described that the transgression of the medial wall of the cavernous sinus is a frequent event, but transgression of the lateral wall and the roof of the cavernous sinus is rare or not possible. He first described the elevation of the dural roof of the cavernous sinus by the pituitary tumors.[1,6] It appears that these descriptions of the dura in the region of the sella and of cavernous sinus helped in the growth of surgery of pituitary tumors and enhanced the scope of surgery from the nasal route.[6] The tumors that were earlier considered to be suitable for transcranial surgery could be operated by transnasal route.

These concepts of anatomy revolutionized surgical approaches to large and giant pituitary tumors in general

and particularly those that extended above the sella and those that invaded into the cavernous sinus. Introduction of endoscope-based surgery assisted in developing this concept further.

Giant Pituitary Tumors

Giant and "invasive" pituitary tumors are among the more complex neurosurgical challenges. Despite the histological benign nature, some of these tumors grow into a massive size and invade into diverse anatomical structures.[2,3] Due to the invasiveness and size of such tumors, surgical resection is difficult and on occasion dangerous.

Classification of Giant Pituitary Tumors[1,7]

Author discussed a classification scheme for giant pituitary tumors on the basis of their dural relationships. The classification helped in characterizing these tumors, assisted in developing a surgical plan, and predicted the surgical and long-term outcome.[7-11]

Grade I Giant Pituitary Tumors

This group of tumors was confined inferiorly to the sellar dura, was underneath the elevated diaphragma sellae, and laterally was bordered by an intact medial wall of the cavernous sinus. Diaphragma sellae can sometimes be elevated up to or even beyond the corpus callosum. Diaphragma sellae was markedly thinned out at places and frequently formed big or small daughter balloons. The rounded superior wall of the tumor was suggestive of the fact that the diaphragma sellae was intact. The diaphragma sellae was elevated superiorly to varying extent. That diaphragma sellae was elevated and not transgressed was identified by the fact that the arteries of the circle of Willis were not encased by the tumor. The presence of an intact diaphragma sella was confirmed during surgery and this feature had significant surgical relevance as it formed an important protective barrier and such tumors could be resected radically through a relatively small exposure by a transnasal transsphenoidal route (**Fig. 13.1**).

Grade II Giant Pituitary Tumors

This group was where the Grade I tumors transgressed medial wall of the cavernous sinus and invaded into the confines of the cavernous sinus. Cavernous sinus invasion could be confirmed on magnetic resonance imaging (MRI) if the tumor extended on both sides of the carotid artery. Although bulged out laterally, transgression of the lateral dural wall of the cavernous sinus was not observed, suggesting the relative firmness and the resistance offered by the lateral dural wall of the cavernous sinus (**Fig. 13.2**).

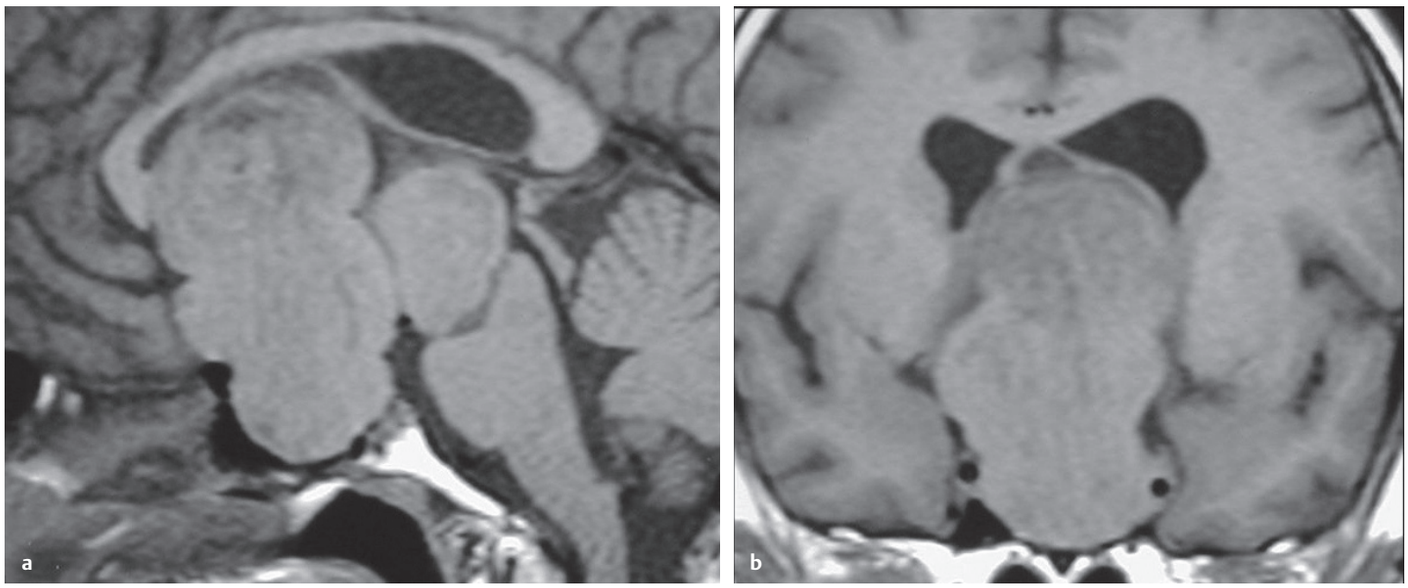

Fig. 13.1 **(a)** Sagittal image showing the large multiloculated suprasellar component of the large grade I tumor. The diaphragma sellae is elevated in a multilobulated fashion. The anterior cerebral artery complex is draped over the tumor. **(b)** Coronal scan shows the tumor. Cavernous sinus is not involved.

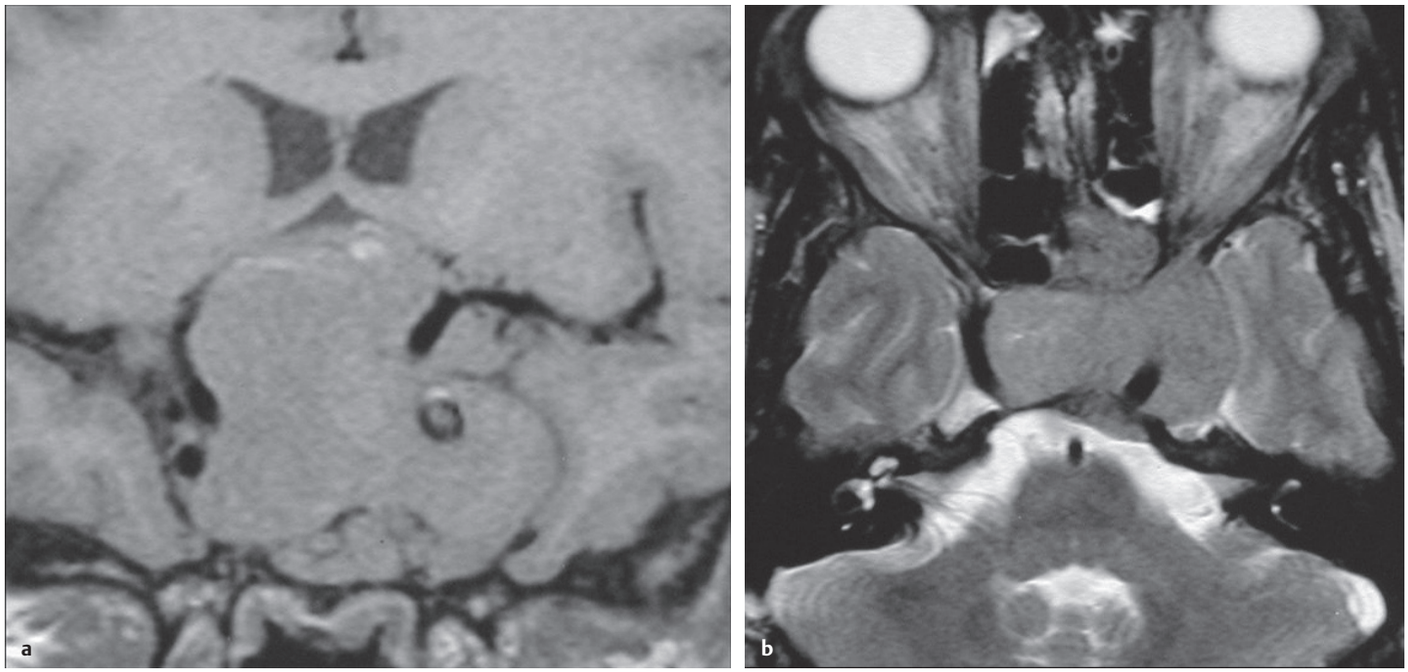

Fig. 13.2 **(a)** Coronal MRI shows grade II giant pituitary tumor. Invasion of the tumor into cavernous sinus is noted. The internal carotid artery is encased by the tumor. The dura of the diaphragm and the lateral wall of the cavernous sinus are displaced by the tumor bulk. **(b)** Axial T2-weighted MRI shows the involvement of cavernous sinus.

Grade III Giant Pituitary Tumors

"Weakness" of the superior wall of the cavernous sinus and its elevation as a result of the presence of an intracavernous sinus meningioma has been described by the author earlier.[12] It was observed that a significant number of giant pituitary tumors, which invaded into the cavernous sinus, elevated the superior dural wall of the cavernous sinus. Such tumors, which selectively elevated the roof of the cavernous sinus, were labeled as grade III pituitary tumors. The author first described the feature of elevation of the dural roof of the cavernous sinus by a pituitary tumor.[7] The superior wall of the cavernous sinus matched in the elasticity but was relatively thinner than the diaphragma sellae. Transsphenoidal surgery was used to resect majority of these tumors. An attempt was made to remove the portion of the tumor extending into the cavernous sinus and along its superior wall. However, radical resection of the part of the tumor along the superior wall of cavernous sinus was relatively complex due to difficulty in adequate exposure of the tumor mass and the narrowness of the dural neck at the level of the roof of the cavernous sinus. Moreover, manipulations in the region of the roof of the cavernous sinus placed the oculomotor nerve in danger of injury due to its anatomical proximity (**Fig. 13.3**).

Grade IV Giant Pituitary Tumors

The giant pituitary tumors, which transgressed the diaphragma sellae boundary and encased the arteries of the circle of Willis, were labeled as grade IV. In these cases, it appeared that the tumor extended into the subarachnoid space of the brain and encased arteries and perforators. The exact site of dural dehiscence could not be confirmed. Invasiveness of such tumors matches an epidermoid tumor, wherein it spreads into the available spaces, engulfs or encircles the blood vessels and cranial nerves without actually invading these structures, rarely compromising the lumen of the artery, and resulting in only moderate displacements. In such cases, surgery and attempts toward radical tumor resection can be dangerous as perforator injury can be an issue. Author has recently identified that a significant number of these patients can have heightened hormonal activity. Prolactinomas can sometime achieve a giant size, and more often these tumors have a bizarre anatomical configuration and some of them may be of grade IV type. As radical resection is difficult in any case, it is advisable to attempt treatment by drugs as a first-choice strategy. Biopsy and radiation treatment is another viable option (**Fig. 13.4**).

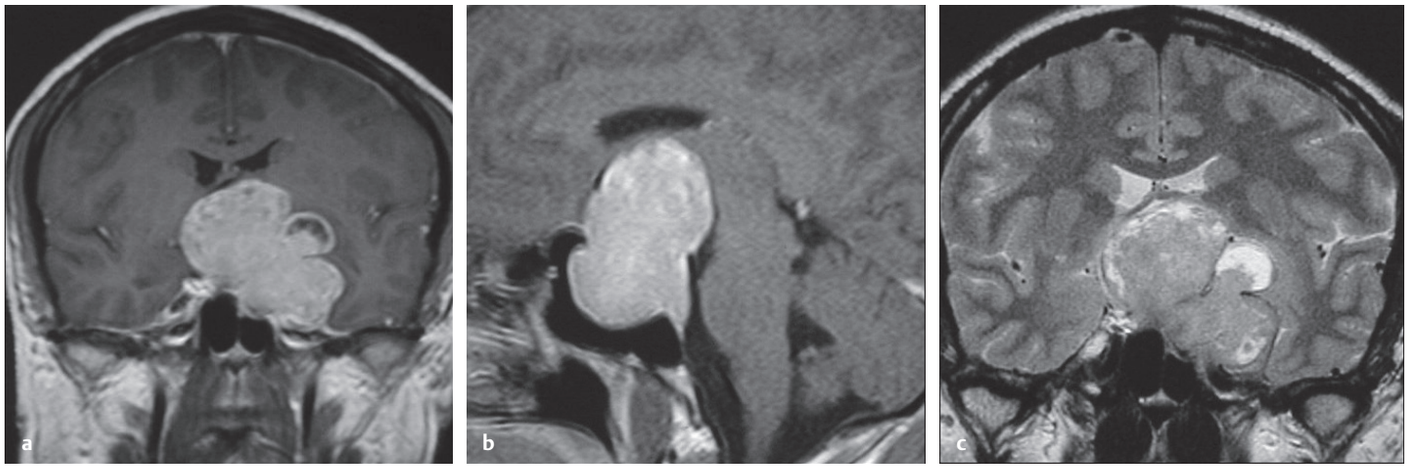

Fig. 13.3 **(a)** Coronal image of the contrast enhanced T1-weighted MRI shows the grade III pituitary tumor. The elevation of the roof of cavernous sinus and diaphragma sellae can be noted. **(b)** Sagittal image of contrast-enhanced MRI shows the elevation of the diaphragma sellae. **(c)** T2-weighted image shows the grade III pituitary tumor with elevation of the roof of cavernous sinus and diaphragma sellae.

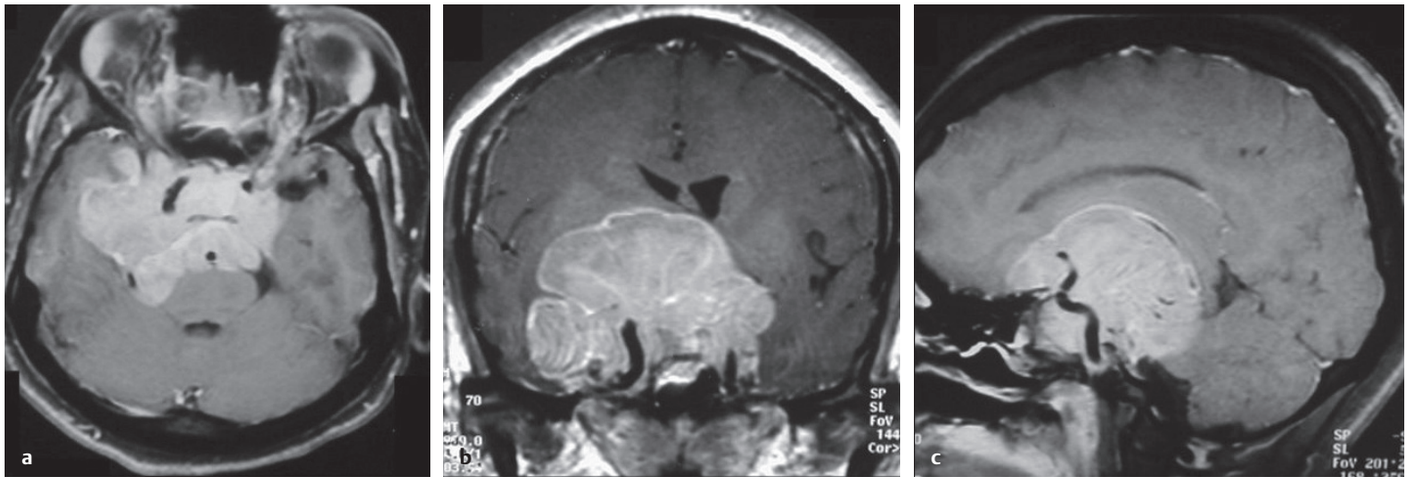

Fig. 13.4 **(a)** Grade IV pituitary tumor. Encasement of the basilar artery can be seen. **(b)** Contrast-enhanced coronal image showing the encasement of the arteries of the circle of Willis. **(c)** Sagittal image.

Tumor invading through the sellar floor dura, sella turcica, and the adjacent bones may extend into the nasopharynx or sphenoid and/or ethmoid sinuses. Extension of the tumor may occur posteroinferiorly in the retropharyngeal space by erosion of the clivus and petrous apices. Larger tumors may extend up to the foramen magnum.

Surgery on Pituitary Tumors

Introduction of the microscope dramatically changed the entire vision of pituitary tumor surgery. Good lighting in the depth and ability to work with comfort and ease made the conduct of the entire operation controlled. Pituitary tumor surgery became one of the most result-oriented neurosurgical operations. Following a successful surgery there can be dramatic and immediate improvement in vision, reversal of acromegalic and cushingoid features, and similar other results. Moreover, resection of these "benign" tumors leads to "cure" from the disease.

Continued Role of Microscope

Sublabial Transsphenoidal Approach

Sublabial-transseptal and transsphenoidal approach to pituitary tumors is an effective surgical approach. The popularity of this approach continues and several surgeons

find it useful, quick, and effective, both for small and for large tumors. Midline approach, wide exposure of the anterior wall of the sella, possibility of lateral extension and exposure of the cavernous sinus, and free and unhindered handling of instruments make this approach popular and effective. Microscope provides good and satisfactory lighting in the depth and a possibility of using both hands freely.

The surgical technique includes wide exposure of the anterior wall of the sella. The anterior sellar wall is then resected widely initially by using a chisel and then rongeurs. After opening the anterior sellar wall, a cruciate incision is taken in the dura. The tumor is then progressively debulked. The tumors are usually soft, friable, and necrotic. This character makes tumor "debulking" safe and relatively quick. Strategic and controlled debulking of the tumor forms the primary surgical technique. The soft and necrotic nature of the tumor permits the possibility of a relatively quick surgical debulking of the tumor. Despite the occasional high vascularity, control of bleeding using hemostats like Gelfoam and *Surgicel* is relatively easily possible. Intratumoral coagulation can be avoided. The tumor resection is first carried out from the sella in the midline. This is followed by tumor resection in the lateral aspect of the sella. The tumor resection is then continued superiorly. As the tumor in the sella is resected, the suprasellar component of the tumor progressively falls in vision and comes down in the operative field. Valsalva maneuver was used during surgery to facilitate the descent of the tumor mass. Getting the tumor inferiorly into the field requires surgical experience and confidence. Frequently the diaphragma sellae has to be superiorly retracted to expose the tumor within the folds of the diaphragma sellae. In grades I to III pituitary tumors, the tumor under the diaphragma sellae can often be resected. Although some tumors are relatively firm and even fibrous and "elastic," they can always be progressively debulked, brought inferiorly into the operative field, and resected. In the early phase of author's experience, to resect the suprasellar component of the tumor, the author preferred to remove the bone of the tuberculum sellae and planum sphenoidale. However, he has realized that removal of bone in the tuberculum sellae and planum sphenoidale is necessary only in minority of patients and can be avoided even in huge tumors (**Figs. 13.5 and 13.6**).

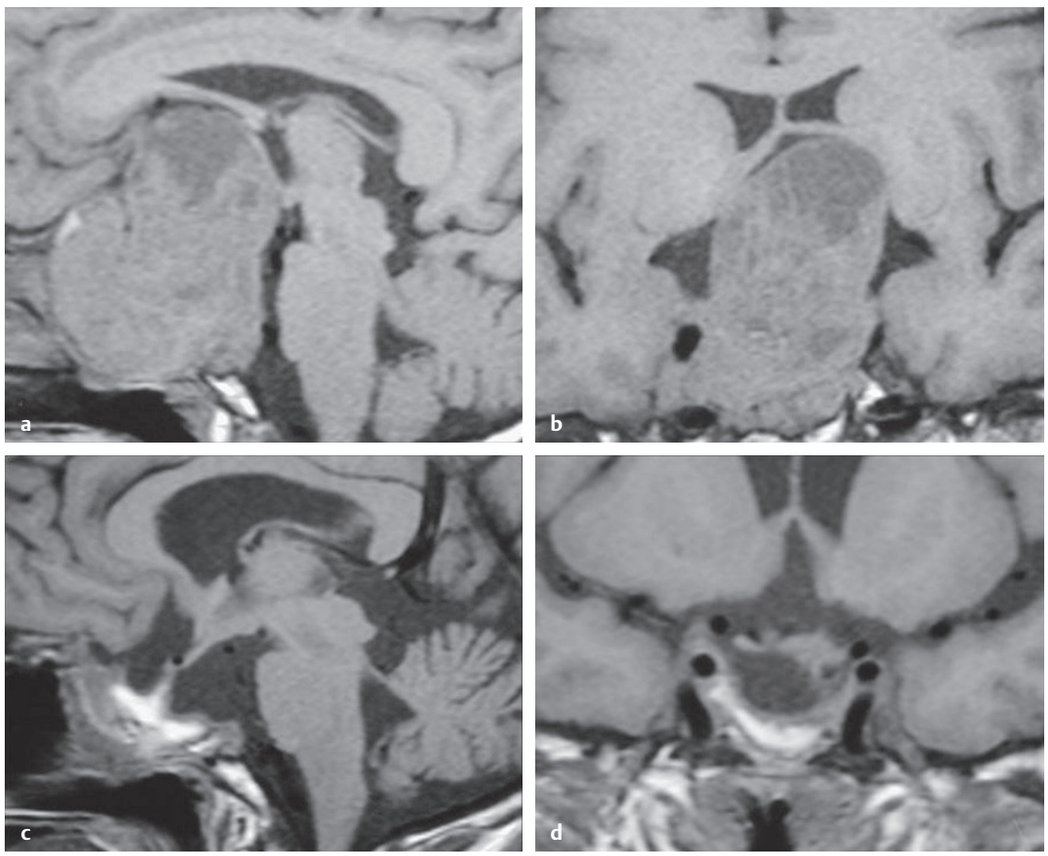

Fig. 13.5 **(a)** Sagittal T1-weighted MRI showing the large giant grade I pituitary tumor. **(b)** Coronal image. Cavernous sinus is not involved. **(c)** Postoperative T1-weighted sagittal image showing tumor resection. **(d)** Postoperative coronal image.

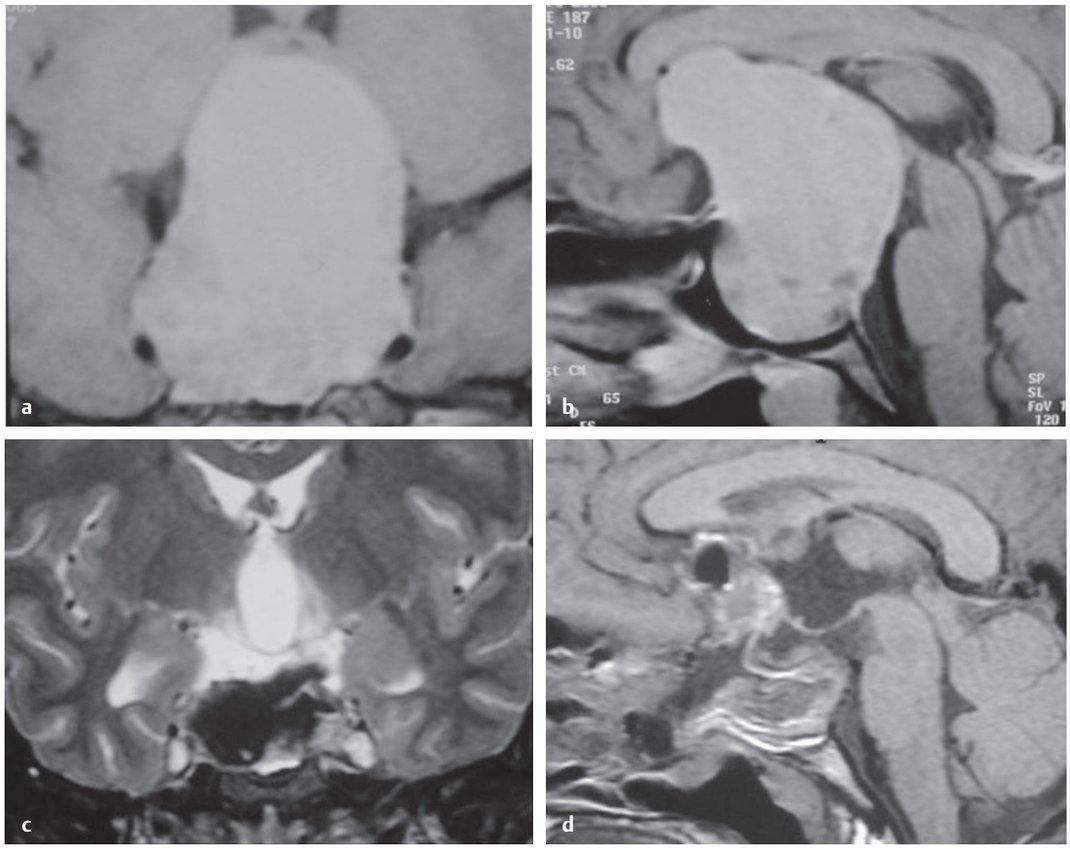

Fig. 13.6 **(a)** Coronal image of contrast-enhanced MRI showing giant grade I pituitary tumor. **(b)** Sagittal image showing the tumor. **(c)** Coronal image of postoperative scan. **(d)** Sagittal image showing tumor resection.

Pituitary forceps and curettes of various angles can help in resection of the tumor located in the lateral aspect of the sella. The art of tumor debulking and bringing the tumor down in to the surgical field by progressive debulking of the tumor has to be learnt by experience.

Lateral Exposure of Sella and of Cavernous Sinus

By extending the midline exposure laterally, one can have the exposure of the anterior wall of the cavernous sinus. Incision over the anterior dural wall is taken protecting the carotid artery. Working anterior and inferior to the anterior loop of the carotid artery exposes the cavernous sinus contents. The extent of resection of the tumor within the cavernous sinus will depend on the consistency of the tumor. The need for radical resection of the tumor from within the confines of the cavernous sinus will depend on the hormonal nature of the tumor. The high probability of injury to the sixth cranial nerve makes the attempt at radical tumor resection highly calculated and philosophical. In general, cavernous sinus manipulations are necessary in hormonally active pituitary tumors. The need and the possibility of resection of the cavernous sinus component of the tumor will depend primarily on the consistency of the tumor. In several situations, the tumors that extend into the cavernous sinus are more necrotic and soft than that encountered in cases where there is no cavernous sinus extension. The tumor in such cases can be resected safely and radically. In desperate situations in cases with functioning pituitary tumors, a lateral basal subtemporal extradural operative route can be adopted to resect this portion of the tumor.

Use of Endoscope in Pituitary Tumor Surgery

Although introduced for quite some time now, endoscopes are currently being recommended for use in a number of neurosurgical operations. The superiority of endoscope in the management of paranasal sinus, clival region, and medial cavernous sinus extradural tumors is now accepted. Several surgeons who have been doing pituitary tumor surgeries using a microscope have identified the use of the endoscope.

It appears that if dural relationships are appropriately understood, particularly as they relate to pituitary tumors and their potential to invade the cavernous sinus,

conventional microsurgery can—if appropriately learned and practiced—provide satisfactory lateral vision to explore the tumor inside the corners of the cavernous sinus in general and also the part of the tumor that is lateral to the internal carotid artery. The radicality of resection of the part of the tumor within the cavernous sinus depends more on tumor characteristics like fragility and vascularity.

Conclusion

Surgery on pituitary tumors is necessarily based on high degree of understanding of dural anatomy and experience in handling and breaking the tumor. Radical tumor resection is associated with quick relief from symptoms and long-term "cure" from the disease.

References

1. Goel A, Nadkarni T. Surgical management of giant pituitary tumours: a review of 30 cases. Acta Neurochir (Wien) 1996; 138(9):1042–1049
2. Krisht AF. Giant invasive pituitary adenomas: management plan. Contemp Neurosurg 1999;21:1–6
3. Symon L, Jakubowski J, Kendall B. Surgical treatment of giant pituitary adenomas. J Neurol Neurosurg Psychiatry 1979; 42(11):973–982
4. Martins AN, Hayes GJ, Kempe LG. Invasive pituitary adenomas. J Neurosurg 1965;22:268–276
5. Mohr G, Hardy J, Comtois R, Beauregard H. Surgical management of giant pituitary adenomas. Can J Neurol Sci 1990;17(1): 62–66
6. Shah A, Mohamed Elsanafiry MS. Diaphragma sellae: Anatomical and surgical implication in surgery for pituitary adenomas: highlighting contributions by Goel. J Craniovertebr Junction Spine 2018;9(3):135–139
7. Goel A, Nadkarni T, Muzumdar D, Desai K, Phalke U, Sharma P. Giant pituitary tumors: a study based on surgical treatment of 118 cases. Surg Neurol 2004;61(5):436–445, discussion 445–446
8. Agrawal A, Cincu R, Goel A. Current concepts and controversies in the management of non-functioning giant pituitary macroadenomas. Clin Neurol Neurosurg 2007;109(8):645–650
9. Goel A. Challenge of giant pituitary tumors. World Neurosurg 2014;82(1-2):e121–e124
10. Goel A. Letter to the Editor: surgical management of pituitary macroadenomas. J Neurosurg 2016;125(2):516–518
11. Goel A. Letter to the Editor: pituitary tumors and cavernous sinus extension. J Neurosurg 2016;124(4):1129–1130
12. Goel A. Meningeal architecture of the cavernous sinus: clinical and surgical implications. Neurosurgery 1998;42(2):430–431 (letter)

Radiation Therapy for Pituitary Tumors

14 *Bhargavi Ilangova, Murali Venkatraman, Murugan Logamuthukrishnan, Babu Rajendran*

Introduction

Radiation therapy is the key adjunct to hormone suppressive pharmacotherapy and surgical excision, the two primary modalities of treatment of pituitary tumors. Radiation therapy has a commendable treatment role to play when endocrine normalization and involution of tumor do not occur following hormone suppressive pharmacotherapy, and when there is residual tumor following surgical excision. It is also used as the primary treatment in the event of contraindication or intolerance to hormone suppressive pharmacotherapy and inoperability due to associated comorbid conditions, and in the treatment of recurrent tumors that are not amenable to surgery. There is also a role for re-irradiation for tumors that recur after radiation therapy, when surgery is not feasible.

An understanding of the basic behavior of these tumors, their anatomical location, and the side-effect profile associated with radiotherapy is essential to decide and plan the multimodal management. The anatomy and physiology of the pituitary gland; incidence, classification, clinical presentation, pathophysiology, radiology, histology, immunohistochemistry, and cytotoxic chemotherapy of pituitary tumors; differential diagnosis of lesions in the sellar and suprasellar region, etc., are discussed elsewhere.

Aims of Therapy

Pituitary adenomas are by far the commonest pituitary tumors. They are benign tumors and are of two types: the hormone hypersecreting/secretory/functional adenomas and the nonsecretory/nonfunctional adenomas.

The aims of hormone suppressive pharmacotherapy (bromocriptine, cabergoline, etc.), surgery, radiation therapy, and cytotoxic chemotherapy (which does not have any role in benign pituitary adenomas) in pituitary tumors are normalization of hypersecretion of pituitary hormones and reduction of tumor size to reduce the pressure effect on adjacent structures, including visual pathways and cavernous sinus, and on the remaining normal pituitary gland to preserve its function.

Some secretory pituitary adenomas tend to present early as microadenomas (less than 10 mm in size), usually confined to the sella turcica, due to the clinical manifestation of the pituitary hormones being secreted in excess, such as hyperprolactinemia, acromegaly, and Cushing's disease. The aim of therapy of such secretory pituitary microadenomas, primarily hormone suppressive pharmacotherapy, is to reverse or control the abnormal systemic clinical manifestations. If this fails, surgery is done; if this too fails, radiation therapy is given.

Other secretory and nonsecretory pituitary tumors tend to present little later as macroadenomas (more than 10 mm in size), usually with suprasellar and parasellar extensions, due to their pressure effect on adjacent structures causing headache and a host of other symptoms. Pressure effect on the optic apparatus causes defects in the visual fields, on the cavernous sinus leads to palsies of ocular nerves, or numbness or pain in the trigeminal nerve distribution, on the remaining normal pituitary gland causes hyposecretion leading to hormonal insufficiency clinical features, and rarely causes hydrocephalus when the ventricular system is blocked. The aim of therapy of such pituitary macroadenomas, primarily surgery, is to reverse the pressure effect, thereby relieving headache, reversing visual field deficits, reversing other cranial nerve palsies and pain, restoring normal pituitary gland hormone secretion, and relieving hydrocephalus. If surgery does not have the desired effect due to the presence of residual tumor, radiation therapy is given.

There are other rare pituitary tumors, such as pituitary carcinoma,[1] pigmented papillary neoplasm of the pituitary fossa,[2] and many other common tumors in the pituitary region, such as craniopharyngioma, meningioma, etc., and incidentalomas (incidental pituitary lesions found during CT or MRI of the brain done for nonpituitary symptoms) that may present in a similar manner needing multimodal therapy.

Nuances That Aid Radiation Therapy

In patients for whom radiation therapy is planned for secretory pituitary adenomas, it has been suggested that hormone suppressive pharmacotherapy be stopped at least a month prior to radiation therapy. This has been associated with higher rates of normalization of hormonal overproduction and also lower rates of hypopituitarism in one study.[3] It has been speculated that the hormone suppressive medications might have a radioprotective effect, thereby reducing the efficacy of radiation therapy.[4] They can be restarted after radiation therapy, if indicated.[3]

In patients for whom radiation therapy is planned for residual pituitary tumor following surgical excision, hypophysopexy is suggested. Hypophysopexy involves the placement of fat and fascia graft to increase the distance between the residual tumor and the normal pituitary gland during surgical excision of pituitary tumors to reduce the radiation to the normal pituitary gland. This has been tried in pituitary tumors involving the cavernous sinus, where the autograft is placed between the cavernous sinus and the pituitary gland. Long-term endocrinological outcomes have been assessed after hypophysopexy. It has been found that even 4 years after the procedure, there has not been any new endocrinological dysfunction in these patients. Long-term follow-up has been suggested.[5]

Also, metallic implants are to be avoided, especially near the site of residual tumor. They could hinder radiation therapy planning due to artifacts seen on imaging, and can also cause scatter of the radiation. The presence of metallic implants does not significantly interfere with photon radiation therapy planning due to the ability of the planning system software to take into consideration the attenuation and scatter by the implants. However, with proton beam therapy, the issues with dose perturbation by the metallic implants need to be explored further.[6]

Timing of Radiation Therapy after Surgery

The decision as to when patients should be irradiated postoperatively for residual tumor is debatable. Early administration of radiation therapy, as against observation for tumor growth postoperatively, has been associated with better tumor control, albeit with an increased risk of hypopituitarism.[7] On tumor progression, if it is not amenable to repeat surgery, the standard of care is to administer radiation therapy. This requires serial follow-up with MRIs of the brain to assess progression. The first follow-up MRI is done at 2 to 3 months postsurgery to enable the postoperative changes seen on MRI to resolve, so that residual tumor can be distinguished from postoperative changes. The 2- to 3-month waiting period also gives time for the surgical wound to heal, especially when cerebrospinal fluid leak repair is done. It is also suggested that at times there is a descent of the suprasellar component of the pituitary adenoma away from the optic chiasm during this period. The indication for immediate radiotherapy is when the tumor is close to the optic apparatus and is causing a threat to vision with potential further growth.

Preradiation Therapy Workup

Radiotherapy for pituitary adenomas involves teamwork of multiple specialties such as the neurosurgeon, otorhinolaryngologist, radiation oncologist, endocrinologist, neuro-ophthalmologist, neuroradiologist, medical physicist, dosimetrist, and radiotherapy technologist.

A complete clinical history, treatment history including details of surgery, hormone suppressive pharmacotherapy, and previous radiation therapy, comorbid conditions, detailed physical examination, including visual fields and hormonal hyper- and hypomanifestations, hormonal assays, review of all pre- and postsurgical/pharmacotherapy brain images, immediate preradiation gadolinium-enhanced contrast MRI of brain in pituitary lesion protocol, histopathology, immunohistochemistry, etc., are essential to provide optimal and holistic care to the patient.

Radiation Dose for Pituitary Adenomas

The radiotherapy dose for nonsecretory pituitary adenomas is in the range of 45 to 50 gray (Gy) in conventional fractionation,[8] 25 Gy/5 # in fractionated stereotactic radiotherapy (FSRT), and a median marginal dose of 18 to 20 Gy in stereotactic radiosurgery (SRS).

The radiotherapy dose for secretory pituitary adenomas is in the range of 50 to 56 Gy in conventional fractionation and a median marginal dose of 23 to 25 Gy in SRS. These tumors require a higher dose of radiotherapy than their nonsecretory counterparts.

Pituitary carcinoma radiotherapy doses are even higher, in the order of 54 to 56 Gy in conventional fractionation.

Care should be taken to ensure that the radiation dosage received by the organ at risk (OAR), such as optic chiasm and brainstem, is well within their tolerated limits. The rest of the brain should optimally receive very minimal radiation dose.

Techniques of Radiotherapy

Radiotherapy can be delivered as a conventionally fractionated radiotherapy regimen or by SRS/hypofractionated radiotherapy. They have been found to be comparable in terms of tumor control in nonsecreting tumors and hormonal control in secretory tumors. The ways by which radiotherapy has been delivered has evolved over the decade. The technical improvement in radiotherapy has been in the delivery of the desired radiation dose to the target volumes with minimal toxicity.[9] With the advent of more conformal techniques, the safety of adjacent structures such as optic chiasm is no longer a concern.

Two-Dimensional Radiotherapy

In the two-dimensional planning, the field is marked by fixing a point 2 cm in front of and 2 cm superior to the tragus. Using this as the center of the field, a 4 × 4 cm box field is marked out on the skin. Lead wires are places on the field borders and a simulation X-ray of the skull is taken to confirm that the sella is covered by the field. The two parallel, opposed fields are used with prescription at the mid-plane depth (**Fig. 14.1**). A dose slightly higher than the prescription dose is received by the temporal lobes as well. The dose to the optic apparatus is also high. In a comparison with the other techniques, 2D technique delivered more doses to the optic apparatus and the temporal lobes than the others.[10] 2D technique is basically a manual calculation and is followed in centers where there is no facility to do computerized planning.

This was commonly used with cobalt 60 machines. With the advent of planning CT scans and linear accelerators (Linac) with multileaf collimators (MLC), 2D radiotherapy has taken a backseat and is not practiced commonly.

Three-Dimensional Conformal Radiotherapy

Three-dimensional conformal radiotherapy (3DCRT) involves planning CT scan obtained after adequately immobilizing the patient using a three-point thermoplastic mask (**Fig. 14.2a**). The slice thickness should be 2 to 3 mm. The tumor is marked out and the field is shaped with MLCs to conform to the shape of the target. As a result, the normal structures getting exposed to the radiation is reduced, thereby minimizing toxicity.

The usual field arrangements are mostly two parallel, opposed lateral fields (**Fig. 14.2b**) and an Antero Superior Oblique (ASO) field (**Fig. 14.2c, d**) to make the dose to

Fig. 14.1 Marking of the beam portal: 2D plan.

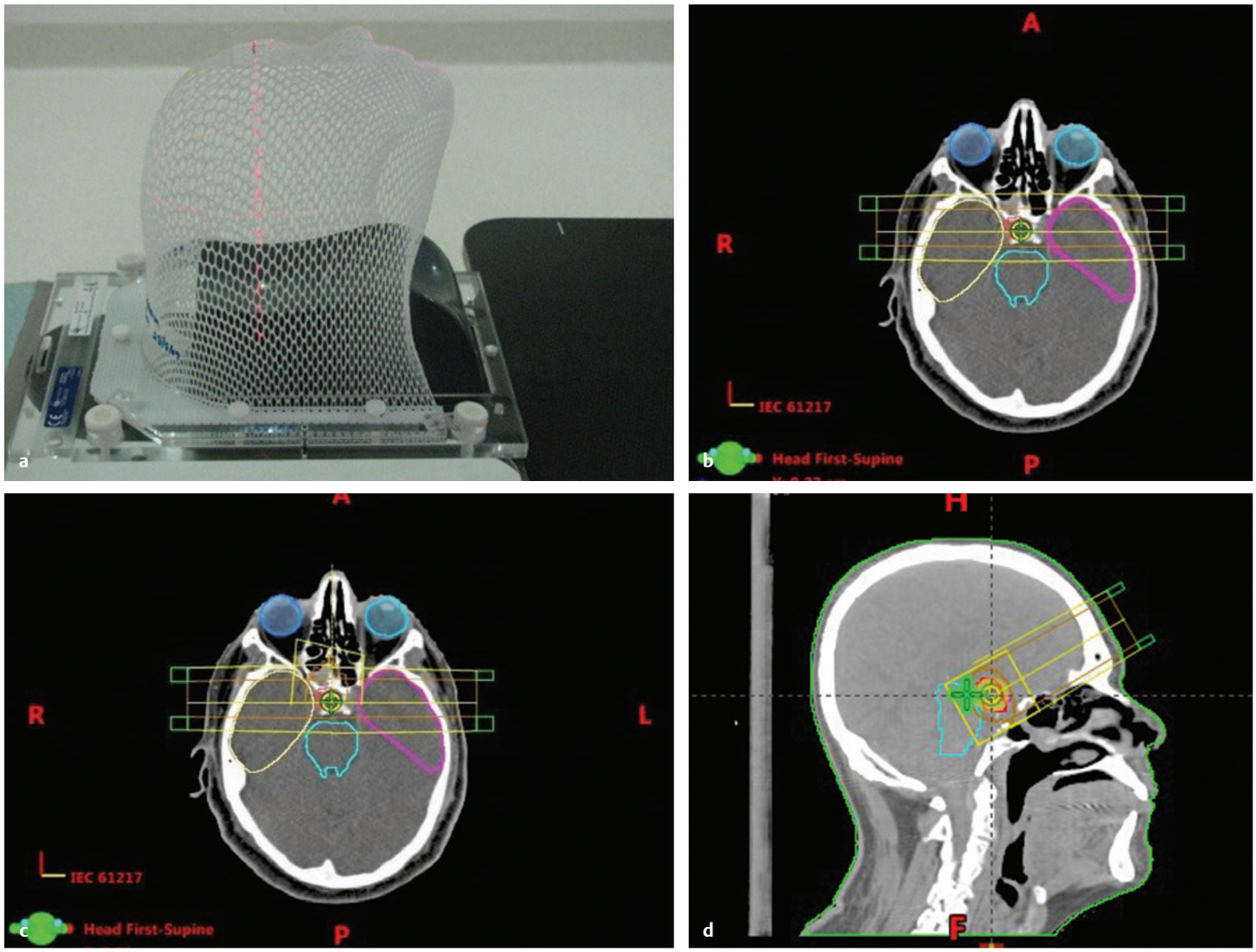

Fig. 14.2 **(a)** Thermoplastic mask; **(b)** two opposing fields; **(c, d)** two opposing fields and an ASO field.

target more conformal. With this arrangement, the dose to the temporal lobes and the optic apparatus is considerably reduced.

Intensity-Modulated Radiotherapy

Intensity-modulated radiotherapy (IMRT) uses multiple small fields with varying intensity/fluence across the beam, aiming to deliver focused radiotherapy to the target with maximal sparing the adjacent critical structures (**Fig. 14.3**). A dose gradient within the target is also achievable with IMRT. This is seldom required in radiotherapy for pituitary adenomas.

There are two ways of dose delivery in IMRT: step-and-shoot method and the sliding window method.

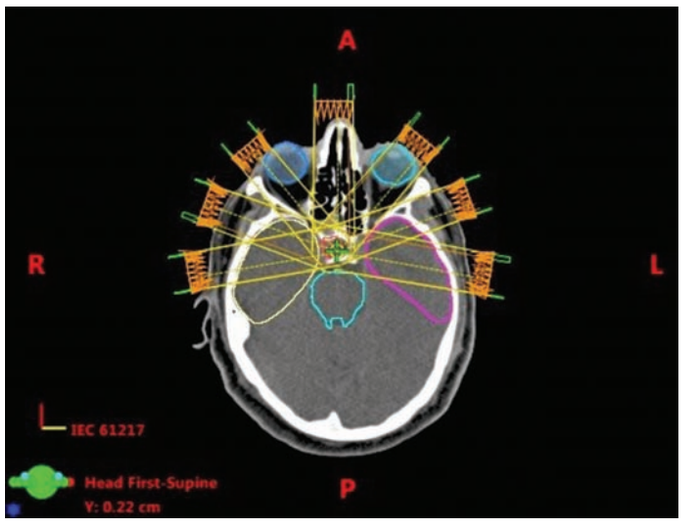

Fig. 14.3 7F IMRT-beam arrangement.

The difference between the two is whether the beam is on during the movement of the MLCs. In step-and-shoot method, the beam is off during the MLC movement, whereas the beam is on during the MLC movement in the sliding window method. The latter produces a better dose distribution due to the continuous modulation of fluence.

The complex dose distribution in IMRT is achieved with the use of MLCs. These MLCs come in various widths. Smaller the width, more conformal is the dose distribution. They are capable of moving independently. As a result of these properties, each beam is divided into multiple beamlets, each with its own fluence, enabling a varied dose deposition across the target. The IMRT uses inverse planning, wherein the user sets the goals for the target dose and dose constraints for the OAR. The close proximity of the chiasm and the cavernous sinuses to the sella makes this technique desirable in terms of normal tissue sparing.

Image-Guided Radiotherapy

The key to a successful radiotherapy schedule is ensuring accurate delivery of the planned dose to the target volume. There are a lot of uncertainties in this, and reproducibility of the daily treatment has been the weakest link in radiotherapy. There are setup uncertainties, intrafraction and interfraction motion of organs, and tumor shrinkage, to name a few. The error introduced due to setup uncertainties and interfraction changes can be overcome to an extent by image guidance. The various ways of image guidance are port films, MV or KV cone beam CT (CBCT) scans obtained using electronic portal imaging devices. They enable us to verify the treatment position before delivering the radiation (**Fig. 14.4**).

Volumetric Modulated Arc Therapy

This is a more sophisticated form of radiotherapy delivery, where the dose is delivered while the gantry and the MLCs move in an arc (complete or partial) (**Fig. 14.5**). The volumetric modulated arc therapy (VMAT) plan has been shown to be better than IMRT or 3DCRT with respect to the homogeneity/conformity indices and the normal tissue doses. However, the low-dose spill is higher than the fixed beam techniques.

Stereotactic Radiosurgery

SRS is the delivery of focused large dose of radiotherapy in a single fraction to a small residual or recurrent tumor. SRS can be delivered with Gamma Knife or Linac-based

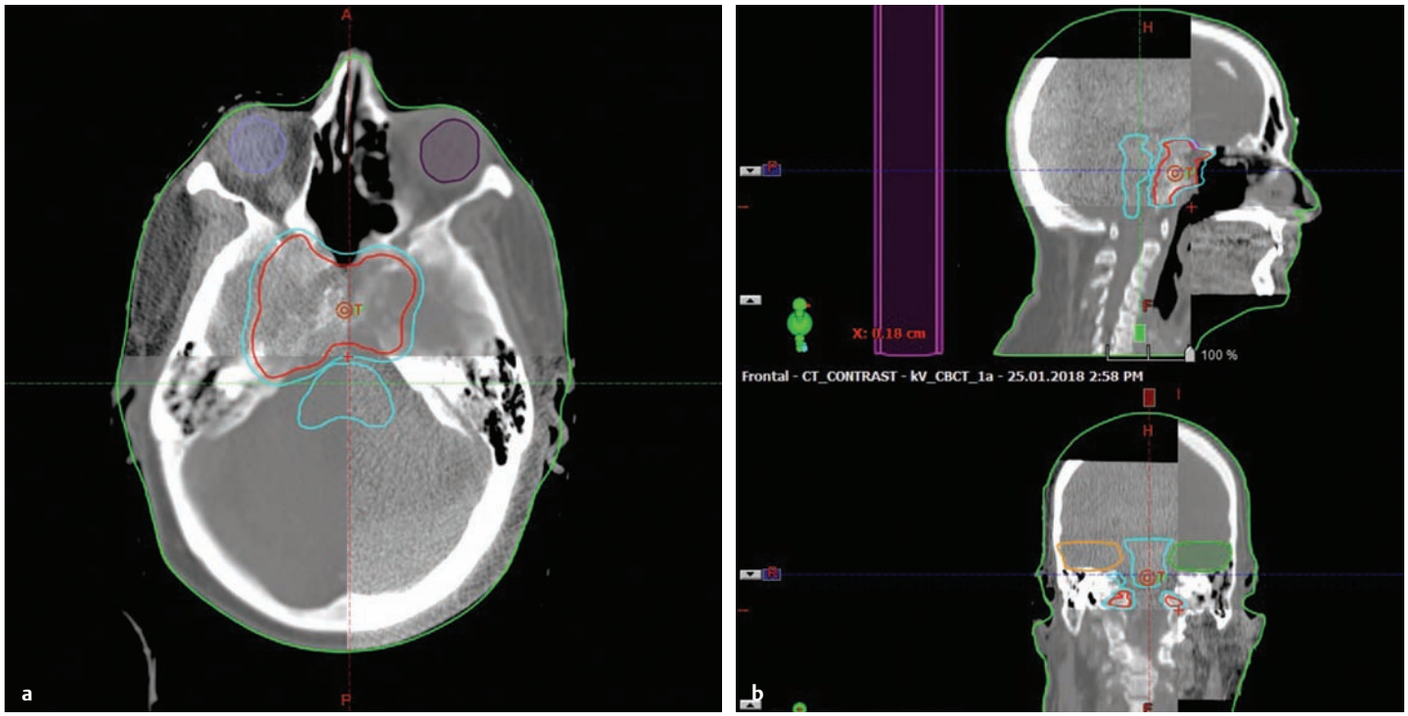

Fig. 14.4 CBCT image guidance. **(a)** Axial images; **(b)** sagittal and coronal images.

techniques. It was first done for pituitary tumors in 1968 using the Leksell Gamma Knife. It uses a helmet which houses 192 to 201 Cobalt 60 sources in a circular array. These sources can be collimated and focused on the target with an accuracy of 3 mm. The target is localized with the help of coordinates on the applicator.[11]

Then came the Linac-based SRS delivery systems. They use head frames (like BRW frame) fixed on the scalp and with the help of stereotactic coordinates the target is localized. Circular cones or micro-MLC, with a width of 2.5 mm at isocenter level, are used to shape the field to conform to the target. Multiple isocenters are used with circular cones to cover larger tumors. With micro-MLC, single isocenter is used irrespective of the tumor size. Mostly noncoplanar beams are used with Linac-based SRS (**Fig. 14.6a**).

CyberKnife (CK) is a miniature Linac, mounted on a robot, which has six degrees of freedom. This does not mandate the frames to be fixed and it exploits real-time tracking techniques with intrafraction image verification. The robotic arm enables the delivery of radiation from multiple noncoplanar (**Fig. 14.6b**) beams, thereby ensuring a highly conformal dose distribution with maximal sparing of adjacent structures.

The main advantages with these techniques are better conformal dose distribution to the target and lesser dose to the critical structures around. Hence, the optic apparatus is better preserved compared to the conventional methods. Radiobiologically, these tumors are believed to have a low alpha/beta. A large dose per fraction is hence desirable for these slow-growing tumors for better tumor control. The radiobiology behind SRS is not the same as conventional fractionation. The mode of cell death in conventionally fractionated radiotherapy is due to single- and double-stranded DNA damage causing lethal, sublethal, and potentially lethal damages. As the tumor cell attempts a division, it succumbs to the damages. The duration between the fractions enables the tissues to recover from the sublethal damage by DNA damage repair. This property, better preserved in the normal tissues in comparison with tumor cells, leads to differential damage to the tumor cells. For doses larger

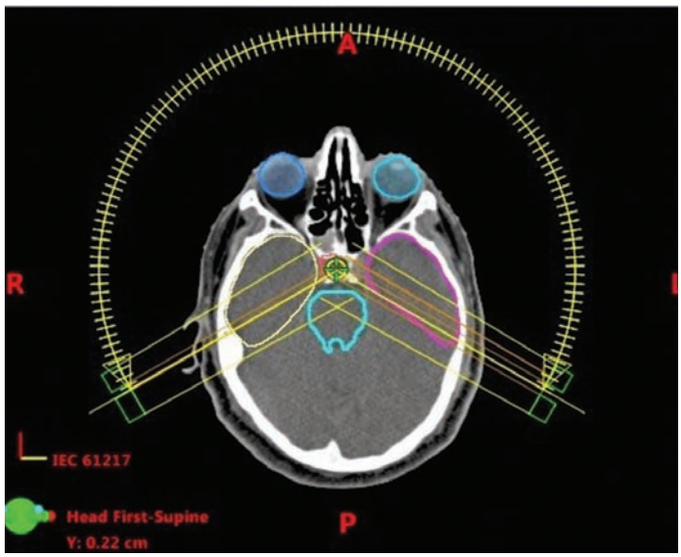

Fig. 14.5 VMAT with two arcs.

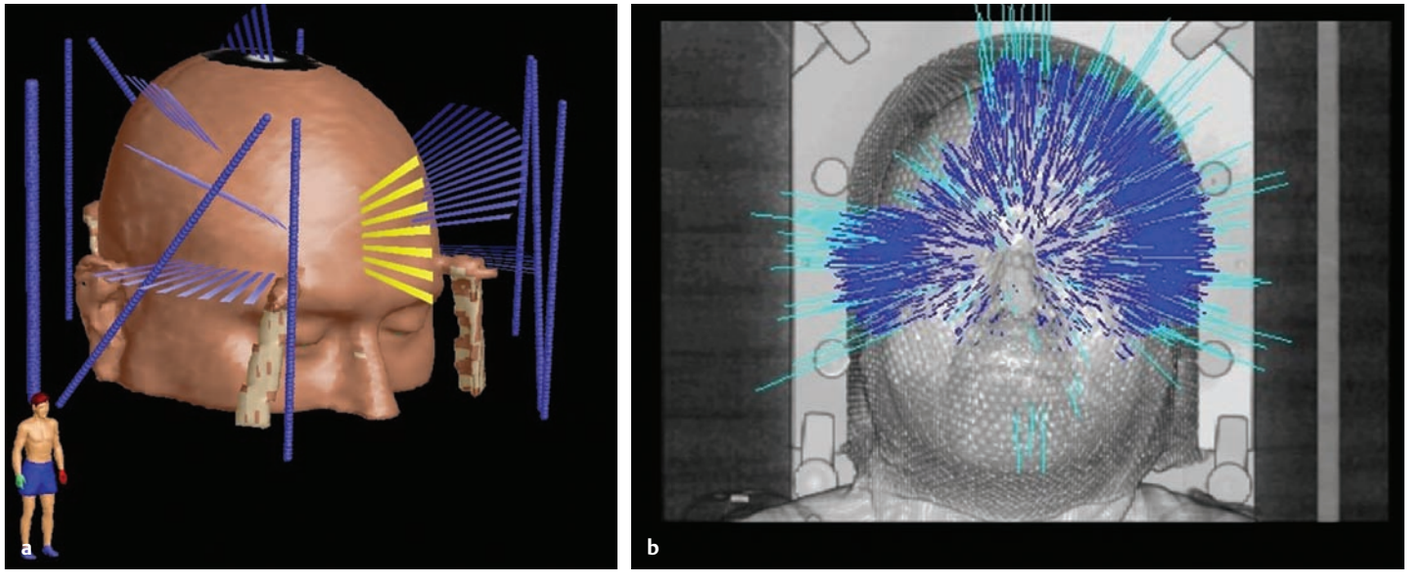

Fig. 14.6 **(a)** Linac-based SRS with frame; **(b)** CyberKnife SRS: frameless.

than 10 Gy, the linear quadratic model does not seem to be applicable. Vascular damage seems to be the mechanism causing cell death apart from apoptosis. This is proposed based on postoperative histopathological examination of benign diseases such as meningioma which were treated with large doses of radiotherapy.

SRS has been found to be equivalent to conventionally fractionated radiotherapy in terms of efficacy and safety profile. The claim that SRS may be superior to the conventionally fractionated radiotherapy has not been proven yet. There have been reports of earlier normalization of hormonal levels with SRS.[12] Likewise, it has not been associated with an increased incidence of side effects.

However, not all cases might be suitable for SRS. Those whose size is less than 4 mL and distance from the chiasm is 2 to 5 mm are recommended for consideration of radiosurgery.[13]

This distance is required to enable a rapid dose falloff, excluding the chiasm from the high-dose region. Failure to do so may increase the risk of optic neuropathy. Careful selection of cases is very important for SRS.

Fractionated Stereotactic Radiotherapy

FSRT combines stereotaxy and fractionation. This has been proven to be as effective as conventional techniques with better conformity. It can be used in cases that do not meet the above-mentioned criteria for SRS.

They can be delivered in conventional fractionation (45–50 Gy /25–28 #) or by a hypofractionated schedule. A dose of 25 Gy /5 # has been evaluated and has been found to be safe for tumor control and vision preservation.[14]

Proton Beam Therapy

Particle therapy has been recently gaining momentum in the field of radiotherapy. Proton beam therapy is being exploited for lesions such as the pituitary adenoma, which is close to many critical structures. Protons travel for a specific distance through the medium, as determined by their energy, and deposit all their energy at the end of their range. This energy deposition is maximum at the end of their range. This is called the Bragg peak. By a selection of energies, the Bragg peak of different proton beams can be made to cover the target. There is practically no exit dose with proton beam therapy. Recent studies have shown similar results with photon-based and proton-based SRS. The benefit will be for larger tumors abutting the optic pathway or the cavernous sinus. The integral dose (the total dose received by the body) is also shown to be less for protons. This may be important in reducing the incidence of second malignancies and neurocognitive defects.[15]

Carbon Ion Therapy

This is another form of particle therapy, which is also characterized by lack of exit dose. Carbon ions and proton beams have been analyzed for the treatment of pituitary tumors. The tumor control was found to be as effective as photons with less acute side effects.[16]

Work Flow

Radiotherapy planning involves acquiring 2- to 3-mm-thick axial CT images with the patient immobilized in supine position with a three-point thermoplastic mask. The CT images are the primary images, on which planning is done, using treatment planning systems. MRI of the brain is acquired and is co-registered with the CT scan images for delineation of the target and critical structures like chiasm and brainstem (**Fig. 14.7**).

The gross tumor volume (GTV) is the residual or recurrent tumor as visible on the MRI. It is delineated in the axial slices. A clinical target volume (CTV), which is the volume that encompasses the microscopic disease, is generally not required, the exception being when there is cavernous sinus involvement in aggressive tumors. In these instances, the entire cavernous sinus is included in the CTV. In other cases, a planning target volume (PTV) is generated by a geometric expansion of the GTV.[17]

This margin is dependent on the immobilization, treatment technique, and verification protocols. In SRS SRT, a 2- to 3-mm margin may suffice due to the stringent imaging and immobilization. For 3DCRT, IMRT, and VMAT, a margin of 5 to 10 mm is usually given to take care of the setup uncertainties.

The OARs, such as the optic nerves, optic chiasm, temporal lobes, hippocampi, lens, and brainstem, are contoured on axial slices. A planning OAR volume may be generated following the same principles of the PTV.

The dose is prescribed based on the technique (conventionally fractionated radiotherapy/SRS/FSRT) and the histology (secretory/nonsecretory/other histologies).

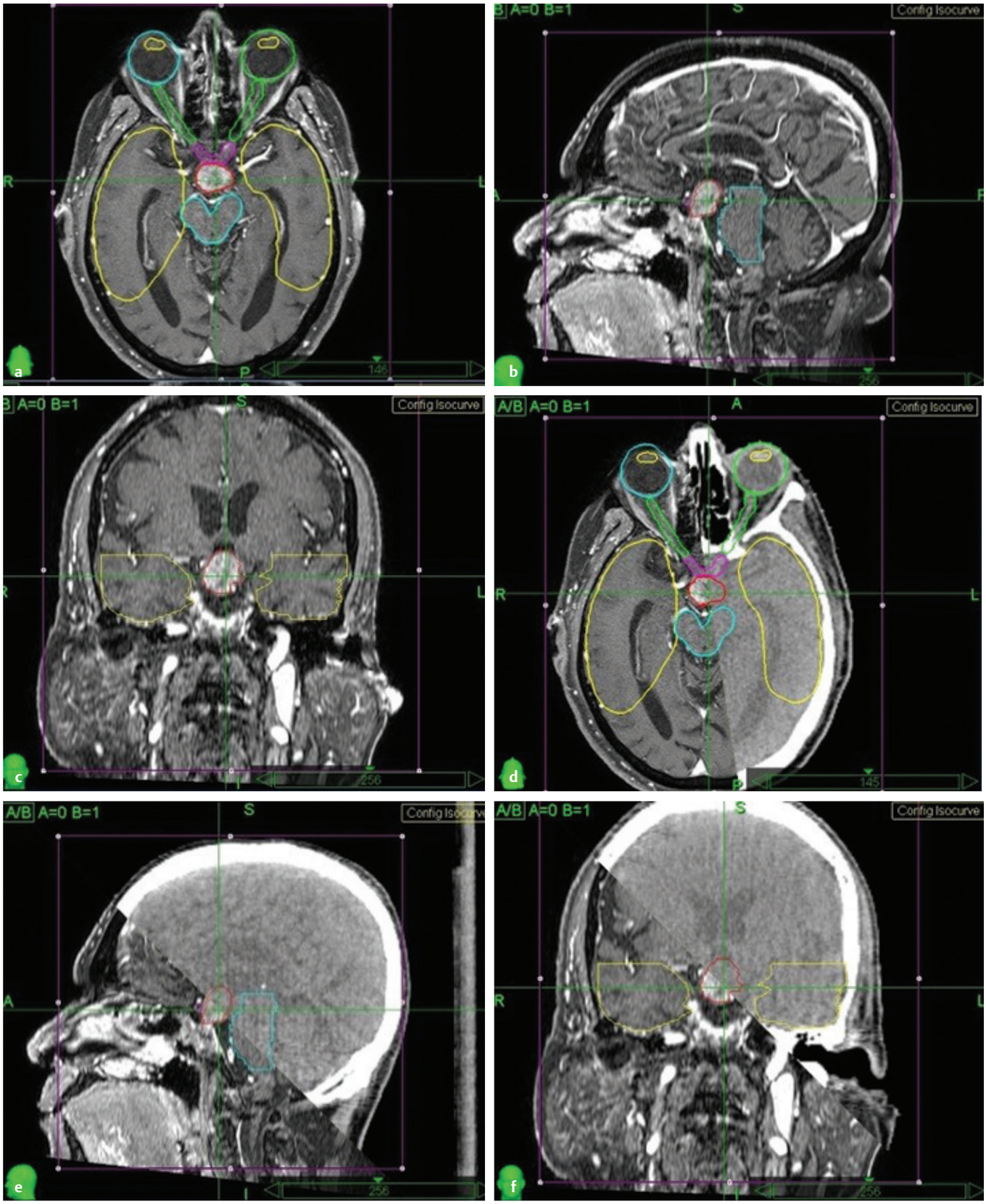

Fig. 14.7 Target volume and OAR images on **(a, b, c)** MR images and **(d, e, f)** fused CT images.

The objectives (the required dose to the target and coverage) and the constraints (the dose limitations for the organs at risk) are provided in **Table 14.1** and **Table 14.2**, respectively. The optic pathways are serial organs. The functional subunits (FSUs) are placed serially and the integrity of the preceding FSU is required for the normal functioning of the following FSU. Hence, the dose constraints for these organs need to be stringent, and therefore the maximum dose is recorded.

Tolerances of the other structures are high enough for the dose prescribed for pituitary tumors. Care should be taken during re-irradiation.

Plan Evaluation

The plan is evaluated slice by slice by examining the isodose distribution and analyzing the dose volume histogram (DVH). The DVH is a graph with the dose plotted against the volume receiving it, for the target and the critical organs. If the plan meets the objective and the constraints, then the plan is approved and is sent for execution.

The treatment is delivered once the setup is satisfactory. This is ensured by the onboard imaging available. The daily setup variations are documented and verified to make sure the PTV margin will be adequate for the case.

Radiation Treatment Plans for Comparative Analysis

Four different case studies were taken for treatment planning and subsequent analysis and comparison. The treatment plans developed are purely for comparison study only and not executed on the patients. Treatment plans were generated for radiotherapy with 6 MV photons using two parallel opposing fields (2F), 3 fields (3F) with 2 opposing, and an ASO noncoplanar field, IMRT, VMAT, and FSRT. An MLC of leaf width 2.5 mm at the isocenter plane was used for shaping the portal. For 2F and 3F, forward planning is done, in which calculation is done first and the dose prescription is done on the isodose which encompasses, say, 95% of the target volume and considering the dose that would be received by the OAR. In IMRT, VMAT, and FSRT where inverse planning is done, the user sets the total dose to the GTV and the OAR, and the treatment planning system does the plan using iterative methods and tries to achieve the goals set. A dose of 45 Gy/25 fractions is prescribed to the GTV.

Table 14.1 PTV objectives

% volume of PTV	% of prescribed dose
99	>90
95	>95
50	100
5	<105
2	<107

Table 14.2 Normal tissue constraints

OAR	Constraints	
	SRT	SRS
Chiasm	D_{max} < 48 Gy	<12 Gy
Lens	<5 Gy	Not specified
Retina	D_{max} < 40 Gy	Not specified

Case 1

A 29-year-old lady was diagnosed to have a pituitary lesion when evaluated for headache. She underwent transsphenoidal surgery for the same. HPE revealed an ACTH secreting tumor. She was started on hormone suppressive pharmacotherapy and was referred for radiotherapy after 1 year for the residual tumor due to rising cortisol levels.

Planning CT scan images were co-registered with the MRI images. The GTV was drawn based on T1-weighted MRI images, which have been fused with CT images. The OARs drawn are chiasm, brainstem, and both temporal lobes.

The dose distribution for all the four techniques with conventional fractionation and CK SRS are shown in **Fig. 14.8a–e**.

Comparison and Analysis

On analyzing the plans, it is seen that the GTV dose coverage does not very significantly differ. The doses to chiasm and brainstem are significantly lower in 2F plan, whereas the doses to both the temporal lobes are 10% above the prescription dose, compared to the 3F plan. The reduction of the dose to temporal lobes is achieved by adding a third field anterosuperiorly. On the other hand, the third field undesirably increases the dose contribution to chiasm and brainstem, but at the same time the 3F conforms the dose to the target. This is the advantage of adding a third field. When these two plans are compared with the IMRT

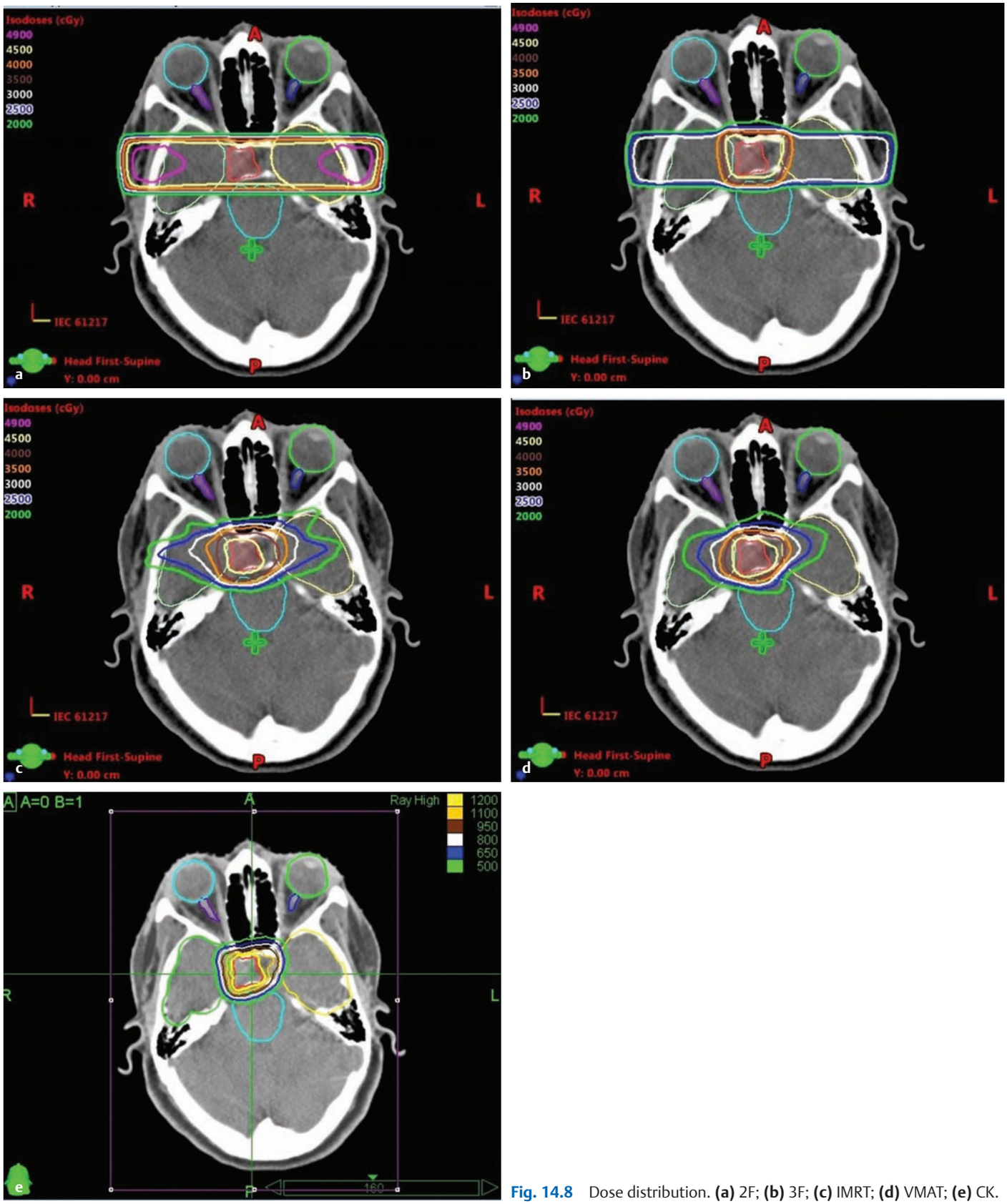

Fig. 14.8 Dose distribution. **(a)** 2F; **(b)** 3F; **(c)** IMRT; **(d)** VMAT; **(e)** CK.

and VMAT plans, it is very evident that, in addition to the target conformity, the doses to chiasm and the temporal lobes are greatly reduced, especially in the region of 25 to 40 Gy (which is 60–90% of the target dose), making IMRT or VMAT the preferred choices of treatment.

A single-fraction SRS plan with CK was also generated for comparison, with a prescription of 12 Gy to the GTV, in view of the proximity of the chiasm. It is seen that the GTV conformity is very much better as the system uses multiple noncoplanar pencil beams. The maximum doses to the chiasm and brainstem, 9.9 and 10.7 Gy, respectively, are well within the limits for an SRS procedure. The dose to GTV could have been increased if hypofractionated FSRT is considered. The dose fall is so rapid that the doses to temporal lobes are very well reduced. For the sake of comparison the DVHs are shown in **Fig. 14.9a–d**, for all the OARs (except the left temporal lobe, as doses received by left and right temporal lobes do not differ much) and the GTV, pertaining to all the plans generated with the conventional fractionation.

Case 2

This 64-year-old gentleman was evaluated for visual disturbances and was found to have a sellar mass with suprasellar extension. He underwent transsphenoidal excision in July 2018. Follow-up MRI in November 2018 showed a gross residue impinging on the chiasm. He was referred for radiotherapy.

Comparison and Analysis

As in the previous case, the doses to chiasm and brainstem are more in 3F plan compared to 2F plan, the reason for which has been explained already. The doses to both the temporal lobes are also less in the 3F plan (**Fig. 14.10a, b**). It is very interesting to note that though the target dose conformity (**Fig. 14.10c, d**) is much better in IMRT and VMAT plans along with a significant reduction of dose to temporal lobes, in the region of 15 Gy to 40 Gy, in the dose region of less than 15 Gy, the dose to temporal lobes is higher with IMRT and VMAT compared to 2F and 3F plan (**Fig. 14.11a–c**). This is due to the usage of multiple fields, which contributes to the more of low-dose volume, and this might be a causative factor for a new tumor. Hence it is very important to consider these factors while choosing an appropriate treatment plan.

A fractionated FSRT plan with CK was also generated for comparison, with a prescription of 25 Gy to the GTV in 5 fractions (**Fig. 14.10e**). It is seen that the dose conformity is very much better as the system uses roughly about 150 noncoplanar pencil beams. The maximum doses to the chiasm and brainstem, 24 Gy and 23 Gy, respectively, are well within the limits for a 5 fractions FSRT procedure. The dose fall is so rapid that the doses to temporal lobes are very well reduced (**Fig. 14.11d**).

Case 3

This 53-year-old gentleman was diagnosed with a pituitary adenoma in 2004, for which he underwent surgery. He recurred again and was operated upon in 2007. He received postoperative radiotherapy to a dose of 48.6 Gy in 27# elsewhere. The doses to the normal structures were not known. He was found to have a recurrent tumor again in December 2017, with suprasellar, parasellar extension and posteroinferior extension along the clivus. He underwent a debulking surgery for the same. Before surgery his visual field assessment showed left temporal hemianopia.

Due to the extensive nature of the disease and to prevent further loss of vision, this patient was referred for re-irradiation. The difficulty in this case was that the optic chiasm could not be clearly made out different from the tumor. This and the fact that the previous radiotherapy details were unknown made it a tricky situation. However, after deliberation with the patient and the neurosurgeon, it was decided to re-irradiate him to prevent the tumor from progressing and causing blindness. Nevertheless, the risk of optic neuropathy due to radiotherapy must also be kept in mind.

The choice of the apt technique in this case will depend on the dose to the chiasm in the various techniques.

Comparison and Analysis

Dose distribution for the conventional fractionation is shown in **Fig. 14.12a–d** and for the CK FSRT in **Fig. 14.12e**.

The point to be noted in this case is that the maximum dose to chiasm dose is more than the prescribed PTV dose due its proximity. Interestingly in this case the dose to chiasm from 3F plan is little lower compared to 2F plan. On comparing all the DVH (**Fig. 14.13a–c**) it is seen that the chiasm dose is lowest in the IMRT plan with a minimum and maximum doses of 13 Gy and 43 Gy, respectively, for a dose of 45 Gy/25#. Even in the CK FSRT plan (**Fig. 14.13d**), the minimum dose to chiasm is 21 Gy and the maximum dose is 26 Gy for a prescription of 25 Gy/5# to the PTV. This suggests that IMRT offers better solution for such large

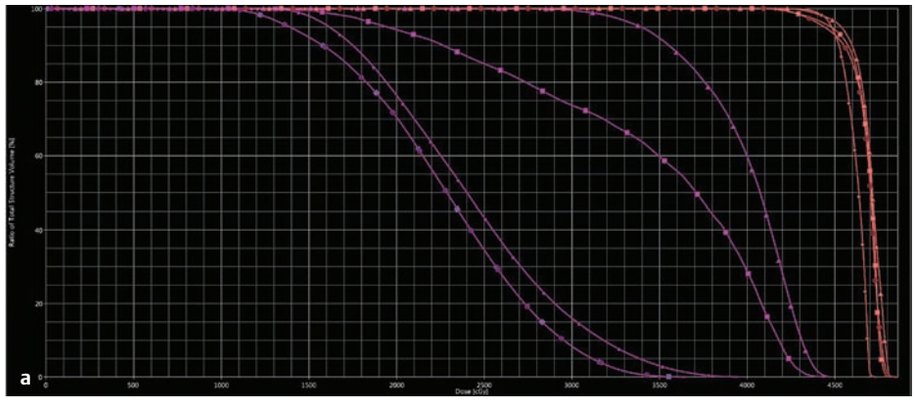

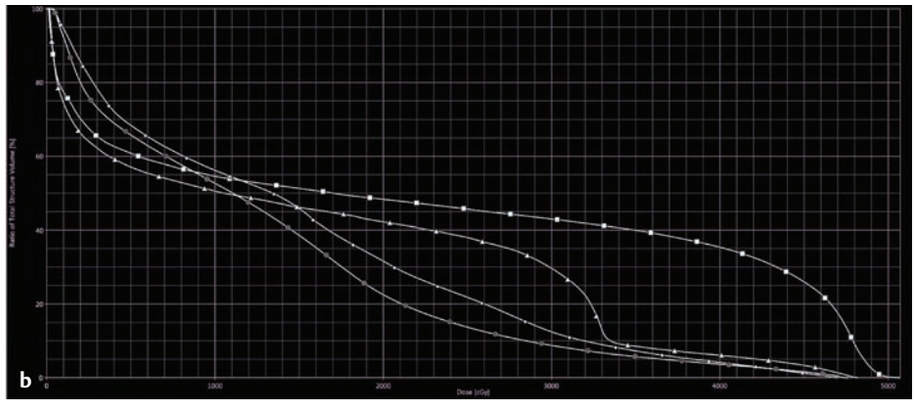

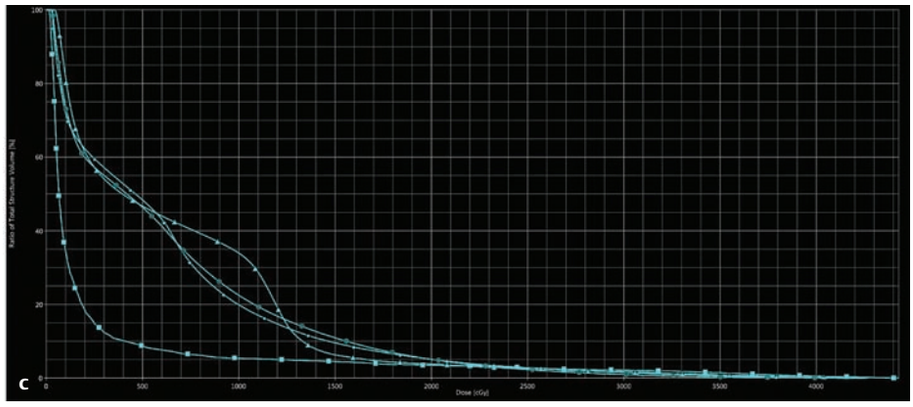

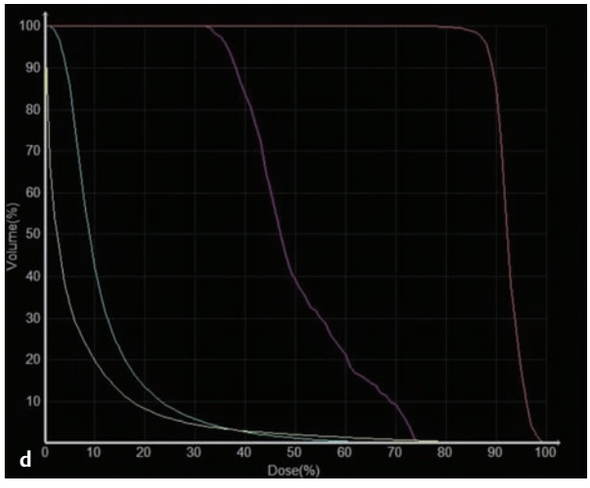

Fig. 14.9 **(a) DVH-GTV:** 2F; 3F; IMRT; VMAT; **chiasm:** 2F; 3F; IMRT; VMAT. **(b) DVH-Rt: temporal lobe:** 2F; 3F; IMRT; VMAT. **(c) DVH-brainstem:** 2F; 3F; IMRT; VMAT. **(d)** DVH-CK SRS plan: GTV ——; Chiasm ——; Rt.temp.lobe ——; Brainstem ——.

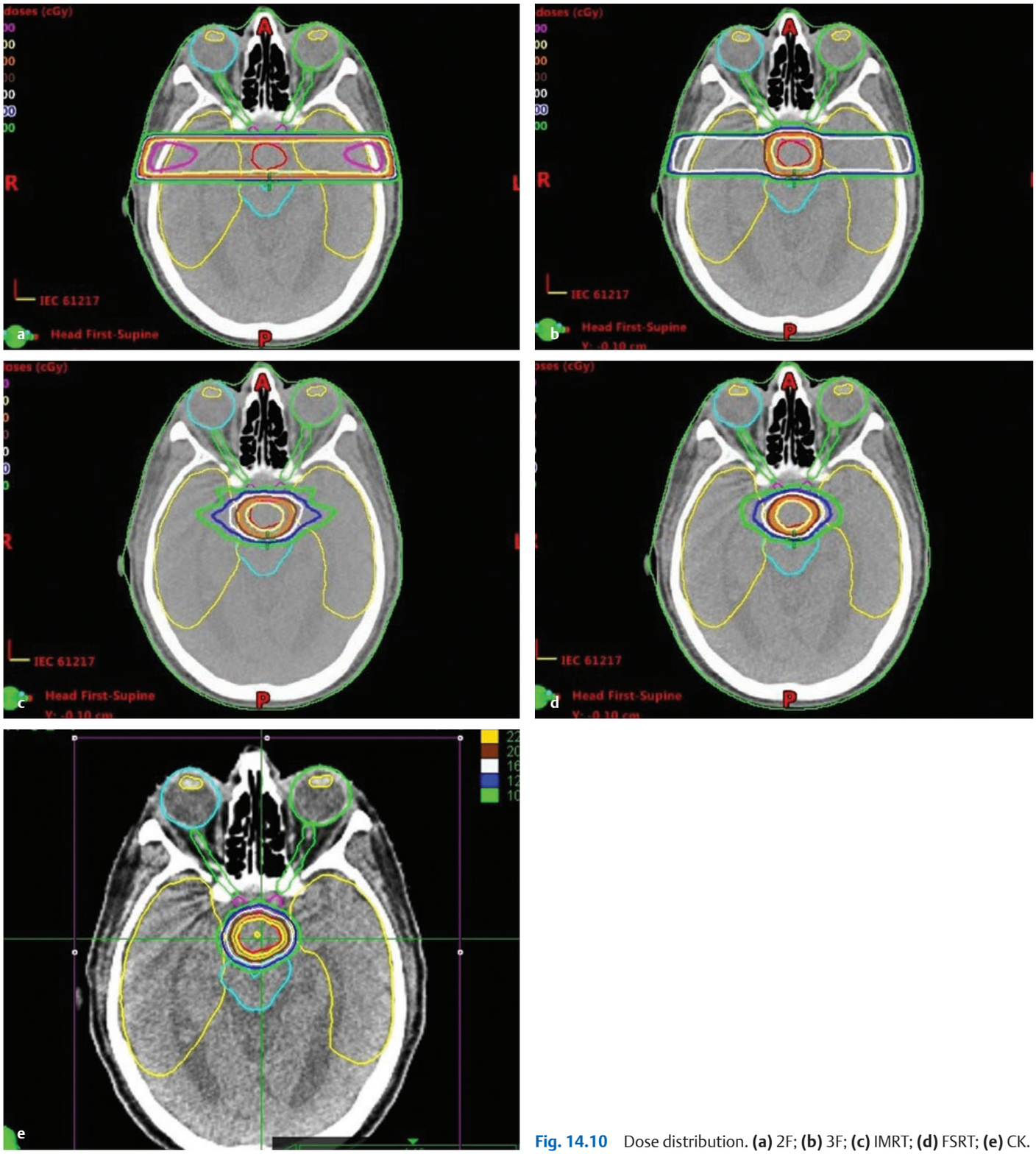

Fig. 14.10 Dose distribution. **(a)** 2F; **(b)** 3F; **(c)** IMRT; **(d)** FSRT; **(e)** CK.

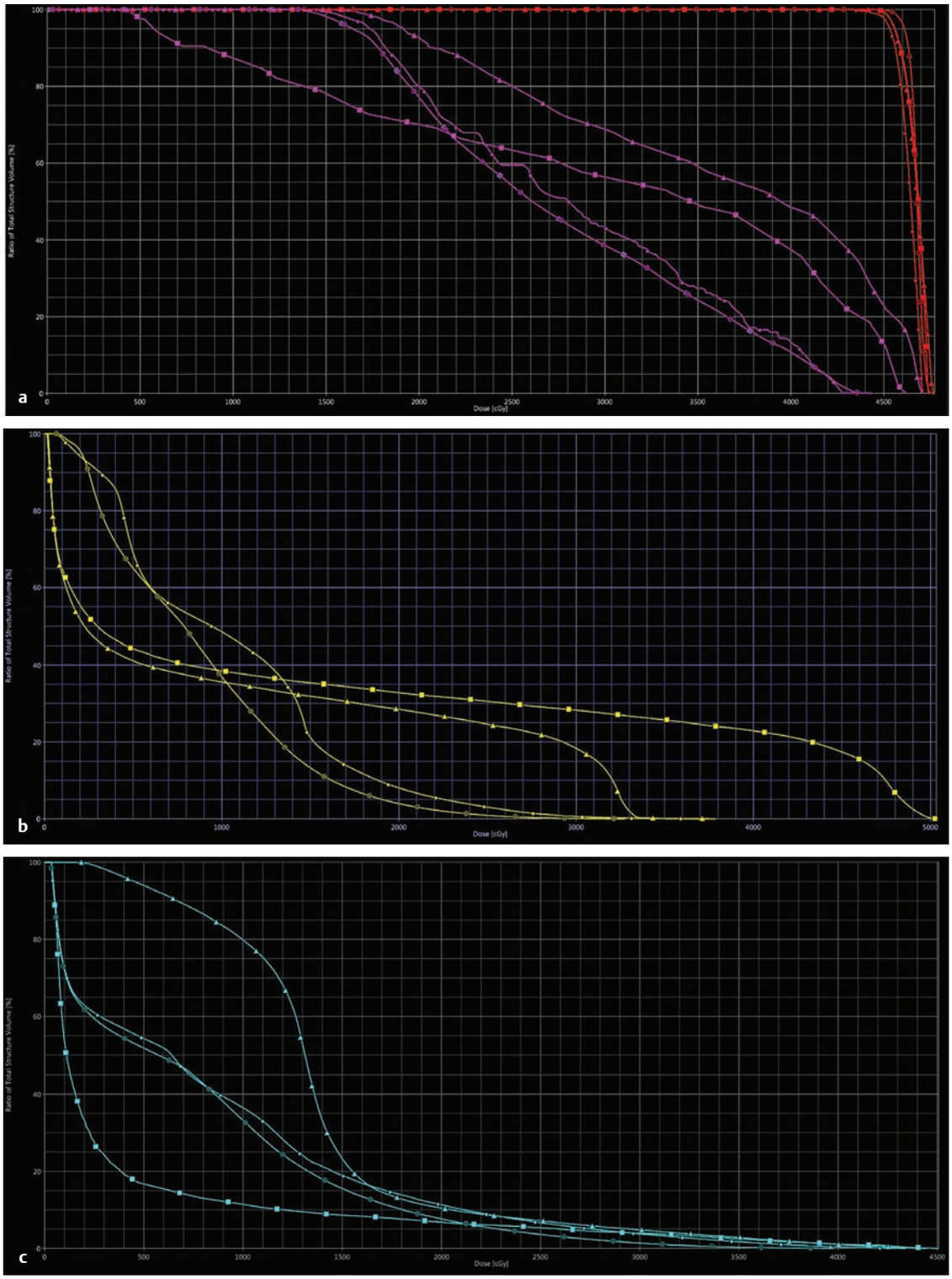

Fig. 14.11 **(a) DVH-GTV:** 2F; 3F; IMRT; VMAT; **chiasm:** 2F; 3F; IMRT; VMAT. **(b) DVH-Rt: temporal lobe:** 2F; 3F; IMRT; VMAT. **(c) DVH-brainstem:** 2F; 3F; IMRT; VMAT.

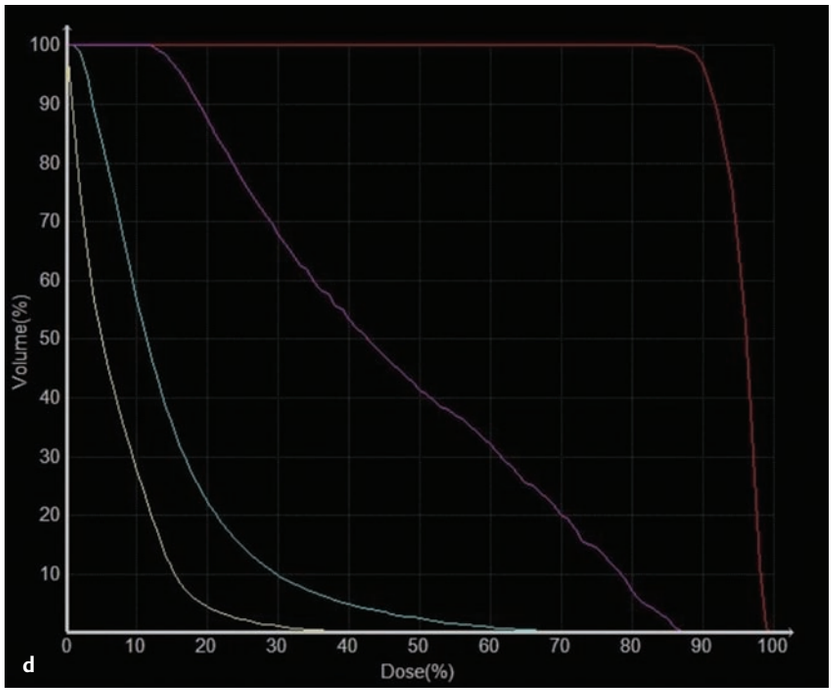

Fig. 14.11 *(continued)* **(d)** DVH-CK FSRT plan: GTV ——; Chiasm ——; Rt.temp.lobe ——; Brainstem ——.

tumors with a proximity to the chiasm. As far as the dose falloff within brainstem and temporal lobes are concerned, the high precision treatments like IMRT, VMAT, and CK offer considerable advantage.

Case 4

This patient had a surgery for recurrent pituitary macroadenoma and came for adjuvant radiation. Patient was planned for adjuvant radiation to a dose of 45 Gy in 25 fractions with VMAT technique and pencil beam spot scanning proton beam therapy (with spot sigma of 3 mm in air of 230 MeV proton beams).

Comparison and Analysis

On comparison of proton and VMAT plan, there was no significant difference in the target coverage and optic apparatus dose. The mean dose received by bilateral hippocampi was significantly lower compared to photon plans (left sided: 540 cGy vs. 1020 cGy, and right sided: 710 cGy vs. 1251 cGy for protons and photons, respectively). The bilateral temporal lobe dose was also lower with proton therapy plans in comparison to VMAT/photon plan (**Fig. 14.14**).

In general, there was very little difference in isodose distribution of higher isodose curves till 70. The difference significantly started to increase beyond 50% isodose lines. **Fig. 14.15** demonstrates the low-dose (30%) isodose lines with proton therapy and VMAT plans.

Results

The 10-year survival rates have been in the order of 95% for both the secretory and nonsecretory tumors. The tumor control rates with radiotherapy, however, have been better in nonsecretory tumors (80%) than their secretory counterpart (45%).[18–20]

Nonsecretory Tumors

The stabilization of tumor size has been the most common pattern of response, with delayed decrease in volume also noted.

Secretory Tumors

In secretory tumors, normalization of hormones is the objective, with changes in size of the tumor also being monitored.[13] In Cushing's disease, the rate of hormonal normalization was found to be about 40% in the median follow-up of 22 months after radiosurgery in one study.[21,22]

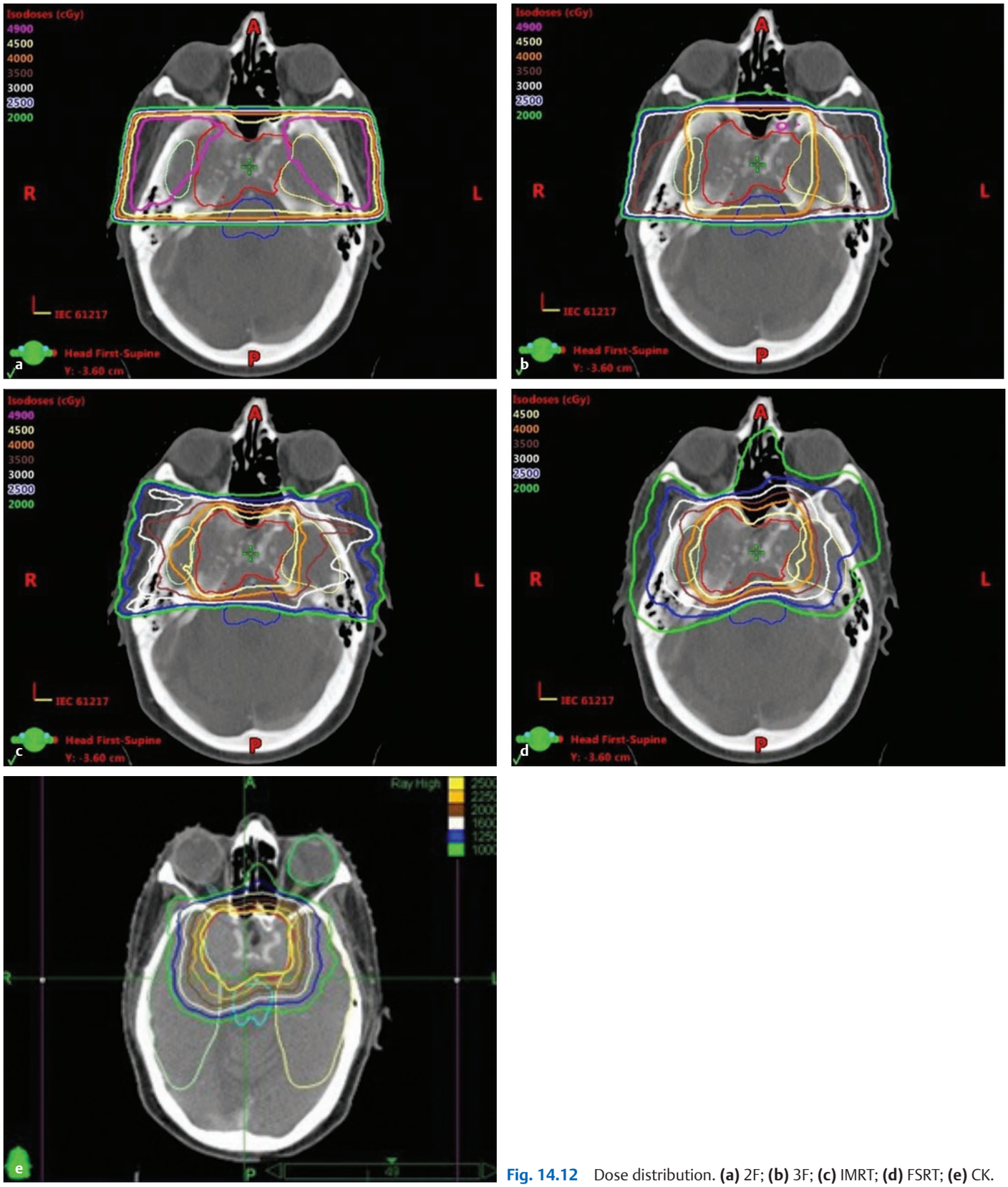

Fig. 14.12 Dose distribution. **(a)** 2F; **(b)** 3F; **(c)** IMRT; **(d)** FSRT; **(e)** CK.

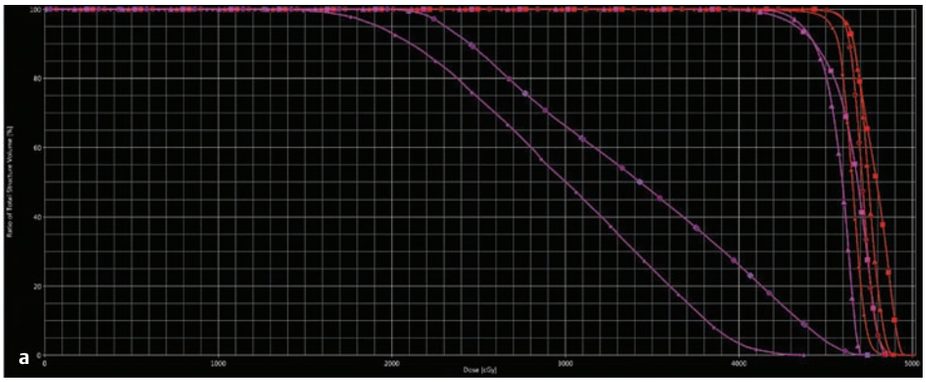

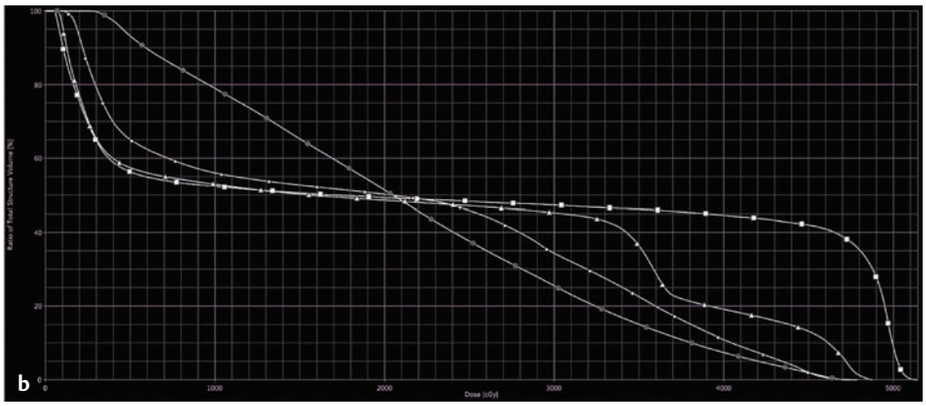

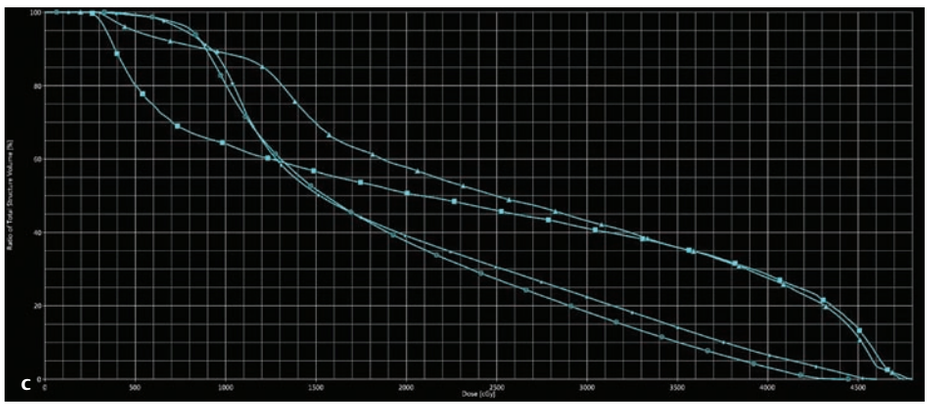

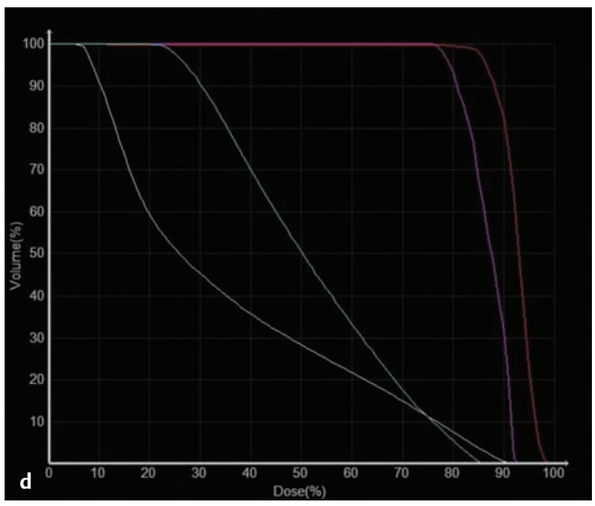

Fig. 14.13 **(a) DVH-PTV:** 2F; 3F; IMRT; VMAT; **chiasm:** 2F; 3F; IMRT; VMAT. **(b) DVH-Rt: temporal lobe:** 2F; 3F; IMRT; VMAT. **(c) DVH-brainstem:** 2F; 3F; IMRT; VMAT. **(d)** DVH-CK FSRT plan: PTV ———; Chiasm ———; Rt.temp.lobe ———; Brainstem ———.

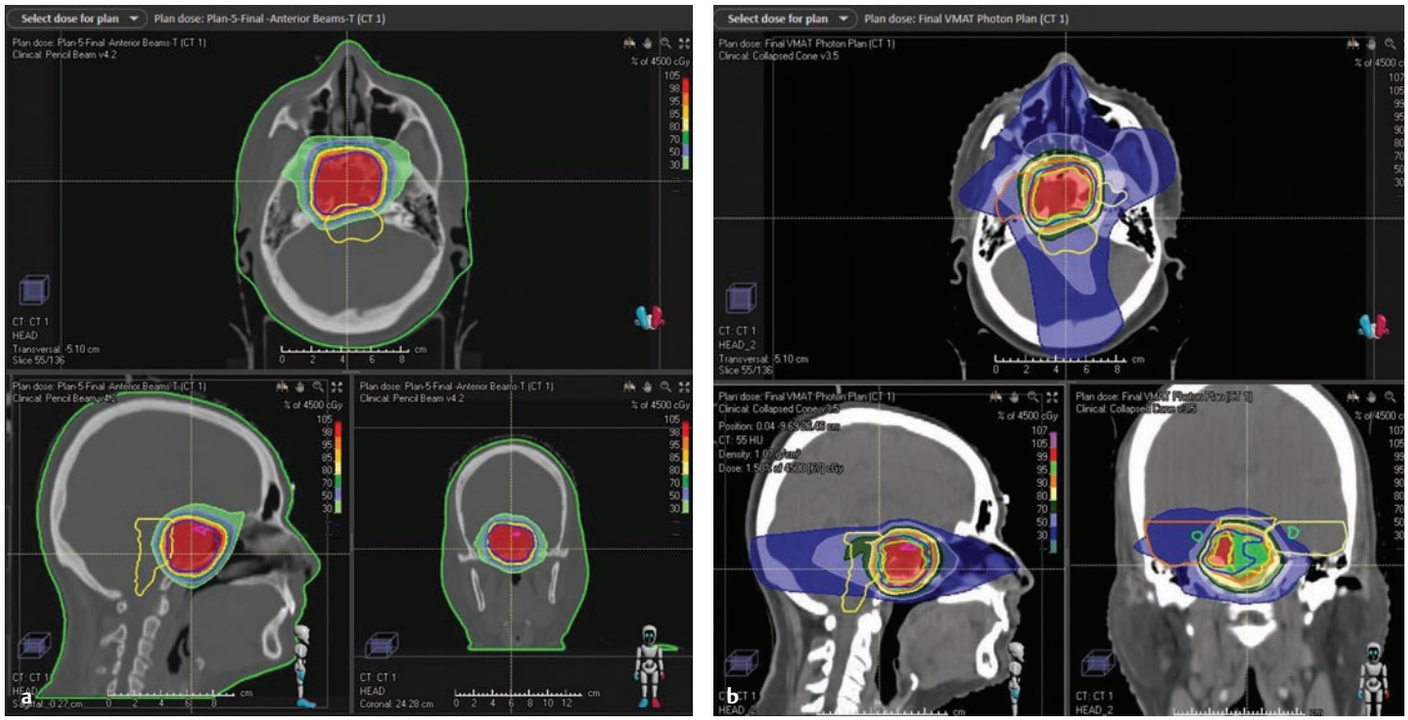
Select dose for plan
Plan dose: Plan-5-Final -Anterior Beams-T (CT 1)
Select dose for plan
Plan dose: Final VMAT Photon Plan (CT 1)
a
b

Fig. 14.14 Isodose distribution. **(a)** Proton plan; **(b)** photon VMAT plan.

Acromegaly: The mean time to normalization after radiosurgery was found to be 27.5 months and the rate of normalization was 65.4% during a median follow-up duration of 61.5 months in one study.[23] In another analysis by Miniti et al, the rate of normalization of GH/IGF 1 ratio was reported to be 48% at 5 years.

Prolactinoma: In one of the large studies by Pan et al, the normalization rate was 52% post-SRS. Certain other studies show normalization rates of 25 to 35%. These are smaller groups with variable follow-up.[24]

The hormone suppressive pharmacotherapy will have to be continued till the normalization of the elevated pituitary hormones.

Side Effects

The side effects were hypopituitarism, cerebrovascular accidents, neurocognitive defects, cranial nerve and brain injury, and second malignancies.[25,26]

Hypopituitarism is the commonest side effect of radiotherapy (30–60%).[20] The incidence of hypopituitarism has been found to be related with the size of the tumor, technique, preexisting hormonal deficits, and the dose delivered. New-onset hypopituitarism has been around 10%. Smaller tumors, treated with SRS have lesser chances of developing hypopituitarism, whereas the larger ones have a higher chance. It has also been increasingly associated with conventional techniques when compared with SRT. The dose to the pituitary stalk determines hypopituitarism. It is not recommended to reduce the dose to prevent hypopituitarism, as this might hamper the tumor control probability.

The incidence of cerebrovascular accidents (4% at 5 years, 11% at 10 years, and 21% at 20 years) has been related to the dose to the tumor and the local extension of the tumor. Radiotherapy has been suggested to cause atherosclerosis in the vessels, leading to cerebrovascular accidents later on. Occlusion of the internal carotid artery leading to hemiparesis has been reported in some patients post-SRS, but there are multiple factors that are contributory as well. The poor compliance in taking the hormone replacements also contribute to the vascular changes. There are no concrete data attributing radiotherapy as a cause of cerebrovascular accidents. However, this should be borne in mind during follow-up.[27,28]

Optic neuropathy is a known complication as a result of injury to the chiasm. Doses of 8 to 12 Gy have been reported to be safe. There have been reports of visual deficits even with 10 Gy, but that is a rare entity.

Plan dose: Plan-5-Final -...
DVH
Volume [%]
Plan dose: Plan-5-Final -Anterior Beams-T (CT 1) [cGy]
Dose axis display options: Absolute values Relative max dose value Relative reference value [cGy]:
Beams (Current) Energy layer (Current) BEV (Current)
Dose Statistics Clinical Goals Biological Response Fractionation Schedule
ROI statistics POI statistics
Dose ROI ROI vol. [cm³] Dose [cGy] D99 D98 D95 Average D50 D2 D1 % outside
Plan dose: Plan-5-Final... BODY 4589.1 0 0 0 215 2 3150 4520 0 %
Plan dose: Plan-5-Final... BRAINSTEM 25.7 1 2 6 1507 720 4604 4628 0 %
Plan dose: Plan-5-Final... EYE L 9.79 4 4 5 64 25 354 422 0 %
Plan dose: Plan-5-Final... EYE R 9.8 2 3 4 65 24 378 461 0 %
Plan dose: Plan-5-Final... HIPPO L 0.96 1 1 1 540 17 4018 4272 0 %
Plan dose: Plan-5-Final... HIPPO R 1.07 2 3 3 710 34 3927 4177 0 %
Plan dose: Plan-5-Final... lens_left 0.16 4 4 4 7 7 11 11 0 %
Plan dose: Plan-5-Final... lens_right 0.19 3 3 3 5 5 8 8 0 %
Plan dose: Plan-5-Final... OPTIC CHIASM 0.82 4099 4125 4328 4527 4554 4641 4648 0 %
Plan dose: Plan-5-Final... OPTIC NERVE L 0.75 537 575 649 2598 2666 4594 4600 0 %
Plan dose: Plan-5-Final... OPTIC NERVE R 0.71 451 493 540 2359 2138 4627 4631 0 %
Plan dose: Plan-5-Final... p45Gy 48.18 4210 4341 4463 4563 4571 4688 4709 0 %
a

Plan dose: Final VMAT P...
DVH
Volume [%]
Plan dose: Final VMAT Photon Plan (CT 1) [cGy]
Dose axis display options: Absolute values Relative max dose value Relative reference value [cGy]:
Beams (Current) Control Points (Current) BEV (Current)
Dose Statistics Clinical Goals Biological Response Fractionation Schedule
ROI statistics POI statistics
ROI ROI vol. [cm³] Dose [cGy] D99 D98 D95 Average D50 D2 D1 % outside grid
inal VMAT... BRAINSTEM 25.68 179 198 875 2958 3042 4489 4527 0 %
inal VMAT... CTV5mm 28.79 4455 4479 4517 4603 4603 4708 4718 0 %
inal VMAT... EYE L 9.79 151 181 272 776 736 1530 1612 0 %
inal VMAT... EYE R 9.81 265 286 359 727 699 1251 1308 0 %
inal VMAT... HIPPO L 0.95 263 264 283 1020 668 3976 4338 0 %
inal VMAT... HIPPO R 1.07 194 199 215 1251 507 4307 4427 0 %
inal VMAT... lens_left 0.16 344 347 355 418 419 483 494 0 %
inal VMAT... lens_right 0.19 366 367 388 450 450 553 572 0 %
inal VMAT... OPTIC CHIASM 0.82 3892 4042 4147 4480 4501 4669 4671 0 %
inal VMAT... OPTIC NERVE L 0.76 1501 1537 1765 2899 2827 4578 4637 0 %
inal VMAT... OPTIC NERVE R 0.71 1141 1179 1219 2450 1994 4682 4705 0 %
inal VMAT... p45Gy 48.16 4181 4244 4336 4548 4576 4704 4716 0 %
inal VMAT... TEMPORAL LOBE L 54.77 359 414 499 1675 1314 4373 4506 0 %
inal VMAT... TEMPORAL LOBE R 62.81 178 209 284 1907 1666 4488 4558 0 %
b

Fig. 14.15 DVH. **(a)** Proton plan; **(b)** photon VMAT plan.

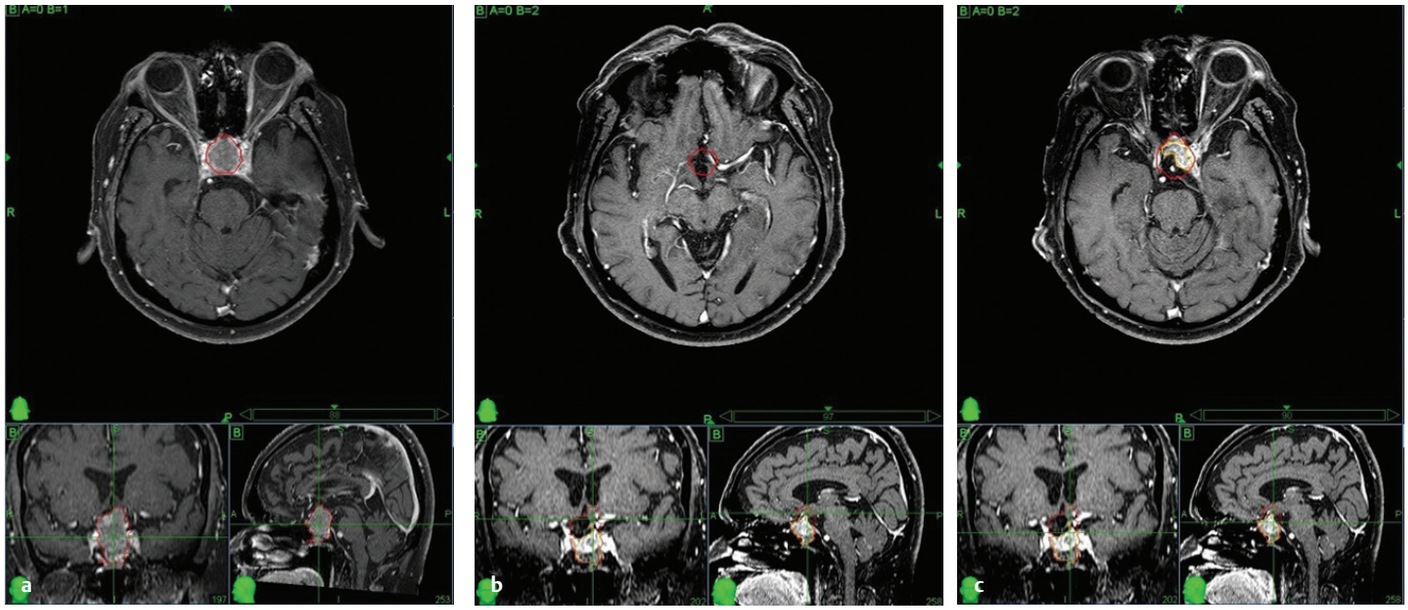

Fig. 14.16 **(a)** Prior to CK treatment; **(b, c)** follow-up after 12 months showing regression of tumor volume.

Brain injuries in the form of seizure have been reported. In cases that have had previous fractionated radiotherapy, re-irradiation with SRS had caused temporal lobe necrosis warranting surgery. There have been reports of hypothalamic injury causing hyperthermia. But these are rare side effects and the dose to the hypothalamus was high in the cases reported.

Follow-up

The follow-up of patients who have undergone radiotherapy for pituitary adenomas should include clinical, radiological, and endocrinological survey. Six monthly follow-up for the first 2 years and annual follow-up thereafter have been advised. Follow-up evaluation includes neuroimaging, visual field and acuity assessment, and hormonal assays. The necessity of long-term hormone replacements in the event of hypopituitarism should be insisted upon (**Fig. 14.16**).

Conclusion

Radiotherapy for pituitary tumors has changed over the years as a result of the technical advances and better selection of cases. Small tumors, away from the chiasm can be safely treated with SRS. For slightly larger tumors, closer to the chiasm, FSRT can be advised (conventionally fractionated or hypofractionated SRT). It is safer to treat larger tumors with cavernous sinus involvement or large suprasellar components or previously irradiated tumors with conventionally fractionated radiotherapy to avoid visual disturbances. Proton beam and carbon ion therapies are new techniques which are said to be associated with less second malignancies and late toxicities. An adequate pre- and postradiotherapy workup, radiological, neurological, visual, and endocrinological follow-up is essential.

References

1. Heaney AP. Clinical review: Pituitary carcinoma: difficult diagnosis and treatment. J Clin Endocrinol Metab 2011; 96(12):3649–3660
2. Fuller CE, Smith M, Miller DC, Schelper R. Pigmented papillary epithelial neoplasm of the pituitary fossa: a distinct lesion of uncertain histogenesis. Arch Pathol Lab Med 2001;125(9): 1242–1245
3. Loeffler JS, Shih HA. Radiation therapy in the management of pituitary adenomas. J Clin Endocrinol Metab 2011;96(7): 1992–2003
4. Pollock BE, Jacob JT, Brown PD, Nippoldt TB. Radiosurgery of growth hormone-producing pituitary adenomas: factors associated with biochemical remission. J Neurosurg 2007; 106(5):833–838
5. Taussky P, Kalra R, Coppens J, Mohebali J, Jensen R, Couldwell WT. Endocrinological outcome after pituitary transposition (hypophysopexy) and adjuvant radiotherapy for tumors

involving the cavernous sinus. J Neurosurg 2011;115(1): 55–62
6. Giantsoudi D, De Man B, Verburg J, et al. Metal artifacts in computed tomography for radiation therapy planning: dosimetric effects and impact of metal artifact reduction. Phys Med Biol 2017;62(8):R49–R80
7. van den Bergh ACM, van den Berg G, Schoorl MA, et al. Immediate postoperative radiotherapy in residual nonfunctioning pituitary adenoma: beneficial effect on local control without additional negative impact on pituitary function and life expectancy. Int J Radiat Oncol Biol Phys 2007;67(3): 863–869
8. Syndikus I, Ashley S, Ph D, Jannoun L. Clinical original contribution. Science 1994;30(4):781–787
9. Minniti G, Gilbert DC, Brada M. Modern techniques for pituitary radiotherapy. Rev Endocr Metab Disord 2009;10(2):135–144
10. Adama D, Gar-elnabi MEM, Aliomer A. The advantages of two dimensional techniques (2D) in pituitary adenoma treatment. J Appl Phys 2014;5(6):49–54
11. Pollock BE, Cochran J, Natt N, et al. Gamma knife radiosurgery for patients with nonfunctioning pituitary adenomas: results from a 15-year experience. Int J Radiat Oncol Biol Phys 2008; 70(5):1325–1329
12. Mitsumori M, Shrieve DC, Alexander E III, et al. Initial clinical results of LINAC-based stereotactic radiosurgery and stereotactic radiotherapy for pituitary adenomas. Int J Radiat Oncol Biol Phys 1998;42(3):573–580
13. Brada M, Jankowska P. Radiotherapy for pituitary adenomas. Endocrinol Metab Clin North Am 2008;37:263–275
14. Killory BD, Kresl JJ, Wait SD, Ponce FA, Porter R, White WL. Hypofractionated cyberknife radiosurgery for perichiasmatic pituitary adenomas: early results. Neurosurgery 2009;64: 19–25
15. Kennedy WR, Dagan R, Rotondo RL, Louis D, Morris CG, Indelicato DJ. Proton therapy for pituitary adenoma. Radiat Oncol Biol. 2014;90(1):S299
16. Combs SE, Kessel K, Habermehl D, Haberer T, Jäkel O, Debus J. Proton and carbon ion radiotherapy for primary brain tumors and tumors of the skull base. Acta Oncol 2013;52(7):1504–1509
17. Minniti G, Osti MF, Niyazi M. Target delineation and optimal radiosurgical dose for pituitary tumors. Radiat Oncol 2016; 11(1):135
18. Rim CH, Yang DS, Park YJ, Yoon WS, Lee JA, Kim CY. Radiotherapy for pituitary adenomas: long-term outcome and complications. Radiat Oncol J 2011;29(3):156–163
19. Minniti G, Clarke E, Scaringi C, Enrici RM. Stereotactic radiotherapy and radiosurgery for non-functioning and secreting pituitary adenomas. Rep Pract Oncol Radiother 2016;21(4): 370–378
20. Brada M, Ajithkumar TV, Minniti G. Radiosurgery for pituitary adenomas. Clin Endocrinol (Oxf) 2004;61(5):531–543
21. Castinetti F, Nagai M, Dufour H, et al. Gamma knife radiosurgery is a successful adjunctive treatment in Cushing's disease. Eur J Endocrinol 2007;156(1):91–98
22. Sheehan JP, Xu Z, Salvetti DJ, Schmitt PJ, Vance ML. Results of gamma knife surgery for Cushing's disease. J Neurosurg 2013; 119(6):1486–1492
23. Lee C, Vance ML, Xu Z, et al. Stereotactic radiosurgery for acromegaly. J Clin Endocrinol Metab 2014;99(4):1273–1281
24. Liu X, Kano H, Kondziolka D, et al. Gamma knife stereotactic radiosurgery for drug resistant or intolerant invasive prolactinomas. Pituitary 2013;16(1):68–75
25. Sebastian P, Balakrishnan R, Yadav B, John S. Outcome of radiotherapy for pituitary adenomas. Rep Pract Oncol Radiother 2016;21(5):466–472
26. Minniti G, Traish D, Ashley S, Gonsalves A, Brada M. Fractionated stereotactic conformal radiotherapy for secreting and nonsecreting pituitary adenomas. Clin Endocrinol (Oxf) 2006;64(5):542–548
27. Brada M, Burchell L, Ashley S, Traish D. The incidence of cerebrovascular accidents in patients with pituitary adenoma. Int J Radiat Oncol Biol Phys 1999;45(3):693–698
28. van Westrhenen A, Muskens IS, Verhoeff JJC, Smith TRS, Broekman MLD. Ischemic stroke after radiation therapy for pituitary adenomas: a systematic review. J Neurooncol 2017; 135(1):1–11

Index

A
acinic cell carcinoma of cavernous sinus, 369–373
airway management, 66, 67–68
anesthetic considerations in surgery, for sellar, suprasellar, and parasellar lesions
  emergence, 67
  induction and maintenance of anesthesia
    monitoring, 67
    prophylactic antibiotics, 67
  intraoperative complications, 67
  postoperative care
    airway management, 67–68
    diabetes insipidus, 68
    hyponatremia, 68–69
    pituitary apoplexy, 68–69
    postoperative analgesia, 68
  preoperative assessment
    airway management, 66
    anesthetic management, 66
    hormone replacement, 66
    lumbar drain, 66
    nasal mucosa, preparation of, 66
    position, 66
  presentation, 65
anesthetic management, 66
anterior clinoidectomy, 421–422
anterior incision, 80
anterior pedicle lateral nasal wall flap, 91–92
anterior skull base reconstruction, vascularized flaps in
  anterior pedicle lateral nasal wall flap, 91–92
  facial buccinator flap, 97
  inferior turbinate flap, 86–88
  middle turbinate flap, 88
  nasoseptal flap, 76–83
  palatal flap, 97
  pericranial flap, 92–94
  posterior pedicled lateral nasal wall flap, 89–91
  rescue nasoseptal flap, 83–84
  reverse nasoseptal rotation flap, 84–86
  temporoparietal fascial flap, 94–97
anterior skull base tumors, perioperative management for
  long-term postoperative management, 62
  perioperative management, 62
  preoperative evaluation, 61
anterior surface, 16

B
binostril transseptal transsphenoidal approach for large solid pediatric adamantinomatous craniopharyngioma involving third ventricle, 404–410
body, 14–15
brain unlocking, in axial and sagittal planes, 419

C
carbon ion therapy, 441
cavernous hemangioma, 374–378
cavernous sinus dural walls, 428–429
cavernous sinus meningioma
  JNA with cavernous extension, 379–383
chordoma, 53–55
craniopharyngioma, 46–51, 265, 280–287
  type 1, 288–291
  type 2, 297–304
  type 3, 266–273, 274–279, 292–296
craniotomy, 418

D
diabetes insipidus, 68
diaphragma sella, 27
displacing the carotid laterally/lateral cavernous sinus, 387–389
donor site care, 83
dynamic contrast MRI
  chordoma, 53–55
  craniopharyngioma, 46–51
  empty sella, 39
  meningioma, 51–52
  miscellaneous lesions, 55–57
  pituitary adenomas, 40–46
  pituitary hyperplasia, 40
  pituitary stalk lesions, 52–53
  Rathke's cleft cysts, 39
  systematic approach to, 38–39

E
embryology of sphenoid ossification center, 12
emergence, 67
empty sella, 39
endoscopic approach, to parasellar lesions
  instrumentation and technical adjuncts, 307
  parasellar area, 306
  preoperative planning, 307
  surgery, indications of, 306
  surgery, limitations of
    anatomical limitations, 306–307
    patient and institution factors, 307
  surgery, rationale of, 307
  surgical technique
    ethmoid-pterygoid-sphenoidal approach
      ethmoid phase, 310
      intracavernous phase, 311
      pterygoid phase, 310–311
      sphenoid phase, 311
      tumor dissection, 311
    midline transsphenoidal endoscopic approach
      sellar phase, 309–310
      tumor dissection, 310
    transmaxilla-pterygoid endoscopic approach, 311–312
endoscopic approach, to sellar lesions
  pituitary adenoma, classification of, 103–104
  preoperative preparation, 100–101
  steps of surgery
    nasal phase, 101–102
    sellar phase, 102–103
    sphenoid phase, 102
  transsphenoidal transsellar approach
    indications for, 99
    limitations of, 100
endoscopic approach, to suprasellar lesions

endoscopic endonasal transsphenoidal approach
contraindications of, 182–183
indications of, 182
patient positioning and preparation, 183
pituitary tumors, 187
preoperative planning, 183
surgical technique
exposure, 183
transplanum approach, 186–187
transtubercular approach, 183–186
endoscopic pituitary surgery
current decade (2011–2019), 7–9
early beginnings (1994–2000), 1–5
next decade (2000–2010), 5–7
endoscopic skull base reconstruction
general principles, 72–75
selection of reconstructive measures, 71–72
vascularized flaps in anterior skull base reconstruction
anterior pedicle lateral nasal wall flap, 91–92
facial buccinator flap, 97
inferior turbinate flap, 86–88
middle turbinate flap, 88
nasoseptal flap, 76–83
palatal flap, 97
pericranial flap, 92–94
posterior pedicled lateral nasal wall flap, 89–91
rescue nasoseptal flap, 83–84
reverse nasoseptal rotation flap, 84–86
temporoparietal fascial flap, 94–97
endoscopic surgery, for sellar and parasellar lesions
binostril transseptal transsphenoidal approach for large solid pediatric adamantinomatous craniopharyngioma involving third ventricle, 404–410
expanded endonasal endoscopic transplanum transtuberculum approach for tuberculum sellae meningioma, 410–415
mononostril transseptal transsphenoidal resection of pituitary macroadenoma, 398–403
ethmoid phase, 310
ethmoid-pterygoid-sphenoidal approach
ethmoid phase, 310
intracavernous phase, 311
pterygoid phase, 310–311
sphenoid phase, 311
tumor dissection, 311
expanded endonasal endoscopic transplanum transtuberculum approach for tuberculum sellae meningioma, 410–415
extended skin incision, 418
extracranial onlay grafting, 72–73

F
facial buccinator flap, 97
fibrous pituitary lesion, 140–146
flap orientation, 75
fractionated stereotactic radiotherapy, 441
free mucosal graft, 73–74

G
giant pituitary tumors
classification of
grade I giant pituitary tumors, 429
grade II giant pituitary tumors, 429
grade III giant pituitary tumors, 430
grade IV giant pituitary tumors, 430–431
grade I giant pituitary tumors, 429
grade II giant pituitary tumors, 429
grade III giant pituitary tumors, 430
grade IV giant pituitary tumors, 430–431
greater wings, 16

H
hormone replacement, 66
hyponatremia, 68–69

I
image-guided radiotherapy, 439
inferior compartment of cavernous sinus, 30–31
Inferior incision, 79–80
inferior surface, 16
inferior turbinate flap, 86–88
inferomedial compartment involvement of cavernous sinus, 320–323
intensity-modulated radiotherapy, 438–439
internal carotid artery engulfment, 390–392
internal carotid artery in relation to skull base, 422–427
intracavernous phase, 311
intracranial inlay grafting, 72
intraoperative magnetic resonance imaging, in endonasal surgery for pituitary adenoma, 394–397
intrinsic ligaments of the sphenoid, 19
involving medial cavernous sinus, 384–386

L
large solid pediatric adamantinomatous craniopharyngioma involving third ventricle, binostril transseptal transsphenoidal approach for, 404–410
lateral compartment of cavernous sinus, 30
lateral opticocarotid recess, 25
lateral pterygoid plate, 19
lateral surface, 16
left sphenoid sinus, pituitary macroadenoma extending to, 147–154
lumbar drain, 66

M
medial opticocarotid recess, 25
medial pterygoid plate, 19
meningioma, 51–52
meningiomas, 242
middle turbinate flap, 88
midline transsphenoidal endoscopic approach
sellar phase, 309–310
tumor dissection, 310
miscellaneous lesions, 55–57
mononostril transseptal transsphenoidal resection of pituitary macroadenoma, 398–403
MRI protocol, 36–37
mucosal decongestion, 78–79

N
nasal mucosa, preparation of, 66
nasal phase, 101–102
nasoseptal flap, 76–83
nonsecretory tumors, 449

O
onodi cell, 22
opening membrane of liliequist, 422
optic canal, 25
optic chiasm, 28
optic strut, 25
orbitomeningeal band dissection, 419

P
palatal flap, 97
paraclinoidal carotid, 25
paraclival internal carotid artery, 24
parasellar anatomy
  inferior compartment of cavernous sinus, 30–31
  lateral compartment of cavernous sinus, 30
  posterior compartment of cavernous sinus, 30
  superior compartment of cavernous sinus, 29–30
parasellar area, 306
parasellar internal carotid artery, 24–25
parasellar lesions, anesthetic considerations in surgery for
  emergence, 67
  induction and maintenance of anesthesia
    monitoring, 67
    prophylactic antibiotics, 67
  intraoperative complications, 67
  postoperative care
    airway management, 67–68
    diabetes insipidus, 68
    hyponatremia, 68–69
    pituitary apoplexy, 68–69
    postoperative analgesia, 68
  preoperative assessment
    airway management, 66
    anesthetic management, 66
    hormone replacement, 66
    lumbar drain, 66
    nasal mucosa, preparation of, 66
    position, 66
  presentation, 65
parasellar lesions, endoscopic approach to
  instrumentation and technical adjuncts, 307
  parasellar area, 306
  preoperative planning, 307
  surgery, indications of, 306
  surgery, limitations of
    anatomical limitations, 306–307
    patient and institution factors, 307
  surgery, rationale of, 307
  surgical technique
    ethmoid-pterygoid-sphenoidal approach
      ethmoid phase, 310
      intracavernous phase, 311
      pterygoid phase, 310–311
      sphenoid phase, 311
      tumor dissection, 311
    midline transsphenoidal endoscopic approach
      sellar phase, 309–310
      tumor dissection, 310
    transmaxilla-pterygoid endoscopic approach, 311–312
parasellar lesions, reconstructive options in surgery for,
  endoscopic skull base reconstruction
    general principles, 72–75
    selection of reconstructive measures, 71–72
    vascularized flaps in anterior skull base reconstruction
      anterior pedicle lateral nasal wall flap, 91–92
      facial buccinator flap, 97
      inferior turbinate flap, 86–88
      middle turbinate flap, 88
      nasoseptal flap, 76–83
      palatal flap, 97
      pericranial flap, 92–94
      posterior pedicled lateral nasal wall flap, 89–91
      rescue nasoseptal flap, 83–84
      reverse nasoseptal rotation flap, 84–86
      temporoparietal fascial flap, 94–97
parasellar lesions, surgery on
  cavernous sinus dural walls, 428–429
  giant pituitary tumors
    classification of
      grade I giant pituitary tumors, 429
      grade II giant pituitary tumors, 429
      grade III giant pituitary tumors, 430
      grade IV giant pituitary tumors, 430–431
  pituitary tumors, surgery on
    continued role of microscope
      lateral exposure of sella and of cavernous sinus, 433
      sublabial transsphenoidal approach, 431–433
    use of endoscope in, 433–434
parasellar regions, anatomical perspectives of
  development, 11–13
  diaphragma sella, 27
  parasellar anatomy
    inferior compartment of cavernous sinus, 30–31
    lateral compartment of cavernous sinus, 30
    posterior compartment of cavernous sinus, 30
    superior compartment of cavernous sinus, 29–30
  pituitary gland, 25–27
  sphenoid bone
    anterior surface, 16
    body, 14–15
    greater wings, 16
    inferior surface, 16
    intrinsic ligaments of the sphenoid, 19
    lateral pterygoid plate, 19
    lateral surface, 16
    medial pterygoid plate, 19
    posterior surface, 16
    pterygoid processes, 19
    lesser wing, 17
  sphenoid ostium
    onodi cell, 22
    posterior wall of sphenoid sinus
      lateral opticocarotid recess, 25
      medial opticocarotid recess, 25
      optic canal, 25
      optic strut, 25
      paraclinoidal carotid, 25
      paraclival internal carotid artery, 24
      parasellar internal carotid artery, 24–25
      planum sphenoidale, 22–23
      tuberculum sella, 23
  sphenoid sinus
    pneumatization patterns of the sphenoid sinus, 20–21
  suprasellar anatomy
    optic chiasm, 28
parasellar regions, radiological protocols in
  anatomy, 33–34
  imaging
    dynamic contrast MRI
      chordoma, 53–55
      craniopharyngioma, 46–51
      empty sella, 39
      meningioma, 51–52
      miscellaneous lesions, 55–57
      pituitary adenomas, 40–46
      pituitary hyperplasia, 40
      pituitary stalk lesions, 52–53
      Rathke's cleft cysts, 39

systematic approach to, 38–39
MRI protocol, 36–37
postoperative imaging, 57–58
parasellar regions, skull base approaches to lesions of
anterior clinoidectomy, 421
brain unlocking in axial and sagittal planes, 419
extended skin incision and craniotomy, 418
internal carotid artery in relation to skull base, 422–427
opening membrane of liliequist, 422
orbitomeningeal band dissection, 419
pericavernous dissection techniques, 419–421
petrous anatomy and anterior petrosectomy, 422
posterior clinoidectomy, 422
pedicle care, 75
pericavernous dissection techniques, 419
pericranial flap, 92–94
petrous anatomy and anterior petrosectomy, 422
pituitary abscess, 124–131
pituitary adenomas, 40–46
classification of, 103–104
pituitary apoplexy, 68–69, 112–117
pituitary gland, 25–27
pituitary hyperplasia, 40
pituitary macroadenoma, 104–111, 118–123, 313–319, 358–363
with acromegaly, 132–139
extending to left sphenoid sinus, 147–154
fibrous type, 193–198, 329–336
invasive, 351–357
mononostril transseptal transsphenoidal resection of, 398–403
parasellar extension, 345–350
suprasellar and parasellar extension, 364–368
with suprasellar and right parasellar extension, 218–224, 225–229
with suprasellar extension, 236–241
with suprasellar extension type A, 188–192, 230–235
with suprasellar extension type B, 199–206
pituitary stalk lesions, 52–53
pituitary tuberculosis, 155–160
pituitary tumors
radiation therapy for
aims of, 435–436
dose of, 437
follow-up, 454
nonsecretory tumors, 449
preradiation therapy workup, 436
radiation treatment plans for comparative analysis, 443–449
secretory tumors, 449–452
side effects, 452–454
techniques of
carbon ion therapy, 441
fractionated stereotactic radiotherapy, 441
image-guided radiotherapy, 439
intensity-modulated radiotherapy, 438–439
proton beam therapy, 441
stereotactic radiosurgery, 439–441
three-dimensional conformal radiotherapy, 437–438
two-dimensional radiotherapy, 437
volumetric modulated arc therapy, 439
timing of, 436
workflow, 441–443
pituitary tumors, surgery on
continued role of microscope
lateral exposure of sella and of cavernous sinus, 433
sublabial transsphenoidal approach, 431–433
use of endoscope in, 433–434
planum sphenoidale, 22–23
planum tuberculum meningioma, 243–246, 247–252, 253–258, 259–264
pneumatization patterns of the sphenoid sinus, 20–21
position, 66
posterior clinoidectomy, 422
posterior compartment of cavernous sinus, 30
posterior pedicled lateral nasal wall flap, 89–91
posterior surface, 16
posterior wall of sphenoid sinus
lateral opticocarotid recess, 25
medial opticocarotid recess, 25
optic canal, 25
optic strut, 25
paraclinoidal carotid, 25
paraclival internal carotid artery, 24
parasellar internal carotid artery, 24–25
planum sphenoidale, 22–23
tuberculum sella, 23
postoperative analgesia, 68
postoperative care
airway management, 67–68
diabetes insipidus, 68
hyponatremia, 68–69
pituitary apoplexy, 68–69
postoperative analgesia, 68
preoperative assessment
airway management, 66
anesthetic management, 66
hormone replacement, 66
lumbar drain, 66
nasal mucosa, preparation of, 66
position, 66
preradiation therapy workup, 436
prophylactic antibiotics, 67
proton beam therapy, 441
pterygoid phase, 310–311
pterygoid processes, 19

R

radiation therapy, for pituitary tumors
aims of, 435–436
dose of, 437
follow-up, 454
nonsecretory tumors, 449
preradiation therapy workup, 436
radiation treatment plans for comparative analysis, 443–449
secretory tumors, 449–452
side effects, 452–454
techniques of
carbon ion therapy, 441
fractionated stereotactic radiotherapy, 441
image-guided radiotherapy, 439
intensity-modulated radiotherapy, 438–439
proton beam therapy, 441
stereotactic radiosurgery, 439–441
three-dimensional conformal radiotherapy, 437–438
two-dimensional radiotherapy, 437
volumetric modulated arc therapy, 439
timing of, 436
workflow, 441–443
radiation treatment plans for comparative analysis, 443–449
Rathke's cleft cysts, 39, 161–166
Rathke's cyst, 167–173
reconstructive options in surgery for sellar, suprasellar, and parasellar lesions

endoscopic skull base reconstruction
general principles, 72–75
selection of reconstructive measures, 71–72
vascularized flaps in anterior skull base reconstruction
anterior pedicle lateral nasal wall flap, 91–92
facial buccinator flap, 97
inferior turbinate flap, 86–88
middle turbinate flap, 88
nasoseptal flap, 76–83
palatal flap, 97
pericranial flap, 92–94
posterior pedicled lateral nasal wall flap, 89–91
rescue nasoseptal flap, 83–84
reverse nasoseptal rotation flap, 84–86
temporoparietal fascial flap, 94–97
rescue nasoseptal flap, 83–84
reverse nasoseptal rotation flap, 84–86
revision pituitary macroadenoma
acromegaly, 337–344
with suprasellar extension, 207–212, 213–217

S

secretory tumors, 449–452
sellar lesions, anesthetic considerations in surgery for
emergence, 67
induction and maintenance of anesthesia
monitoring, 67
prophylactic antibiotics, 67
intraoperative complications, 67
postoperative care
airway management, 67–68
diabetes insipidus, 68
hyponatremia, 68–69
pituitary apoplexy, 68–69
postoperative analgesia, 68
preoperative assessment
airway management, 66
anesthetic management, 66
hormone replacement, 66
lumbar drain, 66
nasal mucosa, preparation of, 66
position, 66
presentation, 65
sellar lesions, endoscopic approach to
pituitary adenoma, classification of, 103–104
preoperative preparation, 100–101
steps of surgery
nasal phase, 101–102
sellar phase, 102–103
sphenoid phase, 102
transsphenoidal transsellar approach
indications for, 99
limitations of, 100
sellar lesions, reconstructive options in surgery for,
endoscopic skull base reconstruction
general principles, 72–75
selection of reconstructive measures, 71–72
vascularized flaps in anterior skull base reconstruction
anterior pedicle lateral nasal wall flap, 91–92
facial buccinator flap, 97
inferior turbinate flap, 86–88
middle turbinate flap, 88
nasoseptal flap, 76–83
palatal flap, 97
pericranial flap, 92–94
posterior pedicled lateral nasal wall flap, 89–91
rescue nasoseptal flap, 83–84
reverse nasoseptal rotation flap, 84–86
temporoparietal fascial flap, 94–97
sellar lesions, surgery on
cavernous sinus dural walls, 428–429
giant pituitary tumors
classification of
grade I giant pituitary tumors, 429
grade II giant pituitary tumors, 429
grade III giant pituitary tumors, 430
grade IV giant pituitary tumors, 430–431
pituitary tumors, surgery on
continued role of microscope
lateral exposure of sella and of cavernous sinus, 433
sublabial transsphenoidal approach, 431–433
use of endoscope in, 433–434
sellar phase, 102–103, 309–310
sellar regions, anatomical perspectives of
development, 11–13
diaphragma sella, 27
parasellar anatomy
inferior compartment of cavernous sinus, 30–31
lateral compartment of cavernous sinus, 30
posterior compartment of cavernous sinus, 30
superior compartment of cavernous sinus, 29–30
pituitary gland, 25–27
sphenoid bone
anterior surface, 16
body, 14–15
greater wings, 16
inferior surface, 16
intrinsic ligaments of the sphenoid, 19
lateral pterygoid plate, 19
lateral surface, 16
medial pterygoid plate, 19
posterior surface, 16
pterygoid processes, 19
lesser wing, 17
sphenoid ostium
onodi cell, 22
posterior wall of sphenoid sinus
lateral opticocarotid recess, 25
medial opticocarotid recess, 25
optic canal, 25
optic strut, 25
paraclinoidal carotid, 25
paraclival internal carotid artery, 24
parasellar internal carotid artery, 24–25
planum sphenoidale, 22–23
tuberculum sella, 23
sphenoid sinus
pneumatization patterns of the sphenoid sinus, 20–21
suprasellar anatomy
optic chiasm, 28
sellar regions, radiological protocols in
anatomy, 33–34
imaging
dynamic contrast MRI
chordoma, 53–55
craniopharyngioma, 46–51
empty sella, 39
meningioma, 51–52
miscellaneous lesions, 55–57
pituitary adenomas, 40–46

pituitary hyperplasia, 40
pituitary stalk lesions, 52–53
Rathke's cleft cysts, 39
systematic approach to, 38–39
MRI protocol, 36–37
postoperative imaging, 57–58
sellar regions, skull base approaches to lesions of
anterior clinoidectomy, 421–422
brain unlocking in axial and sagittal planes, 419
extended skin incision and craniotomy, 418
internal carotid artery in relation to skull base, 422–427
opening membrane of liliequist, 422
orbitomeningeal band dissection, 419
pericavernous dissection techniques, 419–421
petrous anatomy and anterior petrosectomy, 422
posterior clinoidectomy, 422
sellar, suprasellar, and parasellar regions, radiological protocols in
anatomy, 33–34
imaging
dynamic contrast MRI
chordoma, 53–55
craniopharyngioma, 46–51
empty sella, 39
meningioma, 51–52
miscellaneous lesions, 55–57
pituitary adenomas, 40–46
pituitary hyperplasia, 40
pituitary stalk lesions, 52–53
Rathke's cleft cysts, 39
systematic approach to, 38–39
MRI protocol, 36–37
postoperative imaging, 57–58
sellar–suprasellar craniopharyngioma, 174–180
septal factors, 77–78
skull base approaches, to lesions of sellar and parasellar regions
anterior clinoidectomy, 421–422
brain unlocking in axial and sagittal planes, 419
extended skin incision and craniotomy, 418
internal carotid artery in relation to skull base, 422–427
opening membrane of liliequist, 422
orbitomeningeal band dissection, 419
pericavernous dissection techniques, 419–421
petrous anatomy and anterior petrosectomy, 422
posterior clinoidectomy, 422
skull base reconstruction, temporoparietal fascial flap for, 101
lesser wing, 17
sphenoid bone
anterior surface, 16
body, 14–15
greater wings, 16
inferior surface, 16
intrinsic ligaments of the sphenoid, 19
lateral pterygoid plate, 19
lateral surface, 16
medial pterygoid plate, 19
posterior surface, 16
pterygoid processes, 19
lesser wing, 17
sphenoid center ossification, 21
sphenoid ostium
onodi cell, 22
posterior wall of sphenoid sinus
lateral opticocarotid recess, 25
medial opticocarotid recess, 25
optic canal, 25
optic strut, 25
paraclinoidal carotid, 25
paraclival internal carotid artery, 24
parasellar internal carotid artery, 24–25
planum sphenoidale, 22–23
tuberculum sella, 23
sphenoid phase, 102, 311
sphenoid sinus
pneumatization patterns of the sphenoid sinus, 20–21
stereotactic radiosurgery, 439–441
submucoperiosteal elevation, 84
superior compartment of cavernous sinus, 29–30
superior incision, 80
superomedial compartment of cavernous sinus, 324–328
suprasellar lesions, anesthetic considerations in surgery for
emergence, 67
induction and maintenance of anesthesia
monitoring, 67
prophylactic antibiotics, 67
intraoperative complications, 67
postoperative care
airway management, 67–68
diabetes insipidus, 68
hyponatremia, 68–69
pituitary apoplexy, 68–69
postoperative analgesia, 68
preoperative assessment
airway management, 66
anesthetic management, 66
hormone replacement, 66
lumbar drain, 66
nasal mucosa, preparation of, 66
position, 66
presentation, 65
suprasellar lesions, reconstructive options in surgery for,
endoscopic skull base reconstruction
general principles, 72–75
selection of reconstructive measures, 71–72
vascularized flaps in anterior skull base reconstruction
anterior pedicle lateral nasal wall flap, 91–92
inferior turbinate flap, 86–88
middle turbinate flap, 88
nasoseptal flap, 76–83
pericranial flap, 92–94
posterior pedicled lateral nasal wall flap, 89–91
rescue nasoseptal flap, 83–84
reverse nasoseptal rotation flap, 84–86
temporoparietal fascial flap, 94–97
suprasellar regions, anatomical perspectives of
development, 11–13
diaphragma sella, 27
parasellar anatomy
inferior compartment of cavernous sinus, 30–31
lateral compartment of cavernous sinus, 30
posterior compartment of cavernous sinus, 30
superior compartment of cavernous sinus, 29–30
pituitary gland, 25–27
sphenoid bone
anterior surface, 16
body, 14–15
greater wings, 16
inferior surface, 16
intrinsic ligaments of the sphenoid, 19
lateral pterygoid plate, 19
lateral surface, 16

medial pterygoid plate, 19
posterior surface, 16
pterygoid processes, 19
lesser wing, 17
sphenoid ostium
onodi cell, 22
posterior wall of sphenoid sinus
lateral opticocarotid recess, 25
medial opticocarotid recess, 25
optic canal, 25
optic strut, 25
paraclinoidal carotid, 25
paraclival internal carotid artery, 24
parasellar internal carotid artery, 24–25
planum sphenoidale, 22–23
tuberculum sella, 23
sphenoid sinus
pneumatization patterns of the sphenoid sinus, 20–21
suprasellar anatomy
optic chiasm, 28
suprasellar regions, radiological protocols in
anatomy, 33–34
imaging
dynamic contrast MRI
chordoma, 53–55
craniopharyngioma, 46–51
empty sella, 39
meningioma, 51–52
miscellaneous lesions, 55–57
pituitary adenomas, 40–46
pituitary hyperplasia, 40
pituitary stalk lesions, 52–53
Rathke's cleft cysts, 39
systematic approach to, 38–39
MRI protocol, 36–37
postoperative imaging, 57–58
systematic approach to, 38–39

T

temporoparietal fascial flap, 94–97
temporoparietal fascial flap, for skull base reconstruction, 101
three-dimensional conformal radiotherapy, 437–438
transmaxilla-pterygoid endoscopic approach, 311–312
transsphenoidal transsellar approach
indications for, 99
limitations of, 100
tuberculum sella, 23
tumor dissection, 310, 311
two-dimensional radiotherapy, 437

V

vascularized flaps, in anterior skull base reconstruction
anterior pedicle lateral nasal wall flap, 91–92
inferior turbinate flap, 86–88
middle turbinate flap, 88
nasoseptal flap, 76–83
pericranial flap, 92–94
posterior pedicled lateral nasal wall flap, 89–91
rescue nasoseptal flap, 83–84
reverse nasoseptal rotation flap, 84–86
temporoparietal fascial flap, 94–97
vascular pedicle, 76–77
volumetric modulated arc therapy, 439